New Jersey Geological Survey

Bulletin 77

Contributions to the Geology and Hydrogeology of the Newark Basin

State of New Jersey
Department of Environmental Protection
Water Resources Management
New Jersey Geological Survey
2010

For product and ordering information:
World Wide Web: www.state.nj.us/dep/njgs/bulletin77/
Telephone: 609-984-6587

The NJ Geological Survey (NJGS) is a public service and research agency within the NJ Department of Environmental Protection. Founded in 1835, the NJGS has evolved from a mineral resources and topographic mapping agency to a modern environmental organization that collects and provides geoscience information to government, consultants, industry, environmental groups, and the public.
For more information on the NJGS visit us on the World Wide Web at: www.njgeology.org.

Front cover. Geophysical logging of the Springdale Golf Course, Princeton University, Mercer County, NJ by the NJ Geological Survey in December 2003. The Princeton University Carillon (Class of 1892 Bells) looms in the distance.

Contributions to the Geology and Hydrogeology of the Newark Basin

Edited by Gregory C. Herman and Michael E. Serfes, N.J. Geological Survey

Prepared in cooperation with
the U.S. Geological Survey,
Oberlin College, Lafayette College and
Michalski and Associates.

This volume is published as chapters A through F and Appendixes 1 to 4.

N.J. Geological Survey Bulletin 77

State of New Jersey
Department of Environmental Protection
Water Resource Management
New Jersey Geological Survey
2010

Conversion Factors and Datums

Multiply	By	To obtain
	Length	
micrometer (μm)	0.00003937	Inch (in.)
millimeter (mm)	0.03937	Inch (in.)
centimeter (cm)	0.3937	Inch (in.)
meter(m)	3.281	foot (ft)
kilometer (km)	0.6214	mile (mi)
	Area	
square kilometer (km^2)	0.3861	square miles (mi^2)
	Fluid volume	
1 gallon	231	cubic inches (in^3)
1 gallon	0.134	cubic feet (ft^3)
1 liter	0.264	gallon (gal)
	Flow rate (volumetric)	
1 liter per second (L/s)	15.85	gallons per minute (gpm)
1 cubic meter per day (m^3/d)	0.183	gallons per minute (gpm)
1 cubic meter per day (m^3/d)	35.3107	cubic foot per day (cfd)
1 cubic foot per second (cfs)	449	gallons per minute (gpm)
	Hydraulic conductivity	
1 centimeter/second (cm/sec)	1.97	feet per minute (ft/min)
1 centimeter/second (cm/sec)	2837	feet per day (ft/day)
1 centimeter/second (cm/sec)	21200	gallons per day per foot squared (gpd/ft^2)
1 meter/day (m/day)	24.5	gallons per day per foot squared (gpd/ft^2)
1 meter/day (m/day)	3.281	feet per day (ft/day)
	Transmissivity*	
meters squared per day (m^2/day)	**10.765**	feet squared per day (ft^2/d)
	Volume of water in wells	
h = height of water column (ft)	2” well	V = 0.16 h
	4” well	V = 0.65 h
	6” well	V = 1.47h
	8” well	V = 2.61 h
	10” well	V = 4.08 h

Temperature in Fahrenheit (^oF) = (1.8 x ^oC) + 32

*Standard units for transmissivity (T) are cubic foot per day per square foot times foot of aquifer thickness "[(ft^3/d)/ft^2]ft" or cubic meters per day per square meter times meter of aquifer thickness "[(m^3/d)/m^2]m." These mathematical expressions reduce to foot squared per day "ft^2/d" or meter squared per day "m^2/d."

Horizontal coordinate information is referenced to the North American Datum of 1983 (NAD83) unless otherwise stated. Vertical coordinate information is referenced to the North American Vertical Datum of 1988 (NAVD 88) unless otherwise stated.

Contents

[1]US Geological Survey, [2]Oberlin College, [3]West Virginia Dept. of Environmental Protection, [4]Lafayette College, [5]Michalski & Associates, Inc., [6]NJ Geological Survey, [7]Rutgers University

Appendix Contents

Borehole Geophysics and Hydrogeology Studies in the Newark Basin, New Jersey

Photos of organizers and panelists at the hydrogeology workshop at the New Brunswick campus of Rutgers University, November 11-12, 2004.
Workshop organizers (from left to right): Glen Carleton (USGS), Pierre Lacombe (USGS), Ying Fan Reinfelder (Rutgers University), Michael Serfes (NJGS), Zoltan Szabo (USGS), Lisa Senior (USGS), Gregory Herman (NJGS). Not shown are Laura Toran (Temple University), and Andrew Michalski (Michalski Associates).

Panel Discussion, Day 1. From left to right: Pierre LaCombe (USGS), Joseph Smoot (USGS), Paul Olsen (Lamont Doherty Earth Observatory), Roy Schlische (Rutgers University), Robert Bond (Langan Engineering), Andrew Michalski (Michalski & Associates), MaryAnn Malinconico (Lafayette College), and Gregory Herman (NJGS).

Panel Discussion, Day 2. From left to right: Daniel Goode (USGS), Joseph Smoot (USGS), Glen Carleton (USGS), Zoltan Szabo (USGS), Michael Serfes (NJGS), Donna Fennell (Rutgers University), and Danielle Rhine (Rutgers Uinversity). Photographs by Yuri Mun (Rutgers University).

Introduction

New Jersey Geological Survey Bulletin 77 is an outgrowth of a group discussion that took place in early 2004 following a Henry Darcy distinguished lecture given by Dr. Alan Shapiro of the U.S. Geological Survey at the New Brunswick campus of Rutgers University. This discussion focused on hydrogeological work being conducted in the Newark basin, an Early Mesozoic basin filled with fractured sedimentary and igneous bedrock located in eastern Pennsylvania, central New Jersey, and southwest New York State. The basin underlies some of the most densely populated areas in the country, and therefore, is increasingly subject to environmental stresses including increasing groundwater demand and pollution. Discussion revealed that there is a large amount of information being collected by investigators, but there is a lack of awareness and availability of this information, including the diversity of processes studied, the competing views concerning major controls on groundwater flow, flux, and quality, the various advanced tools and techniques currently used to understand these controls. A regional workshop subsequently was convened to address some of these needs on November 11-12, 2004 at the New Brunswick campus of Rutgers University. Participation of various government agencies, universities, and the private sector provided an initial forum for exchanging and integrating ideas and findings (see photos on the opposite page). At this workshop, a NJ Geological Survey publication was proposed to provide a synthesis of the cumulative body of work.

The result, Bulletin 77 contains six articles and four appendixes detailing geological research conducted in the Newark basin during the past 30 years. The purpose of this bulletin is to provide geologists and environmentalists with a more thorough understanding of how the basin formed and evolved, and how these developments affected present day groundwater storage, transmission, and chemistry. The first two articles (chapters A and B) focus on traditional geological aspects including the stratigraphic framework and bedrock composition, and detailed analyses and descriptions of the secondary minerals filling aquifer pores. These are critical aspects of how the basin aquifers formed and evolved into their present state, and provide a sense of dimension, geometry and composition for aquifers throughout the basin. The remaining four articles (chapters C through F) focus on hydrogeological topics. Chapter C addresses basin-scale groundwater movement in early stages of the basin's history using vitrinite-reflectance thermal-alteration indexes for the three primary formations in the basin, together with reported fission-track geothermometry, geochronology, and radiometric-age controls. With respect to modern groundwater issues, chapter D summarizes practical methods of characterizing groundwater flow in the shallow subsurface at contamination sites and discusses conceptual flow models for the fractured-bedrock aquifers. Chapter E focuses on arsenic in groundwater, a recognized public health issue, and summarizes the state of knowledge of its geologic sources, and its mobilization and transport in organic-rich black and gray beds and other red mudstone and siltstone beds. Chapter F summarizes the results of research conducted by NJGS on the types and distribution of subsurface water-bearing features (WBFs) penetrated by water wells throughout the basin. The WBFs are identified, photographed, measured, classified, and related to other aquifer properties using geophysical logs for each well. Detailed results of each project are summarized in the appendixes.

Appendixes 1 to 4 include study results from more than 30 hydrogeology studies of hundreds of water wells in the New Jersey part of the Newark basin from 2001 to 2008. The appendixes provide location maps, borehole-televiewer photographic records of borehole walls and features, and hydrogeological sections detailing the different types and occurrences of WBFs in the subsurface water-bearing zones of each aquifer. The appendixes are based on aquifer groups, including: 1) diabase and basalt igneous rocks, 2) Brunswick aquifer coarse-grained rocks, including conglomerate and sandstone, 3) Brunswick aquifer fine-gained rocks, including mudstone and siltstone and 4) Lockatong argillite and Stockton sandstone. Each appendix includes multiple entries, with each entry detailing the results for a single project.

We are thankful to have had the opportunity to work with the contributors and editors to see this bulletin to completion. This work provides a modern understanding of how the basin aquifers formed, how groundwater is stored and flows in these fractured-bedrock aquifers, and the sources, mobilization, and transport of naturally-occurring arsenic in the basin's groundwater.

Triassic Depositional Facies in the Newark Basin

By Joseph P. Smoot, U.S. Geological Survey

Chapter A of

Contributions to the Geology and Hydrogeology of the Newark Basin

N.J. Geological Survey Bulletin 77

State of New Jersey
Department of Environmental Protection
Water Resource Management
New Jersey Geological Survey
2010

Contents

Figures

Tables

Chapter A

Triassic Depositional Facies in the Newark Basin

Joseph P. Smoot[1]

Abstract

The early Mesozoic Newark basin is a half-graben filled with more than 7 km of continental fluvial and lacustrine deposits intruded by tholeiitic diabase, and interbedded with tholeiitic basalt flows spanning about 35 million years from the late Triassic to the early Jurassic. The Triassic sedimentary rocks include fluvial deposits of the Stockton Formation overlain by a complex assemblage of facies consisting of the Lockatong, Passaic, and Hammer Creek Formations. The Stockton Formation has three major lithologies: conglomerate and conglomeratic sandstone interpreted as low-sinuosity, braided channel deposits, arkosic sandstone comprising upward-fining sequences that are interpreted as lateral accretion deposits of point bars in large meandering rivers, and micaceous sandstone, siltstone, and mudstone sequences that are interpreted as the deposits of avulsion flood plains with intermittent lakes. The central basin facies of the Lockatong and Passaic Formations are a continuum of lithologies that include laminated mudstone, thin-bedded mudstone, and massive mudstone. The lithologies form rhythmic cycles termed Van Houten cycles that are part of a nested hierarchy of cyclicity attributed to climate forcing by orbital eccentricities (Milankovitch cycles). The Lockatong and Passaic Formations are divided into informal members by the third-order periodicities called McLaughlin cycles defined by groupings of more closely spaced laminated mudstone beds versus more closely spaced massive mudstone beds. Laminated mudstone ranges from flat-laminated, black, organic-rich mudstone, interpreted as deposits of very deep lakes, to black or gray mudstone with siltstone to fine sandstone laminae that rhythmically thicken and thin, interpreted as perennial lake deposits that are shallow enough to be affected by surface waves. Thin-bedded mudstone includes gray and red mudstone transitional to laminated mudstone with features indicating wave reworking and intermittent desiccation, and red to gray mudstone with features indicating very shallow water and frequent periods of desiccation. Massive mudstones are red to gray and include types that are brecciated, vesicular, peloidal, burrow-disrupted, and root-disrupted. All except the burrow-disrupted type indicate subaerial exposure, either by disruption of subaqueous deposits, or by accumulation under subaerial conditions. Three types of features indicate the presence of saline minerals in the central basin mudstones. Calcite pseudomorphs after monoclinic minerals are interpreted as cumulate crystals formed in perennial saline lakes; cement-filled crystal casts are interpreted as sediment-enclosed crystals and crystal crusts formed in shallow saline lakes and saline mudflats; and gypsum and anhydrite are interpreted as saline soil features in vegetated mudflats. The basin margin facies of the Lockatong and Passaic Formations include wave-dominated sandstone and deltaic sandstone that are intercalated with Van Houten cycles of mudstones in the central basin facies. Axial sandstone and conglomerate consist of upward-coarsening, basinward-thinning wedges more than a kilometer thick that extend inward from the northeastern and northwestern ends of the basin. They are interpreted as fluvial deposits along the basin axis forming terminal fans that intertongue with the central basin facies. Border conglomerate and sandstone are limited to a narrow area along the faulted northwestern margin of the basin and are interpreted as alluvial fan deposits. Limestone is a minor component of the Newark basin Triassic rocks. Stromatolitic limestone is interpreted as shoreline tufa deposits, nodular limestone is interpreted as soil calcrete, and flat, limestone thin beds are interpreted as lake deposits in areas of low sedimentation.

The Newark basin formed as a half-graben that grew wider and longer with time in response to movement along the border fault system. The Stockton Formation represents the initial capture of river drainage in the subsiding basin. High-energy braided rivers drained the southeastern highlands and exited the basin via outlets cut into the sharp relief at the northwestern end of the basin formed by movement along the border fault system. Limited outflow caused intermittent flooding of the basin floor, so that the braided river channels anastomosed on a broad muddy plain. As the basin became wider, the velocity of rivers draining the southeastern highlands was reduced and they became more sinuous. The lower river velocities also decreased their ability to cut outlets, so that the continued uplift on the northwestern border faults slowly closed off the outlets. This caused the development of lakes that were shallow at first and spilled through the elevated outlets.

[1]US Geological Survey
M.S. 926A, National Center
Reston, VA 20192
jpsmoot@usgs.gov

Eventually they became very deep and only spilled during the highest lake stands. The continued widening of the basin reduced the number of deep lakes from deposition of the Lockatong Formation to deposition of the Passaic Formation. Tectonic movements probably controlled the opening and closing of axial drainage systems during deposition of the Lockatong and Passaic Formations.

Climate change during Triassic sedimentation in the Newark basin was partially controlled by the drift of Pangea from tropical latitudes to dryer latitudes. This climate change is indicated by well-developed rooted soils in the Stockton Formation and in the lowest part of the Lockatong Formation, followed by an interval with deposits in saline lakes and on playa saline mudflats in the Lockatong and lower part of the Passaic Formation. The upper part of the Passaic Formation contains common root-disrupted mudstone indicating vegetated mudflats and the absence of saline lake or dry playa mudflat deposits. Some of these changes could also be attributed to the tectonic development of the basin. The transition from alkaline saline lake and saline mudflat deposits to gypsum and anhydrite saline soils is probably partly due to the opening of evaporite-rich basins east of the Newark basin sometime during deposition of the Passaic Formation.

The tectonic and climatic development of the Newark basin throughout the Triassic explains the distribution of lithologic facies exposed at the surface and their distribution in the downdip direction. Many uncertainties remain due to lack of outcrop and ambiguities in the depositional models.

Introduction

The Newark basin is an early Mesozoic half graben extending 7500 km^2 across Pennsylvania, New Jersey, and New York (fig. A1). It is one of a series of basins that parallel the eastern margin of North America that are collectively referred to as the Newark Supergroup (Froelich and Olsen, 1983). These basins developed from the extensional forces that led to the opening of the Atlantic Ocean and break-up of Pangea. The northwest margin of the Newark basin is dominated by normal faults and folded early Mesozoic strata abutting Precambrian and Paleozoic basement rocks. The southeast margin of the basin is in unconformable contact with the underlying metamorphic rocks. The northeast end of the basin is marked where the basal deposits are truncated by the northwest border fault. The southwest end of the basin is attached to the Gettysburg basin by a narrow belt of sedimentary rocks called the “Narrow Neck”. The eastern margin of the Narrow Neck is defined as the eastern edge of the Morgantown diabase sheet ring (fig. A1).

The Newark basin is divided into four major fault blocks which repeat most of the Triassic section three times (fig. A1). The basin fill consists of more than 7 km of stratigraphic section including upper Triassic through lower Jurassic conglomerate, sandstone, and mudstone that are fluvial and lacustrine deposits. The Triassic strata are intruded by tholeiitic diabase and the Jurassic sedimentary rocks are interbedded with tholeiitic basalt flows. The basin-fill deposits thicken toward the faulted margin of the half graben and thin toward its southeastern margin.

The stratigraphic nomenclature for the Newark basin used in this paper (figs. A1 and A2) was first introduced by Olsen (1980). The basal unit is the Triassic Stockton Formation consisting mostly of sandstone and red mudstone that are interpreted as fluvial deposits. McLaughlin (1945) named four mappable ridge-forming sandstones in the Stockton Formation as members (fig. A2). The Stockton Formation is conformably overlain by the Triassic Lockatong Formation consisting of gray mudstone and black shale with minor red mudstone interpreted as lacustrine deposits. Olsen and others (1996) divided the Lockatong into twelve informal members based upon the distribution of black, gray, and red mudstone beds (fig. A2). The Lockatong Formation is overlain by, and laterally equivalent to, the Passaic Formation, which is mostly Triassic and possibly Jurassic at the top. The Passaic Formation is similar to the Lockatong, but contains predominantly red mudstone and minor black shale and gray mudstone. Olsen and others (1996) divided the Passaic Formation into 40 informal members based on the distribution of gray and black mudstone beds. The Lockatong and Passaic Formations grade laterally into red conglomerates and sandstones interpreted as alluvial fan and fluvial deposits near the faulted basin margin and the northeastern and southwestern ends of the basin. At the southwestern end, in Pennsylvania, conglomerates and sandstones form a wedge that is mapped as the Triassic Hammer Creek Formation, whereas a similar wedge of conglomerate and sandstone in New Jersey is mapped as part of the Passaic Formation. The Passaic Formation is overlain by Jurassic basalt flows that alternate with shale, sandstone, and conglomerate interpreted as lacustrine deposits with lateral fluvial and alluvial fan facies. These are mapped as the Orange Mountain Basalt, the Feltville Formation, the Preakness Basalt, the Towaco Formation, the Hook Mountain Basalt, and the Boonton Formation.

The ages of the rocks in the Newark basin are mostly constrained by palynology (Cornet, 1977), potassium-argon age dates on basalt flows (Hames and others, 2000), potassium-argon and U-Pb dates on diabase dikes interpreted as feeders to the basalts (Sutter, 1988; Dunning and Hodych, 1990), and U-Pb dates from a carbonate tufa stromatolite (Rasbury and

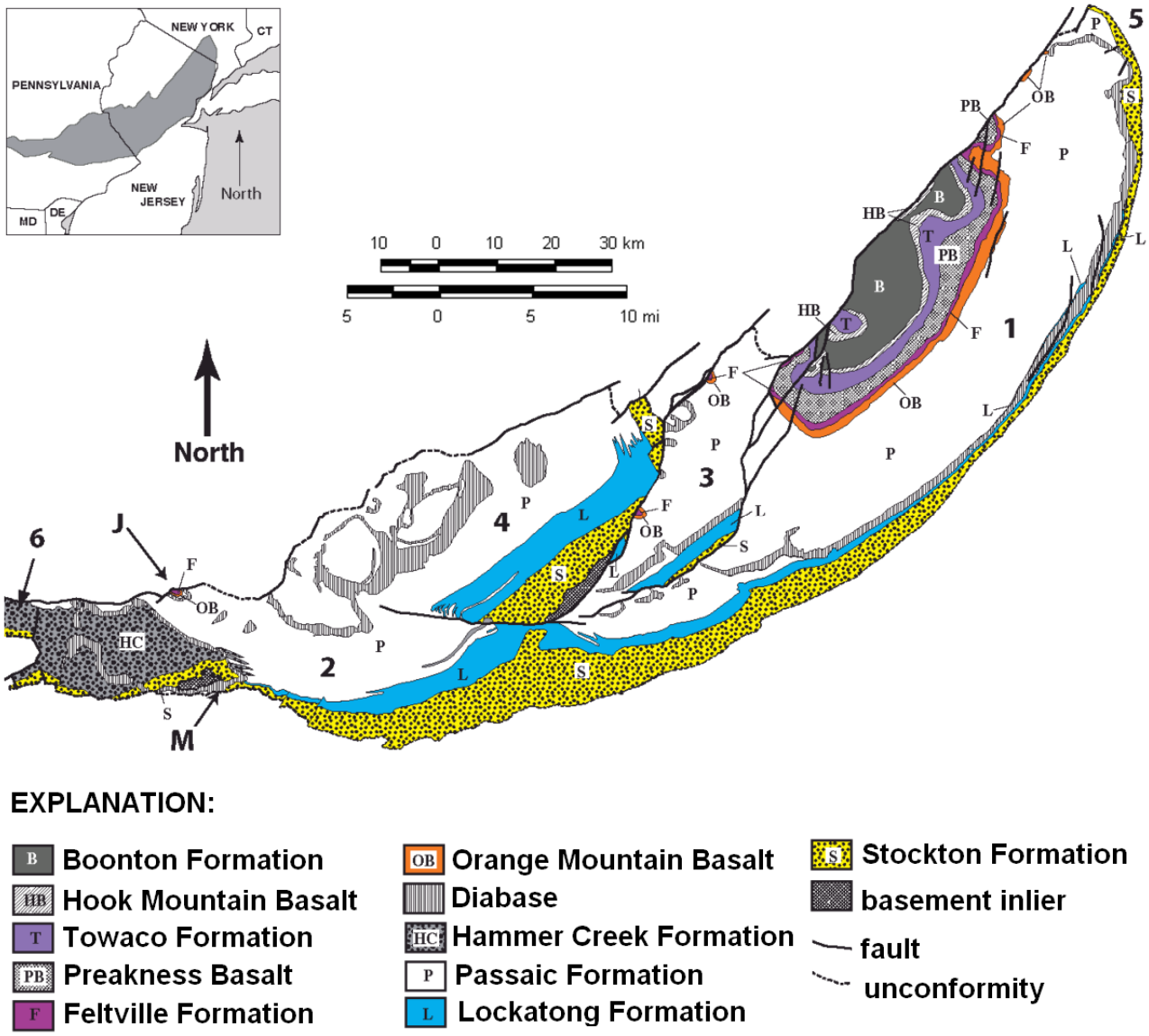

Figure A1. Geologic map of Newark basin in New York, New Jersey, and Pennsylvania (inset). Structural features are: 1) southeastern fault block, 2) southwestern fault block, 3) central fault block, 4) northwestern fault block, 5) eastern axial end, 6) "Narrow Neck" and western axial end. "J" shows location of the Jacksonwald syncline and "M" shows the southern edge of the Morgantown diabase sheet forming a ring at the surface. The southeastern boundary of the basin is an unconformity. Modified from Olsen and others (1996).

others, 2003). Kozur and Weems (2005, 2007) suggest that conchostracans provide biostratigraphic age constraints through correlation with marine and continental strata of the Germanic Basin in Europe. Olsen and others (1996, in press) assign basal strata of the Newark basin to a Carnian age, and the Triassic-Jurassic boundary is placed just below the Orange Mountain Basalt. In contrast, Kozur and Weems (2005, 2007) place the Triassic-Jurassic boundary above the Feltville Formation and the boundary of Olsen and others (1996) as an unconformity separating the Norian (Sevatian) and the upper Rhaetian. Because the work of Kozur and Weems (2005, 2007) is still in its preliminary stages, this paper uses the Triassic-Jurassic boundary of Olsen and others (1996, in press). Olsen and others (1996) believed that the Carnian-Norian boundary is somewhere near the Lockatong-Passaic contact in the central basin, whereas Olsen and others (in press) indicate that the Carnian-Norian boundary is at an unconformity within the Stockton Formation. Kozur and Weems (2007) support the earlier conclusion of Olsen and others (1996).

This paper focuses on the Triassic strata of the Newark basin (fig. A2). Although a significant part of the stratigraphic record is of Jurassic age, the Jurassic

strata are restricted to areas near the border fault and they are poorly exposed. In contrast, the Triassic strata are fairly well exposed along stream and river cuts, in quarries, and in various ephemeral exposures associated with railroads, highways, and building foundations. Individual beds of Triassic strata are traceable along strike using rock chips in the soil (different colors of soil are visible in aerial photographs) and using the topographic expressions of rock units. In addition, uplift of the central and northwestern fault blocks (fig. A1) provide lateral glimpses of the different units approaching the basin border fault. The map distribution of lithologies shown in figures A3 to A5 emphasizes my interpretation of sedimentological associations.

Studies of Triassic strata in the Newark basin include a US Geological Survey (USGS) study of Newark Supergroup basins during the middle 1980's, and ongoing work by Paul Olsen and his students at Lamont-Doherty Earth Observatory of Columbia University. In addition, cooperative mapping projects involving the USGS, New Jersey and Pennsylvania Geological Surveys produced new maps (Drake and others, 1996; Owens and others, 1998) and an overview of early Mesozoic rocks in Pennsylvania (Smoot, 1999; Froelich and Gottfried, 1999). The Newark Basin Coring Project was initiated by Paul Olsen at Columbia University and Dennis Kent at Rutgers University and provides continuous overlapping cores from the base of the Orange Mountain Basalt to less than a hundred meters from the base of Stockton Formation (Olsen and others, 1996). Additional information on the Triassic strata in the Newark basin is provided by a coring transect by the Army Core of Engineers in the northeastern corner of the basin (Fedosh and Smoot, 1988) and by a series of cores at the Naval Air Warfare Center (NAWC) in Trenton, New Jersey (LaCombe, 2000). Finally, two seismic lines (fig. A6, NB-1 and 85SD10) transect the width of the Newark basin in Pennsylvania (Reynolds, 1993; Schlische and Withjack, 2005). A deep well providing information on lithologies and stratigraphic thicknesses is near each seismic line.

Sedimentology of the Triassic rocks of the Newark basin

This paper discusses the sedimentary evolution of the Newark basin and explains the regional distributions of rock types. Each of the Triassic stratigraphic units is described on the basis of current understanding of its sedimentology. The Stockton Formation is described separately although it partly grades into the Lockatong Formation. The Lockatong and Passaic Formations are parts of a continuum with separate facies in the central and marginal parts of the basin. The Hammer Creek Formation is described in the basin margin facies of the Lockatong and Passaic Formations. This work follows the stratigraphic nomenclature of Olsen and others (1996), particularly the use of informal members within each of the formations (fig. A2). Some of the sedimentological information has been previously published (Smoot, 1991, Smoot and Olsen, 1994, and Smoot, 1999).

Stockton Formation

The oldest stratigraphic unit in the Newark basin is the Stockton Formation. It has a maximum thickness of about 1800 m in the central part of the basin, and it thins towards the southeast unconformable boundary as well as to the northeast and southwest ends

(RIGHT) Figure A2. Stratigraphic units and thickness of early Mesozoic rocks in the Newark basin. Two different interpretations of the Triassic-Jurassic boundary are shown: Olsen and others (1996)[1] and Kozur and Weems (2007)[2]. The broad band in the second column on the left represents the boundary of Kozur and Weems (2007) and indicates the uncertainty of its position. Detailed stratigraphy and thickness of the Triassic rocks in the central part of the basin shown to the right. Stockton lithologies include conglomerate, conglomeratic sandstone, and arkosic sandstone (coarse stippling), and micaceous sandstone, siltstone, and mudstone (fine stippling). Lockatong and Passaic lithologies are all mudstones that are black (black bands), dark and medium gray (darker gray bands) or light-gray to purple gray (light-gray bands), or red (white bands). Stockton Formation members are from McLaughlin (1945). Lockatong and Passaic Formation informal members are from Olsen and others (1996). Two different models for the Stages are also shown: Olsen and others (1996)[1] and Olsen and other (in press)[3] which includes substages. The degree of uncertainty on a boundary is indicated by an inclined contact. Kozur and Weems (2005, 2007) place an unconformity between the Sevatian and Rhaetian at the base of the Exeter Township Member and the Carnian-Norian boundary in the Walls Island Member. Modified from Olsen and others (1996), Olsen and Rainforth (2001), and Kozur and Weems (2007).

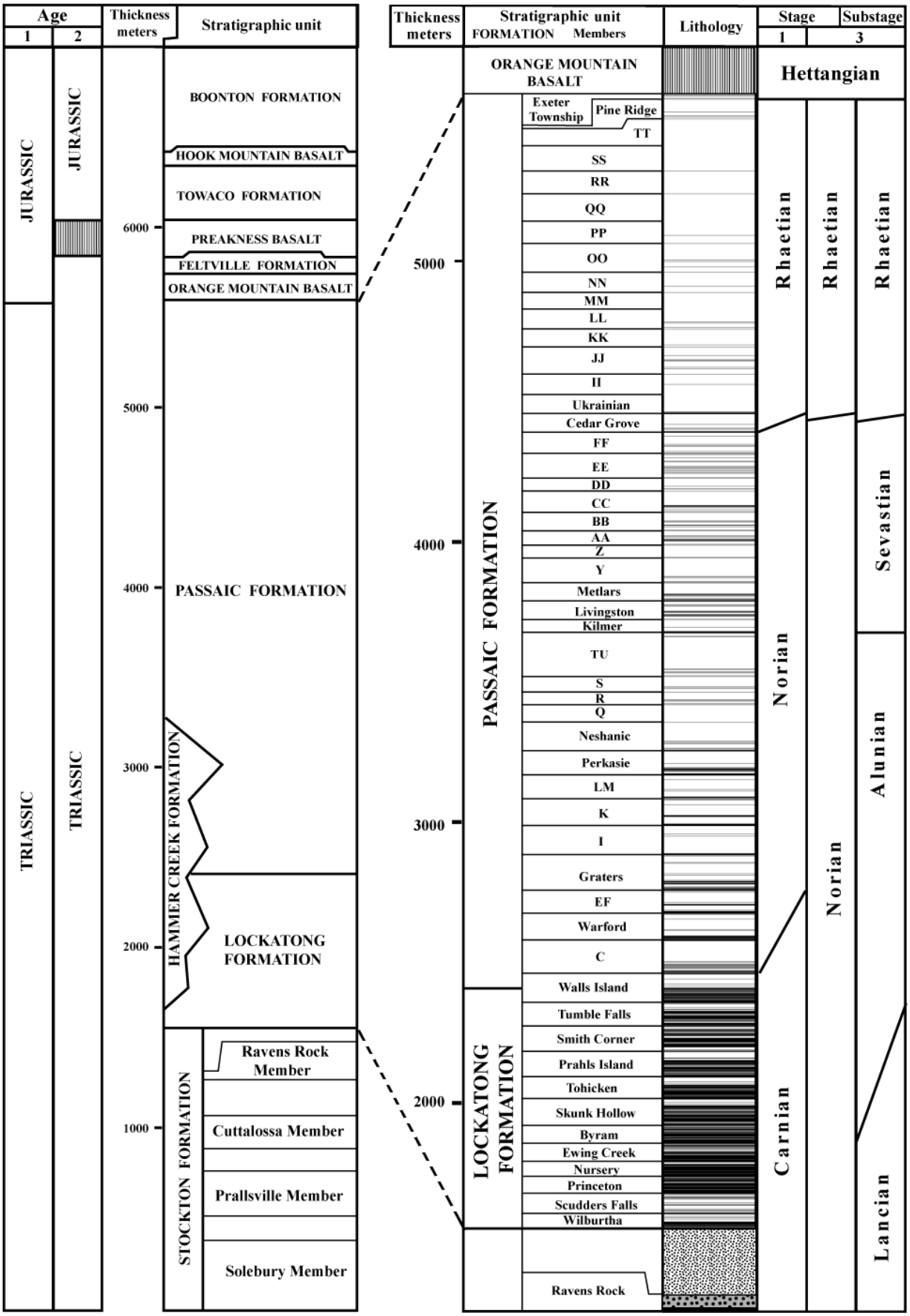
Age
1
2
Thickness meters
Stratigraphic unit
JURASSIC
TRIASSIC
BOONTON FORMATION
HOOK MOUNTAIN BASALT
TOWACO FORMATION
PREAKNESS BASALT
FELTVILLE FORMATION
ORANGE MOUNTAIN BASALT
PASSAIC FORMATION
HAMMER CREEK FORMATION
LOCKATONG FORMATION
STOCKTON FORMATION
Ravens Rock Member
Cuttalossa Member
Prallsville Member
Solebury Member
6000
5000
4000
3000
2000
1000
Thickness meters
Stratigraphic unit
FORMATION Members
Lithology
Stage
Substage
1
3
ORANGE MOUNTAIN BASALT
Hettangian
Exeter Township
Pine Ridge
TT
SS
RR
QQ
PP
OO
NN
MM
LL
KK
JJ
II
Ukrainian
Cedar Grove
FF
EE
DD
CC
BB
AA
Z
Y
Metlars
Livingston
Kilmer
TU
S
R
Q
Neshanic
Perkasie
LM
K
I
Graters
EF
Warford
C
Walls Island
Tumble Falls
Smith Corner
Prahls Island
Tohicken
Skunk Hollow
Byram
Ewing Creek
Nursery
Princeton
Scudders Falls
Wilburtha
Ravens Rock
PASSAIC FORMATION
LOCKATONG FORMATION
5000
4000
3000
2000
Rhaetian
Rhaetian
Rhaetian
Norian
Norian
Carnian
Sevastian
Alunian
Lancian

Table A1. Locations of cores and photographs in figures. Locality numbers are shown in map figures indicated.

Locality	Map Location	Description
1……	Figure A3	Princeton core of the Newark Basin Coring Project
2……	Figure A4	Nursery core of the Newark Basin Coring Project
3……	Figure A4	Titusville core of the Newark Basin Coring Project
4……	Figure A3	Rutgers core of the Newark Basin Coring Project
5……	Figure A3	Somerset core of the Newark Basin Coring Project
6……	Figure A3	Weston core of the Newark Basin Coring Project
7……	Figure A3	Martinsville core of the Newark Basin Coring Project
8……	Figure A4	Naval Air Warfare Center – several cores
9……	Figure A4	Natural outcrop near Stockton, NJ
10……	Figure A5	Roadcut on Pennsylvania Turnpike near King of Prussia, PA
11……	Figure A4	Quarry exposure near Prallsville, NJ
12……	Figure A5	Abandoned quarry exposure in Phoenixville, PA
13……	Figure A4	Road cut on River Road near Lumberville, PA
14……	Figure A4	Quarry exposure near Ravens Rock, NJ
15……	Figure A4	Quarry exposure near Eureka, PA
16……	Figure A4	Quarry exposure near Ottsville, PA
17……	Figure A4	Road cut on Rte 518 southeast of Lambertville, NJ
18……	Figure A4	Quarry exposure near Chalfont, PA
19……	Figure A4	Abandoned quarry exposure along Route 29 near Tumble Falls, NJ
20……	Figure A3	Abandoned quarry and road cut on Route 18 near New Brunswick, NJ
21……	Figure A4	Road cut on Route 29 near Byram, NJ
22……	Figure A4	Natural exposure along Taylorsville Road northwest of Taylorsville
23……	Figures A3 and A4	Road cut on Rte 567 east of Neshanic Station, NJ
24……	Figure A5	Railroad cut near Glasgow, PA
25……	Figure A5	Railroad cut near Gwynedd, PA
26……	Figure A5	Possible location of road cut. Route 422 east of Sanatoga, Pa.
27……	Figure A3	Natural outcrop along Henry Hudson Drive just north of Fort Lee, NJ
28……	Figure A4	Natural outcrop along Route. 627 near Milford, New Jersey
29……	Figure A3	Quarry exposure near Secaucus, NJ
30……	Figure A5	Outcrop on small road along the Schuylkill River near Royersford, Pennsylvania.
31……	Figure A3	Railroad cut near Manville, New Jersey
32……	Figure A3	Roadcut on Interstate I-87 near Suffern, NY
33……	Figures A3 and A4	Stream cut (Cold Brook?) near Oldwick, NJ
34……	Figure A5	Natural outcrop off Wyomissing road near Mohnton, PA
35……	Figure A3	Natural outcrop along Interstate I-280 near East Orange, NJ
36……	Figure A5	Road cut on Interstate I-176 near Beckersville, PA
37……	Figure A5	Quarry exposure near Collegeville, PA
38……	Figure A5	Small exposure along Church Road? near Jacksonwald, PA

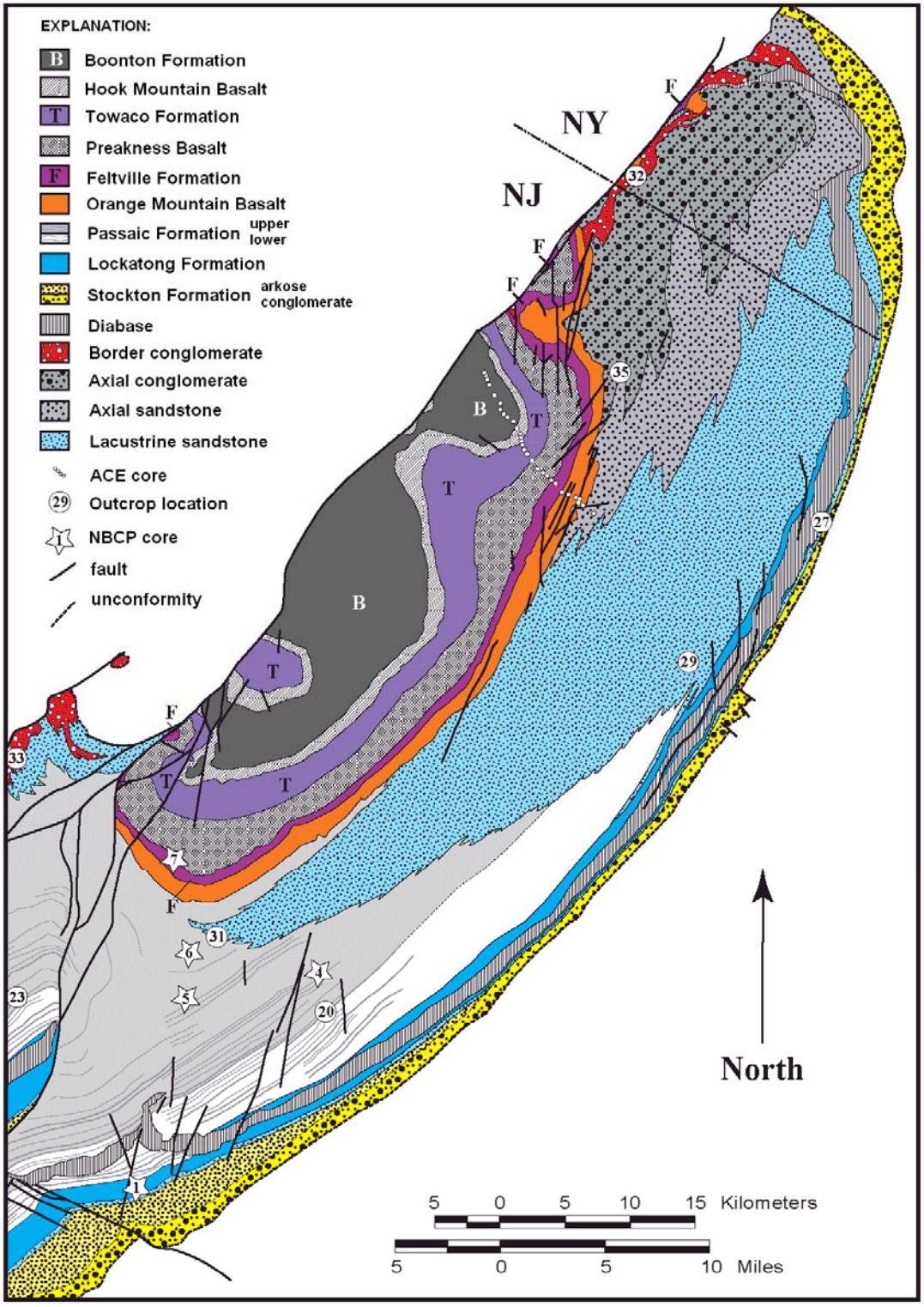

Figure A3. Geologic map of the eastern part of the Newark basin in New Jersey and New York. The upper part of the Passaic Formation, whose base is directly above the lowest two Van Houten cycles of the Perkasie Member, is distinguished from the lower part by abundant root-disrupted mudstone and syndepositional gypsum. Dashed contacts are projections from mapped contacts. Cores collected for the Army Corp of Engineers tunnel project (ACE) are shown. Exposures mentioned in the text or figure captions are also indicated. Numbered sites are listed in table A1. Modified from Olsen and others (1996), Olsen and Rainforth (2001), and Drake and others (1996).

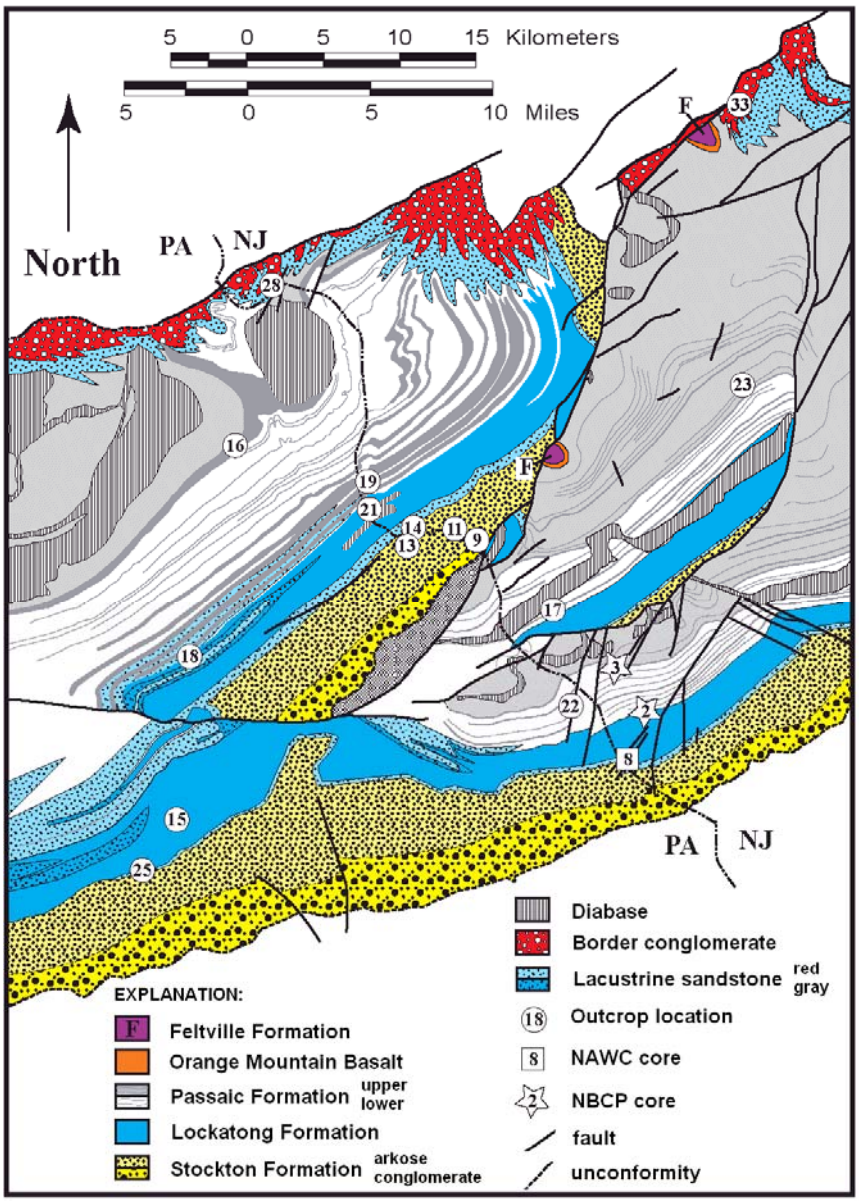

Figure. A4. Geologic map of the central part of the Newark basin in New Jersey and Pennsylvania. Numbered localities include core sites of the Newark Basin Coring Project (NBCP), the Naval Air Warfare Center (NAWC), and exposures mentioned in the text or figure captions. The numbered sites are listed in table A1. Modified from McLaughlin (1945), Rima and others (1962), Olsen and others (1996), Drake and others (1996), Owens and others (1998), and Herman (2006).

of the basin. The minimum thickness of the Stockton Formation is about 100 m. Lithofacies maps of the Stockton were produced by McLaughlin (1945, 1959), Rima and others (1962), and Glaesser (1966). McLaughlin (1945) named four mappable ridge-forming sandstones: the Solebury, Prallsville, Cutalossa, and Ravens Rock Members (fig. A2). Previous work on the Stockton Formation interpreted it as fluvial deposits, and suggested that the coarser facies were deposited as alluvial fans (Rima and others, 1962; Glaesser, 1966; Savage, 1967, 1968; Allen, 1979). Cross-bedding directions and provenance studies indicate that sediment transport was to the northwest throughout deposition of the Stockton (Glaesser, 1966; Savage, 1967, 1968; Allen, 1979; Oshchuldak and Hubert, 1988).

Based on its sedimentary structures and dominant grain sizes, the Stockton is here divided into three major sedimentary facies: 1) conglomerate and conglomeratic sandstone, 2) arkosic sandstone, and 3) micaceous sandstone, siltstone, and mudstone.

Conglomerate and conglomeratic sandstone

Conglomerates and conglomeratic sandstones are dominant in the lower part of the Stockton Formation. They make up more of the formation directly adjacent to the southeastern unconformable boundary than in the other two fault blocks. Conglomerates and conglomeratic sandstones form poorly defined upward-fining sequences that are 2-6 m thick (figs. A7 and A8). The base of the sequences commonly contains

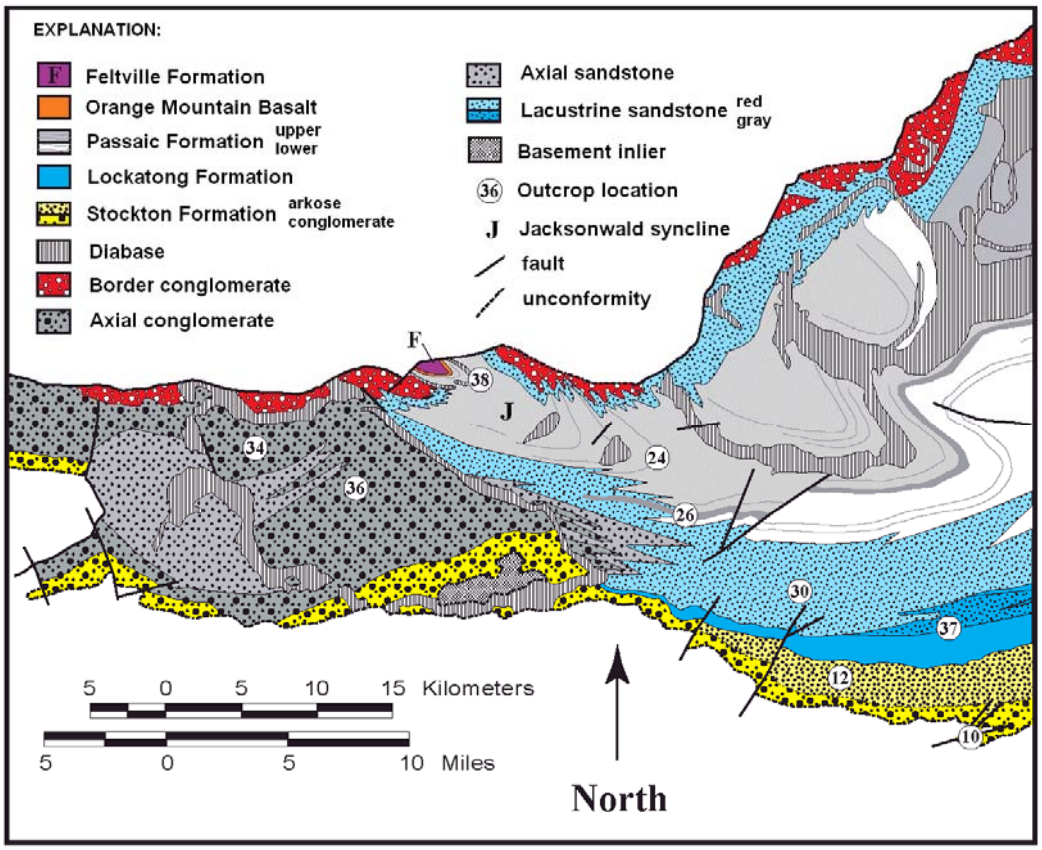

Figure A5. Geologic map of the western part of the Newark basin in Pennsylvania. Numbered localities are exposures mentioned in the text or figure captions. The numbered sites are listed in table A1. Modified from Olsen and others (1996) and Rima and others (1962).

cobble- to pebble-sized clasts whereas the tops are dominated by medium-to-coarse sandstone. Trough cross-bedding is present throughout each upward-fining sequence. The largest trough cross-bed sets near the base are as much as 4 meters wide and 40-100 cm thick, and progressively smaller sets occur near the top (about 50 cm wide and 10-15 cm thick). Tabular foresets are randomly distributed throughout each upward-fining sequence. These foresets are typically less than 1 m thick, but may be as much as 2.5 m thick. Two or more upward-fining sequences of conglomerate and conglomeratic sandstone may be stacked upon each other or the sequences may be separated by mudstone and siltstone units that are several meters to several 10's of meters thick. These units are described in the section on the micaceous sandstone, siltstone, and mudstone facies. The contact between the tops of upward-fining sequences of conglomerate and conglomeratic sandstone and the mudstone and siltstone beds is typically abrupt (fig. A8).

Conglomerates and conglomeratic sandstones in the Stockton Formation are interpreted as deposits of braided stream channels. Upward-fining sequences are attributed to channel-fill successions where the coarsest grain sizes and largest bedforms occur in the thalweg and smaller bedforms composed of finer grain sizes were deposited on and around mid-channel and side-channel bars (Cant and Walker, 1978). Trough cross-bedding probably formed by migration of lower flow-regime, dune-scale bedforms (Harms and others, 1982, chapter 3). Tabular foresets are attributed to accretion on the steep fronts and sides of mid-channel bars (Cant and Walker, 1978). The dearth of ripple cross-bedding and the poorly defined nature of upward-fining sequences are consistent with low channel sinuosity. The coarse grain size and absence of ripple-scale cross-bedding suggest high-gradient drainages.

Arkosic sandstone

Arkosic sandstone in the Stockton Formation occurs in upward-fining sequences which are 10-15 m thick (figs. A9 and A10). These sequences make up about half of the Stockton Formation in the uplifted blocks in the central part of the basin, but are less than a third of the formation that directly overlies the southeastern border of the basin. The basal part of each upward-fining sequence consists of coarse sandstone, which may include some pebbles, grading upward to fine sandstone, then siltstone, which is finally capped by silty mudstone. The coarsest part of each upward-fining sequence contains broad troughs (2-5 m wide and 30-80 cm thick) and low-angle tangential crossbeds (fig. A11A). Trough cross-bedding gradually decreases in

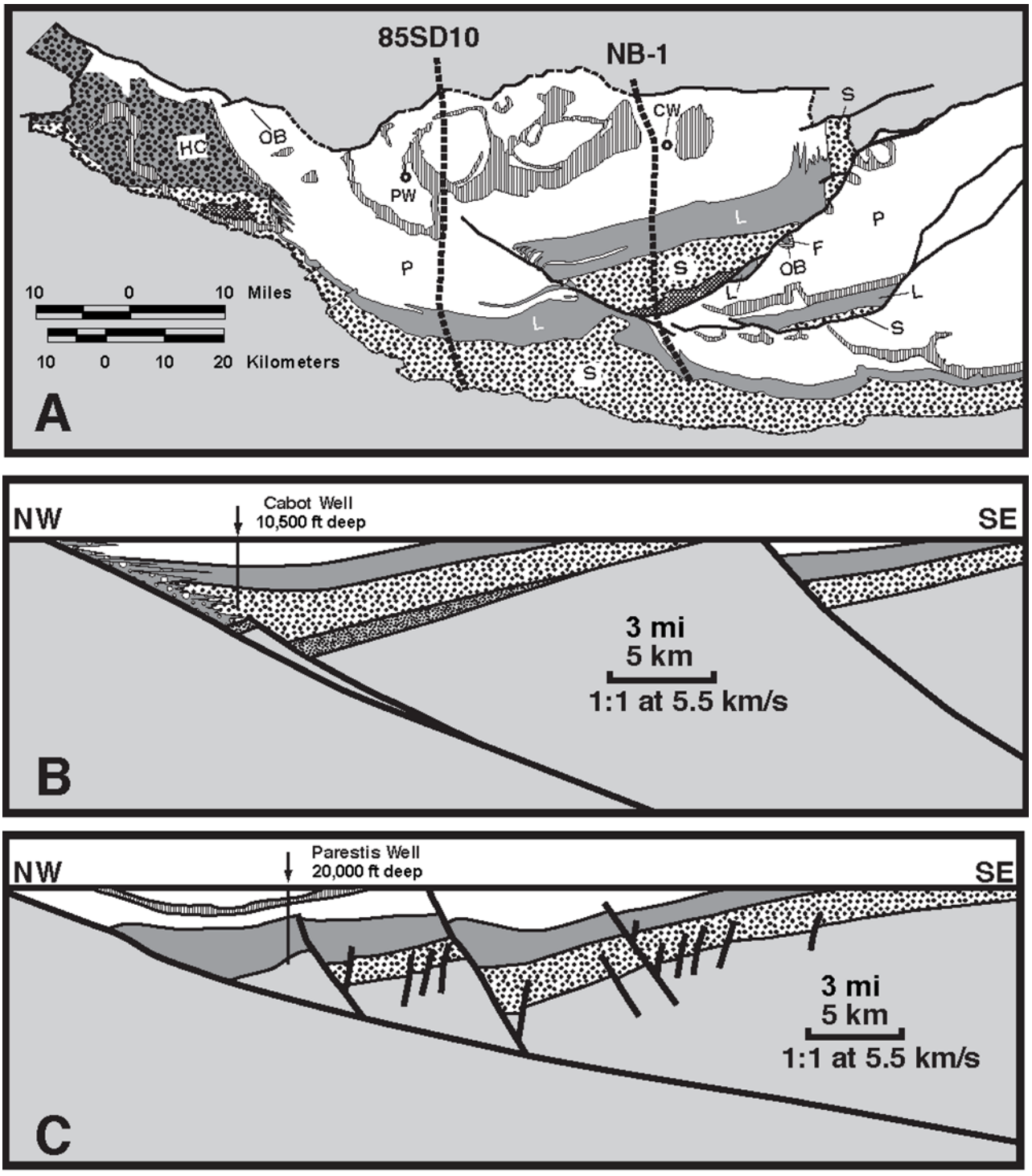

Figure A6. Seismic lines across the Newark basin and nearby wells with geologic logs (CW-Cabot well and PW-Parestis well). Geologic units are the same as in figure A1. B. Sketch of the NB-1 line as interpreted by Schlische and Withjack (2005). Fine stippling is a Stockton Formation facies that is not exposed at the surface, coarse stippling is equivalent to exposed Stockton Formation, light gray is equivalent to the exposed Lockatong Formation, white is equivalent to the exposed Passaic Formation, and dark gray with white circles is interpreted as border conglomerate deposits. The Cabot well is projected onto the line. C. Sketch of the 85SD10 line as interpreted by Reynolds (1993). Lithological interpretations are the same as for 5B, but include vertical line pattern for a diabase intrusive. The Parestis well is projected onto the line. Modified from Schlische and Withjack (2005).

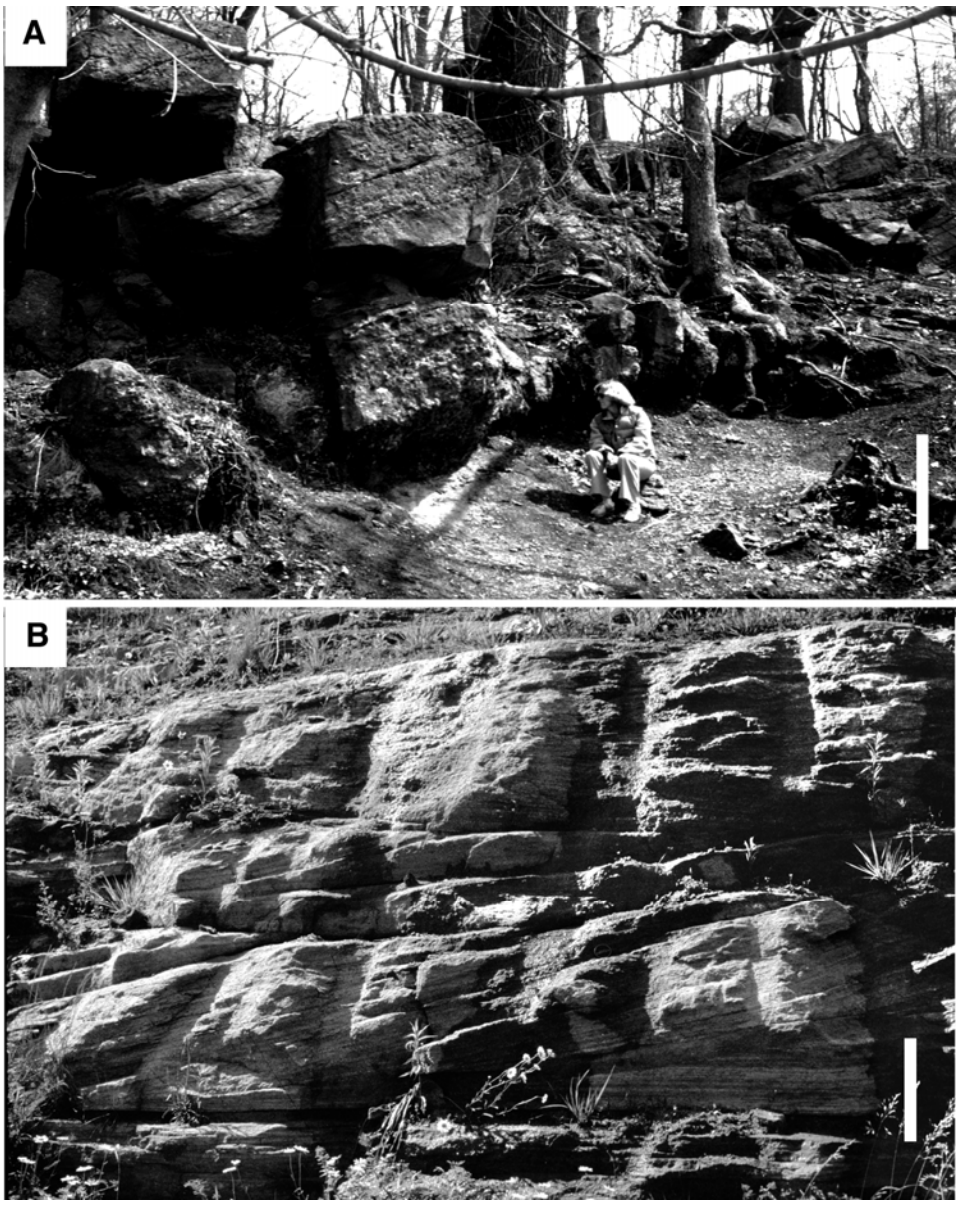

Figure A7. Conglomerate and conglomeratic sandstone of the Stockton Formation. A. Solebury Member conglomerate with tabular foresets (forming ridge) directly overlying bioturbated silty mudstone (lower slope). Note lower-angle trough crossbeds in background to the right. Paleocurrent direction is to the left and out of the picture. Scale bar is 1 m. Locality 9, table A1, fig. A4. B. Lower part of the Stockton Formation conglomeratic sandstone showing alternations of tabular foresets and decimeter-scale trough cross-bedding. Paleocurrent direction is out of the picture. The vegetated area at the top of the picture is silty mudstone, and silty mudstone directly underlies pebbly sandstone at base of the picture. Scale bar is 40 cm. Locality 10, table A1, figure A5.

size upwards within each upward-fining sequence to decimeter-scale-thick troughs about 20 cm wide (fig. A9). The upper fine sandstone and siltstone part of each upward-fining sequence is characteristically dominated by climbing-ripple cross-lamination (figs. A10B and A11B). Each sequence is overlain by several meters to tens of meters of siltstone and mudstone described in the section on the micaceous sandstone, siltstone, and mudstone facies. In a quarry exposure of the Prallsville Member (fig. A9), the upward-fining sequences form a series of laterally offlapping lenses that are amalgamated at the base, suggesting a composite upward-fining sandstone sequence more than 20 m thick. In the Princeton core (fig. A10), stacks of upward-fining successions are progressively finer-grained suggesting a cross section through a similar geometry.

Arkosic sandstone upward-fining sequences are interpreted as point-bar deposits of meandering rivers (Allen, 1970). Large, trough crossbeds with low-angle cross-bedding are interpreted as the deposits of large dunes formed in the channel thalweg. The absence of steeper foresets is attributed to the erosion of most of the dune by the advancement of the next upflow dune as described by Harms and others (1982, Chapter 3). Smaller trough crossbeds were formed by progressively smaller dunes on the submerged point-bar face. Ripple-scale bedforms draped the upper portions of the point bar, producing the climbing-ripple cross-lamination. The regularity of upward-fining sequences with thick intervals of ripple cross-lamination and the occurrence of offlapping lenses are consistent with lateral-accretion sets of meandering-river point bars. The thickness of the upward-fining sequences

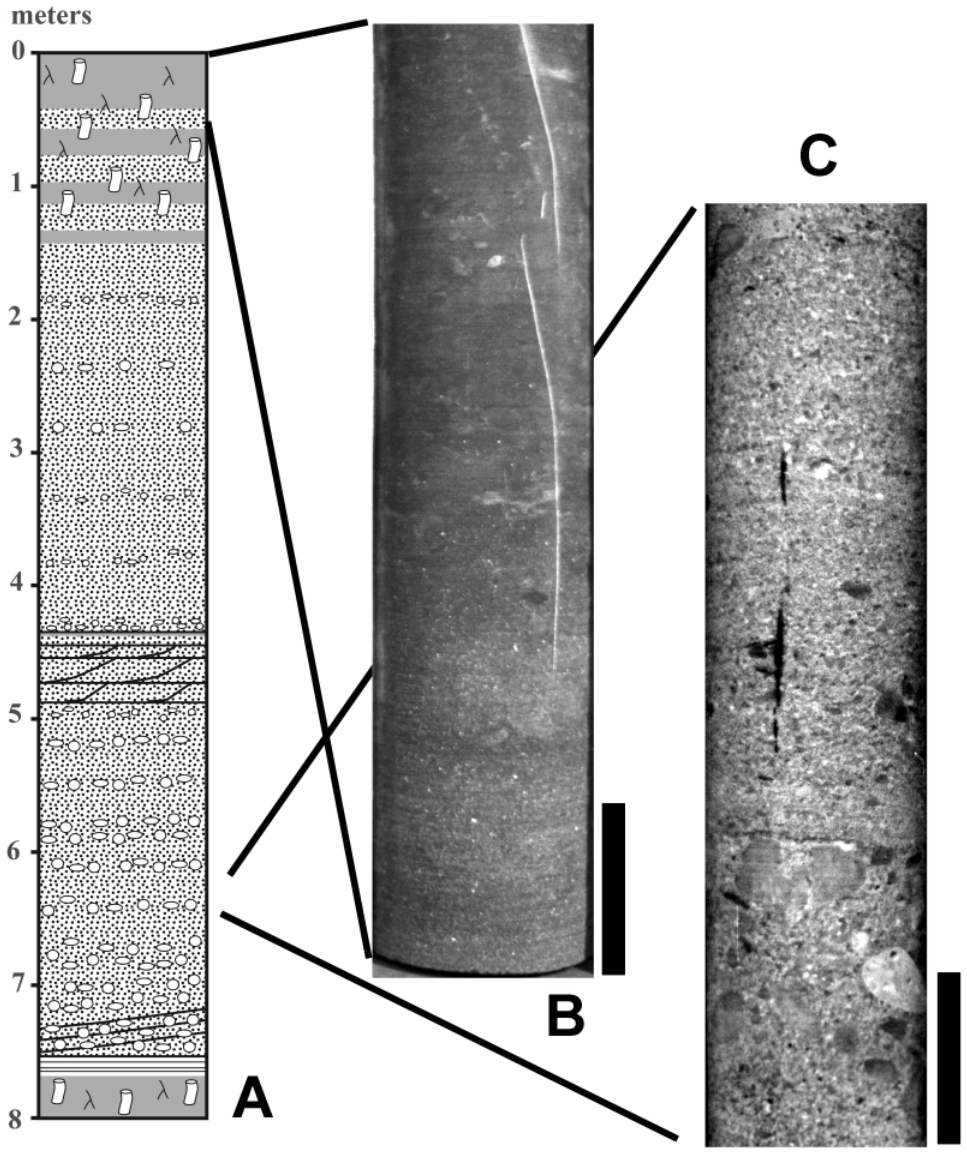

Figure A8. Conglomerate and conglomeratic sandstone of the Stockton Formation. A. Sketch illustrating 6-meter-thick upward fining sequence overlying gray mudstone with irregular lamination and overlain by red mudstone with burrow and root structures. Princeton core interval 3648-3674 ft.
B. Details of the transition from granule-rich sandstone to red mudstone with burrows and root casts at top of sequence shown in A. Linear white features are cement-filled fractures. Scale bar is 5 cm.
C. Detail of pebble conglomerate consisting of a decimeter-scale upward-fining sequence near base of sequence shown in A9A. These upward-fining sequences are cross sections of trough crossbeds. Scale bar is 5 cm. Locality 1, table A1, figure A3.

provides a rough estimate of the river depth at flood stage. Silty mudstone and fine sandstone beds that overlie and underlie upward-fining sequences are interpreted as overbank deposits or muddy plains between channel belts with soil development. These are discussed in more detail in the following section.

Micaceous sandstone, siltstone and mudstone

Micaceous fine sandstone, siltstone, and mudstone occur in the Stockton Formation as interbeds with conglomerate, conglomeratic sandstone, and arkosic sandstone, and as 20-200-m-thick units separating sections dominated by the other rock types. Micaceous sandstone, siltstone, and mudstone comprise about half of the Stockton Formation in the central and northwestern fault blocks, and less than a third of the formation near the unconformable southeastern basin boundary. This facies is very minor in the Stockton Formation near the northeast and southwest ends of the basin. Commonly, it is poorly exposed, forming lowlands between the ridges of arkosic sandstone and conglomerate. All of the sediments in this facies typically are heavily bioturbated, with sediment-filled tubes (figs. A12 and A13). Some tubes have clay lining and they may branch and taper (fig. A12B). Other tubes have uniform diameters and include the ichnofossil, Scoyenia (Olsen, 1984). Mudstones may also contain carbonate nodules, bowl-shaped slickensides, and large, sediment-filled polygonal cracks (fig. A12C). Sandstone beds are 1-40 cm thick and have ripple cross-lamination unless they are completely bioturbated (fig. A13). They occur most commonly as 1-4-m-thick upward-coarsening sequences of progressively thicker beds (figs. A13 and A14A), but

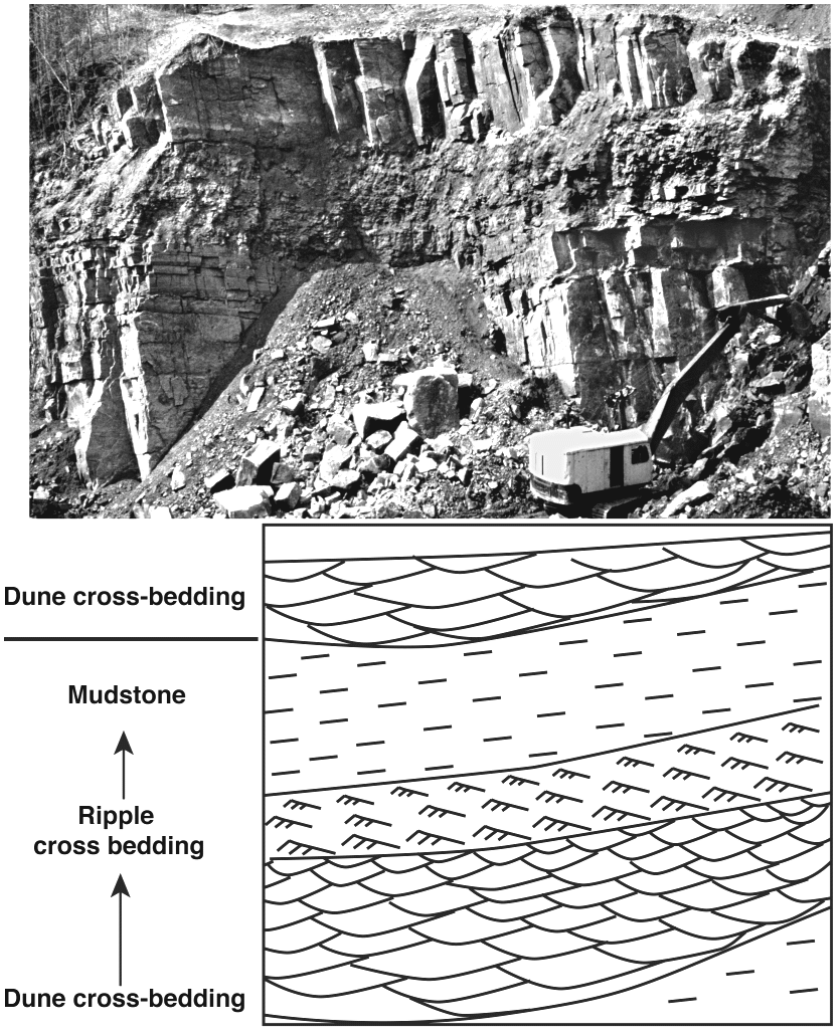

Figure A9. Ridge-forming arkosic sandstone in the Prallsville Member of the Stockton Formation. Upward-fining sequence consists of blocky sandstone at the base grading upward to darker mudstone sharply capped by blocky sandstone. Sandstone sequence begins with large dune-scale trough cross-bedding at the base in coarse sandstone. The trough crossbeds are progressively smaller upwards, grading into ripple cross-lamination. Sketch illustrates the progression of bedforms and the lateral shift to smaller bedforms and finer grain size, interpreted as a lateral accretion surface. Top of backhoe cab is about 3 m. Locality 11, table A1, figure A4.

they also form 5-6-m-thick upward-fining sequences of progressively thinner beds. In the upper few hundred meters of the Stockton Formation, fine sandstone and mudstone beds differ from the typical micaceous sandstone, siltstone, and mudstone.

Fine-sandstone beds that have 2-3-meter-thick foresets consist of deceleration-of-flow climbing-ripple cross-lamination sequences that are finer and have higher angles of climb-down flow (see description in clinoform deltaic sandstone in the basin margin facies). In an outcrop of the Ravens Rock Member, a dark gray mudstone bed that occurs between arkosic sandstone deposits (fig. A14B) contains conchostrachans (Turner-Peterson, 1980). Dark gray to purplish gray mudstone occurs interspersed throughout the Stockton Formation (fig. A15). These mudstones may have irregular lamination (fig. A15A), soft-sediment deformation features (fig. A15C), or are disrupted by large polygonal cracks (fig. A15B).

The sedimentary structures of the micaceous fine sandstone, siltstone, and mudstone units are consistent with low flow velocities and intermittent standing water typical of overbank and flood-plain deposits (Bridge, 1984). Bioturbation includes burrow assemblages, such as Scoyenia, that are consistent with water-saturated soil conditions (Hasiotis, 2002). Tubes that branch and taper are consistent with roots. Clay linings are typical of clay cutans that develop in soil conditions (Retallack, 2001) and carbonate nodules and bowl-shaped slickensides are typical of vertisol soils (Wilding and Puentes, 1988). The large polygonal cracks are consistent with intermittent desiccation of water-saturated sediment. Upward-fining sandstone units within these sections are consistent with small, tightly meandering, muddy streams. Upward-coarsening sandstones with abundant ripple cross-lamination and soil fabrics are probably deposits of crevasse deltas. The thickness and lateral continuity of the micaceous fine sandstone, siltstone, and mudstone deposits are similar to avulsion deposits (Kraus and Wells, 1999). Avulsion deposits are extensive sheets of fine-grained sediment produced in small anabranch channels, that run parallel to major channels rather than fine-grained sediment due to spill over from channel edges. Not

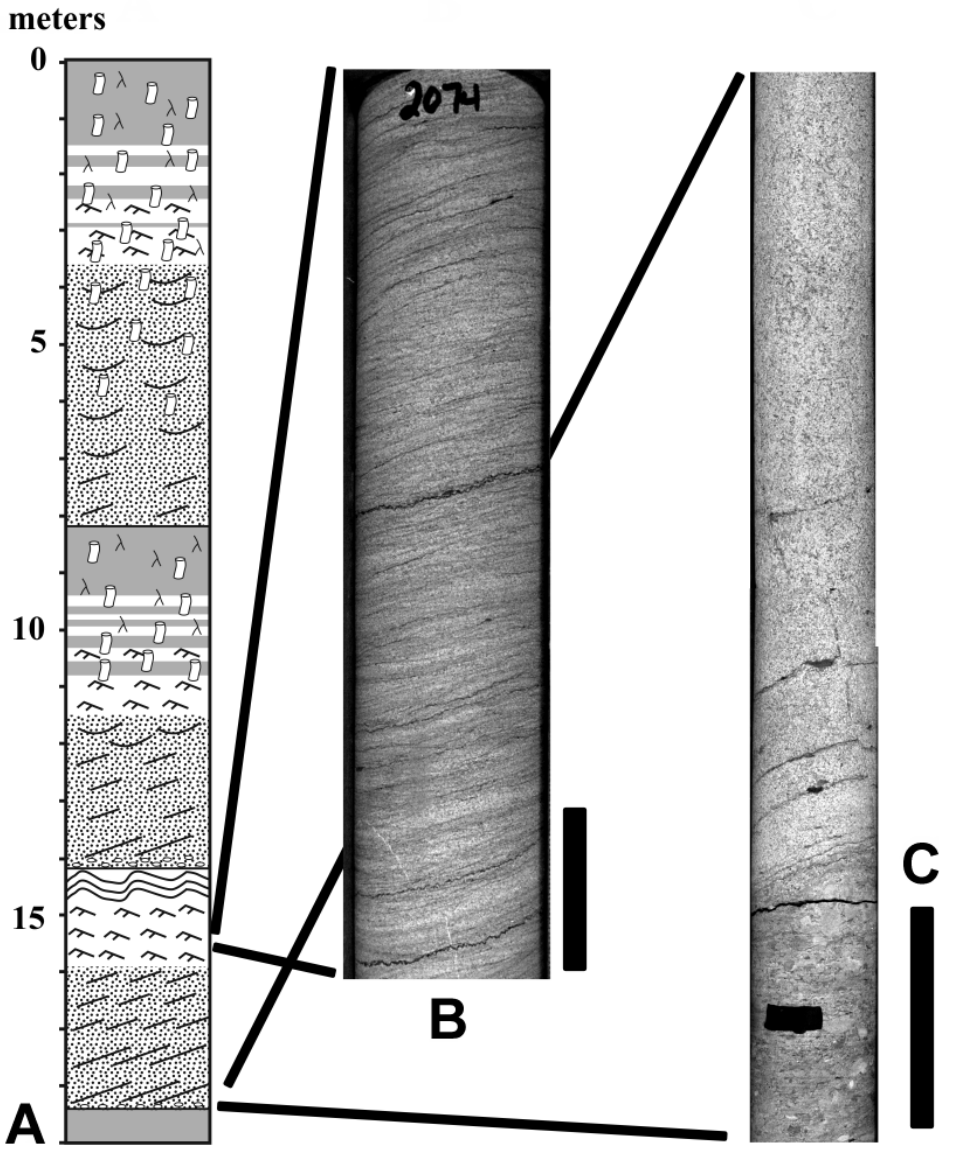

Figure A10. Stockton Formation arkosic sandstone. A. Schematic drawing shows stacked, upward-fining sequences of coarse arkosic sandstone with large scale cross-bedding grading into fine-grained arkosic sandstone with ripple cross-lamination. Each overlying upward-fining sequence is finer-grained at its base and contains more mudstone at its top. Princeton core interval 2023-2086 ft. B. Details of low-angle climbing-ripple cross-lamination near top of first upward-fining sequence in A. Scale bar is 5 cm. C. Details of cross-bedding in coarse sandstone at the base of the first upward-fining sequence in A. Coarse-grained base includes intraclasts of mudstone and micritic carbonate derived from the underlying layer. Scale bar is 10 cm. Locality 1, table A1, figure A3.

enough measurements of paleocurrent indicators in the micaceous fine sandstone have been made to establish that flow is parallel to the regional pattern. Turner-Peterson (1980), Turner-Peterson and Smoot (1985), and Reynolds (1993) suggest that some of the fine-grained sections are lacustrine, particularly those near the top of the Stockton Formation. Gray and purple clay-rich, mudstone beds as much as 30 cm thick indicate standing water and the occurrence of conchostracans in one locality is consistent with a lake deposit. The meters-thick foresets of fine sandstone with well-developed deceleration-of-flow climbing-ripple sequences are consistent with Gilbert-type delta deposits (see Jopling and Walker, 1968). It is possible that the common upward-coarsening sequences of fine sandstone are deposits of small birdfoot deltas in lake margins. These lakes would have been shallow and intermittent, in order to account for the associated fluvial and subaerial indicators previously described.

Lockatong and Passaic Formations - central basin facies

The central basin facies of the Lockatong and Passaic Formations are dominated by shale, mudstone, and silty mudstone that range from 3500-4000 m thick. The two formations are transitional to one another vertically and laterally, with the Lockatong characterized by more common thick beds of black laminated shale and associated gray mudstone, and the Passaic dominated by red mudstone and silty mudstone. Black shale and some gray mudstone owe their color to their organic content. Mudstone overlain by black, organic-rich shale is characteristically gray, even though

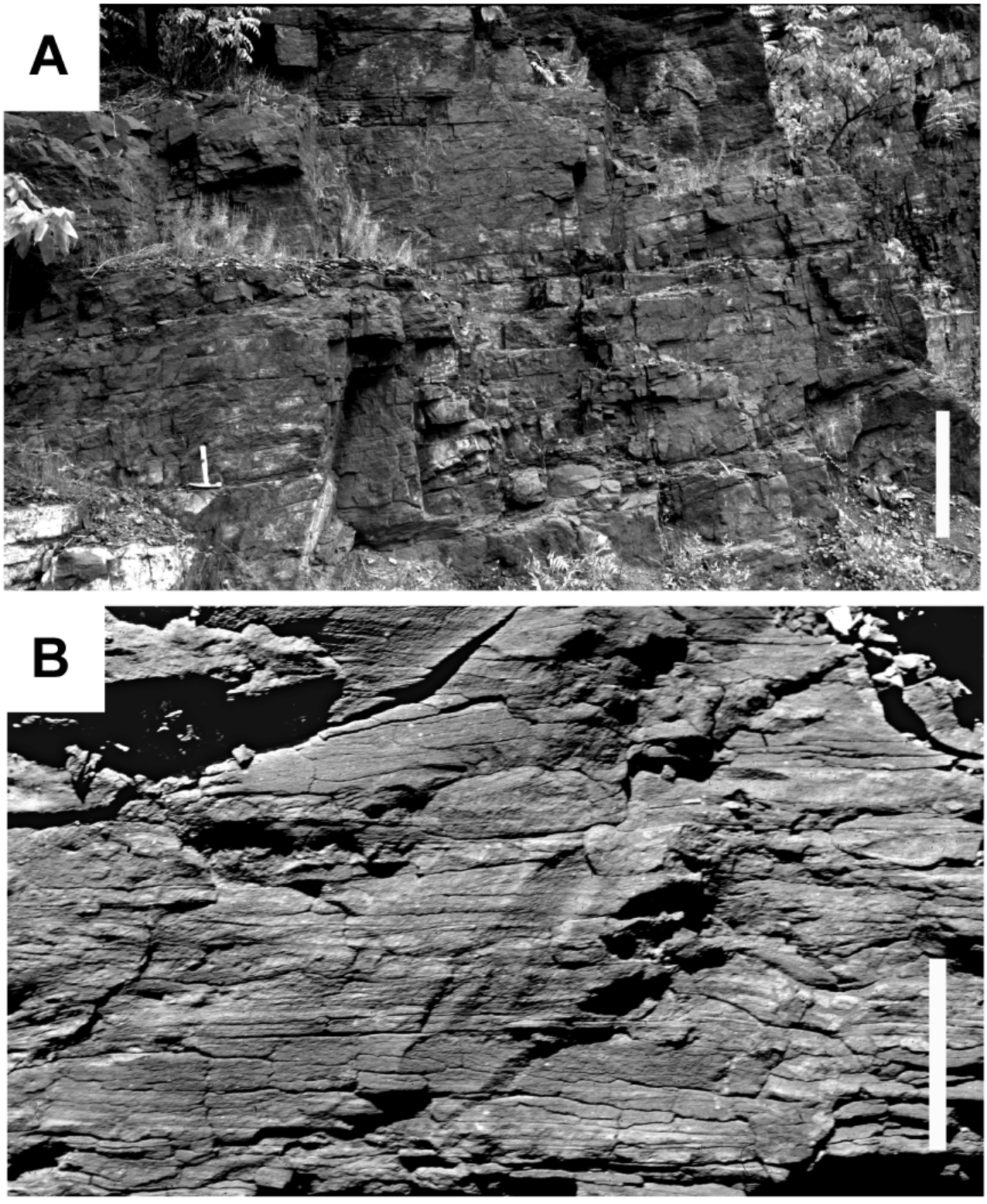

Figure A11. Internal stratification in an upward-fining arkosic sandstone sequence. A. Dune-scale trough cross-bedding (medium size) formed by a paleocurrent that flowed into the page and to the left. Note the width of beds compared to their thickness and low inclination of beds to a tangential contact. Scale bar is about 70 cm. B . Ripple-scale cross-lamination formed by paleocurrent that flowed to the left. Scale bar is about 15 cm. Locality 12, table A1, figure A5.

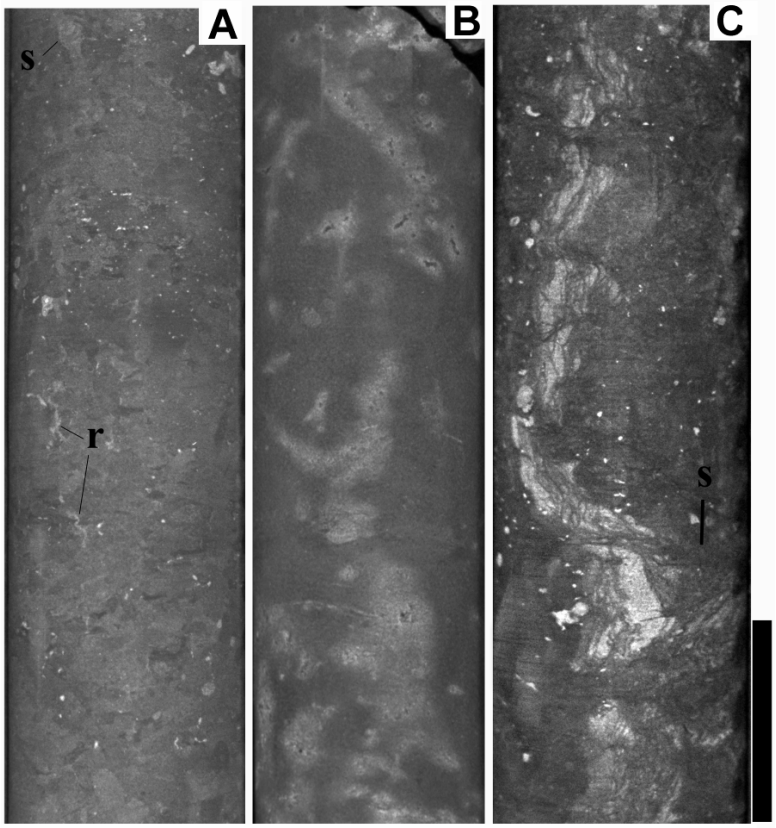

Figure A12. Micaceous siltstone and mudstone in the Stockton Formation. A. Silty mudstone with abundant burrows (light and dark gray ovate features) and root casts (r -light features). Some of the burrow filling show meniscate filling typical of the ichnogenus Scoyenia (s). Princeton core interval 1050 ft. B. Silty mudstone with sediment-filled root casts that have reduction haloes (light). Princeton core interval 1174-1175 ft. C. Silty mudstone with abundant burrows and root casts (faint light and dark ovate and elongate features) and a prominent sand-filled crack (light vertical feature). Crack filling is displaced by arcuate slickenside plane (s). Carbonate concretions (light irregularly circular features) are interpreted as soil features. Scale bar is 5 cm. Locality 1, table A1, figure A3.

it has features similar to those of red mudstone. Here, the thickness of the gray mudstone is directly proportional to the thickness of the overlying black shale. The gray color may grade downward to red away from the contact with the black shale. This color transition is attributed to reduction of iron oxides in the sediment by anoxic pore waters moving downward from an overlying deep lake (Dubiel and Smoot, 1994). In the Lockatong Formation, black shale beds are thicker and more closely spaced, so most of the mudstone is gray, whereas in the Passaic Formation, black shale beds are thinner and more widely spaced, so most of the mudstone is red. The Passaic Formation is siltier upward near to its upper contact with the Orange Mountain Basalt. This is partly exaggerated by the outcrop pattern, exposing deposits closer to the basin-margin border fault, but the trend appears to be consistent in different fault blocks. The central facies consists of a continuum of sedimentary fabrics, mostly mudstone and silty mudstone. The major lithologic types are 1) laminated mudstone, 2) thin-bedded mudstone, and 3) massive mudstone. Evaporite pseudomorphs occur in all three types, and are described separately. Many primary voids and several of the evaporite pseudomorphs are filled with complex cements consisting of silicate and carbonate minerals that are described elsewhere in this volume (Simonson and others, 2010).

The most striking shared characteristic of both formations is a pervasive pattern of 3-7-m cyclic alternations of layered to unbedded mudstone (Van Houten, 1962, 1964; Olsen, 1984, 1986; Olsen and others, 1996) (fig. A16). The layered parts consist of microlaminated black shale to thin-bedded gray mudstone (fig. A16) or poorly bedded red silty mudstone (fig. A17). These grade upward to unbedded mudstone or silty mudstone with abundant indicators of subaerial exposure. Each sequence of layered-to-unbedded sediment with subaerial features was termed a Van Houten cycle by Olsen (1986). Groups of 4 to 6 Van Houten cycles consist of a larger cyclic pattern in which the lower Van Houten cycles have thicker bedded sections and the upper ones have less pronounced bedded intervals and thicker massive mudstones with subaerial exposure. In the Lockatong and Passaic Formations, Olsen and others (1996) identified fifty-two such successions, which they called McLaughlin cycles, and which they designated as informal members of the formations (fig. A2).

Laminated mudstone

The laminated mudstone lithology consists mostly of black to gray mudstone (or shale) with laminae that range in thickness from sub-millimeter (fig. A18) to approximately 1 cm (fig. A19). Laminae are mostly commonly defined by slight differences in grain

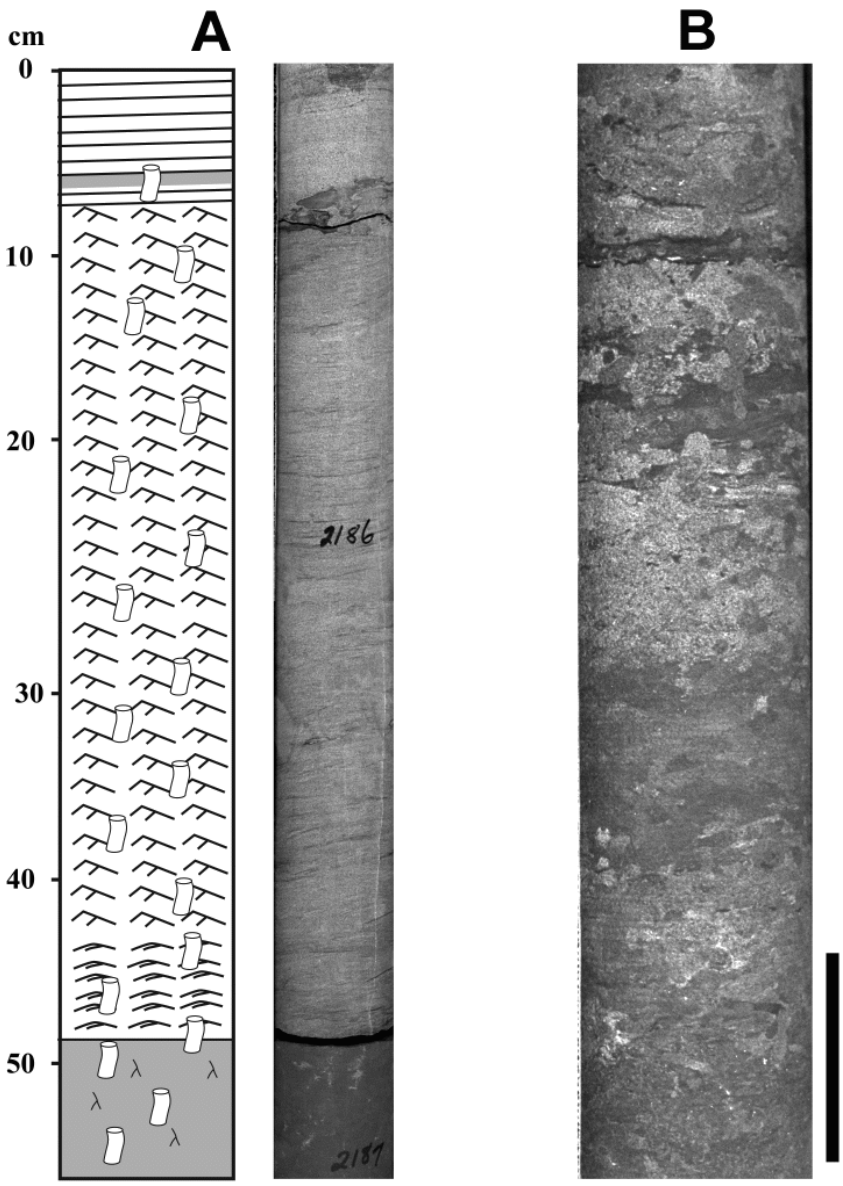

Figure A13. Upward-coarsening sequences in micaceous siltstone, sandstone, and mudstone in the Stockton Formation.
A. Upward-coarsening sequence of micaceous sandstone (light) with ripple cross-lamination. Ripple cross-bedding is smaller at base and uppermost sandstone has tabular inclined bedding. Underlying silty mudstone (dark) contains abundant burrows and root casts. Scale of photo is the same as for sketch. Princeton core interval 2185-2187 ft.
B. Upward-coarsening sequence of micaceous silty mudstone (dark) and micaceous sandstone (light). Internal stratification is obscured by abundant burrows (light and dark ovate features). Scale bar is 5 cm. Princeton core interval 2261-2262 ft.
Locality 1, table 1, figure A3.

size or by variations in carbonate or organic content.

Some laminae are flat, even, and continuous (fig. A18), whereas others consist of graded layers with sharp, silty bases (fig. A19), or clay-sized sediment and organic material alternating with layers of silt- or fine-sand-sized sediment that thicken and thin laterally (pinch-and-swell; fig. A19). These layers of fine sand and silt characteristically have only minor changes in thickness, broad crests and troughs, and no internal stratification. The finest laminae (microlaminae) consist of alternating clay or carbonate and organic material. These laminae are commonly black and contain phosphatic coprolites, fish fossils, and as much as 8 percent organic material. Thick laminae are commonly gray and typically have more conspicuous burrow structures, most of which have millimeter or sub-millimeter diameters and are horizontally oriented (fig. A20). Laminated mudstone is commonly deformed by small fault planes that break layers into discontinuous lenses (loop bedding). These features appear as discontinuous linear gashes in plan view.

Laminated mudstone is interpreted as perennial lake deposits. The differences in the style and composition of laminae may reflect different lake depths or degrees of lake stratification. Sub-millimeter laminae of alternating sediment and organic material probably reflect seasonal variations of suspended sediment inflow into the lake, precipitation of carbonates at the air-water interface, and algal blooms. The laminae may represent more random processes or only partial preservation of seasonal events. Graded laminae represent settling of a range of grain sizes or deposition as a turbidity flow. Thin laminae of consistent thickness are commonly formed by settling of

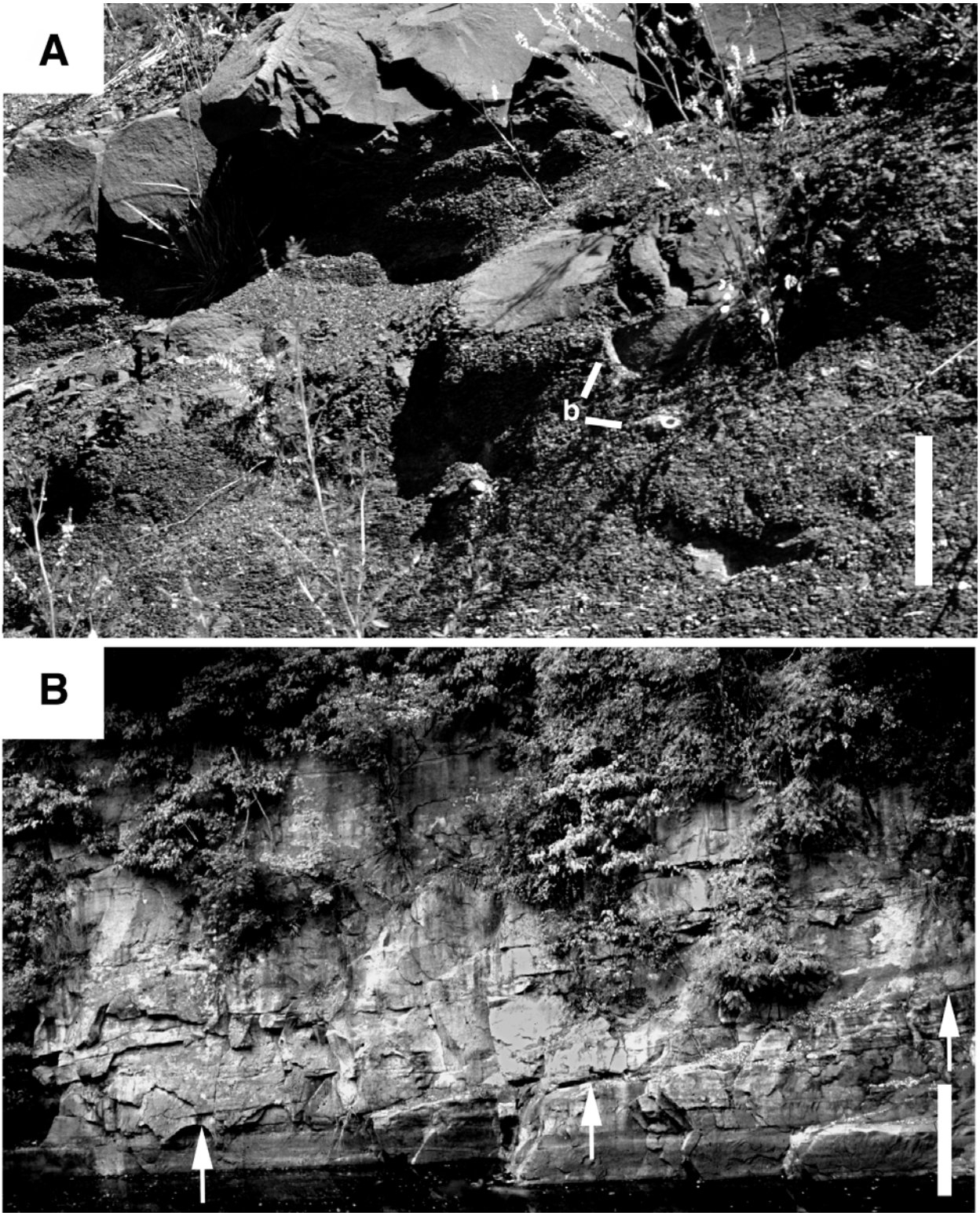

Figure A14. Micaceous sandstone, siltstone, and mudstone in the Stockton Formation. A. Silty mudstone and micaceous fine sandstone (blocky beds) overlying the Cutaloosa member of the Stockton Formation. All beds are heavily bioturbated, including root casts and burrows (b). Sandstone forms an upward-coarsening succession. Scale bar is 30 cm. Locality 13, table A1, figure A4. B. Arkosic trough crossbedded sandstone eroded into mudstone that is dark gray at its base and grades upward into red mudstone with thin siltstone beds in the Ravens Rock Member of the Stockton Formation. Arrows point to base of sandstone. The gray mudstone contains conchostracans, suggesting a shallow lake. Scale bar is 50 cm. Locality 14, table A1, figure A4.

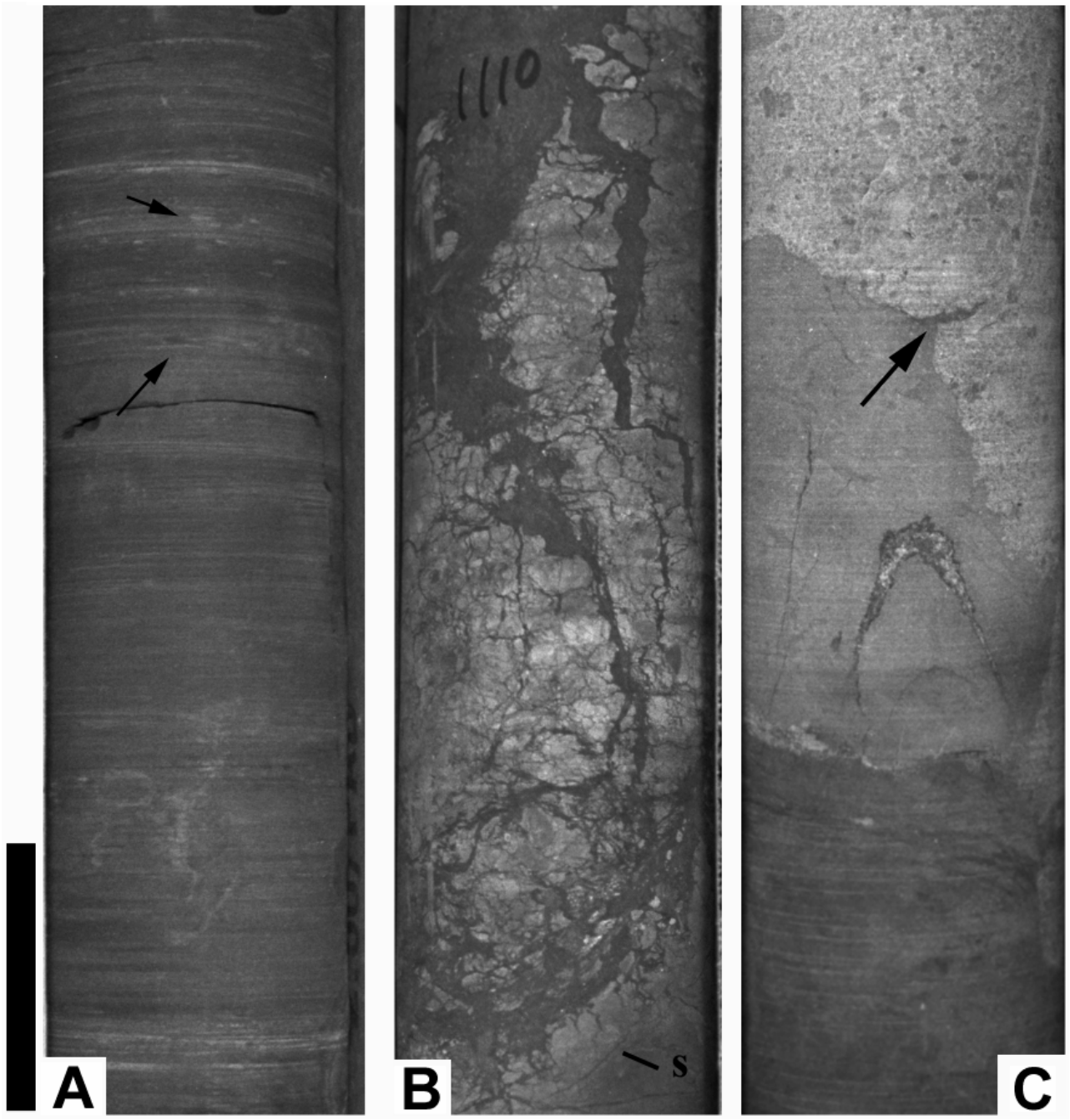

Figure A15. Gray mudstone and silty mudstone in the Stockton Formation. A. Dark gray mudstone shows faint irregular laminae of siltstone (light bands). Small burrows are parallel to the bedding planes (arrows) and larger burrows are more vertical (disruptions near center of section shown). Princeton core interval 2095-2096 ft. B. Purplish gray mudstone (light) disrupted by large cracks filled with red silty mudstone (dark). Breccia-like fabric is due to superimposed desiccation features (see basin-center mudstones). Curved slickenside planes (s) and bioturbation (ovate cross sections) are common. Princeton core interval 1110-1111 ft. C. Gray mudstone (dark) overlain by gray muddy siltstone (lighter gray) and coarse conglomeratic sandstone (light). Burrows are common in the mudstone and siltstone (light and dark ovate features). Coarse sandstone has fluidized the underlying layer as indicated by small flame structures (arrow). Princeton core interval 3609-3610 ft. Scale bar is 5 cm. Locality 1, table A1, figure A3.

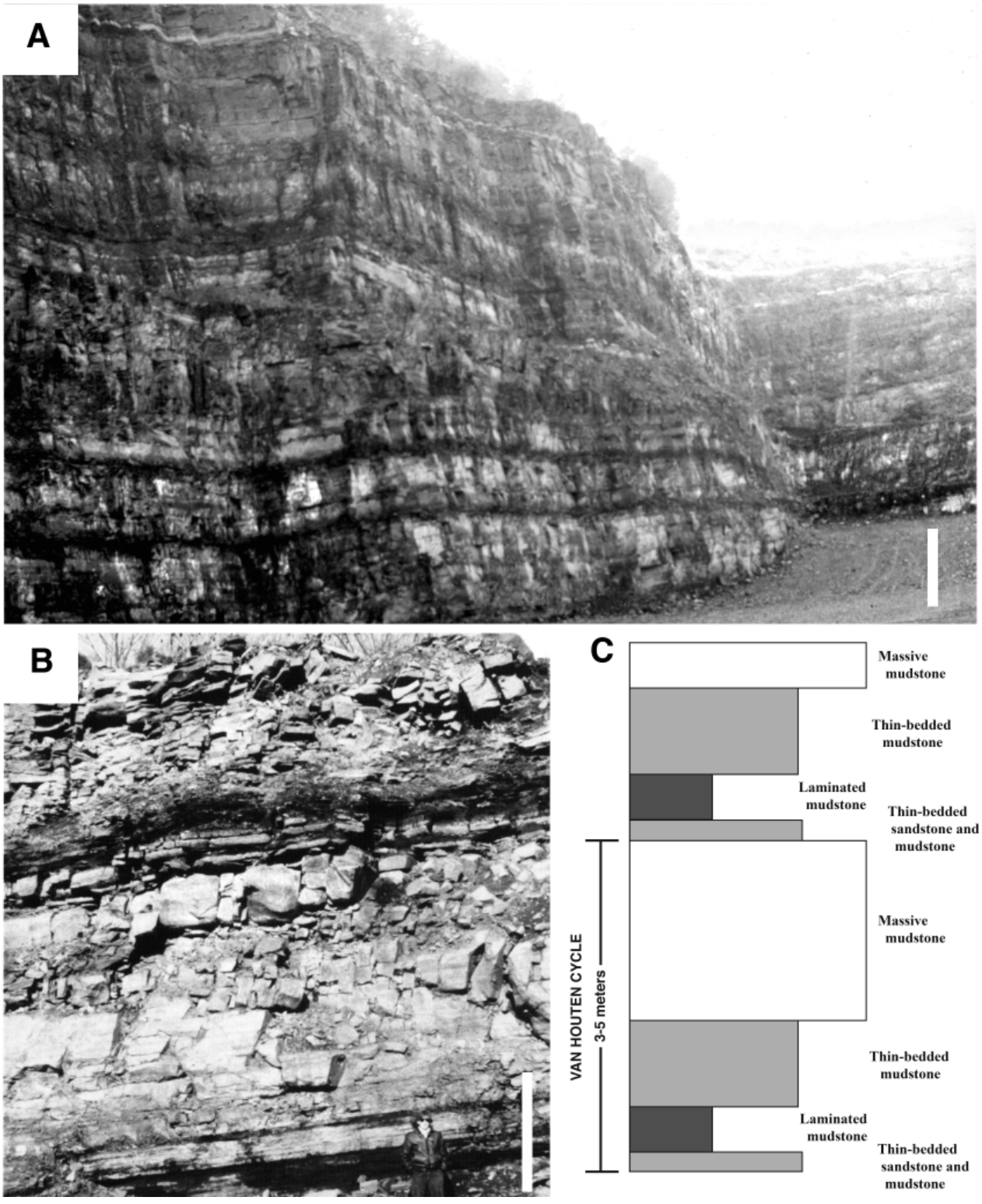

Figure A16. Van Houten cycles in the Newark basin. A. Princeton and Nursery Members of the Lockatong Formation with cyclic alternations of black laminated mudstone (dark bands), and massive mudstone with sedimentary structures indicating subaerial exposure. Scale bar is 5 m. Locality 15, table A1, figure A4. B. Two Van Houten cycles in the Perkasie member of the Passaic Formation. Scale bar is 2 m. Locality 16, table A1, figure A4. C. Lithologies in B. The "massive" layer includes some sandstone beds with boundaries disrupted by bioturbation and polygonal cracks.

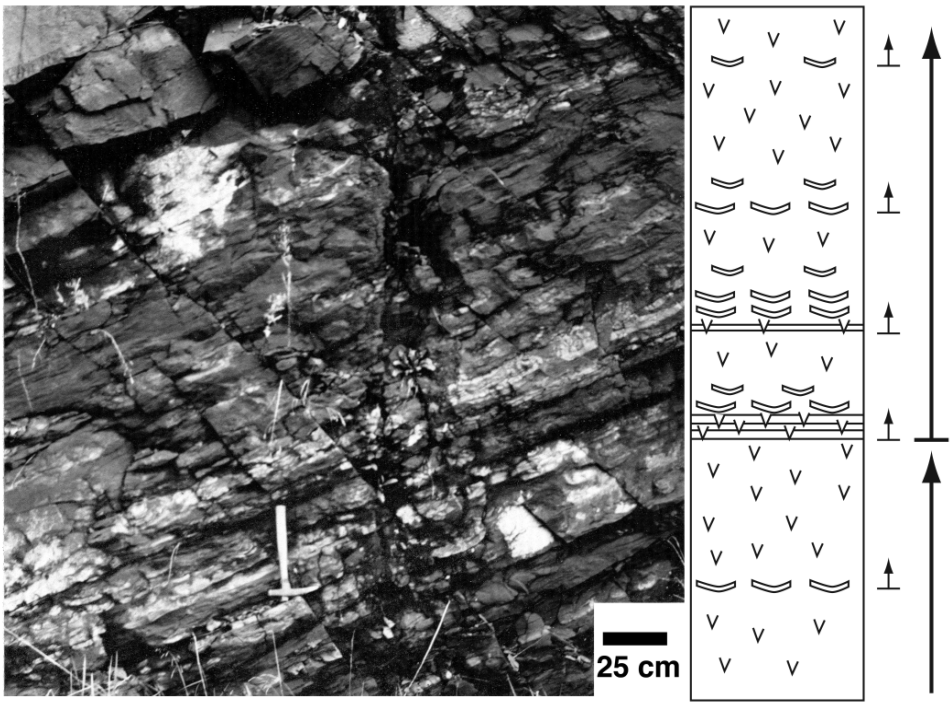

Figure A17. Contact between two Van Houten cycles in the lower part of the Passaic Formation (Member C?) showing a basal succession of thin-bedded mudstone with abundant polygonal cracks grading upward into massive vesicular mudstone. Smaller scale sequences of isolated beds with upcurled edges grading to vesicular mudstone are also visible in the underlying Van Houten cycle. Locality 17, table A1, figure A3.

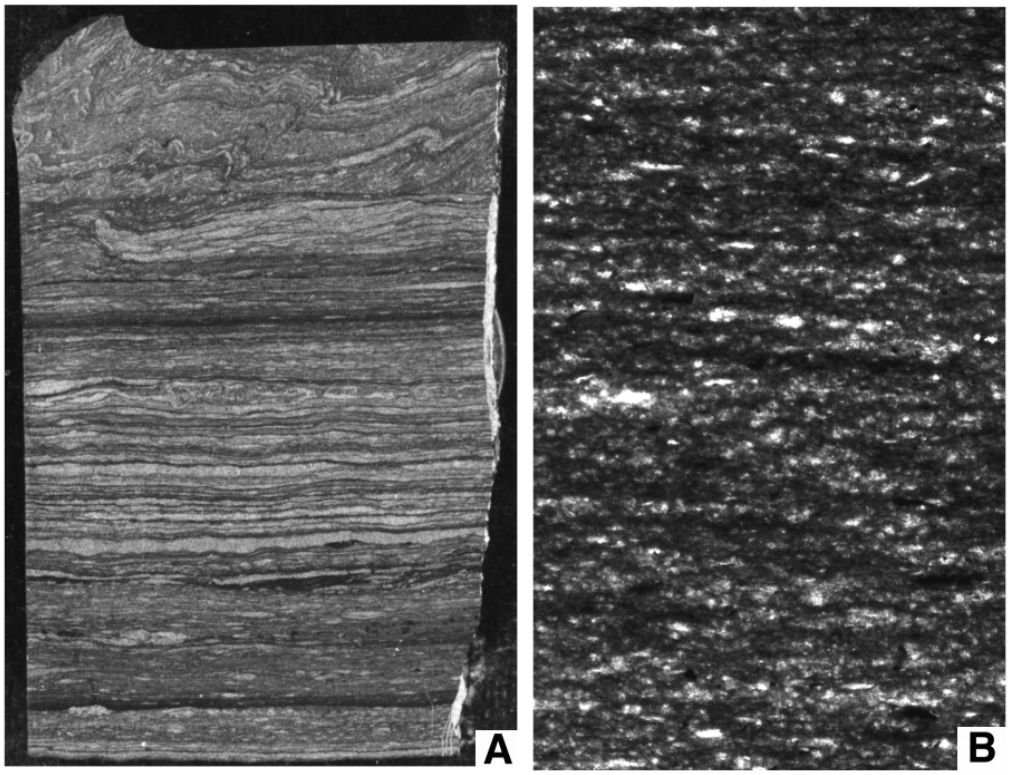

Figure A18. Organic-rich laminated mudstone from the basal part of the Nursery Member of the Lockatong Formation. A. Slabbed specimen about 2 cm thick. Very dark bands consist of finest laminae, lighter bands are more silt-rich and carbonate rich. Some of the discontinuity of layers is due to differential compaction, and some result from low-angle faults (loop bedding). Deformation at the top of the sample is syndepositional. This deformed layer was recognized in an exposure more than 50 km away and is attributed to seismic deformation.
B. Photomicrograph of thin section from the slabbed sample showing microlaminae in the dark bands. Laminae are defined by organic-rich sheets (dark layers) and layers of carbonate and siliciclastic fine silt. About 40 layers occupy the thickness of about 0.2 mm. Locality 15, table A1, figure A4.

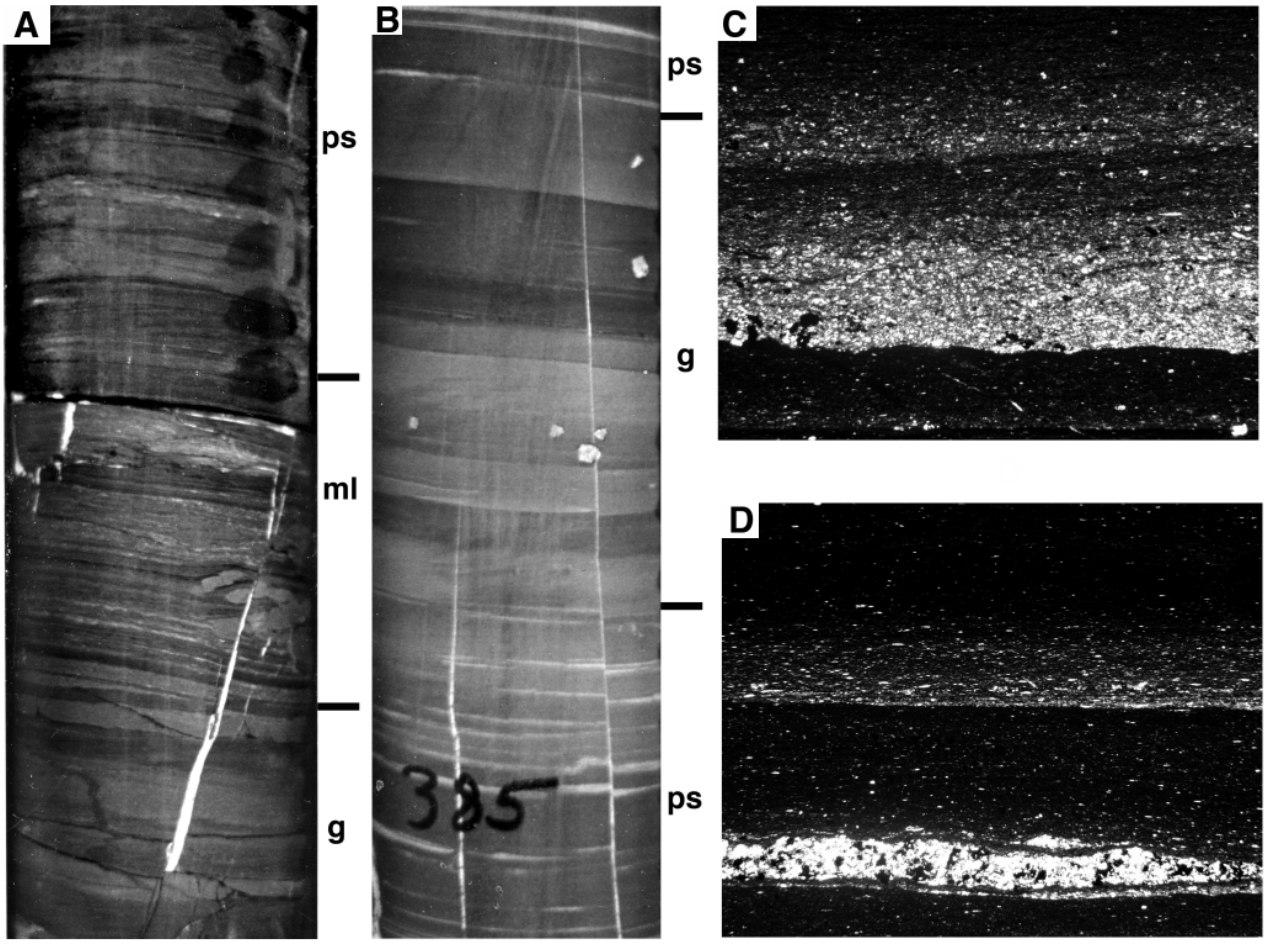

Figure A19. Variations in thickness and style of laminated mudstone. A. Sample from the Nursery Member of the Lockatong Formation showing graded laminae (g) at the base, overlain by organic-rich microlaminae (ml), which are capped by pinch-and-swell lamination (ps). White steeply inclined features are cement-filled fractures. Thickness shown is about 20 cm. Nursery core interval 1738 ft. Locality 2, table A1, figure A4. B. Sample showing thick lamination with pinch-and-swell features (ps) at the base and top and graded laminae (g) in the center in the Ewing Creek Member of the Lockatong Formation. White subvertical features are cement-filled fractures. Thickness shown is about 20 cm. Nursery core interval 385 ft. Locality 2, table A1, figure A4. C. Photomicrograph of thin section showing two graded laminae in the Nursery Member of the Lockatong Formation. Coarse material at the base (light) includes silicate grains and carbonate. Fine-grained top of layers is mostly clay with organic material. Thickness shown is about 0.5 mm. D. Photomicrograph of thin section showing a pinch-and-swell lamina (lower light band) and a graded lamina (upper light band) in the Nursery Member of the Lockatong Formation. The pinch-and-swell lamina consists of well-sorted coarse silt dominated by quartz. Thin clay partings separate a series of lenses that thicken out of the plane of view. Note the sharp upper contact of the silt lens to clay-sized sediment. The base of the graded lamina consists of fine silt-sized silicate minerals and carbonate. Thickness shown is about 0.5 mm. C and D are from locality 15, table A1, figure A4.

sediment from suspension. In contrast, laminae that are thicker, have more variable thickness and lateral erosive bases, are commonly formed by turbidites. Although turbidites may be generated by a variety of processes, they are commonly produced in lakes when sediment is eroded by waves and swept offshore as a plume or by underflows initiated near the lake margins. Laminae that thicken and thin laterally (pinch-and–swell laminae) are produced by waves near the minimum energy level for wave transport. The low relief of the lenses, and lack of steep foresets are characteristic of rolling-grain ripples (Harms and others, 1982, Chapter 2). Pinch-and-swell laminae were probably produced during storm wave events. The presence of burrow fabrics within laminae indicates that the bottom waters were at least partially oxidized. Small burrows that are restricted to a single lamina are typical of low-oxygen conditions, whereas burrows that penetrate several layers suggest more available oxygen (Smoot and Benson, 1998). The loop-bedding discontinuous lenses

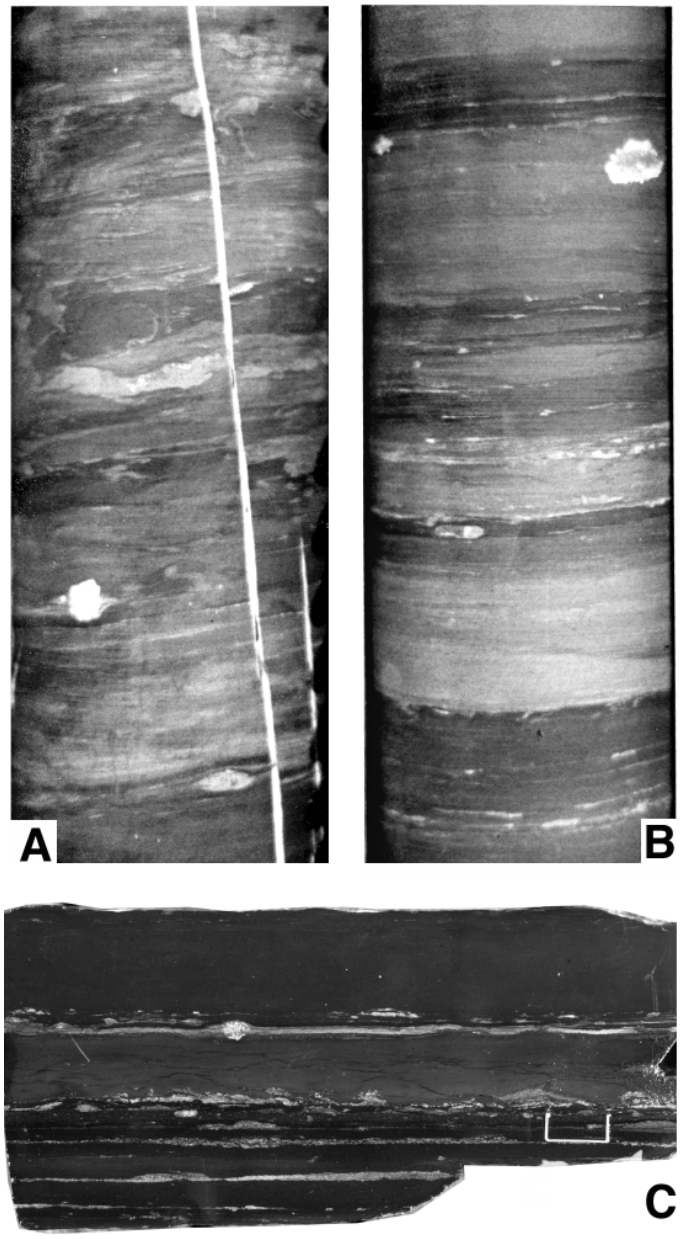

Figure A20. Thick lamination to thin beds with bioturbation. A. Segment of the Skunk Hollow Member of the Lockatong Formation showing thick lamination with alternations of silt-rich mudstone (light) and clay-rich mudstone (dark). Irregular (shredded) contacts are attributed to burrow mixing across grain types. Most ovate cross sections were probably burrows. Nearly vertical, linear white feature is a cement-filled fracture, and circular white mass is framboidal pyrite. Thickness shown is about 20 cm. Nursery core interval 1737 ft. Locality 2, table A1, figure A4. B. Segment of the Ewing Creek Member of the Lockatong Formation showing graded thick laminae and thin beds. Small projections from the base of graded beds (light) are interpreted as sediment-filled burrows. Ovate and circular cross sections and some of the discontinuous layers are all attributed to sediment-filled burrows parallel to bedding. Large circular white feature near top of the sample is framboidal pyrite. Nursery core interval 2235 ft. Locality 2, table A1, figure A4. C. Slabbed sample with pinch-and-swell laminae in the Skunk Hollow Member of the Lockatong Formation. Thick mudstone layers in the upper part of the sample are more silt-rich than the dark mudstone layers in the lower part. Ovate to circular features and irregular bedding contacts are indicators of bioturbation. Irregular dark streaks in the light-gray layer above the staple are also due to bioturbation. The staple is 7 mm wide. Locality 18, table A1, figure A4.

result from differential compaction of the laminated sediments that produces small fault planes. The intersection of the fault planes with the surface produces the gashes (Olsen and others, 1989, p. 43-44). Similar features in the rock record have been attributed to desiccation (Eugster and Surdam, 1973) or to synaeresis (Donovan and Forster, 1972).

The preservation of sub-millimeter laminae generally requires deeper water than that for preservation of thicker laminae. Lamina thickness, however, is not necessarily a direct reflection of the water depth as suggested by Olsen (1984, 1986). Organic material, articulated fish skeletons, and delicate layering will only be preserved in the absence (or near absence) of bioturbating organisms, either through high salinity or anoxia (Anderson and Dean, 1988; Kemp, 1996). Anoxia in bottom waters results from stratification that is difficult to maintain in large lakes without great depth. Wave-induced bottom currents can destroy fine lamination that is not bound by an organic mat. Olsen (1984, p. 278-283) attempted to quantify the maximum water depth to form microlaminae in the Lockatong Formation using the relations for wave height and fetch in Smith and Sinclair (1972). He reasoned that any wave energy reaching the lake floor would disturb the delicate laminae, so water depth must have exceeded half the wave length produced by a given velocity of wind. For an effective fetch of 70 km and 40 m/sec winds, this relation provided a minimum lake depth of about 80 m. Olsen argued, however, that

winds parallel to the long axis of Lake Tanganyika affected sediment to depths of 200 m, and by analogy, the lakes that deposited the Lockatong Formation must have been at least 100 m deep. A more rigorous measure of the maximum depths to which waves can transport sediment is provided by Rowan and others (1992). They used the relation between maximum wave height and effective fetch to determine the maximum depth for transport of silt or coarser material. The shear velocities for transporting grain sizes are based on experimental data of Komar and Miller (1975) that could not be extended to clay-sized sediment due to problems of cohesion and shape. Assuming that the maximum area of a Newark basin lake is equivalent to the preserved basin, the maximum depth for movement of silt-sized sediment is 60 m for a fetch equivalent to the long axis of the basin. This would be the minimum depth for microlaminated mudstone, for instance, at locality 27 (table A1, figure A3). The maximum depth cannot be determined from wave theory without additional data about erodibility of lake-bottom clay and possible binding by organic mats.

Thin-bedded mudstone

Thin-bedded mudstone is part of a continuum from laminated mudstone to massive mudstone. Thin-bedded mudstone that is closer in character to laminated mudstone includes 1) bioturbated beds consisting of alternating mudstone with layers of silt-sized sediment (fig. A20), 2) graded beds of silt- or fine-sand-sized sediment alternating with mudstone (fig. A21), and 3) pinch-and-swell to lenticular beds of silt-to fine-sand-sized sediment alternating with mudstone (fig. A22). Bioturbated thin beds are characterized by bands of lighter, silt-rich beds and darker, clay-rich beds that are disrupted by ovate to circular sediment-filled features and that have irregular contacts with a shredded appearance. The graded beds have sharp bases overlain by sand- or silt-sized sediment that gradually fines up to clay-sized sediment. In some places, the bases of graded beds cut across underlying beds. Elsewhere, the bases of graded beds are deformed into load casts. The basal portion of the graded beds may consist of only thin, discontinuous coarser-grained part and a thicker, more continuous finer-grained part. The coarse-grained part of graded beds is most typically unlayered, but in some cases may include ripple cross-lamination (fig. A21A). The pinch-and-swell layers and the lenticular layers of silt- and fine-sand-sized sediment are as much as a

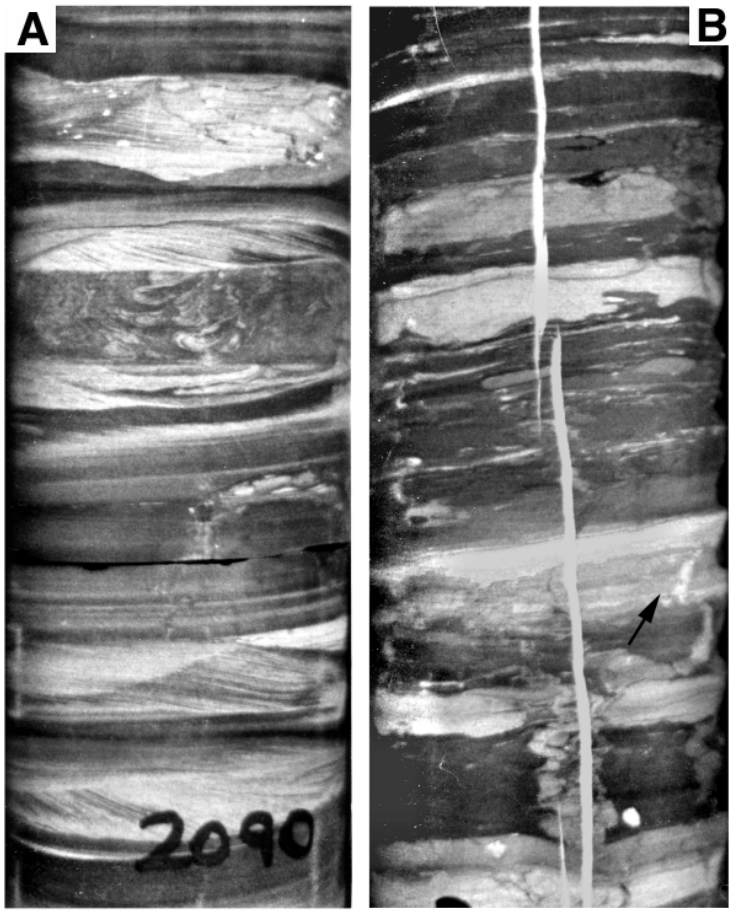

Figure A21. Thin-bedded mudstone with graded thin beds. A. Sample from Member RR of the Passaic Formation showing graded beds of fine sandstone (light) with ripple cross-lamination. The second sand layer from the top is underlain by mudstone with abundant soft-sediment deformation as “pseudonodules”. These form as ripples sink into water-saturated mud as they are moving. Thickness of core is about 20 cm. Martinsville core interval 2090 ft. Locality 7, table A1 figure A3. B. Sample from Perkasie Member of the Passaic Formation of graded beds of fine sandstone (light) with no internal lamination. Irregular bases of sandstone layers are due to soft-sediment loading. Vertical white linear features are cement-filled fractures. Sinuous vertical features near the base are sediment-filled polygonal cracks. Note how the crack cross section on the right (arrow) tapers upwards. Thickness is about 20 cm. Rutgers core interval 2245 ft. Locality 4, table A1, figure A3.

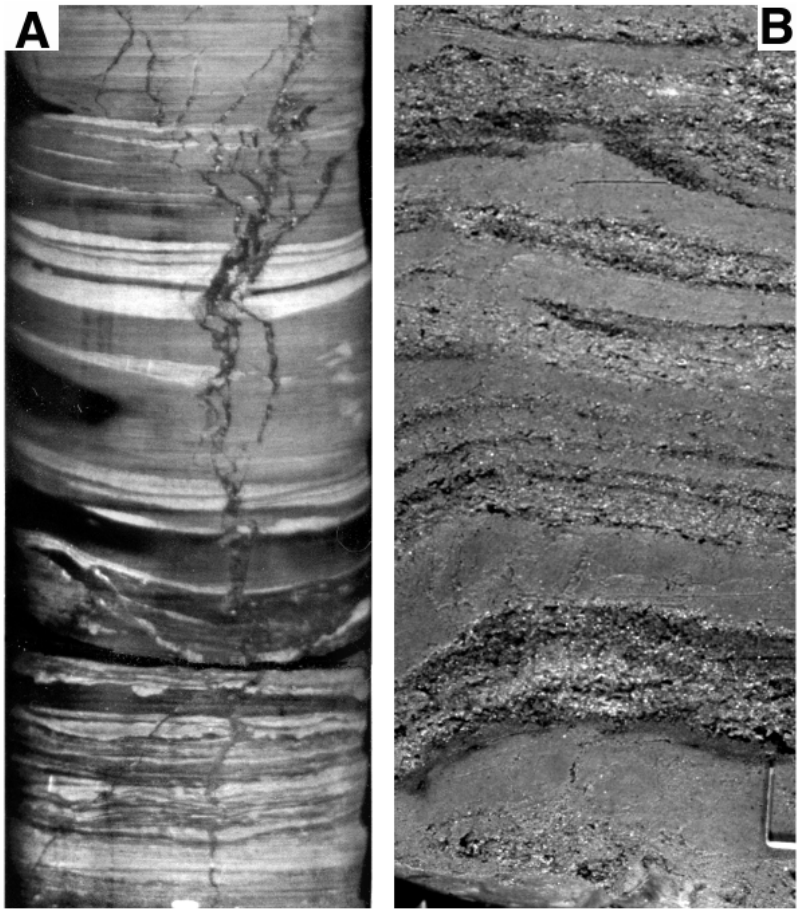

Figure A22. Comparison of thin-bedded mudstone to a Holocene shallow-lake deposit. A. Sample in the Tumble Falls Member of the Lockatong Formation showing pinch-and-swell fine sandstone (light) alternating with mudstone. Vertical disruption features are sediment-filled polygonal cracks. Thickness is about 15 cm. Nursery core interval 486 feet. Locality 2, table A1, figure A4.
B. Sediment core from Owens Lake, California showing late Holocene sand layers (grainy looking layers) formed by storm waves in about 3 m of water. Thickness is about 10 cm.

centimeter in thickness. The base of each coarse layer commonly is gently scalloped into the underlying mudstone layer. In the thicker pinch-and-swell or lenticular layers, internal lamination may consist of sinusoidal to gently inclined layers. Polygonal cracks commonly cross-cut thin-bedded mudstones, particularly those with pinch-and-swell or lenticular bedding. In vertical cross sections, the cracks are typically sinuous and filled with mudstone. Where thin-bedded mudstone is transitional upward from laminated mudstone, crack polygons in plan view have larger diameters (as much as meter scale) and the vertical cross sections are longer (many tens of centimeters) than progressively smaller and shorter cracks in overlying strata. The larger cracks can commonly be traced downward through a great thickness of beds (including laminated mudstone) from the layer of crack initiation, whereas the shorter cracks may originate from several beds. The longer cracks tend to be more sinuous, so that in some cross sections they appear to taper upwards or cause an overlying bed to bulge upward (fig. A21B). The overlapping of cracks from different beds is more common upwards in a succession from laminated mudstone. The overlapping cracks tend to obliterate bedding.

Thin-bedded mudstone that is gradational to laminated mudstone accumulated in the shallow parts of a lake. The abundant circular-to-ovate sediment-filled features in thin-bedded mudstone indicate intense bioturbation, but some layers are still visible as changes in the dominant grain size. The original sediment may have originally been laminated, but the burrows have mostly homogenized the finer structure and disrupted the contacts between contrasting sediment types. Graded beds in thin-bedded mudstone are turbidite deposits from storm waves or rapid sediment fluxes from floods or slumps. The load casts at the base of some graded beds are interpreted to have formed when coarser sediment was deposited rapidly over water-saturated mud. The absence of load casts and erosional contacts at the base of graded beds suggest that the water-saturated mud was eroded before the coarser material was deposited. This may be an indicator of graded beds formed by storm waves (Smoot and Benson, 1998). The graded beds with ripple cross-lamination were probably formed by turbidites that were initiated on a delta front. The pinch-and-swell beds or lenticular beds were produced by waves. In contrast to the pinch-and-swell layers in laminated mudstone, the thicker layers and internal stratification suggest that wave energy was stronger during deposition of thin-bedded mudstone. Internal

stratification in some of these beds indicates that the wave regime moved into the vortex ripple field (Harms and others, 1982, Chapter 2). Polygonal cracks formed when the lake floor was subaerially exposed and the sediment dried. The vertical changes in cracks and some of the variations in character are predictable results of the processes operating during the formation and burial of desiccation cracks. The size of the desiccation-crack polygons and the depth of crack penetration are measures of the wetness of the sediment that was desiccated (Smoot, 1983; Smoot and Lowenstein, 1991, p. 228-229). A thick accumulation of mud in a subaqueous environment may develop large desiccation-crack polygons that penetrate deeply during prolonged subaerial exposure. Some of the sediment that is penetrated by these cracks may have been deposited in hundreds of meters of water. In contrast, a lake margin that is frequently exposed subaerially, with only minor sediment accumulation between episodes of subaerial exposure, will tend to develop smaller desiccation-crack polygons that penetrate less deeply. If a lake transgresses over the desiccated surface before the cracks are filled with sediment, the cracks will collapse when re-saturated, causing them to distort into folds. These folds may be further tightened by compaction of the sediment as it is buried.

Another variety of thin-bedded mudstone is characterized by irregular graded beds and abundant cracks (fig. A23) with circular to flattened-ovate voids (vesicles) filled with diagenetic silicate and carbonate cements. These vesicles are mostly circular or irregularly ovate in plan view, indicating that they are *not* cross-sections of cylindrical roots or burrows. Graded, thin beds of silt- to fine-sand-sized sediment cut into underlying thin beds of mudstone. The coarser-grained parts thicken into scours and thin laterally. In some places, the polygonal cracks are sinuous and V-shaped, elsewhere they are more complex and have flat contacts against the underlying beds. In some cases, the coarser layer is broken into polygonal patches that are curved convex-upward (fig. A24). The areas between these curls are full of vesicles and small complex cracks. The vesicles are rarely circular in vertical cross sections; commonly they are

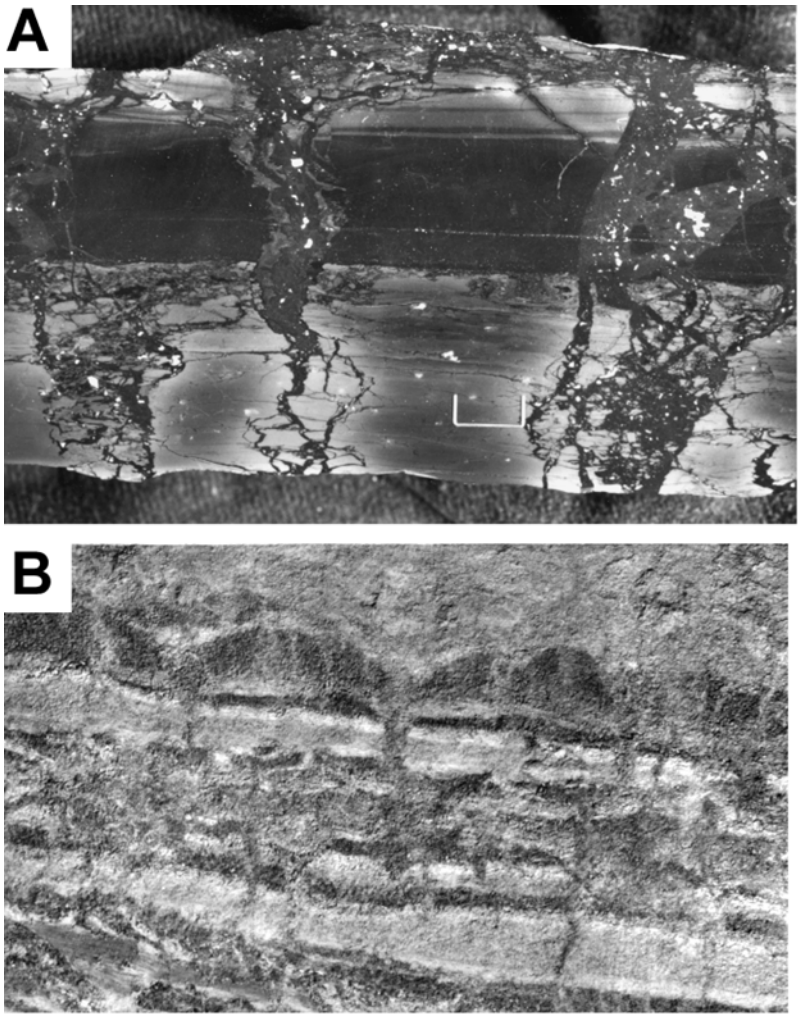

Figure A23. Comparison of thin-bedded mudstone disrupted by polygonal cracks and a Holocene ephemeral lake deposit. A. Tumble Falls Member of the Lockatong Formation showing thin-bedded mudstone with polygonal cracks filled by multiple layers of muddy sediment. White blebs are cement-filled vesicles. Note that polygonal cracks originate in each layer. Sample width is about 20 cm. Locality 19, table A1, figure A5. B. Trench face in a Holocene ephemeral lake deposit in Coyote Valley, California. Note that irregular bedding contacts and sediment-filled cracks originate at each bedding contact. Many of the crack fillings include open vesicles. Vertical section is about 30 cm.

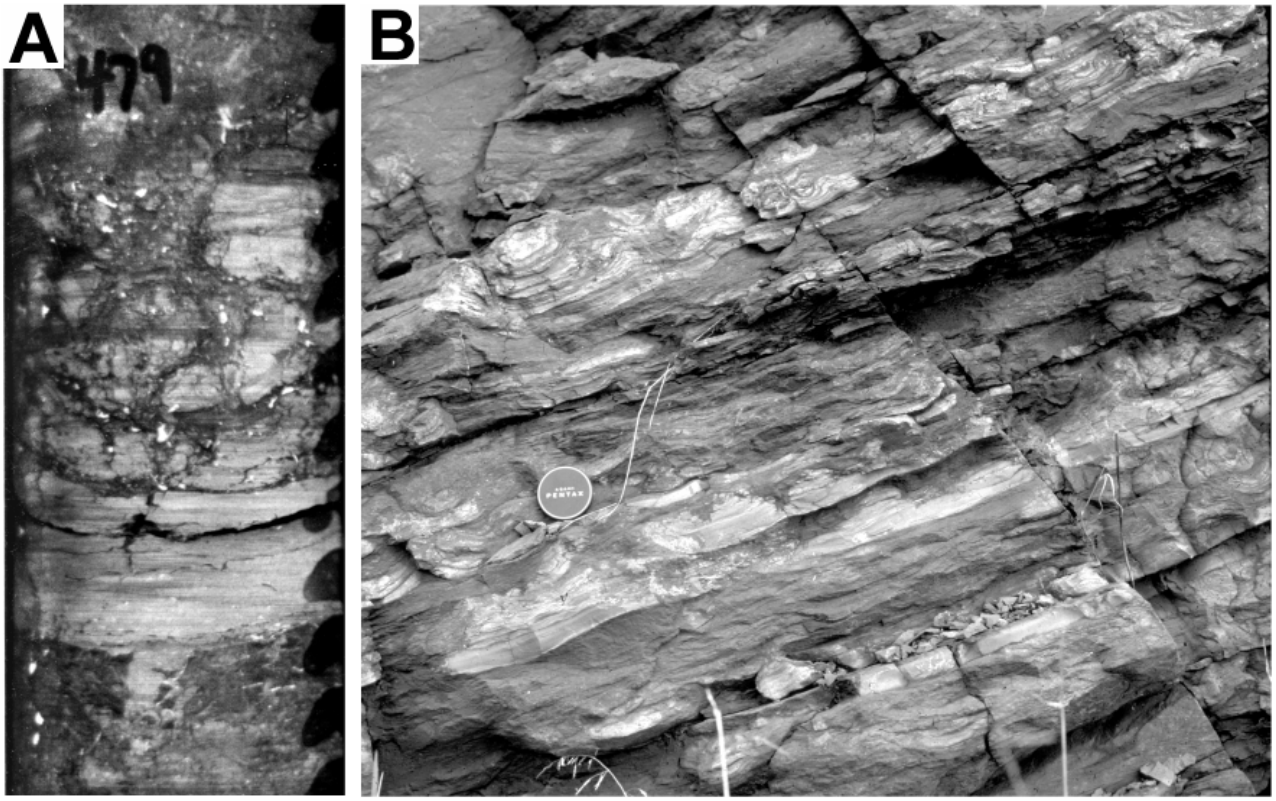

Figure A24. Thin-bedded, vesicular mudstone. A. Sample from the Prahls Island Member of the Lockatong Formation showing siltstone beds (light) alternating with vesicular mudstone (dark with white blotches). Cement-filled vesicles (light blotches) are restricted to polygonal crack fillings. Apparent branching and waviness are partly due to superimposed cracks from multiple layers. Thickness is about 15 cm. Nursery core interval 479 feet. Locality 2, table A1, figure A4. B. Outcrop of irregular siltstone thin beds (light) each cut by polygonal cracks filled with vesicular mudstone (dark) in the lower part of the Passaic Formation (Member C?). Note up-curled edges of siltstone layers and flat bottoms of cracks. Height of photo is about 60 cm. Locality 17, table A1, figure A5.

more ovate or nearly flat. The vesicles are commonly connected by narrow, cement-filled cracks.

Thin-bedded mudstone with irregular scour-based, graded layers and vesicle-filled cracks is interpreted as deposits of shallow, ephemeral lakes. The bedding formed when flood waters eroded the previously desiccated surface and fine-grained sediment settled out of the standing water. In some cases, several layers were deposited in continuous subaqueous conditions before the next desiccation episode. The cracking patterns reflect the frequency of desiccation. In modern ephemeral lakes, sediment that accumulates in lakes with frequent desiccation episodes tends to break up into small polygons with little penetration. In many cases, the polygonal cracks will reform at the site of the previous desiccation cracks, creating complex patterns of sediment fill, similar to the cracks in the vesicular thin-bedded mudstone. The polygonal patches that curve convex-upward in the vesicular thin-bedded mudstone are a thin layer of lake sediment that had curled away from a dry, sun-baked surface which acted as a barrier to crack penetration. Vesicles are common in desiccated mud in ephemeral lakes (Smoot and Lowenstein, 1991). The vesicles form when a completely dry surface is covered with water-saturated mud and escaping air is trapped in the mud as bubbles. The shapes tend to be more elongate and sheet-like in mud filling cracks, probably owing to shrinkage of the sediment filling during drying. Subsequent desiccation hardens the mud around the bubbles and produces tiny cracks that connect them. The bubble shapes are commonly flattened when the mud is re-saturated with water. The close similarity in the size, shape, and distribution of cement-filled vesicles in the Newark basin and the modern open features is strong evidence for a similar origin.

Massive Mudstone

The massive mudstone is named for the common descriptor used in most studies of these largely unbedded deposits (Smoot and Olsen, 1988). The massive mudstone encompasses five types:

1) brecciated massive mudstone, 2) vesicular massive mudstone, 3) peloidal massive mudstone, 4) root-disrupted massive mudstone, and 5) burrowed massive mudstone. There are gradations between each of these types. All of these mudstone types, except the burrowed massive mudstone, indicate subaerial exposures.

Brecciated massive mudstone (fig. A25) is characterized by angular fragments of mudstone separated by narrow, irregular, cracks. The cracks commonly contain silicate and carbonate-cement-filled vesicles (as in the vesicular thin-bedded mudstone), but some have no vesicles, particularly where associated with root-disrupted massive mudstone (see below). Brecciated massive mudstone is commonly transitional from thin-bedded mudstone with abundant polygonal cracks, but in some instances brecciated massive mudstone directly overlies other varieties of massive mudstone. The size of angular mudstone fragments decreases upward, and in some cases, the mudstone fragments have relict bedding from the underlying mudstone. The relict bedding can be traced from one mudstone fragment to another, parallel to regional bedding, even where the fragments are separated by

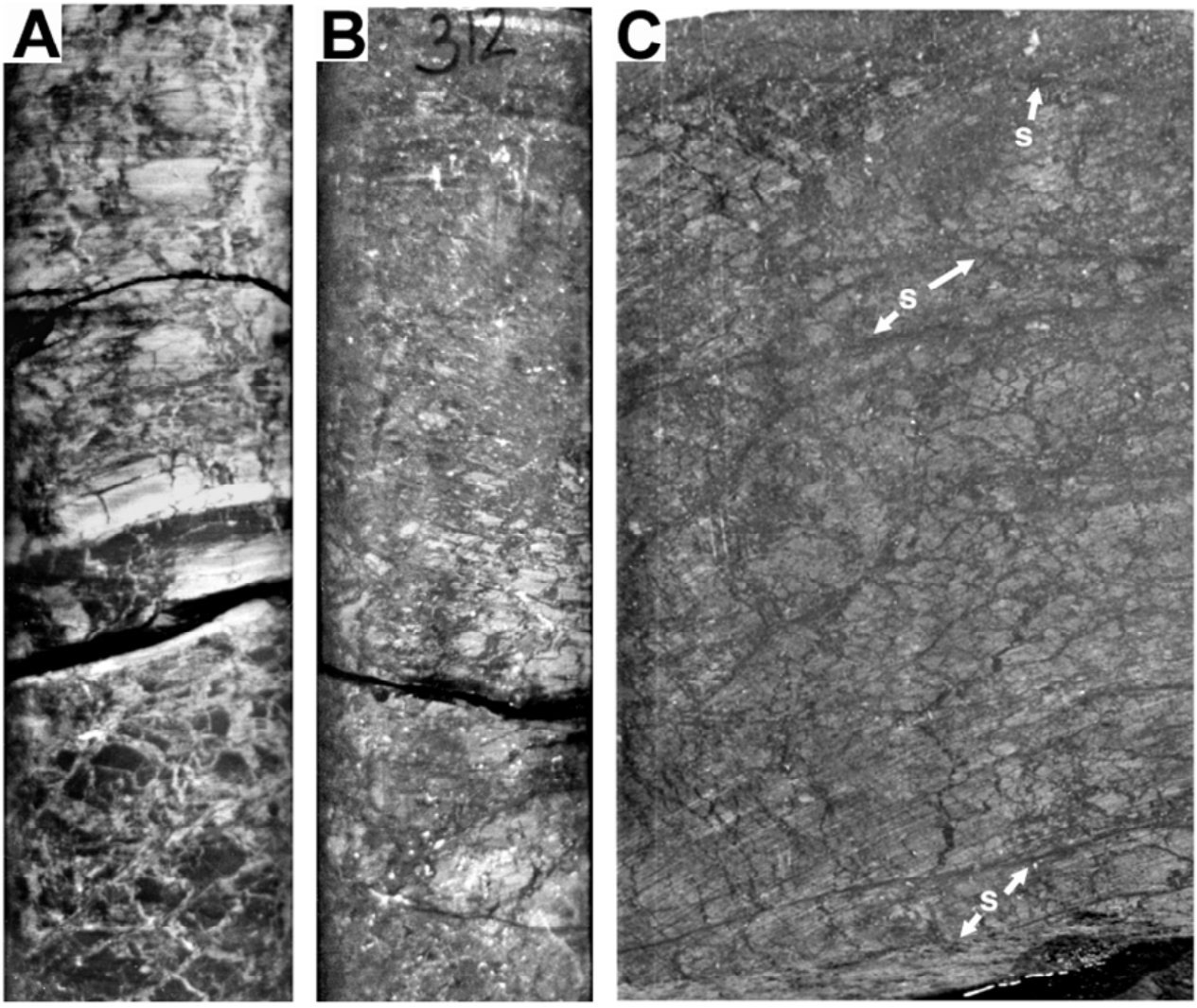

Figure A25. Brecciated massive mudstone. A. Sample in the Smith Corner Member of the Lockatong Formation showing brecciated massive mudstone in gradational contact with thin-bedded mudstone (light bands just below center). Irregular vertical features are sediment-filled polygonal cracks. Thickness is 20 cm. Nursery core interval 853 ft. Locality 2, table A1, figure A4. B. Sample in the L-M Member of the Passaic Formation showing brecciated massive mudstone (base) in gradational contact with vesicular massive mudstone (top). Light clumps are remnant fragments of thin-bedded mudstone cut by sediment-filled polygonal cracks (dark) with cement-filled vesicles (white blebs). Thickness is about 20 cm. Titusville core interval 312 ft. Location 3, table A1, figure A4. C. Slabbed outcrop sample of brecciated massive mudstone with slickenside curved planes (s) in the Tumble Falls Member of the Lockatong Formation. Dark jagged vertical features are sediment-filled desiccation cracks and white blebs are cement-filled vesicles. Thickness is about 30 cm. Locality 19, table A1, figure A5.

wide areas of crack filling (fig. A26). The mudstone fragments tend to be vertically elongated in the lower part of a brecciated massive mudstone with vesicular textures, and the fragments become smaller and more equant upwards. In this type of brecciated massive mudstone, the vesicles commonly are progressively more numerous upwards in the matrix. In brecciated massive mudstone that lacks vesicles, the lower fragments are not vertically oriented and may be horizontally elongated, but grade upward to smaller, more equant fragments. In some brecciated massive mudstone, the brecciated fabric is crosscut by concave-upward planes of slickensided clay (fig. A25C).

Brecciated massive mudstone was formed by the repeated wetting and drying of a mud that was initially deposited in standing water. In modern dry playa mudflats (fig. A26B), the former lake mud deposits are broken up by the superposition of random cracks over the surface (fig. A27). As older open cracks on the surface are gradually filled with sediment during intermittent periods of flooding, newer cracks form that crosscut the old fillings and become new sites for sediment filling. Sediment volume increases by the repeated opening and filling of polygonal cracks. Farther below the desiccation surface, lake mud is less fragmented than that directly beneath the surface because it was not re-saturated with flood water and had fewer episodes of re-cracking. Open vesicles formed by trapped air occur in modern playas. The generation of vesicles within cracks is consistent with the absence of moisture in the sediment between crack-filling events. In brecciated massive mudstone that lacks vesicles, particularly those with horizontally elongated fragments in the lower part, the brecciation is interpreted as displacement by wetting and drying in a vertisol

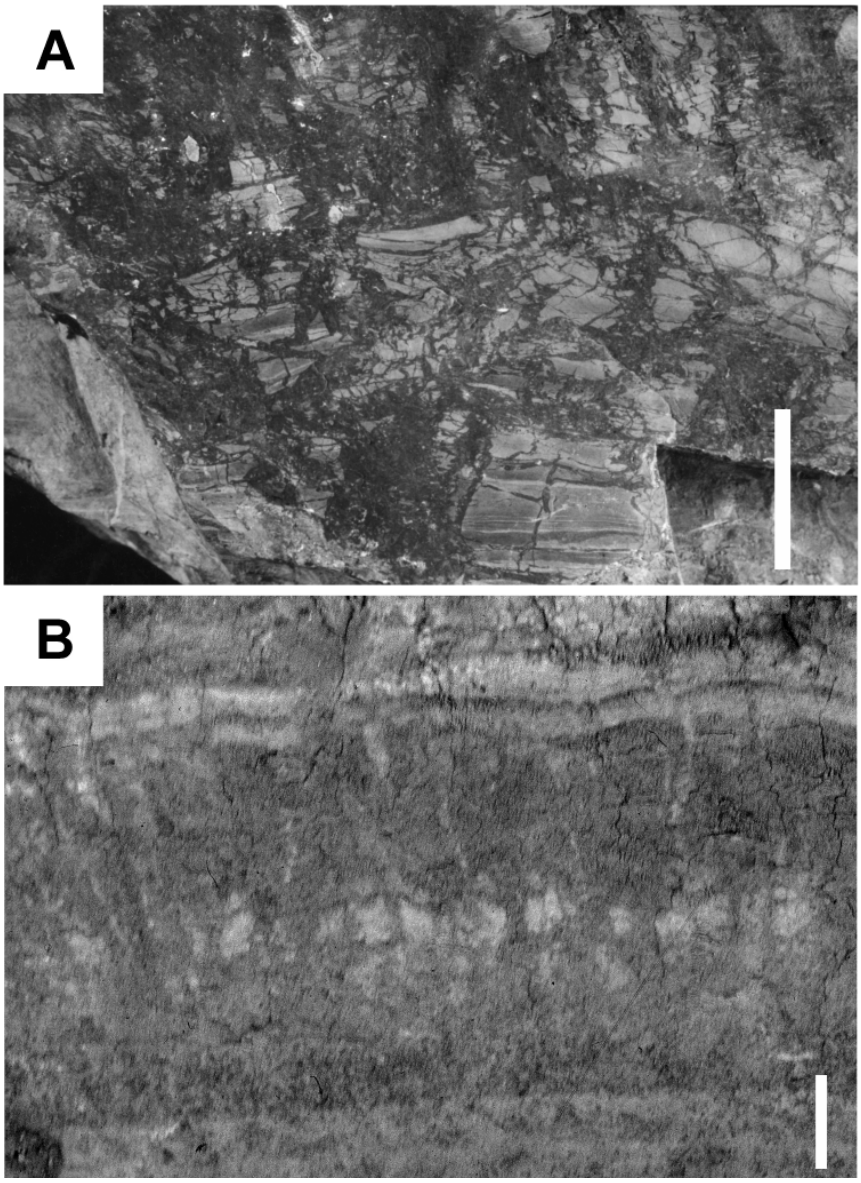

Figure A26. Comparison of brecciated massive mudstone to Holocene playa deposits at Coyote Valley, California. A. Outcrop sample of brecciated mudstone from L-M Member of the Passaic Formation. Thin-bedded gray mudstone clumps (light gray angular blocks) are separated by red vesicular mudstone (dark with white blebs). Note that layers are recognizable in individual, angular blocks at the same level, and the vertically elongated blocks toward top of sample. Scale bar is 5 cm. Locality 20, table A1, figure A4. B. Trench through mud directly below the surface at Coyote Valley. Thin-bedded ephemeral lake deposits at base grades upward into brecciated mud capped by another thin-bedded ephemeral lake deposit. Note traceability of light and dark color bands in angular mud blocks. Vertical light and dark bands are sediment-filled desiccation cracks with open vesicles. Open cracks are visible in the top layer. Scale bar is 5 cm.

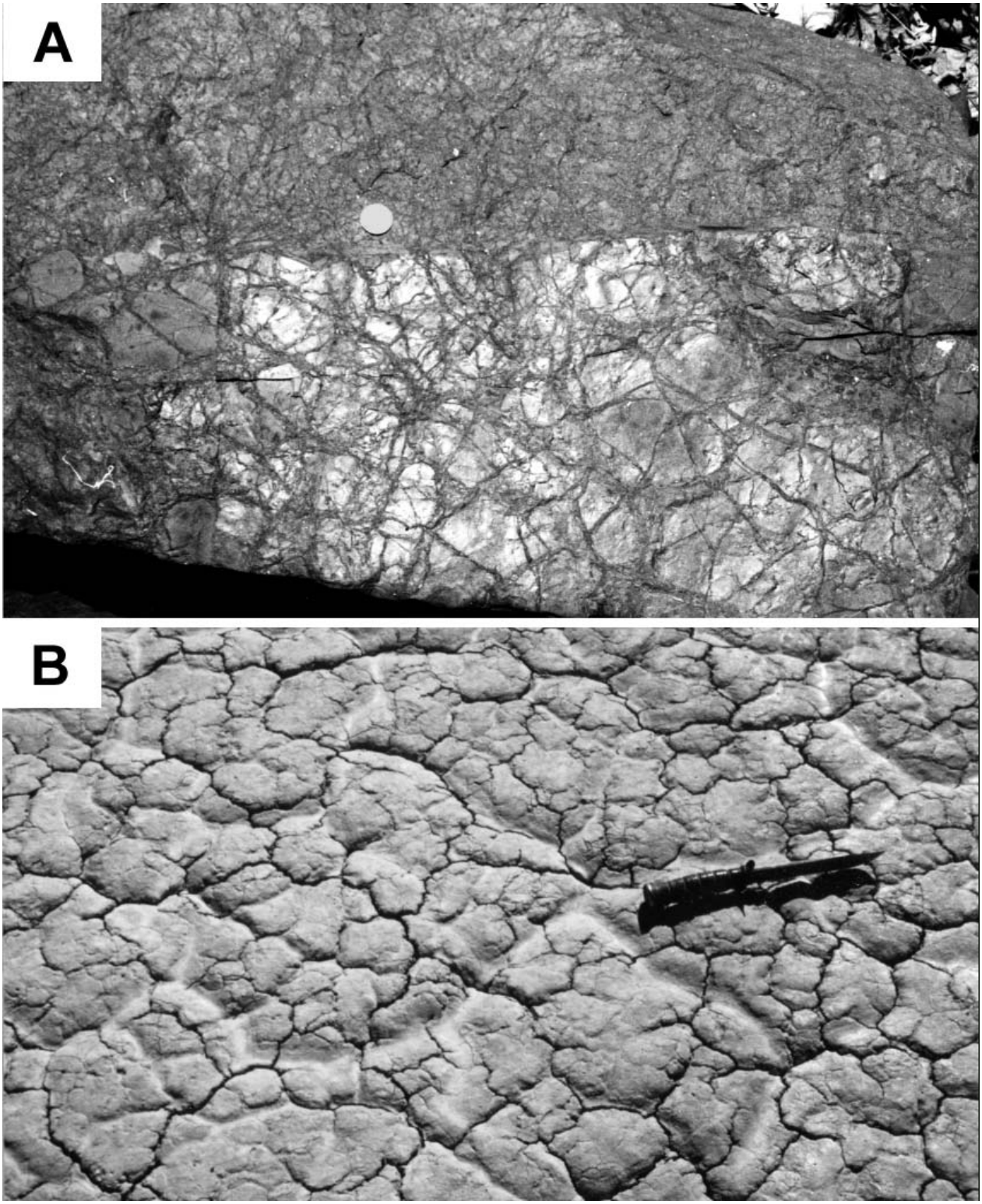

Figure A27. Comparison of plan view of polygonal cracks in brecciated massive mudstone and modern surface of a dry mudflat. A. Plan view of outcrop slab in the Tohicken Member of the Lockatong Formation. Lower part of sample shows multiple cracks cutting a gray thin-bedded mudstone (light) whereas upper part shows overlying transition to more densely crosscutting cracks and isolated mudstone fragments. Area shown is about 50 cm wide. Locality 21, table A1, figure A5. B. Surface at Mud Lake, Nevada, showing sediment-filled polygonal cracks (lighter lines) randomly cut by open polygonal cracks (dark lines). Older crack fillings are barely visible on some of the dark surfaces. Sedimentation is chiefly restricted to filling cracks. Knife is about 30 cm long.

(Wilding and Puentes, 1988). The curved, slickensided planes in some brecciated massive mudstone are slip planes, called gilgae. Gilgae and vesicular fabrics are not mutually exclusive and the two processes may operate together. The absence of vesicular fabrics indicates formation of brecciated massive mudstone in wetter conditions than those for vesicular fabric. The absence of vesicular fabric may be due to lack of preservation by collapse during re-saturation, or to conditions too wet to form vesicles.

Vesicular massive mudstone is a structureless-appearing, poorly sorted mudstone with many silicate and carbonate cement-filled vesicles (fig. A28). The vesicles vary from nearly circular shapes to highly flattened ellipses with vertical or horizontal orientation. In plan view, the vesicles show circular or elliptical cross-sections but no evidence of cylindrical geometry (that is, roots or burrows). The mudstone consists entirely of superimposed small, narrow cracks oriented vertically and horizontally that form cm-scale polygons in plan view. Cracks are mostly filled with mudstone or have small parts filled with silicate and carbonate cement, but they may also have partial filling of silt- or fine-sand-sized sediment. Some crack margins and some edges of vesicles have thin coatings of clay that are parallel to the crack or vesicle margin (fig. A29). Discontinuous layers of silt, fine-sand, or clay-sized sediment in a vesicular massive mudstone are commonly bowl-shaped (fig. A30). Vesicular massive mudstone grades into brecciated massive mudstone or vesicular thin-bedded mudstone. Vesicular massive mudstone tends to be more poorly sorted than brecciated massive mudstone. Curved slickenside planes occur in vesicular massive mudstone in some localities, but they are less common and usually less well developed than those in brecciated massive mudstone. The fabric of vesicular massive mudstone is identical to the fabric in modern playa dry mudflats (Smoot and Lowenstein, 1991), where the groundwater table is well below the surface and where sedimentation events are small and infrequent. The small, narrow cracks and the thin cutans (clay linings) develop on a dry surface that is wetted intermittently. In the modern dry mudflat, sediment accumulates primarily in open cracks during infrequent flooding events. Following a flood, new cracks form that crosscut the old cracks, providing a new locus for sediment accumulation during the next flooding event. Vesicle shapes in the Newark basin resemble those at the surface of modern dry playa mudflats (Smoot and Lowenstein, 1991). The vesicles formed in the wetted mud of a playa surface and within the crack fillings, as trapped air escaped. Some vesicles compacted into ellipses when rewetted. The slickenside planes in the vesicular massive mudstone formed as a result of repeated wetting and drying, but the predominance of dry over wet conditions and the coarse nature of the accumulating sediment retarded the full development of gilgae.

Peloidal massive mudstone consists chiefly of sand- to granule-sized rounded clumps of mudstone (fig. A31). The clumps are commonly separated by interstices filled by silicate and carbonate cement. Where this texture is transitional to another mudstone type, the mudstone clumps are concentrated into cracks with polygonal shapes in plan view, producing a texture similar to that of the brecciated massive mudstone (fig. A32). The polygonal patterns are progressively less distinct upward within a peloidal massive mudstone, where small polygons are defined by different sizes of mudstone clumps crosscutting each other. Unlike the brecciated massive mudstone, slickenside structures and vesicles are absent in the peloidal massive mudstone. Some peloidal massive mudstone occurrences have small (0.1-2.0-mm diameter) anhedral to subhedral crystal pseudomorphs (fig. A33). The peloidal massive mudstone is commonly superimposed upon thin-bedded mudstone (fig. A33) and, more rarely, laminated mudstone.

The peloidal massive mudstone is interpreted as having formed at the surface of saline mudflats with powdery, “puffy ground” salt crusts (fig. A34). In modern saline mudflats with “puffy ground” efflorescence, mud with polygonal desiccation cracks is disrupted by finely crystalline efflorescent salts that break the sediment into small rounded clumps (Smoot and Castens-Seidell, 1994). The brecciated fabrics and the small cross-cutting polygonal cracks in peloidal massive mudstone formed the same way as the previously described brecciated massive mudstone and vesicular massive mudstone, but salts also expanded the surface into a loose, granular mass. Modern “puffy ground” surfaces are easily eroded by wind (Bowler, 1973). Many of the polygonal cracks were filled by mud clumps that were eroded by wind and blown across the surface. The abrupt contacts between peloidal massive mudstone and clearly subaqueous thin-bedded mudstone (fig. A33) or laminated mudstone are attributed to the deflation of some part of the lake regression deposits.

Root-disrupted massive mudstone is characterized by the dominance of cement-filled or sediment-filled tube-shaped features with a wide variety of diameters (fig. A35). Cement filling includes silicates, carbonates, and sulfates in separate tubes or in succession within a single tube (Simonson and Smoot, Chapter B, this volume). The distribution varying these tubes diameters reflects downward tapering and branching into progressively smaller tubes. This mudstone type typically has tubes with millimeter-scale to sub-millimeter-scale diameters in it’s lower part and progressively larger tube shapes upward (fig. A36A). Several decimeter-scale successions of this variety may be within a root-disrupted massive mudstone. The larger tubes are commonly sediment-filled or have only

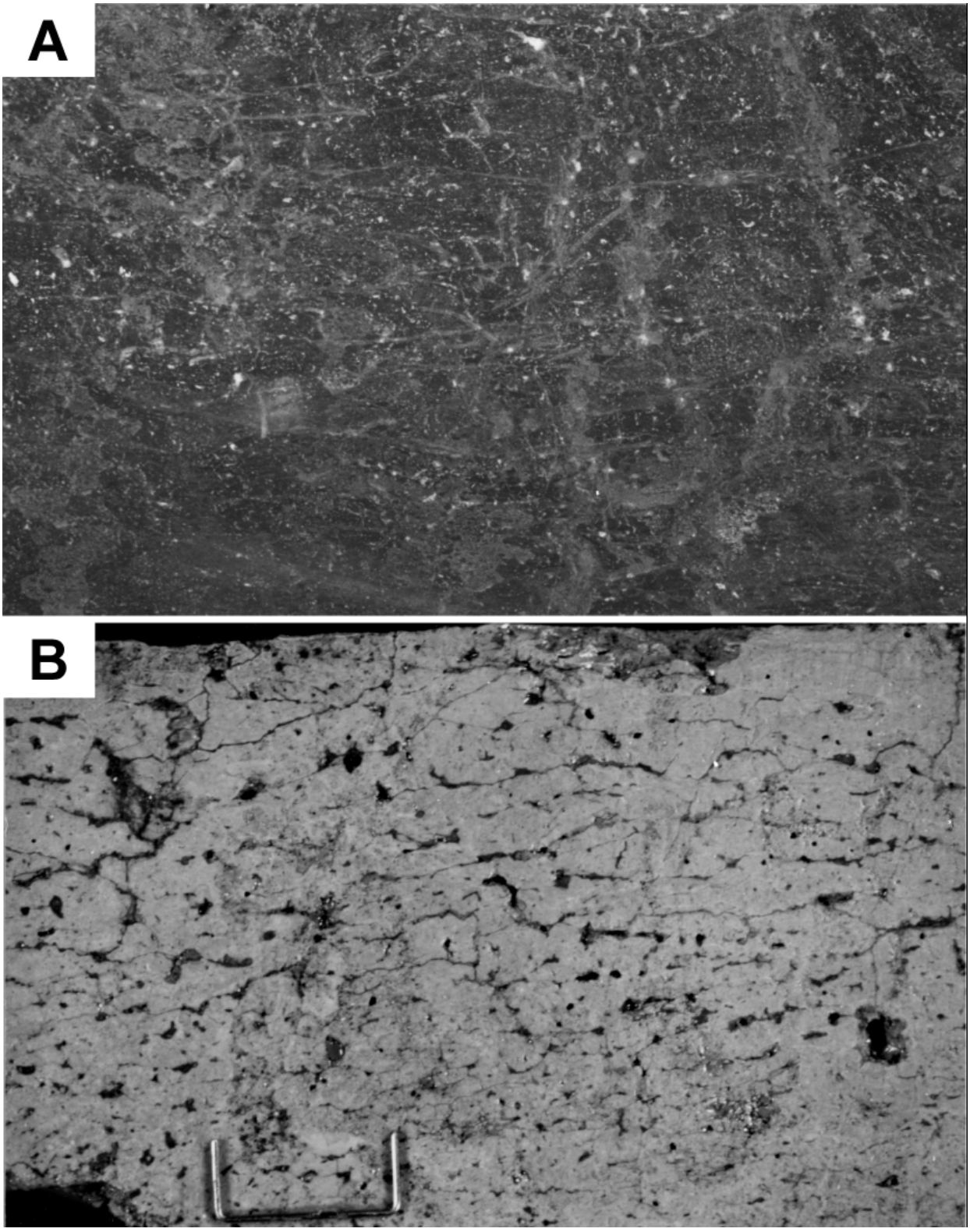

Figure A28. Comparison of vesicular massive mudstone and modern mud from a dry mudflat. A. Slabbed outcrop sample from Skunk Hollow Member of the Lockatong Formation. White blebs are cement-filled vesicles and light, wavy vertical features are sediment-filled polygonal cracks. Note light horizontal features which are cement-filled cracks connecting vesicles. Thickness is 4 cm. Locality 21, table A1, figure A4. B. Slab of modern surface mud from Mud Lake, Nevada, showing open vesicles (black) and sediment-filled cracks (faint darker vertical features). Note horizontal open cracks connecting vesicles. Thickness is 3 cm.

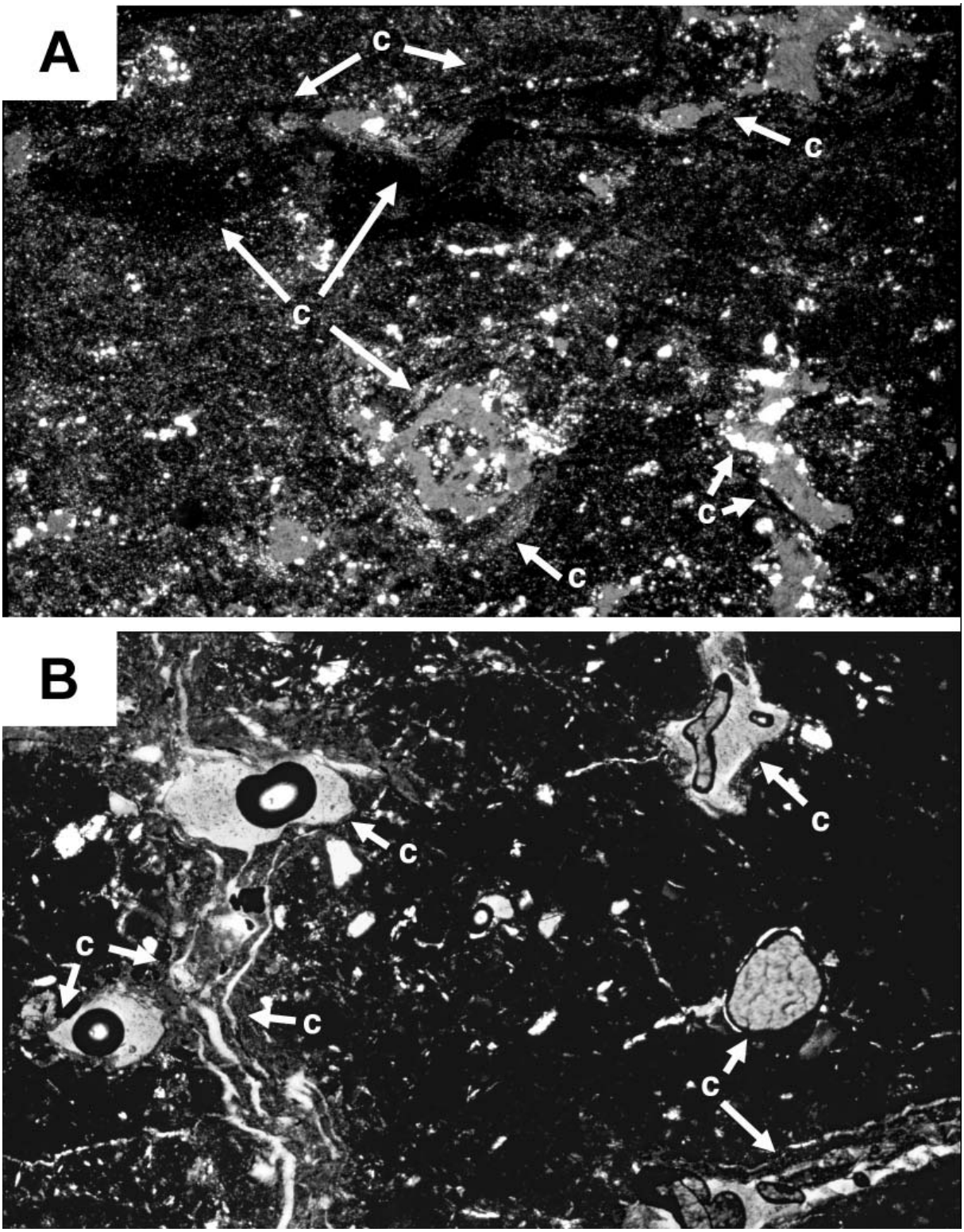

Figure A29. Comparison of photomicrographs of thin-sections of vesicular massive mudstone and mud from a dry mudflat. A. Thin section of vesicular massive mudstone from the Skunk Hollow Member of the Lockatong Formation. Vesicles and small cracks are filled with silicate (gray) and carbonate (white) cements. Clays aligned parallel to cracks and vesicles (c) are cutans. Field of view is about 5 mm wide. Locality 21, table A1, figure A5. B. Thin section of mud from the modern dry mudflat at Mud Lake, Nevada showing open vesicles and cracks (white). Cutans are aligned parallel to cracks and vesicles (c) consisting of material eluviated during prolonged subaerial exposure. Note the sinuosity of vertical crack caused by partial collapse following rewetting. Field of view is about 5 mm wide.

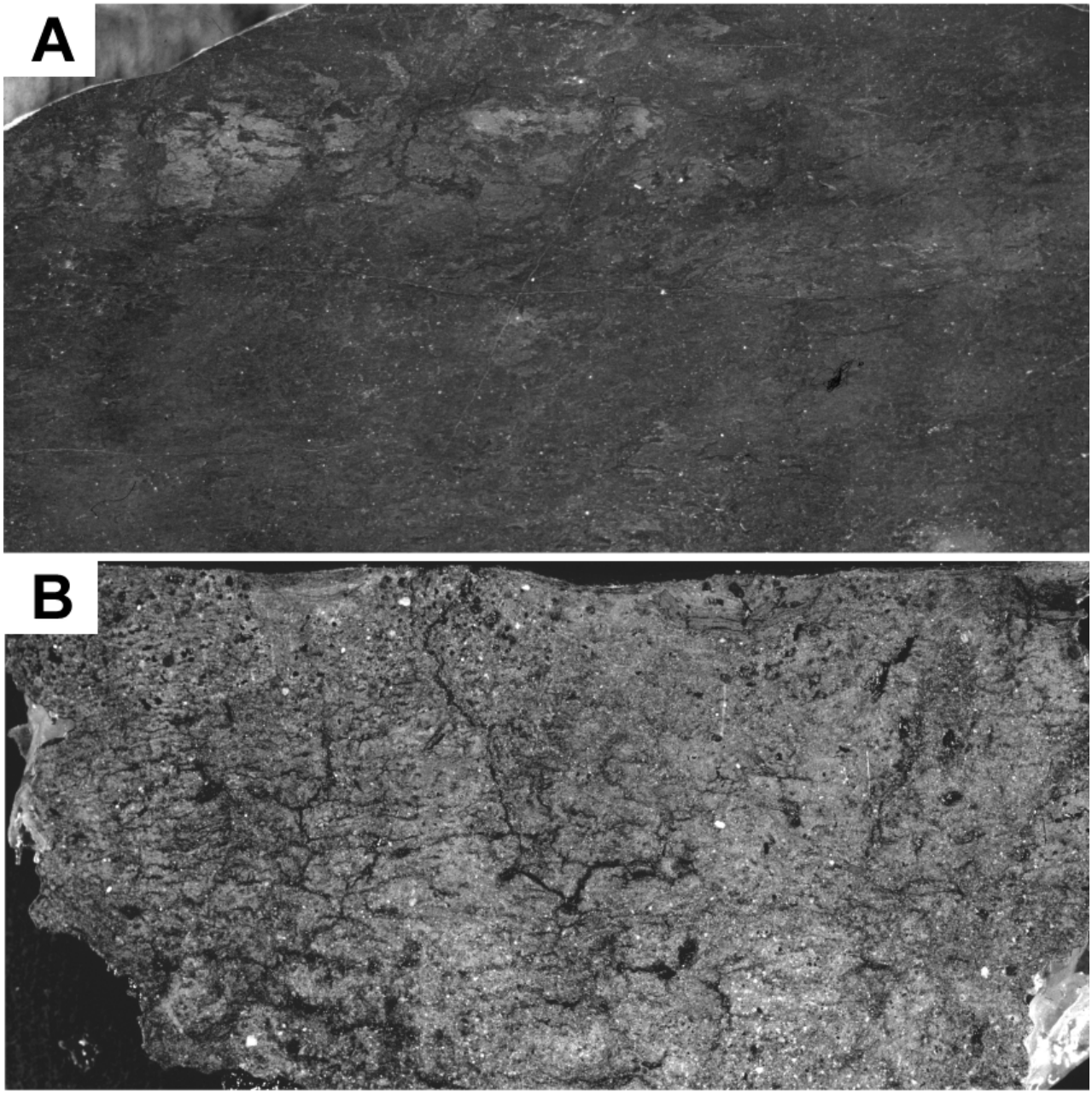

Figure A30. Comparison of vesicular massive mudstone with patches of bedding and modern mud from a dry mudflat. A. Slabbed outcrop sample from the Perkasie Member of the Passaic Formation. Irregular light patches are siltier mudstone forming discontinuous layers. Jagged dark features are sediment-filled polygonal cracks with oriented clay lining. Large dark ovate features are vesicles partially filled with sediment. Numerous white blebs are cement-filled vesicles. Thickness shown is about 10 cm. Locality 20, table A1, figure A3. B. Slabbed sample of surface mud from dry mudflat in Panamint Valley, California. Note isolated layer of silt and clay at top of sample and jagged open cracks with large vesicles (black), and numerous smaller vesicles (black) some of which are sediment filled (gray circular features). Thickness shown is 8 cm.

irregular patches of cement within sediment, whereas smaller tubes are more commonly filled with diagenetic cements. Some root-disrupted massive mudstone includes horizons dominated by large horizontal tubes with only small vertically oriented tubes. Oriented clays commonly line the tube boundaries (fig. A36D) and mm-scale flattened tubes are recognizable by their clay linings. Carbonate concretions and sediment-filled burrows (including Scoyenia) are common in the root-disrupted massive mudstone (fig. A36B), particularly in the upper parts of upward-increasing tube diameters. Well-developed, bowl-shaped slickenside

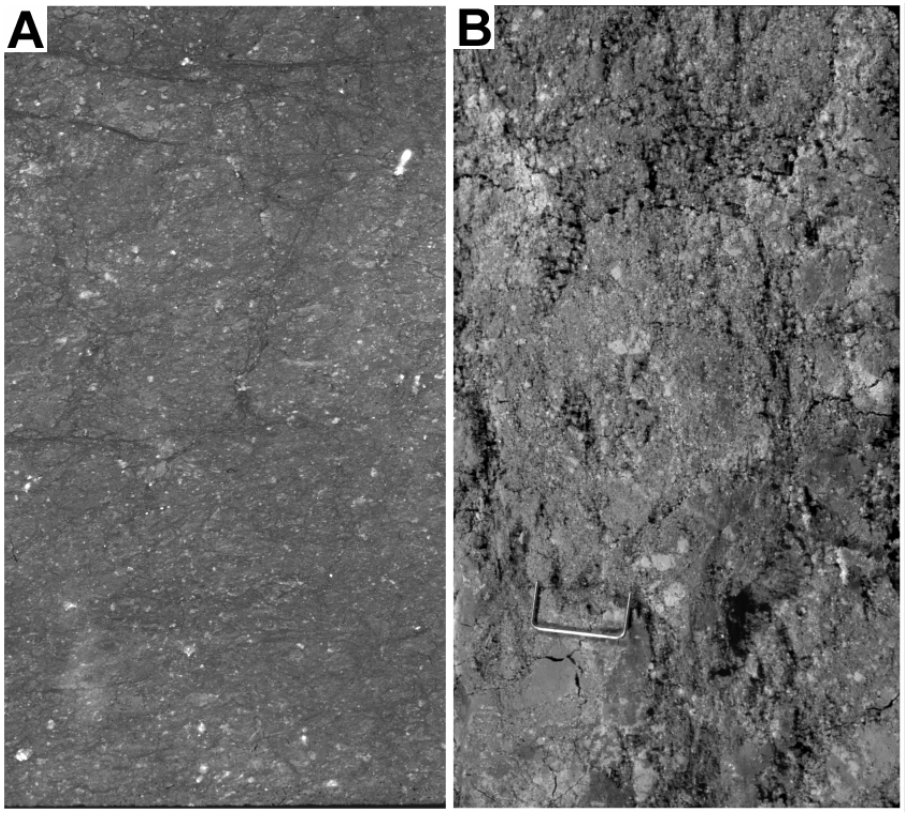

Figure A31. Comparison of peloidal massive mudstone to peloidal fabric produced from puffy ground efflorescence in a modern saline mudflat.
A. Slab of outcrop sample from the Tumble Falls Member of the Lockatong Formation. Granule-sized rounded mud clumps (light gray) are separated by cement (white) and clay (dark). Vertical and horizontal linear features are cement- and clay-filled cracks. Large white blebs are carbonate pseudomorphs after anhedral evaporites and late diagenetic pyrite framboids. Thickness shown is about 15 cm. Locality 19, table A1, figure A5.
B. Cross section of core from Desert Dry Lake, Nevada, showing rounded granule-sized pellets of mud produced by powdery efflorescent crust. Note narrow jagged vertical and horizontal open cracks (black). Thickness shown is 12 cm.

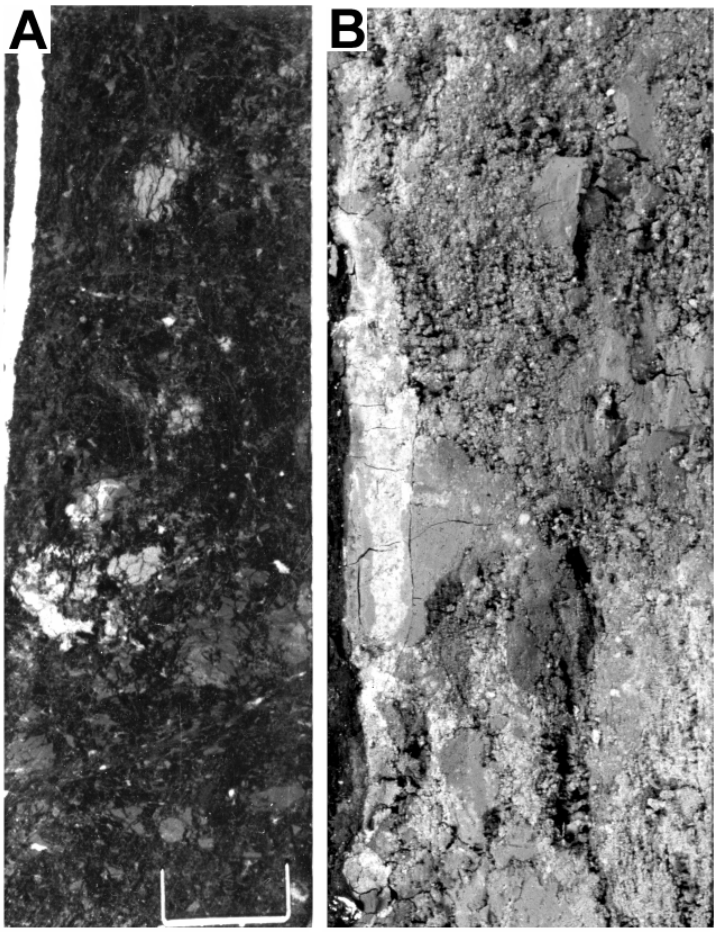

Figure A32. Peloidal massive mudstone with breccia fabric compared to the fabric from a core of a modern saline mudflat with puffy ground salt crust. A. Sample from the Prahls Island Member of the Lockatong Formation of peloidal massive mudstone. Note rounding of some breccia fragments (light) and background of rounded sand- to granule-sized clumps (dark). White, sub-vertical feature is a cement-filled fracture. Thickness shown is about 8 cm. Nursery core interval 1030 ft. Locality 2, table A1, figure A4.
B. Cross section of core from Desert Dry Lake, Nevada, showing breccia of clay clumps surrounded by rounded clay pellets. Brighter vertical feature is a pellet-filled crack from a higher level. Thickness shown is about 8 cm.

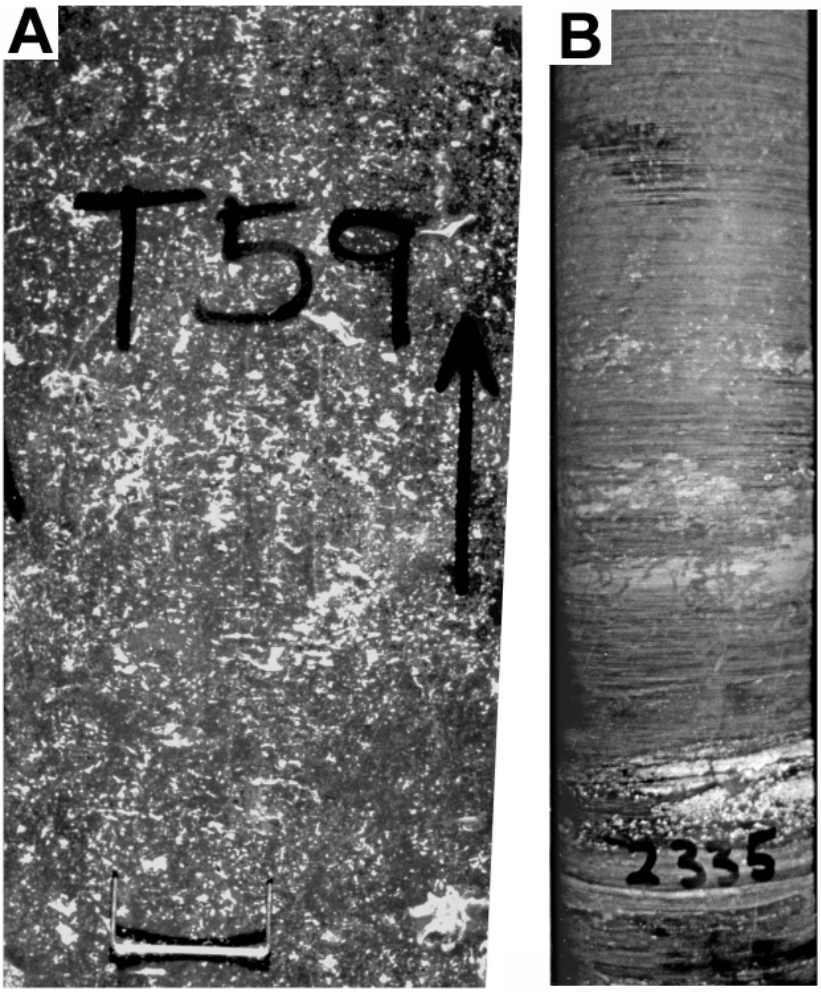

Figure A33. Peloidal massive mudstone fabrics. A. Sample of peloidal massive mudstone with subhedral to anhedral evaporite pseudomorphs (white) in the E-F Member of the Passaic Formation. Dark rounded peloids are visible as matrix and angular crystal faces are evident in some of the white pseudomorphs. Thickness shown is about 5 cm. Titusville core interval 1625 ft. Locality 3, table A1, figure A4. B. Sample from the Ewing Creek Member of the Lockatong Formation showing the transition from thin-bedded mudstone to peloidal massive mudstone. Thin beds at base are disrupted by vertical cracks filled with peloids, grading to mostly peloids with isolated patches of mudstone (light). Compare this to modern puffy ground efflorescence disruption in figure A34. Thickness shown is about 25 cm. Nursery core interval 2335 ft. Locality 2, table A1, figure A4.

planes are also common in the root-disrupted massive mudstone as are a variety of planar to curved planes of variable length and orientation, defined by oriented clays. Root-disrupted massive mudstone in the upper part of the Passaic Formation is commonly silty or sandy with recognizable patches of bedding or cracks filled with sand-sized sediment. Fine-grained, root-disrupted massive mudstone displays large polygonal crack patterns in plan view (tens of centimeter- to meter-scale, fig. A36C) and extends to more than a meter in depth with no change in width. At one locality in the Passaic Formation, carbonized wood forms a stump that is 3 cm in diameter and 10 cm high, which rests directly on root-disrupted massive mudstone and is coated by stromatolitic tufa and capped by lacustrine deposits (fig. A37).

Root-disrupted massive mudstone is interpreted as deposits of a vegetated mudflat, similar to modern vegetated playas in Texas and New Mexico (Holliday and others, 1996; Hovorka, 1997), or soil development superimposed on another depositional environment. Sediment- and cement-filled tubes with a wide variety of diameters and systematic profiles of upward increasing diameters are best interpreted as root casts. In some places, the observed branching and tapering of tubes confirms this interpretation. Modern vegetated playas are intermittently flooded by very shallow lakes; then dry out to soil surfaces covered with plants. The well-developed sequences of upward-increasing tube size with carbonate nodules, short planes of oriented clay, and slickensides in the root-disrupted massive mudstone are probably analogous to features found in modern vertisol soil profiles (Wilding and Puentes, 1988). Less well-developed soils in the root-disrupted massive mudstone are indicated by the root-cast successions associated with the narrow, deep cracks. The cracks in the less well-developed soils may represent a variation on columnar soil peds common to a variety of soils (Retallack, 2001). Root-disrupted massive mudstone dominated by horizontal root casts probably consists of water-saturated soils where plants produced roots that were restricted to the more highly oxidized sediment surface, and vertical penetration was not necessary to obtain water. The decimeter-scale successions of increasing root size in root-disrupted massive mudstone suggest episodes of sediment

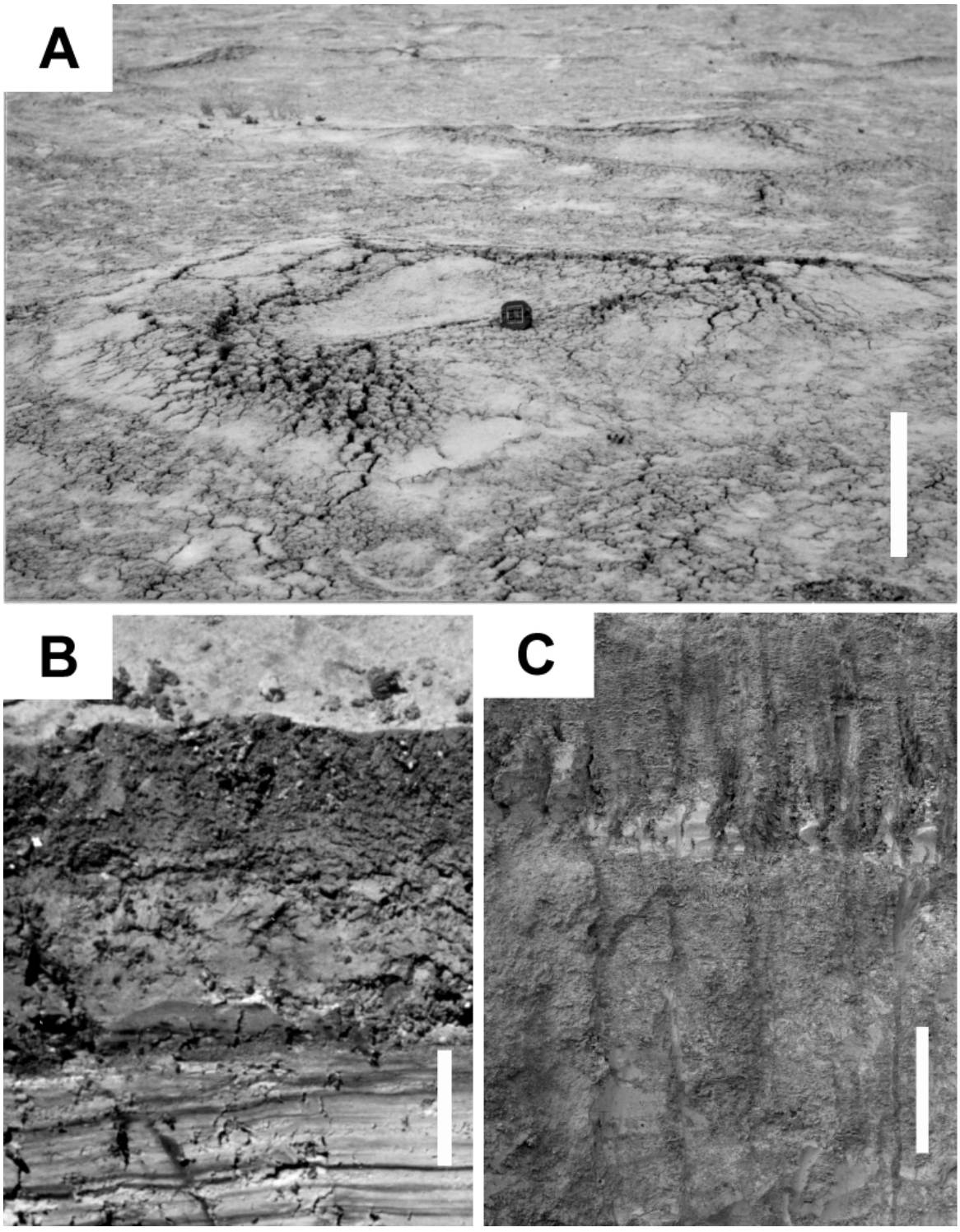

Figure A34. Modern puffy ground efflorescence features. A. Surface of modern saline mudflat at Desert Dry Lake, Nevada, showing puffy ground efflorescence. The surface is loose and powdery because minute sodium carbonate crystals separate rounded mud clumps into polygonal ridges. Scale bar is 30 cm. B. Trench through surface of the Bonneville Salt Flat, Utah, showing peloidal fabric superimposed on Pleistocene lake deposits. Puffy ground efflorescence was produced by halite blown onto the surface from the adjacent salt pan. Sediment was deflated from this surface, contributing to dunes elsewhere on the flat. Scale bar is 10 cm. C. Trench through the surface of a saline mudflat at Desert Dry Lake, Nevada. Lake bed (light gray) separates two thick intervals of peloidal fabric produced by powdery efflorescence. Note the brecciated appearance of the mud layer about a third of the thickness from the top. Scale bar is 30 cm.

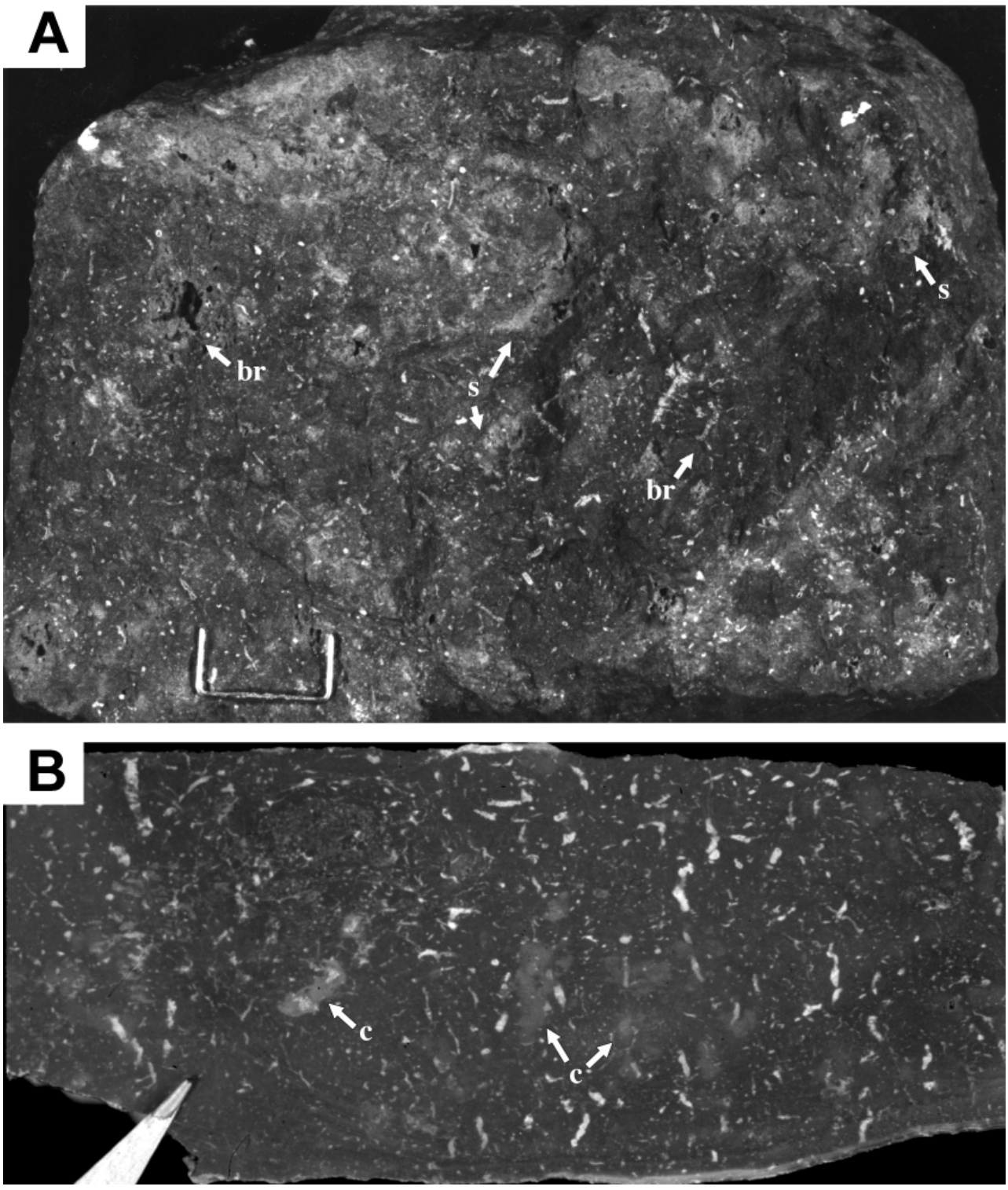

Figure A35. Root-disrupted massive mudstone. A. Outcrop sample of root-disrupted massive mudstone from the lower part of the Passaic Formation (Member F?). Cement-filled root casts (white features) range from 2 mm to less than 0.5 mm in diameter. Some cement has been dissolved, producing open cavities (black). Some of the root casts branch (br). Large root features are filled with sediment (s) producing lighter-colored circular and ovate cross sections. Some of the sediment-filled features may be burrows. Thickness shown is about 10 cm. Locality 22, table A1, figure A5. B. Slabbed outcrop sample of root-disrupted massive mudstone from the Neshanic Member of the Passaic Formation. Root casts (white) are filled with carbonate cement that locally forms diffuse halos around the roots (c), indicating incipient caliche development. Thickness shown is about 4 cm. Locality 23, table A1, figure A4.

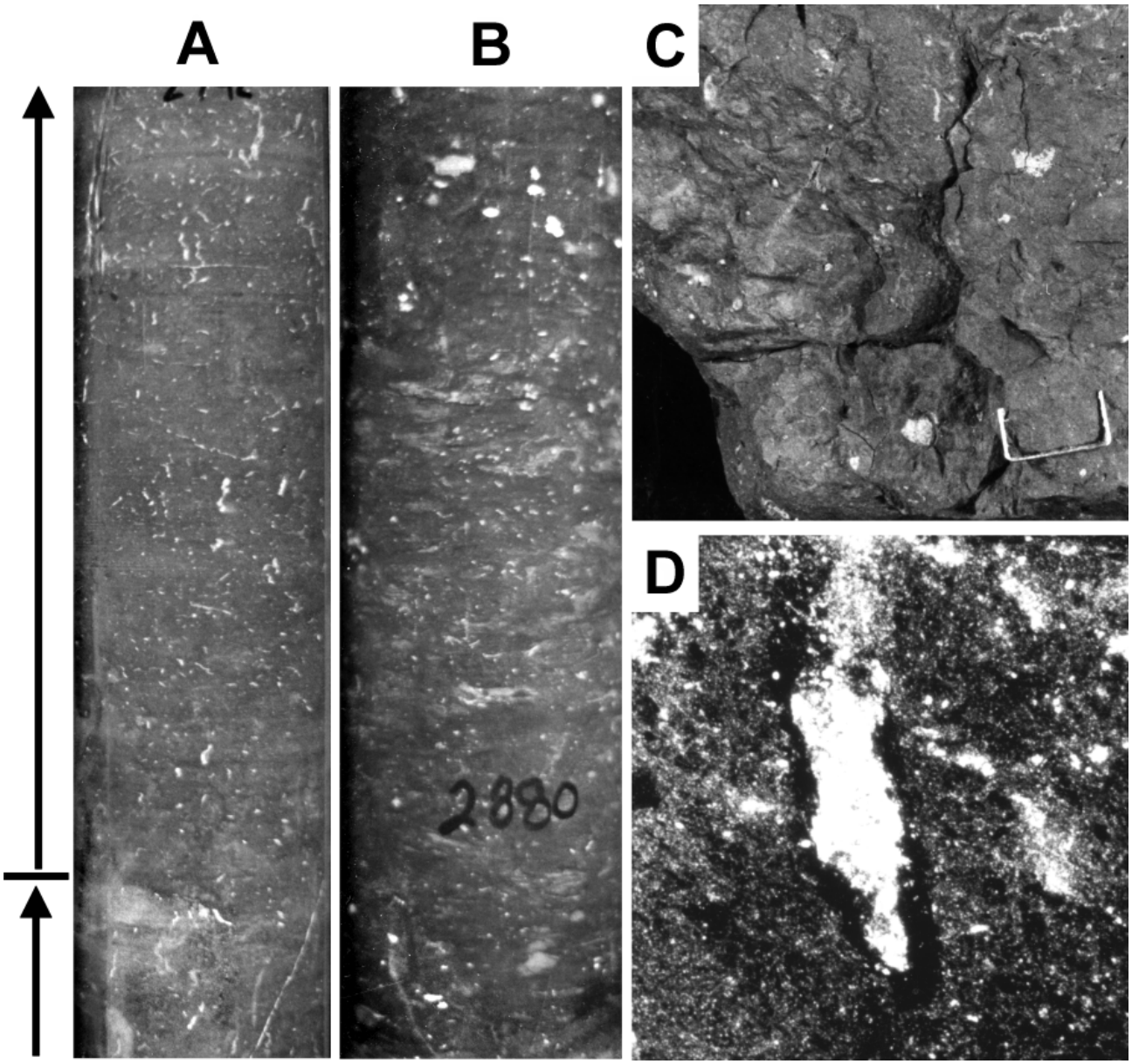

Figure A36. Root-disrupted massive mudstone. A. Sample from Member T-U of the Passaic Formation showing root-disrupted massive mudstone with a succession of upward increasing root-cast diameters (arrows). The largest cement-filled root casts (white) increase in diameter up section, but they are mixed with a variety of tube diameters. The top of the lower root-cast sequence includes carbonate cements around root casts (light gray) interpreted as soil carbonates. Core interval is about 25 cm. Somerset core interval 2912 ft. Locality 5, table A1, figure A3. B. Sample from Member OO of the Passaic Formation of root-disrupted massive mudstone with carbonate nodules. Root casts are cement-filled (white) or sediment-filled (light gray and dark gray circular and ovate cross sections). Some of the dark cross sections are burrows. Carbonate nodules (irregular circular white features) increase in size toward top (a contact with another upward coarsening carbonate nodule sequence is near the base of the sample). Core interval is about 15 cm. Martinsville core interval 2880 ft. Locality 7, table A1, figure A3. C. Outcrop sample of root-disrupted massive mudstone from the lower part of the Passaic Formation (Member F?). Plan view of root-disrupted fabric showing cement-filled tubes (white) and open tube cavities (black) of various diameters. Larger tubes are mostly circles showing their vertical orientation, whereas smaller tubes are also elongate, showing a horizontal component. Large narrow cracks (black linear features) have clay linings and a little sediment filling. Staple is about 7 mm wide. Locality 22, table A1, figure A4. D. Photomicrograph of thin section of root-disrupted massive mudstone in the Perkasie Member of the Passaic Formation. Root casts are filled with silicate cements (white). Clays are oriented parallel to root wall (dark lining). Note smaller root casts (discontinuous white) that project from the larger root cast. Thickness shown is 2 mm. Locality 20, table A1, figure A3.

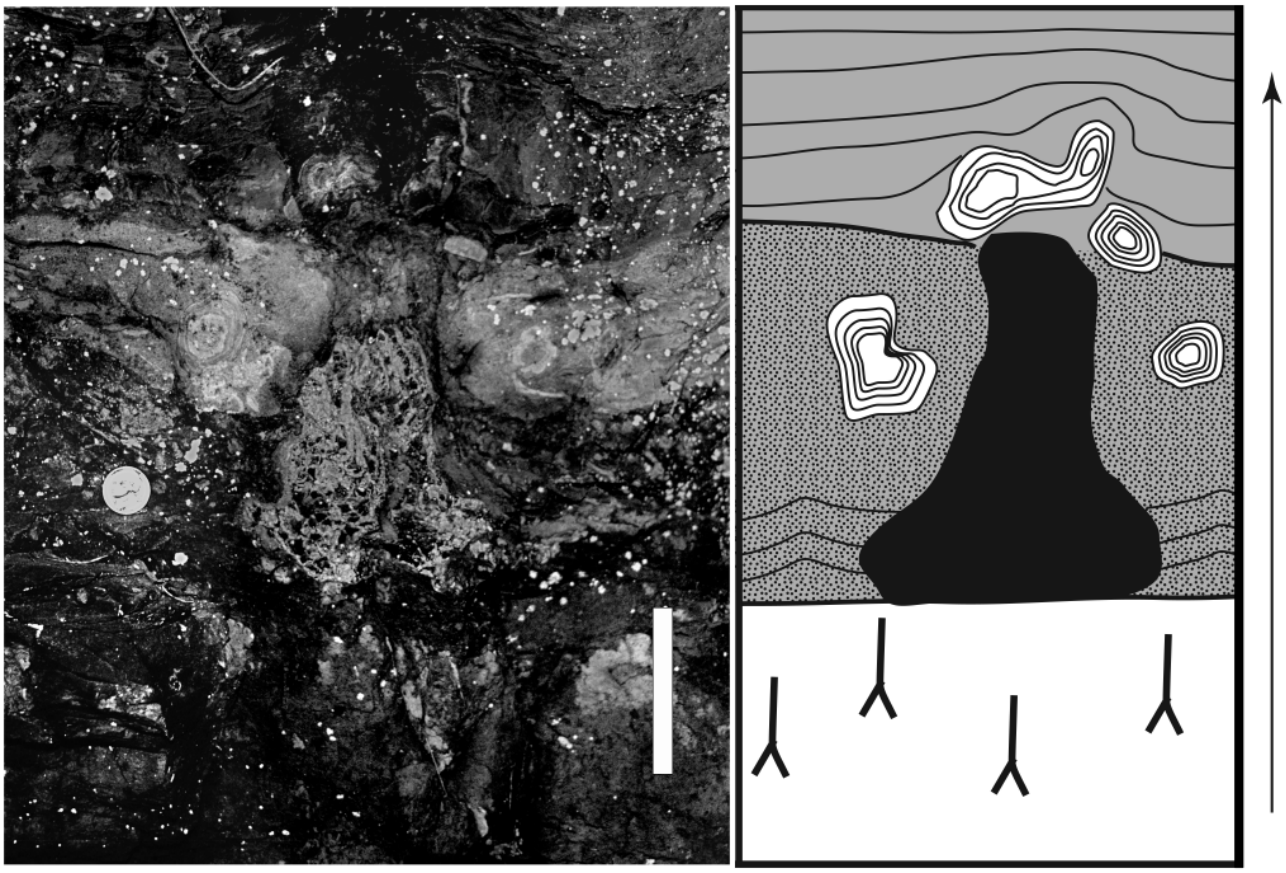

Figure A37. Outcrop of carbonized plant trunk overlying root disrupted mudstone in the Metlars Member of the Passaic Formation. Sketch on right shows distribution of features including root-disrupted mudstone (white), plant trunk (black), wave-rippled oolitic sandstone (stippled), stromatolitic tufa (white banded), and laminated dark gray mudstone (gray). Stromatolitic tufa coats pieces of carbonized wood including the upper part of the trunk. Root casts in the underlying mudstone are all cement-filled. Scale bar is 10 cm. Locality 24, table A1, figure A5.

aggradation, punctuated by soil development. Other than the woody stump in the Passaic Formation, the size and type of plants that formed the root casts are not known.

Burrowed massive mudstone is characterized by many sediment-filled tubes that have a limited number of diameters (fig. A38). They may be straight or sinuous, and may be oriented vertically, horizontally, or randomly, and commonly have less than five different diameters (ranging from 0.5-5 mm). In some cases, the sediment filling the tubes may show arcuate internal lamination (meniscae or spreiten, see Hasiotis, 2002) but most often the fillings consist of one type of sediment or an outer rim of one sediment type and an inner ring of another. Burrowed massive mudstone is commonly transitional from laminated or thin-bedded mudstone by a gradual increase in the density of tube-shaped disruptions. Discontinuous layers or scattered patches of layered sediment are common near the transition. Deep, sinuous, sediment-filled polygonal cracks are typical of burrowed massive mudstone, but are not always present.

Burrowed massive mudstone is interpreted as lacustrine sediment that has been homogenized by the action of burrowing organisms (Smoot and Benson, 1998). Different organisms produce differently shaped burrows and their orientation reflects different purposes such as feeding, shelter, or escape (Hasiotis, 2002). The burrowed massive mudstone has not been examined carefully enough to identify the burrowing organisms or to separate aquatic from terrestrial conditions. Some burrows in the massive mudstone are similar to those in thin-bedded and laminated mudstone, suggesting the organisms lived in a lake, but others have characteristics, particularly meniscate fillings, that Hasiotis (2002) attributes to subaerial insect traces. Deep polygonal cracks observed in some burrowed massive mudstone occurrences are interpreted as evidence of subaerial exposure of water-saturated, lake-floor sediments.

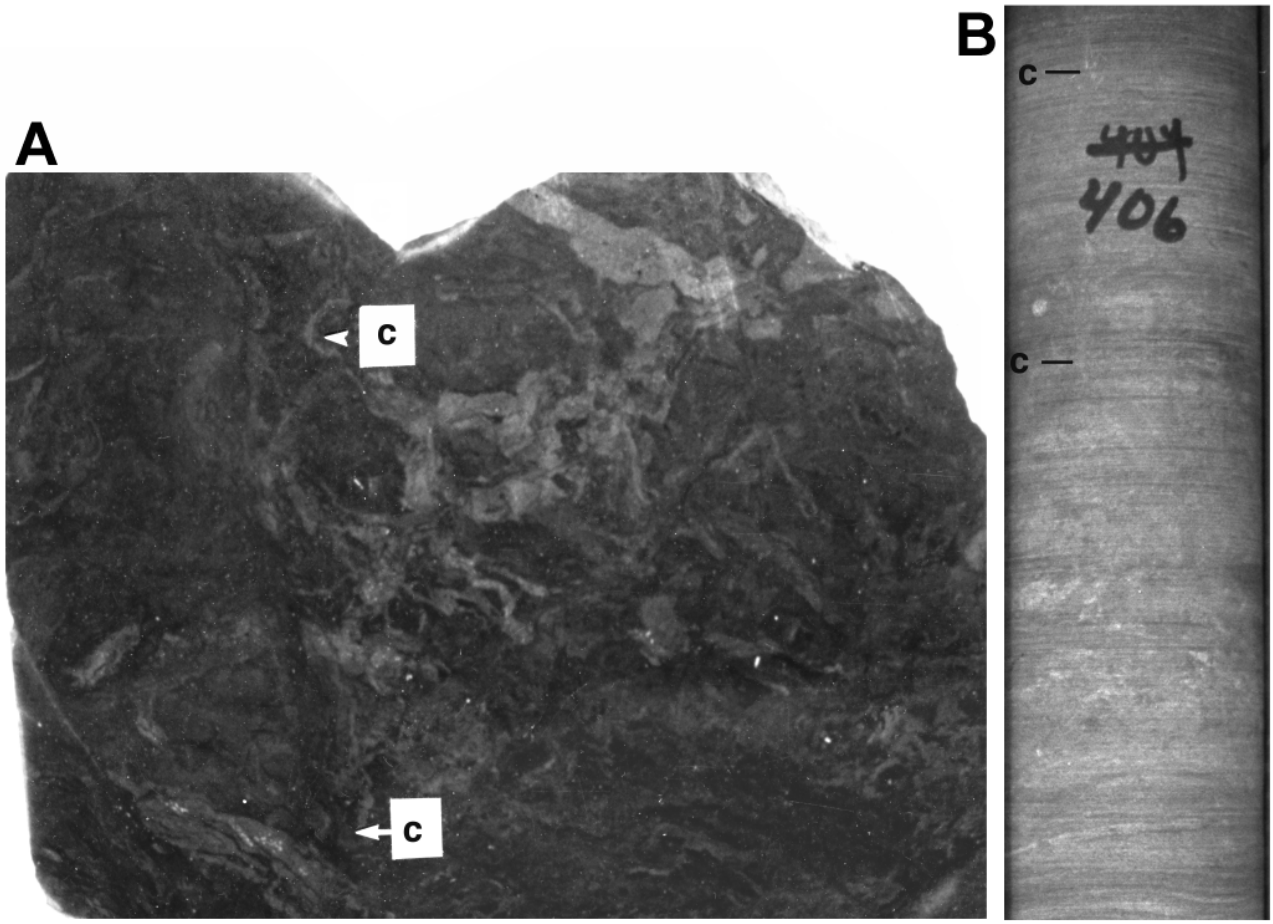

Figure A38. Burrowed massive mudstone. A. Slabbed plan view of an outcrop sample showing burrowed massive mudstone from the Princeton Member of the Lockatong Formation. Sinuous, elongate light gray forms and circular to ovate shapes are interpreted as sediment-filled burrows. A dark, linear, sediment-filled crack is marked by a "c". Light gray linear shape near top of photo is a sediment-filled polygonal crack disrupted by burrows. Sample area shown is about 15 cm wide. Locality 25, table A1, figure A4. B. Sample from the Princeton Member showing burrowed massive mudstone. Faint dark gray ellipses and circles are cross sections of sediment-filled burrows with diameters of about 1 mm, 4 mm, and 9 mm. Narrow, vertical linear shape (marked by "c") is a sediment-filled crack. Thickness shown is about 20 cm. Princeton core interval 406 ft. Locality 1, table A1, figure A3.

Mudstone with saline minerals

Mudstone with saline minerals occurs in many parts of the central basin facies of the Lockatong and Passaic Formations. Saline minerals are indicated by calcite pseudomorphs, silicate and carbonate cement-filled crystal casts, gypsum, and anhydrite. There are two distinct assemblages of evaporite crystal casts. Calcite pseudomorphs and cement-filled crystal casts (fig. A39) are associated with laminated and thin-bedded lake mudstone and are interbedded with, or gradational to, peloidal massive mudstone. Gypsum and anhydrite (fig. A40) exclusively occur in root-disrupted massive mudstone (except for late vein fillings).

Within the organic-rich laminated mudstone, are some laminae of nearly pure calcite or laminae with scattered calcite crystals (fig. A41). The calcite layers include 1) flat laminae with normal- and reverse-grading, 2) irregular laminae with scoured bases, 3) laminae with pinch-and-swell structures, and 4) laminae with dispersed crystals. The calcite crystals have equant hexagonal shapes with uneven sides and uneven interfacial angles (fig. A39). These shapes are inconsistent with calcite and therefore the crystals are interpreted as calcite replacement of a saline mineral. Many of the crystals in the laminated mudstone (particularly in irregular laminae, pinch-and-swell laminae, and dispersed crystals) are subhedral or rounded, suggesting dissolution or abrasion during deposition (fig. A42). Some of the laminated beds associated with laminae or dispersed crystals of calcite pseudomorphs have irregular deformation features, including angular load casts and contorted layers (fig.

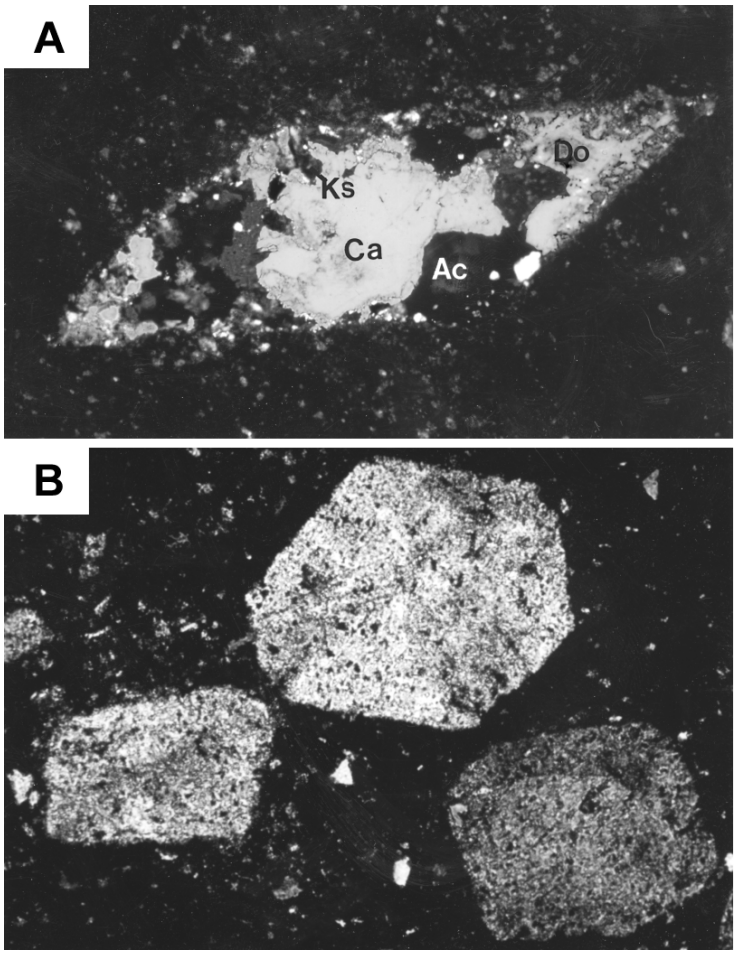

Figure A39. Evaporite crystal pseudomorphs and casts. A. Photomicrograph of thin section of mudstone with a crystal cast filled with silicate and carbonate cements. The cements include analcime (Ac), potassium feldspar (Ks), dolomite (Do), and calcite (Ca). The dolomite and calcite appear to postdate corrosion of analcime and potassium feldspar cements. A rim of small dolomite crystals may represent a cement that predates analcime. Outcrop sample from the Ewing Creek (?) Member of the Lockatong Formation. Field of view is about 2 mm wide. Locality 20, table A1, figure A3. B. Photomicrograph of thin section of laminated mudstone with calcite crystal pseudomorphs (light). Note hexagonal shapes and more tetragonal cross section. These shapes suggest an equant monoclinic mineral that is now calcite. Sample from the Nursery Member of the Lockatong Formation. Field of view is about 0.5 mm. Nursery core interval 2439 ft. Locality 2, table A1, figure A4.

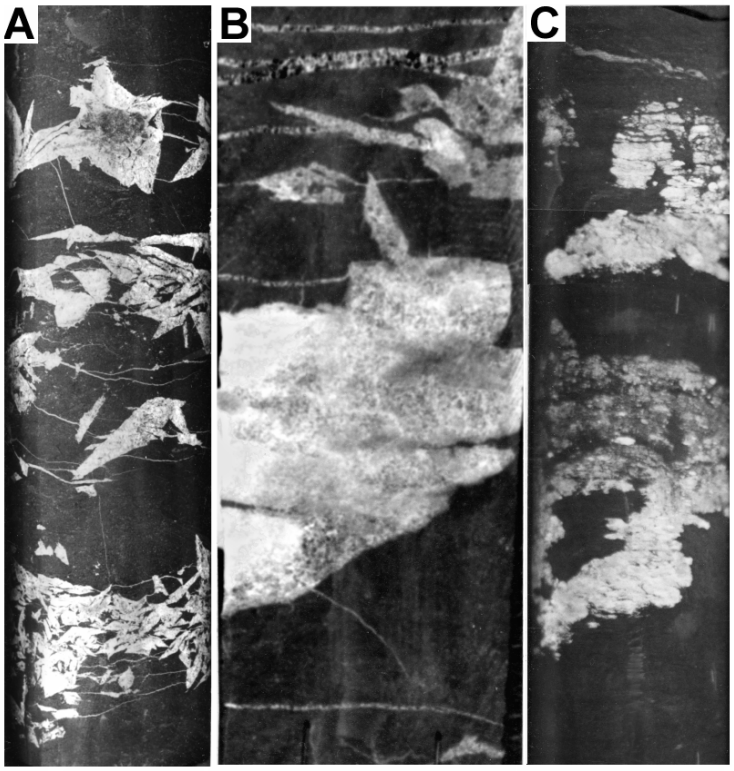

Figure A40. Gypsum crystals and anhydrite replacing gypsum crystals in root-disrupted massive mudstone. A. Sample from Member S of the Passaic Formation showing euhedral gypsum crystals (white) with an upward increase in size. Thickness shown is about 20 cm. Rutgers core interval 1222 ft. Locality 5, table A1, figure A3. B. Sample from Member EE of the Passaic Formation showing euhedral and subhedral gypsum crystal shapes composed of gypsum and anhydrite. Horizontal veins are filled with fibrous gypsum. Thickness shown is 10 cm. Somerset core interval 981 ft. Locality 5, table A1, figure A3. C. Sample from Member OO of the Passaic Formation showing anhedral masses of gypsum. The elongated patterns appear to follow root casts. Thickness shown is about 20 cm. Martinsville core interval 2913 feet. Locality 7, table A1, figure A3.

Figure A41. Laminated mudstone with calcite pseudomorphs after evaporites. A. Sample from the Prahls Island Member of the Lockatong Formation showing laminated mudstone. Calcite layers (white) show erosion, loading, and pinch-and-swell layering. Note beds with a few scattered crystals and irregular blebs of crystals that represent partial dissolution of crystals. Thickness shown is about 25 cm. Nursery core interval above 1106 ft. Locality 2, table A1, figure A4. B. Sample from the upper part of the Nursery Member of the Lockatong Formation of laminated mudstone. Calcite beds include flat beds, pinch-and-swell beds, and layers with scattered crystals. Note angular dark streaks in uppermost white beds reflecting larger crystal shapes filled with calcite pseudomorphs. Smaller versions of these features are in other beds. Vertical white features are cement-filled fractures. Thickness shown is about 10 cm. Nursery core interval 2398 ft. Locality 2, table A1, figure A4.

A43).

Hexagonal calcite crystal forms in the Newark basin were attributed to aragonite by El Tabakh and Schreiber (1998). However, this is unlikely because the common aragonite habit is hexagonal in one cross section and rod-like in the other. More likely, the hexagonal crystal shapes are pseudomorphs after an equant, monoclinic crystal (Smoot, 2006). Flat laminae of small, predominantly euhedral hexagonal crystals suggest that they were precipitated at the surface of a lake and settled to the lake floor as cumulus crystals (fig. A44A, and Smoot and Lowenstein, 1991, p. 204-205). Because supersaturation and crystal growth occurs at the air-water interface, crystals settling in the water column may be partially or completely dissolved before they reach the bottom. Reverse grading in flat crystal laminae may indicate 1) changes in the rate of crystal growth at the water surface, 2) changes in the amount of dissolution as crystals settle through the water column, or 3) crystal overgrowth on the lake floor after settling. Irregularly graded laminae and pinch-and-swell laminae of subhedral to anhedral calcite crystals indicate that they were subjected to mechanical reworking by turbidity currents or waves. The evaporite crystals behaved like sand grains in these types of laminae. In contrast, hexagonal crystals dispersed in mud may represent 1) intrasediment growth of crystals at the lake floor, 2) bioturbation of mixed sediment and evaporite crystals, or 3) partial dissolution of cumulus crystals after they are buried. The angular load casts and contorted layers commonly associated with intrasediment hexagonal crystals are consistent with deformation from crystal growth and collapse following dissolution.

In the central basin facies of the Lockatong and Passaic Formations, crystal casts filled with cements of silicate and carbonate minerals are commonly associated with laminated mudstones that have hexagonal calcite crystals and peloidal massive mudstone. Unlike the calcite crystals, the cement-filled

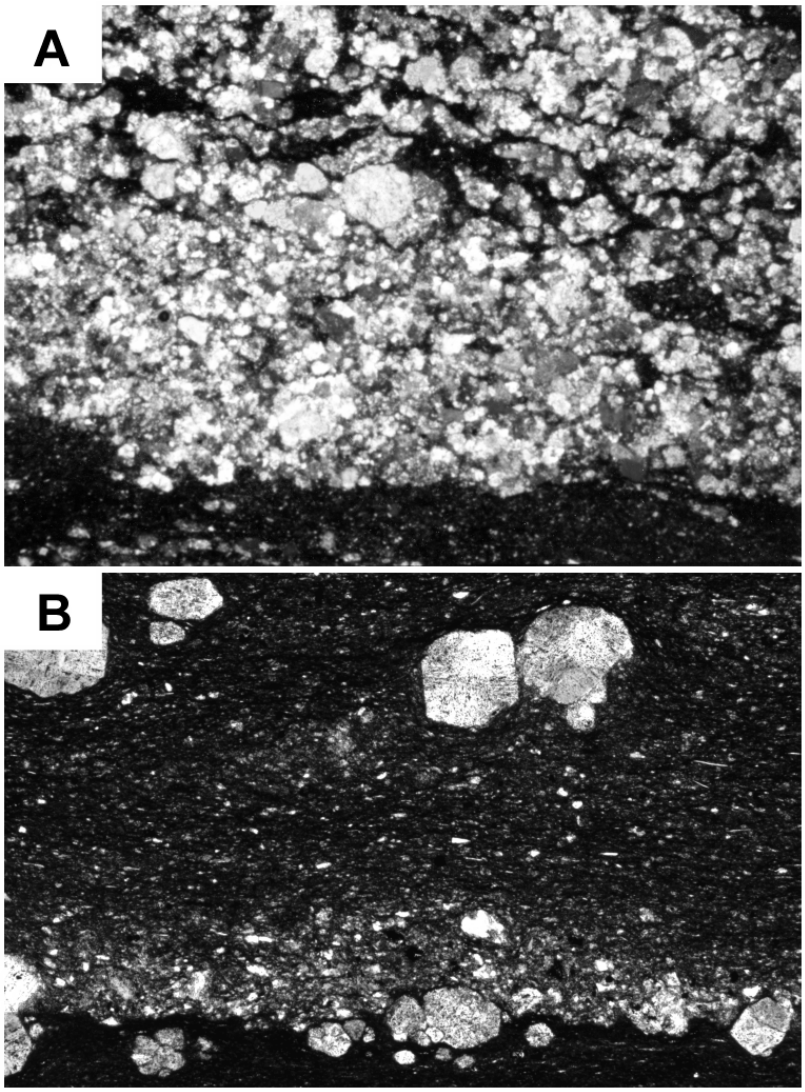

Figure A42. Photomicrographs of thin sections of laminated mudstone with calcite pseudomorphs after evaporites in the Nursery Member of the Lockatong Formation. A. Crystal layer of pinch-and-swell lamina overlain by muddy crystal bed. Note rounded edges of crystals (white and light gray) in pinch-and-swell layer, although some retain crystal angles. Crystals in the overlying layer show irregular jagged shapes suggesting partial dissolution after deposition. Thickness shown is about 0.5 mm. B. Large euhedral crystal shapes in mudstone are partially exhumed by a graded bed with anhedral crystal shapes. This illustrates the syndepositional character of the intrasediment crystals and the effects of reworking of crystals. Thickness shown is about 2 mm. Locality 15, table A1, figure A4.

crystal casts have a variety of crystal shapes and mudstone associations. Cement-filled crystals casts within or adjacent to thin-bedded mudstone include 1) bladed crystals with the long axes roughly perpendicular to the bedding plane and projecting from a common bedding plane, and 2) randomly oriented large euhedral crystals and radial masses of crystals that are independent of bedding (fig. A45). The cement-filled crystal casts oriented perpendicular to bedding may consist of one to three crystals extending upward from a point (fig. A45A and B), or they may consist of a mass of crystals covering tens of centimeters of bedding-plane surface and projecting upward 10's of centimeters with radial dispersion of long axes and progressively larger crystals facing upward from the initial bedding plane (fig. A45B). Randomly oriented crystals concentrated directly below laminated mudstone with hexagonal calcite crystals, or thin-bedded mudstone with perpendicular crystal casts, commonly display a 10-15 cm upward increase of crystal size toward the contact. The most common cement-filled crystal casts are randomly distributed crystals producing successions of upward-decreasing crystal size (fig. A46). These successions of randomly distributed crystal casts are typically within a massive mudstone that chiefly appears to be brecciated massive mudstone or peloidal massive mudstone. The thickness of these successions ranges from about 15 to 30 cm. A typical vertical succession consists of large, randomly oriented bladed or blocky crystals casts overlain by progressively smaller euhedral crystal casts, followed by smaller anhedral crystal casts that are commonly concentrated in cracks (fig. A47) and finally, peloidal massive mudstone with irregular cement-filled blebs. A variation lacks any euhedral crystals, but consists of anhedral crystal casts grading upward to peloidal massive mudstone with cement-filled blebs. Commonly, several of the cement-filled crystal cast successions of decreasing crystal size directly overlie each other (fig. A48). Here, each younger succession

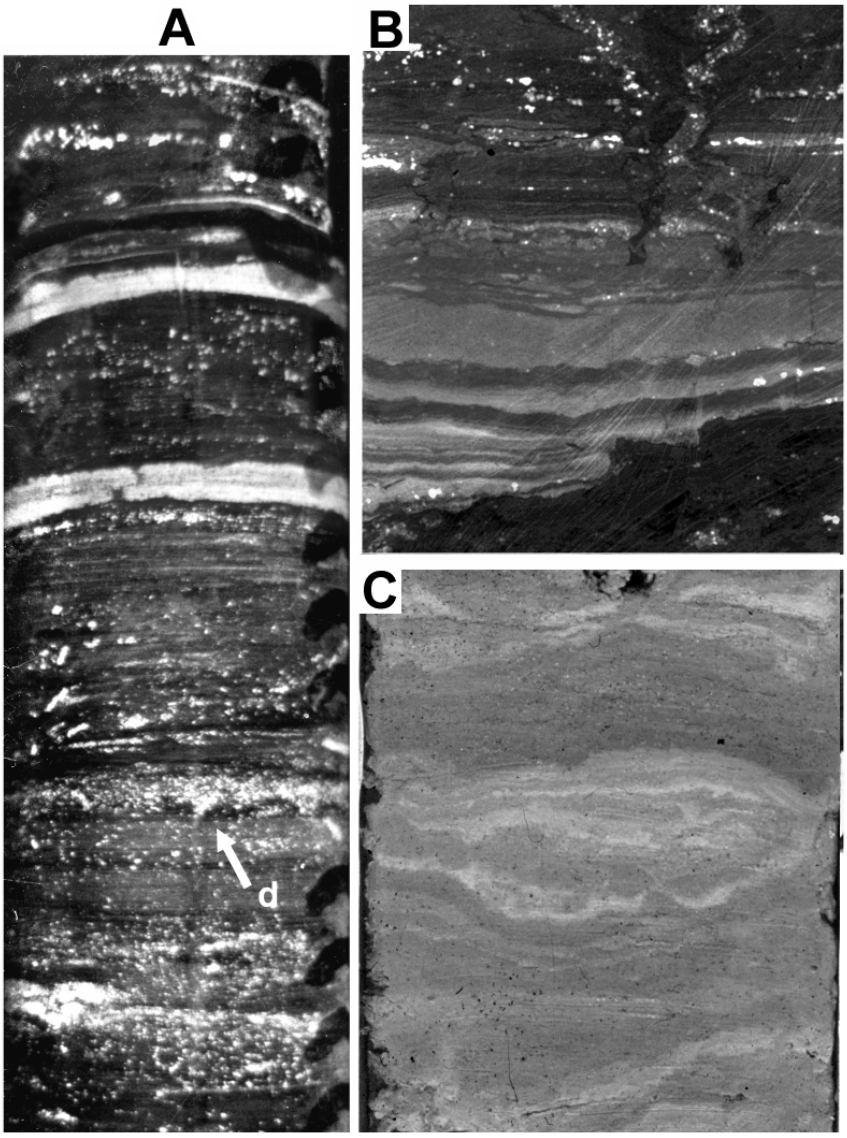

Figure A43. Laminated mudstone with calcite pseudomorphs after evaporites and with dissolution features, compared to a modern example. A. Sample from the Tohickon Member of the Lockatong Formation showing laminated mudstone. Flat continuous beds of calcite (white layers) are cumulus crystal layers. Beds with dispersed crystals include angular projections (d) suggesting some dissolution Thickness shown is about 20 cm. Nursery core interval 1497 ft. Locality 2, table A1, figure A4. B. Sample from the EF Member of the Passaic Formation showing laminated mudstone. Graded silty beds (light gray) overlie angular step-like surface in dark mudstone with anhedral masses of calcite. Small angular projections may also be seen at the base of the graded layers. Vertical wavy features at the top of sample are sediment-filled cracks projecting downward from a horizon about 1 m higher. Thickness shown is about 3 cm. Titusville core interval 1969 feet. Locality 3, table A1, figure A4. C. Cross section of core from Great Salt Lake, Utah, in late Holocene to Recent sediment. Deformed layering is due to dissolution of intrasediment evaporites after burial. Note angular projections and uneven thickness. Thickness shown is about 3 cm. Photo courtesy of Ron Spencer, University of Calgary.

contains smaller euhedral crystals and more anhedral crystals, or progressively fewer anhedral crystals grading to peloidal mudstone.

Cement-filled crystal casts oriented perpendicular to bedding in thin-bedded mudstone are interpreted as evaporites that grew in a saline lake at the sediment-water interface (fig. A44A). In modern saline lakes, this crystal habit occurs where lake water is shallow enough to allow evaporative concentration of the brine at the base of the water column. The larger cement-filled crystal cast masses resemble crystal mounds formed in modern saline lakes at the shoreline (Warren, 1982). Large, euhedral, cement-filled crystal casts that are not oriented to bedding may also occur in association with saline lakes. Large crystals and radial crystal masses that are restricted to polygonal cracks formed where lake brines seeped laterally into adjacent mudflats and preferentially evaporated within open cracks. This resembles modern occurrences of evaporites precipitated where saline lake brines seep into sediment. Near the lake margin, the brines are most concentrated at conduits to open air, such as desiccation cracks; resulting in preferential nucleation along the margins (fig. A44B). Saline lake brines may also sink into the underlying sediment, causing precipitation of euhedral crystals by mixing with pore waters of different chemistry or by change in temperature (fig. A44A). The larger crystals grow closer to the source of sinking solutes. Cement-filled crystal casts consisting of vertical successions of progressively smaller crystals are evaporites formed by the evaporation of groundwater in a saline mudflat setting (fig. A44B). In modern saline mudflats, the brine-saturated phreatic zone promotes slow precipitation of large euhedral crystals and the intermittently wet and dry vadose zone accumulates smaller crystals that are commonly modified by dissolution or dehydration into anhedral forms. Complete evaporation of groundwater at the

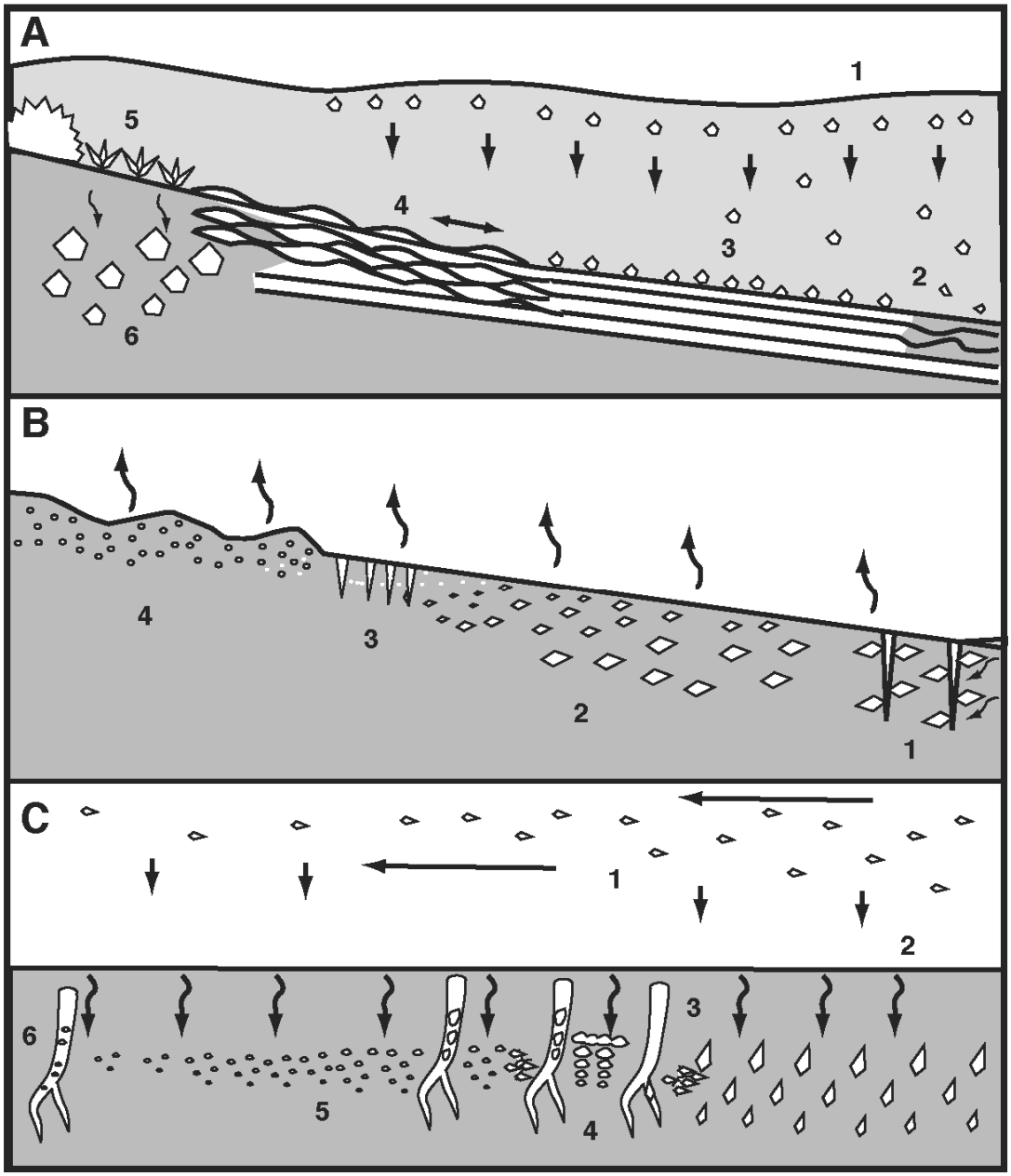

Figure A44. Schematic depiction of depositional environments of evaporites in the Newark basin. A. Saline lake environment. 1) Evaporite crystals precipitate at the air-water interface. 2) Crystals dissolve or partially dissolve in the water column or in the sediment after burial. 3) Crystals produce cumulate beds on the lake floor. 4) Crystals are mechanically reworked by waves or turbidites. 5) Supersaturation at the sediment interface produces bottom crystal growth. 6) Brines sink into the sediment forming intrasediment crystals. B. Saline mudflat environment. 1) Brine-saturated sediment is preferentially evaporated along conduits, such as desiccation cracks, acting as nuclei for precipitating crystals in the surrounding sediment. 2) A near-surface groundwater table is evaporatively wicked into the vadose zone producing a vertical zonation of larger crystals formed slowly at depth and smaller crystals closer to the surface. 3) Vadose- zone crystal formation is restricted to areas of higher porosity such as silty beds and desiccation cracks. Crystals may be partially dissolved by rainfall, making them subhedral to anhedral. 4) Efflorescent crusts form where groundwater completely evaporates to dryness. C. Saline soil environment. 1) The source of solutes is windblown dust. 2) Dust is flushed downward by rainfall, producing the characteristic upward-coarsening succession. 3) Near-surface cementation of soil may produce fractures that form from differential settling or heating-cooling contraction. 4) Conduits such as open cracks or root casts may act as preferred sites for crystallization. Rainfall may cause crystals to partially dissolve or recrystallize into amorphous masses. 5) Lowered influx of windblown solutes produces finer crystalline sequences and increases the likelihood of re-solution by rainfall. 6) Very low solute influx results in crystallization only in conduits.

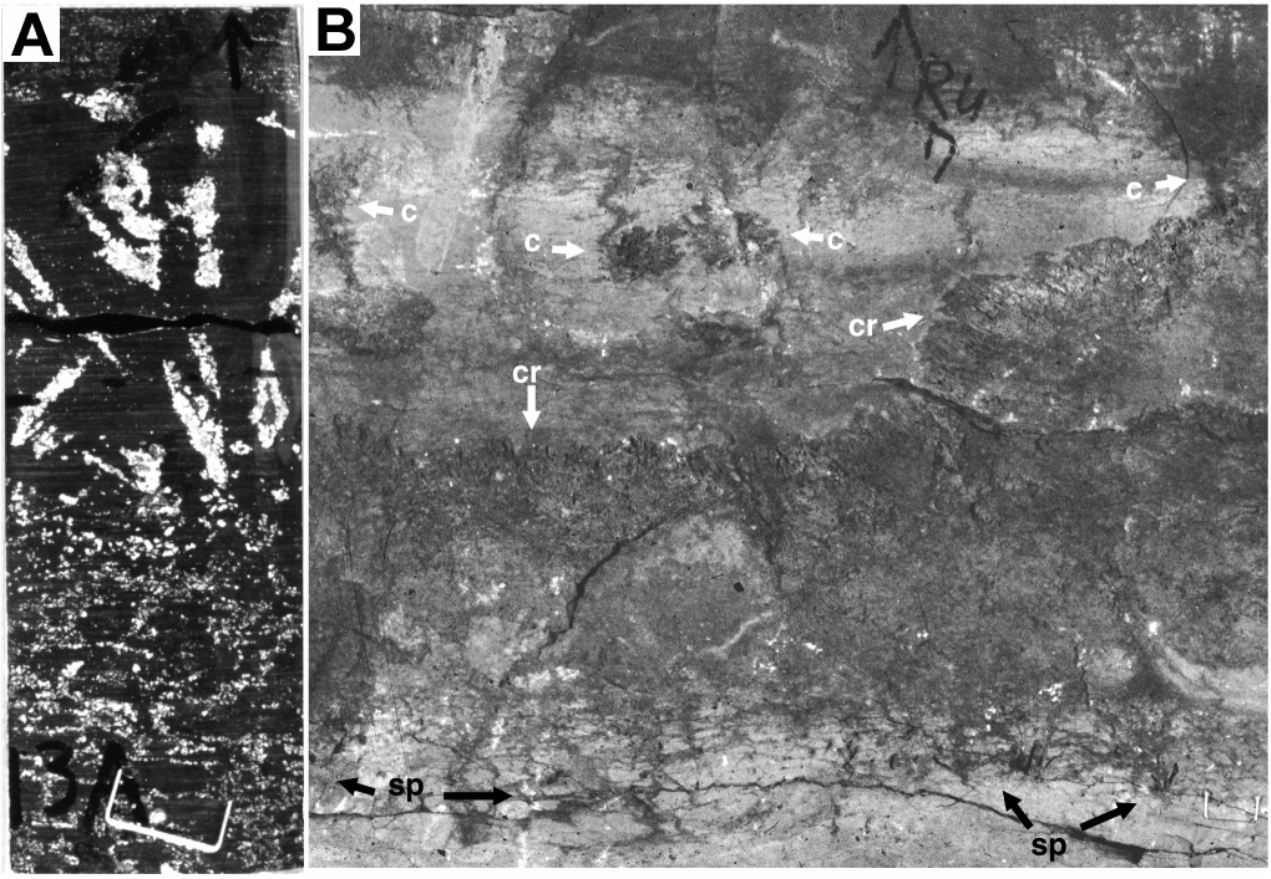

Figure A45. Crystal casts filled with silicate and carbonate cements in thin-bedded mudstone. A. Sample from the Ewing Creek Member of the Lockatong Formation showing vertically oriented crystal splays. The crystal splays sharply overlie mudstone with small subhedral to anhedral crystals at the top of an upward-fining crystal sequence. The splays represent a saline lake transgression over a saline mudflat deposit. Thickness shown is about 6 cm. Princeton core interval 302 ft. Locality 2, table A1, figure A4. B. Outcrop of evaporite crystal habits in the Perkasie Member of the Passaic Formation. The cements filling the crystal casts are dissolved leaving empty (dark) open molds. Base of sample is a thin-bedded gray mudstone with crystal splays (sp) and cracks (dark vertical features at base). The sequence is capped by a thick crust consisting of vertically-oriented crystals (top of crust is shown by arrows (cr). The crust is overlain by thin-bedded gray mudstone with desiccation cracks (c) that have large radial crystal masses growing out of the crack filling into the surrounding mud. Thickness shown is about 35 cm. Locality 20, table A1, figure A3.

sediment-air interface produces efflorescent salt crusts. Another pertinent characteristic of modern saline mudflats is that margins which are well above the groundwater table also contain evaporite minerals and efflorescent crusts. Windblown minerals eroded from the central saline mudflat surface are chemically reworked at the surface by rainfall (fig. A44B). Rain dissolves the minerals, producing brine that is subsequently evaporated, causing preferred crystal growth in open conduits, such as cracks, and the development of efflorescent salt crusts. The vertical successions of cement-filled crystal casts in the Newark basin are interpreted as preserved profiles of these different groundwater settings in a saline mudflat. The vertical repetition of crystal successions, however, has not been observed in modern saline mudflats. The simplest explanation is that the groundwater evaporation profiles were punctuated by episodes of sediment accumulation. Aggradation caused the surface of the subsequent saline-mudflat succession to rise above the regional groundwater table, so that each subsequent succession has progressively more vadose and fewer phreatic components.

The cement-filled crystal casts in the Lockatong and Passaic Formations were initially identified as glauberite ($CaSO_4 \cdot Na_2SO_4$) by Wherry (1916). This has been generally accepted by most subsequent researchers (for example, Schaller; 1932, Van Houten, 1965; El Tabakh, 1994; El Tabakh and Schreiber, 1994; El Tabakh and others, 1997), but some crystals of different shape have been called gypsum ($CaSO_4 \cdot 2H_2O$) and thenardite (Na_2SO_4) (El Tabakh, 1994; El Tabakh and Schreiber, 1994; El Tabakh and others, 1997). Smoot (2006) suggested that the shapes of

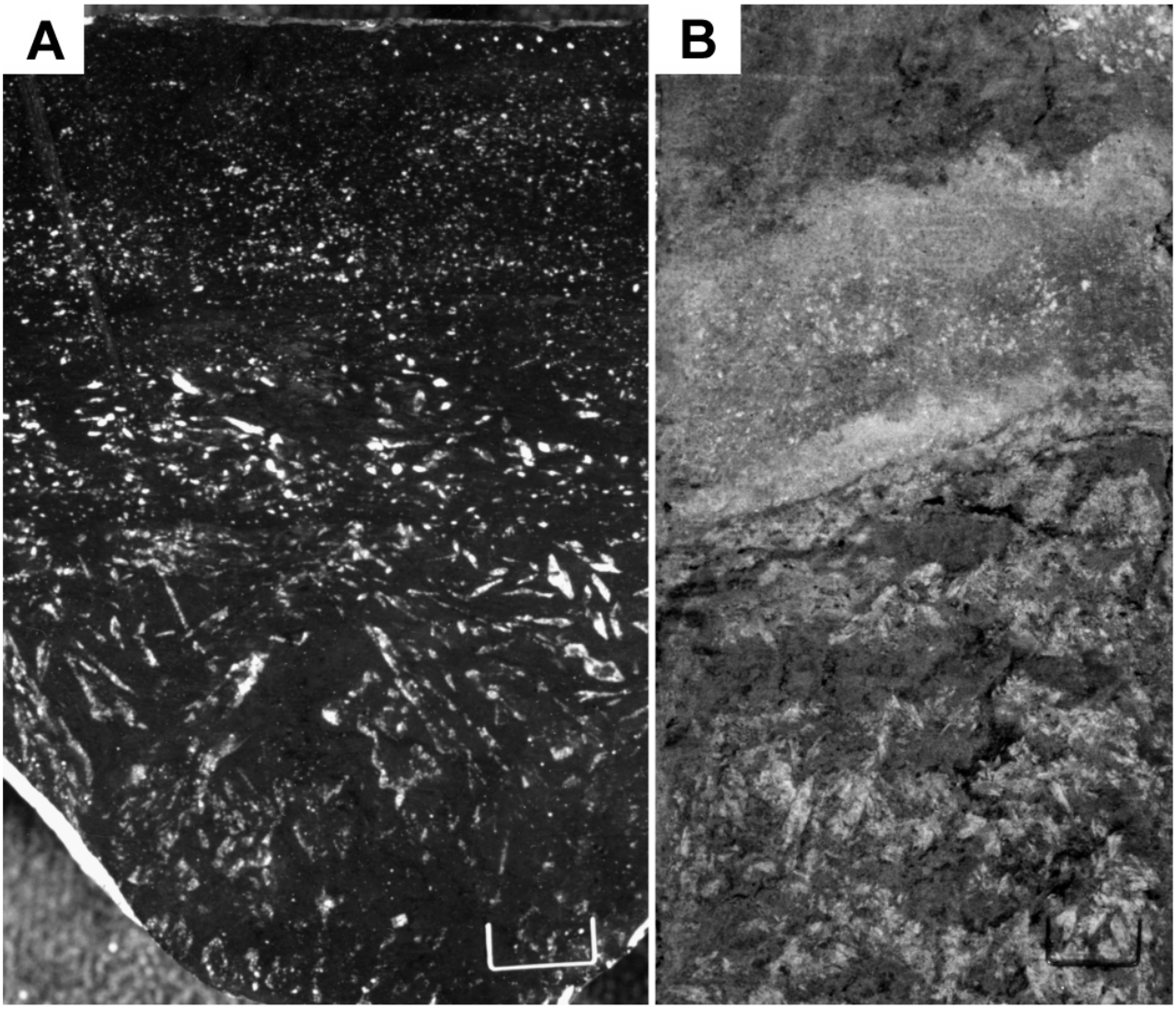

Figure A46. Comparison of mudstone containing upward-fining crystal casts with a core from a modern saline mudflat. A. Outcrop sample of mudstone from the Ewing Creek Member of the Lockatong Formation showing upward-fining crystal sequence. Large, bladed crystals at base (white) have sediment-filled cores. Crystals with vertical orientation are most visible, but others have nearly horizontal long axes (showing as smaller equant shapes in this cross section). Uppermost crystals are anhedral and scattered in a peloidal mudstone. Thickness shown is about 7 cm. Locality 21, table A1, figure A4. B. Core sample from the modern saline mudflat in Death Valley, California. Lower euhedral crystals are in a brine-saturated mud, whereas upper anhedral crystals are in the vadose zone in mud with fabrics produced by efflorescent salt crusts. Note the transition to smaller euhedral crystals below the light band. Thickness shown is about 7 cm.

cement-filled crystal casts are not diagnostic of mineralogy. He argued that the initial mineralogy may have been sodium carbonates, based on four lines of reasoning: 1) the peloidal massive mudstone, interpreted as a product of powdery efflorescent crusts, is more characteristic of an alkaline chemistry than a sulfate-chloride chemistry, 2) the shapes of cement-filled crystals are more similar to natural occurrences of sodium carbonate minerals than to sulfate minerals, 3) the hexagonal calcite crystals are more easily explained as a replacement of a former carbonate mineral having an equant, hexagonal crystal habit (such as pirssonite ($Na_2Ca(CO_3)_2 \cdot 2H_2O$)), and 4) the cements filling the evaporite casts, which include analcime, albite, potassium feldspar, dolomite, and calcite (Simonson and others, Chapter B this volume), are more soluble in highly alkaline brines. Alkaline brines make silica more soluble and accounts for the mobility of solutes to produce that mineral assemblage.

In the Passaic Formation, evaporite crystals and anhedral crystal masses that now consist of gypsum and/or anhydrite occur as 30-50-cm-thick,

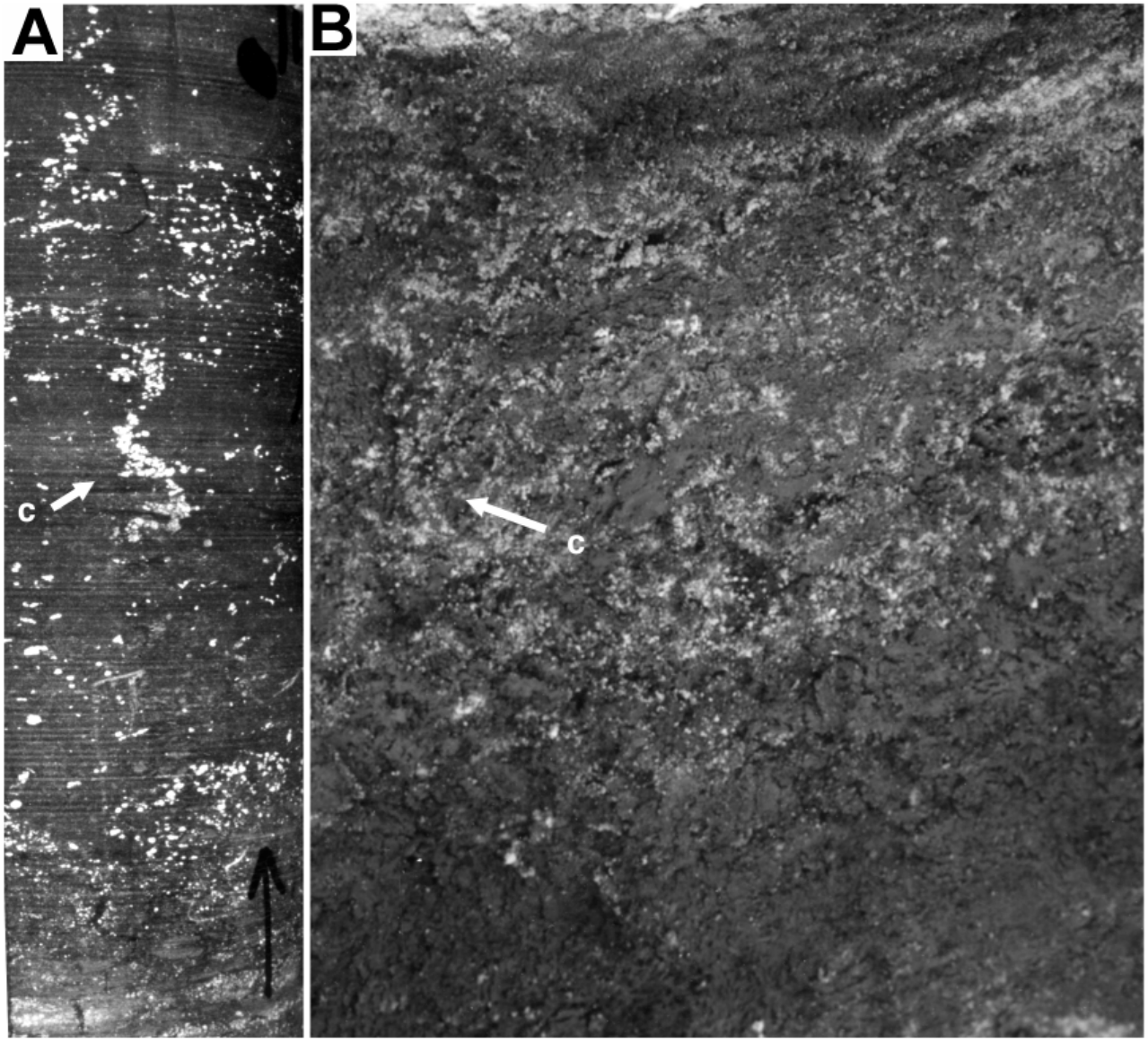

Figure A47. Comparison of mudstone containing anhedral pseudomorphs after evaporites with a trench from a modern saline mudflat. A. Sample from the Tumble Falls Member of the Lockatong Formation showing anhedral pseudomorphs after evaporite minerals. Note concentration of crystals in polygonal crack (c) and concentrations into separate layers. Thickness shown is about 20 cm. Nursery core interval 511 ft. Locality 2, table A1, figure A4. B. Trench in the vadose zone of the saline mudflat in Saline Valley, California. Anhedral crystal masses are concentrated in beds and along desiccation cracks (c). Small euhedral crystals in the lower part of the photo are lighter gray spots. Thickness shown is about 25 cm.

upward-coarsening successions in root-disrupted massive mudstone (fig. A49). A complete succession consists of small euhedral crystals grading upward to large euhedral crystals, or small anhedral crystal masses grading upward to a large mass of anhedral crystals. Some of these crystals appear to be randomly distributed (fig. A40A and B), whereas others are vertically aligned along cracks or tubes that range from 0.5 cm to 5 cm in diameter (fig. A40C). In an upward-coarsening succession of gypsum, irregular fractures or netlike masses of fractures filled with crystals are common (fig. A49C).

The upward-coarsening successions of gypsum and anhydrite in the Passaic Formation have not been recognized as a separate variety of evaporite occurrence by most researchers, and they have been attributed previously to deposition in playa mudflats (El Tabakh, 1994; El Tabakh and Schreiber, 1994; El Tabakh and others, 1997). The crystal styles and upward-coarsening successions, however, closely resemble modern gypsum soil occurrences (Smoot and Lowenstein, 1991) (fig. A50) where gypsum dust is blown onto the surface, and

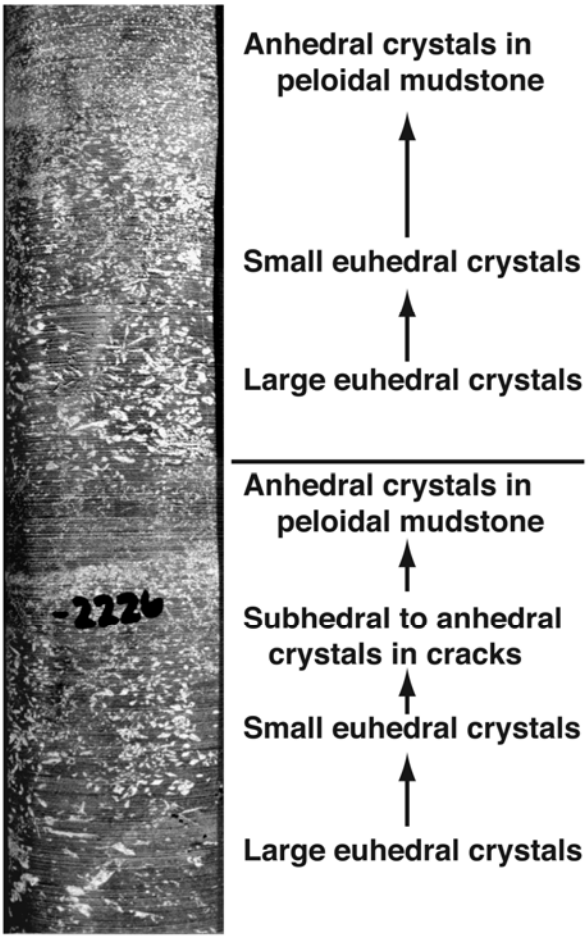

Figure A48. Sample from the Perkasie Member of the Passaic Formation showing upward-fining crystal sequences in mudstone. Each crystal sequence ends with peloidal mudstone containing anhedral crystal casts. Thickness shown is about 30 cm. Rutgers core interval 2226 ft. Locality 4, table A1, figure A3.

then redistributed downward by rainfall (fig. A44C). Rainwater dissolves windblown gypsum at the surface, and then percolates downward into the soil where subsequent evaporation forms new crystals. The largest crystals form at depths most frequently reached by percolating rainwater, with fewer solutes and smaller crystals forming progressively deeper below the surface. Netlike masses of gypsum-filled fractures, such as those in the Passaic Formation, are similar to those in modern gypsum soils resulting from partial cementation of the sediment by gypsum and the expansion and contraction of clays during wetting and drying. Within the Passaic Formation, the upward-coarsening successions of euhedral crystals versus anhedral crystals consisting of gypsum and/or anhydrite probably indicate the difference between slower crystal growth in relatively wet soil versus more rapid crystal growth or crystal dehydration in relatively dry soil.

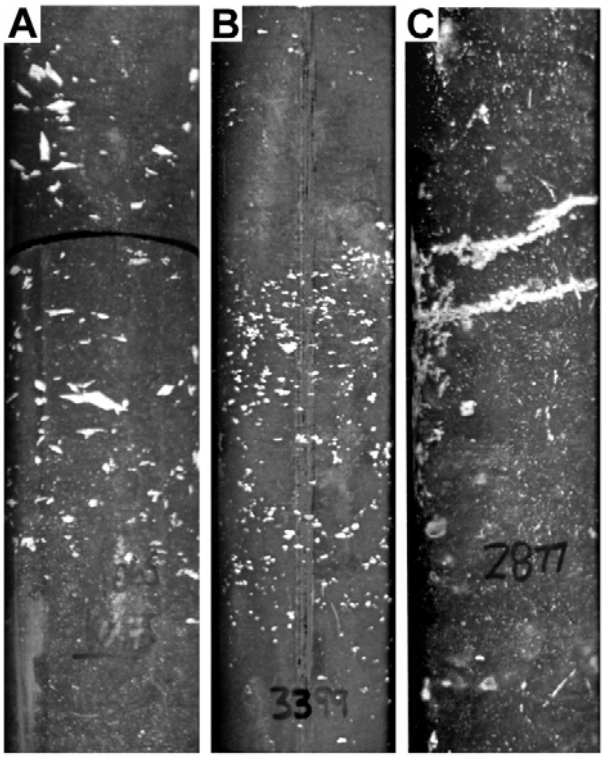

Figure A49. Root-disrupted massive mudstone with syndepositional gypsum. A. Sample from Member DD of the Passaic Formation showing root-disrupted massive mudstone with upward-coarsening euhedral gypsum crystals. Thickness shown is about 20 cm. Somerset core interval 1065 ft. Locality 5, table A1, figure A3. B. Sample from the Member NN of the Passaic Formation showing root-disrupted massive mudstone with upward-coarsening anhedral gypsum crystals. The start of another sequence is at the top of the sample shown. Thickness shown is about 20 cm. Martinsville core interval 3399 ft. Locality 7, table A1, figure A3. C. Sample from Member T-U of the Passaic Formation showing root-disrupted massive mudstone with syndepositional gypsum veins. Gypsum also occurs as anhedral masses and fillings of some roots. Thickness shown is about 20 cm. Somerset core interval 2877 ft. Locality 5, table A1, figure A3.

Lockatong and Passaic Formation – basin margin facies

The basin margin facies of the Lockatong and Passaic Formations are dominated by sandstone and conglomerate that intertongue with the central basin facies. Their thickness is roughly equivalent to that of central basin facies (3000-5000 m) although there is pronounced thinning towards the northeast and southwest ends of the basin, particularly in truncated exposures of the Hammer Creek Formation in the Narrow Neck (fig. A1) where thickness is less than 2000m; also in some localities along the northwestern

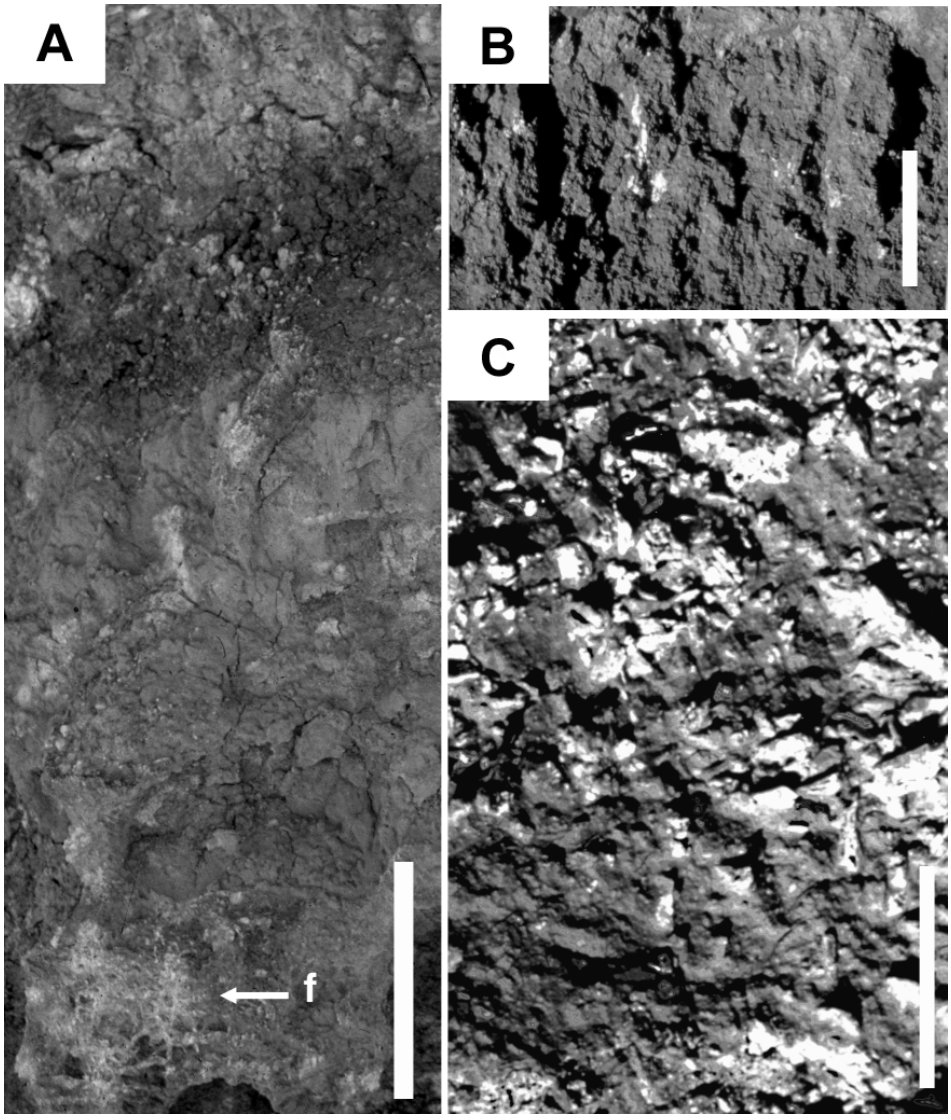

Figure A50. Modern saline soils with gypsum.
A. Trench exposure of saline soil on an alluvial fan surface near Lake Frome, Australia. Subhedral to anhedral crystals (white blebs) form an upward-coarsening sequence in the upper soil; crystals (elongate white features) are preferentially concentrated in root casts near the middle; and fibrous gypsum fills netlike fractures (f) at the base. Scale bar is 30 cm.
B. Trench exposure in interdune flat along the margin of Lake Eyre, Australia. Anhedral gypsum mush (white) fills root casts. Scale bar is 10 cm.
C. Trench exposure of saline soil in central Australia showing an upward-coarsening succession of large, euhedral gypsum crystals (white). Scale bar is 10 cm. Photo courtesy of Daniel Yaalon, The Hebrew University of Jerusalem.

fault-bounded basin margin where basin margin facies unconformably overlie basement rocks. Most of the basin margin facies is included in the Passaic Formation, including those that are laterally equivalent to the Lockatong Formation central basin facies. The exceptions are predominantly thin sandstone-dominated deposits that are integrated with Van Houten cycles. The basin margin facies is divided into five major lithologic types: wave-dominated sandstone, deltaic sandstone, border-fault conglomerate and sandstone, axial sandstone and conglomerate, and limestone.

Wave-dominated sandstone

Wave-dominated sandstone in the Lockatong and Passaic Formations characteristically consists of 0.1-3-m-thick tabular beds forming the top and/or base of Van Houten cycles (fig. A51). The sandstones are typically well-sorted and contain wavy, thin beds of sandstone with mudstone partings (fig. A52) or decimeter beds of sandstone with low-angle inclined lamination or tabular foresets (fig. A53). The thin-bedded wavy sandstones contain sinusoidal cross-lamination (fig. A52) and the associated mudstone partings commonly have sandstone-filled polygonal cracks and trackways of vertebrate animals. The low-angle inclined lamination and tabular foresets of decimeter-thick sandstone beds commonly grade downdip into wavy thin-bedded sandstone (fig. A53). Wave-dominated sandstone at the base of Van Houten cycles typically consists of wavy thin-bedded sandstone consisting of beds 10-30-cm thick that abruptly overlies massive mudstone. Wave-dominated sandstone at the top of Van Houten cycles consist of upward-coarsening successions that overlie thin-bedded mudstone with pinch-and-swell layering grading into thin-bedded wavy sandstone, then decimeter beds of sandstone with low-angle inclined lamination or tabular foresets (fig.

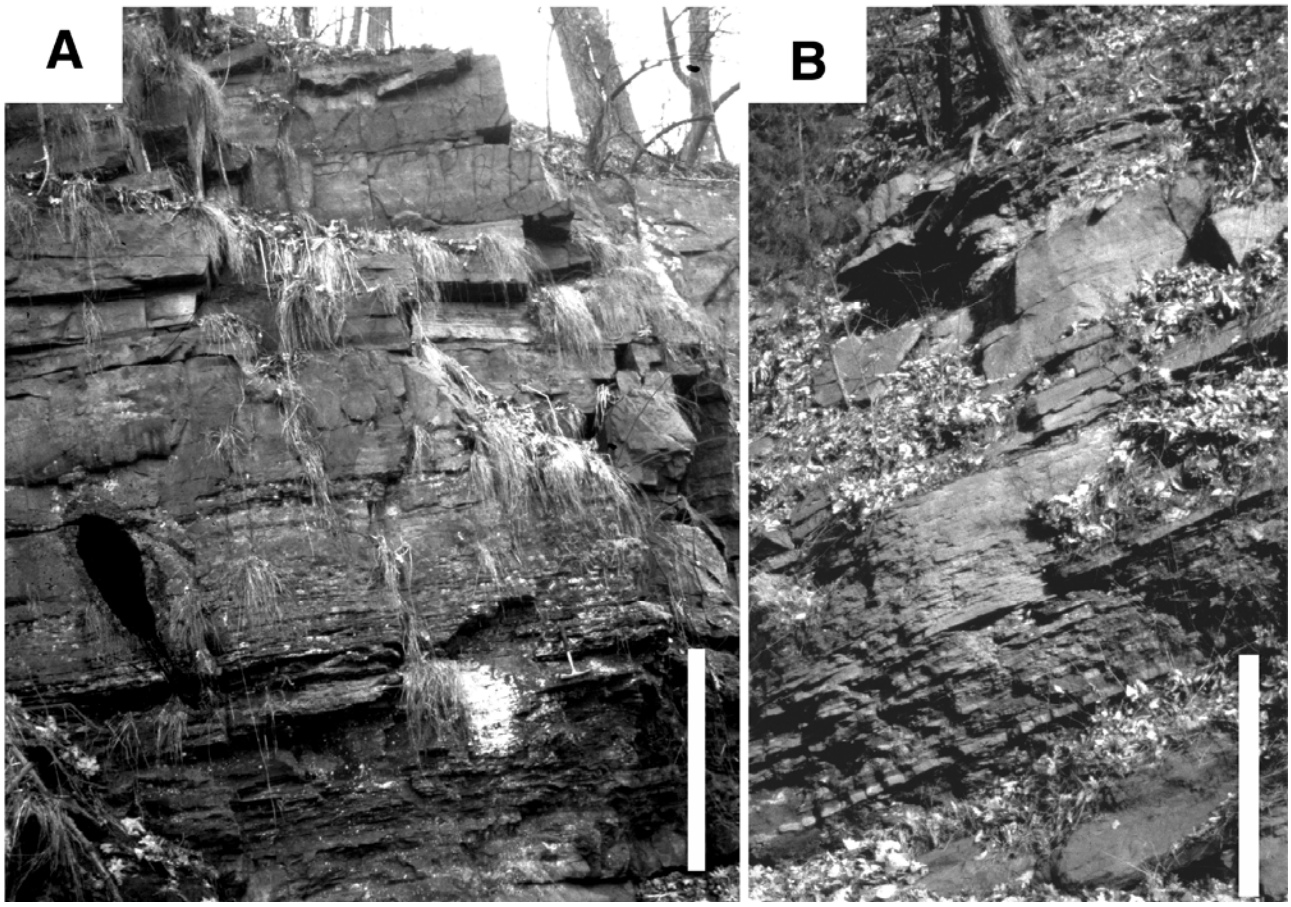

Figure A51. Vertical successions of thin-bedded lacustrine mudstone to wave-dominated sandstone. A. Van Houten cycle in the Metlars Member of the Passaic Formation. Upward-coarsening succession begins with black laminated mudstone grading upward to thin-bedded mudstone with pinch-and-swell layering of fine sandstone. This is overlain by flat-bedded sandstone with wave ripples, then thicker, more tabular sandstone beds that contain low angle foresets and wave-rippled thin beds. Top of cycle includes low-angle delta foresets with climbing-ripple cross-lamination. Scale bar is 1 meter. Locality 24, table A1, figure A5. B. Van Houten cycle capped by sandstone in road cut of the Perkasie (?) Member of the Passaic Formation. Black, laminated mudstone grades upward into thin-bedded mudstone with pinch-and-swell layering, then flat sandstone beds with progressively thinner mudstone partings. Upper blocky beds are wave-sorted sandstone with tabular foresets. Scale bar is 2 meters. Locality 26, table A1, figure A5.

A51). In places along the northwestern fault-bounded margin of the Newark basin, where Van Houten cycles are interbedded with border conglomerates, wave-dominated sandstone is associated with conglomerate that has a matrix consisting of irregular patches of well-sorted sand, granules, and fine pebbles (fig. A54).

Interpretation of wave-dominated sandstone in the Newark basin is based on comparison with modern lake shoreline deposits. Thin-bedded wavy sandstone resembles oscillatory rippled sand in water less than 3 m deep along the margins of lakes with broad, low-slope floors (Smoot and Lowenstein, 1991). Sinusoidal cross-lamination in these beds is diagnostic of wave-formed ripples (Boersma, 1970; Raaf and others, 1977). The ripples formed during episodes of high wind velocities over the lake (such as storms) and mud settled over them during subsequent lulls. Desiccation cracks formed in mud partings of ripples that were formed at the shoreline and were subsequently exposed subaerially. Decimeter-scale sandstone beds with low-angle, inclined lamination or tabular foresets are characteristic of wave-formed bar deposits (fig. A55A). In some cases, inclined lamination indicates beach-face deposits developed on the bar. The relatively small scale of these bar deposits and their intimate association with wave-rippled sandstone in the Newark basin suggests a low slope of the basin floor during lacustrine deposition. Although the lakes had tremendous fetch, the very low slopes of the lake margins caused the waves to rapidly loose energy there. Therefore, most of the shoreline deposits consist of relatively low-energy

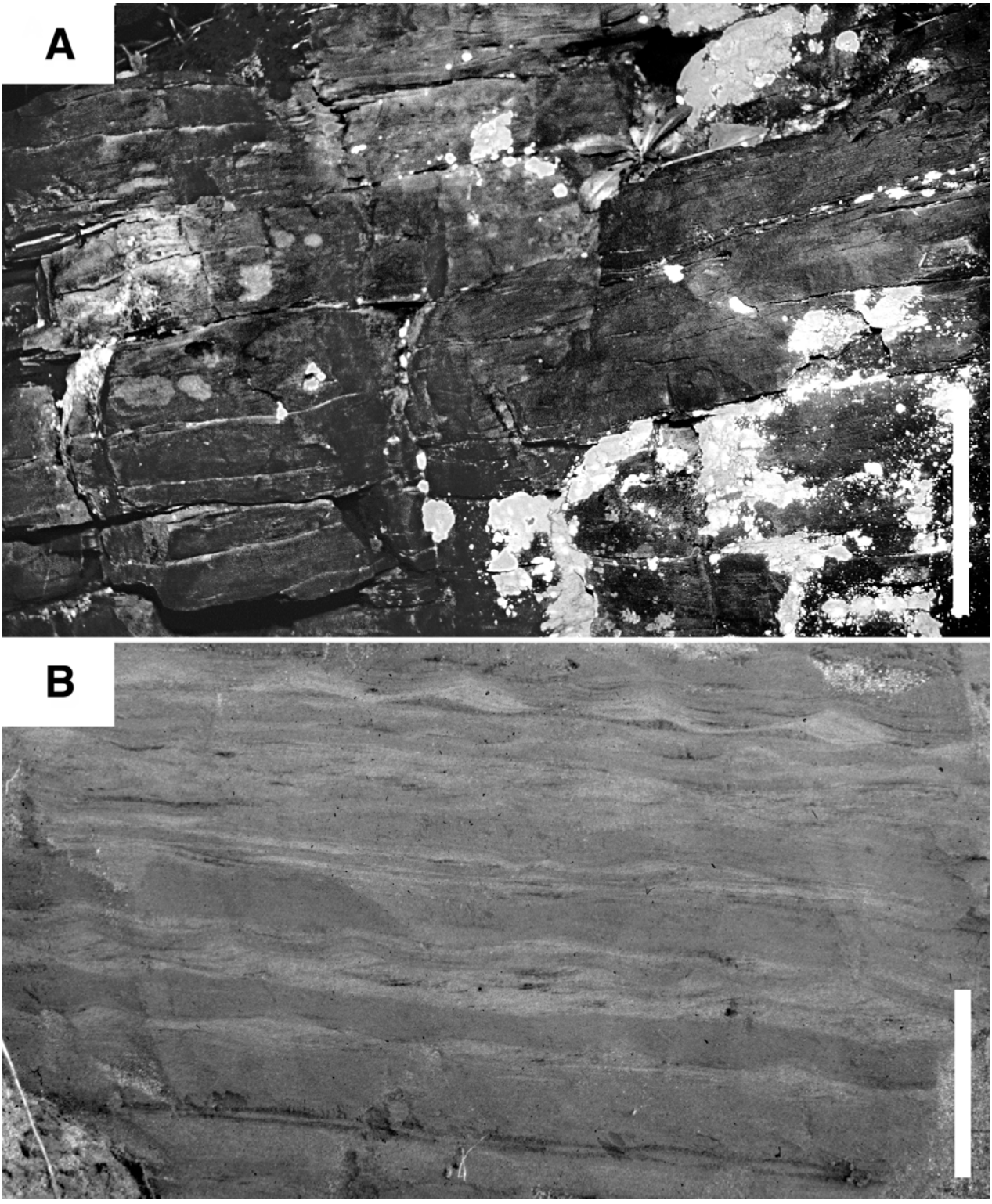

Figure A52. Comparison of wavy-bedded sandstone and modern shoreline sand. A. Sandstone thin beds with mudstone partings in the Metlars Member of the Passaic Formation. Sandstone beds have internal low-angle sinusoidal lamination indicative of wave deposition (see Harms and others, 1982, Chapter 3). Scale is 15 cm. B. Trench exposure of nearshore sand at Walker Lake, Nevada. Wavy beds of sand have internal sinusoidal lamination. Finer-grained sand layers are slightly darker and internal layering is more obscure. Mud partings (dark) are very thin to lenticular in upper beds, and thicker and more continuous in lower beds. This deposit was below two meters of water about two years before this trench was dug. Scale is 15 cm.

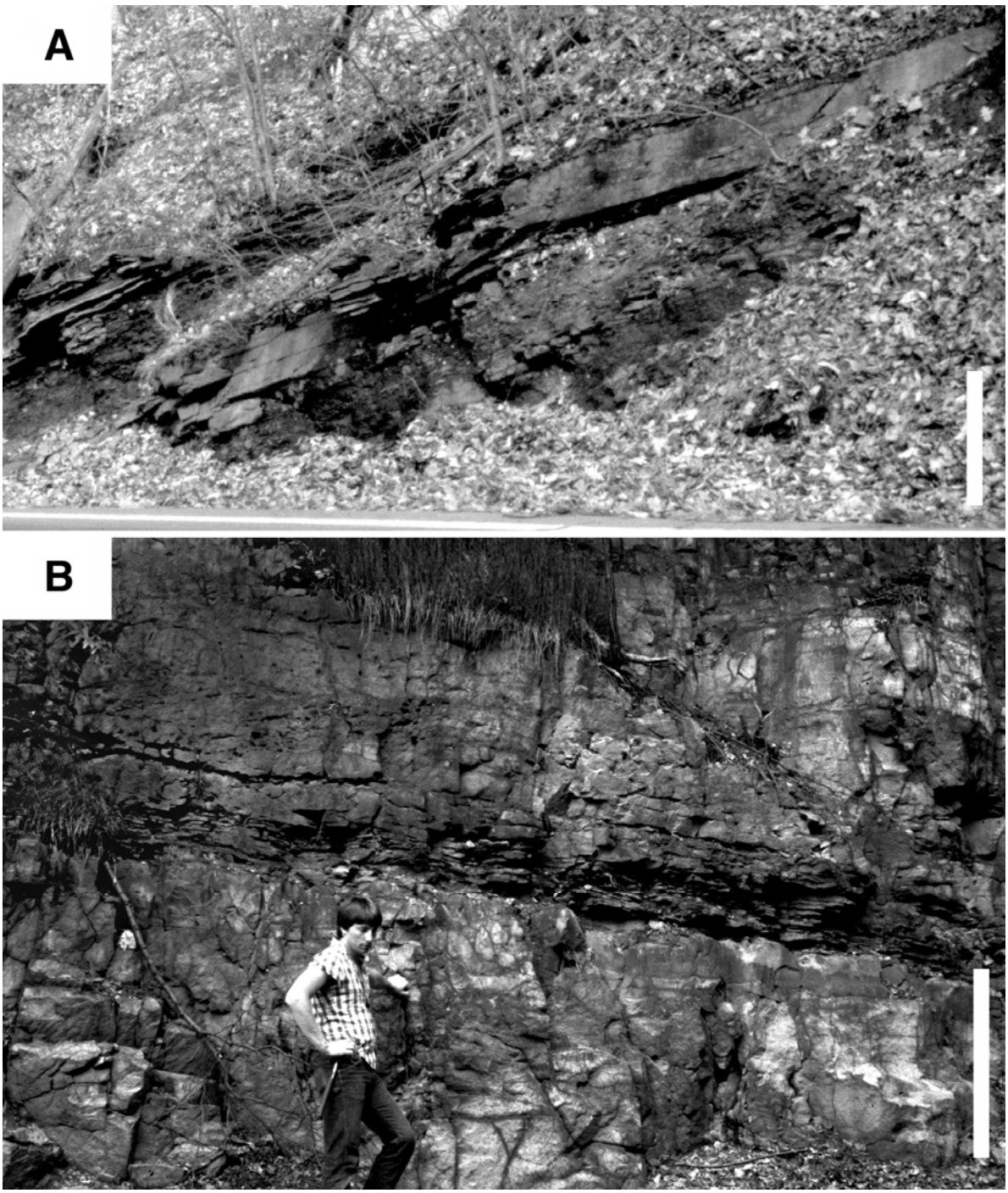

Figure A53. Wave-formed sandstone with tabular foresets. A. Upper part of a Van Houten cycle in the Perkasie (?) Member of the Passaic Formation. Thin-bedded mudstone with pinch-and-swell lamination is sharply overlain by sandstone with low-angle tabular foresets dipping to the right. The sandstone foresets grade laterally into flat wavy beds with sinusoidal lamination. The sandstone is overlain by more mudstone with wavy sandstone interbeds that coarsen upward to blocky sandstone. Scale bar is 1 meter. Locality 26, table A1, figure A6. B. Outcrop of two sandstone beds separated by laminated black mudstone in the Princeton Member of the Lockatong Formation. The rocks are metamorphosed by proximity to a large diabase intrusive sheet. Lower sandstone shows only faint bedding and is disturbed by root casts and bioturbation. Upper sandstone is gradational downward into laminated mudstone through pinch-and-swell layering and wavy sandstone beds. Low-angle foresets of the overlying sandstone grade laterally into wavy sandstone beds, but steep tabular foresets (directly above person) toe out into a single sandstone bed. Overlying sandstone in background (light blocky beds) is also disturbed by bioturbation. Scale bar is 1 meter. Locality 27, table A1, figure A3.

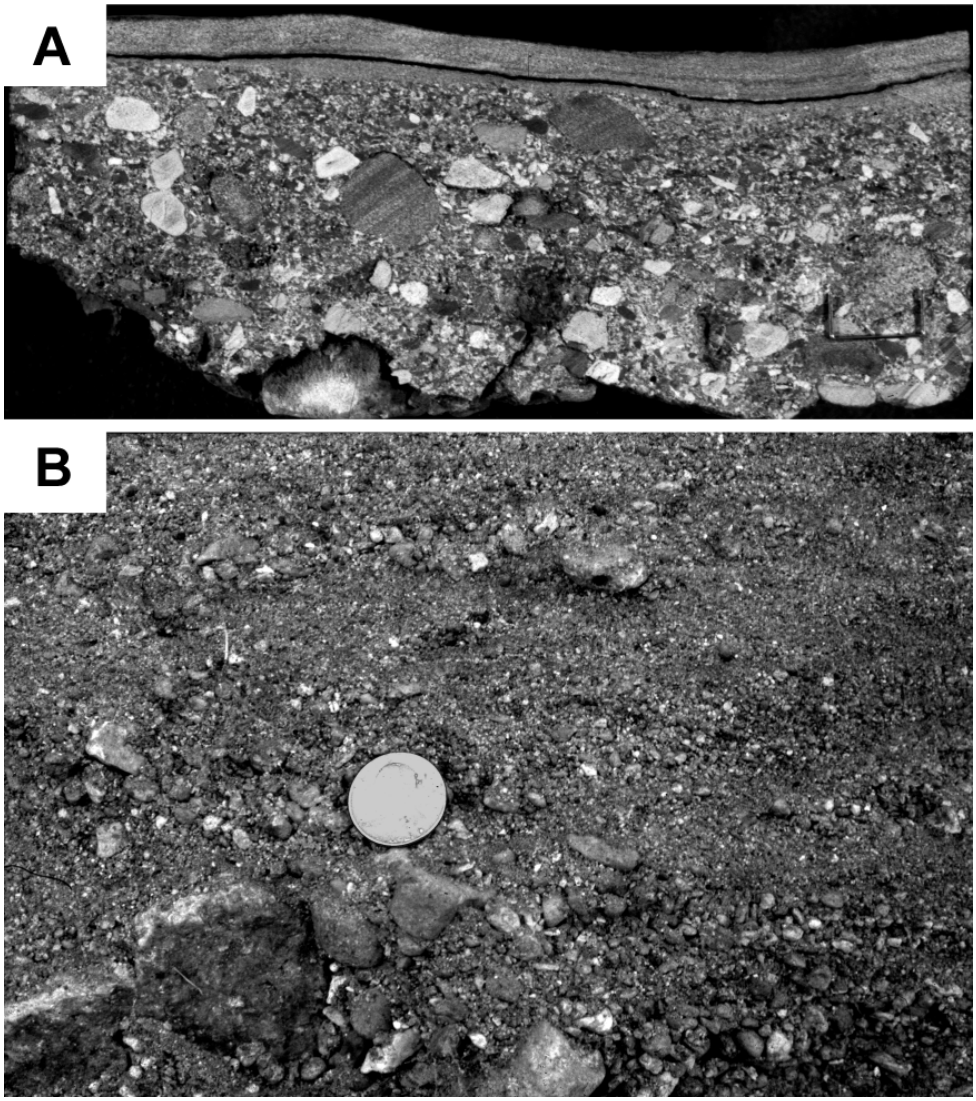

Figure A54. Comparison of a conglomerate that overlies a thin-bedded mudstone and Quaternary wave-reworked alluvial fan deposits. A. Slabbed outcrop sample of conglomerate in the lower part of the Passaic Formation (equivalent to the Perkasie Member?). Largest clasts are poorly sorted, but smaller pebbles and granule-to-coarse sand are well sorted in irregular discontinuous patches. The conglomerate is capped by well-sorted sand with sinusoidal internal lamination indicative of wave deposition. Thickness shown is about 3 cm. Locality 28, table A1, figure A4. B. Trench in Quaternary shoreline deposit on alluvial fan at Walker Lake, Nevada. Largest clasts are unsorted, whereas smallest pebbles and various sand sizes are sorted in irregular patches. Thickness shown is about 12 cm.

sands. Where wave-dominated sandstone is interbedded with border conglomerates in the Newark basin, wave deposits include coarser grain sizes. The patchy sorting of well-sorted granule- and fine-pebble-sized matrix between cobble- and boulder-sized clasts is similar to modern wave-reworked alluvial fan deposits (Smoot and Lowenstein, 1991). In modern settings, boulders and cobbles are generally too large to be moved by waves, so they act as irregular barriers that refract wave energy, producing pockets of different grain size (fig. A55B).

Deltaic Sandstone

Deltaic sandstone in the Newark basin is characterized by fine-sandstone with climbing-ripple cross-lamination in graded beds (fig. A56). Each graded bed of climbing ripples displays an upward decrease of stoss-side erosion and an increase of apparent angle of climb. These sandstones are intimately interbedded with mudstone that has sedimentary features indicating lacustrine deposition. Two major types of deltaic sandstone are in the basin margin facies of the Lockatong and Passaic Formations: 1) steep clinoform deltaic sandstone, and 2) sheet-like deltaic sandstone.

Steep clinoform deltaic sandstones in the Newark basin consist of 2-4-m-high foresets that are bowl-shaped in the perpendicular-to-flow direction (fig. A57). The foresets typically are part of the regressive section of a Van Houten cycle overlying laminated or thin-bedded mudstone. The distribution of grain sizes in clinoform sandstone defines an upward-coarsening succession. In many occurrences, two or three sandstone foresets are stacked, with each one becoming progressively coarser, thicker, and steeper than the underlying ones (fig. A59). Soft-sediment deformation is common in the sandstone beds, particularly where they are interbedded with mudstone (fig. A58). The

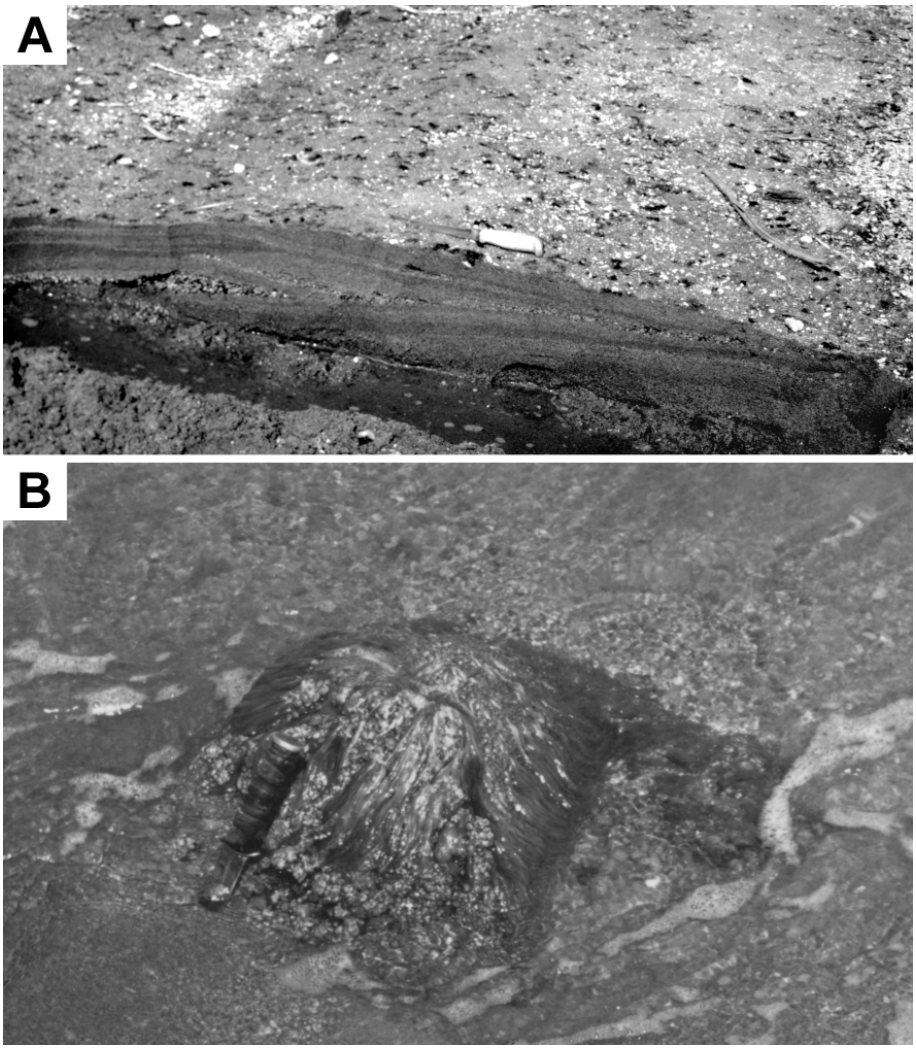

Figure A55. Modern shoreline deposits. A. Trench into small, shoreline bar at Pyramid Lake, Nevada. Tabular foresets dip lakeward (to the left) in a series of offlapping lenses. The base of each foreset grades into wavy bedded sand (under water). Larger barforms develop offshore in a meter or two of water. Field of view is about 1.5 m wide. B. Surface view of the shoreline of Walker Lake, Nevada, where it impinges upon an alluvial fan. Tufa-coated boulder has disrupted waves so that sand and fine gravel were deposited in irregular patches. The shoreline had many such barriers, producing deposits like that in B. Field of view is about 1 m wide.

upper contact of clinoform deltaic sandstone in the Newark basin is commonly a planar erosional surface overlain by finer-grained sediment. Root casts and burrows, including abundant Scoyenia, are common in this type of deltaic sandstone, particularly in the uppermost parts of steep foresets.

Clinoform deltaic sandstone deposits are interpreted as Gilbert-type deltas formed where rivers and streams carrying coarse-grained sediment intersected a lake (Gilbert, 1885, 1890). Gilbert-type deltas build out from the shore by progressive aggradation on the steep delta front. Sediment-laden stream deposits cascade down the steep delta front the way turbidites do (Bouma, 1964). On the steepest part of a Gilbert-type delta, the flow velocities produce only planar lamination, whereas on the lower slopes of the distal part of the delta front, the sediment flows decelerate, producing climbing-ripple cross-lamination. Characteristic graded beds consisting of ripple-cross-lamination with progressive decrease of stoss-side erosion in the Newark basin represent the deceleration-of-flow velocities of a turbidite flow (Bouma, 1964). The down-dip gradation in the thickness, grain size, and stoss-side erosion of climbing-ripples within graded beds in the Newark basin is characteristic of the decreasing flow velocities on a Gilbert-type delta front (Jopling and Walker, 1968). Sediment accumulation on Gilbert-type deltas is commonly rapid and soft-sediment deformation is common in the water-saturated deposits. This is consistent with the occurrence of these features in clinoform deltaic sandstones. The bowl-shaped nature of the foresets in the Newark basin is also consistent with Gilbert-type deltas. Gustavson and others (1975) reported the bowl-shaped geometry from large exposures of Pleistocene Gilbert-type deltas in Massachusetts, and I observed them in Pleistocene and Holocene Gilbert-type delta deposits at Pyramid Lake, Nevada. The bowl shapes appear to be erosional, perhaps due to focusing of density flows on delta lobe margins following distributary channel avulsion. Two features of the Newark basin clinoform deltaic sandstone differ from most modern examples of Gilbert-type deltas. Fluvial topset sandstones are

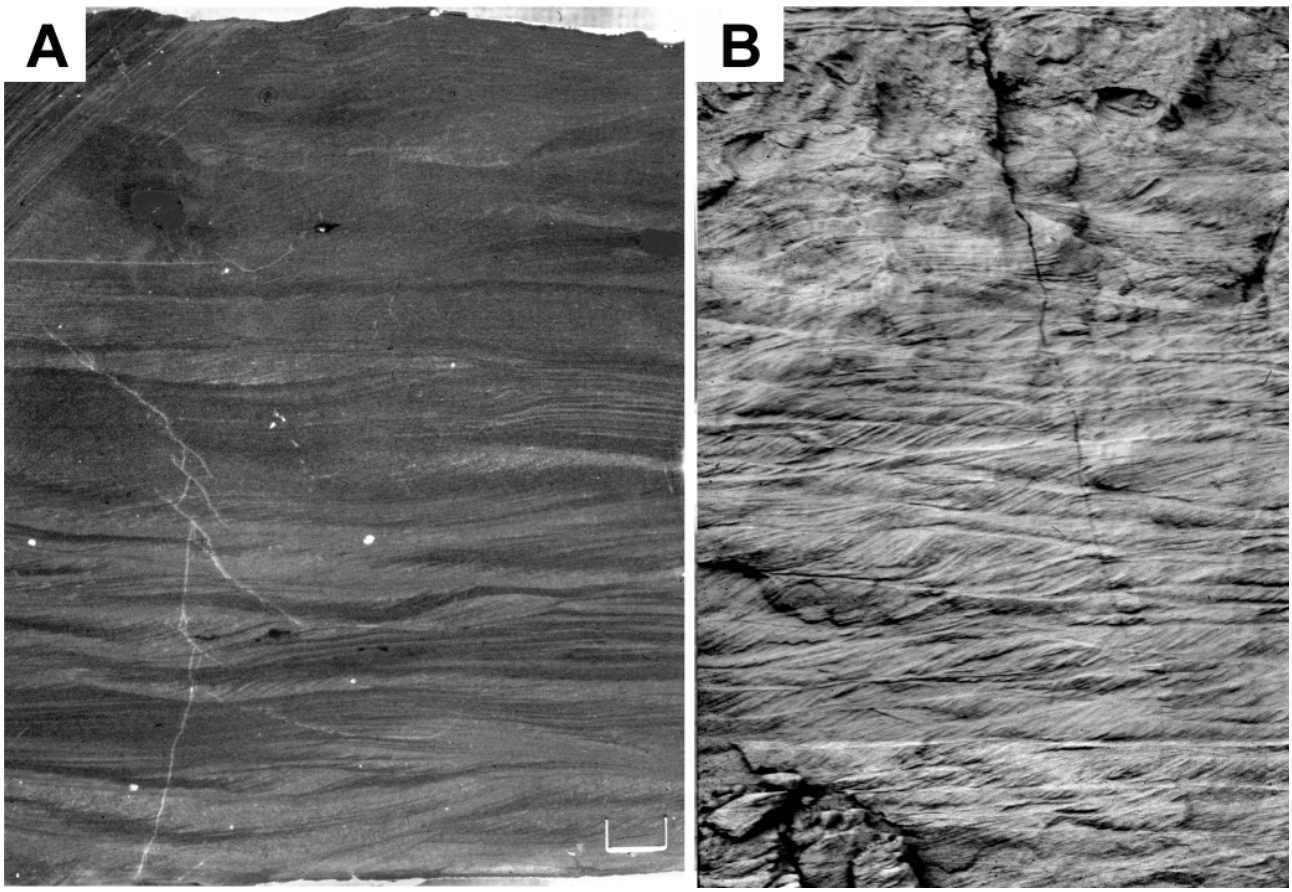

Figure A56. Comparison of internal stratification in deltaic sandstone to that of a Quaternary deltaic deposit. A. Slabbed sandstone sample from the Skunk Hollow Member of the Lockatong Formation. Graded bed of climbing-ripple cross-lamination shows progressive increase of angle-of-climb, as described by Jopling and Walker (1968). The uppermost ripples have no erosion on their stoss side. Flow was to left and out of the page. Thickness shown is 30 cm. Locality 18, table A1, figure A4. B. Outcrop exposure of climbing-ripple cross-lamination in a Quaternary delta deposit of Lake Lahontan, Nevada. The graded bed shows increase of angle-of-climb in ripples, reflecting deposition as an underflow on the delta front. Flow was to the left. Note the soft-sediment deformation at the top of the bed which is due to ripples sinking into fluidized silt. Thickness shown is 40 cm.

generally absent and clinoforms are stacked to form upward-coarsening successions. Both of these features are common in the Gilbert-type delta deposits of hydrologically closed basins (Smoot and Lowenstein, 1991). Stacked Gilbert deltas record delta aggradations during times when lake levels fluctuated over meters or tens of meters in elevation (fig. A60). The deltas built rapidly basinward when lake level fell, but subsequent lake-level rise typically resulted in wave erosion of the topsets. When lake level fell again, new foresets were deposited over the older ones resulting in a gradual aggradation of the delta body. During lake lowstands, the river forming the delta incised into the underlying foresets, making it difficult to intersect the fluvial facies in two-dimensional outcrop sections. Vegetation developed on the subsequently subaerially exposed surface producing the root casts commonly observed.

Sheet-like deltaic sandstone in the Newark basin consists of decimeter-thick, graded sandstone beds separated by cm-thick mudstone beds. The sandstone beds commonly group into upward-thickening successions 1-2 meters thick (fig. A61). Individual beds are continuous throughout the length of an outcrop and groups of beds that are correlated over several square kilometers typically show a basinward thinning of individual beds and upward-thickening successions. Each graded sandstone bed contains climbing-ripple cross-lamination consisting of a deceleration-of-flow sequence (fig. A62) similar to those of the clinoform deltaic sandstone. Soft-sediment deformation is common in the ripple cross-laminated layers. The ripple cross-lamination in these sandstone beds shows similar paleocurrent directions throughout the extent of the sandstone sheets. In some occurrences, the uppermost sandstone beds of upward-thickening sequences include tabular crossbeds, small channel scours, and dune-scale cross-lamination. Mudstone beds between the graded sandstones typically have

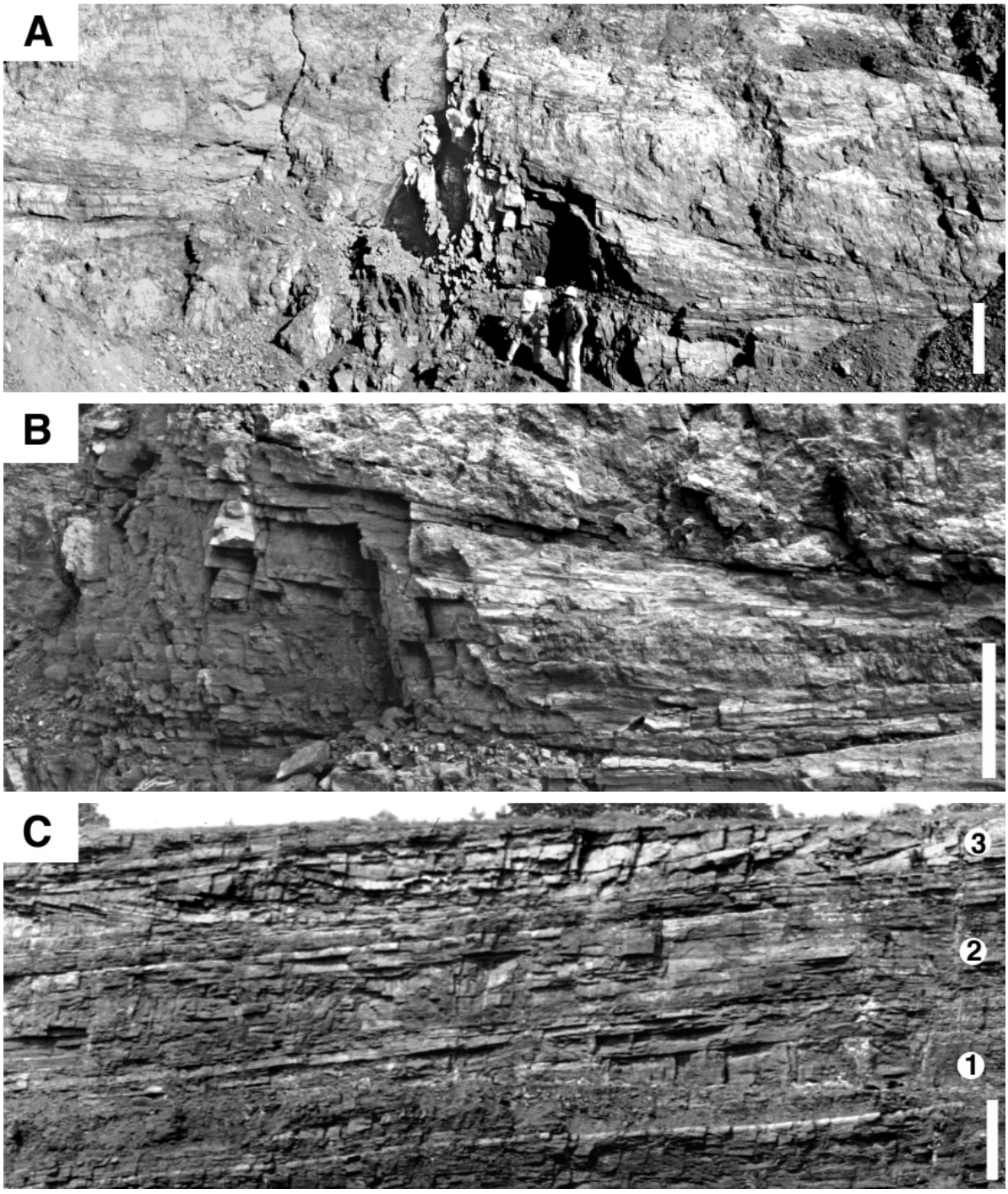

Figure A57. Sandstones showing characteristics of clinoform deltaic sandstone. A. Meter-scale sandstone foresets in the lower part of the Passaic Formation (Neshanic Member?) dipping to the right and out of the page. Thin-bedded mudstone crops out at the base (near figures) and is laterally equivalent to sandstone foresets (transition is visible to right of figures). Steepest foresets (in the middle right of picture) consist of planar lamination. Note transition from foresets to mudstone at higher level in outcrop left of figures. Scale bar is 1 meter. Locality 29, table A1, figure A3. B. Detail of foreset transition to mudstone directly right of figures in A. Sandstone beds thicken upward as they steepen, and thin to the right as they become flatter. Scale bar is 1 meter. C. Van Houten cycle in the Nursery Member of the Lockatong Formation. Black laminated mudstone at base is overlain by three upward-coarsening sequences of mudstone and sandstone defining clinoform deltaic foresets (labeled 1-3). The cross section is perpendicular to the foreset dip direction (into the page). Note how sandstone beds (blockier layers) show steeper inclinations and more bowl-like shapes upward, defining a stacked Gilbert-type delta deposit. Scale bar is 2 meters. Locality 15, table A1, figure A4.

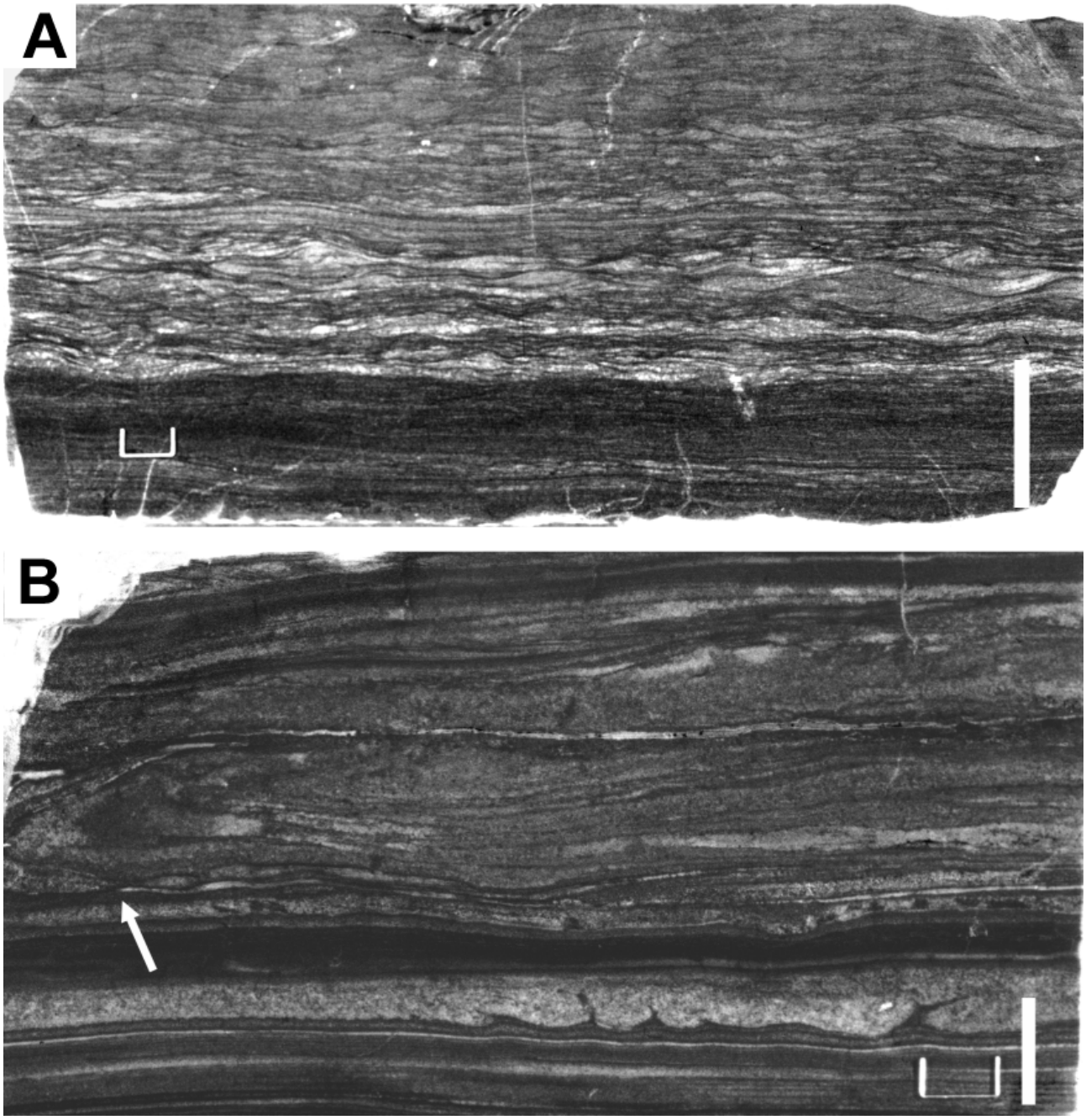

Figure A58. Bedding characteristics of deposits at the base of clinoform deltaic sandstone foresets. A. Slabbed outcrop sample of fine-grained sandstone grading into siltstone in the Nursery Member of the Lockatong Formation. Perpendicular-to-flow cross section shows more lenticular cross sections in low-angle climbing ripples (lowest light-colored layer) becoming progressively more continuous in higher angle of climb. Base of sample is siltstone of vertically climbing ripples with no stoss-side erosion (dark). Scale is 3 cm. Locality 15, table A1, figure A4.
B. Laminated to thin-bedded sandstone and mudstone underlying clinoform deltaic sandstone foresets in the lower part of the Passaic Formation (Neshanic Member?). Base of sample shows sandstone thin beds (light) with ball-and-pillow loading. Upper part of sample is fine sandstone with high-angle climbing-ripple cross-lamination with a soft-sediment fold (arrow). Scale bar is 1 cm. Locality 29, table A1, figure A3.

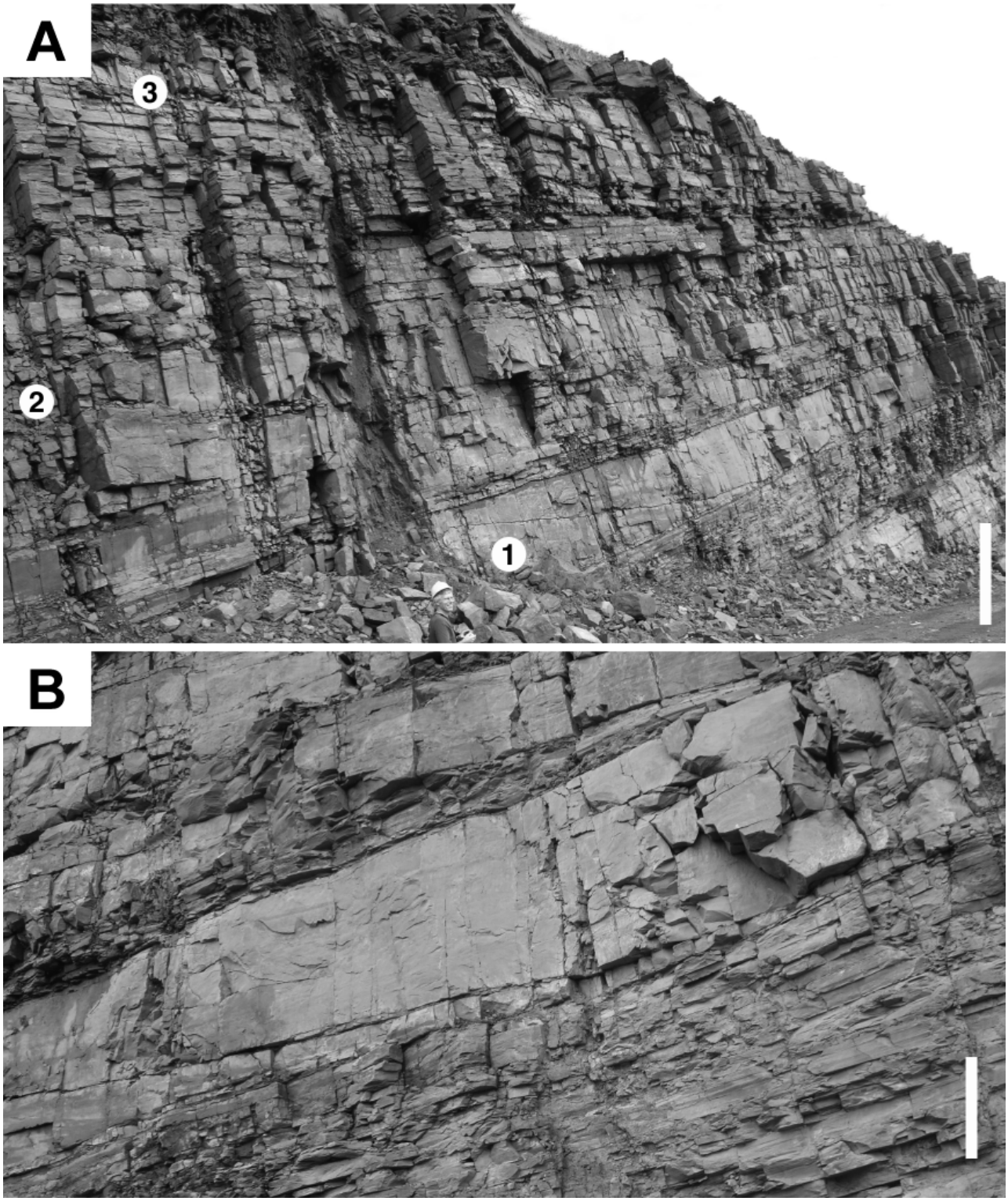

Figure A59. Deltaic sandstone foresets in stacked sequences in the Skunk Hollow Member of the Lockatong Formation. A. View showing three delta foresets (labeled 1-3) stacked on top of black, laminated mudstone grading upward into thin-bedded mudstone. Each successive foreset has less interbedded mudstone at the base. The top of each delta foreset has root casts. Foresets dip to the right and into the page. Scale is 2 m. B. Detail of the base of the lowest sandstone foreset. Note how inclined sandstone beds thin to the right, turning into flat-lying thin beds. Each of the layers is composed of climbing-ripple cross-lamination. Scale is 50 cm. Locality 18, table A1, figure A5 and A7.

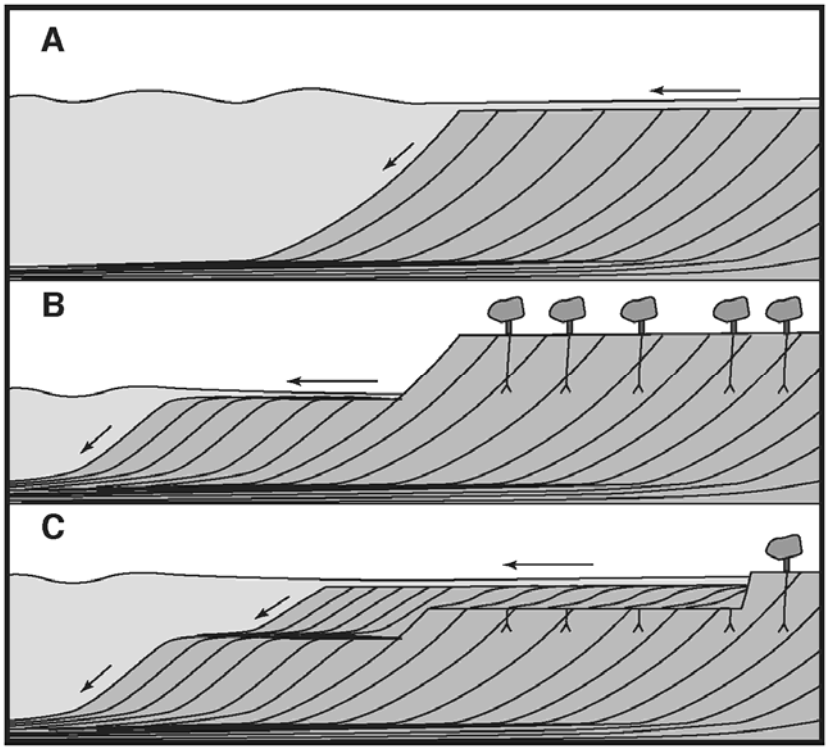

Figure A60. Schematic representation of how stacked Gilbert-type delta deposits are formed. A. Delta forms as river moves sediment into the lake. Foresets are formed by sediment-laden underflows. B. Lake level drops and river cuts down into its old deposits, making a smaller delta. Abundant fine-grained sediment is available for delta deposition because of reworking of the former delta deposits. C. Lake level rises and the topsets are eroded by waves. Delta progradation resumes over the older deposits.

polygonal cracks that are filled by sandstone from the overlying layer. Where sheet-like deltaic sandstone can be traced into mudstone deposits, they are equivalent to thin-bedded vesicular mudstone with siltstone polygonal curls (as in fig. A24B).

Sheet-like deltaic sandstone in the Newark basin is the deposit of low-relief deltas that formed where shallow streams or sheet floods debouched into a rapidly expanding very shallow lake in a hydrologically closed basin (Smoot and Lowenstein, 1991). Low-relief deltas are characteristic of shallow temporary lakes that form in otherwise dry depressions (fig. A63). Graded sand beds form during a single flood event as the delta front is progressively drowned by the advancing lake. The very shallow water of the lake margin and the rapid transgression of the lake result in virtually flat delta foresets. The internal bedding, however, displays the same style of ripple cross-lamination as the more typical deltaic deposits. The lack of relief and decelerating flow result in broad surfaces of ripples moving lakeward, producing paleocurrent patterns like those observed in the Newark basin sheet-like deltaic sandstone. Following each flood event, the lake evaporated and shrank, leaving the recently formed deposits subaerially exposed to produce polygonal desiccation cracks (fig. A64). Saez and others (2007) interpreted similar sandstone sheets with bird tracks in the mudstone partings in the Eocene-Oligocene deposits of the Ebro Basin in Spain as sheet-like deltaic sequences of shallow, fluctuating shoreline of a gypsum-precipitating lake. The upward-thickening successions of graded sandstone beds in the Newark basin are interpreted as evidence of progradation of the sheet-like deltas over time. Scour features, tabular foresets, and dune-scale cross-bedding indicate fluvial deposition in shallow sheetfloods that effectively builds the delta topsets in this type of deposition.

Border-fault conglomerate and sandstone

Conglomerate and sandstone commonly dominate the lithologies along the northern border fault of the Newark basin in strata equivalent to the central basin facies of the Lockatong and Passaic Formations. Conglomerates that are many tens of meters thick rapidly grade basinward into sandstones, often within a kilometer or less, and the sandstones grade into mudstones in another kilometer or two. The coarsest clasts within a boundary-fault conglomerate are boulders more than 50 cm in diameter, but the deposits are dominated mostly by cobble- or pebble-sized clasts. The border-fault conglomerate characteristically is poorly sorted and includes both matrix-supported and clast-supported frameworks (fig. A65). Bedding in the border conglomerate typically consists of overlapping lenses, 0.5-3 m thick, with flat bases and convex tops or scoured concave bases and flat tops (fig. A66). The border-fault conglomerate clasts characteristically reflect rocks of the immediately adjacent highlands, including limestone, dolomite, gneiss, granite, quartzite, and a Devonian pebble conglomerate. Matrix-supported conglomerate consists of deposits with convex tops and

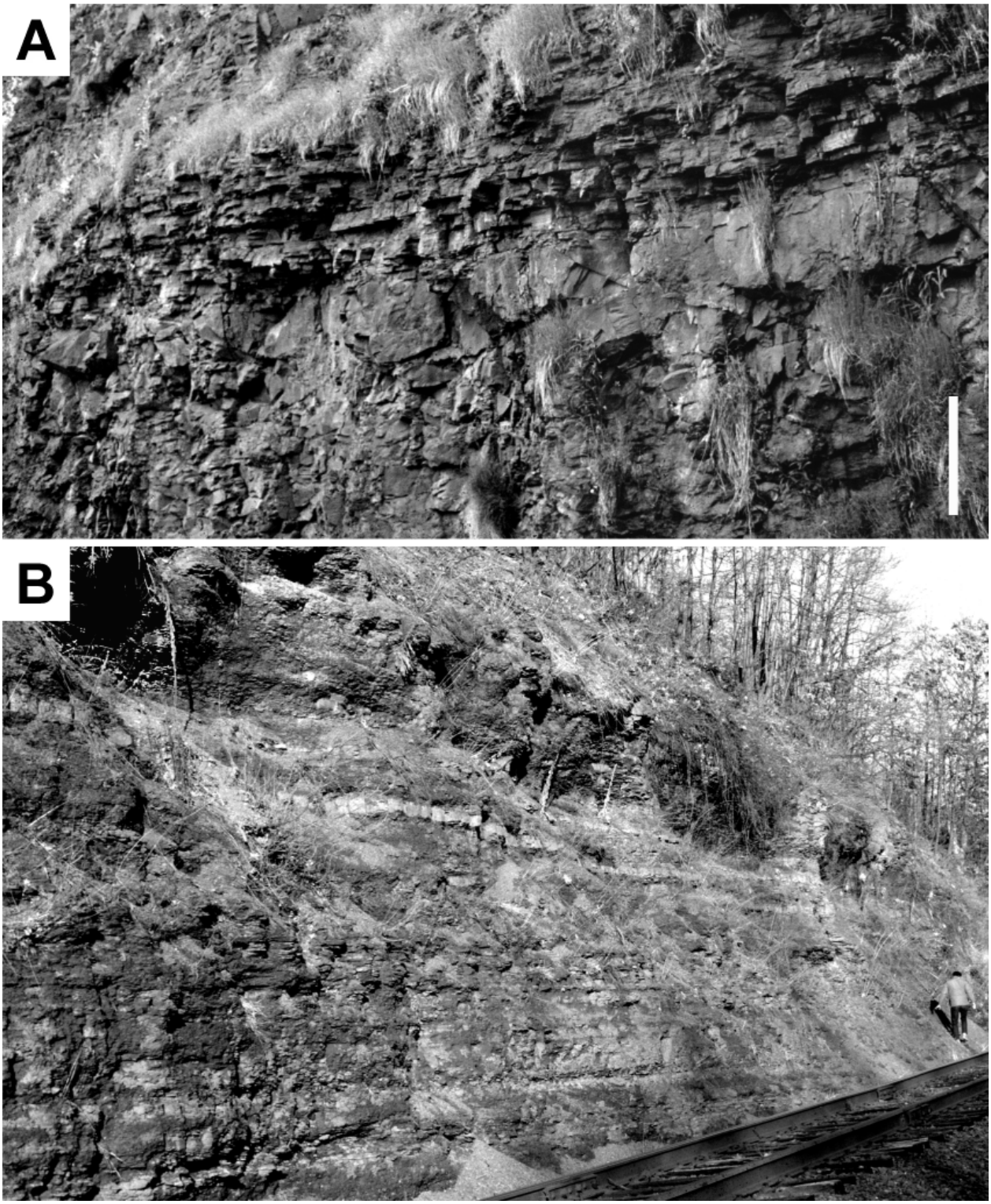

Figure A61. Sheet-like sandstone thin beds with deltaic sedimentary features. A. Outcrop of sandstone thin beds (slabby parting) overlying massive mudstone with vesicular blocky fabric in the lower part of the Passaic Formation (Member C?). Sandstone beds 5-15 cm thick are progressively thicker upwards, making up a unit about 40 cm thick. Mudstone partings between sandstone beds have polygonal cracks. Scale is 30 cm. Locality 30, table A1, figure A6. B. Mudstone with thin-bedded sheets of sandstone (blocky beds) with climbing-ripple cross-lamination in the upper part of the Passaic Formation (Member MM?). Mudstone layers between sandstone beds have polygonal cracks. Ripple cross-laminae in each bed are oriented in the same flow direction. Figure on outcrop is about 1.8 m high. Locality 31, table A1, figures A3 and A5.

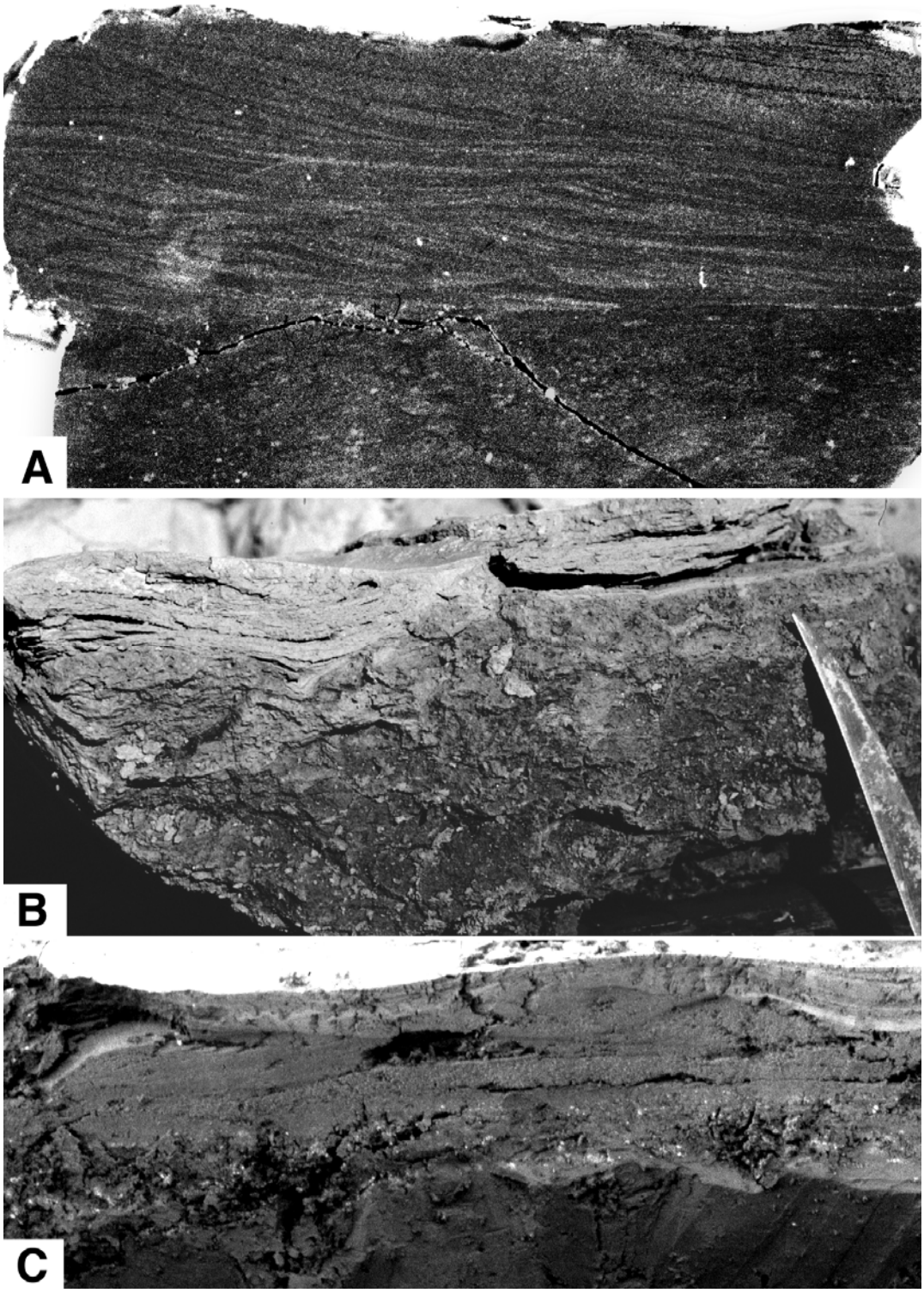

Figure A62. Comparison of internal stratification in sheet sandstone with that of modern sheet delta deposits. A. Slabbed outcrop sample from the upper part of the Passaic Formation shown in B. Base is vesicular mudstone overlain by fine sandstone with low-angle climbing ripples rapidly grading into high-angle climbing ripples. Flow was to the right. Thickness shown is 10 cm. B. Trench cut into the distal part of a small modern sheet delta on a dry mudflat in Panamint Valley, California. Base is vesicular mud overlain by ripple cross-laminated very fine sand (light) with flow direction out of the page. Thickness shown is about 5 cm. C. Trench cut through the proximal part of a small modern sheet delta in Death Valley, California. Graded sand bed (light) shows low-angle climbing ripples at base with progressively less stoss-side erosion to draped mud at top. Flow direction is to the left. The underlying mud is a saline mudflat deposit. Thickness shown is about 15 cm.

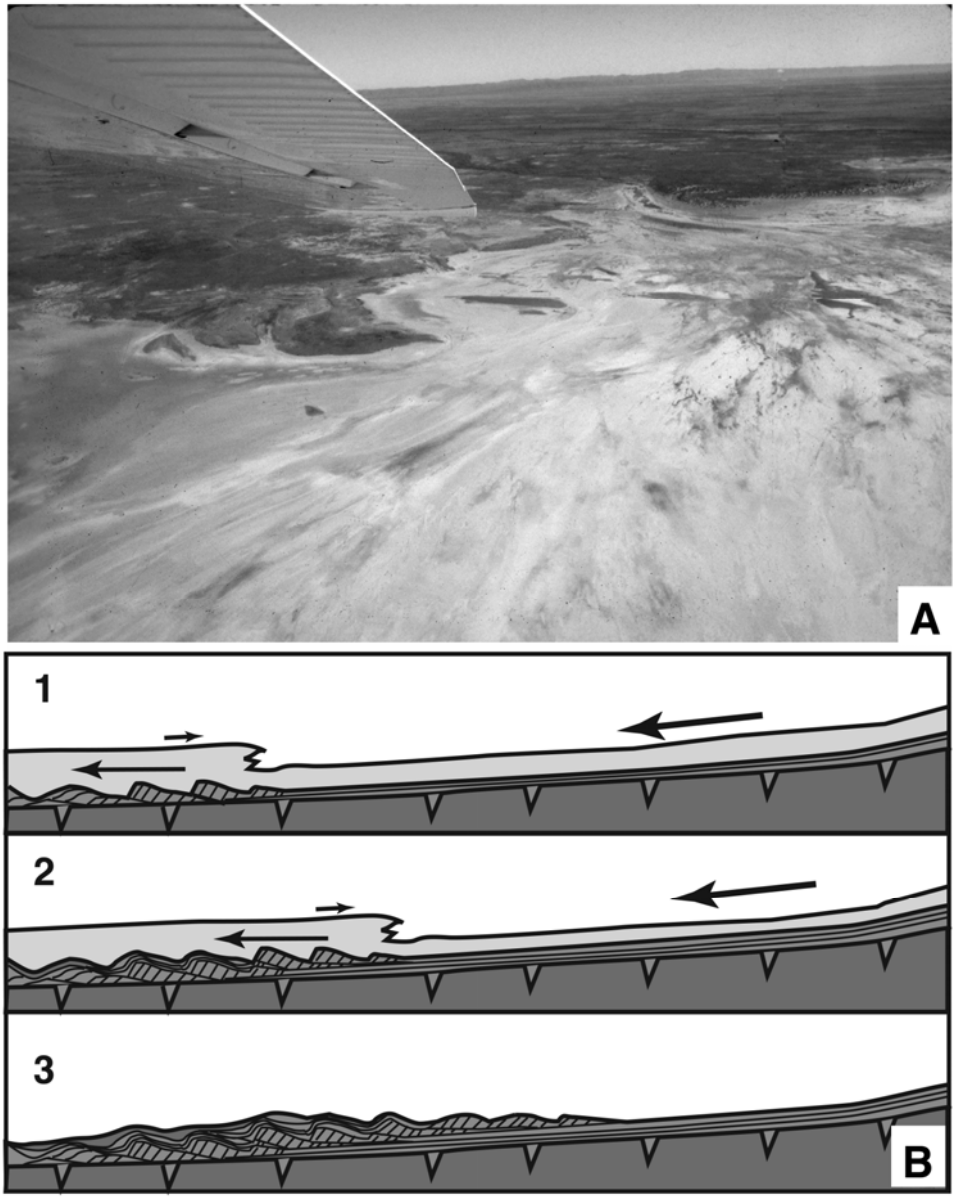

Figure A63. Modern sheet delta with schematic representation of depositional processes. A. Aerial photo shows a sheet delta at intersection of ephemeral stream channels and the Lake Eyre saline mudflat in Australia. The photo shows where the lake expands when the channels flood. Note small channels (dark) on a flat surface and the airplane wing in upper left. Area shown is about 2 km wide. B. Schematic map drawing shows a shallow flood (large heavy arrow) intersecting a shallow lake that is rising and expanding in response (small arrow). 1) Ripples are deposited owing to underflow at the intersection point. 2) Lake continues to rise, causing finer-grained climbing-ripples to be deposited over earlier flood deposits. 3) Following the flood, lake level recedes leaving sheet sand and clay drape subaerially exposed and subsequently desiccated, forming cracks. The length of the rippled zone on a flat playa surface can be as much as tens of kilometers.

concentrations of the largest clasts along the top and edges (fig. A67). The coarse clasts along the edge are steeply imbricated away from the center of the lenses, almost in grain contact. Clast-supported conglomerate fills concave scours and commonly shows imbrication or shadow fabrics and its sandstone matrix commonly has internal flat lamination (fig. A68). Finer-grained conglomerate and conglomeratic sandstone are interbedded with the coarse-grained conglomerates or are basinward of the border fault. These finer-grained deposits typically have flat lamination with trains of isolated cobbles and pebbles whose long axes are nearly vertical or, in some localities, contain convex-upward lenses that are less than 20 cm thick (fig. A69). Sandstone beds along strike with the border-fault conglomerates, and interbedded with the central basin mudstone, are typically 0.2-2-m thick. Root casts and burrows are typically abundant, and bedding, where preseved is dominated by planar lamination (fig. A70).

Border-fault conglomerate and sandstone in the Newark basin are interpreted as alluvial fan deposits because of their abundance along the faulted margin of the basin and their abrupt fining in more basinward exposures. The provenance of the border-fault conglomerates reflects only local source areas consistent with limited drainages at a sharp topographic break. In the coarsest border-fault conglomerate occurrences, there are two major depositional styles. Matrix-supported conglomerates with convex upper surfaces are interpreted as having been deposited as debris flow lobes. The concentration of largest clasts toward the top and outer margins of matrix-supported conglomerate lenses is a diagnostic feature of debris flows and the nearly vertical alignment of long axes of

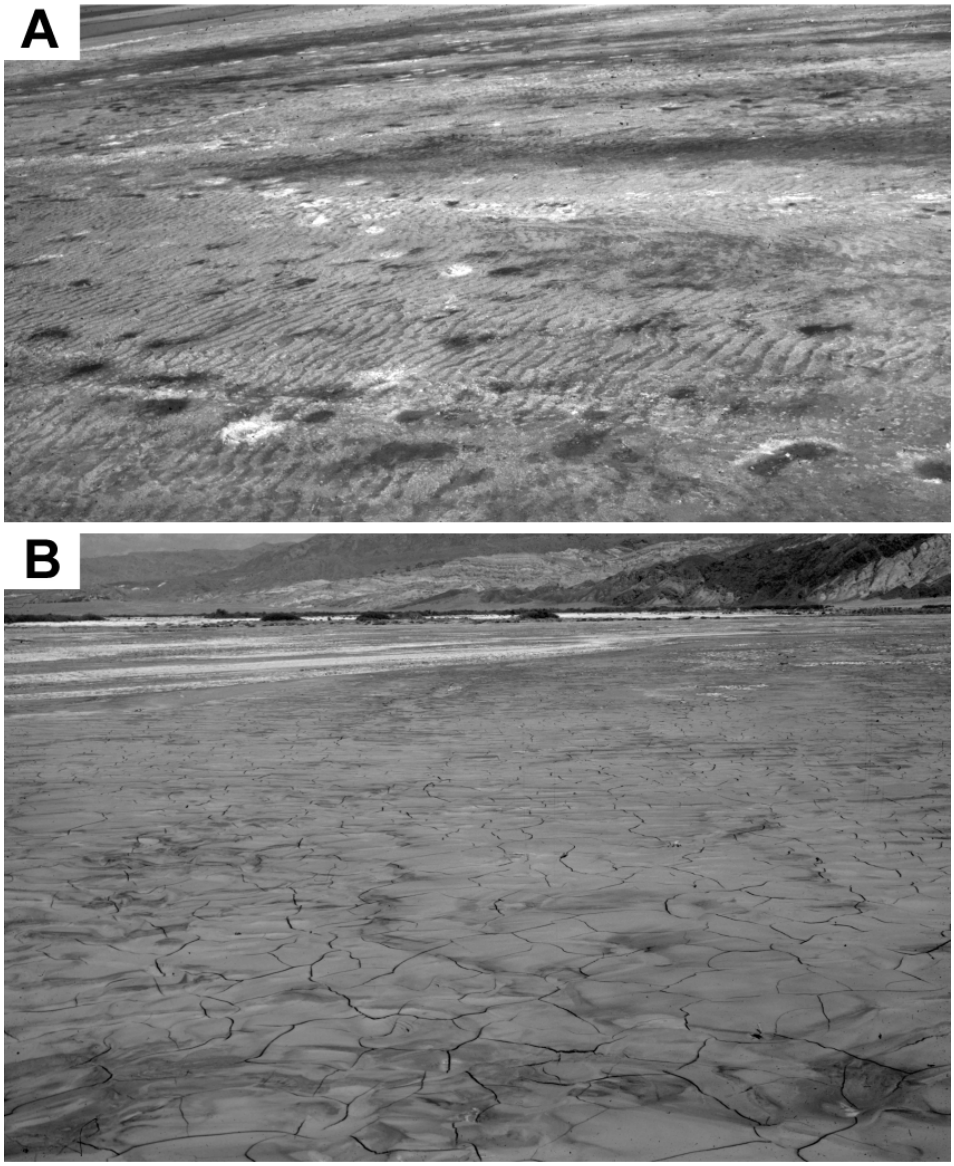

Figure A64. Surface photos of a small sheet delta in Death Valley, California, three days after it was deposited. A. Proximal delta surface with long-crested ripples. This is where trench shown in figure A61C was made. Width of area in foreground is about 10 m. B. Distal delta surface with a thick mud drape and desiccation cracks. Wavy surface of underlying ripples is visible in the foreground. Area in foreground is about 5 m wide.

clasts along the margins is a common trait (Costa, 1988). Clast-supported conglomerates in flat-topped lenses and concave, scoured bases are interpreted as stream channel deposits. Streamflow on alluvial fans is characteristically shallow and short-lived. Bedding produced by ephemeral streams on alluvial fans is commonly flat with imbricated pebbles and cobbles, lenses of planar lamination, and scattered scours filled with boulders and cobbles (Blair and McPherson, 1994). The extremely shallow flow and steep stream profile of alluvial fans preclude extensive development of lower-flow-regime bedforms such as dunes or ripples, and any clasts larger than the flow depth act as barriers that trap coarser material on the upstream side (shadow fabric). In the distal areas of modern alluvial fans, debris flow deposits typically thin to sheet-like lobes that are less than 10 cm thick. These deposits are commonly reworked by more frequent streamflow leaving only the largest clasts of the margins as lags in their original orientation. These debris-flow-margin lags appear as layers of isolated pebbles and cobbles standing on end, or lenses of tightly-packed pebbles and cobbles which have nearly vertical imbrication in stream deposits (fig. A69). The isolated pebbles and cobbles in planar-bedded sandstone in the Newark basin border-fault conglomerate are interpreted as having that origin. Sheet-like sandstones dominated by planar lamination and abundant root casts and burrows that are on strike basinward of border-fault conglomerates are interpreted as distal alluvial fan toes or sheetflats. In modern fan toes and sheetflats, floods initiated on the alluvial fan spread out into unconfined sheets that are only centimeters deep. Planar lamination is deposited under upper flow-regime conditions and it is capped by a thin mud film as the flood ends. The abundance of root casts and burrows in Newark basin sandstones is

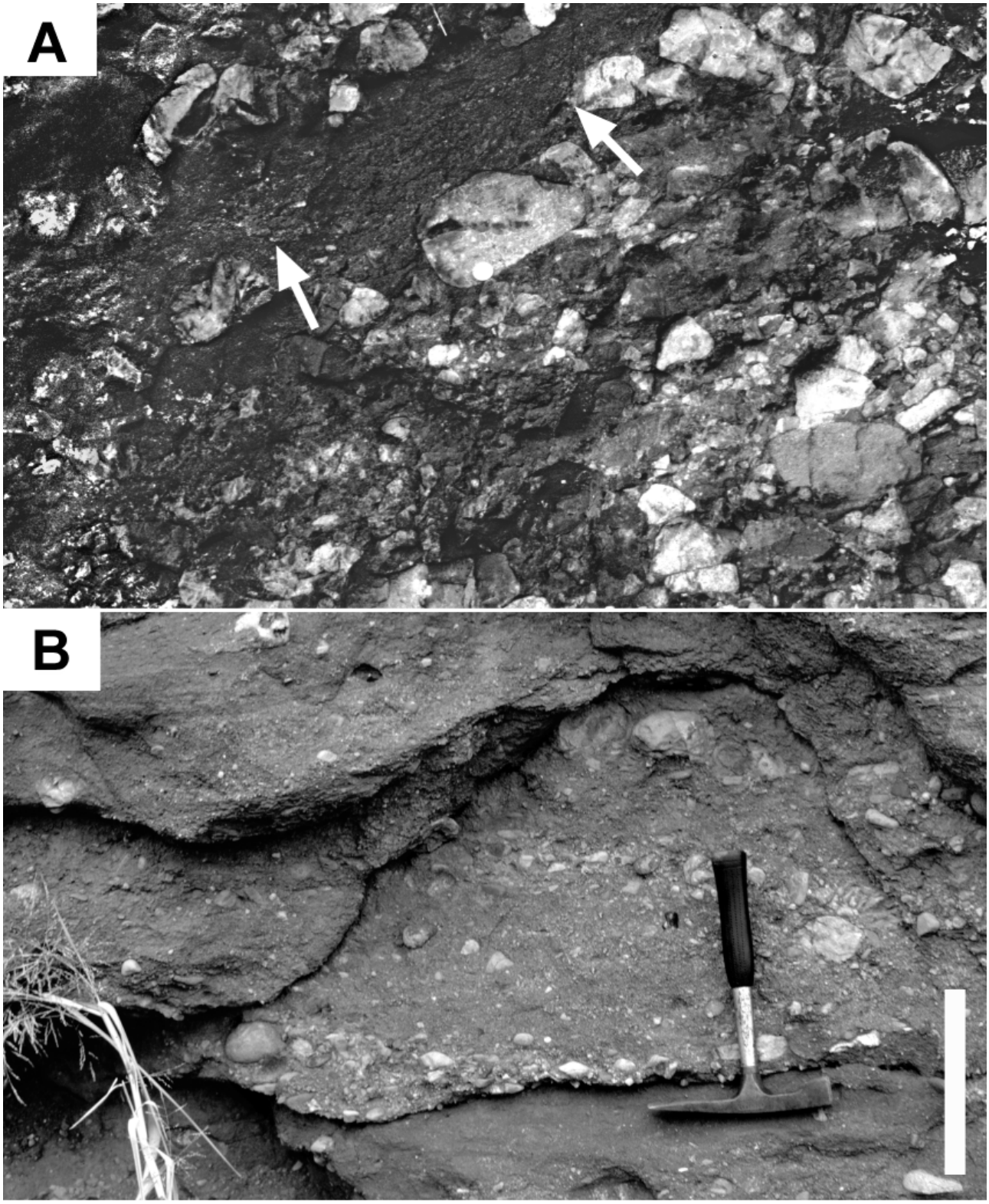

Figure A65. Border conglomerate and sandstone. A. Outcrop of conglomerate showing clasts supported by matrix (lower right side) capped by thin sandstone (arrows), in turn overlain by a clast-supported conglomerate. Thickness shown is about 40 cm. Locality 28, table A1, figure A4. B. Outcrop of conglomerate with lenses of clast-supported pebbles and cobbles separated by pebbly sandstone. Scale is 30 cm. Locality 32, table A1, figure A3.

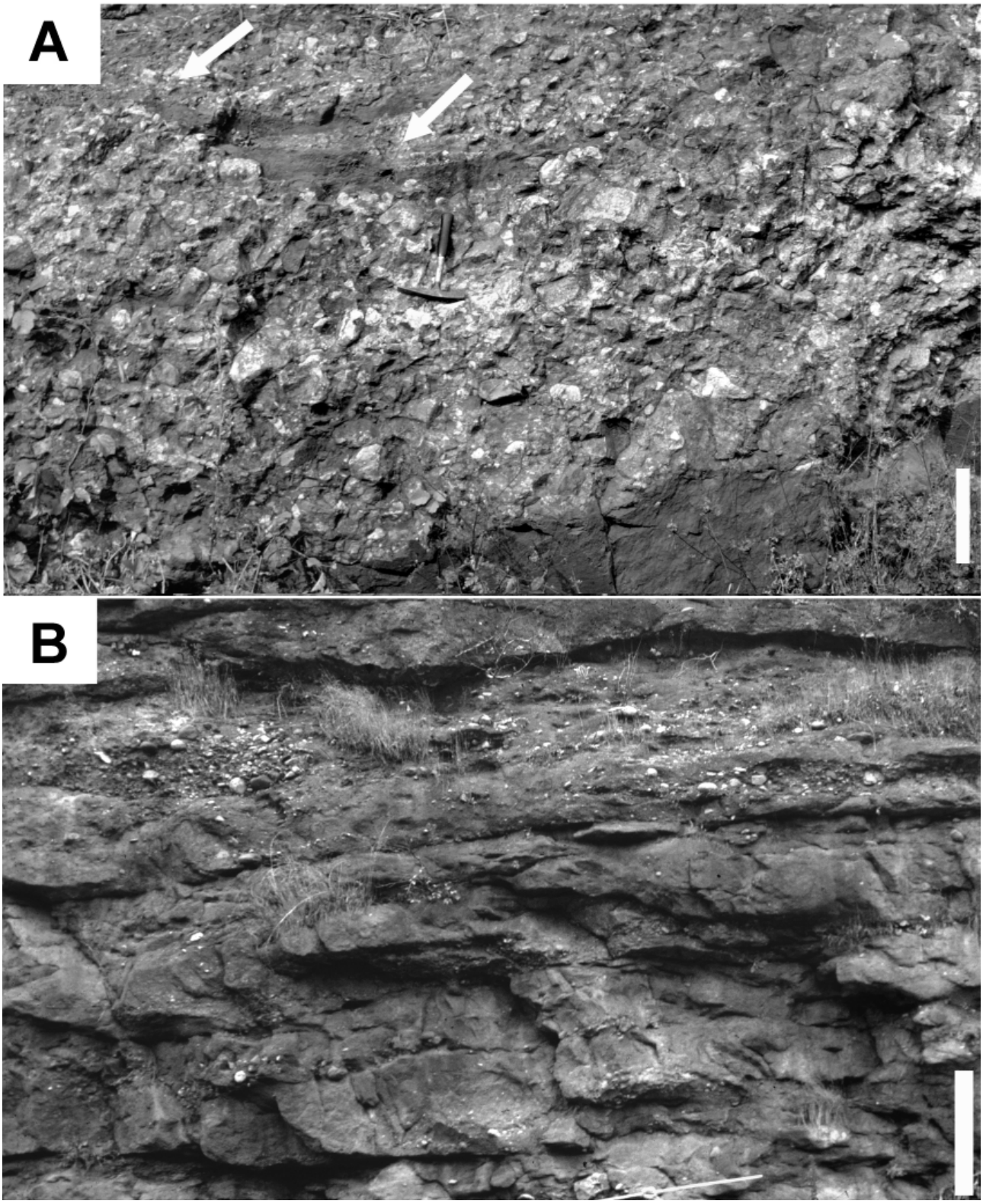

Figure A66. Bedding styles in border conglomerates. A. Conglomerate with a flat base and convex top. Arrows point to sandstone lenses lapping against the convex surface of a matrix-supported conglomerate. Scale bar is 30 cm. Locality 28, table A1, figure A4. B. Conglomerate lenses with concave bases and flat tops. Scale bar is 50 cm. Locality 32, table A1, figure A3.

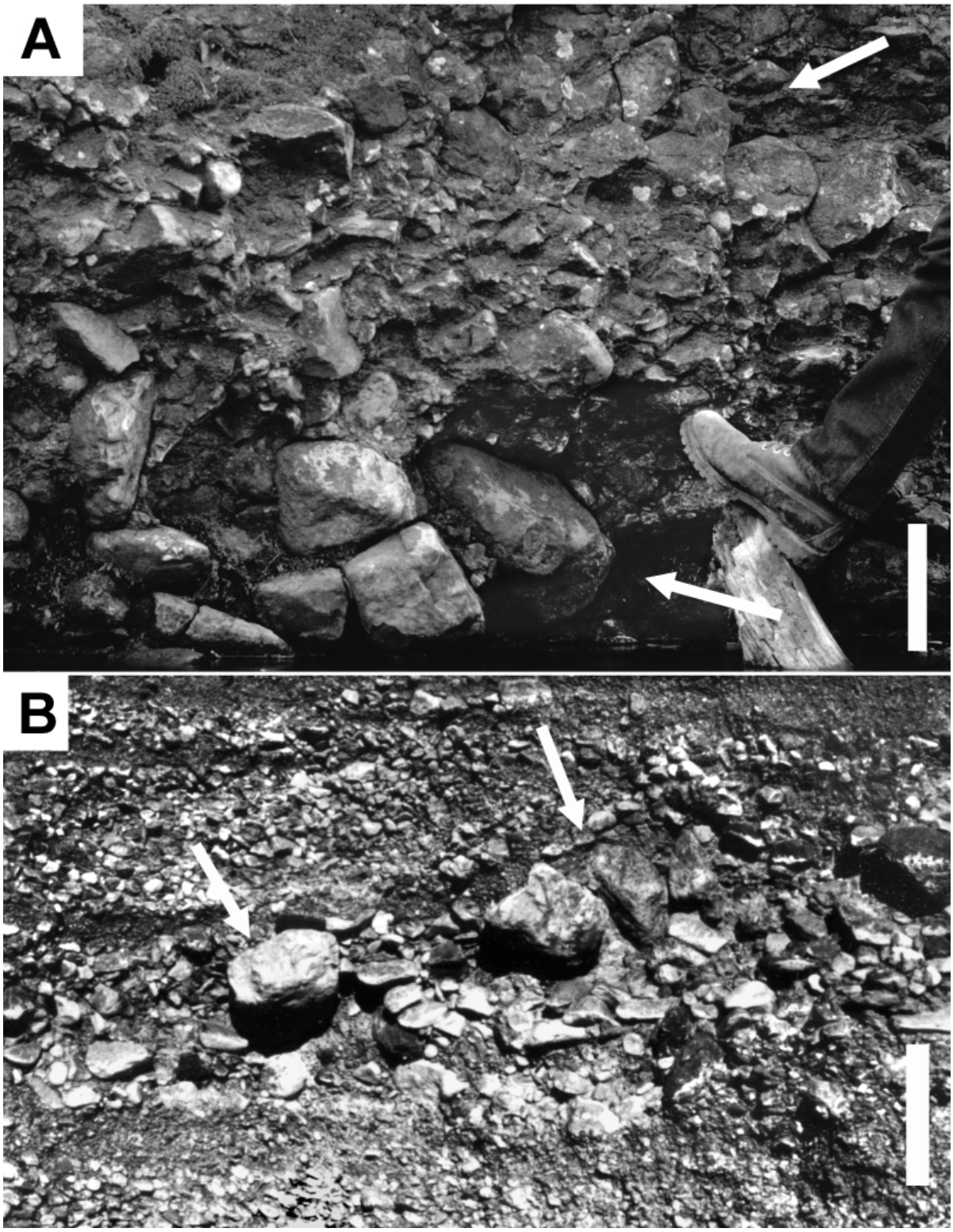

Figure A67. Comparison of matrix-supported border conglomerate and debris-flow deposits in a modern alluvial fan. A. Border conglomerate dominated by limestone clasts with muddy matrix. Margins of convex-upward lenses are made of tightly packed concentrations of the largest clasts (arrows) whose long axes are nearly vertical. Scale is 30 cm. Locality 33, table A1, figures A3 and A4. B. Natural exposure of alluvial fan deposit in Saline Valley, California. Matrix-supported debris-flow lens has concentration of largest clasts along the margins and top with steep (nearly vertical) imbrication (arrows). Surrounding deposits are clast-supported, imbricated gravels and flat-laminated sands. Scale is 30 cm.

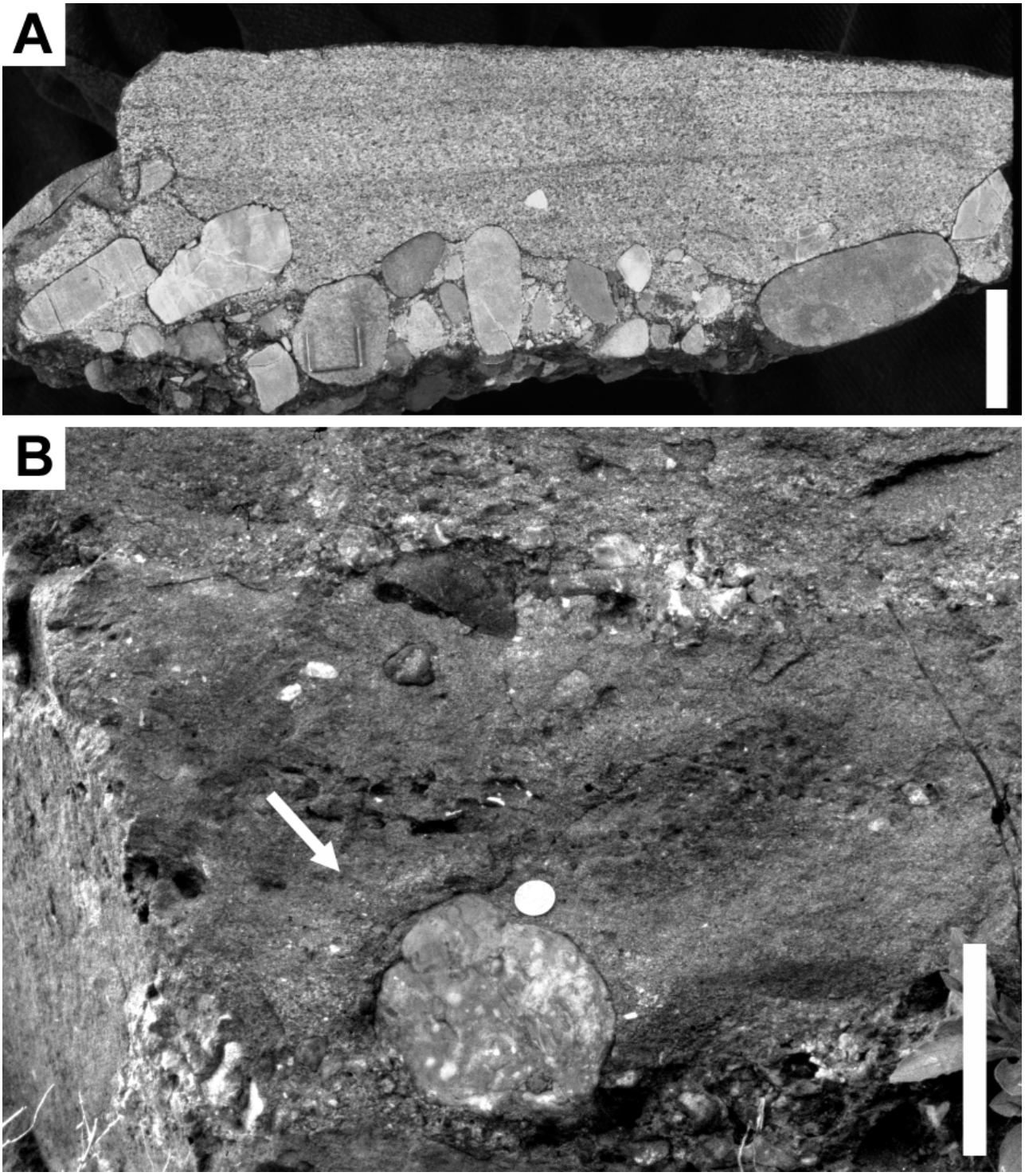

Figure A68. Border conglomerates with clast-supported fabrics. A. Slabbed outcrop sample showing imbricated pebbles (flow direction is left to right) that are overlain by sandstone with flat lamination. Scale bar is 2 cm. Locality 32, table A1, figure A3. B. Outcrop of clast-supported cobbles and pebbles with flat-bedded sandstone. Note concentration of coarse grains on left side of cobble (arrow) and finer sandstone on the right side (flow direction is left to right) called a shadow fabric. Smaller cobble near top shows a similar shadow fabric and imbrication. Scale is 20 cm. Locality 32, table A1, figure A3.

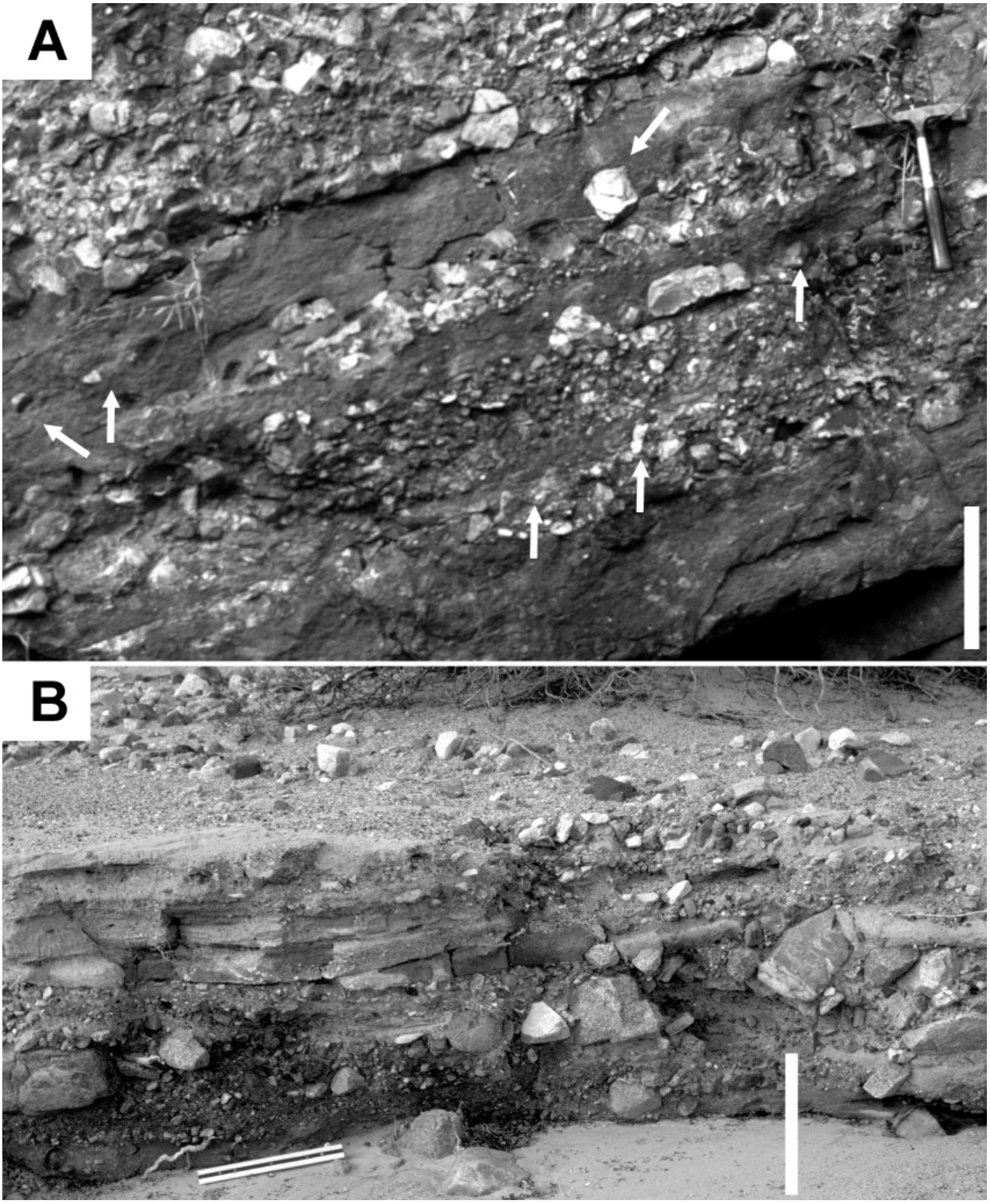

Figure A69. Comparison of fine-grained border conglomerate and modern distal alluvial fan deposit. A. Pebble and cobble conglomerates interbedded with flat-laminated sandstone. Note isolated cobbles and pebbles with steeply inclined long axes (arrows). Flat clast left of hammer is steeply inclined into the plane of the photo. Scale is 30 cm. Locality 28, table A1, figure A4. B. Natural cross section of distal alluvial fan deposit in Saline Valley, CA. Isolated cobbles and pebbles in cross section and on the surface, with long axes steeply inclined, are remnants of thin debris flows whose matrix was removed by subsequent streamflow. Flat-bedded sands and pebbly sands are stream deposits. Scale is 30 cm.

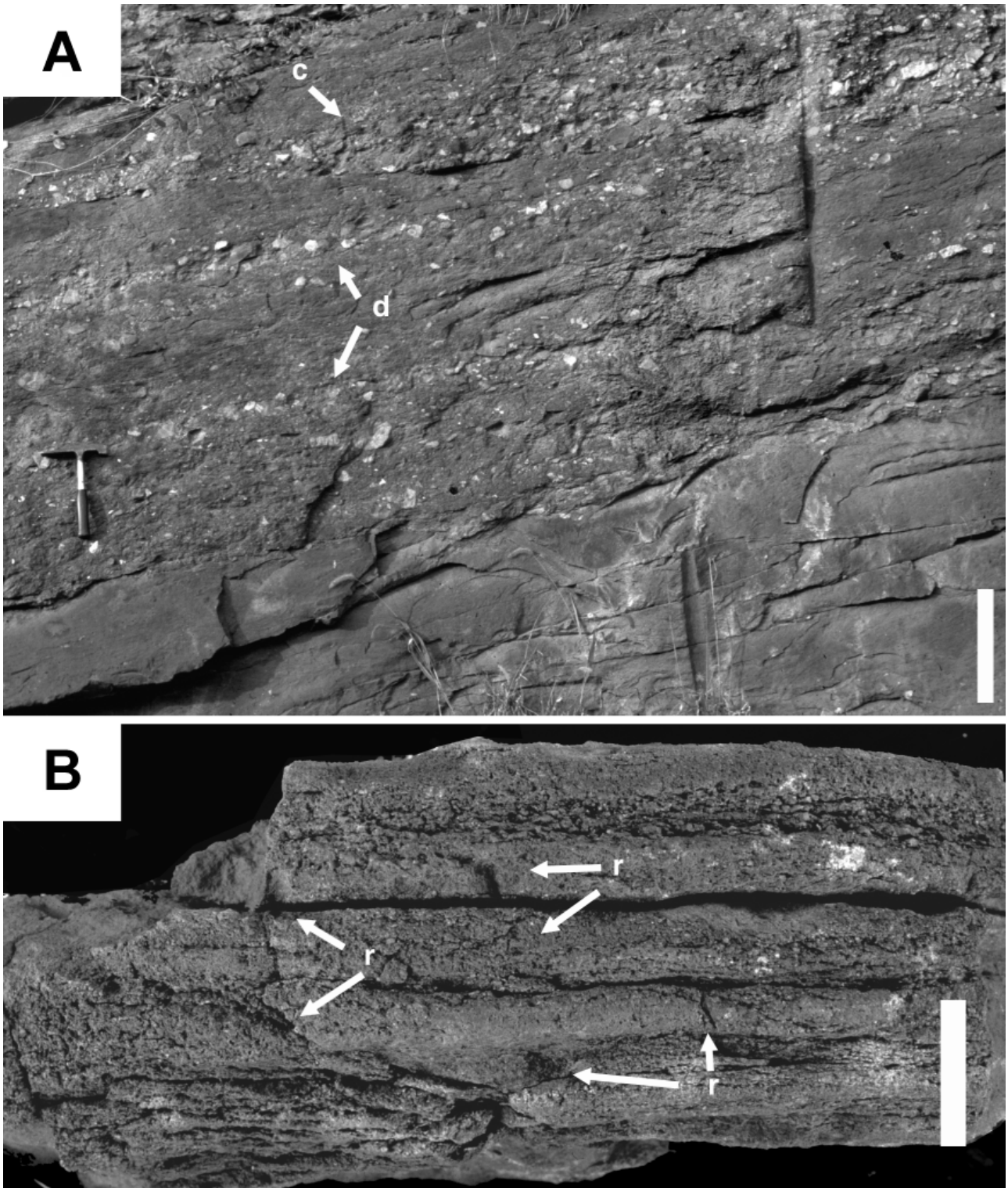

Figure A70. Border conglomerate distal facies. A. Outcrop of interbedded pebble conglomerate and sandstone. Conglomerate includes broad channel lenses (c) and flat beds of isolated pebbles which are remnants of thin debris flows (d). Sandstone at base shows only remnant patches of bedding due to abundant root casts. Scale bar is 30 cm. B. Weathered outcrop sample of flat-bedded sandstone from outcrop above. Root casts (r) are distributed throughout. Scale bar is 1 cm. Locality 28, table A1, figure A4.

also consistent with the fan-toe setting in an arid or semi-arid setting, because vegetation tends to concentrate in those areas, taking advantage of the shallow, fresh groundwater at the intersection of porous alluvial fan deposits and fine-grained basinal deposits.

Axial sandstone and conglomerate

Sandstone and conglomerate are the dominant rocks at the northeastern and southwestern ends of the Newark basin, along strike with central basin mudstone of the Lockatong and Passaic Formations. These deposits are mostly mapped as Passaic Formation (Parker and others, 1988), but include the Hammer Creek Formation at the southwestern end of the Newark basin where it attaches to the "Narrow Neck" (fig. A1). Axial conglomerates are mostly poorly sorted, with grain-supported pebble- and cobble-sized clasts in coarse sandstone matrix. The pebble- and cobble-sized clasts are typically well-rounded and are dominated by quartzite, limestone, and Devonian conglomerate fragments at both ends of the basin. Conglomerate and sandstone form upward-fining successions that are 2-5 m thick with internal decimeter-scale trough cross-bedding and tabular cross-bedding (fig. A71). The trough cross-bedding is thicker where the rock is mostly pebble and cobble conglomerate and thinner where the rock is mostly sandstone. Paleocurrent directions in the trough cross-bedding indicate flow from the northeast basinward in the northeastern end of the basin and from the southwest basinward at the southwestern end of the basin. One or two upward-fining successions are typically separated by silty mudstone interbeds that are 5-20 m thick (fig. A72). In these mudstone interbeds, fine-grained sandstone commonly occurs as decimeter-thick beds that form 1-2-meter-thick upward-coarsening successions by increasing the thickness of sandstone beds and decreasing the thickness of mudstone between them. The mudstone and sandstone beds mostly lack internal layering and have abundant root casts and burrows. Some of the thicker sandstone beds have internal ripple cross-lamination or decimeter-scale tabular foresets that are heavily disturbed by burrows or root casts. Axial sandstone and conglomerate are less dominated by conglomerate and are interbedded with thicker mudstone along strike basinward from the northeastern and southwestern ends of the basin. At the northeastern end of the basin, coarser-grained axial sandstone and conglomerate overlie finer-grained axial sandstone and conglomerate as an upward-coarsening, basinward-thinning wedge that is about 3 km thick and extends basinward about 35 km. At the southwestern end of the basin, there is a suggestion of a similar upward-coarsening wedge in the axial sandstone and conglomerate that extends basinward about 10 km from the "Narrow Neck", with a thickness of about 1.5 km.

Axial sandstone and conglomerate in upward-fining sequences are interpreted as channel deposits of braided rivers. Trough cross-bedding forms by migration of dune-scale bedforms, and tabular foresets are consistent with mid-channel bars. The coarse grain size and poor sorting of the axial sandstone and conglomerate in upward-fining successions suggest that deposition occurred during short, high-discharge floods (Olsen, 1987). Unlike the border conglomerates, the provenance of the clasts suggests relatively large drainage areas and the dune-scale trough cross-bedding indicates lower flow-regime conditions. The poorly defined upward-fining successions, predominance of dune-scale trough cross-bedding mixed with tabular foresets, and dearth of ripple cross-lamination are all consistent with a low sinuosity, high-gradient, braided river environment. The interbedded silty mudstone deposits are not typical of high-gradient drainages, unless the coarse-grained channels avulsed in a broad muddy flood plain (like the anastomosing channels of Smith, 1983; and Makaske, 2001). The upward-coarsening sandstones within the silty mudstone units represent overbank and crevasse delta deposits in an avulsion flood plain (Kraus and Wells, 1999). Paleocurrent data indicate that the coarse-grained channels flowed parallel to the basin axis from the northeastern and southwestern ends of the basin. The net fining of channel deposits basinward from the ends, and the large-scale upward-coarsening successions, suggest that the axial sandstone and conglomerate were formed on terminal fans (Kelly and Olsen, 1993). Terminal fans are large-scale, fan-shaped fluvial deposits that form wedges into a basin terminating in fine-grained deposits.

Limestone

Limestone is a minor component of the Triassic rocks in the Newark basin (DeWet and others, 2002), although many of the laminated mudstones are rich in calcite. Beds of relatively pure limestone are most common in association with basin-margin rocks. These deposits were not carefully examined as part of this study, but are included for completeness. Three kinds of limestone are in the Triassic of the Newark basin: stromatolitic limestone, nodular limestone, and flat limestone thin beds. Stromatolitic limestone (fig. A73) is uncommon in the Triassic rocks and typically occurs at the contact between massive mudstone and laminated to thin-bedded mudstone (fig. A37). Stromatolitic limestone is also in mudstone associated with deltaic sandstone (fig. A73B). The stromatolitic lamination consists of alternating, dense, isopachous micrite and porous micrite with radial and vertical patterns of submillimeter carbonate-lined tubes. The stromatolitic

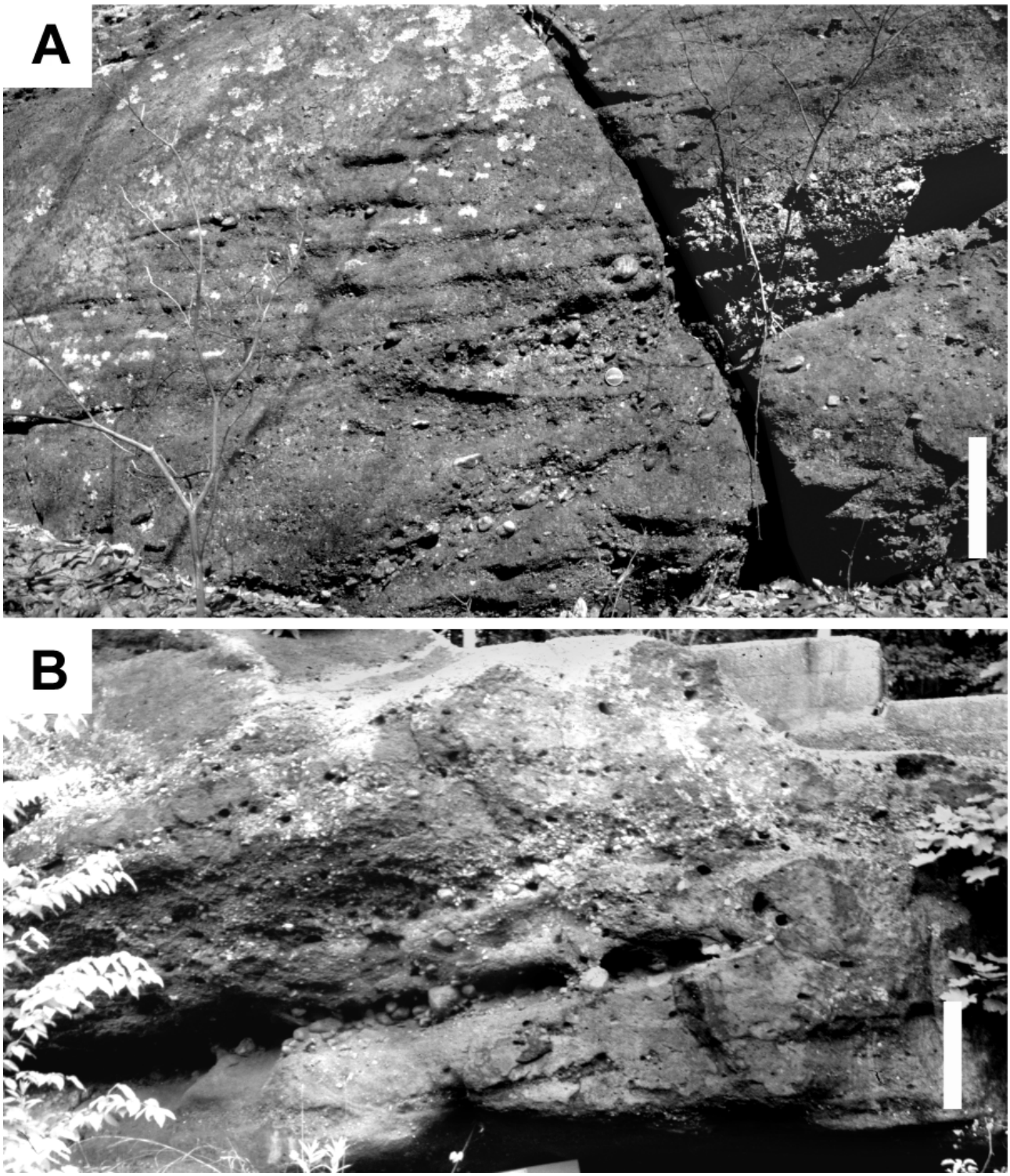

Figure A71. Axial sandstone and conglomerate. A. Outcrop of pebbly sandstone in Hammer Creek Formation. Trough crossbeds are overlain by tabular foresets. Paleocurrent was to right and into page. Scale is 50 cm. Locality 34, table A1, figure A5. B. Pebbly sandstone and conglomerate of the eastern end of the Newark basin. Trough cross-bedding shows flow was to the right and out of page. Scale is 50 cm. Locality 35, table A1, figure A3.

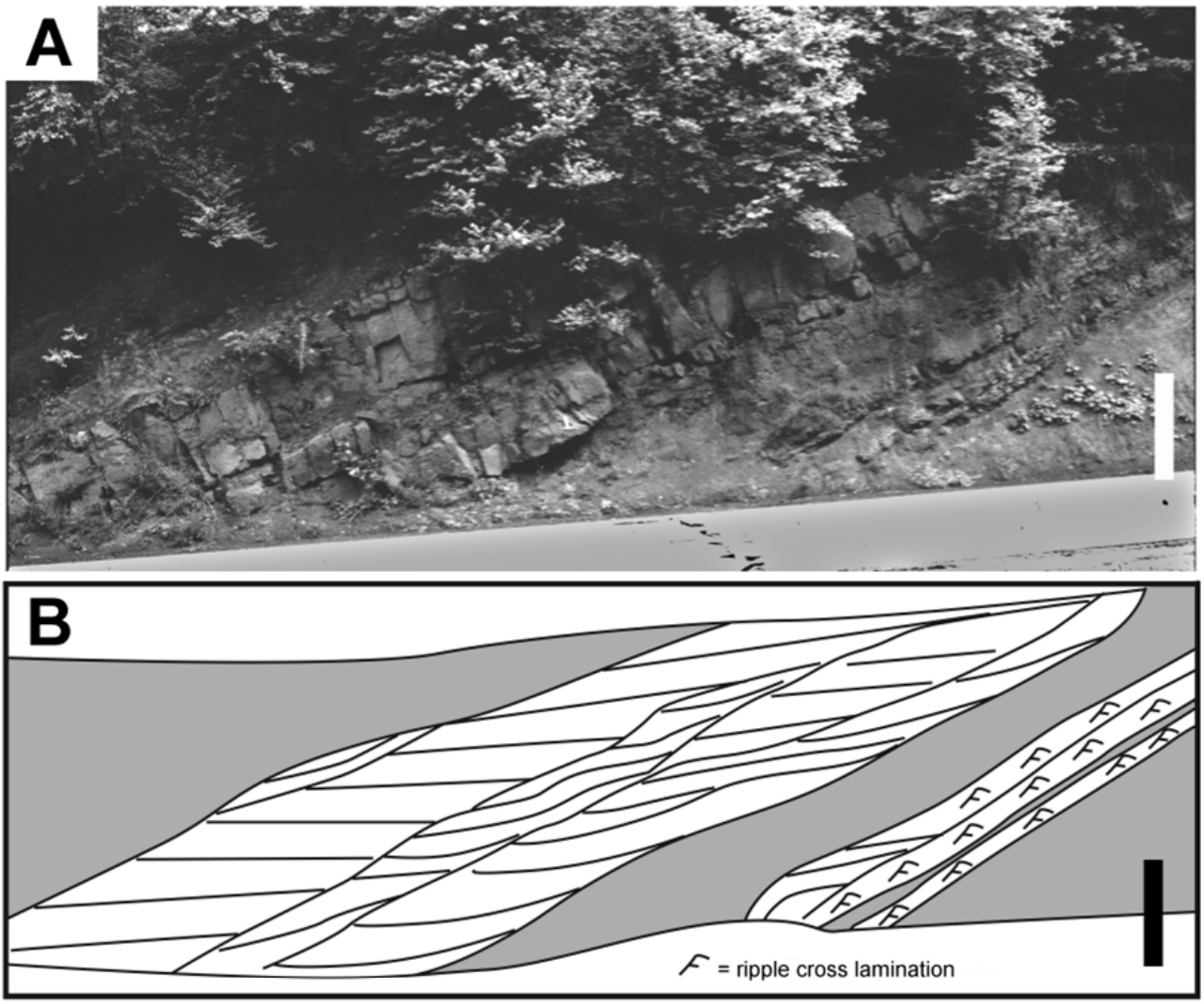

Figure A72. Axial sandstone and conglomerate. A. Outcrop of axial-drainage-facies pebbly sandstone and mudstone in the Hammer Creek Formation. B. Schematic drawing of sandstone and conglomerate (white) and mudstone and siltstone (gray) showing generalized character of internal stratification. Pebbly sandstone is composed of large dune-scale trough cross-bedding grading upward to smaller-scale dune cross-bedding. Thick tabular foresets near the top. Fine-grained sandstone in lower right comprises an upward-coarsening succession of ripple cross-lamination. Mudstone interbeds and the fine-grained sandstone are heavily bioturbated by root structures. Scale is 1 m. Locality 36, table A1, figure A5.

lamination mostly coats woody material or cover irregular surfaces. Siliciclastic sand grains associated with the stromatolitic limestone may have oolitic limestone coatings.

Nodular limestone forms beds within siliciclastic sediment that have a diffuse lower contact and a more dense upper contact (fig. A74). Centimeter-scale nodules may be randomly scattered in the sediment or concentrated into vertical stacks that outline sediment-filled root casts. The upper contact of a nodular limestone bed may be nearly pure limestone with a smooth upper surface and common fractures filled with isopachous lamination (Olsen and Rainforth, 2001, fig. 20). Micrite nodules in nodular limestone commonly have sharp edges, but may also have edges that diffuse into the surrounding sediment. In thin section, the micrite contains small spar-lined tubules and cracks in a clotted micrite matrix with floating grains of silt and sand.

Flat limestone thin beds (fig. A74C) are sheet-like deposits commonly in root-disrupted massive mudstone. The beds have relatively sharp tops and bases and commonly are extensively disrupted by sediment- and spar-filled tubes. The beds consist of micrite and varied mixtures of siliciclastic clay and silt. Thin beds and laminae are visible in some samples (see DeWet and others, 2002); they are defined by concentrations of silt or fine sand, changes in the

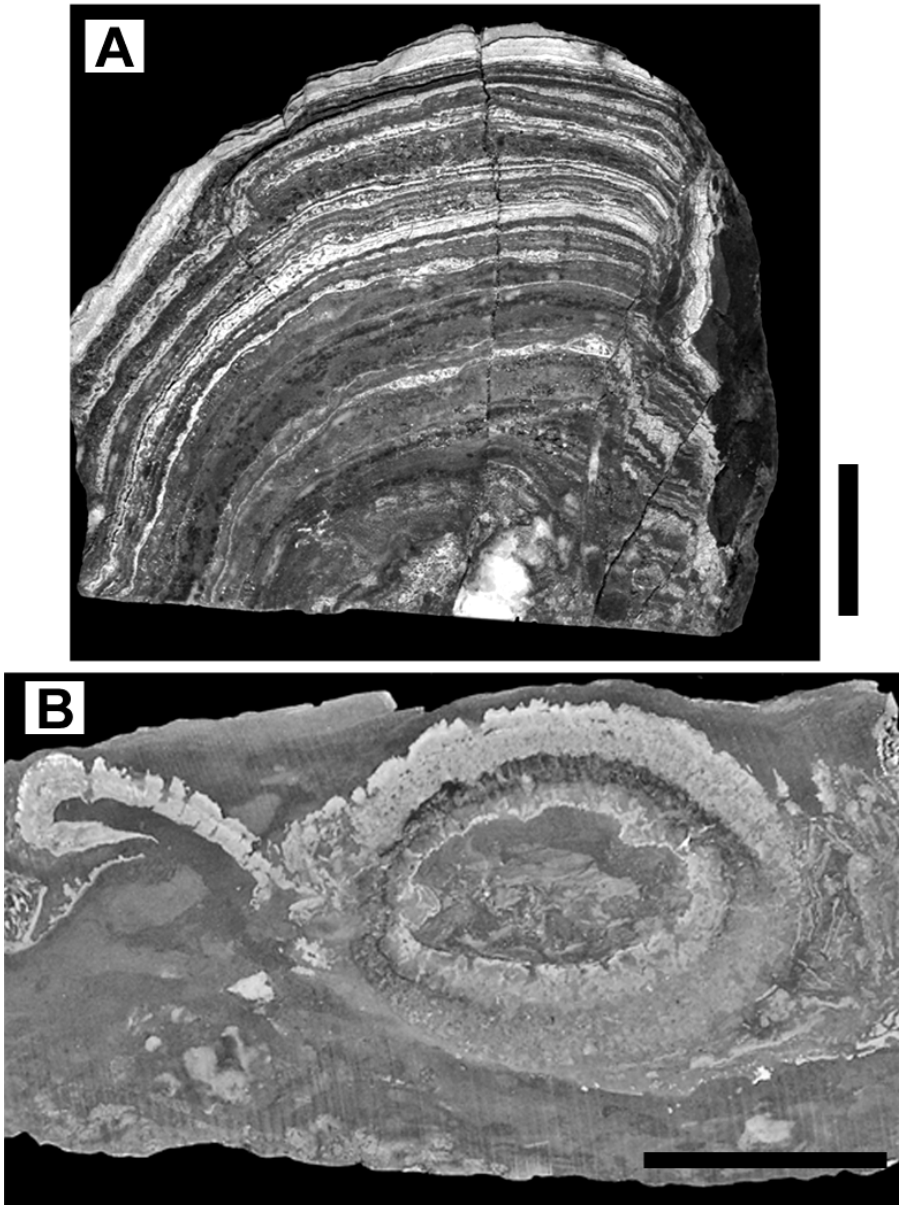

Figure A73. Stromatolitic limestone in the Triassic of the Newark basin. A. Slabbed sample of stromatolitic limestone in the Metlars Member of the Passaic Formation. Light bands are primarily micrite, and the dark bands consist of micrite forming vertical fabrics separated by coarse sparry cement. The lamination overlies the cast of a wood fragment which is chiefly spar-filled (white) but includes some carbonized material (black). Scale bar is 1 cm. Locality 24, table A1, figure A5. B. Slabbed sample of stromatolitic limestone in the Smith Corner Member of the Lockatong Formation. Strong vertical fabric consists of micrite separated by sparry cement. Layering is defined by variations in the amount of micrite or spar. Circular feature to the right is a sediment filled cast of wood coated by stromatolitic limestone. To the left, more micrite-rich stromatolitic limestone overlies an irregular surface of burrowed muddy siltstone. Intraclasts of stromatolitic limestone occur near the base of the sample. Scale bar is 5 cm long. Locality 37, table A1, figure A5. Photo courtesy of Paul Olsen, Lamont-Doherty Earth Observatory of Columbia University.

amount of siliciclastic clay, or in concentrations of ostracodes.

Limestone in the Triassic of the Newark basin primarily formed in areas with low sedimentation rates. Stromatolitic limestone was deposited in shallow shoreline areas during periods of lake transgression. The stromatolites are chemical deposits formed by precipitation of calcite around algal mats (Bertrand-Sarfati and others, 1994). The rarity of these deposits in the Triassic of the Newark basin suggests that their development was controlled by local processes, such as spring-water mixing (Casanova, 1994; DeWet and others, 2002). Nodular limestone is interpreted as soil concretions formed by chemical reworking of dust into the soil K horizon (Retallack, 2001). The accumulation of carbonate in a soil reflects the relative length of time of soil development if there are no changes in source material or climate (Birkeland, 1999; Retallack, 2001). The development of carbonate pavements with internal fractures and lamination are late-stage soil carbonate features (Machette, 1985).

Flat limestone thin beds are interpreted as lake deposits where carbonate accumulated as cumulus crystals. Most of the layering observed in the flat limestone thin beds indicates either intermittent wave action that eroded the underlying strata, or concentrated coarser grain sizes or changes in the suspended siliciclastic sediment in the lake. The sediment- and spar-filled tubes in the flat limestone thin beds appear to be root casts following the criteria for the root-disrupted massive mudstone. In places, flat limestone thin beds with ostracodes overlie nodular limestone beds, suggesting that the soil carbonates may have provided poor local drainage and shallow lake development (see

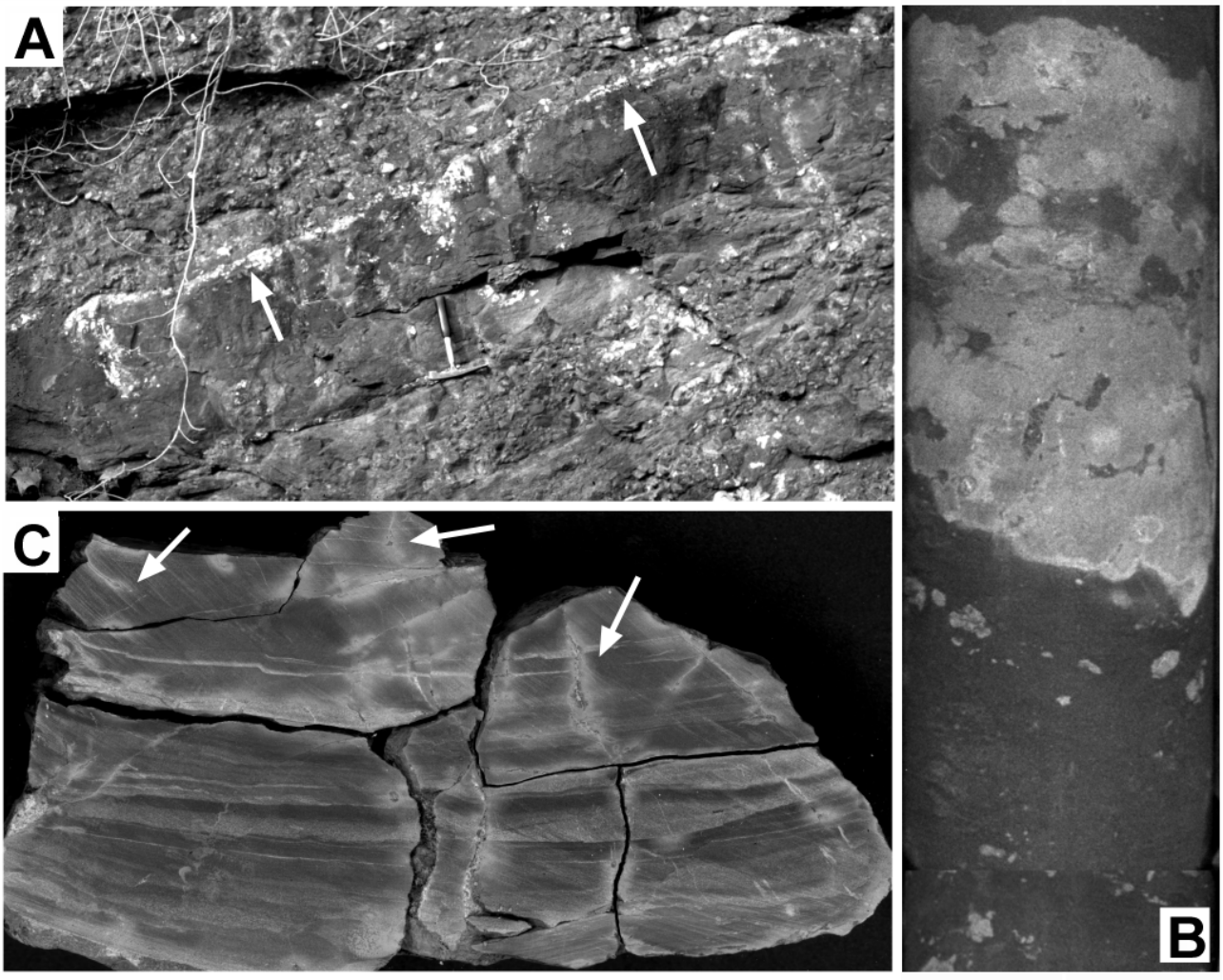

Figure A74. Limestone in the Triassic of the Newark basin. A. Nodular limestone in a border conglomerate and sandstone. Thin layer (arrows) consists of amalgamated nodules. Vertical projections of nodules below the layer are interpreted as root casts lined by carbonate nodules. Hammer is 35 cm long. Locality 28, table A1, figure A4. B. Nodular limestone (light) forms a layer in micaceous siltstone and mudstone of the Stockton Formation. Layer is composed of spherical micrite nodules that are amalgamated. Note sediment within the limestone layer and isolated nodules in the mudstone. Princeton core interval 2188-2189 ft. Locality 1, table A1, figure A3. C. Slabbed outcrop sample of a 10 cm-thick flat limestone bed from the upper part of the Passaic Formation (Member SS?). Limestone layering consists of alternating fine-grained clay-rich limestone (dark) and coarser-grained limestone (light) that contains siliciclastic sand grains. Coarse layers form pinch-and-swell lamination. The upper part of the bed has only faint lamination and abundant root casts (arrows). Thickness shown is about 6 cm. Locality 38, table A1, figure A5.

Olsen and Rainforth, 2001, p. 94). Thin lacustrine limestone beds with pedogenic overprints probably indicate shallow lakes in areas with low clastic sediment input (for instance, Armenteros and Huerta, 2006).

Stratigraphic and geographic distribution of facies

This discussion highlights details of lithofacies distribution that are visible in maps (figs. A3, A4 and A5) as well as features that do not show on these maps. Lithofacies variations include those controlled by geographic location as well as those that reflect changes in climatic or tectonic conditions through time. The fault blocks and other locations discussed below are shown in figure A1.

Stockton Formation

The Stockton Formation differs radically in thickness in different parts of the basin. The thickest

Stockton Formation section (about 1800 m) appears to be in the northwestern fault block, from there the unit appears to thin both toward the southeastern unconformable margin of the basin and toward the northeast and southwest ends of the basin. The Princeton core, located in the southeastern fault block (fig. A3, table A1), penetrated about 870 m of Stockton Formation, ending about 100 m above the unconformable contact with basement (Olsen and others, 1996). The small exposure of Stockton Formation in the northeastern fault block appears to be thinner than the exposed sequence in the northwestern fault block. The 85SD10 seismic line (as interpreted by Reynolds, 1993) shows significant thinning of the Stockton Formation towards the border fault and its complete absence on a basement block at the border fault (fig. A6C). The NB-1 seismic line (as interpreted by Schlische and Withjack, 2005), in contrast, shows strata equivalent to the exposed Stockton Formation thickening toward the faulted basin boundary (fig. A6B). Reynolds (1993) earlier examined the same NB-1 seismic line and concluded that the Stockton Formation fluvial deposits grade into lacustrine strata downdip toward the border fault.

The distribution of different lithologies in the Stockton Formation is only roughly known. McLaughlin (1945) mapped ridge-forming units of the Stockton Formation in the northwestern fault block that are dominated by arkosic sandstone or conglomerate and conglomeratic sandstone. The intervening depressions are dominated by micaceous sandstone, siltstone, and mudstone. McLaughlin was able to trace the ridges laterally for as much as 30 km in the northwestern fault block, but was unable to recognize similar ridge patterns in the southwestern fault block, presumably due to poor exposure. McLaughlin (1945, 1959) noted that the Stockton Formation is generally coarser-grained towards the basal unconformity and that it is progressively finer-grained upsection. Micaceous sandstone, siltstone, and mudstone units, however, are also interbedded with the coarser ridge-forming deposits, but as thinner units. Rima and others (1962) focused on the Stockton Formation in the southeastern and southwestern fault blocks. They divided the formation into three members: a lower arkose member dominated by coarse sandstone and conglomerate with interbeds of siltstone and mudstone, a middle arkose member with roughly equal abundance of medium- to fine-grained sandstone, siltstone, and mudstone, and an upper shale member dominated by red mudstone and siltstone. These members are roughly equivalent to the conglomerate and conglomeratic sandstone, arkosic sandstone, and micaceous sandstone, siltstone, and mudstone lithologies described earlier. The maps of Rima and others (1962) show little continuity of beds and lateral intertonguing of the members, including a radical thickening of the coarse sandstone and conglomerate near Rambler, Pennsylvania in the southwestern fault block that intertongues laterally with finer-grained deposits within a few kilometers to the northeast and the southwest. Olsen and others (1996) noted that the Princeton core has sections many tens of meters thick consisting chiefly of conglomerate, conglomeratic sandstone, and coarse- to fine-grained sandstone that alternate with sections of similar thickness consisting chiefly of fine-grained sandstone, siltstone, and mudstone. They suggested that these alternations are equivalent to the ridge-forming units and finer-grained intervals mapped by McLaughlin (1945). Their correlation suggests that the ridge-forming sandstones in the northwestern fault block can be traced over 30 km to the southeast. Olsen and Rainforth (2001) divide the upper 190 m of the Stockton Formation in the Princeton core into eight subunits, with gray or black rocks at the base and red rocks at the top. They suggest that these alternations are similar to McLaughlin cycles in the Lockatong and Passaic Formation. The gray or black rocks include mudstone, sandstone, and conglomerate. Based on his interpretation of the NB-1 seismic line, Reynolds (1993) argued that the Cutaloosa Member of McLaughlin (1945) overlies an angular unconformity in the Stockton Formation. LeTourneau (2003) also inferred a stratigraphic break in the Stockton Formation at the base of the Cutaloosa Member, based on his correlation of magnetic reversals in the Taylorsville basin to those in the Newark basin. There is no direct evidence of this inferred unconformity in outcrops of the Stockton Formation.

The distribution of rock types in the Stockton Formation also varies in the basin. Rima and others (1962) indicate lithologies equivalent to conglomerate and conglomeratic sandstone dominating the lowest 450-900 m of the Stockton Formation in the southwestern fault block, whereas the Princeton core described by Olsen and others (1996) accounts for only about 240 m of conglomerate and conglomeratic sandstone in the southeastern fault block (including about 100 m of uncored section from the base of the core to the basal unconformity with basement rocks). The measured thickness of predominately conglomerate and conglomeratic sandstone in the northwestern fault block is about 400-700 m (McLaughlin, 1945). Micaceous sandstone, siltstone, and mudstone are intimately interbedded with the conglomerate and conglomeratic sandstone in beds that are 2-20 m thick. Conglomerate and conglomeratic sandstone also appear to dominate the Stockton Formation where it thins at the northeastern and southwestern ends of the basin. Upward-fining arkosic sandstone sequences in the northwestern fault block dominate four ledge-forming units that are 150, 60, 120, and 110 m thick (McLaughlin, 1945). These ledge-forming units are separated by micaceous sandstone, siltstone, and

mudstone-dominated intervals that are 135, 115, and 240 m thick and are overlain by a section of micaceous sandstone, siltstone, and mudstone that is over 200 m thick. The middle arkose member of Rima and others (1962), in the southeastern fault block, is about 200 m thick and presumably about half is composed of arkosic sandstone and half of micaceous sandstone, siltstone, and mudstone. This is overlain by the upper shale member that is about 100 m thick. For the Princeton core, Olsen and others (1996) indicate 610 m of Stockton Formation, with mostly arkosic sandstone in upward-fining sequences and relatively thin interbeds of micaceous sandstone, siltstone, and mudstone. The upper 100 m of the Stockton Formation in the Princeton core is dominated by the finer-grained rocks. Descriptions of the Stockton Formation in the northeastern fault block by Drake and others (1996) suggest that an undetermined thickness of the upward-fining arkose is also present there.

The distribution of micaceous sandstone, siltstone, and mudstone deposits in the Stockton Formation indicates that most of the basin floor, even in areas with high-gradient braided river channels, was covered by a muddy flood plain throughout deposition. The distribution suggests that braided-river and meandering-river-channel belts were separated by avulsion flood plains similar to anastomosing river systems (Smith, 1983; Makaske, 2001). Braided-river-channel belts appear to be stratigraphically older than meandering-river-channel belts at any one locality, but the relative proportion of the total thickness of the Stockton Formation dominated by the braided channels decreases towards the northwestern border fault of the basin. The percentage of the Stockton Formation dominated by micaceous sandstone, siltstone, and mudstone increases toward the northwestern border fault.

The published record on the Stockton Formation at this time (2010) is not detailed enough to clarify the geometry of the various lithofacies in it. To guess at possible geometries, it is necessary to choose among several models that explain the known record. The relative ages of the deposits are mostly unknown outside of the broad constraints of paleontology. Schlische (1992) argued that the NB-1 seismic line (fig. A6B) shows the Stockton Formation onlapping the unconformable basin margin so that the basal deposits on the southeastern margin are younger than those exposed in the northwestern fault block. He also explains the thinning of Stockton Formation on the northeastern and southwestern ends of the basin as evidence of onlap. The implication of this interpretation is that conglomerate and conglomeratic sandstone in the Stockton Formation are laterally equivalent to arkosic sandstone (fig. A75A). The correlation of the ridge-forming sandstone members of McLaughlin (1945) to sandstone and conglomerate units in the Princeton core by Olsen and others (1996) suggests that the Stockton Formation thins toward the southeastern basin margin while maintaining the same succession of lithologies (fig. A75B). The implication of this interpretation is that thinning is more a function of accommodation space than of onlap. Several early workers in the Stockton Formation interpreted the conglomerate and conglomeratic sandstone as alluvial fan deposits (Rima and others, 1962; Glaesser, 1966; Savage, 1967, 1968; Allen, 1979), and Rima and others (1962) suggested that the thick section of the Stockton Formation near Rambler, Pennsylvania was an alluvial fan lobe deposit. Most, if not all, of this apparent increase in thickness, however, is due to structural complications (Schlische, 1992) rather than depositional patterns. Reynolds (1993) in his interpretation of the NB-1 seismic line (fig. A6B) argued that parallel reflectors in the Stockton Formation near the western border fault indicate a more lacustrine character. Olsen and others (1996) suggested that gray siltstone and mudstone beds in the Stockton Formation are lateral equivalents of thicker lacustrine units downdip near the western boarder fault. If lacustrine onlap is interstratified with the fluvial deposits, the observed alternation of coarser-grained and finer-grained deposits may represent shifts in local base level rather than the more arbitrary channel avulsion model. Several different scenarios for the geometry of Stockton Formation lithologies are discussed below.

If the outcrop pattern of the Stockton Formation lithologies is due to onlap (fig. A75A), then the smaller braided channels must have coalesced into larger meandering channels toward the central basin. On the other hand, if the outcrop pattern of the Stockton Formation is due to decreased accommodation space away from the border fault (fig. A75B), then larger, more closely spaced braided channels in the southeastern end of the basin split into smaller, more widely spaced channels toward the basin center, with wider areas of avulsion flood plain. In this model, the southeastern margin of the basin was an area of frequent erosion and reworking, and the northeastern and southeastern ends of the basin received very little sediment. This model also suggests that the meandering river channels belts are separated by larger amounts of avulsion deposits in the central basin than at the southeastern unconformable margin, and that the youngest deposits of the Stockton Formation are absent near the northeastern and southwestern ends of the basin. If the distribution of coarse-grained and fine-grained lithologies is controlled by lake transgressions and regressions (fig. A76), the micaceous fine sandstone, siltstone, and mudstone units consist of laterally continuous units that thin toward the southeastern basin margin, and separate units that have more abundant sandstone or conglomerate lenses.

The vertical and lateral scales of conglomerate

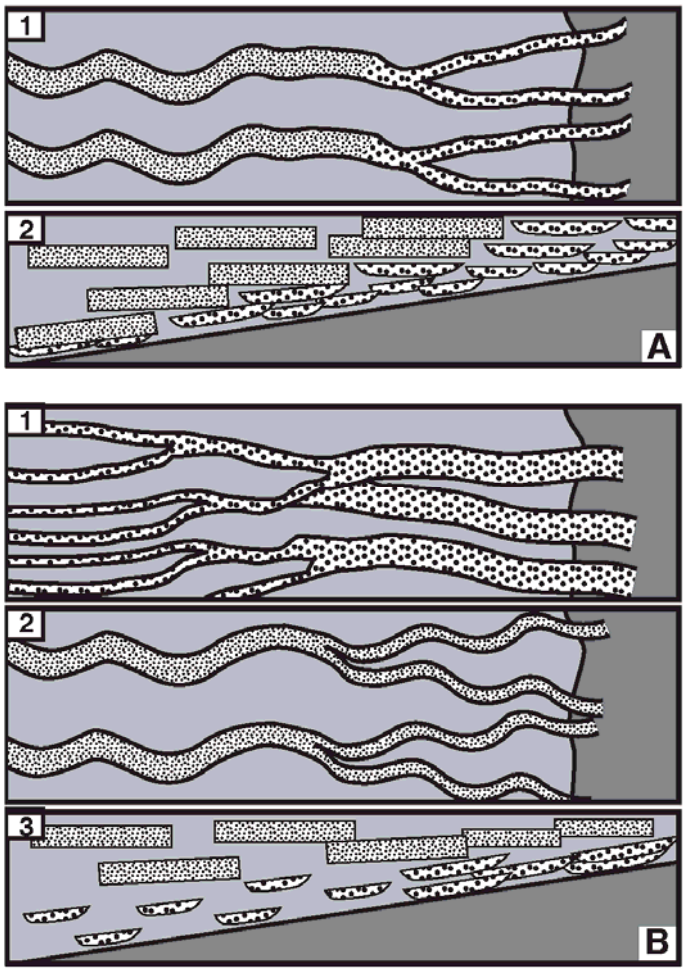

Figure A75. Schematic representation of channel deposits in the Stockton Formation, assuming that the micaceous sandstone, siltstone, and mudstone lithology is primarily the result of random avulsion. A. Channel distribution if thinning of the Stockton Formation to the southeast (right) was due to relative, progressive onlap onto basement rocks (dark gray). (1) Low-sinuosity conglomeratic channel deposits (coarse stippling) coalesce basinward to form larger channels that become more sinuous basinward and form meandering river channel belts (fine stippling). (2) In cross section, small lenses of conglomeratic sandstone are laterally equivalent to larger lenses of conglomeratic sandstone and progressively larger sheets of arkosic sandstone from the onlap contact into the basin. B. Channel distribution assuming that thinning of the Stockton Formation to the southeast reflects reduced accommodation space. (1) Early in basin development, large low-sinuosity rivers draining the southeast highlands split into numerous smaller branches basinward. (2) Later in basin development, small meandering rivers coalesced into larger meandering rivers basinward. (3) In cross section, a lower stratum consists of large conglomeratic lenses that are closely spaced near the southeast margin that correlate basinward with smaller, more widely spaced conglomeratic lenses that have more intercalated fine-grained deposits. An upper stratum consists of thinner, narrower meander belts of thin intercalated fine-grained deposits near the southeastern margin that correlate basinward with thicker, wider, arkosic meander belts of thicker, intercalated fine-grained sediment.

and conglomeratic sandstone or arkosic sandstone beds are not known. The ridges of sandstone and conglomerate mapped by McLaughlin (1945, 1959) are composite features with stratigraphic thicknesses of 60-150 m of multiple channel-fill deposits that are separated by relatively thin sequences of overbank deposits. The ridges are topographically distinct over lateral distances of 30 km. If the sandstone ridges represent a response to base-level fluctuations of a rising and falling lake, then it is reasonable to expect that coarse-grained channel deposits and finer-grained lacustrine and overbank deposits would show similar scale alternations that are laterally traceable everywhere in the subsurface, with a less pronounced differentiation in the southeastern part of the basin. This model also predicts that the sandstone beds are thinner and less abundant in the downdip areas that are near the northwestern border-fault margin of the basin. If the sandstone ridges are amalgamated channel belts randomly separated by avulsion plain deposits, their vertical and lateral expressions are less predictable. Gibling (2006) compiled data on the published dimensions of modern and ancient fluvial channel deposits. For mobile channel belts (channel systems not constrained by bedrock or valley walls), braided and low-sinuosity rivers have width-to-thickness ratios ranging between 20 and 20,000, whereas meandering rivers have width-to-thickness ratios ranging between 10 and 3000. The width-to-thickness ratio trends toward higher numbers in areas of lower subsidence, and it trends toward lower numbers where channels are more like delta distributaries. Sedimentary data for the Stockton Formation indicate conditions are more likely that result in narrow, thick channel belts in the central basin and slightly wider and thinner belts toward the southeastern basin margin. The data of Gibling (2006) show that most of the low-sinuosity rivers have width-to-depth ratios between 100 and 1000. If the Stockton Formation's braided channels on the southeastern margin had similar dimensions, the conglomerate and conglomeratic sandstone channel lenses (2-5 m thick) would have widths of 200-5000 m in cross sections perpendicular to flow. In contrast, arkosic sandstone in upward-fining sequences (10-15 m thick) would have widths of 300-3000 m in cross sections perpendicular to flow. The mappable ridges are oriented perpendicular to flow and are more than ten times wider, supporting the model where channel

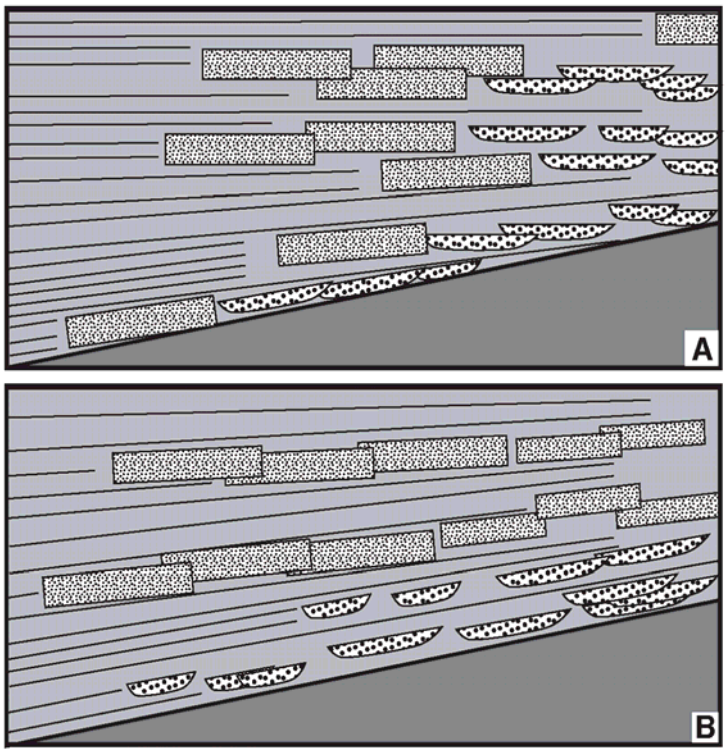

Figure A76. Schematic representation of channel deposits in the Stockton Formation, assuming that the micaceous sandstone, siltstone, and mudstone lithology is primarily controlled by lake transgression and regression on the northwestern end of the basin. A. Cross section of conglomeratic sandstone lenses (coarse stippling) and arkosic sandstone meander belts (fine stippling) if thinning of the Stockton Formation to the southeast was due to progressive onlap onto basement rocks (dark gray). Lenses of conglomeratic sandstone are laterally equivalent to sheets of arkosic sandstone separated by continuous beds of lacustrine mudstone (parallel black lines) toward the northwestern edge. The coarse-grained stratigraphic units are separated by lacustrine mudstone. B. Cross section of conglomeratic sandstone lenses and arkosic meander belts if thinning of the Stockton Formation to the southeast reflects reduced accommodation space in the subsiding basin. Lower stratigraphic units are dominated by conglomeratic sandstone lenses that are thinner and more widely spaced basinward, whereas upper stratigraphic units are dominated by arkosic sandstone sheets that are thinner and narrower near the southeastern basin margin.

development is punctuated by changing base level rather than by random channel avulsion.

The final problem in the distribution of Stockton Formation lithologies is the possibility of lateral correlation to Lockatong Formation lithologies. Reynolds (1993) argued that seismic reflectors equivalent to the Stockton Formation are more continuous near the border faults, indicating a lateral change to lacustrine deposits. This is similar to the facies models of Faill (1973, 2003, and 2005) and Turner-Peterson (1980) wherein the Stockton Formation is a lateral facies of the Lockatong Formation. Rocks previously mapped as Stockton Formation in the northernmost part of the southeastern fault block include sandstones with sedimentary features indicating deltaic and wave deposition that are correlative to mudstone in the lower part of the Lockatong Formation (see discussion below). Parker and others (1988) show sandstones of Stockton Formation lithology overlying and laterally equivalent to the Lockatong Formation. Olsen and Rainforth (2001) correlate conglomerate and conglomeratic sandstone near the northeastern end of the basin in New York to the Nursery or Ewing Creek Members of the Lockatong Formation. They argue that the coarse-grained deposits are on strike with cyclic Lockatong mudstone and that they have “hints of lacustrine influence”. The Ravens Rock Member of McLaughlin (1945) contains gray mudstone with conchostracans, and sandstone with clinoform delta features, both indicating lacustrine conditions. In the Princeton core, the upper 200 m of the Stockton Formation contains numerous clay-rich gray and purple mudstones that may be lacustrine. These data indicate that, at least during the final stage of the Stockton deposition, the fluvial deposits were covered by lakes. There are no observations, however, that distinguish between small lakes on extensive avulsion flood plains and large bodies of water that inundated most of the basin floor.

Lockatong and Passaic Formations – central basin facies

The central basin facies of the Lockatong and Passaic Formations are characterized by Van Houten cycles and McLaughlin cycles. The central basin facies of the Lockatong and Passaic Formations intertongue with basin margin facies at the northeastern and southwestern ends of the basin, along the northwestern border fault of the basin, and along the basal contact of the Lockatong Formation with the Stockton Formation. Detailed mapping has demonstrated that at least several of the organic-rich laminated mudstone beds of the Lockatong and Passaic Formations are continuous for more than 75 km, and comparison of detailed measured sections indicates that thin-bedded mudstone and massive mudstone features have lateral continuity on the scale of 30 km or more (McLaughlin, 1946; Olsen, 1988; Olsen and others, 1996). McLaughlin cycles are distinguished in outcrop by the succession of laminated and thin-bedded mudstone in the Van Houten cycles,

and by the type of massive mudstone units within them. Although the lateral continuity of every McLaughlin cycle has not been verified in outcrop, those within overlapping sections of the Newark Coring Project and the cores at the NAWC site (fig. A4) can easily be matched. Several McLaughlin cycles with very distinctive patterns of organic-rich laminated mudstone have been mapped throughout most of the Newark basin (figs. A3 through A5), and some of those have been verified by measured magnetic reversals in core and outcrop (for instance the Perkasie Member and the Ukranian Member, Olsen and others, 1996). Most of the members of the Lockatong Formation are distinguishable in large parts of the basin floor, except for the Wilburtha and Scudders Falls Members. The Nursery Creek Member is easily the most readily traceable McLaughlin cycle in the Lockatong Formation. In the Passaic Formation, the Warford, Graters, Perkasie, Neshanic, Kilmer, Livingston, Metlars, Cedar Grove, Ukranian, Pine Ridge, and Exeter Township Members are all traceable throughout much of the basin. In general, Van Houten cycles tend to be thicker in the central and northwestern fault blocks than in the southeastern and southwestern fault blocks (Schlische, 1992). There is a decided thinning of Van Houten cycles in the lower part of the Lockatong Formation toward the northeastern end of the Newark basin (Olsen and others, 1996). The thickness of a Van Houten cycle is commonly proportional to the thickness of laminated mudstone within it, but thin-bedded mudstone or massive mudstone components may be missing in thinner parts of these cycles.

Smoot and Olsen (1994) described five general types of Van Houten cycles, based on descriptions from the Newark Coring Project cores (figs. A77 through A80): 1) cycles dominated by organic-rich laminated

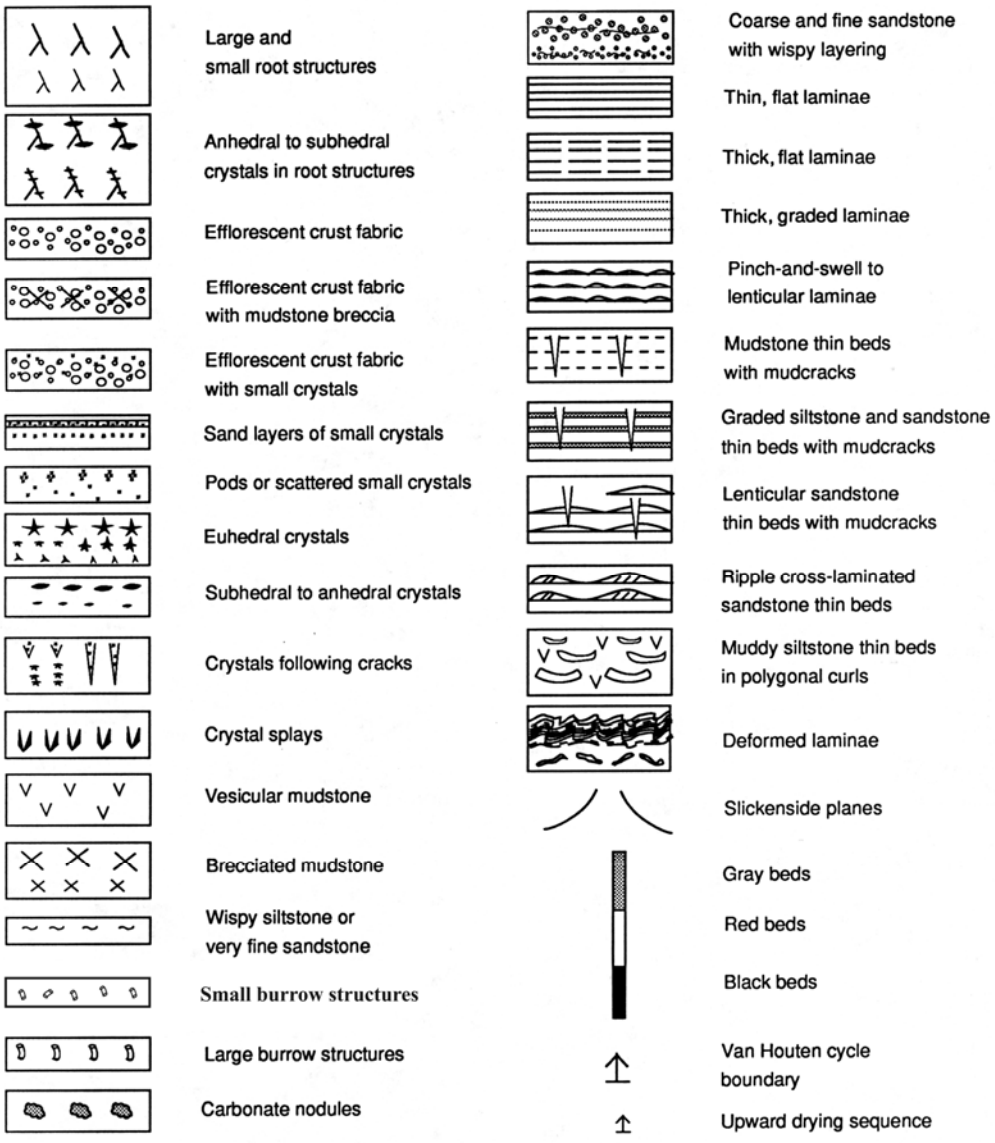

Figure A77. Explanantion of symbols used for cores in figures A78 through A80.

mudstone grading into thin-bedded mudstone and peloidal massive mudstone at the top (figs. A78A and A81), 2) cycles similar to the first type but with more thin-bedded mudstone, brecciated massive mudstone, and evaporite pseudomorphs (fig. A78B and A82), 3) cycles with laminated mudstone or thin-bedded mudstone grading into brecciated massive mudstone and vesicular massive mudstone (figs. A78B and A82), 4) cycles similar to the previous type but with root-disrupted massive mudstone at the top (figs. A79A and A83), and 5) cycles dominated by root-disrupted massive mudstone (commonly with gypsum crystals) directly overlying laminated and/or thin-bedded mudstone (figs. A79B and A84). A sixth type of cycle in the central basin facies of the Lockatong and Passaic Formations (type VI) is less well documented. It consists of organic-rich laminated mudstone grading upward into thin-bedded mudstone that has abundant burrows and deep polygonal cracks (figs. A80 and A85). Type I cycles are common in the upper part of the Princeton and lower part of the Nursery Members and are present throughout the basal part of the Perkasie Member. Type II cycles are present in the upper part of the Princeton and lower part of the Nursery Members and are common in the upper part of the Nursery Member and through the lower part of the Perkasie Member. The stratigraphically highest occurrence of type II cycles is in the basal part of the Metlars Member. Type III cycles are common in the upper part of the Nursery Member through the Warford Member. Type IV cycles first appear in the Warford Member and are the dominant cycle through the base of the Perkasie Member and are present in the Metlars Member. Type V cycles dominate from the upper part of the Perkasie Member through the rest of the Passaic Formation. Type VI cycles are dominant in the lower part of the Princeton Member and possibly in the Scudders Falls and Wilburtha Members, which consist chiefly of mudstone in the central and northwestern fault blocks but are sandstone-rich where penetrated by the Princeton and Nursery cores. In each type of cycle, the succession of sediment types suggests a rise in lake level or increase in wetness, followed by a drop in lake level or increase in dryness. McLaughlin cycles are defined by groupings of Van Houten cycles, with greater thicknesses of laminated or thin-bedded mudstone in the lower Van Houten cycles, and greater thicknesses of massive mudstone in the upper Van Houten cycles. The McLaughlin cycle, therefore, mimics the pattern of greater wetness giving way to greater dryness in the Van Houten cycles, but at a greater thickness of section. The oscillation of wetness and dryness in the Van Houten and McLaughlin cycles is attributed to climate change, and the pervasive multi-level periodicity is cited as evidence of Milankovitch climate forcing (Olsen, 1986; Olsen and others, 1996).

Van Houten cycles in the central basin facies of the Lockatong and Passaic Formations commonly contain decimeter-scale successions of sedimentary fabrics that also appear to represent changes in water depth or changes in wetness and dryness (figs. A78 through A85). In some laminated mudstones, the decimeter-scale changes include gradations from flat very fine lamination to thicker lamination with some bioturbation, followed by lamination with pinch-and-swell layering, overlain again by flat very fine lamination. In some thin-bedded mudstone, the decimeter-scale changes include an increase in the number of bedding planes from which polygonal cracks extend downward in transition to brecciated massive mudstone overlain again by thin-bedded mudstone. In some massive mudstones, decimeter-scale alternations of brecciated massive mudstone and vesicular massive mudstone, or rooted massive mudstone with no gypsum, grade upward into root-disrupted massive mudstone with abundant gypsum, indicating changes in degree of dryness. The periodicity of decimeter-scale cyclic changes does not show up in the Fourier analyses of Olsen (1986). This may indicate that the changes are random, but the depth-rank model used by Olsen (1986) does not include variations in massive mudstone (they are all depth rank 0) so the pattern would only be intermittently sampled within the layered parts of Van Houten cycles.

Calcite pseudomorphs after evaporites, and cement-filled crystal casts, are stratigraphically separated from gypsum and anhydrite in the Newark basin. Calcite pseudomorphs and cement-filled crystal casts indicate deposition in saline lakes and saline mudflats, whereas gypsum and anhydrite consistently indicate root-disrupted saline soils. The first occurrence of calcite pseudomorphs and cement-filled crystals is in the upper part of the Princeton Member and they are common into the lower Van Houten cycles of the Perkasie Member of the Passaic Formation where they are almost always associated with peloidal massive mudstone. The same Van Houten cycles that have deltaic sandstone generally lack these features or have only minor occurrences. Cement-filled crystal casts are also found in the lowest Van Houten cycles of the Metlars Member of the Passaic Formation. Gypsum and anhydrite are absent from the lower Van Houten cycles of the Metlars Member and are common in the upper Van Houten cycles. Gypsum and anhydrite first occur in the upper Van Houten cycles of the Perkasie Member and are common in the rest of the Passaic Formation. Gypsum and anhydrite are rarely preserved in outcrop, and mudstone beds that had large amounts of these minerals tend to crumble in outcrop. Depositional gypsum and anhydrite appear to be scarcer or absent in mudstones that are near the northeastern or southwestern axial sandstone and conglomerate wedges or the border conglomerate and sandstone units. Gypsum and anhydrite also appear to be relatively

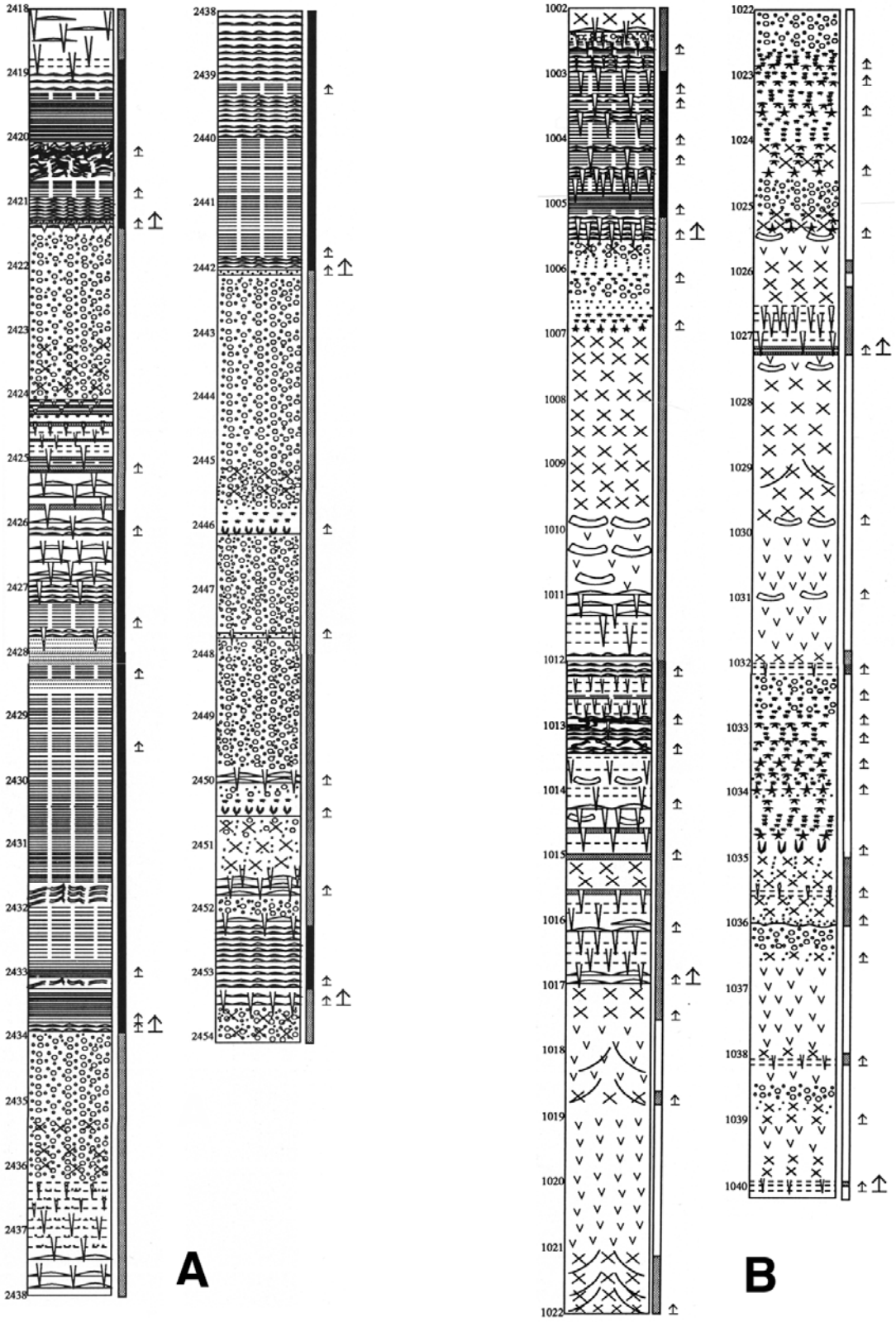

Figure A78. Examples of Van Houten cycles in the Lockatong Formation. A. An example of type I cycles in the Nursery Member. Nursery core interval 2418-2454 ft. Locality 2, table A1, figure A4. B. An example of type II and type III cycles in the Prahls Island Member and the base of the Smith Corner Member. The lowest Van Houten cycle is type II, whereas the overlying Van Houten cycle is type III. Nursery core interval 1002-1040 ft. Locality 2, table A1, figure A4. Sections are modified from Smoot and Olsen (1994).

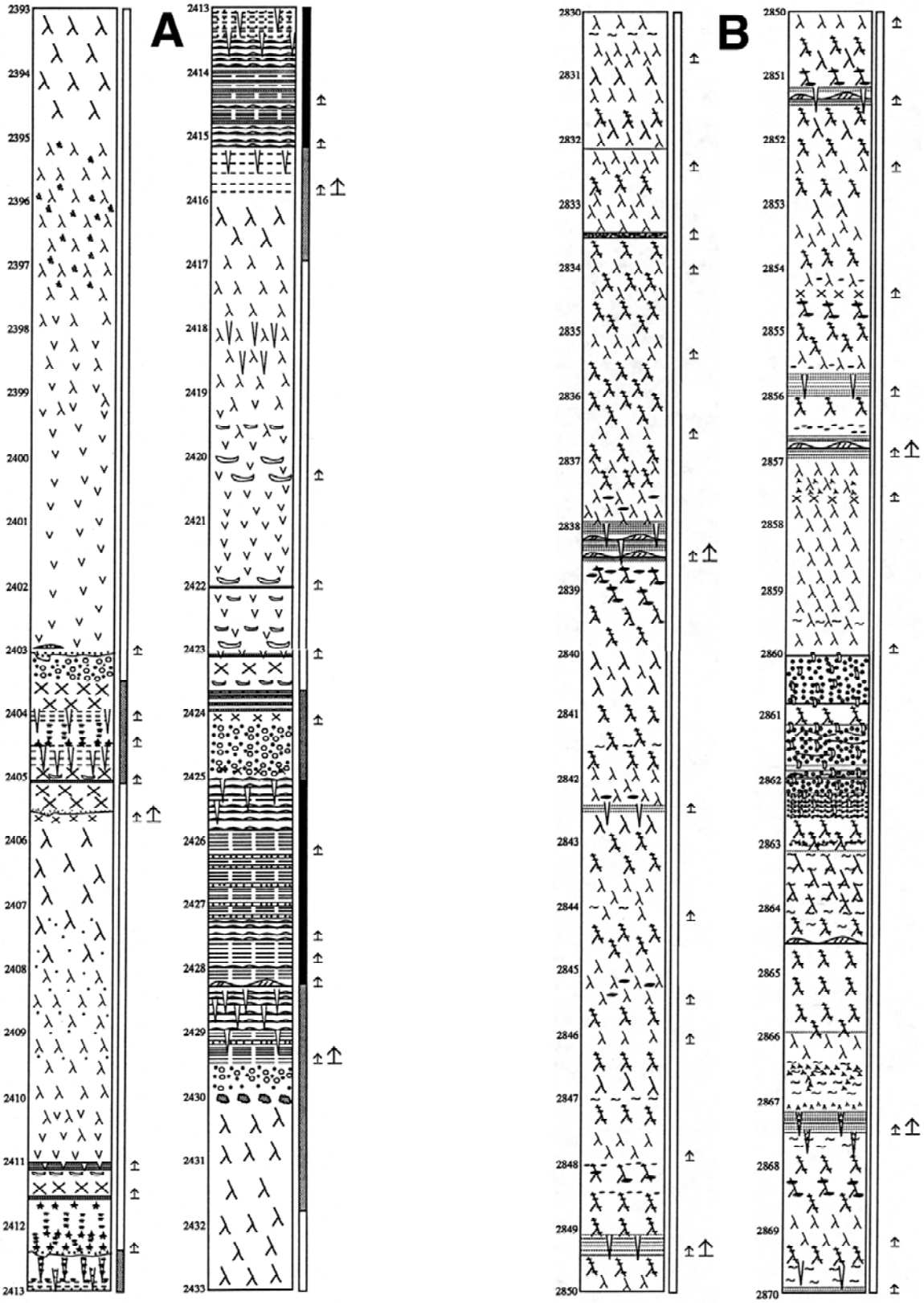

Figure A79. Examples of Van Houten cycles in the Passaic Formation. A. An example of type IV cycles in the Metlars Member. Somerset core interval 2395-2433 ft. Locality 5, table A1, figure A3. B. An example of type V cycles in Member PP. Martinsville core interval 2830-2870 ft. Locality 7, table A1, figure A3. Sections are modified from Smoot and Olsen (1994).

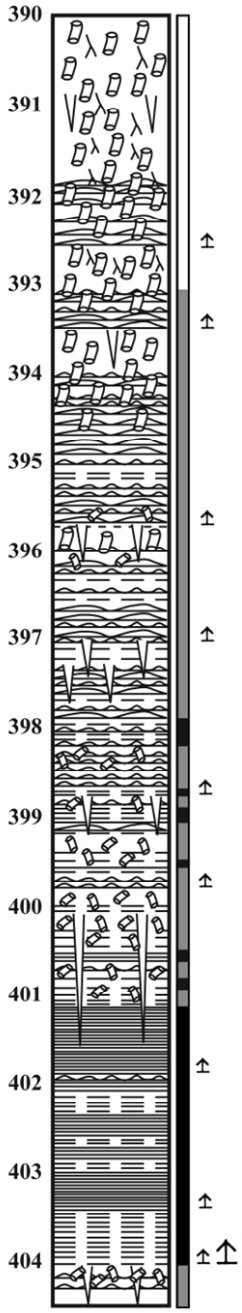

Figure A80. An example of type VI cycles in the Princeton Member of the Lockatong Formation. Princeton core interval 390-404 ft. Locality 1, table A1, figure A3.

unimportant in central basin mudstone exposed in the Jacksonwald syncline. This could be an artifact of preservation, but crystal molds were not observed in strata overlying the Metlars Member and they are uncommon in rocks of the Passaic Formation overlying the Perkasie Member directly south of the Jacksonwald syncline. In contrast, crystal molds after gypsum and anhydrite were observed in outcrops in the central and northwest fault blocks. This suggests that gypsum and anhydrite may be more abundant in the eastern part of the basin.

Lockatong and Passaic Formations – basin margin facies

The relationship between basin margin facies and central basin facies of the Lockatong and Passaic Formations is recognizable where they intertongue (figs. A5A and A5B), but it is less certain where mudstone is mostly replaced by sandstone or conglomerate. The distinctive patterns of Van Houten cycles in the central basin facies are obscured by sandstone and conglomerate beds of varied thickness, and it is likely that some cycles are locally eroded. Therefore, the discussion of the basin margin facies of the Lockatong and Passaic Formations is more concerned with broad stratigraphic zonations and their geographic distribution.

Four major sources of coarse-grained sediment in the Lockatong and Passaic Formations in the Newark basin are: 1) alluvial fans along the northwestern margin of the basin, 2) the southeastern margin of the basin, 3) axial drainage from the Narrow Neck and the southwestern end of the basin, and 4) axial drainage from the northeastern end of the basin. The distribution of wave-dominated sandstone and deltaic sandstone within Van Houten cycles is controlled by intercalation of lacustrine mudstone with coarse-grained deposits from these source areas.

Border conglomerate and sandstone deposits indicate alluvial fans that developed along the faulted northwestern margin of the basin. Border conglomerate and sandstone are stratigraphically equivalent to all of the members of the Lockatong and Passaic Formations. In the northwest fault block (fig. A1), border conglomerate appears to be on strike with at least the uppermost Stockton Formation. The interpretation of the NB-1 seismic line by Schlische and Withjack (2005) indicates that border conglomerate intertongues with the entire thickness of the Stockton Formation (fig. A6B). Border conglomerate is discontinuous along the northwestern border of the Newark basin, and areas along the border are occupied by sandstone and mudstone. This pattern is attributed to compressive folds with axes perpendicular to the border that expose vertical successions of conglomerate and finer-grained strata in anticlines and synclines. The stratigraphic alternations are on the scale of 200-300 m, consisting mostly of conglomerate near the border fault and mostly sandstone and silty mudstone a few kilometers from the boundary. In a few scattered localities, border conglomerate unconformably overlies basement. Lockatong directly overlies basement in the Parestis well (fig. A6C), and Paul Olsen (oral communication, 2007) noted the Perkasie Member of the Passaic Formation directly overlying basement near the northwestern border. Schlische (1992) interpreted this border as a series of fault segments with relay ramps connecting them. Rider blocks within these segments have Triassic sediments of different ages

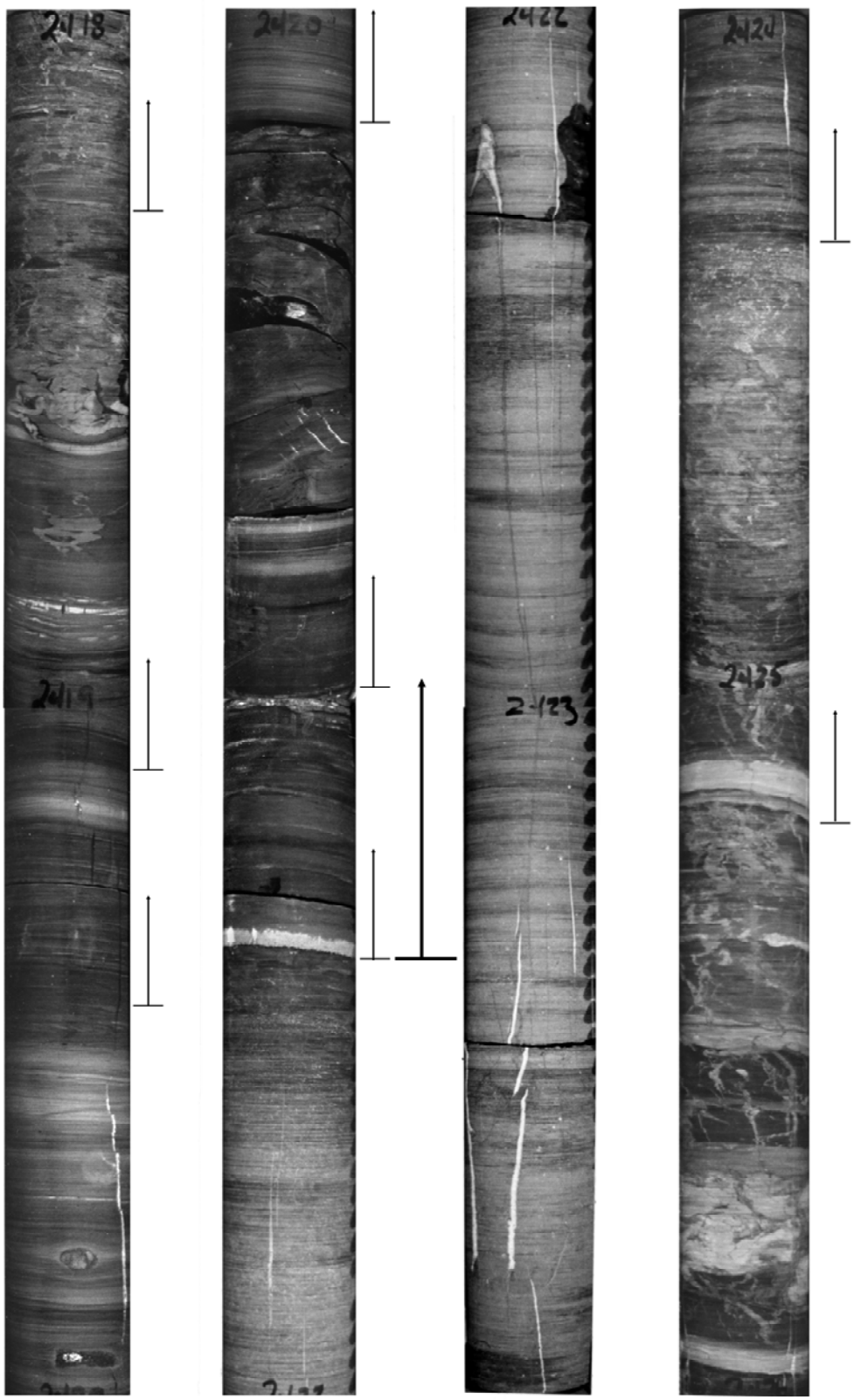

Figure A81. Type I cycles in the Nursery Member of the Lockatong Formation from the core interval illustrated in figure A78A. The large, heavy arrow shows a Van Houten cycle contact, and the smaller, thinner arrows denote the contacts of sedimentary sequences indicating shallower water or more desiccation upward. Note the abrupt transition from laminated mudstone to peloidal massive mudstone in the lower Van Houten cycle. Numbers on the cores are depths in feet below the land surface that are equivalent to depths in figure A78A.

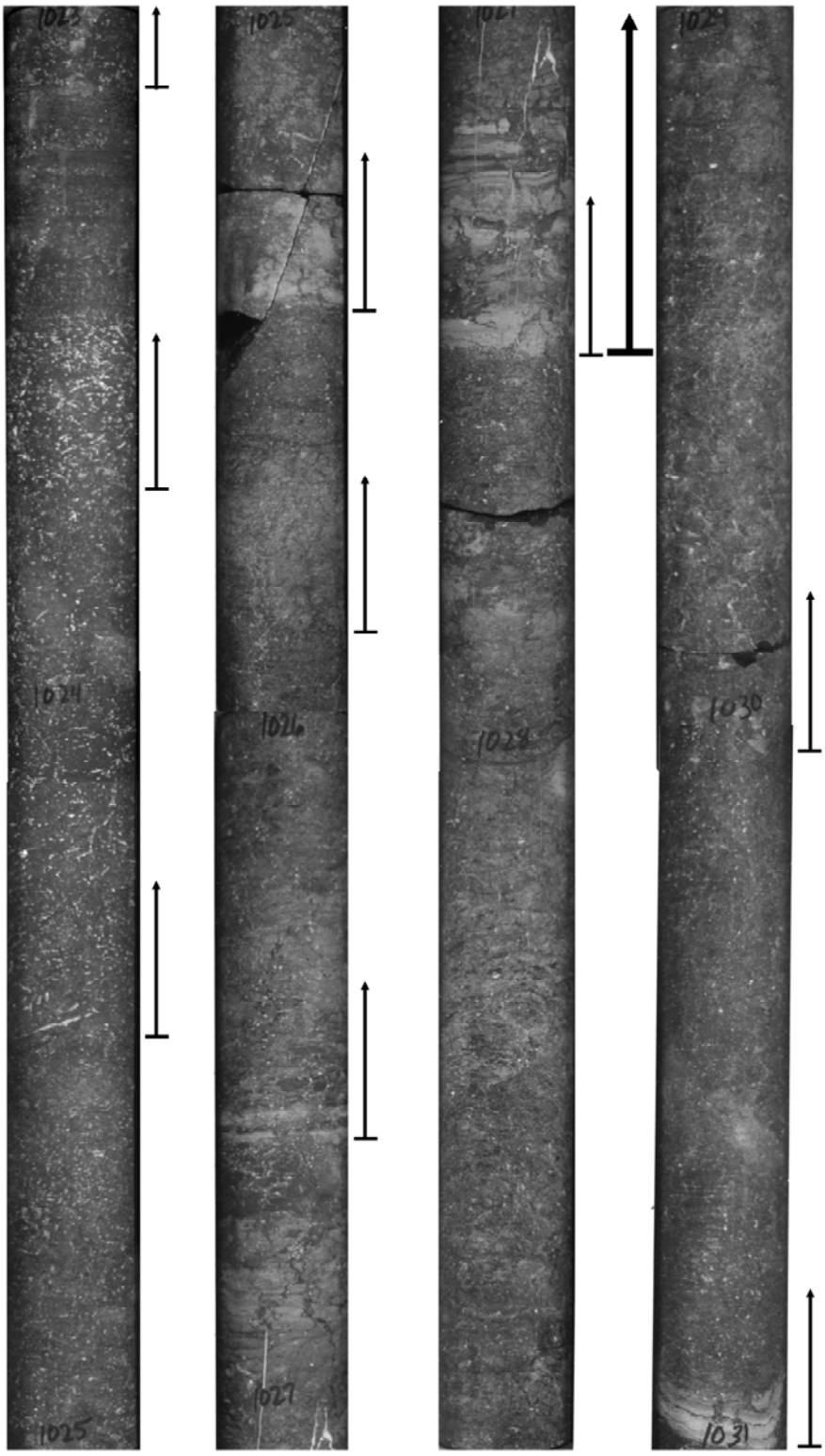

Figure A82. Type II and type III cycles in the Prahls Island Member of the Lockatong Formation illustrated in figure A78B. The large, heavy arrow shows a Van Houten cycle contact, and the smaller, thinner arrows denote the contacts of sedimentary sequences indicating shallower water or more desiccation upward. The lower Van Houten cycle is type III, with smaller sedimentary sequences of brecciated massive mudstone or thin-bedded vesicular mudstone grading upward into vesicular massive mudstone. The upper cycle is type II, with smaller sedimentary sequences indicating large euhedral crystals grading into smaller anhedral crystals or peloidal massive mudstone. Numbers on the cores are depths in feet below the land surface that are equivalent to depths in figure A78B.

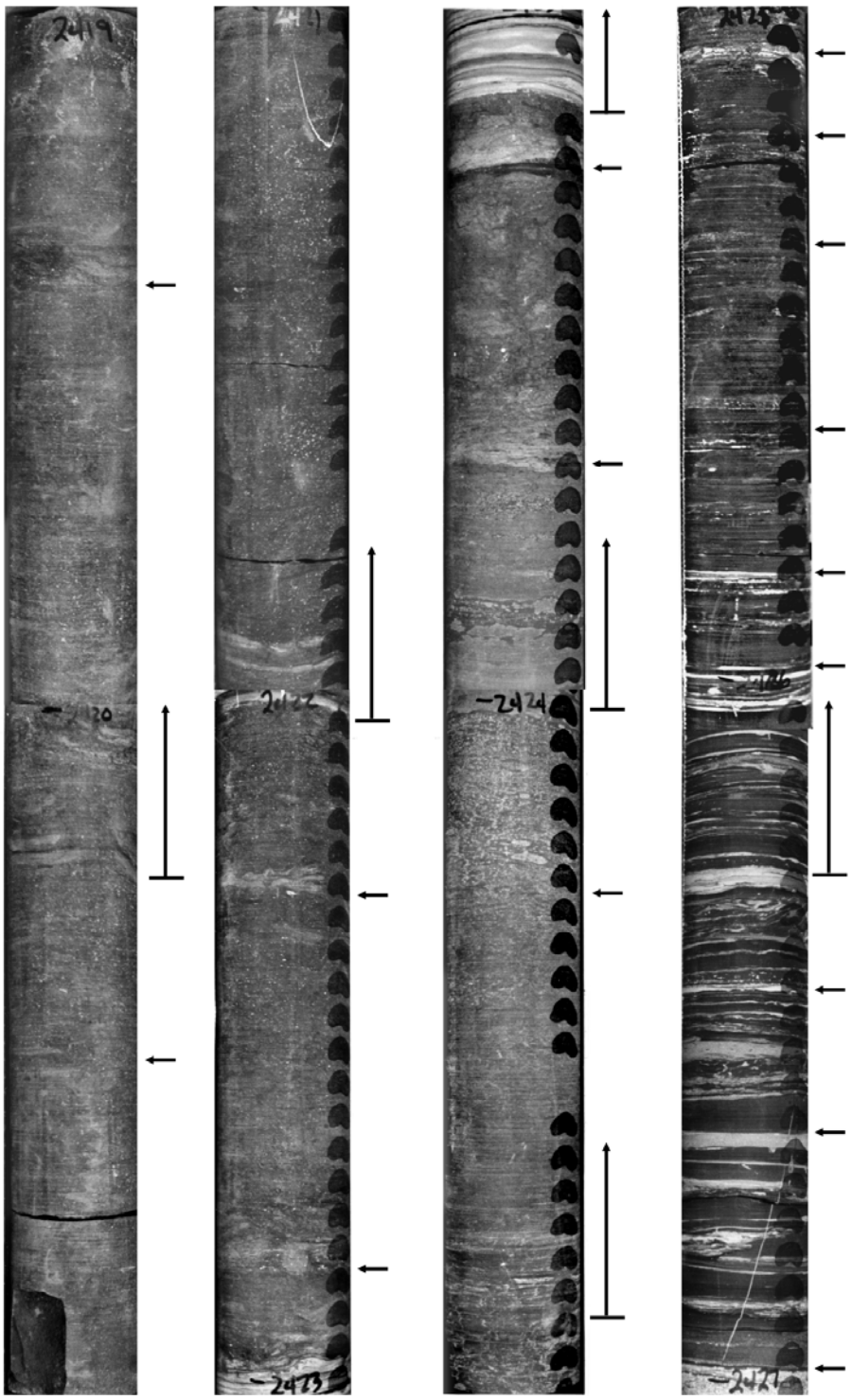

Figure A83. Type IV cycles in the Metlars Member of the Passaic Formation illustrated in figure A79A. The section shown is in a single Van Houten cycle. The vertical arrows denote the contacts of sedimentary sequences indicating shallower water or more desiccation upward, and horizontal arrows indicate boundaries of smaller sections that suggest shallower water or more desiccation. The sequences indicated by vertical arrows include grading from flat lamination to pinch-and-swell lamination at the base of the section, an abrupt transition from laminated mudstone to peloidal massive mudstone in the next sequence, and several transitions from vesicular thin-bedded mudstone to vesicular massive mudstone. Small horizontal arrows chiefly indicate change from thin lamination to thicker lamination, or suggestions of layering in vesicular massive mudstone. Root-disrupted massive mudstone is only at the top of the section that is near the top of the Van Houten cycle. Numbers on the cores are depths in feet below the surface that are equivalent to depths in figure A79A.

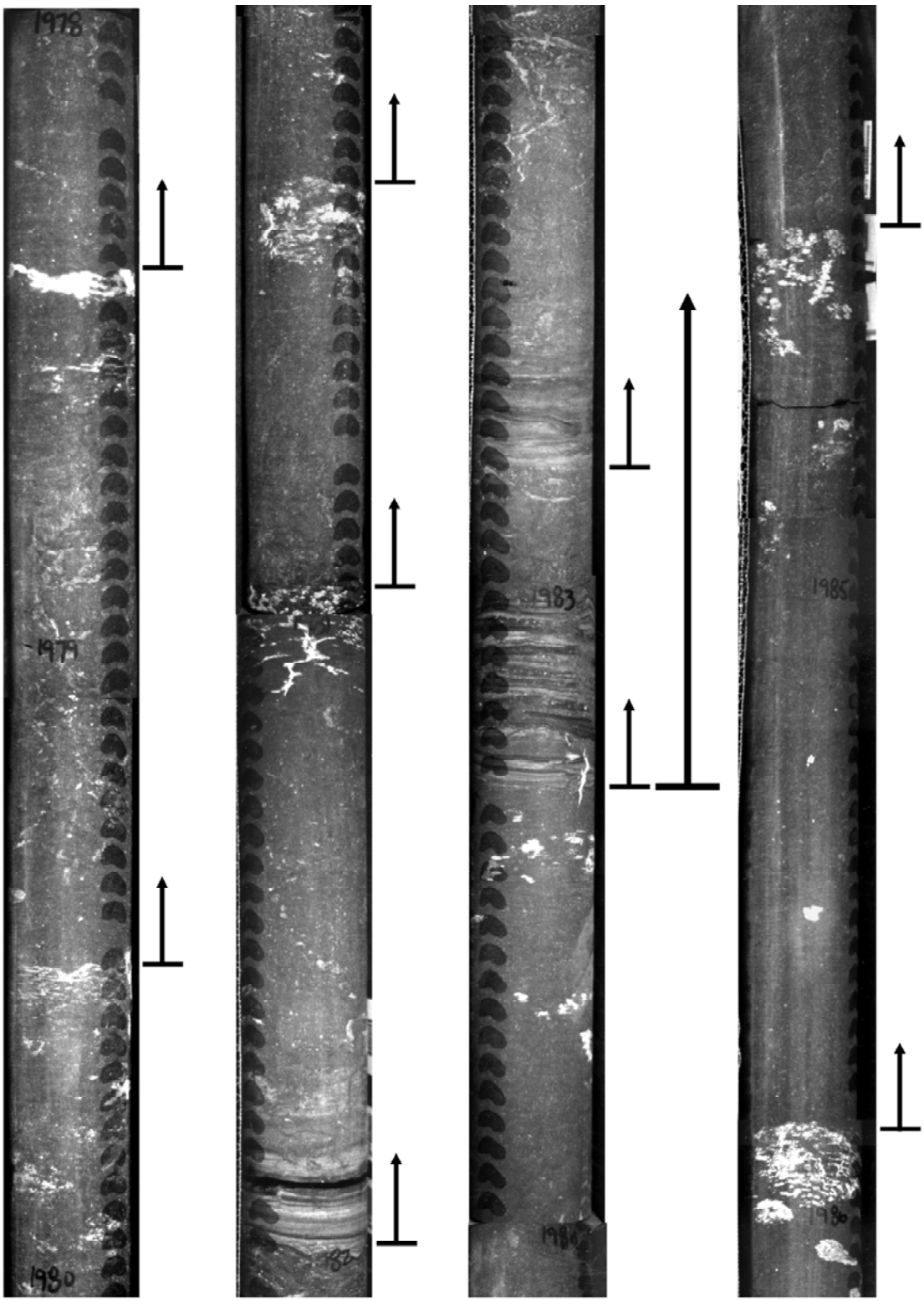

Figure A84. Type V cycles in Member PP of the Passaic Formation as illustrated in figure A79B. The long, heavy arrow shows a Van Houten cycle contact, and the smaller, thinner arrows denote the contacts of sedimentary sequences indicating shallower water or more desiccation upward. Smaller sequences in the lower part and upper part of the section shown indicate upward increase of root-cast diameters and larger size and abundance of gypsum nodules. Smaller sequences near the base of the Van Houten cycle include laminated to thin-bedded mudstone, with root structures superimposed on top. Numbers on the cores are depths in feet below the surface that are equivalent to depths in figure A79B.

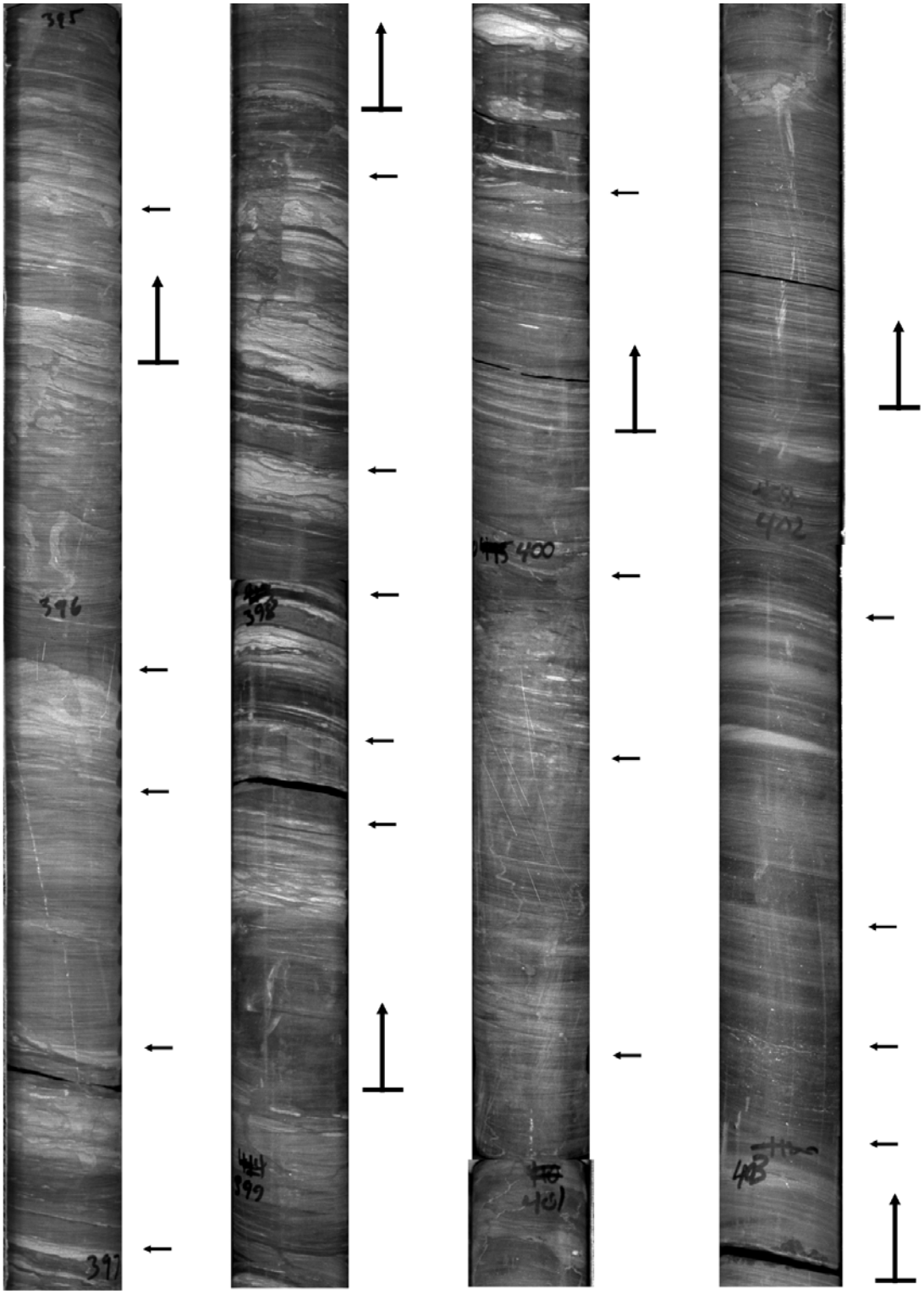

Figure A85. Type VI cycles in the Princeton Member of the Lockatong Formation as illustrated in figure A80. The section shown is in a single Van Houten cycle. The vertical arrows denote the contacts of sedimentary sequences indicating shallower water or more desiccation upward, and horizontal arrows indicate boundaries of smaller sequences that suggest shallower water or more desiccation. The vertical arrows indicate sequences of changes from laminated mudstone to burrowed thin-bedded mudstone, or burrowed massive mudstone. The smaller sequences include changes from flat laminated mudstone to pinch-and-swell lamination, and burrowed thin-bedded mudstone to burrowed massive mudstone. Numbers on the cores are depth in feet below the land surface that are equivalent to depths in figure A80.

unconformably overlying basement. The distribution of conglomerate and finer-grained strata along the northwestern border suggests that the current basin boundary was not the boundary during time of deposition. Ratcliffe and Burton (1985) and Ratcliffe and others (1986) observed that extensional faults located several kilometers northwest of the basin have veins similar in composition to those of the border faults, and suggested they formed at the same time. The apices of alluvial fans may have developed outside of the current basin boundaries, so that only the distal parts of alluvial fans are preserved. This accounts for the comparatively fine grain size of conglomerates compared to that in modern proximal alluvial fans (Blair and McPherson, 1994).

The lower part of the Lockatong Formation (underlying the Ewing Member) is more sandstone-rich in the southeastern and southwestern fault blocks than in the central and northwestern fault blocks. The sandstone in this part of the Lockatong Formation is similar to sandstone of the Stockton Formation. As noted earlier, Olsen and Rainforth (2001) correlated cross-bedded conglomerate and conglomeratic sandstone with the Nursery or Ewing Members near the northeastern end of the basin. No other fluvial sandstone or conglomerate in the southeastern side of the basin can be correlated to the Lockatong Formation. The interpretation is that the river deposits were restricted to an area near the southeastern edge of the basin and they were subsequently eroded. Axial sandstone and conglomerate near the southwestern end of the Newark basin includes the Hammer Creek Formation and several tongues of conglomerate and sandstone that extend eastward into the Newark basin about 10 km from the Narrow Neck (fig. A5). Paleocurrent data from the sandstone and conglomerate indicate that flow was into the basin from the northwest. The Hammer Creek Formation rests directly on the Stockton Formation in the Narrow Neck, but, east of eastern side of the Morgantown diabase sheet, axial sandstone and conglomerate overlie the lowest part of the Lockatong Formation. The exposure in this area is very poor and it is unclear exactly what part of the Lockatong Formation underlies the axial sandstone and conglomerate. The strike belt suggests that it probably includes the Princeton Member and possibly the lower part of the Nursery Member. The maximum basinward extent of the axial sandstone in the southwest end of the basin is on strike with the Smith Corner Member of the Lockatong Formation. Therefore, the axial sandstone and conglomerate lithology in the basin may cover the stratigraphic section from the Byram Member of the Lockatong Formation to the Perkasie Member of the Passaic Formation. Van Houten cycles in these lacustrine rocks are all sandstone-rich.

There is no overlap of provenance for the Stockton Formation and the Hammer Creek Formation in the Narrow Neck, suggesting that the contact may be an unconformity. The occurrence of basement in the rocks overlying the Morgantown diabase sheet in the Narrow Neck indicates that this area was uplifted with respect to the rest of the basin to the east. The axial sandstone and conglomerate are interpreted as terminal fan deposits (Kelly and Olsen, 1993) that built basinward during deposition of the Lockatong Formation deposition and receded during the early Passaic Formation. Based on the data of Kelly and Olsen (1993), proximal channels have width/thickness ratios near 50 whereas more distal channels have ratios near 200. Data provided by Gibling (2006) suggest that channels on terminal fans tend to avulse more frequently so sheet-like channel belts are unlikely. This is particularly true for the distal terminal fan where lake transgressions produce deltaic conditions. The density of sandstone and conglomerate beds in the Hammer Creek Formation indicates that they are proximal and medial terminal-fan deposits, so the perpendicular-to-flow widths of sandstone and conglomerate beds are probably on the scale of 200-500 m. In the area east of the Morgantown diabase sheet (fig. A5), the channel deposits are probably thinner, with greater widths perpendicular to flow (fig. A86) and the mudstone interbeds are much thicker. The absence of mappable Lockatong Formation or of McLaughlin cycles in the area east of the axial sandstone and conglomerate is interpreted as an indication of local erosional relief during deposition, making the cyclic pattern difficult to trace.

The axial sandstone and conglomerate at the northeastern end of the Newark basin extends about 35 km basinward as an upward-coarsening wedge whose top is approximately aligned with the Ukranian Member of the Passaic Formation. Axial sandstone and conglomerate also occurs up to the base of the Orange Mountain Basalt in the Army Corp of Engineers cores (fig. A3), although the sandstones are fine-grained and there are purple mudstones for about 20 m below the basalt. The base of the axial sandstone and conglomerate is not well known. Parker and others (1988) did not distinguish between border conglomerate and sandstone versus the axial sandstone and conglomerate. Border conglomerate near the New York-New Jersey state line has similar provenance to the axial sandstone and conglomerate, but lacks the large-scale cross-stratification. Olsen and Rainforth (2001) noted that fine-grained red mudstone with limestone interbeds underlie the axial sandstone and conglomerate. They interpreted the fine-grained deposits as part of the Passaic Formation. A map in Olsen and Rainforth (2001) shows that the base of the axial sandstone and conglomerate is approximately equivalent to the Graters Member of the Passaic Formation or higher. Like the axial sandstone and conglomerate at the southwestern end of the basin, the

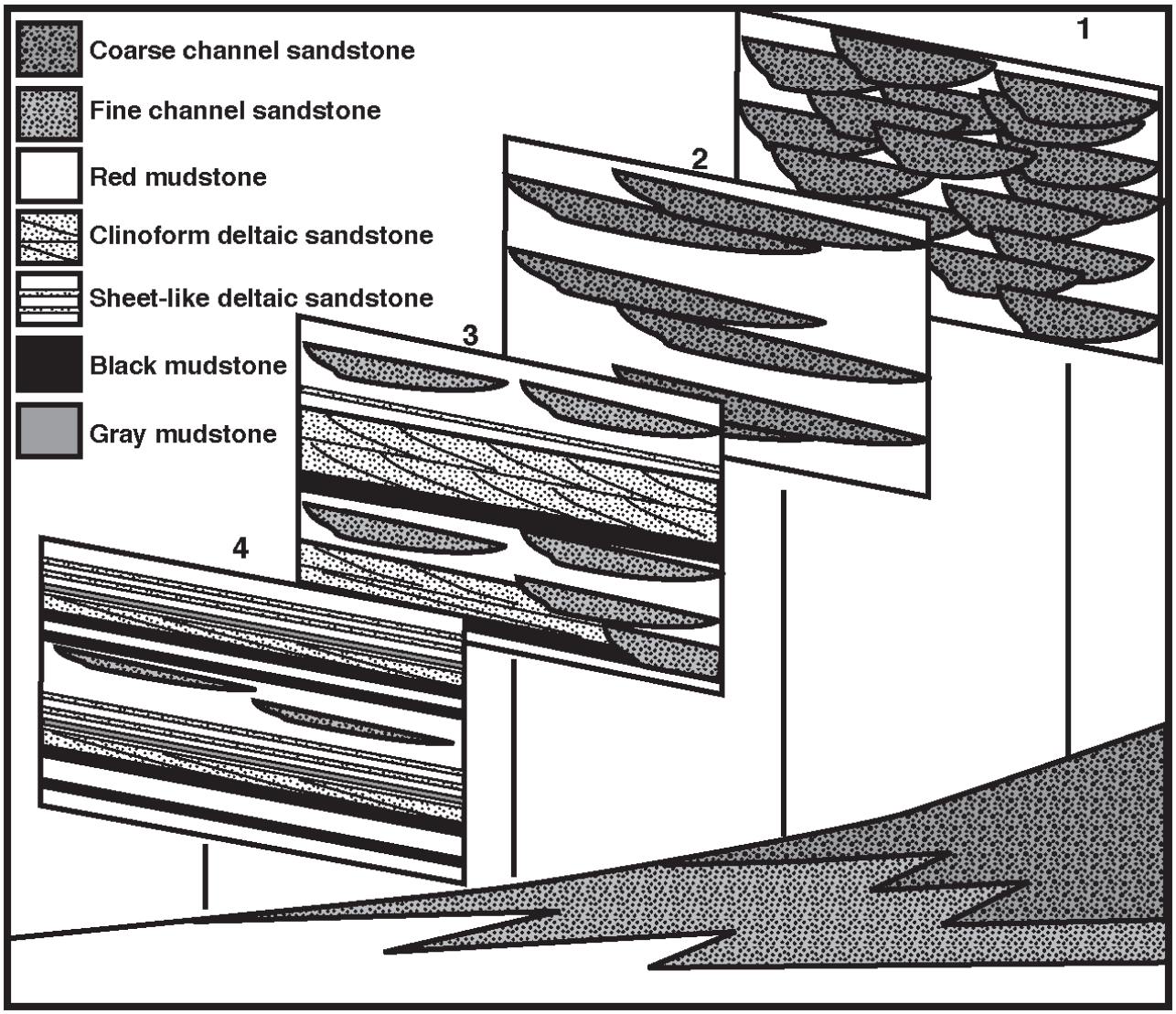

Figure A86. Schematic representation of axial sandstone and conglomerate deposits as they intertongue with lacustrine mudstones. Vertical cross section at base is parallel to flow, showing the wedge-shaped geometry of the coarser-grained deposits and the upward-coarsening character of a terminal fan. Boxes (numbered 1-4) illustrate the width and thickness of channel sandstone deposits and deltaic sandstone deposits perpendicular to flow. 1) Thick conglomeratic sandstone channel deposits are closely spaced with only patches of fine-grained deposits between them. 2) Conglomeratic sandstone deposits are thinner, but form broader lenses. Fine-grained deposits are thicker and more continuous between channel deposits. 3) Channel sandstones are narrower and are interbedded with thick clinoform deltaic sandstone deposits associated with black laminated mudstone. 4) Channel sandstones are thinner and scarcer in fine-grained deposits, and deltaic sandstone includes sheet deltaic sandstone associated with red lacustrine mudstone and thin clinoform deltaic sandstone associated with black laminated mudstone.

northeastern occurrence is interpreted as terminal fan deposits with similar channel geometries. The proximal facies, however, may be better represented in the uppermost exposures near the New York-New Jersey state line. The sandstone and conglomerate bodies probably consist of overlapping lenses that are 5-10 m thick and 50-100 m wide with only minor mudstone interbeds in this area. Parker and others (1988) report channel widths at the scale of 5-15 m in these deposits, but they may have been observing bedforms (trough crossbeds) or bar deposits in a channel deposit. The sandstone and conglomerate deposits southwest of this area probably have width/thickness ratios of about 100 in the thicker lenses and 250 in the thinner lenses, and the fine-sandstone, siltstone, and mudstone sections are even thicker.

Deltaic sandstone is incorporated in Van Houten cycles in which the central basin facies of the Lockatong and Passaic Formations intertongues with any of the coarse-grained deposits from the four source

areas. The thickest deltaic sandstone deposits are related to the axial sandstone and conglomerate wedges (fig. A86-1). Most of the lacustrine sandstone mapped in the northeastern and southwestern ends of the basin (figs. A5A and A5B) is dominated by deltaic sandstone in Van Houten cycles, although it also includes significant amounts of channel sandstone bodies and wave-dominated sandstone.

Clinoform deltaic sandstone units are best developed in Van Houten cycles with black laminated mudstone, whereas sheet-like deltaic sandstone is found in Van Houten cycles that have thin-bedded mudstone. Clinoform deltaic sandstone units are also found in the lowest part of the Lockatong Formation (below the Ewing Member) in the southeastern and southwestern fault blocks. Sheet-like deltaic sandstone is most common in Van Houten cycles interbedded with border conglomerate and sandstone. Clinoform deltaic sandstone also occurs in the upper part of the Stockton Formation in the northwestern fault block. Clinoform deltaic sandstone beds are thin and have low-angle foresets in the most northeastern extents of Stockton lacustrine sandstone in the northwestern and southwestern fault blocks. The more proximal occurrences of clinoform deltaic sandstone are characterized by thicker, steeper foresets and thicker successions of stacked foresets. The proximal areas of sheet-like deltaic sandstone are transitional to the mudstone-rich axial sandstone and conglomerate channels or to sheet sandstone distal to border conglomerate.

Clinoform deltaic sandstone bodies are associated with deep lakes and substantial influx of fluvial sediment. Sheet-like deltaic sandstone bodies are associated with shallow lakes and intermittent fluvial influx. The large lateral extent of deltaic sandstones away from the fluvial source areas is interpreted as a reflection of fluctuating lake levels during deposition. During falling lake levels, deltaic deposits from previous higher lake levels were reworked into new delta fronts. The repeated rise and fall of lake levels resulted in multiple delta fronts at various locations, producing a large sheet of superimposed delta wedges. In the sheet-like deltaic sandstone, the initial geometry was a sheet, but the rise and fall of lake level accentuated the broadness of the delta front wedges.

Wave-dominated sandstones make up the base and top of Van Houten cycles containing black laminated mudstone or gray thin-bedded mudstone. Wave-dominated sandstones are typically thinner at the base of Van Houten cycles (10-20 cm thick) and thicker at their tops (1-1.5 m thick) where the central basin facies of the Lockatong and Passaic Formations intertongue with border conglomerate or with either of the axial sandstone and conglomerate wedges. In the areas intertonguing with the axial sandstone and conglomerate, the regressive parts of Van Houten cycles are deltaic sandstone more often than wave-dominated sandstone. The thickest sequences (several meters thick) of wave-dominated sandstone make up the tops of Van Houten cycles in two areas of the basin. The first is in the northeastern end where the lower part of the Lockatong Formation (Ewing Member and lower) becomes progressively more sandstone-rich toward the northeast. Here, sandstone with Stockton Formation provenance overlies recognizable Lockatong Formation. The other area with thick wave-dominated sandstone beds in Van Houten cycles is near the southwestern end of the basin where the Passaic Formation, above the Perkasie Member, overlies the axial sandstone and conglomerate wedge. The stratigraphically highest occurrences of thick wave-dominated sandstone here are in the Metlars Member of the Passaic Formation, or directly above it.

Wave-dominated sandstone forms during the transgressive and regressive stages of Van Houten cycles in areas where sand was available for distribution by waves. In areas of where there was active fluvial sediment deposition, such as in the axial drainages, deltaic deposits overwhelmed the wave-formed deposits during lake regressions. Near the border conglomerate and sandstone deposits, wave-dominated sandstone and conglomerate indicate the intermittent deposition of sediment. Thick sequences of wave-dominated sandstone in the northeastern part of the basin are associated with exceptionally thin Van Houten cycles in the lower part of the Lockatong Formation (Olsen and others, 1996). This suggests that fluvial deposits from the southeastern margin or the axial drainage were not very large during that time. If fluvial conglomerate and conglomeratic sandstone are correlative with the Lockatong Formation, as suggested by Olsen and Rainforth (2001), the fluvial activity must have been very sporadic and short-lived to account for the lack of deltaic deposits and the much lower sedimentation rates. The situation near the southwestern margin is similar in some ways. The wave-formed sandstones appear to replace deltaic sandstones above axial sandstone and conglomerate in that area (fig. A5). The Van Houten cycles, however, are not condensed, as they are in the northeastern end of the basin.

The distribution of limestone in the basin margin facies of the Lockatong and Passaic Formations is similar to that of wave-dominated sandstone. Stromatolitic limestone is associated with oolitic wave-dominated sandstone at the base of a Van Houten cycle in the Metlars Member of the Passaic Formation near the Jacksonwald Syncline (fig. A5). The only other known stromatolitic limestone occurs in the Lockatong Formation as clasts within clinoform deltaic sandstone near the southwestern end of the basin. Nodular limestone forms thin beds in border conglomerate and sandstone, but thick beds of nodular limestone occur with flat limestone thin-beds in the

northeastern end of the basin, in rocks below the axial sandstone and conglomerate, and in the Jacksonwald Syncline in strata above the Metlars Member of the Passaic Formation.

The distribution of limestone in the Lockatong and Passaic Formations probably indicates areas of low sedimentation or sporadic sedimentation. The depositional characteristics of border conglomerate and sandstone are consistent with intermittent flow on alluvial fans. The limestone in the northeastern end of the basin is below the axial sandstone and conglomerate, and the Van Houten cycles of the Lockatong Formation directly below them are very thin, suggesting low sedimentation rates. At the southwestern end of the basin, the limestone is above the axial sandstone and conglomerate, indicating that sediment influx from the axial drainage was much lower there at that time. The flat limestone thin-beds may be lateral equivalents to laminated mudstone in Van Houten cycles, but their relationship to specific cycles is unknown.

Tectonic and climatic controls on facies distribution

Triassic deposition in the Newark basin lasted about 35 million years. The basin evolved from its initial narrow opening to one whose remnant area exceeds 7600 km^2. The basin was subjected to climatic variation throughout this time as the North American plate migrated, so that the Newark basin shifted from an equatorial paleolatitude to one nearly 20^o north of the paleoequator (Kent and Tauxe, 2005). Given the prolonged time frame and the distribution of facies in the Newark basin, the successive stratigraphic units cannot be viewed simply as laterally adjacent environments (Turner-Peterson, 1980; Faill, 2003). The climatic record indicates unstable conditions with a highly dynamic system that varied through time in response to changing latitude and to changes in world climate. Distinguishing sedimentary features controlled by tectonics versus those controlled by climate is still under debate. Most researchers would agree that the Van Houten cycles indicate climate change, but changes in their component facies may not be exclusively climatic. Improved age constraints should help to interpret some of the variation correctly and limit the number of interpretations.

Tectonic origin of the Newark basin

Schlische and Olsen (1990), Schlische (1992), Withjack and others (2002), and Schlische and Withjack (2005) envisioned the Newark basin as a half-graben that became wider and longer with an evolving system of border faults. They related sedimentation to continuous filling of the available space, which progressively increased through time. The oldest sediments were continuously dropped and rotated downward along the border faults during basin growth, with younger sediments progressively onlapping newly-depressed basement on the opposite side of the basin. Although Faill (1973, 2003, and 2005) envisioned the basin as a pre-existing depression of unstated origin that was subsequently filled by Mesozoic sediments, seismic lines (fig. A6) show that older rocks are rotated downward towards the border faults to greater extents than younger rocks, indicating that the border faults were active during deposition. Greater sediment thickness toward the northwestern border is also consistent with syndepositional fault movement. The repeated occurrence of alluvial fan conglomerates adjacent to the northwestern border faults indicates that depositional relief was sharp, although this does not confirm that the fault was syndepositionally active. Alternations of sandstone and mudstone with border conglomerates, however, are readily explained by alluvial fan deposition with intermittent fault uplift (Heward, 1978). Active movement along the border fault system is also suggested by “rider blocks” of basement here that are overlain by Lockatong or Passaic Formation rocks (Schlische, 1992).

Although the interpretation of the NB-1 seismic line by Schlische and Withjack (2005) suggests onlap of the Stockton Formation onto basement rocks (fig. A6B), this has not been confirmed in outcrop. As indicated earlier, it is difficult to distinguish between lower net sedimentation in the Stockton Formation owing to relative subsidence rates, and onlap. No internal age controls in the Stockton Formation enable differentiation of ages. Although Stockton Formation is much thinner in the northeastern end of the Newark basin than in the central area, continuous Van Houten cycles in the Lockatong Formation also show thinning in this direction. The correlation of members from the northwestern fault block with those of the Princeton core by Olsen and others (1996) also suggests a thinning of each depositional unit away from the central basin. Some of the variability in the thickness of Stockton Formation (and possibly the Lockatong Formation) may be related to paleotopography of the basin floor or to drainage locations, rather than to different age of deposits onlapping basement.

Schlische and Olsen (1990) proposed that the transition from the fluvial Stockton Formation to the cyclic lacustrine Lockatong Formation is a typical response to basin evolution in a half-graben. The half-graben sedimentation model envisioned by Schlische and Olsen (1990) suggests that deposition in the basin is primarily a function of accommodation

space that systematically changes with time. Early in basin development, rivers, such as those that formed the Stockton Formation, could continuously fill the expanding accommodation space of the basin, thus preventing the development of lakes. However, as the basin became continuously wider, a time came when fluvial sedimentation could no longer keep up with expansion and subsidence, and lakes formed in the remaining accommodation space (see also Schlische, 1992; Withjack and others, 2002). Beyond this time, lakes would become progressively deeper in response to the reduced sedimentation rates and growing accommodation space, as long as sufficient water was available to fill the basin. The model of Schlische and Olsen (1990) predicts that at some point a basin becomes too wide for any inflow to form deep lakes, so that lakes would become progressively shallower until the basin fills or some tectonic perturbation changes the balance. They attribute the transition from the Lockatong Formation, with abundant black laminated mudstone units, to the upper part of the Passaic Formation where laminated mudstone beds are rare, to this model. Similar models of accommodation space filled by sediment and water have been proposed by Lambiase (1990) and Bohacs and others (2000).

Although the model of Schlische and Olsen (1990) successfully explains the vertical transition from fluvial to lacustrine deposits in the Newark basin, the control of accommodation space on fluvial sedimentary style does not realistically explain the distribution of sedimentary facies. Smoot (1991) suggested some modifications to this model to explain some of the fluvial characteristics of the Stockton Formation (fig. A87) and similar basal fluvial deposits in other Newark Supergroup basins. The important characteristics shared by the basal fluvial deposits in most of Newark Supergroup basins are: 1) the oldest fluvial deposits have conglomeratic channel deposits indicative of braided rivers, 2) the overlying fluvial deposits have finer-grained meandering river-channel deposits that are finer-grained and more sinuous in the youngest deposits before grading upward into lacustrine deposits, and 3) all channel sandstones, from the base of the fluvial units to the top, have thick interbeds of siltstone and mudstone that are consistent with avulsion flood plains. Smoot (1991) also noted that the direction of fluvial drainage in other Newark Supergroup basins was not always towards the border faults. Furthermore, the basal, fluvial deposits intertongue with border conglomerates in some basins. Restricted fluvial outflow through outlets cut into the surrounding highlands of a developing basin can explain most of these characteristics. Early in the formation of a basin, the relatively narrow depression randomly captured regional drainages. The drainages were high energy due to the new relief and they had sufficient stream power to cut outlets out of the basin. Whenever the combined discharge of rivers entering the basin exceeded the outlets capacity, the basin floor would be covered by standing water. The distribution of sediment in the basin could be even and its outlets were not necessarily at the same elevation. As the basin grew larger, streams had to flow greater distances to reach the outlets. Streams lost some of their momentum from the source-area highlands over the extended travel distances and they developed meanders. Lower stream power and broader basin floor both acted to decrease the number of outlets, because of the loss of cutting power and the combination of drainages. With time, the scale of the basin would be too large to enable rivers to cut outlets, allowing permanent lakes to develop. This model suggests that the transition from fluvial to lacustrine deposition in a half-graben basin is inevitable. Furthermore, the Stockton Formation geometry of fluvial drainage with flow toward the border fault is not the only possibility, but it is the geometry that would produce the most rapid transition from fluvial to lacustrine conditions. The major difference between the outlet model and the accommodation space models is that sediment and water supply do not need to keep up with subsidence in order to maintain fluvial deposition. Therefore, even during fluvial deposition, there could be considerable relief on the basin margins, allowing alluvial fan deposition. The outlet model predicts that shallow spilling lakes would form early in the transition from fluvial conditions, and deep lakes and closed-basin conditions would follow as fault uplift raised the former outlets relative to the basin floor. This aspect of the outlet model is virtually the same as predicted by the accommodation space models. In the Newark basin, this transition is represented by the uppermost Stockton Formation (shallow lakes near the northwestern fault boundary and no recognizable Van Houten cycles) and by the Scudders Falls and Wilburtha Members of the Lockatong Formation (progressive shift of laminated mudstone towards the southeastern basin margin and pronounced Van Houten cycles).

Schlische and Olsen (1990) attributed the decrease in frequency and thickness of black laminated mudstones progressively upward from the Lockatong Formation into the Passaic Formation as a function of the increasing size of the Newark basin with time. The smaller, narrower basin during deposition of the Lockatong Formation needed less water to form a deep lake than the larger, wider basin during deposition of the Passaic Formation. The extensional-widening model of Schlische and Olsen (1990) also predicts that Van Houten cycles and McLaughlin cycles in the Passaic Formation should be thinner than those in the Lockatong Formation because sediment was spread out over a greater surface area. According to thicknesses reported in Olsen and others (1996) from the Newark Basin Project cores, the average thickness of McLaughlin cycles in the Passaic Formation is about 10

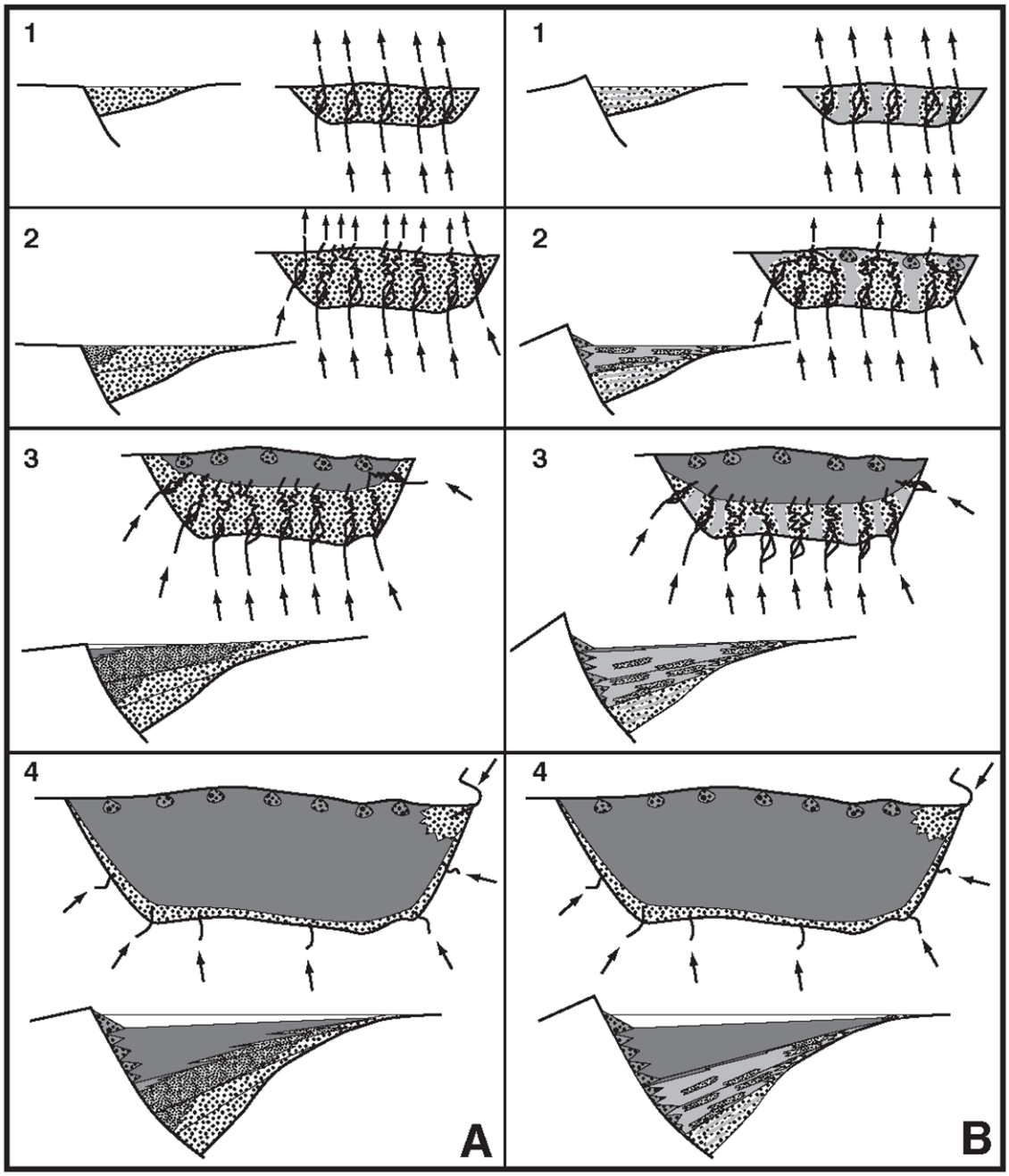

Figure A87. Schematic representation in vertical and map view of differences between the basin evolution model of Schlische and Olsen (1990) based on accommodation space (A) and that of Smoot (1991) based on outlet cutting (B). A. The initial basin (1) is drained by braided streams, and sedimentation is equal to subsidence. As the basin widens (2), streamflow includes finer-grained meanders but sedimentation is still equivalent to subsidence. When basin width makes it impossible for stream deposition to keep up with subsidence (3), lakes develop in the remaining accommodation space. The area of lake deposition progressively increases as the basin becomes wider and sediment accumulation falls behind subsidence (4). The lakes become deeper until basin width outgrows available water volume, lakes then become shallower. B. The subsiding basin captures drainages (1) which exit through outlets cut into the developing highland. The limited drainage exits promote back flooding into shallow lakes and anastomosing channels. As the basin widens (2), the travel distance for rivers to the outlets is greater, resulting in meandering channels with lowered velocities, less efficient outlet cutting, fewer outlets, and more standing flood water that leads to thicker mud deposits. At some point, the rivers can no longer cut outlets (3) and lakes develop. Their depths are controlled by the spillway on the northwestern margin of the basin. The transition from fluvial anastomosing to alternating lake and dry mudflat is relatively abrupt. The lakes become deeper and cover larger areas as the basin continues to grow as shown in A. Arrows indicate directions of streamflow.

m greater than that of McLaughlin cycles in the Lockatong Formation. Two factors may influence this observation: 1) cores in the Lockatong Formation are mostly from the southeast and southwest fault blocks, whereas those in the Passaic Formation are from areas closer to the northwestern border fault system, and 2) cores from the uppermost Passaic Formation are closer to the wedge of the northeastern axial sandstone and conglomerate than those in the Lockatong Formation. Both of these factors could increase the relative sedimentation rates of the Passaic Formation. Another possible effect on the sedimentation rate in the Lockatong Formation and lowermost Passaic Formation is the frequent occurrence of peloidal massive mudstone. The depositional conditions associated with peloidal massive mudstone include common deflation of subaerially exposed surfaces. The Lockatong cycles may appear thinner in part owing to removal of material between lake transgressions. This effect is discussed more fully in the section on climatic influences.

Olsen (1997) has suggested that there were four major tectonic events in the central Pangean area from the late Permian through the early Jurassic. The resulting four tectonostratigraphic units are separated by angular unconformities in the Argana basin of Morocco. Olsen and Rainforth (2001) indicated that three of these tectonostratigraphic units are present in the exposed rocks of the Newark basin. Tectonostratigraphic unit II is interpreted as the exposed Stockton Formation underlying an unconformity at the base of the Cutaloosa Member. Tectonostratigraphic unit III consists of the rest of the Stockton Formation, all of the Lockatong Formation and most of the Passaic Formations. The contact between tectonostratigraphic unit III and IV is placed at the base of the Pine Ridge Member of the Passaic Formation. Tectonostratigraphic unit IV consists of the Pine Ridge Member, the remaining Passaic Formation, and the overlying basaltic and sedimentary rocks of the basin fill. The evidence for these tectonostratigraphic units in the Newark basin, however, is not particularly strong.

The unconformity postulated for the base of the Cutaloosa Member in the Stockton formation is based on two observations. Reynolds (1993) believed that reflectors in the NB-1 seismic line that project to the outcrop position of the Cutaloosa Member in the northwestern block dip less steeply toward the northwest than those below it. This unconformity is difficult to see, even in the highly depth-migrated interpretation shown in Schlische and Withjack (2005). There is no evidence of an unconformity in the Stockton outcrop, and the rocks below the proposed unconformity are similar in character to those above it. LeTourneau (2003) compared the pattern of magnetic reversals in cores from the Taylorsville basin in Virginia to that of the Newark basin (Olsen and others, 1996). He found that the thicknesses of the reversal bands in the Taylorsville basin cores were nearly identical to those in the Newark basin cores, except for a thick reversed sequence near the base of the Newfound Formation. He attributed the difference in the two magnetic reversal patterns to the absence of a section of the Stockton Formation comparable to the difference in the thickness of the two reversed sections. The proposed missing section is directly below the Cutaloosa Member of Olsen and others (1996) in the Princeton core. LeTourneau (2003) also noted that the magnetic reversal profiles in the Locaktong Formation correlated with those in lacustrine units in the Taylorsville basin, and that the vertebrate and pollen fossil records of the two basins were in agreement with this correlation. This interpretation requires that sedimentation rates in the two basins were identical, including fluvial sedimentation in the Leedstown Formation in the Taylorsville basin and central basin facies lacustrine sedimentation in the Passaic Formation. Given the very different modes of sediment delivery and distribution in fluvial and lacustrine environments, it is unlikely that they could have identical sedimentation rates. The only reasonable explanation for comparable accumulation rates in the two basins is that subsidence and accommodation space were the controls on accumulation. Given some of the lateral variation in thickness in Van Houten cycles noted by Olsen and others (1996), it is also fortuitous that the intervals selected for magnetic measurements are identical. Finally, the proposed unconformable contact shows no changes in sedimentation style or unusual lithology to indicate nearly 200 m of missing section. The coincidence of the seismic line unconformity and the proposed gap for comparable magnetic reversal patterns cannot easily be dismissed, but the physical supporting evidence and the depositional implications need to be explained.

The base of tectonostratigraphic unit IV in the Newark basin was identified by Olsen and Rainforth (2001) in the cores drilled by the Army Corp of Engineers (fig. A3) as an abrupt transition from predominantly conglomerate and conglomeratic sandstone to a thick succession of rocks dominated by sandstone and siltstone. In the Jacksonwald syncline (fig. A5), they marked the contact at the base of the Pine Ridge Member of the Passaic Formation above which black laminated mudstone is common and below which there are many hundreds of meters of mudstone with no black or gray mudstone intervals. In both places, Olsen and Rainforth (2001) argue that a tectonic event changed the depositional style. Extrusive basalt flows are also attributed to the ongoing effects of that event. The base of the Pine Ridge Member in the Martinsville core (fig. A3) is less distinct than in the Jacksonwald syncline, consisting of a hundreds of meters of red mudstone changing upward to red mudstone with thin intervals of purple or gray mudstone (Olsen and others,

1996). The sedimentary changes above the base of the Pine Ridge Member at both localities are not different from those in other parts of the Passaic Formation that are attributed to climatic fluctuations. Furthermore, the change in fluvial style in the Army Corp of Engineers cores has not been conclusively correlated to the base of the Pine Ridge Member and a similar abrupt transition in terminal fan progradation earlier in deposition of the Passaic Formation (described below) is not correlated to one of the regional tectonic events of Olsen (1997).

Smoot (1999) suggested that the southwestern drainage switched from primarily flowing into the Newark basin to mostly flowing into the adjacent Gettysburg basin during the time of deposition of the lower part of the Passaic Formation. This argument is supported by the occurrence of a conglomeratic wedge in the Gettysburg basin whose age roughly correlates with the time that the Hammer Creek axial sandstone and conglomerate wedge stopped building into the Newark basin. There is no stratigraphic control on the age of the Hammer Creek in the "Narrow Neck", but the thickness of section there is small compared to the thickness of stratigraphic sections with which it intertongues in both basins. This implies that the "Narrow Neck" was a tectonic high area (Anders and Schlische, 1994). The abrupt end of the southwestern terminal fan deposition and the initiation of the northeastern terminal fan are about the same stratigraphic level. This suggests that the tectonic event inferred to have switched the southwestern drainage into the Gettysburg basin may have also caused the capture of a new drainage in the northeastern part of the basin. The timing of this possible tectonic event does not correlate with any of the regional events envisioned by Olsen (1997).

Climate change and sedimentation

Cyclic changes in the deposits of the Lockatong and Passaic Formations have been interpreted as the products of climate change (Van Houten, 1962, 1964; Olsen, 1986; Olsen and Kent, 1996; Olsen and others, 1996). Olsen (1986), Olsen and Kent (1996), and Olsen and others (1996) linked these cycles to Milankovitch periodicities of eccentricity in the earth's orbit by generating curves of sediment thickness versus a "depth rank" bedding index and assuming a constant sedimentation rate. The major Milankovitch periodicities of 20,000 years and 405,000 years, and several less pronounced minor periodicities, were identified using Fourier analysis of "depth-rank" data and time constraints from biostratigraphic correlation and radiometric dates. We assume from the Milankovitch model that net sediment accumulation rates in the Newark basin were constant for periods of millions of years, and that the Newark basin lacustrine strata have no erosional gaps that exceed 20,000 years. Olsen and others (1996) named informal members for the groupings of cyclic strata comparable to the 400,000 year orbital periodicity (fig. A3). Based on the Milankovitch cycle model, Lockatong lacustrine sediment accumulation began about 226 Ma and Passaic sediment accumulation ended about 200 Ma. The Milankovitch forcing-of-climate model predicted the multiple levels of periodicity that were subsequently observed in the Newark Coring Project (Olsen and others, 1996). However, considerable uncertainty remains on the ages of the strata, and some disagreement remains on the reliability of biostratigraphic markers (Kozur and Weems, 2005, 2007). A possible source of error in this mathematical treatment may result from the relative weighting of the depth-rank indicators. More than 70 percent of the composited thickness of the Lockatong and Passaic Formations in the Newark Coring Project cores falls in the zero depth rank. The percentage is even higher for most of the upper half of the Passaic Formation. It is possible that the scale of periodicities between cycles could shift in the strata with lower percentages of depth ranks above 0 and not be recognized in the Fourier analysis. A grouping of five Van Houten cycles forming a 100,000-year eccentricity cycle may not be distinctive enough to be separated from a grouping of four 100,000-year eccentricity cycles forming a McLaughlin cycle if little or no contrast is in the depth rank indicators. This scale of misinterpreting cycle patterns in the upper part of the Passaic Formation is unlikely, however, because of the multiple levels of cyclicity that are maintained from the more well-constrained patterns in the Lockatong Formation and lower part of the Passaic Formation. Also, a uranium-lead age of the Metlars Member of the Passaic Formation (Rasbury and others, 2003) is very similar to the age predicted by Milankovitch periodicity (Olsen and others, 1996).

The decimeter-scale changes in sedimentary character in Van Houten cycles do not register in the mathematical analysis of Olsen (1986) because a large part of them consist entirely of depth rank zero. Even regular patterns of depositional change would appear random with thick intervals of periodic change not registering in the analysis. If Van Houten cycles are assumed to last 20,000 years, these smaller patterns have durations of one to five thousand years. Such periodicities have been noted in Holocene and Pleistocene lacustrine sequences (Benson, 1999). Some debate lingers about the regularity of these events, their global extent, actual causes, and their applicability through geologic time (see Cohen, 2003, Chapter 13 for a clear summary).

An important implication of the Milankovitch model is that, at least in the central part of the basin,

there were no major erosional surfaces and also that sedimentation rates were relatively constant during deposition of thousands of meters of sediment. These conditions seem unlikely in the Newark basin, given the frequency of subaerial exposure, the changing conditions of sedimentation, and the presence of destructional fabrics such as those in brecciated and peloidal massive mudstone. Peloidal massive mudstone fabrics are commonly superimposed directly on laminated mudstone without transitional beds of thin-bedded mudstone that have an upward-increasing abundance of polygonal cracks. If peloidal massive mudstone is correctly interpreted as a puffy ground deposit, then the abrupt transitions from deposits interpreted as perennial lakes probably reflect deflation. The amount of section removed by deflation is difficult to gauge, but Van Houten cycles and McLaughlin cycles with intervals of peloidal massive mudstone are notably thinner than those lacking them. The presence of peloidal massive mudstone, however, does not appear to disrupt the pattern of depth rank at a scale recognizable by the Fourier analysis. Furthermore, field evidence indicates that most of the Van Houten and McLaughlin cycles in the Lockatong and Passaic Formations are continuous across most of the basin floor. Therefore, the amount of erosion due to deflation must be too small to impact the larger pattern of lake transgressions and regressions. The only places where the cycle patterns are not recognizable are areas that are close to the northeastern or southwestern axial sandstone and conglomerate wedges. In these areas, black laminated mudstone occurs in cycles interbedded with deltaic sandstone, but the patterns of black laminated mudstone and gray thin-bedded mudstone that make McLaughlin cycles recognizable are not preserved. A likely reason for the loss of cycle patterns is that erosion and irregular depositional topography resulted in only partial preservation. It is also possible that the poor outcrop preservation of sandstone-rich strata makes it difficult to find the cycles in these areas.

The stratigraphic transition in the types of cycles may represent a larger-scale climatic signal (fig. A88). Smoot (1991) suggested that the Stockton Formation and the lowest Lockatong Formation, with abundant rooted mudstones and burrows, represent wetter climatic conditions than the parts of the Lockatong and Passaic Formations with indications of saline lakes and dry mudflats. The occurrence of root-disrupted massive mudstone in the Passaic Formation followed by the absence of saline-lake and dry-mudflat indicators higher in the formation was cited by Smoot (1991) as evidence of a return to wetter conditions heading into the Jurassic. During deposition of the Stockton Formation and lowest Lockatong Formation, the Newark basin paleolatitude was equatorial, but the basin drifted to more northerly latitudes throughout deposition of the Lockatong and Passaic Formations (Kent and Tauxe, 2005). Terrestrial vertebrate fossils are most common in the Stockton Formation, the upper part of the Passaic Formation, and in Jurassic strata, suggesting that these sections had the most favorable conditions for nonlacustrine vertebrates in the Newark basin. Vertebrate tracks are common throughout the stratigraphic succession of the basin, but are commonly limited to transgressive wave-dominated sandstone or deltaic sandstone beds in the Lockatong and Passaic Formations. Similarly, features interpreted as root casts are common in deltaic sandstones that correlate with central basin facies of the Lockatong and Passaic Formations that lack root casts in the subaerial deposits. The absence of vesicular massive mudstone and cement-filled crystal casts in lacustrine mudstone of the upper part of the Passaic Formation may be due to lack of preservation. If sedimentation rates were generally lower in this part of the stratigraphic sequence, root fabrics may have obliterated any signs of the other subaerial features or evidence of shallow saline lakes. The lowest Van Houten cycles of the Metlars Member of the Passaic Formation contain vesicular massive mudstone, indicating dry mudflats, and cement-filled crystal casts, indicating saline lakes and saline mudflats. Seven members between the Metlars Member and the Perkasie Member lack these fabrics and have well-developed gypsum upward-coarsening profiles. There are no gypsum crystals in the lowest Van Houten cycles of the Metlars Member. The lack of any transitional features argues against the overprint hypothesis, and the absence of vesicular mudstone and cement-filled crystal casts probably indicates major changes in the depositional environments.

The Stockton Formation was deposited in an open, spilling drainage, and lakes in the lower part of the Lockatong Formation were probably small and spilling. In these conditions, water would not have had enough residence time to precipitate brines through evaporation. Furthermore, dry mudflats would have been limited to a narrow strip near the border fault, currently unexposed in outcrop. The transition to a closed basin would facilitate the development of saline lakes, saline mudflats, and extensive dry mudflats without a significant change in climate. The transition to root-disrupted mudstones could also be interpreted as an artifact of the structural evolution of the basin. In a narrow basin, a change to wetter conditions would cause growth of a lake, whereas in a much wider basin, a change to wetter conditions would result in a shallower groundwater table throughout broad areas of subaerial exposure before lake transgression. Finally, the changing basin geometry may have changed the amount of groundwater entering the basin or changed its chemistry. Calcite pseudomorphs and cement-filled crystal casts associated with peloidal massive mudstone suggest an alkaline mineral suite (Smoot, 2006), whereas the gypsum and anhydrite indicate a change in

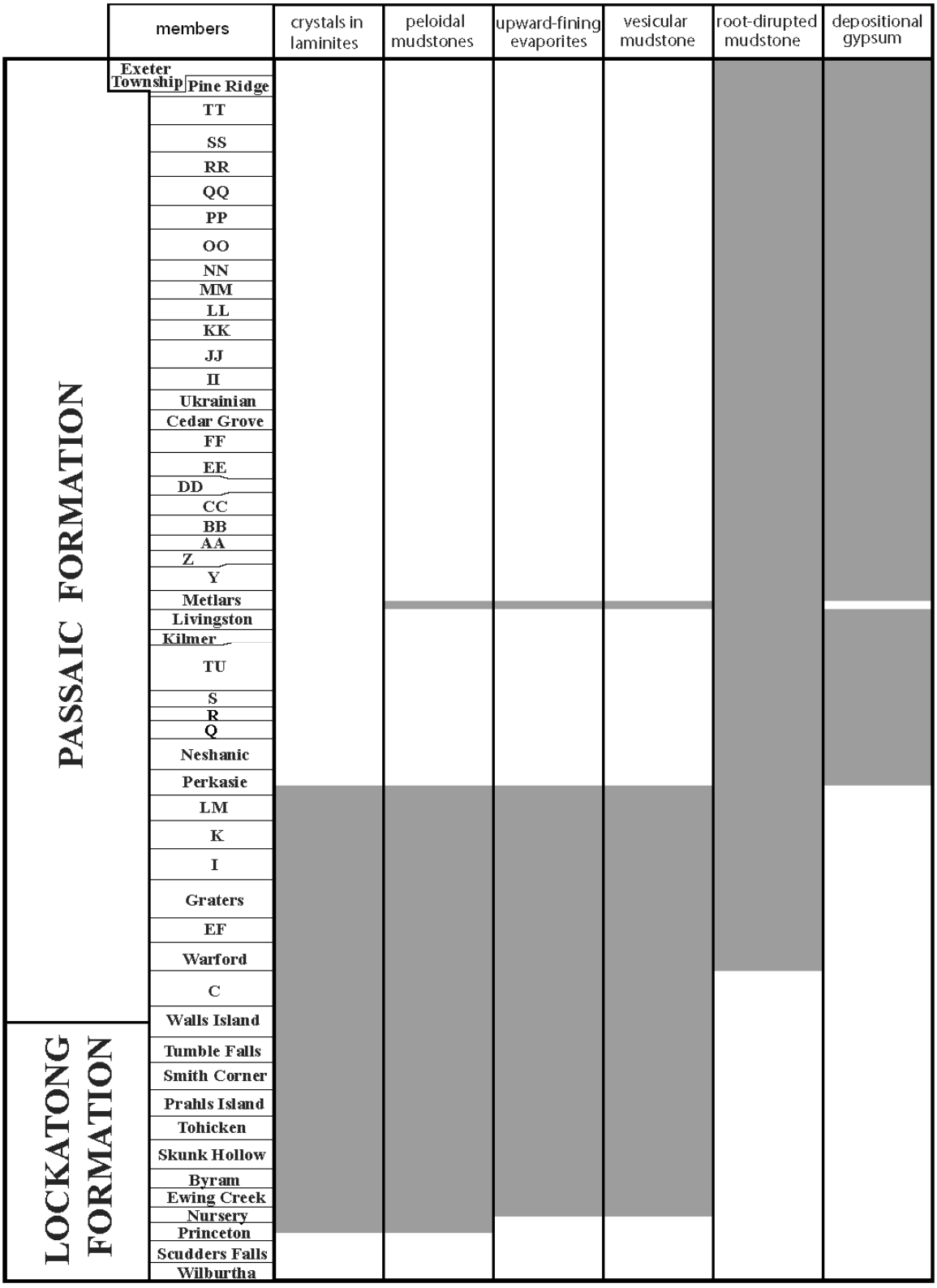

Figure A88. Distribution of subaerial sedimentary fabrics in the central facies of the Lockatong and Passaic Formations. Abundance of saline mudflat and dry mudflat fabrics in the section between the upper part of the Princeton and lower part of the Perkasie Members suggests greater aridity than in the lowest part of the Lockatong Formation and upper part of the Passaic Formation, which are dominated by root-disrupted horizons. The oldest deposits of the Lockatong Formation may appear wetter, due to a low basin spill level. The lack of saline mudflat and dry mudflat fabrics in the upper part of the Passaic Formation may be due in part to tectonic causes.

chemistry. Calcite pseudomorphs and cement-filled crystal casts were formed in saline lakes and saline mudflats, whereas gypsum and anhydrite crystallized and accumulated in root-disrupted soils by downward percolating rainwater. Gypsum and anhydrite are not indicators of groundwater, but they may indicate some other change in the basin. One possibility is that they represent an influx of windblown dust and aerosols from evaporite basins now buried beneath the continental shelf (Holser and others, 1988). These basins apparently developed sometime during deposition of the Passaic Formation and they are dominated by gypsum and halite. This model would account for the apparent decrease in gypsum in the deposits in the western part of the Newark basin.

Summary

Triassic sedimentation in the Newark basin spanned about 35 million years in a half-graben that became broader and longer as it developed. A fault complex that probably extended tens of kilometers northwest of the preserved basin boundary created abrupt relief along the northwestern margin of the basin which was bounded on the southeastern side by highlands of lower relief. The initial deposits in the basin forming the Stockton Formation were in high-energy braided-river channels initiated in the southeastern highlands that anastomosed across broad muddy avulsion plains before exiting via incised outlets in the northwestern boundary fault system (figs. A87 and A89A). The Stockton Formation rivers became more sinuous and of lower energy as the basin broadened and the rivers lost hydraulic momentum crossing the valley floor. A tectonic event may have caused an angular unconformity during deposition of the Stockton Formation, but the evidence for it is inconclusive. The progressive loss of hydraulic head in the streams entering the Newark basin during deposition of the Stockton Formation ultimately led to lake development as the rivers were no longer able to cut their outlets in the continuously uplifted northwestern basin boundary. The initial lakes were shallow and spilled through outlets in the northwestern boundary (fig. A89A). The deposits of these early Newark basin lakes are thickest near the northwestern boundary, thinning southeastward where they were incised by channels of meandering rivers during low stands. The lakes enlarged and deepened as subsidence exceeded sedimentation along the northwestern basin boundary in part due to entrapment of coarse sediment from the southeast in deltas along the lake shorelines. These deposits are part of the youngest Stockton Formation

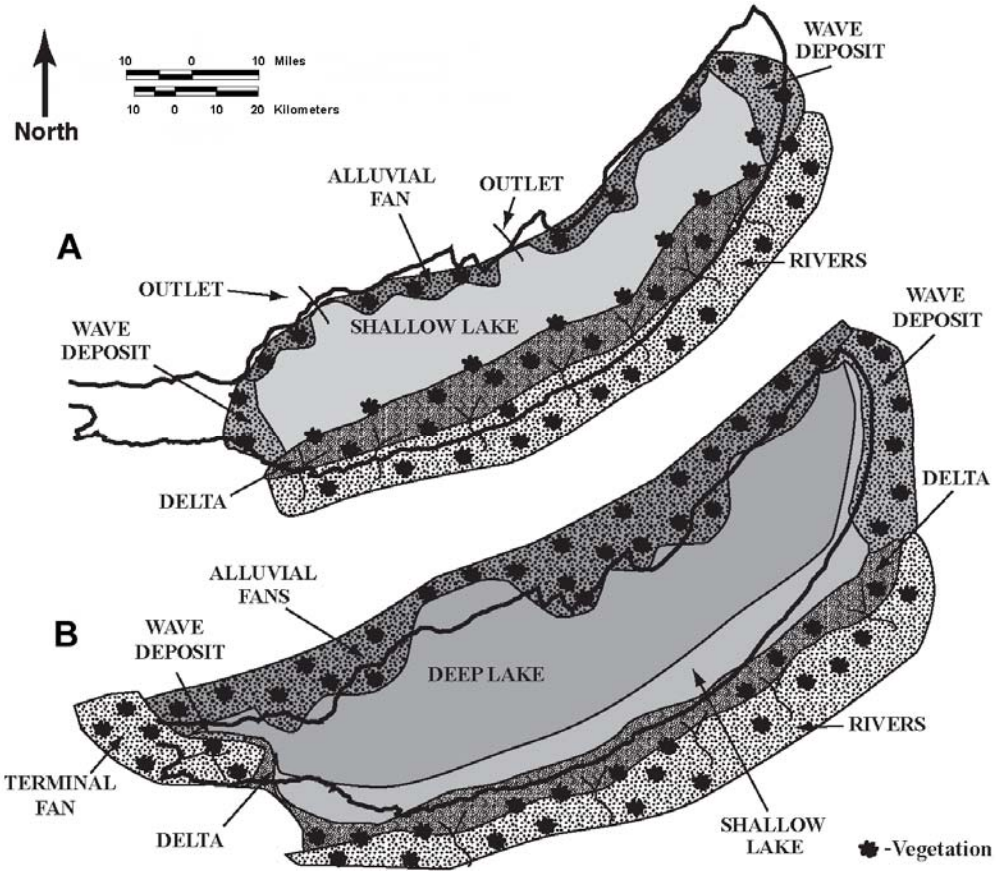

Figure A89. Schematic drawings of facies distribution in the Newark basin. Thick black lines show current basin limits.
A. shrinking lake of the Scudders Falls Member of the Lockatong Formation. Rivers from the southeast feed a shallow lake that spills to the northwest.
B. A shrinking lake of the Nursery Member of the Lockatong Formation. A lake covers most of the basin floor and a terminal fan is built from the southwestern end of the basin.

and the Wilburtha and Scudders Falls Members of the Lockatong Formation. During deposition of the Princeton Member of the Lockatong Formation, the outlets were high enough above the basin floor to form deep lakes covering most of the basin floor (fig. A89B). The lakes spilled only during the highest lake stands, and the basin became hydrologically closed during low stands. This resulted in episodes of complete desiccation of the basin floor (fig. A90). This pattern continued throughout deposition of the remainder of the Lockatong Formation and deposition of the Passaic Formation. The gradual growth of the Newark basin is shown by the frequency with which lakes became deep enough to become permanently stratified, allowing preservation of abundant organic material. During deposition of the Lockatong Formation, stratified-lake conditions were common, whereas during deposition of the Passaic Formation, stratified-lake deposition became progressively scarcer until just before the end of the Triassic. This change is attributed to the progressive growth of the basin area, requiring progressively larger amounts of water to reach spillway elevations.

A river was captured sometime early during deposition of the Lockatong Formation. It entered the basin from the southwestern end and produced a terminal fan complex (figs. A89 and A90). This drainage shifted away from the Newark basin during the early part of the deposition of the Passaic Formation, probably due to tectonic uplift of the Narrow Neck between the Newark and Gettysburg basins. Another river was captured early in the deposition of the Passaic Formation that entered the basin from the northeastern end, producing a terminal fan complex (fig. A91). The terminal fan built basinward until late in deposition of the Passaic Formation, when it abruptly decreased in size in response to a tectonic event that may have affected most of central Pangea.

During the initial opening of the Newark basin, its paleolatitude was near the equator and it received enough rainfall to support vegetated floodplains with terrestrial fauna. It was arid enough, however, for periods of time during which soil carbonates accumulated in vertisols. Climatic variability probably caused a pattern of thick beds of closely spaced channel-fill conglomerate and sandstone alternating with thick beds of mudstone and siltstone. However, this could also be caused by random avulsion across a broad muddy plain. The Newark basin drifted northward in paleolatitude throughout the remainder of the Triassic so that it passed into the arid horse latitudes.

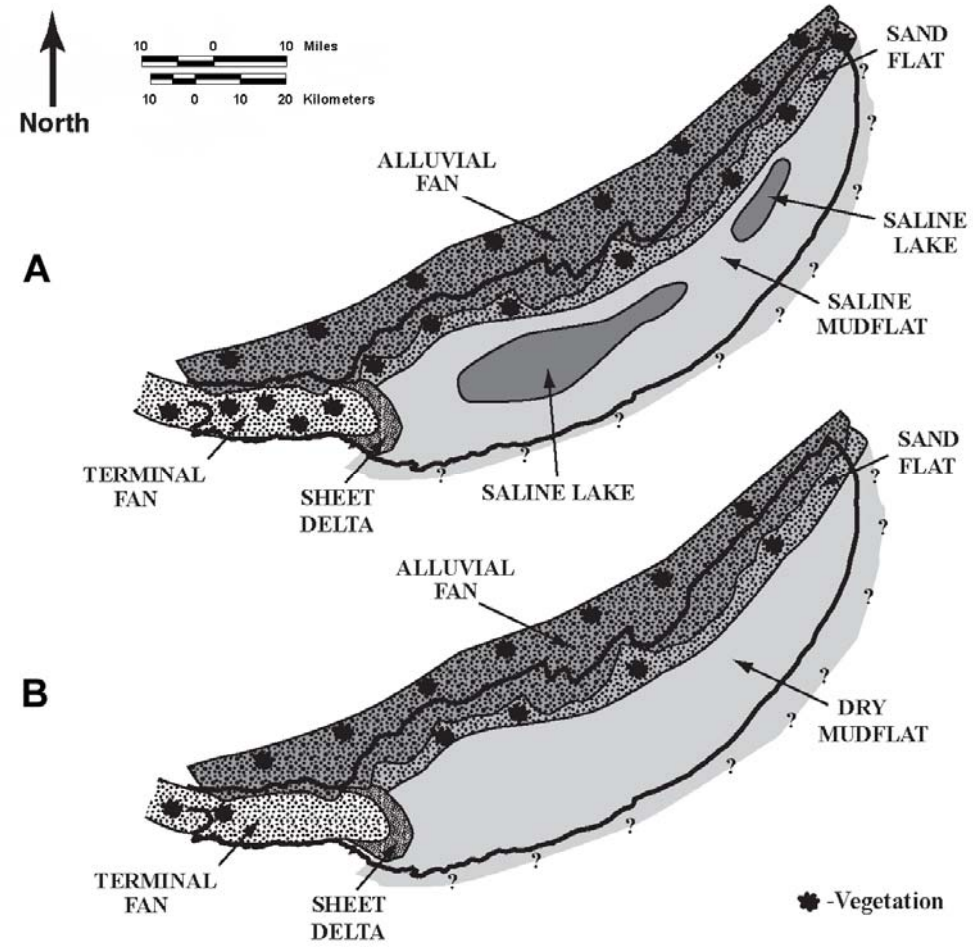

Figure A90. Schematic drawings of the facies distribution in the Newark basin. Thick black lines show current basin limits. A. A shrinking saline lake of the Skunk Hollow Member of the Lockatong Formation. Shallow saline lakes are surrounded by flats covered by powdery efflorescent salt crusts. Sheet deltas form during intermittent flooding of the terminal fan. B. A dry mudflat period of the Skunk Hollow Member of the Lockatong Formation. Most of the basin floor is a vegetation-free mud-cracked flat. Sheet deltas form during intermittent flooding of the terminal fan.

During deposition of the latest Stockton Formation, shallow lakes frequently formed on the muddy plain during wet periods and their deposits were subsequently cut by channel systems during dryer periods. During deposition of the Wilburtha and Scudders Falls Members of the Lockatong Formation, relatively deep lakes formed during wet periods and the basin floor may have become intermittently dry. Wet and dry episodes throughout deposition of the Lockatong and Passaic Formations were highly rhythmic throughout several periodicities that may coincide with climate oscillations initiated by orbital eccentricity cycles (Milankovitch cycles). During deposition of the late part of the Princeton Member of the Lockatong Formation and lasting until the early part of the Perkasie Member of the Passaic Formation, some deep lakes were balanced by evaporation long enough to become saline and precipitate alkaline evaporite minerals. When the lakes dried, saline mudflats formed on the basin floor with powdery efflorescent salt crusts (fig. A90A). During this same period, some lakes were less saline and their floors were covered by evaporite-free dry mudflats (fig. A90B). Vegetation was absent on the basin floor during lake-desiccation stages, but it occurred in shoreline deposits during high lake stands. During deposition of the Warford Member, and lasting through deposition of the Perkasie Member of the Passaic Formation, vegetation developed on dry mudflat deposits just prior to lake transgressions (fig. A91B). This change from the earlier vegetation-free cycles is probably from more frequent rainfall providing a shallow, fresh, groundwater table. The change may also result from the tectonic increase of basin floor area, enabling more freshwater to be stored in sediment before ponding into a lake. During deposition of the upper part of the Perkasie Member and the rest of the Passaic Formation, the deposits of saline lakes, saline mudflats, and dry mudflats are absent (with the exception of the lower part of the Metlars Member). Laminated and thin-bedded lacustrine mudstones alternate with root-disrupted mudstone containing gypsum and anhydrite. These saline soils are attributed to gypsum dust blown from saline basins east of the Newark basin that was reworked in the prevailing semiarid conditions. The absence of saline lake deposits at this time may reflect the short periods of standing water or longer periods of lake water spilling out of the basin, preventing solute accumulation.

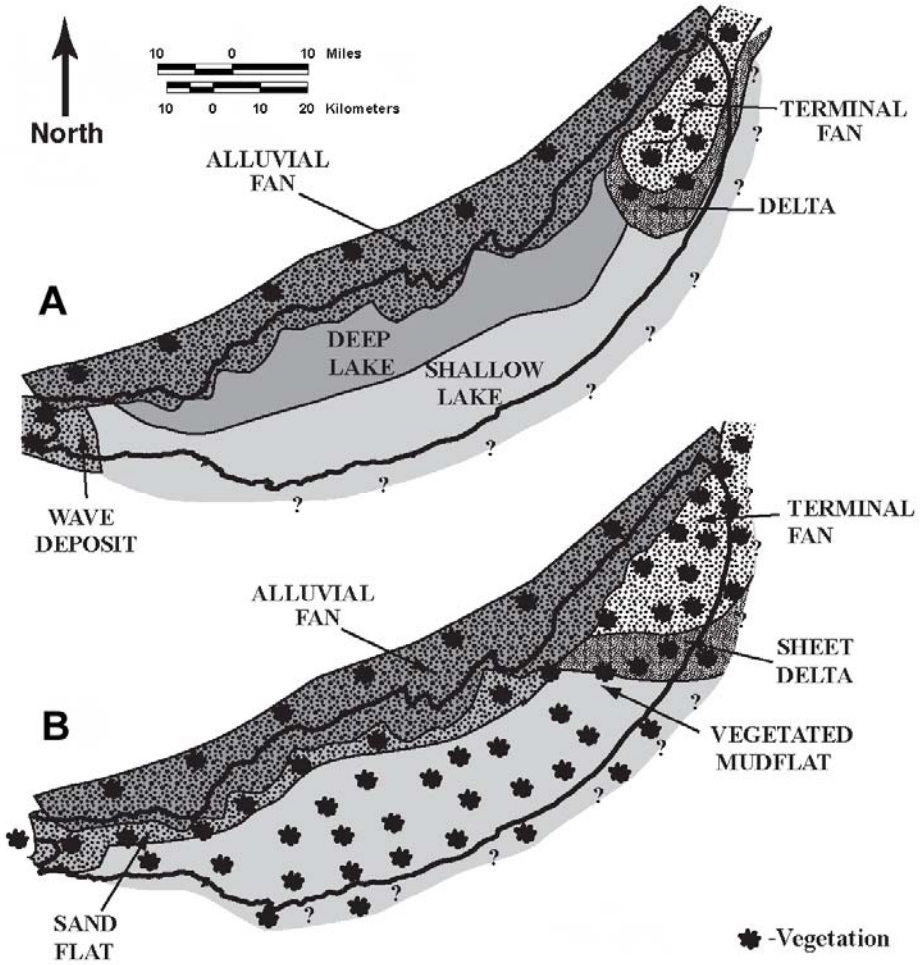

Figure A91. Schematic drawings of facies distribution in the Newark basin. Thick black lines show current basin limits. A. A shrinking lake of the Perkasie Member of the Passaic Formation. Shallow-lake conditions are more widespread than during deposition of the Lockatong. A terminal fan at the northeast end of the basin forms deltas into the lake. Wave-formed deposits occupy the southwestern end of the basin. B. A dry mudflat period of the Neshanic Member of the Passaic Formation. Most of the basin surface is covered by a heavily-vegetated mudflat. Intermittent flooding of the terminal fan produced sheet delta deposits. Gypsum soils formed in most of the vegetated mudflat, but are best developed to the east away from the terminal fan.

The distribution of rocks in the Newark basin records the complex interplay of tectonic forces and climatic changes during deposition. Sandstone geometries are difficult to predict due to uncertainties in the depositional models and to the lack of outcrops. Stockton Formation sandstones and conglomerates are channel deposits that consist of individual channel lenses including ribbons of sandstone that are 1-5 km wide in the lower part of the formation and much wider channel belts (10-30 km wide) in the upper part of the formation, at least in the central part of the basin. The spacing of channel deposits depends upon the relative importance of depositional onlap versus differential subsidence. Sandstones in the Lockatong and Passaic Formations, or their stratigraphic equivalents, include sheets of wave-dominated sandstone that parallel lake margins and are thickest in the northeastern end of the basin (equivalent to the Lockatong and lowest Passaic Formations) and in a broader area on the southwestern side of the basin (equivalent to the upper part of the Passaic Formation). Fluvial sandstone and conglomerate occurs in two upward-coarsening, basinward-thinning wedges beginning at the northeastern and southeastern ends of the basin. Sandstone and conglomerate in the wedges occur as isolated lenses that overlap where closest to the end of the basin and are more isolated in siltstone and mudstone units basinward. The lenses are ribbons of sandstone probably less than 500 m wide. Deltaic sandstone in the Lockatong and Passaic Formations includes thick units of clinoform delta fronts or thin units of sheet-like delta fronts. The clinoform delta sandstones form composite upward-coarsening sequences several meters thick that may laterally extend several kilometers both parallel to and perpendicular to their fluvial source area. These deposits are best developed basinward of the axial sandstone and conglomerate wedges, and near the central part of the southeastern margin of the basin, in the lowest part of the Lockatong Formation. Conglomerate and sandstone form thick units within a few kilometers of the northwestern fault boundary of the basin. They are interbedded with central-basin mudstone of the Lockatong and Passaic Formations, and possibly with siltstone and mudstone of the Stockton Formation. Most of the Newark basin Triassic deposits are cyclic mudstone. Most of the mudstone is unbedded and tightly cemented. Organic-rich, laminated-mudstone beds and gray, laminated to thin-bedded mudstone beds are most abundant in the Lockatong Formation and progressively less common in the Passaic Formation. These weather to shaly bodies on exposure and are also subject to bedding-parallel veins caused by tectonism. Massive mudstone in the Lockatong and Passaic Formations has cement-filled crystal molds in some beds that may weather to open cavities where exposed. Massive mudstone in the upper part of the Passaic Formation tends to be silty and commonly contains gypsum and anhydrite. These rocks weather into chips, and the gypsum and anhydrite may be dissolved to form open cavities as much as tens of meters below the land surface. The gypsum and anhydrite horizons in massive mudstone are most common in the western part of the southeastern fault block, the central fault block, and the eastern parts of the southwestern and northwestern fault blocks. They are less common near the northwestern border fault, near the sandstone-rich areas basinward of the axial sandstone and conglomerate wedges, and the western part of the basin.

The Triassic rocks in the Newark basin record repeated fluctuations in depositional conditions. Although most types of sedimentary features are in conformable vertical successions, they do not represent laterally adjacent facies (table A2). In some stratigraphic levels, organic-rich, flat-laminated mudstone beds appear to have been deposited throughout the entire preserved basin with no laterally-equivalent facies preserved. In other levels, however, organic-rich flat laminated mudstone is equivalent to laminated mudstone with pinch-and-well layers, thin-bedded mudstone with mudcracks, and sandstone with deltaic and wave-formed features. Sedimentary fabrics of dry mudflats are not coeval with perennial lake deposits or saline mudflat deposits. The transition from one set of climate conditions to another probably occurred rapidly with little lateral facies shift over the broad, flat surfaces. Many fabrics represent overprints of processes during periods of desiccation or increased moisture, rather than aggradation during a climatic setting. This complicated overprint of depositional conditions and record of rapid facies changes through time are characteristic of closed-basin conditions and should be expected in other sedimentary deposits in similar settings.

Acknowledgments

I would like to thank Paul Olsen for his extensive aid in showing me exposures, discussing the significance of observations, and providing the free exchange of scientific data and ideas necessary to complete this kind of study. He and Dennis Kent graciously provided access to the Newark Drilling Project cores for description and sampling and provided photographs of the cores. The late Al Froelich provided initial guidance in research of the Newark Supergroup and provided “free rein” for my investigations in the Newark basin. I appreciate the cooperation of the New Jersey and Pennsylvania Geological Surveys during the years that I conducted this study. The paper was greatly improved through thoughtful reviews by Beth Gierlowski-Kordesch, Chris Swezey, Rob Weems, Paul

Table A2. Time equivalent association of the different Triassic mudstone types in the Newark basin. Numbers in the top row refer to the mudstone types in the left-hand column.

Types of mudstone	1	2	3	4	5	6	7	8	9	10	11	12	13	14	15	16	17
1. Flat continuous laminae……		X	X	X	X	X											
2. Pinch-and-swell laminae……....	X		X	X	X	X			X								
3. Graded laminae……	X	X		X	X	X			X								
4. Thin-bedded burrowed……..	X	X	X		X	X			X	X							
5. Thin-bedded graded……..	X	X	X	X		X			X	X							
6. Thin-bedded lenticular……..	X	X	X	X	X				X	X							
7. Thin-bedded vesicular, flat……...								X		X	X						
8. Thin-bedded vesicular, curled……							X			X	X		X				
9. Massive, burrowed……		X	X	X	X	X							X				
10. Massive, brecciated……					X	X	X	X	X		X		X				
11. Massive, vesicular……..							X	X		X			X				
12. Massive, peloidal……														X	X	X	
13. Massive with root structures……..								X	X	X	X						X
14. Laminated with crystals……..												X			X	X	
15. Thin-bedded with crystals……												X		X		X	
16. Massive with graded crystals……												X		X	X		
17. Massive with root structures and gypsum…													X				

Olsen, Irving Grossman, and Gregory Herman. U.S. Geological Survey funding for this research includes the Newark Supergroup Project under Al Froelich and Rob Robinson (1983-1990), a Gilbert Fellowship award (1992-1993), and the Bedrock Regional Aquifer Systems (BRASS) project under Bill Burton (2002-2005).

References

Allen, J.F., 1979, Paleocurrent and facies analysis of the Triassic Stockton Formation in western New Jersey: Rutgers University M.S. thesis, New Brunswick, New Jersey, 84 p.

Allen, J.L., 1970, Studies in fluviatile sedimentation: a comparison of fining-upwards cyclothems, with special reference to coarse-member composition and interpretation: Journal of Sedimentary Petrology, v. 40, p. 298-323.

Anders, M.H., and Schlische, R.W., 1994, Overlapping faults, intrabasin highs, and the growth of normal faults: Journal of Geology, v. 102, p. 165-179.

Anderson, R.Y., and Dean, W.E., 1988, Lacustrine varve formation through time: Palaeogeography, Palaeoclimatology, Palaeoecology, v. 62, p. 215-235.

Armenteros, I., and Huerta, P., 2006, The role of clastic sediment influx in the formation of calcrete and palustrine facies: A response to paleogeographic and climatic conditions in the southeastern Tertiary Duero basin (northern Spain), *in* Alonzo-Zarza, A.M., and Tanner, L.H., eds., Paleoenvironmental Record and Applications of Calcretes and Palustrine Carbonates: Geological Society of America, Special Paper 416, p. 119-132.

Benson, L.V., 1999, Records of millennial-scale climate change from the Great Basin in the western United States, *in* Clark, P.U., Webb, R.S., and Keigwin, L.D., eds., Mechanisms of Global Climate Change at Millenial Time Scales: American Geophysical Union, Geophysical Monograph 112, p. 203-225.

Bertrand-Sarfati, J., Freytet, P., and Plaziat, J.C., 1994, Microstructures in Tertiary nonmarine stromatolites (France). Comparison with Proterozoic, *in* Bertrand-Sarfati, J., and Monty, C., eds., Phanerozoic Stromatolites II: Kluwer Academic Publishers, Dordrecht, The Netherlands, p. 155-191.

Birkeland, P.W., 1999, Soils and Geomorphology, 3rd edition, Oxford University Press, New York, 430 p.

Blair, T.C. and McPherson, J.G., 1994, Alluvial fans and their natural distinction from rivers based on morphology, hydraulic processes, sedimentary processes, and facies assemblages: Journal of Sedimentary Research, v. A64, p. 450-489.

Boersma, J.R., 1970, Distinguishing features of wave ripple cross-stratification and morphology: Geologie en Mijnbouw, v. 49, p. 534-535.

Bohacs, K.M., Carroll, A.R., Neal, J.E., and Mankiewicz, P.J., 2000, Lake-basin type, source

potential, and hydrocarbon character: an integrated sequence-stratigraphic-geochemical framework, *in* Gierlowski-Kordesch, E.H. and Kelts, K.R., eds., Lake Basins Through Space and Time: American Association of Petroleum Geologists Studies in Geology 46, p. 3-33.

Bouma, A.H., 1964, Ancient and recent turbidites: Geologie en Mijnbouw, v. 43, p. 375-379.

Bowler, J.M., 1973, Clay dunes: Their occurrence, formation and environmental significance: Earth Science Reviews, v. 9, p. 315-338.

Bridge, J.S., 1984, Large-scale facies sequences in alluvial overbank environments: Journal of Sedimentary Petrology, v. 54, p. 583-588.

Cant, D.J., and Walker, R.G., 1978, Fluvial processes and facies sequences in the sandy braided South Saskatchewan River, Canada: Sedimentology, v. 25, p. 625-648.

Casanova, J., 1994, Stromatolites from the East African Rift: A synopsis, *in* Bertrand-Sarfati, J., and. Monty, C., eds., Phanerozoic Stromatolites II: Kluwer Academic Publishers, Dordrecht, The Netherlands, p. 193-226.

Cohen, A.S., 2003, Paleolimnology: The History and Evolution of Lake Systems: Oxford University Press, New York, New York, 500 p.

Cornet, B., 1977, The palynostratigraphy and age of the Newark Supergroup: Pennsylvania State University Ph.D. disseration, Pennsylvania, 504 p.

Costa, J.E., 1988, Rheologic, geomorphic, and sedimentologic differentiation of water floods, hyperconcentrated flows, and debris flows, *in* Baker, V.R., Kochel, R.C., and Patton, P.C., eds., Flood Geomorphology: Wiley, New York, New York, p. 113-122.

DeWet, C.B., Mora, C.I., Gore, P.J.W., Gierlowski-Kordesch, E., and Cucolo, S.J., 2002, Deposition and geochemistry of lacustrine and spring carbonates in Mesozoic rift basins, eastern North America, *in* Renaut, R.W. and Ashley, G.M., eds., Sedimentation in Continental Rifts: Society of Economic Paleontologists and Mineralogists Special Publication No. 73, p. 309-325.

Donovan, R.N., and Forster, R.J., 1972, Subaqueous shrinkage cracks from the Caithness Flagstone Series (Middle Devonian) of Northeast Scotland: Journal of Sedimentary Petrology, v. 42, p. 309-317.

Drake, A.A., Volkert, R.A., Monteverde, D.H. Herman, G.C., Houghton, H.F., Parker, R.A., and Dalton, R.F., 1996, Bedrock geologic map of northern New Jersey: U.S. Geological Survey, Miscellaneous Investigation Series Report I-2540-A, 2 sheets, scale 1:100,000.

Dubiel, R.F., and Smoot, J.P., 1994, Criteria for interpreting paleoclimate from red beds – a tool for Pangean reconstructions, *in* Embry, A.F., Beauchamp, B., and Glass, D.J., eds., Pangea: Global Environments and Resources: Canadian Society of Petroleum Geologists, Memoir 17, Calgary, Canada, p. 295-310.

Dunning, G.R., and Hodych, J.P., 1990, U/Pb zircon and baddelyite ages for the Palisades and Gettysburg sills of the northeastern United States: Implications for the age of the Triassic/Jurassic boundary: Geology, v. 18, p. 795-798.

El Tabakh, M., 1994, Early rift-basin deposition: Triassic-Jurassic sedimentation and subsequent diagenesis in the Newark basin, New Jersey: City University of New York Ph.D. dissertation, New York, New York, 382 p.

El Tabakh, M., Riccioni, R., and Schreiber, B.C., 1997, Evolution of late Triassic rift basin evaporites (Passaic Formation): Newark Basin, Eastern North America: Sedimentology, v. 44, p. 767-790.

El Tabakh, M., and Schreiber, B.C., 1994, Lithologies and diagenesis of the lacustrine sediments of the Lockatong Formation (Upper Triassic) in the Newark rift basin, *in* Lomando, A.J., Schreiber, B.C., and Harris, P.M., eds., Lacustrine Reservoirs and Depositional Systems: Society of Economic Paleontologists and Mineralogists Core Workshop 19, p. 239-295.

El Tabakh, M., and Schreiber, B.C., 1998, Diagenesis of the Newark rift basin, Eastern North America: Sedimentology, v. 45, p. 855-874.

Eugster, H.P., and Surdam, R.C., 1973, Depositional environment of the Green River Formation of Wyoming: a preliminary report: Geological Society of America Bulletin, v. 86, p. 319-334.

Faill, R.T., 1973, Tectonic development of the Triassic Newark-Gettysburg basin in Pennsylvania: Geological Society of America Bulletin, v. 84, p. 725-740.

Faill, R.T., 2003, The early Mesozoic Birdsboro central Atlantic margin basin in the Mid-Atlantic region, eastern United States: Geological Society of America Bulletin, v. 115, p. 406-421.

Faill, R.T., 2005, The early Mesozoic Birdsboro central Atlantic margin basin in the Mid-Atlantic region, eastern United States: Reply: Geological Society of America Bulletin, v. 117, p. 829-832.

Fedosh, M.S., and Smoot, J.P., 1988, A cored stratigraphic section through the northern Newark basin, New Jersey, *in* Froelich, A.J. and Robinson, G.R., eds., Studies of the Early Mesozoic Basins of the Eastern United States: U.S. Geological Survey Bulletin 1776, p. 19-24.

Froelich, A.J., and Gottfried, D., 1999, Chapter 12B: Early Mesozoic – Igneous and Contact Metamorphic Rocks, *in* Schultz, C.H., ed., The Geology of Pennsylvania, Special Publication 1, Pennsylvania Geological Survey and Pittsburgh Geological Society, p. 202-209.

Froelich, A.J., and Olsen, P.E., 1983, Newark

Supergroup, a revision of the Newark Group in eastern North America: U.S. Geological Survey Bulletin 1537-A, p. A55-A58.

Gibling, M.R., 2006, Width and thickness of fluvial channel bodies and valley fills in the geological record; a literature compilation and classification: Journal of Sedimentary Research, v. 76, p. 731-770.

Gilbert, G.K., 1885, The topographic features of lake shores: U.S. Geological Survey, 5th Annual Report, p. 69-123.

Gilbert, G.K., 1890, Lake Bonneville, U.S. Geological Survey, Monograph 1, 438 p.

Glaesser, J.D., 1966, Provenance, dispersal and depositional environments of Triassic sediments in the Newark-Gettysburg basin: Pennsylvania Topographic and Geologic Survey, 4th Series, Bulletin G-43, 168 p.

Gustavson, T.C., Ashley, G.M., and Boothroyd, J.C., 1975, Depositional sequences in glaciolacustrine deltas, *in* Jopling, A.V., and McDonald, B.C., eds., Glaciofluvial and Glaciolacustrine Sedimentation: Society of Economic Paleontologists and Mineralogists Special Publication 23, 264-280.

Hames, W.E., Renne, P.R., and Ruppel, C., 2000, New evidence for geologically-instantaneous emplacement of the earliest Jurassic Central Atlantic Magmatic Province basalts on the North American margin: Geology, v. 28, p. 859-862.

Harms, J.C., Southard, J.B., and Walker, R.G., 1982, Structures and sequences in clastic rocks: Society of Economic Paleontologists and Mineralogists Short Course 9, Tulsa, Oklahoma, 225 p.

Hasiotis, S.T., 2002, Continental Trace Fossils, Society of Economic Paleontologists and Mineralogists Short Course Notes, v. 51, 132 p.

Herman, G.C., 2006, Joints and veins in the Newark basin, New Jersey in regional perspective, *in* Gates, A.E. ed., Newark Basin – View from the 21st Century: Field Guide and Proceedings of the 22nd Annual Meeting of the Geological Association of New Jersey, p. 75-116.

Heward, A.P., 1978, Alluvial fan sequence and megasequence models: with examples from Westphalian D – Stephanian B coalfields, northern Spain, *in* Miall, A.D., ed., Fluvial Sedimentology: Canadian Society of Petroleum Geologists, Memoir 5, p. 669-702.

Holliday, V.T., Hovorka, S.D., and Gustavson, T.C., 1996, Lithostratigraphy and geochronology of fills in small playa basins on the Southern High Plains, United States: Geological Society of America Bulletin, v. 108, p. 953-965.

Holser, W.T., Clement, G.P., Jansa, L.F., and Wade, J.F., 1988, Evaporite deposits of the North Atlantic Rift, *in* Manspeizer, W., ed., Triassic-Jurassic Rifting: Continental Breakup and the Origin of the Atlantic Ocean and Passive Margins: Elsevier, Amsterdam, The Netherlands, p. 525-556.

Hovorka, S.D., 1997, Quaternary evolution of ephemeral playa lakes on the Southern High Plains of Texas: cyclic variation in lake level recorded in sediments: Journal of Paleolimnology, v. 17, p. 131-146.

Jopling, A.V., and Walker, R.G., 1968, Morphology and origin of ripple-drift cross-lamination with examples from the Pleistocene of Massachusetts: Journal of Sedimentary Petrology, v. 38, p. 971-984.

Kelly, S.B., and Olsen, H., 1993, Terminal fans – a review with reference to Devonian examples: Sedimentary Geology, v. 85, p. 339-374.

Kemp, A.E.S., 1996, Laminated sediments as palaeo-indicators, in A.E.S. Kemp, ed., Palaeoclimatology and Palaeooceanography from Laminated Sediments: Geological Society of London Special Publication No. 116, p. vii-xii.

Kent, D.V., and Tauxe, L., 2005, Corrected Late Triassic latitudes for continents adjacent to the North Atlantic: Science, v. 307, p. 240-244.

Komar, P.D., and Miller, M.C., 1975, Sediment threshold under oscillatory waves: Proceedings 14th Conference on Coastal Engineering, p. 1101-1110.

Kozur, H.W., and Weems, R.E., 2005, Conchostracan evidence for a late Rhaetian to early Hettangian age for the CAMP volcanic event in the Newark Supergroup, and a Sevatian (late Norian) are for the immediately underlying beds: Hallesches Jahrbuch fur Geowissenschaften, v. 27, p. 21-51.

Kozur, H.W., and Weems, R.E., 2007, Upper Triassic conchostracan biostratigraphy of the continental rift deposits of eastern North America: Its importance for correlating Newark Supergroup events with the Germanic Basin and the International Geologic Time Scale, *in* Lucas, S.G. and Spielmann, J.A., eds., The Global Triassic: New Mexico Museum of Natural History and Science Bulletin 41, p. 137-188.

Kraus, M.J., and Wells, T.M., 1999, Recognizing avulsion deposits in the ancient stratigraphical record, *in* Smith, N.D. and Rogers, J., eds., Fluvial Sedimentology VI: Special Publication 28, International Association of Sedimentologists, Blackwell, Oxford, England, p. 251-268.

LaCombe, P.J., 2000, Hydrogeologic framework, water levels, and trichloroethylene contamination, Naval Air Warfare Center, West Trenton, New Jersey, 1993-1997: U.S. Geological Survey Water-Resources Investigations Report 98-4167, 139 p.

Lambiase, J.J., 1990, A model for tectonic control of lacustrine stratigraphic sequences in continental rift basins, *in* Katz, B.J., ed., Lacustrine Basin Exploration – Case Studies and Modern Analogs: American Association of Petroleum Geologists, Memoir 50, p. 265-276.

LeTourneau, P.M., 2003, Stratigraphic architecture and

paleomagnetic reversal stratigraphy of the Late Triassic Taylorsville basin, Virginia and Maryland, USA, *in* LeTourneau, P.M. and Olsen, P.E., eds., The Great Rift Valleys of Pangea in Eastern North America, v. 2, Sedimentology, Stratigraphy, and Paleontology: Columbia University Press, New York, New York, p. 12-58.

Machette, M.N., 1985, Calcic soils of the southwestern United States, *in* Weide, D.L., ed., Soils and Quaternary Geology of the Southwestern United States: Geological Society of America, Special Paper 203, p. 1-21.

Makaske, B., 2001, Anastomosing rivers: a review of their classification, origin and sedimentary products: Earth Science Reviews, v. 53, p. 149-196.

McLaughlin, D.B., 1945, Type sections of the Stockton and Lockatong Formations: Pennsylvania Academy of Sciences Proceedings, v. 19, p. 102-113.

McLaughlin, D.B., 1946, Continuity of strata in the Newark Series: Michigan Academy of Science, Arts and Letters, v. 32, p. 295-303.

McLaughlin, D.B., 1959, Mesozoic rocks, *in* Willard, B., ed., Geology and Mineral Resources of Bucks County, Pennsylvania: Pennsylvania Geological Survey, 4th series, Bulletin C9, p. 55-162.

Olsen, H., 1987, Ancient ephemeral stream deposits: A local terminal fan model from the Bunter Sandstone Formation (L. Triassic) in the Tonder-3, -4, and -5 wells, Denmark, *in* Frostick, L. and Reid, I., eds., Desert Sediments: Ancient and Modern: Geological Society of London, Special Publication 35, p. 69-86.

Olsen, P.E., 1980, The latest Triassic and Jurassic formations of the Newark basin (eastern North America Newark Supergroup): stratigraphy, structure, and correlation: New Jersey Academy of Sciences Bulletin, v. 25, p. 25-51.

Olsen, P.E., 1984, Comparative paleolimnology of the Newark Supergroup – A study of ecosystem evolution: Yale University Ph.D. disseration, New Haven, Connecticut, 726 p.

Olsen, P.E., 1986, A 40-million year lake record of early Mesozoic orbital climate forcing: Science, v. 234, p. 842-848.

Olsen, P.E., 1988, Continuity of strata in the Newark and Hartford basins, *in* Froelich, A.J. and Robinson, G.R., eds., Studies of the Early Mesozoic Basins of the Eastern United States: U.S. Geological Survey Bulletin 1776, p. 6-18.

Olsen, P.E., 1997, Stratigraphic record of the early Mesozoic breakup of Pangea in the Laurasia-Gondwana rift system: Earth and Planetary Science Review, v. 25, p. 337-401.

Olsen, P.E., and Kent, D.V., 1996, Milankovitch climate forcing in the tropics of Pangea during the Late Triassic: Palaeogeography, Palaeoclimatology, Palaeoecology, v. 122, p. 1-26.

Olsen, P.E., Kent, D.V., Cornet, B., Witte, W.K., and Schlische, R.W., 1996, High-resolution stratigraphy of the Newark rift basin (early Mesozoic, eastern North America): Geological Society of America Bulletin, v. 108, p. 40-77.

Olsen, P.E., and Rainforth, E.C., 2001, The "Age of Dinosaurs" in the Newark basin, with special reference to the lower Hudson Valley: 2001 New York State Geological Association Guidebook, p. 59-176.

Olsen, P.E., Schlische, R.W., and Gore, P.J.W., 1989, Tectonic, depositional, and paleoecological history of early Mesozoic rift basins, eastern North America: 28th International Geological Congress, Field Trip Guidebook T351, 174 p.

Olsen, P.E., Whiteside, J.H., and Smoot, J.P., in press, Lacustrine cyclicity and the Triassic-Jurassic transition: The Mosasaur

Oshchuldak, M.E., and Hubert, J.F., 1988, Petrology of Mesozoic sandstones in the Newark basin, central New Jersey and adjacent New York, *in* Manspeizer, W., ed., Triassic-Jurassic Rifting: Continental Breakup and the Origin of the Atlantic Ocean and Passive Margins: Elsevier, Amsterdam, The Netherlands, p. 333-352.

Owens, J.P., Sugarman, P.J., Sohl, N.F., Parker, R.A., Houghton, H.F., Volkert, R.A., Drake, A.A., Orndorff, R.C., Bybell, L.M., Andrews, G.W., Bukry, D., Zapecza, O.S., Paulachok, G.N., and Mullikin, L., 1998, Bedrock geologic map of central and southern New Jersey: U.S. Geological Survey, Miscellaneous Investigation Series Report I-2540-B, 4 sheets, 1:100,000.

Parker, R.A., Houghton, H.F., and McDowell, R.C., 1988, Stratigraphic framework and distribution of early Mesozoic rocks of the northern Newark basin, New Jersey and New York, *in* Froelich, A.J. and Robinson, G.R., eds., Studies of the Early Mesozoic Basins of the Eastern United States: U.S. Geological Survey Bulletin 1776, p. 31-39.

Pietras, J.T., and Carroll, A.R., 2006, High-resolution stratigraphy of an underfilled lake basin: Wilkins Peak Member, Eocene Green River Formation, Wyoming, U.S.A.: Journal of Sedimentary Research, v. 76, p. 1197-1214.

Raaf, J.F.M., de, Boersma, J.R., and Gelder, A., van, 1977, Wave-generated structures and sequences from a shallow marine succession, Lower Carboniferous, County Cork, Ireland: Sedimentology, v. 24, p. 451-483.

Rasbury, E.T., de Wet, C.B., and Nienstedt, J., 2003, U-Pb age of stromatolite calcite from the Triassic Passaic Formation of the Newark basin: Geological Society of America, Abstracts with Programs, National Meeting, v. 34, p. 508.

Ratcliffe, N.M., and Burton, W.C., 1985, Fault reactivation models for origin of the Newark basin and studies related to Eastern U.S. seismicity, *in*

Robinson, G.R. and Froelich, A.J., eds., Proceedings of the second U.S. Geological Survey Workshop on the Early Mesozoic Basins of the Eastern United States: U.S. Geological Survey Circular 946, p. 36-45.

Ratcliffe, N.M., Burton, W.C., D'Angelo, R.M., and Costain, J.K., 1986, Low-angle extensional faulting, reactivated mylonites, and seismic reflection geometry of the Newark basin margin in eastern Pennsylvania: Geology, v. 14, p. 766-770.

Retallack, G.J., 2001, Soils of the Past: Blackwell Science Ltd., Oxford, England, 404 p.

Reynolds, D.J., 1993, Sedimentary basin evolution: tectonic and climatic interaction: Columbia University Ph.D. dissertation, New York, New York, 215 p.

Rima, D.R., Meisler, H., and Longwill, S., 1962, Geology and hydrology of the Stockton Formation in southeastern Pennsylvania: Pennsylvania Topographic and Geologic Survey, Bulletin W-14, 111 p.

Rowan, D.J., Kalff, J., and Rasmussen, J.B., 1992, Estimating the mud deposition boundary depth in lakes from wave theory: Canadian Journal of Fisheries and Aquatic Science, v. 49, p. 2490-2497.

Saez, A., Anadon, P., Herrero, M.J., and Moscariello, A., 2007, Variable style of transition between Palaeogene fluvial fan and lacustrine systems, southern Pyrenean foreland, NE Spain: Sedimentology, v. 54, p. 367-390.

Savage, E.L., 1967, The Triassic sediments of Rockland County, New York: Rutgers University Ph.D. disseration, New Brunswick, New Jersey, 193 p.

Savage, E.L., 1968, Triassic rocks of the northern Newark Basin, Trip C: New York Geological Association, Guidebook for Field Excursions, p. 49-68.

Schaller, W.T., 1932, The crystal cavities of the New Jersey zeolite region: U.S. Geological Survey Bulletin 832, 85 p.

Schlische, R.W., 1992, Structural and stratigraphic development of the Newark extensional basin, eastern North America: Evidence for the growth of the basin and its bounding structures: Geological Society of America Bulletin, v. 104, p. 1246-1263.

Schlische, R.W., and Olsen, P.E., 1990, Quantitative filling model for continental extensional basins with applications to early Mesozoic rifts of eastern North America: Journal of Geology, v. 98, p. 135-155.

Schlische, R.W., and Withjack, M.O., 2005, The early Mesozoic Birdsboro central Atlantic margin basin in the Mid-Atlantic region, eastern United States: Discussion: Geological Society of America Bulletin, v. 117, p. 823-828.

Simonson, B.M., Smoot, J.P., and Hughes, J., 2010, Paragenesis of authigenic minerals in macropores and veins in Late Triassic mudstone of the Newark basin: implications of late digenetic fluid migration through mudstone, *in* Herman, G.C., and Serfes, M.E., N.J. Geological Survey Bulletin 77, p. B1-B26.

Smith, D.G., 1983, Anastomosed fluvial deposits: modern examples from western Canada, *in* Collinson, J.D. and Lewin, J., eds., Modern and Ancient Fluvial Systems: International Association of Sedimentology Special Publication 6, p. 155-168.

Smith, I.R., and Sinclair, I.J., 1972, Deep water waves in lakes: Freshwater Biology, v. 2, p. 387-399.

Smoot, J.P., 1983, Depositional environments in an arid closed basin: the Wilkins Peak Member of the Green River Formation (Eocene), Wyoming, U.S.A.: Sedimentology, v. 30, p. 801-827.

Smoot, J.P., 1991, Sedimentary facies and depositional environments of early Mesozoic Newark Supergroup basins, eastern North America: Palaeogeography, Palaeoclimatology, Palaeoecology, v. 84, p. 369-423.

Smoot, J.P., 1999, Chapter 12A: Early Mesozoic - Sedimentary Rocks, *in* Schultz, C.H., ed., The Geology of Pennsylvania, Special Publication 1, Pennsylvania Geological Survey and Pittsburgh Geological Society, p. 180-201.

Smoot, J.P., 2006, Late Triassic evaporite minerals of the Newark basin, New Jersey and Pennsylvania: Geological Society of America, Abstracts with Programs, v. 38, p. 85.

Smoot, J.P., and Benson, L.V., 1998, Sedimentary structures as indicators of paleoclimatic fluctuations, Pyramid Lake, Nevada, *in* Pitman, J.K. and Carroll, A.R., eds., Modern and Ancient Lake Systems: Utah Geological Association, Guidebook 26, Salt Lake City, Utah, p. 131-161.

Smoot, J.P., and Castens-Seidell, B., 1994, Sedimentary features produced by efflorescent salt crusts, Saline Valley and Death Valley, California, *in* Renaut, R. and Last, W.M., eds., Sedimentology and Geochemistry of Modern and Ancient Saline Lakes: Society of Economic Paleontologists and Mineralogists Special Publication 50, p. 73-90.

Smoot, J.P., and Lowenstein, T.K., 1991, Depositional environments of non-marine evaporites, in J.L. Melvin, ed., Evaporites, Petroleum and Mineral Resources: Devolpments in Sedimentology 50: Elsevier, Amsterdam, The Netherlands, p. 189-347.

Smoot, J.P. and Olsen, P.E., 1988, Massive mudstones in basin analysis and paleoclimatic interpretation of the Newark Supergroup, *in* Manspeizer, W., ed., Triassic-Jurassic Rifting: Continental Breakup and the Origin of the Atlantic Ocean and Passive Margins: Elsevier, Amsterdam, The Netherlands, p. 249-274.

Smoot, J.P., and Olsen, P.E., 1994, Climatic cycles as sedimentary controls of rift-basin lacustrine deposits in the early Mesozoic Newark basin based on

continuous core, *in* Lomando, A.J. , Schreiber, B.C., and Harris, P.M., eds., Lacustrine Reservoirs and Depositional Systems: Society of Economic Paleontologists and Mineralogists Core Workshop 19, p. 201-237.

Sutter, J.F., 1988, Innovative approaches to the dating of igneous events in the Early Mesozoic basins of the eastern United States, *in* Froelich, A.J. and Robinson, G.R., eds., Studies of the Early Mesozoic Basins of the Eastern United States: U.S. Geological Survey Bulletin 1776, p. 194-200.

Turner-Peterson, C.E., 1980, Sedimentology and uranium mineralization in the Triassic-Jurassic Newark basin, Pennsylvania and New Jersey, *in* Peterson, C.E., ed., Uranium in Sedimentary Rocks: Application of the Facies Concept in Exploration: Society of Economic Paleontologists and Mineralogists Short Course Notes, Rocky Mountain Section, p. 149-170.

Turner-Peterson, C.E., and Smoot, J.P., 1985, New thoughts on facies relationships in the Triassic Stockton and Lockatong Formations, Pennsylvania and New Jersey, *in* Robinson, G.R. and Froelich, A.J., eds., Proceedings of the second U.S. Geological Survey Workshop on the Early Mesozoic Basins of the Eastern United States: U.S. Geological Survey Circular 946, p. 10-17.

Van Houten, F.B., 1962, Cyclic sedimentation and the origin of analcime-rich Upper Triassic Lockatong Formation, west-central New Jersey and adjacent Pennsylvania: American Journal of Science, v. 260, p. 561-576.

Van Houten, F.B., 1964, Cyclic lacustrine sedimentation, Upper Triassic Lockatong Formation, New Jersey and adjacent Pennsylvania, *in* Merriam, D.F., ed., Symposium on Cyclic Sedimentation: Kansas Geological Survey Bulletin 169, p. 497-531.

Van Houten, F.B., 1965, Crystal casts in Upper Triassic Lockatong and Brunswick Formations: Sedimentology, v. 4, p. 301-313.

Warren, J.K., 1982, The hydrological setting, occurrence and significance of gypsum in Late Quaternary salt lakes in South Australia: Sedimentology, v. 29, p. 609-637.

Wherry, E.T., 1916, Glauberite crystal-cavities in the Triassic rocks of eastern Pennsylvania: American Mineralogist, v. 1, p. 114-125.

Wilding, L.P., and Puentes, R., 1988, Vertisols: Their Distribution, Properties, Classification and Management. Technical Monograph 18: Texas A&M, College Station, Texas, 193 p.

Withjack, M.O., Schlische, R.W., and Olsen, P.E., 2002, Rift-basin structure and its influence on sedimentation systems, *in* Renault, R.W. and Ashley, G.M., eds., Sedimentation in Continental Rifts: Society of Economic Paleontologists and Mineralogists Special Publication 73, Tulsa, Oklahoma, p. 57-81.

Authigenic Minerals in Macropores and Veins in Late Triassic Mudstones of the Newark Basin: Implications for Fluid Migration through Mudstone

By Bruce M. Simonson, Oberlin College,
Joseph P. Smoot, U.S. Geological Survey and
Jennifer L. Hughes, West Virginia Dept. Environmental Protection

Chapter B of

Contributions to the Geology and Hydrogeology of the Newark Basin

N.J. Geological Survey Bulletin 77

State of New Jersey
Department of Environmental Protection
Water Resource Management
New Jersey Geological Survey
2010

Contents

Figures

Table

Chapter B

Authigenic Minerals in Macropores and Veins in Late Triassic Mudstones of the Newark Basin: Implications for Fluid Migration through Mudstone

Bruce M. Simonson[1], Joseph P. Smoot[2] and Jennifer L. Hughes[3]

Abstract

At the time of deposition, many of the nonmarine mudstones in the early Mesozoic Newark Supergroup of eastern North America contained abundant millimeter-scale macropores in the form of desiccation cracks, trapped air bubbles (vesicles), and/or root tubules. Most of these macropores are currently filled with coarsely crystalline authigenic minerals, most commonly analcime, K-feldspar, albite, calcite, dolomite, gypsum, and (or) anhydrite. Some of these fillings display textures typical of void-filling cements, but there is also ample petrographic evidence of a long and complex diagenetic history involving major changes in chemical composition. For example, carbonate rhombs are pseudomorphed by analcime or feldspar, analcime euhedra are invaded by K-feldspar, and K-feldspar is replaced by carbonate. Widespread veins and veinlets with mineral assemblages and parageneses very similar to those of the macropores indicate the fluids responsible for these phases were circulating primarily through fractures. Authigenic K-feldspars in the macropores yield $^{40}Ar/^{39}Ar$ dates of ca. 195 Ma, indicating reactive solutions were still circulating through these mudstones 20 million years or more after deposition. K-rich phases in the mafic intrusions and extrusions of the Newark basin succession yield comparable ages, indicating some of the diagenetic phases and probably some of the fractures formed at the time the plutons were emplaced. However, the fact that other phases predate and postdate the K-feldspar suggests fluids were circulating through the mudstones and precipitating authigenic minerals over a longer time span. Unlike most marine mudstones, these mudstones have not been strongly compacted; we attribute this to fabrics produced during subaerial exposure and (or) to early partial cementation. Therefore, external sources of material are required to occlude most of the macropore porosity. However, the authigenic minerals form three discrete assemblages that appear to be tied to the stratigraphy on a broad scale, suggesting they are related in some way to depositional environments. The apparent contradiction of late diagenetic cements and stratigraphically controlled mineralogy can be resolved if the authigenic minerals precipitated from solutions that originated as brines in alkaline lake environments, then evolved progressively over long periods of time by back-reacting with the sediments. Maturation of organic matter may have also played a role in changing the chemistry of the authigenic minerals. The precise causes of fracturing and fluid migration are not known with certainty. Possible causes include the progressive release of strain from continued extension of the basin during sedimentation, gravity-driven fluid flows, fracturing related to fluid overpressuring by emplacement of mafic intrusions, and shifts in stress orientation during later Jurassic compression and erosion of the basin. More recently, dissolution of soluble minerals from both macropores and fractures has helped to create effective conduits for groundwater flow and exerts a negative influence on local groundwater quality.

Introduction

The early Mesozoic Newark Supergroup of eastern North America consists of nonmarine strata deposited in a series of rift basins, the best exposed of which is the Newark basin (fig. B1). The dominant lithology in many of the stratigraphic units in these basins is mudstone, such as in the Lockatong and Passaic Formations of the Newark basin (fig. B2). Occurrences of coarsely crystalline (that is, sparry) authigenic minerals are widespread in the mudstones of the Newark Supergroup. They were first described from the Lockatong Formation by Van Houten (1962, 1964), who noted an abundance of authigenic analcime and

[1]Oberlin College
Dept. of Geology
52 West Lorain St., Oberlin, OH 44074
bsimonso@oberlin.edu

[2]U.S. Geological Survey.
M.S. 926A, National Center
Reston, VA 20192

[3]West Virginia Dept. Environmental Protection
601 57th Street
Charleston, WV 25304

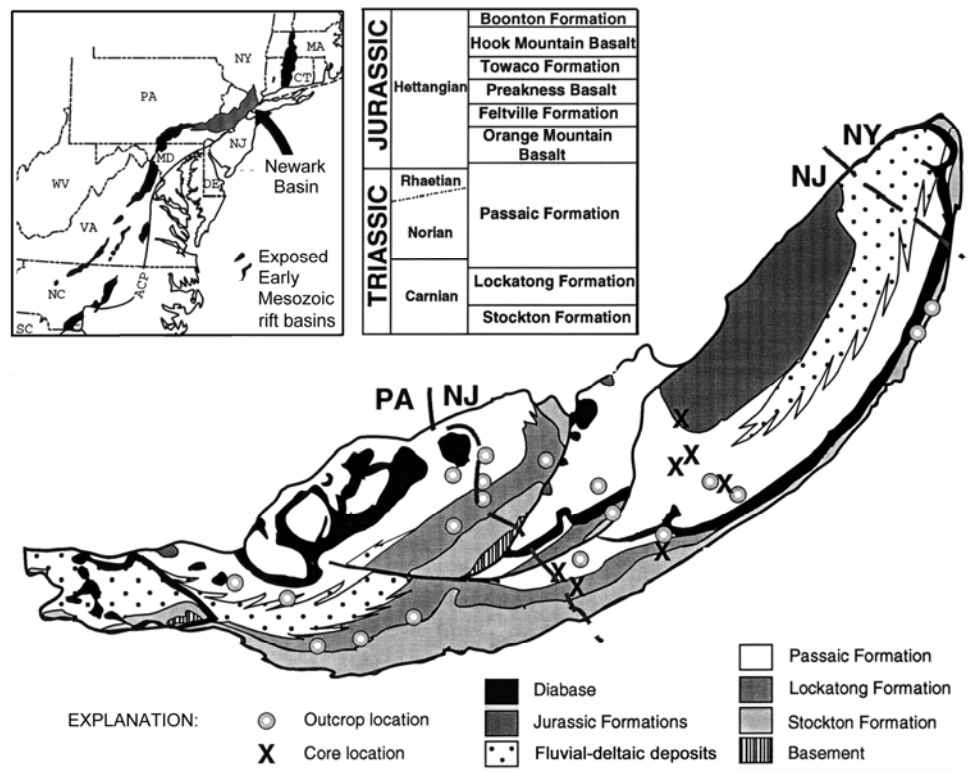

Figure B1. Map of the Newark basin showing general geology and sites where samples were collected for this study. Insets in upper left show the exposed portions of the Newark Supergroup basins and the age and stratigraphy of the Newark basin proper. Fluvial-deltaic deposits were formed at several different times by several different major inputs into the basin (Smoot, 2010).

dolomite and interpreted them as syndepositional precipitates formed from surface and (or) very shallow subsurface waters. He further proposed that the Lockatong mudstones were deposited in alkaline lakes because of the abundance of sodium-rich tectosilicates and associated magnesium-rich carbonate, an interpretation that gained wide acceptance (for example, Turner-Peterson, 1980; Lorenz, 1988).

Much of the authigenic material in the Newark mudstones is coarsely crystalline and in macropores that are locally abundant (table B1). Coarse crystals growing in mudstones seem counterintuitive since they generally have small pores and serve as barriers to subsurface fluid flow, but the incongruity of having sparry authigenic minerals in the Newark basin mudstones has not been perceived as a problem, presumably because of the syngenetic interpretation proposed by Van Houten (1962, 1964). The presence of coarse crystals of authigenic tectosilicates in macropores is particularly problematic. In addition to analcime, authigenic potassium-feldspar (K-feldspar) and albite are also abundant in the nonmarine mudstones of the Lockatong and Passaic Formations (Simonson and Smoot, 1994, 1995; van de Kamp and Leake, 1996). Both authigenic analcime and K-feldspar have been detected in late Tertiary and younger sediments, but only as extremely fine crystals (Surdam and Eugster, 1976; Surdam and Sheppard, 1978; Gude and Sheppard, 1988; Stamatikis, 1989; Renaut, 1993; Mees and others, 2005). Moreover, to our knowledge, albite has not been documented as a synsedimentary authigenic phase in any modern environment. Data presented in this paper indicate the syngenetic interpretation is no longer tenable for these and many of the other coarsely crystalline authigenic minerals in the Newark mudstones and, therefore, an origin later in diagenesis is proposed. Given this interpretation, the ability of nonmarine mudstones to serve as conduits for, instead of barriers to, subsurface fluid flow needs to be reassessed. Dissolution of secondary minerals in macropores and associated veins has also produced major water-bearing zones throughout the Newark basin fill (Rima, 1955; Herman, 2001) and alters water chemistry by increasing the amount of total dissolved solids (Michalski and Britton, 1997; Serfes, 2005). Moreover, the dissolution of these minerals contributes to the mobilization of major and trace elements, such as arsenic, by exposing the matrix surface to weakly acidic groundwater.

This study of the mudstones in the Newark basin was made possible by cores drilled during the Newark Basin Coring Project (NBCP) of the Continental Scientific Drilling Program. Olsen and others (1996) obtained more than 6,770 m of continuous core representing a composite section of about 5,200 m in thickness that includes most of the Newark basin fill. They achieved this using an ingenious offset coring technique involving the drilling of a series of cores, each about 1.5 km deep, at 7 sites at progressively deeper stratigraphic levels, with about 15-percent stratigraphic overlap between adjacent cores. Of the approximately 5.2-km thickness of section cored, about 0.83 km lies within the Lockatong Formation and 3.26

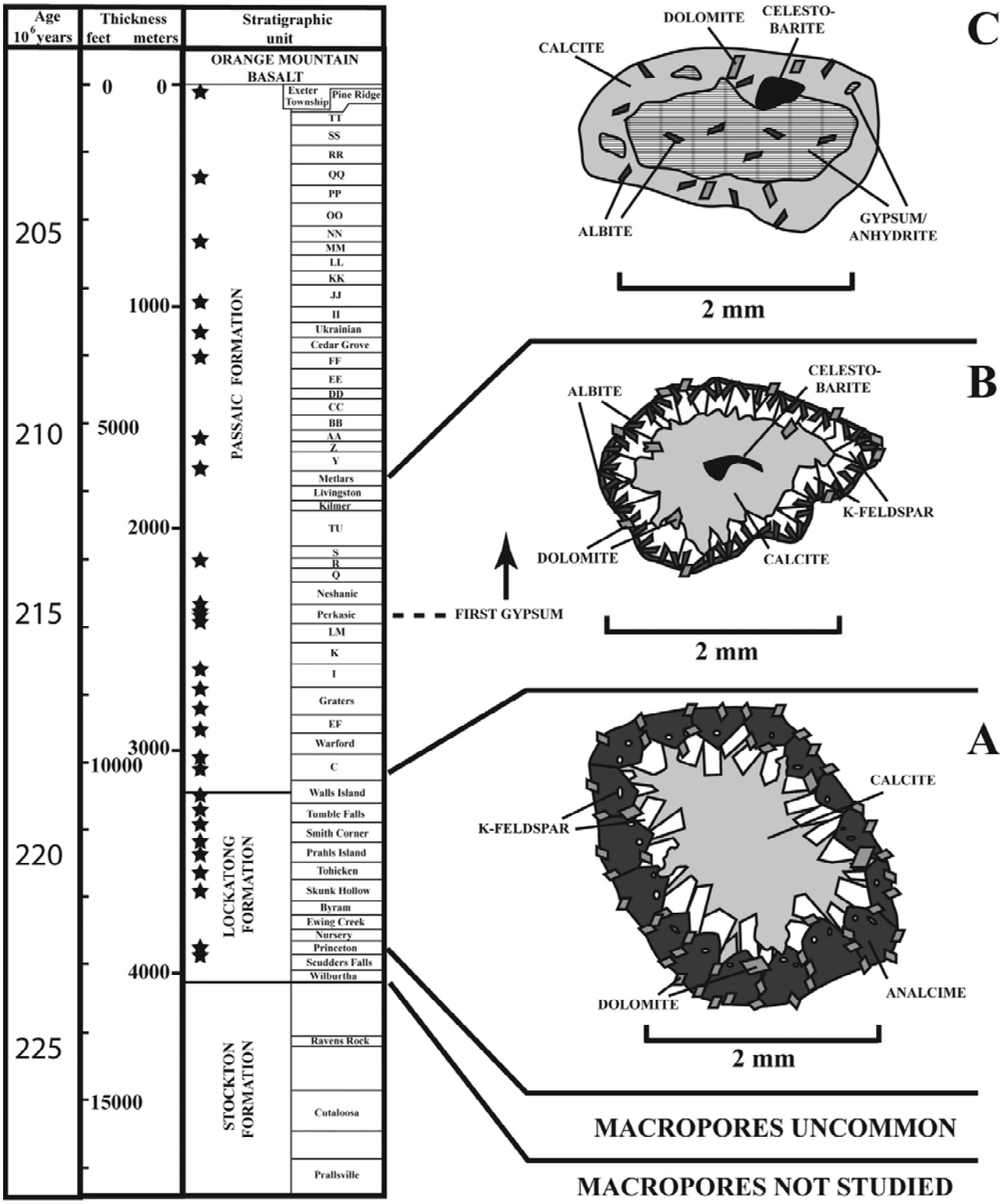

Figure B2. Stratigraphic column of Newark basin succession showing 3 discrete zones (A, B, and C) defined by progressive changes in the nature of coarsely crystalline authigenic minerals filling macropores in mudstones of the Lockatong and Passaic Formations; paragenesis typical for each zone is shown schematically on right (see text for further explanation). Lowest stratigraphic occurrence of gypsum in macropores is indicated by dashed line below arrow. Black stars left of formation names indicate the principal stratigraphic levels sampled. Age estimates on left are from Olsen and Rainforth (2001); stratigraphic nomenclature is after Olsen and others (1996).

Table B1. Relative abundances of depositional macropores and coarsely crystalline minerals filling them in selected Newark basin mudstones (see text for additional discussion).

Formation and member[2] (where known)	sample number	source[†]	volume (%) of individual minerals in macropores[1]					macropores[1] total sample volume (%)
			analcime	'diseased' analcime	feldspar	carbonate	other	
Passaic Formation Perkasie Member……..	A 48-4	S	--	--	13.4	2.6	0.9	16.9
Passaic Formation Member EF……..	T5A	C	--	--	P[§]	P[§]	--	21.1
Lower Passaic Formation member unknown…….	A 67-1	S	*	--	9.6	7.0	--	16.6
Lower Passaic Formation member unknown…….	A 81-3	S	--	--	10.1	5.3	--	15.4
Lower Passaic Formation member unknown…….	A 80-1	S	*	--	8.1	5.6	--	13.7
Lockatong Formation Prahl's Island Member…….	LK-13	S	1.4	3.2	0.4	1.4	1.4	7.8
Lockatong Formation Prahl's Island Member…….	LK-11	S	4.7	1.9	0.9	4.1	--	11.6
Lockatong Formation Prahl's Island Member…….	N38	C	12.0	--	--	7.5	--	19.5
Lockatong Formation Skunk Hollow Member…….	B9-1	S	9.2	--	trace	6.6	--	15.8

[1]expressed as a percentage of total sample volume
[2]stratigraphic nomenclature according to Olsen and others (1996)
* no analcime in macropores, but present in veins
[†] S = surface sample, C = core sample
[§] P = present but amount not quantified

km within the overlying Passaic Formation (fig. B2). Both of these stratigraphic units consist predominantly of nonmarine mudstones deposited in a variety of related subenvironments (Smoot and Olsen, 1988, 1994; Smoot, 1991, 2010). These mudstones contain mineral-filled macropores and fractures that are the focus of our study. Because of their coarser grain size, coeval fluvial-deltaic deposits (fig. B1) lack significant macroporosity, so they were not included in our study.

Alteration by surface weathering is only evident in samples from the uppermost parts of the cores. The most obvious evidence of weathering is the selective dissolution of gypsum in about the upper 100 m of the cores (although the cutoff depth varied from core to core). Nearly horizontal "satin spar" veins of fibrous gypsum are present between depths of about 100 and 300 m below ground surface. El Tabakh and others (1998) attribute these veins to precipitation in extensional fractures created by exhumation and unloading. Goldberg and others (2003) noted that horizontal veins are restricted to cores from more central parts of the basin and suggested post-rift erosion controlled their distribution. Herman (2005, 2009) suggests that the gypsum veins may in part stem from basin compression sometime after the lower Jurassic. The restriction of significant deviations in modern temperature profiles to the upper 200-300 m of the boreholes suggests there has been no hydrologic disturbance related to the current land surface at greater depths (Goldberg and others, 1994).

Methods

More than 700 samples were collected and examined for the present study. More than 400 of these samples were from the NBCP cores, where members throughout the Lockatong and Passaic Formations were targeted to ensure complete coverage of all the mudstones (fig. B2). At least one petrographic thin section was made from 95 percent of the core samples, and then examined via transmitted light microscope to determine the types of authigenic phases present and their parageneses. Polished full-size thin sections (2x3 inches) were then prepared from about 10 core samples with textures representing the commonest paragenetic assemblages. These were examined via scanning electron microscope (SEM), at which time semi-quantitative analyses of the coarsely crystalline authigenic phases were made using energy-dispersive

x-ray analysis (EDAX). The latter was used to confirm optical identifications of minerals and to determine the approximate compositions of minerals with variable cationic ratios, such as carbonate. These analyses provided the basis for our tabulation of the distribution of the coarsely crystalline authigenic minerals (fig. B2). No element maps were made to determine the actual volume percentages of the various phases. Lastly, the mineralogies of 5 bulk samples of mudstones lacking obvious sparry mineralization were determined via x-ray diffraction (XRD) to see if the sparry phases observed in the macropores were also present in the matrix.

Thin sections were also prepared from most of the surface samples collected and examined via the same methods as the core samples. This included the preparation of polished, full-size thin sections from about 10 samples to analyze via SEM and EDAX. To determine the maximum volumetric abundance of the coarsely crystalline phases, 20 core and surface samples with what appeared to be the greatest local abundance of spar-filled macropores were selected from multiple stratigraphic levels for point counts. On average, roughly 800 points were counted per thin section using a polarized light microscope. Only the cement-filled macropores and their constituent minerals were tallied; representative results are presented in table B1. As some mudstones have essentially no spar-filled macropores, the mean volume of macropores in the Newark mudstones as a whole is clearly less than the values in table B1, but not known.

Most of the data presented here were collected from the core samples. Many of the surface samples showed signs that more soluble phases (especially sulfates and carbonates) have been selectively dissolved, presumably via leaching during surface weathering. Moreover, the stratigraphic positions of the surface samples were often not as well constrained as those of the core samples. Therefore surface samples served primarily to provide a broader context.

Finally, ten samples of mudstones with the coarsest and most abundant authigenic K-feldspar crystals were selected for age dating via $^{40}Ar/^{39}Ar$ using step heating. These results were reported in Kunk and others (1995) and are only addressed briefly herein.

Coarsely crystalline authigenic minerals

General characteristics of non-vein spar

Excluding vein-filling phases, the coarsely crystalline authigenic minerals of the Newark mudstones can be subdivided into three textural categories:

1) pseudomorphs of euhedral evaporite crystals (Van Houten, 1965b; Smoot, 1991, 2010)

2) millimeter- to centimeter-scale nodules, many of which may also have originated as evaporites (Smoot and Olsen, 1994), and

3) sparry authigenic minerals that occupy former voids in the mudstones. The authigenic minerals in the third category are the main focus of this paper.

The mudstones of the Newark basin were deposited in a broad spectrum of nonmarine paleoenvironments ranging from deep perennial lakes to dry playa mudflats (Smoot and Olsen, 1988, 1994; Smoot, 2010). In terms of thickness, over 70 percent of the mudstones in the Newark basin accumulated in paleoenvironments that were dominantly subaerial rather than subaqueous (Olsen, 1986; Smoot and Olsen, 1994; Smoot, 2010). Modern muds deposited in analogous subaerial environments are commonly riddled with millimeter-scale macropores of three general types (fig. B3A; see Smoot, 2010 for more discussion). Spherical to ovate voids known as vesicles are one type; they form where air bubbles are trapped in mud. This can happen either during deposition, or as air escapes upwards from partially saturated muds during subsequent flooding events. Desiccation of freshly deposited mud gives rise to a second type of macropore, fine cracks that generally trend either vertically or horizontally. Finally, biogenic activity can give rise to cylindrical voids, either through burrowing by animals or, more commonly, by the growth and decay of root tubules. The mudstones of the Newark basin contain cement-filled analogs to all three types of macropores (fig. B3B and Smoot, 2010). There are eight widespread macropore-filling minerals in the mudstones of the Newark basin: analcime, K-feldspar, albite, calcite, dolomite, gypsum, anhydrite, and celesto-barite. On a broad scale, both the types of macropores present in the mudstones and the minerals that fill them vary as a function of stratigraphic position (fig. B2), as summarized in the next section. In contrast, the macropores and their fillings are impressively consistent when traced laterally across the Newark basin at a constant stratigraphic level, or when they are studied over stratigraphic sections no more than tens of meters thick. Where they are most abundant, macropores filled with coarsely crystalline minerals make up about 20 percent by volume of individual samples of mudstone (table B1).

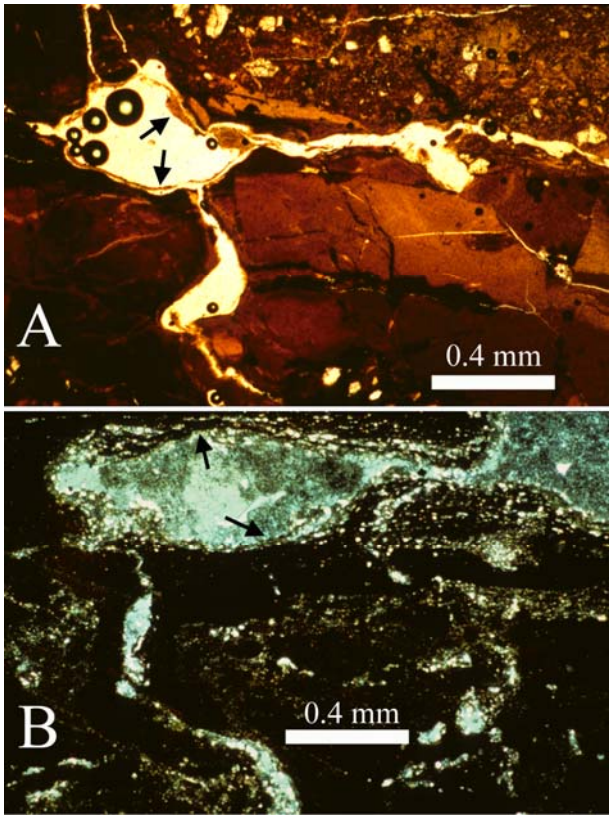

Figure B3. Photomicrographs of comparable textures in modern mud and Triassic mudstone. A. Sediment from the surface of a dry playa mudflat at Mud Lake, Nevada viewed in plane polarized light that has open voids (white areas) consisting of a large vesicle (upper left with black circles that are air bubbles in epoxy) connecting to a sinuous vertical crack downwards and sideways to a horizontal sheet crack. Most voids are lined with thin coatings of clay known as cutans (examples indicated by arrows) that are partly spalled off due to desiccation. B. Mudstone from the Tumble Falls Member (upper zone A) viewed between partially crossed polarizers showing vesicles and cracks like those in A, except that they are filled with coarsely crystalline analcime and dolomite (light gray); cutans, again present (examples at arrows) have been impregnated with iron oxide (black) and small authigenic crystals, mainly dolomite (bright dots).

Paragenetic relationships in depositional macropores

In general, the coarsely crystalline minerals filling the depositional macropores in the Newark mudstone fall naturally into three broad assemblages or zones that succeed one another stratigraphically (fig. B2). Macropores are scarce in about the lowest fourth of the Lockatong Formation stratigraphically, but they are present to abundant in most mudstones in the upper 75 percent of the Lockatong Formation and throughout the entire Passaic Formation. The lowest of the three assemblages stratigraphically, here designated zone A, extends through most of the Lockatong Formation and up into the basal units of the Passaic Formation (fig. B2). Most of the macropores in zone A are filled with analcime, which invariably occurs as coarse, equidimensional crystals (figs. B4A). In the largest macropores, which are as much as 4 mm long, individual analcime crystals reach diameters of 0.7 mm

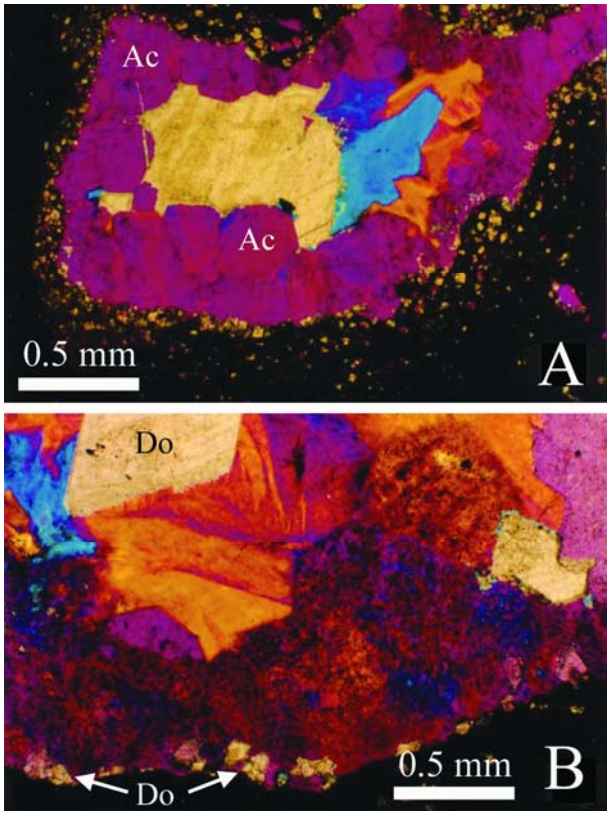

Figure B4. Photomicrographs of depositional macropores from the Lockatong Formation (middle of zone A) viewed between crossed polarizers with gypsum plate inserted. A. Typical vesicle-type macropore from the Tohicken Member lined with inward-directed euhedra of analcime (Ac, all magenta); center of void is filled with a coarsely crystalline mixture of K-feldspar (yellow and blue) and calcite and dolomite (bright high-order colors). Carbonate crystals invade and replace the K-feldspar and analcime crystals along their mutual contacts. Small dolomite crystals (bright rhombs) are scattered around the edge of the macropore (probably within former cutans) and replace the analcime locally. B. Macropore from Prahls Island Member with analcime euhedra (magenta) growing inward that have “feldspar disease,” that is, they are riddled with K-feldspar inclusions (yellow and blue). Larger K-feldspar crystals fill the center of the macropore. Dolomite crystals (Do; bright high-order colors) crosscut both K-feldspar (large rhomb in upper left) and analcime (small crystals near bottom).

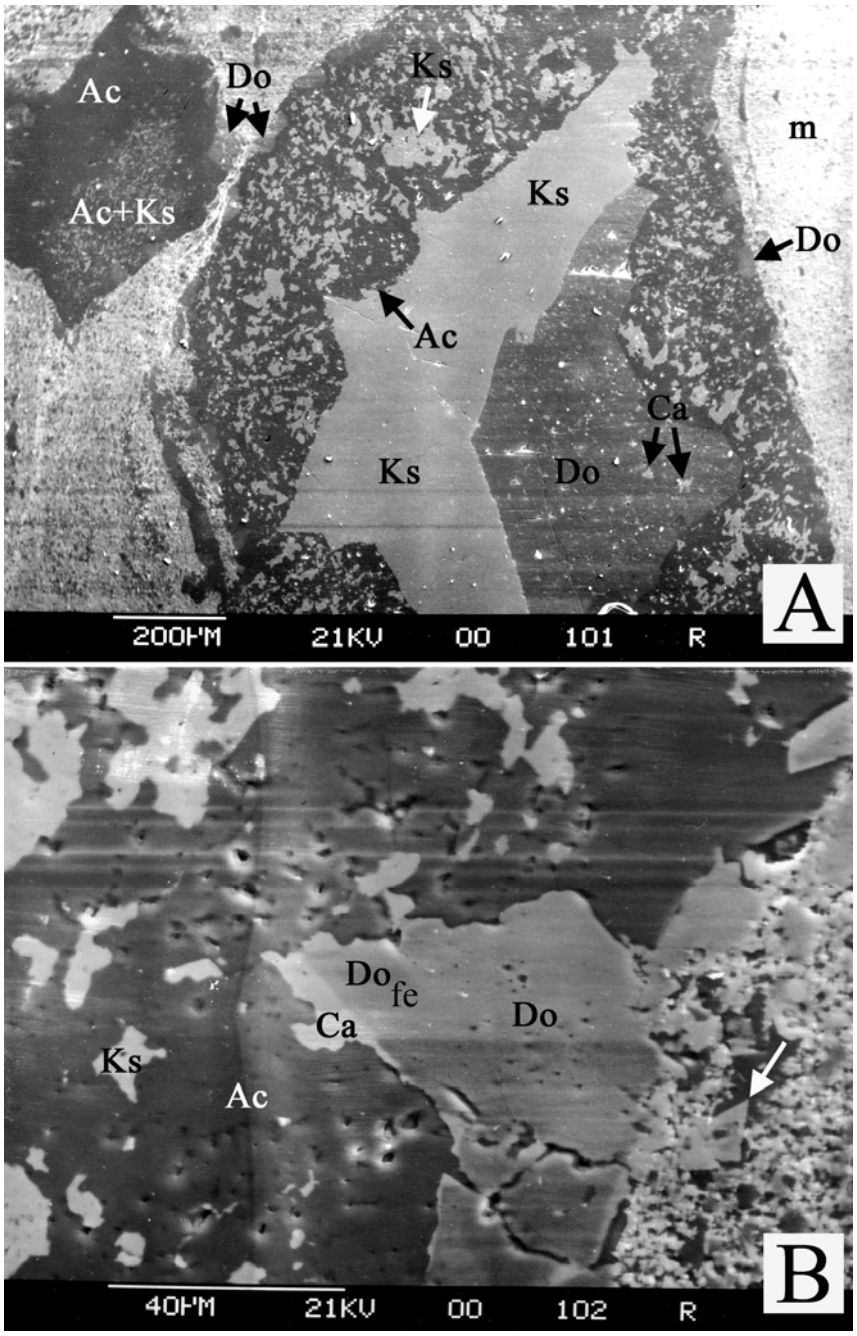

Figure B5. Backscattered SEM photomicrographs of depositional macropores in a sample from the Prahls Island Member, Lockatong Formation (middle of zone A); mineral identification based on EDAX. A. Macropores like those in fig. B4B are lined with analcime (Ac) crystals riddled with K-feldspar inclusions (example at Ks arrow); as in B4B, large K-feldspar crystals (Ks) fill the center and dolomite (Do) corrodes contacts between K-feldspar and analcime, especially along their contact with the matrix (m). Dolomite crystals contain small inclusions of calcite (Ca). Labeled scale bar is 200 microns. B. Detail of margin of macropore. Dolomite crystal (Do) protrudes from the matrix (in lower right corner) into the macropore filling and cuts across analcime crystals (Ac) with K-feldspar (Ks) inclusions. The dolomite crystal has an outer rim of high-iron dolomite (Do_{fe}) that is overlain by calcite (Ca). Matrix also contains small dolomite rhomb (arrow). Labeled scale bar is 40 microns.

or more and may surround a central area of coarsely crystalline K-feldspar, dolomite and (or) calcite crystals (fig. B4A). The analcime crystals in such macropores have well-developed crystal faces on their inward-directed edges, whereas the minerals in the central area tend to be euhedral dolomite rhombs, anhedral calcite, and (or) interlocking masses of bladed K-feldspar crystals showing few if any euhedral faces (fig. B4). The margins of both the dolomite and calcite crystals tend to cut indiscriminately across the K-feldspar crystals. In addition, fine crystals of K-feldspar and carbonate replace the outer edges of analcime crystals (fig. B5). Replacement of analcime is minor in the lower part of zone A but becomes progressively more widespread moving upwards. Although analcime crystals are clear and unaltered in the lower part of the zone (fig. B4A), they are riddled with inclusions of K-feldspar (informally known as "feldspar disease"; figs. B4B and B5A) by the top of zone A. Although the K-feldspar inclusions in the analcime are generally small, they are typically in optical continuity with coarse K-feldspar crystals in central areas (fig. B4B). Albite, gypsum, and anhydrite were not observed in any of the macropore fillings in zone A.

The overlying assemblage, here designated zone

B, extends from the top of zone A well up into the Passaic Formation (fig. B2). The paragenetic sequence of the macropore fillings in zone B is more complex than in A, but is consistent throughout the zone. Most of the macropores are filled with coarsely crystalline carbonate and abundant feldspar crystals, the latter including both albite and K-feldspar. The morphology and distribution of dolomite and calcite crystals are generally similar to those of zone A. In contrast, albite occurs in isolated crystals, generally laths to stubby rectangles that tend to be more abundant on the margins of the macropores and project inward at various angles (figs. B6A and B7). In addition to large central crystals like those of zone A, K-feldspars also occur in mosaics of finer crystals rich in disseminated inclusions (mostly carbonates) along the margins of former macropores.

Obvious pseudomorphs of analcime are present along some margins in zones of K-feldspar rich in inclusions ± albite (figs. B6B and C). In fact, much of the macropore filling, especially low in zone B, could represent replaced analcime. Coarsely crystalline celesto-barite is also present in the centers of some of the larger macropores (fig. B7B). Gypsum and anhydrite first appear in the middle of zone B (fig. B2) and increase progressively in abundance upsection to zone C.

The uppermost zone, here designated as C, extends from the top of zone B to the top of the Passaic Formation. Macropores were less abundant and smaller in zone C than in the underlying zones, primarily because the upper Passaic Formation tends to be sandier than the strata below (Smoot and Olsen, 1994; Smoot, 2010). Macropores are simply scarcer and smaller in sandy sediments than they are in purer muds. Nevertheless, some macropores were present, and they are mostly filled with a combination of gypsum, anhydrite, and calcite (fig. B8). Small amounts of albite and dolomite are also present, but K-feldspar is either very scarce or absent altogether. Neither analcime nor any pseudomorphs indicating its former presence were observed in any of the macropore fillings in zone C. Paragenetic relationships indicate calcite both replaces and is replaced by gypsum, whereas small euhedra of albite appear to replace gypsum and anhydrite randomly in the centers of former macropores (fig. B8B).

As noted above, coarsely crystalline authigenic minerals also occur in evaporite pseudomorphs throughout the Lockatong and Passaic Formations. In a given zone, these pseudomorphs consist of the same minerals as the macropore fillings, for example, they are dominantly analcime and dolomite in zone A (fig. B9A) versus gypsum and anhydrite in zone C (fig. B9B).

Within a given zone, however, minerals in macropores versus pseudomorphs commonly differ in their relative abundances. In zone A, for example, dolomite is more abundant than analcime in the crystal pseudomorphs, whereas analcime is more abundant than carbonate in the macropore fillings. Crystal pseudomorphs include euhedral rhombs of dolomite that are partially to wholly replaced by analcime in zone A and by feldspar in zone B (fig. B10).

Primary or secondary?

Many of the macropore fillings in Newark mudstones have centripetal zonation and include crystals whose shapes suggest they formed by inward directed growth (figs. B4A and B6A). These are classic characteristics of true cements, that is, void-filling precipitates (Grigor'ev, 1965). However, given their coarse crystal size and complex parageneses, it is highly unlikely the macropore-filling assemblages precipitated at or near the depositional surface. It is much more likely that coarsely crystalline tectosilicates such as these formed slowly and later in the diagenetic history.

The formation of all of these minerals as void-filling precipitates is also inconsistent with the fact that most or all of the coarsely crystalline authigenic minerals show petrographic evidence of having formed via replacement in one or more contexts. Specifically, analcime replaced evaporite crystals (fig. B9A) and carbonate rhombs; K-feldspar replaced analcime (figs. B4B, B5, and B9A) and dolomite rhombs (fig. B10); and dolomite and calcite replaced analcime, K-feldspar, and albite in the macropore fillings (figs. B4, B5, B6, and B7). Such complex parageneses suggest these coarsely crystalline assemblages formed over a long time span involving multiple migrations of aqueous solutions whose solute compositions changed through time.

A long history of diagenetic reaction for the macropore fillings of the Newark mudstones is confirmed by radiometric age dates from the coarsely crystalline authigenic K-feldspars. Macropore-filling K-feldspars were separated from mudstones of the Perkasie Member of the Passaic Formation and yielded an $^{40}Ar/^{39}Ar$ age of 196 ± 1 million years (Kunk and others, 1995). Inasmuch as the Perkasie mudstones were deposited about 209-213 million years ago (Olsen and others, 1996) and many of the K-feldspars that yielded the age date were subsequently replaced by calcite and dolomite, reactive fluids must have continued to move through these mudstones for some 20 million years or more after deposition. Dates obtained from authigenic K-feldspars from mudstones in the upper part of the underlying Lockatong Formation, deposited ca. 213 to 217 million years ago, are also in the neighborhood of 196 million years (Kunk and others, 1995). This implies that the authigenic minerals were reacting with pore fluids for even longer time spans and that the growth of the K-feldspar in zones A and B was coeval.

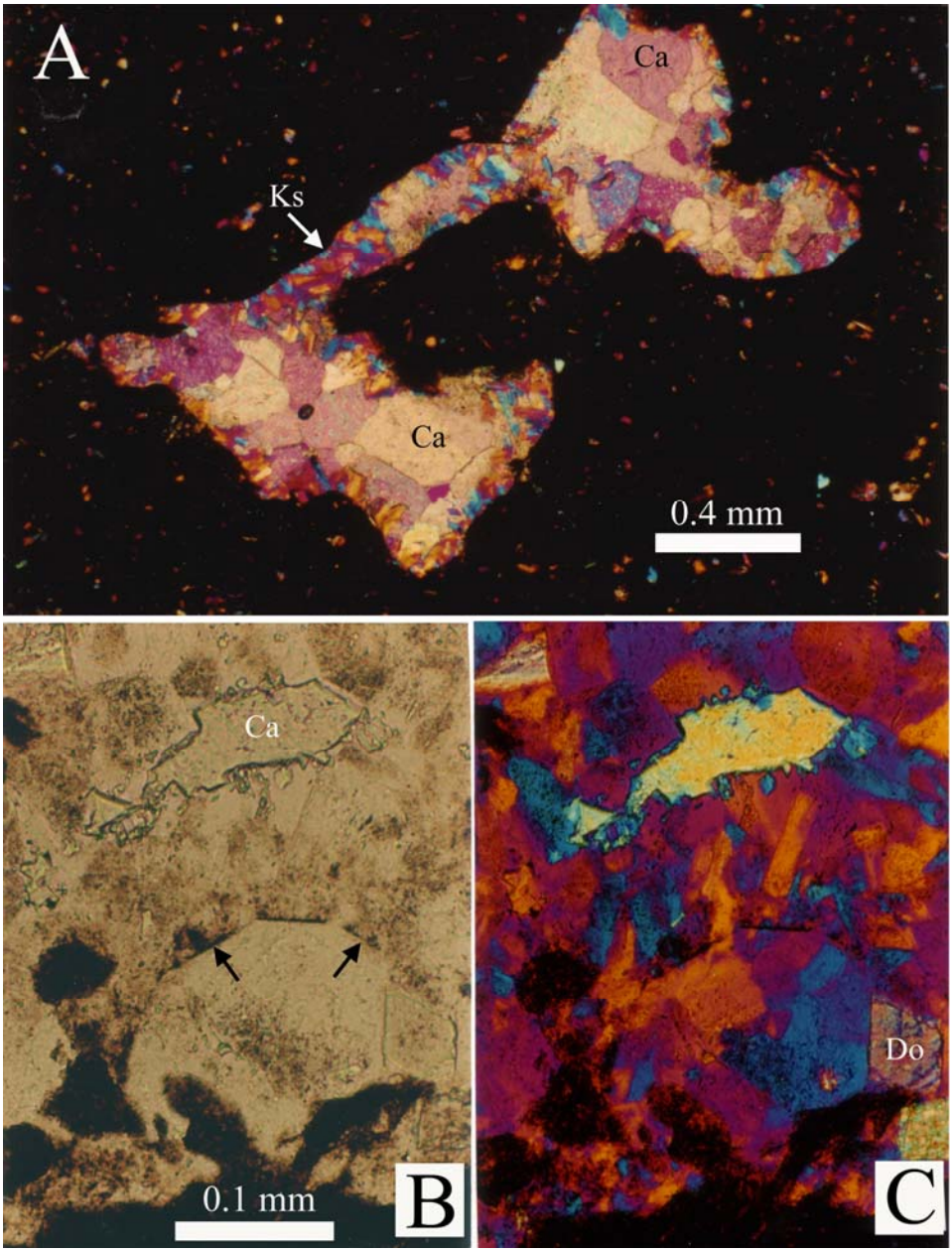

Figure B6. Polarized-light photomicrographs of depositional macropores from the Passaic Formation (middle of zone B). A and C viewed between crossed polarizers with gypsum plate inserted, B viewed in plane polarized light. A. Root cast macropore from Member LM with lining of small, lath-shaped albite crystals overlain in places by larger patches of K-feldspar (example at Ks arrow; all feldspars are yellow, blue, or magenta). Calcite (Ca) both replaces the K-feldspar and fills the remainder of the macropore. Matrix (dark) has bright spots that are mostly silt-size detrital grains of tectosilicates. B and C. Pseudomorph of euhedral analcime crystal in a root-cast macropore from Perkasie Member whose shape is preserved within a combination of albite and K-feldspar. Outer edge of former analcime crystal (indicated by arrows) and others like it are encrusted by albite laths that in turn are encrusted by K-feldspar; center of macropore is filled with calcite (Ca in B, yellow in C). All silicates are crosscut locally by euhedral dolomite rhombs (Do).

Spar-filled veins

General characteristics

Veins consisting of minerals similar to those filling the depositional macropores are widespread in cores of the Newark mudstones. Goldberg and others (2003) demonstrated that veins dipping 75° to 80° in the NBDP cores are more abundant through the lower Passaic to Stockton Formations, whereas nearly horizontal veins (5° to 25° dip) dominate in the uppermost Passaic Formation. We identified 131 different veins in the core samples we studied, the largest of which was 4 cm in width. In our samples, 79 percent of the veins are close to vertical and almost all the rest are nearly horizontal. Eight major minerals were recognized in the veins, but one mineral almost always makes up at least half of a given vein (figs. B11 and B12). Vertically oriented veins mainly consist of either fibrous or non-fibrous carbonate, whereas horizontal veins mainly consist of fibrous gypsum, that is, satin spar. Overall, 45 percent of the veins in our core samples were partially or entirely fibrous. We observed a few instances of horizontal veins cutting across vertical ones (fig. B12C) but samples with cross-cutting relationships are rare.

Herman (2005, 2009) identified three groups of steeply dipping veins based on field work, core, and borehole televiewer images in the central part of the basin in New Jersey. The oldest veins (S1) are

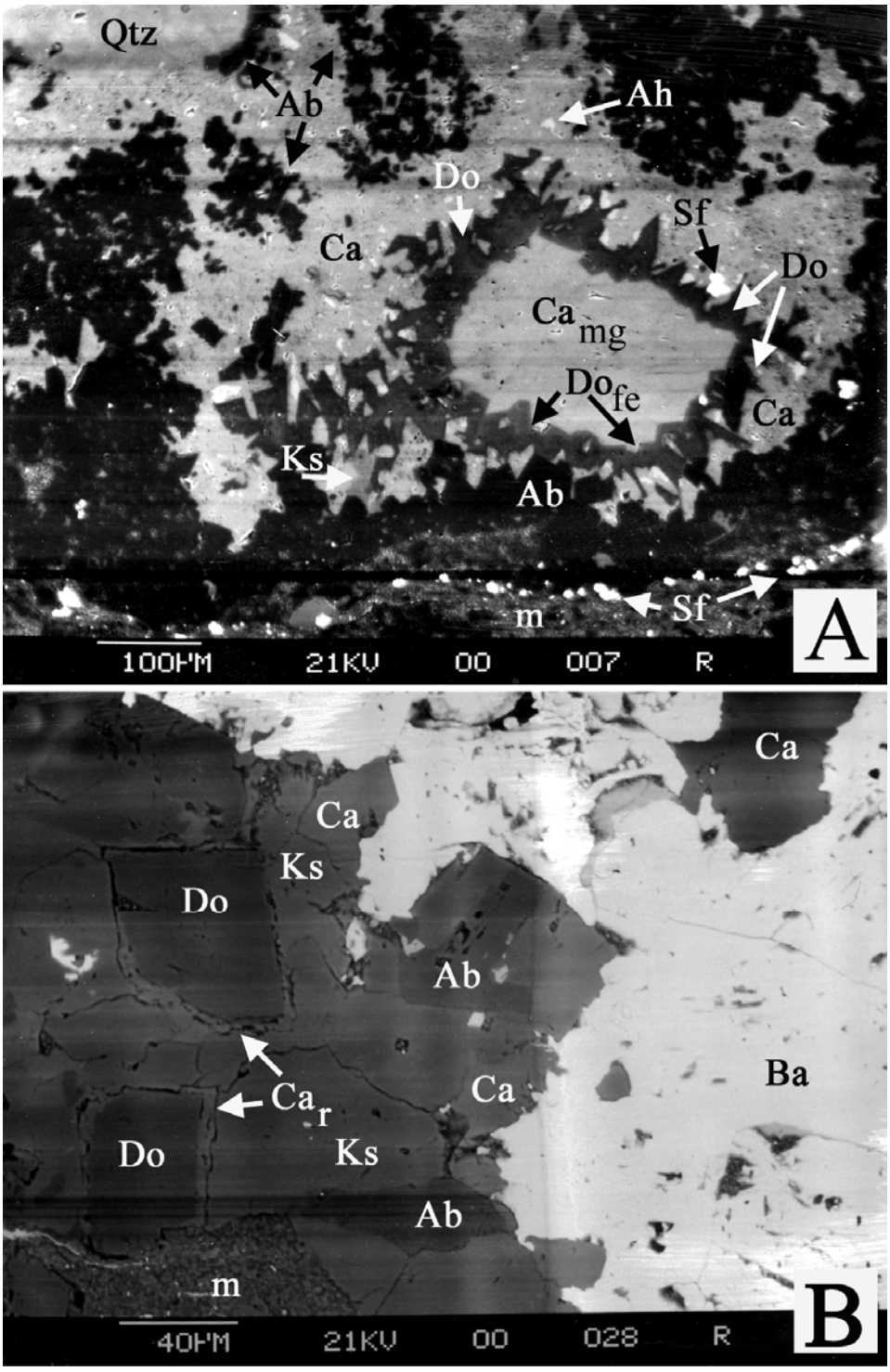

Figure B7. Backscattered SEM photomicrographs of depositional macropores from the Passaic Formation (zone B); mineral identification based on EDAX. A. Most of a single macropore in a matrix of sandy mud (m) from the Livingston Member with a rim of albite crystals (Ab) overlain by minor K-feldspar (Ks). Most of the void is filled with calcite (Ca) that is overlain by dolomite (Do) with an outer rim of high-iron dolomite (Do_{fe}), and finally high-magnesium calcite (Ca_{mg}). The calcite includes numerous bright white specks of anhydrite (Ah). Brightest specks (mostly along base of macropore) are sulfide minerals (Sf). One detrital quartz grain (Qtz) protrudes into the top of the macropore from the matrix. Labeled scale bar is 100 microns. B. Detail of macropore margin from the Perkasie Member in similar matrix (m). Albite laths (Ab) are overlain by K-feldspar (Ks). Silicates are irregularly embayed by calcite (Ca) and dolomite rhombs (Do) with calcite rims (Ca_r). The carbonate minerals are overlain and embayed by celesto-barite (Ba). Labeled scale bar is 40 microns.

complexly filled with calcite and tectosilicates (primarily albite), and oriented roughly parallel to the northwestern faulted margin of the basin. They occur in the Stockton, Lockatong, and Passaic Formations and also cut some diabase bodies. The next younger set of veins (S2) rotated about thirty degrees relative to the S1 fractures, and is more abundant near large intrabasin cross faults in the Passaic Formation, and throughout the Jurassic basalts and formations. The S2 veins characteristically consist of fibrous calcite. The youngest set of steeply dipping veins (S3) is also dominated by fibrous calcite, is oriented roughly N-S, and is associated with features indicating compression and wrench faulting. Herman (2005, 2009) argued that horizontal satin spar veins are the youngest features and that they could reflect unloading and exhumation (as in

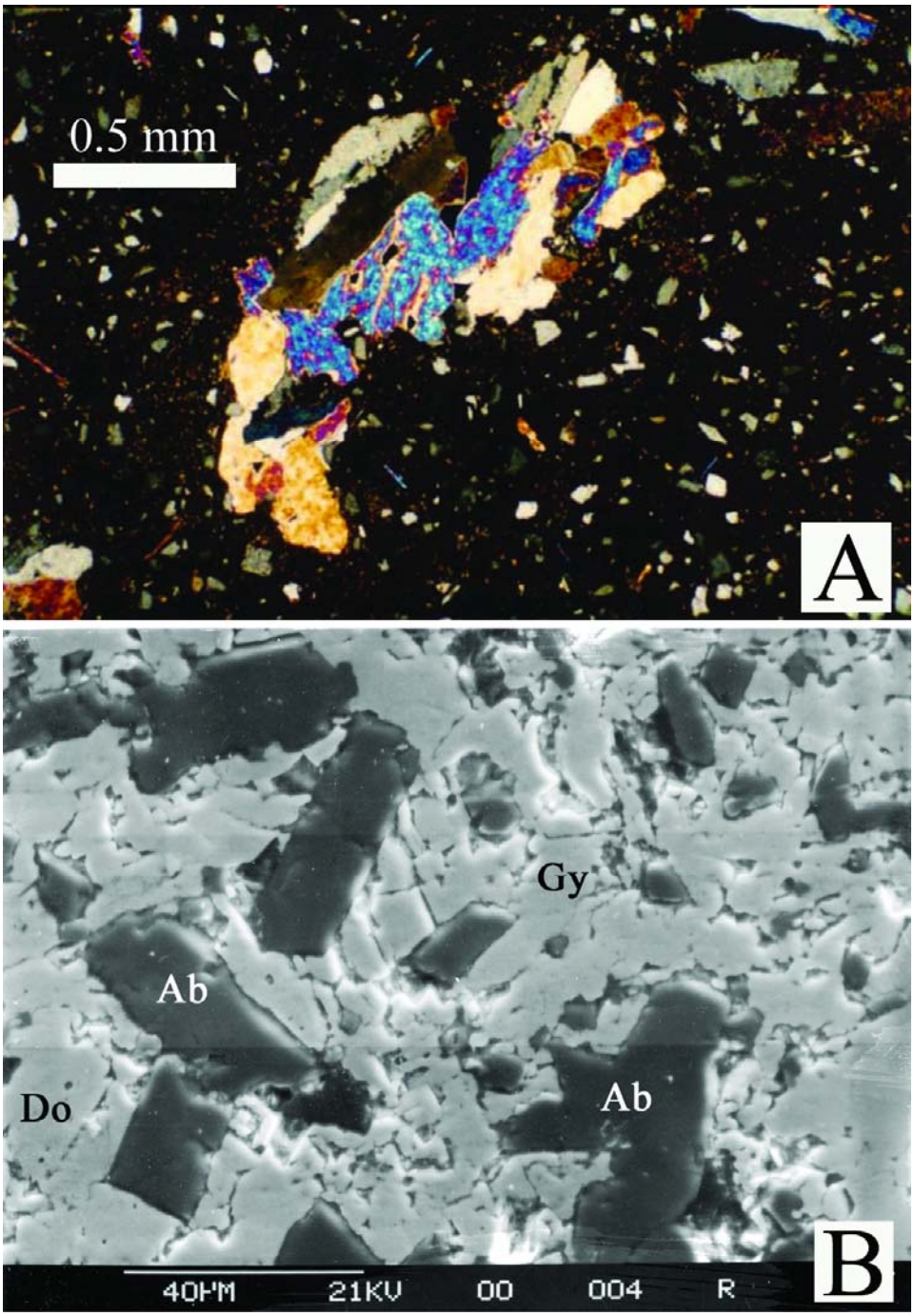

Figure B8. Photomicrographs of depositional macropores from Member PP in the upper Passaic Formation (upper zone C). A. View between crossed polarizers of a root cast macropore filled with two kinds of sulfates, gypsum (gray and brown) and anhydrite (bright colors). Surrounding matrix (dark) contains abundant silt- to very fine sand-size detrital grains of quartz and feldspar (white and gray specks) and some muscovite flakes (blue and red).
B. Backscattered SEM image of depositional macropore; mineral identification based on EDAX. Gypsum (Gy) fills most of the macropore and includes scattered laths of albite (Ab) and rhombs of dolomite (Do). Labeled scale bar is 40 microns.

El Tabakh and others, 1998, and Goldberg and others, 2003) or compression of the basin.

We confirmed the observation of El Tabakh and others (1998) that virtually all of the horizontal satin spar veins in the NBCP cores are located in a zone from 100 to 400 meters deep in five cores in particular (namely, Martinsville, Weston Canal, Somerset, Rutgers, and Titusville). These veins are broadly parallel to the present ground surface, suggesting they are a younger feature.

Internal textures

As noted above, veins show a combination of fibrous and non-fibrous textures internally. Many of the fibrous veins display crack-seal textures internally, that is, bands of minute inclusions parallel to the walls (figs. B11A and C and B12). These indicate that the fractures opened gradually through repeated fracturing, with the addition of a small increment of material to each of the fibers each time they opened (Ramsey, 1980). Although carbonates dominate the vertical veins, many contain

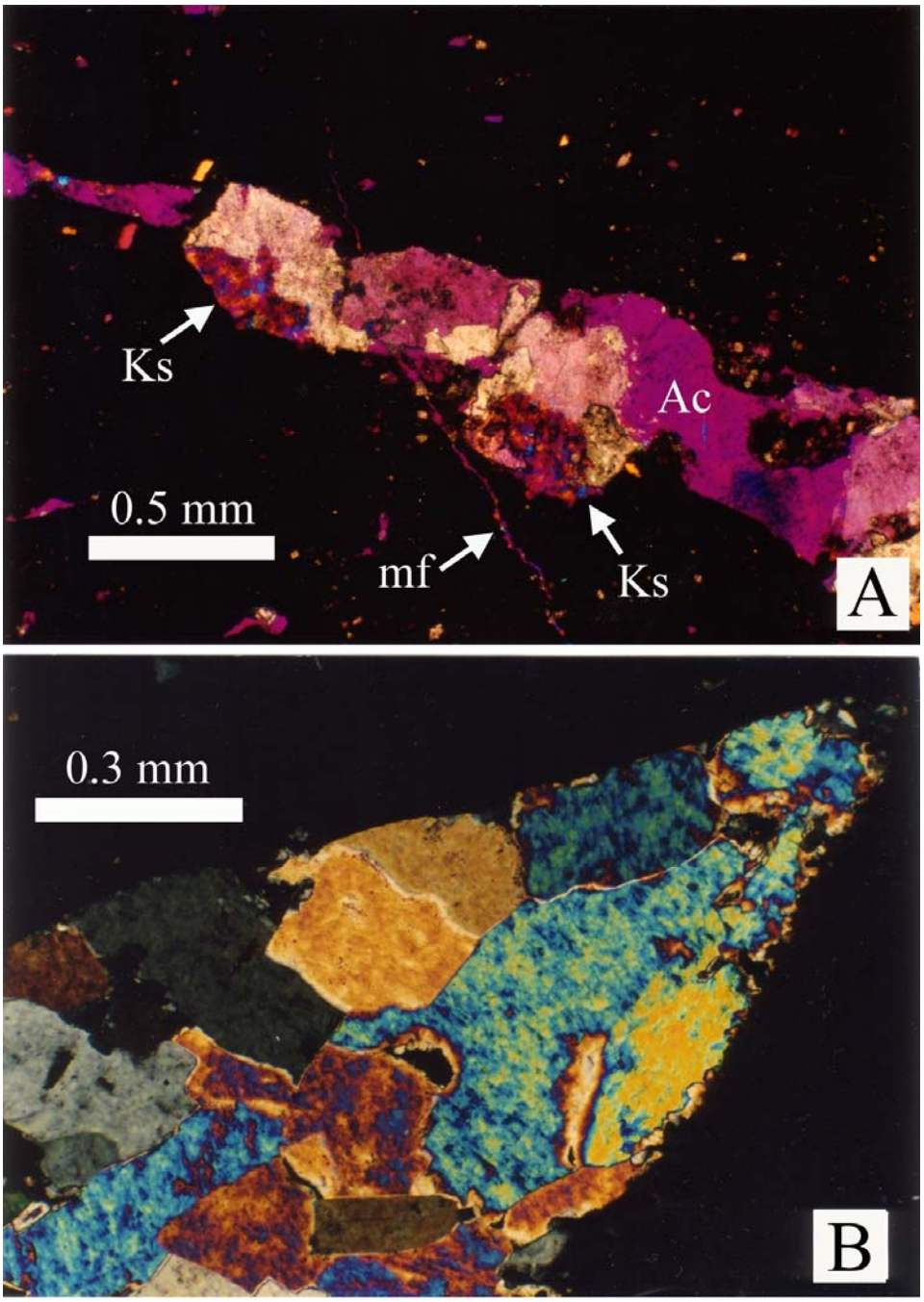

Figure B9. Photomicrographs of evaporite crystal pseudomorphs viewed between crossed polarizers; gypsum plate is inserted in A but not in B. A. Evaporite crystal pseudomorph from Prahls Island Member (middle of zone A) consisting of analcime (Ac) partially replaced by K-feldspar (mottled yellow and blue next to Ks arrows) and calcite (bright high-order colors); dolomite rhombs (also bright high-order colors) cross cut all other minerals. Note paper-thin analcime-filled microfracture (mf arrow). B. Evaporite crystal pseudomorph from Member DD (low in zone C) formed by a mixture of anhydrite (brightly mottled colors) and gypsum (gray and brown).

thin selvedges of feldspar along their edges that predate the carbonate and (or) replaced the tips of the fibers (figs. B11A, B and C and B12A). The fact that most fibers grew normal to fracture walls indicates the vertical veins formed largely via horizontal extension, whereas the horizontal veins grew largely through vertical extension.

Compared to the fibrous veins, the non-fibrous veins are more coarsely crystalline, and many display competitive-growth textures typical of void-filling precipitates such as geodes. This includes crystal growth directed outwards from fracture walls (figs. B12B and D and B13D) and centripetal zoning with successive generations of different minerals (figs. B11B, B12B and D, and B13D). A small minority of the veins show both fibrous and nonfibrous textures (figs. B11B and B13B). The existence of open voids during the formation of some of the veins is indicated by occurrences of disoriented vein-filling crystals that were fractured or folded, then displaced (presumably downward). Among the latter are pieces of analcime euhedra (fig. B12D), thin selvedges of feldspar (fig. B13C), and an entire vein of fibrous calcite that buckled, indicating the support of the walls must have

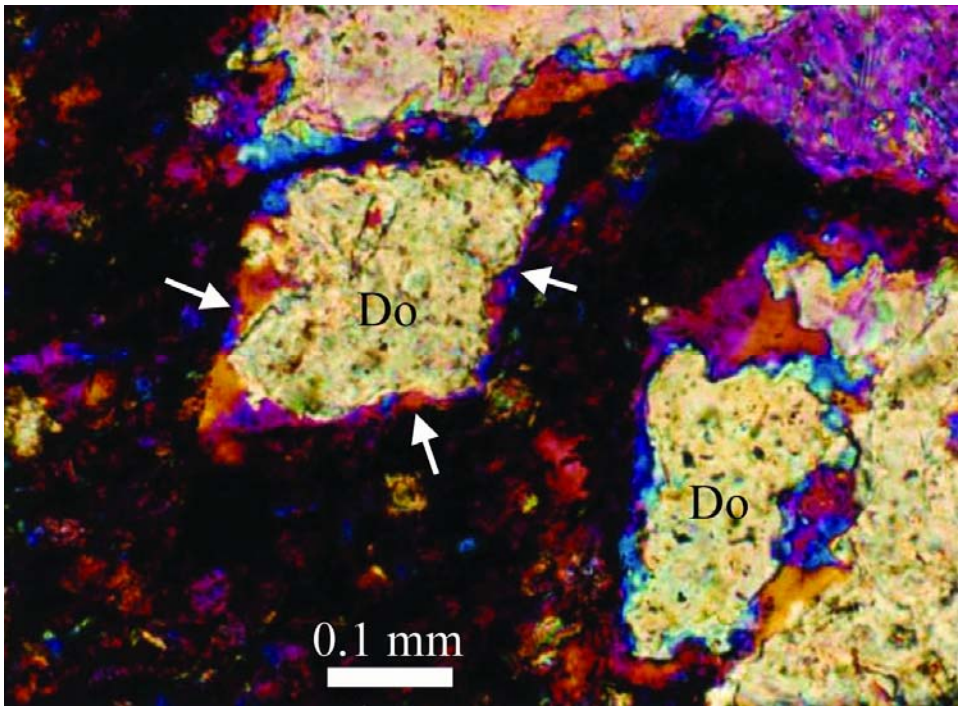

Figure B10. Polarized-light photomicrograph between crossed polarizers with gypsum plate inserted of coarse dolomite crystals (Do), whose margins are replaced by K-feldspar (blue, yellow, and magenta), in matrix of silty mud in Member EF (low in zone B); arrows indicate planar limits of K-feldspar that outline original edges of one dolomite rhomb.

been removed (fig. B13D). The latter indicates fractures were at times rapidly enlarged after some phases had precipitated. The fact that some of the displaced crystal pieces are embedded in other types of minerals indicates the composition of the fluids utilizing these fractures changed over time, again implying the fractures had a long and complex history of use as fluid conduits.

In addition to crystals, some of the veins in the stratigraphically lower mudstones contain bitumen (figs. B13A and B), indicating liquid hydrocarbons must have migrated through some fractures. The restriction of the bitumen to deep stratigraphic levels can be ascribed to the fact that organic-rich deep lake deposits are thickest and most abundant low in the Newark succession (Olsen and others, 1996). The hydrocarbons were clearly using fractures (primarily vertical ones) as an escape route. The mobility of the hydrocarbons was probably limited by the fact that many fractures taper out and overlap in en echelon fashion (figs. B11C and B13A). Hydrocarbons would have to traverse low-permeability mudstones to get from one fracture to the next in such an arrangement; this is evidenced by high concentrations of residual bitumen in some crossover zones (fig. B13A). The paragenetic relationships of the bitumen and mineral phases again imply a surprisingly complex and long-lived history of migration by multiple fluid types through the fractures. For example, liquid hydrocarbons were clearly migrating through some fractures in which carbonates and tectosilicates had already precipitated (fig. B13A). In contrast, the bitumen itself is fractured in some veins, and carbonate minerals precipitated in the resulting gaps (fig. B13B). These relationships indicate mineral-precipitating water was passing through the fractures both before and after the migration of the liquid hydrocarbons. Moreover, enough time passed between mineral-precipitating events and the temperature increased enough for the liquid hydrocarbons to solidify into bitumen (Tissot and Welte, 1978) before additional mineralization.

Comparison of veins with macropores

Both the veins and the depositional macropores are largely filled with the same eight minerals. Moreover, the dominant minerals filling the veins vary as a function of stratigraphic position in a way that matches the assemblages observed in the macropores fairly well. In other words, the minerals filling the veins form three assemblages that succeed one another vertically and match the assemblages of the coarsely crystalline authigenic minerals rather closely (fig. B2). However, the transitions from one assemblage to the next in the veins appear to be offset to slightly lower stratigraphic levels relative to comparable transitions in the macropores. This could be an actual difference reflecting original patterns of fluid migration and (or) mineral precipitation through time, but our sampling was not dense enough to exclude the possibility that it may be an artifact of incomplete or selective sampling in the transition areas. Despite this possible discrepancy, the minerals filling the veins and the pores are remarkably similar, indicating that they are likely to share a common origin.

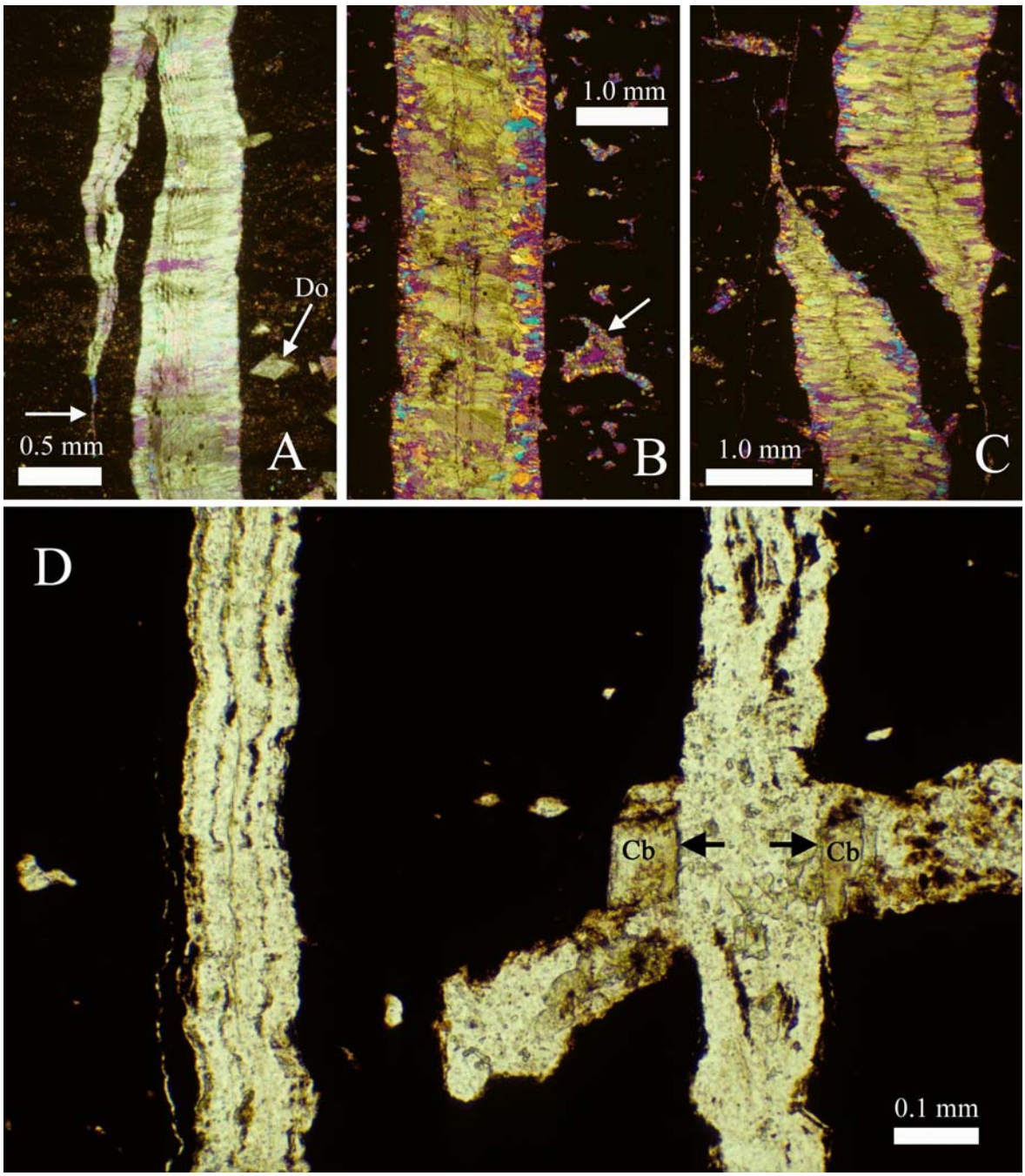

Figure B11. Photomicrographs of vertical crack-seal veins from Passaic Formation (low in zone B) viewed between crossed polarizers with gypsum plate inserted (in A, B and C) or in plane polarized light (in D). A is from Member EF and B, C, and D are from Member C. Original vertical direction is towards top in all images. A. Vein with crack-seal texture (described in text) consisting largely of coarsely fibrous carbonate, but minute K-feldspar crystals (yellow and blue) are present along edges and in hairline crack (arrow in lower left) where vein pinches out. Scattered dolomite rhombs (Do) replace matrix. B. Vein consisting of coarsely fibrous carbonate (in center) with larger and more abundant tectosilicate crystals (mainly albite) lining the edges. Crack-seal textures are present, but not as extensive as in A. Macropore in lower right (arrow) has a centripetally zoned filling with albite laths on outside (yellow and blue) and larger central crystal K-feldspar (magenta). C. Tapered tips of two en echelon veins consisting of coarsely fibrous carbonate with fine tectosilicates along edges. Note how one vein thickens as the other thins so the amount of horizontal extension stays constant at all levels. D. Two thin, non-fibrous veins consisting largely of K-feldspar with small carbonate inclusions; both veins display crack-seal textures despite the lack of fibrous textures. Vein on right bisects a macropore filled (like the vein itself) with coarsely crystalline K-feldspar and carbonates; two halves of a single carbonate crystal (Cb) were separated horizontally by the vein (matching points indicated by arrows).

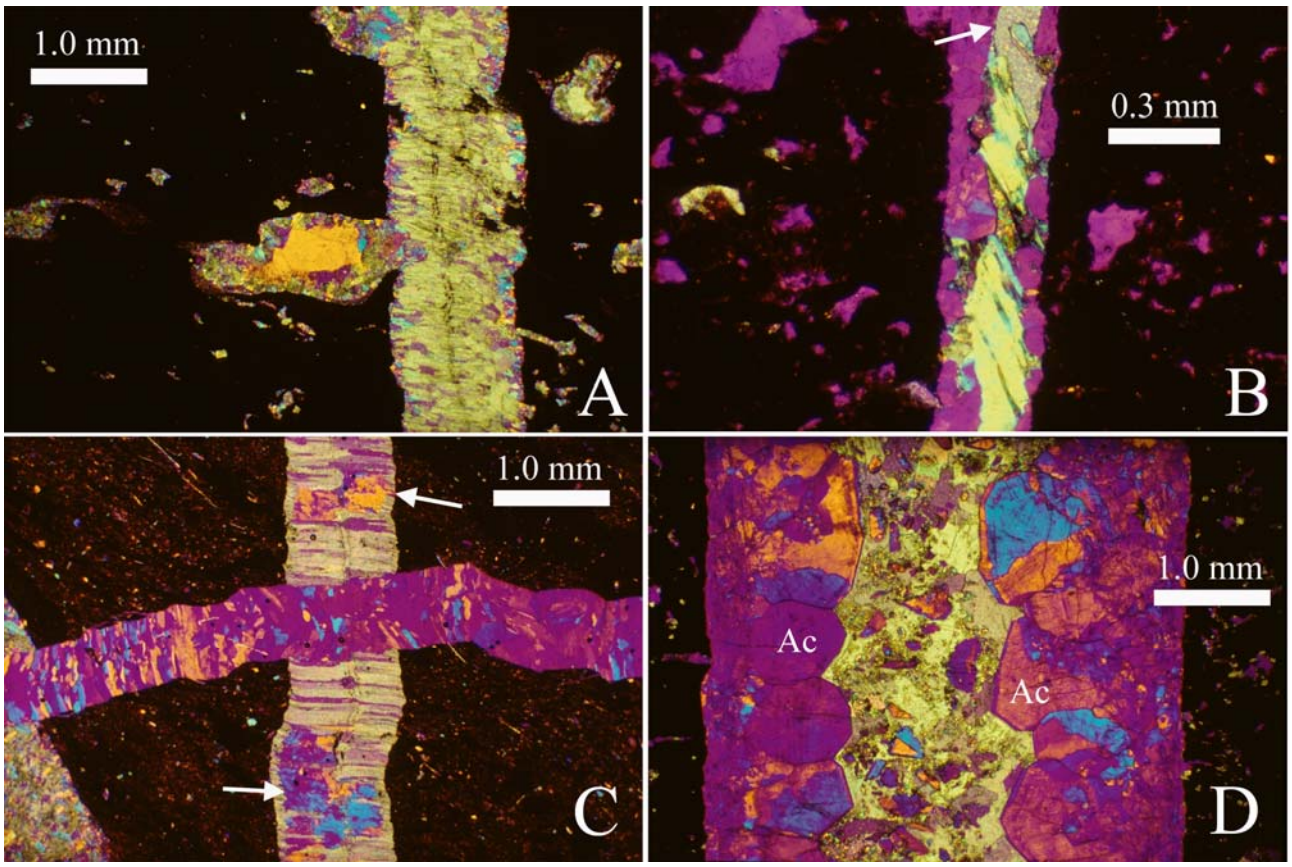

Figure B12. Photomicrographs of veins from all 3 zones viewed between crossed polarizers with gypsum plate inserted. Original vertical direction is towards top in all images. A. Vein from same sample as in fig. B11C (low in zone B) that impinges on a macropore; very similar minerals fill vein and macropore, but the macropore is filled with albite laths and finely crystalline carbonate around a larger crystal of K-feldspar (yellow) whereas carbonate dominates the vein fill. B. Vein from Skunk Hollow Member (zone A) with coarse analcime crystals (magenta) on edges, some euhedral and some broken. Coarse crystals of carbonate (arrow) and celesto-barite (pale green) fill the center; few if any fibrous textures are present. Analcime-filled macropores (magenta) are abundant in the surrounding matrix. C. Intersecting veins from Member EE (zone C); quasi-horizontal vein of fibrous gypsum ("satin spar") (magenta, blue and yellow) cross-cuts vertical vein of coarsely fibrous carbonate (bright high-order colors) locally replaced by gypsum (arrows). D. Vein from Tohicken Member (middle of zone A) lined with coarse analcime euhedra (Ac), some showing anomalously high birefringence (magenta, blue and yellow). Coarsely crystalline carbonate (bright high-order colors) in center of vein contains jagged pieces of analcime in varied orientations that appear to be fragments of crystals that broke off and fell from higher in the fracture.

Constraints on interpretation of authigenic minerals

External source of mass necessary

The paragenetic evidence presented above combined with the radiometric age dates of Kunk and others (1995) indicates that most or all of the coarsely crystalline authigenic minerals in the nonmarine mudstones of the Newark Supergroup precipitated long after deposition. Many of the minerals formed via replacement reactions involving large changes in major element chemistry, for example, the replacement of analcime by K-feldspar and the replacement of K-feldspar by dolomite. Such wholesale changes in chemical composition are unlikely to proceed by the local redistribution of material within the mudstones.

Two other reasons help rule out an internal source for the coarsely crystalline authigenic minerals in the Newark mudstones. One reason is the lack of evidence for significant compaction in most of the Newark mudstones. Roughly 30 percent of the Newark mudstones were deposited in subaqueous paleoenvironments (Olsen, 1986; Smoot and Olsen, 1994), and like marine muds, they show ample evidence of compaction. This includes laminae deformed around rigid objects (like bones, and concretions) and folded vertical structures (like burrows and mud cracks). Using

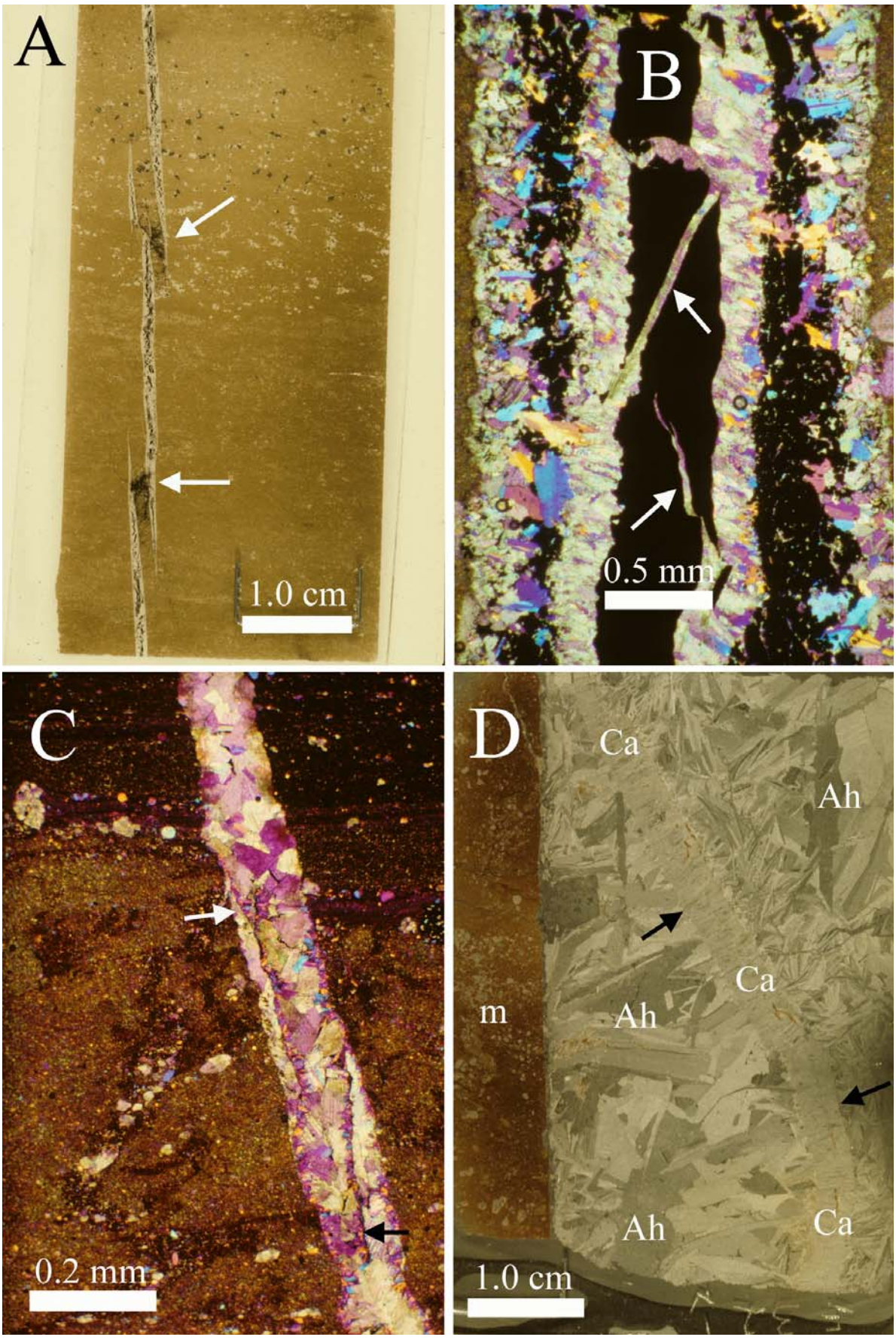
A
1.0 cm
B
0.5 mm
C
0.2 mm
D
Ca
Ah
Ca
m
Ah
Ah
Ca
1.0 cm

Figure B13. (Opposite page) Photomicrographs of veins showing evidence of hydrocarbon migration and/or late reactivation. A, B, and C are from Nursery Member (low in zone A) and D is from Member EE (zone C). A and D show entire thin sections viewed in reflected light; B and C are viewed in transmitted light between crossed polarizers with gypsum plate inserted. Original vertical direction is towards top in all images. A. Short, en echelon veins filled with carbonate and minor feldspar (clear) plus fractured bitumen (black) in center; mudstone between tips of adjacent cracks is impregnated with bitumen (arrows). B. Vein filled in multiple stages with two generations of bitumen (black) and at least two generations of carbonate (bright high-order colors); complex marginal zone consists of both feldspar (yellow and blue) and coarsely crystalline carbonate. Where central bitumen strip was fractured, it was healed with calcite (arrows) that probably predates coarsely fibrous carbonate on either side of strip. C. Non-fibrous vein consisting largely of coarsely crystalline carbonate in a silty mudstone. Thin plates of feldspar “swimming” in the carbonate appear to be selvedges (like those on vein edges in figs. B11B and B12A) that spalled off the sides and fell into an open fissure. D. Vein in sandy mud (m) that consists largely of carbonate and anhydrite. A fibrous calcite vein about 0.4 cm thick (Ca; edges indicated by arrows) apparently formed first, then buckled downward into a series of folds after a catastrophic reopening of the fracture; bladed crystals of anhydrite (Ah) subsequently filled the newly created void space between the folded vein and walls of the reopened fracture.

strain markers such as these, compactive shortening is estimated to be around 50 to 60 percent in marine mudstones (Rieke and Chilingarian, 1974; O'Brien and Slatt, 1990, p. 91-95). However, roughly 70 percent of the Newark mudstones were deposited in subaerial paleoenvironments or have subaerial overprints. The shapes of mud cracks and other strain markers in the subaerial Newark mudstones are virtually identical to those in analogous modern muds (fig. B3; see also figs. 11 and 12 in Smoot, 1991). The depositional porosities of subaerial muds in comparable modern environments are estimated at 50 to 60 percent, whereas most Newark mudstones have very little porosity. Given the minimal vertical shortening, this implies that something approaching half of the Newark mudstones by volume represents occluded porosity, and total porosity cannot be decreased by an internal redistribution of material. Compactive expulsion of water from the subaqueous Newark mudstones could have supplied some material, but not nearly enough to occlude all of the pores in the much thicker section of subaerial mudstones. In summary, based on their minimal compaction we estimate roughly half the mass of the subaerial Newark mudstones was imported during diagenesis. The coarsely crystalline authigenic minerals filling macropores are the most obvious component.

A second line of evidence militating against an internal source is the lack of any correlation between the coarsely crystalline authigenic minerals in the Newark mudstones and gross variations in the composition of Newark strata reflecting major changes in provenance through time. As explained in Smoot (1991, 2010), fluvio-deltaic sands were deposited in different parts of the Newark basin (fig. B1) at different times, and their composition varies as a reflection of compositional differences in the source areas that were being eroded. If the solutes needed to make the authigenic minerals were derived locally, their composition should mirror these gross changes in provenance, but the macropore-filling authigenic minerals do not show any changes that correlate with the geographic distribution of the fluvio-deltaic deposits either vertically or laterally. In fact, the clay minerals of the Lockatong and Passaic mudstones basinwide are more uniform compositionally than either the sandy fluvial deltaic deposits or the coarsely crystalline authigenic minerals filling their macropores. The mudstones consist almost exclusively of well-ordered illite (Van Houten, 1965a; Schamel and Hubbard, 1985; Gottfried and Kotra, 1988). As discussed below, the original clay minerals were probably more variable in composition, then were replaced wholesale by illite during diagenesis.

Timing and scale of fluid circulation

The data presented here strongly suggest that the emplacement of the coarsely crystalline authigenic minerals involved the passage of large volumes of fluid through these mudstones for long periods of time after they were deposited. Continued circulation over a time span of tens of millions of years is indicated by the radiometric age dates in Kunk and others (1995). Circulation to depths of hundreds of meters to kilometers is suggested by the stratigraphic thicknesses of the mudstones in the Newark basin (fig. B2). At the time the dated authigenic K-feldspars precipitated, the mudstones of the Perkasie Member were overlain by about 2200 m of strata. Given the minimal compaction of the subaerial mudstones, this 2200 m is roughly equivalent to the burial depth of the Perkasie. The fact that authigenic K-feldspars in the underlying Lockatong mudstones yielded similar age dates suggests fluids circulated to even greater depths, on the order of 3 km underground. In contrast to the vertical variation, the coarsely crystalline authigenic minerals at a given stratigraphic level appear to be similar throughout the Newark basin, suggesting lateral flow on the scale of tens to hundreds of kilometers. This is consistent with the fact most sedimentary strata are strongly anisotropic with respect to groundwater flow, that is, hydraulic conductivity along bedding is generally much higher than it is across bedding. At such depths, the most likely conduits for fluid migration through mudstone are fractures. We believe the abundant veins filled with the same minerals as the macropores represent those fractures.

Possible causes of fracturing

Recent work suggests a tectonic origin for many of the fractures in the Newark mudstones. Herman (2005, 2009) argued that steeply dipping fractures formed throughout basin development in response to extensional stress perpendicular to the northwest bounding fault. He envisioned the fractures as part of the mechanism for stretching as the headwall moved away from the footwall, and he cited the orientation and dip of the fractures as support for this mechanism. The fractures he observed with this orientation (S1) included those lined with tectosilicates and those showing some evidence of compaction. A younger set of steeply dipping fractures (S2) are oriented more in alignment with intrabasinal cross faults and they cut across basalts. Herman attributed these fractures to an abrupt rotation of the extensional axis sometime in the Early to Middle Jurassic. These fractures are characteristically lined with fibrous calcite. The youngest set of fractures (S3) is also lined with fibrous calcite, but shows evidence of compression of the Newark basin.

The release of overburden on a succession of strata undergoing erosion is another mechanism that can

form fractures, but they would be dominantly horizontal. In the Newark basin, as much as 6 km of overlying sediment have been eroded in places (Malinconico, 2010). The dominantly horizontal set of satin-spar veins probably formed in this way (El Tabakh and others, 1998; Goldberg and others, 2003), although Herman (2005, 2009) suggests some of these veins may be due to fractures growing in a compressional state long after deposition of the Newark basin rocks. In any event, any mechanism involving erosional unloading would only be effective close to the present-day erosional surface and is highly unlikely to play a role in fracturing at great depth.

Another mechanism that can give rise to fractures is pore fluid overpressures that exceed the strength of the host sediment (Du Rouchet, 1981). Several different situations can elevate pore pressures (see Magara, 1978; Chapter 4), and one or more may have played a role in the Newark basin. Differential compaction of mudstone can create overpressured layers. In the Newark basin, there is a major contrast in the degree of compaction of the subaqueously deposited lacustrine mudstones versus the subaerial mudstones as described above (also see Smoot, 2010). A similar disparity in compaction between soils and subaqueously deposited muds was noted by Caudill and others (1997). Differential compaction would have been most likely in the Lockatong and lower Passaic Formations inasmuch as they contain most of the lacustrine mudstones. Another situation that can elevate pore pressure is the release of water when hydrous clays or evaporites convert to anhydrous phases. All of the Triassic mudstones in the Newark basin are presently illite, but originally they almost certainly were smectites (see discussion below). Even small differences in clay mineralogy have been cited as sufficient to create significant overpressuring (Marcussen and others, 2009). A third possibility is that hydrocarbon production increased pore pressures by releasing water and gas. Evidence presented here (figs. B13A and B) clearly indicates liquid hydrocarbons migrated through fractures in the lower Newark succession. Finally, pore overpressures may have developed as a thermal effect of the injection of mafic magma into the Newark succession. Ryan and others (1997) describe how the intrusion of diabase dikes and sills in Hawaii elevated groundwater pressures at depth.

Possible causes of fluid circulation

Whatever was responsible for creating the fractures, they served as conduits for the movement of large volumes of fluid over a prolonged period of time. In Person and Garvin's (1994) generalized model for deep groundwater flow in an extensional basin, flow is driven by the hydraulic head provided by topographic highs along the faulted margin. Steckler and others (1993) noted that zircons in Newark basin sediments adjacent to the border fault were not thermally reset, whereas those away from the fault were. They attributed this to the downward circulation of relatively cool waters along the border fault followed by hydrothermal heating within the basin. Malinconico (2002, 2010) argued that reflectance values of organic material support a model where cool waters moving downward along the border fault were heated geothermally, then moved laterally into the basin within sandstones of the Stockton Formation. Hydraulic head in the Stockton Formation would have increased progressively as the basin subsided until the time of maximum burial. The distribution of vitrinite reflectance values observed by Malinconico (2002, 2010) indicates some of the fluids in the Stockton Formation were siphoned off along faults. Fractures forming throughout the extension of the basin (Herman, 2005, 2009) probably also acted as avenues of upward fluid escape from the Stockton Formation.

Hydrothermal circulation induced by the widespread emplacement of mafic sills and dikes in the Jurassic may have also been responsible for fluid movement. Vitrinite reflectance data from the Lockatong and Passaic Formations suggest a hydrothermal fluid pulse was associated with the Jurassic volcanic event (Katz and others, 1988; Pratt and others 1988; Huntoon and Furlong, 1992). Further support for a connection between fluid movement and the diabase intrusions is provided by the congruence of radiometric age dates obtained from K-feldspars in both the intrusions and mudstones (Kunk and others, 1995). However, the compositions and textures of the coarsely crystalline authigenic minerals in the Newark mudstones do not vary as a function of proximity to the intrusions, excluding contact-metamorphosed rocks that are located within meters of major diabase sheets such as the Palisades Sill (Van Houten, 1965a). The overpressuring associated with diabase intrusion may have distributed fractures more evenly across the basin, allowing for fluid movement in areas not in the immediate vicinity of an intrusion. Modeling of the basin thermal structure by Malinconico (2002, 2010) indicates that the Jurassic thermal event is not necessary to account for the observed distribution of vitrinite reflectance values and therefore may have had only localized impacts on hydrothermal fluid flow.

Fluid expulsion by overpressuring may have also occurred late in the basin's burial history. The increased fluid pressures due to conversion of smectitic clays to illite and the formation of petroleum from organics may have been sufficient to force movement along planes of weakness, such as pre-existing fractures. Traces of kerogen are associated with calcite-filled veins that postdate veins initially lined with K-feldspars that were broken and corroded by a younger

vein-filling event. This late event may also have been triggered by the compressional event that led to uplift and erosion of the Newark basin that probably occurred after the Middle Jurassic (Schlische and others, 2003; Herman, 2005, 2009).

Provisional Interpretation

Previous interpretations of the coarsely crystalline authigenic minerals in the Newark mudstones have diverged widely in terms of the inferred timing of their emplacement. Some researchers argued one or more of the minerals were formed as synsedimentary precipitates whereas others interpreted them as late diagenetic phases, sometimes on an *ad hoc* basis. For example, El Tabakh and Schreiber (1994) suggested that analcime replaced calcite within the depositional environment, whereas van de Kamp and Leake (1996) envisioned a later diagenetic reaction (sodium metasomatism) that included albitization of feldspar grains, although both argued that the analcime crystals formed from the interaction of alkaline lake brines with clays. Based on the data presented here, we believe that alkaline brines formed in the basin during deposition did play an important role in the precipitation of the coarsely crystalline authigenic minerals. However, their distribution is independent of specific depositional environments, other than selectively creating large pores in which large crystals could precipitate. Moreover, the coarsely crystalline minerals filling depositional macropores and nearby veins are quite similar. These and other lines of evidence indicate analcime is part of a diagenetic continuum that lasted more than 20 million years and included the subsequent precipitation of large volumes of albite and K-feldspar. Illite, the predominant clay mineral in the mudstones, has also been interpreted as a diagenetic mineral replacing smectite clays (El Tabakh and Schreiber, 1994; van de Kamp and Leake, 1996). We agree with this interpretation, and this conversion plays an important role in our revised model as outlined below.

During deposition of the Lockatong Formation and the lower part of the Passaic Formation, perennial lakes evolved into saline lakes that produced saline mudflats upon desiccation (Smoot and Olsen, 1994; Smoot, 2010). The mineral casts found in these deposits have been interpreted by most researchers as pseudomorphs after sulfate minerals such as gypsum, glauberite, and thenardite (Wherry, 1916; Hawkins, 1928; Schaller, 1932; Van Houten, 1965b; El Tabakh and Schreiber, 1994; El Tabakh and others, 1997). Smoot (2010) argues that they could equally well represent former sodium carbonate minerals, borates, or other monoclinic minerals instead. Furthermore, some of the Newark mudstones deposited in saline mudflat environments display sedimentary fabrics indicating "puffy ground" efflorescent salt crusts were present (Smoot and Olsen, 1994; Smoot, 2010). This style of efflorescence is more likely to develop with alkali mineral suites than with sulfate-chloride mineral suites (Smoot and Lowenstein, 1991; Smoot and Castens-Seidell, 1994).

The importance of making this distinction lies in the fact that sodium carbonate and mixed sodium carbonate-sulfate evaporites only form in basins that are intermittently inundated with highly alkaline brines (pH of 10 or higher). If such evaporites were present in the Newark basin, the pore waters near the surface of the saline lake and saline mudflat environments would have been enriched in Na, K, Si, and lesser Mg. Whatever their original composition, detrital clays exposed to such waters generally react to form poorly ordered, high-sodium smectite clays such as $Na_{0.54}\ K_{0.22}\ (Mg_{0.7}\ Fe_{0.6}\ Al_{0.78})\ (Si_{3.8}\ Al_{0.2})\ O_{10}\ (OH)_2$ (Jones and Weir, 1983). As they are buried, such poorly ordered clays readily alter to more stable sodium smectites such as beidellite $[Na_{0.33}\ Al_{2.33}\ Si_{3.67}\ O_{10}\ (OH)_2]$ and sodium-rich montmorillonite $[Na_{0.33}\ (Mg_{0.33}\ Al_{1.67})\ Si_4\ O_{10}\ (OH)_2]$ (Chamley, 1989). The conversion process releases Na, Al, and Si into the pore waters, which is favorable for the precipitation of analcime. The presence of abundant smectite-type clays at the time of deposition is supported by the common occurrence of well-developed slickenside bowls in these strata. Such bowls typically form in response to wetting and drying of fine-grained expandable clays, especially smectites (Wilding and Puentes, 1988, p. 65). Evidence of former saline lakes is rare in the upper Passaic Formation, but slickenside bowls are still relatively common (Smoot, 2010). This suggests expandable clays like smectites were originally abundant in the younger mudstones as well. However, they would not have been as disordered as the older clays if they were not associated with alkali evaporites, and therefore not as likely to elevate the concentrations of Na, Al and Si in the pore waters during burial.

Although analcime could theoretically form in a depositional environment under conditions like those outlined above, there is no evidence of disseminated analcime in the clays, nor are there variations in analcime distribution reflecting synsedimentary interaction of lake brines with underlying layers like those reported for the Lake Bogoria occurrence (Renaut, 1993). Had they formed as synsedimentary precipitates, we would expect the analcime crystals in the Newark mudstones to be largest and most abundant directly below alkaline lake deposits and get progressively smaller and less abundant downward and outward. This is not what we observed; the only systematic variations we detected in analcime crystal size and abundance in the Newark mudstones are those dependent on variations in the abundance and size of depositional macropores. In fact, the textures in the macropores of the Newark mudstones are impressively uniform and

independent of depositional fabrics in their host mudstones on a local scale.

Some diagenetic precipitation of silicates probably began relatively early in the sediment-burial history. Some alkaline brine probably sank into the subsurface and began reacting with the Stockton Formation sandstones. Oshchudlak and Hubert (1988) report albite overgrowths, albitized plagioclase, and albite replacement of K-feldspars that were probably aided by these fluids. This early cementation may have allowed the sandstones of the Stockton Formation to retain some permeability and thereby serve as aquifers even after burial to a depth of some kilometers, as envisioned by Malinconico (2002, 2010). As explained above, burial of disordered smectite-rich lake clays to several tens of meters or a few hundreds of meters would cause them to convert to more ordered smectite clays. This would release solutes into the remaining pore water that would promote the precipitation of analcime in any available pore space. Fractures opened by the ongoing extension of the basin and (or) differential compaction of the lake and subaerial muds would have caused these fluids to move upward into stratigraphic levels where macropores were still open. We infer that this occurred under relatively shallow burial conditions because some analcime-lined fractures show evidence of subsequent compaction.

One byproduct of the precipitation of analcime from alkaline pore fluids in the Lockatong and lower Passaic Formations would be relative enrichment of the residual fluids in Si and K. These evolving fluids would circulate to progressively higher levels through time due to compaction of clays and partial occlusion of pore space by analcime, and as they evolved, albite would ultimately be a more stable mineral than analcime. A gradual stratigraphic transition consistent with this scenario is indicated by a succession, in ascending order, from unaltered analcime (figs. B4A and B12B) to analcime with “feldspar disease” (figs. B4B and B5A), then finally no trace of analcime other than stray pseudomorphs in authigenic feldspars in the lower Passaic Formation (figs. B6B and C). The latter presumably reflects initial precipitation of analcime in the early diagenetic stages that back-reacts later with more silica-rich fluids.

Another factor that may have helped change the composition of the initial authigenic phase from analcime to albite was an increase in temperature. At higher temperatures, the albite stability field expands greatly at the expense of the analcime field (Liou, 1971; Thompson, 1971). It is possible that the transition from analcime to albite was due to the opening of fractures that led deeply buried fluids in the Stockton Formation up into the middle and upper Passaic Formation. In either case, the precipitation of albite from the pore fluids had the effect of increasing the concentration of K in the solution still further, which would have increased the likelihood that K-feldspar would precipitate. The volcanic event that produced the diabase intrusions and the basalt flows at the beginning of the Jurassic was almost certainly linked to the precipitation of the K-feldspar cements. Increases in both fluid pressure and temperature allowed K-feldspar to fill additional space in the larger macropores and to fill any open fractures. The addition of heat also hastened the conversion of any remaining smectites into illite.

Gypsum becomes an important component of the macropore-filling cements in the upper part of zone B and dominates them in zone C. This shift from silicates to sulfates coincides with the first appearance of synsedimentary gypsum crystals; the lowest occurrences stratigraphically are in the Perkasie Member of the Passaic Formation (Smoot, 2010). Unlike the evaporite crystals replaced by silicates and carbonates deeper in the Newark succession, the gypsum was probably transported into the basin physically as windblown dust rather than as solutes in surface or groundwater from nearby source areas (Smoot and Olsen, 1994; Smoot, 2010). A series of basins in the area now occupied by the Atlantic shelf, where gypsum-halite deposits were accumulating sometime during the Norian (Evans, 1978), represents a plausible source of eolian gypsum dust. The gypsum in zone C mainly accumulated in saline soils, and once it was buried below the water table, it could have been recycled into pore-filling cement within a few tens of meters of the surface (Drever and Smith, 1978; Smoot and Lowenstein, 1991). Sulfate-rich waters may also have moved upward from greater depths along fractures still forming due to basin extension.

The change from a silicate-dominated macropore assemblage to one rich in carbonates signals another major shift in diagenetic fluid composition. It cannot be attributed to the igneous event that produced basalts and diabase intrusions for several reasons. One is the fact that carbonates precipitated in reactivated veins, some of which were lined with K-feldspar (fig. 13C). Moreover, carbonates occur in a series of fractures (S2) that are rotated thirty degrees counterclockwise from the earlier veins (Herman, 2005, 2009). The carbonate-precipitating fluids were aggressive, with crystals embaying the older silicates in the macropore cements and in veins. Carbonate minerals also partially replaced detrital quartz grains (fig. B14) in the Stockton, Lockatong, and lower Passaic Formations. Lastly, multiple types of carbonate may be present within a single macropore, including ferroan dolomite, ferroan calcite, and non-ferroan calcite (figs. B5B and B7A). The late carbonate minerals in veins and macropores are also associated with bitumen and sulfides (fig. B13B).

The change in fluid chemistry from an alkaline, silicate-precipitating fluid to a silicate-dissolving, carbonate-precipitating fluid was probably due to a

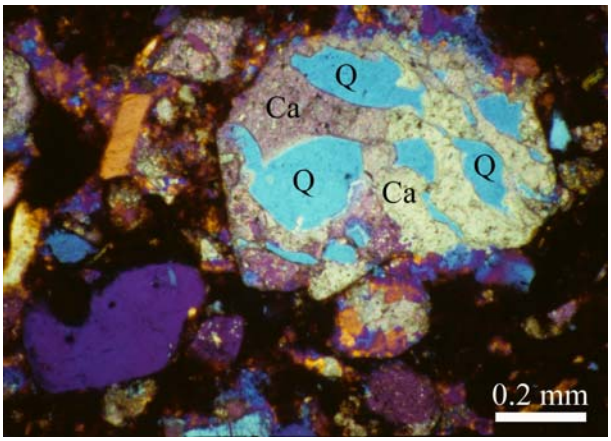

Figure B14. Photomicrograph between crossed polarizers with gypsum plate inserted of sandy sediment from the Passaic Formation (middle of zone B) with detrital quartz grains replaced by carbonate; what was originally one coarse sand grain now appears to be multiple pieces quartz (Q) separated by strips of coarsely crystalline calcite (Ca), but the quartz remnants retain their uniform crystallographic orientation (evidenced by their consistent blue interference color).

massive infusion of dissolved CO_2 which made the waters more acidic at first, then provided the CO_3 necessary to precipitate calcite and dolomite cements. A late diagenetic transition from kerogen to oil could account for the release of CO_2 (Tissot and Welte, 1978, p. 162-163) as well as the association of bitumen with later cements. Malinconico (2002, 2010) combined observations of vitrinite reflectance with published zircon and apatite fission-track-closure data (Roden and Miller, 1991; Kohn and others, 1993; Steckler and others, 1993) to estimate a basinwide geothermal gradient of about 25^{o}-27^{o}C/km during burial. If catagenesis initiated at about 100 ^{o}C (Verweij, 1993, p. 94-97), this gradient would put the organic-rich shales at the base of the Lockatong Formation into the oil window after burial to a depth of 3.7-4.0 km. Based on stratigraphic thicknesses, they would have been buried to roughly this depth at the beginning of the Jurassic. However, Malinconico (2002, 2010) indicated that the basal 150 m of the Lockatong Formation was thermally altered by heat flowing up from the Stockton Formation because the latter acted as a conduit for heated fluids escaping from greater depths near the border fault. This resulted in an effective thermal gradient of 35 ^{o}C/km for these lower deposits, in which case oil production could have begun after burial to only 2.8 km. This implies that some of the Lockatong Formation petroleum could have gone beyond the liquid window, but the organics in the upper Lockatong Formation and lower Passaic Formation would have still been a viable source of oil. Oil and CO_2-charged formation waters may have then been able to migrate to lower stratigraphic levels by traveling updip from border faults, then moving to stratigraphically lower but physically higher strata where they intersected faults and fractures. A similar mechanism involving updip migration would allow the gypsum-rich mudstones of the upper Passaic Formation to provide Ca, Fe, and S for the precipitation of calcite and pyrite in deeper stratigraphic units. Malinconico (2002, 2010) cited evidence of thermal fluids from the Stockton Formation moving along faults and entering the overlying Lockatong and Passaic Formation, which includes the precipitation of base metal deposits. Herman (2005, 2009) noted that the S2 fractures were probably generated during a short period of time, suggesting a possible tectonic triggering mechanism for the release of the carbonate-precipitating fluids.

Summary and conclusions

The Newark basin contains nearly 6 km of late Triassic to early Jurassic mudstones deposited in a hydrologically closed basin. Some of this mud was deposited in deep to shallow perennial lakes, but most of it accumulated on subaerially exposed mudflats and contained as much as 20 percent by volume primary macroporosity in the form of millimeter-scale air bubbles (vesicles), desiccation cracks, and root tubules. Coarsely crystalline authigenic minerals fill many of these depositional macropores, and their composition changes systematically on a broad scale as a function of stratigraphic position. In ascending stratigraphic order, the three main assemblages we recognized (fig. B2) are zone A with analcime, K-feldspar, and carbonate but no albite or gypsum-anhydrite; zone B with albite, K-feldspar, and carbonate but no analcime and gypsum-anhydrite only in the uppermost part; and zone C with calcite and gypsum and traces of albite and dolomite but no analcime or K-feldspar. Although our analysis is based largely on samples from the NBCP drill cores, samples from surface exposures suggest these assemblages persist throughout the Newark basin. Other authigenic minerals are also present in minor amounts, most notably celesto-barite that postdates calcite, and base-metal sulfides that postdate dolomite and are synchronous with or predate calcite. Some of these authigenic minerals were previously interpreted as precipitating from saline surface waters essentially in the depositional environment, but this interpretation is no longer tenable. Despite the broad correlation between mineral assemblages and stratigraphic position, the coarsely crystalline nature of the assemblages and their complex parageneses indicate that few if any formed near the depositional interface. Moreover, $^{40}Ar/^{39}Ar$ ages indicate the K-feldspars were growing about 20 million years after deposition. These characteristics require a long and complex history of

fluid migration through the Newark mudstones.

The mudstones also contain an abundance of veins with mineral assemblages very similar to those filling the macropores. We interpret the veins as paleofractures that served as conduits for the postulated late diagenetic fluid flow. Although there appears to be a small stratigraphic offset between the assemblage transitions in the macropores versus the veins, our sample coverage is not sufficiently dense to rule out the possibility that this is an artifact of sampling. The parageneses of the vein-filling minerals require a long and complex history that we suggest proceeded as follows. Veins containing analcime and albite appear to be equivalent to the S1 fractures of Herman (2005; 2009) that are attributed to extension occurring throughout deposition of the Newark basin rocks. Fluid movement upward along these fractures may have been generated by differential compaction via the rupturing of basin-scale aquifers whose hydraulic head was controlled by relief along the faulted margin. We think the fluids from which the macropore- and vein-filling minerals precipitated originated as alkaline brines in saline lakes and saline mudflats, and then were progressively modified over time by the conversion of unstable smectite clays to more stable phases. We attribute the veins with gypsum and anhydrite in the upper Passaic Formation to the redistribution of gypsum originally precipitated in saline soils by groundwater moving through the S1 fractures. Veins lined with K-feldspar apparently formed during the volcanic event at the beginning of the Jurassic, owing in part to a surge of fluid pressure that resulted from diabase intrusion. The fluid injected during this period had evolved from the earlier Na-silicate precipitating fluids, in part by alteration of the smectites to illite. Both the formation of some carbonate-filled veins and the reactivation of older veins filled with silicates occurred sometime after deposition of the Jurassic part of the basin fill in a stress field rotated from that of the basin margin (Herman, 2005, 2009). The carbonate-rich fluids were generated by CO_2 released by oil formation. These fluids also transported base metals and petroleum along the fractures and into open pores partially formed by dissolution of framework grains and earlier cements. Horizontal veins only occur within 100 to 400 m of the modern surface and are mostly filled with fibrous gypsum (satin spar). These probably formed after erosion of overlying rocks during formation of the post-rift unconformity. Most recently, dissolution of sparry calcite and gypsum minerals from both macropores and fractures has increased the permeability of the Newark mudstones to the point where strata rich in these minerals locally control groundwater flow and chemistry (Rima, 1955; Herman, 2001).

Acknowledgments

Field and lab work were supported by NSF Grant EAR-9105788 (to BMS) and a U.S. Geological Survey Gilbert Fellowship (to JPS). Many Oberlin students aided us in the field and/or lab, most notably Amanda Zola Mosala, Karen Carney, Sarah Webb, Jack Williams, Justin Mog, and Brooke Wilkerson. Students were supported by NSF and various Oberlin College grants including a Mellon Minority Fellowship and a BP America Research Assistantship. We thank Paul Olsen and Dennis Kent for access to the NBCP cores and Paul Olsen for suggesting suitable outcrops for sampling and providing detailed instructions for finding them. The manuscript benefited from thoughtful reviews by Blair Jones, Bob Burruss, Randy Steinen, Michael Serfes, Gregory Herman, and Irving Grossman. We thank MaryAnn Malinconico and Gregory Herman for providing copies of unpublished manuscripts to help us with our interpretations.

References

Caudill, M.R., Driese, S.G., and Mora, C.I., 1997, Physical compaction of vertic palaeosols: implications for burial diagenesis and palaeo-precipitation estimates: Sedimentology, v. 44, p. 673-685.

Chamley, H., 1989, Clay Sedimentology: Springer-Verlag, New York, New York, 623 p.

Drever, J.I. and Smith, C.L., 1978, Cyclic wetting and drying of the soil zone as an influence on the chemistry of groundwater in arid terrains: American Journal of Science, v. 278, p. 1448-1454.

Du Rouchet, J., 1981, Stress fields, a key to oil migration: American Association of Petroleum Geologists Bulletin, v. 65, p. 74-85.

El Tabakh, M., Riccioni, R.B., and Schreiber, B.C., 1997, Evolution of late Triassic rift basin evaporites (Passaic Formation), Newark Basin, eastern North America: Sedimentology, v. 44, p. 767-790.

El Tabakh, M., and Schreiber, B.C., 1994, Lithologies and diagenesis of the lacustrine sediments of the Lockatong Formation (Upper Triassic) in the Newark rift basin, *in* Lomando, A.J., Schreiber, B.C., and Harris, P.M., eds., Lacustrine Reservoirs and Depositional Systems: Society of Economic Paleontologists and Mineralogists Core Workshop no. 19, , Tulsa, Oklahoma, p. 239-295.

El Tabakh, M., Schreiber, B.C., and Warren, J.K., 1998, Origin of fibrous gypsum in the Newark Rift Basin, eastern North America: Journal of Sedimentary Research, v. 68, p. 88-99.

Evans, R., 1978, Origin and significance of evaporites in basins around the Atlantic margin: American

Association of Petroleum Geologists Bulletin, v. 62, p. 223-234.

Goldberg, D.S., Lupo, T. , Caputi, M., Barton, C., and Seeber, L., 2003, Stress regimes in the Newark basin rift: Evidence from core and downhole data, *in* LeTourneau, P.M. and Olsen, P.E., eds., The Great Rift Valleys of Pangea in Eastern North America, vol. 1, Tectonics, Structure, and Volcanism: Columbia University Press, New York, New York, p. 104-117.

Goldberg, D.S., Reynolds, D.J., Williams, C.F., Witte, W.K., Olsen, P.E., and Kent, D.V., 1994, Well-logging results from the Newark rift basin coring project: Scientific Drilling, v. 4, p. 267-279.

Gottfried, R.M. and Kotra, R.K., 1988, Comparative mineralogy of clay-rich strata in selected early Mesozoic basins of the eastern United States, *in* Froelich, A.J., and G.R Robinson. Jr., eds. Studies of the Early Mesozoic Basins of the Eastern United States: U.S. Geological Survey Bulletin 1776, p. 99-103.

Grigor'ev, D.P., 1965, Ontogeny of minerals: Israel Program for Scientific Translations, Ltd., Jerusalem, Israel, 250 p.

Gude, A.J., and Sheppard, R.A., 1988, A zeolitic tuff in a lacustrine facies of the Gila Conglomerate near Buckhorn, Grant County, New Mexico: U.S. Geological Survey Bulletin 1763, 22 p.

Hawkins, A.C., 1928, Halite and glauberite and included minerals from central New Jersey: American Mineralogist, v. 23, p. 145-176.

Herman, G.C., 2001, Hydrogeological framework of bedrock aquifers in the Newark basin, New Jersey: *in* LaCombe, P.J., and Herman, G.C., eds., Geology in Service to Public Health, 18th Annual Meeting of the Geological Association of New Jersey, p. 6-45.

Herman, G.C., 2005, Joints and veins in the Newark basin, New Jersey in regional tectonic perspective, *in* Gates, A.E., ed., View from the 21st Century, 22nd Annual Meeting of the Geological Association of New Jersey, p. 75-116.

Herman, G.C., 2009, Steeply-dipping extension fractures in the Newark basin, New Jersey: Journal of Structural Geology v. 31 p. 996-1011.

Huntoon, J.E., and Furlong, K.P., 1992, Thermal evolution of the Newark basin: Journal of Geology, v. 100, p. 579-591.

Jones, B.F., and Weir, A.H., 1983, Clay minerals of Lake Abert, an alkaline, saline lake: Clays and Clay Minerals, v. 31, p. 161-172.

Katz, B.J., Robison, C.R. , Jorjorian, T., and Foley, F.D., 1988, The level of organic maturity within the Newark basin and its associated implications, *in* Manspeizer, W., ed., Triassic-Jurassic Rifting: Continental Breakup and the Origin of the Atlantic Ocean and Passive Margins, Part B: Elsevier, Amsterdam, The Netherlands, Developments in Geotectonics v. 22, p. 683-696.

Kohn, B.P., Wagner, M.E., Lutz, T.M., and Organist, G., 1993, Anomalous Mesozoic thermal regime, central Appalachian Piedmont: Evidence from sphene and zircon fission-track dating: Journal of Geology, v. 101, p. 779-794.

Kunk, M.J., Simonson B.M., and Smoot, J.P., 1995, $^{40}Ar/^{39}Ar$ constraints on the age of K-feldspar cementation in non-marine sediments of the Newark, Gettysburg, and Culpeper basins: Geological Society of America Meeting Abstracts with Program, Northeastern Section, v. 27, p. 62.

Liou, J.G., 1971, Analcime equilibria: Lithos, v. 4, p. 389-402.

Lorenz, J.C., 1988, Triassic-Jurassic Rift-Basin Sedimentology: Van Nostrand Reinhold Company, New York, 315 p.

Magara, K., 1978, Compaction and Fluid Migration, Practical Petroleum Geology: Elsevier, Amsterdam, Developments in Petroleum Science 9, 319 p.

Malinconico, M.L., 2002, Lacustrine organic sedimentation, organic metamorphism, and thermal history of selected early Mesozoic Newark supergroup basins, eastern U.S.A.: Columbia University Ph.D. dissertation, New York, New York, 419 p.

Malinconico, M.L., 2010, Synrift to early postrift basin-scale groundwater history of the Newark basin based on surface and borehole vitrinite reflectance data, *in* Herman, G.C., and M.E. Serfes, eds., Contributions to the Geology and Hydrogeology of the Newark Basin: N.J. Geological Survey Bulletin 77, Chapter C., p. C1-C38.

Marcussen, O., Thyberg, B.I., Peltonen, C., Jahren, J. , Bjorlykke, K. , and Faleide, J.I., 2009, Physical properties of Cenozoic mudstone from the northern North Sea; impact of clay mineralogy on compaction trends: American Association of Petroleum Geologists Bulletin, v. 93, p. 127-150.

Mees, F., Stoops, G., Van Ranst, E., Paepe, R., and. Van Overloop, E., 2005, The nature of zeolite occurrences in deposits of the Olduvai Basin, northern Tanzania: Clays and Clay Minerals, v. 53, p. 659-673.

Michalski, A., and Britton, R., 1997, The role of sedimentary bedding in the hydrogeology of sedimentary bedrock – Evidence from the Newark basin, New Jersey: Ground Water, v. 35, p. 318-327.

O'Brien, N.R. and Slatt, R.M., 1990, Argillaceous Rock Atlas: Springer-Verlag, New York, New York, 141 p.

Olsen, P.E., 1986, A 40-million year record of early Mesozoic climate forcing: Science, v. 234, p. 842-848.

Olsen, P.E., Kent, D.V., Cornet, B., Witte, W.K., and Schlische, R.W., 1996, High-resolution stratigraphy of the more than 5000 m Newark rift section (early

Mesozoic, eastern North America): Geological Society of America Bulletin, v. 108, p. 40-77.

Olsen, P.E., and Rainforth, E.C., 2001, The "Age of Dinosaurs" in the Newark basin, with special reference to the lower Hudson Valley, *in* Gates, A.E., ed., Geology of the Lower Hudson Valley, 2001; New York State Geological Association Field Trip Guidebook, p. 59-176.

Oshchudlak, M.E., and Hubert, J.F., 1988, Petrology of Mesozoic sandstones in the Newark basin, central New Jersey and adjacent New York, *in* Manspeizer, W., ed., Triassic-Jurassic Rifting: Continental Breakup and the Origin of the Atlantic Ocean and Passive Margins, Part A, Developments in Geotectonics 22: Elsevier, Amsterdam, The Netherlands, p. 333-352.

Person, M. and Garven, G., 1994, A sensitivity study of the driving forces on fluid flow during continental-rift basin evolution: Geological Society of America Bulletin, v. 106, p. 461-475.

Pratt, L.M., Shaw, C.A., and Burruss, R.C., 1988, Thermal histories of the Hartford and Newark basins inferred from maturation indices of organic matter, *in* Froelich, A.J., and Robinson, G.R. Jr., eds. Studies of the Early Mesozoic Basins of the Eastern United States: U.S. Geological Survey Bulletin 1776, p. 58-63.

Ramsey, J.G., 1980, The crack-seal mechanism of rock deformation: Nature, v. 284, p. 135-139.

Renaut, R.W., 1993, Zeolitic diagenesis of late Quaternary fluviolacustrine sediments and associated calcrete formation in Lake Bogoria Basin, Kenya Rift Valley: Sedimentology, v. 40, p. 271-301.

Rieke, H.H. III, and Chilingarian, G.V., 1974, Compaction of Argillaceous Sediments: Elsevier, Amsterdam, The Netherlands, 424 p.

Rima, D.R., 1955, Ground water resources of the Lansdale area, Pennsylvania: Pennsylvania Geological Survey Fourth Series, Progress Report 146, 17 p.

Roden, M.K., and Miller, D.S., 1991, Tectono-thermal history of Hartford, Deerfield, Newark, and Taylorsville basins, eastern United States, using fission-track analysis: Schweizerische Mineralogische und Petrographische Mitteilungen, v. 71, p. 187-203.

Ryan, M.P., Yang, J., and Edwards, R.N., 1997, Dike-forming intrusions and hydrothermal circulation in compartmentalized volcanic systems: Evolutionary patterns in internal porous media convection and external heat flow: EOS Transactions of the American Geophysical Union, Fall Meeting Program, v. 78, p. F-765.

Schaller, W.T., 1932, The crystal cavities of the New Jersey zeolite region: U.S. Geological Survey Bulletin 832, 90 p.

Schamel, S., and Hubbard, I.G., 1985, Thermal maturity of Newark Supergroup basins from vitrinite reflectance and clay mineralogy [abstract]: Bulletin of the American Association of Petroleum Geologists, v. 69, p. 1447.

Schlische, R.W., Withjack, M.O., and Olsen, P.E., 2003, Relative timing of CAMP, rifting, continental breakup, and basin inversion: Tectonic significance, *in* Hames, W.E., McHone, J.G., Renne, P.R., and Ruppel, C., eds., The Central Atlantic Magmatic Province, Insights from fragments of Pangea: American Geophysical Union, Geophysical Monograph 136, p. 33-59.

Serfes, M.E., 2005, Arsenic occurrence, sources, mobilization, transport, and prediction in the major bedrock aquifers in the Newark basin: Rutgers University Ph.D. dissertation, New Brunswick, New Jersey, 122 p.

Simonson, B.M., and Smoot, J.P., 1994, Distribution and origin of macropore-filling cements in non-marine mudstones, Early Mesozoic Newark Basin, New Jersey and Pennsylvania: Geological Society of America Abstracts with Program, v. 26, p. A-337.

Simonson, B.M., and Smoot, J.P., 1995, Are coarsely crystalline authigenic minerals in the mudstones of the Early Mesozoic Newark Supergroup truly cements?: Geological Society of America Abstracts with Program, v. 27, p. 81.

Smoot, J.P., 1991, Sedimentary facies and depositional environments of early Mesozoic Newark Supergroup basins, eastern North America: Palaeogeography, Palaeoclimatology, Palaeoecology, v. 84, p. 369-423.

Smoot, J.P., 2010, Triassic depositional facies in the Newark basin, *in* Herman, G.C., and Serfes, M.E., eds., Contributions to the Geology and Hydrogeology of the Newark Basin: New Jersey Geological Survey Bulletin 77, Chapter A, p. A1-A109.

Smoot, J.P., and Castens-Seidell, B., 1994, Sedimentary features produced by efflorescent salt crusts, Saline Valley and Death Valley, California: *in* Renaut, R.W., and Last, W.M., eds., Sedimentology and Geochemistry of Modern and Ancient Saline Lakes: Society of Economic Paleontologists and Mineralogists Special Publication 50, p. 73-90.

Smoot, J.P. and Lowenstein, T.K., 1991, Depositional environments of non-marine evaporites, in Melvin, J.L., ed., Evaporites, Petroleum and Mineral Resources, Developments in Sedimentology 50: Elsevier, Amsterdam, The Netherlands, p. 189-347.

Smoot, J.P., and Olsen, P.E., 1988, Massive mudstones in basin analysis and paleoclimatic interpretation of the Newark Supergroup, *in* Manspeizer, W., ed., Triassic-Jurassic Rifting: Continental Breakup and the Origin of the Atlantic Ocean and Passive

Margins, Part A, Developments in Geotectonics 22: Elsevier, Amsterdam, The Netherlands, p. 249-274.

Smoot, J.P. and Olsen, P.E., 1994, Climatic cycles as sedimentary controls of rift-basin lacustrine deposits in the early Mesozoic Newark basin based on continuous cores, *in* Lomando, A.J., Schreiber, B.C., and Harris, P.M., eds., Lacustrine Reservoirs and Depositional Systems: Society of Economic Paleontologists and Mineralogists Core Workshop no. 19, p. 201-237.

Stamatikis, M.G., 1989, Authigenic silicates and silica pseudomorphs in the Miocene saline-alkaline deposits of the Karlovassi Basin, Samos, Greece: Economic Geology, v. 84, p. 788-798.

Steckler, M.S., Omar, G.I., Karmer, G.D., and Kohn, B.P., 1993, Pattern of hydrothermal circulation within the Newark basin from fission-track analysis: Geology, v. 21, p. 735-738.

Surdam, R.C., and Eugster, H.P., 1976, Mineral reactions in the sedimentary deposits of the Lake Magadi region, Kenya: Geological Society of America Bulletin, v. 87, p. 1739-1752.

Surdam, R.C., and Sheppard, R.A., 1978, Zeolites in saline, alkaline-lake deposits, *in* Sand, L.B., and Mumpton, F.A., eds., Zeolites: Occurrence, Properties, Use: Pergamon Press, Oxford, England, p. 145-174.

Thompson, A.B., 1971, Analcite-albite equilibria at low temperatures: American Journal of Science, v. 271, p. 79-92.

Tissot, B.P., and Welte, D.H., 1978, Petroleum Formation and Occurrences, Springer-Verlag, New York, 538 p.

Turner-Peterson, C.E., 1980, Sedimentology and uranium mineralization in the Triassic-Jurassic Newark basin, Pennsylvania and New Jersey, *in* Turner-Peterson, C.E., ed., Uranium in Sedimentary Rocks: Applications of the Facies Concept to Exploration: Society of Economic Paleontologists and Mineralogists, Rocky Mountain Section Short Course Notes, p. 149-175.

van de Kamp, P.C., and Leake, B.E., 1996, Petrology, geochemistry, and Na metasomatism of Triassic-Jurassic non-marine clastic sediments in the Newark, Hartford, and Deerfield rift basins, northeastern USA: Chemical Geology, v. 133, p. 89-124.

Van Houten, F.B., 1962, Cyclic sedimentation and the origin of analcime-rich Upper Triassic Lockatong Formation, west-central New Jersey and adjacent Pennsylvania: American Journal of Science, v. 260, p. 561-576.

Van Houten, F.B., 1964, Cyclic lacustrine sedimentation, Upper Triassic Lockatong Formation, central New Jersey and adjacent Pennsylvania, *in* Merriam, D.F., ed., Symposium on Cyclic Sedimentation: Kansas Geological Survey Bulletin 169, p. 497-531.

Van Houten, F.B., 1965a, Composition of Triassic Lockatong and related formations of the Newark Group, central New Jersey and adjacent Pennsylvania: American Journal of Science, v. 263, p. 825-863.

Van Houten, F.B., 1965b, Crystal casts in Upper Triassic Lockatong Formation, west-central New Jersey and adjacent Pennsylvania: Sedimentology, v. 4, p. 301-313.

Verweij, J.M., 1993, Hydrocarbon Migration Systems Analysis: Developments in Petroleum Science 35, Elsevier, Amsterdam, The Netherlands, 276 p.

Wherry, E.T., 1916, Glauberite crystal-cavities in the Triassic rocks of eastern Pennsylvania: American Mineralogist, v. 1, p. 37-43.

Wilding, L.P., and Puentes, R., 1988, Vertisols: Their Distribution, Properties, Classification and Management: Technical Monograph no. 18, Soil Management Support Services, Texas A&M University, College Station, Texas, 193 p.

Synrift to Early Postrift Basin-Scale Groundwater History of the Newark Basin Based on Surface and Borehole Vitrinite Reflectance Data

By MaryAnn Love Malinconico, Lafayette College

Chapter C of

Contributions to the Geology and Hydrogeology of the Newark Basin

N.J. Geological Survey Bulletin 77

State of New Jersey
Department of Environmental Protection
Water Resource Management
New Jersey Geological Survey
2010

Contents

Figures

Tables

Chapter C

Synrift to Early Postrift Basin-Scale Groundwater History of the Newark Basin Based on Surface and Borehole Vitrinite-Reflectance Data

MaryAnn Love Malinconico[1]

Abstract

The pattern of synrift to early postrift steady-state and transient basin-scale groundwater flow in the Newark basin is evident in its paleomaximum temperature structure, recorded in surface and borehole vitrinite-reflectance data. Flow in the Late Triassic to Early Jurassic occurred primarily through coarse porous clastic sedimentary units and along faults. Downwelling meteoric waters, gravity driven by topographic highs at the western border fault, flowed down the fault through permeable alluvial fan sediments, but were restricted from basinward flow by low-permeability lacustrine mudstones, until they reached the basal coarse fluvial Stockton Formation. There, fluids, heated to approximately 235˚C, flowed cross-basin and updip through the Stockton, cooling to below 210˚C before discharging along the hanging wall basin edge. Vertical vitrinite-reflectance profiles from three boreholes that intersect the Stockton Formation indicate that this unit, at the time of paleomaximum temperature, functioned as a well-mixed, confined, horizontal/lateral aquifer that was vertically isothermal at any given distance from the border fault. Heated flow through the Stockton lasted long enough for overlying strata to reach a steady-state conductive gradient of ~35˚C/km; the background synrift conductive geothermal gradient of the basin was ~25˚C/km. Modeling of basin thermal history and vitrinite-reflectance evolution indicates maximum steady-state temperatures occurred at the end of synrift sedimentary deposition (194 $\pm$ 5 Ma).

Seismic pumping during early postrift basin structural inversion and exhumation produced transient advective high heat flow in thin permeable units within cyclic lacustrine sediments intersected by faults tapping the basal Stockton aquifer. Evidence for these events includes high vitrinite reflectance anomalies, commonly also associated with epigenetic stratabound copper mineralization. Trace metal analyses of these black-shale-associated base-metal concentrations also show a positive correlation with arsenic. The vitrinite reflectance data, plus published fluid inclusion temperatures from Newark lead-zinc vein deposits, indicate ore deposition began while heated flow through the Stockton was still at thermal maximum. Zircon fission-track ages by other authors suggest that the maximum temperature of the Stockton aquifer and the basin-scale groundwater system cooled below 180˚-220˚C about 185-175 Ma. The demise of this groundwater system was most likely due to erosional destruction of border-fault topographic highs, which had provided the hydraulic head, and the occlusion of formation permeability by mineral cements.

Introduction

The Early Mesozoic Newark basin is one of the most intensely studied continental rift basins, including, in the past twenty years, several studies on basin thermal history and thermal indicators (Katz and others, 1988b, Pratt and others, 1988; Sutter, 1988; Walters and Kotra, 1990; Roden and Miller, 1991; Huntoon and Furlong, 1992; Kohn and others, 1993; Steckler and others, 1993; El-Tabakh and others, 1997; Smith and Faill, 2000). The impetus for these studies has been exploration for domestic fossil fuel resources and interest in the tectonic evolution of the western Atlantic passive margin. Conclusions are varied and include transient thermal pulses (initial basin extension, igneous or hydrothermal activity), or long-term events (elevated conductive basement heat flow or basin groundwater circulation).

Data for nearly all these previous studies, however, have been obtained from surface samples. Following the acquisition of several thousand meters of core from seven offset but stratigraphically overlapping coreholes of the Newark Basin coring project (NBCP; table C1), a third dimension has become available for sampling (Olsen and others, 1996a) The study presented here combines new borehole vitrinite-reflectance data from six ~1000m NBCP cores, plus data from a deep (~3200 m) industry drill hole, with expanded Newark basin surface vitrinite-reflectance coverage. Vitrinite reflectance is an organic low-grade metamorphic

[1]Lafayette College
Department of Geology and Environmental Geosciences
Easton, Pa 18042
lovem@lafayette.edu

Table C1. Deep rock cores and a petroleum exploration well in the Newark basin.

Name	Latitude	Longitude	County, State	Total depth below land surface (feet)	Total depth below land surface (meters)
Martinsville….....	40˚ 37' 09" N	74˚ 34' 22" W	Somerset, NJ	4015.0	1223.8
Weston Canal…..	40˚ 32' 33" N	74˚ 33' 49" W	Somerset, NJ	2602.0	793.1
Somerset……..	40˚ 30' 31" N	74˚ 33' 58" W	Somerset, NJ	3010.0	917.4
Rutgers……..	40˚ 32' 33" N	74˚ 26' 00" W	Middlesex, NJ	3095.0	943.4
Titusville…….....	40˚ 19' 35" N	74˚ 51' 02" W	Mercer, NJ	3035.0	925.1
Nursery……..	40˚ 18' 03" N	74˚ 49' 27" W	Mercer, NJ	3310.0	1008.9
Princeton……..	40˚ 22' 09" N	74˚ 36' 49" W	Middlesex, NJ	3697.0	1126.8
Cabot #1*……	~40˚ 30' 37" N	~75˚ 09' 15" W	Bucks, PA	10500.0	3200.4

Note: All cores, except Cabot #1, were part of the Newark Basin Coring Project (NBCP).
Latitude, longitude and depth of NBCP cores from Olsen and others (1996a).
*Cabot #1, a petroleum exploration well, has its location based on 1985 well-location map filed with PA Dept. of Environmental Resources and obtained from the Pennsylvania Geological Survey. Well drilled on former property of Cabot Corp, Revere, PA.

indicator and is used here to evaluate the paleomaximum thermal structure of the basin and to test previous thermal history hypotheses. The results of this study indicate that, during the basin's synrift to early postrift history (221-180 Ma), a steady-state, gravity-driven, basin-scale groundwater system modified the distribution of heat in the basin sediments and was punctuated by late transient advective flow events.

Background

The Newark basin of New Jersey, Pennsylvania and New York is the largest of the exposed Late Triassic-Early Jurassic Newark-Supergroup-type basins along the Atlantic continental margin of the United States and Canada (fig. C1). The basins in this wide rift zone (Hutchinson and Klitgord, 1988) formed between the end of the Carboniferous-Permian Alleghany orogeny and the Early-to-Middle-Jurassic opening of the modern Atlantic Ocean. The border faults of the half-graben are normally-reactivated thrust faults (Robinson, 1979; Ratcliffe and others, 1986; Gates, 1997; Withjack and others, 1998; Schlische, 2003). Rifting began at least as early as the Middle Triassic, based on paleontological dating of sediments (Olsen and others, 1989) and $^{40}Ar/^{39}Ar$ dating of fault breccia (Altamura, 1996).

Sedimentary fill of the Newark Supergroup rift basins is entirely continental and consists of fluvial and lacustrine sedimentary formations and basalt flows (Olsen and others, 1996a; Olsen, 1997). The sedimentary rocks are organized in large-scale unconformity-bounded tripartite fluvial-lacustrine-fluvial tectonostratigraphic sequences (Olsen, 1997). Such tripartite basin-fill sequences are typical of tectonically active nonmarine basins and have been described for the Mesozoic Central Atlantic margin (CAM) rift basins of eastern North America and of Morocco (Olsen, 1997) and for lacustrine sequences in general (Katz and Liu, 1998). These sequences are predicted by basin filling models of increasing basin capacity with time, with accompanying constant sediment and water-supply rates (Schlische and Olsen, 1990; Schlische, 2003). Four tectonostratigraphic sequences have been identified in the CAM basins: sequences III and IV are found in core and outcrop in the Newark basin. Sequence I is only currently identified in the Fundy basin (Nova Scotia, Canada) and the Argana basin (Morocco); sequence II is limited to basins south of the Newark basin (Olsen, 1997).

The Newark basin is the type area of the latest Triassic tectonostratigraphic sequence III (TS III) and includes, from older to younger, the basal sandstone-rich fluvial Stockton Formation, the gray-black deep lacustrine Lockatong Formation, and the mostly red lacustrine to playa Passaic Formation (Olsen and others, 1996a; Olsen, 1997 and fig. C2a). The Lockatong and Passaic Formations are predominantly mudstone. The tectonically-forced sequences are overprinted by orbitally-forced climate cyclicity of which the approximately 20,000-year transgressive-regressive Van Houten lake cycle is the basic unit (Olsen, 1986, 1997). The Van Houten cycles display a hierarchy of expression: that is, relative lake depth, indicated by sediment color and degree of bioturbation, is modulated by longer term orbital cycles of ca. 100 ka, 400 ka, and 2000 ka (Olsen, 1986, 1997). The members of the Lockatong and Passaic Formations are bundles of Van Houten cycles controlled by the ca. 400 ka orbital eccentricity cycle (Olsen and others, 1996a).

Tectonostratigraphic sequence IV begins with a

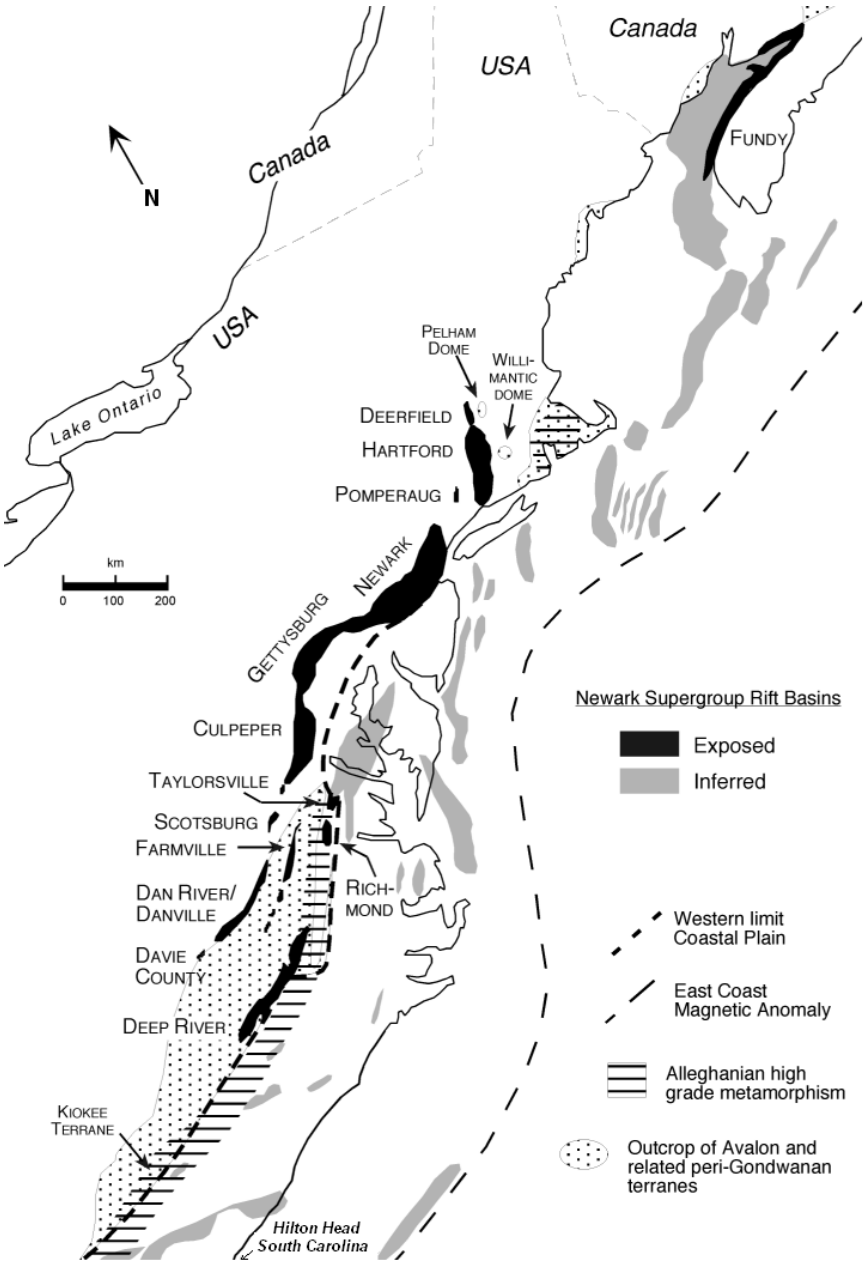

Figure C1. Location map of early Mesozoic Newark Supergroup rift basins (after Klitgord and others, 1988; Olsen, 1990), along the east coast of the United States and maritime Canada, also showing surface exposures of Avalon and related peri-Gondwanan terranes (Hatcher and others, 1990; Nance and Thompson, 1996), region of Alleghanian amphibolite-grade metamorphism (Hatcher and others, 1990), coastal plain (Hatcher and others, 1990), and the East Coast Magnetic Anomaly assumed to mark the transition to oceanic crust (Hutchinson and Klitgord, 1988).

sedimentation rate increase in the two latest Triassic members of the Passaic Formation, succeeded by three Jurassic basalt flows and three intervening lacustrine formations (Feltville, Towaco and Boonton Formations (fig. C2a)). The basalt flows and accompanying diabase sills and dikes are part of a giant igneous province (Central Atlantic Magmatic Province- "CAMP") produced during a short-lived (0.58 $\pm$ 0.1 m.y.) and well-dated extrusive event at about 201 Ma (Sutter, 1988; Dunning and Hodych, 1990; Olsen and others 1996b; Marzoli and others, 1999; Hames and others, 2000). The sedimentation rate increase has been interpreted as an increase or rejuvenation in extension rate accompanying the magmatic event (Schlische and Olsen, 1990; Olsen, 1997 and Schlische, 2003).

Several Newark Supergroup basins show evidence of postrift compression and basin structural inversion: the Taylorsville (LeTourneau, 1999) and Richmond (Withjack and others, 1998) basins of Virginia, and the Fundy (Withjack and others, 1995; 1998) basin, of maritime Canada. A consensus definition of basin inversion is "a basin controlled by a fault system that has been subsequently compressed-transpressed, producing uplift and partial extrusion of the basin fill"; the change in the stress system from extension to compression results in "extensive re-use of the pre-existing fault (system), with the uplift affecting the hanging wall rather than the

footwall" (Cooper and others, 1989). The shift from an extensional to compressional regime in the Early Mesozoic basins of Virginia and southward, and, by inference, the rift-drift transition, occurred before the intrusion of diabase dikes associated with the CAMP igneous event (202-201 Ma). The evidence is cross-cutting relationships of dikes and reverse-fault propagation folds, and the general northwest strike of the dikes, indicating the maximum horizontal stress was also in that orientation (Schlische and Ackermann, 1995; Withjack and others, 1998). Duration-of-sedimentation calculations for the Taylorsville basin, suggesting synrift sedimentation ended between 208-202 Ma (Malinconico, 2003), and apatite fission-track modeling indicating cooling, most likely due to uplift, along the eastern edge of that basin at ca. 200 Ma (Tseng and others, 1999) also support this hypothesis.

On the other hand, diabase dikes north of Virginia into maritime Canada strike generally northeast, indicating that the minimum horizontal stress was still northwest-southeast at the time of emplacement. The rift-drift transition along the Atlantic margin of North America is, consequently, diachronous (Withjack and others, 1998), occurring at or just prior to the Triassic-Jurassic boundary (ca. 202 Ma) from the Taylorsville basin south (fig. C1), and about 185 Ma off the northeastern United States and maritime Canada (including offshore of the Newark and Fundy basins), based on the oldest postrift strata in the Georges Bank and Scotian basins. Inversion in the Early Mesozoic Newark Supergroup basins has been attributed to incipient ridge-push forces and continental resistance to plate motion associated with the beginning of modern Atlantic sea-floor spreading (de Boer and Clifton, 1988; Withjack and others, 1998).

One consequence of postrift inversion and exhumation in the Newark basin is erosion of the synrift basin fill prior to the deposition of passive margin coastal plain sediments. Postrift basin erosion estimates, based on thermal indicators, have been previously made by several authors. Katz and others (1988b), Pratt and others (1988), Walters and Kotra (1990) and Huntoon and Furlong (1992) have suggested that less than 1 to 3 km of synrift Jurassic strata have been eroded above the youngest extant Newark Jurassic formation. Steckler and others (1993), in their fission-track study, concluded a minimum of 3 km of denudation over the Newark basin and surrounding region. El-Tabakh and others (1997) assumed that the Passaic Formation at the NBCP core sites (fig. C2) had been covered by a maximum of 3 km of synrift sediment above the current surface. Although the oldest coastal plain sediments that onlap the eroded hanging wall eastern edge of the basin are Cenomanian (97.5-91 Ma; Drake and others, 1998), basin erosion and exhumation were probably complete by the time of the Barremian (124-118 Ma) deposition of the oldest New Jersey Coastal Plain formations in the subsurface east of the basin (Steckler and others, 1993; Owens and others, 1998).

Numerous hypotheses of the synrift and postrift thermal evolution of the Newark basin have been put forward in the last two decades. Data for nearly all these studies (fission-track cooling ages and/or organic maturation indicators) were obtained from surface samples. Conclusions of these studies are diverse, including high heat flow at initial stages of rifting (Katz and others, 1988b), thermal pulse associated with earliest Jurassic (ca. 202 Ma) tholeiitic flood-basalt event with or without associated hydrothermal activity (Pratt and others, 1988; Roden and Miller, 1991; Huntoon and Furlong, 1992), regionally elevated conductive geothermal gradient (Kohn and others, 1993; Smith and Faill, 2000), postrift hydrothermal event about 176 Ma (Sutter, 1988; Walters and Kotra, 1990; El-Tabakh and others, 1997), and basin-scale topographically driven hydrothermal circulation (Steckler and others, 1993). However, despite the variety of published thermal scenarios for the Newark basin, there is a consensus that an average stable continental geotherm, 15-25˚C/km or 41-61 mW/m^2 (Morgan and Sass, 1984), is not sufficient to produce the level of maturity seen in the various thermal indicators. Either long-term elevated heat flow or a late synrift or postrift thermal pulse is essential.

A few of the Newark basin thermal evolution hypotheses include or suggest some type of long distance or basin-scale hydrothermal groundwater flow. It should be noted that "hydrothermal" refers to "heated or hot aqueous-rich solutions; …of diverse sources, including magmatic, meteoric, and connate waters" (American Geological Institute, 1976): it is not exclusively or solely related to igneous processes. The past twenty-five years have seen an increase in both attention to and understanding of large-scale groundwater systems in ancient basins and their effect on the distribution of heat and chemical mass, particularly the formation of fossil fuel and metalliferous ore deposits. Facilitating this interest in basin paleohydrology has been the development of sophisticated groundwater computer modeling programs (Garven and Freeze, 1984; Bethke, 1985). Early research focused on foreland basins: sources of hydraulic head or drive, the formation and location of stratabound ore deposits, particularly Mississippi Valley-type lead zinc deposits, and petroleum migration and maturation patterns (Garven, 1989; Bethke and others, 1991; Qing and Mountjoy, 1992; Shelton and others, 1992; Garven and others, 1993; Hitzman and others, 1998). Hypotheses for hydraulic drive included the "squeegee" effect, the expulsion of fluids from beneath thrust sheets into the foreland basin (Oliver, 1986). However, although faulting may produce short-term fluid expulsion events, it is now generally

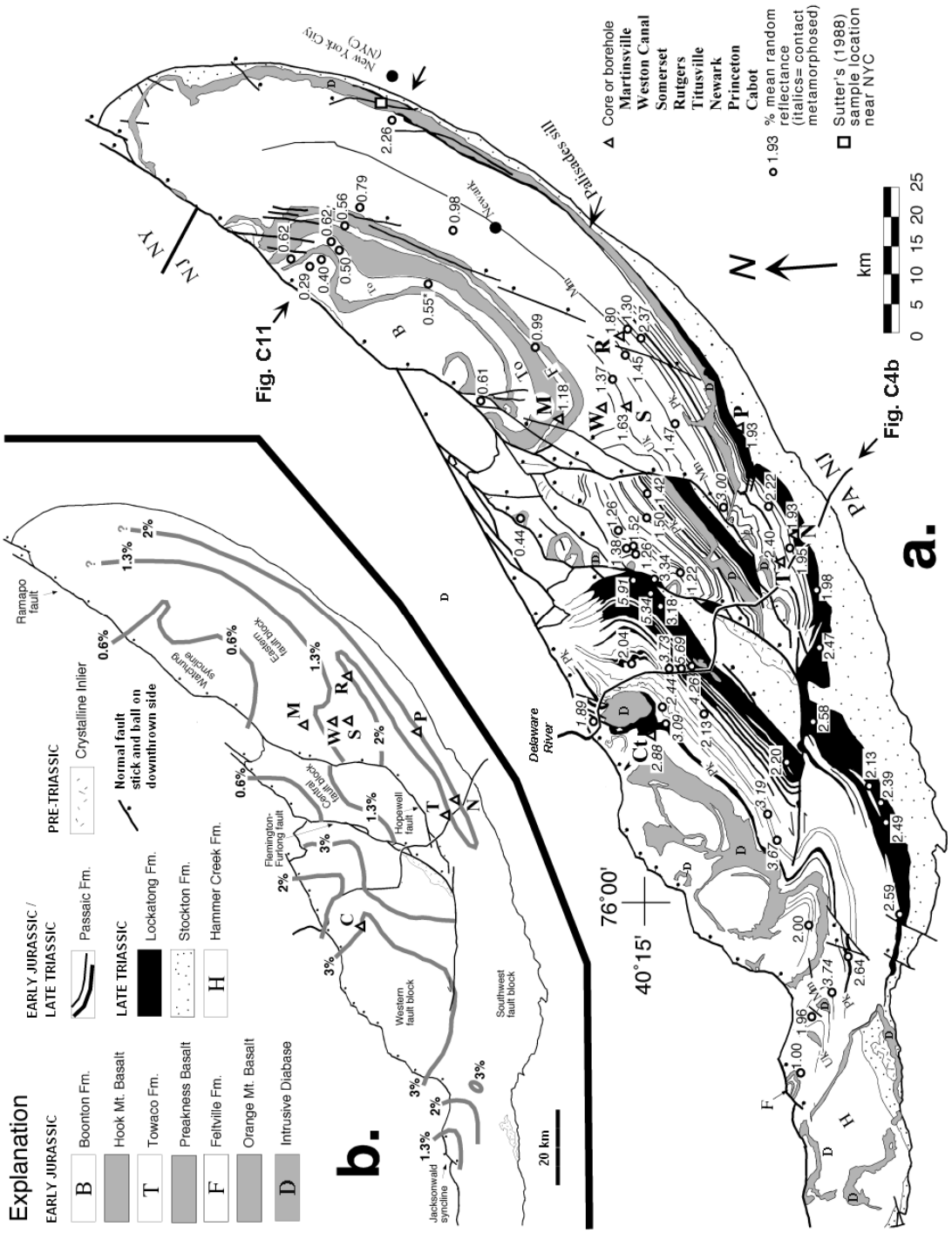

Figure C2. a) Newark basin bedrock geology map showing borehole locations (table C1), and surface mean random vitrinite-reflectance data. Reflectance values in italics due to contact metamorphism; value with asterisk (*) is corrected for reflectance suppression (Lo, 1993). Values at borehole locations (open triangles) are the shallowest measured values in cores or cuttings, except for Weston Canal, as noted in text. NBCP cores (Table C1) are M-Martinsville, W-Weston Canal, S-Somerset, R-Rutgers, T-Titusville, N-Nursery, P-Princeton. Ct-Cabot borehole (North Central Oil). b) Names are of basin geologic features and contours of surface vitrinite-reflectance data. Birth line of oil= 0.6%; death line= 1.3%. Passaic Formation member abbreviations: Pk-Perkasie, Uk-Ukrainian, Mm-Metlars.

agreed that to produce the necessary continuous flow for long distance transport of heat and mass, basin margin topographic highs produces the required hydraulic head. In foreland basins, the rising orogenic thrust belt provides the highs for gravity-driven recharge of meteoric water.

In contrast to basins formed in compressional tectonic settings, Person and Garven (1994) did sensitivity modeling of hydrologic systems in extensional rift basins. They primarily tested the effect of horizontal differences in stratigraphic permeability on patterns of temperature and discharge. The hydraulic head in rift basins is provided by footwall topographic highs at the border fault. In both rift and foreland basins, heat flow is depressed in the recharge area, owing to the downward flow of cooler meteoric waters (Person and Garven, 1994; Deming, 1994b). Meteoric water is eventually heated at depth and advection of heat may occur across the basin and/or in the discharge area if flow velocity exceeds the rate of fluid cooling.

One tool for discerning patterns of ancient fluid flow is thermal maturation, diagenetic or low-grade metamorphic indicators that provide information on patterns of maximum temperature. These methods may include vitrinite reflectance, spore-based thermal alteration indices, conodont alteration indices, clay crystallinity, and apatite and zircon fission-track analysis. This study uses vitrinite reflectance, the measured percentage of incident light reflected at a wavelength of 546 nm (green) under oil immersion microscopy from a polished surface of vitrinite. Vitrinite is fossil woody land plant matter deposited, preserved, and coalified in a reducing environment (coal swamp or low oxygen sediment) and not oxidized by composting, long-term transport through aerobic environments, or combustion. It can be found in sediments, sedimentary rocks, and very low-grade metasedimentary rocks. The logarithm of reflectance increases linearly with burial depth under a constant geothermal gradient, owing to increasing aromatization of carbon molecular structures and loss of volatiles. The level of reflectance is determined by the length of time the rock spends within 15˚C of maximum temperature. Vitrinite reflectance is a reliable thermal maturation indicator from 50˚C to about 400˚C, which includes the windows of oil and gas generation, lignite to anthracite coal ranks, and sediment diagenesis to prehnite-pumpellyite metamorphism (Taylor and others, 1998). The downhole and expanded surface vitrinite- reflectance data from this study will constrain the conductive and advective processes responsible for the pattern and level of Newark basin thermal maturity.

Methods

All vitrinite reflectance data were collected by the author, except for those of the Cabot borehole. Cabot borehole vitrinite-reflectance data were produced by Brown and Ruth Laboratories, Houston, Texas, and are published with the permission (1998) of North Central Oil Corporation, Inc., Houston, Texas.

Samples used for vitrinite reflectance in this study are well cuttings or pieces of whole rock from core and surface samples mounted in epoxy and polished. Surface sample locations are listed in Malinconico (2002). Reflectance was measured under oil immersion in plane polarized light at 546 nm on a Leitz MPV II microscope at the Coal Characterization Laboratory, Department of Geology, Southern Illinois University (SIU), Carbondale, Illinois; on a Leitz MPV I at the Department of Geological Sciences, University of Missouri (MU), Columbia, Missouri; and on a Leitz MPV II in the Coal and Organic Petrology Laboratories, Energy Institute, Penn State University (PSU), University Park, Pennsylvania. The first two microscopes were outfitted with rotational polarization as described in Bensley and Crelling (1991) and Houseknecht and others (1993). In reflectance measurement with rotational polarization, the maximum, minimum, and random (polarizer position at 45˚) reflectances of a particle are measured during computer-guided motorized rotation of the polarizer, rather than manual rotation of the microscope stage with fixed polarizer. Appropriate corrections for polarizer and optical path anisotropy are made by the computer during routine standardization procedures. Macerals believed to be first-cycle indigenous vitrinite appropriate for maturation determination were initially chosen for measurement using the microscopist edit method of Barker and Pawlewicz (1993). Maximum and minimum reflectance data collected using rotational polarization at SIU and MU were then used to construct reflectance crossplots (Kilby, 1988) to identify vitrinite particles with similar reflectance indicatrices and, therefore, assumably similar chemical and physical properties (Malinconico, 2000). This method is believed to be more useful in determining the first-cycle or indigenous vitrinite population than the traditional histogram method (Barker and Pawlewicz, 1993), especially in samples with an abundance of reworked, recycled, pseudo-, and oxidized vitrinite and semi-inertinite (Malinconico, 2000). Once the indigenous vitrinite population of a sample was identified, corresponding random reflectances for those particles were used to calculate the mean random reflectance (% R_O). Random reflectance traditionally is the reflectance measured on a particle of vitrinite without rotating the sample or microscope stage to find the maximum or minimum reflectance value of this uniaxial or biaxial material.

At Penn State, apparent maximum and minimum reflectance data were collected by manual rotation of the microscope stage (polarizer fixed at 45˚)

on several indigenous vitrinites in each sample. From those that appeared to have a similar reflectance indicatrix, the true maximum and true minimum reflectances were then chosen. Subsequent vitrinites with random reflectances between the true maximum and true minimum values were assumed to also be optically similar and were used to calculate the mean random reflectance for the sample.

Amounts of eroded synrift strata were calculated using the method of Dow (1977) which extrapolates the regressed line of a semi-logarithmic borehole reflectance-depth profile back to 0.2% R_O, the reflectance of recently deposited woody plant matter or low grade peat; the $\log_{10}$ of vitrinite reflectance is linear with depth under conditions of a constant geothermal gradient. The stratigraphic difference between the 0.2% intercept and the erosional unconformity in question is the estimate of missing section, assuming no changes in the reflectance slope in the eroded strata. A detailed discussion of assumptions in the Dow (1977) method versus other overburden estimate methods can be found in Malinconico (2003). Error in missing strata estimates was calculated using the parametric bootstrap technique of Efron and Tibshirani (1993).

Vitrinite-reflectance-evolution modeling was done using EASY%R_o (Sweeney and Burnham, 1990), a simplified first-order Arrhenius kinetic model of vitrinite reflectance evolution. Initial temperature estimates for vitrinite reflectance used the vitrinite geothermometer of Barker and Pawlewicz (1994) that is based on correlation of vitrinite reflectance and fluid inclusion homogenization temperatures (fig. C3). However, the vitrinite geothermometer does not take into account the effect of maximum temperature duration on vitrinite-reflectance evolution. The reflectance of vitrinite when held at constant temperature for at least a few million years will continue to increase a few to several tenths of percent, depending on maturation level, and asymptotically approach a maximum value for that temperature. When tested against reflectance evolution using a kinetic

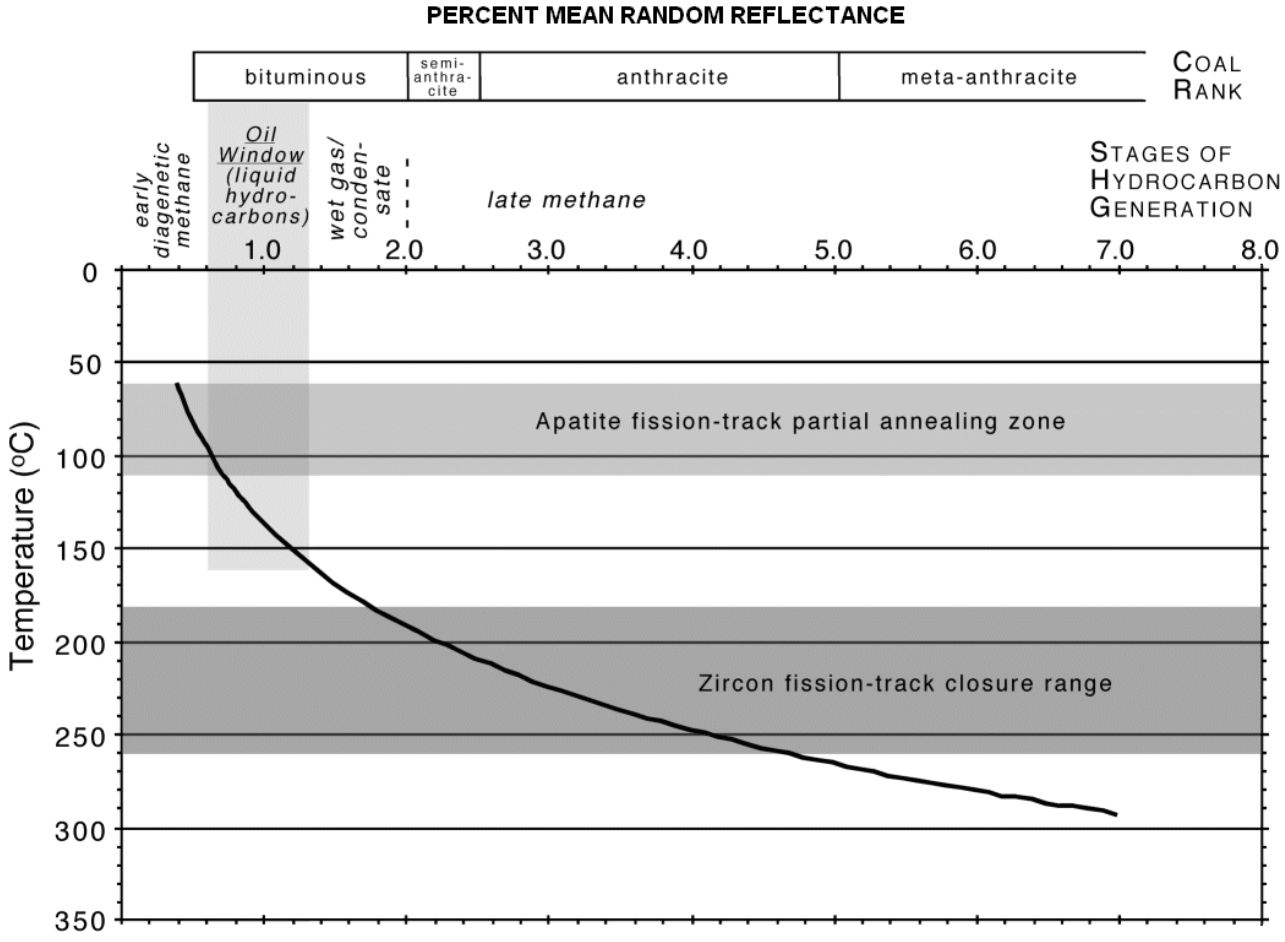

Figure C3. Chart of Barker and Pawlewicz (1994) vitrinite geothermometer showing peak temperature estimated from vitrinite reflectance for a burial or slow heating rate. Error in temperature estimates is ± 10° C (Barker, oral communication, 1994). Coal ranks, stages of hydrocarbon generation, and annealing zones for zircon and apatite fission-tracks are also shown.

vitrinite-reflectance modeling algorithm, such as EASY%R_o (Sweeney and Burnham, 1990), the given reflectances for the burial (slow) heating rate of the Barker and Pawlewicz (1994) vitrinite geothermometer would only be reached after 5-10 million years at the corresponding peak temperature. Therefore, at shorter heating durations, the Barker and Pawlewicz (1994) vitrinite geothermometer underestimates temperature, whereas for longer times it overestimates temperature. However, it is a reasonable initial estimate of temperature relative to vitrinite reflectance. The empirical error in the temperatures from the vitrinite reflectance geothermometer is $\pm$ 10˚C (Charles Barker, oral communication, 1994)

The Weston Canal copper and trace element data were obtained commercially at Acme Analytical Laboratories, Ltd. (ISO 9002 certified), Vancouver, British Columbia, by inductively coupled plasma (ICP) with an aqua regia leach.

Results of vitrinite-reflectance data

The mean random vitrinite-reflectance (%R_O) data for the six NBCP cores and one industry borehole (Cabot #1) are listed in table C2. Surface sample locations and results are shown in figure C2; downhole data plotted in figures C4 to C6. Only one vitrinite-bearing horizon was found in the Martinsville core: the Washington Valley Member of the Lower Jurassic Feltville Formation. Because the mean random vitrinite reflectance measured within this unit, 1.18% at 162.7 m, is shallow, it is marked only on the map of surface reflectance (fig. C2a). The shallowest values in all other cores, except Weston Canal, are also on the surface map (fig. C2a) in addition to the downhole reflectance profiles (figs. C4 to C6). The shallowest Weston Canal sample is from 546.8 m and is not considered representative of the surface maturation at that location. In this section, the reflectance data for the cores and surface samples are described, followed by cross-basin estimates of erosion, and thermal modeling results.

Nursery, Princeton, Titusville cores and Cabot borehole: Steady-state advective flow through a confined horizontal aquifer.

The Nursery, Princeton and Titusville coreholes near the central southeastern edge of the basin (fig. C2a), include the lower Passaic, Lockatong, and Stockton Formations and have planned stratigraphic overlap between them (Olsen and others, 1996a). The Cabot borehole penetrates these same formations but is close to the western border fault (fig. C2a). Significantly, part or all of the vitrinite reflectance profiles (figs. C4 and C5) have vertical slopes that imply a 0˚C/km geothermal gradient, interpreted to result from horizontal fluid flow that is vertically isothermal at any point along the aquifer.

In the Princeton core (fig. C4), the $\log_{10}$ of mean random vitrinite reflectance generally increases linearly downward through the lower Lockatong (0-290m). However, within the Stockton Formation, the reflectance is fairly constant at 2.4-2.5%, slightly lower at the top of the formation and the bottom of the core. The shape of the reflectance profile within the Stockton Formation in the Princeton core mimics heated, lateral fluid flow in a confined thick horizontal aquifer with an isothermal core (0˚ C/km gradient) and enclosing boundary layers (Ziagos and Blackwell, 1986). Heat transfer into impermeable layers above such an aquifer is by conduction only, and, at steady-state conditions, the temperature profile between the aquifer heat source and the ground surface is that of a constant geothermal gradient (fig. C7). The estimated temperature of the 2.4 %R_o isothermal core of the Stockton aquifer at the Princeton core location is 207 $\pm$ 10˚C (Barker and Pawlewicz, 1994). The estimated geothermal gradient in the Lockatong of the Princeton core is 32.9˚C/km, also based on conversion of reflectance to temperature using the Barker and Pawlewicz (1994) vitrinite geothermometer; this gradient is assumed to be due to conduction from the aquifer heat source below rather than representative of the basin burial geothermal gradient. The Barker and Pawlewicz (1994) burial-heating-rate vitrinite geothermometer can appropriately be used as an estimate of temperature here since the reflectance pattern indicates long-term steady-state flow rather than short-term transient flow.

In the Nursery core, the vertical isoreflectance (2.4%) section is of the same magnitude as in the Princeton core and includes the drilled part of the Stockton and the Lockatong Formation below the Princeton Member. The Princeton and older Scudders Falls and Wilburtha Members of the Lockatong Formation have a higher sandstone content than younger Lockatong members, reflecting the sedimentological transition from the underlying predominantly fluvial Stockton to the lacustrine Lockatong (Olsen and others, 1996a), and apparently can act as effective aquifers, like the Stockton. Although the reflectance data from the lower Lockatong of the Princeton core does not indicate similar fluid transfer, the high reflectance spike (2.6%) within the Scudders Falls Member at 211.8 m may indicate some limited lateral advective heat flow through correlative strata. Above the Princeton Member in the Nursery core, the reflectance profile is log linear with depth (R^2= 0.73), and the estimated geothermal gradient, using the Barker and Pawlewicz (1994) vitrinite geothermometer, is 36.8˚C/km.

Table C2. Subsurface vitrinite-reflectance data, Newark basin

Depth (feet)	Depth (meters)	%Ro[1]	Standard deviation
NURSERY CORE			
383.8	117.0	1.94	0.18
503.0	153.3	2.28	0.24
561.2	171.1	1.98	0.15
794.7	242.2	2.06	0.12
1005.7	306.5	2.05	0.17
1142.1	348.1	2.21	0.20
1410.9	430.0	2.10	0.23
1540.4	469.5	2.20	0.14
1698.9	517.8	2.51	0.17
1783.8	543.7	2.41	0.17
1932.4	589.0	2.56	0.11
2190.6	667.7	2.48	0.18
2356.1	718.1	2.69	0.24
2585.0	787.9	2.61	0.16
2722.4	829.8	2.37	0.36
2805.5	855.1	2.71	0.32
2897.0	883.0	2.67	0.23
3073.8	936.9	2.42	0.28
3176.5	968.2	2.37	0.42
TITUSVILLE CORE			
75.0	22.9	2.42	0.16
225.1	68.6	2.25	0.22
340.7	103.8	2.81	0.21
670.3	204.3	2.47	0.13
1009.0	307.5	2.52	0.17
2011.0	613.0	2.53	0.20
2372.7	723.2	2.39	0.23
2727.0	831.2	2.39	0.17
WESTON CANAL CORE			
1794.0	546.8	1.61	0.11
2030.0	618.7	2.66	*
2034.0	620.0	1.77	0.14
2035.3	620.4	1.99	1.50
2474.0	754.1	1.74	0.08
2596.7	791.5	1.42	0.07

Depth (feet)	Depth (meters)	%Ro[1]	Standard deviation
PRINCETON CORE			
80.2	24.4	1.93	0.14
310.0	94.5	2.01	0.11
384.8	117.3	2.17	0.11
578.4	176.3	1.99	0.10
634.9	193.5	2.13	0.26
694.9	211.8	2.60	0.17
728.0	221.9	1.90	0.19
834.0	254.2	2.20	0.17
969.6	295.5	2.11	0.22
970.0	295.7	2.30	0.29
1751.7	533.9	2.52	0.13
1751.9	534.0	2.32	0.26
2941.9	896.7	2.40	0.25
2942.8	897.0	2.53	0.18
3340.6	1018.2	2.42	0.37
3420.5	1042.6	2.28	0.41
RUTGERS CORE			
262.9	80.1	1.80	0.12
375.8	114.5	1.73	0.07
599.8	182.8	1.79	0.09
601.2	183.2	1.64	0.12
2011.0	613.0	2.22	0.24
2013.8	613.8	2.21	0.32
2230.3	679.8	2.58	0.18
2247.0	684.9	2.70	0.22
2788.8	850.0	2.46	0.24
2791.0	850.7	2.20	0.30
2791.2	850.8	2.38	0.19

Depth (feet)	Depth (meters)	%Ro[1]	Standard deviation
SOMERSET CORE			
255.8	78.0	1.63	0.10
481.0	146.6	1.72	0.13
730.4	222.6	1.56	0.09
874.7	266.6	1.79	0.11
1317.9	401.7	1.48	0.09
1720.0	524.3	1.74	0.09
2210.8	673.9	1.99	0.09
2414.7	736.0	2.48	0.15
2546.3	776.1	2.32	0.12
2596.1	791.3	2.32	0.14
2637.6	803.9	2.14	0.08
2739.8	835.1	1.96	0.21
2791.0	850.7	2.46	0.19
2792.5	851.2	2.69	0.24
CABOT #1 BOREHOLE**			
700	213.4	2.88	0.52
1610	490.7	2.84	0.23
2270	691.9	3.17	0.22
3060	932.7	2.81	0.23
3660	1115.6	2.83	0.17
4320	1316.7	3.03	0.28
4920	1499.6	3.03	0.16
5580	1700.8	3.41	0.18
6150	1874.5	3.54	0.30
6810	2075.7	3.05	0.31
8240	2511.5	3.38	0.28
9250	2819.4	3.34	0.36
10090	3075.4	3.38	0.31
10330	3148.6	3.41	0.29

[1]% mean random vitrinite reflectance.
*Vitrinite-reflectance equivalent (Landis and Castaño,1995) of solid bitumen reflectance 2.43%.
** With permission of North Central Oil, Inc.

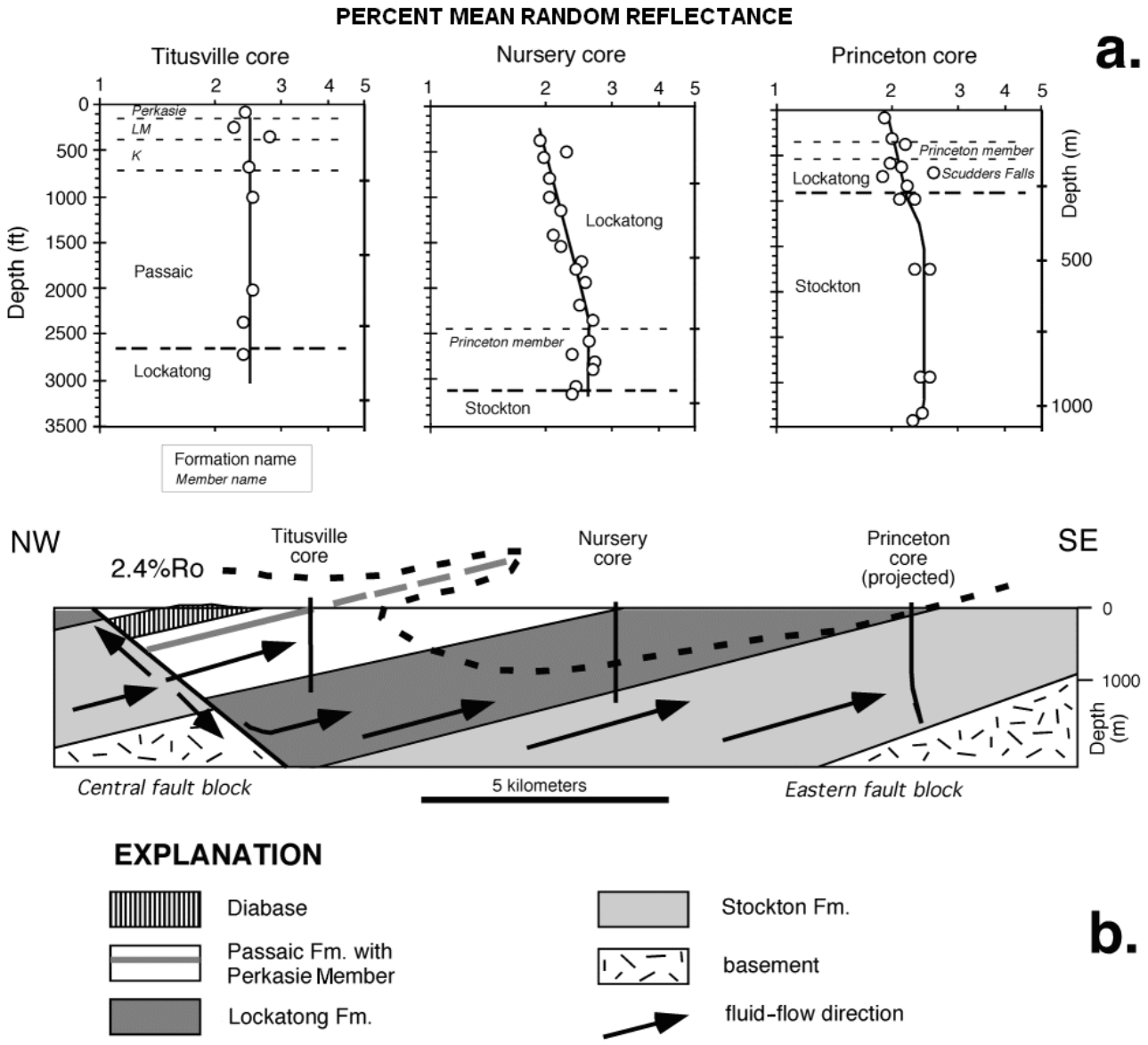

Figure C4. a) Downhole mean random vitrinite-reflectance data for the Titusville, Nursery and Princeton NBCP cores (data listed in table C2). Lines through data in Nursery core (Lockatong Formation above the Princeton Member) and Princeton core (Lockatong Formation) are the calculated regression lines; b) Cross section through Titusville, Nursery, and projected Princeton cores showing the 2.4% R_o isoreflectance contour and pattern of subsurface advective fluid flow based on vitrinite-reflectance data. Cross section based on Olsen and others (1996a).

In the Titusville core, even though the mudstone-dominated lithology of the Passaic and Lockatong Formations is similar to that of the Upper Lockatong in the Nursery core (Olsen and others, 1996a), the reflectance profile throughout the cored interval is vertical (actual calculated regression slope = 2˚C/km), like that within the Stockton or sandy Lower Lockatong in the Nursery and Princeton cores and is of similar magnitude (2.4% R_o). Isoreflectance or isothermal temperature profiles may result from horizontal/lateral fluid flow, as mentioned earlier, or vertical flow (Freeze and Cherry, 1979; Ziagos and Blackwell, 1986; Law and others, 1989). Flow at the Titusville core location is assumed to lateral because 1) the downhole reflectance patterns in the Princeton and Nursery cores suggest lateral advective flow in the gently-dipping Stockton Formation and coarse, lower part of the overlying Lockatong Formation across several kilometers, and 2) the hydraulic conductivity of shale is greatest parallel to bedding strike (Freeze and Cherry, 1979). A cross section of the basin through the Titusville, Nursery, and Princeton (projected) core sites (fig. C4b) shows the 2.4% iso-reflectance contour.

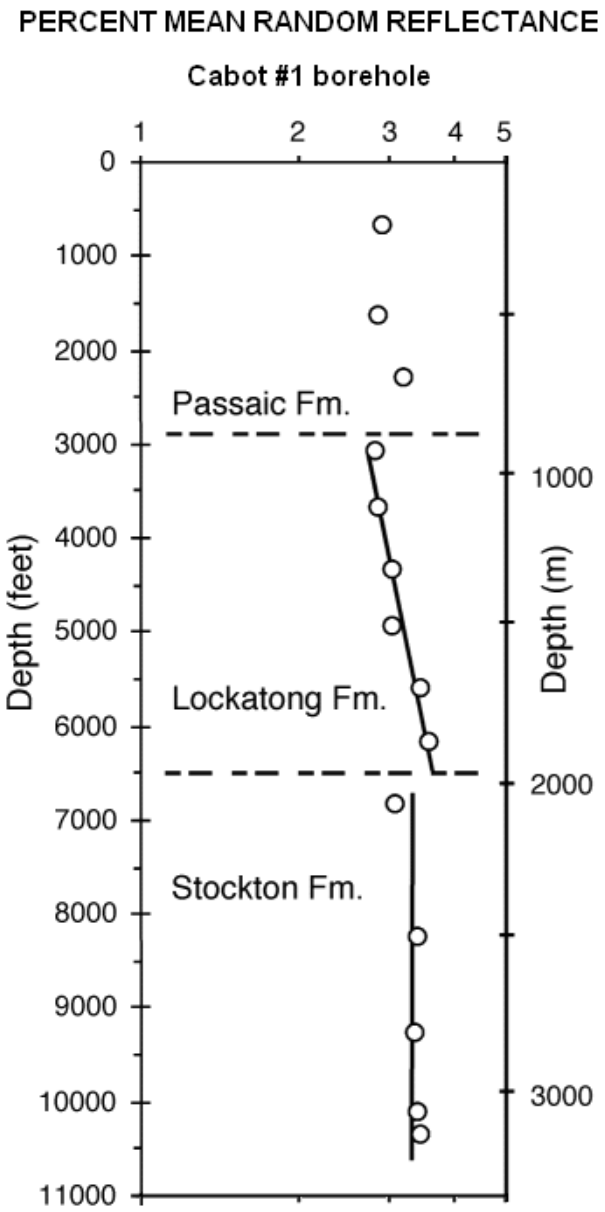

Figure C5. Downhole mean random vitrinite-reflectance data from the Cabot #1 borehole (with permission of North Central Oil). Line through Lockatong Formation data is a calculated regression line. Data listed in table C2.

It suggests that heated fluids from the Stockton Formation in the Central Fault block (fig. C2b), flowed across and along the Hopewell fault, and laterally permeated the Passaic and Lockatong Formations directly opposite the Stockton of the Central Fault block for some distance through the Titusville core site. With increasing distance from the Hopewell fault, heated fluids slowed and cooled through most of the less permeable Passaic and Lockatong shale, but heat was still advected through the sandier more permeable lower Lockatong and Stockton Nursery core) and eventually, at the Princeton core location, through the coarser parts of the Stockton Formation.

A diabase sill crops out near, but stratigraphically above, the Titusville core site (fig. C4b). Contact metamorphism combined with burial heating and heat conduction from the Stockton aquifer would produce a concave, not a vertical reflectance or paleomaximum temperature profile (Malinconico, 2002), indicating that the hypothesis of lateral advective heat flow is reasonable.

The Cabot drill hole, near the western border fault, penetrates the Passaic Formation below the Perkasie Member, the Lockatong Formation, and a significant part of the Stockton Formation (fig. C5). The reflectance gradient in the Stockton Formation in the Cabot borehole, like that in the Princeton core, is vertical with no decrease at the bottom. The reflectance in the Stockton is 3.4% (table C2), an estimated paleomaximum temperature of 235 $\pm$ 10˚ C (Barker and Pawlewicz, 1994). The reflectance profile above the isothermal section from 915 to 1980 m has an estimated gradient of 21.1˚ C/km. Above 760 m, the reflectance profile is nearly vertical again. Thick diabase sills crop out adjacent to the drill hole, and contact metamorphic effects are apparent in nearby surface reflectance data (fig. C2a). In contrast to thermal models of the Titusville core, the reflectance gradient in the Lockatong and Passaic Formations of the Cabot borehole may be reproduced by a combination of burial heating, conduction from an underlying heated aquifer and contact metamorphism of an overlying sill (Malinconico, 2002). The section with the low 21˚C/km gradient is, therefore, a result of contact metamorphism.

The vertical reflectance profile in the Stockton of the Cabot borehole, combined with the data from the Nursery and Princeton cores, indicates that advective flow occurred in the Stockton Formation across the basin from the western border fault to the eastern hanging wall edge of the basin. The paleoflow direction is considered to be from northwest to southeast (current coordinates). Fluid flow is due to recharge of meteoric water, driven by the hydraulic head of the rift flank footwall topographic high, in coarse sediments adjacent to the border fault, similar to that found in other rift basins (Person and Garven, 1994). The meteoric water was heated at depth, at the basin/basement contact, and then flowed across the basin through the basal permeable Stockton Formation, ultimately discharging at the hanging-wall basin edge. At steady-state, the conductive geothermal gradient of post-Stockton formations increased over background because the temperature at the top of the Stockton was the same as at the bottom of the formation (fig. C7). Depending on the cooling rate of the heated Stockton flow along the shallowing hanging-wall basement-basin contact, the temperature of fluids in the Stockton aquifer towards the hanging wall edge of the basin may have been warmer

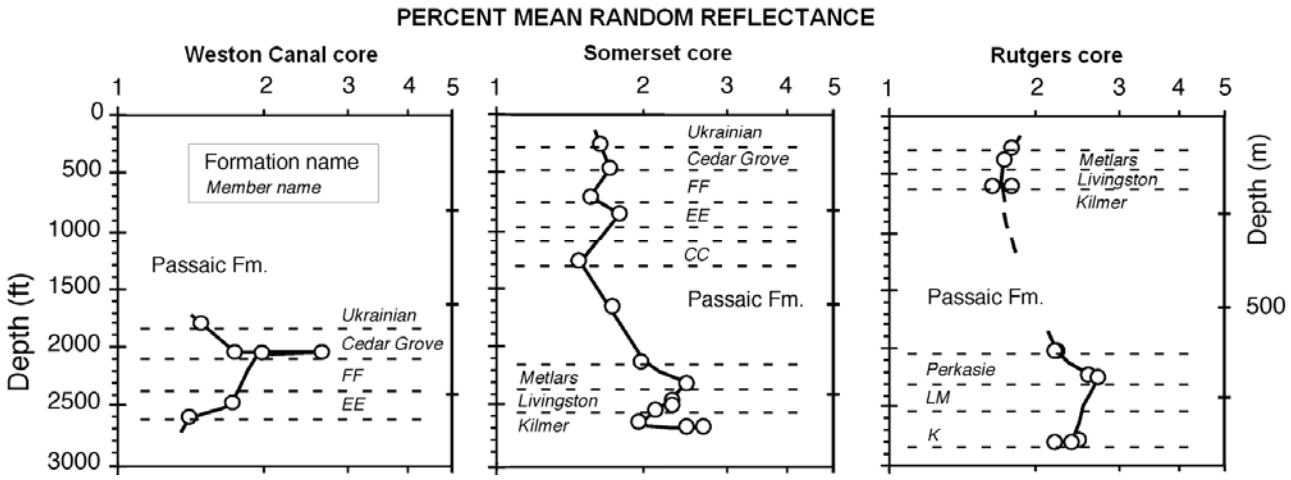

Figure C6. Downhole mean random vitrinite-reflectance data for the Weston Canal, Somerset and Rutgers NBCP cores (data listed in table C2).

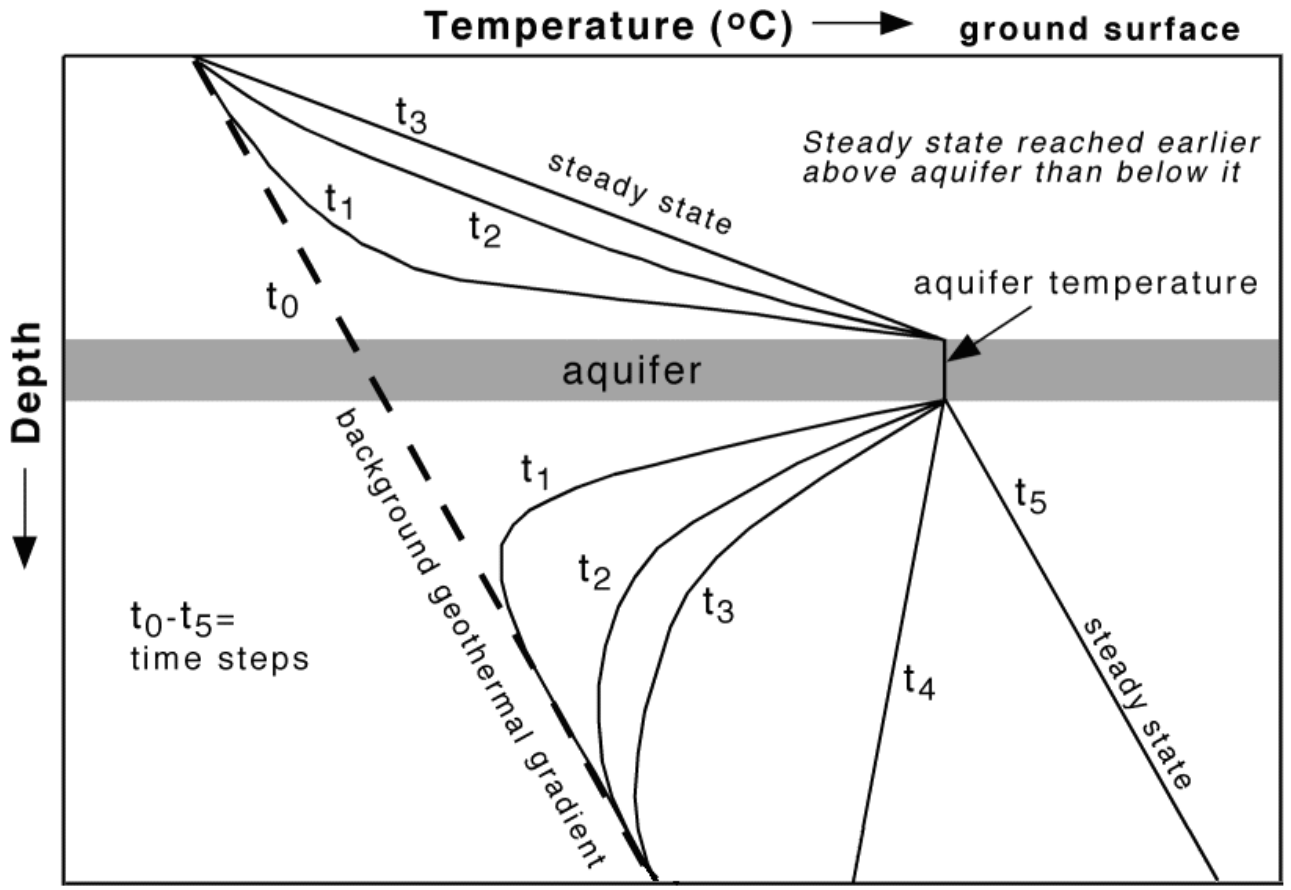

Figure C7. Theoretical temperature vs. depth profiles for times t1-t5 at a single location above and below a confined, horizontal heated aquifer, based on Ziagos and Blackwell (1986). Heat transfer into the half space below the aquifer and into the strata above the aquifer up to the ground surface is by conduction only. Steady-state heat transfer above the aquifer is achieved before steady state is reached in the half space below.

than pre-flow basement temperature. Importantly, the estimated paleomaximum temperature of 235 ± 10° C in the Stockton of the Cabot borehole should also define the limit on the maximum fluid temperature in the Newark basin topographically-driven groundwater system.

Weston Canal, Somerset, and Rutgers cores: transient advective heat flow and associated base-metal mineralization.

The Weston Canal, Somerset and Rutgers cores sample the upper two-thirds of the Passaic Formation, which is mostly red mudstone punctuated by gray-to-black, deep-lake sediments. The cores have irregular downhole reflectance profiles indicative of high temperature excursions (fig. C6). The nonlinear reflectance profiles in strata above the anomalies are typical of transient channelized fluid flow and indicate that, in contrast to conditions of advective flow through the Stockton Formation, long-term steady-state conductive heat flow from the thin Passaic aquifer layers was not achieved (fig. C7 and Ziagos and Blackwell, 1986; Lampe and Person, 2000; Lampe and others, 2001).

The lack of igneous intrusions and the association of sediment-hosted copper mineralization with many of the reflectance anomalies also point to an advective origin. Stratabound copper mineralization is currently understood to be epigenetic: formed when hot migrating metalliferous brines contact and are reduced by organic matter and/ or associated pyrite in sedimentary rocks (White, 1971; Püttmann and Merz, 1989; Mauk and Hieshima, 1992). The origin of known Newark basin stratabound base metal deposits, in particular, has also been ascribed to this process (Smoot and Robinson, 1988).

The Weston Canal core is the best example of the association of high reflectance anomalies and copper mineralization. Vitrinite-bearing strata (fig. C6) were not found above 525 m, but reflectance data below that depth show an increase in reflectance with depth (>1.6 %), apart from anomalously high values in the Cedar Grove Member, down to the bottom of the core where reflectance decreases to 1.4 %. The highest reflectance value in the Weston Canal core (2.66 %) is the vitrinite-reflectance equivalent (Landis and Castaño, 1995) of that measured on pore-filling bitumen. Weston Canal copper data are listed in table C3 and plotted versus depth in figure C8. Copper concentrations are generally highest in purple, white, and gray sandstone, siltstone and shale underlying more organic-rich, but less permeable, black, deep-lake sediment (fig. C8). This finding is similar to that of Smoot and Robinson (1988) who found that, in Culpeper basin stratabound lacustrine mudstone copper deposits, the highest metal abundances were in coarse (sandy root-rich mudstone) units directly below black shale.

The organic matter available for reduction of metal species and formation of sulfides in the more permeable lacustrine units (siltstone to sandstone) consisted of organic particulates (algal or land-plant debris) or liquid hydrocarbons. A study of organic matter distribution through 20,000-year, orbitally forced lake cycles of the Jurassic Towaco Formation (Malinconico, 2002) shows that hydrocarbon fluid inclusions and pore-filling bitumen are most common in coarser sediments directly below deep lake black shale, identifying these units as hydrocarbon migration pathways also. Where more permeable sediments are lacking at the bottom of the Weston Canal core in the lowermost Member EE, a thin gray/black shale enclosed by red shale, vitrinite reflectance ($\%R_O$ = 1.4) and copper concentration (table C3, figs. C6 and C8) are also low, indicating both inefficient heat and chemical transport by fluids.

In the Somerset and Rutgers cores, the presence of copper sulfides in some black shale samples suggests that flow of metalliferous brines lasted long enough to infiltrate or leak into these lithologies, either through micropermeability or by dissolution/ replacement of carbonate or other soluble minerals (Seward and Barnes, 1997). Economic concentrations in the classic stratabound copper deposits at White Pine, Michigan, and at the Kupferschiefer of Germany and Poland are in the lower sections of black shaly siltstone or black dolomitic shale, respectively (Maynard, 1983). Both of these rock types are more permeable or more soluble than pure shale, and the mineralizing brines entered shale from underlying sandstone (White, 1971; Püttmann and Merz, 1989). In the Newark basin, cyclic, deep lacustrine organic-rich black shale is carbonate-rich and has higher carbonate content than the transgressive and regressive lake sediment enclosing it (Olsen, 1986). The elevated copper concentrations in the Newark basin are again not considered to be syngenetic; although the reducing syndepositional conditions of organic-rich sediment can also concentrate metals, the typical black shale copper concentration is only 95 ppm (Maynard, 1983), at least an order of magnitude less than much of the data reported in table C3.

The copper minerals identified microscopically in the NBCP cores and surface samples include chalcopyrite ($CuFeS_2$), covellite (CuS), chalcocite (Cu_2S) and bornite (Cu_5FeS_4). In some samples, concentrically zoned copper sulfides with chalcopyrite cores rimmed by covellite, then chalcocite, indicate increasing Cu:S ratio during paragenesis. Pyrite was occasionally found as nuclei in chalcopyrite, indicating it was active in the reduction of metal brines or copper mineralization formed by replacement of pyrite (Mauk and Hieshima, 1992). Concentrations of other economic

Table C3. Weston Canal core trace-metal concentrations (parts per million)

Depth (feet)	Depth (meters)	Arsenic	Copper	Lead	Zinc	Silver	Cadmium	Molybdenum
1789.8	545.5	4	522	13	143	0.4	0.3	5
1790.3	545.7	35	1384	80	139	2.4	0.8	11
1793.1	546.5	41	69	142	300	1.4	6.4	20
1794.0	546.8	36	184	101	278	0.8	7.6	43
1795.0	547.1	20	1333	26	135	1.0	0.7	21
2030.0	618.7	1	83	7	195	<0.3	0.4	1
2031.8	619.3	1	1245	9	136	<0.3	0.5	1
2032.5	619.5	1	289	11	146	<0.3	0.2	1
2034.0	620.0	12	219	23	149	<0.3	0.1	1
2034.3	620.1	1	592	6	281	<0.3	0.4	1
2035.3	620.4	117	706	56	382	2.6	9.6	30
2035.3	620.4	14	234	40	161	<0.3	0.8	1
2036.6	620.8	20	4194	23	97	1.7	0.3	28
2085.3	635.6	2	27	9	76	<0.3	0.6	2
2457.7	749.1	1	37	13	131	<0.3	1.1	1
2458.0	749.2	6	5	10	95	<0.3	0.7	1
2474.0	754.1	1	1583	8	267	1.7	0.1	1
2475.2	754.4	1	35889	28	295	24.0	0.1	1
2596.7	791.5	4	425	10	154	0.4	0.2	6

Note: Data by Acme Analytical Laboratories, Ltd., Vancouver, British Columbia, using inductively coupled plasma (ICP) with an aqua regia leach.

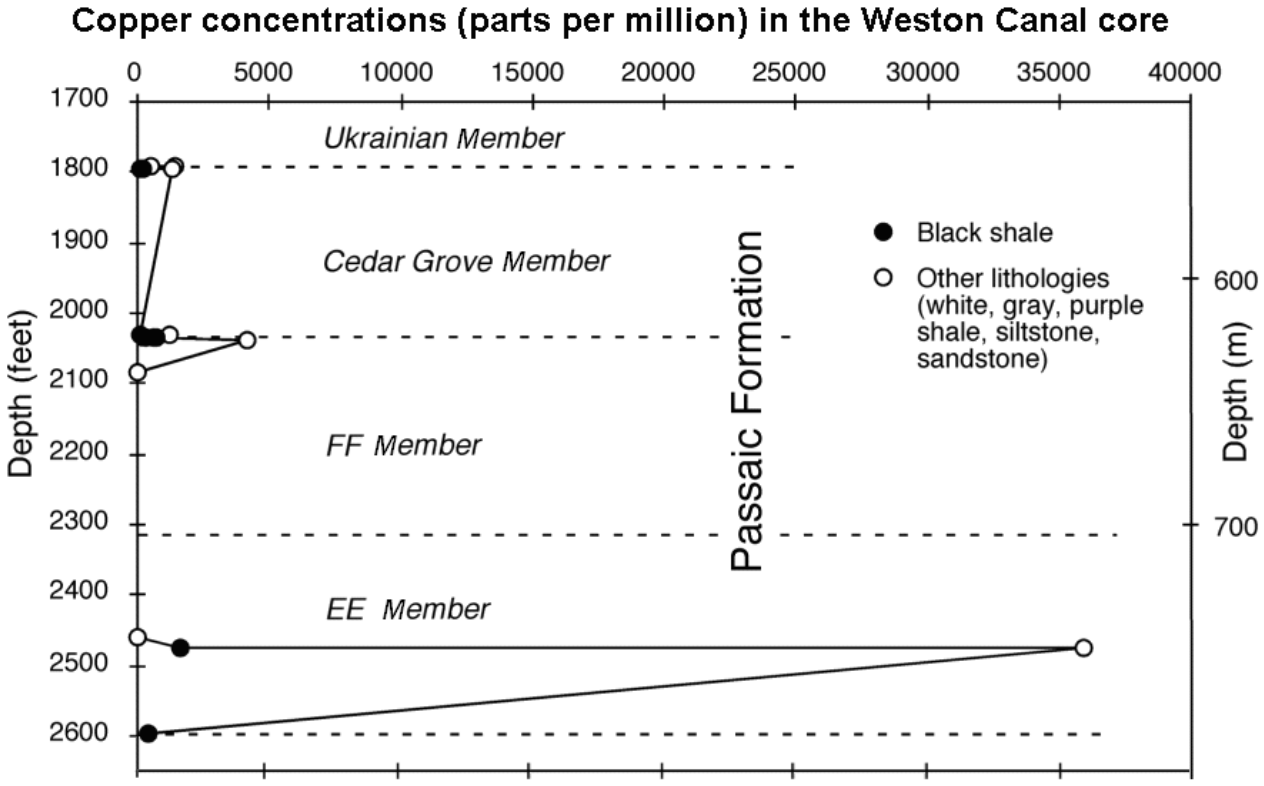

Figure C8. Graph of copper concentration versus core depth (table C3) and lithology in several members of the Passaic Formation in the Weston Canal core.

metals: lead, zinc, and silver, in the Weston Canal samples are also listed in table C3. Cross plots of pairs of metals from the drill core as a whole and from individual stratigraphic members indicate that silver is generally correlated with copper, and lead with zinc. However, other major metal concentrations are not consistent between or within stratigraphic members, as noted by Smoot and Robinson (1988) in lacustrine mudstones of the Culpeper basin.

Arsenic, a toxic element of environmental and medical concern, is associated with the base metal mineralization (table C3). Figure C9 shows the downhole concentrations of arsenic, copper and lead. Although arsenic appears to generally increase with both metals, the cross plot of figure C10 indicates a poor correlation of arsenic with zinc (R^2 = 0.32) and copper (R^2 = 0.02), but a strong, linear correlation with lead (R^2 = 0.85, excluding the highest arsenic value).

High radiogenic element concentration in black shale is not a cause of elevated reflectance values in these cores. The uppermost deep lake black shale in the Perkasie Member, present in the Rutgers and Titusville cores, is moderately radioactive in outcrop except at one site adjacent to the border fault along the Delaware River (Olsen, 1988). Such internal heat sources could produce a vitrinite-reflectance anomaly. However, data from the Rutgers core show similar reflectance in both the uppermost Perkasie black shale (2.58% at 679.8 m (2230.3 ft)) and older black shale (2.70% at 684.9 m (2247.0 ft)) in the same member. In addition, reflectance values in the more radiogenic Nursery core Lockatong Formation (most $\geq$ 600 API units) are lower than in the less radiogenic Rutgers Perkasie (~ 300 API units; Goldberg and others, 1994). Therefore, the Perkasie reflectance anomaly is interpreted to be due to advective fluid flow.

It is noted that the data in this paper identify temperature anomalies in sampled vitrinite-bearing strata. El-Tabakh and others (1997) reported fluid inclusion homogenization temperatures ranging from 150-280˚C in recrystallized anhydrite in red shale, typically barren of organic matter, from the Somerset and Rutgers cores. This suggests that there were permeable pathways in strata deposited not only during precipitation maxima which produced deep lakes, but also during arid evaporite-forming conditions. Therefore, the downhole paleomaximum temperature profiles probably have more perturbations than the vitrinite-reflectance data alone indicate.

Sulfide mineralization, plus solid bitumen, are also found in veins in Newark basin cores and outcrop (Robinson and Woodruff, 1988; Parnell and Monson, 1995; Herman, 2005; and Simonson and others, 2010). These vein occurrences indicate important vertical or fracture fluid pathways, but the vitrinite-reflectance data from the Weston Canal, Somerset and Rutgers cores demonstrate that bed-parallel lateral fluid flow was also an instrumental component in early basin heat and chemical transfer.

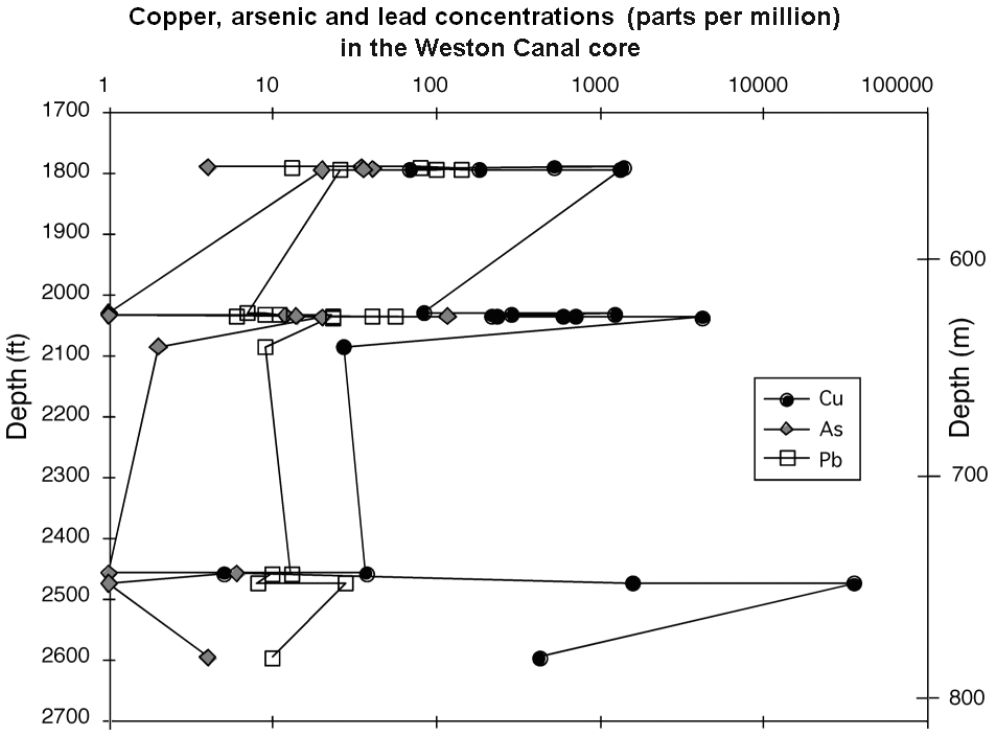

Figure C9. Copper, arsenic and lead concentrations in the Weston Canal core (table C3).

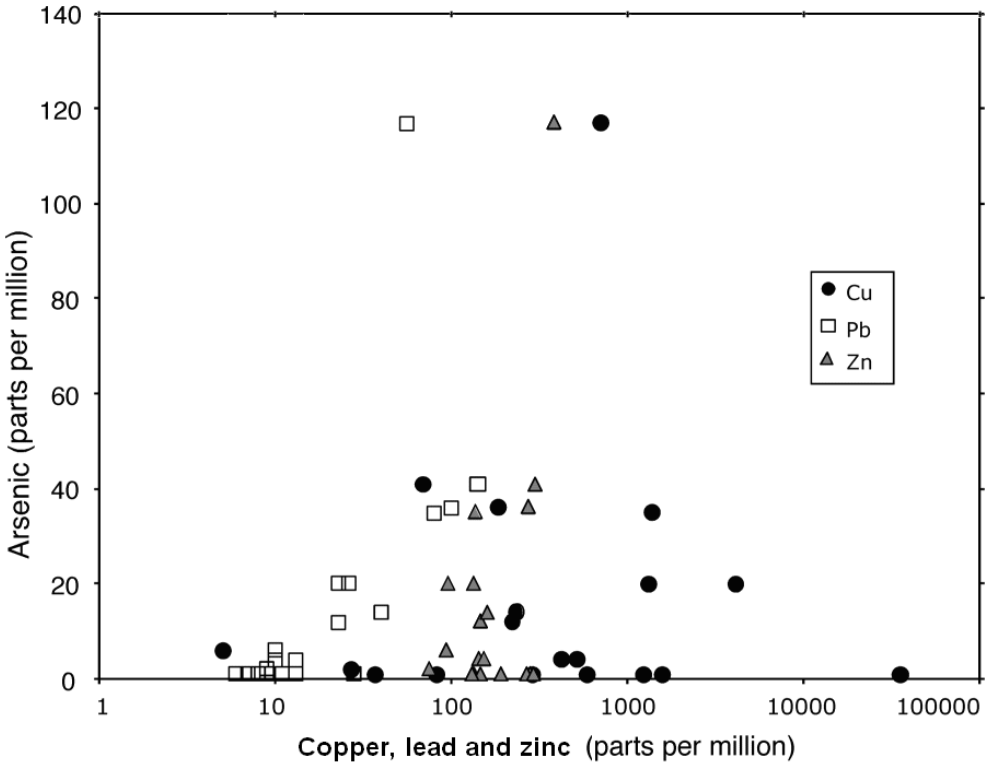

Figure C10. Crossplot of copper, lead and zinc concentrations with arsenic concentrations for the Weston Canal core (table C3).

Surface vitrinite-reflectance data.

Vitrinite reflectance data from Newark basin surface samples and the shallowest values from all cores, except Weston Canal, are shown in figure C2a. Surface sample locations are listed in Malinconico (2002). The outcrop reflectance data of this study expands the limited reflectance coverage of Pratt and others (1988) and Katz and others (1988b) with similar results obtained at common localities. The data are contoured in figure C2b, using the iso-reflectance contours 0.6% (birth line of oil), 1.3% (death line of oil), 2.0% and 3.0%. The boundaries of the oil window are convenient isograds of very low-grade metamorphism or late diagenesis. The general surface reflectance pattern shows an increase in reflectance with stratigraphic age. Within a formation, reflectance increases towards the center of the basin adjacent to the border fault, as expected in a half graben, and displays a similar pattern to the increase in Van Houten cycle thickness illustrated in figure 10 of Schlische (1992).

Elevated reflectance values from contact metamorphism are marked in italics in figure C2a where they occur in the western fault block (fig. C2b) near diabase sheets in Pennsylvania and along the Delaware River in the lower Passaic and Lockatong type sections in the vicinity of various dikes and a small exposed sill (south of $\%R_o$=4.26). Many samples collected within the hornfels contact aureoles of these and other basin intrusions, including the Palisades sill, are barren of vitrinite and other organic macerals, probably owing to metamorphic reactions. Contact metamorphism in the western fault block along the Delaware River may be due to cross-cutting dike connections, either subsurface or now eroded, between major diabase sheets or, in the case of the small exposed sill and the Lockatong Formation to the northeast, metamorphism around crack-tip edges of a buried or eroded sill.

The lowest surface reflectance values, not unexpectedly, are in the Jurassic Feltville, Towaco and Boonton Formations. Jurassic samples are from outcrops and from shallow cores of the U.S. Army Core of Engineers (ACE) Passaic River Flood project. The mean random reflectance of 0.55% in the Towaco Formation in the central Watchung syncline at Roseland, New Jersey (marked by an asterisk in fig. C2a) was corrected from a measured value 0.46%, because of vitrinite reflectance suppression. Pratt and others (1988) reported a similar value of 0.40% from the same location. Reflectances of 0.40-0.46 % at Roseland are lower than expected, based on Towaco data to the northeast. The Roseland sample is the only immature-to-low-maturity black shale used for reflectance measurement in this study; in such rocks with an abundance of hydrogen-rich organic matter, the suppression of vitrinite reflectance can be important (Lo, 1993). The corrected reflectance value of 0.55% was obtained using the guidelines of Lo (1993) and the Rock-Eval pyrolysis hydrogen index data of Pratt and others (1986) for Roseland dark shale.

From the abundant Jurassic reflectance data, the estimated paleogeothermal gradient in the northern

Watchung syncline was determined two ways: 1) data from four Jurassic ACE cores plus the Passaic Formation Exeter Township Member, directly underlying the Orange Mountain basalt in Clifton, New Jersey, plotted against the core-based composite Jurassic stratigraphic column in Olsen and others (1996b); and 2) a surface cross-basin section (fig. C11, marked on fig. C2a) including five Jurassic ACE cores, the Passaic Formation Exeter Township Member, and Lockatong Formation Ewing Creek Member plotted against surface distance between westernmost and easternmost points and using a northern basin dip of 10˚ (Schlische, 1992). Mean random reflectance was converted to temperature using the vitrinite geothermometer of Barker and Pawlewicz (1994). In the first case, linear regression gives an estimated paleomaximum gradient of 31.7˚ C/km; in the latter instance, the gradient is 33.6˚ C/km, both similar to that in the Lockatong of the Princeton core (32.9˚ C/km).

In the Triassic Passaic Formation, reflectance data from the central fault block (fig. C2a) show it is mature (within the oil window) to barely over mature (1.2-1.5% R_O) above the death line of oil (fig. C3). The data do show a general increase with stratigraphic age, but there is scatter that may be due to transient advective fluid flow within some members, like reflectance trends in the Somerset, Rutgers and Weston Canal cores; comparable scatter is seen in Passaic surface-sample data from the eastern fault block. Although reflectances lower than expected in surface samples could be attributed to weathering, optical and physical features typical of vitrinite weathering were not seen. Reflectance suppression is not an issue in this reflectance range (Lo, 1993).

Notably, the thermal anomaly found in the Passaic Formation Perkasie Member in the Rutgers core also occurs in the surface data. A reflectance of 2.37% was measured in an outcrop sample south of the Rutgers core location. Iso-reflectance contours (fig. C2b) suggest that this advective thermal anomaly may originate at the Hopewell fault, and is a more channelized or focused extension of the advective signature in the Titusville core (fig. C6).

Estimates of eroded synrift strata from borehole and surface vitrinite-reflectance data

Estimates of eroded synrift overburden in the Newark basin were calculated on the assumption that the reflectance-vs.-depth gradient in the upper Nursery core (< 720 m depth), the longest interval in any NBCP core that has a log linear increase in reflectance with depth, is valid for the whole basin. Similarity of calculated geothermal gradients from the upper Princeton core and the Jurassic of the northern Watchung syncline to that of the Nursery core indicate that this is a reasonable assumption. The amount of eroded overburden at the Nursery core site was calculated using the method of Dow (1977), which

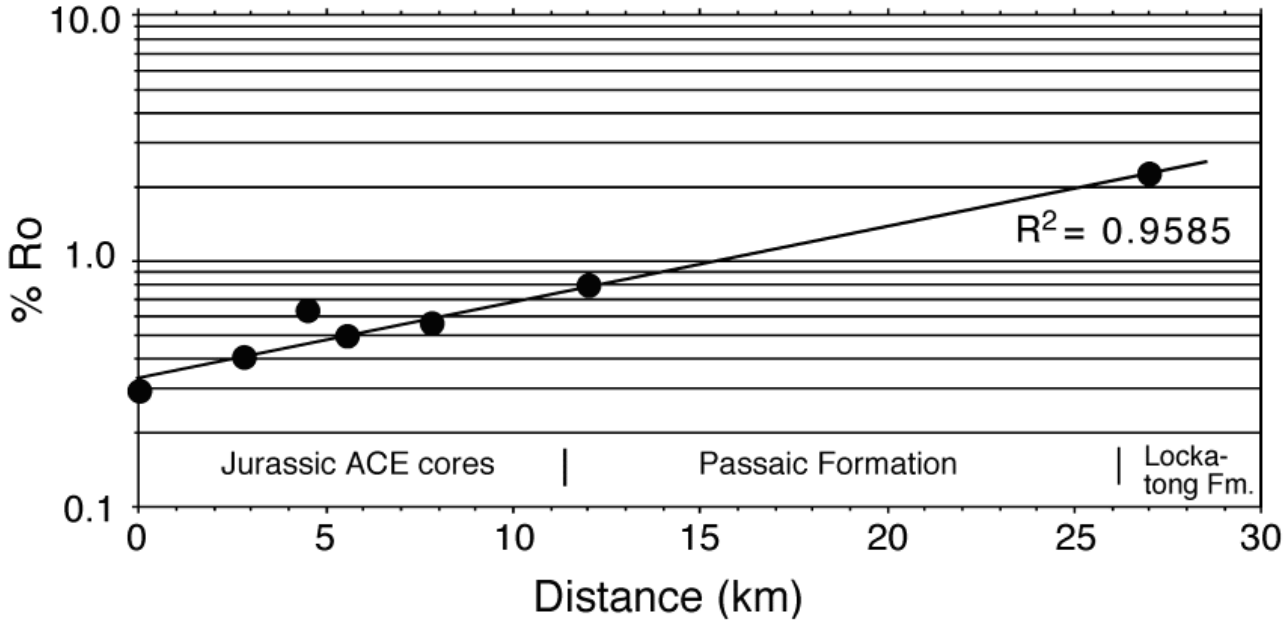

Figure C11. Graph of distance versus vitrinite reflectance for a surface transect, marked in figure C2a, from the Watchung syncline southeast to a sample location in the Lockatong Formation (fig. 2C, 2.26 value) demonstrating a log-linear reflectance gradient with distance and, therefore, a linear geothermal gradient in post-Stockton formations in the northern part of the northern Newark basin.

extrapolates the linear regression of the $\log_{10}$ of reflectance versus depth back to a pre- to early burial reflectance of 0.2% (fig. C12). The geothermal gradient in the missing section is assumed to be the same as that in the extant section. A complete discussion of this method compared to others used for estimating eroded section can be found in Malinconico (2003). The estimated eroded synrift section at the Nursery core, using log linear data from strata above the Princeton Member, is 4914 m. The error in this estimate is 1713 m, calculated using the parametric bootstrap method of Efron and Tibshirani (1993). Figure C12 also shows another example of estimating the eroded synrift strata over the Exeter Township Member (Jacksonwald syncline, southwestern Newark basin) where the measured reflectance is 1.0%.

Resulting contours of estimated eroded synrift strata are found in figure C13. The reflectance-depth gradient of the Nursery core was used to calculate missing section for all surface reflectance data points considered to be unaffected by contact metamorphism or transient advective fluid flow. Estimates range from less than one kilometer at a small outcrop area of the Jurassic Boonton Formation in the northern Watchung syncline to more than 6 km in the lower Lockatong and Stockton Formations along the Delaware River. The general range of 1-2 km of missing strata overlying the extant Boonton (fig. C13), the youngest synrift formation, is in good agreement with the estimates of Pratt and others (1988) and Katz and others (1988b). The erosion estimates, like the general reflectance pattern, increase with formation age and increase within a single formation toward the border fault and the center of the basin.

Summary of vitrinite-reflectance results

The pattern of vitrinite-reflectance data from borehole and surface samples, described above, indicates that the primarily fluvial Stockton Formation functioned as a major aquifer through which heated fluids migrated long enough for steady state to be reached: that is, the strata between the Stockton and the ground surface were conductively heated to a constant linear geothermal gradient. Flow direction was from the border fault towards the hanging wall edge of the basin (modern

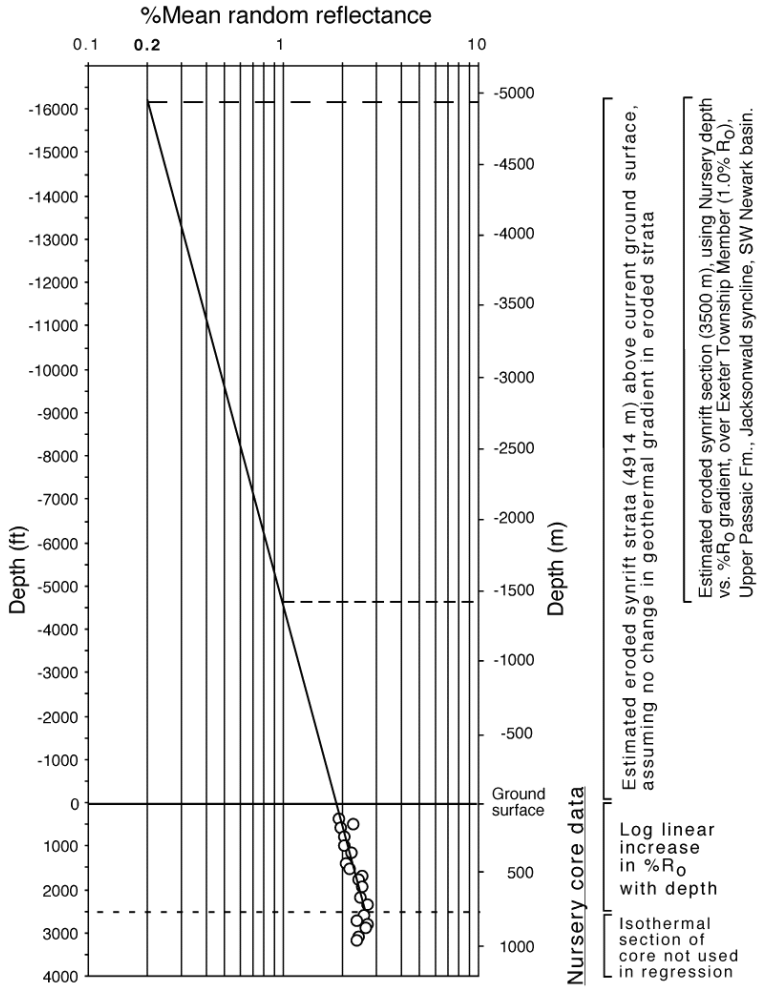

Figure C12. Determination of eroded synrift strata using the method of Dow (1977). The regression line for log(10) reflectance vs. depth is extrapolated back to 0.2% Ro, the reflectance of recently-deposited woody plant matter. The Nursery core reflectance data is used in this example. The reflectance data below 720 m (2360 ft) is not included in regression since the reflectance gradient there is vertical due to lateral confined advective heat flow. Also shown is an application of the Nursery reflectance-vs.-depth gradient for estimating eroded overburden for surface reflectance sample locations.

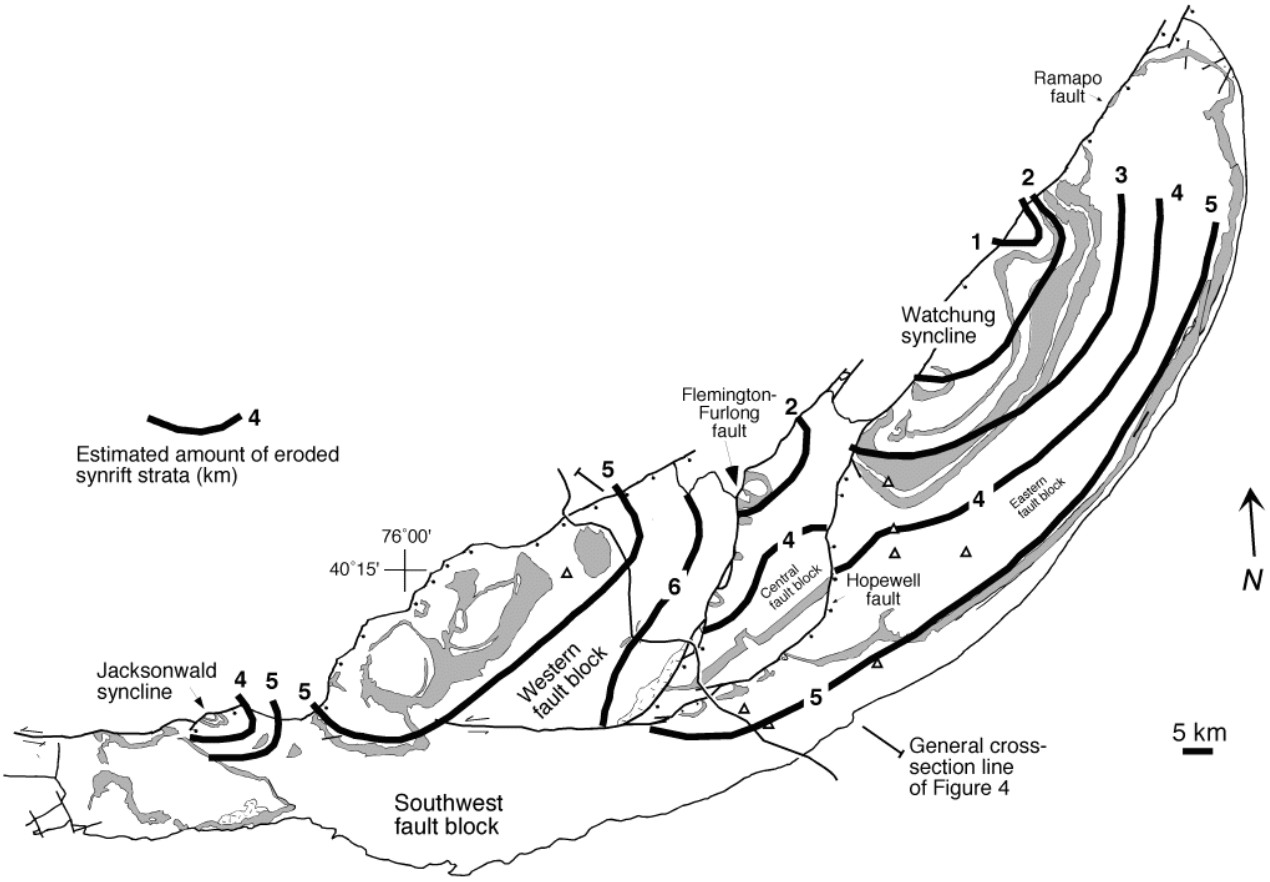

Figure C13. Generalized map of the Newark basin showing estimated thickness (km) of eroded Newark basin synrift strata based on surface reflectance values not affected by contact metamorphism and transient advective heat flow. Estimates calculated using Nursery core depth vs. $\log_{10}$ %R_o gradient (fig. C12). Igneous basalt and diabase shaded gray for reference. Locations of NBCP cores and Cabot well shown as open triangles.

direction northwest to southeast). The resulting estimated geothermal gradients in the Lockatong of the Nursery and Princeton cores, and the Jurassic of the northern Watchung syncline fall within a narrow range of 32-37˚C/km. Reflectance anomalies in the Passaic Formation of the Weston Canal, Somerset, and Rutgers cores identify non-steady-state or short-lived high-temperature advective fluid flow associated with several deep lacustrine sedimentary units. The map pattern of surface-sample reflectance data suggests that this transient advective flow, spatially associated with stratabound copper mineralization, was fed from permeable intrabasin faults that tapped the basal Stockton aquifer. Hydrothermal mineralization along the Furlong fault, Bucks Country, Pennsylvania, also confirms that basin faults were conduits, not seals (Ratcliffe and Burton, 1988).

Vitrinite-reflectance evolution and basin thermal history

The estimates of geothermal gradient or maximum temperature of various strata were initially based on the vitrinite geothermometer of Barker and Pawlewicz (1994). Kinetic vitrinite-reflectance modeling (Sweeney and Burnham, 1990) will test these temperature estimates by combining chemical rate-based vitrinite-reflectance evolution algorithms with plausible burial/heating/cooling histories. Specifically, the models will test various thermal scenarios to see if the required level of maturation can be reproduced, and if the timing of the initiation or duration of steady-state flow and transient advective events can be constrained. Reflectance evolution modeling of the steady-state groundwater system (burial heating plus conductive heat flow from the Stockton aquifer) will be done using Nursery core data from the Lockatong Formation, varying the time of initiation of the steady-state system and the duration of heating at maximum temperature. For transient advective events,

duration versus peak temperature will be modeled both in a thin aquifer (Cedar Grove Member, Weston Canal core) and in strata overlying a thin aquifer in the Passaic Formation (CC and Metlars Members, Somerset core).

Certain input parameters have to be assumed or calculated and will be discussed below. These include: 1) the pre-rift heat flow or geothermal gradient, 2) thermal conductivity, 3) time of end of synrift sedimentation or maximum burial, 4) the time it would take to conductively heat up to about 6 km of basin strata above a basal aquifer, 5) cooling ages, and 6) relative age range of transient flow.

Pre-advection geothermal gradient

Previous studies of Newark basin thermal history (Walters and Kotra, 1990; Huntoon and Furlong, 1992; El-Tabakh and others, 1997) have assumed a standard pre-rift gradient of 15-20˚C/km, based on average continental geotherms or current passive margin heat flow. The Newark basin, however, was formed relatively soon after the Alleghanian orogeny (end ca. 275-260 Ma) (Daniels and others, 1994; Stamatakos and others, 1996), and lies within the thrusted terrain between the folded foreland to the west and the metamorphic internides, which are offshore and under the coastal plain to the southeast. The high synrift geothermal gradient (50-55˚ C/km) of the Triassic Taylorsville basin, Virginia (Malinconico, 2002), was probably inherited from this underlying high grade Alleghanian metamorphic belt and processes of post-orogenic collapse along the same zone (Wintsch and others, 1992; Hames and others, 2000). Because metamorphic gradients decreased to the west of that belt (Vynhal and McSween, 1990), any relict orogenic heat flow under the Newark basin would be expected to be lower also.

The pre-rift or pre-advection (before initiation of basin-scale gravity-driven groundwater flow) geothermal gradient of the Newark basin is estimated using data from the Cabot borehole (fig. C5) that is adjacent to the western border fault and at the recharge end of the basin groundwater flow system. Recharge of meteoric water, gravity-driven by border-fault footwall topographic highs, initially cools or suppresses the heat flow in the vicinity of the fault. However, at depth, the recharged fluids eventually heat up to ambient temperature. The temperature at the Stockton/basement contact at the Cabot location, theoretically due to basement heat flow only, should be the maximum temperature to which meteoric water descending at the border fault would be heated before flowing updip across the basin through the Stockton due to buoyancy and hydraulic gradients. (The Stockton paleomaximum temperature (about 207˚C) in the Nursery and Princeton cores, closer to the eastern edge of the basin, may not be representative of the basement heat flow if the velocity of groundwater flow exceeded the rate at which the heated fluid could equilibrate with basement.)

At the Cabot site, the difference in temperature between the paleo-ground surface and the Stockton/basement contact divided by the total thickness of synrift sedimentation should approximate the basin geothermal gradient due solely to basement heat flow. The maximum temperature at the Stockton/basement contact at the Cabot site is estimated as 235˚C, using the vitrinite reflectance geothermometer of Barker and Pawlewicz (1994) to convert a reflectance of 3.4%. The vertical (isothermal) reflectance profile in the Stockton Formation of the Cabot borehole indicates that the Stockton aquifer is well-mixed, therefore, the vitrinite reflectance value at the basement/Stockton contact is assumed to be the same (3.4%) as it is at the upper Stockton/Lockatong contact. The paleo-surface temperature used is 21˚C/km, reasonable for the ice-cap-free late Triassic Earth (Olsen, 1997). The total estimated synrift sedimentary section thickness of 7.8 to 8.8 km equals: 1) the thickness of Stockton in borehole (1.1 km) plus 2) the estimated post-Stockton synrift strata (about 6.2 km using the Nursery core reflectance vs. depth gradient and the method of Dow, 1977) from the bottom of Lockatong Formation in the Cabot well, plus 3) estimated Stockton thickness below drill hole, based on cross sections constrained by seismic-reflection data (0.5 to 1.5 km, M.O. Withjack, written communication, 2001). Using these parameters, the calculated range of the pre-advection geothermal gradient is therefore about 24.3 to 27.5˚C/km.

In the thermal models of post-Stockton strata, this pre-advection geothermal gradient (25˚C/km), due to basement heat flow only, is assumed to be constant from the initiation of rifting until conductive heating by hydrothermal flow through the Stockton. A quickly decaying thermal pulse during early stages of rifting (McKenzie, 1978) would not be retained in downhole reflectance data after the first several million years of basin history, according to both Deming (1994b) and simple tests of reflectance maturation using the Sweeney and Burnham (1990) EASY%R_o program for a Newark Supergroup-type basin with a 20-to-30 million year old synrift history. Similarly, any early changes in heating rate due to compaction-related factors, relevant to maturation and degree of petroleum generation in young basins, would not be material for the Newark basin.

Thermal conductivity

Thermal conductivity is necessary to calculate heat flow values from geothermal gradient; heat flow (W/m/˚C) is a useful value for comparisons with other rift basins or tectonic regimes. Thermal conductivity

data on the NBCP cores by Williams and others (1991; C.F. Williams, written communication, 1999) shows a range of 1.44-2.12 W/m/°C for red to dark gray mudstones and siltstones. Gypsum-bearing siltstones, and a mudstone and sandstone from the Stockton Formation had thermal conductivities greater than 2.5 W/m/°C, but the bulk of the basin sediments neither average the 2.5 W/m/°C assumed in various basin thermal models or interpretations (Huntoon and Furlong, 1992; Kohn and others, 1993) nor show a contrast between red and gray shale. The notable carbonate content of Newark basin black shale (Olsen, 1986) would increase the bulk conductivity of the shale and possibly diminish any thermal conductivity contrast with other lithologies. Assuming a basin average thermal conductivity of 2.0 W/m/°C, the estimated pre-advective background geothermal gradient of 23-27.5°C/km is equivalent to heat flow of 46-55 mW/m^2.

Because there is no apparent thermal conductivity contrast between lacustrine basin lithologies, differences or variations in heating rate due to thermal conductivity will not be considered in the reflectance evolution modeling.

End of synrift sedimentation

The date of the end of rifting or synrift sedimentation in the Newark basin is not known. However, an estimate of age of maximum basin depth or maximum sediment burial is necessary for basin thermal modeling. Here, the termination of sedimentation is calculated using estimates of total synrift sediment over the Jurassic middle Towaco Formation (201.6 Ma; Olsen and others, 1996b) and a logarithmically decreasing rift-basin-sedimentation-rate equation (Contreras and others, 1997). This equation is consistent with a documented decrease in compacted sedimentation rate from the Towaco Formation into the overlying Boonton Formation (Schlische and Olsen, 1990). The exact geographical location used for this calculation is the Towaco surface vitrinite reflectance sample site ($\%R_O$ = 0.50) in the northern Watchung syncline (fig. C2b) where the calculated missing synrift overburden is 2490 m.

The resulting calculated end of synrift sedimentation is 194.3 Ma. With a bootstrap calculated error in the 2.49-km overburden estimate of 1.1 km, the termination age range becomes 198.2-189.4 Ma. When the $\pm$ 1 m.y. error in the radiometric age (201-202 Ma) of the Palisades sill (Sutter, 1988; Dunning and Hodych, 1990), and by inference the coeval Newark basin lava flows and the Triassic / Jurassic boundary (Olsen and others, 1996b) are taken into consideration, the estimated age range of the end of sedimentation becomes larger by 2 m.y.

Period of time to reach thermal steady state over a planar advective heat source

The time required for the entire stratigraphic or rock column overlying a heated aquifer to reach conductive steady state (linear geothermal gradient) can significantly affect the evolution of vitrinite reflectance and petroleum generation because it may materially lengthen or shorten the "effective heating time" (time spent within 15°C of maximum temperature) (Hood and others, 1975). The long-time Laplace transform approximate solution of Ziagos and Blackwell (1986) was used to determine the time to conductively heat 5.5 km of overburden over the Stockton aquifer. Although the referenced solution assumes a very thin aquifer, it can also be used for any thick aquifer that is well-mixed and vertically isothermal (Ziagos and Blackwell, 1986). The calculated time to reach steady state for 5.5 km of overburden above a heated lateral aquifer is 400,000-500,000 years. This heating time is a maximum limit, if heated flow through the Stockton began instantaneously at maximum burial or afterwards.

Cooling ages

Cooling ages to be used in the Newark basin thermal models consist of previously published data from zircon and apatite fission-track studies. These provide constraints on the "effective heating time" that strata remain near maximum temperature and the rate of cooling from maximum temperature, both of which influence the maturation of the rock and, therefore, the vitrinite reflectance.

The closure temperature under which fission tracks from the spontaneous fission of trace ^{238}U are retained in zircons is 220° $\pm$ 40°C, and the number of tracks is related to the time since cooling below the closure temperature (Naeser, 1979; Hurford and Green, 1983). The range of published zircon fission-track ages for the Newark basin and enclosing basement is 196-150 Ma (mean = 182 $\pm$ 10 Ma), although most ages are between 195-170 Ma (fig. C14) (Roden and Miller, 1991; Kohn and others, 1993; Steckler and others, 1993). The calculated end of Newark synrift sedimentation, 194.3 Ma, falls at the older end of the Jurassic zircon fission-track age range; the rift-drift transition for the central north Atlantic (about 185 Ma) is in the middle (fig. C14). The mean of the six intrabasin zircon fission-track ages only is 177 Ma. Five of these basin samples are from along the border fault or in the Stockton Formation, the remaining sample (185 Ma) is from the uppermost Passaic Formation in northern New Jersey (Steckler and others, 1993). The 176 Ma $^{40}Ar/^{39}Ar$ date on potassium feldspar (closure

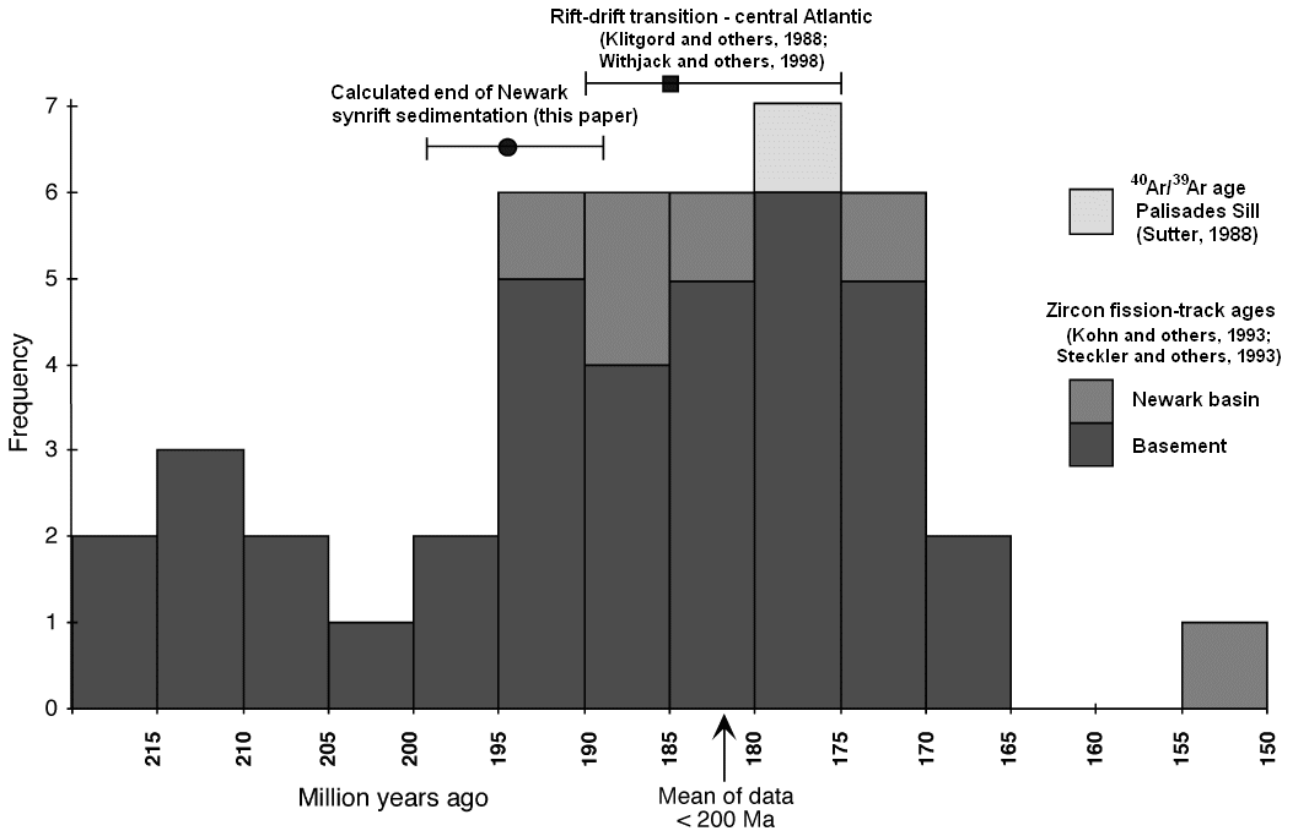

Figure C14. Histogram of published zircon fission-track ages for the Newark basin (Kohn and others, 1993; Steckler and others, 1993) plus Palisades sill granophyre $^{40}Ar/^{39}Ar$ cooling age of Sutter (1988) with estimated end of Newark basin synrift sedimentation (this paper) and rift-drift transition for eastern North America (Withjack and others, 1998).

temperature ca. 200˚C) from a granophyric segregation in the Palisades sill (fig. C2a, and Sutter, 1988) is consistent with the zircon fission-track data.

For the thermal model, the age of cooling below zircon fission-track annealing temperature is the regional average 182 Ma. The zircon fission-track closure temperature used is 180˚C, the minimum of the estimated zircon fission-track closure temperature range. This choice is based on geologically derived estimates of minimum closure temperature (Harrison and others, 1979; Naeser, 1979).

The apatite fission-track partial annealing zone is 60-120˚C (Arne and Zentilli, 1994). The range of Newark basin apatite fission-track ages found by Roden and Miller (1991) and Steckler and others (1993) is 170-126 Ma. Hoek (1997) and Hoek and others (1998) found a similar range except for very young ages (~72 Ma) in part of the Martinsville core interpreted as resulting from late fluid flow through a horizontal fracture system (currently 150-600m depth). The date of cooling below apatite fission-track closure temperature for modeling of the Nursery core Lockatong strata is 134 Ma, the cooling age for a nearby Stockton Formation surface sample (Steckler and others, 1993); for Passaic Formation units the basin average, 154 Ma (Steckler and others, 1993) is used. The apatite fission-track closure temperature used in modeling is 100˚ C (Roden and Miller, 1991).

In the models, surface temperature at deposition in the greenhouse Triassic/ Jurassic world is an assumed 21˚C. Modern day surface temperature is 15˚C with a current basin geothermal gradient of ca. 25˚C/km (Goldberg and others, 1994).

Constraints on the relative age, age limits, and temperature of transient advective flow events

The main purpose of the kinetic vitrinite-reflectance modeling of the transient advective heat flow events is to determine the range of possible temperatures and the duration of heating necessary to produce the measured maturity. The time frame in which these events occurred can first be narrowed from crosscutting relationships and previously published thermal data.

As stated previously, copper, lead, and zinc mineralization is associated with several of the high

vitrinite reflectance anomalies, marking pathways of transient advective fluid flow. Besides occurrences in Newark basin Triassic rocks, chalcopyrite ($CuFeS_2$) was observed microscopically in samples of the Early Jurassic (about 202 Ma) Towaco Formation. Smoot and Simonsen (2004) reported base metal sulfides late in the paragenetic sequence of void-filling basin cements (analcime/ albite-- potassium feldspar-- dolomite/calcite ± sulfides). The older potassium feldspar cements of that sequence have $^{40}Ar/^{39}Ar$ age dates of 196-195 Ma with an error of ± 1 m.y. (Kunk and others, 1995). Copper mineralization and, therefore, transient advective fluid flow is earliest Jurassic or younger.

Basin fluid-inclusion homogenization temperatures restrict the high temperature (>180˚C) transient flow events to being older than zircon fission ages (196-150 Ma; mean = 182 ± 10 Ma). Homogenization temperatures (T_h) from moderately saline aqueous fluid inclusions in sphalerite and quartz from southwestern Newark basin lead-zinc deposits in Pennsylvania at New Galena in Bucks County, Phoenixville in Chester County, and Audubon in Chester and Montgomery Counties generally range from 135-210˚C; calculated hydrostatic inclusion formation temperatures are 165-243˚C (Lawler, 1981). The high temperature inclusions are assumed to represent maximum ore fluid temperature. El-Tabakh and others (1997) reported T_h, ranging from 150-280˚C, from aqueous inclusions in anhydrite of the Somerset and Rutgers cores. That homogenization temperature distribution has two populations, one with a median of about 180˚C and a second of about 240˚C. Many of these fluid inclusion temperatures are within or slightly above the zircon fission-track annealing zone (220˚C ± 40˚) (Naeser, 1979; Hurford and Green, 1983), so represent fluid events that are older than zircon fission-track cooling ages. The minimum probable temperatures of 175-215˚C (Barker and Pawlewicz, 1994) of high-reflectance excursions of 1.6-2.7% R_O in the Weston Canal, Somerset and Rutgers cores are consistent with the fluid-inclusion data.

As noted from the surface-reflectance map pattern (fig. C2) and the Titusville/Nursery/Princeton core cross section (fig. C4), the steady-state and transient advective-heat-flow events are linked spatially, so are part of the same system. The similarity in range of maximum anomalous reflectances in both the Passaic Formation cores (Weston Canal, Somerset, Rutgers) and the surface samples (2.4-2.8%) with the reflectance data from the Stockton and Lower Lockatong in the Nursery and Princeton cores suggests that transient-advective-heat flow in the Passaic occurred during paleomaximum temperature in the Stockton aquifer. However, when basin and Stockton paleomaximum temperature was achieved and how long it lasted can only be limited to the time between the Early Jurassic end of synrift sedimentation / age of maximum burial (194.3 ± 5 Ma) and age of cooling through zircon fission-track closure temperature, basin average 182 Ma. Modeling the effects of transient advective fluid flow on vitrinite reflectance evolution sets limits on the duration of those events and, therefore, how long before cooling below minimum zircon fission-track closure temperature (about ~180˚C) a transient flow event could have occurred or begun.

Reflectance modeling of burial plus steady-state conductive heating of the Lockatong Formation resulting from heated fluid flow in the underlying Stockton aquifer- Nursery core

A primary goal of the Lockatong model is to ascertain whether the initiation of the steady-state advective groundwater flow through the Stockton Formation can be constrained to Triassic or earliest Jurassic time. Reflectance modeling was done on two Lockatong Formation members in the Nursery core: the Walls Island Member (current depth 117.0 m; age: 218.5 Ma), and the Nursery Member (718.1 m; age: 222 Ma). Both lie above the heated lateral aquifer in the lower Lockatong and Stockton Formation (fig. C4). Depositional ages of the members of the Lockatong and other units used in subsequent models are based on Kent and others (1995, table C4)). Burial rate is assumed to be constant. The reflectances to be reproduced by the kinetic reflectance evolution modeling (Walls Island $\%R_o$=1.98; Nursery Member $\%R_o$=2.60) are calculated from linear regression of the Nursery core reflectance data.

The model thermal histories are illustrated in standard time-temperature charts in figure C15; the specific parameters and numerical results are also listed in table C4. The graphs show the burial history of the Walls Island and Nursery Members through time. On the assumption that cooling of the post-Stockton basin sediments resulted from cooling of the Stockton aquifer during postrift exhumation, the end of maximum burial time is coincident with the initiation of cooling. The time spent at maximum burial was manipulated in the model so that the Walls Island Member crossed the 180˚C isotherm at 182 Ma (because the Nursery Member is deeper, it is at 200˚C at 182 Ma.). The resultant maximum burial duration is 6 m.y. (194.3-188.3 Ma). Inasmuch as Cretaceous coastal plain sediments onlap the hanging wall edge of the basin, basin exhumation is assumed to have been completed by 120 Ma, the approximate age of the oldest New Jersey passive margin coastal plain sediments (Steckler and others, 1993; Owens and others, 1998): the current basin surface and core depths at 120 Ma are assumed,

Table C4. Parameters and results of reflectance modeling for the Nursery core

Stratigraphic Member	Walls Island		Nursery	
Current depth (meters)……	117.0		718.1	
Calculated $\%R_O$……	1.98		2.60	
Member deposition age (Ma)……..	218.5		222.0	
End of rift sediment deposition (Ma)……..	194.3		194.3	
Time of maximum temperature (Ma)[1]……	194.3		194.3	
Temperature at 182 Ma[2] (^oC)……	180		200	
Temperature at 134 Ma[3] (^oC)……	100		120	
Average surface temperature – Triassic/Early Jurassic (^oC)…	21		21	
Modern surface temperature (^oC)……..	15		15	
Current estimated temperature at member depth (^oC)……..	18		27	
Eroded synrift strata (km)……	5.0		5.6	
	Model 1	**Model 2**	**Model 1**	**Model 2**
Time of geothermal gradient increase to ~35^{o}C/km (Ma)[4] ……	218.5	201.0	222.0	201.0
Resulting modeled maximum temperature (^oC)……..	187	187	209	209
Estimated geothermal gradient (^oC/km) between stratigraphic member and top of synrift section……..	34.1	34.1	33.5	33.5
Estimated geothermal gradient (^oC/km) between Walls Island and Nursery Members……..	N/A	N/A	36.6	36.6

[1] Maximum temperature held for 6 m.y. to 188.3 Ma
[2] Age of cooling below zircon fission-track closure temperature
[3] Age of cooling below apatite fission-track closure temperature
[4] Due to conduction from heated fluid flow through Stockton Fm.: Model 1-35^{o}C/km existed before member deposition; Model 2 – steady-state conductive conditions reached after 0.5 m.y. from initiation of heated Stockton flow at 201 Ma.

therefore, to be the same as they are now. Cretaceous-Tertiary reburial under the Atlantic Coastal Plain did not position the current surface or shallow sediments within the apatite fission-track partial annealing zone (60˚-120˚C) and re-exhumation with erosion of the coastal plain may have begun between 65-42 Ma (Miller and others, 1998).

The two models (fig. C15) differ in the initiation time of steady-state fluid flow through the Stockton aquifer with accompanying heat conduction and development of a 35˚C/km geothermal gradient in overlying strata. The EASY%R_o vitrinite-reflectance modeling program uses temperature and time as the material input data so the benchmarks for heating and cooling are ages of deposition, end of basin sedimentation, and cooling through zircon and apatite fission-track closure temperatures. The maximum temperature at maximum burial for each member was manipulated in the program until the required vitrinite-reflectance level was matched.

In the first model (fig. C15a), steady-state conduction began in early Lockatong time (post-Stockton) at or before deposition of the Nursery Member so that a constant geothermal gradient of 35˚C/km existed during burial. The isotherms mark various increments under this temperature regime. Modeled paleomaximum temperature for the Walls Island Member is 187˚C, for the Nursery Member, 209˚C. In figure C15b, initial burial occurred under a 25˚C/km geothermal gradient, which later increased over 500,000 years to 35˚C/km at 201 Ma; in this case, cross-basin groundwater flow began during the Latest Triassic/ Earliest Jurassic increase in extension. In this model also, the paleomaximum temperature for the Walls Island Member is 187˚C, for the Nursery Member, 209˚C.

Other maximum burial durations and times of initiation of cooling from maximum temperature were modeled, including immediate exhumation after reaching maximum burial. However, the maximum temperature did not change by more than 3˚C; the error in EASY%R_o temperatures is $\pm$5˚ (Sweeney, written communication, 2001). Numerous scenarios are reasonable for time and duration of maximum burial, particularly in light of the error in the calculated end of synrift sedimentation (194.3 $\pm$ 5 Ma) and of cooling through 180˚C (182 $\pm$ 10 Ma). Figure C15 shows two models based on average ages.

Because of the manipulation of maximum temperature to match the required vitrinite reflectance,

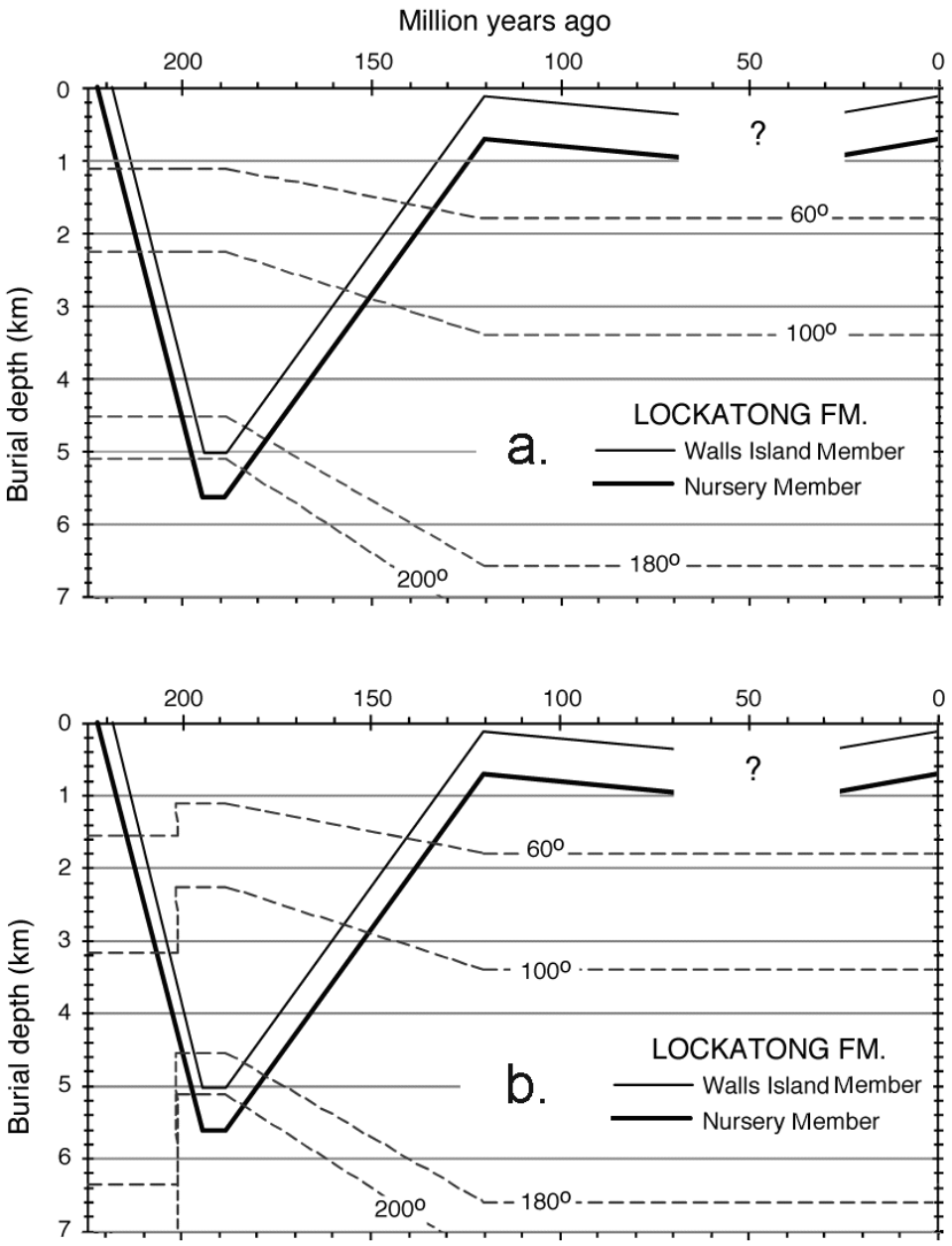

Figure C15. Time-temperature-depth plots for the Walls Island and Nursery Members of the Lockatong Formation. a) Burial under ~35°C/km geothermal gradient owing to heated groundwater flow through the underlying Stockton Formation aquifer that began at or before Nursery Member deposition; b) Burial under an initial 25°C/km geothermal gradient with increase to ~35°C/km owing to heated fluid flow through the Stockton beginning during the Earliest Jurassic increase in basin extension. Calculations indicate steady-state conduction from the Stockton aquifer was reached within 500,000 years. Duration of heating at maximum temperature and depth of burial determined by model is 6 m.y. Cooling of Lockatong members based on averages of published zircon and apatite fission-track age data (see text). Geothermal gradient assumed to be 25° C/km by 120 Ma. Model parameters listed in table C4.

the final calculated maximum geothermal gradient is not exactly 35˚C/km. The paleomaximum geothermal gradients (table C4) were calculated from the two modeled histories; the first for between each member and the top of the estimated total synrift section (from Walls Island = 33.5˚C/km; from Nursery Member = 34.1˚C/km) and the second, between the Walls Island and Nursery Members (36.6˚C/km). A large error in the former calculation is attributed to error in calculating eroded overburden. The gradient in the latter case, calculated between the members, importantly lacks the error in depth. The modeled estimates in paleogeothermal gradient are similar to the 36.8˚C/km calculated previously for the Nursery core using the vitrinite geothermometer of Barker and Pawlewicz (1994). The estimated heat flow, therefore, is 68-73 mW/m^2.

Figure C16 illustrates the change of vitrinite reflectance with time for the two Walls Island Member thermal histories of figure C15. It importantly shows that in models where burial and temperature history are the same, except for whether heated-fluid flow through the Stockton begins early in the basin history in the Triassic or during extensional rejuvenation ca. 201 Ma, the percent vitrinite reflectance (level of maturation) is the same by maximum burial, 194.3 Ma. Therefore, these modeling results, and the available data, cannot constrain the time of the initiation of heated-fluid flow through the Stockton and resultant conductive heating of the overlying Lockatong.

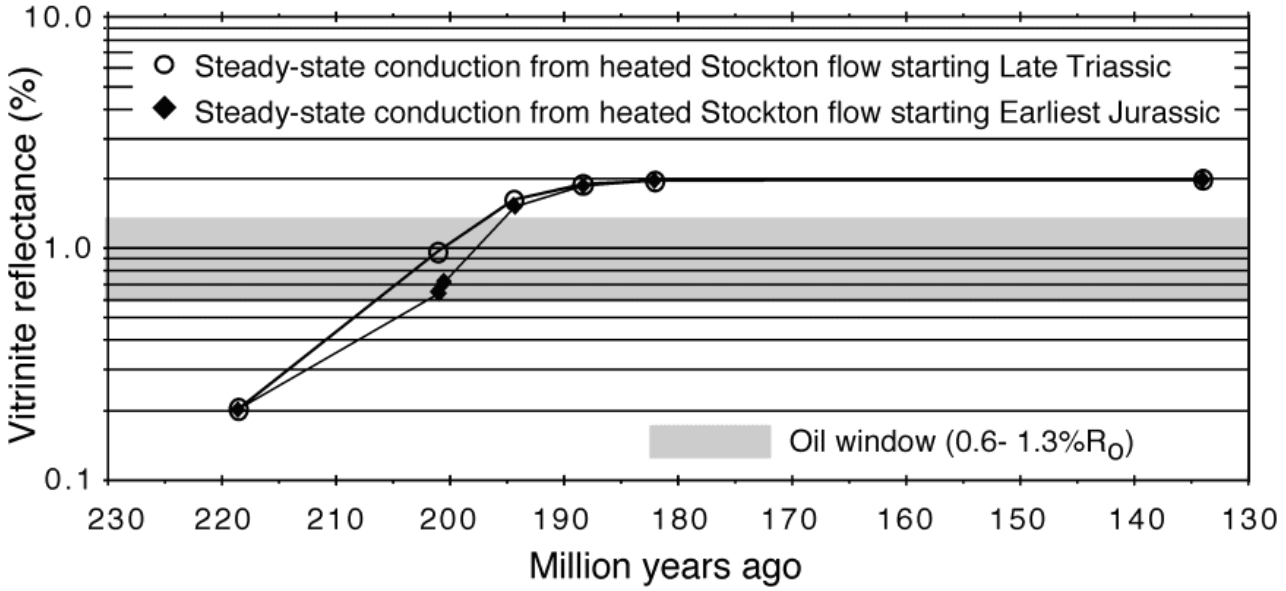

Figure C16. Vitrinite-reflectance evolution of Walls Island Member for the two thermal histories shown in figure C15 demonstrating same level of maturation by 194 Ma, whether Stockton Formation heated groundwater flow began in the Triassic or Early Jurassic. The oil window (0.6-1.3% reflectance) is shown for reference (fig. C3).

A third model was run in which a 25˚C/km geotherm persisted from deposition through and beyond maximum burial with increase to 35˚C/km (and the initiation of Stockton heated flow) occurring just before cooling through zircon fission-track closure temperature at 182 Ma. In this model, peak temperature was chosen as 235˚C/km, the maximum estimated at the bottom of the Cabot core, and the time at this temperature manipulated in EASY%R_o to match the required reflectances in the Walls Island and Nursery Members. The peak temperature of the third model would have to occur only 1.5 m.y. before cooling below zircon fission-track closure temperature to be consistent with the published cooling age data. However, because maximum footwall uplift to provide the topographic hydraulic head for sustained basin-scale fluid from the border fault in rift basins is typical of the synrift period (Person and Garven (1994), a ca. 182 Ma postrift initiation of heated fluid flow through the Stockton appears to be less viable than the two synrift scenarios.

Reflectance modeling of a transient advective fluid flow event - Weston Canal core, Passaic Formation, Cedar Grove Member

The Cedar Grove Member (547.0-620.5 m; age = 208 Ma) shows the highest anomalous vitrinite-reflectance values in the Weston Canal core (1.73, 1.99, 2.66%) (fig. C6; table C2) owing to transient or non-steady-state advective heat flow that also occurred in enclosing stratigraphic members (Ukrainian and CC Members). It is a useful example for testing the duration of a zircon fission-track resetting hydrothermal event because the estimated background reflectance suggests a pre-transient heat flow event temperature below 180˚C. The basin mean zircon fission-track age, therefore, defines the end of the high temperature advective events, assuming that the reset Early Jurassic fission-track ages apply to the basin as a whole.

In the Weston Canal core, the general reflectance signature of lateral advective fluid flow is 1.61-1.75%, stratigraphically spanning more than a couple of hundred meters. The abrupt anomalous excursions of 2.66% (VRE) and 1.99% in the Cedar Grove Member indicate more highly permeable pathways and very short duration of flow, based on predicted maximum temperature patterns surrounding heated lateral aquifers (fig. C7).

The reflectance of the Cedar Grove Member without transient advective overprint is estimated to be 1.31%, using the Nursery core reflectance-vs.-depth gradient through the measured 1.40% R_o of Weston Canal Member EE, assumed to have been unaffected by advective or conductive effects of transient fluids through other Weston Canal strata. From the Barker and Pawlewicz (1994) vitrinite geothermometer, 1.31% corresponds to a temperature of ca. 158˚C. The associated geothermal gradient, ~35˚C/km, would be due to steady-state conductive effects of heated groundwater flow through the Stockton Formation, and is assumed, in these models, to have existed since

before Upper Triassic Cedar Grove deposition, as in figure C15a.

For the overprinting transient hydrothermal event, six possible time-temperature histories that reproduce the measured Cedar Grove reflectance of 1.73% were constructed with EASY%R_o using maximum temperatures of 280˚, 265˚, 245˚, 200˚, 190˚ and 176˚C. In each instance, the peak advective-flow temperature was reached in 100 years and cooled back to ambient in 100 years. The duration of heating at maximum temperature was manipulated in the model program until the measured reflectance was reproduced. The results indicate that higher temperatures produce the same level of maturity or organic metamorphism over shorter heating intervals (fig. C17). For example, the total duration of the transient pulse that peaked at 245˚C was 2,900 years, and for 200˚C, about 560,000 years (fig. C17). The highest possible peak temperature for the longest possible duration, 194.3 Ma (end of sedimentation) to 182 Ma, is 176˚C, barely at the minimum zircon annealing temperature. Therefore, any advective thermal pulse >180˚C within the Passaic Formation was short-lived and would have occurred close in time to the reset zircon fission-track ages.

Reflectance modeling was also done for the VRE of 2.66% (solid bitumen reflectance of 2.43%), 1.3 m above the 1.73% sample modeled above. Two resulting heating rate scenarios for a peak temperature of 245˚C are illustrated in figure C18. The first represents an increase to 245˚C and immediate decrease to 180˚C with a cycle duration of 2 My. The second represents an instantaneous increase (in 100 years) to 245˚C which was maintained for 190,000 years before instantaneous decrease to 180˚C. In the former case, the effective heating time (Hood and others, 1975) within 15˚C of peak temperature is 340,000 years. This demonstrates that heating rate (~instantaneous for model 1 versus extended in model 2) can have a material effect on required duration at maximum temperature.

These duration results represent only a few possible thermal scenarios for the Cedar Grove Member in the Weston Canal core. Thermal anomalies in other members of the Passaic, however, may have different durations of flow at any given peak temperature. In any case, as stated previously, the advective thermal pulse creating the reflectance anomalies would have to occur shortly prior to cooling below zircon fission-track closure temperature to be consistent with the fission-track ages.

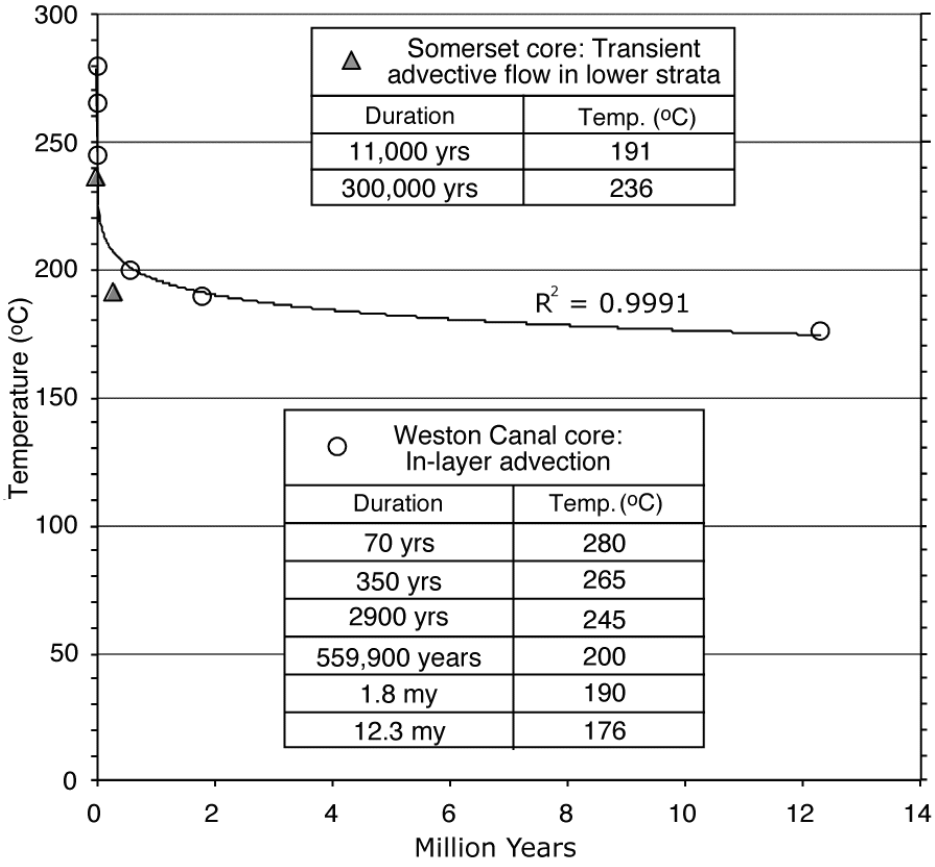

Figure C17. Graph and table showing possible temperatures and corresponding heating durations of transient advective fluid flow (circles) that reproduce the measured vitrinite reflectance in the Cedar Grove Member of the Passaic Formation from the Weston Canal core. Heating to and cooling from maximum temperature occurs over 100 years. Triangles show conductive heating duration for the CC Member of the Passaic Formation from the Somerset core, 334 m above the Metlars Member, a heated thin lateral aquifer, before background vitrinite reflectance was exceeded.

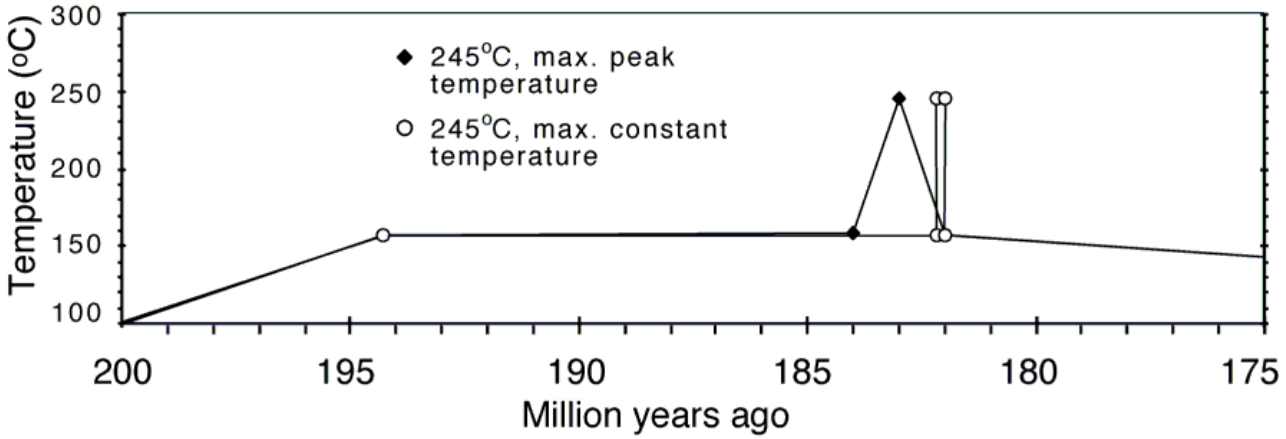

Figure C18. Two possible time-temperature histories for advective heat flow in the Passaic Formation, Cedar Grove Member, Weston Canal core (618.7 m), with different heating rates and maximum temperature (245°C) duration that both reproduce the solid bitumen vitrinite reflectance equivalent (VRE) of 2.66%. The models indicate that to be compatible with zircon fission-track cooling ages (mean age 182 Ma; closure temperature 220 ± 40°C) a transient advective pulse would have to occur just prior to 182 Ma.

Modeling vitrinite-reflectance evolution caused by conductive effects from a transient, advective heat-flow event in strata overlying a confined, transient-heated aquifer - Somerset core, Passaic Formation, CC and Metlars Members

The Metlars Member in the Somerset core also shows a reflectance anomaly (2.48%) attributed to transient advective heat flow. The CC Member (1.48% R_o; age = 209 Ma) lies about 334 m stratigraphically above the Metlars and is similar to the lowermost EE Member in the Weston Canal core because it is interpreted to be thermally unaffected by the transient fluid flow through surrounding lithologies. This means that steady-state conditions were not reached during the Metlars flow event and that limits on the duration of the event may be determined by calculating the maximum time before the reflectance in Member CC is exceeded. The change in temperature with time in Member CC due to conduction from heated lateral flow through the Metlars Member was calculated using the long-time Laplace transform approximate solution of Ziagos and Blackwell (1986). The resulting heating rate information was then used to model reflectance evolution (Sweeney and Burnham, 1990).

The estimated temperature for a reflectance of 1.48% in the CC Member under a 35˚C/km geothermal gradient (Nursery core gradient) and a surface temperature of 21˚C is 160˚C. This temperature and reflectance would be due to steady-state conduction of heat from the Stockton aquifer. The underlying Metlars Member temperature, before the transient advective event, would be ca. 171˚C. Two models were run, one for a transient aquifer temperature of 191˚C (Δ20˚) and a second for 236˚C (Δ65˚).

In the lower temperature model (Δ20˚), the temperature of the CC Member starts to increase after 1000 years of constant-temperature heated-fluid flow through the Metlars Member. However, because of the time dependence of vitrinite-reflectance evolution, particularly because the measured reflectance of any sample is due to its cumulative heating and cooling history, heated fluid flow at 191˚C through the Metlars could last 300,000 years before the vitrinite reflectance of the CC Member would increase over that from a thermal history lacking a transient heat flow event.

Cooling in the model was essentially instantaneous (10 years). In the higher temperature example (Δ65˚), initial temperature increase begins 726 years after beginning of heated fluid flow through the Metlars, but the event could last as much as 11,000 years before exceeding the measured reflectance of the CC Member. These calculations again demonstrate that an advective event with temperatures within the zircon fission-track annealing zone (220˚ ± 40˚C) is relatively short-lived and, therefore, would have to occur in a narrow time window preceding basin zircon fission-track age (mean 182 Ma). It is also important to note that fluid inclusion data (Lawler, 1981; El-Tabakh and others, 1997) include homogenization temperatures below zircon fission-track closure temperature so that transient events hotter than ambient but below 180˚C did occur.

In all the examples of transient heat flow events, a single overprinting event has been modeled. Realistically, there may be several episodes of shorter duration that exceeded the background conductive temperature of a unit. Zonation in sphalerite (Lawler,

1981), non-correlation of lead-zinc to copper-silver concentrations (Smoot and Robinson, 1988), and vein mineralogy zonation (Parnell and Monson, 1995) all indicate several fluid pulses, but only those with temperatures higher than or within the effective heating range of a previous paleomaximum temperature (± 15˚C) could materially effect vitrinite reflectance (Katz and others, 1988a).

Discussion

The Newark basin borehole and surface vitrinite-reflectance data plus modeling results indicate organic metamorphism in the basin due to steady-state conductive heating above a heated basal aquifer overprinted by transient lateral advective heat flow in some units. The direction of flow within the basal Stockton aquifer was from the western border fault to the east and southeast (current coordinates) across the hanging wall, presumably driven by footwall topography, as found in other rift basins. The only effect of the 201-202 Ma magmatic event preserved in the thermal indicators is contact metamorphism adjacent to diabase dikes and sills.

The synrift structural, hydrological and thermal evolution of the Newark basin cannot be considered as an isolated geologic event, but occurred within the context of the transition from the end of the Alleghanian orogeny to the opening of the modern Atlantic ocean. During the post-orogenic period, ca. 275-235 Ma (Wintsch and others, 1992), orogenic collapse, ductile exhumation, and possible mantle delamination were concentrated along the Alleghanian metamorphic internides, which run through eastern South Carolina and Virginia and offshore north into Rhode Island (fig. C1). The high heat flow (80-100 mW/m^2) before, during, and after rifting in the Late Triassic Taylorsville basin of Virginia (Malinconico, 2002), astride the Alleghanian metamorphic belt, is attributed to these processes. Brittle deformation following ductile exhumation, however, affected a wider region (Hutchinson and Klitgord, 1988) including the thrusted region of Grenville basement allochthons where the Newark basin is situated. This transition from ductile exhumation to a wide zone of brittle rifting to, ultimately, a narrow rift zone and seafloor spreading is predicted by numerical extension models (Hopper and Buck, 1996) of lithosphere with decreasing lithospheric thickness and heat flow. That the Newark basin lies off and west of the Alleghanian metamorphic belt is supported by the Rb-Sr biotite cooling age patterns of Kohn and others (1993): late-to-post-Alleghanian ages indicating cooling below biotite closure temperature of 300-320˚C since 300 Ma occur to the southeast of the basin near Wilmington and Baltimore whereas older ages enclose the basin.

Figure C19 illustrates the general thermal history of the Newark basin from this study. The calculated background pre-rift to early synrift Triassic geothermal gradient is ca. 25˚C/km (fig. C19a), consistent with the basin's location west and off the Alleghanian metamorphic axis. Intrabasin faults prior to the Jurassic were minimally active: Triassic lake cycles thicken towards the border fault less than predicted for more active faulting (Schlische, 1992). In the earliest Jurassic, however, sedimentation rate increased (Schlische and Olsen, 1990; Olsen, 1997), indicating an increase in extension rate and in major movement on intrabasin faults (M.O. Withjack and R.W. Schlische, oral communication, 2002), and resulted in varied thickness of Jurassic sediments between faults blocks (figs. C13 and C19b). At some time during the synrift period, the geothermal gradient, in the Triassic Lockatong and Passaic and Jurassic formations, was raised to 32-37˚C/km owing to steady-state conduction from gravity-driven heated fluid flow through the basal fluvial Stockton Formation. The maximum fluid temperature of the Stockton Formation horizontal aquifer was about 235˚C near the border fault and decreased to 205-210˚C near the exposed eastern basin edge on the hanging wall. The Stockton cooled below zircon fission-track closure temperature about 180 Ma (regional mean age 182 Ma, basin-only mean age 177 Ma). Thermal modeling alone of the Lockatong in the Nursery core cannot discriminate whether this long-term hydrothermal system began during the Triassic or the Earliest Jurassic: both long and shorter durations of heating under a ca. 35˚C/km geothermal gradient would produce the same maturity or vitrinite reflectance-value by the time of maximum basin-sediment burial, 194 Ma (fig. C16).

Estimates of paleomaximum geothermal gradient in the Lockatong Formation of the Nursery (36.8˚C/km) and Princeton (32.9˚C/km) cores, and the Jurassic section of the northern Watchung syncline (31.7-33.6˚C/km), show that any depression in heat flow due to gravity-driven meteoric-water recharging in coarse facies at the border fault did not extend far (<5 km) into the basin. Steckler and others (1993) also suggested this based on their apatite fission-track data. This is consistent with rock permeability contrasts inherent in the idealized Newark-type lacustrine facies complex (Olsen, 1990) in which, during lacustrine deposition, less permeable mudstones dominate the basin-fill, and coarse clastic rocks are restricted to basin margins. This lithologic permeability structure would restrict the basinward migration of descending meteoric waters until they reached the basal, fluvial, early-basin fill. The downhole vitrinite reflectance patterns of the Newark basin show that recharging fluid was heated at the basin floor adjacent to the border fault; the heated fluid then flowed across the hanging wall within the Stockton Formation, which functioned as a confined

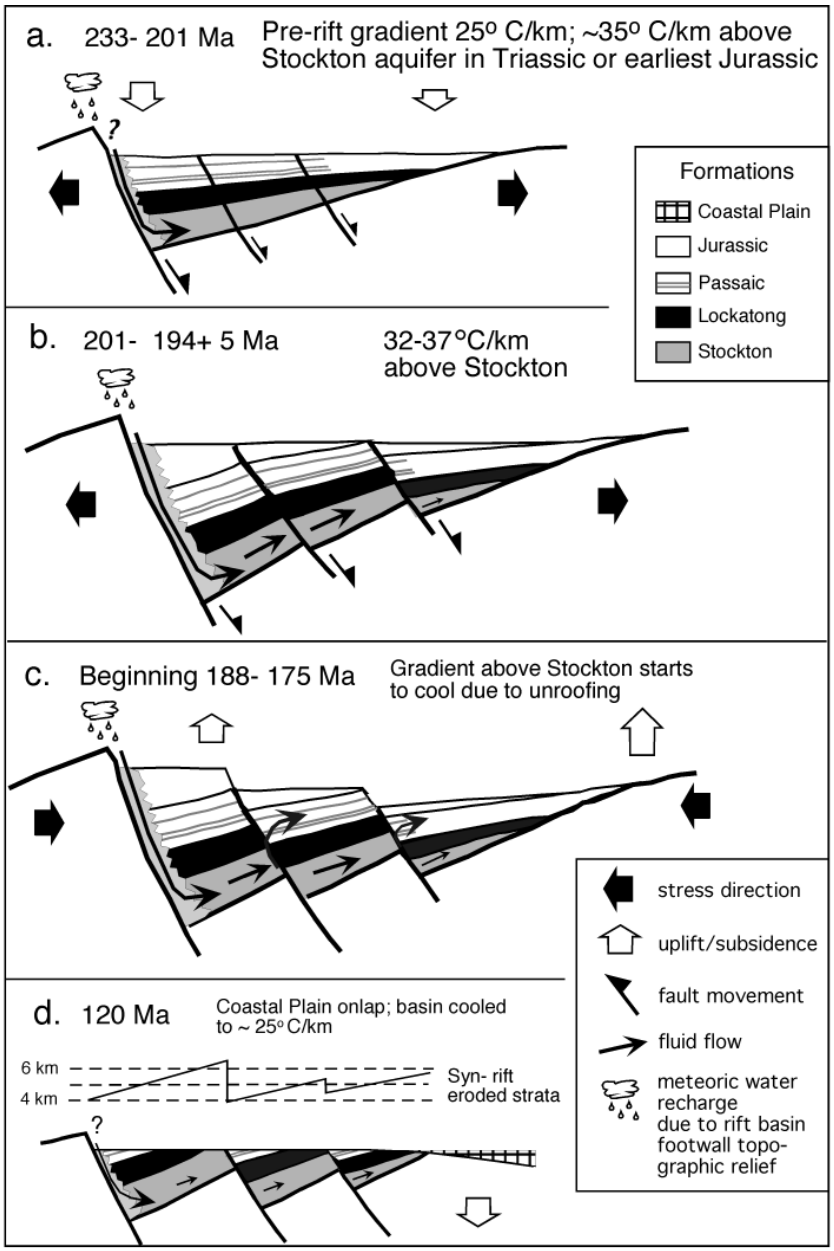

Figure C19. Summary cartoon of Newark basin thermal history. a) Synrift subsidence and sediment deposition under a calculated conductive geothermal gradient of ca. 25°C/km, compatible with the basin's position off the axis of Alleghanian metamorphism and post-orogenic (275-235 Ma) ductile extension and exhumation. The groundwater flow system, topographically-driven by footwall uplift, may have begun at this time. The geothermal gradient would then have conductively increased in Lockatong, Passaic and Jurassic formations to 32-37°C/km due to steady-state heated fluid flow through the Stockton Formation aquifer. b) Increase in sedimentation rate in latest Triassic and Early Jurassic accompanied by major displacement along intrabasin faults. If not begun earlier, the gravity-driven groundwater flow through the Stockton Formation could have started at this time of the rejuvenation of extension. c) Compression and exhumation due to structural inversion of the Atlantic margin during the rift-drift transition and early stages of seafloor spreading (Withjack and others, 1998). Seismically-induced, lateral, episodic or transient advective heat flow events in more permeable members of the Passaic Formation, fed by faults tapping the Stockton aquifer, are spatially associated with stratabound copper mineralization and high reflectance anomalies (Weston Canal, Somerset, Rutgers cores, fig. C5). d) Onlap of passive margin coastal plain sediments after exhumation and erosion of synrift sediments. Graph of cross-basin synrift erosion based on figure C13.

horizontal aquifer. On the other hand, the Taylorsville basin, Virginia, contains Richmond-type lacustrine sequences, formed under generally more humid equatorial climatic conditions; here thick coarse alluvial fans and fan deltas prograded far into the basin during lake highstands throughout synrift time (Olsen, 1990). Borehole vitrinite-reflectance data from the Taylorsville basin (Malinconico, 2002) show that synrift paleogeothermal gradients were lower (about 40˚C/km) in the western basin within 15-20 km of the border fault than in the eastern part of the basin (50-55˚C/km), owing to flow of cool meteoric recharge from the border fault far into the basin through the permeable fluvio-deltaic facies. The hydrostratigraphy or location of aquifers within the basin fill of the Newark and Taylorsville basins, and the thermal signature of the subsequent groundwater-flow systems, is a direct effect of latitudinal climate on stratigraphic architecture.

Transient advective fluid-flow events preserved as vitrinite-reflectance anomalies (fig. C6), are attributed to postrift inversion, the change in stress regime from northwest-southeast extension to compression and related faulting (fig. C19c). In the Rhinegraben, Lampe and others (2001) attributed episodic advective heat-flow events, producing similar reflectance anomalies, to tectonically-related changes in fault permeability, or seismic strain-cycling (Muir Wood, 1994). The vitrinite-reflectance modeling of

transient higher temperature fluid-flow events producing reflectance anomalies in the Passaic Formation of the Weston Canal, Somerset, and Rutgers cores indicates that similar events in Newark basin were of short duration, on the order of 11,000-360,000 years, and would have to occur just before cooling below 180˚C to be compatible with the zircon fission-track data. Although the average of the zircon fission-track data for the basin and immediately adjacent region is 182 Ma, the flat distribution from 196-150 Ma suggests a long history of transient events overprinting tectonic exhumation. This exhumation was complete by the time of Early Cretaceous onlap of passive-margin coastal plain sediments (fig. C19d).

The steady-state Stockton flow system and the transient lateral heated-fluid flow through younger mudstone-rich formations are linked spatially as seen in cross section through the Titusville core (fig. C4) and in the map view (fig. C2), particularly the 2.0% R_O contour that begins at the Hopewell fault near the Perkasie Member at the top of the Titusville core and extends eastward over 40 km enclosing the Perkasie Member at least as far as the Rutgers core location. This pattern indicates that faults were major conduits of heated fluids, tapping the Stockton aquifer, while it was still at paleomaximum temperature, and that fault movement placing the Passaic of the Titusville core adjacent to the Stockton Formation across Hopewell fault also occurred before or during maximum aquifer temperature. The spatial relationship of Newark basin lateral fluid flow to faults tapping the Stockton suggests that transient flow events related to faulting would also have a force contribution from the hydraulic head of the gravity-driven hydrologic system, possibly increasing the distance of heated fluid migration before cooling to background temperatures.

As seen in the high reflectance anomalies in the Weston Canal, Somerset and Rutgers cores, lateral fluid flow in these formations at temperatures higher than background was confined to certain more permeable units (fig. C8). Permeable layers included interconnected shallow playa evaporites (El-Tabakh and others, 1997), coarser siltstones or sandstones associated with deep lacustrine black shale (Smoot and Robinson, 1988), and the black shales themselves, through which fluids may have advanced by replacement of component carbonate. Stratabound copper mineralization is associated with the high reflectance anomalies (1.6-2.7%) in the Passaic Formation cores (Weston Canal, Somerset, Rutgers, and Titusville), but is also found in the Lockatong of the Nursery and Princeton cores where the mineralizing fluids were not hotter in temperature than that produced by steady-state conduction from advective flow through the underlying Stockton Formation.

High arsenic content of base metal deposits in the Newark basin (figs. C9, C10 and table C3) suggests that its concentration in that association is also related to ore-forming fluids. Serfes (2005) found two major sources of arsenic in the basin: hematite coatings in red mudstone and pyrite in black shale. The poor correlation of arsenic with some major metals such as copper (fig. C10) suggests it may be more preferentially incorporated into gangue pyrite during base metal deposition rather than into ore minerals.

The advective fluid flow around 180 Ma and its association with ore deposition were not confined solely to lateral and vertical *intrabasin* pathways. Vein deposits associated with Early Mesozoic basins, including the Phoenixville ores of the southern Newark basin, intrude basement from New Hampshire to Virginia, with isolated occurrences in North Carolina (Lawler, 1981; Robinson and Woodruff, 1988). This indicates that the basement was not hydrologically impermeable. Rock permeability can vary dramatically from low at the core scale to high at the regional scale, due to faults and fractures (Deming, 1994a). In the Rio Grande rift, Mailloux and others (1999) found that hydrologic modeling results best matched paleo- and present-day heat flow data if the upper two km of crystalline basement were moderately permeable. This is in contrast to many basin models that assume an impermeable basement. Therefore, the ca. 180 Ma fluid-flow event in the Newark basin/ central Appalachian Piedmont region, which probably extended into southern New England as well, appears to be regional in scale, utilizing moderate fracture permeability of the basement, but concentrated in the more highly permeable Mesozoic sedimentary basins.

Cooling of the Newark basin, in particular the interpretation of Early Jurassic postrift zircon fission-track and $^{40}Ar/^{39}Ar$ ages, has been controversial. Sutter (1988) proposed that a 176 Ma, $^{40}Ar/^{39}Ar$ cooling age on potassium feldspar (closure temperature ~200˚C) from a granophyric segregation in the Palisades sill (located in fig. C2a) was due to hydrothermal flow resulting from regional tilting, since post-intrusion cooling of the enclosing 202 Ma Palisades diabase sill below 200˚C would have occurred much earlier. Kohn and others (1993) and Smith and Faill (2000), on the other hand, suggested that early Jurassic cooling ages were due to a regional reheating event related to extension and rift-basin formation. This paper, however, shows that the basin-scale groundwater flow system had temperatures >180˚C in the Stockton aquifer and raised temperatures conductively above 180˚C in the Lockatong Formation by maximum burial about 194 Ma. Cooling of that system, starting probably around 188 Ma, based on the thermal modeling of the Lockatong Formation in this paper, is consistent with the published zircon fission-track and $^{40}Ar/^{39}Ar$ data. Decay of the groundwater system would be concomitant with general basin exhumation and accompanying erosion and decrease in topographic relief (hydraulic

head). The exhumation results from basin structural inversion and the change in stress regime from extension to compression owing to the initiation of sea-floor spreading in the north central Atlantic (Withjack and others, 1995). The development of the Newark Supergroup basin rift system, as stated earlier, also is seen as part of a continuum from the collapse of the Alleghanian orogen, ductile exhumation and dome formation (for example the Willimantic dome in Connecticut) accompanied by advection of isotherms along the orogen's old metamorphic belt, followed by brittle wide-area rift-basin formation, and ultimately, seafloor spreading (Wintsch and others, 1992; Hopper and Buck, 1996), without a separate extensional reheating/thermal event.

Recognition of the degree of fluid flow and maturation in the Newark basin also has implications for inorganic geochemical studies of early basin lacustrine sediments. The bulk of the Triassic formations of the basin are well indurated, having undergone non-contact very low-grade metamorphic temperatures of as much as 235˚ ± 10˚C (upper zeolite to lower prehnite-pumpellyite facies metamorphism) in places, although in the Lockatong Formation, the metamorphic reaction of analcime with quartz to form albite plus water (ca. 180-200˚C) (Zen and Thompson, 1974) apparently did not take place owing to lack of excess silica (Van Houten, 1965). In addition, geochemical mass transport by fluids has been suggested in previous studies of both Newark basin ore deposits (Smoot and Robinson, 1988) and chemical remagnetization (Witte and Kent, 1991) and is supported by this study. These observations, therefore, have to be taken into consideration when drawing conclusions about depositional and early diagenetic basin sediment chemistry.

Conclusions

The results of this study indicate the Newark rift basin sediments were deposited under an initially low regional geothermal gradient of about 25˚C/km that increased to 32-37˚C/km owing to synrift steady-state gravity-driven heated-fluid flow through the basal rift-fill fluvial Stockton Formation. Footwall uplift is assumed to provide the topographic gradient for meteoric recharge at the border fault. Initiation of this system cannot be dated or constrained by modeling, but it may have existed either from early rift history in the Triassic, or begun in the earliest Jurassic, during a rejuvenation of extension and major displacement on intrabasin faults.

The steady-state conductive heat-flow regime in formations overlying the Stockton Formation was overprinted in places by transient advective heat flow marked by anomalous high vitrinite-reflectance excursions. The map pattern of surface-sample reflectance data suggests that this transient advective flow, spatially associated with epigenetic stratabound copper mineralization, was fed from permeable intrabasin faults that tapped the basal Stockton aquifer. Thermal modeling of the possible duration of transient events indicates that they occurred in the postrift period in the few million years before the reset Jurassic zircon fission-track ages (mean 182 Ma), when the entire basin groundwater flow system began to cool due to unroofing.

The probable episodic faulting causing the transient flow events is attributed to postrift structural inversion related to the initial stages of Atlantic sea-floor spreading, ca. 185-175 Ma. Inversion-related unroofing also resulted in significant erosion of synrift sediments varying from less than one kilometer over youngest extant Jurassic Formations along the border fault to five-to-six kilometers where the oldest synrift Stockton Formation is exposed along the eastern hanging-wall edge of the basin and along the Delaware River at the eastern edge of the intrabasin western fault block. Exhumation was essentially complete before the Early Cretaceous onlap of the coastal plain. Bed-parallel intraformational groundwater flow probably lasted into the Cretaceous, terminated presumably by both loss of topographic hydraulic head and occlusion of intergranular porosity by mineral cements.

Acknowledgements

This thermal history of the Newark basin was part of the author's dissertation research at the Lamont-Doherty Earth Observatory and the Department of Earth and Environmental Science (DEES) of Columbia University in the City of New York. The research was financially supported in part by student research grants from the Geological Society of America (1995) and the American Association of Petroleum Geologists (1997), and a grant from the DEES's student field fund (1996).

Machine time for vitrinite-reflectance data collection was donated by the Coal Characterization Lab, Dept. of Geology, Southern Illinois University, Carbondale, Illinois (John Crelling, Director); the Dept. of Geological Sciences, University of Missouri, Columbia, Missouri (Michael Underwood); and the Coal and Organic Petrology Laboratory of the Pennsylvania State University, University Park, Pennsylvania (Gareth Mitchell, Director). Thanks also to William Huggett (Coal Characterization Lab, SIU) for polishing hundreds of sample pellets.

I would like to thank my adviser, Paul Olsen, and other members of my dissertation committee, Michael Steckler, Roger Buck, and Nicholas

Christie-Blick. Many other people also gave their time for discussions, looking at samples, or providing samples or access to samples: Donald Monteverde, Wallace Dow, Charles Barker, Charles Landis, Gareth Mitchell, John Castaño, Kevin Shelton, Roy Schlische, Martha Withjack, Douglas Martinsen (error determination and the bootstrap technique), Richard Volkert, Peter LeTourneau, Emma Rainforth, and various persons listed as providing "oral or written communications" information not found in published articles. The Army Corps of Engineers granted access to their Newark basin cores when stored at the U. S. Army depot in Bayonne, New Jersey. I also thank North Central Oil for permission to publish the Cabot well-reflectance data, and Michael E. Serfes and Robert C. Smith II for thoughtful scientific reviews. Irving Grossman provided thorough editorial reviews.

This paper is dedicated to my economic geology professor during Master's degree study at Dartmouth College, Half Zantop.

References

Altamura, R.J., 1996, Tectonics of the Lantern Hill fault, southeastern Connecticut: Evidence for the embryonic opening of the Atlantic Ocean, *in* LeTourneau, P.M., and Olsen, P.E., eds., Aspects of Triassic-Jurassic Rift Basin Geoscience-Abstracts: State Geological and Natural History Survey of Connecticut Miscellaneous Reports 1, p. 5.

American Geological Institute, 1976, Dictionary of Geologic Terms: Anchor Press/ Doubleday, Garden City, New York, 467 p.

Arne, D., and Zentilli, M., 1994, Apatite fission-track thermochronology integrated with vitrinite reflectance, *in* Mukhopadhyay, P.K., and Dow, W.G., eds., Vitrinite reflectance as a maturity parameter: American Chemical Society Symposium Series, v. 570, p. 249-265.

Barker, C.E. and Pawlewicz, M.J., 1993, An empirical determination of the minimum number of measurements needed to estimate the mean random vitrinite reflectance of disseminated organic matter: Organic Geochemistry, v. 20, p. 643-651.

Barker, C.E. and Pawlewicz, M.J., 1994, Calculation of vitrinite reflectance from thermal histories and peak temperature: A comparison of methods, *in* Mukhopadhyay, P.K., and Dow, W.G., eds., Vitrinite reflectance as a maturity parameter: Applications and limitations, American Chemical Society Symposium Series, v. 570, p. 216-220.

Bensley, D.F., and Crelling, J.C., 1991, The interpretation of vitrinite reflectance measurements using rotational polarization: Proceedings, Annual Meeting of the Society for Organic Petrology, v. 8, p. 29.

Bethke, C.M., 1985, A numerical model of compaction-driven groundwater flow and heat transfer and its application to the paleohydrology of intracratonic sedimentary basins: Journal of Geophysical Research, v. 90, p. 6817-6828.

Bethke, C.M., Reed, J.D., and Oltz, D.F., 1991, Long-range petroleum migration in the Illinois basin: American Association of Petroleum Geologists Bulletin, v. 75, p. 925-945.

Contreras, J., Scholz, C., and King, G.C.P., 1997, A model of rift basin evolution constrained by first order stratigraphic observations: Journal of Geophysical Research, v. 102, p. 7673-7690.

Cooper, M.A., Williams, G.D., de Graciansky, P.C., Murphy, R.W., Needham, T., de Paor, D., Stoneley, R., Todd, S.P., Turner, J.P., Ziegler, P.A., 1989, Inversion tectonics - a discussion, *in* Cooper, M.A., and Williams, C.D., eds., Inversion tectonics: Geological Society Special Publication 44, p. 335-351.

Daniels, E.J., Aronson, J.L., Altaner, S.P., Clauer, N., 1994, Late Permian age of NH4-bearing illite in anthracite from eastern Pennsylvania: Temporal limits on coalification in the central Appalachians: Geological Society of America Bulletin, v. 106, p. 760-766.

de Boer, J.S., and Clifton, A.E., 1988, Mesozoic tectogenesis: development and deformation of 'Newark' rift zones in the Appalachians (with special emphasis on the Hartford basin, Connecticut), *in* Manspeizer, Warren, ed., Triassic-Jurassic Rifting, Continental Breakup and the Origin of the Atlantic Ocean and Passive Margins: Elsevier, Amsterdam, The Netherlands, p. 275-306.

Deming, D., 1994a, Fluid flow and heat transport in the upper continental crust, in Parnell, J. ed., Geofluids: origin, migration, and evolution of fluid in sedimentary basins: Geological Society Special Publication 78, p. 27-42.

Deming, D., 1994b, Overburden rock, temperature and heat flow, in Magoon, L., and Dow, W.G., eds., The petroleum system-From source to trap, American Association of Petroleum Geologists Memoir 60, p. 165-186.

Dow, W.G., 1977, Kerogen studies and geological interpretations, Journal of Geochemical Exploration, v. 7, p. 79-99.

Drake, A.A., Jr., Volkert, R.A., Monteverde, D.H., Herman, G.C., Houghton, H. F., Parker, R.A., Dalton, R.F., 1998, Bedrock geologic map of northern New Jersey: U.S. Geological Survey Miscellaneous Investigation Series Map I-2540A.

Dunning, G.R., and Hodych, J.P., 1990, U/Pb zircon and baddeleyite ages for the Palisades and Gettysburg sills of the northeastern United States: Implications for the age of the Triassic/Jurassic

boundary: Geology, v. 18, p. 795-798.

Efron, B., and Tibshirani, R. J., 1993, An Introduction to the Bootstrap, Monograph on Statistics and Applied Probability 57: Chapman & Hall, New York, New York, 436 pages.

El-Tabakh, M., Riccioni, R., and Schreiber, C.B., 1997, Evolution of Late Triassic rift basin evaporites (Passaic Formation): Newark Basin, eastern North America: Sedimentology, v. 44, p. 767-790.

Freeze, R.A., and Cherry, J.A., 1979, Groundwater: Prentice Hall, Englewood Cliffs, New Jersey, 604 pages.

Garven, G., 1989, A hydrogeological model for the formation of the giant oil sands deposits of the Western Canada Sedimentary Basin: American Journal of Science, v. 289, p. 105-166.

Garven, G., and Freeze, R.A., 1984, Theoretical analysis of the role of groundwater flow in the genesis of stratabound ore deposits: 1. Mathematical and numerical model: American Journal of Science, v. 284, p. 1085-1124.

Garven, G., Ge, S., Person, M.A., Sverjensky, D.A., 1993, Genesis of stratabound ore deposits in the mid-continent basins of North America. 1. The role of regional groundwater flow: American Journal of Science, v. 293, p. 497-568.

Gates, A.E., 1997, Multiple reactivations of accreted terrane boundaries: An example from the Carolina terrane, Brookneal, Virginia *in* Glover, L. III, and Gates, A.E., eds., Central and southern Appalachian sutures: Results of the EDGE Project and related studies: Geological Society of America Special Paper 314, p. 49-64.

Goldberg, D.S., Reynolds, D.J., Williams, C.F., Witte, W.K., Olsen, P.E., and Kent, D.V., 1994, Well-logging results from the Newark rift basin coring project: Scientific Drilling, v. 4, p. 267-279.

Hames, W.E., Renne, P.R., and Ruppel, P.R., 2000, New evidence for geologically instantaneous emplacement of earliest Jurassic central atlantic magmatic province basalts on the North American margin: Geology, v. 28, p. 859-862.

Harrison, M., Armstrong, R.L., Naeser, C.W., and Hanakal, J. E., 1979, Geochronology and thermal history of the Coast Plutonic Complex near Prince Rupert, British Columbia: Canadian Journal of Earth Science, v. 16, p. 400-410.

Hatcher, R.D., Osberg, P.H., Drake, A.A., Jr., Robinson, P., and Thomas, W. A., 1990, Tectonic Map of the U.S. Appalachians, *in* Hatcher, R.D., Thomas, W.A., and Viele, G.W., eds., The Appalachian-Ouachita Orogen in the United States: Geological Society of America, The Geology of North America, v. F-2, Plate 1.

Herman, G.C., 2005, Joints and veins in the Newark Basin, New Jersey, in regional tectonic perspective: *in* Gates, A.E., ed., Newark Basin—View from the 21st Centrury: 22nd Annual meeting of the Geological Association of New Jersey, p. 76-116.

Hitzman, M.W., Allan, J.R., and Beaty, D.W., 1998, Regional dolomitization of the Waulsortian Limestone in southeastern Ireland: evidence of large-scale fluid flow driven by the Hercynian Orogeny: Geology, v. 26, p. 547-550.

Hoek, J., 1997, Thermal history of the Passaic Formation, Newark basin, USA, from drill cores using apatite-fission-track analysis: University of Pennsylvania Masters thesis, Philadelphia, Pennsylvania, 96 pages.

Hoek, J., Omar, G., Steckler, M., and Karner, G., 1998, Thermal and hydrogeologic history of the Newark basin, U.S.A., during Mesozoic time: An apatite fission track study: Geological Society of America Abstracts with Program, v. 30, p. 26.

Hood, A., Gutjahr, C.M., and Peacock, R.L., 1975, Organic metamorphism and the generation of petroleum: American Association of Petroleum Geologists Bulletin, v. 59, p. 986-996.

Hopper, J.R., and Buck, W.R., 1996, The effect of lower crustal flow on continental extension and passive margin formation: Journal of Geophysical Research, v. 101, p. 20174-20194.

Houseknecht, D.W., Bensley, D.F., Hathon, L.A., and Kastens, P.H., 1993, Rotational reflectance properties of Arkoma basin dispersed vitrinite: insights for understanding reflectance populations in high thermal maturity regions: Organic Geochemistry, v. 20, p. 187-196.

Huntoon, J.E., and Furlong, K.P., 1992, Thermal evolution of the Newark basin: Journal of Geology, v. 100, p. 579-591.

Hurford, A.J., and Green, P.F., 1983, The zeta age calibration of fission-track dating: Chemical Geology, v. 1, p. 285-317.

Hutchinson, D.R., and Klitgord, K.D., 1988, Evolution of the rift basins on the continental margin off southern New England, *in* Manspeizer, Warren, ed., Triassic-Jurassic Rifting, Continental Breakup and the Origin of the Atlantic Ocean and Passive Margins: Elsevier, Amsterdam, The Netherlands, p. 81-98.

Katz, B.J. and Liu, X., 1998, Summary of the AAPG research symposium on lacustrine basin exploration in China and Southeast Asia: American Association of Petroleum Geologists Bulletin, v. 82, p. 1300-1307.

Katz, B.J., Pheifer, R.N., and Schunk, D.J., 1988a, Interpretation of discontinuous vitrinite reflectance profiles: American Association of Petroleum Geologists Bulletin, v. 71, p. 926-931.

Katz, B.J., Robison, C.R., Jorjorian, T., and Foley, F.D., 1988b, The level of organic maturity within the Newark basin and its associated implications, *in* Manspeizer, Warren., ed., Triassic-Jurassic Rifting,

Continental Breakup and the Origin of the Atlantic Ocean and Passive Margins: Elsevier, Amsterdam, The Netherlands, p. 683-696.

Kent, D.V., Olsen, P.E., Witte, W.K., 1995, Late Triassic-Early Jurassic geomagnetic polarity sequence and paleolatitudes from drill cores in the Newark rift basin, eastern North America: Journal of Geophysical Research, v. 100, no. B8, p. 14965-14998.

Kilby, W.E., 1988, Recognition of vitrinite with non-uniaxial negative reflectance characteristics: International Journal of Coal Geology, v. 9, p. 267-285.

Klitgord, K.D., Hutchinson, D.R., and Schouten, H., 1988, Tectonic features and geophysical lineaments, *in* Sheridan, R.E., and Grow, J.A., eds., The Atlantic Continental Margin: Geological Society of America, The Geology of North America, v. I-2, Plate 2C.

Kohn, B. P., Wagner, M. E., Lutz, T. M., and Organist, G., 1993, Anomalous Mesozoic thermal regime, central Appalachian Piedmont: Evidence from sphene and zircon fission-track dating: Journal of Geology, v. 101, p. 779-794.

Kunk, M.J., Simonson, B.M., Smoot, J.P., 1995, 40Ar/39Ar constraints on the age of K-feldspar cementation in non-marine sediments of the Newark, Gettysburg and Culpepper basins: Geological Society of America Abstracts with Program, v. 27, p. 62.

Lampe, C., and Person, M., 2000, Episodic fluid flow in the Upper Rhinegraben (Germany): Journal of Geochemical Exploration, v. 69-70, p. 37-40.

Lampe, C., Person, M., Nöth, S., and Ricken, W., 2001, Episodic fluid flow within continental rift basins: Some insights from field data and mathematical models of the Rhinegraben: Geofluids, v. 1, p. 42-52.

Landis, C.R., and Castaño, J.C., 1995, Maturation and bulk chemical properties of a suite of solid hydrocarbons: Organic Geochemistry, v. 22, p. 137-149.

Law, B.E., Nuccio, V.F., and Barker, C.E., 1989, Kinky vitrinite reflectance well profiles: Evidence of paleopore pressure in low-permeability, gas-bearing sequences in Rocky Mountain foreland basins: American Association of Petroleum Geologists Bulletin, v. 73, p. 999-1010.

Lawler, J.P., 1981, Fluid inclusion evidence of ore-forming solutions: Phoenixville, Audubon, and New Galena mine districts, Pennsylvania: Bryn Mawr College Masters thesis, Pennsylvania, 73 p.

LeTourneau, P.M., 1999, Depositional history and tectonic evolution of Late Triassic age rift of the U.S. Atlantic margin: result of an integrated stratigraphic, structural, and paleomagnetic analysis of the Taylorsville and Richmond basins: Columbia University Ph.D. dissertation, New York, New York, 294 pages.

Lo, H.B., 1993, Correction criteria for the suppression of vitrinite reflectance in hydrogen-rich kerogen: preliminary guidelines: Organic Geochemistry, v. 20, p. 653-657.

Mailloux, B J., Person, M., Kelley, S., Dunbar, N., Cather, S., Strayer, L., Hudleston, P., 1999, Tectonic controls on the hydrology of the Rio Grande Rift, New Mexico: Water Resources Research, v. 35, p. 2641-2659.

Malinconico, M.L., 2000, Using reflectance crossplots and rotational polarization for determination of first-cycle vitrinite for maturation studies: Int. Journal of Coal Geology, v. 43, p. 105-120.

Malinconico, M.L., 2002, Lacustrine organic sedimentation, organic metamorphism, and thermal history of selected Early Mesozoic Newark Supergroup basins, Eastern U.S.A: Columbia University Ph.D. dissertation, New York, New York, 419 pages.

Malinconico, M.L., 2003, Estimates of eroded strata using borehole vitrinite reflectance data, Triassic Taylorsville rift basin, Virginia: Implications for duration of synrift sedimentation and evidence of structural inversion *in* LeTourneau, P.M., and Olsen, P.E., eds., The Great Rift Valleys of Pangea in eastern North America, v.1, Tectonics, structure, and volcanism: Columbia University Press, New York, New York, p. 80-103.

Marzoli, A., Renne, P.R., Piccirillo, E.M., Ernesto, M., Bellieni, G., de Min, A., 1999, Extensive 200 million year old continental flood basalts of the Central Atlantic Margin Province: Science, v. 284, p. 616-618.

Mauk, J.L., and Hieshima, G.B., 1992, Organic matter and copper mineralization at White Pine, Michigan, U.S.A.: Chemical Geology, v. 99, p. 189-211.

Maynard, J.B., 1983, Geochemistry of sedimentary ore deposits: Springer Verlag, New York, 305 pages.

McKenzie, D., 1978, Some remarks on the development of sedimentary basins: Earth and Planetary Science Letters, v. 40, p. 25-32.

Miller, K.G., Mountain, G.S., Browning, J.V., Kominz, M., Sugarman, P.J., Christie-Blick, N., Katz, M.E., Wright, J.D., 1998, Cenozoic global sea level, sequences, and the New Jersey transect: Results from coastal plain and continental slope drilling: Reviews of Geophysics, v. 36, p. 569-601.

Morgan, P., and Sass, J.H., 1984, Thermal regime of the continental lithosphere: Journal of Geodynamics, v. 1, p. 143-166.

Muir Wood, R., 1994, Earthquakes, strain cycling and the mobilization of fluids, *in* Parnell, J., ed., Geofluids: Origin, migration, and evolution of fluid in sedimentary basins: Geological Society Special Publication 78, p. 85-98.

Naeser, C.W., 1979, Fission-track dating and geologic

annealing of fission-tracks, *in* Jager, E. and Hunziker, J. C., eds., Lectures in isotope geology: Springer Verlag, Heidelberg, Germany, p. 154-169.

Nance, R.D., and Thompson, M.D., 1996, Avalonian and related peri-Gondwanan terranes of the circum-North Atlantic: An introduction, *in* Nance, R.D., and Thompson, M.D., eds., Avalonian and related peri-Gondwanan terranes of the circum-North Atlantic: Geological Society of America Special Paper 304, p. 1-7.

Oliver, J., 1986, Fluids expelled tectonically from orogenic belts: Their role in hydrocarbon migration and other geologic phenomena: Geology, v. 14, p. 99-102.

Olsen, P.E., 1986, A 40-million year lake record of early Mesozoic climatic forcing: Science, v. 234, p. 842-848.

Olsen, P.E., 1988, Continuity of strata in the Newark and Hartford basins, *in* Froelich, A.J., and Robinson, G.R., eds., Studies of the Early Mesozoic Basins of the Eastern United States: U.S. Geological Survey Bulletin 1776, p. 6-18.

Olsen, P.E., 1990, Tectonic, climatic and biotic modulation of lacustrine ecosystems: examples from the Newark Supergroup of eastern North America, *in* Katz, B.J., ed., Lacustrine Basin Exploration: Case Studies and Modern Analogs: American Association of Petroleum Geologists Memoir 50, p. 209-224.

Olsen, P.E., 1997, Stratigraphic record of the Early Mesozoic breakup of Pangea in the Laurasia-Gondwana rift system: Annual Reviews of Earth and Planetary Sciences, v. 25, p. 337-401.

Olsen, P.E., Kent, D.V., Cornet, B., Witte, W.K., Schlische, R.W., 1996a, High-resolution stratigraphy of the Newark rift basin (early Mesozoic, eastern North America): Geological Society of America Bulletin, v. 108, no. 1, p. 40-77.

Olsen, P.E., Schlische, R.W., and Fedosh, M.S., 1996b, 580 Ky duration of the Early Jurassic flood basalt event in eastern North America estimated using Milankovitch cyclostratigraphy, *in* Morales, M., ed., The Continental Jurassic: Museum of Northern Arizona Bulletin v. 60, p. 11-22.

Olsen, P.E., Schlische, R.W., and Gore, P.J.W., eds., 1989, Tectonic, depositional and paleoecological history of early Mesozoic rift basins, eastern North America: International Geological Congress Field Trip T351, Washington, D.C., American Geophysical Union, 174 pages.

Owens, J.P., Sugarman, P.J., Sohl, N.F., Parker, R.A., Houghton, H.F., Volkert, R.A., Drake, A.A. Jr., Orndorff, R.C., 1998, Bedrock geologic map of central and southern New Jersey: U.S. Geological Survey Miscellaneous Investigation Series Map I-2540-B.

Parnell, J., and Monson, J., 1995, Paragenesis of hydrocarbon, metalliferous, and other fluids in Newark Group basins, eastern U.S.A.: Transaction of the Institution of Mining and Metallurgy Section, v. 104, p. B136-144.

Person, M., and Garven, G., 1994, A sensitivity study of the driving forces on fluid flow during continental-rift basin evolution: Geological Society of America Bulletin, v. 106, p. 461-475.

Pratt, L.M., Shaw, C.A., and Burruss, R.C., 1988, Thermal histories of the Hartford and Newark Basins inferred from maturation indices of organic matter, *in* Froelich, A.J., and Robinson, G.R., eds., Studies of the Early Mesozoic Basins of the Eastern United States: U.S. Geological Survey Bulletin 1776, p. 58-62.

Pratt, L.M., Vuletich, A.K., Shaw, C.A., 1986, Preliminary results of organic geochemical and stable isotope analyses of Newark Supergroup rocks in the Hartford and Newark basins, eastern U.S. Geological Survey Open-File report 86-284, 29 pages.

Püttmann, W., and Merz, C., 1989, The secondary oxidation of organic material and its influence on Kupferschiefer mineralization of southwest Poland: Applied Geochemistry, v. 4, p. 151-161.

Qing, H., and Mountjoy, E., 1992, Large-scale fluid flow in the Middle Devonian Presqui'ile barrier, Western Canada Sedimentary Basin: Geology, v. 20, p. 903-906.

Ratcliffe, N.M., and Burton, W.C., 1988, Structural analysis of the Furlong fault and the relation of mineralization to faulting and diabase intrusion, Newark basin, Pennsylvania, *in* Froelich, A.J., and Robinson, G.R., eds., Studies of the Early Mesozoic Basins of the Eastern United States: U.S. Geological Survey Bulletin 1776, p. 176-193.

Ratcliffe, N.M., Burton, W.C., D'Angelo, R.M., and Costain, J.K., 1986, Low-angle extensional faulting, reactivated mylonites, and seismic reflection geometry of the Newark basin margin in eastern Pennsylvania: Geology, v. 14, p. 766-770.

Robinson, G.R., and Woodruff, L.G., 1988, Characteristics of base-metal and barite vein deposits associated with rift basins, with examples from some Early Mesozoic basins of eastern North America, *in* Froelich, A.J. and Robinson, G.R., eds., Studies of the Early Mesozoic Basins of the Eastern United States: U.S. Geological Survey Bulletin 1776, p. 77-390.

Robinson, G.R., Jr., 1979, Pegmatite cutting mylonite--Evidence supporting pre-Triassic faulting along the western border of the Danville Triassic basin, southern Virginia: Geological Society of America Abstracts with Program, v. 11, p. 210.

Roden, M.K. and Miller, D.S., 1991, Tectono-thermal history of Hartford, Deerfield, Newark and Taylorsville Basins, eastern United States, using

fission-track analysis: Schweizerische Mineralogische und Petrographische Mitteilungen, v. 71, p. 187-203.

Schlische, R.W., 1992, Structural and stratigraphic development of the Newark extensional basin, eastern North America: Evidence for the growth of the basin and its bounding structures: Geological Society of America Bulletin, v. 104, p. 1246-63.

Schlische, R.W., 2003, Progress in understanding the structural geology, basin evolution, and tectonic history of the eastern North American rift system, *in* LeTourneau, P.M., and Olsen, P.E., eds., The Great Rift Valleys of Pangea in eastern North America, v.1 Tectonics, structure, and volcanism: Columbia University Press, New York, New York, p. 80-103.

Schlische, R.W., and Ackermann, R.V., 1995, Rift basin inversion around the margins of the North Atlantic Ocean: Chronology, causes, and consequences: Geological Society of America Abstracts with Programs, v. 27, no. 1, p. 80.

Schlische, R.W., and Olsen, P.E., 1990, Quantitative filling models for continental extensional basins with application to the early Mesozoic rifts of eastern North America: Journal of Geology, v. 98, p. 135-155.

Serfes, M.E., 2005, Arsenic occurrence, sources, mobilization, transport and prediction in the major bedrock aquifers of the Newark basin: Rutgers University Ph.D. dissertation, New Brunswick, New Jersey, 122 pages.

Seward, T.M., and Barnes, H.L., 1997, Metal transport by hydrothermal ore fluids, *in* Barnes, H.L., ed., Geochemistry of hydrothermal ore deposits, 3rd edition: John Wiley & Sons, New York, New York, p. 435-486.

Shelton, K.L., Bauer, R.M., Gregg, J.M., 1992, Fluid-inclusion studies of regionally extensive epigenetic dolomites, Bonneterre Dolomite (Cambrian), southeast Missouri: Evidence of multiple fluids during dolomitization and lead-zinc mineralization: Geological Society of America Bulletin, v. 104, p. 675-683.

Simonson, B.M., Smoot, J.P. and Hughes, J.L., 2010, Paragenesis of authigenic minerals in macropores and veins in Late Triassic mudstones of the Newark basin: Implications for late diagenetic fluid migration trough mudstone, *in* Herman, G.C. and Serfes, M.E., eds.: N.J. Geological Survey Bulletin 77, Chapter B, p. B1-B25.

Smith, R.C. II, and Faill, R., 2000, The Mesozoic heating event in the mid-Atlantic region, U.S.A.: Geological Society of America Abstracts with Program, v. 32, p. A-75.

Smoot, J.P., and Robinson, G.R., Jr., 1988, Sedimentology of stratabound base-metal occurrences in the Newark Supergroup, *in* Froelich, A. J., and Robinson, G. R., eds., Studies of the Early Mesozoic Basins of the Eastern United States: U.S. Geological Survey Bulletin 1776, p. 356-376.

Smoot, J.P. and Simonson, B., 2004, Possible lithologic controls on groundwater quality in the Triassic rocks of the Newark basin, *in* Hydrogeology of the Newark basin – A regional workshop, November 2004: New Brunswick, NJ, Rutgers University, http:///geology.rutgers.edu/nbhydro/agenda.html

Stamatakos, J., Hirt, A.M. and Lowrie, W., 1996, The age and timing of folding in the central Appalachians from paleomagnetic results: Geological Society of America Bulletin, v. 108, p. 815-829.

Steckler, M.S., Omar, G. I., Karner, G.D., and Kohn, B. P., 1993, Pattern of hydrothermal circulation with the Newark basin from fission-track analysis: Geology, v. 21, p. 735-38.

Sutter, J.F., 1988, Innovative approaches to the dating of igneous events in the early Mesozoic basins of the eastern United States, *in* Froelich, A.J., and Robinson, G.R., eds., Studies of the Early Mesozoic Basins of the Eastern United States: U.S. Geological Survey Bulletin 1776, p. 194-200.

Sweeney, J.J. and Burnham, A.K., 1990, Evaluation of a simple model of vitrinite reflectance based on chemical kinetics: American Association of Petroleum Geologists Bulletin, v. 74, p. 1559-1570.

Taylor, G.H., Teichmüller, M., Davis, A., Diessel, C.F. K., Littke, R., Robert, P., 1998, Organic petrology: Gebrüder Borntraeger, Berlin, 704 pages.

Tissot, B.P., and Welte, D.H., 1984, Petroleum formation and occurrence (2nd. edition): Springer Verlag, Berlin, Germany, 699 pages.

Tseng, H.Y., Burruss, R.C., Onstott, T.C., and Omar, G., 1999, Paleofluid flow circulation within a Triassic rift basin: Evidence from oil inclusions and thermal histories: Geological Society of America Bulletin, v. 111, p. 275-290.

Van Houten, F.B., 1965, Composition of Triassic Lockatong and associated formations of Newark Group, central New Jersey and adjacent Pennsylvania: American Journal of Science, v. 263, p. 825-863.

Vynhal, C.R., and McSween, H.Y., 1990, Constraints on Alleghanian vertical displacements in the southern Appalachian Piedmont, based on aluminum-in-hornblende barometry: Geology, v. 18, p. 938-941.

Walters, C.C., and Kotra, R.K., 1990, Thermal maturity of Jurassic shales from the Newark Basin, U.S.A.: influence of hydrothermal fluids and implications to basin modeling: Applied Geochemistry, v. 5, p. 211-225.

White, W.S., 1971, A paleohydrologic model for mineralization of the White Pine copper deposit, northern Michigan: Economic Geology, v. 66, p. 1-13.

Williams, C.F., Sass, J.H., Moses, T.H., Jr., and Goldberg, D., 1991, Preliminary heat flow results from the Newark Rift Basin Coring Project: Eos, Transactions American Geophysical Union, v. 72, no. 44 supplement, p. 504.

Wintsch, R.P., Sutter, J. F., Kunk, M. J., Aleinikoff, J.N., Dorais, M. J., 1992, Contrasting P-T-t paths: Thermochronologic evidence for a late Paleozoic final assembly of the Avalon composite terrane in the New England Appalachians: Tectonics, v. 11, p. 672-689.

Withjack, M.O., Olsen, P.E., and Schlische, R.W., 1995, Tectonic evolution of the Fundy rift basin, Canada: Evidence of extension and shortening during passive margin development: Tectonics, v. 14, p. 390-405.

Withjack, M.O., Schlische, R.W., and Olsen, P.E., 1998, Diachronous rifting, drifting, and inversion on the passive margin of central eastern North America: An analog for other passive margins: American Association of Petroleum Geologists Bulletin, v. 82, no. 5A, p. 817-835.

Witte, W.K., and Kent, D>V., 1991, Tectonic implications of remagnetization event in the Newark basin: Journal of Geophysical Research, v. 96 (B12), p. 19569-19852.

Zen, E., and Thompson, A.B., 1974, Low grade regional metamorphism: mineral equilibrium relations: Annual Review of Earth and Planetary Science, v. 2, p. 179-212.

Ziagos, J.P., and Blackwell, D.D., 1986, A model for the transient temperature effects of horizontal fluid flow in geothermal systems: Journal of Volcanology and Geothermal Research, v. 27, p. 371-97.

Hydrogeologic Characterization of Contaminated- Bedrock Sites in the Newark Basin: Selecting Conceptual Flow Model and Characterization Tools

By Andrew Michalski, Michalski & Associates, Inc.

Chapter D of

Contributions to the Geology and Hydrogeology of the Newark Basin

N.J. Geological Survey Bulletin 77

State of New Jersey
Department of Environmental Protection
Water Resource Management
New Jersey Geological Survey
2010

Contents

Figures

Table

Chapter D

Hydrogeologic Characterization of Contaminated-Bedrock Sites in the Newark Basin: Selecting Conceptual Flow Model and Characterization Tools

Andrew Michalski[1]

Abstract

The development of a realistic conceptual flow and transport model is the key factor for effective groundwater monitoring, numerical modeling, and remediation of contaminated bedrock sites in the Newark basin. Incorrect conceptualization of groundwater flow commonly results in misdelineation of contaminant plumes, induced migration of non-aqueous phase liquids and dissolved contaminants through well bores or across aquitards, and ultimately in failed remediation efforts. Although the storage and permeability of the bedrock are chiefly fracture-controlled, most conceptual flow models used for bedrock sites are based on an equivalent porous medium (EPM) concept. This concept includes: 1) uniform flow; 2) two-zone and three-zone aquifers; 3) strike-aligned anisotropy (Herpers and Barksdale, 1951); and 4) dipping multilayer models.

The prominent role of bedding fractures in transmitting the bulk of groundwater through the bedrock is conceptualized by a hybrid model of a leaky multi-unit aquifer (LMA) (Michalski 1990). These fractures function as discrete tabular aquifers (high T but very low S) and as collectors of flow from sub-vertical joints in adjacent beds that function as aquitards. Such major bedding fractures occur at uneven stratigraphic intervals of tens to hundreds of feet. A zone of weathered shale and mudstone bedrock, commonly 30 ft to 100 ft thick, contains more numerous but poorly integrated fractures, which increases its porosity and storage but reduces its permeability. In recharge areas, this weathered zone is drained by updip extensions of underlying major bedding fractures. Below this zone, groundwater flow within such bedding fractures follows the strike of bedding. The LMA framework can significantly improve the effectiveness of groundwater characterization, remediation, and monitoring at contaminated-bedrock sites.

Expedited hydrogeologic characterization of contaminated-bedrock sites relies on deep temporary test holes (TTHs) for investigating controlled short-circuiting in transmissive (water-bearing) bedrock fractures. The characterization toolbox for the TTHs includes: televiewer, caliper, electrical conductivity and temperature logs, in-hole flow tracing (or flow-meter log), depth-discrete sampling of the cross flows, and packer testing. This approach enables the hydrogeologist not only to locate transmissive fractures within the TTH, but also to quantify transmissivity and hydraulic head for any such fractures, and to determine contaminant concentrations in inflow-producing fractures. The TTH data, together with the generic LMA framework, provide the basis for formulating a flow-and-transport model for the site and converting the TTHs to short-screen monitoring wells. The validity of this site-specific model is then verified by comparing predicted and observed hydraulic responses to short-term pumping stress generated during routine purging of the monitoring wells.

Introduction

The Newark basin is a gently-tilted block filled with sedimentary and igneous rocks that is faulted and locally folded (Olsen, 1980; Schlische, 1992: Herman, 2001). The sedimentary formations consist of repeated sequences of sandstone, shale and mudstone beds, in varying proportions, which reflect climate-driven oscillation from fluvial to lacustrine deposition. The basin includes the highly urbanized areas of New Jersey, New York (Rockland County) and Pennsylvania. Numerous bedrock wells in the region have been contaminated by industrial activities. Chlorinated solvents and gasoline constituents are the most common groundwater contaminants. Remedial attempts are commonly ineffective because hydrogeologic complexities of the fractured bedrock result in inadequate characterization efforts.

This paper outlines a practical approach to a comprehensive hydrogeologic bedrock characterization, which was tested at several contaminated sites in the Newark basin. It is based on a realistic conceptualization of a multi-unit aquifer, and it focuses on identification and characterization of controlling

[1]Michalski & Associates, Inc.
South Plainfield, NJ 07080-2450
amichalski@comcast.net

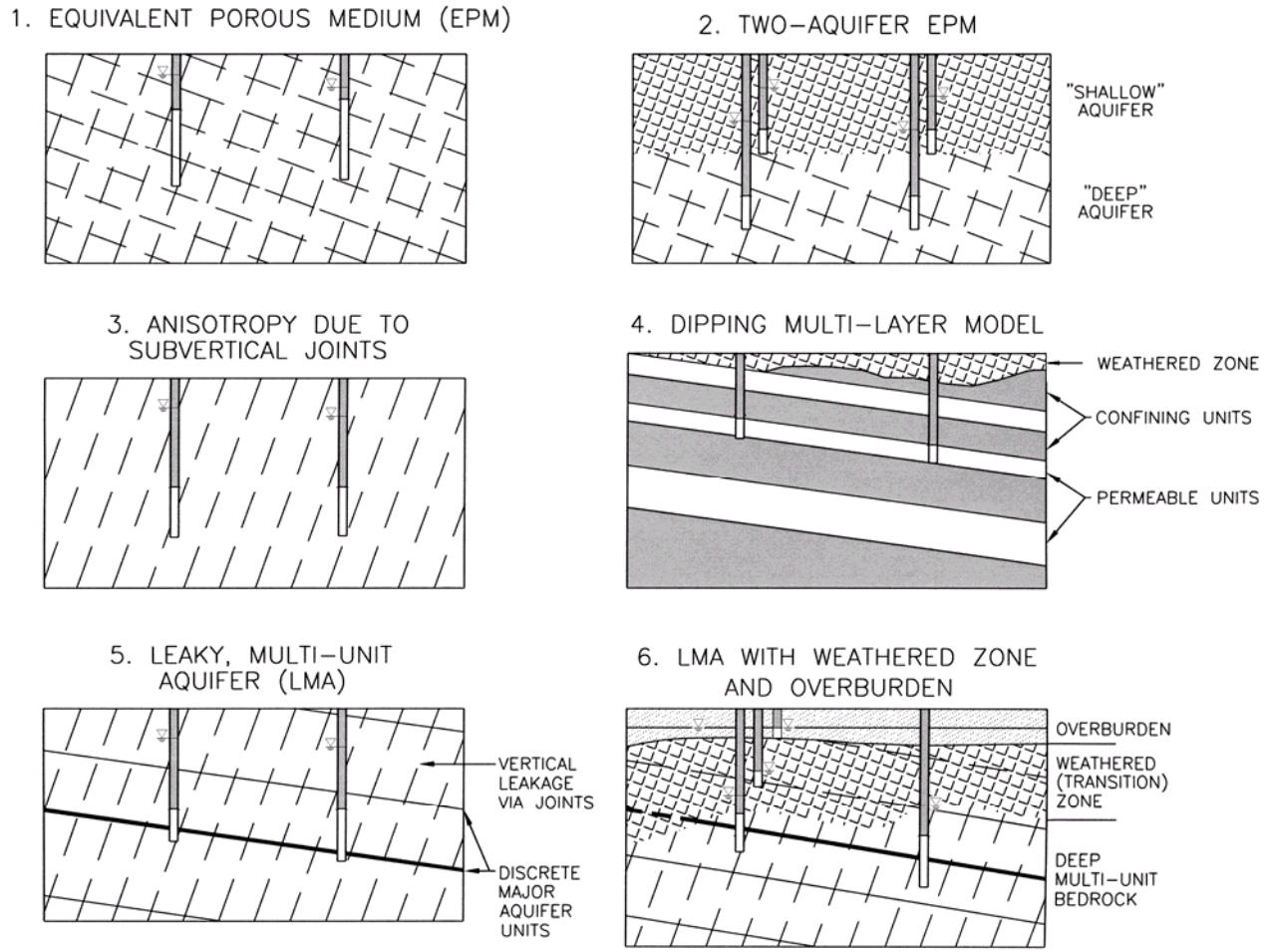

Figure D1. Conceptual groundwater flow models (1-6) for sites in the Newark Basin (modified from Michalski and Britton, 1997).

bedding fractures that provide preferential flow and contaminant-migration pathways. Construction of temporary test holes (TTHs), which are subsequently converted to short-screen monitoring wells, permits rapid and comprehensive characterization of the multi-unit bedrock and the development of a realistic site model. The site-specific model is then verified, and fine-tuned if needed, by short-term pumping tests. This characterization strategy is also applicable to wellhead-protection and water-supply-allocation projects in the Newark basin, and is transferable to other fractured bedrock sites marked by layered-type bedrock heterogeneities.

Conceptual models of groundwater flow in the Newark basin

Various models have been used to conceptualize the flow of ground water at sites in fractured bedrock of the Newark basin (fig. D1). The equivalent-porous-medium (EPM) concept extends the flow and transport analyses from granular porous media to fractured bedrock. Model 1 in figure D1 is commonly a default model during initial site characterization. A two-aquifer EPM model (fig. D1; model 2) accounts for significant differences in groundwater elevations between "shallow" and "deep" wells at many bedrock sites. This model is sometimes expanded to a three-aquifer EPM system featuring “shallow”, “intermediate”, and “deep” aquifer zones sliced horizontally (fig. D1). Although still utilized, the depth-based EPM model ignores the effects of structural dip, and fracture permeability within the bedrock section. EPM is inadequate as transport model for most remediation or wellhead-protection cases.

Another conceptual model (fig. D1; model 3) postulates that near-vertical joints subparallel to the strike of beds provide primary flow pathways through the bedrock and produce its anisotropic behavior. This model was first proposed by Herpers and Barksdale (1951) to explain an elliptical drawdown response

during a pumping test in Newark, NJ. However, the observed drawdown anisotropy is more accurately explained by the penetration by multiple observation wells of multiple water-bearing units in a dipping multi-unit bedrock aquifer: observation wells aligned along the strike of bedding of a pumping well tend to intercept the same beds/aquifer units as the pumping well, whereas wells of similar depth but aligned perpendicular to the strike penetrate different beds/aquifer units. Any model with homoclinal dip of beds (fig. D1; models 4, 5, and 6) can explain the observed anisotropic response to pumping.

A dipping multilayer model (fig. D1; model 4) recognizes the lithostratigraphic and structural controls on groundwater flow in a dipping set of permeable layers and low-permeability beds (LaCombe, 2000). This conceptualization is often used for MODFLOW-based flow simulations for sites in the Newark basin (for example, Lewis-Brown and dePaul, 2000). However, it neglects the prominent role of bedding fractures in many bedrock wells in the region.

The fifth and sixth models in figure D1 feature a leaky, multi-unit aquifer (LMA) concept (Michalski, 1990). Bedding-plane partings form discrete aquifer units in the layered bedrock. Owing to their high transmissivity and large areal extent, such large-aperture bedding fractures become low-head centers and discrete aquifer units. Near-vertical jointing in adjacent beds results in leakage between the adjacent aquifer units, but such cross-bed leakage is commonly retarded by the termination of most joints at bed boundaries. The major bedding fractures show transmissivity values exceeding 1,000 gpd/ft (15,000 gpd/ft in one case), and occur at varied stratigraphic intervals of tens to hundreds of feet. Measured storativity values for such major fractures are very low ($1x10^{-5}$ - $1x10^{-6}$). Some major bedding partings can be traced for more than 1,500 feet (Michalski and Britton, 1997). Groundwater velocity in such preferential fracture-flow pathways exceeds 10 ft/d at low ambient horizontal hydraulic gradients (0.001-0.0001).

Bedding fractures of much lower transmissivity may also act as major preferential pathways for contaminant migration. Such minor transmissive fractures are common in low-permeability bedrock sections that are regional aquitards (for example, parts of the Lockatong Formation). Because these bedding fractures facilitate horizontal flow and contaminant migration within the low-permeability bedrock section (rather than the vertical flow commonly expected in an aquitard), they function as preferential flow pathways within the layered aquitard section.

A more realistic representation of the LMA model is obtained by superposition of a weathered zone, and a saturated overburden, if present, overlying the bedrock consisting of discrete aquifer units (fig. D1; model 6). Weathering of mudstone and shale beds produces numerous poorly integrated fractures. Major fractures may become clogged, resulting in a weathered zone of much lower permeability but much greater storage capacity than the deep bedrock. Nevertheless, extensions of the major bedding fractures into the weathered zone (fig. D1; model 6) are the principal pathways for down-dip flow and drainage of the weathered zone. Below this zone, the prevailing groundwater flow direction in the discrete aquifer units turns to parallel the strike of bedding, as the local down-dip flow merges with the strike-parallel regional flow and farther downdip flow is impeded by a reduction of bedding parting apertures and permeability with depth. Plumes of dissolved contaminants in such units extend along strike for thousands of feet. Updip flow from the discrete aquifer units prevails in groundwater discharge zones. Figure D2 applies the LMA generic model to a site tested by the methodology described in this paper.

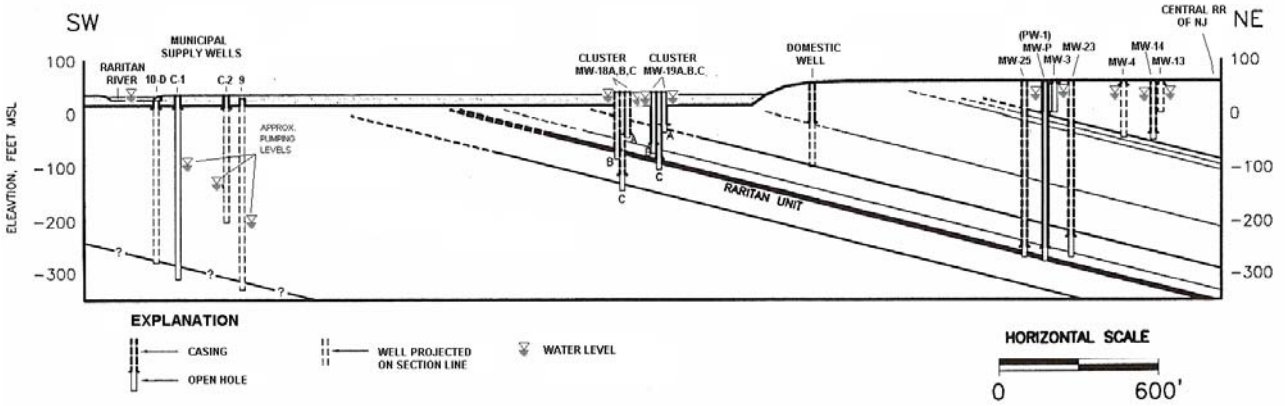

Figure D2. Hydrostratigraphy of the Passaic Formation at a site in Bridgewater, NJ (after Michalski and Britton, 1997). Several minor bedding-controlled discrete aquifer units and one major unit (labeled as Raritan Unit) are unevenly distributed within the cross section. Confining units make up most of the section. The left part of the section is based on limited data.

Misapplication of EPM

Where an open hole/well penetrates two or more major bedding fractures (aquifer units) of the multi-unit bedrock system, vertical crossflows commonly develop in the hole. Such crossflows can significantly alter pre-existing head distribution and contaminant migration patterns. Through this mechanism, deep open holes of inactive bedrock-supply wells and old monitoring wells have commonly played a major role in spreading contaminants in bedrock. The cross-flow problems of the past largely stem from the convenience of using the EPM approach in lieu of more realistic conceptual models that recognize the multi-unit structure of bedrock aquifer systems in the area. To reduce potential crossflows, current drilling regulations in New Jersey restrict the length of the open-hole (or screened) interval in bedrock-monitoring wells to 25 feet. Hydrogeologic characterization of sites with pre-existing bedrock supply wells or deep open-hole monitoring wells poses additional challenges, as the impact of such wells on flow and contaminant migration needs to be evaluated.

Ignoring a discrete, multi-unit hydrostratigraphy and structural dip model for the convenience of the EPM model commonly results in other adverse consequences, including:1) distorted potentiometric data and flow direction; 2) underestimated contaminant migration velocity along unrecognized preferential flow pathways; 3) misdelineated contaminant plumes; and 4) failed remediation efforts. Because of these adverse effects, the LMA framework (fig. D1; models 5 and 6) should be considered as a default conceptual model for groundwater characterization, remediation, monitoring, and groundwater protection.

The LMA model also clarifies some apparent hydraulic anomalies observed in the region, such as downward hydraulic gradient (and downward flow in open holes) in a groundwater discharge area (fig. D3). 3). This anomaly results from opposite directions of structural dip of the bedding fractures and river/topographic grade. The sketch shows a setup typical of sites in lower reaches of the Raritan, Rahway and Passaic Rivers (where a downward gradient would be least expected), but the situation depicted is common in upland areas where ΔH (fig. 3D) is higher.

Bedrock characterization with temporary test holes (TTHs)

Approach

Although vertical cross flows in bedrock wells may be harmful and should generally be avoided, they also offer an opportunity for rapid hydrogeologic exploration and characterization of bedrock sites, provided that two conditions for long open holes are satisfied: 1) TTHs are installed and tested under controlled conditions so that any harm from cross flows is assessed and harmful cross flows are terminated (for example, by inflating a temporary packer); and 2) The holes remain open only for a limited testing time (a few days to weeks) and then are converted to bedrock monitoring wells or are properly sealed. The scope of characterization testing is outlined in table 1; generally in the order the testing is conducted.

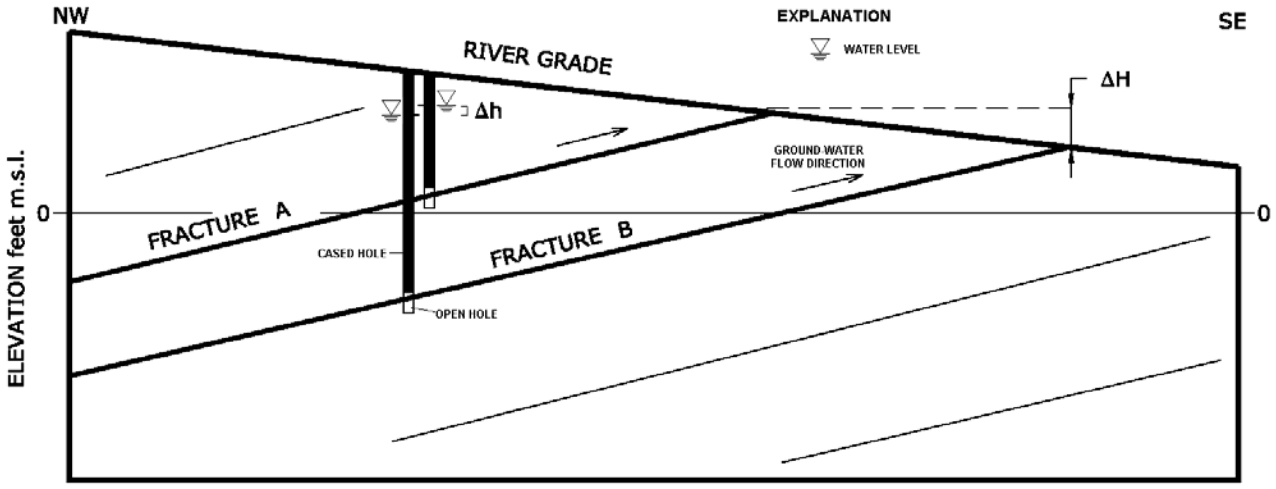

Figure D3. Groundwater discharge from bedding fractures to a river grade opposing structural dip. Although upward/updip flow prevails in each of the two transmissive bedding fractures shown, a downward vertical gradient exists between fractures A and B because of the lower elevation of fracture B at the discharge location.

Identification of transmissive fractures

Fracture identification in test holes is ordinarily the domain of borehole geophysics (for example, Keys, 1990; Hsieh and others, 1993; Paillet and Crowder, 1996). Although numerous fractures are commonly observed in rock cores or on borehole walls in the Newark basin, only a few locally transmit ground water (for example Michalski 1990; Morin and others, 1997). Identification of such transmissive fractures is successfully accomplished by use of flow-sensitive methods, specifically the following: 1) Observation of water flows during air-rotary drilling, 2) Logging/profiling of fluid specific electrical conductance (EC) and temperature, and 3) In-well flow tracing or flow-meter measurements.

Fluid electrical conductivity logging

The usefulness of EC and temperature logging stems from the principle that water entering the test hole from a transmissive fracture may exhibit a slightly different mineralization (thus different EC) and temperature than the water already in the hole. The resulting mixing can produce inflections of the EC and temperature profiles at inflow locations. Profile segments with constant EC values generally correspond to active but constant vertical flow across confining/aquitard units. Similarity of two consecutive background EC logs in a new test hole indicates that vertical crossflows and mixing have reached a near-steady state. This generally takes several hours to several days following hole completion. Although the EC log is not as revealing for locating water-exit fractures, it provides a rapid way of selecting target depths for flow-meter measurements or injection of saline slugs to trace in-well cross flows (fig. D4).

Vertical flow tracing

In-well flow tracing tests can measure the amount of cross flows and their directions in the water column

Table D1. Recommended testing program for comprehensive hydrogeologic characterization of sedimentary bedrock in a temporary test hole.

Characterization tool	Information and data sought
Drilling (Air Rotary)	Location of water-producing zones, yield estimates; lithologic variations.
Downhole Video Survey or Borehole Imaging	Location and orientation of visible fractures; lithologic variations; seeps and wet walls above the standing water.
Borehole Geophysics - Fluid Electrical Conductance and Temperature Logs - Gamma Ray Log - Caliper Log	Location of hydraulically active fractures. Marker beds for stratigraphic correlation between TTHs. Hole-diameter profile changes.
In-well Flow Tracing / Flow-meter Logs	Direction and amount of ambient vertical cross flows; Location of inflow and outflow fractures.
Discrete-Depth Flow Sampling & Analysis	Vertical distribution of contaminant concentrations, and estimate of contaminant contribution from individual inflow zones.
Packer Testing of Selected Zones in the TTH	Hydraulic head distribution along the TTH. Transmissivity estimate for fracture zones. Contaminant concentrations and water-quality data (for inflow fracture zones only).

Note: Underlined procedures show the scope of testing necessary for a limited characterization of vertical contaminant distribution.

(Michalski and Klepp, 1990), thus providing additional data on locations of evidently transmissive fractures producing the flows. Typically, the tracing test starts with the pouring of a small amount of saline tracer (30 to 60 grams of NaCl in 0.2-0.5 gallon of water for a 6-inch-diameter hole) through weighted small-diameter PVC tubing lowered to a target release depth. Fresh water "chaser" is then poured in to displace any tracer residue from the tubing before the tubing is gently pulled from the hole.

The first image of the injected tracer is then obtained through EC profiling of the water column (fig. D4; the first image 4 minutes after the injection). This first tracer image provides a reference for determining the direction and the amount of vertical flow in the hole from a series of subsequent images of the tracer obtained by repeated EC profiling over time. Location of water inflow and exit zones, and the type of inflow or exit flow (discrete versus diffuse) can be interpreted from changes in the shape and the size of the sequence of images. Evidence of an inflow zone/fracture may include persisting disturbance of the sequential tracer images at the inflow location (fig. D4) and an increased tracer velocity downstream of the inflow location. A flow-exit-zone/fracture is recognized by a decreasing size and disappearance of the tracer image at the exit zone (the loss of tracer mass from the hole), and/or by slower tracer velocity beyond the exit location (fig. D4). Local tracer velocity value is calculated from the vertical distance traveled by a selected segment of two tracer images and the elapsed time difference. Vertical flow is calculated as a product of the local velocity and the cross-sectional area of the hole.

In-well flow tracing enables detection of inflow and vertical flow velocity as low as 0.1 cm/min, approximately 20 times more precise than the reported resolution of a high-resolution heat-pulse flow meter (2 cm/min; Hess, 1985). The latter resolution corresponds to an undetected vertical flow of about 130 gal/day in a 6-inch-diameter well. Some commercial flowmeters are unreliable for measuring flows below 1,000 gal/day (0.7 gpm), and are about 80 percent accurate for upward flows rated at 0.7 to 25 gpm (Herman, 2006). Most bedrock wells in the region, when tested under non-pumping conditions, have vertical flows that are important for long-term contaminant migration at a site but are below the resolution of commercial flow meters. In addition to its enhanced accuracy, in-well flow tracing provides a continuous record of vertical flow and an average vertical flow velocity for selected hole segments. The vertical flow record provides some information on the vertical distribution of hydraulic head in the tested open hole relative to a composite water level based on this simple rule: the head in any inflow-producing zone or fracture is higher than the composite head and lower in any outflow fracture/zone.

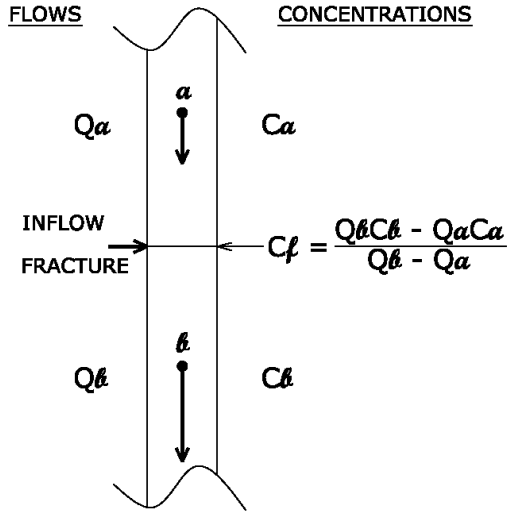

Figure D5. Contaminant concentration in an inflow-producing fracture (Cf) based on measured flows in open hole above (Qa) and below (Qb) the fracture and contaminant concentrations in depth-discrete water samples above (Ca) and below (Cb) it.

Characterization of individual transmissive fractures (aquifer units)

Depth-discrete vertical-flow sampling

Where water quality is of major concern, depth-discrete sampling permits a rapid screening-level assessment of contaminant concentrations in all inflow fractures/zones identified in the TTH through in-well flow tracing. Figure D5 shows a segment of an open hole with an inflow-producing fracture and a formula for calculating a contaminant concentration in the inflow fracture. The calculation is based on the measured vertical flow above and below the fracture, and contaminant concentrations in depth-discrete flow samples collected above and below the inflow fracture. The formula is derived from the principle of contaminant mass preservation upon simple mixing under an assumed steady-state vertical flow in the hole. The computational setup in figure D5 is comparable to determining the contaminant concentration in an inaccessible tributary stream based on the measured flows and contaminant concentrations in the main river at sections located upstream and downstream of the confluence.

The depth-discrete analytical samples obtained above and below the inflow fracture should be collected outside a zone of inflow mixing with water moving through the hole. An existing baseline EC log can be used to assess the extent of the mixing zone. The

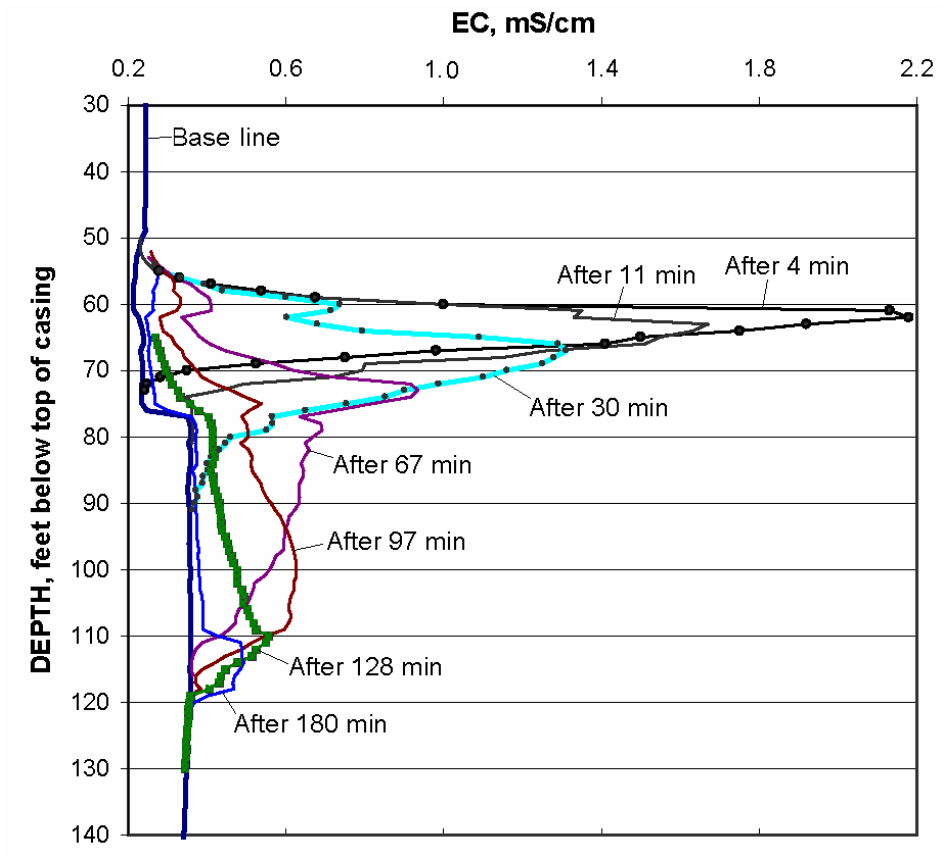

Figure D4. Series of tracer images obtained with a hand-held EC probe during in-well flow tracing test in a TTH. Saline tracer solution was injected to straddle a bedding fracture at a depth of 62 ft. Fresh water inflow from this fracture not only produced a downward migration of the tracer but also produced a disturbance on each consecutive tracer image at the inflow depth – an indication of discrete nature of the inflow. Another inflow from a fracture at 76 ft depth is indicated by faster migration of the tracer toward exit fractures at 110 ft and 118 ft. Calculated downward flow was 0.35 gpm below 62 ft depth and 1.3gpm below 76 ft depth.

depth-discrete sampling should also be conducted in a way that limits disturbance to the cross-flows. A low-flow sampling technique is suitable for collection of such samples, if purging is limited to a small submersible pump and connecting tubing. Alternatively, a Kemmerer sampler may be used (Michalski and others, 1992). The depth-discrete sampling, if conducted after completion of in-well flow tracing, offers an inexpensive but powerful tool for speedy determination of vertical distribution of contaminants within the TTH. Experience from several sites shows this tool yields very similar contaminant concentrations as those derived from standard straddle-packer sampling of inflow zones. Results of depth-discrete sampling, together with measured vertical cross flows, enable one to quantify possible contaminant migration through the TTH and to decide whether the test hole may be kept open for additional testing. Early determination of contaminant concentrations in inflow-producing fractures intersecting the hole may also aid in locating migration pathways and source(s) of the detected contamination.

Packer testing

Although packer tests are commonly used in bedrock wells and test holes, their role is usually limited to sampling of packer-isolated test zones. For a complete characterization of individual transmissive fractures, packer testing can easily be expanded to include hydraulic-head measurement (head profiling) and transmissivity determination of specific transmissive fractures identified in a TTH, as outlined below.

A complete packer test setup includes three pressure transducers that are set 1) within, 2) directly above and 3) directly below the packer-isolated interval that contains a transmissive fracture. It is helpful to reset all transducer readings to zero prior to inflation of the packers (fig. D6). A stabilized reading of the test-zone transducer upon inflation of the packers (but prior to any pumping) corresponds to the hydraulic head value in the fracture tested relative to an ambient water level in the test hole measured just prior to the inflating of the packers. This ambient head is actually a composite of the heads in all transmissive fractures involved in the crossflows.

A constant-rate pumping of the packed-off fracture interval, performed as part of a purging routine prior to sampling, is used to calculate the transmissivity (T) of the fracture-straddling length of test interval (L) in a given radius (r) of the test hole, and the measured stabilized drawdown value (s) at the applied constant pumping rate (q), based on the following form of the steady-state (Thiem) formula (National Research

Council, 1996; Cedergren, 1986; p. 53):

$$T = (q/2\pi s) \ln (L/r).$$

A water-quality sample is collected from the test zone upon its proper purging near the end of the pumping. The full packer test record can also provide useful information on hydraulic relations of the packer-isolated bedding fracture to other transmissive bedding fractures (aquifer units), including degree of vertical confinement or leakage, position of a controlling fracture within the TTH, and recharge conditions (fig. D6).

Figure D7 summarizes the calculated transmissivity values for seven packer-tested zones in a TTH. The most highly transmissive fracture, at a depth of 122 feet, yielded a transmissivity value of 7,900 gpd/ft and accounts for an estimated 95 percent of the total transmissivity of this 200-foot-deep test hole. Three other transmissive fractures above that fracture yielded transmissivity values typical of minor aquifer units.

Although packer samples from inflow-producing fractures are representative of native water quality, those from zones straddling outflow/exit fractures generally are not because of the quantities of water injected into such fractures by spontaneous cross flows in the TTH prior to packer testing. Purging of packer-isolated outflow zones may be inadequate to eliminate prior cross-flow impacts. Any packer sampling that neglects such impacts may provide misleading representation of vertical contaminant distribution. For this reason, results of in-well flow tracing and depth-discrete sampling are important for planning and interpreting packer sampling results.

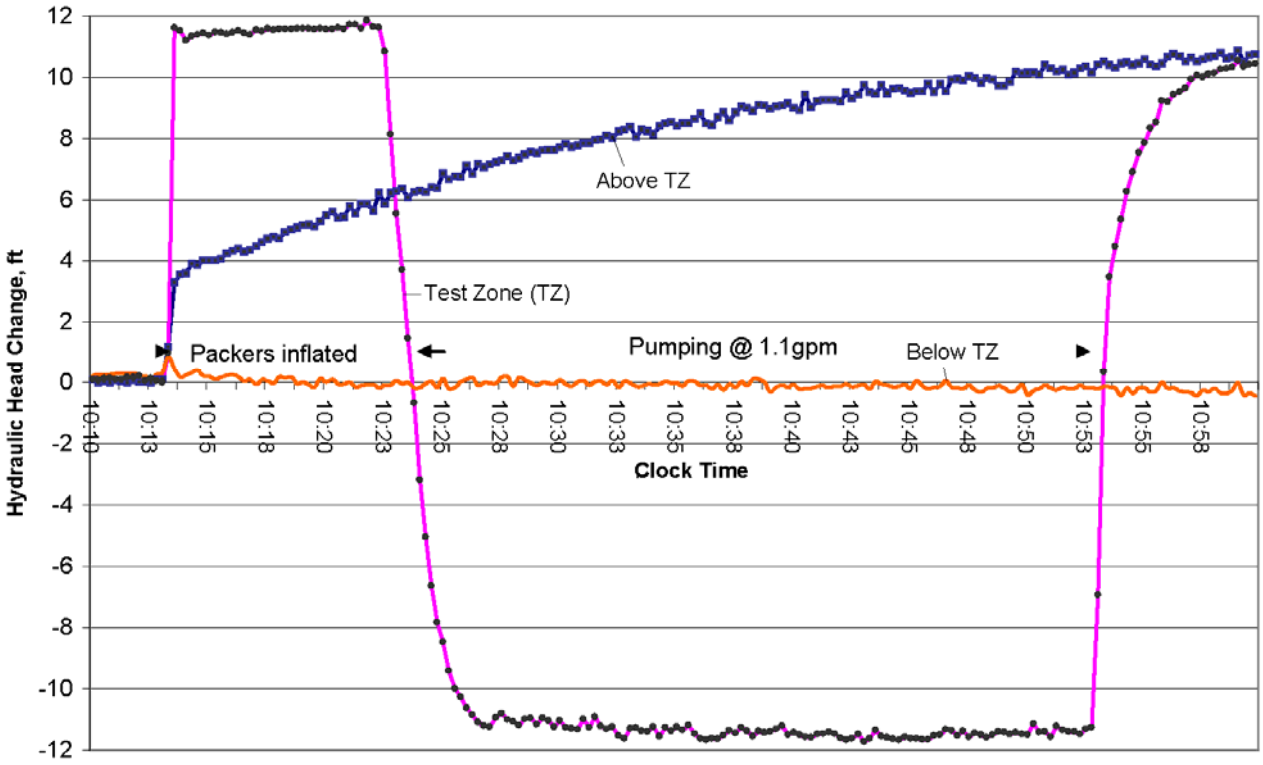

Figure D6. Pressure transducers records during a packer test straddling a minor bedding fracture. All three transducers were zeroed prior to inflating the two packers at 10:14. Upon inflating, the head in the test zone increased by nearly 12 ft above an ambient water level in the open hole. Constant rate pumping from the test zone started at 10:23 and continued for 30 minutes. Note that this pumping had practically no impact on the transducer readings above and below the test zone, indicating its hydraulic confinement. This test zone straddled the 62-ft inflow fracture identified in figure D4. The transducer readings above the test zone continued to rise, responding to continued water buildup above the upper packer after suppression of prior downward flow. Slightly negative readings below the test zone reflected a new composite head in fractures below the lower packer. Main outflow fracture from this test hole was at a depth of 110 ft (fig. D4).

Conversion of TTHs to monitoring wells

Native water quality and contaminant concentrations in the exit fracture can be determined only after this fracture interval is targeted for permanent monitoring at the completion of the TTH testing program, and sufficient time has elapsed to clear the impact of prior cross-flow injection. The criteria for selecting intervals for permanent groundwater monitoring follow this sequence: 1) water-exit fracture, 2) the most transmissive fracture, 3) the most contaminated interval, 4) hydraulic head distribution, and 5) vertical delineation required for contaminants of concern. Because of a common overlap of two or more of these criteria (for example, a water exit fracture may be the most transmissive and also exhibit the lowest hydraulic head), two or three intervals selected for permanent monitoring may suffice for most TTHs.

In order to monitor water levels (for horizontal gradient and flow direction) and contaminant concentrations (for plume delineation), at least three short-screen wells/piezometers need to be installed in each transmissive bedding fracture (aquifer unit) selected for monitoring.

Development of site-specific LMA model and its verification

Information on depth of transmissive fractures in individual TTHs, together with data on fracture-transmissivity values, cross flows, relative

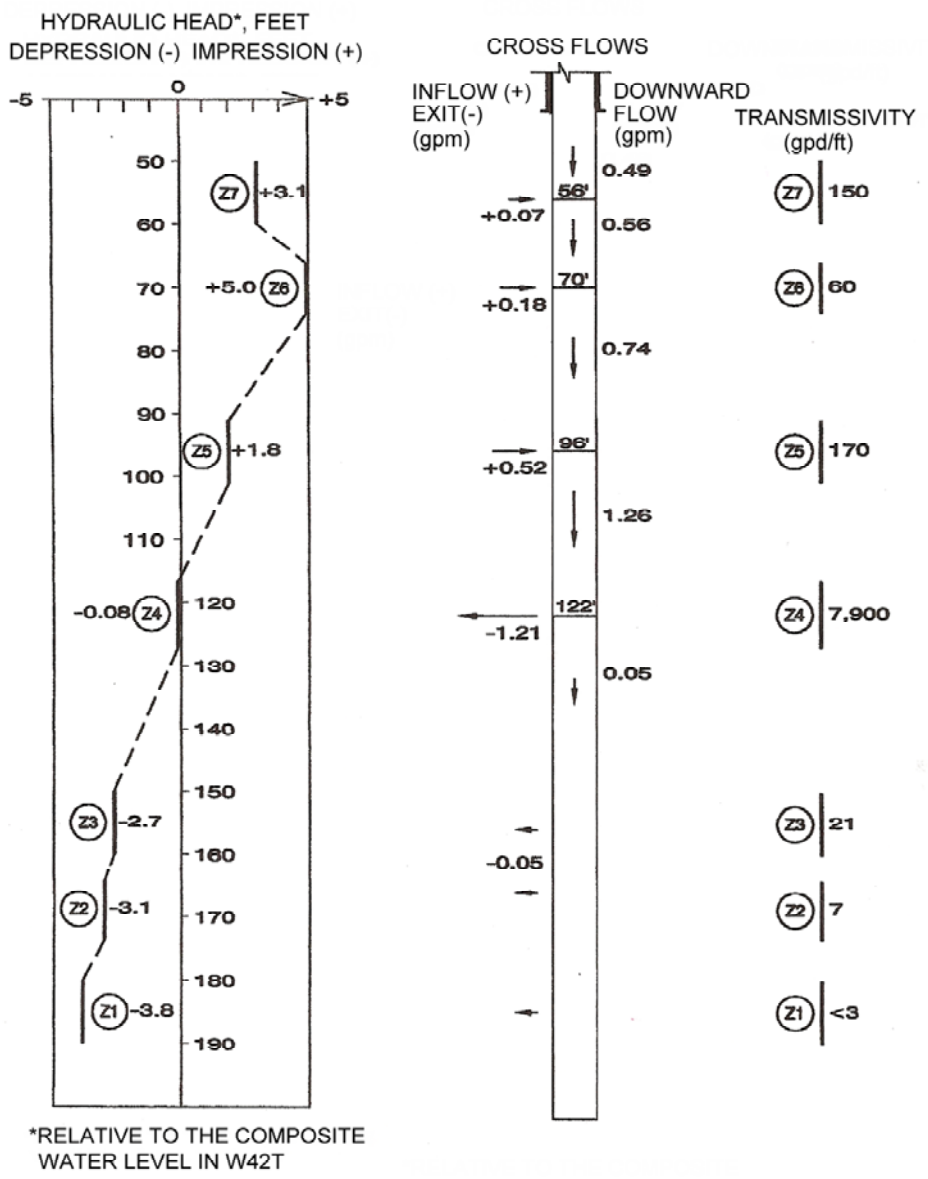

Figure D7. Synthesis of packer-testing (left figure) and in-well flow tracing (middle figure) results (hydraulic-head profile and transmissivity distribution) at another site in northern New Jersey. Note a very high transmissivity for the main exit fracture at a depth of 122 ft. Lower heads and slight downward flow in an aquitard section below this fracture was attributed to regional pumping.

heads (fig. D7) and contaminant distribution, provide the basis for a site-specific conceptual model of groundwater flow and contaminant transport in the bedrock. Relevant information from each TTH is projected on a cross section perpendicular to the local strike of beds. Traces of all significantly transmissive fractures are plotted on the cross section to identify those that follow the trace of the bedding plane in several holes. Major confining units (aquitards) are also identified in the cross section. An early model of site-specific bedrock hydrogeology is important, even if it may need major refinements following additional inter-well verification tests. Such refinements generally require additional TTHs, monitoring wells or piezometers to resolve specific issues of concern. Short-term pumping tests and contaminant plumes provide adequate verification tools for a site-specific LMA flow model. A short-term pumping test can verify the presence or absence of a direct hydraulic connection of a major transmissive fracture between test holes/wells: Owing to the low storativity but high transmissivity of such a fracture, it takes only seconds to a few minutes for the pumping stress to propagate over distances of as much as 1,600 ft (Michalski and Britton, 1997). Routine well purging prior to sampling can be treated as a short-term pumping test. Such verification tests can disclose suspected breaks in the continuity of a bedding fracture tested between the pumping and observation holes, either due to faulting (for example LaCombe, 2000) or to mineralization clogging the fracture. The latter may consist of locally tight areas of residual gypsum and calcite mineralization within an otherwise transmissive bedding fracture, which this author has observed at some sites. Dissolution of mineral infilling from fractures and sedimentologic features, such as root holes and mudcracks, are considered important in the development of secondary porosity (Herman, 2001).

Costly standard-duration pumping tests, interpreted in terms of standard computational models overlooking the multi-unit structure of bedrock, may lead to confusing interpretations and ambiguous results. For a multi-unit bedrock system, the determinations of hydraulic parameters, hydraulic gradients and an accurate direction of groundwater flow (and dissolved plume migration), need to take into account specific major transmissive fractures treated as aquifer units. Unless a multi-unit aquifer structure is properly recognized and accounted for in a remedial action design, long-term remedial pumping may result in

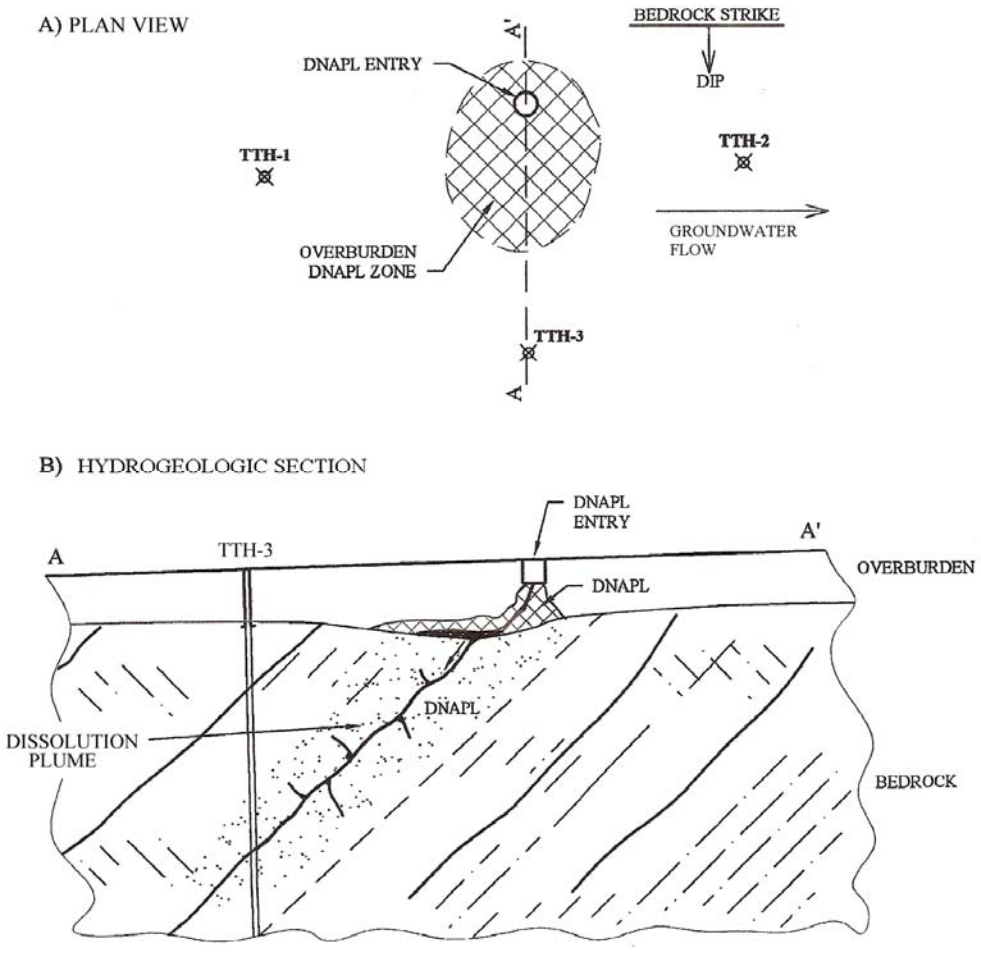

Figure D8. Three TTHs at a suspected DNAPL bedrock site positioned with regard for the suspected source location, bedrock structure and presumed groundwater-flow direction.

inadvertent spreading of contaminants into previously uncontaminated aquitard and aquifer units.

Use of TTHs for characterization of DNAPL sites

A strategy of employing TTHs on a site believed to be contaminated by dense solvents (DNAPL) is presented in figure D8. The key factors considered in the placement of TTHs are: 1) the strike of bedding, which controls groundwater flow and dissolved-plume migration within transmissive bedrock fractures, and 2) location of a suspected DNAPL entry area and possible DNAPL zone in the overburden. The first test hole (TTH-1) is situated upgradient of the DNAPL zone. This pilot hole is intended to identify and characterize discrete aquifer units penetrated, including background (upgradient) water quality in individual units. The second hole (TTH-2) is located downgradient of the overburden DNAPL zone and along strike with respect to TTH-1 (fig. D8). These two holes provide information on bedrock hydrostratigraphy in the suspected source area and on source impacts on downgradient groundwater quality in transmissive bedrock fractures (aquifer units) identified in these test holes.

The third hole (TTH-3) is installed to explore the depth of possible solvent product penetration in downdip direction. As the DNAPL tends to preferentially invade large-aperture fractures (Kueper and McWhorter, 1991), any major bedding fracture (that is any major aquifer unit in the LMA concept) with its subcrop connected to the overlying DNAPL zone becomes a potential preferential pathway for a downward (downdip) product migration. Therefore, TTH-3 should be installed down-section of the overburden DNAPL zone (fig. D8). This deeper hole should intercept, at a minimum, a major aquifer unit whose subcrop is directly beneath the overburden DNAPL zone. In figure D8B, the dashed line parallel to the bedding gives a graphical estimate of the depth of TTH-3. The determination of possible DNAPL penetration is commonly based on comparing dissolved-solvent concentrations obtained from the discrete-depth cross-flow samples from TTH-3 against solvent aqueous solubility (Pankow and Cherry, 1996).

This strategy incorporates the "outside-in" approach (Pankow and Cherry, 1996) to minimize the potential for inducing contaminant migration during investigation of suspected DNAPL sites. The investigation starts with assessing impacts of the DNAPL zone on the dissolved plume and then proceeds to assess the DNAPL source itself. The three-hole strategy enables the hydrogeologist to complete a fast, cost-effective and comprehensive characterization of bedrock hydrostratigraphy and vertical contaminant distribution, in the framework of a site-specific LMA model.

Implications for site remediation

The bedrock-characterization strategy outlined here is rooted in a generic model of sedimentary bedrock as a leaky multi-unit aquifer, in which a few transmissive bedding fractures function as aquifer units and preferential-flow pathways. The use of temporary test holes (TTHs), and their subsequent conversion to permanent monitoring wells, facilitates a rapid and comprehensive hydrogeologic characterization of bedrock sites and the development of realistic and verifiable site-specific flow and transport models for such sites. Several parameters, such as vertical flow, transmissivity, hydraulic head, and contaminant distribution are simultaneously characterized, which offer cost-savings in remedial investigations. This approach can also be extended to other problem sites, including those with old supply wells and a record of unsuccessful remediation efforts. Such sites may require hydrogeologic re-evaluation based on the LMA model that offers a realistic and testable representation of bedrock hydrogeology and the contamination problem.

This practical characterization strategy was developed and tested at many sedimentary-bedrock sites in the Newark basin, including suspected DNAPL sites that commonly pose the greatest characterization challenge. It may also be applicable to other bedrock settings marked by preferential groundwater flow along a few transmissive fractures.

References

Cedergren, H.R., 1986, Seepage, drainage, and flow nets. 3rd edition: Wiley-Interscience, New York, New York, 465 p.

Herman, G.C., 2001, Hydrogeologic framework of bedrock aquifers in the Newark basin: *in* LaCombe, P.J. and Herman, G.C., eds., Geology in Service to Public Health, 18th Annual Meeting of the Geological Association of New Jersey, p. 6-45.

Herman, G.C., 2006, Field tests using a heat-pulse flow meter to determine its accuracy for flow measurements in bedrock wells. N.J. Geological Survey Technical Memorandum TM 06-1, 8 p.

Herpers, H. and Barksdale, H.C., 1951, Preliminary report on the geology and ground water supply of the Newark, New Jersey, area. N.J. Department of Conservation and Economic Development Division of Water Policy and Supply Special Report 10, 52 p.

Hess, A.E. 1985, Identifying hydraulically-conductive

fractures with a low-velocity borehole flowmeter: Canadian Geotechnical Journal. v.23, no.1, p. 69-78.

Hsieh, P.A., Shapiro, A.M., Barton, C.C., Haeni, F.P., Johnson, C.D., Martin, C.W., Paillet, F.L., Winter, T.C. and Wright, D.L., 1993. Methods for characterizing fluid movement and transport in fractured rocks: Field Trip Guidebook for the Northeastern United States: 1993 Boston, v. 2, contr. no. 67, Dept. of Geology and Geography, Univ. of Mass., Amherst, Mass.

Keys, W.S., 1990, Borehole geophysics applied to groundwater investigations: U.S. Geological Survey Techniques of Water-Resources Investigations, Book 2, Ch. E2, 150 p.

Kueper, B.H. and McWhorter, D.W., 1991, The behavior of dense, non-aqueous phase liquids in fractured clay and rock: Ground Water, v. 31, p. 716-728.

LaCombe, P.J. 2000, Hydrogeologic framework, water levels, and trichloroethylene contamination, Naval Air Warfare Center, West Trenton, New Jersey, 1993-97: U.S. Geological Survey Water- Resources Investigations Report 98-4167, 139 p.

Lewis-Brown, J. and dePaul, V. T., 2000, Groundwater flow and distribution of volatile organic compounds, Rutgers University Bush Campus and vicinity, Piscataway Township, New Jersey: U.S. Geological Survey Water Resources Investigations Report 99-4256, 72 p.

Michalski, A., 1990, Hydrogeology of the Brunswick (Passaic) Formation and implications for ground water monitoring practice: Ground Water Monitoring Review, vol. X, no. 4, p. 134-143.

Michalski, A. and Britton, R., 1997, The role of bedding fractures in the hydrogeology of sedimentary bedrock - evidence from the Newark basin, New Jersey: Ground Water, v. 35, p. 318-327.

Michalski, A., Britton, R. and Uminski, A.H., 1992, Integrated use of multiple techniques for contaminant investigations in fractured aquifers: A case study from the Newark basin, New Jersey: Proc. Focus Conf. on Eastern Reg. Ground Water Issues, Oct. 13-15, Boston Mass., published by NGWA, Dublin, OH, p. 809-826.

Michalski, A. and Klepp, G.M., 1990, Characterization of transmissive fracture by simple tracing of in-well flow: Ground Water, v. 28, no. 2, p. 191-108.

Morin, R.H., Carleton, G.B. and Poirier, S., 1997, Fractured-aquifer hydrogeology from geophysical logs; the Passaic Formation, New Jersey: Ground Water, v. 35, p. 328-338.

National Research Council, 1996, Rock fractures and fluid flow – Contemporary understanding and applications: National Academy Press, Washington D.C., 551 p.

Olsen, P.E., 1980, The Latest Triassic and Early Jurassic formations of the Newark basin (Eastern North America, Newark Supergroup): stratigraphy, structure, and correlation: New Jersey Academy of Science Bulletin, v. 25, p. 25-51.

Paillet R.F. and Crowder, R.E., 1996, A generalized approach for the interpretation of geophysical well logs in groundwater studies - theory and application: Ground Water, v. 34, no. 5, p. 883-898.

Pankow, F.J. and Cherry, J.A., 1996, Dense chlorinated solvents and other DNAPLs in groundwater: history, behavior and remediation: Waterloo Press, Portland, Oregon, 522 p.

Schlische, R.W., 1992, Structural and stratigraphic development of the Newark extensional basin, eastern North America: Evidence for the growth of the basin and its bounding structures: Geological Society of America Bulletin, v. 104, p. 1026-1042.

Sources, Mobilization and Transport of Arsenic in Groundwater in the Passaic and Lockatong Formations of the Newark basin, New Jersey

By Michael E. Serfes, N.J. Geological Survey,
Gregory C. Herman, N.J. Geological Survey,
Steven E. Spayd, N.J. Geological Survey, and
John Reinfelder, Rutgers University

Chapter E of

Contributions to the Geology and Hydrogeology of the Newark Basin

N.J. Geological Survey Bulletin 77

State of New Jersey
Department of Environmental Protection
Water Resource Management
New Jersey Geological Survey
2010

Contents

Figures

Tables

Chapter E

Sources, Mobilization and Transport of Arsenic in Groundwater in the Passaic and Lockatong Formations of the Newark Basin, New Jersey

Michael E. Serfes[1], Gregory C. Herman[1], Steven E. Spayd[1] and John Reinfelder[2]

Abstract

Arsenic (As) concentrations as high as 215 µg/L occur in bedrock aquifers of the Newark basin in New Jersey. This basin is a Mesozoic half graben filled with continental strata and intrusive and extrusive basaltic rocks. Arsenic exceeding 10 µg/L in groundwater occurs in the shallow-lake/playa-derived red mudstone and siltstone of the Passaic Formation and the black and gray shale of the underlying Lockatong Formation. As(V) is the dominant aqueous species in the more oxic red strata and As(III), in the less oxic black-gray strata. Analyses of black shale, gray shale, and red mudstone show maximum arsenic concentrations of 240, 50 and 14.8 mg/kg respectively (crustal average, 1.8 mg/kg). Electron microanalyses of pyrite in black shale confirmed that it is the major mineral source of the arsenic, containing as much as 4 weight percent. It is hypothesized that most arsenic in groundwater of the black/gray-shale-dominated Lockatong Formation is mobilized when pyrite oxidizes. Chemical equilibrium modeling based on MINEQL+ V4.5 was used to conclude that less than 50 percent of As(III) mobilized from pyrite is adsorbed on associated Fe_2O_3 products at circumneutral pHs. Elevated arsenic concentrations in groundwater in the Passaic, however, commonly occur in thick sequences of red strata that appear to be hydraulically sealed off from the intermittent beds of pyritic black-gray shale. Therefore, pyrite is not the major mineral source of arsenic in the red strata. Geochemical analyses of 15 red mudstones and siltstones (4.5 to 14.8 mg/kg arsenic) from the middle and upper Passaic revealed a very strong statistical correlation, using the Pearson product-moment correlation coefficients (r), between arsenic and REE (sum La to Lu) (r = 0.94), and strong ones respectively between arsenic and REE with Al_2O_3[clay] (r = 0.82 and 0.81) and Fe_2O_3 (r = 0.83 and 0.84). Also, a strong correlation between Al_2O_3[clay] and Fe_2O_3 (r = 0.92) indicates a clay-and-iron oxide association. Other workers have observed first-generation hematite coating clay surfaces in these rocks and it is hypothesized that arsenic is enriched in this hematite. Abiotic leach experiments targeting the water-soluble fraction in a red mudstone (14.8 mg/kg arsenic) demonstrated that the major arsenic mobilization mechanism in the red beds is desorption, and maximum aqueous concentrations occur at pH 8.0. The presence of the competitive ion phosphate further enhances maximum arsenic concentrations. These results suggest that arsenic concentrations in groundwater in contact with red strata are mainly controlled by adsorption-desorption onto hematite/goethite with a ZPC (about 7.8 to 8.5), and that competition with other oxyanions naturally occurring in groundwater, such as dihydrogen borate ($H_2BO_3^-$), molybdate (MoO_4^{2-}), and carbonate (CO_3^{2-}) could potentially enhance arsenic mobilization. High yielding dissolution-type water-bearing zones in some red strata tapped by wells optimize arsenic mobility and steady-state concentrations because an alkaline pH results when carbonate minerals dissolve and first-generation hematite is continuously exposed in the honeycombed groundwater-flow network.

Introduction

The Newark basin is a Mesozoic half graben filled with Mesozoic continental sediments extending along the mid-Atlantic coast of the United States (fig. E1.). Arsenic concentrations as high as 215 µg/L have been measured in groundwater in the basin in New Jersey (Serfes and others, 2005). The United States Environmental Protection Agency (USEPA) primary drinking water standard for arsenic in public-water supplies is 10 µg/L (USEPA, 2002). Human exposure to inorganic arsenic in drinking water has been linked to internal and external cancers and non cancer-related health impacts (IARC, 1987; NRC, 2001). Harmful arsenic concentrations in groundwater supplies are a global issue because countries on all continents are reported to be affected (Smedley and Kinniburgh, 2002).

[1]NJ Geological Survey
29 Arctic Parkway, Box 427
Trenton, NJ, 08625

[2]Rutgers University
Department of Environmental Sciences
14 College Farm Road, New Brunswick, NJ 08901

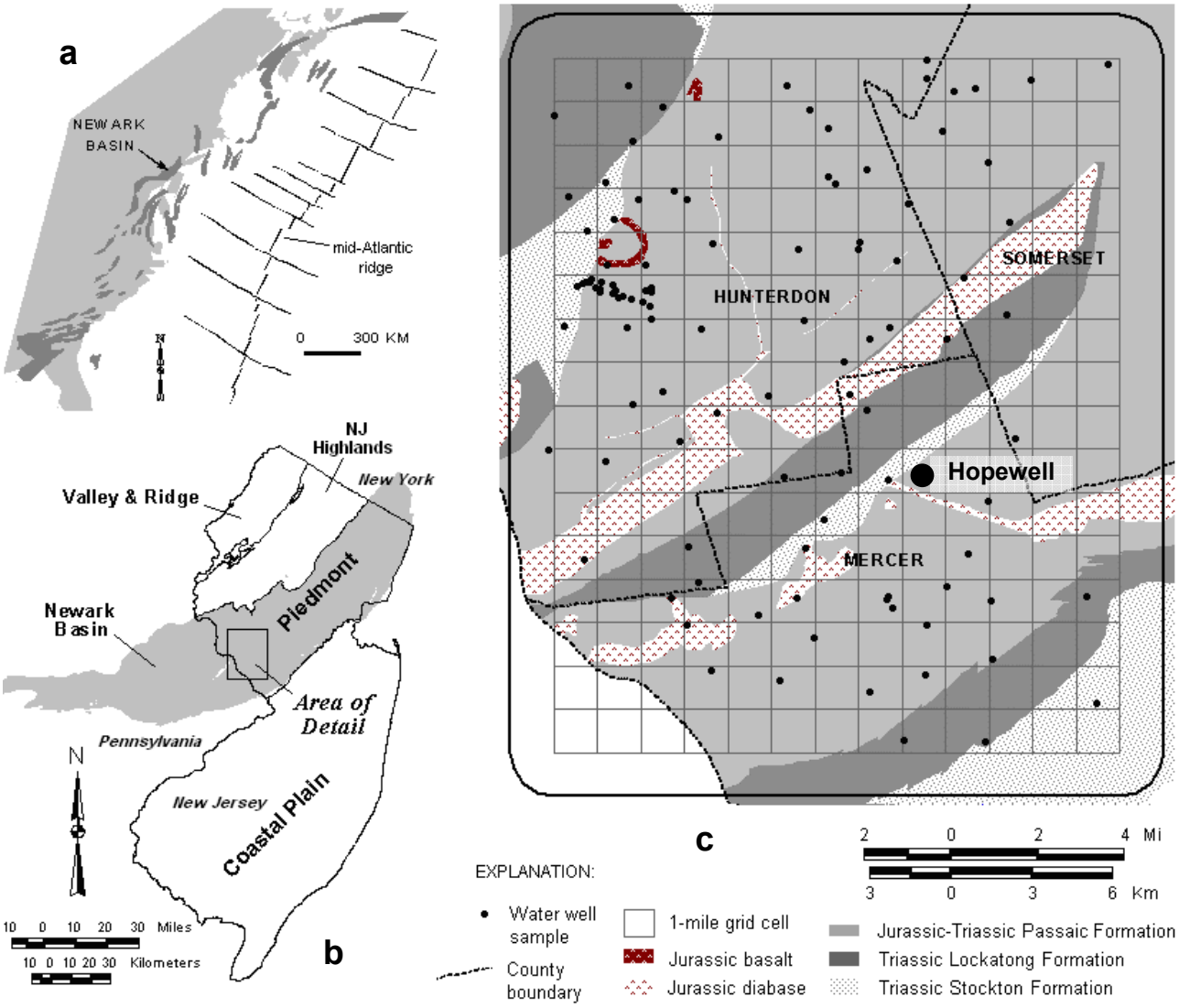

Figure E1. a) Rift basins of eastern North America and the Newark basin (modified from Schlische, 1992). b). Newark basin in relation to New Jersey. c) The 520-square-kilometer study area and location of wells sampled. Fifteen percent of wells sampled had water exceeding 10 µg/L arsenic. The Passaic and Lockatong Formations had highest occurrence and concentrations of arsenic. A detailed study was done in Hopewell.

To better understand the cause and scope of this problem in the Newark basin, this paper focuses on the following four key questions:

1. What is the spatial distribution, and hydrologic and aqueous geochemical settings associated with arsenic concentrations greater than 10 µg/L in the major bedrock aquifers of the Newark basin?

2. What are the major lithogenic sources of arsenic in those aquifers?

3. What chemical mechanisms and hydrogeologic settings favor the mobilization of arsenic from these sources?

4. What physical and chemical processes control the mass transport of arsenic in these aquifers?

Most of the focus of this paper is on the New Jersey part of the basin. However, the same formations also extend into Pennsylvania and New York. Therefore, the findings presented here may be somewhat applicable to similar geologic settings throughout the basin and perhaps also to other Mesozoic rift basins in eastern North America. Much of the information in this report is from Serfes (2005) and Serfes and others (2005).

Background

This section presents information on potential arsenic sources contaminating groundwater, the geochemistry of arsenic, and, the spatial distribution, concentration and hydrologic and aqueous geochemical settings of arsenic in the major bedrock aquifers of the Newark basin.

Arsenic sources

The first evaluation of the spatial distribution and concentrations of arsenic in the basin was made in 1998, based on data from New Jersey's ambient groundwater quality network (Serfes, 1994). The widespread detection of arsenic in the basin suggested that it was derived from dispersed nonpoint sources rather than isolated point sources of contamination. Two obvious potential nonpoint sources are arsenical pesticides in agricultural areas and naturally occurring minerals containing arsenic. Arsenical pesticides were widely used in this country, including New Jersey, from the late 1800s until the mid-to-late 1900s (Murphy and Aucott, 1998). The most extensive use in New Jersey was in fruit orchards (NJDEP, 1999). However, arsenical pesticides are only barely water-soluble, and the arsenate binds tightly to soil particles. Studies in North Dakota, South Dakota, Wisconsin and Minnesota show that groundwater is largely unaffected by past arsenical pesticide use (Welch and others, 2000). Therefore, arsenical pesticides are not considered a major source of arsenic to groundwater. The application of phosphate fertilizers however may release slugs of arsenic from those soils via competitive adsorption, resulting in seasonal spikes in arsenic concentrations in groundwater (Welch and others, 2000). This mobilization mechanism is not supported however, because concentrations in water from wells in the basin suggest they are steady-state (Serfes and others, 2005). Studies have demonstrated that sulfide mineral oxidation and iron oxide reduction are the most important mechanisms for mobilizing arsenic in groundwater (Welch and others, 2000). Therefore arsenic in groundwater in the basin is hypothesized to be mobilized from natural mineral sources, rather than arsenic-bearing pesticides. These sources are discussed in later sections.

Arsenic geochemistry

Arsenic is a heavy metalloid element with atomic number 33, one natural isotope with atomic mass number 75, and five valence states in the natural environment: -3, -1, 0, +3 and +5 (Jones and Nesbitt, 2002). It ranks fifty-second in crustal abundance, can substitute for Si^{4+}, Al^{3+}, Fe^{3+} and Ti^{4+} in many rock forming minerals and has an average crustal concentration of 1.8 mg/kg or parts per million (ppm) (Demayo, 1985; Smedley and Kinniburgh, 2002). Geological processes can enrich some rock types with arsenic relative to others. For example, arsenic is significantly enriched in fine-grained, organic-rich, sedimentary rocks, and their metamorphic equivalents compared to igneous rocks (table E1).

The occurrence, concentration and species of arsenic in groundwater are related to their locations, type and significance of their sources and their hydrogeochemical environments. In natural aqueous environments, which include low-temperature surface, ground and hydrothermal water, arsenic generally forms dissolved inorganic oxyanions (polyatomic ions that contain oxygen) including arsenite (As(III), [$H_3AsO_3^o$ at pH < 9.2]) under chemically reducing conditions, and arsenate (As(V), [$H_2AsO_4^-$ at pH < 6.9 and $HAsO_4^{2-}$ at pH > 6.9]) under more oxidizing conditions (Smedley and Kinniburgh, 2002). Both species commonly occur together because the abiotic transformation of one to the other is kinetically hindered (Masscheleyn and others,

Table E1. Range in arsenic concentrations in rock and earth materials.

Rock type	Arsenic concentration range (mg/kg)	Average concentration mg/kg	Number of samples
Basalt……	0.2 to 113	2.3	78
Granite……..	0.2 to 15	1.3	116
Slate and phyllite…….	0.5 to 143	18.1	75
Shale and argillite……	0.3 to 500	14.5	116
Coals…….	0.3 to 35,000	Not given	Not given
Iron-rich rock..……..	1 to 2900	Not given	45

From Boyle and Jonasson (1973), and Palmer and Klizas (1997).

1991). However, manganese oxides, which commonly coat hydraulic conduits in the basin, are known to rapidly oxidize As(III) to As(V) (Driehaus and others, 1995; Scott and Morgan, 1995). Although not significant for most waters, organically bound arsenic such as the methylated species monomethylarsonic acid (MMA) and dimethylarsonic acid (DMA), may be produced by microbial detoxification where arsenic and organic matter occur together (Oremland and Stolz, 2003). Arsenic is particularly mobile in the pH range 6.5 to 8.5 that is common in groundwater and some surface water. It may be mobile under both reducing and oxidizing conditions; however, the neutral complex arsenite is generally more mobile than the arsenate anion.

The fate of mobile arsenic is closely tied to the geochemical cycles of iron and sulfur and the occurrence of clay minerals (Stollenwerk, 2003). Eh, pH, and possibly microbiological activity mainly determine the redox state of arsenic, iron, and sulfur, and therefore the stability of arsenic-bearing mineral phases. Iron oxide minerals such as hematite, sulfide minerals such as pyrite, and the surface of clay minerals are all potential sinks and sources of arsenic. The reduction of iron oxides and the oxidation of sulfide minerals such as pyrite are considered the most significant mechanisms for the mobilization of arsenic into groundwater (Welch and others, 2000).

Under aerobic conditions where oxides are stable, dissolved oxyanions and hydroxy complexes of arsenic can readily adsorb to iron, aluminum, and manganese oxides, particularly iron oxides, because of their ubiquitous occurrence, and therefore they can concentrate on and in them in surface and subsurface environments (Smedley and Kinniburgh, 2002). Concentrations of arsenic in hematite and ferric oxyhydroxides may be as high as 160 and 76,000 mg/kg respectively (Baur and Onishi, 1969; Pichler and others, 1999). Metal ions exposed on oxide surfaces in aqueous environments complete their coordination shells with OH groups that bind or release H^+, depending on the pH (Stumm, 1992). The pH-dependent density of the surface functional groups OH_2^+, OH, and O^-, makes up the active binding sites and affects the overall surface charge of the absorbent. Therefore, at pH values below the adsorbents point of zero charge (PZC), pH at which the net surface charge is zero, the surface is dominated by OH_2^+, and above it O^-, yielding a net positive and negative charge respectively. For example, goethite (FeOOH) and hematite (Fe_2O_3) have a point of zero charge of ~7.8 and 8.5 respectively (Stumm, 1992). The complexation of arsenite and arsenate at the metal-oxide surface is mainly associated with ligand exchange with those functional groups. The anion arsenate ($H_2AsO_4^-$) is more strongly retained at lower pH values when the net surface charge is positive, and arsenite ($H_3AsO_3^o$) is at higher pH values (Wilkie and Hering, 1996). Experimental work using goethite as an absorbent showed that the adsorption of As(V) is more likely than that of As(III) below pH 5-6, and above pH 7-8 As(III) has a greater affinity for absorption onto the solid (Dixit and Hering, 2003). Both arsenic species mainly form bidentate binuclear surface complexes (Manning and others, 1998, Sun and Doner, 1996). Like oxide minerals, the Al ions exposed at clay mineral edges can also form inner sphere complexes with adsorbed arsenic (Foster, 1999). Other oxyanion, hydroxy complex, and anion forming elements that may also be adsorbed onto iron oxide surfaces, and possibly trapped as absorbed impurities and onto clay edges include vanadium, boron, fluorine, molybdenum, selenium, uranium, chromium, rhenium and phosphorus (Smedley and Kinniburgh, 2002). Aqueous complexes of these elements can compete with arsenic for adsorption sites.

The nucleation and growth of pyrite occurs in anoxic environments where sulfide and ferrous iron are stable. Arsenic is a chalcophile (sulfur loving) element that substitutes for sulfur as As(-1) in the structure of pyrite (Savage and others, 2000). Arseniferous pyrite is generally the most ubiquitous arsenic-bearing sulfide mineral, and micron-scale spot concentrations have been shown to occur as high as 8.50 and 9.97 weight percent in sedimentary and hydrothermal pyrite, respectively (Kolker and others., 1998; Plumlee 1989).

The types and significance of arsenic sources and the hydrogeochemical and hydrologic settings that exist in the Newark basin ultimately control the occurrence of arsenic in its aquifers. These sources and settings are directly related to the original depositional and diagenetic environments that preserved some primary minerals, altered others, and to varying degrees controlled the formation of secondary minerals. A summary of the analytical methods used here and the geologic, hydrogeologic, and hydrogeochemical settings in the basin follows.

Analytical methods

The water-quality characteristics in tables E2, E3 and E4 are for the Passaic, Lockatong and Stockton Formations respectively and are described in Serfes (1994) along with a reference to the analytical methods used. Water samples collected from domestic wells for the spatial analysis of arsenic occurrence were analyzed using inductively coupled plasma-mass spectroscopy (ICP-MS), EPA Method 200.8 at Environmental Health Laboratories, a New Jersey certified laboratory, in Indiana. Aqueous samples from the Hopewell 6 case study were analyzed for arsenic and other elements using ICP-MS, ICP-OES techniques at Activation Laboratories in Ancastor, Ontario in Canada. Whole-rock geochemical analyses of all rock samples discussed in this paper were determined using the MER

Table E2. Chemical and physical groundwater summary for the Passaic Formation (Serfes, 1994).

Characteristic or constituent	Number of samples	Minimum	25th percentile	Median	75th percentile	Maximum
Temperature (^{o}C) ……..	94	9.5	12.5	13	13.5	14.5
Specific conductance (µS/cm)[1]…	94	155	374	450	632	2040
Dissolved Oxygen (mg/L)[2]……..	94	<0.1	0.7	2.9	5	14.7
PH (standard units)…….	95	6	7.4	7.6	7.8	9.3
Field alkalinity (mg/L as $CaCO_3$)..	95	21	112	141	161	338
Major and minor dissolved constituents in mg/L (water filtered through a 0.45-micron filter)						
Calcium…….	94	3	40	50	73	365
Magnesium……..	94	1.4	12	16	21	69
Sodium……..	94	2.1	12	15	27	270
Potassium…….	94	0.4	1	1.3	1.9	6.6
Chloride…….	94	2.8	12	18	32	110
Sulfate…….	94	1.1	29	44	78	1200
Silica……..	94	11	19	22	25	45
Trace and minor dissolved constituents in µg/L[3] (water filtered through a 0.45-micron filter)						
Barium……..	71	<2	27	80	205	1100
Iron…….	94	<3	<3	22	60	11000
Lithium……..	71	<4	18	24	33	100
Manganese……..	94	<1	<1	2	46	1600
Strontium ……	71	50	225	530	925	11000
Zinc……....	94	<3	6	18	50	740

[1]µS/cm - microsiemens per centimeter, [2]mg/L - milligrams per liter, [3]µg/L - micrograms per liter

Table E3. Chemical and physical groundwater summary for the Lockatong Formation (Serfes, 1994).

Characteristic or constituent	Number of samples	Minimum	25th percentile	Median	75th percentile	Maximum
Temperature (^{o}C) ……..….	22	10.5	12.5	13	13.5	17
Specific conductance (µS/cm)[1]....	22	221	336	447	585	900
Dissolved Oxygen (mg/L)[2]……..	22	<0.1	0.2	0.5	2.5	7.5
PH (standard units)…….	22	6.6	7.2	7.6	7.7	8.8
Field alkalinity (mg/L as $CaCO_3$).	21	61	93	151	220	321
Major and minor dissolved constituents in mg/L (water filtered through a 0.45-micron filter)						
Calcium…….	22	2.50	30	46	55	79
Magnesium……..	22	1.2	7.8	11	21	37
Sodium……..	22	7	12	27	35	140
Potassium…….	22	0.8	1.5	2.7	4.7	6.6
Chloride…….	22	1.7	6.2	11.5	26	70
Sulfate…….	22	10	17	41	62	135
Silica……..	23	13	20	26	34	42
Trace and minor dissolved constituents in µg/L[3] (water filtered through a 0.45-micron filter)						
Barium……..	21	10	33	73	153	1200
Iron…….	22	<3	7	19	260	2900
Lithium……..	21	6	9	16	25	96
Manganese……..	22	<2	11	26	260	790
Strontium ……..	20	78	240	460	520	730
Zinc…….	22	7	12	30	170	1100

[1]µS/cm - microsiemens per centimeter, [2]mg/L - milligrams per liter, [3]µg/L - micrograms per liter

Table E4. Chemical and physical groundwater summary for the Stockton Formation (Serfes, 1994).

Characteristic or constituent	Number of samples	Minimum	25th percentile	Median	75th percentile	Maximum
Temperature (°C).....	29	11.5	12.5	13	13.5	16.5
Specific conductance (µS/cm)[1]....	29	140	287	346	400	808
Dissolved Oxygen (mg/L)[2].....	29	0.1	1.0	2.9	5.1	7.7
PH (standard units).....	29	5.5	6.6	7	7.6	8.6
Field alkalinity (mg/L as $CaCO_3$)..	29	21	85	104	145	177
Major and minor dissolved constituents in mg/L (water filtered through a 0.45-micron filter)						
Calcium.....	29	7.8	27	36	43	47
Magnesium.....	29	0.27	10	13	16	25
Sodium.....	27	7.8	9.1	13	15	155
Potassium.....	29	0.8	1	1.3	1.7	302
Chloride.....	29	3.3	11	13	21	130
Sulfate.....	29	5.1	18	23	37	94
Silica.....	29	11	19	23	26	29
Trace and minor dissolved constituents in µg/L[3] (water filtered through a 0.45-micron filter)						
Barium.....	25	26	135	160	220	390
Iron.....	29	<3	<3	6	17	1200
Lithium.....	25	4	6	8	9	47
Manganese.....	29	<1	<1	4	40	500
Strontium.....	25	71	168	290	423	580
Zinc.....	29	<3	11	21	43	140

[1]µS/cm - microsiemens per centimeter, [2]mg/L - milligrams per liter, [3]µg/L - micrograms per liter

method at XRAL Laboratories in Don Mills,Ontario Canada. This multi-method, multi-element analysis uses X-ray fluorescence, ICP, Neutron Activation Analysis, ICP-MS and atomic adsorption spectrophotometry to obtain high-quality quantitative analyses of as many as 64 elements. Standard procedure is to dry, crush to 2mm, riffle to a maximum split of 250g, and mill in chrome steel equipment to 75µ. Silica sand cleaners were used between samples to minimize the risk of contamination from mineralized samples. Approximately 20 grams or more of each sample were sent to XRAL, this exceeds their required 5-gram minimum.

Samples were also collected for analysis of arsenic species from select wells using opaque containers and an ethylenediaminetetraacetic acid (EDTA) preservative to minimize metal oxyhydroxide precipitation, as described in Bednar and others, (2002). These samples were analyzed at the U.S. Geological Survey Laboratory in Denver Colorado using a liquid chromatograph with an anion exchange column to separate the arsenic species As(III), dimethylarsinate (DMA), monomethylarsonate (MMA), and As(V), followed by analysis using ICP-MS to quantify species concentrations.

Hydrogeologic setting

Geology

The Newark basin (fig. E1a) occupies a belt of tectonic-fault-bounded extensional basins that formed along eastern North America during the Late Triassic and Early Jurassic periods (Olsen, 1980). These basins are filled with continental sedimentary strata and igneous rocks, and are graben structures that reflect the western limit of continental rifting during the opening of the Atlantic Ocean. Some are exposed at the surface, others are buried under coastal-plain and glacial sediments, and some are buried on the continental shelf. The Newark basin is the largest of those exposed, covering about 7500 km^2, and extending about 190 km from eastern Pennsylvania through New Jersey and into southwestern New York, with a maximum width of about 50 km (fig. E2).

The basin is characterized as a half-graben with northeast striking and southeast dipping faults along its northwestern border (fig. E2). These border faults probably originated as Paleozoic thrust faults and were later reactivated with normal dip-slip movement during continental extension beginning approximately 230 Ma (Schlische, 1992). As the depth, width and length of the basin increased,

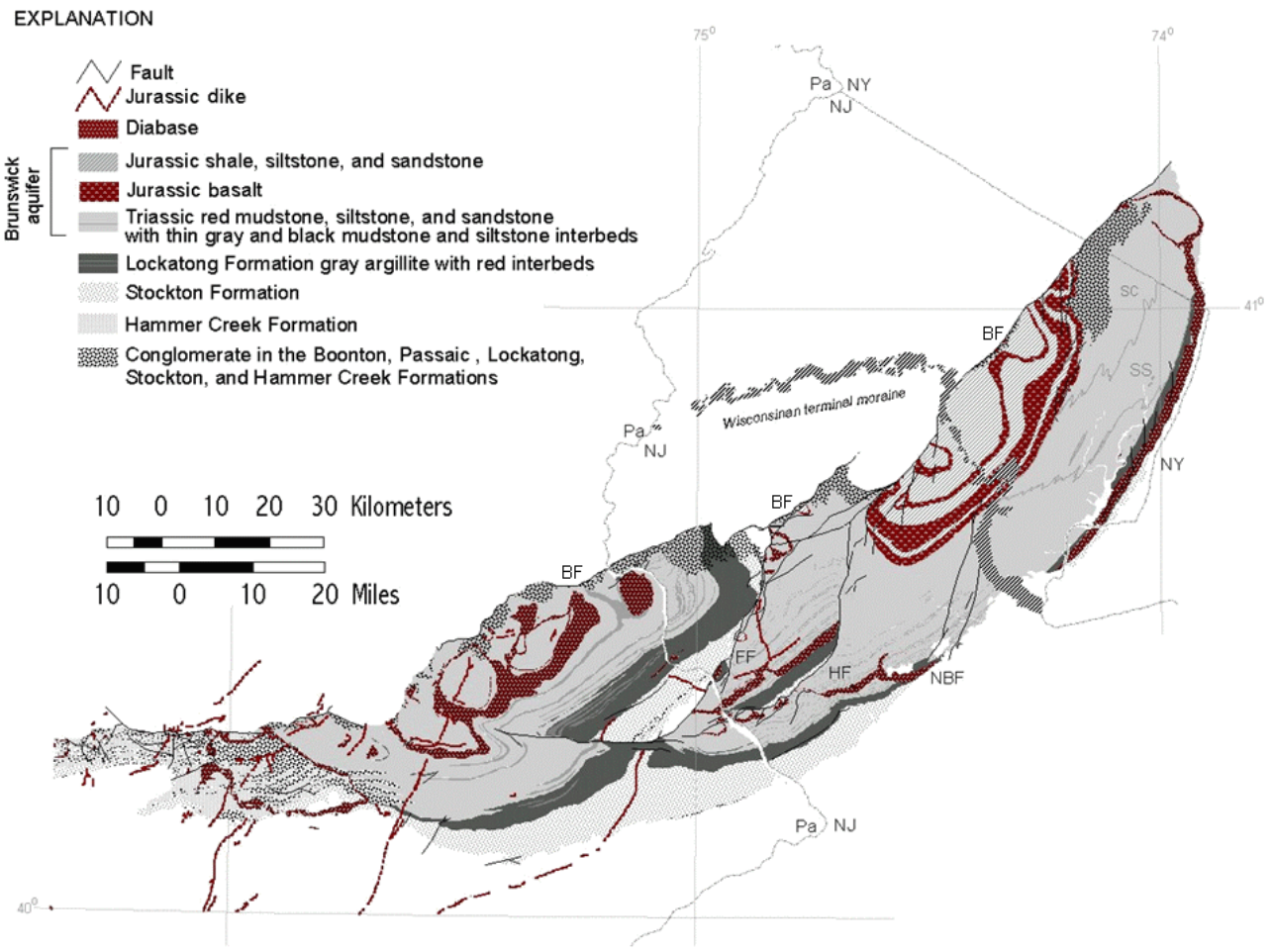

Figure E2. Geology of the Newark basin showing the Wisconsinan terminal moraine. BF – border fault, FF – Flemington fault, HF – Hopewell fault, NBF – New Brunswick fault, SC – sandstone and conglomerate facies of the Passaic Formation, SS – sandstone and siltstone facies of the Passaic Formation.

reflecting syndepositional fault movement, it filled with as much as 6-8 km of fluvial and lacustrine continental sediments derived from the surrounding Precambrian and Paleozoic uplands, as well as mafic igneous flows and intrusions (Schlische and Olsen, 1990).

The stratigraphic and structural features of the basin are important to understand because they make up the hydrogeological framework for the storage and movement of groundwater. Syndepositional rotation of the hanging walls of the border faults resulted in increased sediment thickness adjacent to the faults and a decrease in dip from older to younger strata. The average dip is 10^{o} to 15^{o} northwest in exposed sections. Differential movement along the border and other, synthetic, intrabasin faults produced localized folding with axes oriented orthogonal to the faults. At approximately 201 $\pm$ 1 Ma a short-lived igneous event emplaced diabase sills and dikes and basalt flows, and resulted in localized contact-metamorphic effects (Sutter, 1988; Olsen and Fedosh, 1988, Schlische and Le Tourneau, 2003). It is uncertain if this igneous event resulted in basin-wide versus local hydrothermal effects that may have mobilized many elements, including arsenic.

Tectonic rifting imparted systematic sets of steeply-dipping, en echelon, extension fractures in basin strata, including ordinary and mineralized joints (Herman, 2009). They contributed to crustal stretching, sagging, and eventual faulting of basin rift deposits. They cluster into three prominent structural groups including early, NE-SW striking; intermediate, NNE-SSW striking; and late, N-S striking fractures reflecting 50^{o} to 60^{o} of counterclockwise rotation of incremental stretching directions during the Early Triassic.

Unweathered fractures are generally healed with sparry, secondary crystalline minerals (Parnell and Monson, 1995; Herman, 2001, 2010; Simonson and others, 2010). An approximately 185-to-175-Ma tectonic-compression event, attributable to the rift-to-drift transition (Withjack and others, 1998), produced basin inversion and resulted in topographic

highs that promoted a fault-guided hydrothermal flow system, with a pre-180-Ma maximum temperature of about 250ºC, that persisted in the basin for tens of millions of years (Steckler and others, 1993; Malinconico, 2002). Therefore the geochemical processes associated with varying depositional, diagenetic and hydrothermal environments controlled the early fate of mobile arsenic in the basin.

An estimated upper limit of approximately 6 km of material was subsequently eroded from the uplifted strata, and by 120 Ma the hydrothermal system effectively shut down (Steckler and others, 1993; Malinconico, 2002). The surface bedrock pattern of the Newark basin has varied little since that time (fig. E2). A stratigraphic column (fig. E3) based on data from the Newark Basin Coring Project (NBCP) shows geologic formations and members in the basin (Olsen and others, 1996). Of the approximately 7500 km^2 of basin exposure, 55 percent consists of the Passaic (4127 km^2), 9 percent the Lockatong (~ 703 km^2), and 12 percent the Stockton Formation (~ 909 km^2).

Depositional environments

The depositional geochemical environments and subsequent diagenetic processes that affected the stability of primary and secondary minerals in part control the present-day hydrogeochemical setting, and the occurrence, and mobilization of arsenic. The reactivity of primary and authigenic minerals during water-rock contact in the basin groundwater systems imparts a characteristic geochemical flavor to the water, and in some settings also affects the occurrence of intermittent but significant dissolution-type water-bearing zones which are sometimes associated with high arsenic concentrations. Therefore, an understanding of these depositional environments is important.

The Newark basin was hydraulically open during deposition of the Stockton Formation and closed for the remainder of its depositional history, and the sediments filling it generally have the same upland provenance (Schlische and Olsen, 1990). Stream sediment and dissolved loads flowing into the basin were mainly derived from the flanking calc-alkalic Precambrian basement rocks, with some contribution from Paleozoic rocks consisting of conglomerates along the northwest border facies (Van Houten, 1965; van de Kamp and Leake, 1996). The Precambrian rocks include sodic-plagioclase-rich granitic gneisses and schists with minor mafic varieties. Weathered mafic and sulfide minerals are likely sources of many of the metals and arsenic in the basin and sodium-rich feldspars provided the sodium that is particularly enriched in the Stockton, Lockatong and Passaic Formations (Van Houten, 1965; El Tabakh and Schreiber, 1998).

Evolving basin geometry coupled with orbitally forced climatic fluctuations controlled the long- and short-period depositional environments (Olsen and others, 1996). The basin was near the equator and exposed to cyclical wet-dry (monsoonal climate) conditions during deposition of the Lockatong and younger formations (Olsen, 1980). Varying water supply and sediment rates, coupled with the dynamic tectonic basin geometry yielded the classic tripartite stratigraphy of basal fluvial (Stockton Formation) followed by deep lacustrine (Lockatong) and shallow lacustrine (Passaic) sedimentary environments (Schlische and Olsen, 1990).

The depositional environments and four major lithic groups in the basin shown in figure E3 and table E5 are listed from oldest to youngest:

1. Stockton Formation (late Triassic) - Alluvial arkosic sandstone, arkosic conglomerate and red mudstone and siltstone. High-gradient braided streams, meandering streams, intermittent basin flooding, lower energy streams when basin became closed.

2. Lockatong Formation (late Triassic) - Cyclic sequences of black (organic-rich), gray and red argillitic mudstone, siltstone and shale. Mainly deep anoxic lake environments with the preservation of organic-rich detrital sediments. Periodic shallow and playa-lake environments.

3. Passaic Formation (late Triassic) - Cyclic sequences of red mudstone, siltstone and sandstone with intermittent gray mudstone and black shale. Shallow-water and playa-lake margin (particularly in younger rocks) with intermittent deep anoxic lake environments.

4. Meridan Group (early Jurassic) - Depositional environment similar to that of lower Passaic formation. Basalt interlayered with sedimentary rock including mudstone, siltstone, sandstone and conglomerate.

The wet-dry orbital cycles of about 20,000 (Van Houten), 100,000 and 400,000 (McLaughlin) years are evident in the rock record of the Lockatong, Passaic and younger formations as repetitive fluctuations in color, sedimentary fabrics, and organic carbon content that are associated with various lake levels (Olsen and others, 1996). Formations, members and strata-specific hydrogeological and geochemical environments are a reflection of these cyclic depositional environments.

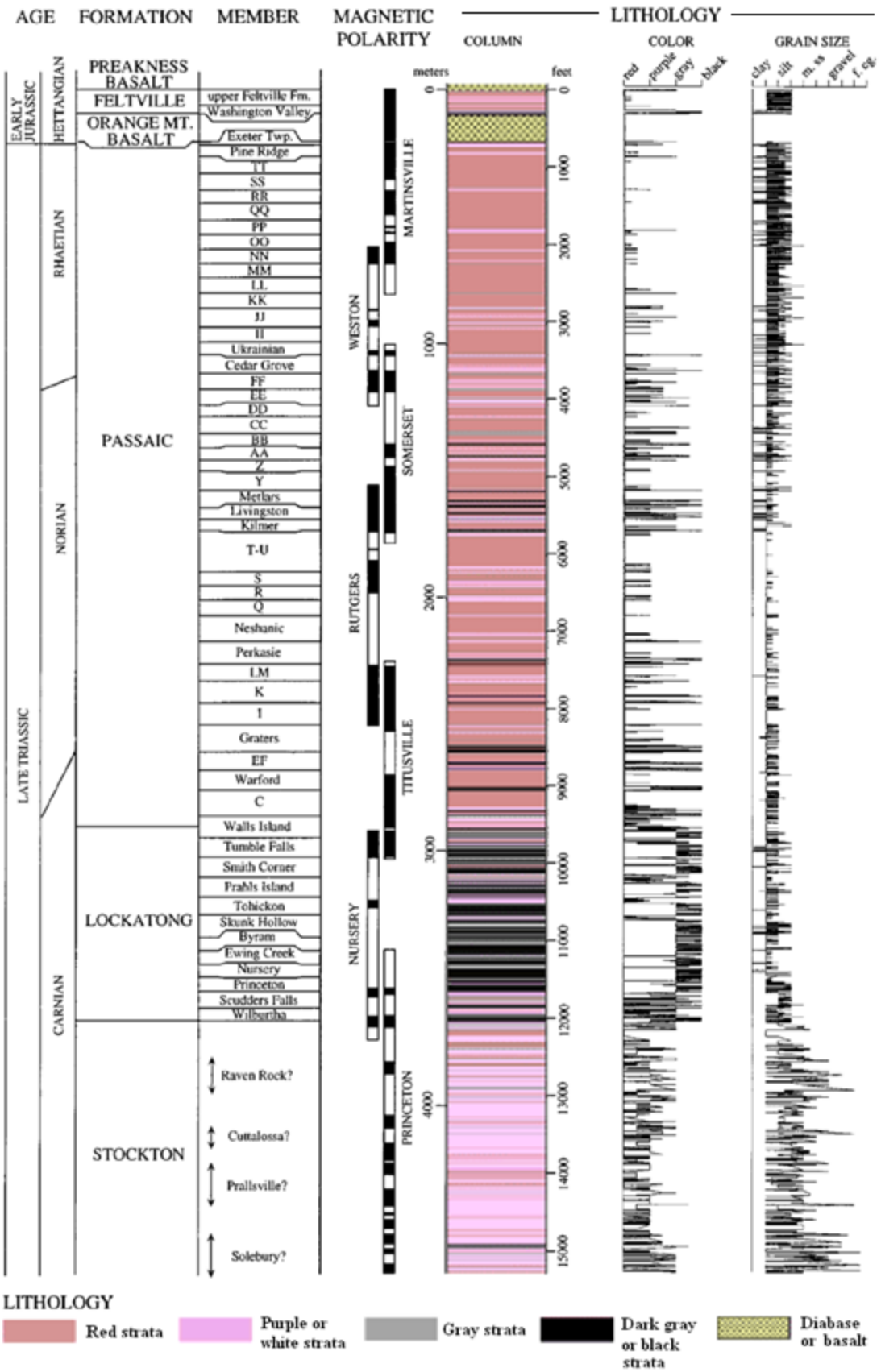

Figure E3. Newark basin stratigraphy and magnetic polarity (Olsen and others, 1996).

Table E5. Stratigraphy of the Newark basin in New Jersey showing major depositional environments, lithologies, and secondary minerals.

Era	Period	Stratigraphic units with Late Triassic depositional environments		Jurassic predominant lithologies and Triassic descriptive lithologies
Mesozoic (Active extension, basin filled with 6 to 8 km of nonmarine, sedimentary and igneous rocks	**Lower Jurassic** (201 +/- 1 Ma)	**Meridan Group** (Weems and Olsen, 1997)	Boonton Formation	Sandstone, siltstone, shale, conglomerate
			Hook Mountain Basalt	Basalt with intercalated sedimentary rock
			Towaco Formation	Sandstone, siltstone, shale, conglomerate
			Preakness Basalt	Basalt with intercalated sedimentary rock
			Feltville Formation	Sandstone, siltstone, shale, conglomerate
			Orange Mountain Basalt	Basalt
	Upper Triassic (~ 225 to 200 Ma)	**Passaic Formation** Thickness ≤ 9000 ft Mostly oxic shallow lakes and vegetated and dry playa mud flats with intermittent suboxic to anoxic deep lakes Similar to upper Lockatong but mostly oxic shallow saline lakes and saline mud flats with periodic suboxic to anoxic fresh and saline deep lakes		Mostly red mudstone, siltstone, sandstone and conglomerate with lesser gray and black shale Secondary diagenetic and hydrothermal minerals and cements filling fractures, cavities and intergranular voids, including: early and late hematite and calcite, early pyrite and late hydrothermal sulfide minerals associated with organic material, albite, k-spar, quartz, ferroan dolomite, and anhydrite/gypsum
		Lockatong Formation Thickness ≤ 2500 ft Mostly suboxic to anoxic fresh and saline deep lakes with oxic shallow saline lakes and saline mud flats		Mostly gray and black mudstone with lesser red beds Secondary diagenetic and hydrothermal minerals similar to those of the Passaic but also analcime
		Stockton Formation Thickness ≤ 3200 ft Mostly oxic fluvial and meandering streams and deltaic environments		Arkosic sandstone, siltstone, shale, conglomerate Secondary diagenetic and hydrothermal minerals similar to those of the Passaic.

Groundwater flow

Groundwater in the Newark basin is mainly stored in, and transmitted through, interconnected conduits such as joints, faults, bedding-plane partings, solution channels and, too a lesser extent, interstitial pore spaces. It flows from upland recharge areas to lowland discharge areas such as streams. Wells completed in the basin are cased through the regolith and shallow bedrock and open to various depths in the deeper bedrock. Water flows to the well bore from the uncased water-bearing zones it intersects. Well-yield data from Houghton and Flynn (1988) show that the average yields are: Stockton (20.0 gpm) > Passaic (16.3 gpm) > basalt (11.8 gpm) > Lockatong (9.5 gpm) > diabase (7.4 gpm). These average yields provide indirect information about the hydraulic conductivity of these aquifers and potentially the relative residence time of groundwater in them; high conductivity is indicative of younger water. The water-rock contact time may affect the water chemistry.

The Passaic, Lockatong and Stockton Formations are the three major aquifers in the basin. Below the shallow weathered zone, the Passaic Formation, and probably the Lockatong Formation, are generally characterized as anisotropic, leaky, multilayered aquifer systems (LMAS) with bed-parallel water-bearing zones (WBZs) sandwiched between thicker nonconductive zones (Michalski and Britton, 1997; Herman, 2001, 2010; appendixes 2-4). Flow between WBZs occurs as leakage via fractures that cross stratigraphic layering or as cross flow in well boreholes. Hydraulic conductivity, and therefore velocity of flow, is greatest parallel to bedding strike, somewhat less so in the dip direction and least of all perpendicular to bedding (Morin and others, 1997; Morin and others, 2000). Weathered bedrock near the surface is more hydraulically isotropic, and possesses greater storage but is considered less permeable than deeper bedrock because of the clogging of potential

conduits with clays and silt (Michalski and Britton, 1997). Hydrogeologic investigations in shallow weathered sedimentary rock with dipping beds at the Oak Ridge National Laboratory facility yielded a comprehensive understanding of contaminant transport in that setting (Soloman and others, 1992; Driese and others, 2001). There, both the near-surface storm flow in the shallow weathered zone and the deeper water-table flow are largely controlled by topography, with permeable, weathered WBZs acting as conduits between the two. Groundwater recharge into the deeper and less-weathered bedrock aquifer mainly occurs where WBZs intersect the shallow weathered zone. Despite uncertainties, this conceptual flow model also probably applies to the Passaic and Lockatong Formations. The more coarse-grained Stockton Formation has the highest well yields of the three aquifers. This is attributed to the occurrence of more intergranular pore spaces, open fractures, and thicker regolith and weathered zones in the arkosic sandstones than in the finer-grained rocks making up the Passaic and Lockatong Formations (Rima and others, 1962; Herman, 2010).

Interestingly, strata-bound dissolution zones containing sparry minerals (calcite, dolomite, gypsum and albite) that fill interconnected root cavities in red mudstones and siltstones of the Passaic Formation may be significant WBZs after these minerals dissolve out (Herman, 2001). This type of WBZ has been observed to produce water with high arsenic concentrations at several locations (Serfes and others, 2005).

Groundwater chemistry

Groundwater chemistry is a function of (1) the composition of precipitation, (2) the natural and anthropogenic chemical conditions the precipitation encounters at the land surface and in the unsaturated zone, (3) the degree of water-rock contact and residence time in the aquifer, and (4) most important, the composition and mineralogy of subsurface materials that the groundwater contacts as it flows through the aquifer (Serfes, 1994). The composition and mineralogy of the subsurface materials in the Newark basin are a direct reflection of the original depositional and diagenetic environments described in table E5 and in the text above. The lithogenic fate of arsenic in sedimentary environments is generally tied to that of iron, sulfur and clay minerals. Therefore, iron oxides, sulfide minerals such as pyrite, and clay mineral surfaces; are all potential sources and sinks for arsenic. The aqueous geochemical environment; coupled with the hydrogeological setting, controls the mobilization and transport of arsenic from those sources and through the groundwater system. Chemical parameters such pH, oxidation-reduction potential and competing ions affect the stability of minerals and mineral surfaces containing arsenic. The chemical character and presence or absence of certain chemical species in groundwater lend clues to the fate of minerals that may contain arsenic. Therefore, it is important to delineate the hydrogeochemical character of the major aquifers in the Newark basin.

A statistical summary of important groundwater-quality characteristics of the Passaic, Lockatong, and Stockton Formations is given in tables E2, E3, and E4 respectively. Differences in groundwater chemistry of the three formations are related to their unique rock and mineral composition and to their hydrogeological character. Based on the median concentrations listed in these tables, some of the more obvious differences are: (1) Water from the Passaic Formation is highest in calcium, magnesium, chlorine, lithium and sulfate, and in specific conductance. (2) Water from the Lockatong Formation is highest in potassium, sodium, silicon, iron, manganese, and alkalinity, and lowest in dissolved oxygen and chloride. (3) Water from the Stockton Formation is highest in barium, and lowest in pH, specific conductance and alkalinity.

Piper diagrams classify the hydrogeochemical type of water in an aquifer by comparing the percent equivalents of the dominant cations and anions on a trilinear diagram (Back, 1960). Based on these plots, the Stockton, Lockatong and Passaic formations all mainly contain calcium-magnesium-sodium-bicarbonate-type waters (Serfes, 1994). However, calcium-sulfate-type water with high specific conductance in the Passaic formation and sodium bicarbonate water in the Lockatong formation also occur. The calcium-sulfate-type water common in certain stratigraphic sections in the Passaic Formation is the direct result of the dissolution of gypsum. The high sodium in water from the Lockatong Formation is likely due to the dissolution of analcime ($NaAlSi_2O_6 \cdot H_2O$).

Arsenic in groundwater in the New Jersey part of the Newark basin

Regional occurrence

Figure E4 shows the approximate locations (points not digitized) of New Jersey public-supply wells sampled in 1995 to 2000, and private wells sampled as part of the New Jersey Private Well Testing Act from September 2002 to March 2003, that had arsenic concentrations in their water exceeding 10 µg/L. Most of the wells with arsenic concentrations greater than 10 µg/L tap the Lockatong and Passaic Formations. A preliminary conclusion is that most of the wells in the Passaic Formation with concentrations exceeding 10µg/L appear to be associated with the Metlars, and older members (figure E3). However, wells intersecting

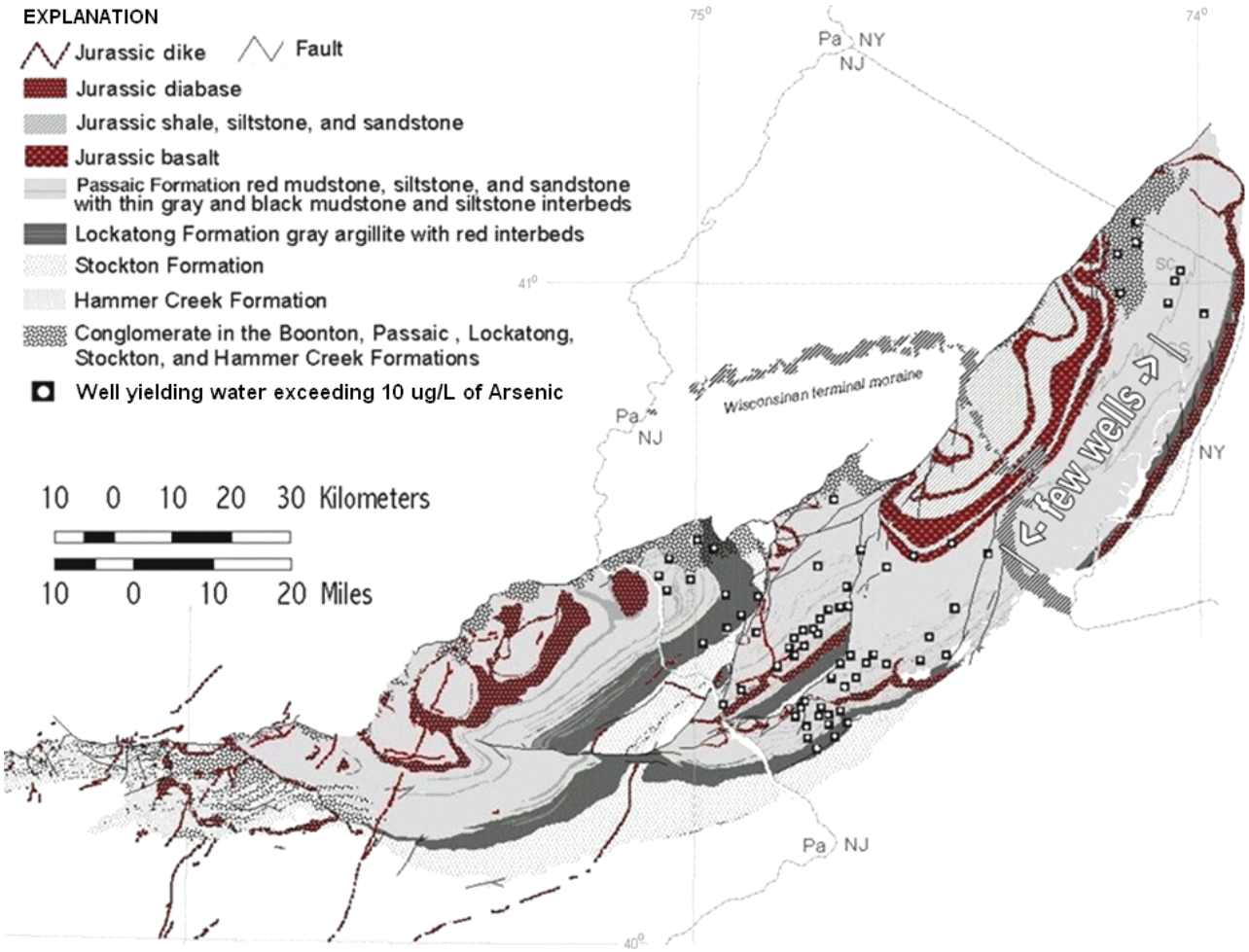

Figure E4. Distribution of wells sampled from 1995 to 2003 showing those exceeding 10 µg/L arsenic. Domestic wells were sampled as part of public-supply-well sampling from 1995 to 2000 and the Private Well Testing Act (http://www.nj.gov/dep/pwta/) from September 2002 to March 2003.

younger members of the Passaic Formation have arsenic concentrations as much as 215 µg/L. Field parameters such as pH, dissolved oxygen (DO) and specific conductance (SC) that would aid in characterizing the hydrogeochemical environment were not collected during these regulatory samplings.

A hydrologic study by Sloto and Schreffler (1994) in the Newark basin in northern Bucks County Pennsylvania found wells with concentrations of arsenic as much as 28 µg/L. Of the 35 wells with results for arsenic, four (11 percent) have arsenic concentrations exceeding 10 µg/L. Two wells in the Passaic Formation have 24 and 28 µg/L arsenic, one in the Lockatong Formation has 11 µg/L arsenic, and one in the diabase has 13 µg/L arsenic.

Distribution of arsenic in the central part of the basin

In 1999 to 2000, the NJGS conducted a detailed investigation of arsenic in groundwater as a function of bedrock lithology using a geographic information system (fig. E1). The study encompassed a 200-square-mile (518 km^2) region in western New Jersey marked by high concentrations of arsenic in groundwater (fig. E1c).

A grid-based approach using square-mile cells, and random selection within blocks, assured that the sampling was spatially distributed within the study area rather than being mainly clustered in high-population areas as it would have been if a simple random approach had been used (Alley, 1993). The goal was to collect representative groundwater samples and field parameter data: pH, DO, SC, and temperature (T) from at least one domestic well per cell. Samples were obtained mainly from outside taps after water had discharged for at least

15 minutes and field parameters had stabilized. Three well records were obtained per cell, for a total of 600 records, by conducting a search using the NJ Department of Environmental Protection, Division of Water Supply well-record database. Generally, the most recent records in each cell identify the current property owner. Volunteers were sought for this project for each of the 200 cells and 94 volunteers responded. Cluster sampling was also conducted in two areas (appendix 3D and 3M) where at least one well had water with an arsenic concentration exceeding 40 µg/L.

Of the 94 wells sampled, 15 percent had arsenic concentrations exceeding 10 µg/L (fig. E5). Groundwater from the Passaic and Lockatong Formations had the highest arsenic concentrations and frequency of occurrence (Serfes and others, 2005). The Passaic Formation is much more areally extensive than the Lockatong and therefore the number of wells with concentrations of arsenic exceeding the drinking water standards is greater (fig. E4).

Based on the pH and dissolved oxygen (DO) concentrations measured at the time of sampling, arsenic concentrations exceeding 10µg/L in water from the Passaic Formation were associated with pH ranging from 7.5 to 8.2 and low DO concentrations (< 3 mg/L, fig. E6). Arsenic concentrations exceeding 40 µg/L are associated with suboxic concentrations (DO < 1.0 mg/L) and a pH of about 8 in the Passaic Formation. These values fall into the lower and upper percentiles respectively for that formation (table E2). However, for the Lockatong Formation, 15 of 16 water samples had DO < 3 mg/L and 11 were < 1 mg/L regardless of the arsenic concentration (fig. E6). Also, the pH corresponding to the highest arsenic concentrations was

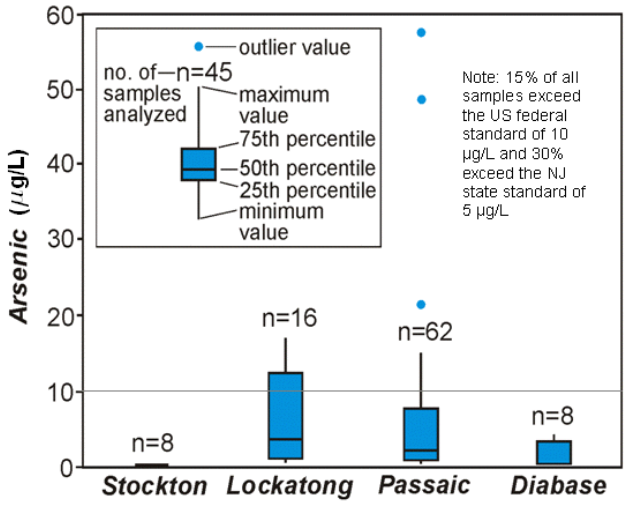

Figure E5. Box-and-pin diagrams summarizing arsenic concentrations in groundwater from 1999 to 2000 for the Stockton, Lockatong and Passaic Formations and diabase. Maximum concentrations for each unit formation were as much as 95, 120 and 215 µg/L respectively.

not well defined. The low DO is characteristic of this formation and is related to the more anoxic nature of the organic-rich and pyritic deep-water lake-derived strata (table E5). The geochemical character of the Passaic and Lockatong Formations defined during the arsenic reconnaissance study is comparable to that given in tables E2 and E3. Subsequent sampling also identified areas in the Newark basin where some wells had higher concentrations than those found in the original reconnaissance. Several wells tapping diabase near its contact with sedimentary rock in the southwestern part of the basin in New Jersey had as much as 95 µg/L arsenic. Approximately 10 miles east of these wells, a well tapping the Lockatong Formation had as much as 120 µg/L arsenic. Also, wells drawing water from a mineralized zone in the Passaic Formation underlying a basalt flow in the north-central Newark basin in New Jersey (appendix 1F1) had arsenic concentrations as much as 215 µg/L.

Groundwater collected from a 400 ft-deep, public-supply well in the Passaic Formation in the Borough of Hopewell (appendix 3G1), has consistently had arsenic concentrations of 45 $\pm$ 5 µg/L since the well was installed in 1995. Samples collected periodically over months and years from other wells in another arsenic treatment study in the basin also have had less than a 20 percent variation in arsenic concentrations. These uniform concentrations indicate that a steady-state geochemical condition prevails between groundwater and the rock matrix. The few exceptions are several wells penetrating the Passaic Formation beneath Orange Mt. basalt that yield water with high arsenic concentrations and show large concentration fluctuations. In those wells, a correlation between precipitation events and decreasing concentrations has been noted and may reflect a more open fracture network that is directly connected to the near-surface system.

Arsenic speciation analysis showed that arsenic in groundwater in the Passaic Formation is predominantly arsenate even under suboxic conditions (table E6). The occurrence of oxidized arsenic species in the Passaic Formation could be due to reactive contact with Mn-oxide coatings that were found on bedrock fracture surfaces in the Passaic Formation from analysis using energy dispersion spectroscopy (EDS). Manganese oxides are known to rapidly oxidize arsenic from As(III) to As(V) (Driehaus and others, 1995; Scott and Morgan, 1995). Arsenic species analyses of 23 public-supply wells in the Passaic Formation known to have elevated arsenic concentrations showed the same, As(V). However, arsenite (As(III)) was the dominant species in two domestic and two public-supply wells in the Lockatong Formation where it made up more than 63 percent of total arsenic concentrations that ranged from 11.9 to 45.0 µg/L in the four wells. Water from these wells also had a hydrogen sulfide odor, indicating

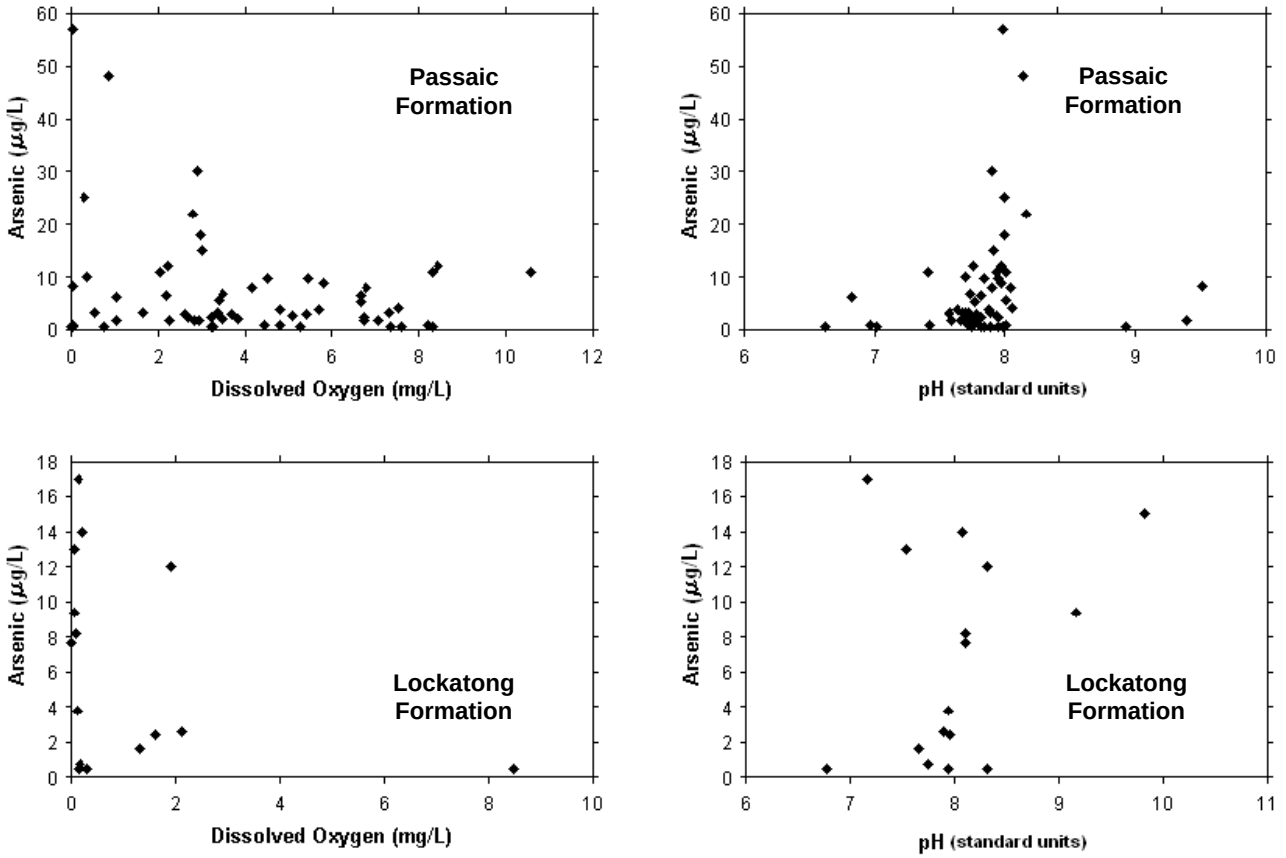

Figure E6. Arsenic versus dissolved oxygen and pH in groundwater from the Passaic and Lockatong Formations in the central part of the Newark basin in New Jersey.

strong reducing conditions. The methylated arsenic species monomethylarsonic acid (MMA) and dimethylarsinic acid (DMA) were all less than 0.5 µg/L.

Case Study: The Borough of Hopewell well HW-6.

The Borough of Hopewell well 6 (HW-6) is a 400-ft-deep public-supply well in Mercer County (figs. E1 and E7) that was installed in the Passaic Formation in 1995 to meet growing water-supply needs. In December 1995, a 72-hour pump test was conducted using two nearby 6-in.-diameter, deep observation wells. Well OBS-1 is 400 ft deep, located about 75 ft northeast and along strike with HW-6. Well OBS-2 is 300 ft deep, located about 286 ft to the north and downdip of HW-6 (appendix 3G3). All of these wells are cased to a depth of 50 ft and are open to bedrock from the bottom of the casing to the total depth of the well. The pump test showed that the aquifer is heterogeneous and anisotropic. The greatest drawdown was along strike, and the boundaries are leaky. Also, HW-6 can produce 140 gallons per minute without any detrimental impact on other nearby producing wells. Nonpumping deep local flow is assumed to parallel bedding strike and local topography (fig. E7). Groundwater flows from the diabase uplands to the

Table E6. Arsenic speciation in water from nine residential wells in the Passaic Formation. Concentrations in µg/L.

Species	Well 1	2	3	4	5	6	7	8	9
Arsenic total.	22.3	31.8	61.9	39.8	19.5	5.2	40.5	9.7	22.7
As(III)……	0.3	0.1	0.5	1.6	<0.1	<0.1	0.3	<0.1	0.2
As(V)……	22.0	31.4	59.6	37.9	19.2	4.9	39.9	9.3	22.5
MMA[1]……	<0.1	0.1	0.4	<0.1	0.1	<0.1	0.1	0.2	<0.1
DMA[2]……	<0.1	0.2	0.4	0.2	0.2	0.2	0.2	0.2	<0.1

[1] monomethylarsonic acid, [2] dimethylarsinic acid.

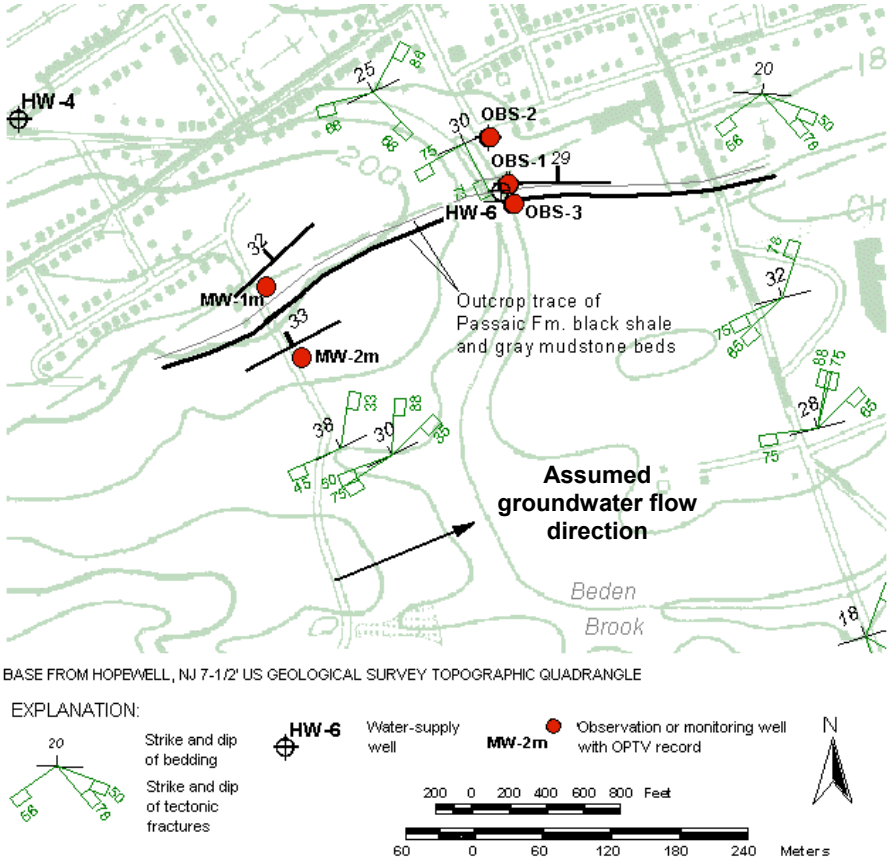

Figure E7. Geologic map of study area in the Borough of Hopewell showing locations of the 400-ft-deep public-supply well HW-6, deep observation wells OBS-1 and OBS-2, shallow observation well OBS-3 and strike and dip of bedding and fractures. Bedrock structure mapped by Don Monteverde, NJ Geological Survey. Regional location of the Hopewell study shown in figure E1.

southwest, downhill along the strike of bedding to the northeast where it eventually discharges to Beden Brook (fig. E7). Most of the recharge to the stratabound water-bearing zones intersected by these wells takes place uphill where bedrock strata crop out below regolith. An analysis of water from HW-6 in November 1995 yielded an arsenic concentration of 44 µg/L. This concentration has generally varied by less than 20 percent since that time. The well was taken off line because of the high arsenic concentrations.

In 1999 the NJGS collected a 400-ft long rock core (HW CORE) approximately 50 ft from HW-6 to investigate the stratigraphic and structural features of the water-bearing zones and their effects on the hydraulics of that well (Herman, 2001). An optical televiewer study of OBS-1 enabled comparison of features in the core with those in the well. The HW CORE penetrated pyritic black and gray shale of the Kilmer Member and the underlying T-U Member of the Passaic Formation, consisting mainly of red mudstones and siltstones (figs. E3 and E8). HW-6, OBS-1 and HW CORE are located within 100 ft of each other, are aligned close to the strike of bedding, penetrate the same stratigraphic section, and have a strong hydraulic connection, so comparison is reasonable.

Downhole geophysical logging was also used to assess flow (appendix 3G3 and 3G4). An important finding was that in OBS-1 (and therefore HW-6), most groundwater flow is in mineral-dissolution cavities (fig. E9 and appendix 3G3-3G7, 3G9 and 3G10). Microanalysis of pyrite in the black shale showed that concentrations of arsenic were as high as 3000 mg/Kg (Serfes, 2005). These findings led to a tentative hypothesis that the pyrite in the black shale was the source of the arsenic in HW-6. To test the hypothesis, an intensive investigation of the hydraulics and hydrochemistry of HW-6 was conducted.

In September 2002 the NJGS installed a 35-ft-deep well located less than 100 ft from, and slightly updip from, HW-6 (appendix 3G1) as part of the ongoing investigation of arsenic in groundwater. This shallow well is cased to a depth of 10 ft and is open to the black and gray shale approximately 16 to 24-ft below land surface. It was tested on October 2, 2002, approximately one month after installation, for pH and redox variations with depth (table E7).

From September to November of 2002 the NJGS conducted a hydrologic and water-quality investigation of HW-6 and the nearby observation wells to determine where and in which water-bearing zones arsenic is being transported (see appendix entry 3G). As part of this investigation, a single hydraulic packer, along with transducers and pumps above and below the packer, were used to collect hydraulic-head data and

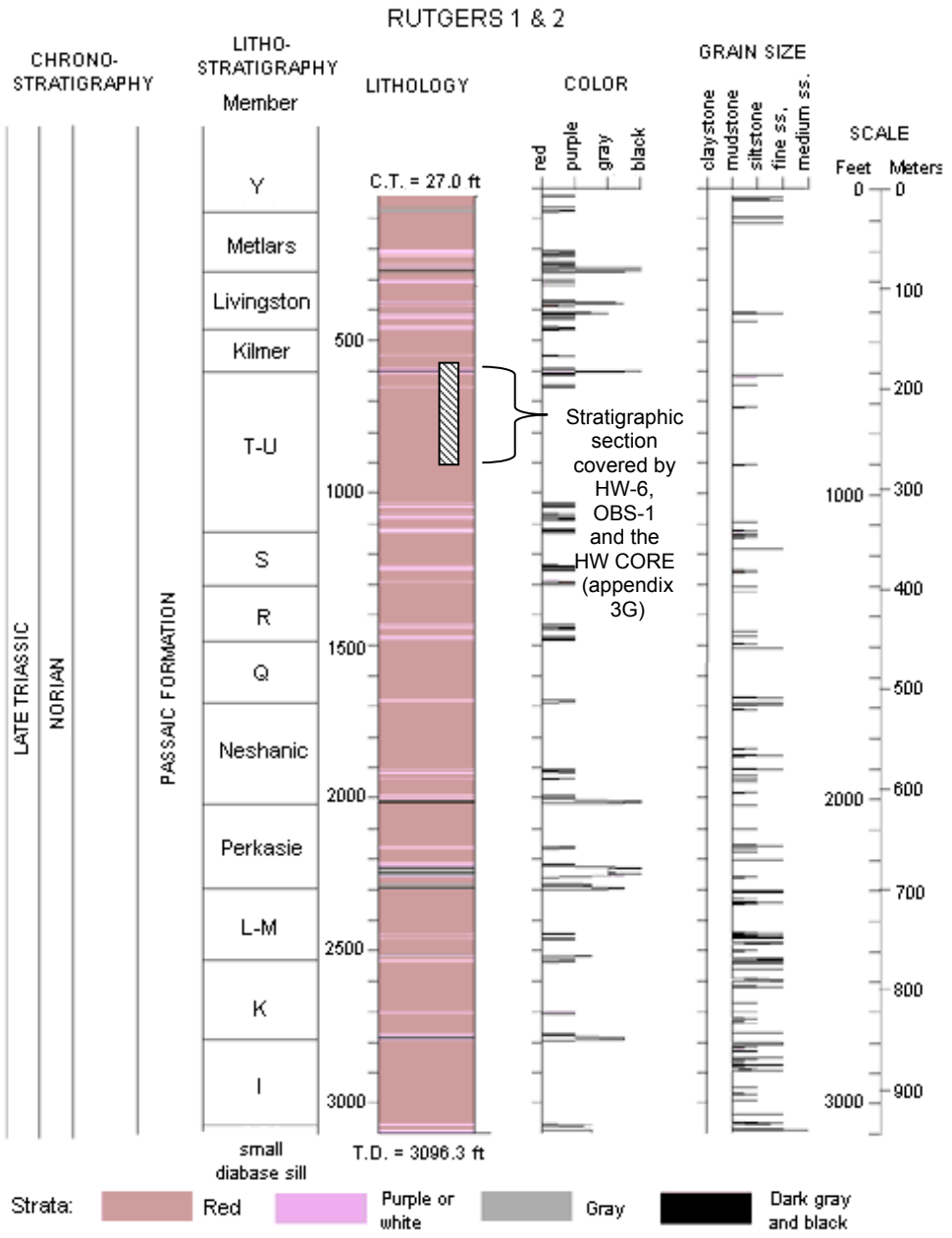

Figure E8. Stratigraphic section including wells HW-6, OBS-1 and the HW CORE in relation to the Rutgers # 1 & 2 cores (Olsen and others, 1996 and fig. E3). The section for the Hopewell study is based on a local bedding dip of 29°.

Table E7. Physical and chemical characteristics of groundwater from OBS-3, October 2, 2002. Well is 35 ft. deep and cased to about 11 ft. Parameters measured using a Horiba X-22 meter .

	steel casing	black-gray beds	gray-purple beds	purple-red beds	red beds
Depth (ft below land surface)……..	10.92	18.92	24.92	15.92	33.92
Temperature (°C)……..	17.8	15.3	14.2	16.2	12.7
Specific conductance (µS/cm)……	330	430	440	410	520
Dissolved Oxygen (mg/L)……	0.0	0.0	0.0	0.0	0.09
PH (standard units)……..	6.56	6.95	6.96	6.80	7.06
Oxidation-reduction potential (mvolts)…..	-47	-95	-94	-84	-4

Table E8. Physical and chemical characteristics of groundwater from Hopewell investigation wells HW-6, OBS-1, OBS-2, and OBS-3 from September2001 to October 2002.

Well (p, if packer used)	HW-6	OBS-1	OBS-1p				OBS-2	OBS-2p		OBS-3
Depth to top of sample interval (ft)……....	50	50	50	50	50	291	50	50	60	10
Depth to bottom of sample interval (ft)….....	400	400	60	400	291	400	300	60	300	35
Chlorofluorocarbon 11, 12, 113 model age										
Age (+/-2 years)……..	21	23	--	--	--	--	22	--	--	30
Characteristics										
Temperature (°C)……	14.4	13.4	12.9	13.9	--	--	12.9	12.9	13.6	15.4
Specific conductance (µS/cm)[1]...	380	420	530	430	--	--	339	390	330	380
Dissolved Oxygen (mg/L)……..	0.0	0.0	0.0	0.21	--	--	3.62	1.45	2.3	0.0
Ph (standard units)……	7.87	7.71	7.43	7.65	--	--	7.79	8.0	7.47	7.25
ORP (mvolts)……	105	31	-61	128	--	--	--	108	130	-44
Field Alkalinity (mg/L as CaCO3).	142	150	203	127	111	94	--	101	99	115
Major and minor dissolved constituents (mg/L)[2]										
Calcium……	49.4	59.1	80.4	52.8	47	50.1	28.9	44.5	37.4	83.9
Magnesium……..	14.3	16.3	30.1	17	16.8	12.9	15.6	21	16.5	23.6
Sodium……	18.6	24.4	14.1	23.6	19	24.6	9.7	12.7	10.7	15.5
Potassium……	1.17	1.04	1.59	1.07	1.18	0.88	0.97	1.15	1.1	1.61
Chloride……	8.7	11.2	25.1	11.9	12.4	10.2	12.6	18.8	11.9	15.2
Sulfate……..	43.4	40.3	29.5	49.2	25.4	38.5	22.1	24.2	21.5	30.2
Silica……	11.3	11.9	11.7	10.5	11.0	11.3	10.8	11.6	12.2	10.0
Strontium……..	2.56	2.58	0.95	2.53	1.79	2.40	1.15	1.26	1.13	0.49
Nitrate……	1.73	1.11	0.59	0.71	1.46	1.57	--	3.01	2.26	.52
Phosphorous (ND = <0.04)……	ND	ND	ND	ND	ND	ND	ND	ND	ND	ND
Trace and minor dissolved constituents (µg/L)[3]										
Arsenic……..	41.9	33.8	3.01	29.4	27.3	36.4	9.2	7.03	8.5	1.06
Barium……..	133	136	226	149	170	109	153	165	170	372
Iron……	<0.5	<0.5	<0.5	<0.5	<0.5	<0.5	<0.5	<0.5	<0.5	<0.5
Manganese……..	1.2	0.5	38.1	<0.5	2.4	0.7	<0.5	3.4	0.2	303
Molybdenum……	14.7	16.4	18.2	16.5	12.9	23.2	1.9	1.5	1.5	17.2

Notes: Samples for OBS-1 were collected September 14, 2001, whereas samples for HW-6 were collected during September and October 2002. A single hydraulic packer was used in OBS-1 and OBS-2. Samples were not filtered. Chlorofluorocarbon analyses were made at the University of Miami Tritium laboratory. Field parameters measured using Horiba X-22 meter and Hach Alkalinity titration. Analyte analyses conducted at Activation Laboratories in Ancastor, Canada. - - indicates that no measurement was taken. Depth in ft below land surface. ORP - oxidation reduction potential. ND – nondetect. [1]µS/cm - microsiemens per centimeter, [2]mg/L - milligrams per liter, [3]µg/L - micrograms per liter

water-quality samples. Field water-quality data, samples for age dating using chlorofluorocarbons (CFCs) and for comprehensive water analyses, were collected and analyzed (table E8). Semiquantitative testing disclosed variations in yield within the well bore. Most of the hydraulic testing related to HW-6 took place in OBS-1 because a turbine pump in the supply well blocked access to it.

Hopewell HW-6 hydraulics and water-chemistry results

Hydraulics

1. Hydraulic head in wells 1 and 2 measured above and below packers showed a downward vertical gradient. This is the expected head distribution as the stratabound water-bearing zones dip in a direction opposite to the slope of the hill.

2. The yields from OBS-1are approximately the same from the 50-to-291-ft. section as they are from 291 to 400 ft. , showing that the yields are higher in the deeper strata.

3. Core samples show more dissolution zones in the deeper strata (fig. E9). This corroborates the finding that yields increase with depth.

Water Chemistry

1. In general, all of the groundwater is of the calcium bicarbonate type, which is characteristic of water from the Passaic Formation. A comparison of the quality-of-water parameters of HW-6 with OBS-1 & 2 (table E8) with those from similar wells in the Passaic Formation (table E2) shows that the these wells fall between the 25th and 75th percentiles for the Passaic Formation, except for a lower DO in HW-6 and OBS-1, and a slightly higher pH and strontium concentration and a lower silicon concentration in the Hopewell wells. HW-6 and OBS-1also have very high arsenic concentrations whereas OBS-2 is approximately 4 times lower, but still higher than most of the wells sampled during the reconnaissance study (fig.E5).

Figure E9. Examples of spar minerals filling voids, including fractures and root cavities, in the HW CORE at depths of 253 ft and 359 ft below land surface (bls). Dissolution-type water-bearing zones also occur at depth such as shown above at 324 ft and 359 ft bls (from Herman, 2001).

2. Arsenic concentrations are highest in HW-6 and OBS-1. They increase with depth in OBS-1, and are much lower in OBS-3, which penetrates the black and gray strata at shallow depths and has the highest whole-rock concentrations of arsenic (table E9). Therefore, arsenic is entering HW-6 and OBS-1 from the deep, high-yielding dissolution zones in the red mudstone and not from the more shallow gray and black beds.

3. Water from wells HW-6, OBS-1 and OBS-3 is suboxic to anoxic whereas that from OBS-2 has a DO concentration similar to that of the median for the Passaic Formation (tables E2 and E8).

4. Analyte measurements of water from well OBS-3 showed that it is generally chemically reducing compared to that from the deeper wells and that water taken from black and gray beds is the most reducing (tables E7 and E8).

5. Chemistry of water from well OBS-1 at a depth of 50 to 60 ft. is similar to that of water from well OBS-3, which is uncased from 10 to 35 ft. Both have a much lower oxidation reduction potential, lower arsenic, strontium, and sulfate concentrations, a lower pH, and higher calcium, magnesium, barium and manganese concentrations than the other wells (table E8). This suggests that pyrite is stable in the more reduced environment but carbonate minerals are unstable at the lower pH. The lower strontium concentration may indicate that it is associated with calcium in gypsum ($CaSO_4$. $2H_2O$) rather than with calcite ($CaCO_3$) or dolomite ($CaMg(CO_3)_2$). Not surprisingly, alkalinity, 203 mg/L, is higher in the shallow zones of OBS-1, at depths of 50 to 60 ft, than it is in the deeper zones at depths of 291 to 400 ft (94 mg/L).

6. Age of groundwater, using CFCs, was approximately 22 years in HW-6, OBS-1 and OBS-2. Groundwater in OBS-3, which is much shallower, had a model age of 30 years. The older age of water in OBS-3 is probably due to the relatively low permeability in its source zone, or it may reflect CFC degradation in relatively higher-reducing waters.

7. The deeper zones in OBS-1 are much higher in arsenic, strontium, and sulfate, higher in pH and lower in alkalinity and manganese concentrations.

8. Nitrate values in water from all of the wells suggest anthropogenic impacts. All of the beds intersected

by these wells crop out in former and current agricultural fields.

These findings demonstrate that arsenic concentrations in groundwater may differ considerably even between closely spaced wells unless they tap the same strata. Wells that mainly intersect high-yielding WBZs that are transporting elevated concentrations of arsenic have elevated concentrations in their water.

Introductory findings and conclusions

The results from the reconnaissance sampling of domestic wells in the 200-square-mile study area, the study at HW-6 and related work, provide the following findings and conclusions that address key question no. 1 in the introduction.

1. Of the three major formations, the Passaic and Lockatong have the highest arsenic concentrations in their water: more than 15 percent of the wells exceed 10 µg/L, and 30 percent 5 µg/L arsenic.

2. Arsenic concentrations in some wells, sampled many times over periods of months and years, have generally varied by less than 20 percent, indicating steady-state geochemical conditions.

3. Study of wells near HW-6 showed that arsenic concentrations in water, even from closely spaced wells, may differ considerably unless the wells tap the same major WBZs.

4. Groundwater in the Lockatong Formation is characterized by low DO: 15 of 16 samples are below 3 mg/L and 11 are below 1 mg/L regardless of their arsenic concentration. Also, the pH at which the highest arsenic concentrations occur is not well defined and ranges from 7 to 10. Arsenite is the dominant species.

5. Groundwater in the Passaic Formation with arsenic concentrations exceeding 10 µg/L is characterized by:

    a) Ca-Mg,-Na bicarbonate type water, as is most groundwater in the Passaic Formation, regardless of arsenic concentration.
    b) Dissolved oxygen concentrations less than 3.0 mg/L
    c) Arsenate, As(V), ($HAsO_4^{2-}$) exceeds 95-percent of total arsenic (table E6).
    d) pH range is 7.5 to 8.2 .
    e) Generally low iron and manganese concentrations.
    f) Sulfate and total dissolved solids concentrations are average.

6. Water from wells in the Passaic Formation exceeding 20 µg/L arsenic is typically characterized by:

    a) pH of approximately 8.0.
    b) DO commonly less than 1.0 mg/L.
    c) Association with dissolution zones of interconnected voids formed by the solution of secondary calcite +/- dolomite +/- gypsum.

Questions 2, 3 and 4 in the introduction concern the sources, mobilization and transport of arsenic in the black, organic-rich, deep-water-lake-derived shale that makes up most of the Lockatong Formation and the shallow-water lake and playa-derived red mudstone and siltstone that make up most of the Passaic Formation. These questions are addressed in the following sections.

Lithochemistry

Arsenic concentrations from whole-rock analyses of the Stockton, Lockatong and Passaic Formations are shown in figure E10. Black shale and gray mudstone from the Passaic and Lockatong formations are highest in arsenic and some pyrite-rich portions of the black shale exceed 200 ppm (Szabo and others, 1997; Serfes and others, 2005). The Stockton Formation and red mudstone and siltstone of the Passaic Formation generally are lower in arsenic. Arsenic concentrations in groundwater are highest in the Lockatong and Passaic Formations.

Although black and gray shale are the dominant lithology in the Lockatong Formation, red strata dominate the Passaic Formation, where red and purple beds make up close to 98 percent of the formation. Water from many wells tapping red beds in the Passaic Formation has concentrations of arsenic that exceed Federal and State drinking water standards. The following two sections focus on the major sources of arsenic in these formations.

Arsenic in black and gray shale

Black and gray shale are the dominant rocks in the Lockatong Formation. Although samples discussed here are from the Passaic, they are representative of similar shale in the Lockatong. The fine-grained nature of shale, mudstone and siltstone hampers geochemical characterization of all except the coarser individual

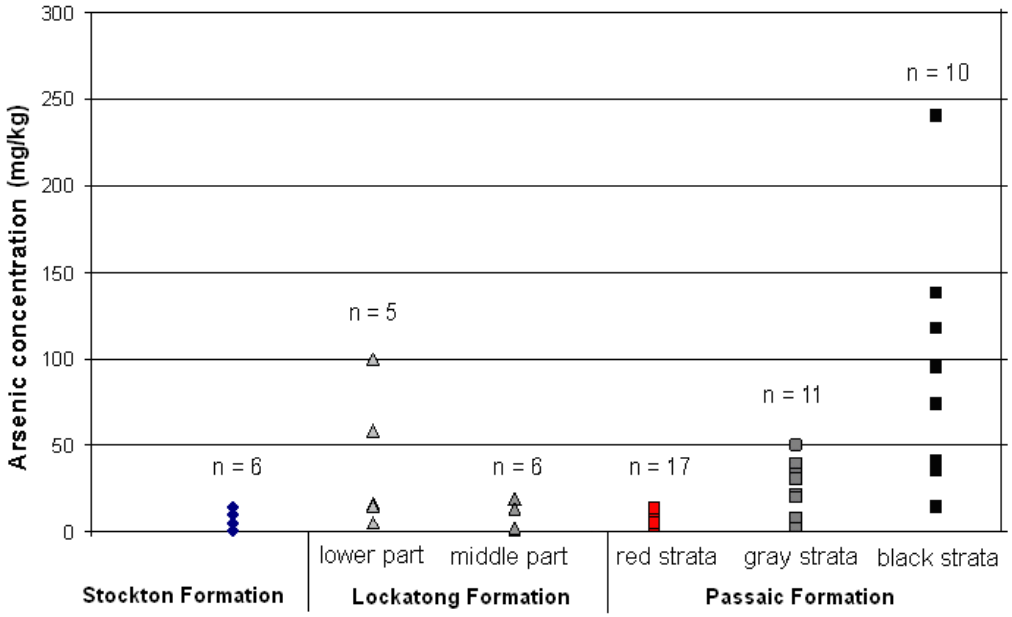

Figure E10. Arsenic whole-rock concentrations in three major bedrock formations in the New Jersey part of the Newark basin. Data from Serfes and others, (2005, table E10), Malinconico (2002) and Szabo and others (1997).

minerals. Electron microprobe analysis of black and gray shale in the Warford Member of the lower Passaic Formation (core sample provided by Zoltan Szabo, USGS) and in the Kilmer Member of the middle Passaic HW CORE, identified the mineral pyrite (FeS_2) as the major source of arsenic in both (fig. E11). These two black and gray shale units have measured maximum arsenic concentrations in pyrite of 40,000 and 3000 mg/Kg, respectively. Arsenic concentrations vary considerably within and between pyrite grains, and smaller grains generally had higher concentrations than the larger ones. Pyrite cores and small micron-sized grains were observed to have the highest concentrations of arsenic, and rims around the cores had the lowest (fig. E12). For example, a pyrite grain less than two microns in diameter had 4 -weight percent arsenic. This suggests that most of the mobile arsenic was readily incorporated into pyrite early on as it nucleated and grew. Under sulfide-reducing conditions, the nucleation and growth of low-temperature pyrite in the deep lake sediments acts as a sink for many metals and arsenic (Berner, 1984). Presumably, early diagenetic nucleation and growth of pyrite in the anoxic deep lake sediments caused scavenging of most of the available mobile

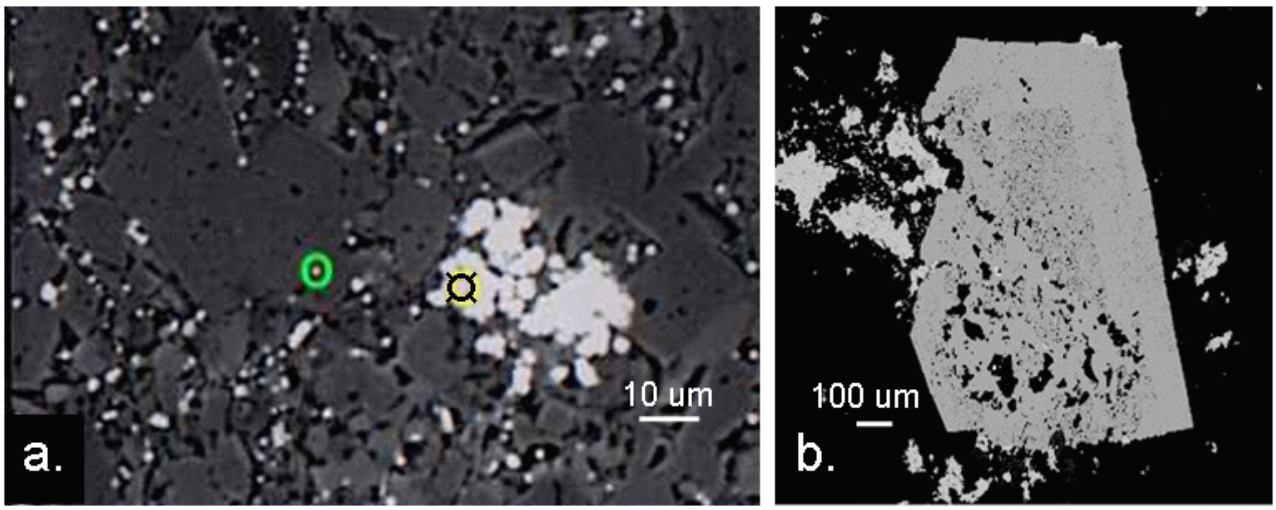

Figure E11. Scanning electron micrographs (SEM) of pyrite in black shale and gray mudstone from two members in the lower part of the Passaic Formation. a) SEM of shale from the Warford Member. Pyrite appears as bright areas in the dark gray calcite matrix. Arsenic concentrations in pyrite are 11,500 in the green circle to the left and 15,860 in the yellow mark (¤) to the right (in mg/kg. b). SEM of large pyrite crystal (medium gray) with chalcopyrite (light gray) in mudstone matrix from the Kilmer Member. Arsenic concentrations in some pyrite are as much as 3000 mg/kg.

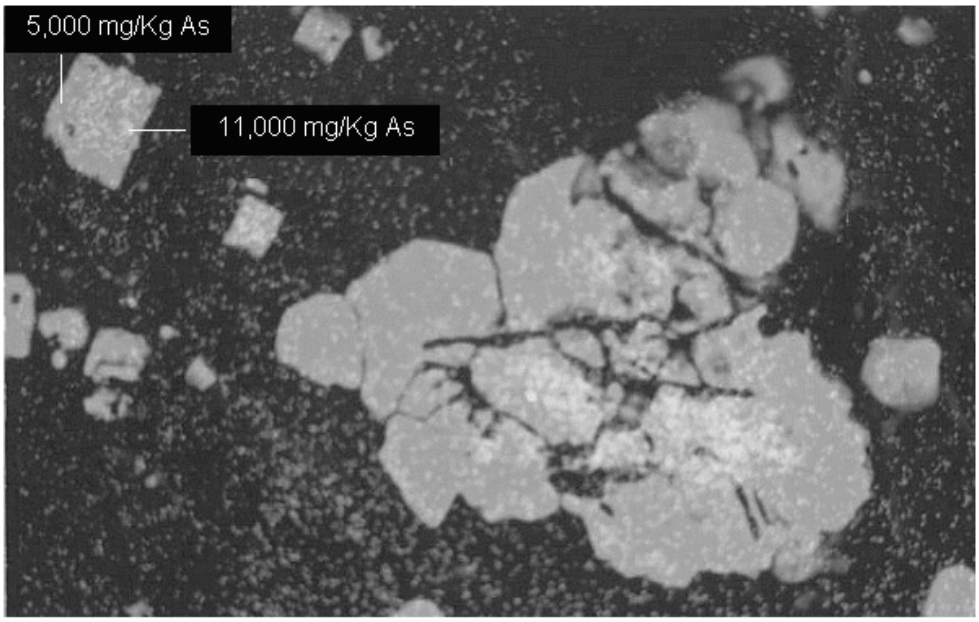

Figure E12. Arsenic element map of pyrite (medium gray) in dark gray matrix of black shale from the Warford Member of the lower part of the Passaic Formation. Arsenic appears as light gray specks on pyrite. A higher density of light gray specks indicates higher arsenic concentrations.

arsenic. The subsequent growth of pyrite was in pore fluids depleted in arsenic and therefore the rims have lower concentrations. Some late-stage mobilization and enrichment of arsenic in sulfide minerals occurred during the hydrothermal event(s) (Smoot and Robinson, 1988). Hydrogeochemical and experimental investigations to evaluate pyrite as a source of arsenic in groundwater in the Newark basin include Zhu and others (2008) and Zhu (2009).

Arsenic in red mudstone and siltstone in the Passaic Formation

Red mudstone and siltstone in the Passaic Formation have much lower arsenic concentrations than the pyrite-bearing black and gray shale do (fig. E10). These red rocks consist mainly of the minerals listed in table E9. Of these, hematite and illite are probably the major sources of arsenic because of their documented affinity for it (Stollenwerk, 2003). Direct measurement of arsenic concentrations in these fine-grained and dispersed minerals using electron microanalytical techniques is difficult because they are below the detection limits. Therefore, multi-element statistical correlation analysis and geochemical interpretation are used to evaluate the potential sources of arsenic in these rocks.

Table E9 lists the concentration of chemical components in 14 samples from the 400-ft Hopewell rock core (HW CORE). This core penetrated approximately 10 ft of black and gray shale and 390 ft of massive red mudstone and siltstone in the middle part of the Passaic Formation (Herman, 2001). The core was collected within 50 ft of HW-6, with water containing about 45 µg/L of arsenic (figs. E1 and E7). The table includes chemical data on four samples from the upper Passaic Formation. Three samples are from a core (SS) collected within 50 ft of a domestic well yielding water containing about 57 µg/L of arsenic and one is from directly below the Orange Mountain basalt in the Martinsville core (Olsen and others, 1996). The Martinsville core is from the stratigraphic horizon where another distant well produces water containing 216 µg/L of arsenic (appendix 1F).

The black-and-gray shale samples HW-26 and HW-28.5 in table E9 have the highest weight percent arsenic, sulfur and organic carbon content in the HW CORE. Also, HW 30-33 is a red siltstone with high concentrations of sulfur (0.17 weight percent) and copper (2420 mg/Kg) compared to the other red rocks. The copper and sulfur in this sample are in a geochemical setting similar to those in other stratabound red-bed copper deposits in the basin as well as other Mesozoic rift basins, indicating element transport and precipitation in these strata (for example: Kummel, 1901; Smoot and Robinson, 1988). These rocks were tested in the aqueous leach experiment, detailed later, to assess arsenic mobility in black, gray and red mudstones and siltstones.

The major mineral sources of arsenic in the red mudstone and siltstone are hematite, illite and chlorite (table E10). The statistical relationships between the mass of arsenic and these minerals in the bulk rocks are obtained by relating the appropriate proportion of the chemical component mass in table E10 to the appropriate mineral. Most of the weight percent Fe_2O_3 in the bulk rocks is in the mineral hematite. Based on the mineral types and their relative percentile abundance, most of the Al_2O_3, designated Al_2O_3[total] in the bulk rock, is partitioned among illite, chlorite and

Table E9. Geochemistry of rock in middle and upper parts of the Passaic Formation

Depth of core (ft)	rock color	As	REE[2]	Fe_2O_3[3]	Al_2O_3	P_2O_3	K_2O	Na_2O	S
		mg/kg		weight percent					
HW-26……..	black	95	112.1	4.91	11.1	0.06	1.17	4.66	1.82
HW-28.5……	gray	18	150.8	6.19	13	0.1	1.32	4.87	0.57
HW-29.5……	red	10.0	209.60	8.94	20.2	0.17	4.89	3.23	0.02
HW-30-33[1]……	red	4.5	167.18	8.47	18.9	0.16	4.88	2.9	0.17
HW-33……..	red	7.0	184.27	7.45	17.9	0.16	4.25	3.15	0.05
HW-83.6……	red	5.1	167.68	5.71	14.03	0.11	2.22	3.9	0.00
HW-144…….	red	12.1	254.07	8.74	20.3	0.19	5.19	2.74	0.02
HW-161…….	red	10.4	235.93	8.10	19.5	0.17	4.63	2.91	0.02
HW-213.4-214[1]……	red	11.1	249.46	8.84	19.98	0.18	3.65	4	0.02
HW-225.6……	red	10.3	241.10	8.65	19.98	0.16	4.23	3.93	0.00
HW-286……	red	11.0	229.00	7.36	20.1	0.2	4.45	3.53	0.02
HW-334…….	red	11.7	246.88	8.72	20.21	0.19	5.21	2.75	0.02
HW-392-393[1]……..	red	14.8	255.50	8.91	20.75	0.18	5.26	3.07	0.02
HW-394…….	red	13.0	248.56	8.34	20.1	0.18	4.44	3.7	0.01
SS-96.5…….	red	11.1	235.17	8.47	19.89	0.18	5.12	1.9	0.02
SS-144-145[1]…….	red	9.6	230.52	8.83	20.16	0.22	5.02	2.66	0.02
SS-147……..	red	8.6	208.65	6.5	16.75	0.18	2.82	4.12	0.02
M-1127……..	red	4.5	169.59	4.76	14.89	0.11	1.57	4.7	0.04

[1]Composite sample
[2]REE, sum of the rare earth element concentrations of La, Ce, Pr, Nd, Sm, Eu, Gd, Tb, Dy, Ho, Er, Tm, Yb and Lu.
[3]Iron reported as Fe_2O_3 regardless of actual oxidation state.
Notes: HW CORE is from the middle part of the Passaic Formation and the Hopewell investigation.
Cores SS- and M- are from the upper part of the Passaic Formation.

plagioclase. For this analysis, illite and chlorite are lumped together as clay minerals, and their constituent mass of Al_2O_3, designated Al_2O_3[clay], can be determined by subtracting the mass of Al_2O_3 in plagioclase from Al_2O_3[total]. Most of the plagioclase in the red strata of the Passaic Formation is albite ($NaAlSi_3O_8$) and most of the Na_2O in the bulk rock is partitioned in this mineral (Van Houten, 1965). For each mineral listed in table E10, Al_2O_3[clay] is determined by partitioning all the mass of Na_2O into albite, then calculating the weight percent Al_2O_3[albite] needed for the albite and subtracting this from Al_2O_3[total]. Most of the weight percent K_2O in the red rocks is associated with the illite clay fraction (Van Houten, 1965), and a comparison of its statistical significance with Al_2O_3[total] versus Al_2O_3[clay] is used to validate this approach. The Pearson product-moment correlation coefficient (r) for the linear correlation analysis among the geochemical variables arsenic, REE (sum of lanthanum (La) to lutetium (Lu) in mg/Kg) in mg/Kg and Al_2O_3total], Al_2O_3[clay], Fe_2O_3, P_2O_3, K_2O, Na_2O and sulfur in weight percent is shown in table E11 and graphically represented in figure E13. These variables are chemical components and/or indicators of hematite and clay (illite and chlorite) and other minerals such as apatite [$Ca_5(PO_4)_3$ (OH,F,Cl)] and sulfides such as pyrite that may contain arsenic. Although sulfide minerals are seldom observed in these oxic red rocks, comparison of the mass of S to that of arsenic, in addition to the other comparisons, encompasses the complete range of potential major arsenic hosts recognized in these rocks. For discussion purposes, the correlation coefficient (r) is considered very strong if it ranges from 0.9 to 1, strong from 0.8 to 0.89 and moderate from 0.7 to 0.79.

Very strong positive statistical correlations prevail between Al_2O_3[clay] and K_2O (r = 0.98), REE and arsenic (r = 0.94) and, Al_2O_3 [clay] and Fe_2O_3 (r = 0.92). Strong correlations prevail among arsenic and REE with Al_2O_3[clay] (r = 0.82 and 0.81) and Fe_2O_3 (r = 0.83 and 0.84) respectively, and, di-phosphurus trioxide (P_2O_3) with Al_2O_3[clay] (r = 0.81). Moderate correlation among P_2O_3 and the chemical components K_2O (r = 0.78), Fe_2O_3 (r = 0.75), REE (r = 0.75), and arsenic (r = 0.72) also exist. No correlation exists between sulfur percent and any other component (r ranges from – 0.34 for REE to -0.05 for P_2O_3).

The statistical correlation between K_2O and Al_2O_3[clay] (r = 0.98) versus Al_2O_3[total] (r = 0.91) is stronger, suggesting that it is a more valid indicator of

Table E10. General mineral and chemical composition of red mudstones and siltstones in the Passaic Formation

Mineral	Formula	Percent
Quartz…….....	SiO_2	29.6
Plagioclase…….....	$(Na, Ca)AlSi_3O_8$	30.4
Microcline……..	$KAlSi_3O_8$	< 5.0
Anhydrite/gypsum……	$CaSO_4$//$CaSO_4 \cdot 2H_2O$	<1.0
Calcite…….....	$CaCO_3$	2.9
Ferroan dolomite……..	$(Ca, Mg)CO_3 \cdot (Fe, Mn)\ CO_3$	<1.0
Hematite…….....	Fe_2O_3	8.0
Illite……..	$(H_3O, K)_y(Al_4 \cdot Fe_4 \cdot Mg_4 \cdot Mg_6)(Si_{8-y} \cdot Al_y)O_{20}(OH)_4$	25.5
Chlorite……	$(Mg, Fe^{2+}, Fe^{3+})_6(AlSi)_4O_{10}(OH)_8$	3.5

Mainly after van de Kamp and Leake (1996), also Van Houten (1965), and Oshchudlak and Hubert (1988).
Actual mineral percentages in individual rocks may vary.

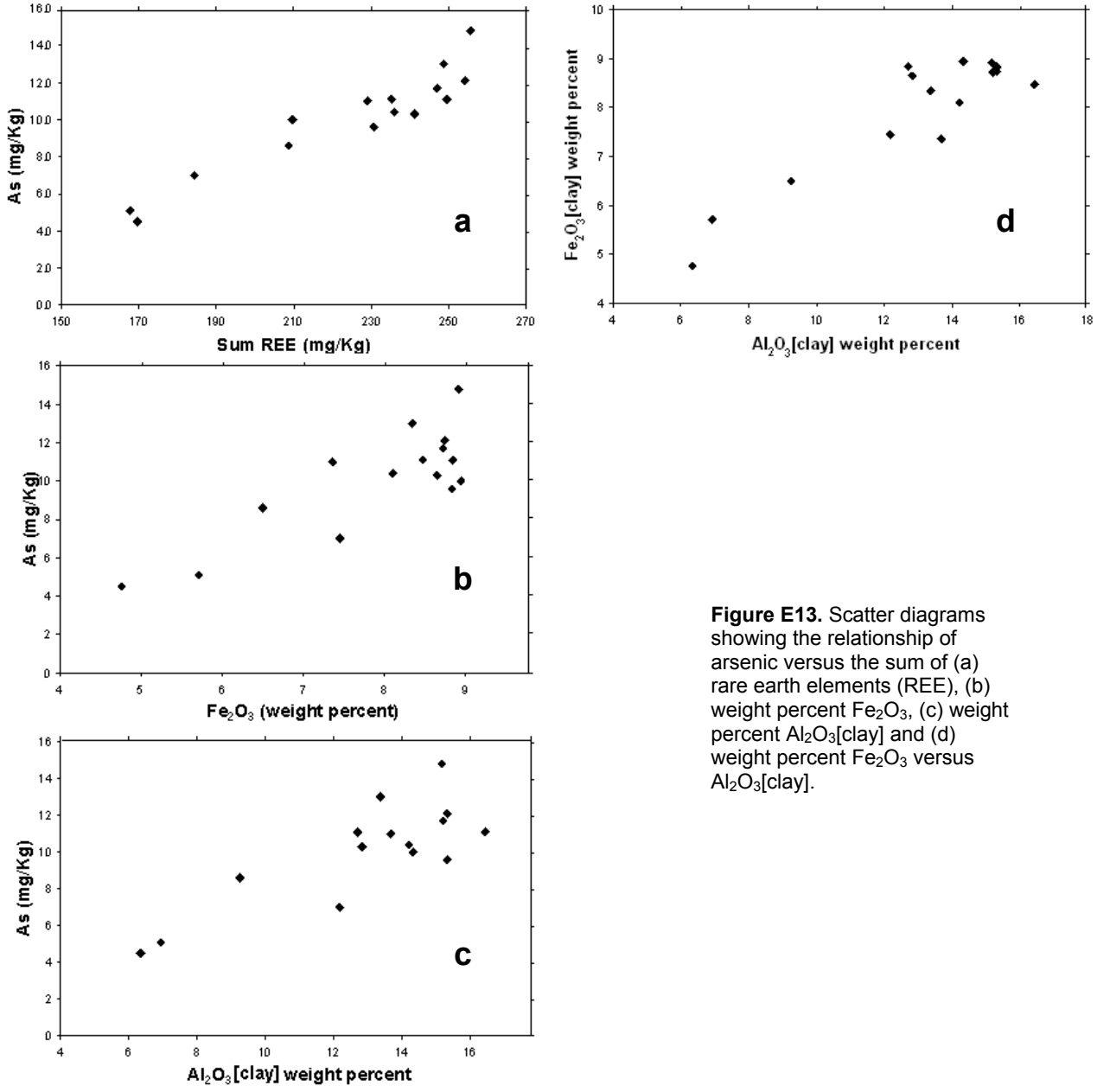

Figure E13. Scatter diagrams showing the relationship of arsenic versus the sum of (a) rare earth elements (REE), (b) weight percent Fe_2O_3, (c) weight percent Al_2O_3[clay] and (d) weight percent Fe_2O_3 versus Al_2O_3[clay].

Table E11. Correlation analysis showing the correlation coefficient r, in the concentration of 8 chemical constituents of 16 red mudstones and siltstones shown in table E10.

Chemical constituent	As	sum REE[1]	Al_2O_3 [total]	Al_2O_3 [clay][2]	Fe_2O_3	K_2O	P_2O_3	S	Zr	B
As……..	1.00									
Sum REE…….	0.94	1.00								
Al_2O_3[total]……	0.89	0.89	1.00							
Al_2O_3[clay][2]……..	0.82	0.81	0.94	1.00						
Fe_2O_3……	0.83	0.84	0.94	0.92	1.00					
K_2O……	0.81	0.76	0.91	0.98	0.90	1.00				
P_2O_3……..	0.72	0.75	0.82	0.81	0.75	0.78	1.00			
S…….	-0.29	-0.34	-0.13	-0.08	-0.23	-0.08	-0.05	1.00		
Zr……	-0.20	-0.21	-0.21	-0.31	-0.45	-0.38	-0.27	0.38	1.00	
B…….	0.66	0.76	0.69	0.52	0.61	0.46	0.53	-0.26	-0.23	1.00

[1] REE Rare Earth Elements
[2] Al_2O_3(clay) determined by subtracting Al_2O_3 in albite (NaAlSi3 O8) from Al_2O_3 (total). All whole-rock Na assumed to be from albite.

the clay fraction than Al_2O_3[total] (table E11). Al_2O_3[clay] and Fe_2O_3also strongly correlate (r = 0.92) and therefore the relative abundance of clay minerals and hematite in the bulk rock is directly related. This finding is not surprising because a direct positive relationship between clay mineral content and iron is observed in river, offshore and marine sediments (Moore, 1963; Yan and others, 1991). Most of the hematite in the red mudstones of the Newark basin is microcrystalline and specular and both characteristics are primarily associated with the matrix clay minerals (McIntosh and others, 1985). Those workers concluded that the microcrystalline hematite formed by the dehydration of iron hydroxide that coated the detrital clay particles. It is important to note that because the masses of Al_2O_3[clay] and Fe_2O_3 are strongly associated, geochemical components that are strongly associated with only one, but not the other of these major components, may falsely yield a statistically significant correlation with the other, and with other similarly associated components. Therefore, for those geochemical components that can arguably be associated with both Al_2O_3[clay] and Fe_2O_3, such as arsenic and REE, it may be impossible to differentiate their true degree of association between the two using statistical analyses alone.

REE and arsenic are very strongly correlated (r = 0.94). This can be interpreted as indicating proportional mass partitioning of these elements among host minerals (table E11). Clay mineral structures are important for the accumulation of the trivalent REE, and the bulk of REE is associated with the silt-and-clay-size sediment fractions (McLennan, 1989; Condie, 1991; van de Kamp and Leake, 1996). However, coatings of manganese and iron oxides and organic matter on particles are the dominant scavengers of REE in rivers and the ocean (Elderfield and others, 1990; Sholkovitz, 1995, p. 94; Lerche and Nozaki, 1998; Ingri and others, 2000). Strong correlations exist in the red mudstones and siltstones between arsenic and REE with Al_22O_3[clay] (r = 0.82 and 0.81) and Fe_22O_3 (r = 0.83 and 0.84) respectively. Based on the physical association of hematite with silt and clay-sized particles in these rocks and the geochemical affinity of arsenic and REE for hematite in particular, but also for clays, it is concluded that arsenic and REE are mainly associated with the hematite-coated clay minerals. Other abundant minerals making up these rocks, such as albite, probably contain crustal abundances of arsenic (arsenic about 1.8 mg/Kg). Some accessory minerals such as apatite may contain arsenic and REE; others, such as pyrite, and still others, such as zircons, REE only.

REE from zircon and apatite in shale is generally considered less important than clay control (Condie, 1991). This generalization holds true for zircon because REE and zirconium correlate poorly (r = -0.21) in these rocks. However, moderate correlations of r = 0.72 and 0.75 do however exist between P_2O_3 with arsenic and REE respectively. Nevertheless, these moderate correlations may be misleading because a stronger statistical correlation between P_2O_3 and Al_22O_3 in clay (r = 0.81) and a moderate one with Fe_22O_3 (r = 0.75) suggest P_2O_3 also has a geochemical association with hematite-coated clay. An acid leach experiment conducted by Serfes (2005) removed more than 95 percent of the total P_2O_3 from a pulverized sample of HW-394, suggesting that any apatite in the rock was dissolved, but only 50 percent of the arsenic

and 25 percent of the REE was. These results indicate that although apatite may be a minor source of arsenic and REE, it is not the major source. Percentage sulfur lacks correlation with any other component (r ranges from –0.34 for REE to -0.05 for P_2O_3) and therefore pyrite is not associated with arsenic in these rocks.

Arsenic mobilization mechanisms in the Lockatong Formation

The Lockatong Formation mainly consists of black and gray shale with fewer red rocks. This section focuses on the mobilization of arsenic from pyrite, which is most common in the black shale. Naturally occurring arsenic concentrations in water are governed by abiotic and/or microbially controlled mineral-water interactions. These are mainly: 1) precipitation-dissolution reactions and 2) adsorption-desorption reactions. Two main processes are thought to control the mobilization of arsenic in the black shale outcrop area: (1) dissolution of pyrite; which releases arsenic into solution, and (2) adsorption of arsenic onto adsorbents such as hydrous ferrous oxide (HFO); which reduces its concentration. Each of these processes is discussed below.

Pyrite Dissolution

During the nucleation and growth of pyrite in reducing environments, available oxy-anions of arsenic are reduced first by sulfide before replacing sulfur in the pyrite structure (Morse and Luther, 1999). After this, arsenic can be released back into the environment, but its host pyrite must be oxidized first. Arsenic is generally the most abundant minor constituent of pyrite and research is being conducted by the US Geological Survey to assess the degree to which it destabilizes pyrite, making it more reactive (USGS, 2002). The dominant oxidizer of this decomposition is O_2, however secondary oxidants such as Fe^{3+} and NO_3^- may also play a role. When exposed to air and water, pyrite oxidizes by the following generally accepted overall reaction (Howard, 1998).

equation 1:

$$FeS_2 + 15/4O_2 + 7/2H_2O \rightarrow Fe(OH)_3(s) + 2SO_4^{2-} + 4H^+$$

For every mole of pyrite oxidized, 4 equivalents of acidity are released. The major multiple reactions leading to the overall reaction are:

$$FeS_2 + 7/2O_2 + H_2O \rightarrow Fe^{2+} + 2SO_4^{2-} + 2H^+$$
(oxidation of pyrite sulfur)

$$Fe^{2+} + 0.25O_2 + H^+ \rightarrow Fe^{3+} + 0.5H_2O$$
(rate-limiting step, oxidation of Fe^{2+} to Fe^{3+})

$$Fe^{3+} + 3H_2O \rightarrow Fe(OH)_3(s) + 2H^+$$ (Fe^{3+} is hydrolyzed),
or
$$FeS_2(s) + 14Fe^{3+} + 8H_2O \rightarrow 15Fe^{2+} + 2SO_4^{2-} + 16H^+$$
(Fe^{3+} acts as a secondary oxidant)

Therefore, the principle pyrite decomposition reactions involve the oxidation of both sulfide (S^{-2}) and ferrous iron (Fe^{2+}). The rate-limiting step is the oxidation of ferrous to ferric iron. At pH lower than 4, the rate of pyrite oxidation is largely controlled by the metabolism of bacteria such as Thiobacillus ferrooxidans (Singer and Stumm, 1968). At pH values higher than this, the abiotic rate of pyrite oxidation rapidly increases so that bacterial catalysis is not needed to explain the observed rate of aqueous iron oxidation. Therefore, at circumneutral pH, pyrite oxidation is mainly controlled by the amount of molecular oxygen in the recharge water. Inasmuch as calcite ($CaCO_3$) occurs in lenses, pore fillings and fracture fillings in rock associated with the pyritic-black shale of the Newark basin, it is assumed that it will readily react and buffer the pH. Therefore, a circumneutral pH is assumed and microbial metabolism is not considered to be a major control of pyrite oxidation.

A general rate law for the oxidation of pyrite at 25°C was developed by Williamson and Rimstidt (1994) by comparison of data from several previous investigations. This law assumes a constant supply of oxygen and no rate reduction due to potential diffusion limitations imposed by reaction-product surface coatings such as HFO on the pyrite surface. The law is:

equation 2:

$$-d[py]/dt = r(mol/m^2/s) =$$

$$10^{-8.19\ (\pm 0.1)}\ [O_2]^{0.5\ (\pm 0.04)}\ [H+]^{-0.11\ (\pm 0.01)}$$

The reaction rate of pyrite oxidation was also investigated experimentally by Kamei and Ohmoto, (2000) who measured decreasing O_2 concentrations during the reaction in a closed system. The rate of reaction (1) at a pH 5.7 $\pm$ .03 and T = 25°C was determined to be:

$$-d[py]/dt = 10^{-6.0\ (+/-0.5)}\ [O_2]\ (mol/m^2/s).$$

Therefore pyrite in water at equilibrium with atmospheric oxygen (8.58 milligrams per liter or 0.00026 moles per liter) and at pH = 5.7 decomposes as described in *equation 1* at a rate of 2.6 x 10^{-10} moles of pyrite/m^2/s, which compares well with a rate of 6.1 x 10^{-10} moles of pyrite/m^2/s determined using *equation 2*. These rate equations are instructive but difficult to apply

in field settings because it is difficult to determine the surface area of reactive pyrite in a particular rock and its hydrogeological setting. Variables such as the size and geometric distribution of pyrite grains, the thickness of the weathered bedrock zone, and the geometry of the hydraulic conduit network pervading the rock, among others, would have to be determined first.

Adsorption of arsenic onto HFO

As indicated in the reaction detailed in *equation 1*, hydrous ferrous oxide is formed during the oxidation of pyrite. Numerous workers have noted the importance of HFO as a major adsorbent of arsenic, and Dzombak and Morel (1990) compiled adsorption constants for the generalize two-layer model for HFO. Studies of mechanisms of arsenic adsorption onto HFO at the molecular scale have been made to better understand its uptake and release. The complexation of arsenite and arsenate at the HFO surface is pH dependent and mainly associated with ligand exchange with OH_2 and OH^- at binding sites. Therefore, arsenic forms inner sphere complexes with HFO. Arsenate is more strongly retained at lower pH and arsenite at higher pH (Wilkie and Hering, 1996). Both arsenic species mainly form bidentate binuclear surface complexes (Manning and others, 1998, Sun and Doner, 1996). Reaction mechanisms of arsenic with HFO have been investigated by assessing surface-charge variations and the release stoichiometry of H^+/OH^- during complexation reactions (Jain and others, 1999). One of their findings is that at low pH (< 6.0), oxygen involved in the Fe-O-As bond of arsenite remains partly protonated, resulting in neutral complexes ($Fe\text{-}O(H)As(OH)_2$) that are less strongly bound than the -1 or -2 charged arsenate species. Above pH 7.0 a considerable increase in surface charge reduction is related to a change in arsenate surface species from $Fe\text{-}OAs(O)_2\text{-}(OH)$ to $Fe\text{-}OAs(O_3)$. This increased negative charge of the arsenate surface species coupled with a hydroxylated surface inhibits arsenate adsorption. Above pH 7.0, arsenite species do not form surface species that reduce the surface charge and therefore are more strongly retained than arsenate.

The adsorption of arsenic onto HFO as a function of adsorbate/adsorbent ratios and co-occurring solutes (Ca^{2+} and SO_4^{2-}) was investigated using experimental and modeling techniques (MINEQL+ v.3.01) over a pH range of 4 to 9 (Wilkie and Hering, 1996). Major experimental findings are that competition for sorption sites with SO_4^{2-} for arsenate, and particularly arsenite, was greatest at low pH and the adsorption of Ca^{2+} at high pH enhanced the adsorption of arsenate. This enhanced adsorption of arsenate was attributed to the favorable electrostatic surface effects (positive charge) associated with Ca^{2+} adsorption. Model predictions overestimated, but were qualitatively consistent with, the competitive effect of SO_4^{2-} on both arsenic species and the enhanced adsorption of arsenate associated with Ca^{2+} adsorption.

Site-specific model

A simple geochemical model based on data from the lower Passaic Formation in the Hopewell HW-6 study was used to evaluate the equilibrium chemistry resulting from the weathering of pyrite and calcite in a black bed. This bed is slightly above the Lockatong Formation stratigraphically and is therefore assumed to be comparable from a geochemical perspective. This site was selected because ample data are available and local groundwater is contaminated with as much as 48 ppb arsenic. A whole-rock arsenic concentration of 138 ppm and 1.11 weight percent sulfur was obtained from a core sample of the black shale. For this model it is assumed that all the arsenic and sulfur in this rock are associated with pyrite. In that case the rock contains 2.14 weight percent pyrite with an average pyritic arsenic content of 6440 ppm. Concentrations of arsenic in pyrite obtained using electron microprobe techniques from the same rock are shown in figure E11a, they appear to be consistent with the above estimate. Interestingly, arsenic concentrations in soils in the same area increase from a mean of 11.4 mg/kg 0 to 2 ft below land surface to 56.2 mg/kg directly above bedrock at 6 to 8 ft below land surface where a maximum of 359 mg/kg was found (NJDEP, 1998). The increase in arsenic concentration with depth supports a natural rather than anthropogenic source for most, if not all, of it in soil here. It also indicates that some of the arsenic released during bedrock weathering remained in the soil, probably adsorbed onto mineral surfaces.

The movement of water from the atmosphere to groundwater at the site can be divided into four chemically distinct zones:

1) Precipitation zone: acidic dilute solution, arsenic < 1 µg/L

2) Soil zone: unsaturated, acidic solution less dilute than precipitation, arsenic < 1 µg/L

3) Highly weathered bedrock zone: variable saturation, calcite + pyrite occur, circumneutral pH, increased dissolved solids, arsenic mobilized (> 1 µg/L)

4) Slightly weathered and unweathered bedrock zone: circumneutral pH, saturated, arsenic transported by groundwater mainly through fractures.

This model focuses on determining the potential for arsenic mobilization in the highly weathered bedrock zone. It is based on the minimum volume of pyrite that is weathered per square ft per year to account for 50 µg/L arsenic in water recharging the groundwater reservoir at this site. This approach is practical in that it provides background on the volume of pyrite involved and the amount of released arsenic that is mobile.

A groundwater recharge rate of approximately 10 inches per year is estimated for this rock type and area. Using equation 3 below, the minimum volume of pyrite that must be weathered, in cubic centimeters (cc) per square ft., to produce a concentration of 50 µg/L arsenic in water recharging the groundwater reservoir is 0.035 cc. This assumes that all the arsenic released from pyrite containing 6440 mg/Kg arsenic goes into solution and none is diluted.

equation 3:

Minimum volume of pyrite
decomposed per square foot per year (in cc) =

[recharge (inches/year) x 144 inches^2 x 16.38 x arsenic concentration in water (µg/L)] / [(5.2 gm/cc) x arsenic in pyrite (µg/Kg)]

Model parameters

MINEQL+ (ver. 4.5; see references) was used to evaluate the concentration and speciation of mobile and adsorbed arsenic after .035 cc of pyrite with an arsenic concentration of 6440 mg/Kg is decomposed. Molarity concentrations were determined assuming complete dissociation of 6.6e-5 moles of pyrite and 1.32e-4 moles of $CaCO_3$ in 23.6 liters of recharge water (table E12). It is assumed that pyrite (0.183 gms) is completely oxidized as are all released iron and sulfur.

Model results and discussion

The model results shown in tables E13 and E14 indicate that arsenic, particularly arsenite, is mobile over a wide pH range. A circumneutral pH of 6 to 8 is expected for this system; therefore this range is more detailed. Some of the important model results are:

1) All the Fe^{3+} was precipitated as hematite (Fe_2O_3) throughout the entire pH range.

2) Arsenic species were mainly bound to the HFO weak binding sites (Serfes, 2005) and the percentages are similar at I = .001M and .01M

3) At equilibrium, the pH = 7.0 (equal acid and base) and I = .003. It is estimated that the pH in the highly weathered bedrock zone is circumneutral, pH 6 to 8. For comparison, the median pH in this aquifer is 7.6 (Serfes, 1994).

4) At circumneutral pH, as much as 75 percent of arsenite is mobile as opposed to only 4 percent arsenate.

5) At circumneutral pH, SO_4^{2-} competition for adsorption sites is minor compared to that at the lower pH range (see appendix C in Serfes, 2005 for graph and data).

Table E12. Constituents and physical characteristics used to model the speciation and mobilization of arsenic in highly weathered black shale in the middle of the Passaic Formation.

Comstituents and physical charactersitics	Modeling procedures and parameters	Concentration and temperature
Fe^{3+}……	Released in 0.035 cc pyrite (0.183 grams)	6.6e-5M
SO_4^{2-}……..	Released in 0.035 cc pyrite (0.183 grams)	1.3e-4M
AsO_3^{3-}…….....	Released in 0.035 cc pyrite (0.183 grams)	6.54e-7M
Ca^{2+}……...	Released during calcite dissolution[1]	1.32e-4M
CO_3^{2-}…….	Released during calcite dissolution[1]	1.32e-4M
Fe(wk)OH…….	0.2 mole sites/mole Fe	1.32e-05M
Fe(st)OH……..	0.005 mole sites/mole Fe	3.3e-07
O_2……..	All Fe and S in oxidized state	Not applicable
Ionic Strength……..	I = 0.001 and .01, also calculated	Calculated
pH……..	Range 4 – 10, also calculated	Calculated
Temperature…….....	Approximate groundwater temperature	12 °C

[1] Based on equation: $FeS_2 + 2CaCO_3 + 15/4O_{2\,(g)} + 3/2H_2O \rightarrow Fe(OH)_{3(s)} + 2Ca_{2+} + 2SO_4^{2-} + 2CO_{2\,(aq)}$

Table E13. Percentage of arsenite species as a function of pH.

pH	Adsorbed As (%)	Mobile As (%)	
	$Fe(wk)H_2AsO_3$	$\% H_3AsO_3$	$\% H_2AsO_3^-$
4……	1	99	0
6……	24	76	0
7……	36	64	0
8……	36	61	3
10……	2	22	76

Note: Total As = 6.54e-7M, only species > or = 10% within pH range 4 to 10 are shown.

Table E14. Percentage of arsenate species as a function of pH.

pH	Adsorbed As (%)			Mobile As (%)	
	$Fe(wk)HAsO_4$	$Fe(wk)H_2AsO4$	$Fe(wk)OH\text{-}AsO_4$	$H_2AsO_4^{2-}$	$HAsO_4^{2-}$
4……	27	32	0	38	0
6……	3	0	94	0	0
7……	0	0	97	0	0
8……	0	0	95	0	4
10……	0	0	95	0	5

Note: Total As = 6.54e-7M, only species > or = 10% within pH range 4 to 10 are shown.

6) At circumneutral pH and higher, the increased calcium adsorption appeared to maintain arsenate adsorption at the concentrations used for this model.

Based on these results, figure E14 depicts a conceptual model of arsenic mobilization resulting from pyrite oxidation and calcite dissolution in black shale in the basin. If arsenite is the major arsenic species at the circumneutral pH modeled for the highly weathered bedrock zone, minimal pyrite oxidation is required to explain the high concentrations of arsenic in local groundwater.

Conclusions

A simplified model of chemical equilibrium in the

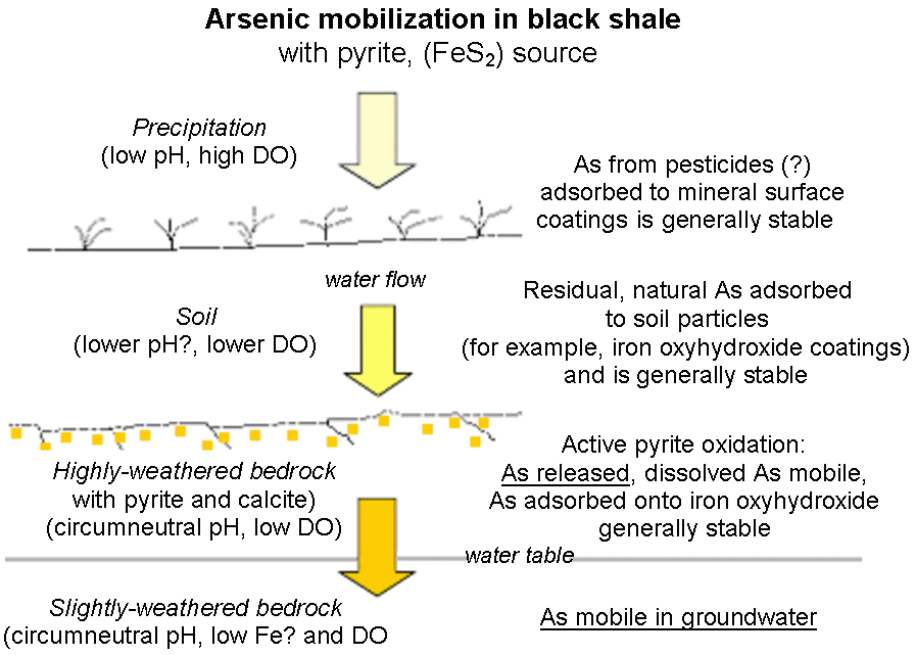

Figure E14. Conceptual model of arsenic mobilization in black shale containing pyrite and calcite in the Newark basin. DO, dissolved oxygen.

highly-weathered bedrock zone (fig. E14) based on MINEQL+ v. 4.5 produced the following results:

1) under the chemical conditions used for the model simulation, the oxidation of pyrite may be a prolific source of As in groundwater if arsenite is the major arsenic species present. In this simulation less than 0.05cc of pyrite/ft^2/year would need to decompose to account for 50 µg/L of arsenic in water.

2) At the circumneutral pH estimated for this system, as much as 75 percent of the neutral arsenite species (H_3AsO_3) is in solution and mobile. Arsenate ($H_2AsO_4^-$) is almost 100 percent adsorbed as Fe(wk)OH-AsO_4^{3-} within the same pH range.

3) Field data indicate that dissolved oxygen and iron concentrations are generally low in groundwater and arsenic concentrations exceed 10 µg/L. One possibility is that most of the iron is oxidized and DO is consumed in water recharging the groundwater reservoir as shown in figure E15.

4) Arsenic bound to HFO in the soil and in the highly-weathered bedrock zone is a potential source of contamination if exposed to competing ions such as phosphate, or to reducing conditions resulting from organic pollution.

5) The volume of pyrite decomposition required to account for the arsenic concentrations in groundwater is related to:

   a) The lateral and vertical distribution of arsenic -bearing pyrite in bedrock.
   b) The concentration of arsenic in the pyrite.
   c) The surface area of reactive pyrite exposed in the highly weathered zone.
   d) The volume of groundwater recharge and the hydrodynamic setting.
   e) The pH and Eh of water in the highly weathered bedrock zone, which controls reaction rates and products.

6) A deterministic contaminant-transport model is needed that can predict arsenic mobilization and flux in the unsaturated and saturated zones associated with the pyritic black shale. The hydrodynamic and geochemical model parameters should be determined and supported by field investigations. Field calibration and validation are also required.

Arsenic mobilization mechanisms in the Passaic Formation

Leach experiments

An initial water-rock leach experiment was designed and used to evaluate and compare potential arsenic mobilization from red, gray, and black strata in the Passaic Formation. Powdered samples of red (4.5 mg/kg arsenic), gray (12.6 mg/kg arsenic) and black (52.4 mg/kg arsenic) strata in the HW CORE from depths of 18 to 31 ft were used. Pyrite is ubiquitous in the black shale and point concentrations of as much as 3000 mg/L of arsenic were analyzed using electron microprobe techniques (Serfes and others, 2005; Serfes, 2005).

This experiment exposed 500 grams of pulverized rock to 500 ml of air-equilibrated, doubly-distilled deionized water for one hour per week for 20 weeks, following the Accelerated Weathering of

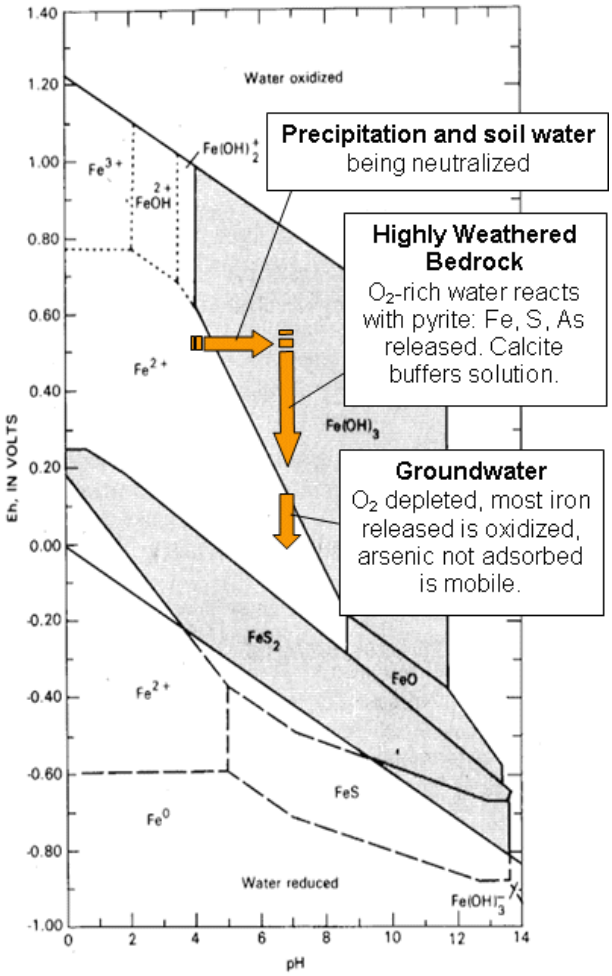

Figure E15. Fields of stability for solid and dissolved forms of Fe as a function of Eh and Ph at 25°C and one atmosphere pressure. From Hem (1985).

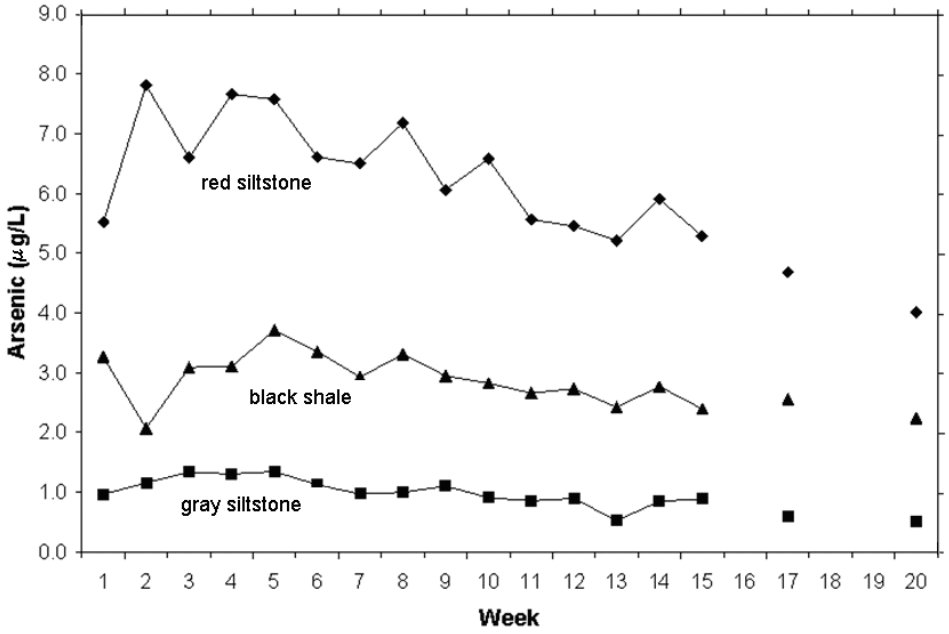

Figure E16. Arsenic concentration versus duration of leaching. Five hundred g pulverized rock exposed to 500 ml of air-equilibrated doubly distilled deionized water for 1 hr per week (American Society for Testing and Materials 2001). Analytical precision and accuracy is ± 10 percent.

Solid Materials procedure (ASTM, 2001). Arsenic concentrations in leachate versus collection week are shown in figure E16. Average arsenic concentrations in leachate of about 6 µg/L from the red siltstone are higher than those from the black (about 3 µg/L) and gray (about 1 µg/L) shale. Microscopic examination of pyrite in the pulverized black shale (52.4 mg/kg, arsenic) showed that it had not oxidized after 20 weeks and was presumably not contributing arsenic to the leachate. However, the higher values of leached arsenic in the red rocks prompted further studies using powdered red rock samples from the Passaic Formation.

Comparison of whole rock arsenic concentration versus arsenic mobilization

The concentration of arsenic in six samples of pulverized red mudstone and siltstone from the two rock cores shown in table E9; the HW CORE, and the SS core, collected adjacent to a domestic well with water containing 57 µg/L arsenic (appendix 3D9), is compared with the concentration of arsenic in leachate from these rocks. Five grams of pulverized rock was mixed with 200ml of doubly distilled deionized water and the mixture was agitated for 16 hours.

Arsenic concentrations in pulverized rock from

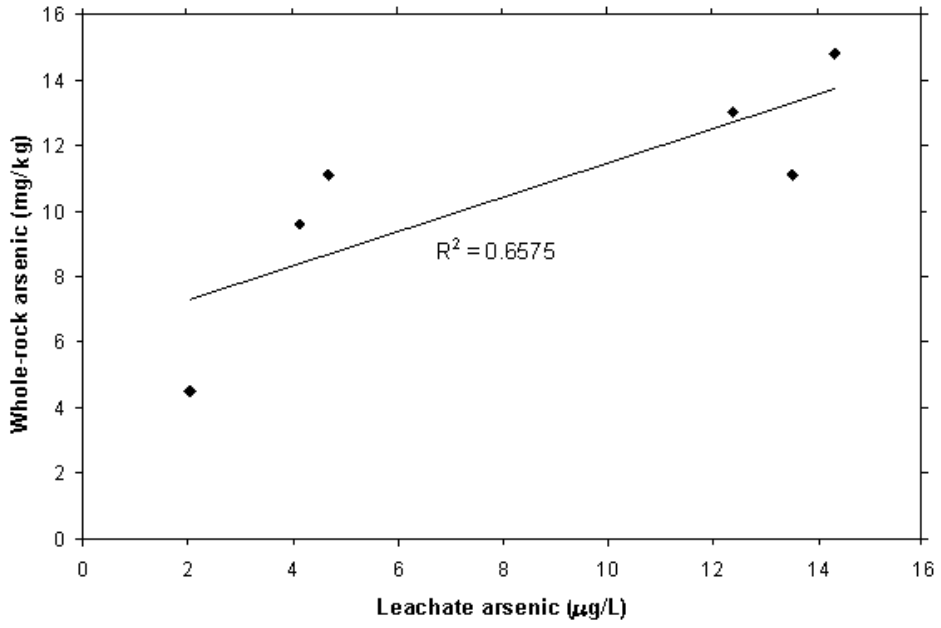

Figure E17. Whole-rock arsenic concentrations versus leachate arsenic concentrations (diamonds) from 6 samples using 5-grams of pulverized rock in 200 ml of doubly distilled deionized water followed by a 16-hour agitation procedure. Analytical precision and accuracy are within ± 10 percent.

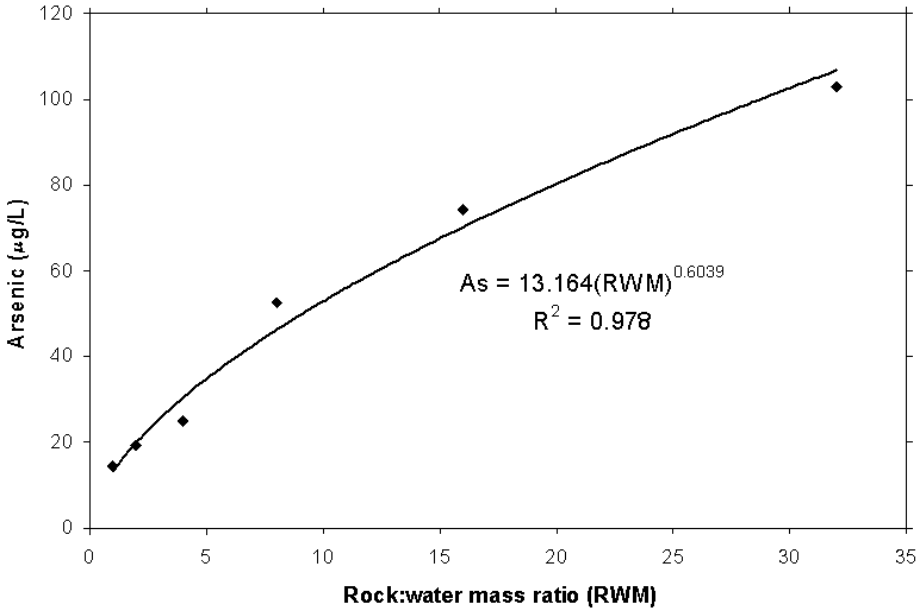

Figure E18. Arsenic concentrations versus rock-to-water mass ratio. A relative ratio of 1 is equal to 1:40 pulverized red mudstone (15 mg/kg arsenic) to water. Experiment shows the effect of varying water-rock contact. Analytical precision and accuracy within +/-10 percent.

six separate red mudstones and siltstones, and associated leachate after a 16-hour leach procedure, are shown in figure E17. These data show a strong linear correlation, r = 0.81, between arsenic concentrations in the rock and in the leachate. The graph of whole rock concentrations of arsenic in red mudstone and siltstone versus those in leachate using the procedure described above shows a positive trend.

Comparison of surface area versus arsenic mobilization

To evaluate the concentration of arsenic in the water-soluble fraction as a function of surface area: 5, 10, 20, 40, 80, and 160 grams of pulverized red mudstone (HW 392-393) containing 14.8 mg/kg arsenic were mixed with 200ml of doubly distilled deionized water and agitated for 16 hours.

The variation of arsenic concentration in aqueous solution relative to rock surface area (RSA) is shown in figure E18. Arsenic concentrations in leachate ranged from 14.3 µg/L, for a pulverized-rock-to-water ratio of 1:40, to barely over 103 µg/L, for a ratio of 0.8:1 for a 16-hour exposure time.

Evaluating arsenic mobilization at various pH values and also with $Na_2H_2PO_4$

Arsenic concentration versus stable pH in the aqueous leachate was evaluated to understand the mechanisms involved in the mobilization of arsenic in the natural groundwater reservoir. Stabilized pH values of 8.0, 8.5 and 9.0 were maintained using a 50-micromolar bicine, $C_6H_{13}NO_4$, buffer solution (pK_a = 8.35). A 50-micromolar hepes, $C_8H_{17}N_2SO_3$, buffer

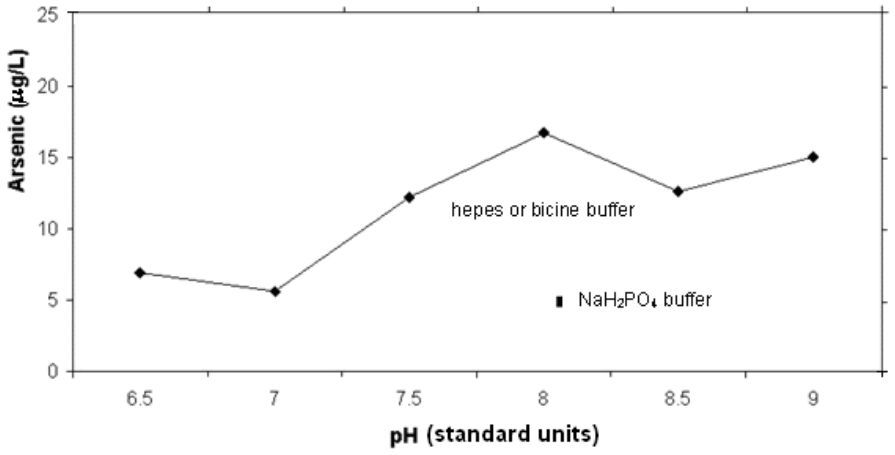

Figure E19. Arsenic concentration versus pH using 5 grams of pulverized red mudstone in 200-ml doubly distilled deionized water. Organic buffers hepes and bicine, and NaH_2PO_4 used to buffer pH. Analytical precision and accuracy within 10 percent.

solution (pK_a = 7.55) maintained pHs of 6.5, 7.0 and 7.5. Initially, each sample mixture contained 5 grams of sample HW392-393 containing 14.8 mg/kg arsenic, with 200 ml of DDW. This initial mixture was agitated for two hours to allow the solution to reach pseudo-equilibrium with the solid. Each sample was then titrated up to the target pH values using KOH. If the target pH was exceeded, HCl was added to lower the pH and thereby adjust it to the target value. This procedure took approximately one hour. The pH-adjusted samples were then agitated for an additional 21 hours for a total of 24 hours of contact time. In order to assess the competitive desorption of arsenic from the rock material, a solution containing 50 micromolar of NaH_2PO_4 buffer (pK_{a2} = 7.21) adjusted to a pH of 7.5 was also used. Results from the leach experiments that assessed arsenic mobilization versus pH and the competitive ion phosphate, are shown in figure E19. All final leachate pH values were within 0.05 of the original KOH-adjusted pH. Arsenic mobilization clearly increased from a pH of 6.5 to 8.0 and then decreased slightly at higher pH values. The maximum arsenic concentration, at a pH of 8.0, was 16.7 µg/L. The NaH_2PO_4 buffer (50 micromolar) was adjusted to pH 7.5 and produced an arsenic concentration of 30 µg/L; about 2.5 times more than in the non-phosphate sample at the same pH. This indicates that competitive ions such as phosphate can enhance the mobilization of arsenic from these rocks.

Arsenic mobilization in the Passaic Formation

Geochemical data from whole rock mineral analyses and water-rock leach experiments are interpreted to evaluate the sources and mobilization mechanisms of arsenic in the Passaic Formation in the New Jersey part of the Newark basin. This formation covers more than 50 percent of the basin area, has the most wells with arsenic concentrations exceeding federal and NJ state drinking water standards, and has the highest concentration of arsenic (216 µg/L) in groundwater in New Jersey (Serfes and others., 2005; Serfes 2005). Whole-rock concentrations of arsenic in the black shale (maximum 240 mg/kg) and gray shale (maximum 50 mg/kg) tend to be higher than those in the red mudstone and siltstone (maximum 14.8 mg/kg) in this formation. Pyrite is the major source of arsenic in the black shale, measured concentrations are as much as 4 weight percent, based on electron microprobe measurements. One preliminary hypothesis proposed by Serfes and others, (2005) is that the pyritic black shale that is variably intercalated with the red strata may be the major source of arsenic in groundwater in the Passaic Formation. The red strata (including purple beds) total about 97.5 percent of the volume of the formation but field observations and leach experiment results do not support this hypothesis (Serfes, 2005). For example, arsenic concentrations range from 35 to 45 µg/L in water from Hopewell HW-6, a deep well tapping solely red strata, and range similarly in water from adjacent well OBS-1 (figure E7). Two nearby observation wells, OBS-2 and OBS-3, penetrate black shale and red mudstone and siltstone beds of the Kilmer and T-U Members of the Passaic Formation, but have arsenic concentrations in their water of only 9 and 2 µg/L arsenic, respectively (Serfes, 2005). Arsenic concentrations exceeding 10 µg/L are common in water from wells tapping only red strata, although black and gray strata occur locally (Serfes and others, 2005). The leach experiment to evaluate the mobilization potential of arsenic demonstrates that during a 20-week procedure, red siltstone releases more arsenic than does the black or gray shale (fig. E16). These results indicate that the red strata, particularly the mudstones and siltstones that make up most of the Passaic Formation, are the major sources of labile arsenic in that formation's groundwater.

Sources of arsenic in the red mudstone and siltstone

Strong statistical correlations exist between arsenic and REE with Al_2O_3[clay] (r = 0.82 and 0.81) and Fe_2O_3 (r = 0.83 and 0.84) respectively in the red mudstones and siltstones (table E11). Based on the physical association of hematite with silt-sized and clay-sized particles in these rocks, and the geochemical affinity of arsenic and REE for hematite in particular but also for clays, it is concluded that arsenic and REE are mainly associated with the hematite-coated clay minerals. Other abundant minerals composing these rocks, such as albite, probably contain only crustal abundances of arsenic (~ 1.8 mg/kg). Some accessory minerals such as apatite may contain arsenic and REE; others, such as pyrite, arsenic only; and still others such as zircons, REE only. This interpretation is also supported by findings in hydraulically open and closed alluvial basins in the semi-arid southwestern United States. Some of these basins are modern analogs of the shallow lake/playa vegetated mud flats preserved in the upper two-thirds of the Passaic Formation (Smoot and Olsen, 1994; Smoot, 2010). Groundwater in alluvial basins in Arizona has arsenic concentrations of as much as 1300 µg/L (Robertson, 1989). Aqueous arsenic is associated with red clay beds that contain as much as 88 mg/Kg of arsenic. Arsenic occurs as arsenate ($HAsO_4^{-2}$) in these oxic groundwaters and concentrations are controlled by pH and redox conditions that affect the stability of iron oxyhydroxide and the

adsorption-desorption of As. Although the concentrations of arsenic anions, and oxyanions; such as fluorine, vanadium, selenium, and molybdenum are associated with iron oxyhydroxides, ubiquitous clay minerals such as montmorillonite are believed to also play a role (Robertson, 1989). Another modern analog is the Carson River area in the Carson Desert in Nevada where concentrations of arsenic and uranium in shallow groundwater locally exceed 1000 µg/L (Welch and Lico, 1998). These high concentrations are interpreted to be the result of evaporative concentration of Carson River water because concentrations of arsenic and uranium correlate positively with chlorine. Arsenic and uranium mobility are associated with adsorption/desorption on iron oxide phases and on their stability. Therefore, association of arsenic with hematite-coated clay in red mudstone and siltstone in the Newark basin is reasonable. The evaporative concentration of arsenic and other elements in the playa environments may have enhanced their adsorptive enrichment onto the iron phases coating clays and other particles.

Mobilization of arsenic from red mudstone and siltstone

The concentration of arsenic in leachate measured in red-rock–water-contact experiments is approximately proportional to that in the rock (fig. E17). However, slight variations in the proportional exposure of arsenic-rich surfaces among these pulverized rock samples may have affected arsenic concentrations in the leachate. Accordingly, during subsequent experiments, a red mudstone associated with WBZs transmitting water exceeding 45 µg/L arsenic, and with an arsenic concentration of 14.8 mg/kg arsenic (HW CORE 392-393 ft), was tested. The results of the relative surface area versus arsenic mobilization shown in figure E18 illustrate that the extent of water-rock contact is directly and positively related to the arsenic concentration. This indicates that water-rock contact along the groundwater flow path promotes arsenic mobilization and therefore a higher arsenic concentration in groundwater. The pH dependence of arsenic mobilization shown in figure E19 is similar to that from field data collected from domestic wells, as shown in figure E6, where maximum arsenic mobilization is at a pH of approximately 8.0. A maximum arsenic concentration at pH 8.0 suggests that goethite/hematite, with a point of zero charge of about 7.8 to 8.5, controls the arsenic concentration via adsorption-desorption reactions (Stumm, 1992). Arsenic desorbed from early hematite-source coatings on clays and/or adsorbed onto later hydrothermally-derived late hematite cements, as described in Oshchudlak and Hubert (1988), are possible mechanisms for this pH control of aqueous arsenic concentrations. The competitive nature of arsenic mobilization by phosphate in these rocks is also evident in figure E19 which shows an almost 250-percent increase in mobilized arsenic compared to the non-phosphate-buffered sample at the same pH. Speciation analyses described in Serfes and others (2005) and Serfes (2005) showed that arsenic in groundwater in the Passaic Formation and in the red siltstone leachate is dominantly As(V). Analyses of groundwater from wells in the Passaic Formation for this study have measured <0.04 mg/L phosphate. Low concentrations of phosphate in groundwater elsewhere in the Newark basin are also reported in Serfes (1994). Therefore, dissolved phosphate is probably not a major control on arsenic concentrations in the Passaic Formation. However, other oxyanions such as boron and molybdenum that locally occur in this groundwater are likely to compete with arsenic for sorption sites and thereby control its aqueous concentration (Senior and Sloto, 2006; Serfes and others, 2005). The pH and competition-dependent control on arsenic mobilization of this aquifer material, and the generally low iron concentrations in groundwater from the Passaic, indicate that desorption from, but not dissolution of, soluble iron phases, is the major release mechanism of labile arsenic.

Based on the leach experiments described here, arsenic mobilization in groundwater of the red strata in the Passaic Formation is controlled by the following master variables:

1) pH,
2) As concentration in the red rock strata,
3) intensity of water-rock contact,
4) duration of water-rock contact, and
5) competing ions.

Some red strata in the Passaic Formation contain flow zones where secondary sparry, carbonate and sulfate minerals are dissolved by groundwater (fig. E9). These zones are likely sources for the mobilization and transport of lithogenic arsenic that was initially adsorbed and absorbed on and in iron-oxide mineral coatings during the Triassic Period and is currently being released via water-rock contact. Sparry minerals in these zones such as calcite and dolomite buffer and control aqueous pH by dissolution, thereby providing greater surface exposure to matrix hematite coating clay minerals and other minerals. Such zones of high hydraulic conductivity supply high yields to wells. If the arsenic concentrations in the aquifer matrix are high, wells tapping these permeable zones are likely to supply water with high arsenic concentrations.

Conclusions

1. This leach-experiment study has been confined to the Passaic Formation in the New Jersey part of the Newark basin; however, the results and conclusions are believed to be applicable to comparable parts of the formation in Pennsylvania and New York.

2. Whole-rock concentrations of arsenic in the black shale (maximum 240 mg/kg) and gray shale (maximum 50 mg/kg) tend to be higher than those in the red mudstone and siltstone (maximum 14.8 mg/kg).

3. Pyrite is the major source of arsenic in the black shale, with measured concentrations as much as 4 weight percent based on electron microprobe analysis.

4. Hematite that coats clays and other minerals, and possibly the clay surfaces themselves, is inferred to be the major source of arsenic in the red mudstone and siltstone.

5. Aqueous leach experiments performed on pulverized rock samples indicate that:
    a. Arsenic is more readily leached into dilute aqueous solution from red mudstone and siltstone than from gray or black shale.
    b. Arsenic concentrations in the aqueous leachate correlate directly with their concentration in red mudstone and siltstone.
    c. A pH of 8.0 maximizes arsenic concentrations in water contacting red mudstone. Maximum mobilization of arsenic at pH 8.0 is consistent with field observations and suggests that the adsorption/desorption of arsenic on hematite/goethite, with a PZC ~ 8.0 to 8.5, moderates its concentration in solution.
    d. Dissolved phosphate increases the arsenic concentration in a water contacting red mudstone.
    e. Conclusions c. and d. indicate that desorption mechanisms, not dissolution of an arsenic-bearing phase, are the main cause of mobilization. Competing ions such as boron, molybdenum, fluorine, selenium, uranium, chromium, rhenium, vanadium, sulfate, carbonate and others probably increase arsenic concentrations in solution.

6. Some red strata in the Passaic Formation contain stratigraphic flow zones where secondary, sparry, carbonate and sulfate minerals are dissolved by groundwater. These zones are likely sources for lithogenic arsenic in wells because they buffer and control aqueous pH, provide maximum surface exposure to matrix hematite-coated clays, and enhance hydraulic conductivity and yields of wells.

Summary

This paper focused on answering the following four key questions:

1. What is the distribution, concentration, hydrology, and, geochemical setting associated with arsenic concentrations greater than 10 µg/L in the major bedrock aquifers of the Newark basin?

2. What are the major lithogenic sources of arsenic in those aquifers?

3. What chemical mechanisms and hydrogeologic settings promote the mobilization of arsenic from those sources?

4. What physical and chemical processes control the mass transport of arsenic in these aquifers? Can arsenic concentrations in groundwater be predicted?

The summary below briefly describes the findings in this paper as they relate to questions 1 to 3 above. A conceptual model of arsenic transport in groundwater in the Lockatong and Passaic Formation in the Newark basin follows. The final section briefly discusses needs for further work.

Hypotheses concerning what and how natural sources of arsenic contaminate groundwater in the Newark basin continue to evolve; those presented here are supported by recent and extensive observations and experimentation. The updated hypotheses are based on findings from groundwater samples, whole-rock and mineral-geochemical analyses, and leach experiments. Groundwater reconnaissance sampling showed that the Lockatong and Passaic formations have the highest percentage of wells exceeding 10 µg/L arsenic (fig. E5). Maximum concentrations of arsenic measured in black, gray and red mudstones and siltstones of the Lockatong and Passaic formations are 240, 50, and 14.8 mg/kg respectively. An important discovery during the early work was that pyrite associated with black and gray mudstone and siltstone in the basin contains as much as 4-weight percent arsenic. Therefore, black and gray shale were originally hypothesized to be the major source of arsenic in groundwater in both the Lockatong and Passaic formations. In the Passaic Formation, thick sections of red strata are intercalated with thinner layers of pyrite-rich gray and black units. In the original

hypothesis, wells tapping only the red mudstone units were thought to be cross-contaminated along complex flow paths that intersect the pyritic, black mudstone units. Because of the hematite-rich nature of the red beds, and the untenable nature of the flow paths required to support some black-bed-to-red-bed flow in some locations, hematite in the red units also became a suspected source of arsenic. Subsequent statistical analysis of whole rock geochemical data from red beds in the Passaic Formation revealed a very strong correlation, based on the Pearson product-moment correlation coefficients (r), between REE and arsenic (r = 0.94), and strong correlations respectively between arsenic and REE with Al_2O_3[clay] (r = 0.82 and 0.81) and Fe_2O_3 (r = 0.83 and 0.84). Also, a strong correlation of Al_2O_3[clay] and Fe_2O_3 (r = 0.92) indicated a clay-and-iron-oxide association. Arsenic appears associated with early hematite coating clay, so it was concluded that the major hematite source of arsenic is the early, rather than the more abundant late, hydrothermal hematite. This conclusion needs to be validated using sophisticated analytical techniques such as laser-ablation ICP-MS. Although the arsenic in groundwater in the Passaic Formation may be associated with hematite-coated clay minerals, pyrite in the Lockatong Formation may still be the ultimate source there.

Results from the leach experiments on red mudstone and siltstone demonstrated that arsenic concentrations in the aqueous leachate directly correlate with 1) the surface area of water-rock contact, 2) the concentration of arsenic in the source rock and 3) the duration of contact. Competitive ions such as phosphate, and a pH of 8.0, maximize arsenic concentrations in solution, showing that desorption and not dissolution is the master mobilization mechanism. A maximum arsenic concentration at pH 8.0 is consistent with field data and suggests that hematite/goethite, with a point of zero charge of about 7.8 to 8.5, moderates the arsenic concentration via adsorption-desorption reactions. Some red units in the Passaic Formation contain strata-bound flow zones in which secondary, sparry, carbonate and sulfate minerals are dissolved by the recharge and flux of weakly acidic groundwater, forming an interconnected anastomosing conduit network. These zones are likely sources for lithogenic arsenic in wells tapping them because they buffer and control aqueous pH, provide maximum surface exposure to matrix clays, and by their high hydraulic conductivity, provide high yields to wells tapping them. Models describing the flux of arsenic in the Passaic and Lockatong formations in the Newark basin must take these findings into account.

Transport of arsenic in the Lockatong and Passaic Formations

Figure E20 shows conceptual models summarizing arsenic sources, mobilization, and transport in black and gray shale, and red mudstone and siltstone. These models are representative of the Passaic Formation, consisting largely of red units, and the Lockatong Formation, consisting largely of black and gray strata. According to the leaky, multlayered aquifer system flow model of Michalski and Britton

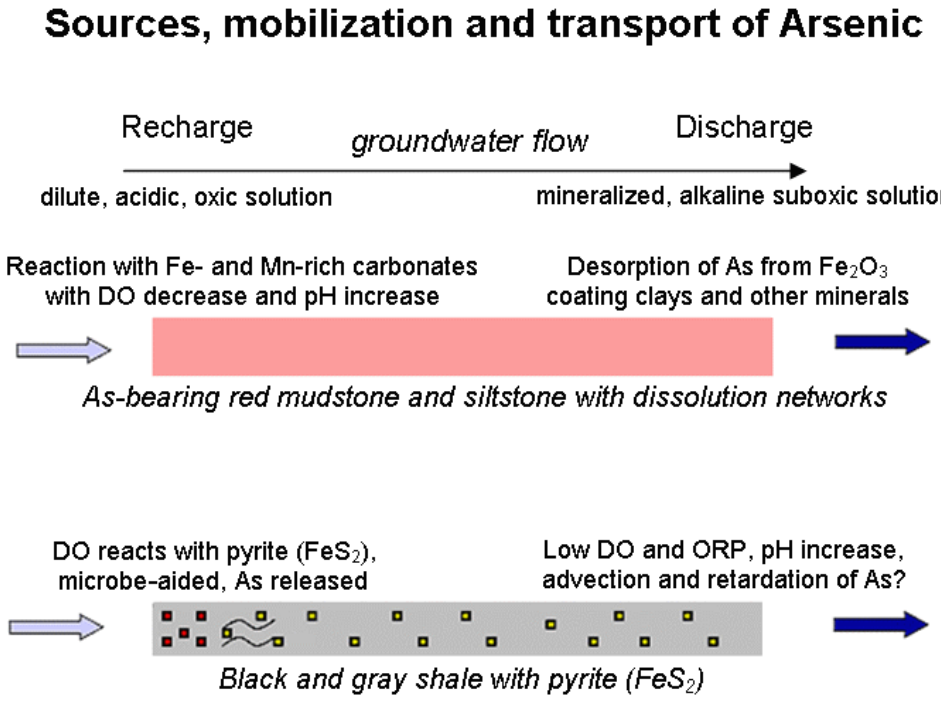

Figure E20. Diagram illustrating the conceptual models for the sources, mobilization and transport of arsenic in red mudstone and siltstone of the Passaic Formation and black and gray shale of the Lockatong and Passaic Formations in the Newark basin.

(1997), the advective flow in the Passaic is assumed to be mostly stratabound and anisotropic. This model is also assumed to represent flow in the multilayered strata of the Lockatong Formation. Both model flow paths in figure E20 start with dilute, acidic, oxygen-bearing recharge water infiltrating the aquifers.

In the red strata, the dissolution of sparry minerals such as calcite and iron/manganese-bearing dolomite in the water-bearing zones raises the pH and releases reduced iron and manganese that can react with, and lower, the concentration of dissolved oxygen. The removal of these phases also provides fresh clay surfaces for water contact. The leach experiments indicate that the arsenic concentrations along the flow path are mainly a function of the arsenic concentration in the rock with which the water is in contact, the degree of the water/rock contact, and the aqueous pH. Although not explored in this paper, the concentration of dissolved oxygen, the oxidation-reduction potential and microbes in these natural aqueous systems may also play a role in arsenic mobilization. Arsenic becomes adsorbed to the hematite coating of clay minerals during deposition and diagenesis and then is released into solution via desorption. For example, the following equation relates surface adsorption (≡Surf) to a mineral surface:

$$\equiv\text{Surf}\,HAsO_4^- + H_2O \rightarrow \equiv\text{Surf}\,OH + H_2AsO_4^-$$

In the black and gray strata, pyrite is oxidized during exposure to oxic recharge waters following the generally accepted overall reaction as shown by Howard (1998):

$$FeS_2 + 15/4O_2 + 7/2H_2O \rightarrow Fe(OH)_3(s) + SO_4^{2-} + 4H^+$$

Arsenic in the pyrite is then available for mobilization if the geochemical conditions are favorable. If pyrite is the major source of arsenic to groundwater in the black and gray shale, its mobilization is expected mainly when it is oxidized at the start of the flow path, when dissolved oxygen is available. Downgradient from that zone, dispersion, retardation via adsorption, and possibly, mineral precipitation decrease aqueous arsenic concentrations.

Need for Further Work

Further work that will lead to a better understanding of the sources, mobilization and transport of As in groundwater in the Passaic and Lockatong formations in the Newark basin includes:

1. Verifying the major hematite source of early versus late arsenic in the Passaic Formation. This may be accomplished by using analytical techniques such as laser ablation ICP-MS to quantify low level arsenic concentrations in early hematite coating clays and other minerals, and comparing them to those in late hydrothermal hematite.

2. Determining if pyrite is the major source of arsenic to groundwater in the Lockatong Formation. Although pyrite is the major mineral source of arsenic in the black and gray shale, it has not been proven to be the major source of arsenic in groundwater associated with these rocks. Work to verify the major natural arsenic source(s) contaminating groundwater in the Lockatong Formation is needed.

3. Determining what role the oxidation-reduction potential (ORP) of groundwater in the Passaic and Lockatong Formations has on the mobilization of arsenic. It is possible that the destabilization of metal oxide surfaces as a function of ORP could affect the adsorption and desorption of arsenic in solution.

4. Determining the microbiological control(s) of arsenic mobilization and speciation in the Passaic and Lockatong Formations. Work by Zhu and others (2008) is improving our understanding of biotic controls.

Acknowledgments

Many people and groups deserve recognition for their direct and indirect contributions to this project, starting with the citizens who volunteered to have their domestic water supplies studied by the NJGS. People we would like to thank on a program level include Karl Muessig, State Geologist of the NJ Geological Survey (NJGS), for recognizing the importance of this research and facilitating its pursuit. Also, Ying Fan Reinfelder, professor in the Department of Earth and Planetary Sciences, Rutgers University, provided unwaivering interest, advice, guidance and financial support as the main author's PhD advisor throughout this research. John Curran and Greg Steidl of the NJGS provided drilling, borehole geophysics and hydraulic-testing support. John Dooley and Don Monteverde of the NJGS helped with X-ray analyses and geologic mapping support respectively. Raymond Bousenberry of the NJGS assisted in the sampling and borehole-testing efforts. Judy Lewis and Eileen Murphy of the NJ Department of Environmental Protection (NJDEP) Science and Research program provided some initial funds with a research grant in the early phase of this

study. Jeremy Delaney of Rutgers University provided microprobe support. Zolton Szabo from the US Geological Survey provided stimulating discussion and access to some of the core samples used in this study. We also thank Bay Weber of the Stony Brook – Millstone Watershed Association and Jim Kinsel of Honey Brook Organic Farms for frequent access to water wells located on these respective properties. We acknowledge the Borough of Hopewell Water department and its Supervisor of Water, Dave Misolek, for taking time to provide access and facilitate study of well HW-6. And finally, a special "thank you" to Paul Olsen of Columbia University for his many detailed studies of Newark basin stratigraphy that provided a thorough stratigraphic framework that constrained many aspects of this research.

References

Alley, W.M., 1993, Regional groundwater quality, Chapter 3; Groundwater Quality Surveys: Van Nostrand Reinhold, New York, New York, 634 p.

American Society for Testing and Materials (ASTM), 2001, ASTM Designation: D 5744 – 96(2001) - Standard test method for accelerated weathering of solid materials using a modified humidity cell, ASTM, West Conshohocken, Pennsylvania, 13 p.

Back, W. 1960, Origin of hydrochemical facies in groundwater in the Atlantic coastal plain: International Geological Congress Proceedings, Copenhagen, Denmark, p. 87-95.

Baur, W.H. and Onishi, B.M., 1969, Arsenic, i*n*, Wedepohl, K.H, ed.: Handbook of Geochemistry. Springer-Verlag, Berlin, Germany, p. 33-A-31-33-30-35

Bednar, A.J., Garbarino, J.R., Ranville, J.F. and Wildeman, T. R., 2002, Preserving the distribution of inorganic Arsenic species in groundwater and acid mine drainage samples: Environmental Science and Technology, v. 36, p. 2213 -2218

Berner, R.A., 1984, Sedimentary pyrite formation: An update: Geochimica et Cosmochimica Acta, v. 48, p. 605-615.

Boyle, R.W. and Jonasson, I.R., 1973, The geochemistry of As and its use as an indicator element in geochemical prospecting. Journal of Geochemical Exploration, v. 2, p. 251-296.

Condie, K.C., 1991, Another look at rare earth elements in shales: Geochimica et Cosmochemica Acta, v. 55, p. 2527-2531.

Demayo, A., 1985, Elements in the earths crust, In: CRC Handbook of Chemistry and Physics, 66th Edition, Weast, R.C., ed., CRC Press Inc., Boca Ratan, Florida, p. F145.

Dixit, S., and Hering, J.G., 2003, Comparison of arsenic (V) and arsenic (III) sorption onto iron oxide minerals: Implications for arsenic mobility: Environmental Science amd Technology, v. 37, p. 4182-4189.

Driehaus, W., Seith, R, and Jenkel, M., 1995, Oxidation of arsenate (III) with manganese oxides in water treatment: Water Research, v.1, p. 297-305.

Driese, S.G., McKay, L.D., and Penfield, C.P., 2001, Lithologic and pedogenic influences on porosity distribution and groundwater flow in fractured sedimentary saprolite: an application of environmental sedimentology. Journal of Sedimentary Research, v. 71, no. 5, p. 843-857.

Dzombak, D.A., and Morel, F.M., 1990, Surface Complexation Modeling, Hydrous Ferric Oxide. John Wiley & Sons, New York, New York.

Elderfield, H., Upstill-Goddard, R., and Sholovitz, E., 1990, The rare earth elements in rivers, estuaries, and coastal seas and their significance to the composition of ocean waters: Geochimica et Cosmochimica Acta, v. 54, no. 4, p. 971-991.

El Tabakh, M., and Schreiber, B.C., 1998, Diagenesis of the Newark rift basin, eastern North America: Sedimentology, v. 45, p. 855-874.

Foster, A.L., 1999, Partitioning and transformations of arsenic and selenium in natural and laboratory systems: Stanford University PhD dissertation, 225 p.

Hem, J.D., 1985, Study and interpretation of the chemical characteristics of natural water (3rd edition): U.S. Geological Survey Water-Supply Paper 2254, 263 p.

Herman, G.C., 2001, Hydrogeological framework of bedrock aquifers in the Newark basin, New Jersey: *in* LaCombe, P.J., and Herman, G.C., eds. Geology in Service to Public Health, Field Guide and Proceedings of the 18th Annual Meeting of the Geological Association of New Jersey, p. 6-45.

Herman, G.C. 2009, Steeply-dipping extension fractures in the Newark basin, New Jersey: Journal of Structural Geology, v. 31, no. 9, p. 996-1011.

Herman, G.C. 2010, Hydrogeology and borehole geophysics of fractured-bedrock aquifers, Newark basin, New Jersey, *in* Herman, G.C., and M.E. Serfes, eds., Contributions to the geology and hydrogeology of the Newark basin: N.J. Geological Survey Bulletin 77, Chapter F., p. F1-F45.

Houghton, H.F., and Flynn, J.J., 1988, Geology and hydrogeology of the Piedmont Lowlands Province: The early Mesozoic Newark basin in New Jersey: Proceedings, Geology and hydrology of New Jersey – A two day field course presented by Rutgers University, Department of Geological Sciences in cooperation with Cook College, New Brunswick, New Jersey, p. E1-E57.

Howard, A.G., 1998, Aquatic Environmental Chemistry, Oxford University Press, New York, New York

Ingri, J., Widerlund, A., Land, M., Gustafsson, O., Andersson, P., and Ohlander, B., 2000, Temporal variations in the fractionation of the rare earth elements in a boreal river; the role of colloidal particles: Chemical Geology, v. 166, no. 1, p. 23-45.

International Agency for Research on Cancer (IARC), 1987, Arsenic and arsenic compounds: IARC Monograph on the evaluation of carcinogenic risks to humans-overall evaluations of carcinogenicity: an update of the IARC Monographs 1 to 42, Lyon, France, Supplemental 7, p.100-106.

Jain, A., Raven, K.P., and Leoppert, R.P., 1999, Arsenite and arsenate adsorption on ferrihydrite: Surface charge reduction and new OH-release stoichiometry: Environmental Science and Technology, v. 33, p 1179-1184.

Jones, R.A., and Nesbitt, H.W., 2002, XPS evidence for Fe and As oxidation states and electronic states in loellingite ($FeAs_2$): American Mineralogist, v. 87, nos. 11-12, p. 1692-1698.

Kamei, G., and Ohmoto, H., 2000, The kinetics of reactions between pyrite and O^2-bearing water revealed from in situ monitoring of DO, Eh and pH in a closed system: Geochimica et Cosmochimica Acta, v. 64, p. 2585-2601.

Kolker, A., Cannon, W.F., Westjohn, D.B., and Woodruff, L.G., 1998, Arsenic-rich pyrite in the Mississippian Marshall Sandstone: Source of anomalous arsenic in southeastern Michigan groundwater: Geological Society of America, Abstracts with Programs, v. 30, no. 7, p. A-59.

Kummel, H.S., 1901, Mining industry of New Jersey: New Jersey Geological Survey, Annual Report of the State Geologist, p. 150-156.

Lerche, D., and Nozaki, Y., 1998, Rare earth elements of sinking particulate matter in the Japan Trench: Earth and Planetary Science Letters, v. 159, nos. 1-2, p. 71-86.

Malinconico, M.L., 2002, Lacustrine organic sedimentation, organic metamorphism and thermal history of selected Early Mesozoic Newark Supergroup basins, Eastern U.S.A.: Columbia University Ph.D. dissertation, New York, New York, 419 p.

Manning, B.A., Fendorf, S.E., and Goldberg, S., 1998, Surface structures and stability of arsenic (III) on goethite: Spectroscopic evidence for inner-sphere complexes, Environmental Science & Technology, v. 32, p. 2383-2388.

Masscheleyn, P.H., Delaune, R.D., and Patrick, W.H., Jr., 1991, Effect of redox potential and pH on arsenic speciation and solubility in a contaminated soil: Environmental Science and Technology, v. 25, p. 1414-1419.

McIntosh, W., Hargraves, R., and West, C., 1985. Paleomagnetism and oxide mineralogy of Upper Triassic to Lower Jurassic red beds and basalts in the Newark basin: Geologic Society of America Bulletin, v. 96, p. 463-480.

McLennan, S.M., 1989, Rare earth elements in sedimentary rocks: influence of provenance and sedimentary processes, *in* Lipin, B.R., and McKay, G.A., eds.: Geochemistry and Mineralogy of Rare Earth Elements: Reviews in Mineralogy, v. 21, chapter 7, p. 170-199.

Michalski, A., and Britton, R., 1997, The role of bedding fractures in the hydrogeology of sedimentary bedrock-evidence from the Newark basin, New Jersey: Groundwater, v. 35, no. 2, p. 318-327.

MINEQL+(ver.4.5). Chemical equilibrium modeling software: (www.mineql.com/noframes/mineql.html)

Moore, R.A., 1963, Bottom sediment studies, Buzzards Bay, Massachusetts: Journal of Sedimentary Petrology, v. 33, p. 511-558.

Morin, R.H., Carlton, G.B., and Poirier, S., 1997, Fractured-Aquifer Hydrogeology from Geophysical Logs; The Passaic Formation, New Jersey: Groundwater, v. 35, no. 2, p. 328-338.

Morin, R.H., Senior, L.A., and Decker, E.R., 2000, Fractured-aquifer hydrogeology from geophysical logs: Brunswick Group and Lockatong Formation, Pennsylvania: Groundwater, v. 38, no. 2, p 182-192.

Morse, J.W. and Luther,G.W., III, 1999, Chemical influences on trace metal-sulfide interactions in anoxic sediments: Geochimica et Cosmochimica Acta, v. 63, p. 3373-3378.

Murphy, E.A., and Aucott, M., 1998, An assessment of the amounts of arsenical pesticides used historically in a geographic area: The Science of the Total Environment, v. 218, p. 89-101.

NRC, National Academy of Sciences National Research Council (NAS), 2001, Arsenic in Drinking Water: 2001 Update, National Academy Press.

NJDEP, 1998, Unpublished letter from Thomas R. Vetrano of ENVIRON to Mr. Michael Tompkins of NJDEP: Arsenic sampling data, Bristol-Myers Squibb Company-Scotch Road Property, Hopewell Township, New Jersey, Case N0. 98-05-29-0140-30.

NJDEP, 1999, Findings and Recommendations for the Remediation of Historic Pesticide Contamination - Final Report, March.

Olsen, P.E., 1980, The latest Triassic and Early Jurassic formations of the Newark basin (eastern North America, Newark Supergroup; stratigraphy, structure, and correlation: The New Jersey Academy of Science Bulletin, v. 25, p. 25-51.

Olsen, P.E., 1986, A 40-million-year lake record of early Mesozoic climatic forcing: Science: v. 234, p. 842-848.

Olsen, P.E. and Fedosh, M.S., 1988, Duration of the early Mesozoic extrusive igneous episode in eastern North America determined by use of Milankovitch-type lake level cycles: Geological

Society of America, Abstracts with Programs, v. 20, no. 1, p. 59.

Olsen, P.E., Kent, D.V., Cornet, B., Witte W.K., and Schlische, R.W, 1996, High–resolution stratigraphy of the Newark rift basin (early Mesozoic, eastern North America): Geological Society of America Bulletin, v. 108, no. 1, p. 40-77.

Oremland, R.S., and Stolz, J.F., 2003, The ecology of arsenic: Science: v. 300, p. 939-944.

Oshchudlak, M.E., and Hubert, J.F., 1988, Petrology of Mesozoic sandstones in the Newark basin, central New Jersey and adjacent New York: Developments *in* W. Manspeizer, ed., Triassic-Jurassic Rifting: Continental Breakup and the Origin of the Atlantic Ocean and Passive Margins: Elsevier, Amsterdam,The Netherlands, Chapter 13, | p. 333-351.

Palmer, C.A. and Klizas, S.A., 1997, The chemical analysis of Argonne premium coal samples: U.S. Geological Survey Bulletin 2144, 106 p.

Parnell, J., and Monson, B., 1995, Paragenesis of hydrocarbon, metalliferous and other fluids in Newark Group basins, Eastern U.S.A: Applied Earth Science; v. 104, p. 136-144.

Pichler, T., Veizer, J., and Hall, G.M., 1999, Natural input of arsenic into a coral reef ecosystem by hydrothermal fluids and its removal by Fe(III) oxyhydroxides: Environmental Science & Technology, v. 33, p. 1373-1378.

Plumlee, G.S., 1989, Processes controlling epithermal mineral distribution in the Creede mining district, Colorado: Harvard University Ph.D. dissertation, 378 p.

Rima, R.J., Meisler, H., and Logwill, S., 1962, Geology and hydrology of the Stockton Formation in southeastern Pennsylvania: Pennsylvania Geological Survey Bulletin W-14, 111 p.

Robertson, F.N., 1989, Arsenic in groundwater under oxidizing conditions, south-west United States: Environmental Geochemistry and Health, v. 11, p. 171-185.

Savage, K.S., Tingle, T.N., O'Day, P.A., Waychunas, G.A., and Bird, D.K., 2000, Arsenic speciation in pyrite and secondary weathering phases, Southern Mother Lode Gold District, Tuolumne County, California: Applied Geochemistry, v. 15, no. 8, p. 1219-1244.

Schlische, R.W., 1992, Structural and stratigraphic development of the Newark extensional basin, eastern North America; Implications for the growth of the basin and its bounding structures: Geological Society of America Bulletin, v. 104, p. 1246-1263.

Schlische, R.W., and Le Tourneau, P.M., 2003, Progress in understanding the structural geology, basin evolution, and tectonic history of the eastern North American rift system, *in* P.M. LeTourneau and P.E. Olsen, eds., The Great Rift Valleys of Pangea in Eastern North America, v. 1, -Tectonics, Structure, and Volcanism: Columbia University Press, New York, New York, p. 21-64.

Schlische, R.W., and Olsen, P.E., 1990, Tectonic development of the Newark rift basin: implications for the growth and evolution of half graben and their boundary faults: EOS: Transactions of the American Geophysical Union, v. 71, no. 43, p. 1606.

Scott, M.J., and J.J. Morgan, 1995, Reactions at the oxide surfaces. 1. Oxidation of As(III) by synthentic birnessite: Environmental Science and Technology: v. 29, no. 8, p. 1898-1905.

Senior, L.A., and Sloto, R.A., 2006, Arsenic and boron in groundwater in and near diabase intrusions, Newark basin, Southeastern Pennsylvania: Geological Society of America, Abstracts with Programs, v. 38, no. 7, p. 320.

Serfes, M.E., 1994, Natural groundwater quality in bedrock of the Newark basin, New Jersey, N.J. Geological Survey Report GSR 35, 28 p.

Serfes, M.E.., 2005, Arsenic occurrence, sources, mobilization, transport and prediction in the major bedrock aquifers in the Newark basin. Rutgers University Ph.D. dissertation, New Brunswick, New Jersey, 122 p.

Serfes, M.E., Spayd, S.E., and Herman, G.C., 2005, Arsenic in New Jersey Groundwater: Advances in Arsenic research: Integration of experimental and observational studies and implications for mitigation, *in* ODay, P.A., Vlassopoulos, D., Meng, X., and Benning, L.G., eds: American Chemical Society Symposium Series 915, chapter 13, p. 175-190.

Sholkavitz, E., 1995, The aquatic chemistry of rare earth elements in rivers and estuaries. Aquatic Geochemistry, v. 1, no. 1, p. 1-34.

Simonson, B.M., Smoot, J.P., and Hughes, J.L., 2010, Authigenic minerals in macropores and veins in late Triassic mudstones of the Newark basin: Implications for fluid migration through mudstone, *in* Herman, G.C., and M.E. Serfes, eds., Contributions to the Geology and Hydrogeology of the Newark Basin: N.J. Geological Survey Bulletin 77, Chapter B, p. B1-B26.

Singer, P.C., and Stumm, W., 1968, Kinetics of the oxidation of ferrous iron. Second Symposium on Coal Mine Drainage Research: Mellon Institute, Pittsburgh, Pensylvania, p. 12-34.

Sloto, R.A., and Schreffler, C.L., 1994, Geohydrology and groundwater quality of northern Bucks County, Pennsylvania: U.S. Geological Survey Water-Resources Investigations Report 94-4109, 85 p.

Smedley, P.L., and Kinniburgh, D.G., 2002, A review of the source, behavior and distribution of arsenic in natural waters: Applied Geochemistry, v. 17, no. 5, p. 517-568.

Smoot, J.P., and Olsen, P.E., 1994, Climatic cycles as sedimentary controls of rift-basin lacustrine deposits in the early Mesozoic basin based on continuous core, *in* Lomando, T., and Harris, M., eds., Lacustrine depositional systems: Society of Economic Paleontologists and Mineralogists Core Workshop Notes, v. 19, p. 201-237.

Smoot, J.P., and Robinson, G.R. Jr., 1988, Sedimentology of stratabound base-metal occurrences in the Newark Supergroup: US Geological Survey Bulletin, 1776, p. 356-376.

Smoot, J.P., and Simonson, B.M., 1994, Alkaline authigenic minerals in the early Mesozoic, Newark basin, NY, NJ, PA; evidence for late fluid movement through mudstones. American Association of Petroleum Geologists and Society of Economic Paleontologists and Mineralogists, v. 1994, p. 261-262.

Soloman, D.K., Moore, G.K., Toran, L.E., Dreier, R.B., ans McMaster, W.M., 1992, Status report: A hydrologic framework for the Oak Ridge Reservation: Oak Ridge National Laboratory, Environmental Sciences Division, Publication no. 3815.

Steckler, M.S., Omar, G.I., Karner, G.D., and Kohn, B.P., 1993, Pattern of hydrothermal circulation within the Newark basin from fission-track analysis: Geology, v. 21, p. 735-738.

Stollenwerk, K.G., 2003, Spectrographic investigations of arsenic species in solid phases, *in* Welch, A.H., and Stollenwerk, K.G., eds.: Arsenic in Groundwater, Geochemistry and Occurrence, Kluwer Academic Publishers, Boston, chapter 3, p. 67-100.

Stumm, W., 1992., Chemistry of the solid-water interface: Wiley Interscience, New York, New York, p. 428.

Sun, X., and Doner, H.E., 1996, An investigation of arsenate and arsenite bonding structures on goethite by FTIR: Soil Science, v. 161, no. 12, p. 865-872.

Sutter, J. F., 1988, Innovative approaches to dating igneous events in the early Mesozoic basins of the eastern United States, *in* Froelich, A.J., and Robinson, G.R., Jr., eds., Studies of the Early Mesozoic basins of the eastern United States: U.S. Geological Survey Bulletin 1776, p. 94-200.

Szabo, Z., Taylor, T.A., Payne, D.F., and Ivahnenko, T., 1997, Relation of hydrogeologic characteristics to distribution of radioactivity in groundwater, Newark basin, New Jersey: U.S. Geological Survey Water Resources Investigations Report 95-4136, p. 134.

USEPA, 2002, Implementation Guidance for the Arsenic Rule - Drinking Water Regulations for Arsenic and Clarifications to Compliance and New Source Contaminants Monitoring - (EPA-816-K-02-018). 83 p.

van de Kamp, P.C., and Leake, B.E., 1996, Petrology, geochemistry, and Na metasomatism of Triassic-Jurassic non-marine clastic sediments in the Newark, Hartford, and Deerfield rift basins, northeastern USA: Chemical Geology, v. 133, p. 89-124.

Van Houten, F.B., 1965, Composition of Triassic Lockatong and associated formations of Newark Group, central New Jersey and adjacent Pennsylvania: American Journal of Science, v. 263, p. 825-863.

Weems, R. E., and Olsen, P. E., 1997, Synthesis and revision of groups within the Newark Supergroup, eastern North America: Geological Society of America Bulletin, v. 109, no. 2, p. 195-209.

Welch, A.H., and Lico, M.S., 1998, Factors controlling As and U in shallow groundwater, southern Carson Desert, Nevada: Applied Geochemistry, v. 13, no. 4, p. 521-539.

Welch, A.H., Westjohn, D.B., Helsel, D.R., and Wanty, R.B., 2000, Arsenic in groundwater of the United States: occurrence and geochemistry: Groundwater, v. 38, p. 589-604.

Wilkie, J.A., and Hering, J.G., 1996, Adsorption of arsenic onto hydrous ferric oxide: Effects of adsorbate/adsorbent ratios and co-occurring solutes. Colloids and Surfaces A-Physicochemical and Engineering Aspects, v. 107, p. 97-110.

Williamson, M.A., and Rimstidt, J.D., 1994, The kinetics and electrochemical rate-determining step of aqueous pyrite oxidation: Geochimica et Cosmochimica Acta, v. 58, p. 5443-5454.

Withjack, M.O., Schlische, R.W., and Olsen, P.E., 1998, Diachronous rifting, drifting, and inversion on the passive margin of central eastern North America: An analog for other passive margins: American Association of Petroleum Geologists Bulletin, v. 82, no. 5A, p. 817-835.

Yan, L., Stallard, R., Key, R., and Crerar, D., 1991, Trace metals and dissolved organic carbon in estuaries and offshore waters of New Jersey, USA: Geochimica et Cosmochimica Acta v. 55, p. 3647-3656.

Zhu, W.Y., 2009, Chemical and microbial control of pyrite weathering and its implications to arsenic mobility and sulfur and iron geochemistry: Rutgers University Ph.D. dissertation, New Brunswick, NJ.

Zhu, W.Y., Young, L.Y., Yee, N., Serfes, M.E., Rhine, E.D., and Reinfelder J.R., 2008, Sulfide-driven arsenic and mobilization from arsenopyrite and black shale pyrite, Geochimica et Cosmochimica Acta, v. 72, p. 5243-5250.

Hydrogeology and Borehole Geophysics of Fractured-Bedrock Aquifers, Newark Basin, New Jersey

By Gregory C. Herman, NJ Geological Survey

Chapter F of

Contributions to the Geology and Hydrogeology of the Newark Basin

N.J. Geological Survey Bulletin 77

State of New Jersey
Department of Environmental Protection
Water Resource Management
New Jersey Geological Survey
2010

Contents

Figures

Tables

Chapter F

Hydrogeology and Borehole Geophysics of Fractured-Bedrock Aquifers, Newark Basin, New Jersey

Gregory C. Herman[1]

Abstract

This report summarizes the results of 36 hydrogeologic projects in which fractured-bedrock aquifers in the Newark basin were studied by the NJ Geological Survey from 2001 through 2008. These studies utilized geophysical logs of 128 water wells to determine the character, spatial distribution and continuity of geologic features that store and transmit groundwater. These water-bearing features (WBFs) are stratigraphic and structural in nature and were identified using an optical televiewer, a heat-pulse flowmeter, traditional geophysical logs, rock cores and other data. The geophysical records of each study are detailed in appendixes as hydrogeologic sections that chart WBFs in each well and aquifer.

The New Jersey part of the Newark basin includes the Stockton, Lockatong, Brunswick, and diabase aquifers. The Stockton, Lockatong and diabase aquifers correspond directly to the respective geologic formations. The Stockton is of alluvial origin and consists of arkosic sandstone with lesser amounts of siltstone and mudstone. The Lockatong is of lacustrine origin and is consists of gray, red and black argillite. The Stockton and Lockatong locally include alluvial fanglomerate and sandstone near the northwest, faulted margin of the basin. Diabase is of igneous origin and it intruded the Stockton, Lockatong and Passaic Formations as thick sills and thin dikes. The Brunswick aquifer includes rocks of lacustrine, alluvial and igneous origin that are, in ascending order: the Passaic, Orange Mt. Basalt, Feltville, Preakness Basalt, Towaco, Hook Mt. Basalt and Boonton Formations. The Brunswick consists of seven aquifer zones that differ in composition and texture in various parts of the basin. Four zones in the central part of the basin are underlain by fine-grained sedimentary beds of the Passaic Formation. These are the lower and middle, gray and red zones respectively, and consist of red and gray siltstone and mudstone and gray and black shale, arranged in stacked, cyclical sequences. These rocks were formerly mud, silt and sand deposited in shallow to deep lakes during alternating dry and wet climate cycles. Gray zones contain proportionately more gray and black shale than the red ones. Three other Brunswick zones in the peripheral margins of the basin contain coarse-grained sedimentary rocks mapped in the Passaic and Boonton Formations. These are conglomerate, conglomerate-and-sandstone, and sandstone zones and consist of red beds of alluvial and shallow lacustrine origin. The sedimentary and basalt formations of Early Jurassic age are included in the Watching zone. The basalt formations in the Watchung zone are designated basalt units in the Brunswick aquifer, rather than basalt aquifers.

WBFs in 119 of the 128 wells in the study were identified using optical and acoustic borehole televiewer images. Three types of WBFs were identified:

1) bedding planes and layers,
2) fracture planes, and
3) linear intersections of bedding and fracture planes.

Type 1 WBFs include planar fractures resulting from mechanical breaking along stratigraphic contacts between beds of varied texture and thickness. Type 1 also includes sedimentary beds and igneous layers that are highly porous and permeable owing to the dissolution and removal of secondary sparry minerals from fracture interstices and/or the rock matrix by interaction with weakly-acidic groundwater. Type 2 WBFs includes transmissive extension and shear fractures not parallel to the stratigraphic plane. Fractures are grouped here by gentle (1^o to 29^o), moderate (30^o to 59^o) and steep (60^o to 89^o) dip angles. Most conductive fractures are steeply-dipping tectonic extension fractures, including ordinary joints with fracture interstices that are free of secondary authigenic minerals that seal gaps. Type 3 features are intersections of strata and fracture planes that channel water along linear conduits. Examples of WBFs and their physical link to geological strata and structures are illustrated using two- and three-dimensional diagrams, photographs, and hydrogeologic sections, most of which are included in a set of appendixes.

Measured geophysical responses and types of

[1]NJ Geological Survey
29 Arctic Parkway, Box 427
Trenton, NJ 08825
greg.herman@dep.state.nj.us

WBFs in each aquifer and aquifer zone are summarized in tables. All types of WBFs occur in all bedrock aquifers. However, type 1 WBFs are most common in basalt (52 percent) and red, coarse-grained sedimentary units (48 percent). Type 2 features are most common in all aquifers (54 percent) and the highest percentage is in Brunswick fine-grained, gray units (70 percent). Type 3 features are the least common in all aquifers (about 12 percent) but are most common in the red, coarse-grained sedimentary beds (26 percent) including coarse-grained sandstone (24 percent) and conglomerate (48 percent).

Closely spaced wells make it feasible to construct hydrogeologic sections illustrating subsurface and topographic conditions. These sections include interpretations of the shallow and deep aquifer sections. The shallow section includes weathered bedrock to depths of about 60 to 100 ft below land surface (bls) in areas having less than 20 ft overburden. Groundwater flowing in shallow bedrock under natural, nonpumping conditions is generally controlled by local topographic gradients and nearby surface-water drainage. Topographic gradients stem from the differential erosion of gently-dipping strata. Groundwater flowing in deep bedrock is semiconfined. Deep wells tapping semiconfined strata have complex, nonpumping cross flows with water entering and leaving uncased parts of the boreholes at different depths and flow rates. Hydrogeological sections normal to the strike of bedding demonstrate how these nonpumping cross flows result from gently-dipping, semiconfined beds cropping out at various elevations with differing hydraulic potentials.

Stratigraphic unconformities within thick accumulations of red mudstone locally include mineralized paleosoil. These horizons commonly have dense accumulations of authigenic minerals subsequently removed locally from the rock matrix by mineral dissolution to form highly-transmissive, type 1 WBFs and strata-parallel water-bearing zones. Paleosols also form stratigraphic pinchouts where strata are cut off at gentle angles by superjacent beds forming hydrologic boundaries that locally retard groundwater recharge in poorly productive aquifers.

Introduction

Bedrock aquifers of Early Mesozoic age in the Newark basin (figs. F1 and F2) underlie some of the most densely populated and heavily industrialized areas in the United States. They also supply vast quantities of groundwater for domestic, commercial, and industrial needs (Hoffman and Lieberman, 2000). Protecting these aquifers from pollution and overpumping requires an understanding of the hydrogeological framework, that is, the configuration of the various bedrock strata and fractures that store and transmit groundwater.

The purpose of this report is to provide a fuller understanding of the hydrogeologic framework of fractured-bedrock aquifers in the Newark basin by summarizing the types, spatial distribution and continuity of water-bearing features (WBFs) identified in water wells in the New Jersey part of the basin (fig. F3). Identification of these features relies on borehole geophysical data that were collected, analyzed and catalogued for 36 hydrogeologic projects involving 128 water wells drilled into the Stockton, Lockatong, Brunswick and diabase aquifers (table F1, figs. F2 and F3, and appendix table A1). These projects were conducted by the NJ Geological Survey (NJGS) in support of publicly-funded pollution investigations and water-supply-permit activities by the NJ Dept. of Environmental Protection (NJDEP), or were NJGS research projects funded by the NJDEP Hazardous Waste Spill Fund. Most of the geophysical data were collected by the NJGS in water-supply and water-monitoring wells with uncased, open boreholes of 6- to- 8 inch diameter, appendix table A1). Most wells are less than 600 ft deep and were drilled into bedrock overlain by thin (< 20 ft) overburden. Some borehole records were generated by secondary parties and donated to the NJGS or were part of third-party geotechnical investigations that were reanalyzed and incorporated here. The hydrogeologic effects of thick unconsolidated deposits overlying bedrock are not considered in this report.

Identification of WBFs relies on the use of borehole imaging systems, including optical and acoustical televiewer probes, and a multidirectional video camera. Of these, the optical televiewer (OPTV) is the most useful because it provides an oriented, digital photographic record of the strata penetrated in a well plus secondary structures such as fractures and faults. The digital data files are processed and interpreted for structural analysis of the aquifer as seen in the borehole walls. A tally is kept of the types of WBFs within the various aquifer units and zones, and the ranges of observed geophysical responses for the various types of geophysical logs employed in these analyses. Photographs and schematic diagrams of the OPTV used by the NJGS are included in a section

Table F1. Number of projects and wells for each major aquifer.

Aquifer	Projects	Wells
Diabase……..	4	7
Brunswick……..	24	102
Lockatong……..	4	9
Stockton…….	5	12
Total*……..	**36**	**128**

* Some projects and wells cover more than one aquifer so that total values are less than column totals.

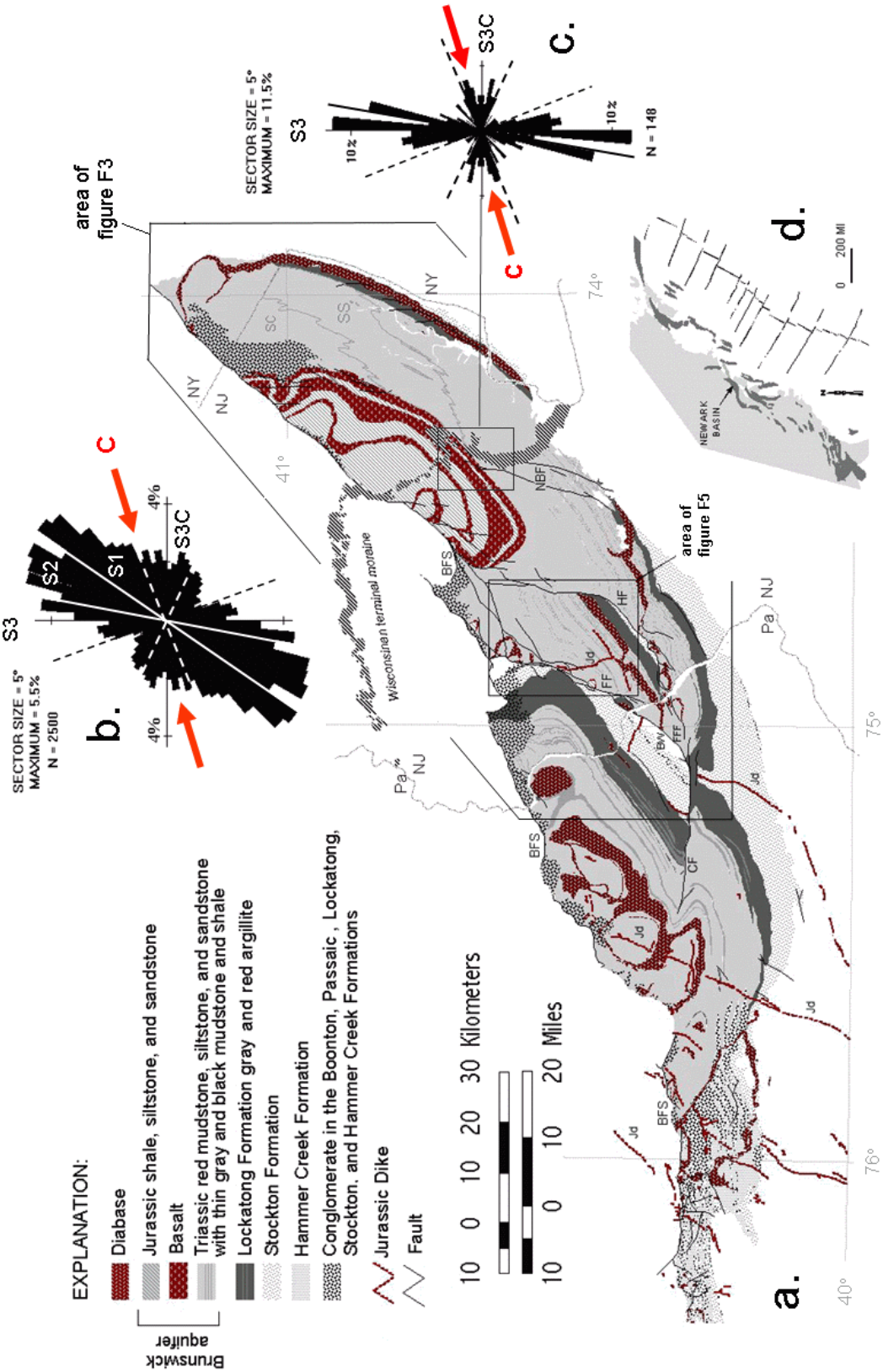

Figure F1. Bedrock geology of the Newark basin (**a.**) showing stratigraphic formations, sedimentary facies, faults, dikes, and circular histograms of extension fractures. Bedrock map compiled from geographic information system shape files for New Jersey (http://www.state.nj.us/dep/njgs/geodata/dgs04-6.htm), New York http://www.nysm.nysed.gov/data/lhud_bedr1a.zip), and Pennsylvania (http://www.dcnr.state.pa.us/topogeo/map1/bedmap.aspx#entirestate). Histogram **b.** shows plane strike for 2500 sets of tectonic extension and shear fractures in about 1300 outcrops in the center of the basin. Extension fractures in Late Triassic rocks predominantly strike N20°E to N65°E whereas those in younger Early Jurassic rocks strike more northerly (histogram (**c.**). adapted from Monteverde and Volkert (2005). SC – sandstone and conglomerate facies, SS – sandstone and siltstone facies, NBF – New Brunswick fault, HF – Hopewell fault, FF – Flemington-fault, FRF - Furlong fault, CF - Chalfont fault, RF - Ramapo fault. Index map of Mesozoic basins on the East Coast (**d.**) adapted from Schlische (1992).

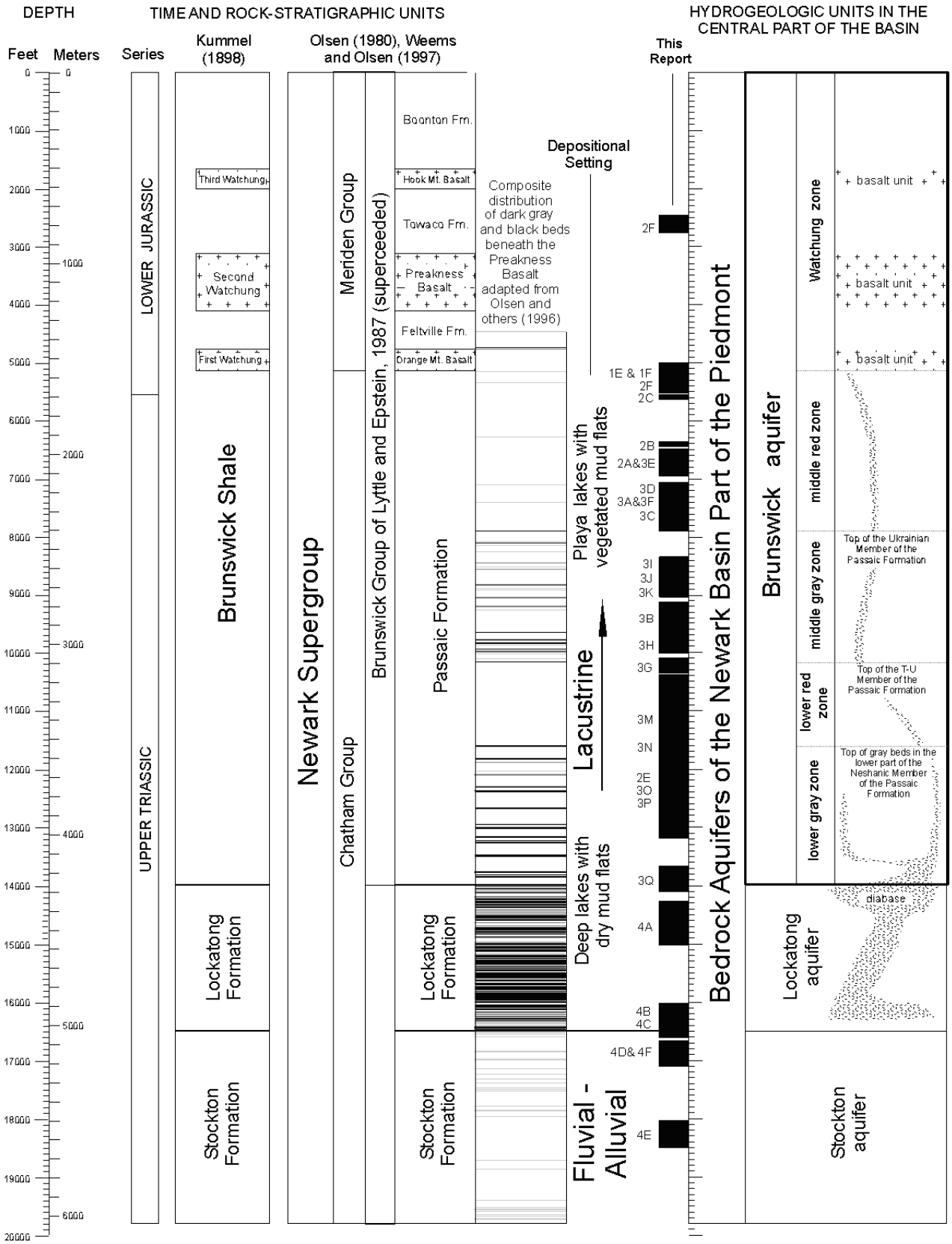

Figure F2. Summary of time, rock and hydrogeologic units in the central part of the Newark basin showing approximate stratigraphic intervals covered in this report and earlier studies.

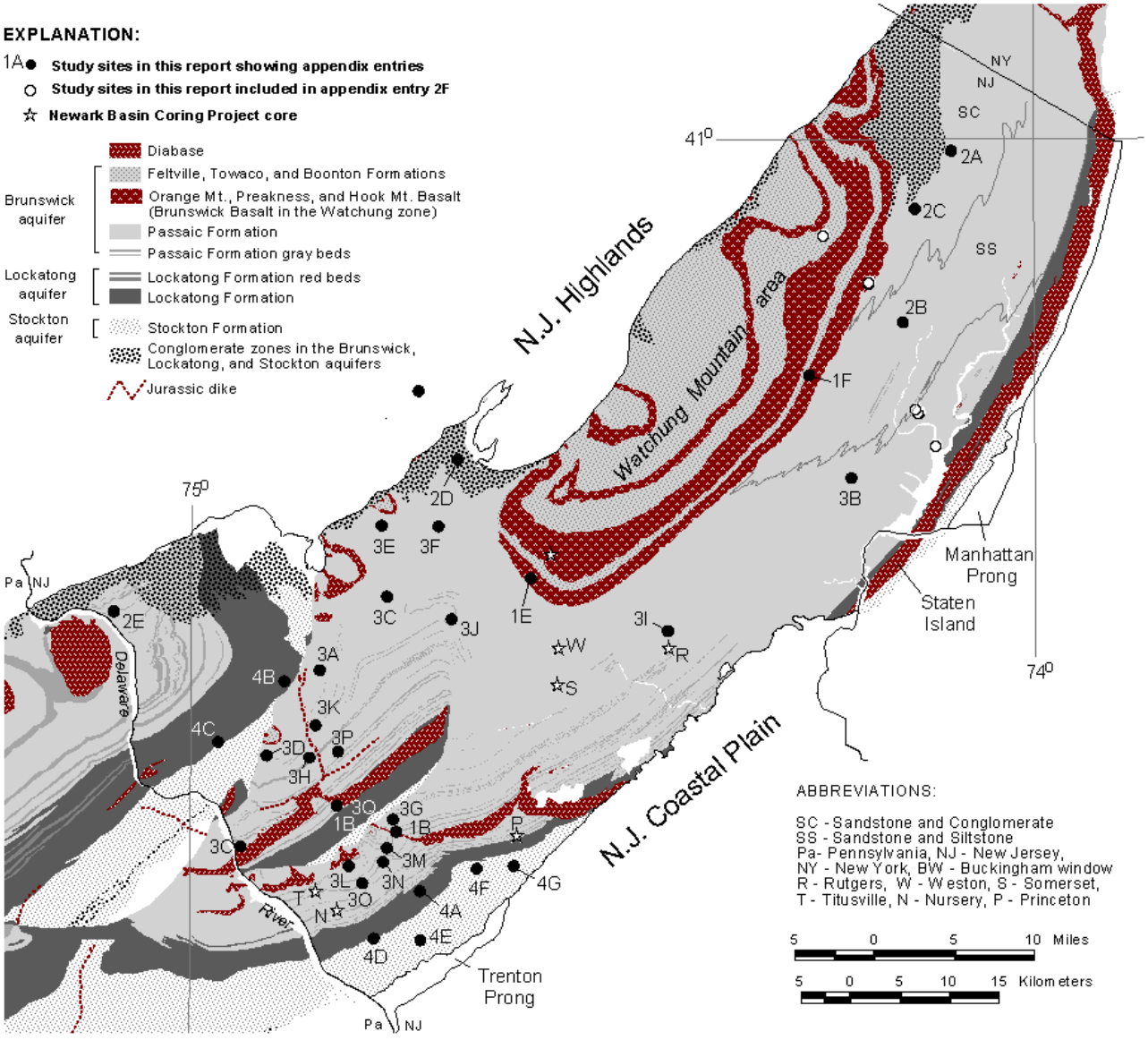

Figure F3. Map of study locations showing core locations for the Newark Basin Coring Project (Olsen and others, 1996). Geology compiled from sources listed in figure F1.

on borehole geophysics.

Each borehole analysis is unique. The WBFs in each well differ from one another in their characteristics and spatial distribution. Some WBFs are simply bedding planes whereas others are tectonic fractures or intersections of bedding and structural features. Where two or more boreholes are closely spaced, their WBFs can be compared and represented in profile, or in 3D perspective, as a hydrogeological framework. This delineates the continuity and orientation of the WBFs and bedrock features constituting the stacked set of aquifers and less-permeable layers in a multilayer aquifer system.

Other data collected for this report include heat-pulse flowmeter (HPFM) studies of borehole cross flows, bedrock core samples, and straddle-packer tests with information on groundwater yield for specific bedrock intervals. Local differences in land elevation are also shown to affect the direction and rate of borehole cross flows in different areas. Cross flows were mostly measured under nonpumping conditions but some projects include flow measurements that were taken while pumping.

This work builds on fracture mapping (Herman, 1997) and uses customized computer programs (Herman, 2000; 2001a) to represent geological structures and hydrogeological data in map,

profile and three-dimensional (3D) perspectives. Computer-generated, 3D models may be used to illustrate the spatial distribution and geometry of interpreted hydrogeologic features, and how they locally interact to transmit groundwater or result in borehole cross flows.

Detailed records for each project are presented in appendixes 1 to 4. These records include a location map of logged wells, detailed structural analyses of stratigraphic layering and fractures from OPTV records, and hydrogeologic sections based on geophysical logs that illustrate specific examples of the types and distributions of WBFs. The appendixes are used throughout the report to illustrate relationships.

Geologic setting

The Newark basin is a sedimentary basin of Early Mesozoic age formed on the eastern North American continental margin during tectonic rifting and breakup of the supercontinent Pangea prior to the onset of sea-floor spreading and formation of the Atlantic Ocean (Dietz, 1961; Sanders 1963). The basin covers about 2900 mi^2 extending from southern New York across New Jersey and into southeastern Pennsylvania (fig. F1). It is filled with as much as 20,000 ft of Upper Triassic to Lower Jurassic sedimentary and igneous rocks (fig. F2) that are tilted gently northwestward, faulted, and locally folded (Schlische and Olsen, 1988, Schlische 1992; and Olsen and others, 1996). Multiple tectonic movements have affected the basin (Lucas and others, 1988; de Boer and Clifford, 1988; Schlische, 1992; Herman, 2005). Tectonic extension peaked from the latest Triassic to the earliest Jurassic with widespread igneous activity (tholeiitic basalt and diabase) and a marked increase in sediment-accumulation rates (Schlische, 1992). Tectonic deformation and synchronous sedimentation continued at least into the Middle Jurassic (Schlische, 1992) when extensional faulting and associated tilting and folding were succeeded by periods of contraction, uplift and erosion, similar to events in other areas of the continental margin (de Boer and Clifford, 1988; Withjack and others, 1995; Olsen and others, 1992). Coastal plain sediment deposited on the underlying Mesozoic rocks resulted in flexural loading of the continental margin during the Late Mesozoic through Early Cenozoic (Owens and Sohl, 1969; Owens and others, 1998). Late Cenozoic glacial and fluvial deposits and erosion landforms in the Newark basin form buried valleys, till plains, upland surfaces, fluvial terraces and scarps (Stanford, 2000; Stanford and others, 2001).

The Newark basin is underlain by three sedimentary formations of Late Triassic to Early Jurassic age and overlying and discontinuous sedimentary rocks of early Jurassic age interlayered with basalt flows (figs. F1 and F3). The primary bedrock units include in ascending order: the Stockton, Lockatong, and Passaic Formations (fig. F2). The Stockton Formation unconformably overlies basement rocks of Proterozoic and Paleozoic age. Basal conglomerates of the Stockton fine upward into sandstone and progressively thicker mudstone interbeds. The unit reaches a maximum thickness of about 4000 ft. The Lockatong Formation includes black, gray, and red argillite (highly indurated shale), and gray mudstone and siltstone; the red units are progressively more abundant higher in the sequence. The formation reaches a maximum thickness of about 3500 ft. The Passaic Formation in central parts of the basin is mostly red mudstone and siltstone with lesser amounts of gray and black shale (Olsen and others, 1996). These fine-grained facies grade laterally into sandstone and conglomerate in the southwest and northeast margins of the basin. The maximum thickness of the Passaic Formation is about 11,800 ft.

The sequence of interlayered basalt and clastic sedimentary rocks of early Jurassic age includes in ascending order: the Orange Mt. Basalt, Feltville Formation, Preakness Basalt, Towaco Formation, Hook Mt. Basalt, and Boonton Formation. Each basalt formation consists of several basalt flows (Tollo and Gottfried, 1992) that were fed by diabase sheets and dikes that intruded and thermally metamorphosed older sedimentary deposits in the basin. The sedimentary rocks of Jurassic age are fluvial-deltaic sandstone, siltstone, and lacustrine mudstone. The combined maximum thickness of Jurassic bedrock in the Newark basin is about 4920 ft. All sedimentary formations in the center of the basin grade into alluvial fanconglomerate to the northwest along the border fault system (figs. F1 and F3).

The succession of lacustrine sedimentary rocks in the Lockatong and Passaic Formations reflects a gradual climatic change during a 30-million-year period from arid conditions in a narrow basin to subhumid ones in a broad basin (Smoot and Olsen, 1994). Sediment deposited in deep lakes bordered by dry, saline mud flats was gradually succeeded upwards by sediment deposited in shallow lakes flanked by wetter, vegetated mud flats (Smoot and Olsen, 1985; 1988). Included in this succession is a series of graduated sedimentary cycles that reflects the rise and fall of lake level (Van Houten, 1962), largely in response to periodic and cyclical climatic changes occurring over tens of thousands to millions of years (Olsen, 1986; 1988). The detailed stratigraphy of the Newark basin is based on outcrop mapping and an extensive, regional rock-coring program referred to as the Newark Basin Coring Project (fig. F1, and Olsen and others; 1996). The basic rock-stratigraphic cycle of sedimentary units in the basin is the 'Van Houten' or 'precession' cycle (Olsen,

1986). It marks the successive, gradational accumulation of mudstone and siltstone during transgressive, highstand, and regressive lake stages controlled by a 21,000-year precession cycle of the earth's axis. Precession cycles are arranged in a series of large-order compound sedimentation cycles resulting from orbital variations occurring over 109,000-, 413,000-, and ~2,000,000-year periods. A typical Van Houten cycle in Late Triassic sedimentary bedrock includes a middle high-water sequence marked by fine-grained shale, mudstone and siltstone sandwiched between other sequences of mudstone, siltstone, and sandstone deposited in shallow transgressive, then regressive waters. The upper unit reflects lowstand periods when the lake was at least occasionally dry, with incipient soil development in a subaerial environment.

Sedimentary beds and igneous layers dip gently 1° to 29° northwest in the basin except near faults and folds, where strata dip more moderately (30° to 59°) to steeply (60° to 89°) as a result of tectonic strain. Gently-dipping strata commonly are cut by secondary bedrock fractures that dip steeply and are mapped as joints (fig. F4). In those areas containing more moderately-to-steeply-dipping strata, these secondary fractures dip more gently, suggesting that most extension fractures formed early in subhorizontal strata, then were locally tilted together with bedding during later stages of deformation. Herman (2001) reported that the average dip of extension fractures (joints) in pre-tilted beds in the center of the basin is about 70°, the ideal angle of inclined shear failure reported for extended rocks (Xiao and Suppe, 1992; Dula, 1991; Withjack and others, 1995).

Figure F4. Joints in the Passaic Formation (location 3Q, fig. F3). Joints are elliptical, systematic extension fractures that form in clustered sets. They dip steeply and form in conjugate arrays. Photograph provided by Matthew Mulhall.

Four groups of faults and steeply- to moderately-dipping extension fractures have been mapped in the basin (Herman, 2005). The groups are differentiated by structural strike and relative age. The first and oldest set (S1) strikes N.35°E. to N.70°E. subparallel to the basin's northwestern, faulted margin (fig. F1). The group of faults defining the northwest margin is referred to as the border-fault system (BFS of Schlische, 1992). Individual fault segments generally show a progressive counterclockwise change of strike from about E.-W. in the southwest part of the basin to N.40°E. in the northeast. Fault dips steepen from about 25° to 30°S.E. near the Delaware River (Ratcliffe and others, 1986) to about 60° to 70°S.E. in the northeastern parts of the basin (Ratcliffe, 1980). The BFS displays a right-stepping geometry of individual fault segments in map view (fig. F1). Parts of the northwestern margin lacking mapped faults are interpreted to be underlain by buried and hidden, or 'blind' fault splays covered by younger sediment (Schlische, 1992; Drake and others, 1996). Fault movement along the BFS is thought to be predominantly normal dip-slip with a maximum stratigraphic offset exceeding 3.5 miles in the northeast. Detailed studies of fault slip from core drilling along the BFS show complex fault movements with oblique dip-slip commonly reported (Burton and Ratcliffe, 1985; Ratcliffe and others, 1990).

The second structural group (S2) includes intrabasinal faults and associated extension fractures striking ~N.10°E. to N.35°E. (fig. F1). S2 intrabasinal faults include isolated and interconnected splay faults that cluster into fault systems separated by 10 to 20 miles along the basin's transverse axis (fig. F1). In New Jersey, from west to east, they are referred to as the Flemington (FF), Hopewell (HF), and New Brunswick (NBF) faults. These faults decrease in stratigraphic displacement eastward, the FF having the greatest displacement and the NB the least. The FF links up with the Furlong (FRF) and Chalfont (CF) faults in Pennsylvania (Schlische, 1992). The CF-FRF-FF system of faults displays a curved map trend veering from about E.-W. in Pennsylvania to N.-S. in New Jersey before connecting with the BFS (Houghton and others, 1992). A window of Paleozoic bedrock crops out midway along its trace at the point of maximum curvature (fig. F1). The FF has component faults interpreted to dip about 40° to 70°E. with predominant normal slip and lesser right-lateral oblique slip (Drake and others, 1996). Maximum stratigraphic

offset exceeds 2.5 miles near Flemington. The HF is interpreted as dipping 50° to 70°E, with normal and right-lateral oblique slip (Drake and others, 1996; Laney, 2005; Laney and others, 1995). Some of the western faults in the HF system are normal faults with westerly dips of about 70° (Monteverde and others, 2003). The NBF is interpreted to have predominantly normal slip on steeply-inclined faults (Stanford and others, 1998) and maximum stratigraphic offset of about 1.5 miles near New Brunswick (Owens and others, 1998).

The third structural group (S3) includes faults and fractures striking from about N.20°W. to N.15°E. in the northeast part of the basin near the Watchung Mountains (Monteverde and Volkert, 2005; Volkert, 2006). A fourth group of extension fractures (SC3) and oblique-slip faults strikes about E.-W. in complimentary directions to S3 structures. S3C mineralized cross fractures in New Jersey occur southeast of the HF and north of the Trenton Prong (Herman, 2005). They may represent late-stage dilation and mineralization of earlier, curviplanar, nonsystematic cross fractures optimally aligned for reactivation and growth in the present compressive-stress field (C in fig. F1). The interactions between the different fault, fold, and fracture sequences record episodes of extension and collapse followed by periods of compression and uplift (de Boer and Clifford, 1988; Schlische 1992; Herman, 2006;2008).

Hydrogeologic units and the leaky, multi-unit aquifer system

Hydrogeologic units in the New Jersey part of the Newark Basin reflect local stratigraphy and consist of four principle aquifers including the Stockton, Lockatong, diabase and Brunswick (fig. F2). The Stockton, Lockatong and diabase coincide with the respective geologic formations. The Stockton is of alluvial origin and consists of arkosic sandstone with lesser amounts of siltstone and mudstone. The Lockatong is of lacustrine origin and consists of gray, red and black argillite. The Stockton and Lockatong locally include alluvial fanglomerate and sandstone near the northwest, faulted margin of the basin. Diabase is of igneous origin and it intruded the Stockton, Lockatong and Brunswick as thick sills and thin dikes (figs. F1 and F3). The Brunswick is of lacustrine, alluvial and igneous origin and includes, in ascending order: the Passaic, Orange Mt. Basalt, Feltville, Preakness Basalt, Towaco, Hook Mt. Basalt and Boonton Formations.

Shale is typically used by well drillers and geologists working in the basin to describe many of the fine-grained red beds in the Brunswick, but Van Houten (1965) and Smoot and Olsen (1988) have shown that most of it is massive mudstone and siltstone. Much of the fissility of the red beds has been destroyed by repeated episodes of wetting and drying of sediment on mud flats, by bioturbation, and by the accumulation and growth of secondary authigenic minerals, including gypsum and calcite, in the shallow subsurface during diagenesis. Shale-like bed partings commonly develop in these massive rocks following prolonged weathering near the surface. The term shale is historically embedded in the literature and existing databases, but ‘mudstone and siltstone’ are used here to refer to red fine-grained beds. ‘Gray’ and ‘black’ beds in the Brunswick aquifer consist of gray mudstone and shale, dark gray shale, and black, laminated to thin-bedded shale rarely exceeding 6 ft in stratigraphic thickness. Other colors recorded for these beds, such as brown, yellow and green, are called gray here as they commonly represent weathered gray and black beds. Black beds are mapped as part of the ‘gray beds’ on geologic maps but it is important to note them separately in subsurface investigations. For example, unusually high radioactivity, radon and concentrations of arsenic have been found in dark gray and black shale in the basin (Szabo and others, 1997; Serfes and others, 2005). These beds typically act as units confining adjacent red-bed aquifers. This is apparent where fluid electrical conductivity and resistivity logs show stepped values at contacts between red and gray beds (appendix 3G8, 3H2, 3I2, 3I3, 3K3, 3K6, 3K7, 3M10, 3N5, 3N13 and 3P4).

The Brunswick is subdivided into eight aquifer zones to facilitate aquifer mapping and cataloguing of aquifer parameters. These zones reflect variations in bedrock composition and texture in the different formations and parts of the basin. A conglomerate zone is used for the northwestern, faulted margin of the basin containing cobble fanglomerate in the Passaic Formation and the sedimentary formations of Jurassic age in the Watchung Mountain region (figs. F2 and F3). A second zone is used for this same region for the fine-grained sedimentary rocks and interlayered basalt formations (figs. F2 and F3). This Watchung zone also occurs as small stratigraphic outliers along the Flemington fault system (Houghton and others, 1992; Drake and others, 1996). The remaining six zones are used for areas underlain exclusively by the Passaic Formation. Of these, two occur in the northeast margin of the basin underlain by pebble conglomerate and sandstone red beds of alluvial origin (figs. F2 and F3). The four remaining zones are used for the central part of the basin underlain by fine-grained sedimentary beds of lacustrine origin. They are, in ascending order: the lower gray, lower red, middle gray and middle red zones (fig. F2). The middle zones were previously defined to be upper zones (Herman, 2001b) but are redefined here because they physically occupy middle sections of the aquifer, and also to avoid confusion

when referring to red strata of Jurassic age in the upper part of the Brunswick. These four zones show a pronounced stratigraphic cyclicity (Olsen and others, 1996) that facilitates aquifer subdivision where distinct sets of bed-strike-parallel topographic ridges formed as a result of differential erosion of the red, gray, and black strata (fig. F5). Hard beds of siltstone, mudstone and shale form ridge tops whereas softer or extremely fractured mudstone and shale underlie valleys. Typically, in areas underlain by fine-grained lacustrine beds, stratigraphic sequences having abundant black and gray shale form prominent ridges with dark shale underlying northwest-facing hill slopes (Appendix 3G1, 3H1, 3K1, 3N1, 3N2 and 3P1).

The lower gray zone of the Brunswick aquifer consists of red and gray mudstone and siltstone, and gray and black shale. It correlates with the lower part of the Passaic Formation, from the top of the Lockatong Formation to the top of two, thick gray-bed sequences in the bottom of the Neshanic Member (fig. F2). These gray beds form a prominent topographic ridge in the center of the basin. The upper contact of the lower gray zone is mapped at the base of this ridge (fig. F5). The lower red zone consists of red mudstone and siltstone with minor gray mudstone and shale, and includes the remainder of the Neshanic Member upwards to the base of the Kilmer Member (fig. F2). The middle gray zone consists of red mudstone and minor siltstone, gray mudstone, and gray and black shale. It correlates with the middle part of the Passaic Formation, including the Kilmer Member, upward to the top of gray beds in the bottom of the Ukrainian Member (fig. F2). The middle red zone consists of red mudstone and micaceous siltstone, with minor amounts of gray mudstone and shale. It includes the remainder of the Ukrainian Member and the Passaic Formation upward to the base of the Orange Mt. Basalt.

Figure F5. Shaded relief map of the Amwell Valley showing four zones in the Brunswick aquifer with contacts following pronounced topographic ridges. db – diabase, sf – Stockton Formation, lf – Lockatong Formation, ba - Brunswick aquifer, cg – conglomerate, rv – Round Valley reservoir.

The directional hydraulic property of fractured sedimentary bedrock aquifers in the Newark basin has been repeatedly demonstrated since Herpers and Barksdale (1951) first reported that wells aligned along bedding strike could affect one another. During the past twenty years, Andrew Michalski and colleagues have defined the *Leaky Multi-Layer Aquifer System* (LMAS) model for Triassic mudstone and siltstone in the basin along with an outline of useful approaches for conducting hydrogeological investigations at groundwater pollution sites (see Chapter D and Michalski, 1990; Michalski, 2001; Michalski and Klepp, 1990; Michalski and Gerber, 1992; Michalski and Britton, 1997). The LMAS model describes the tendency of groundwater to flow along gently inclined bedding fractures in deep, multi-unit bedrock (fig. F6). These transmissive, bed-parallel features are nonuniformly distributed in a vertical direction by distances ranging from about 30 ft to more than 150 ft. They are separated by thick, leaky stratigraphic layers with subvertical extension fractures that are developed throughout the basin but differ spatially in density and orientation (Herman, 1997; 2001). These fractures are locally open and conductive and they provide pathways for groundwater to infiltrate and flow between highly transmissive units. In some instances, the steeply dipping fractures have been reported to be the principle conduits for groundwater recharge, storage and flow (Knapp, 1904; Vecchioli, 1965; Spayd, 1985). Both bedding and fracture components of the LMAS are discussed in detail below and illustrated in the appendexes.

Overburden and weathered bedrock overlie LMAS components and provide storage and pathways for groundwater to recharge deeper aquifers. Permeable fractures in weathered bedrock include the steeply-dipping extension fractures from which secondary cements such as calcite have been removed by weakly acidic, recharging groundwater (Herman, 2001b). Deep flow zones are recharged with groundwater where transmissive beds extend upward to shallow depths (Michalski and Britton, 1997).

Groundwater infiltrates fracture apertures in the weathered bedrock that may extend from the surface to depths exceeding 60 ft in parts of the basin with thin

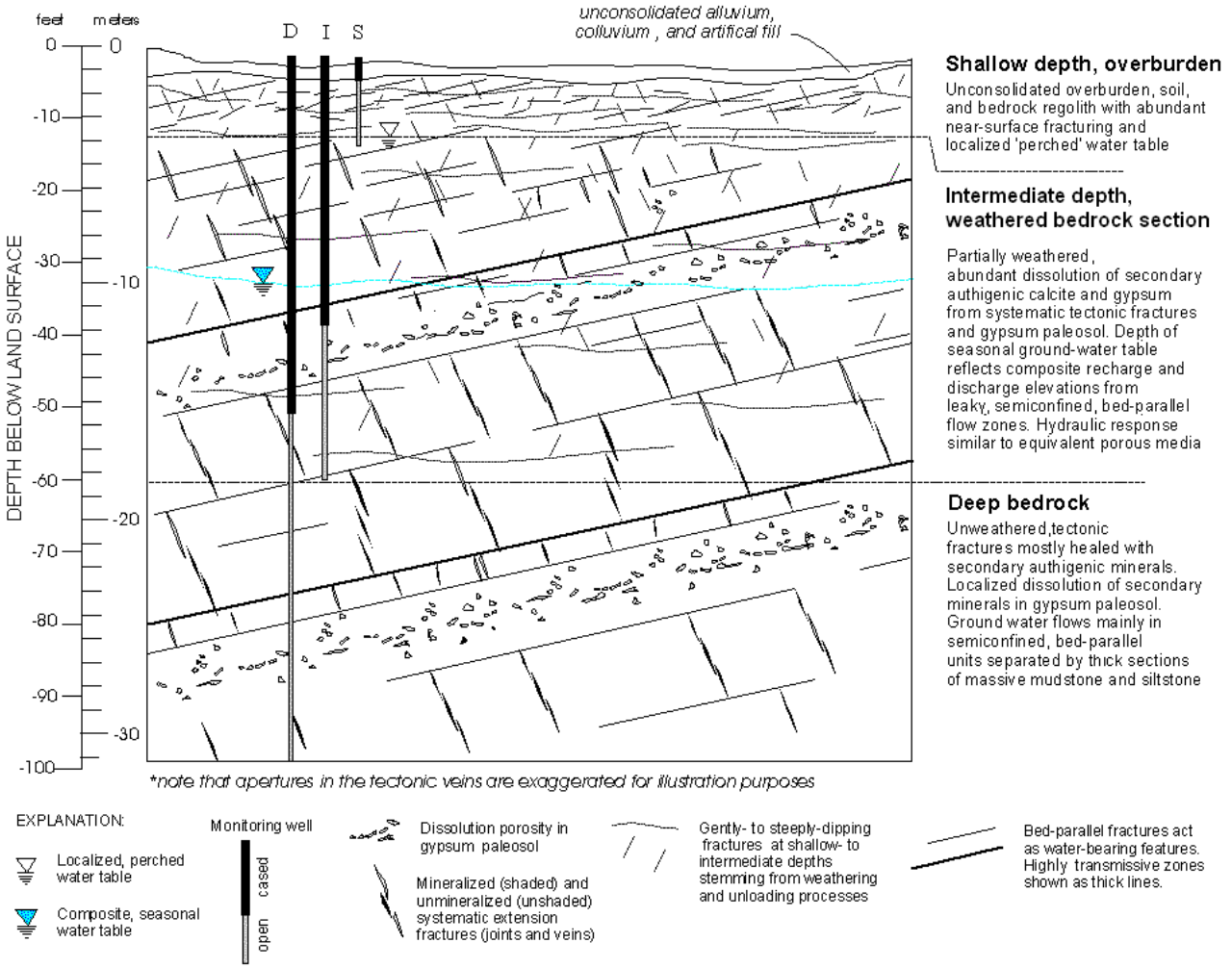

Figure F6. Profile view of a three-tiered conceptual framework of fractured sedimentary aquifers in the Newark basin as modified from the leaky, multi-unit aquifer system (LMAS) model of Michalski and Britton (1997) for areas lacking thick (>50 ft) overburden. Steeply-dipping extension fractures occur as joints near land surface where they are open and permeable. They are mostly plugged by secondary minerals in the subsurface except where these were removed by dissolution. Transmissive WBZs mostly occur along fractures developed between stratigraphic layers, shown above as dipping gently right-to-left. Other layer-parallel WBZs occur as permeable fracture sets preferentially developed within specific strata or as tabular strata with abundant secondary porosity resulting form the dissolution of secondary, authigenic minerals from the bedrock matrix. The latter are referred to as gypsum paleosoil that increases in abundance in the lower and middle red zones of the Brunswick aquifer. Gently-dipping fractures stemming from weathering and unroofing are common near land surface to intermediate depths in weathered bedrock. Groundwater flow is progressively more anisotropic at depth, reflecting the gradual change from many open, interconnecting flow conduits near land surface to very few, widely spaced conduits in deep bedrock that lie along bed partings or in paleosol horizons. Layered WBZs in deep bedrock are generally separated by thick confining beds. Deep (D), intermediate (I) and shallow (S) wells are used to monitor each tier.

overburden (Herman, 2001b). In contrast, buried-valley aquifers are thick accumulations of glacial sediment locally overlying bedrock that can store and transmit significant volumes of deep water. These aquifers commonly are saturated and overlie weathered bedrock. The depth and hydrogeological properties of weathered bedrock underlying buried-valley aquifers in glaciated terrain are not well documented.

Borehole geophysics

The identification and classification of WBFs rely on the use of slim-line geophysical tools to measure the various physical properties of the formation and its water. Most of the geophysical logs detailed in the appendixes were collected by the NJGS. Logs collected by others are so noted in appendix table A1 along with

NJGS project names and well parameters, including location coordinates, uses and construction details. Conventional geophysical logs typically include borehole diameter (caliper-inches), single-point electrical resistance (ohms), natural gamma-ray emissions (counts per second - cps), water temperature (^{o}F), fluid electrical conductivity (microsiemens/cm) and resistivity (ohm-m). Oriented borehole images were acquired using optical and acoustical borehole televiewer (BTV) systems manufactured by Robertson Geologging Ltd.. The basic design and components of the OPTV system are shown in figure F7. The OPTV provides a continuous, orientated, 360º digital image of the strata and structures in the borehole wall. Figure F8 shows how OPTV data are processed and displayed as digital records. The cylindrical image is processed and transformed into rectangular coordinates using Robertson Geologging Ltd. proprietary computer software (fig. F8a). Planar structures penetrated by the borehole are interpreted on the 'unwrapped and flattened' image (fig. F8b). Hard-copy outputs of the interpreted images are generated at 1/12 (fig. F8c) and/or 1/8 scales using the Joint Photographic Experts Group (JPEG) image format and are then catalogued as NJGS library records. Structural interpretations include the description and 3D location and orientation of planes intersecting the borehole, including plane dip and strike (Fig. F8c and Table F2).

The structural analysis of WBFs using BTV technology is based on a selective-sampling procedure of imaged borehole features. Stratigraphic layers and fractures were measured in ~16-ft stacked intervals such

A

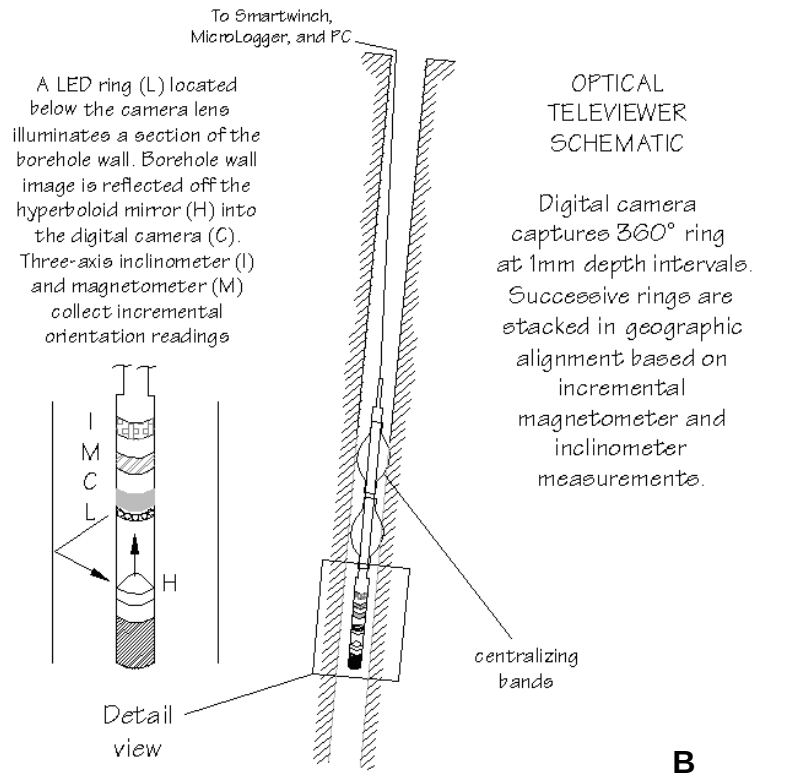

B

Figure F7. The NJGS OPTV is used for mapping subsurface geological features in 6- and 8-inch water wells. A. Photos of the sonde assembly showing how the tool is deployed. B. Illustrations show that light from the diode source (L) illuminates the borehole wall and reflects the wall image off the hyperbolic mirror (H) into the digital camera (C). Cabled-depth readings together with magnetometer (M) and inclinometer (I) incremental readings provide a 3D orientation for each pixel. Data are transmitted up a coaxial cable for data storage and processing on a personal computer.

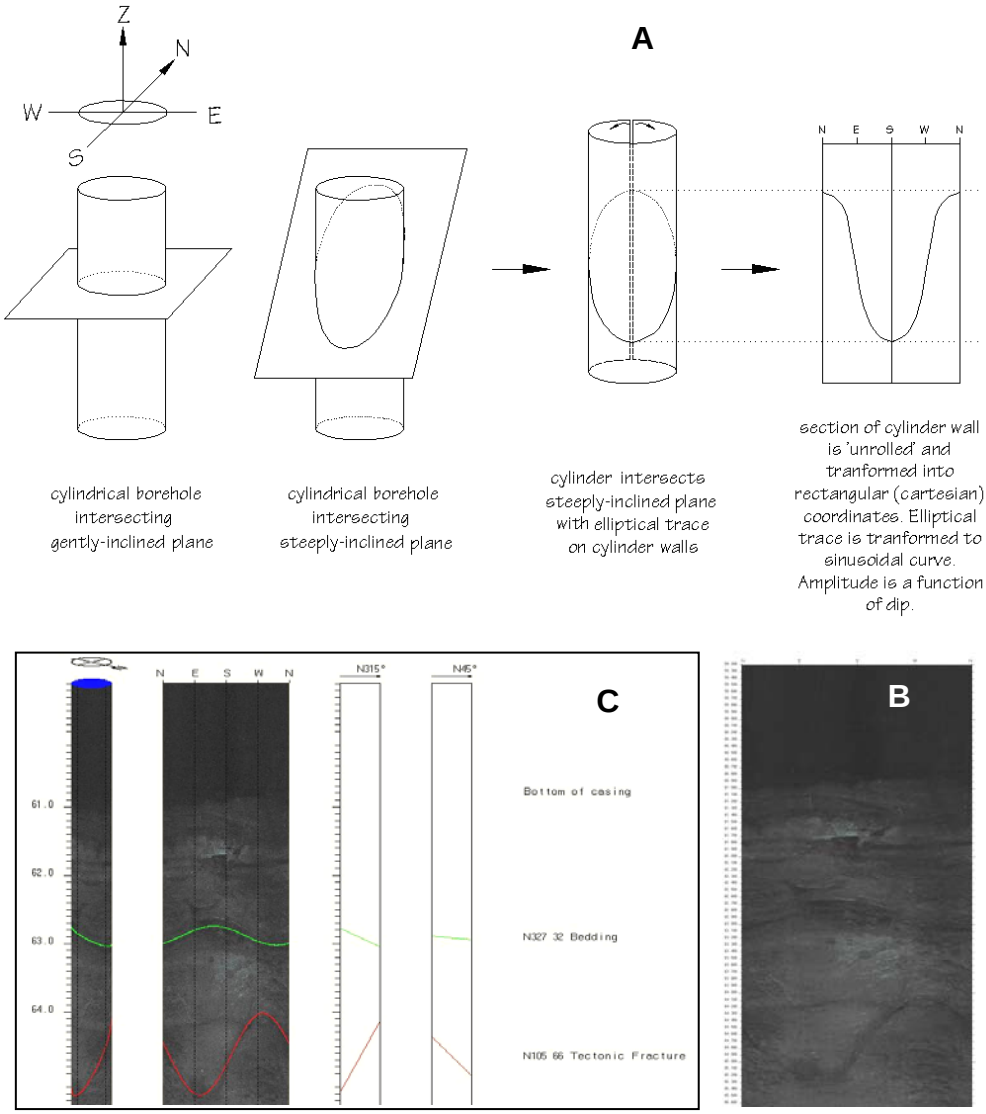

Figure F8. BTV diagrams and images showing how OPTV records are processed interpreted, and output as data records. A. Schematic diagram showing how a cylindrical BTV image is 'unrolled' for display during data processing. B. Uninterpreted OPTV record. C. Interpreted OPTV record including stick diagrams and feature parameters output at 1/12-scale using a JPEG image format.

Table F2. Example of data fields and parameters for interpreted geological features output using BTV processing software. Column headings are explained below.

ID	DEPTH	INC	BRG	CODE	AZM	DEV	CO	C1	C2
1..	28.388	23	188	2	213.99	3	Fracture	Gently-inclined	Vein
2..	32.138	34	25	0	208.00	3	Bedding		
3..	33.403	52	198	2	211.40	3	Fracture	Moderately-inclined	Conductive
4..	35.922	15	19	0	218.66	4	Bedding		Conductive
5..	43.290	77	185	2	220.06	4	Fracture	Steeply-inclined	Vein

ID – Feature-identification sequential integer
DEPTH – Depth (feet) below log reference datum to center of measurement point
INC - Inclination or dip (degrees) of the measured plane
BRG - Bearing or dip azimuth (degrees) of measured plane
CODE - Integer used to differentiate between stratigraphic layering and fracturing
AZM - Azimuth bearing (degrees) of borehole drift
DEV - Angular deviation (degrees) of borehole from vertical
C0, **C1** and **C2** – Text variables for classifying geological features

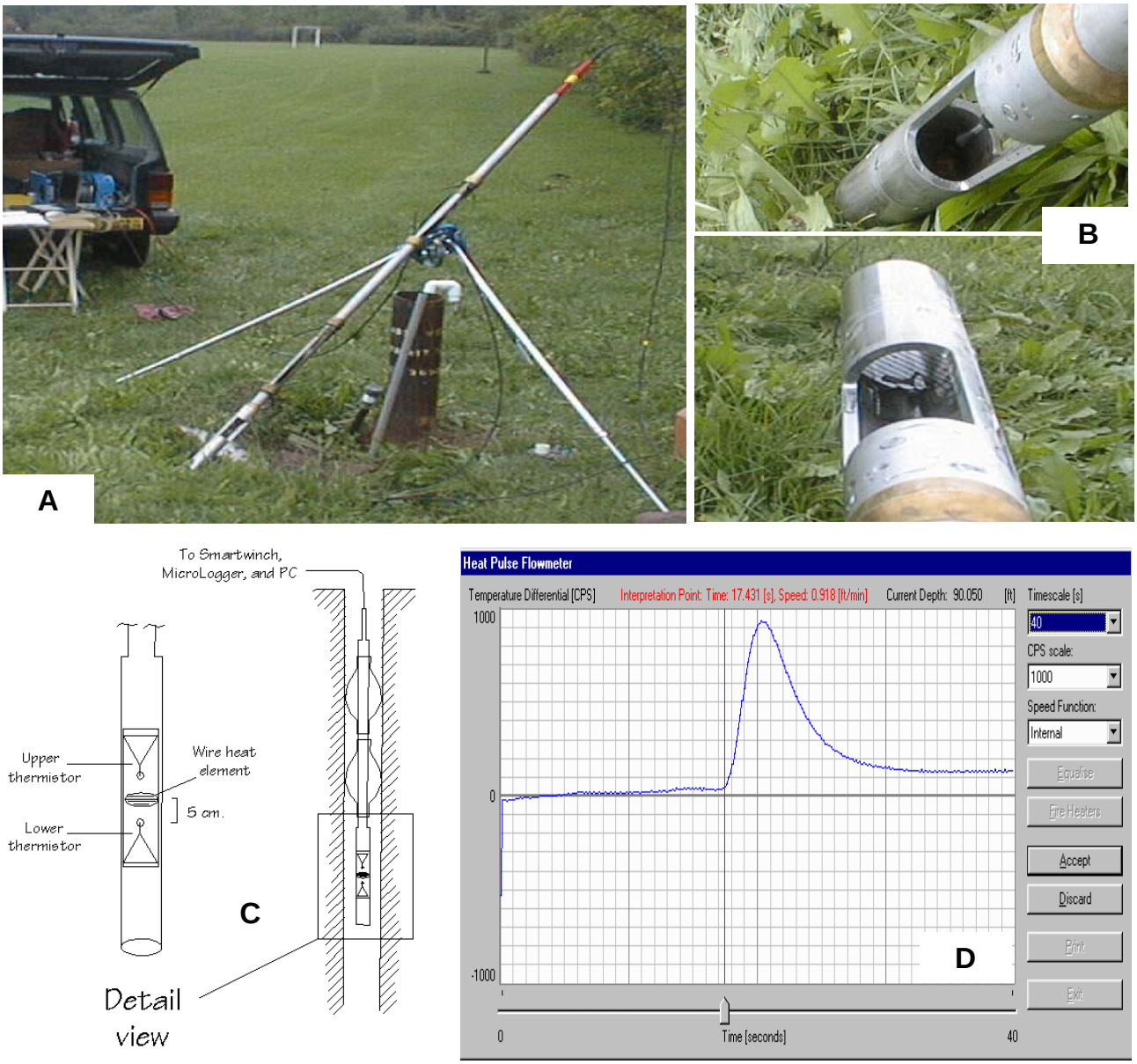

Figure F9. Photos and diagrams of the Robertson Geologging, Ltd. HPFM used by the NJGS. A. Photo of the sonde resting on the tripod/pulley and connected with a coaxial cable to the winch located in the Jeep. B. Details of the sonde assembly including the tool aperture, upper thermistor and heating grid. C. Schematic diagram illustrating the details of the sonde assembly and a profile of the instrument as deployed in a well. D. The data-acquisition interface showing a graph of the HPFM response time (x-axis, seconds) and the temperature differential between upper and lower thermistors (y-axis, counts-per-second (CPS)). Graph axes are scaled using pull-down menus shown on the upper right part of the display. The HPFM response time and fluid speed values (ft/min) are determined by sliding the cursor control along the base of the x-axis to the first deflection point where the arriving heat pulse produces a large positive-count differential for the upward thermistor as charted above. A downward-deflected curve indicates downward flow.

that a particular, measured feature was commonly taken to represent closely-spaced sets of subparallel features within the sample interval. For example, elliptical fracture surfaces cluster in spaced sets within stratigraphic intervals (fig. F4). For BTV interpretations, a single fracture measurement represents a fracture set if strikes or dips of multiple fractures are within 5° of each other. Five-degree histogram bins are the basis of graphical structural analyses reported in the appendixes. Structural planes identified in BTV records as stratigraphic layers, fractures, or faults are included in output tables using an ASCII text-file format (table F2). Data fields in these text files include depth of a feature, plane inclination (dip) and bearing (dip

azimuth). The azimuth bearing and deviation of the borehole from vertical is also recorded for each feature. These data tables are used for subsequent structural analysis of feature orientations and for investigating subsurface spatial relationships of geological features and well-field components using GIS (NJ Geological Survey, 2001).

Water flow rates in some boreholes were measured using a heat-pulse flowmeter (HPFM). HPFM technology was developed in the early 1970's and is in widespread use today. Unlike other probes used in this study, the HPFM is deployed in a well in a stationary mode at specific depths rather than actively trolling upward or downward in the well at a constant rate (fig. F9). The HPFM is selectively positioned to bracket potential WBFs identified using OPTV records, trace anomalies from fluid logs, or enlarged openings in the borehole indicated by caliper logs. The data-acquisition assembly of the HPFM probe contains a horizontal wire-grid heating element and thermistors positioned above and below it (figs. F9B and C). Apertures in the device (fig. F9B) permit the free flow of well fluid through the assembly. The flow velocity of the fluid column is determined when a pulse of electric current is emitted to the heating grid, which in turn warms the water column in the vicinity of the grid. The warm-fluid front migrates within the moving fluid column past a thermistor where it is detected, then registered as a response curve on a system display of the sonde log (F9D). Depending on the direction of flow in the borehole, either the upper or lower thermistor detects the warm fluid front first. An upward-flow response is measured at the first break point of an upward deflection (fig F9D) and vice versa for downward flow. Response time is computed in seconds and calculated fluid speed in feet per minute (ft/min). The HPFM is repeatedly equalized and fired at a specific depth until reproducible or similar results are obtained (table F3). Multiple values of traveltime and fluid velocity are measured and recorded at each depth, then combined later to determine an average time and fluid velocity at each depth of measurement (table F3). These values are then compared to other geophysical and geological records to construct profiles of borehole flow as part of the hydrogeologic interpretation of geophysical logs (table F3 and appendixes 1 to 4). The HPFM used by the NJGS has been tested and found to be about 75 percent accurate for measuring fluid velocities ranging from 0.3 to 17.0 ft/min (~0.5 to 25 gpm in a 6-inch well). Flow velocities below the 0.3 ft/min minimum threshold value are reported as no measurable flow.

Fractures, bedding in sedimentary rocks, and layering in basalt and diabase, are described as hydraulically conductive in illustrations titled

Table F3. Heat-pulse flowmeter data for well 4 (appendix 1B5)

Multiple heat-pulse arrival-time measurements at various depths[3]		**Average heat-pulse arrival time (HPAT) and calculated fluid velocity and flow rates at various depths. Average arrival time > 14 sec and < 32 seconds**			
Depth[1] (ft)	heat-pulse arrival time (seconds)	Depth[1] (ft)	HPAT (seconds)	Calculated fluid velocity[2] (ft/min)	Calculated flow rate[3] (gpm)[4]
85.10	26.880	85.10	26.88	0.20	0.30
99.95	20.625	99.95	21.72	0.38	0.56
99.95	22.813	119.60	18.18	0.53	0.79
119.60	15.000	160.00	16.98	0.59	0.87
119.60	17.569	200.00	16.50	0.62	0.91
119.60	18.472	240.00	18.09	0.54	0.79
119.60	20.417				
119.60	20.417				
160.00	16.979				
200.00	15.885				
200.00	17.656				
200.00	15.313				
200.00	17.135				
240.00	16.771				
240.00	18.229				
240.00	19.271				

[1]Depths are below land surface

[2]Calculated fluid velocity = ((-.85*(Log(HPAT)+3)) modified from Herman (2006)

[3]Rate calculated for a 6-in. well

[4] gpm - gallons per minute

The average results are charted to the right.

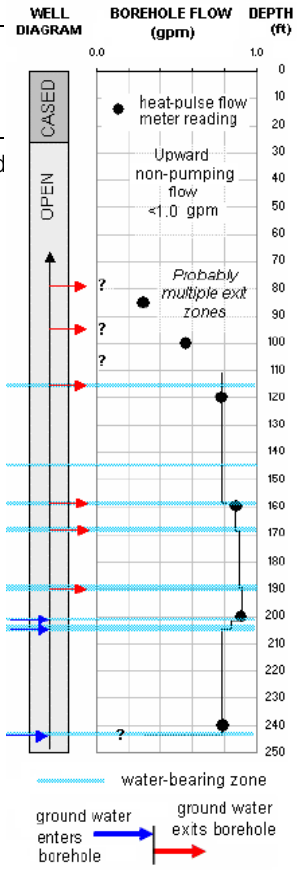

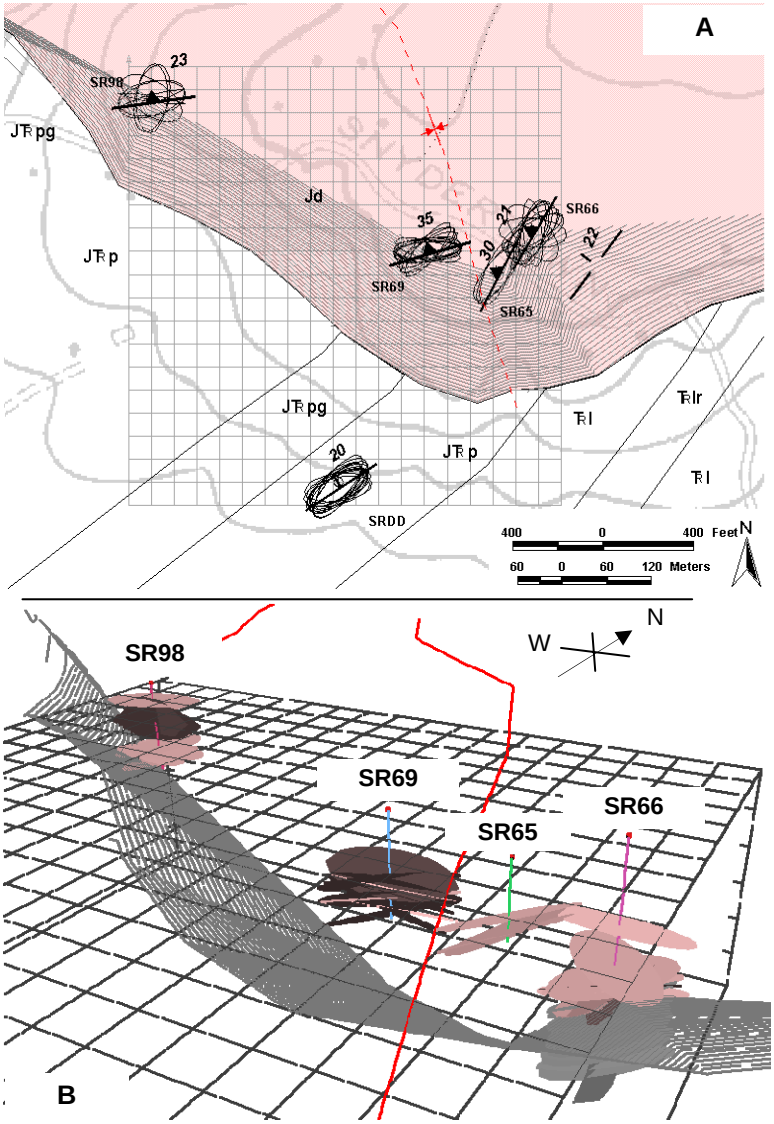

Figure F10. Geologic map (A) and 3D display (B) of the Snydertown Road domestic-well study (appendix entry 1B). The map view shows average strike and dip of compositional layering in diabase (Jd) and bedding in underlying mudstone and shale (wells SR66 & SRDD) determined from the five OPTV surveys. The bottom contact of the diabase sill with the underlying Passaic Formation was penetrated in well SR66.Compositional layering (pink) and sedimentary bedding (gray) are shown using 3D ellipses in B. An elliptical plane was generated at the point of interpretation of each structure and plotted along its borehole trace. Planes have 300-ft major axes oriented along strike and a 2:1 strike-to-dip aspect ratio. The orientations of layer ellipses in diabase are outlined on the map. Ellipses plot on top of one another when projected to the land surface and show that compositional layering varies considerably in strike in the vertical direction over small distances. The 3D perspective is viewed looking slightly down and a little West of North. Grid cells and tick marks are 100ft. Part of the sill base is mapped above using 5 ft contours and represented below in 3D. Axial traces of nearby folds are dashed red lines in the map and solid red lines below. The folds are gentle warps in the diabase layering and therefore postdate intrusion.

"Hydrogeologic interpretation of geophysical logs" in appendixes 1 to 4. A water-bearing zone (WBZ) is identified as a continuous section of the open hole where two or more WBFs intersect, based on visual evidence in OPTV records (appendix 3A3, 3D4, 3J4 and 3N7). Flow in and out of these zones typically produces trace fluctuations on fluid temperature, electrical conductivity/resistivity and flow logs (appendix 3D7, 3D9, 3K3 and 3K5). These anomalies are used to position the HPFM and straddle-packer assemblies for measuring the section fluid velocity and volumetric flow rates.

Groundwater chemistry within each WBZ or WBF commonly differs from that in the other isolated subsurface flows but mixing takes places in the open borehole. Dissolved minerals from inflows may sometimes precipitate on the borehole wall adjacent to the entry point in response to the chemical mixing of formerly isolated waters. Examples of borehole stains originating from WBFs are shown in the appendixes for the following units:

Diabase – figs. 1A3 and 1B6
Brunswick basalt units – 1E6 (left)
Brunswick sedimentary units – figs. 2E6, 2E7, 3C2, 3D13 (well 53), 3G5, 3H3, 3J4 (well 84), 3M12 and 3M18
Lockatong – 4B3 (left) and 4B7

Staining originating from WBFs may sometimes indicate both upward and downward flow directions (appendix 1A3) caused by the combined influence of natural cross flows and pumping that temporarily reverses borehole flow directions. Staining from pumping-induced flows appears subordinate to that stemming from natural, nonpumping cross flows, based on consideration of where the pump is set relative to the conductive feature. Nonpumping cross-flow velocities

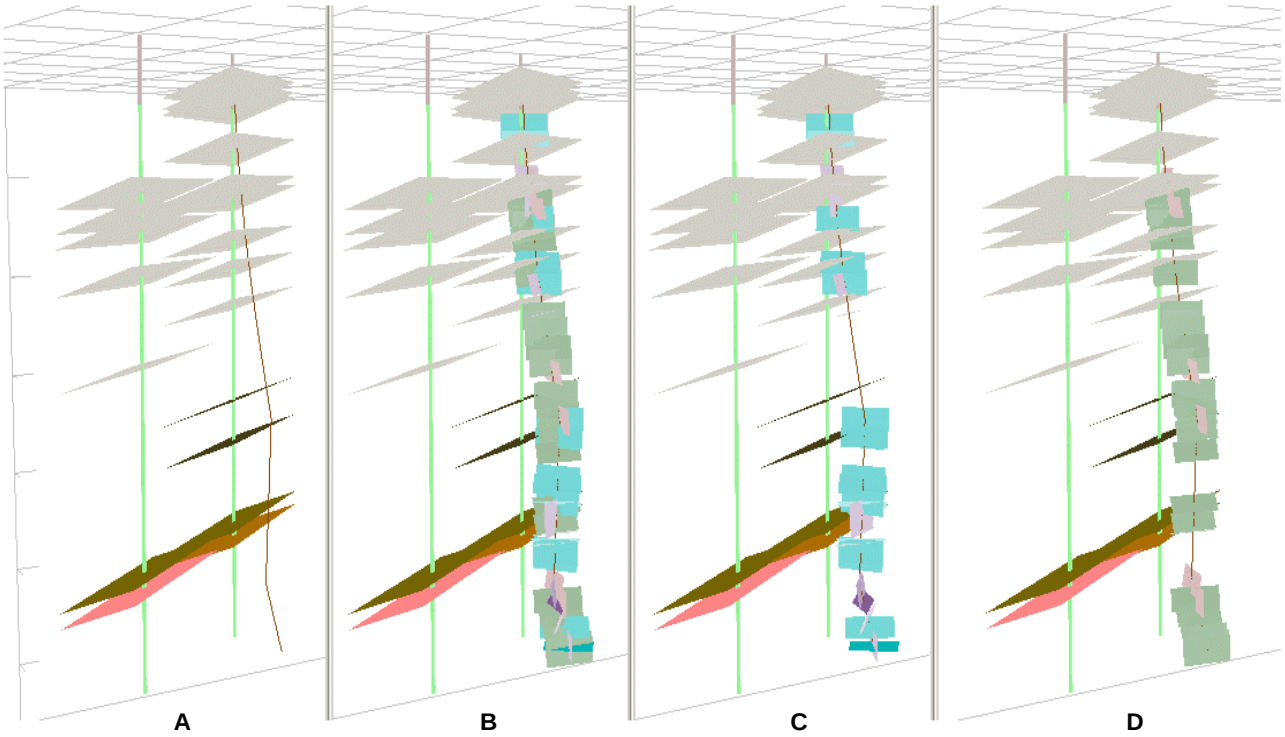

Figure F11. Paneled views from a 3D-GIS computer model of two wells in the lower part of the Passaic Formation (appendix entry 3P). Grid cells at the top of each panel and tick marks to the left mark 100-ft. intervals. Driller-reported WBZs are shown to parallel sedimentary bedding and are plotted along the vertical projection of two wells with cased (pink at top) and open (green) intervals . WBZs dip gently northwest (right-to-left). Dark planes at bottom represent high-yield zones. The actual borehole geometry of the well on the right is shown with a thin, crooked line that was generated using an OPTV record. It shows that the well has an irregular shape that drifts in a direction opposite to bed dip (A). All measured fracture sets are plotted along the borehole trace in B. Fractures are rectangular with a 50 ft strike and 25 ft dip length. One set of fractures (S1) is plotted in C whereas a different fracture set (S2) is plotted in D. This demonstrates that specific fracture sets may be local only, or may overlap. Borehole drift is affected by fracture distribution; major deviations in the borehole trace coincide with the distribution of different fracture sets. Highest-yielding WBZs correspond to sections containing overlapping fracture sets.

in poorly productive units are generally below about 0.3 gpm, the instrument detection limits of the NJGS HPFM (Herman, 2006). Low flow rates may cause more uniform log responses for the fluid column because only one or two entry streams are mixed.

Each BTV survey and interpretation generates structural geological data for the set of interpreted OPTV records and borehole-orientation information (table F2). Computer programs are used to statistically analyze these structural data and visualize their interrelationships using geographic information systems (GIS) and other computer-aided drafting software (figs. F10 and F11). Structural analyses of BTV data in the appendixes include circular histograms and stereonet diagrams that show map trends and 3D orientations, respectively. Mean strike, dip, and/or dip direction (azimuth) of bedding, layering, and fractures are included in these analyses for individual wells or groups of wells in a well field. Statistical maximums are interpreted for the 3D stereonet diagrams then used to represent primary map orientations of stratigraphic layering and secondary fractures on project-site maps throughout the appendixes.

Water-bearing features

WBFs have been identified in all four major aquifers, all zones in the Brunswick aquifer and in groups of igneous and sedimentary rocks (tables F4 and F5). A total of 650 WBFs are identified in the hydrogeologic sections, based on geophysical logs for 35 of the 36 projects and 119 of the 128 wells detailed in the appendixes. Detailed examples of diverse types of WBFs are presented using OPTV records for each study. Each project summary includes examples of interpreted features for at least one well. Some projects include multiple wells, and some feature interval-flow data derived from HPFM logs and/or from

straddle-packer tests. Projects having the most complete data include a hydrogeological profile and/or a 3D graphic interpretation showing the spatial distribution of WBFs in the subsurface. Studies with hydrogeologic interpretations of multiple wells having detailed subsurface information are indexed as hydrogeologic framework studies. Of the 36 projects (table F1), 12 are presented as framework studies, with 10 for the Brunswick and one each for the Lockatong and Stockton aquifers. Of the 10 for the Brunswick, 3 involve basalt units in the Watchung zone.

Three types of WBFs are identified including:

1) bedding planes and layers,
2) fracture planes, and
3) linear intersections of bedding planes and fracture planes

The assignment of a particular WBF to a specific group based on borehole imagery is a highly subjective exercise. In many instances, a feature or set of features can be assigned to more than one group. For example, networks of hydraulically conductive fractures having the same orientation locally occur within specific stratigraphic horizons (appendix 3D13 and 3D14). In such cases, there are both stratigraphic and fracture controls on the occurrence of a WBZ and it is difficult to assign WBF classification to solely one feature. They are therefore identified as being both a conductive bed and conductive fractures. Primary considerations for classifying WBFs are: what specific feature stores and conducts groundwater, and, if features are nonlayering fractures, is there good evidence showing stratigraphic control of their occurrence and distribution? In the examples noted above, the features are included as type 3, layer-fracture intersections, though arguments may be made for both stratigraphic and structural control. A common problem is that these relationships are demonstrated locally for a single well, but the continuity of features within a specific stratigraphic interval in a specific area requires BTV coverage in many wells with overlapping stratigraphic coverage; this however is not common. Designation of a feature simply as a ‘conductive tectonic fracture’ may not capture its essence as part of a group of features restricted to a particular stratigraphic horizon and lying just beyond the physical limits of the borehole record. In general, hydraulically conductive intersections of both strata and fracture planes are probably undermeasured in the summary geostatistics listed in tables F5 and F6.

Type 1 WBFs – Bedding planes and layers

WBFs classified as bedding planes and layers include planar features and tabular units lying parallel to sedimentary beds or compositional layering in igneous basalt and diabase. No distinction is made between the planar and tabular varieties in the hydrogeologic interpretations of borehole geophysical logs included in the appendixes; WBFs are simply noted as either conductive bedding (cb) or conductive layering (cl). However, the different varieties of these features are discussed here to promote an understanding of how groundwater is stored and conveyed in the Newark basin aquifers.

The permeable geological features related to stratigraphic layering include bed partings, or simple, planar mechanical breaks along contacts between strata composed of differing grain size and bed thickness. Examples from the different aquifers listed below are referenced to figures in the appendixes:

Diabase – 1B4-left, 1B6 and 1C3-left
Basalt – 1E6 and 1F3
Brunswick – 2A2 (well 15), 2A3, 2BC2, 2C2, 2D3, 2D4-left, 2E6-left, 2E7-right, 3C2, 3C5, 3J4-right, 3J5-right, 3M17-right, 3N6-left, 3N10-left, 3N12-right, 3P2 and 3E6-left
Lockatong - appendix 4B3-left and 4C3
Stockton – appendix 4C4 and 4D3.

Features having millimeter thickness are commonly noted by logging technicians as bedding fractures or ‘hairline’ fractures lying in the stratigraphic plane. They can be locally enlarged as a result of weathering and drilling operations to appear on BTV records as being a few centimeters thick (appendix 4D3 and 2E6-left and 2E-right). The lateral continuity of these mechanical breaks can be seen in BTV surveys of closely-spaced wells, and their subsurface continuity and capacity to be conductive planes extends hundreds to thousands of feet (appendix 4F9-left, 3N11-left and 3N12-right). Conductive bed partings commonly occur near stratigraphic contacts between gray and black beds with massive red mudstone and siltstone (appendix 3E6-left and 3H3)). Two additional types of WBFs noted as conductive bedding or layering include tabular units with thickness of as much as a few feet and lateral continuity over distances of hundreds of feet. These tabular units include highly-fractured transmissive strata lying between adjacent, confining mudstone and siltstone layers (appendix 3D13 and 3D14) and fine-grained sedimentary beds containing mineral-dissolution zones within gypsum paleosoil horizons (appendix 3F4--right and 3M7).

Massive mudstone beds make up a large part of the Brunswick aquifer (Smoot and Olsen, 1985; 1994). They list three types of massive mudstone common in the Newark basin including burrowed, mud-cracked and root-disrupted varieties. Each represents an end member having dominant, distinctive fabrics that denote specific depositional environments (Smoot and Olsen,

Table F4. Summary of projects, wells and WBFs, geophysical logs collected and ranges of log values

PROJECTS, WELLS AND WATER-BEARING FEATURES							GEOPHYSICAL LOGS COLLECTED												LOG-RESPONSE VALUES				
Appendix Entry	NJGS Project	Aquifer or aquifer zone(s)	no. of wells	number of WBFs by type			Imaging			Fluid				HPFM		Formation				fluid resistivity (ohm-m)	fluid conductivity (μs/cm)	HPFM borehole flow (np) (gpm)	formation natural gamma bswl (cps)	formation single-point resistance bswl (ohms)
				1	2	3	O	A	B	FC	FR	FT	PA	np	pu	C	G	SP	SL					
1A	258 S. Franklin AGW	diabase	1	7	3	1	X		X	X	X	X		X	X		X	X		14-30	328-700	0.3	20-105	1595-2074
1B	Snydertown Rd AGW	diabase	4	3	18	1	X		X	X	X	X		X		X	X	X		12-56	185-900	0.9	4-55	370-2900
1C	Crusher Rd.WS	diabase	1	1	4		X			X		X									205-475			
1D	Block 38, Lot 16 WS	diabase	1		7		X		X	X	X	X				X	X	X		7-71	141-1410		5-86	2920-2994
1E	Essex County CC WS	BWB	3	15	4	3	X		X	X	X	X		X				X		18-40	257-545	5.6	7-61	70-1550
1E	Essex County CC WS	BSS	1	3	1	1	X		X	X	X	X		X				X		22-36	280-285	0.5	30-160	123-300
1F	1163 Delaware AGW	BWB	1		6	1	X		X	X	X	X		X		X	X	X		7-28	354-1385	ND	6-42	500-2270
1F	1163 Delaware AGW	BMR	1				X		X	X	X	X		X		X	X	X		28-29	349-354	ND	15-195	140-234
2A	Ridgewood Shell GWI	BSC	9	4			X																	
2B	Sandos-Clariant GWI	BSS	2	6	4		X																	
2C	Hoffman-LaRoche GWI	BSC	3	3	6		X																	
2D	Hamilton Farms WS	BC	3	8	7	14	X			X		X		X							120-234	0.3		
2E	Milford Boro WS	BLGSC	5	22	8	8	X		X	X	X	X		X		X	X	X		15-43	230-1370	ND	44-560	1240-4288
2F	Passaic Flood Tunnel GI	BWS-BMR-BLR	9								X	X	X			X	X		X	1-41			20-234	
3A	Flemington Boro WS	BMR	1	12	3		X		X	X	X	X				X	X	X		1-10	345-15000		52-208	1514-1564
3B	Hillside Car Wash WS	BMR	1	2			X			X		X									1742-1820			
3C	Readington Twp GWI	BMR	5	18	12	1	X		X	X	X	X		X		X	X	X		28-103	65-290	3.8		
3D	Delaware Twp AGW	BMR	5	6	7		X		X	X	X	X		X			X	X		22-38	200-211	2.5	40-220	150-1020
3E	Potterstown Rt 22 GWI	BMR	6	10	10		X		X	X		X			X					2-28	300-576	ND	17-320	120-450

Aquifer abbreviations: BWB - Brunswick Watchung basalt, BWS- Brunswick Watchung sedimentary rock, BC - Brunswick conglomerate, BSC - Brunswick sandstone and conglomerate, BLGSC - Brunswick lower gray zone with sandstone and conglomerate, BMR - Brunswick middle red zone, BMG - Brunswick middle gray zone, BSS - Brunswick sandstone, BLR - Brunswick lower red zone, BLG - Brunswick lower gray zone

Water-bearing feature (WBF) key: Type 1 - bedding planes and layers, Type 2 - fracture planes, Type 3 - linear intersection of bed and fracture planes

Geophysical log abbreviations: O - optical televiewer, A - acoustic televiewer, B - borehole video camera, FC - fluid conductivity FR - fluid resistivity, FT - fluid temperature, PA straddle packed, HPFM - heat-pulse flow meter, np - nonpumping, pu - pumping, C - caliper, G- natural gamma, ND - not determined, SP - singe-point resistance, SL - short-long normal resistivity

Log-response abbreviations: μs/cm - microsiemens per centimeter, gpm - gallons per minute, cps - counts per second, bswl - below static-water level

(continued on next page)

(continued from previous page)

Table F4. Summary of projects, wells and WBFs, geophysical logs collected and ranges of log values

PROJECTS, WELLS AND WATER-BEARING FEATURES							GEOPHYSICAL LOGS COLLECTED													LOG-RESPONSE VALUES				
Appendix Entry	NJGS Project	Aquifer or aquifer zone(s)	no. of wells	number of WBFs by type			Imaging			Fluid				HPFM		Formation				fluid resistivity (ohm-m)	fluid conductivity (μs/cm)	HPFM borehole flow (np) (gpm)	formation natural gamma bswl (cps)	formation single-point resistance bswl (ohms)
				1	2	3	O	A	B	FC	FR	FT	PA	np	pu	C	G	SP	SL					
3F	Trump National GC WS	BMR	7	1	32		X																	
3G	Hopewell Boro AGW	BMR	7	21	15	4	X		X	X	X	X	X	X	X	X	X	X	X	15-44	79-325	0.5	80-200	125-340
3H	Larison's Corner GWI	BMG	1	2	9	1	X			X	X	X	X			X	X		X	28-36	870-895		58-300	103-386
3I	Home Depot GWI	BMG	3	6	8	2	X			X	X	X		X		X	X	X		1-31	325-12000	ND	55-240	250-675
3J	Branchburg Rt202 GWI	BMG	6	8	24		X																	
3K	Heron Glen GC-QNS WS	BMG	4	5	7		X		X	X	X	X			X	X	X	X		29-44	230-336	8.0*	75-320	630-760
3L	Harbat Farms WS	BLR	1		5		X		X	X											220-228			
3M	Stony/Honey Brook WS	BLR	10	20	29	9	X	X		X	X	X	X	X						9-60	264-448	2.4	50-367	47-933
3N	Bristol Meyers-Squibb GWI	BLG		4	33	9	X	X		X		X	X	X							230-950	ND		
3O	Pennington Boro WS	BLG	1	2	7		X			X		X		X							325-335	ND		
3P	The Ridge GC WS	BLG	2	3	8		X			X		X					X				250-850		15-4012	
3Q	Snydertown Rd GWS	BLG-L	2		2	1	X			X	X	X				X	X	X		18-38	263-538		30-2686	310-1685
4A	Terhune Orchards GWS	L	2	2	3	3	X			X		X				X	X	X			225-390		50-960	439-1717
4B	Hilltop Development WS	L	5	2	24	2	X			X		X		X		X	X	X			255-820	ND	50-1750	350-1400
4C	29 Pine Hill Rd. AGW	L-S	1	6	5	1	X			X	X	X	X	X			X	X		14-24	431-690	0.9	75-650	10-1250
4D	Ewingville Rd & Rt31 GWI	S	3		1		X																	
4E	Green Acres CC WS	S	2	3	12	3	X			X	X	X		X	X	X	X	X		14-55	280-857	3.8	5-540	540-860
4F	Springdale GC WS	S	3	8	11	7	X			X	X	X		X		X	X	X	X	14-55	250-425	15.0	50-600	100-600
4G	Princeton Plasma Physics	S	3					X												1-103	2-15000	ND	1-4012	10-4288
		Totals	128	213	335	72																		

Aquifer abbreviations: BMR - Brunswick middle red zone, BMG - Brunswick middle gray zone, BLR - Brunswick lower red zone, BLG - Brunswick lower gray zone, L - Lockatong, S - Stockton

Water-bearing feature (WBF) key: Type 1 - bedding planes and layers, Type 2 - fracture planes, Type 3 - linear intersection of bed and fracture planes

Geophysical log abbreviations: O - optical televiewer, A - acoustic televiewer, B - borehole video camera, FC - fluid conductivity
FR - fluid resistivity, FT - fluid temperature, PA straddle packed, HPFM - heat-pulse flow meter, np - nonpumping, pu - pumping,
C - caliper, G- natural gamma, ND - not determined, SP - singe-point resistance, SL - short-long normal resistivity

Log-response abbreviations: μs/cm - microsiemens per centimeter, gpm - gallons per minute, cps - counts per second, bswl - below static-water level

* flow measured while two irrigation wells were pumping nearby

1994). Cycle thickness also increases from the hinged and lateral basin margins inward toward the center (Schlische, 1992). The basic Van Houten precession cycle thickens upward in the basin, reflecting a gradual upward increase in sediment-accumulation rates throughout time (Schlische, 1992). Generally, the Lockatong precession cycles are about 5 to 20 ft thick. The Passaic cycles range in thickness from about 10 to 30 ft. The Jurassic lacustrine cycles are the thickest, ranging from about 30 to 75 ft (Schlische, 1992). Identifying precession cycles in the lower and middle red zones of the Brunswick aquifer is complicated by the abundance of red beds and the scarcity of gray and black marker beds (fig. F2). Thick red beds were deposited during prolonged arid conditions resulting from the overlapping effects of larger-order climate cycles. Cycle thickness of a stratigraphic section differs in different parts of the basin, probably in response to a combination of tectonic and climatic controls (Schlische and Olsen, 1990; Schlische, 1992).

Mud-cracked and burrowed mudstone is mostly restricted to the Lockatong aquifer and lower gray part of the Brunswick aquifer and indicates deposition of sediment on dry or occasionally wetted mud flats (Smoot and Olsen, 1994). Root-disrupted mudstone is progressively more abundant in the middle-to-upper-red zones in the Brunswick aquifer (Herman, 2005) and results from deposition on wet mud flats having periodic, fresh, groundwater tables (Smoot and Olsen, 1994). All varieties of mudstone locally contain assemblages of millimeter-to-centimeter scale crystal casts and linear to ovate syndepositional sedimentary features filled with secondary, sparry cements locally including calcite ($CaCO_3$), gypsum ($CaSO_4 \cdot 2H_2O$), analcime [$Na_{16}(Al_{16}Si_{32}O_{96}) \cdot 16H_2O$)], albite ($NaAlSi_3O_8$), potassium feldspar ($KAlSi_3O_8$), and dolomite ($CaMg(CO_3)_2$)(Van Houten, 1965; Smoot and Olsen, 1994; Tabakh and Schreiber, 1998). Secondary, authigenic calcite and gypsum are most abundant in the middle part of the Brunswick aquifer where sedimentary vesicles, evaporite-crystal casts, desiccation cracks, and root structures form networks of type 1 conduits (fig. F12 and appendix 3M7).

Dense accumulations of calcite and gypsum grew locally in relict soil horizons, but and are now partially dissolved in bedrock to depths exceeding 400 ft below the land surface, leaving vuggy, tabular beds of siltstone and mudstone capable of storing and transmitting significant quantities of water (appendix 3M7, 3M8, 3M12-right, 3G5-right, 3G7-right). These horizons are collectively referred to as gypsum paleosols. This term is also applied to red beds whose appearance and hydraulic properties are inherited from past accumulations of evaporite minerals in a subsurface stratigraphic horizon. These horizons may be cemented with salts of carbonate, sulfate and other evaporites in

Table F5. Types[1] of WBFs by aquifers, zones, units and groups of rocks

Aquifer	Zones, units and groups	No. of Wells	Type 1	Type 2	Type 3	Total	%1	%2	%3
Diabase…..	……	7	11	32	2	45	24	71	4
Brunswick...	……	93	181	247	54	482	38	51	11
Lockatong..	……	10	8	31	6	45	18	69	13
Stockton…..	……	12	13	25	10	48	27	52	21
TOTAL[2]…..	……	**119**	**213**	**335**	**72**	**620**	**34**	**54**	**12**
Brunswick	Basalt units in the Watchung zone (BWB)……..	4	15	10	4	29	52	34	14
Brunswick	Conglomerate and Sandstone (BC and BSC)…..	20	37	21	22	80	47	26	26
Brunswick	Sandstone (BSS)……..	3	9	5	1	15	60	33	7
Brunswick	Middle Red zone (BMR)……..	33	70	79	5	154	45	51	3
Brunswick	Middle Gray zone (BMG)……	14	21	48	3	72	29	67	4
Brunswick	Lower Red zone (BLR)……	11	20	34	9	63	32	54	14
Brunswick	Lower Gray zone (BLG)……..	10	9	50	10	69	13	72	14
Brunswick	Coarse-grained units (BC, BSC and BSS)……	23	46	26	23	95	48	27	24
Brunswick	Fine-grained units (BMR, BMG, BLR and BLG)..	68	120	211	27	358	33	59	8
Brunswick	Red Units (BC, BSC, BSS, BMR and BLR)……..	67	136	139	37	312	43	45	12
Brunswick	Gray Units (BMG and BLG)……	24	30	98	13	141	21	70	9
	Igneous rocks (diabase and basalt)……..	11	26	42	6	74	35	57	8
	Sedimentary rocks……	110	187	295	67	549	34	54	12

[1]Type 1 – bedding planes and layers, type 2 – fracture planes, type 3 – linear intersections of bed and fracture planes

[2] Some wells penetrate more than one aquifer, group or unit so that the total number of wells and WBFs may not equal column totals.

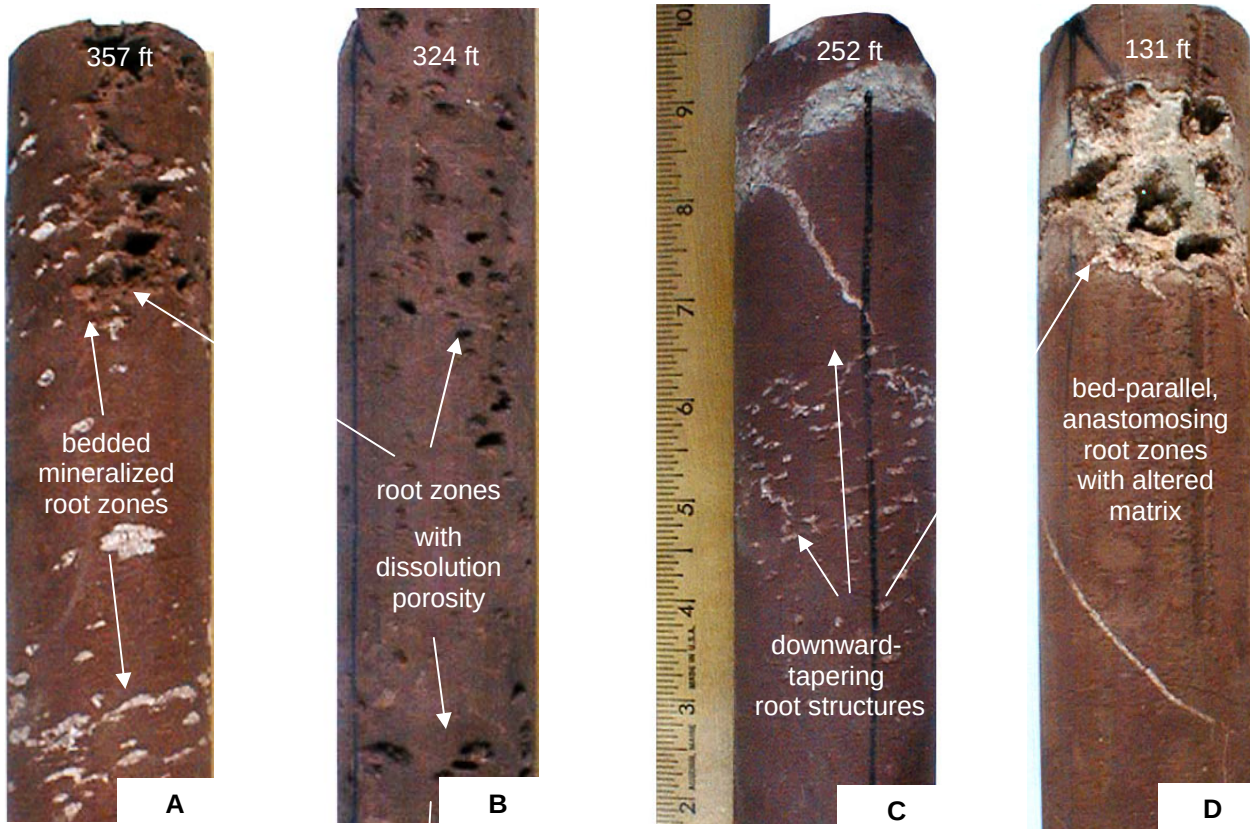

Figure F12. Examples of cores showing stratified gypsum paleosols from the lower red zone of the Brunswick aquifer. A, B, and D show beds having effective secondary porosity stemming from dissolution of soluble minerals from matrix pores. C and D show downward-tapering root structures within these soil horizons. Secondary tectonic vein cuts the lower part of D from upper left to lower right. Ruler shows scale in inches.

arid settings, such as those on margins of deserts and playa lakes (Retallack, 2001). Such minerals are readily soluble in fresh water. In many beds, all that remains of these ancient evaporite beds are pseudomorphs of crystals or breccia layers where the sediment collapsed into the dissolved salt layers producing breccia and 'crumb' fabrics during diagenesis (Smoot and Olsen, 1985). In other beds, mineralized nodules and root tubes form anastomosing networks of secondary authigenic minerals (appendix 3M7). Their hydrogeological significance is illustrated in appendix entries for the Stony Brook-Millstone Watershed Association research well field (3M), the Hopewell Borough Supply Well 6 study (3G) and Trump National Golf Course (3F) as previously described by Herman (2001).

Layering in diabase and basalt is more varied in strike over small distances than sedimentary bedding. For example, compositional layering in diabase in the Sourland Mt. sill has a wider variety of orientations (fig. 1B1) than underlying mudstone and shale in the Passaic Formation (fig. 3Q1). Basalt layers are more varied in strike than adjacent sedimentary beds (appendix 1E2). The variation in compositional layering reflects the complex flow paths followed during the injection and extrusion of magma into and onto other strata. Their varied orientations reflect limited subsurface continuity of layering, with the likelihood of adjacent layers being onlapped and truncated. This limits continuity in the subsurface in an average strike direction and decreases horizontal conductivity. Complex layering contributes to the 3D heterogeneity of these igneous aquifers except where layer boundaries are more continuous along contacts of major sills and flows resulting from large magma pulses, or the development of thick cumulate layers during fractionation and cooling processes. These stratigraphic intervals have varied textures, colors and/or fracture densities (appendix 1A2, 1B3, 1B5, 1B7, 1C2 and 1D2, 1E3, 1E5, 1E7, 1E9 and 1F2). Increased structural heterogeneity results in decreased horizontal and vertical conductivity and in groundwater recharge potential in comparison to the fine-grained sedimentary beds having continuity in the basin subsurface over distances of miles (Olsen and others, 1996).

Type 2 WBFs: Fracture planes

WBFs classified as conductive fractures (cf) are those that have visible secondary porosity along most or the entire entire fracture plane that is not oriented parallel to the bedding plane. All fractures in bedrock are secondary geological features postdating sedimentary bedding and igneous layering. Natural fractures occur as a brittle strain response in the Earth's crust from deep-seated tectonic stresses or as a response to near-surface stresses stemming from the removal of overburden by erosion and weathering. Other bedrock fractures can be artificially induced in rock cores (Kulander and others, 1990) and in well boreholes following drilling and hydrofracturing. However, this section is focused on sets of naturally-occurring, systematic, tectonic fractures that store and transmit groundwater in deep, relatively unweathered bedrock, as seen in wells having uncased sections ranging from about 20 to 50 ft bls. Fractures are considered systematic where they occur in sets that are parallel or subparallel (Hodgson, 1961).

Systematic fractures in the basin include sets of steeply- to moderately-dipping extension fractures and gently- to moderately-dipping tectonic shear fractures. Of these, the steeply-dipping extension fractures, commonly referred to as joints in outcrop (figs. F6, F13, F14a, F15 and F16), are the most abundant in the Newark basin and are shown below to be an important part of the aquifer framework.

Sets of steeply-dipping extension fractures formed in basin bedrock as a brittle strain response to tensile stretching of the crust along what is now the eastern margin of North America during the Early Mesozoic (Herman, 2005; 2008). These fractures are classified as 1) joints if the two sides of the fracture show no differential displacement to the naked eye, 2) as healed joints if the fracture walls are completely or partially joined together by secondary crystalline minerals or 3) as tectonic veins if secondary minerals completely fill the space between fracture walls (Ramsay and Huber, 1987). Extension fractures are mostly or entirely filled with secondary albite (fig. F14b) and calcite (fig. F18) in bedrock excavations (figs. F4, F13b, F14a, F15 and F16a, b and d), rock cores (figs. F12, F17 and F18) and BTV records. obtained below near-surface depths (~6 ft bls). However, these fractures are typically mapped as joints because any secondary minerals that formerly filled them are weathered out (Herman, 2001b). Their tensile origin is confirmed by their characteristic markings in outcrop that include plumose (feather) patterns, rib marks and hackles (Pollard and Aydin, 1988; Herman, 2005). Multiple sets of steeply-dipping extension fractures of different orientations occur throughout the basin so that two to four different fracture sets occur at a single location (figs. F11, F14b, F17a, F18; Herman, 2005). The spacing, arrangement, and density of these fractures also differ as a result of mechanical layering of strata (fig. F15) and proximity to large normal faults (Herman, 1997). Fracture spacing and fracture-strike lengths vary with layer thickness so that fracture

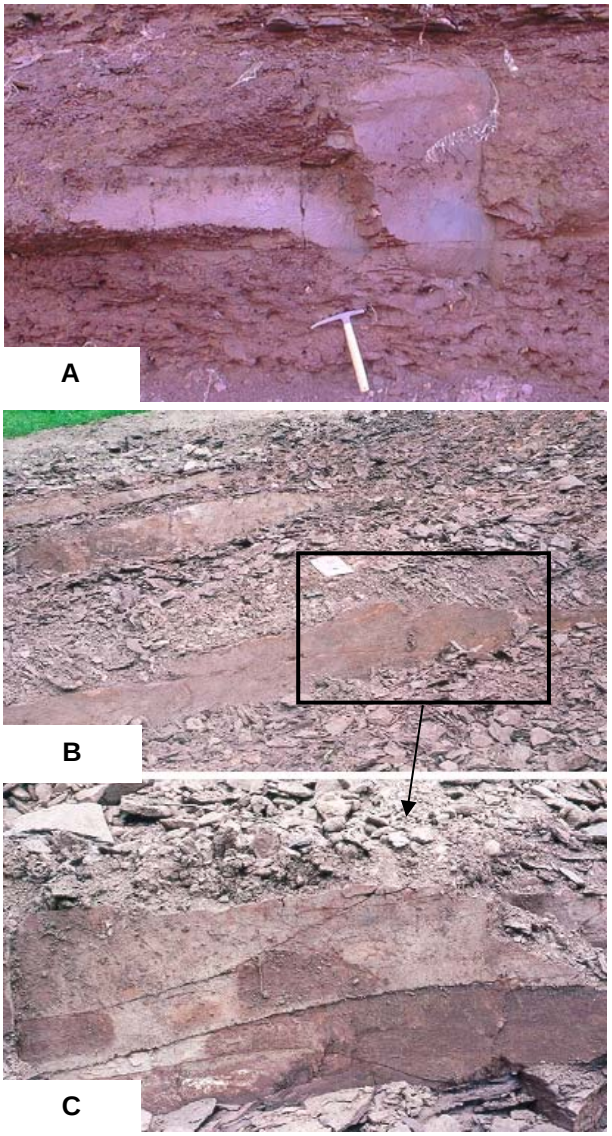

Figure F13. Extension fractures in Passaic Formation mudstone red beds. A. Stream-bank outcrop showing a pitted paleosol horizon overlain by a fractured mudstone (near appendix entry 3F). Note how the two joints span different heights within the fractured layer. B and C show a shallow bedrock excavation (appendix entry 3P). The rectangle in B approximates the area covered by C. The latter highlights a steeply-dipping fracture face having a trace length of about 3 meters and a height of about 3 feet for the fractured stratigraphic interval. Two, gently-dipping, curviplanar fractures intersecting the steep face are typical of gently-dipping fractures in shallow bedrock stemming from stratigraphic unroofing and weathering.

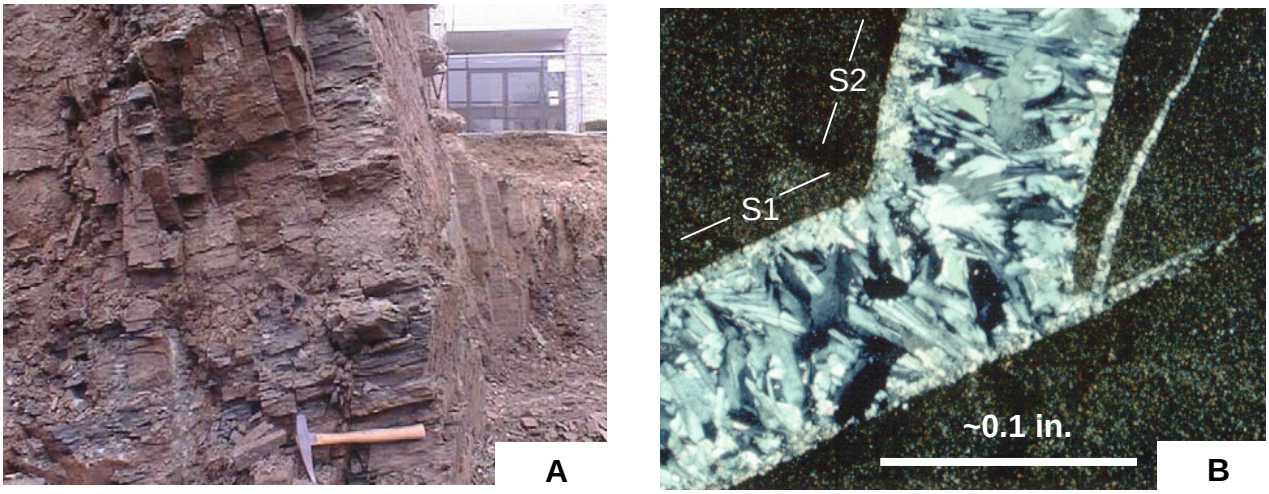

Figure F14. Extension fractures in the Lockatong Formation exposed in a foundation excavation (A) along Route 31N in Ewing, NJ. B. Photomicrograph (crossed nicols) of a tectonic vein from A showing sodium-silicate (albite) filling fracture interstices having both S1 and S2 fracture orientations.

Figure F15. Extension fractures in mudstone and siltstone of the Passaic Formation (Brunswick Middle Red zone) exposed in vertical face cuts during excavation of a commercial pipeline, Somerset County. Plastic netting on the upper benches is about 4 feet in height. Note the difference in thickness between bedding and fractured layers and how fracture density and dimensions differ. Photograph courtesy of Don Monteverde, NJGS.

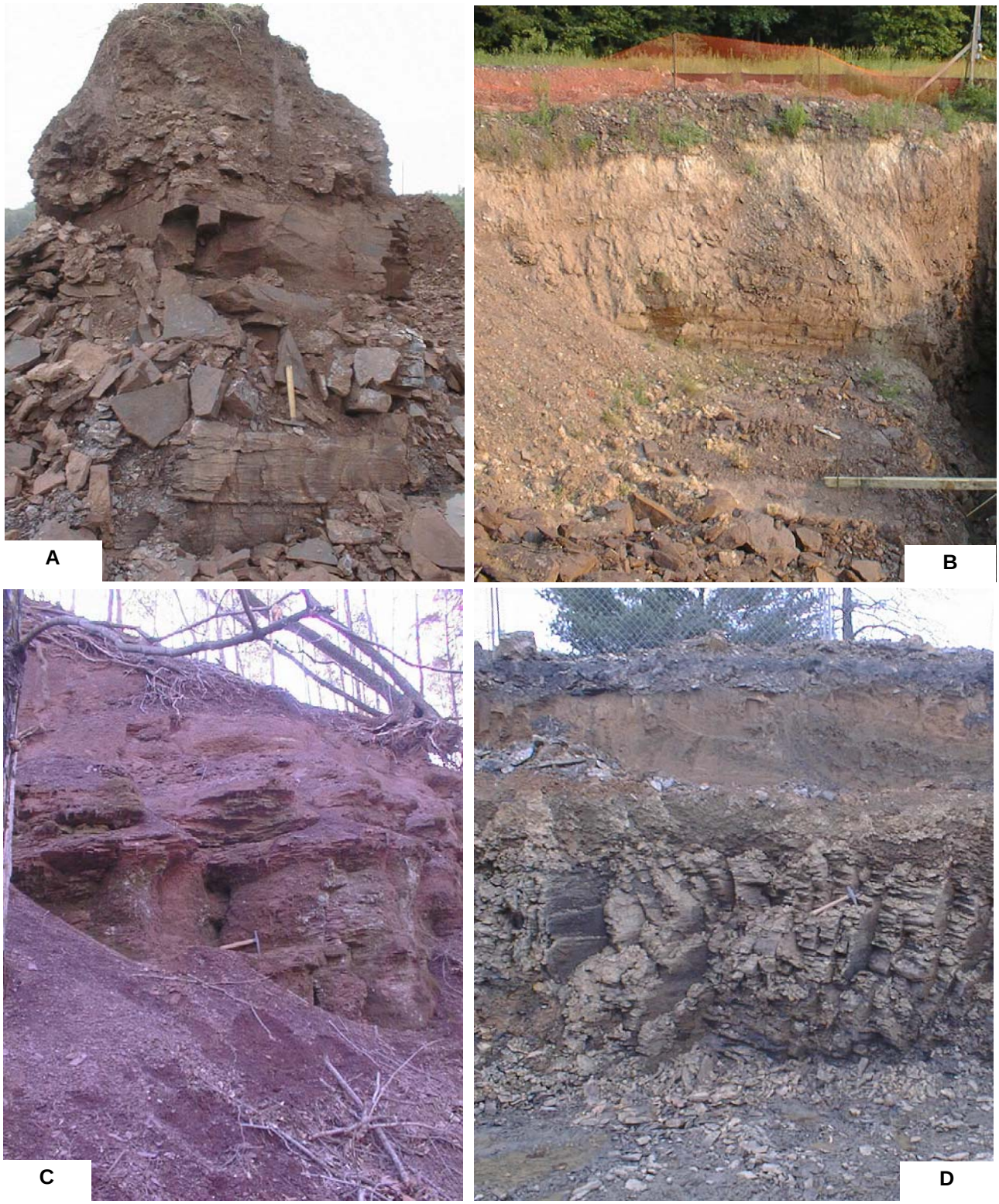

Figure F16. Photographs showing regolith overlying weathered bedrock in the lower gray (A) and middle red (B and C) zones of the Brunswick aquifer, and the Lockatong aquifer (D). A, B and D are in excavations whereas C is a stream-bank outcrop.

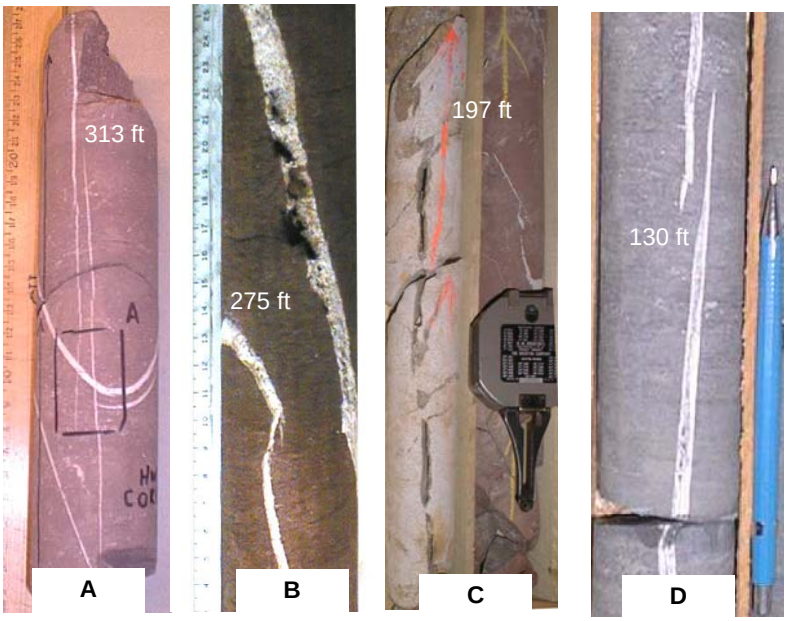

Figure F17. Core photos showing mineralized extension fractures (tectonic veins) that are locally conductive. Fractures are permeable where secondary minerals that otherwise fill veins are dissolved out. A and B are from Hopewell Boro (appendix 3G). A shows multiple sets of crosscutting veins. B shows where secondary minerals are locally dissolved from veins that are hydraulically conductive. C shows open and conductive extension fractures in the Stockton Formation, Mercer County. D shows tectonic veins in gray mudstone of the Brunswick aquifer in Mercer County. Approximate depth to top of core sample indicated on each photo. Ruler shows centimeter scale for A and B.

density generally increases as the thickness of the fractured layer decreases as shown by fracture-spacing studies conducted in sedimentary rocks elsewhere (Pollard and Adyin, 1988; Huang and Angelier, 1989; Narr and Suppe, 1991, Gross, 1993). Fracture density also increases from an average of <1 fracture per meter in areas remote from faults to >50 fractures per meter near large fault traces (Herman, 1997).

Secondary fracture-fill minerals are locally dissolved and removed from extension-fracture interstices in deep bedrock (figs. F17b and F17c) by weakly-acidic groundwater. Notable examples of conductive extension fractures are included in the appendixes for the following aquifers:

Diabase – 1A3-right, 1B4-right, 1B8, 1D3-right and 1D4-left
Basalt – 1E6-right
Brunswick – 2B3-left, 2D3, 2D5, 2E7-left, 2E8-right, 3C2, 3C3, 3C4, 3C5-left, 3D8, 3D10, 3D12, 3D14, 3E6-right, 3F5-right, 3F6-right, 3H3-right, 3I4-left, 3J3, 3J4, 3J6, 3M6, 3M11, 3M17, 3M18, 3N6-right, 3N7, 3N10, 3N14, 3O2 and 3P5
Lockatong – 4B6 and 4B7
Stockton – 4C3-left, 4E3, 4E5, 4E6, 4F4, 4F5 and 4F7.

Open, conductive, extension fractures occur randomly throughout Newark basin aquifer systems and commonly provide leakage between primary WBZs aligned with stratigraphic planes. Statistically, they act as primary WBFs in the gray units of the Brunswick aquifer and in the Lockatong aquifer (table F5). Overall, they make up just over half of the WBFs in this study (table F5).

Late sets of gently- to moderately-dipping, systematic, tectonic shear fractures and veins occur locally in areas of gently-folded rocks (appendix 3M2 and 3N3) and igneous intrusions (fig. 1B1). These fractures are also largely filled with secondary minerals, especially in the sedimentary units, but are less significant in providing cross-layer leakage than the steeply-dipping fractures because of their gentler dips

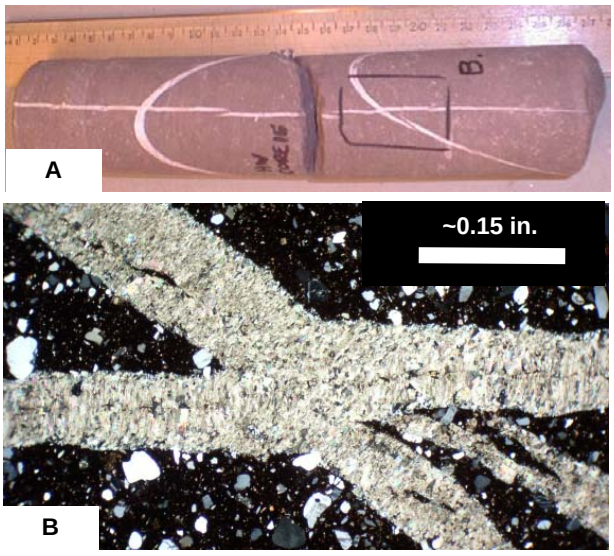

Figure F18. Photos of calcite-filled tectonic veins from Hopewell Boro (appendix 3G). Red mudstone core contains young veins striking/dipping N10^{o}W dipping 86^{o}E that crosscut older veins striking N45^{o}E dipping 66^{o}S and striking N75^{o}E dipping 62^{o}S. Black rectangle in A is the sample area of photomicrograph B. Fibrous calcite fills fracture interstices. Younger vein(horizontal in B cuts across older ones and helps establish the relative timing of fracturing in the basin. Photomicrograph taken using crossed nicols.

and limited vertical extent. Their restricted distribution also limits their hydrogeologic importance. Other nonlayering, nonsystematic fractures (Groshong, 1988) do not appear to contribute significantly to the hydrologic framework of unweathered bedrock, based on the inspection of the BTV records. Most are steeply-dipping cross fractures striking normal to the clustered arrays of systematic extension fractures. Cross fractures are irregular, curviplanar and discontinuous surfaces that commonly terminate against bedding and other fractures (Hodgson, 1961; Herman 2005). They also have little or no separation of the fracture walls and very few secondary mineral accumulations.

Another set of fractures in the subsurface includes subhorizontal gypsum veins reportedly originating from stratigraphic unroofing (Tabakh and others, 1998). They are filled with satin spar (gypsum) fibers that are commonly straight and oriented nearly normal to the fracture walls (fig. F19). They occur in the Passaic Formation at depths ranging from about 300 ft to 700 ft bls and range in thickness from less than an inch to several inches. Localized curved fibers indicate vein growth accompanying stratigraphic tilting and/or flexural slip (Tabakh and others, 1998). These veins are thought to have precipitated in a 'mixed phreatic zone' from saturated diagenetic brines originating in a shallow 'dissolution zone' (Tabakh and others, 1998; fig.8). These gypsum veins can reduce an aquifer's productivity. For example, packer-tested intervals in subsurface borings for the Passaic Flood Tunnel geotechnical investigation (appendix 2F) show that stratigraphic sections with these veins (appendix 2F3) have very low transmissivity in comparison to adjacent intervals that lack them. Subhorizontal gypsum veins were seen in only one well having an OPTV record as part of this study (appendix 3B). They strike and dip at very low angles to sedimentary bedding and mostly dip gently north (appendix 3B2). Their strike orientation parallels many other late-stage tectonic shear planes in diabase and suggests that they may have originated in response to late stage, compressive stresses resulting in basin inversion. More work is needed to identify their occurrence, origin, and hydraulic importance. Subhorizontal cracks stemming from basin exhumation and stratigraphic unloading also occur at shallow depths (fig. F13c) within the unsaturated and active phreatic zone but are difficult to detect and differentiate from other fractures due to the lack of secondary vein fill and small fracture apertures.

Bedrock weathers near the land surface because of the many physical, chemical and biological processes that alter it into regolith. These processes include freeze-thaw cracking, erosion, mineral precipitation and dissolution, alteration and transformation, and root growth. The deterioration produces networks of secondary pores that enhance groundwater storage and movement in the weathered bedrock interval that commonly reaches, and in some cases exceeds, depths of about 60 ft bls in areas poor in unconsolidated sedimentary cover (Herman, 2005). Other nonsystematic fractures in the shallow subsurface stem from freeze-thaw cracking, sedimentary and glacial unloading, and occur as intermittently permeable fractures of limited extent. The sum total of fracture systems interconnect at different densities and orientations in different places to form a network of hydraulically conductive planes and linear intersections of planes that generally channel shallow groundwater down topographic slope.

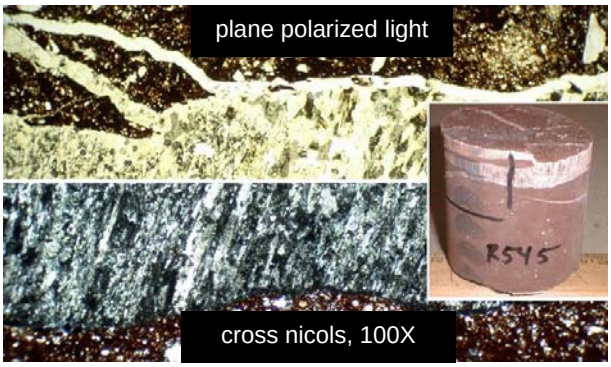

Figure F19. Photo and photomicrographs of gypsum veins from the Rutgers NBCP core (fig. F3) from 545 ft depth. Gypsum veins are as much as a few inches thick iin wells and rock cores from the Passaic Formation in northeast and central parts of the basin. They occur at depths of about 320 to 700 feet and are late structures oriented subparallel to land surface. Satin-spar gypsum fibers are subvertical and locally show shear fabrics. These structures tend to reduce an aquifer's productivity.

Type 3 WBFs: Linear intersections of bedding and fracture planes

A third type of WBF includes hydraulic conduits formed by the intersections of fracture planes with other fractures and with stratigraphic planes. The intersection of two planes forms a line that intersects a plane at a point. Therefore, many of these features appear as points of secondary porosity on the borehole wall (appendix 2E5-right @ 382 ft, 3H4-right @ 250 ft, 3M6 @ 52 ft and 3N10-left @ 176 ft). These features are also barely visible at the scale of the typical hydrogeologic section because they appear as points in the profile plane.

Potential permeable conduits situated at intersections of stratigraphic and fracture planes display a wide range of orientations. This is demonstrated in the appendixes using cyclographic stereonet plots of fracture planes measured in the BTV records (for example, appendix 3M2, 3N3 and 3N4). Hydraulically conductive plane-intersections are an important part of the hydrogeologic framework because they provide steeply-plunging pathways for groundwater to infiltrate and recharge deep bedrock. The trends and plunges of intersecting, potentially permeable structures in an area can be generated and plotted to visualize them on maps and 3D diagrams (fig. F20).

Other WBFs of this type include examples where secondary porosity has preferentially developed in fracture interstices within a specific stratigraphic horizon (appendix 3D13-left, 3D14, 3J3, 3J4 and 3M17-left), where fractures terminate against stratigraphic contacts (appendix 3P3-right and 4F5) and where fractures intersect other fractures of different orientations (appendix 3M11, 3M14-left, 3N7-left, and 4E3-left). In one case, sets of open, permeable fractures occur within a specific stratigraphic section that is continuous over a distance of more than 1000 ft (appendix 3D14).

Hydrogeologic analyses

The methods of developing hydrogeologic sections and 3D framework depictions included in the appendixes are described below. 2D and 3D visualization methods are used to illustrate standard and advanced hydrogeological concepts such as the development of stratigraphic unconformities in massive mudstone beds (appendix 3F2 and 3F3), and the influence of geological structures on the drift of well boreholes (fig. F11). Specific examples of framework interpretations for each major aquifer follow a discussion on groundwater recharge and discharge and

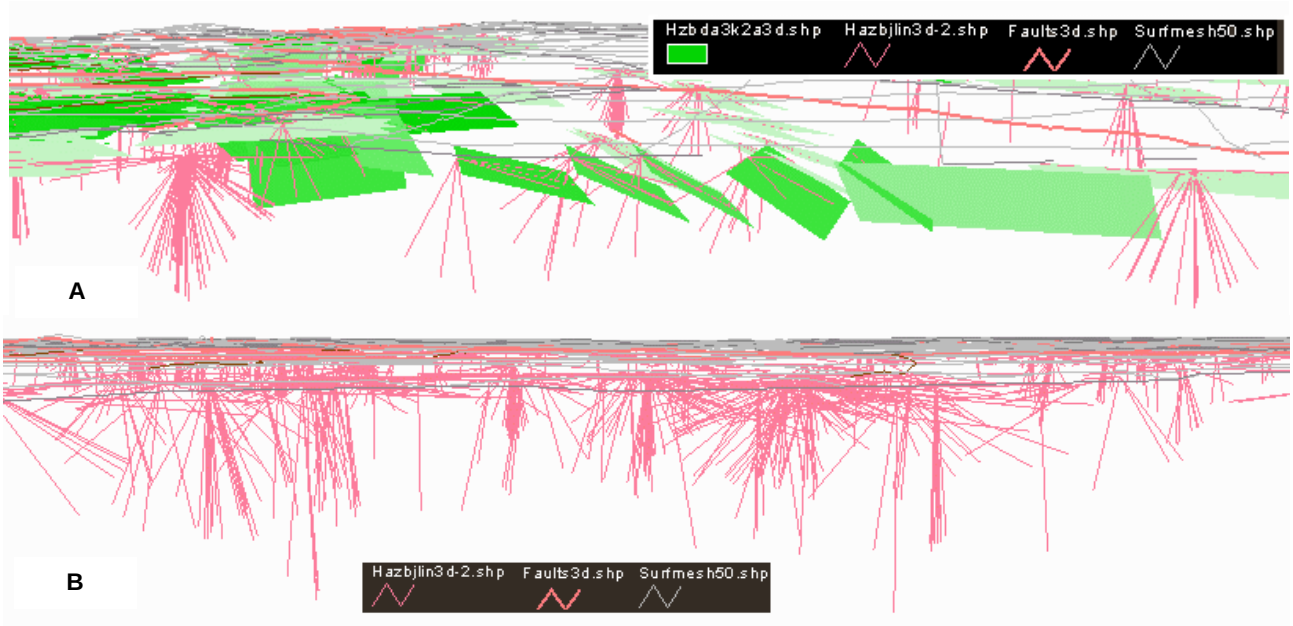

Figure F20. ArcView GIS 3D visualizations of layer-fracture and fracture-fracture intersections calculated for two areas of the basin based on structural measurements in outcrop. Linear intersections of two or more planes are potential permeable conduits, many of which plunge steeply and facilitate groundwater recharge to deep bedrock. A. Northeast view through part of the Flemington fault zone showing bedding (green, rectangular planes dipping left-to-right) and intersection lineation (pink lines) with respect to the trace of the Flemington fault (heavy red line). Planes are 3000 ft wide and 1000 ft long. Intersection lines are about 1000 ft to 1300 ft long. B. Northwest view through the Stony Brook-Millstone research well field (appendix entry 3M).

borehole cross flows. Stratigraphic descriptions included in figures stemming from OPTV interpretations rely on a description of unit color, textures, and layering characteristics. A list of the descriptive adjectives used here and in the appendixes is included in table F6.

Table F6. Lithologic description of geological features

Rock……..	shale, mudstone, siltstone, sandstone, conglomerate, basalt, diabase
Color……..	red, gray, black, orange
Textures...	fine (<.5mm), medium (.5-1mm)-, coarse (.5-1mm) very coarse (1-4mm), pebble (4-16mm), cobble (16-64mm)
Layering...	conductive, laminated (<0.5 in), thin (0.5-4 in), medium (4-12 in), thick (1-3 ft), very thick (>3 ft)
Fractures..	conductive, altered, mineralized, vein, dipping gently (1^o to 29^o), moderately (30^o to 59^o) and steeply (60^o to 89^o)

Map and cross-section components

The hydrogeological framework for the different aquifers is illustrated in the appendixes, using maps, hydrogeologic cross sections, and 3D diagrams. Map elements include the location of a well, or a group of wells, on a topographic or aerial-photographic base map together with the key planar features including stratigraphic contacts, structures such as fractures, faults, and folds and the line traces of cross sections. In some instances, lines extending from the wells normal to stratigraphic dip indicate the extent of the penetrated stratigraphic interval (for example, see appendix 2E1). Cross-section traces are aligned normal to stratigraphic strike to minimize distortions in the dip of strata-parallel WBZs. Features situated off the profile trace are projected into the plane of cross section. In these instances, apparent-dip angles of strata or structures striking at angles other than normal to the profile trace are calculated using trigonometric relationships derived from Ragan (1985).

Land surface is used as the uppermost boundary of the profile and is extracted from the topographic map along the profile trace using standard cross-section construction methods. The representative elevation of a projected well can vary depending upon the focus of the interpretation. Given the absence of subsurface control points that tie a well into another with identified stratigraphic markers, projected wells are drawn at their current surface elevations and therefore may lie above or below the land surface as depicted in cross section (appendix 3N2 and 3F3). The trace of a well in profile is ordinarily plotted vertically from the elevation of the top of casing to the total well depth (TD) as determined from geophysical logs, well-permit records, or from drillers' logs for those wells lacking geophysical logs. For the Brunswick, Lockatong, and diabase aquifers, weathered bedrock extends below overburden to about 60 ft bls unless direct evidence indicates otherwise. Weathered bedrock in the Stockton aquifer extends to a depth of 100 ft, as explained below. Hachuring makes it visually distinct (fig. F21). Other subsurface features represented in profile include WBFs oriented parallel to sedimentary bedding (fig. F21). Depths of WBFs and annotation of any observed borehole features are derived from the geophysical summaries for each well or set of wells in the appendixes. WBFs classified as stratigraphic planes and layers (type 1) are traced parallel to stratigraphic dip from control points identified and labeled on the geophysical log diagrams. Lengths of WBF traces are determined by interpolating between, and extrapolating from, control points to distances that are supported by the bulk of data. WBFs identified as fractures (type 2) are drawn using the same criteria but are shortened by a factor of ½ relative to type 1 features. This reflects their subordinate hydraulic role because they are smaller than stratigraphic planes. For the hydrogeologic section covering the Bristol-Meyers Squibb, Honey Brook Farm, and Stonybrook-Millstone Watershed Nature Reserve well fields (appendix 3N1 and 3N2) the interpretation includes the use of dip-domains. These are panels of parallel strata separated from others along sharp, subvertical lines (kink planes) bisecting panels of rock that dip at various angles. Boundaries between these domains are represented as flexures in an otherwise monoclinal stratigraphic sequence. Other map and profile components are added to reflect local conditions. For example, unconformity surfaces occur in gypsic mudstones near the border fault at Bedminster, NJ (appendix 3F2 and 3F3). Other framework elements may include the traces of gray and black beds in maps and cross sections with arrows indicating the direction of cross flows in wells (fig. F21). WBFs stemming from the intersection of layers and fractures are omitted on cross sections because most would appear as points rather than line traces.

Topographic controls on borehole cross flows

Surface water recharges groundwater in basin aquifers through the diverse, open and permeable features. Precipitation percolates downward under the

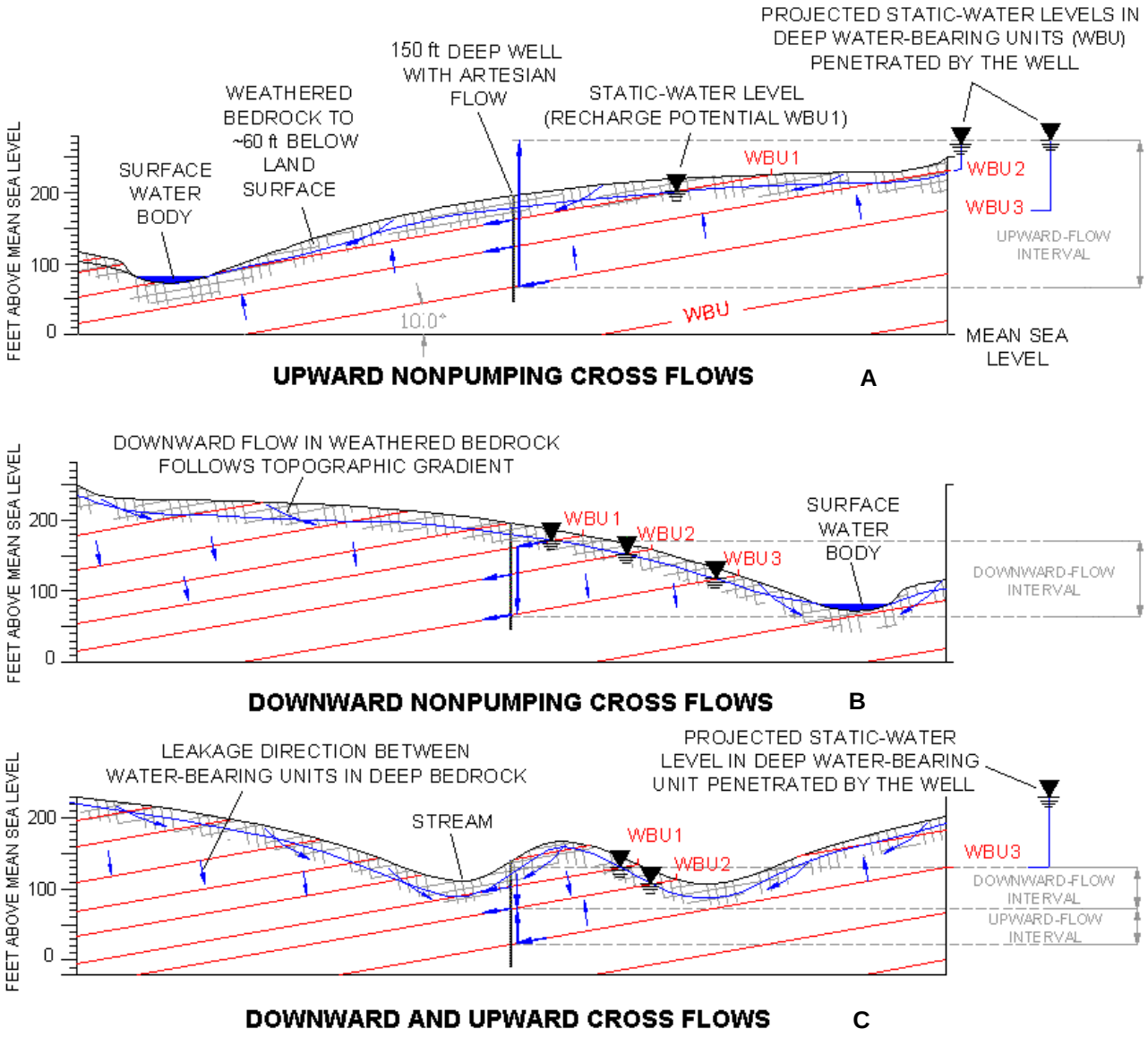

Figure F21. Profile diagrams illustrating the relationship between topographic grade and direction of cross flows in wells under natural (nonpumping) conditions. A. Upward cross flows occur in wells that penetrate deep aquifers with strata dipping in the same direction as topographic grade over long distances. B. Downward cross flows occur where strata dip in a direction opposite to long topographic grades. C. Wells that penetrate strata intersecting both recharge areas on hilltops and hill slopes and discharge areas in valleys can have both upward and downward cross flows. In general, cross flows can be expected to coincide with the direction of leakage in thick sequences of poorly conductive strata that confine bed-parallel WBZs.

influence of gravity into gently-dipping bedrock where permeable bed partings and layers are confined at depth by intervening thick, leaky and less permeable layers (fig. F6, Michalski and Britton, 1997; Michalski, 2001). Natural hydraulic gradients prevail between groundwater recharge and discharge areas in strata that crop out at different elevations in hilltops, hillsides and valleys. Cross flows between WBFs exist where natural flow systems are short-circuited by wells that penetrate different layers that are recharged at different elevations and so have different hydraulic potentials (figs. F21, F22 and appendix 3K2). Wells situated on large hilltops and hillsides sloping in a direction opposite to the dip of bedding have weak, downward cross flows (fig. F21B) that seldom exceed the minimum flow rate that the NJGS HPFM instrument can measure (~0.33 gpm in a 6-inch well). Wells situated in large valleys or hillsides sloping in a direction parallel to bedding dip tap pressurized, semiconfined water-bearing units with upward cross flows that are locally artesian (figs. F21A,

appendix 4C1 and 4C2). Wells in areas of many smaller ridges and valleys may produce upward and downward cross flows because they tap strata that crop out in both recharge and discharge areas (figs. F21C and F22B). For deep wells in hilly topography that tap several discharge and recharge areas, one may measure multiple cross-flow intervals in the well with different flow directions (appendix 3D7 and 3M10). The direction of cross flows may be based on knowledge of the vertical extent of the cased and open sections and on projection of the open sections to the surface.

Diabase

Seven wells in diabase were logged as part of four projects (table F1) in Mercer and Hunterdon Counties (fig. F3). The local surface-water drainage follows the measured fracture orientations in all projects (appendix 1A1, 1B1, 1C1 and 1D1). Groundwater flows mainly in tectonic fractures (71 percent) and to lesser extent along breaks between compositional layering (24 percent) and plane intersections (4 percent).

Diabase layering is thin to very thick and moderately inclined, probably about twice as steeply as

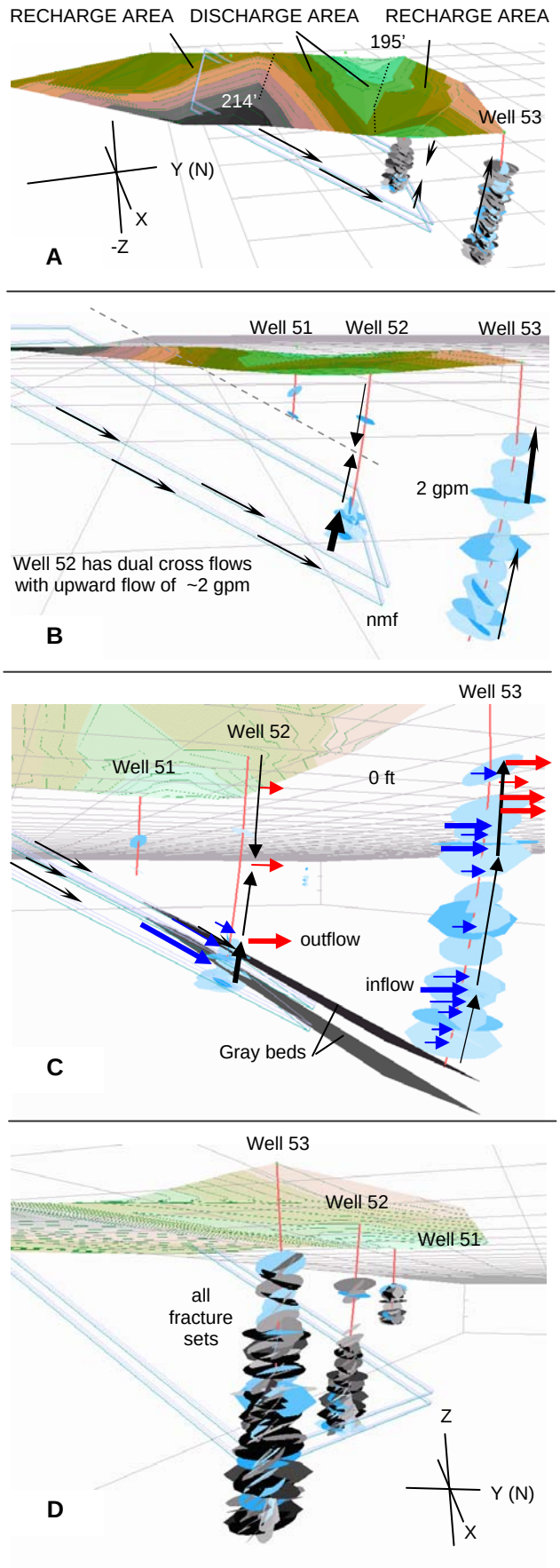

Figure F22 (right). West-looking 3D –GIS perspectives for an arsenic-in-groundwater study, Delaware Twp, Hunterdon County (appendix entry 3D). Topographic survey by Joe Rich and Walt Marzulli, NJGS. Well-field-grid cells are 100-ft and the wells range in depth from 175 ft to 250 ft. Sedimentary bedding and secondary fractures measured with the OPTV are plotted as elliptical planes along each borehole trace, shown as gently-curving, subvertical lines. Elliptical planes were generated using 50-ft major axes oriented along plane strike and using a 2:1 strike-to-dip aspect ratio. Hydraulically conductive bedding and fracture surfaces are shown as light-colored ellipses in B and C, but combined with all other measured fractures in A and D (dark ellipses). Bedding dips gently to moderately northeastward (left to right). Well 52 shows the cross-flow scenario illustrated in Figure F21C with dual cross-flow directions. Upward flows proceed from WBFs in fractured red beds that recharge at high topographic elevations and are confined by overlying gray beds. Downward flows occur in red beds that recharge at lower elevations with lower hydraulic potentials than other semiconfined units. Rates of nonpumping upward cross flows in well 52 reach about 2 gpm (C) in lower depths where water exits the borehole and units above begin to have weak downward cross flows. Cross flows are upward in well 53 because the well intercepts two recharge zones. Topography is modeled as a shaded surface ranging in elevation from 214 ft to 195 ft.

when originally intruded. Layering is locally complex as seen near the base of the Sourland Mt. sill (fig. F10) and in a thin sill at the west end of the Rocky Hill diabase sheet (appendix 1C1), with both NW and SE dips. Diabase layers alternate from light-gray to dark-gray with varying degrees of fracturing (appendix 1A2, 1B3, 1B5, 1B7, 1C2 and 1D2), but diabase shade is unrelated to the fracture density. Shaded layers range in thickness from about 2 ft to more than 100 ft whereas fractured layers range in thickness from a few feet to about 40 ft. The thickest set of fractures seen in BTV records is only about 6 ft in height but correlative fracture surfaces mapped in nearby diabase quarries exceed 20 ft in height and in width (Herman, 2005). The most densely fractured bedrock is near outcrops that show slickensided shear planes associated with nearby faulting (appendix 1C1). The strike of steeply-dipping extension fractures in diabase clusters in the S2 and S3 regional directions and reflects late ENE-WSW to E-W stretching in the basin (Herman, 2005).

Cross flows measured in diabase with the HPFM were less than 1 gpm (table F4). Fluid electrical conductivity and natural-gamma ray emissions are likewise low compared to other aquifers but formation electrical resistivity values are among the highest in the basin (table F4). Diabase is the least productive bedrock aquifer and has the poorest aquifer ranking in New Jersey (Herman and others, 1998).

Brunswick aquifer

Appendixes 1 to 3 include the results of 24 studies of the Brunswick aquifer, including 102 wells (table F1). Table F5 details the number of wells studied in the different zones and units. A detailed discussion of each of the zones in the Brunswick aquifer follows a brief discussion of the Passaic Flood Tunnel geotechnical evaluation summarized in appendix 2F.

An extensive borehole geophysical data set was generated for the Brunswick aquifer by the IT Corporation in 1995 as part of the Passaic Flood Tunnel geotechnical evaluation in the Passaic River valley. The results are on file at the NJGS office. Digital records of the borehole geophysical logs recompiled by the NJGS in 2003 are included in appendix 2F. These data are presented as a set of 4 geophysical log summaries based on data for 10 borings drilled near a set of 4 work shafts (appendix 2F1). The borings penetrated fine- to coarse-grained sedimentary units of the Brunswick aquifer in the northeastern part of the basin, and Lower Jurassic shale and siltstone in the Watchung Mt. area (fig. F3). The logs are the only records of geophysical responses from the Lower Jurassic sedimentary rocks in this study. The geophysical logs measure both formation and fluid properties and include some density logs and straddle-packer flow tests, in addition to detailed description of the drill cuttings. Gamma-ray logs and electrical-resistivity logs from nearby wells record lateral and vertical changes in the bedded mudstone, siltstone, and sandstone strata (appendix 2F2 to 2F6). Coaxial plots of logs of adjacent wells were made to compare changes in stratigraphy over short distances. The geophysical heterogeneity reflects the cumulative set of lacustrine and alluvial sedimentary processes resulting in the deposition of shallow-lake clay, silt and sand and massive mudstone on semi-arid mud flats. Descriptions of mineralized, vuggy mudstone and siltstone are assumed to mark gypsum paleosols. Records for workshaft 2B (appendix 2F3) show that deep parts of the aquifer below 320 ft have numerous horizontal gypsum veins and are poorly permeable, with transmissivity <1 gpd/ft, whereas vuggy beds above this depth are highly permeable, with transmissivity of ~30,000 gpd/ft.

Basalt units in the Watchung zone

Two studies were made of the Orange Mt. basalt in the Watchung zone of the Brunswick aquifer. One was on irrigation and monitoring wells at the Essex County Country Club (appendix 1E) where one well penetrated the base of the Orange Mt. basalt and finished about 150 ft in the uppermost Passaic Formation. The Orange Mt. basalt is the oldest, lowermost unit of the three in the Watchung Mountain area (fig. F3) and lies just atop the Triassic-Jurassic contact (fig. F2). The other study was on a domestic well in Somerset County (appendix entry 1F) that also penetrated the base of the Orange Mt basalt and 28 ft of the Passaic Fm. Although both studies involved wells that were finished in the uppermost Passaic Formation, the Essex study involved Brunswick sandstone whereas the Somerset study involved mudstone in the middle red zone (fig. F3). Sedimentary cross beds and cut-and-fill fluvial structures occur in fine-grained sandstone directly below the contact to the east (appendix 1E8) whereas massive mudstone underlies the contact farther west (appendix 1F4). At the latter, half-inch-sized ovoid accumulations of secondary minerals show hydrothermal alteration rinds that pock the shale. This contact is nonuniform in the basin and reflects both high-energy (sandstone) and low-energy (mudstone) sedimentary environments of deposition.

Analysis of WBFs of basalt shows that about half consist of type 1 fractures (table F5) between basalt layers of differing compositions and thicknesses. About one-third of the remainder are type 2 features, and type 3 features the least numerous at 14 percent. Cross flows measured with the HPFM reached more than 5 gpm in one 8-in-diameter supply well in the Essex study (appendix 1E3) but otherwise, measured flows were less

than 1 gpm. Gamma ray emissions from basalt are low in comparison to those from sedimentary units (table F4).

The geophysical results also show varied hydrogeology, reflecting stratigraphic heterogeneity and secondary structural controls. The Essex study (appendix 1E) showed that type 1 features were most abundant, whereas the Somerset study (appendix 1F) disclosed that type 2 WBFs can be locally dominant. In both locations, layering in basalt varies in thickness from laminated to thick-bedded, with textual and color changes. Measurable cross flows were found associated with both type 1 and 2 features (appendix 1E3 and 1E5) but flow rates in Well 11 for the Somerset study were considerably higher in the Passaic Fm than in the overlying basalt (appendix 1F2). This shows that basalt locally confines underlying sedimentary beds. Basalt has a poor aquifer ranking (Herman and others, 1998).

The local hydrogeological framework in basalt also depends on the proximity to local faulting and associated dense fracturing as seen elsewhere in the basin (Herman, 1997). Away from fault zones, bedding control of flow is strong, but within fault zones, fracture control is dominant. The N15^{o} to N30^{o}E strike of fracturing is the intermediate phase of extension fracturing in the basin (S2) and is the most common orientation of extension fractures in basalt and diabase in New Jersey; it is also a dominant regional trend (Herman, 2005).

Conglomerate, sandstone, siltstone, mudstone and shale

Coarse-grained units in the Brunswick aquifer occur in the conglomerate, conglomerate-and-sandstone, and sandstone zones mapped in the northwest and northeast margins of the basin (figs F1 and F3). About half (48 percent) of the WBFs in coarse-grained red beds are type 1 planes (table F5) resulting from mechanical parting along the interface between beds of differing thicknesses and grain sizes (appendix 2A2, 2A3, 2B2, 2B3, 2C2, 2C3, 2D3, 2D4, 2D5, 2E5, and 2E6). The remainder is about equally distributed among types 2 and 3 WBFs (table F5). Brunswick coarse-grained units have the highest proportion of type 1 and 3 WBFs of any sedimentary aquifer in the basin (table F5). Borehole cross flows in these units were measured in two projects (appendix 2D and 2E) and both had measured flows of less than 1 gpm (table F4). The vertical spacing of WBZs in sandstone ranged from about 2 ft to 50 ft (appendix 2D2, 2F2, 2E2, 2E3 and 2E4). The highest transmissivity of sandstone red beds was 700 gpd/ft from a straddle-packer test of a 20-ft section near workshaft 2C of the Passaic Flood Tunnel Geotechnical investigation (appendix 2F5).

Fine-grained units in the Brunswick aquifer include siltstone, mudstone and shale. They vary in the character, distribution, and continuity of WBFs in the red and gray beds. About 60 percent of all WBFs in siltstone, mudstone and shale are type 2 steeply-dipping extension fractures (table F5). Type 2 features are most common in all fine-grained units including those in the lower and middle zones (table F5). However, the middle red zone has the highest percentage (45) of type 1 WBFs, followed by the lower red zone (32 percent). Type 1 paleosol dissolution zones appear to locally transmit the most water of any features in sedimentary units: cross flows commonly reach 1 to 3 gpm (table F4; entries 3C, 3D and 3M). They first appear in thick red beds in the upper part of the lower red zone (fig. F12 and appendix 3G5 and 3G7) and are most abundant in the middle red zone (appendix 3A3, 3B3, 3C5, 3D4, 3D12, 3F4, 3F5, 3G5, 3G7, and 3G) where an overall upward increase in dissolution-enhanced WBZs coincides with the increase in root-disrupted, massive red mudstone in the Passaic Formation reported by Smoot and Olsen (1985). Layered dissolution zones in the middle red zone also coincide with elevated levels of sulfate in groundwater as noted by Michalski and Britton (1997) and signal a bulk chemistry change from a silicate and sodium-dominant depositional environment for the Lockatong Formation and the lowermost part of the Passaic Formation to a more calcium carbonate and sulfate environment for the playa lake deposits in the upper part of the Passaic Formation and middle red zone of the Brunswick aquifer (Smoot and Olsen, 1994; Herman, 2001b). A regional analysis of the quality of ambient groundwater from wells in the Passaic Formation part of the Brunswick aquifer showed that calcium-bicarbonate and calcium-sulfate waters dominate (Serfes, 1994).

Type 2 WBFs are most common in gray zones containing abundant gray mudstone and gray and black shale (table F5; BLG, BMG and gray units). Gray beds range from less than a few feet to about 50 ft in thickness. They locally include multiple, thin to thick red beds that transmit water principally through steeply-dipping extension fractures (appendix 3M18, 3N5, 3N8, 3N13, 3O2, 3P2, 3P4, and 3Q2). The effects of groundwater flow in these fractures are clearly seen in the Brunswick gray zones (table F5). Borehole geophysical data repeatedly show marked contrasts in fluid temperatures and electrical conductance/resistance between adjacent, thick red beds and thin gray and black beds (appendix 3K3, 3K6, 3K7, 3N5 and 3N13). This suggests that flow cells develop within thick sequences of red mudstone and siltstone separated by gray-bed sequences that act as regional confining layers. This interpretation is supported by outcrops where copper minerals locally occur in the base of some gray beds overlying thick red-bed sequences (Monteverde and others, 2003). Oxygenated groundwater circulating in

red beds may carry dissolved metals that precipitate out where they come into contact with overlying, confining gray beds in a reducing geochemical environment due to the elevated organic carbon content at or near the red-gray redox boundary. As seen in borehole imagery, permeable extension fractures within the red beds seldom penetrate adjacent gray and black layers which develop their own sets of fractures (appendix 3N6). Stratigraphic heterogeneity likely plays an important role in concentrating other metals, radionuclides, and elements such as arsenic in specific stratigraphic horizons.

Groundwater electrical resistivity/conductivity profiles of specific stratigraphic sequences also vary between wells within short distances (appendix 3N8 and 4B8) with anomalous log traces corresponding to where groundwater enters or exits boreholes through WBFs and WBZs. In some places, type 2 WBFs develop in specific, correlative stratigraphic horizons (appendix 3D13, 3D14 and 3N8). However, type 1 WBFs in gray beds typically develop along or near contacts with red beds (appendix 3N5, 3N8, 3O2 and 3P4) that appear to transmit groundwater over great distances through type 1 features. But in general, groundwater leaks through thick gray-bed confining units in the Brunswick gray zones that are largely disconnected from major strata-parallel WBZs. This may result from insoluble silica based matrix cements in deep lake beds (see Chapter B) and the high degree of compaction and hardening of the formation resulting from deep burial (see Chapter C). This is important because thick confining units separate a small number of type 1 WBFs that owe their permeability to fracture porosity along the interface of fracture layering. Consequently, vertical flux in fine-grained units containing many gray beds is weak and groundwater recharge is limited. However, certain beds are more prone to develop transmissive type 2 fractures than others (appendix 3D14).

The most extensive hydrogeologic studies involving BTV technology in New Jersey spanned 14 wells in three adjacent projects near Hopewell and Pennington in Mercer County. The projects cover the Bristol Meyers-Squibb Research Campus, the Honey Brook Organics Farm, and the Stonybrook-Millstone Watershed Association Preserve (appendix 3N1). The combined wells extend over the zsection between the lower red and gray zones (fig. F2) resulting in a map span of about 1 mile (appendix 3N1). The profile interpretation includes a series of marker beds in the OPTV data records that help establish area-wide stratigraphic correlation. The distribution and names of the geological formations and members mapped in these projects are based on Olsen and others (1996). Figure F23 illustrates how strike and dip in red beds in the lower red zone of the Brunswick aquifer vary in 3D at the Stony-brook-Millstone site and exhibit layering heterogeneity that limits hydraulic conductivity along the strike of bedding. This group of wells is also useful in demonstrating the depth of weathering in fine-grained, fractured sedimentary bedrock based on fluid-temperature differences in profiles of many close wells (fig. F24). These wells were drilled when regulations required only 20 ft of casing rather than the current requirement of 50 ft, and therefore enable measurements to be made of hydraulic responses in the weathered bedrock that are ordinarily unattainable with deeper casings. Fluid-temperature differences plotted in the vertical direction show many fluctuations of greater intensity in the upper 60 ft than at deeper sections. This indicates an enhanced connection between surface and groundwater in this upper, weathered section. This depth of weathering is supported by large fluid-temperature anomalies measured just below casing under pumping conditions in wells having only 50 ft of casing (fig. F25). In some locations, upward flows are lost into WBZs located directly below casing in the 50-to-60-ft interval (appendix 3D5, 3D9).

Lockatong aquifer

The Lockatong aquifer was studied in Hunterdon and Mercer Counties (figs. F2, F3 and appendix 3Q, 4A, 4B and 4C). Appendix entries 3Q and 4C involve Wells 108 and 116 that penetrated the upper and lower stratigraphic contacts with the Passaic and Stockton Formations. The other two projects involved two and five observation and test wells respectively (appendix 4A and 4B). More than two-thirds of all WBFs in the Lockatong are tectonic fractures (table F5; 69 percent). The remaining third is divided between type 1 (19 percent) and type 3 (14 percent). The Lockatong is similar to the lower gray zone of the Brunswick in most respects but with overall thicker gray beds and thinner red beds. BTV studies show that small-scale normal faulting is common in the Lockatong Formation; small faults strike N20^{o} to 50^{o}E in two separate fault blocks (appendix 4A4, 4A6, 4B4, and 4B6). The geophysical logs generally show that WBFs are scarcer and more widely spaced vertically than they are in the Brunswick aquifer. Fluid temperature and electrical logs typically display wavy gradients that gradually stabilize at depth into more uniform values with narrowly-focused sections having pronounced log-value shifts (appendix 4A2, 4A5, 4B2, 4B5 and 4C2) due to the small number of WBFs intersecting a well. This is consistent with the Lockatong aquifer having the lowest aquifer ranking of any sedimentary unit in the basin (Herman and others, 1998). Cross flows were below the minimum threshold of detection (~0.5 ft/min) with the NJGS HPFM (Herman, 2006).

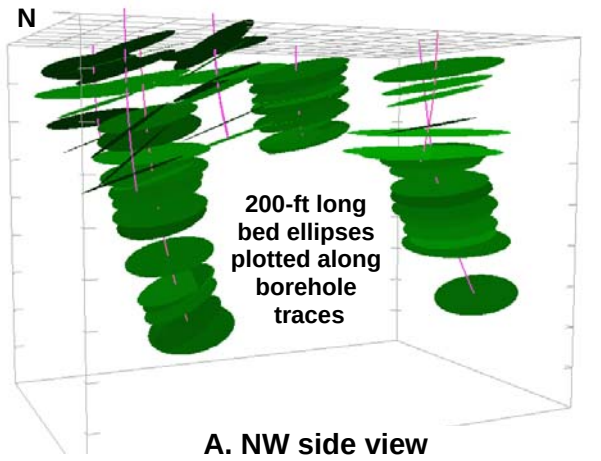

A. NW side view

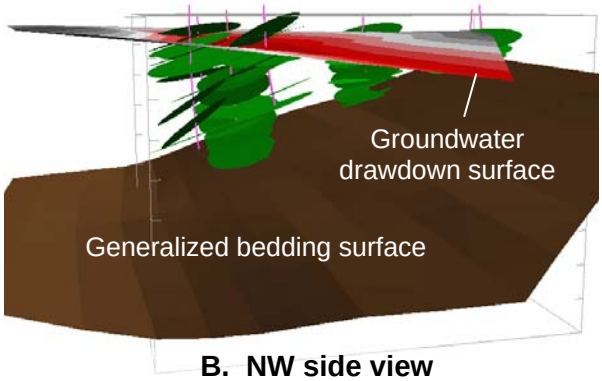

B. NW side view

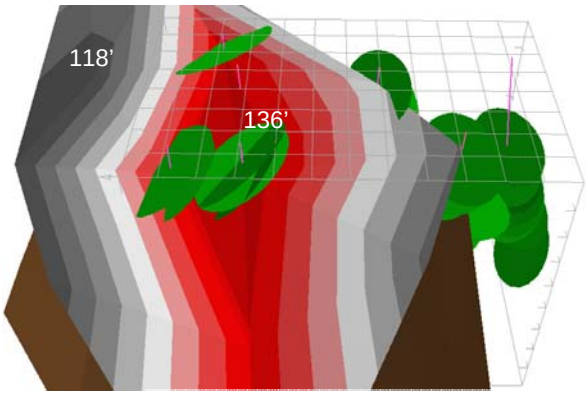

C. NW top-side view

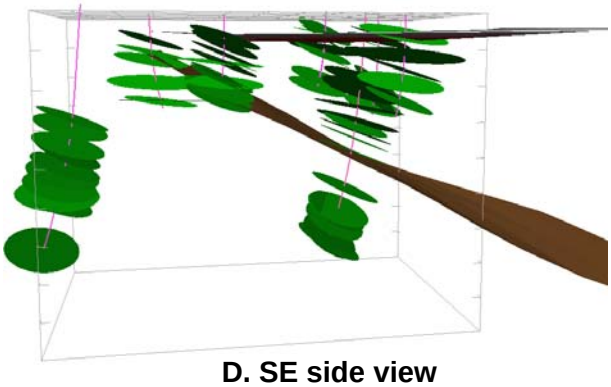

D. SE side view

Stockton aquifer

The Stockton Formation is the basal stratigraphic unit in the basin. BTV data for the Stockton aquifer are spotty and are mostly from north of the Trenton Prong between Trenton and Princeton, in Mercer County (fig. F3). The most extensive data stem from two framework studies using golf course irrigation wells and observation wells (appendix 4E and 4F). Other BTV analyses were made on third-party data from groundwater pollution investigations in Mercer County (appendix 4D and 4G). The upper contact with the overlying Lockatong aquifer was covered by an OPTV survey in Hunterdon County (appendix 4C). Analyses of WBFs in the Stockton show that just more than half are tectonic extension fractures and the remainder are about equally divided between types 1 (27 percent) and 3 (21 percent, table F5). HPFM data show that all types of WBFs may be highly transmissive (appendix 4E4, 4F3, and 4F5) and cross flows commonly exceed 3 gpm (table F4), and one 8-in-diameter well yielded about 15 gpm (appendix 4F5).

Geophysical logs of the Stockton aquifer generally show fluctuating hydraulic responses that commonly extend about 100 ft bls (appendix 4C2, 4E2, 4E4, 4F3, 4F5 and 4F7). Such responses are attributable to many WBFs intersecting the boreholes in the near-surface, weathered-bedrock section. This results from the removal of secondary authigenic minerals from fracture interstices, and the local weathering of bedrock along fracture surfaces to clay and silt. Fluid temperature and electrical logs typically display wavy gradients that gradually stabilize at depths below about 100 ft into more uniform values, with narrowly-focused sections having pronounced log-value shifts corresponding to WBFs and WBZs, as seen in other aquifers. High fluid temperatures above 100 ft depth in

Figure F23 (left). 3D-GIS perspectives of sedimentary bedding interpreted from OPTV records of part of the Stony Brook-Millstone Research well field (Appendix A entry 1C2). Cross-stratification of red beds is illustrated by bedding planes plotted as 3D ellipses along borehole traces, represented as gently-curving subvertical lines. Ellipses were generated using 200-ft major axes oriented along bedding strike and a 2:1 strike-to- dip aspect ratio. Grid tics and well-field grid cells are 50 ft. Top three views look southeast. The upper, shaded surface in figures B and C is a groundwater equipotential surface after a nine-day aquifer test conducted on the central well in the well field (Carlton and others, 1999). The lower surface is a generalized bedding surface representing average bedding orientations throughout the well field. Cross-stratification helps account for an irregular drawdown surface that is generally elongate along bedding strike but limited in its extent because of stratigraphic heterogeneity.

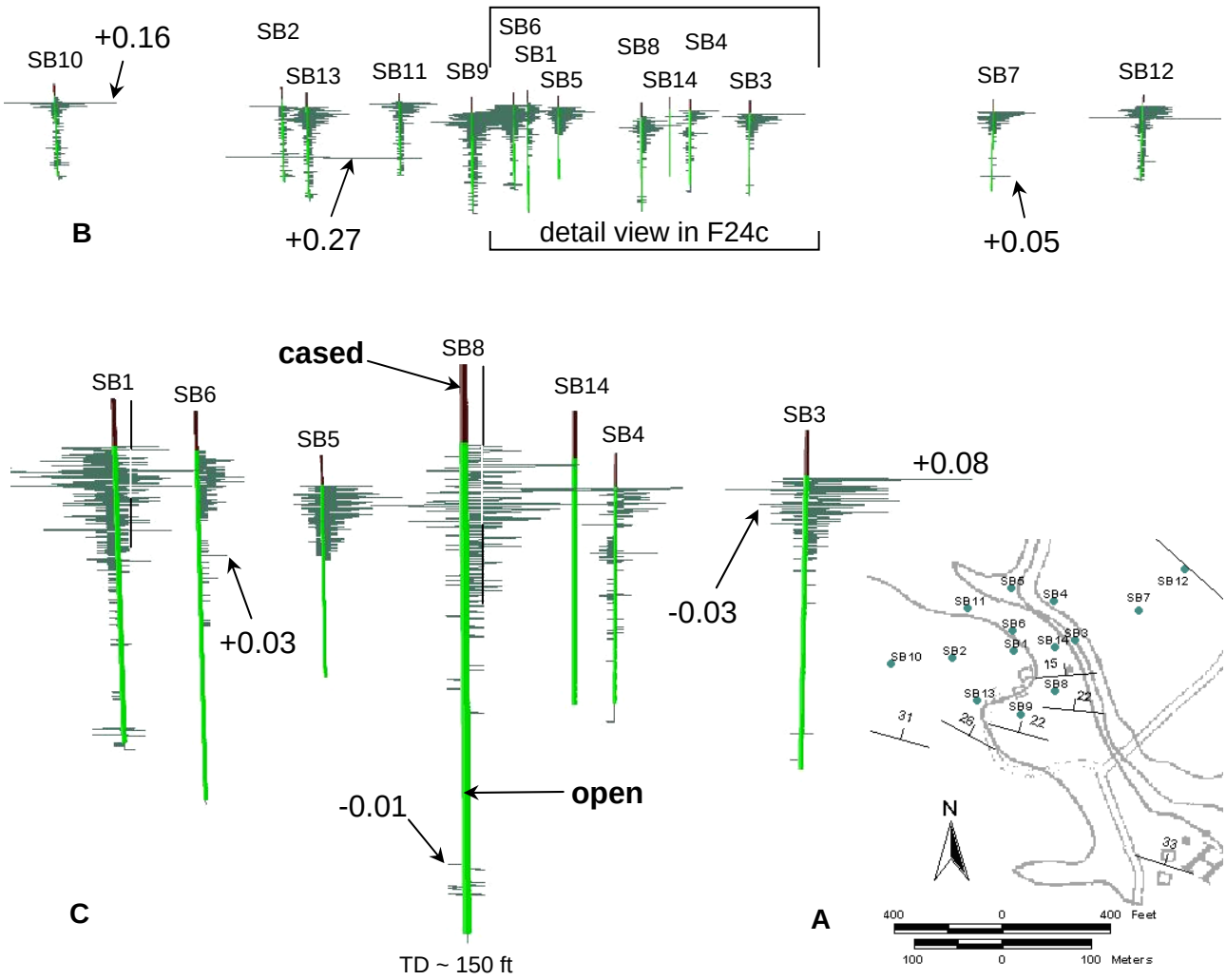

Figure F24. 3D-GIS perspective diagrams (looking northwest) showing fluid-temperature-difference profiles in the Stony Brook-Millstone Watershed Association preserve well field (Appendix 3M). A. Part of the US Geological Survey Hopewell, NJ 7-1/2' topographic map shows well locations and bedrock strike and dip. B. 3D perspective for the entire well field. The top of casing approximates land surface. Each well is about 150 ft deep with about 20 ft of casing. Horizontal spikes are fluid-temperature differences (^{o}F) plotted below casing. Temperature differences were calculated by subtracting successive readings taken at each 0.1-ft-depth interval. Line lengths are proportional to temperature differences that range from -0.45^{o} to +0.27^{o}. C. Detailed view of the part of the well field shown within bracketed area of B. Vertical black and white bar scales show 20-ft-depth increments for SB1 and SB8. The vertical distribution of temperature changes is used as a measure of entry and exit points of groundwater into and out of the open borehole and helps constrain the depth of the weathered zone in bedrock aquifers. Fluid-temperature differences decrease in frequency and magnitude downward to about 60 ft bls, near the base of the weathered zone. Intermittent temperature anomalies below this depth correspond to semiconfined-flow sections in deep bedrock. Well data and fluid-temperature logs provided courtesy of Glen Carleton, U.S. Geological Survey.

wells logged during warm summer months (appendix 4E4, 4F3 to 4F7) also suggest that the Stockton locally has a direct hydraulic connection between surface water and groundwater to that depth. The Stockton therefore has a deep water-table aquifer partly owing to its many fractured beds of deeply-weathered arkosic sandstone. The fractured layers provide highly permeable pathways for groundwater flow and, combined with secondary fractures, result in hydraulic gradients strongly reflecting topographic slope (appendix 4D1).

Outcrops of the Stockton in the southern Piedmont province near Trenton are scarce. Fractures are best characterized by use of BTV equipment. The strike of fractures in the Stockton is generally parallel and normal to bed strike (appendix 4D1, 4E1 and 4G1). Other, localized fracture sets reflect secondary structural strains near faults and folds. For example, fracture

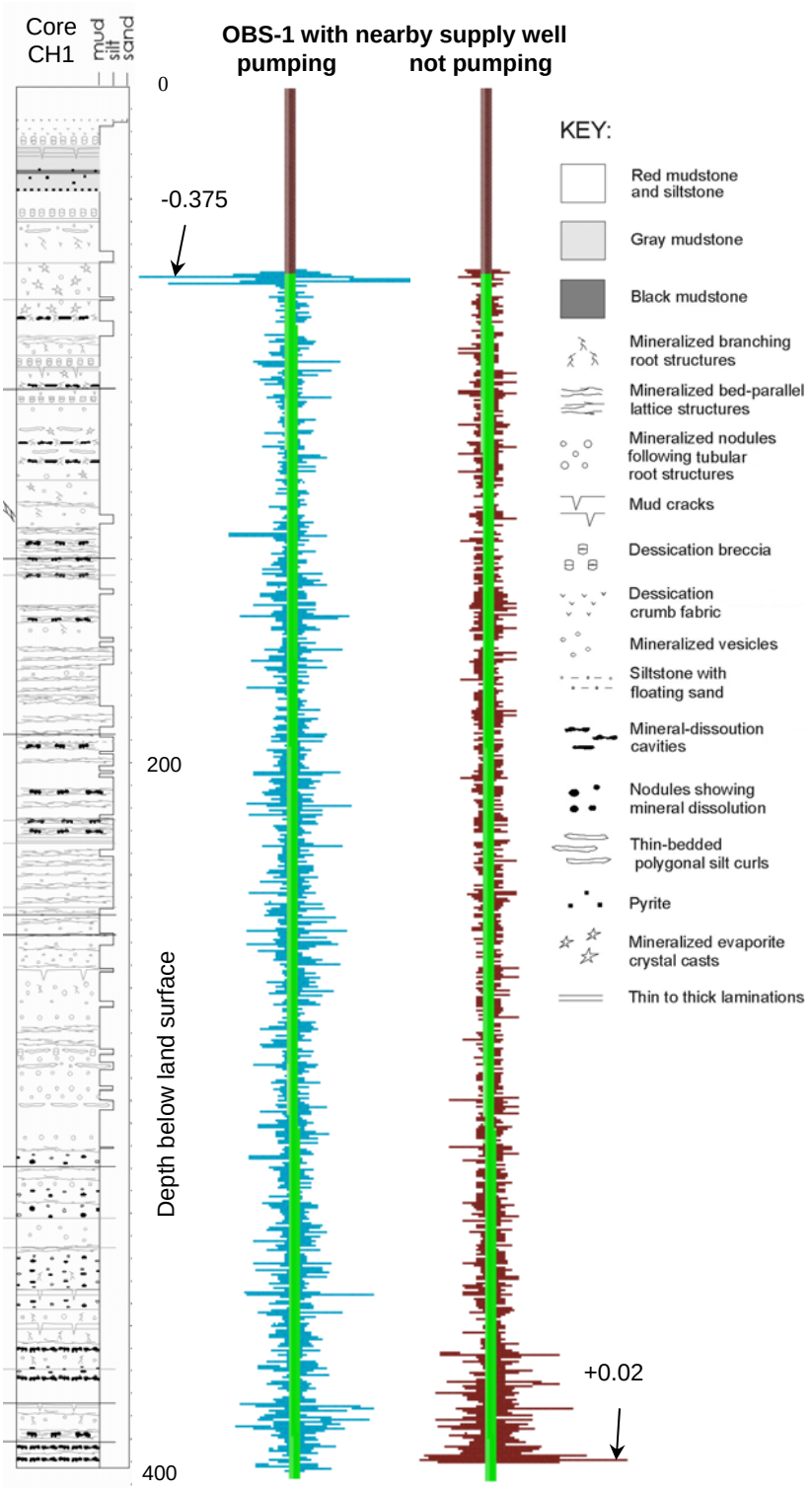

Figure F25. Diagrams comparing fluid-temperature differences (^{o}F) in Hopewell Borough well OBS-1 (Well 69, Appendix 3G) for pumping (left) and non-pumping (right) conditions. Diagrams are plotted next to stratigraphic diagram of nearby core (left). Temperature differences under nonpumping conditions are an order of magnitude lower than those for pumping conditions. Note the correlation between temperature anomalies and dissolution zones in the core and the pronounced temperature differences directly below casing under pumping conditions.

strikes for the Princeton study (fig. F26 and appendix 4F1) occur in all orientations but with strike maximums that agree with other, nearby but less fractured rocks. Concealed faults in this area are interpreted using surface-water drainage patterns, air-photo lineament analyses (fig. F26), and geophysical aeromagnetic coverage (Ghatge, 2004; Herman 2005). The Piedmont region was probably faulted and fractured during many incremental tectonic stages with faults and fracture zones striking in many directions (fig. F26).

BTV data of the Stockton show that cross bedding is common and bedding dip directions range over 180^{o} (appendix 4D1). Very thick sequences of alternating red and white sandstone are demonstrably continuous in the subsurface over hundreds of feet and include some stratigraphic pinch-outs interpreted by use of OPTV records and stratigraphic marker horizons for studies having two or more wells with overlapping stratigraphic coverage (appendix 4E6 and 4F2). These pinch-outs occur within larger belts of similar strata and do not appear to be as sharp in reducing horizontal conductivity in the Stockton aquifer as in the gypsic-paleosol unconformities in the Brunswick aquifer.

Open, permeable, steeply-dipping extension fractures penetrated by boreholes drilled into the Stockton reach maximum vertical dimensions of about 5 to 6 ft (appendix 4E3-right, 4F6-left and 4F8-left). Many type 1 WBFs in the Stockton occur at the contact between sandstone beds of different colors and compositions (appendix 4C2, 4C4-right, 4C3, 4E2 and 4F5). Many type 2 features also occur close to stratigraphic contacts (appendix 4C3 4C4-left, 4E2, 4E3, 4E5, 4E6, 4F4 and 4F5). The vertical spacing of water-bearing units is highly varied and ranges from inches to tens of feet of separation. The Stockton is typically able to supply hundreds of gpm of water to high-capacity wells and therefore has an intermediate-aquifer ranking in New Jersey (Herman and others 1998)

Relict hydrocarbon (bitumen)

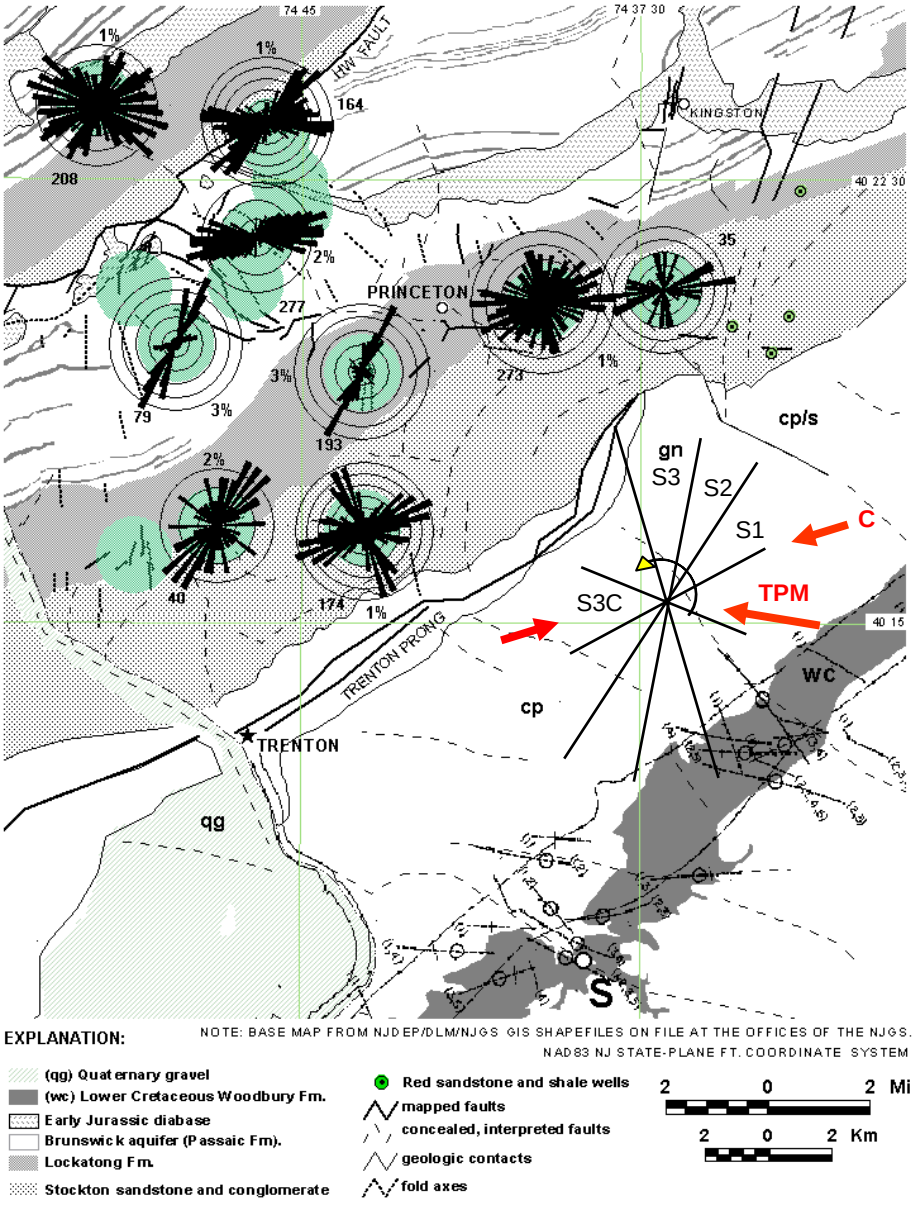

Figure F26. Bedrock geology of the Trenton area (modified from Drake and others, 1996; Herman 2005). Histograms show strike of nonbedding-plane fractures measured in OPTV records for selected projects detailed in figure F3. Histogram numbers indicate the number of measurements at each site; percentages indicate ring increments. Structural lineament analysis of the Woodbury Clay Formation (**wc**) by unpublished source on file at the NJGS. **S** – Site where overturned and contorted clay is reported in NJGS permanent notes. Histograms show different fracture strikes throughout the region. Diagram at center right summarizes the proposed sequence of extension-fracture development in the basin (S1 to S3, then SC3) in comparison to present-day, horizontal crustal compression determined from earthquake analyses (**C**; Goldberg and others, 2003) and current tectonic-plate motion (**TPM**) based on 12 years of GPS data NASA,2009). Abbreviations: qg – quaternary gravel, cp – coastal plain, cp/s coastal plain overlying Stockton Formation, gn – gneiss.

has been reported in authigenic mineral fill of tectonic fractures in the basin (Parnell and Monson, 1995; Herman, 2005, and Chapter C). OPTV images of bitumen clots and stringers in Stockton beds (appendix 4E3-left, 4E7-left, 4F6-lower right, 4F8-right, 4F9-right and 4F10-left) and in fractures (appendix 4F8-left) were collected in the area north of Trenton (fig. F3). The sedimentary matrix near bitumen accumulations is locally altered and stained by mineral-enriched fluids (appendix 4F5-right, 4F6-left and 4E7-left).

Discussion

Bedrock aquifers in the Newark basin, where unconsolidated overburden is generally thin (< 20 ft) include shallow, intermediate, and deep sections having variable hydraulic properties (fig. F6). Shallow overburden includes unconsolidated alluvium, colluvium, artificial fill, and regolith. Regolith in most sedimentary formations includes red, brown, orange, yellow, and gray silty clay to clayey silt residuum containing angular bedrock fragments above bedrock (fig. F16). Weathered conglomerate includes loose cobbles and gravel at the surface. The shallow section extends to depths of ~3 to 15 ft and commonly has a perched, transient water table near its base that discharges to streams and other surface-water bodies (fig. F6). Ackermann (1997) demonstrated a strong correlation between surface-water drainage patterns and the strike of fractures in bedrock overlain by thin cover. This relationship is further demonstrated by comparing

fracture strikes determined form BTV analysis to topographic trends (appendix 1A1, 1D1, 1E1, 1F1, 2E1, 3A1, 3D1 among others).

The intermediate or 'weathered' bedrock section is subject to prolonged episodes of weathering during wide fluctuations of climate, including permafrost during past glacial epochs. Conductive features in weathered bedrock included 1) gently dipping fractures resulting from erosion and pressure release (fig. F13c) in addition to those found in deeper bedrock including, 2) bedding fractures focused near stratigraphic contacts, 3) strata containing porous gypsum paleosols, and 4) fractured layers with secondary porosity stemming from mineral dissolution from both the rock matrix and fracture interstices. Abundant, connected pathways for groundwater flow in the weathered section commonly result in water-table or unconfined conditions and natural hydraulic gradients aligned down topographic slope (fig. F21 and appendix 2D1). Groundwater flow in the shallow bedrock is therefore more uniformly distributed than it is under the anisotropic conditions in deep bedrock that favor horizontal flow directions along stratigraphic strike (Vecchioli and others, 1969; Michalski and Britton, 1997; Carlton and others, 1999). Weathered bedrock commonly reaches depths of 60 to 100 ft in the Brunswick and Stockton aquifers respectively, based on groundwater temperature and electrical logs (see previous discussion for the Stockton aquifer. Also, Morin and others (1997 and 2000) reported high yields at depths of about 60 ft in basin wells. Water-temperature logs of the other aquifers, including the Lockatong, diabase, and basalt zones in the Brunswick aquifer, show no evidence of having as deep a weathered zone as that in the Stockton and therefore are assumed to have more shallow weathered sections like those in the Brunswick. Most wells in these other aquifers in this study have a minimum of 50 ft of casing that makes hydrogeologic evaluation of the weathered section difficult.

The hydrologic connection between open boreholes and weathered bedrock is an important consideration in addressing near-surface groundwater pollution because the depth of weathering may exceed the depths to which water wells are commonly cased. The weathered section in the Brunswick red beds and the Stockton Formation is shown here to range from about 60 to100 ft bls. As a result, about 10 to 50 ft of open borehole may be connected to the water-table aquifer and a likelihood of a strong hydraulic connection to near-surface waters, especially during pumping. This has been verified by large fluid-temperature and electrical log responses recorded directly below casing during pumping (fig. F25). Based on these findings, water-supply wells should be cased to a depth of at least 60 ft in all aquifers, and to about 100 ft in the Stockton aquifer.

The infiltration of water from precipitation through shallow fractures may be impeded in some places to less than it is in deep bedrock by silt and clay residuum of weathered rock in and along fractures (fig. F27 and Kasabach, 1966; Lewis-Brown and dePaul, 2000). However, vertical hydraulic-conductivity values of the weathered section exceed those in the deep zone by two orders of magnitude in nearby areas (Lewis-Brown and Jacobsen, 1995). This apparent anomaly points to the need for more hydrogeologic research on weathered bedrock to clarify aspects of groundwater recharge and contaminant transport in the shallow subsurface.

Groundwater exhibits anisotropic, confined-flow characteristics in deep bedrock mostly because gently-dipping strata exert primary control on the hydrogeologic framework. Groundwater is principally stored in myriad fractures but is transmitted long distances by bed partings and highly permeable layers between confining beds. Olsen and others (1996) demonstrated the continuity of lacustrine beds deposited in deep-water environments throughout the basin so that dark shale extended to distances of tens of miles. In comparison, the vertical fracture is limited to the vertical thickness of the fractured layer that is at least an order of magnitude smaller than the bedding plane (fig. F15). The maximum vertical extent of individual fractures measured in small-diameter boreholes for this study was about 6 ft (appendix 3N7, 3O2). This is an important aspect of borehole hydrogeology because the geometric relation between steeply-dipping fractures and a steeply-inclined borehole limits the thickness of the fractured layer (fig. F28). It also demonstrates that the 3D extent and hydraulic connection between steeply-dipping fractures in a fractured layer is difficult to determine from borehole BTV studies alone.

Reported transmissivity (T) values of deep bedrock vary significantly, commonly as much as three orders of magnitude among the different aquifers and discreet sections of a single aquifer (appendix 2F3, 2F4, 2F5, 2F6 and Morin and others, 1997; Lewis-Brown and dePaul, 2000; Lewis-Brown and others, 2004; Michalski, 2001; and Michalski, 2009). This varied character results from geological heterogeneity and from the different methods used for calculating T. For example, T values of an aquifer commonly are calculated from pumping tests based on the entire saturated interval penetrated by a well. It is important to note that these aquifer characteristics are only average values of a composite flow system consisting of many thin aquifers separated by some thick confining layers. Detailed hydrogeological studies using methods for determining intervals flows, such as HPFM studies and straddle packer tests produce more accurate determinations of aquifer characteristics for discrete WBZs. Parameter values of individual parts of the section should be determined and used for

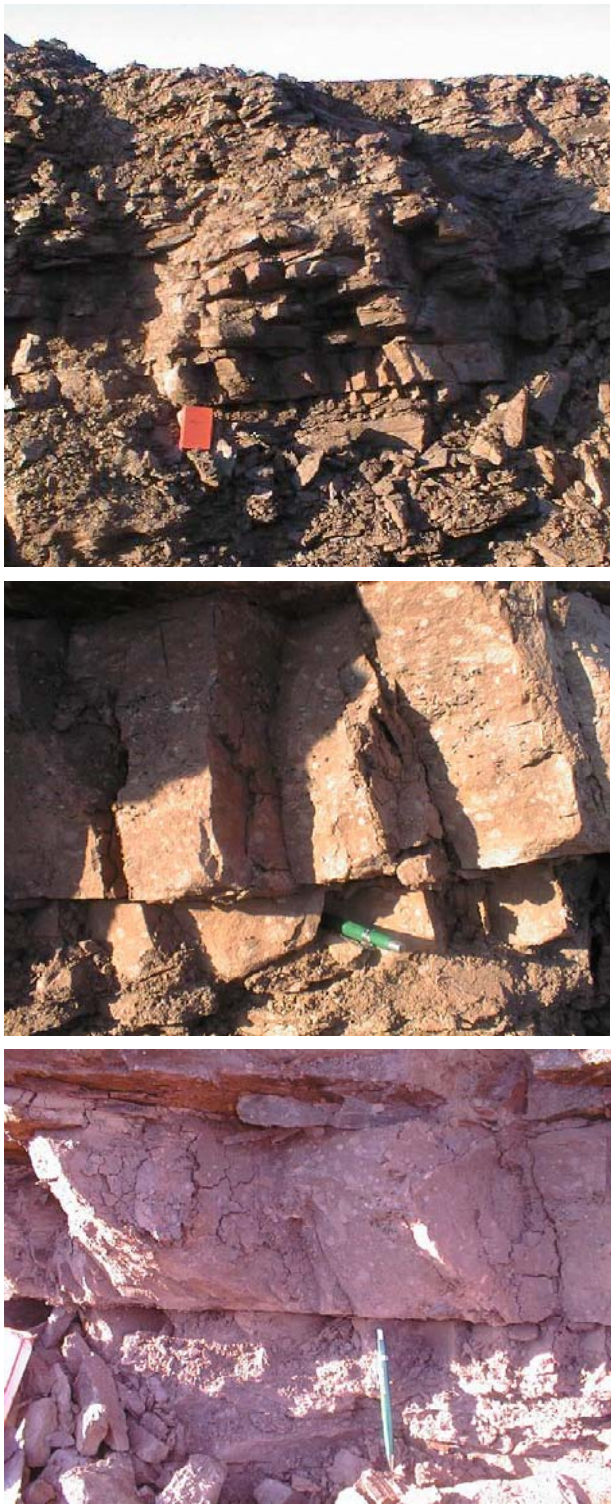

Figure F27. Bedrock excavations in the Passaic Formation during construction of the Heron Glen Golf Course, Hunterdon County (appendix 3K). Shortly after excavation, polygonal mudcracks formed along fracture walls in desiccated silt and clay residuum of siltstone and mudstone. This shows that silt and clay infilling shallow fractures originate directly from degradation and weathering of bedrock.

characterizing the distribution, fate, and transport of groundwater contaminants when possible. Average values based on large intervals of open borehole may result in underestimating T and therefore both the distribution and velocity of contaminants in highly transmissive units.

A benefit of recorded OPTV records is that they may help to constrain the vertical extent of the section for which aquifer parameters are required. Based on OPTV records for this study, the maximum vertical extent of any specific WBF intersected by a well is about 10 ft regardless of whether it is classified as large-aspect extension fractures or a thick gypsum-paleosol bed. This needs to be taken into consideration when assembling straddle packers for conducting environmentally sensitive hydrogeologic studies, because straddle-packer tests commonly employ assemblies having 20-ft of separation, possibly leading to underestimation of T values by a factor of at least two.

Cross flows in water wells in the Newark basin stem mostly from topographic irregularities at the land surface resulting from differential erosion of gently-dipping, layered strata. Ambient flow volumes measured in small-diameter water wells in the basin range from no measurable flow (NMF) to about 15 gpm in the Stockton aquifer, 8 gpm in the Brunswick aquifer, 5 gpm in basalt, and 1 gpm in the Lockatong Fm. and diabase (table F4). The 8 gpm measured in the Brunswick aquifer was from a 6-inch-diameter observation well located near two irrigation wells that were pumping at a combined rate of about 500 gpm (appendix 3K1). The 8 gpm value is therefore probably more than it would be under nonpumping conditions based on other studies where cross-flow rates for the same section were 2 to 6 times greater under pumping conditions in comparison to those for nonpumping conditions (appendix 3D5 and 3G6). Most of the gray beds in the Brunswick and Lockatong aquifers yield meager flows too low to detect using the NJGS HPFM, whereas the highest cross flows are from red beds in the Brunswick aquifer, particularly from the middle red zone, where gypsum paleosol is abundant. It is notable that the respective flows cited for each aquifer resemble the aquifer rankings in the basin (Herman and others, 1998); the Stockton (C-ranking) and Brunswick (C) aquifers produce the highest flows and high-capacity yields, followed in decreasing order by the Lockatong (D) and basalt (D), then diabase (E).

Hydrogeological framework characterization of red beds in the Brunswick formation needs to take into account the distribution of gypsum-soil beds with unconformity surfaces and dissolution-enhanced WBZs. These features are common in massive red mudstone and are important because their occurrence and geometry can diminish or enhance the ability of an aquifer to supply groundwater. Angular unconformities

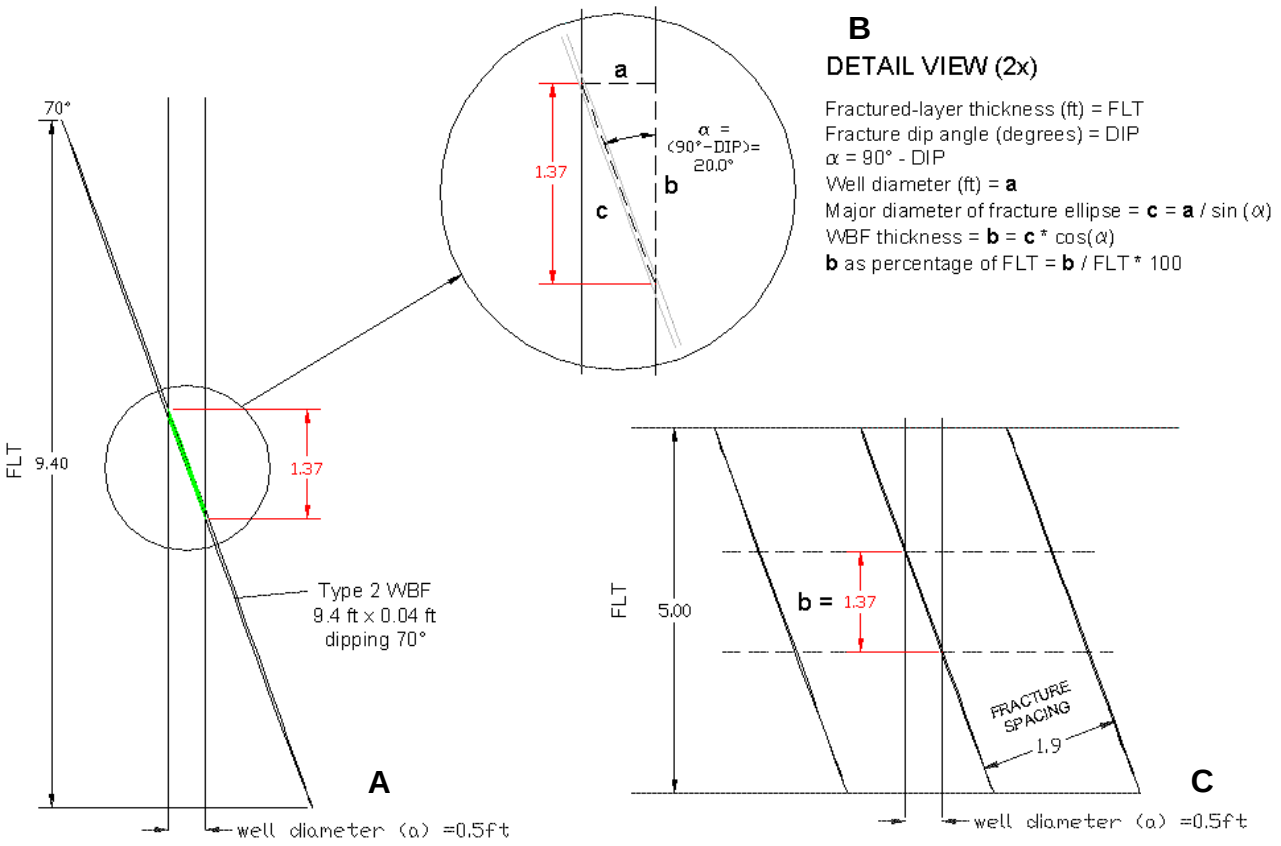

Figure 28. Profile views of dipping type 2 WBFs in relation to the thickness of fractured layers and a vertical well. A. A 9.4 ft-thick fractured layer penetrated by a 6-inch diameter well bisects one steeply-dipping and permeable extension fracture with a maximum, 4 mm-wide interstice. In this example, the measured thickness of the WBF in the borehole is only ~15% (1.37/9.40) the actual thickness of the fractured, permeable layer. B. Details of the geometric relationships for the approximate vertical thickness of the WBF (b), the diameter of the borehole (a) and the partial length of the fracture ellipse (c). C. A second example of a type 2 WBF dipping 70° with only a 5.0 ft fractured-layer thickness and a fracture-spacing of about 2.0 ft; a typical value mapped in the basin for medium-to thick sedimentary beds. In this example, the vertical thickness of the WBF is about 27% that of the permeable layer. Flow rates and contaminant concentrations for partially-penetrated type 2 WBFs are therefore apparent values that represent conditions for the entire fractured layer when fracture interstices are open and hydraulically conductive throughout the layer. Measured flow rates and analyte concentrations for a partially-penetrated type 2 WBF, or an interval containing such a feature, must be used with caution because of differences between the apparent (b) and true (FLT) thicknesses of the permeable unit; measured flow and constituent concentrations associated with a dipping, type 2 feature reflect conditions over a much thicker interval than directly sampled by a well. Similarly, if the well fails to penetrate such a feature, the interval may be misinterpreted as being impermeable and unpolluted.

can locally truncate paths of groundwater recharge to deep aquifers (appendix 3F4) and thereby diminish well yields, whereas conductive dissolution zones locally form high-yielding WBZs over distances of thousands of feet (appendix 3M7, 3D14, 3F3 and 3F4). Dissolution enhancement of gypsum-soil beds and fractured layers can result in highly productive aquifers capable of conveying groundwater pollution over great distance in relatively short time periods.

More work is needed to evaluate aquifer characteristics in areas of dense tectonic fractures near large-scale faults. In outcrops, multiple sets of tightly spaced fractures exhibit iridescent-blue manganese minerals coating fracture surfaces. Clearly, groundwater flow is vigorous in tectonically active areas and fault zones may contain anomalous groundwater that deviates geochemically from the LMAS groundwater flow model, at least to the extent that fractures exert primary hydrogeological control. If so, the horizontal component of hydraulic conductivity may be preferentially aligned along the strike of the fault rather than bedding strike if bedding and faults strike do not coincide. Nevertheless, stratigraphic bedding is the dominant control on the storage and movement of groundwater in most of the basin and the primary consideration in determining the direction of groundwater flow below the

weathered-bedrock interval.

Acknowledgements

Many people helped find and gain access to the project sites used for this research. In this regard, I thank Matt Mulhall, Penelope Althoff, Vince Uhl, Greg Bakeman, Frank Source, Nick Sodano, Carole Chatelain, Jill Dunphy, Marc Romanell, Greg Giles, Jason Pierce, Bay Weber, Jim Kinsell, Pierre LaCombe, Glen Carleton, Tony Hauk, Rob Sheneman, Dave Misiolek, Charles Dey, Roger Stewart, Michael Gornnert, Robert Weiss, David Stout, and Ken Luperi. I acknowledge and thank all homeowners who provided access to their domestic water-supply wells. Steve Laney provided a valuable review of the early manuscript and appendixes. Paul Sanders and Kevin Schick of the NJDEP provided program coordination and administered research funds used to support this work. Below I acknowledge the efforts and contributions of fellow NJGS employees. Many enjoyable field days were spent pulling and replacing water pumps and packer strings, and logging wells with Steve Spayd, John Curran and Gregg Steidl, Brian McCann, and Mark French. Michael Serfes and Jim Boyle contributed valuable discussions and insights with regard to hydrogeologic relationships and analyses. Joe Rich and Walter Marzulli provided surface elevation surveys for some projects. I thank Don Monteverde, Hugh Houghton, Jim Mitchell, and Seth Fankhauser of the NJGS for their use of their structural data and bedrock maps. Dave Hall, Robert Canace, Dave Pasiczynk, and Karl Muessig supervised these efforts and provided program support. I give special recognition and thanks to Irving, 'Butch' Grossman, and Bill Graff for providing thorough and helpful reviews of this manuscript. Butch's review, in particular, resulted in a much more presentable and clear report.

References

Ackermann, R.V., 1997, Spatial distribution of rift-related fractures: field observations, experimental modeling, and influence on drainage networks: Rutgers University Ph.D. dissertation, New Brunswick, New Jersey, 136 p.

Brown, J.C., and dePaul, V.T., 2000, Groundwater flow and distribution of volatile organic compounds, Rutgers University Busch Campus and vicinity, Piscataway township, New Jersey: U.S. Geological Survey Water-Resources Investigations Report 99-4256, 72 p.

Burton, W.C., and Ratcliffe, N.M., 1985, Attitude, movement history, and structure of cataclastic rocks of the Flemington fault--Results of core drilling near Oldwick, New Jersey: U.S. Geological Survey Miscellaneous Field Studies Map MF-1781.

Carlton, G.B., Welty, C., and Buxton, H.T., 1999, Design and analysis of tracer tests to determine effective porosity and dispersivity in fractured sedimentary rocks, Newark Basin, New Jersey: U.S. Geological Survey Water-Resources Investigations Report 98-4126, 80 p.

de Boer, J.Z., and Clifford, A.E., 1988, Mesozoic tectogenesis: Development and deformation of 'Newark' rift zones in the Appalachians (with special emphasis on the Hartford basin, Connecticut), *in* Manspeizer, Warren, ed., Triassic-Jurassic Rifting, Continental Breakup, and the Origin of the Atlantic Ocean and Passive Margin: Elsevier, New York, New York, p. 275-306.

Dietz, R.S., 1961, Continent and ocean basin evolution by spreading of the sea floor: Nature, v. 190, p. 854-857

Drake, A.A., Jr., Volkert, R.A., Monteverde, D.H., Herman, G.C., Houghton, H.H., and Parker, R.A., 1996, Bedrock geologic map of northern New Jersey: U.S. Geological Survey Miscellaneous Investigation Series Map I-2540-A, scale 1:100,000; 2 sheets.

Dula, W.F., 1991, Geometric models of listric normal faults and rollover folds: American Association of Petroleum Geologists Bulletin, v. 75, no. 10, p. 1609-1625.

Ghatge, S.L., 2004, Magnetic anomalies of New Jersey, N.J. Geological Survey Digital Geodata Series DGS04-3, ArcView shapefile coverage, scale 1:500,000.

Goldberg, D., Lupo, T., Caputi, M., Barton, C., and Seeber L., 2003. Stress regimes in the Newark basin rift: Evidence from core and downhole data: *in* LeTourneau, M., Olsen, P.E., eds., The great rift valleys of Pangea in eastern North America 1, Tectonics, Structure, and Volcanism, Chapter 7: Columbia University Press, New York, New York, p. 104-117.

Groshong, R.H., 1988, Low-temperature deformation mechanisms and their interpretation: Geological Society of America Bulletin, v. 100, p. 1329-1360.

Gross, M.R., 1993, The origin and spacing of cross joints: examples from the Monterey Formation, Santa Barbara Coastline, California: Journal of Structural Geology, v. 15, p. 737-751.

Herman, G.C., 1997, Digital mapping of fractures in the Mesozoic Newark basin, New Jersey: Developing a geological framework for interpreting movement of groundwater contaminants: Environmental Geosciences, v. 4, no. 2, p. 68-84.

Herman, G.C., 2000, ArcView 3.X Extension for making 2D and 3D structural geologic shapefiles: NJ Geological Survey Digital Geodata Series DGS00-5. Computer program for use with ESRI

ArcView 3.x Geographic Information System.

Herman, G.C., 2001a, ArcView 3.X Extension for making 2D and 3D structural geologic shapefiles: N.J. Geological Survey Digital Geodata Series DGS01-1. 1. Computer program for use with ESRI ArcView 3.x Geographic Information System.

Herman, G.C., 2001b, Hydrogeological framework of bedrock aquifers in the Newark basin, New Jersey: *in* LaCombe, P.J. and Herman, G.C., eds. Geology in Service to Public Health, Field Guide and Proceedings of the 18th Annual Meeting of the Geological Association of New Jersey, p. 6-45.

Herman, G.C., 2005, Joints and veins in the Newark basin, New Jersey, in regional tectonic perspective: *in* Gates, A. E., ed., Newark basin – View from the 21st Century: Field Guide and Proceedings of the 22nd Annual Meeting of the Geological Association of New Jersey, p. 75-116.

Herman, G.C., 2006, Field tests using a heat-pulse flow meter to determine its accuracy for flow measurements in bedrock wells: N.J. Geological Survey Technical Memorandum TM06-1, 8 p.

Herman, G.C., Canace, R.J., Stanford, S.D., Pristas, R.S., Sugarman, P.J., French, M.A., Hoffman, J.L., Serfes, M.S., and Mennel, W.J., 1998, Aquifers of New Jersey: N.J. Geological Survey Open-File Map 24, scale 1:500,000, 1 sheet.

Herpers, H., and Barksdale, H.C., 1951, Preliminary report on the geology and groundwater supply of the Newark, New Jersey, Area: N.J. Department of Conservation and Economic Development, Special Report 10, 52 p.

Hodgson, R.A., 1961, Regional study of jointing in Comb ridge-Navajo Mountain Area, Arizona and Utah: American Association of Petroleum Geologists Bulletin, v. 45, 1-38.

Hoffman, J.L., and Lieberman, S.E., 2000, New Jersey Water Withdrawals 1990-1996: N.J. Geological Survey Open-File Report OFR 00-1, 123p.

Houghton, H.F., 1990, Hydrogeology of the early Mesozoic rocks of the Newark basin, New Jersey, *in* Brown, J.O., and Kroll, R. L., eds. Aspects of Groundwater in New Jersey: Field Guide and Proceedings of the 7th Annual Meeting of the Geological Association of New Jersey, p. E1-E36.

Houghton, H.F., Herman, G.C., and Volkert, R.A., 1992, Igneous rocks of the Flemington Fault zone: Geochemistry, structure, and stratigraphy, in Puffer J.H. and Ragland, P.C., eds., Eastern North American Mesozoic Magmatism, Geological Society of America Special Paper 268, p. 219-232.

Huang, Q., and Angelier, J., 1989, Fracture spacing and its relation to bed thickness: Geological Magazine, v. 126, p. 355-362.

Kasabach, H.F., 1966, Geology and Groundwater Resources of Hunterdon County, New Jersey: N.J. Geological Survey Special report no. 24, 128 p.

Knapp, G.N., 1904, Underground waters of New Jersey, Wells drilled in 1903: Annual report of the State Geologist for 1903, N.J. Geological Survey, p. 73-93.

Kulander, B.R., Dean, S.L., and Ward, B.J., 1990, Fractured core analysis: Interpretation, logging, and use of natural and induced fractures in core: American Association of Petroleum Geologists Methods in Exploration Series, no. 8, Tulsa, Oklahoma, USA, 88 p.

Kummel, H.B., 1898, The Newark System or red sandstone belt: N.J. Geological Survey Annual Report of the State Geologist for the Year of 1897, p. 23-159.

Laney, S.E., 2005, Stop 4. Structure of the Hopewell fault, North segment, Belle Mead, N.J., *in* Gates, A.E., ed., Newark basin – View from the 21st Century: Field Guide and Proceedings of the 22nd Annual Meeting of the Geological Association of New Jersey, p. 145-159.

Laney, S.E., Husch, J.M., and Coffee, C.,1995, The petrology, geochemistry and structural analysis of late-stage dikes and veins in the Lambertville sill, Belle Mead, New Jersey: Northeastern Geology and Environmental Sciences, v. 17, no. 2., p. 130-145.

Lewis-Brown, J.C., and dePaul, V.T., 2000, Groundwater flow and distribution of volatile organic compounds, Rutgers University Busch campus and vicinity, Piscataway Township, New Jersey: U.S. Geological Survey Water-Resources Investigations Report 99-4256, 72 p.

Lewis-Brown, J.C., and Jacobsen, E., 1995, Hydrogeology and groundwater flow, fractured Mesozoic structural-basin rocks, Stony Brook, Bedens Brook, and Jacobs Creek drainage basins, west-central New Jersey: U.S. Geological Survey Water-Resources Investigations Report 94-4147, 83 p.

Lewis-Brown, J.C., Rice, D.E., Rosman, R., and Smith N.P., 2004, Hydrogeological framework, groundwater quality, and simulation of groundwater flow at the Fair Lawn well field Superfund site, Bergen County, New Jersey: U.S. Geological Survey Scientific Investigations Report 2004-5280, 109 p.

Lucas, M., Hull, J., and Manspeizer, W., 1988, A foreland-type fold and related structures of the Newark rift basin, *in* Manspeizer, W., ed., Triassic-Jurassic Rifting, Continental Breakup, and the Origin of the Atlantic Ocean and Passive Margin: Elsevier, New York, New York, p. 307-332.

Michalski, A., 1990, Hydrogeology of the Brunswick (Passaic) formation and implications for groundwater monitoring practice: Groundwater Monitoring Review, v. 10, no. 4, p.134-143.

Michalski, A., 2001, A practical approach to bedrock aquifer characterization in the Newark basin, *in*

LaCombe, P.J. and Herman, G.C., eds., Geology in Service to Public Health: Field Guide and Proceedings of the 18th Annual Meeting of the Geological Association of New Jersey p. 46-59.

Michalski, A., 2010, Hydrogeologic characterization of contaminated sites in the Newark basin: Selecting conceptual flow model and characterization tools, *in* Herman, G.C. and Serfes, M.E., eds., Contributions to the geology and hydrogeology of the Newark basin, Chapter D: N.J. Geological Survey Bulletin 77, Trenton, N.J., p. D1-D12.

Michalski, A., and Britton, R., 1997, The role of sedimentary bedding in the hydrogeology of sedimentary bedrock - Evidence from the Newark basin, New Jersey: Groundwater, v. 35, no. 2. p. 318-327.

Michalski, A., and Gerber, T., 1992, Fracture flow velocities in the Passaic Formation in light of interwell tracer tests: *in* Ashley, G.M. and Halsey, S.D, eds., Field Guide and Proceedings of the 9th Annual Meeting of the Geological Association of New Jersey, p. 1-7.

Michalski, A., and Klepp, G.M., 1990, Characterization of transmissive fractures by simple tracing of in-well flow: Groundwater, v. 28, no. 2, p. 191-198.

Monteverde, D.H., Stanford, S.D., and Volkert, R.A., 2003, Geologic Map of the Raritan Quadrangle, Hunterdon and Somerset Counties, New Jersey: N.J. Geological Survey Geologic Map Series GMS 03-2, scale 1:24,000.

Monteverde, D.H. and Volkert, R.A., 2005, Bedrock Geology of the Chatham Quadrangle, Morris, Somerset, and Union Counties, New Jersey, N.J. Geological Survey Geological Map Series Map GMS04-2, scale 1:24,000.

Morin, R.H., Carleton, G.B., and Poirier, S., 1997, Fractured-aquifer hydrogeology from geophysical logs; the Passaic Formation, New Jersey: Groundwater, v. 35, no. 2, p. 328-338.

Morin, R.H., Senior, L.A., and Decker, E.R., 2000, Fractured-aquifer hydrogeology from geophysical logs: Brunswick Group and Lockatong Formation, Pennsylvania: Groundwater, v. 38, no. 2, p. 182-192.

Narr, W., and Suppe, J., 1991, Joint spacing in sedimentary rocks: Journal of Structural Geology, v. 13, p. 1037-1048

NASA (National Aeronautics and Space Administration), 2009, GPS Time-series data: http://sideshow.jpl.nasa.gov/mbh/series.html.

Olsen, P.E., 1980, The latest Triassic and early Jurassic Formations of the Newark basin (Eastern North America, Newark Supergroup): Stratigraphy, structure, and correlation: New Jersey Academy of Sciences, v. 25, no. 2, p. 25-51.

Olsen, P.E., 1986, A 40-million year lake record of orbital climate forcing: Science, v. 234, p. 842-847.

Olsen, P.E., 1988, Continuity of strata in the Newark and Hartford Basins, *in* Froelich, A.J., and Robinson, G.P., Jr., eds., Studies of the Early Mesozoic Basins of the Eastern United States: U.S. Geological Survey Bulletin 1776, p. 6-18.

Olsen, P.E., Kent, D.V., Cornet, Bruce, Witte, W.K., and Schlische, R.W., 1996, High-resolution stratigraphy of the Newark rift basin (early Mesozoic, eastern North America): Geological Society of America Bulletin, v. 108, no. 1, p. 40-77.

Olsen, P.E., Withjack, M.O., and Schlische, R.W., 1992: Inversion as an integral part of rifting: An outcrop perspective from the Fundy basin, eastern North America: Eos-American Geophysical Union Transactions, v. 73, n. 43, p. 562.

Owens, J.P., and Sohl, N.F., 1969, Shelf and deltaic paleoenvironments in the Cretaceous-Tertiary Formations of the New Jersey Coastal Plain, *in* Subitzky, Seymour, ed., Geology of selected areas in New Jersey and Eastern Pennsylvania and guide book: Rutgers University Press, New Brunswick, New Jersey, p. 235-278.

Owens, J.P., Sugarman, P.J., Sohl, N.F., Parker, R.A., Houghton, H.F., Volkert, R.A., Drake, A.A., Jr., and Orndorff, R.C., 1998, Bedrock geologic map of central and southern New Jersey: U.S. Geological Survey Miscellaneous Investigation Series Map I-2540-B, scale 1:100,000; 3 sheets.

Pollard, D.P., and Aydin, A., 1988, Progress in understanding jointing over the past century: Geological Society of America Bulletin, v. 100, p. 1181-1024.

Parnell, J., and Monson, B., 1995, Paragenesis of hydrocarbon, metalliferous and other fluids in Newark Group basins, Eastern U.S.A., Institute of Mining and Metallurgy, Transactions, Section B: Applied Earth Science; v. 104, p. 136-144.

Ragan, D.M., 1985, Structural Geology; an Introduction to Geometric Techniques, 3rd Edition: John Wiley & Sons, Inc., New York, New York, 393 p.

Ramsay, J.G., and Huber, M. I., 1987, The techniques of modern structural geology, v. 2: Folds and fractures: Academic Press, London, England, 700 p.

Ratcliffe, N.M. 1980, Brittle faults (Ramapo fault) and phyllonitic ductile shear zones in basement rocks of the Ramapo seismic zone, New York and New Jersey, and their relationship to current seismicity, *in* Manspeizer, Warren, ed., Field studies of New Jersey geology and guide to field trips, 52nd annual meeting of the New York State Geological Association, p. 278-311.

Ratcliffe, N.M., Burton, W.C., D'Angelo, R.M., and Costain, J.K., 1986, Low-angle extensional faulting, reactivated mylonites, and seismic reflection geometry of the Newark basin margin in eastern Pennsylvania: Geology, v. 14, p. 766-770.

Ratcliffe, N.M., Burton, W.C., and Pavich, M.J., 1990,

Orientation, movement history, and cataclastic rocks of the Ramapo fault based on core drilling, and trenching along the western margin of the Newark basin near Bernardsville, New Jersey: U.S. Geological Survey Miscellaneous Investigation Series Map I-1982.

Retallack, G.J., 2001, Soils of the Past, and Introduction to Paleopedology: Blackwell Science Ltd., Osney Mead, Oxford, England, 404. P.

Sanders, J.E., 1963, Late Triassic tectonic history of northeastern United States: American Journal of Science, v. 261, p. 501-524.

Schlische, R.W., 1992, Structural and stratigraphic development of the Newark extensional basin, eastern North America: Evidence for the growth of the basin and its bounding structures: Geological Society of America Bulletin, v. 104, p. 1246-1263.

Schlische, R.W., and Olsen, P.E., 1988, Structural evolution of the Newark basin, *in* Husch, J. M., and Hozik, M.J., eds., Geology of the central Newark basin: Field guide and proceedings of the 5th Annual meeting of the Geological Association of New Jersey, p. 43-65.

Schlische, R.W., and Olsen, P.E., 1990, Quantitative filling model for continental extensional basins with application to the early Mesozoic rifts of eastern North America: Journal of Geology, v. 98, p. 135-155.

Serfes, M.E., 1994, Natural groundwater quality in bedrock of the Newark basin: N.J. Geological Survey Report GSR 35, 32 p.

Serfes, M.E., Spayd, S. E., Herman, G.C., and Monteverde, D. H., 2000, Arsenic occurrence, source and possible mobilization mechanisms in groundwater of the piedmont physiographic province in New Jersey: EOS, Transactions of the American Geophysical Union Fall Meeting, v. 81, no. 48, p. F525-H210-08.

Serfes, M.E., Spayd., S.E., Herman, G.C., 2005, The occurrence, sources, mobilization, and transport of groundwater in the Newark basin of New Jersey, *in* O'Day, P.A., Vlassopoulos, Meng, Xiaoguang, and Benning, L.G., eds., Advances in Arsenic Research; Integration of Experimental and Observational Studies and Implications for Mitigation, Chapter 13: American Chemical Society Symposium Series 915, Washington, District of Columbia, p. 175-190.

Smoot, J.P., and Olsen, P. E., 1985, Massive mudstones in basin analysis and paleoclimatic interpretation of the Newark Supergroup, *in* Robinson, G. R., and Froelich, A. J., eds., Proceedings of the second U.S. Geological Survey workshop on the Early Mesozoic basins of the Eastern United States: U. S. Geological Survey Circular 946., p. 29-33.

Smoot, J.P., and Olsen, P.E., 1988, Massive mudstones in basin analysis and paleoclimatic interpretations, *in* Manspeizer, W., ed., Triassic-Jurassic rifting, continental breakup, and the origin of the Atlantic Ocean and passive margins, Part A: , Elsevier, Amsterdam, The Netherlands, p. 249-274.

Smoot, J.P., and Olsen, P.E., 1994, Climatic cycles as sedimentary controls of rift-basin lacustrine deposits in the early Mesozoic Newark basin based on continuous core, *in* Lomando, T., and Harris, M., eds. Lacustrine depositional systems: Society of Economic Paleontologists and Mineralogists Core Workshop Notes, v. 19, p. 201-237.

Spayd, S.E., 1985, Movement of volatile organics through a fractured rock aquifer: Groundwater, v. 23, no. 4, p. 496-502.

Stanford, S.D., 2000, Overview of the glacial geology of New Jersey, *in* Harper, D. P. and Goldstein, F. R., eds., Glacial Geology of New Jersey: Field Guide and Proceedings for the 7th Annual Meeting of the Geological Association of New Jersey, p. II-1 to II-24.

Stanford, S.D., Ashley, G. M., and Brenner, G. J., 2001, Late Cenozoic fluvial stratigraphy of the New Jersey Piedmont: A record of glacioeustacy, planation, and incision on a low-relief passive margin: Journal of Geology, v. 109, p. 265-276.

Stanford, S.D., Monteverde, D.H., Volkert, R.A., Sugarman, P.J., and Brenner, G.J, 1998, Geology of the New Brunswick quadrangle, Middlesex and Somerset Counties, New Jersey: N.J. Geological Survey Open-file Map 23, scale 1:24,000 scale; 3 sheets.

Szabo, Z., Taylor, T.A., Payne, D.F., and Ivanchenko, T., 1997, Relation of hydrogeologic characteristics to distribution of radioactivity in groundwater, Newark basin, New Jersey: U.S. Geological Survey Water-Resources Investigations Report 95-4136, 134 p.

Tabakh, M. El, and Schreiber, B.C., 1998, Diagenesis of the Newark rift basin, Eastern North America: Sedimentology v. 45, p. 855-874.

Tabakh, M. El, Schreiber, B.C., and Warren, J.K., 1998, Origin of fibrous gypsum in the Newark basin, eastern North America: Journal of Sedimentary Research, v. 68, p. 88-99.

Tollo, R.P., and Gottfried, D., 1992, Petrochemistry of Jurassic basalt from eight drill cores, Newark basin, New Jersey: Implications for the volcanic petrogenesis of the Newark Supergroup, *in* Puffer, J. H. and Ragland, P. C., eds., Eastern North American Mesozoic Magmatism: Geological Society of America Special Paper 268, p. 233-259.

Van Houten, F.B., 1962, Cyclic sedimentation, Upper Triassic Lockatong Formation, central New Jersey and adjacent Pennsylvania: American Journal of Science, v. 260, p. 561-576.

Van Houten, F.B., 1965, Composition of Triassic Lockatong and associated formations of Newark Group, central New Jersey and adjacent

Pennsylvania: American Journal of Science, v. 263, p. 825-863

Vecchioli, J., 1965, Directional hydraulic behaviour of a fractured-shale aquifer in New Jersey: International Association of scientific hydrology; Symposium of Dubrovnik, Croatia, p. 318-326.

Vecchioli, J., Carswell, L.D., and Kasabach, H.F., 1969, Occurrence and movement of groundwater in the Brunswick Shale at a site near Trenton, New Jersey: U.S. Geological Survey Professional Paper 650-B, p. B154-B157.

Volkert, R.A., 2006, Bedrock Geologic map of the Paterson quadrangle, Passaic, Essex and Bergen Counties, New Jersey: N.J. Geological Survey Geologic Map Series GMS 06-6, scale 1: 24,000.

Weems, R.E., and Olsen, P.E., 1997, Synthesis and revision of groups within the Newark Supergroup, eastern North America: Geological Society of America Bulletin, v. 109, no. 2, p. 195-209.

Withjack, M.O., Islam, Q.T., and La Pointe, P.R., 1995, Normal faults and their hanging-wall deformation: An experimental study: American Association of Petroleum Geologists Bulletin, v.79, no. 1, p. 1-18.

Xiao, H., and Suppe, J., 1992, Origin of rollover: American Association of Petroleum Geologists Bulletin, v. 76, no. 4, p. 509-529.

Borehole Geophysics and Hydrogeology Studies in the Newark Basin, New Jersey

By Gregory C. Herman and John F. Curran, N.J. Geological Survey

Appendixes 1 to 4 of

Contributions to the Geology and Hydrogeology of the Newark Basin

N.J. Geological Survey Bulletin 77

State of New Jersey
Department of Environmental Protection
Water Resource Management
New Jersey Geological Survey
2010

Appendixes Contents

Borehole Geophysics and Hydrogeology Studies in the Newark Basin, New Jersey

Appendixes 1 to 4

Borehole Geophysics and Hydrogeology Studies in the Newark Basin, New Jersey

Gregory C. Herman and John F. Curran[1]

Description of Contents

Appendixes 1 to 4 include study results from 36 hydrogeology projects involving 127 water wells in the New Jersey part of the Newark basin from 2001 to 2008. The studies are based on geophysical logs collected in open-hole parts of the wells for aquifer-characterization research and ground-water supply and pollution projects supported and/or regulated by the NJ Dept. of Environmental Protection.

The purpose of these appendixes is to provide location maps, visual records and hydrogeologic sections detailing the different types of hydraulically-conductive bedrock features in the subsurface water-bearing zones (WBZs) of each aquifer. Appendixes 1 through 4 are organized using aquifer groups including: 1) diabase and basalt igneous rocks, 2) Brunswick aquifer coarse-grained rocks including conglomerate and sandstone, 3) Brunswick aquifer fine-gained rocks including mudstone and siltstone and 4) Lockatong argillite and Stockton sandstone. Each appendix includes entries detailing the results for a single project. The location and nature of the projects are listed in table AP1 and shown on figures AP1 and AP2 below. Table AP1 includes construction and location details for each well.

An appendix entry includes a map showing well locations and illustrations of the hydrogeologic aspects of the local aquifer, based on the geophysical logs acquired for each study. The suite of geophysical logs collected at each site varies, but commonly includes a caliper (borehole-diameter) log, water temperature and electrical conductivity or resistivity logs, bedrock natural gamma radiation and single-point electrical-resistance logs, and borehole televiewer (BTV) logs. BTV logs are collected using optical televiewer (OPTV) and acoustical televiewer (ATV) probes. The OPTV captures oriented camera images of the borehole walls and therefore, visual records of the bedrock strata and structures penetrated by a well. ATV probes capture oriented images of the borehole walls using reflected sound-waves. BTV logs therefore provide direct measurements of bedrock features that store and convey ground water, and serve as the primary basis for conducting a detailed hydrogeologic assessment of the aquifer. Beds, layers and fractures are traced in BTV imagery, then measured and statistically analyzed using circular histograms and stereonet diagrams to determine orientations of the most common structural features in a well. The location maps include oriented bedding, layering and fracture symbols stemming from these structural analyses that are plotted on a topographic base to demonstrate the link between bedrock strata, structures and topographic landforms.

The hydrogeologic sections relate the various geophysical-log responses in a well to bedrock features of the aquifer. They include geologic interpretation of the geophysical logs, summarize aspects of well construction, depict the types and spatial distribution of subsurface water-bearing features in a well and therefore relate stratigraphic and structural heterogeneity of the aquifer to observed anomalies in the geophysical logs. Some hydrogeologic sections incorporate the results of borehole flow studies detailing flow rates and directions determined using a heat-pulse flowmeter and/or straddle-packers.

Projects having many wells in close proximity may provide enough information to construct a hydrogeologic framework interpretation for an area. These entries are noted as framework studies in the list of appendix contents and include hydrogeologic cross-section interpretations showing the location and extent of WBZs in relative stratigraphic context. They commonly rely on the use of stratigraphic marker beds seen in OPTV records to constrain the stratigraphic framework and depict the continuity of WBZs in the subsurface. These diagrams therefore illustrate how permeable features are arranged in the subsurface between wells and provide a basic framework to relate borehole cross flows to local topographic variations, ground-water recharge and discharge areas, weathered- and deep-bedrock intervals. Other appendix entries detail the results for only one or two wells, or lack the necessary logs to conduct a framework analysis.

Appendix entry 2F is unique because it includes results of an unpublished geotechnical investigation conducted in the 1990s for the proposed Passaic flood tunnel project. It lacks BTV records and relies upon

[1]NJ Geological Survey
PO Box 427,
Trenton, NJ 08625
greg.herman@dep.state.nj.us

third-party geotechnical documentation.

References

Kummel, H. B., 1898, The Newark System or red sandstone belt: New Jersey Geological Survey Annual Report of the State Geologist for the Year of 1897, p. 23-159.

Lyttle, P. T., and Epstein, J. B., 1987, Geologic map of the Newark 1 x 2 quadrangle, New Jersey, Pennsylvania and New York, USGS Misc. Invest. 1715, two sheets, map scale 1:250,000.

New Jersey Geological Survey, 2000, Bedrock geology and topographic base maps of New Jersey: N.J. Geological Survey CD Series CD00-1, 1 Compact Disk.

Olsen, P. E., 1980, The latest Triassic and early Jurassic Formations of the Newark Basin (Eastern North America, Newark Supergroup): Stratigraphy, structure, and correlation: New Jersey Academy of Sciences, vol. 25, no. 2, p. 25-51.

Olsen, P. E., Kent, D. V., Cornet, Bruce, Witte, W. K., and Schlische, R. W., 1996, High-resolution stratigraphy of the Newark rift basin (early Mesozoic, eastern North America): Geological Society of America Bulletin, v. 108, no. 1, p. 40-77.

Weems, R. E., and Olsen, P. E., 1997, Synthesis and revision of groups within the Newark Supergroup, eastern North America: Geological Society of America Bulletin, v. 109, no. 2, p. 195-20.

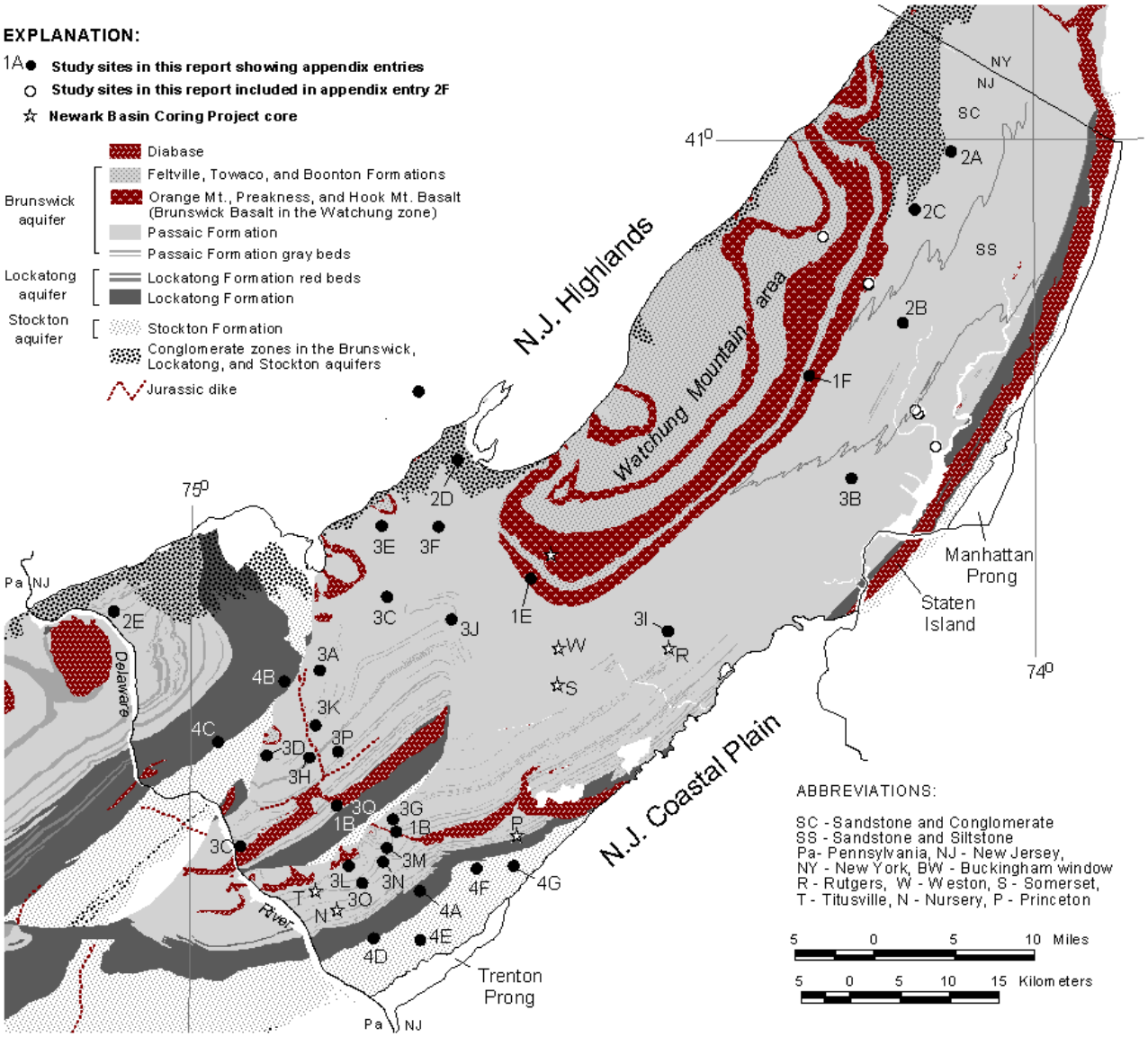

Figure AP1. Map of study locations in the appendixes with core locations for the Newark Basin Coring Project (Olsen and others, 1996). Geology compiled from Geographic Information Systems coverage of the basin from Pennsylvania (Pennsylvania Geological Survey written communication, February 2000; New Jersey (NJ Geological Survey, 2000) and New York (http://www.nysm.nysed.gov/data/lhud_bedr1a.zip).

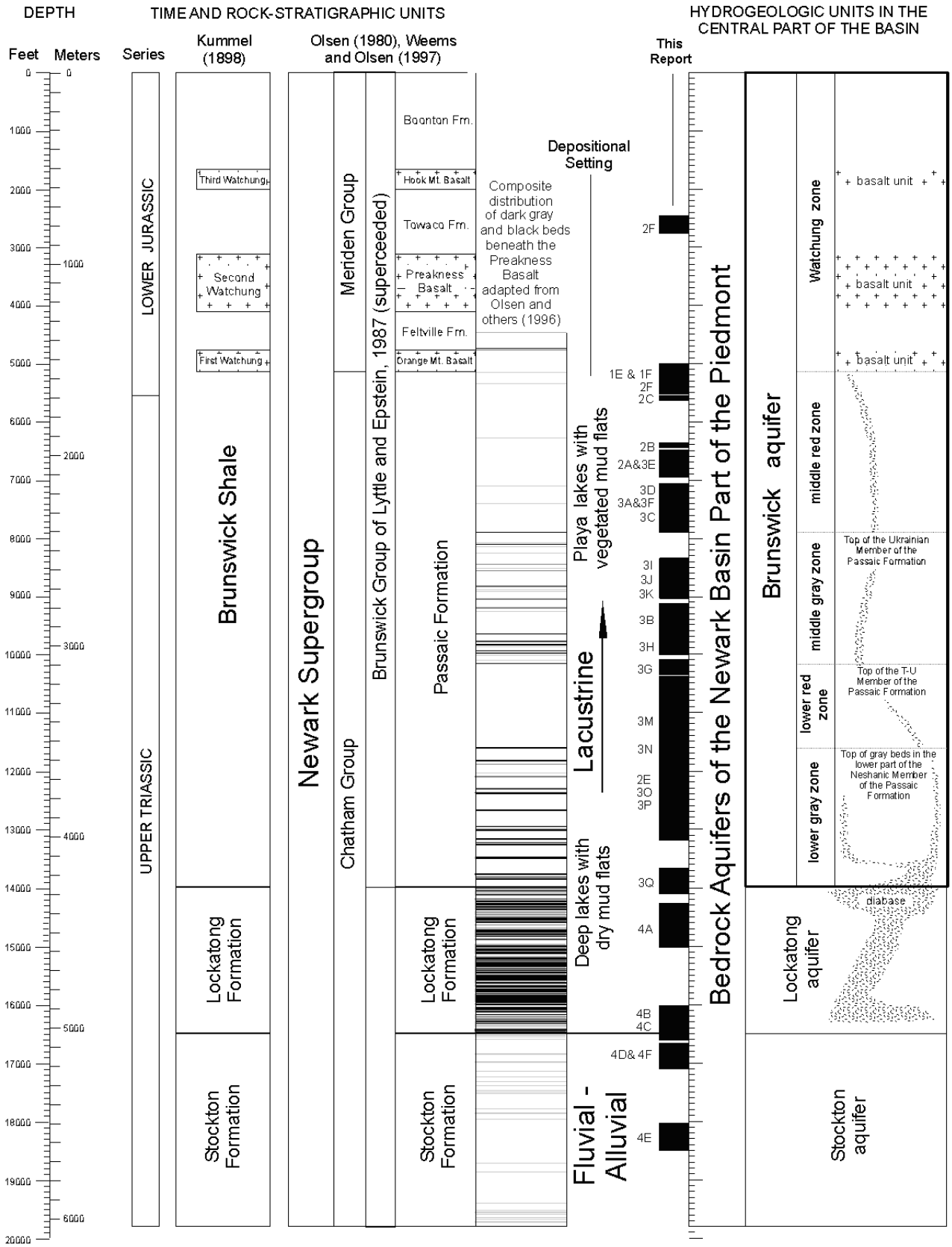

Figure AP2. Summary of time, rock and hydrogeologic units in the central part of the Newark basin showing approximate stratigraphic intervals covered by each study.

TABLE AP1. RECORDS OF WELLS AND CORES IN THE NEWARK BASIN, NEW JERSEY INCLUDED IN APPENDIXES 1 TO 4

Well	Appendix Entry	NJGS Project	Project Identification or Location	Diameter (inches)	Well Type	Log Source	Aquifer or Aquifer Zone
1	1A	258 S. Franklin St.AGW	258 S. Franklin St.	6	Domestic	NJGS	Diabase
2	1B	Snydertown Rd. AGW	SR65	6	Domestic	NJGS	Diabase
3	1B	Snydertown Rd. AGW	SR66	6	Domestic	NJGS	Diabase overlying Brunswick lower gray
4	1B	Snydertown Rd. AGW	SR69	6	Domestic	NJGS	Diabase
5	1B	Snydertown Rd. AGW	SR98	6	Domestic	NJGS	Diabase
6	1C	Crusher Rd. WS	Crusher Rd.	6	Domestic	NJGS	Diabase
7	1D	East Amwell WS	Block 38, Lot 16	6	Domestic	NJGS	Diabase
8	1E	Essex County Country Club WS	Well 1	8	Irrigation	NJGS	Brunswick Watchung basalt and middle red
9	1E	Essex County Country Club WS	Well 2	8	Irrigation	NJGS	Brunswick Watchung basalt and middle red
10	1E	Essex County Country Club WS	Well 3	8	Irrigation	NJGS	Brunswick Watchung basalt and middle red
11	1F	1163 Delaware AGW	1163 Delaware Ave	6	Domestic	NJGS	Brunswick Watchung basalt and middle red
12	2A	Ridgewood Shell GWI	MW-9D	6	Monitoring	DEP/SRP	Brunswick sandstone conglomerate
13	2A	Ridgewood Shell GWI	MW-27	6	Monitoring	DEP/SRP	Brunswick sandstone conglomerate
14	2A	Ridgewood Shell GWI	MW-29	6	Monitoring	DEP/SRP	Brunswick sandstone conglomerate
15	2A	Ridgewood Shell GWI	MW-30	6	Monitoring	DEP/SRP	Brunswick sandstone conglomerate
16	2A	Ridgewood Shell GWI	MW-32	6	Monitoring	DEP/SRP	Brunswick sandstone conglomerate
17	2A	Ridgewood Shell GWI	MW-33	6	Monitoring	DEP/SRP	Brunswick sandstone conglomerate
18	2A	Ridgewood Shell GWI	MW-37	6	Monitoring	DEP/SRP	Brunswick sandstone conglomerate
19	2A	Ridgewood Shell GWI	MW-38	6	Monitoring	DEP/SRP	Brunswick sandstone conglomerate
20	2A	Ridgewood Shell GWI	MW-43	6	Monitoring	DEP/SRP	Brunswick sandstone conglomerate
21	2B	Sandos_Clariant GWI	MW-29R	8	Monitoring	DEP/SRP	Brunswick sandstone conglomerate
22	2B	Sandos_Clariant GWI	MW-30R	8	Monitoring	DEP/SRP	Brunswick sandstone conglomerate
23	2C	Hoffman-LaRoche GWI	CH-1	8	Monitoring	DEP/SRP	Brunswick sandstone
24	2C	Hoffman-LaRoche GWI	CH-2	8	Monitoring	DEP/SRP	Brunswick sandstone
25	2C	Hoffman-LaRoche GWI	60 Princeton Place	5	Domestic	DEP/SRP	Brunswick sandstone
26	2D	Hamilton Farms Golf Course WS	HF2	8	Irrigation	NJGS	Brunswick conglomerate
27	2D	Hamilton Farms Golf Course WS	HF3	8	Irrigation	NJGS	Brunswick conglomerate
28	2D	Hamilton Farms Golf Course WS	HF5	6	Observation	NJGS	Brunswick conglomerate
29	2E	Private Housing Development WS	7032	6	Test	NJGS	Brunswick lower gray (coarse)
30	2E	Private Housing Development WS	7034	6	Test	NJGS	Brunswick lower gray (coarse)
31	2E	Milford Boro WS	Milford Boro OBS-A	6	Observation	NJGS	Brunswick lower gray (coarse)
32	2E	Milford Boro WS	Milford Boro OBS-B	6	Observation	NJGS	Brunswick lower gray (coarse)
33	2E	Milford Boro WS	Milford Boro OBS-D	6	Observation	NJGS	Brunswick lower gray (coarse)
34	2F	Passaic Flood Tunnel GI	Workshaft 2 IT-2-PB	4	Test	IT Corp.	Brunswick sandstone
35	2F	Passaic Flood Tunnel GI	Workshaft 2 IT-2-PW	8	Test	IT Corp.	Brunswick sandstone
36	2F	Passaic Flood Tunnel GI	Workshaft 2B core C-23	3	Core	ACE	Brunswick lower red
37	2F	Passaic Flood Tunnel GI	Workshaft 2B IT-2-BK-PB01	4	Test	IT Corp.	Brunswick lower red
38	2F	Passaic Flood Tunnel GI	Workshaft 2B IT-2-BF-PW01	8	Test	IT Corp.	Brunswick lower red
39	2F	Passaic Flood Tunnel GI	Workshaft 2C IT-2C-PB	4	Test	IT Corp.	Brunswick lower red
40	2F	Passaic Flood Tunnel GI	Workshaft 2C IT-2C-PW	8	Test	IT Corp.	Brunswick lower red
41	2F	Passaic Flood Tunnel GI	Workshaft 3 IT-3-PB01	4	Test	IT Corp.	Brunswick Watchung siltstone and mudstone
42	2F	Passaic Flood Tunnel GI	Workshaft 3 IT-3-PW01	8	Test	IT Corp.	Brunswick Watchung siltstone and mudstone
43	3A	Flemington Boro WS	OBS-1	6	Observation	NJGS	Brunswick middle red
44	3B	Hillside Car Wash WS	1260 North Broad St.	6	Commercial	NJGS	Brunswick middle red
45	3C	Readington Twp. GWI	15 Roosevelt Rd.	6	Domestic	NJGS	Brunswick middle red
46	3C	Readington Twp. GWI	16 Arrowhead Dr.	6	Domestic	NJGS	Brunswick middle red
47	3C	Readington Twp. GWI	39 42nd Str.	6	Domestic	NJGS	Brunswick middle red
48	3C	Readington Twp. GWI	Readington Middle School	6	Public NC	NJGS	Brunswick middle red
49	3C	Readington Twp. GWI	Rusinksi Farm	6	Test	NJGS	Brunswick middle red
50	3D	Delaware Twp. AGW	74 Lambert Rd.	6	Domestic	NJGS	Brunswick middle red
51	3D	Delaware Twp. AGW	81 Dunkard Church Rd.	6	Domestic	NJGS	Brunswick middle red
52	3D	Delaware Twp. AGW	79 Dunkard Church Rd.	6	Domestic	NJGS	Brunswick middle red
53	3D	Delaware Twp. AGW	77 Dunkard Church Rd.	6	Domestic	NJGS	Brunswick middle red
54	3D	Delaware Twp. AGW	32-34 Haines Rd.	6	Domestic	NJGS	Brunswick middle red
55	3E	Rt 22 Potterstown GWI	24-40973 Hartsell	6	Monitoring	NJGS	Brunswick middle red
56	3E	Rt 22 Potterstown GWI	24-40974 Huska	6	Monitoring	NJGS	Brunswick middle red
57	3E	Rt 22 Potterstown GWI	24-40975	6	Monitoring	NJGS	Brunswick middle red
58	3E	Rt 22 Potterstown GWI	287-4 Rt 22	6	Domestic	NJGS	Brunswick middle red
59	3E	Rt 22 Potterstown GWI	Salem B2	6	Test	NJGS	Brunswick middle red
60	3E	Rt 22 Potterstown GWI	Salem Supply	6	Public NC	NJGS	Brunswick middle red
61	3F	Trump National Golf Course WS	A2	6	Observation	Mid-Atlantic	Brunswick middle red
62	3F	Trump National Golf Course WS	C3	6	Observation	Mid-Atlantic	Brunswick middle red
63	3F	Trump National Golf Course WS	C9	6	Observation	Mid-Atlantic	Brunswick middle red
64	3F	Trump National Golf Course WS	D2	6	Observation	Mid-Atlantic	Brunswick middle red

TABLE AP1. (continued)

County	Municipality	USGS 7-1/2' Quadrangle	XY Source	GEOGRAPHIC (degrees) Latitude	Longitude	NAD83 NJSPF X_coord	Y_coord	NGVD88 Land elev (ft)	Elev. Source	Total Depth (ft)[1]	Casing (ft)[1]
Hunterdon	Lambertville	Lambertville, Pa-NJ	Map	39.8470978	74.2735330	369301.85	555707.65	269.53	DEM	370.0	48.5
Hunterdon	East Amwell	Hopewell, NJ	GPS	40.3973192	74.8244674	401759.26	569809.38	406.25	DEM	172.0	39.3
Hunterdon	East Amwell	Hopewell, NJ	GPS	40.3978303	74.8239106	401915.00	569995.00	409.20	DEM	591.0	46.1
Hunterdon	East Amwell	Hopewell, NJ	GPS	40.3975830	74.8255657	401453.71	569906.60	406.23	DEM	246.0	25.0
Hunterdon	East Amwell	Hopewell, NJ	GPS	40.3993800	74.8299300	400240.69	570565.72	376.00	DEM	283.0	30.0
Mercer	Hopewell	Pennington, NJ	Map	40.3739328	74.7575905	420360.00	561229.00	325.00	MAP	521.0	49.7
Hunterdon	East Amwell	Hopewell, NJ	GPS	40.4366880	74.7749039	415607.55	584103.74	490.00	DEM	493.5	45.1
Essex	West Orange	Orange, NJ	GPS	40.7829916	74.2647840	558141.67	710552.77	544.83	DEM	110.0	19.5
Essex	West Orange	Orange, NJ	GPS	40.7829916	74.2647840	557258.49	710226.32	516.82	DEM	317.4	17.9
Essex	West Orange	Orange, NJ	GPS	40.7842234	74.2618569	558067.82	710677.24	543.91	DEM	500.0	49.4
Somerset	Somerset	Bound Brook, NJ	Map	40.1084272	73.9533597	464880.00	645016.00	422.00	MAP	298.5	26.1
Bergen	Ridgewood	Hackensack, NJ	Map	40.9875499	74.0943230	604115.46	784920.77	108.25	DEM	84.4	26.7
Bergen	Ridgewood	Hackensack, NJ	Map	40.9869448	74.0940572	604189.86	784700.68	109.26	DEM	82.8	53.5
Bergen	Ridgewood	Hackensack, NJ	Map	40.9879161	74.0940012	604203.67	785054.62	108.93	DEM	67.8	47.9
Bergen	Ridgewood	Hackensack, NJ	Map	40.9875221	74.0948540	603968.92	784909.99	109.20	DEM	80.6	42.7
Bergen	Ridgewood	Hackensack, NJ	Map	40.9865378	74.0934963	604345.39	784553.14	109.62	DEM	84.1	47.2
Bergen	Ridgewood	Hackensack, NJ	Map	40.9863766	74.0941528	604164.42	784493.55	109.66	DEM	78.6	45.3
Bergen	Ridgewood	Hackensack, NJ	Map	40.9861891	74.0930351	604473.30	784426.68	107.90	DEM	88.3	44.0
Bergen	Ridgewood	Hackensack, NJ	Map	40.9857001	74.0940964	604181.14	784247.17	105.70	DEM	79.5	53.0
Bergen	Ridgewood	Hackensack, NJ	Map	40.9838796	74.0925265	604617.63	783585.96	94.35	DEM	69.3	44.0
Bergen	Fairlawn	Paterson, NJ	Map	40.9358056	74.1398888	591614.30	766014.60	42.08	DEM	163.8	68.3
Bergen	Fairlawn	Paterson, NJ	Map	40.9344168	74.1392223	591800.50	765509.40	47.49	DEM	165.5	41.4
Essex	Nutley	Orange, NJ	Map	40.8344695	74.1580233	586748.41	729077.07	103.23	DEM	638.1	100.3
Passaic	Clifton	Orange, NJ	Map	40.8383097	74.1592703	586397.95	730474.72	131.28	DEM	638.6	80.5
Passaic	Clifton	Orange, NJ	Map	40.8328891	74.1516463	588515.20	728508.28	137.69	DEM	170.0	34.1
Somerset	Bedminster	Gladstone, NJ	Map	40.0458747	73.8095045	442374.54	685428.27	367.03	DEM	296.0	51.7
Somerset	Bedminster	Gladstone, NJ	Map	40.0452714	73.8129509	442147.34	684465.15	323.07	DEM	297.2	
Somerset	Bedminster	Gladstone, NJ	Map	40.0439260	73.8142072	441654.53	684117.20	322.79	DEM	302.0	57.7
Hunterdon	Milford Boro	Frenchtown, NJ-Pa	GPS	39.7374866	74.0090849	329675.00	630173.00	275.74	DEM	415.0	49.0
Hunterdon	Milford Boro	Frenchtown, NJ-Pa	GPS	39.7369054	74.0079830	329465.00	630484.00	284.29	DEM	418.0	48.6
Hunterdon	Milford Boro	Frenchtown, NJ-Pa	GPS	39.7366802	74.0053816	329387.00	631216.00	266.87	DEM	216.0	48.6
Hunterdon	Milford Boro	Frenchtown, NJ-Pa	GPS	39.7360533	73.9930858	329178.00	634675.00	401.03	DEM	378.0	57.6
Hunterdon	Milford Boro	Frenchtown, NJ-Pa	GPS	39.7347064	73.9908376	328691.00	635310.00	386.88	DEM	434.0	48.6
Passaic	Little Falls	Orange, NJ	Map	40.4117712	73.6026173	576176.68	741998.43	391.08	DEM	517.0	
Passaic	Little Falls	Orange, NJ	*							526.0	10.0
Hudson	Kearny	Orange, NJ	Map	40.4548126	73.7495025	591474.56	700965.10	5.00	DEM	470.0	
Hudson	Kearny	Orange, NJ	Map	40.4578337	73.7554285	592561.12	699306.78	7.65	DEM	505.0	145.0
Hudson	Kearny	Orange, NJ	*							407.0	78.0
Hudson	Kearny	Jersey City, NJ-NY	Map	40.4753376	73.799304	598837.60	687047.43	6.00	DEM	504.0	87.0
Hudson	Kearny	Jersey City, NJ-NY	*							506.0	
Passaic	Wayne	Pompton Plains, NJ	Map	40.3701181	73.5472901	561164.45	757567.85	174.06	DEM	360.0	
Passaic	Wayne	Pompton Plains, NJ	*							357.0	105.0
Hunterdon	Raritan	Flemington, NJ	GPS	40.5203700	74.8461700	395891.00	614657.00	129.00	DEM	339.0	58.3
Union	Hillside	Elizabeth, NJ-NY	Map	40.6932604	74.21659145	570709.00	677577.00	71.00	DEM	385.0	137.0
Hunterdon	Readington	Flemington, NJ	Map	39.9832548	73.9813126	419238.47	637463.34	209.60	Map	89.0	30.4
Hunterdon	Readington	Flemington, NJ	Map	39.9753370	73.9847749	416348.80	636509.83	197.32	Map	117.0	49.0
Hunterdon	Readington	Flemington, NJ	Map	39.9828710	73.9689427	419119.09	640930.28	267.42	Map	104.7	44.6
Hunterdon	Readington	Flemington, NJ	Map	39.9861400	73.9699979	420308.06	640627.53	234.57	Map	98.0	51.2
Hunterdon	Readington	Flemington, NJ	Map	39.9805345	73.9671432	418271.01	641439.59	239.82	Map	149.0	24.5
Hunterdon	Delaware	Stockton, NJ	GPS	39.8663238	74.1568425	376409.13	588442.73	219.81	DEM	198.0	50.7
Hunterdon	Delaware	Stockton, NJ	GPS	39.8755772	74.1632664	379772.74	586626.94	204.09	DEM	172.0	48.0
Hunterdon	Delaware	Stockton, NJ	GPS	39.8763267	74.1631564	380045.88	586656.80	204.51	DEM	195.0	48.2
Hunterdon	Delaware	Stockton, NJ	GPS	39.8770174	74.1630627	380297.54	586682.15	206.13	DEM	196.6	49.0
Hunterdon	East Amwell	Stockton, NJ	GPS	39.8806616	74.1639552	381623.98	586426.69	179.95	DEM	245.0	59.4
Hunterdon	Readington	Califon, NJ	GPS	39.9602140	73.9116848	410966.97	657028.80	217.56	DEM	69.6	45.8
Hunterdon	Readington	Califon, NJ	GPS	39.9566048	73.9084316	409658.34	657949.38	248.09	DEM	69.0	44.6
Hunterdon	Readington	Califon, NJ	GPS	39.9601320	73.9089167	410942.20	657804.89	230.03	DEM	69.0	45.7
Hunterdon	Readington	Califon, NJ	Map	39.9575706	73.9088700	410009.30	657824.18	249.01	DEM	165.0	21.1
Hunterdon	Readington	Califon, NJ	GPS	39.9583499	73.9100671	410290.96	657486.74	232.17	DEM	145.0	19.3
Hunterdon	Readington	Califon, NJ	GPS	39.9593811	73.9105874	410665.61	657338.41	244.92	DEM	248.0	65.5
Somerset	Bedminster	Gladstone, NJ	Map	40.0268383	73.8838555	435287.71	664661.62	186.50	DEM	514.0	50.0
Somerset	Bedminster	Gladstone, NJ	Map	40.0341279	73.8947355	437922.12	661596.89	196.54	DEM	252.0	15.5
Somerset	Bedminster	Gladstone, NJ	Map	40.0335830	73.8946976	437723.69	661608.83	199.72	DEM	498.3	52.1
Somerset	Bedminster	Gladstone, NJ	Map	40.0299752	73.8831712	436431.68	664845.33	148.11	DEM	511.8	52.9

TABLE A1. RECORDS OF WELLS AND CORES IN THE NEWARK BASIN, NEW JERSEY INCLUDED IN APPENDICES 1 - 4

Well	Appendix Entry	NJGS Project	Project Identification or Location	Diameter (inches)	Well Type	Log Source	Aquifer or Aquifer Zone
65	3F	Trump National Golf Course WS	F	6	Observation	Mid-Atlantic	Brunswick middle red
66	3F	Trump National Golf Course WS	H	6	Observation	Mid-Atlantic	Brunswick middle red
67	3F	Trump National Golf Course WS	P	6	Observation	Mid-Atlantic	Brunswick middle red
68	3G	Hopewell Boro Supply Well 6 AGW	CH-1	2	Core	NJGS	Brunswick middle gray and middle red
69	3G	Hopewell Boro Supply Well 6 AGW	OBS-1	6	Observation	NJGS	Brunswick middle gray and middle red
70	3G	Hopewell Boro Supply Well 6 AGW	OBS-2	6	Observation	NJGS	Brunswick middle gray
71	3G	Hopewell Boro Supply AGW	MW-1m	6	Monitoring	NJGS	Brunswick middle gray and middle red
72	3G	Hopewell Boro Supply AGW	MW-2m	6	Monitoring	NJGS	Brunswick middle gray and middle red
73	3G	Hopewell Boro Rockwell	MW-24	6	Monitoring	BBL	Brunswick middle gray and middle red
74	3G	Hopewell Boro Rockwell	VO-7	6	Monitoring	BBL	Brunswick middle gray and middle red
75	3H	Larison's Corner GWI	S-1	6	Domestic	NJGS	Brunswick middle gray
76	3I	Home Depot/Vitaulic GWI	MW-10	6	Monitoring	NJGS	Brunswick middle gray
77	3I	Home Depot/Vitaulic GWI	MW-11	6	Monitoring	NJGS	Brunswick middle gray
78	3I	Home Depot/Vitaulic GWI	MW-12	6	Monitoring	NJGS	Brunswick middle gray
79	3J	Branchburg Rt. 202 GWI	1011 Rt. 202	6	Domestic	NJGS	Brunswick middle gray
80	3J	Branchburg Rt. 202 GWI	75 North Branch Rd.	6	Domestic	NJGS	Brunswick middle gray
81	3J	Branchburg Rt. 202 GWI	941 Route 202	6	Domestic	NJGS	Brunswick middle gray
82	3J	Branchburg Rt. 202 GWI	947 Route 202	6	Domestic	NJGS	Brunswick middle gray
83	3J	Branchburg Rt. 202 GWI	954 Route 202	6	Domestic	NJGS	Brunswick middle gray
84	3J	Branchburg Rt. 202 GWI	971 Route 202	6	Domestic	NJGS	Brunswick middle gray
85	3K	Heron Glen Golf Course WS	Heron Glen N	6	Observation	NJGS	Brunswick middle gray
86	3K	Heron Glen Golf Course WS	Heron Glen B	6	Public NC	NJGS	Brunswick middle gray
87	3K	Heron Glen Golf Course WS	Heron Glen L	6	Observation	NJGS	Brunswick middle gray
88	3K	Private Housing Development WS	QNS	6	Test	NJGS	Brunswick lower red
89	3L	Harbat Farms WS	East well in field	6	Domestic	NJGS	Brunswick lower red
90	3M	Stony Brook-Millstone Reserve AGW	SB1	6	Test	NJGS	Brunswick lower red
91	3M	Stony Brook-Millstone Reserve AGW	SB3	6	Test	NJGS	Brunswick lower red
92	3M	Stony Brook-Millstone Reserve AGW	SB6	6	Test	NJGS	Brunswick lower red
93	3M	Stony Brook-Millstone Reserve AGW	SB8	6	Test	NJGS	Brunswick lower red
94	3M	Stony Brook-Millstone Reserve AGW	SB9	6	Test	NJGS	Brunswick lower red
95	3M	Stony Brook-Millstone Reserve AGW	SB11	6	Test	NJGS	Brunswick lower red
96	3M	Stony Brook-Millstone Reserve AGW	SB14	6	Test	NJGS	Brunswick lower red
97	3M	Stony Brook-Millstone Reserve WS	OFW-2	8	Test	NJGS	Brunswick lower red
98	3M	Honey Brook Organic Farm WS	OFHW	6	Domestic	NJGS	Brunswick lower red
99	3M	Honey Brook Organic Farm WS	OFW-1	8	Test	NJGS	Brunswick lower red and lower gray
100	3N	Bristol-Myers Squibb GWI	POW-1	6	Observation	NJGS	Brunswick lower gray
101	3N	Bristol-Myers Squibb GWI	POW-2	6	Observation	NJGS	Brunswick lower gray
102	3N	Bristol-Myers Squibb GWI	TB-1	6	Observation	NJGS	Brunswick lower gray
103	3N	Bristol-Myers Squibb GWI	TB-4	6	Observation	NJGS	Brunswick lower gray
104	3N	Bristol-Myers Squibb GWI	TB-5	6	Observation	NJGS	Brunswick lower gray
105	3O	Pennington Boro WS	OBS-2	6	Observation	NJGS	Brunswick lower gray
106	3P	The Ridge Golf Club WS	CH	6	Public NC	NJGS	Brunswick lower gray
107	3P	The Ridge Golf Club WS	MWA	6	Observation	NJGS	Brunswick lower gray
108	3Q	Snydertown Rd. WS	SRDD	6	Domestic	NJGS	Brunswick lower gray and Lockatong
109	4A	Terhune Orchards WS	Well 1	6	Test	NJGS	Lockatong
110	4A	Terhune Orchards WS	Well 2	8	Test	NJGS	Lockatong
111	4B	Domestic Supply Well	241 Route 12	6	Domestic	NJGS	Lockatong
112	4B	Hilltop Development WS	HT24-24	6	Test	NJGS	Lockatong
113	4B	Hilltop Development WS	HT24-18	6	Test	NJGS	Lockatong
114	4B	Hilltop Development WS	HT24-17	6	Test	NJGS	Lockatong
115	4B	Hilltop Development WS	HT6	6	Test	NJGS	Lockatong
116	4C	29 Pine Hill Rd. AGW	29 Pine Hill Rd.	6	Domestic	NJGS	Lockatong and Stockton
117	4D	Ewingville Rd & Rt31 GWI	EMmw12d	6	Monitoring	NJGS	Stockton
118	4D	Ewingville Rd & Rt31 GWI	EMmw13d	6	Monitoring	NJGS	Stockton
119	4D	Ewingville Rd & Rt31 GWI	EMmw14dd	6	Monitoring	NJGS	Stockton
120	4E	Greenacres County Club WS	OW-1	8	Observation	NJGS	Stockton
121	4E	Greenacres County Club WS	OW-2	6	Observation	NJGS	Stockton
122	4F	Springdale Golf Course WS	IW1	8	Irrigation	NJGS	Stockton
123	4F	Springdale Golf Course WS	IW2	8	Irrigation	NJGS	Stockton
124	4F	Springdale Golf Course WS	MW1	6	Observation	NJGS	Stockton
125	4G	Princeton Plasma Physics GWI	MW-22	6	Monitoring	Secor Intl.	Stockton
126	4G	Princeton Plasma Physics GWI	MW-24	6	Monitoring	Secor Intl.	Stockton
127	4G	Princeton Plasma Physics GWI	MW-28	6	Monitoring	Secor Intl.	Stockton

Abbreviations: AGW - arsenic in ground water, DEM - Digital Elevation Model, GI - Geotechnical investigation, GPS - Global Positioning System,
* approximate location for a well cluster, [1]Below land surface

TABLE AP1. (continued)

County	Municipality	Quadrangle	XY Source	GEOGRAPHIC (degrees) Latitude	Longitude	NAD83 NJSPF X_coord	Y_coord	NGVD88 Land elev (ft)	Elev. Source	Total Depth(ft)[1]	Casing (ft)[1]
Somerset	Bedminster	Gladstone, NJ	Map	40.0319501	73.8911383	437135.69	662609.52	225.25	DEM	333.0	19.3
Somerset	Bedminster	Gladstone, NJ	Map	40.0346112	73.8952620	438097.15	661448.27	187.16	DEM	97.6	41.5
Somerset	Bedminster	Gladstone, NJ	Map	40.0347871	73.8918457	438167.72	662404.38	185.67	DEM	243.6	50.8
Mercer	Hopewell Boro	Hopewell, NJ	GPS	39.9852041	74.2371006	419634.40	565788.27	180.00	MAP	402.7	27.5
Mercer	Hopewell Boro	Hopewell, NJ	GPS	39.9852311	74.2371015	419644.23	565787.99	170.00	MAP	400.0	44.6
Mercer	Hopewell Boro	Hopewell, NJ	GPS	39.9849321	74.2362354	419536.03	566030.97	180.00	MAP	300.0	51.5
Mercer	Hopewell Boro	Hopewell, NJ	GPS	39.9817463	74.2390144	418373.33	565255.70	215.00	MAP	105.0	34.9
Mercer	Hopewell Boro	Hopewell, NJ	GPS	39.9822532	74.2403494	418556.87	564881.10	193.00	DEM	72.0	14.4
Mercer	Hopewell Boro	Hopewell, NJ	GPS	40.3932450	74.7579150	420290.00	568264.12	177.00	DEM	199.0	20.1
Mercer	Hopewell Boro	Hopewell, NJ	GPS	40.3939790	74.7571750	420496.99	568530.86	181.00	DEM	192.8	25.2
Hunterdon	East Amwell	Hopewell, NJ	MAP	40.4408584	74.8585932	392319.38	585706.44	262.00	Map	314.0	19.7
Middlesex	South Plainfield	Plainfield, NJ	GPS	40.2338653	74.0126721	510476.00	628176.00	103.35	DEM	99.0	25.7
Middlesex	South Plainfield	Plainfield, NJ	GPS	40.2360773	74.0125237	511282.00	628213.00	101.36	DEM	109.0	25.4
Middlesex	South Plainfield	Plainfield, NJ	GPS	40.2366887	74.0103665	511508.00	628814.00	95.16	DEM	114.0	25.6
Somerset	Somerset	Raritan, NJ	Map	40.0376831	74.0051844	439026.11	630664.25	105.05	MAP	161.7	22.6
Somerset	Somerset	Raritan, NJ	Map	40.0403593	74.0061734	439999.40	630381.92	69.44	MAP	99.3	22.0
Somerset	Somerset	Raritan, NJ	Map	40.0442549	74.0013954	441425.85	631711.70	89.00	MAP	86.0	26.6
Somerset	Somerset	Raritan, NJ	Map	40.0438828	74.0018208	441289.65	631593.36	88.00	MAP	92.8	19.8
Somerset	Somerset	Raritan, NJ	Map	40.0422735	74.0011516	440704.50	631783.98	81.96	MAP	198.4	69.2
Somerset	Somerset	Raritan, NJ	Map	40.0412186	74.0031495	440317.12	631226.79	80.30	MAP	122.7	64.2
Hunterdon	Raritan	Hopewell, NJ	GPS	39.9138643	74.1291829	393756.47	596134.37	202.26	DEM	394.0	50.4
Hunterdon	Raritan	Hopewell, NJ	GPS	39.9150252	74.1291437	394179.39	596143.61	211.75	DEM	296.0	56.0
Hunterdon	Raritan	Hopewell, NJ	GPS	39.9171783	74.1245455	394969.04	597430.05	206.22	DEM	178.0	40.2
Hunterdon	Raritan	Hopewell, NJ	Map	39.9312613	74.1204691	400103.54	598551.56	155.00	MAP	195.0	58.5
Mercer	Hopewell	Pennington, NJ	GPS	40.3450575	74.8105410	405571.00	550757.88	223.00	GPS	293.0	48.2
Mercer	Hopewell	Hopewell, NJ	GPS	39.9797880	74.2728721	417634.03	555770.25	166.89	DEM	152.0	21.0
Mercer	Hopewell	Hopewell, NJ	GPS	39.9805987	74.2726821	417929.47	555822.75	168.42	DEM	148.5	20.9
Mercer	Hopewell	Hopewell, NJ	GPS	39.9797685	74.2725267	417627.19	555867.06	155.10	DEM	189.0	18.6
Mercer	Hopewell	Hopewell, NJ	GPS	39.9803370	74.2735653	417833.50	555575.50	157.00	DEM	148.5	17.5
Mercer	Hopewell	Hopewell, NJ	GPS	39.9798856	74.2739618	417668.81	555464.81	163.23	DEM	146.5	25.0
Mercer	Hopewell	Hopewell, NJ	GPS	40.3593940	74.7684970	417305.24	555941.92	171.00	DEM		
Mercer	Hopewell	Hopewell, NJ	GPS	39.9803307	74.2727983	417831.78	555790.44	161.20	DEM	370.0	58.5
Mercer	Hopewell	Hopewell, NJ	GPS	39.9803754	74.2742856	417846.99	555373.64	169.00	DEM	395.0	68.0
Mercer	Hopewell	Hopewell, NJ	GPS	39.9821135	74.2758906	418478.97	554922.29	158.00	DEM	207.0	69.7
Mercer	Hopewell	Hopewell, NJ	GPS	39.9826013	74.2772170	418655.72	554550.19	163.00	DEM	600.0	124.0
Mercer	Hopewell	Pennington, NJ	GPS	39.9722499	74.2931797	414874.46	550086.08	145.64	DEM	335.0	49.9
Mercer	Hopewell	Pennington, NJ	GPS	39.9731079	74.2986592	415183.46	548549.74	159.58	DEM	440.0	50.5
Mercer	Hopewell	Pennington, NJ	GPS	39.9740105	74.2867373	415520.00	551890.00	180.31	DEM	302.0	18.2
Mercer	Hopewell	Pennington, NJ	GPS	39.9824170	74.2898517	418580.00	551010.00	209.74	DEM	297.0	21.5
Mercer	Hopewell	Pennington, NJ	GPS	39.9762539	74.2846718	416338.54	552466.89	196.12	DEM	274.0	17.1
Mercer	Pennington	Pennington, NJ	GPS	39.9582072	74.3098755	409749.00	545418.00	200.00	GPS	298.0	49.4
Hunterdon	East Amwell	Hopewell, NJ	GPS	40.4436100	74.8219400	402524.58	586669.50	242.00	MAP	560.0	56.2
Hunterdon	East Amwell	Hopewell, NJ	GPS	40.4458300	74.8280600	400824.30	587484.47	139.00	MAP	555.0	52.7
Hunterdon	East Amwell	Hopewell, NJ	GPS	40.3948300	74.8269500	401064.48	568905.18	342.42	DEM	478.0	51.7
Mercer	Lawrence	Princeton, NJ	GPS	40.0106200	74.3225724	428833.00	541821.00	180.45	DEM	402.0	48.8
Mercer	Lawrence	Princeton, NJ	GPS	40.0079273	74.3228757	427852.00	541738.00	187.02	DEM	484.0	48.3
Hunterdon	Raritan	Pittstown, NJ	GPS	39.8901642	74.0805706	385184.17	609810.08	389.12	DEM	700.0	48.9
Hunterdon	Raritan	Pittstown, NJ	GPS	39.8898258	74.0787269	385063.32	610327.98	431.30	DEM	516.0	45.0
Hunterdon	Raritan	Pittstown, NJ	GPS	39.8878562	74.0767849	384348.51	610876.26	450.47	DEM	291.0	49.0
Hunterdon	Raritan	Pittstown, NJ	GPS	39.8876016	74.0772645	384255.12	610742.14	450.57	DEM	256.9	46.4
Hunterdon	Raritan	Pittstown, NJ	GPS	39.8843129	74.0777503	383056.60	610611.49	469.42	DEM	494.1	48.2
Hunterdon	Delaware	Stockton, NJ	Map	40.4551039	74.9964407	362330.00	591036.00	411.00	MAP	395.6	49.1
Mercer	Ewing	Pennington, NJ	SURVEY	39.9689957	74.3804627	413644.36	525626.73	132.81	SURVEY	361.0	52.3
Mercer	Ewing	Pennington, NJ	SURVEY	39.9689709	74.3795106	413635.67	525893.57	136.18	SURVEY	354.0	48.6
Mercer	Ewing	Pennington, NJ	SURVEY	39.9694125	74.3796441	413796.47	525855.93	139.80	SURVEY	68.0	20.0
Mercer	Lawrence	Princeton, NJ	GPS	40.2769700	74.7263900	428962.00	525885.00	79.00	MAP	66.5	26.0
Mercer	Lawrence	Princeton, NJ	GPS	40.2761000	74.7264300	428950.00	525568.00	79.00	MAP	87.0	18.5
Mercer	Princeton	Princeton, NJ	GPS	40.0609909	74.2960729	447196.59	549201.28	127.15	DEM	352.0	43.1
Mercer	Princeton	Princeton, NJ	GPS	40.0612208	74.2965596	447280.03	549064.86	130.82	DEM	486.4	49.5
Mercer	Princeton	Princeton, NJ	GPS	40.0622153	74.2980332	447641.32	548651.60	111.95	DEM	492.0	51.1
Middlesex	Plainsboro	Hightstown, NJ	Map	40.0960176	74.2949487	459955.97	549486.52	97.69	DEM	85.0	24.5
Middlesex	Plainsboro	Hightstown, NJ	Map	40.0971045	74.2899032	460355.19	550897.03	108.78	DEM	50.0	28.0
Middlesex	Plainsboro	Hightstown, NJ	Map	40.0961881	74.2923956	460019.73	550200.60	106.00	DEM	91.0	26.2

GWI - Ground-water contaminant investigation, WS- Water Supply , NAD83 NJSPF - 1983 North American Datum New Jersey State Plane Coordinate Feet
NGVD88 -National Geodetic Vertical Datum 1988

Appendixes 1 to 4, Figures

Appendix 2 List of Figures (continued)

Appendix 3 List of Figures (continued) figure and page

Appendix 3 List of Figures (continued)

APPENDIX 4. Lockatong and Stockton

Appendix 4 List of Figures (continued)

Summary of Borehole Geophysical Studies in the Newark Basin, New Jersey:

Diabase and Brunswick Basalt in the Watching Zone

By Gregory C. Herman and John F. Curran, N.J. Geological Survey

Appendix 1 of

Contributions to the Geology and Hydrogeology of the Newark Basin

N.J. Geological Survey Bulletin 77

State of New Jersey
N.J. Department of Environmental Protection
Water Resource Management
N.J. Geological Survey
2010

Well 1 – Diabase

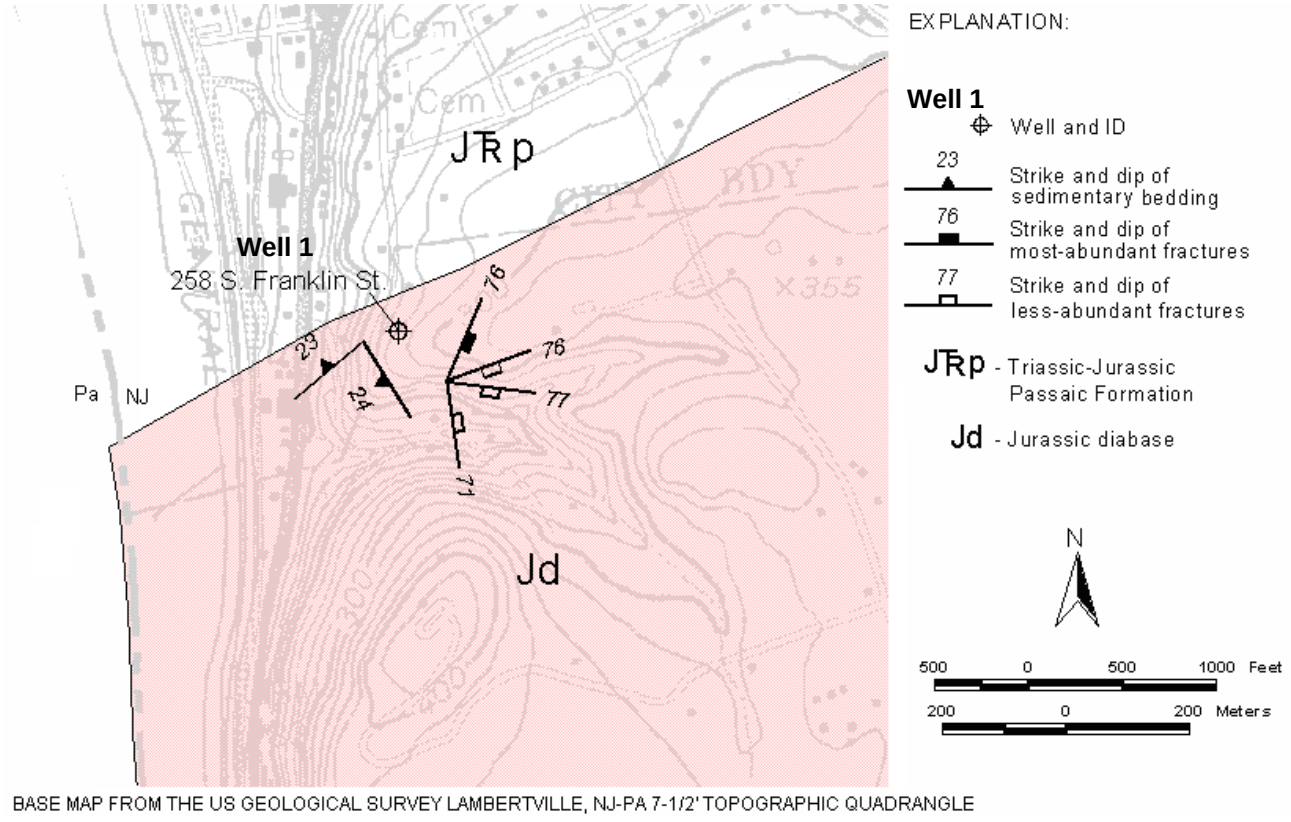

BASE MAP FROM THE US GEOLOGICAL SURVEY LAMBERTVILLE, NJ-PA 7-1/2' TOPOGRAPHIC QUADRANGLE

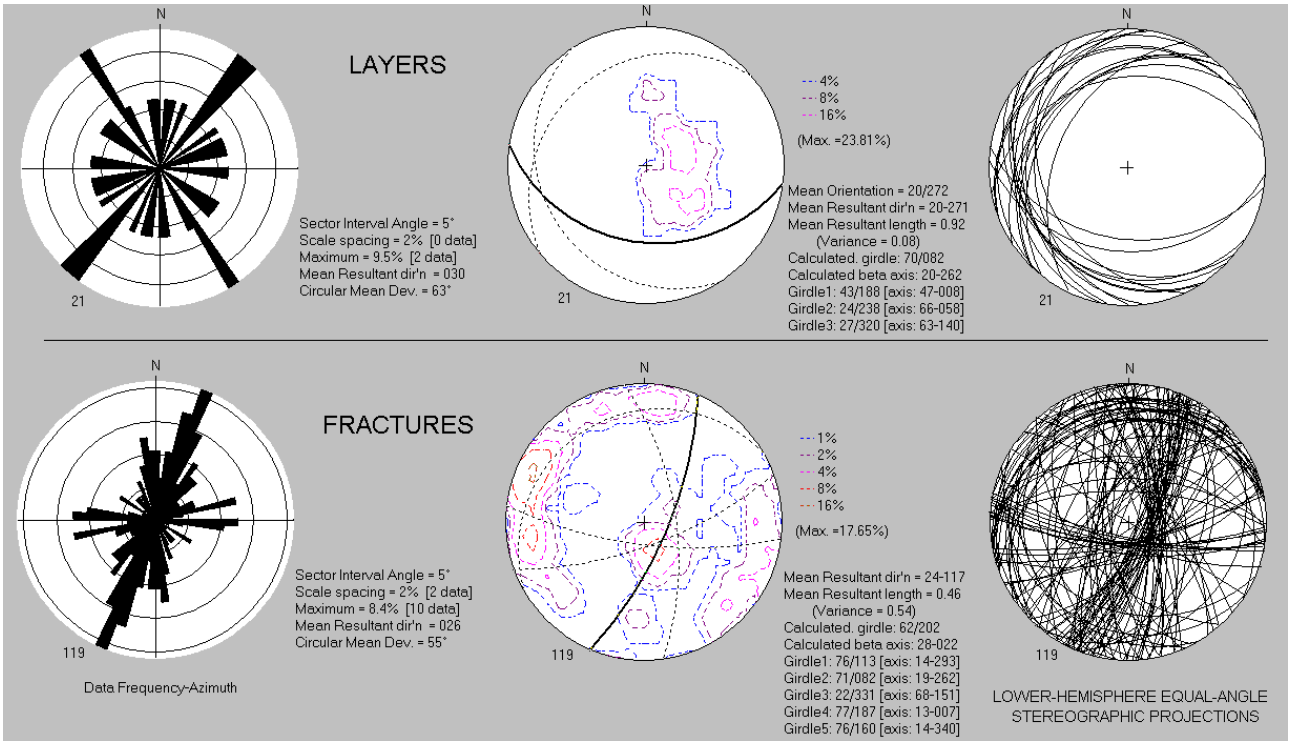

Figure 1A1. Map (above) shows well 1 at 258 South Franklin St., Lambertville, Hunterdon County, NJ. Mapped bedrock structures based on a structural analysis (below) of the OPTV record. Note that topographic ridges and streams parallel structural trends.

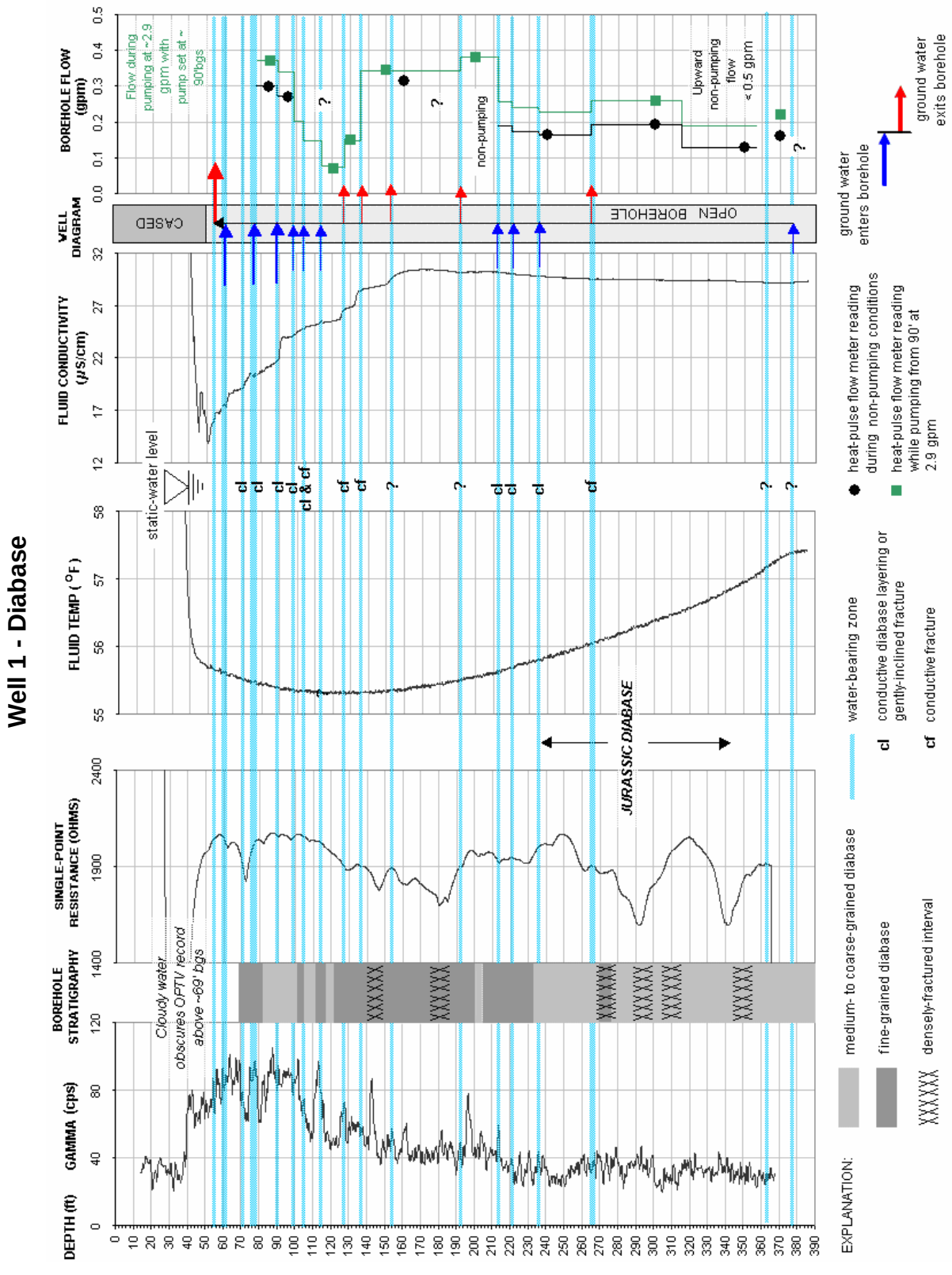

FIGURE 1A2. Hydrogeologic section based on geophysical logs for well 1 showing the vertical distribution and types of hydraulically-conductive features and water-bearing zones. Depth values are in feet below land surface.

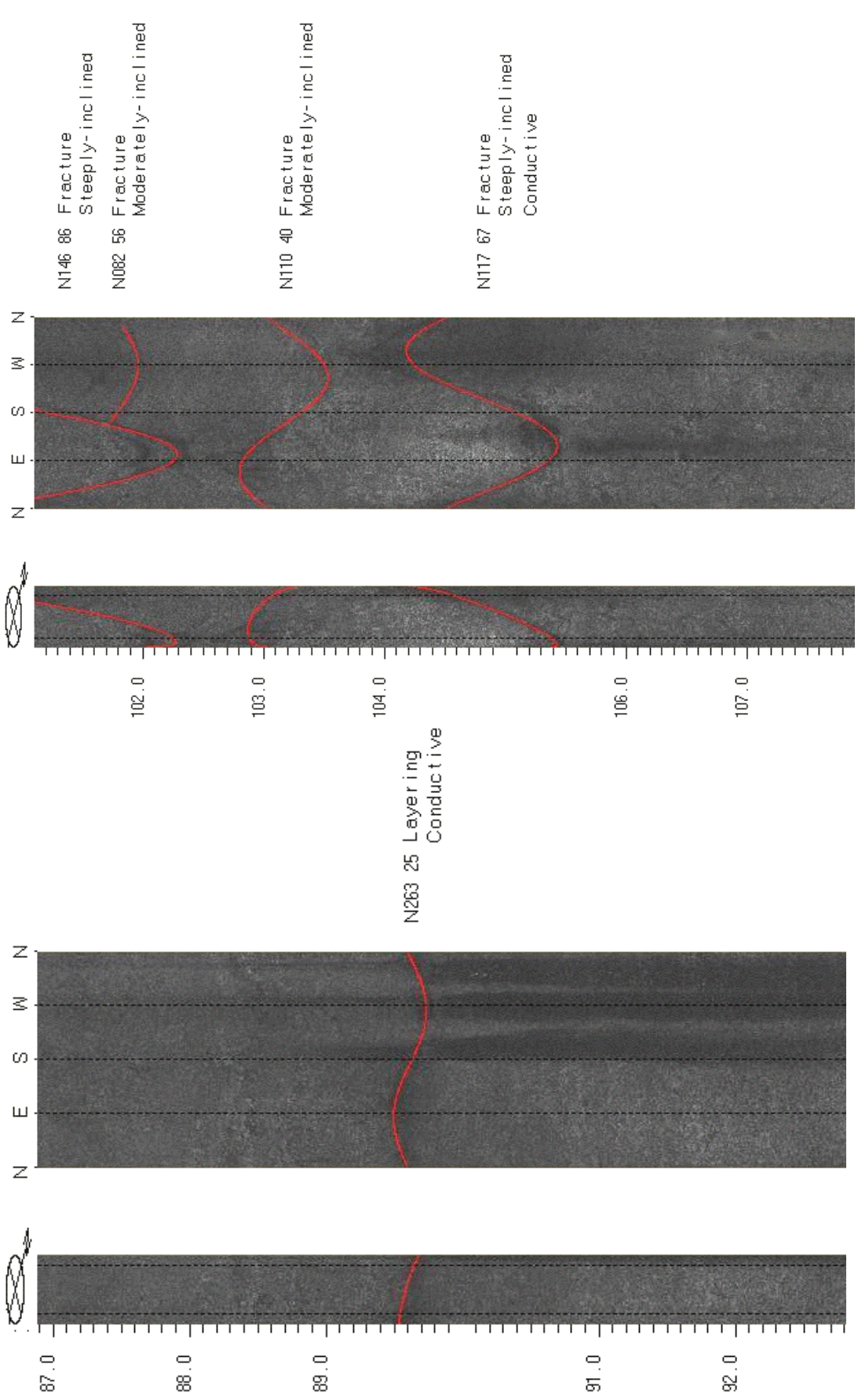

FIGURE 1A3. OPTV records of the 6-inch diameter well 1showing bedrock structures and hydraulically-conductive features in diabase. Mineral deposits seen as dark stains on the borehole wall emanate from conductive features and taper off in the direction of water flow. Upward-tapering stains are less pronounced than downward ones, indicating upward non-pumping cross flows are less than pumping-induced downward flows where the conductive features occur above the pump depth. Depth values are in feet below land surface.

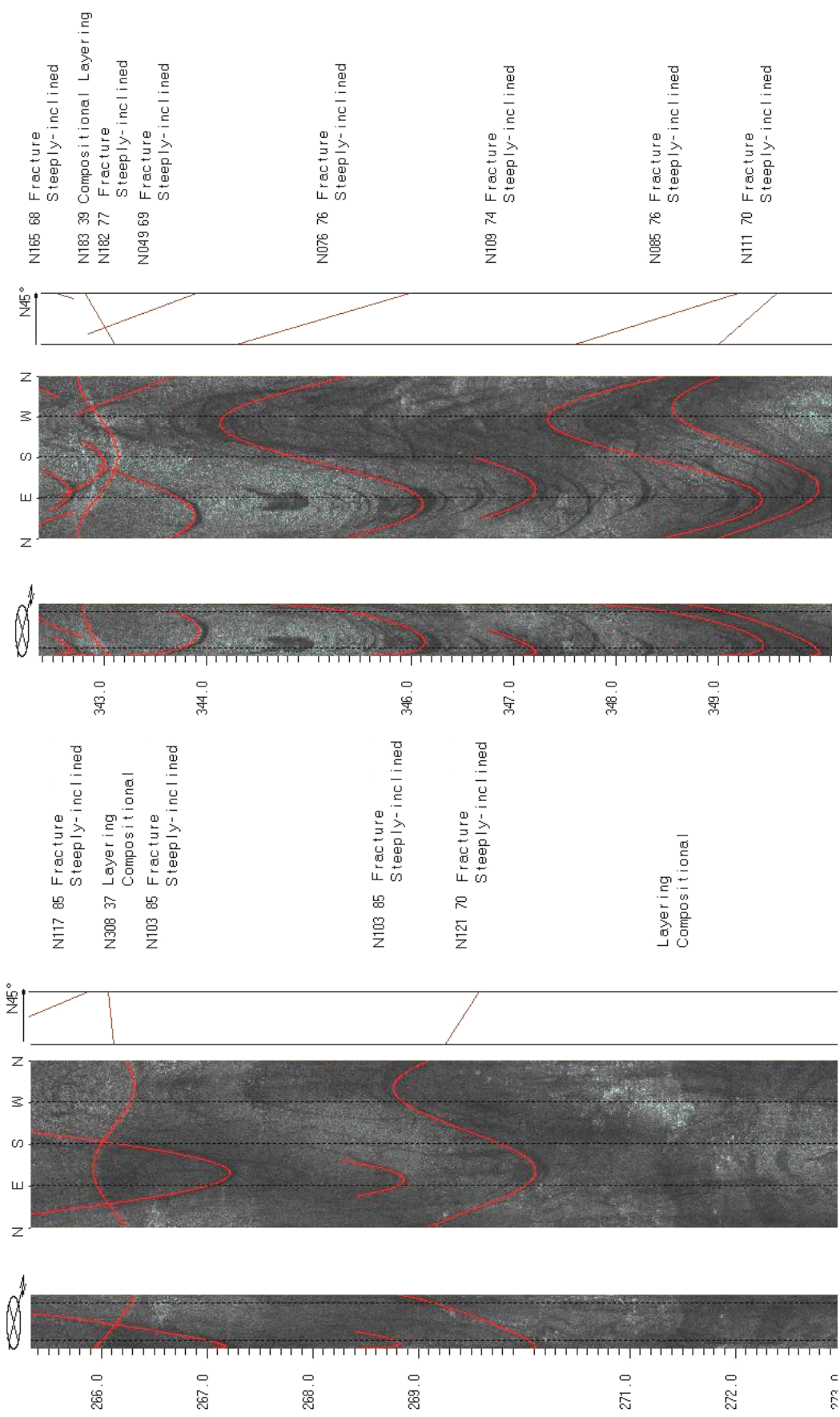

FIGURE 1A4. OPTV records of the 6-inch diameter well 1 showing bedrock structures in diabase. Depth values are in feet below land surface.

Wells 2 to 5 – Diabase overlying the Brunswick lower gray zone and Lockatong aquifers

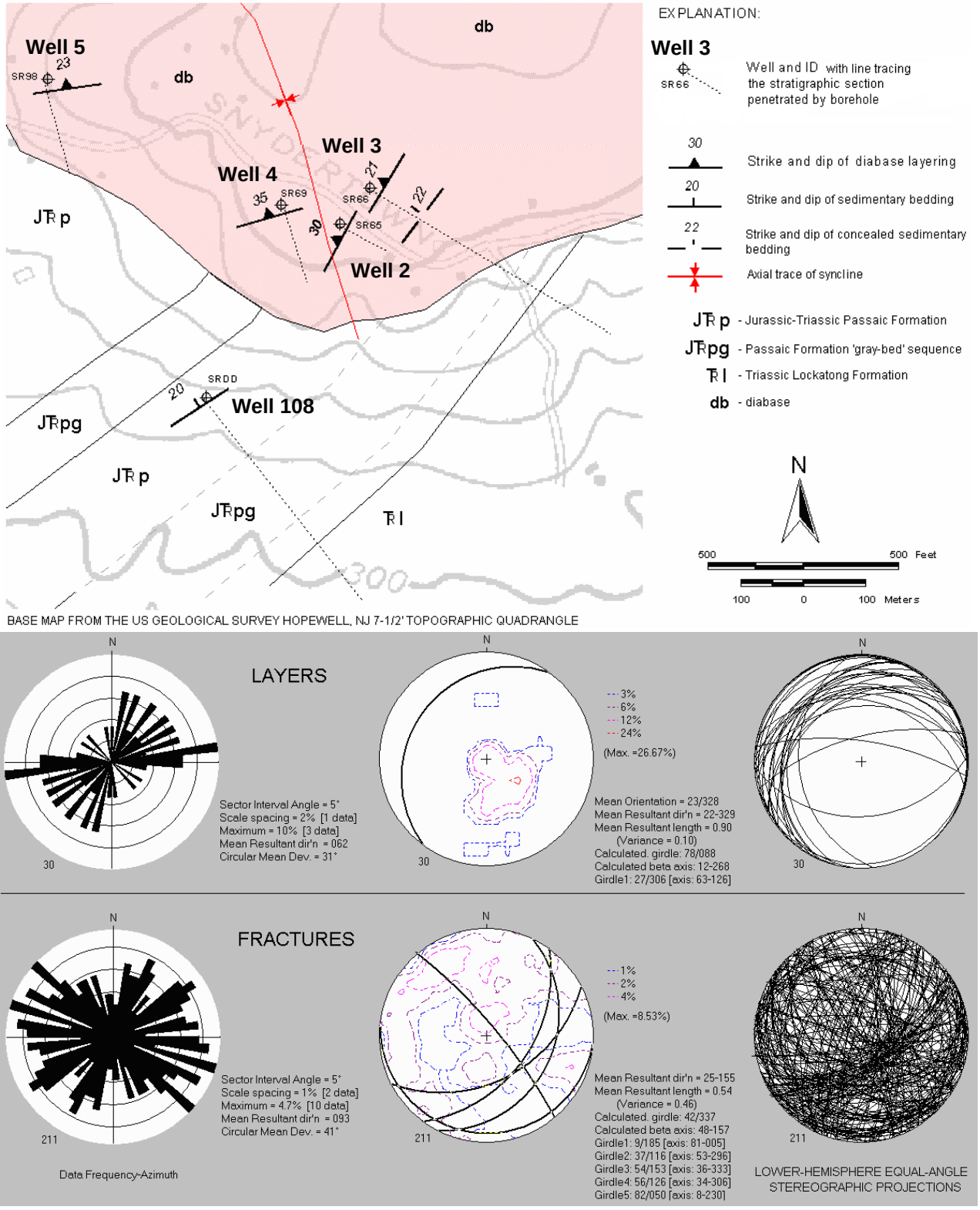

Figure 1B1. Map (above) shows wells 2 through 5 and 112 along Snydertown Rd., East Amwell Twp., Hunterdon Country, NJ. Mapped bedrock structures are based on a structural analysis (bottom) of the OPTV records. Hydrogeologic analysis of well 108 is in appendix entry 3Q.

Wells 2 to 5 – Diabase overlying the Brunswick lower gray zone and Lockatong aquifers

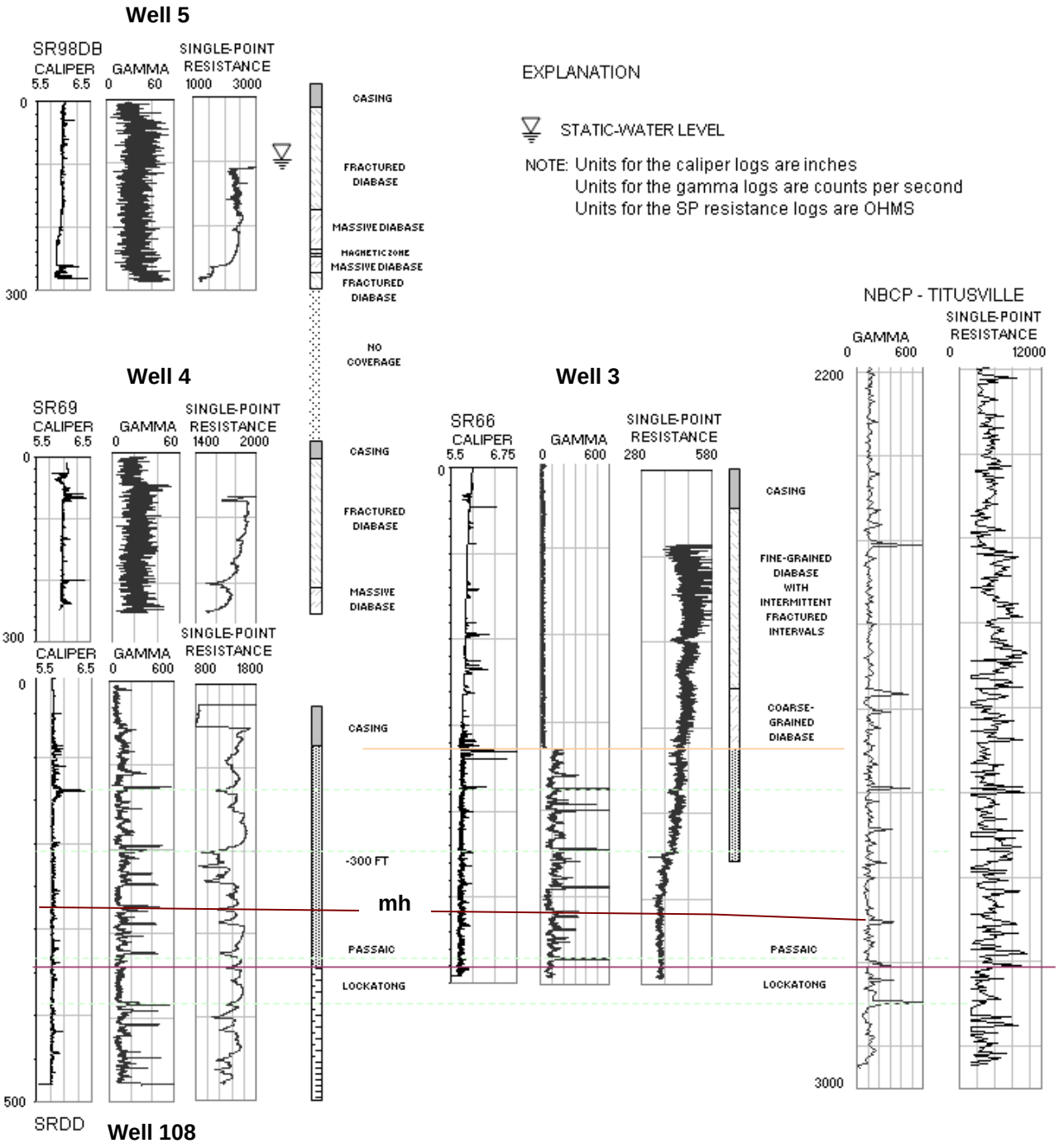

FIGURE 1B2. Stratigraphic section based on geophysical logs for wells 3, 4, 5 and 108 showing diabase overlying the Passaic and Lockatong Formations. Wells 3 and 108 are correlated with the Titusville core hole of Olsen and others (1996) using natural gamma and electrical resistance logs. Depth values are in feet below land surface. Marker horizon (mh) shown using OPTV records in figure 3Q3.

Well 3 – Diabase overlying Brunswick lower gray zone and Lockatong aquifers

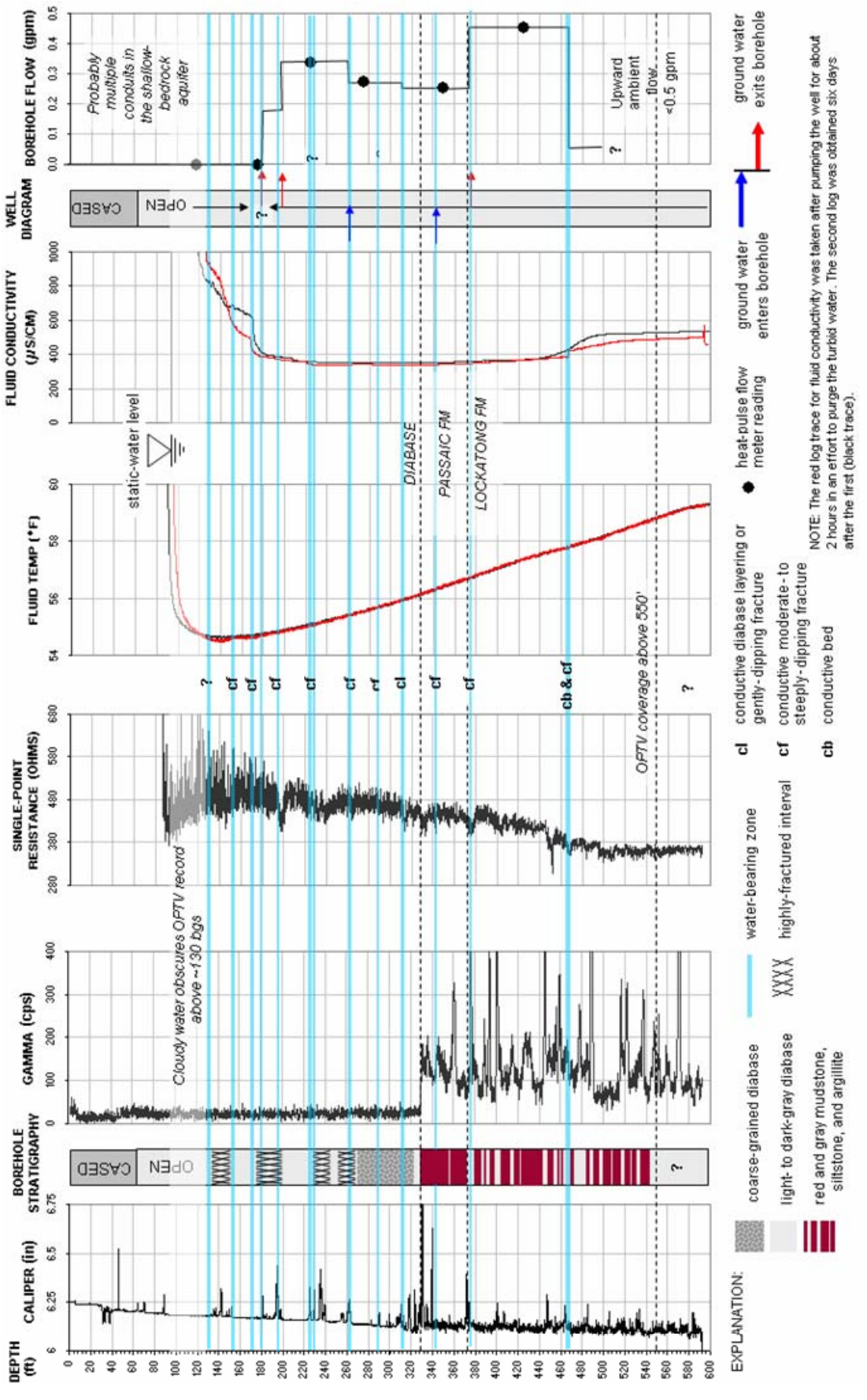

FIGURE 1B3. Hydrogeologic section based on geophysical logs for well 3 showing the vertical distribution and types of hydraulically-conductive features and water-bearing zones in diabase, the lower gray zone of the Brunswick aquifer and the Lockatong aquifer, Depth values are in feet below land surface.

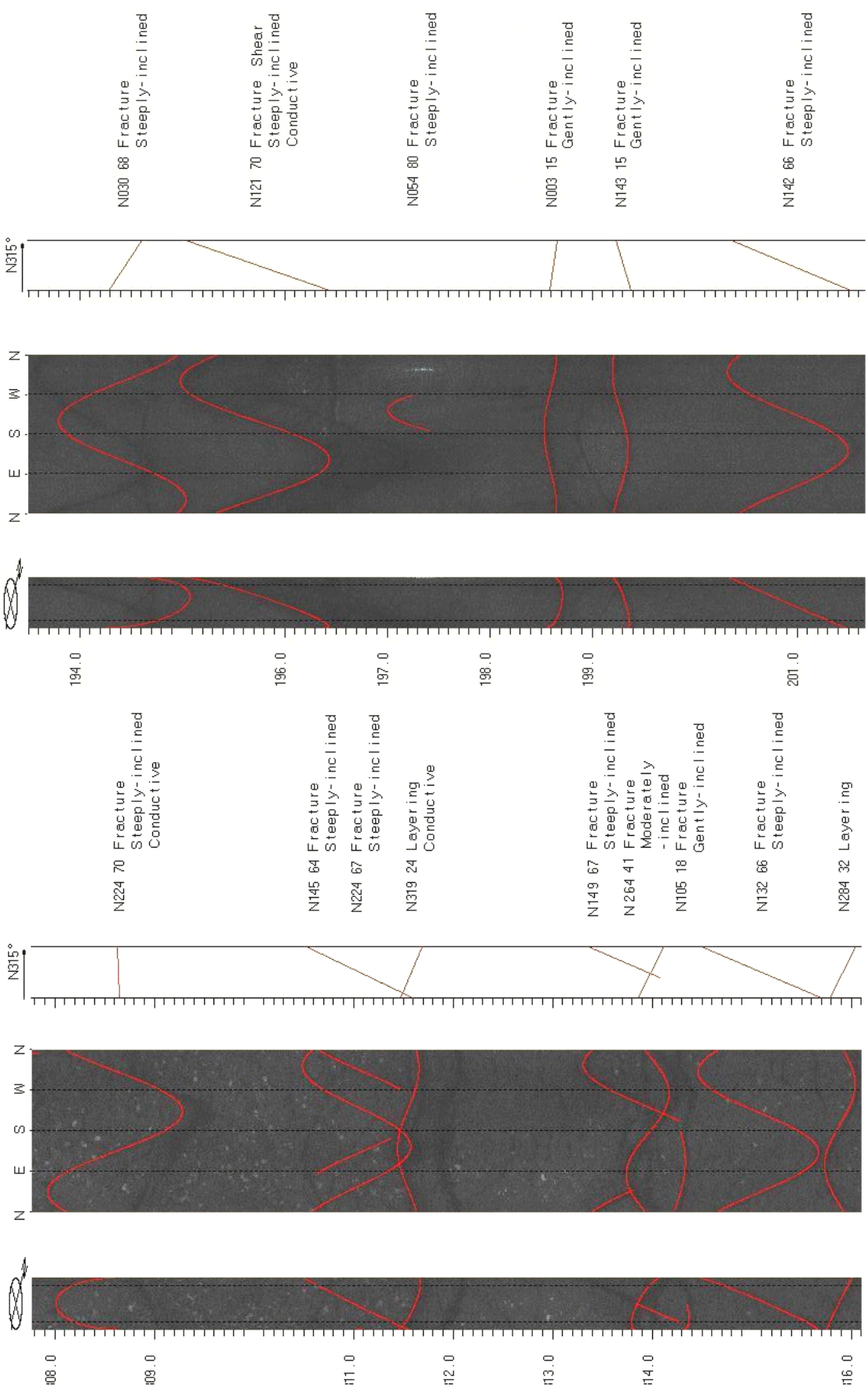

FIGURE 1B4. OPTV records of the 6-inch diameter well 3 showing bedrock structures and hydraulically-conductive features in diabase. Depth values are in feet below land surface.

Well 4 - Diabase

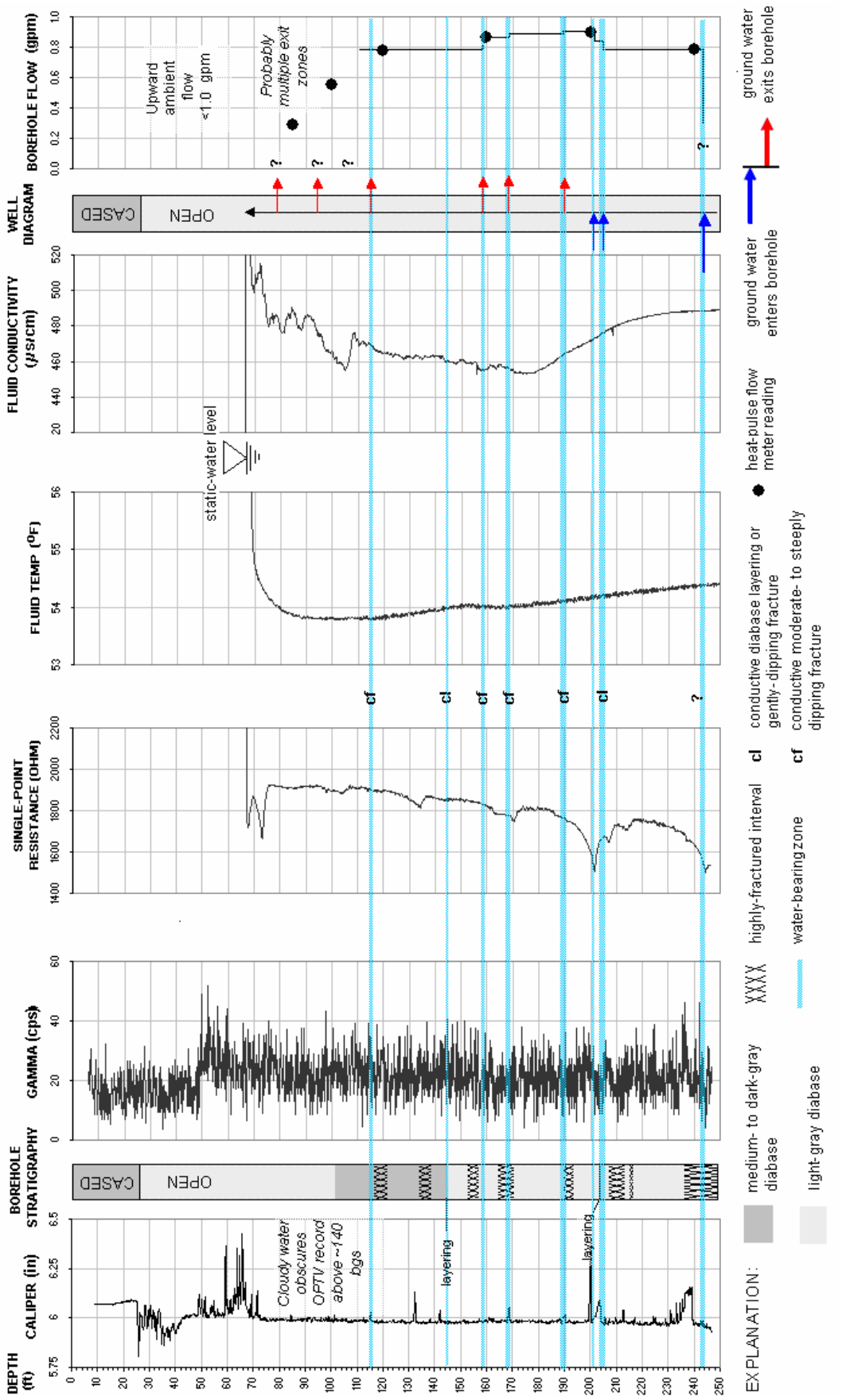

FIGURE 1B5. Hydrogeologic section based on geophysical logs for well 4 showing the vertical distribution and types of hydraulically-conductive features and water-bearing zones in diabase. Depth values are in feet below land surface.

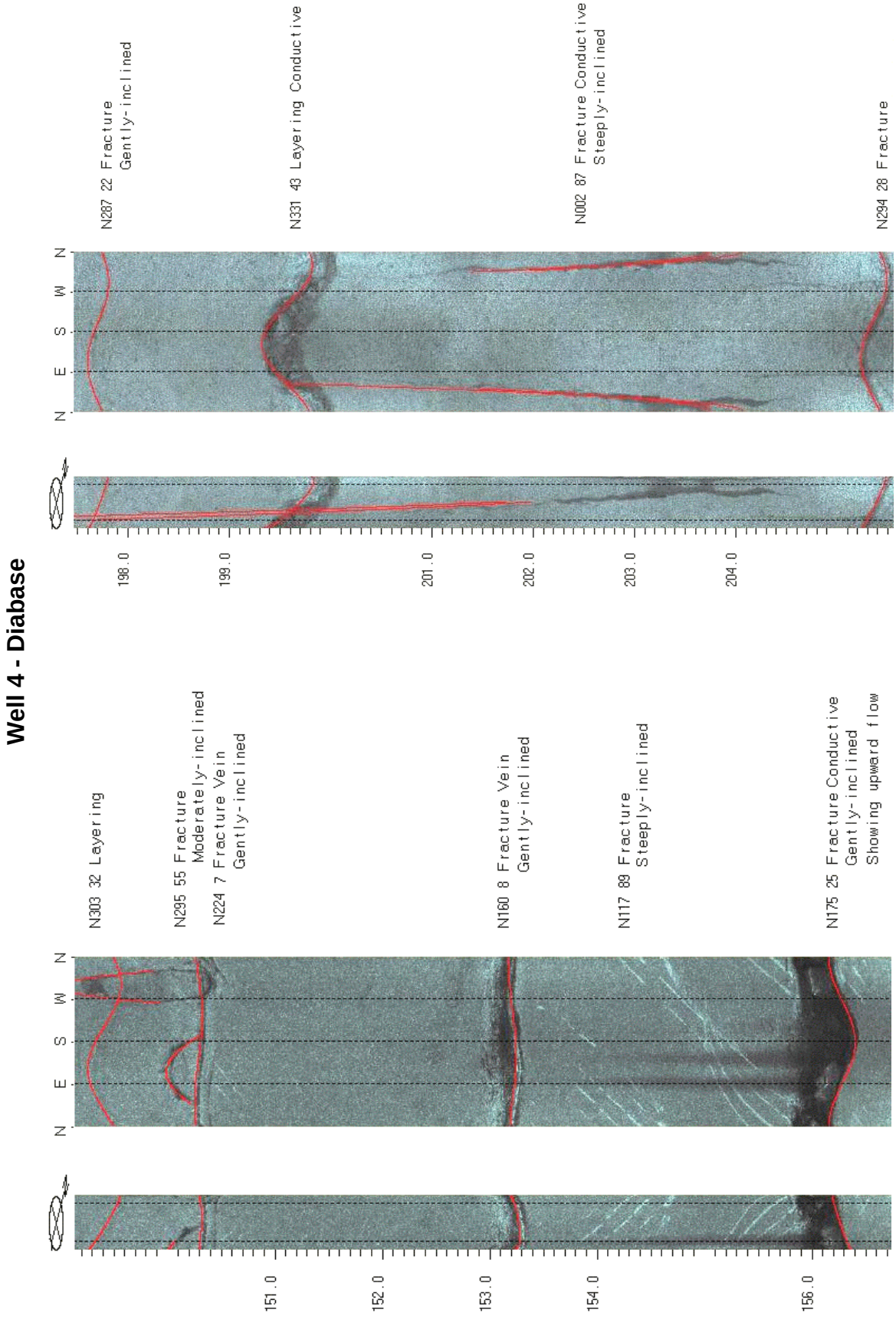

FIGURE 1B6. OPTV records of the 6-inch diameter well 4 showing bedrock structures and hydraulically-conductive features in diabase. Mineral deposits seen as dark stains on the borehole wall (left) emanate from a conductive layer and taper upward in the direction of water flow. These stains indicate upward, non-pumping cross flows that are confirmed by HPFM readings (fig. 1B5). Depth values are in feet below land surface.

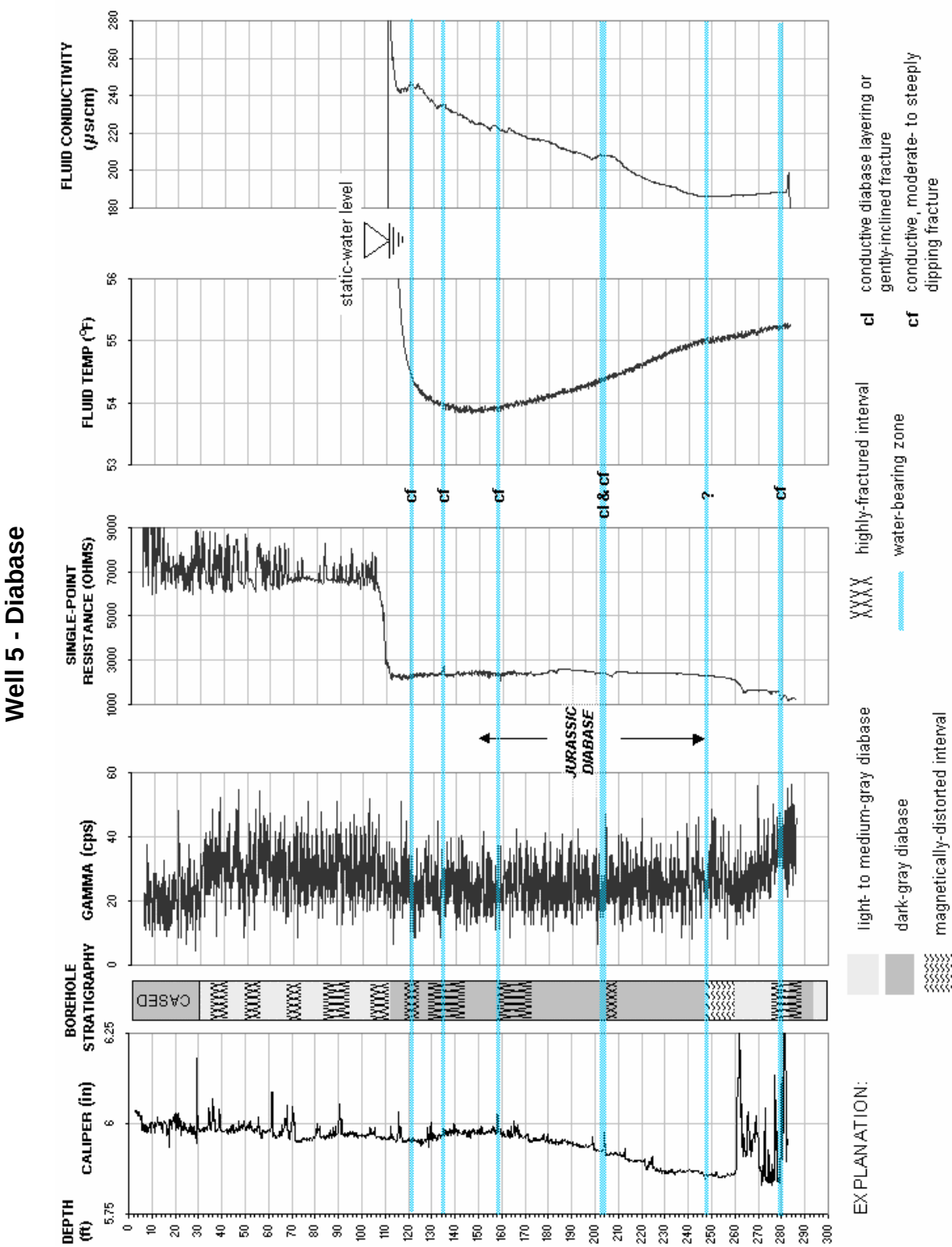

FIGURE 1B7. Hydrogeologic section based on geophysical logs for well 5 showing the vertical distribution and types of hydraulically-conductive features and water-bearing zones in diabase. Depth values are in feet below land surface.

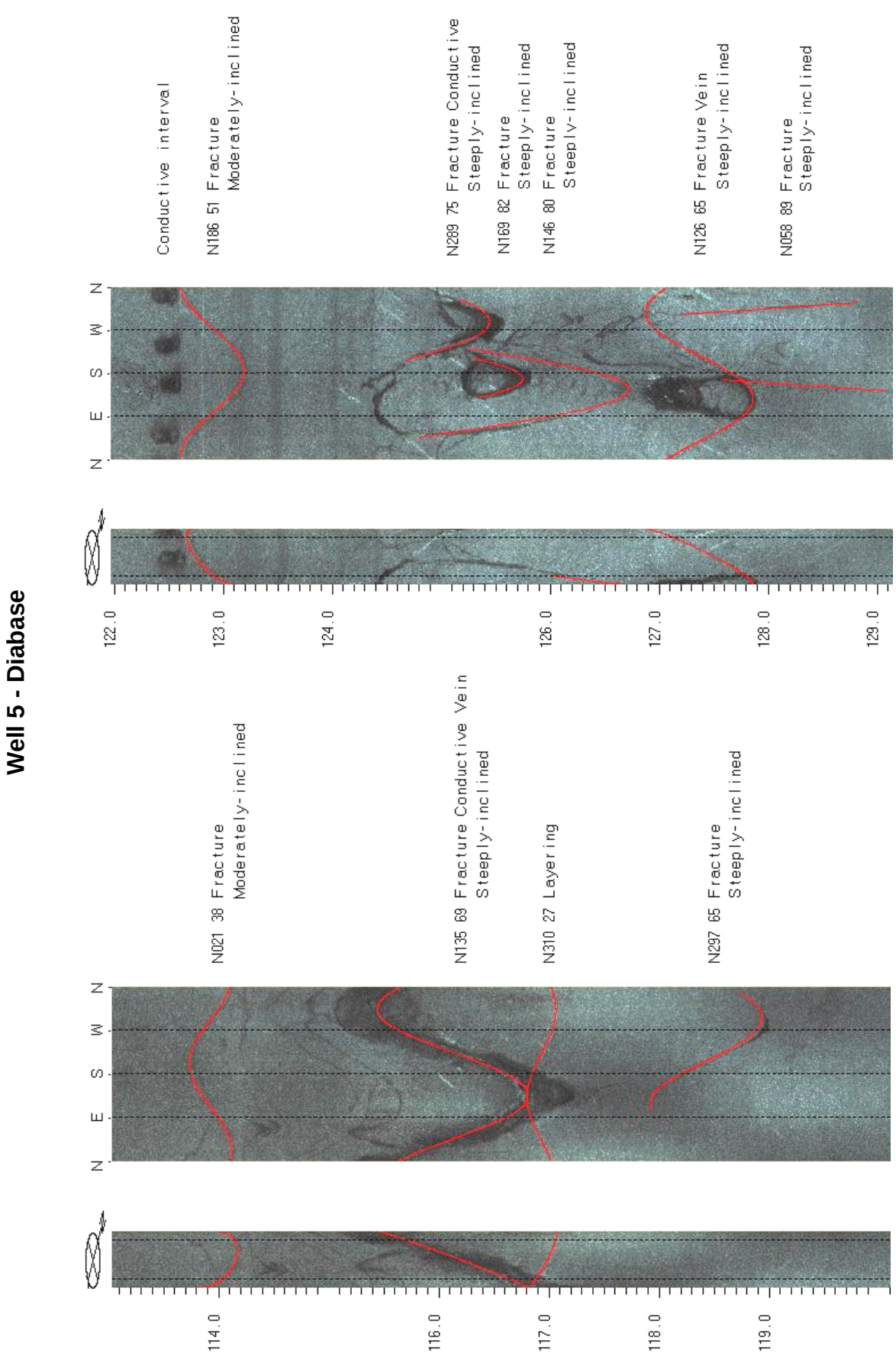

FIGURE 1B8. OPTV records of the 6-inch diameter well 5 showing bedrock structures and hydraulically-conductive features in diabase. Depth values are in feet below land surface.

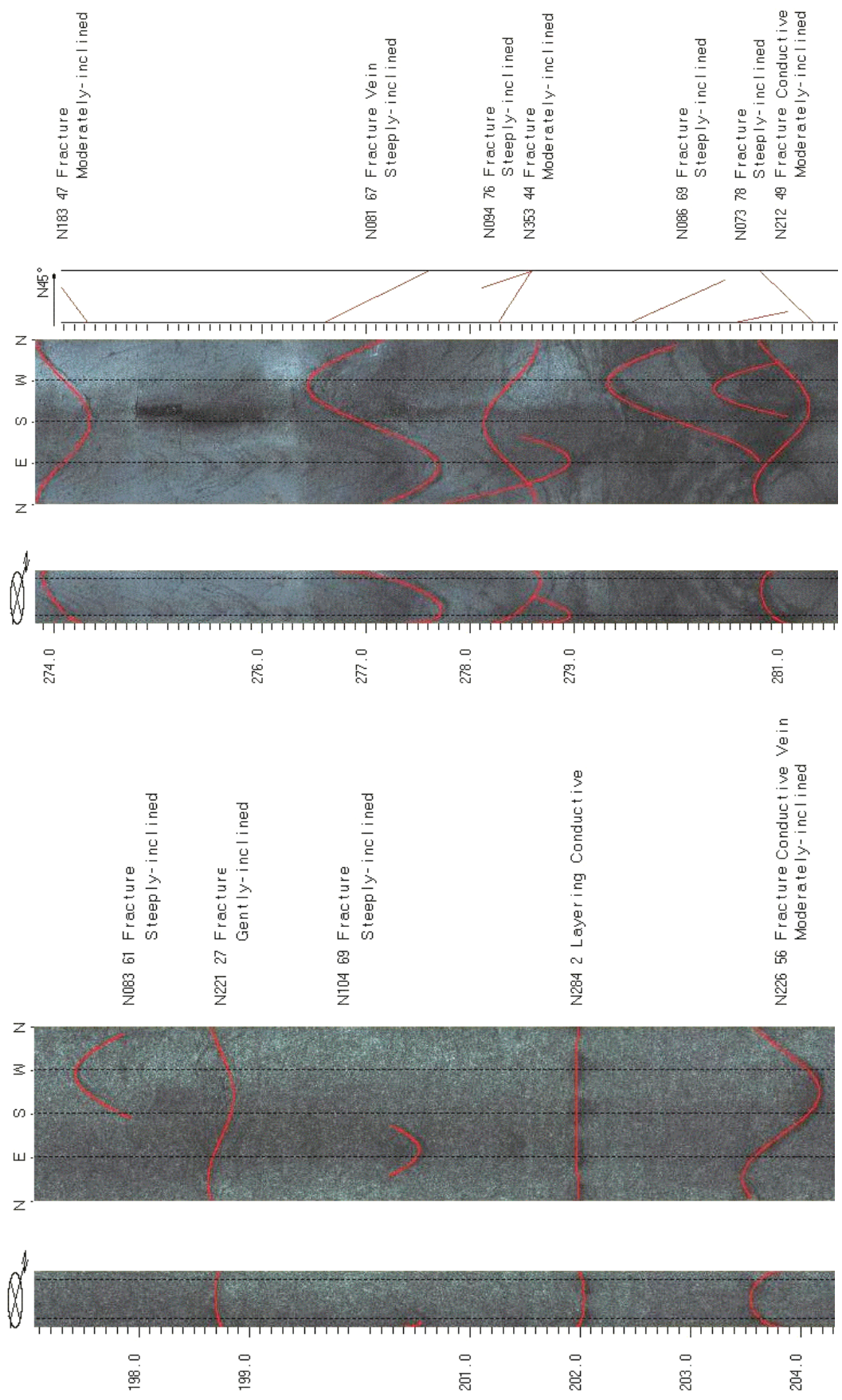

FIGURE 1B9. OPTV records of the 6-inch diameter well 5 showing bedrock structures and hydraulically-conductive features in diabase. Depth values are in feet below land surface.

Well 6 - Diabase

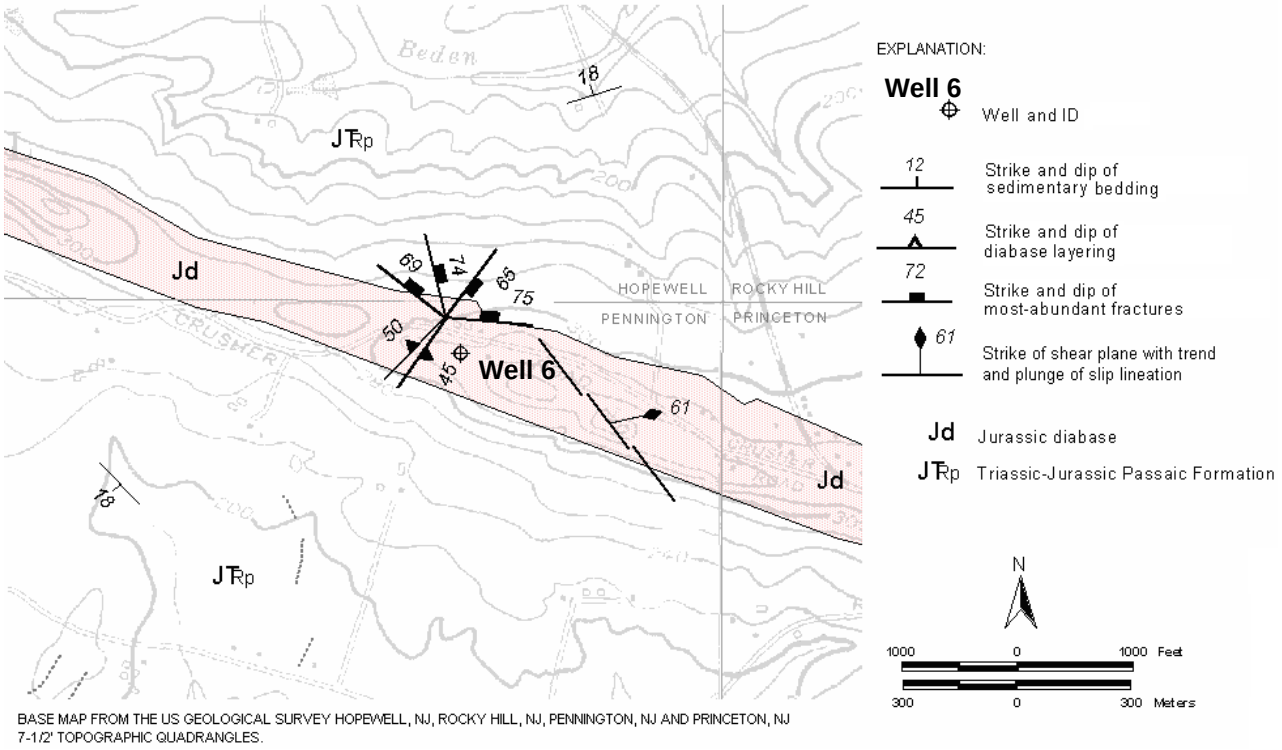

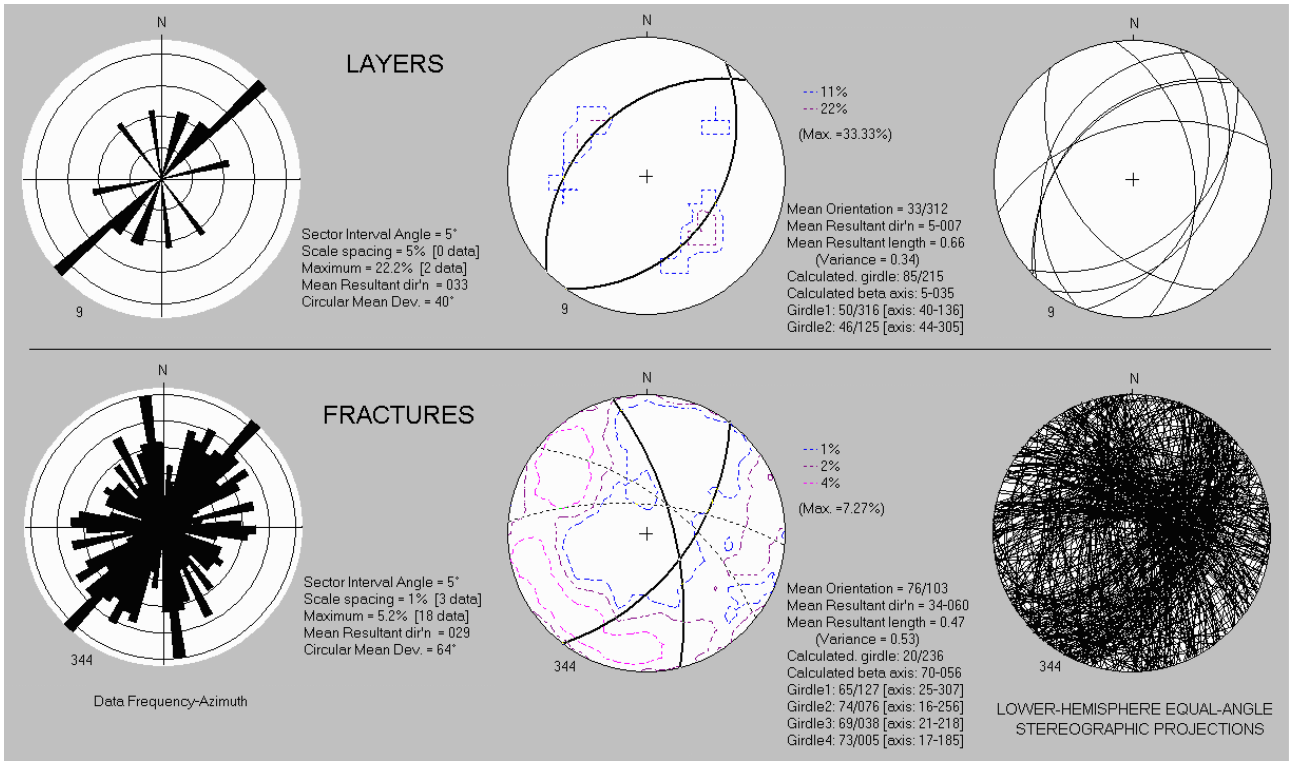

Figure 1C1. Map (above) shows well 6 at 65 Crusher Rd., Hopewell Twp., Mercer County, NJ. Mapped bedrock structures are based on a structural analysis (bottom) of the OPTV record.

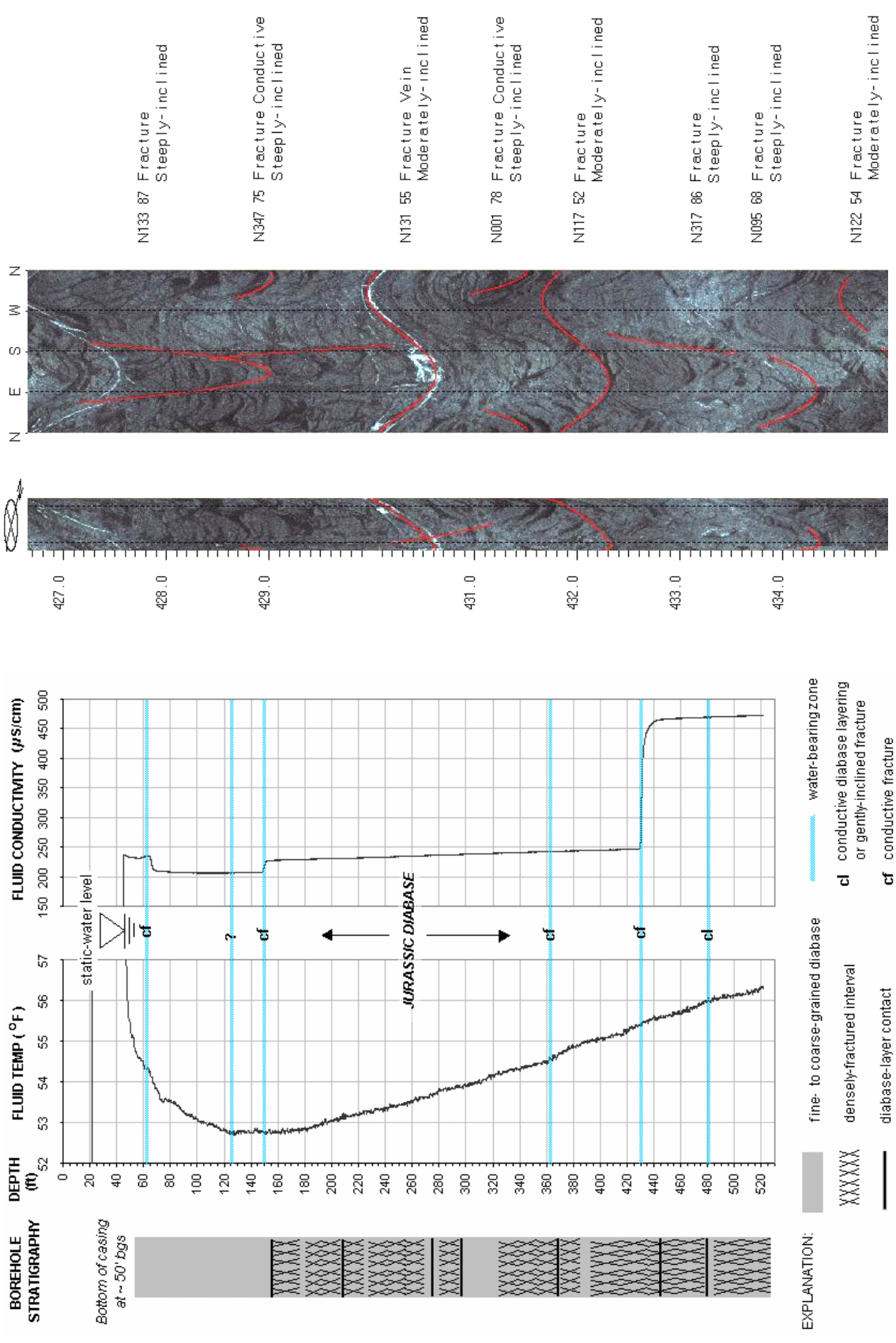

FIGURE 1C2. Hydrogeologic section based on geophysical logs for well 6 (left) shows the vertical distribution and types of hydraulically-conductive features and water-bearing zones in diabase. OPTV record (right) of the 6-inch diameter well shows bedrock structures in diabase. Depth values are in feet below land surface.

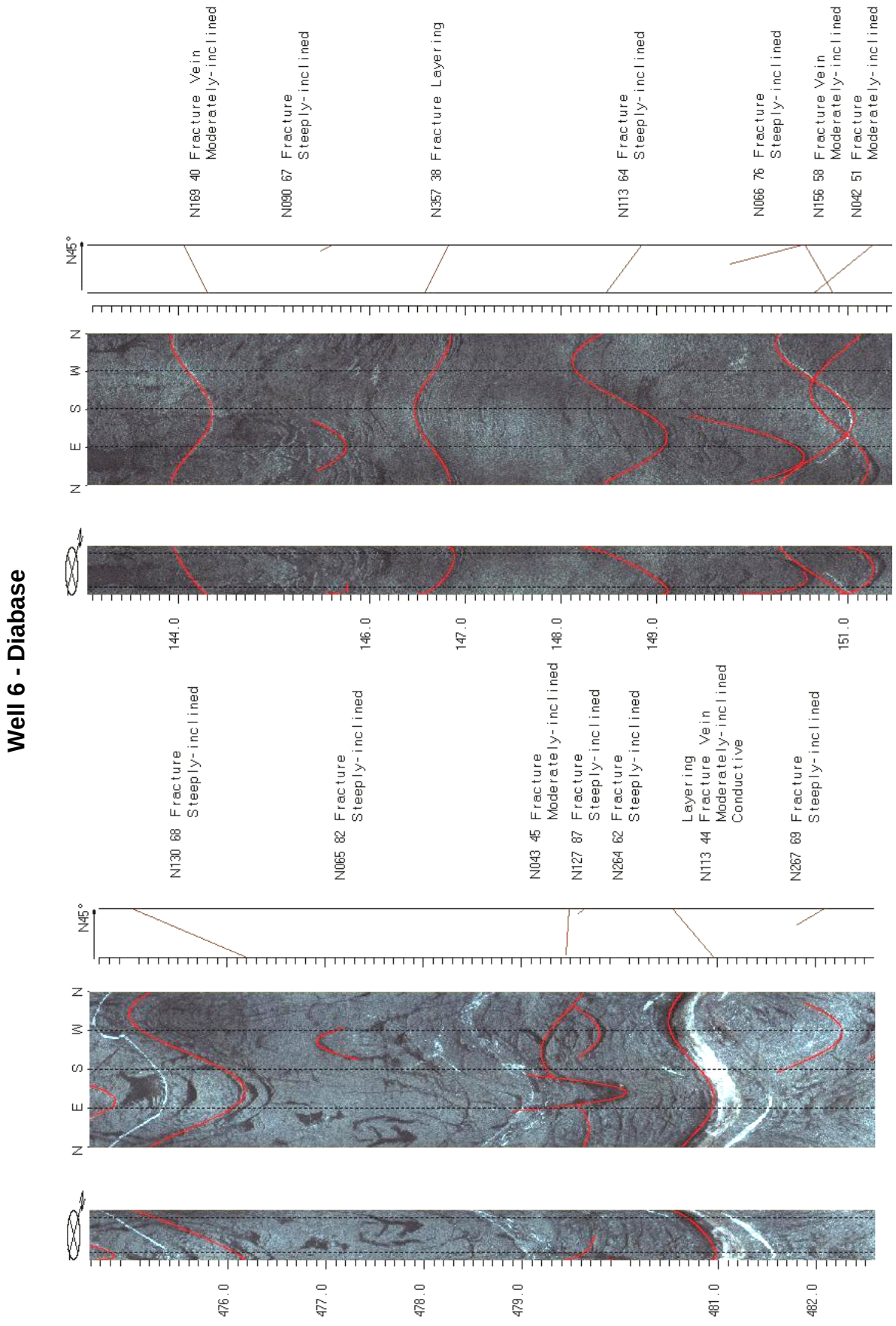

FIGURE 1C3. OPTV records of the 6-inch diameter well 6 showing bedrock structures and hydraulically-conductive features in diabase. Depth values are in feet below land surface.

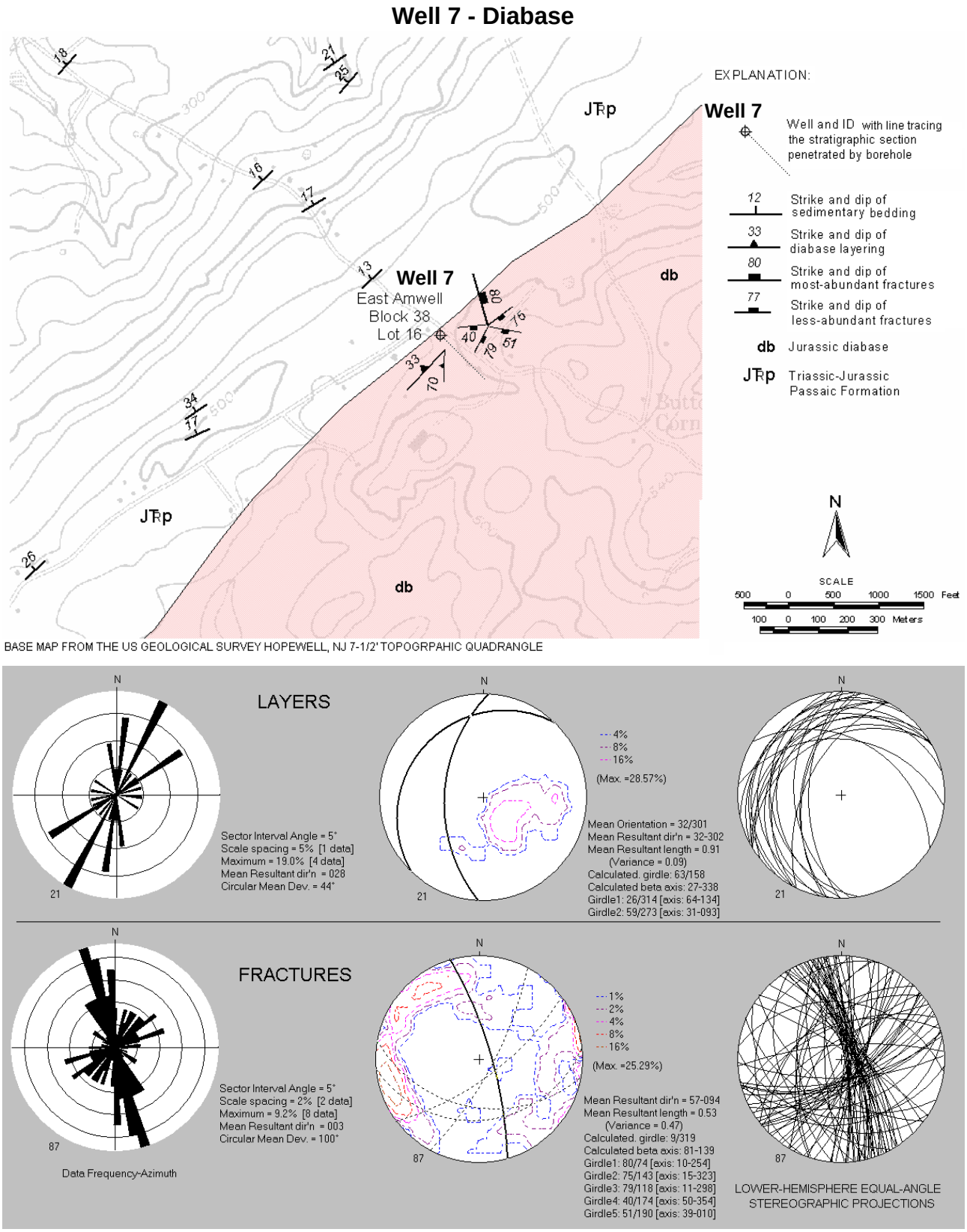

Figure 1D1. Map (above) shows well 7 on Block 38, Lot 16, East Amwell Twp., Hunterdon County, NJ. Bedrock structures mapped near the well are based on a structural analysis (bottom) of the OPTV record. Strike and dip of nearby sedimentary beds from outcrop measurements compiled by the NJ Geological Survey, Trenton, NJ.

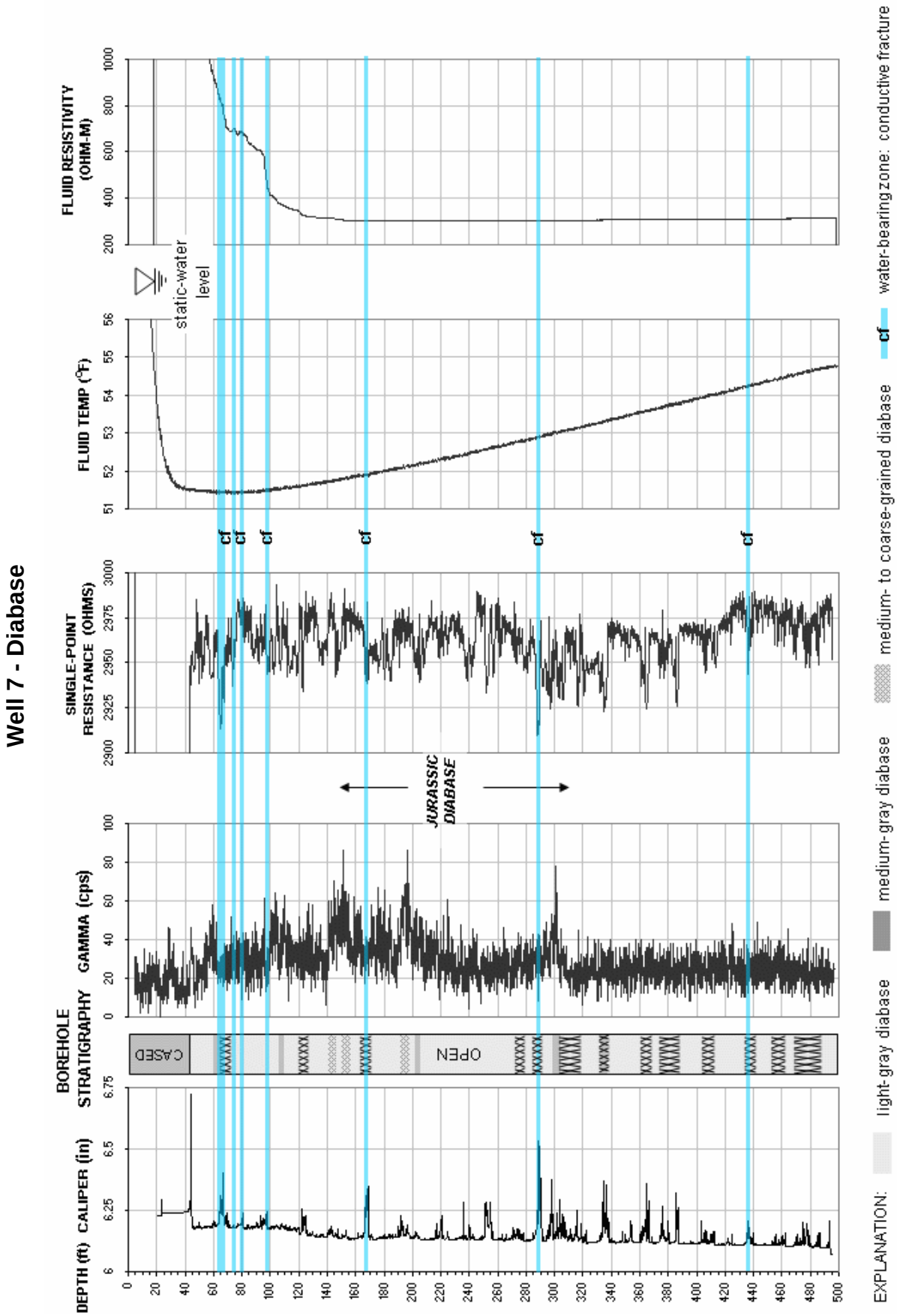

FIGURE 1D2. Hydrogeologic section based on geophysical logs for well 7 showing the vertical distribution of hydraulically-conductive fractures and water-bearing zones in diabase. Depth values are in feet below land surface.

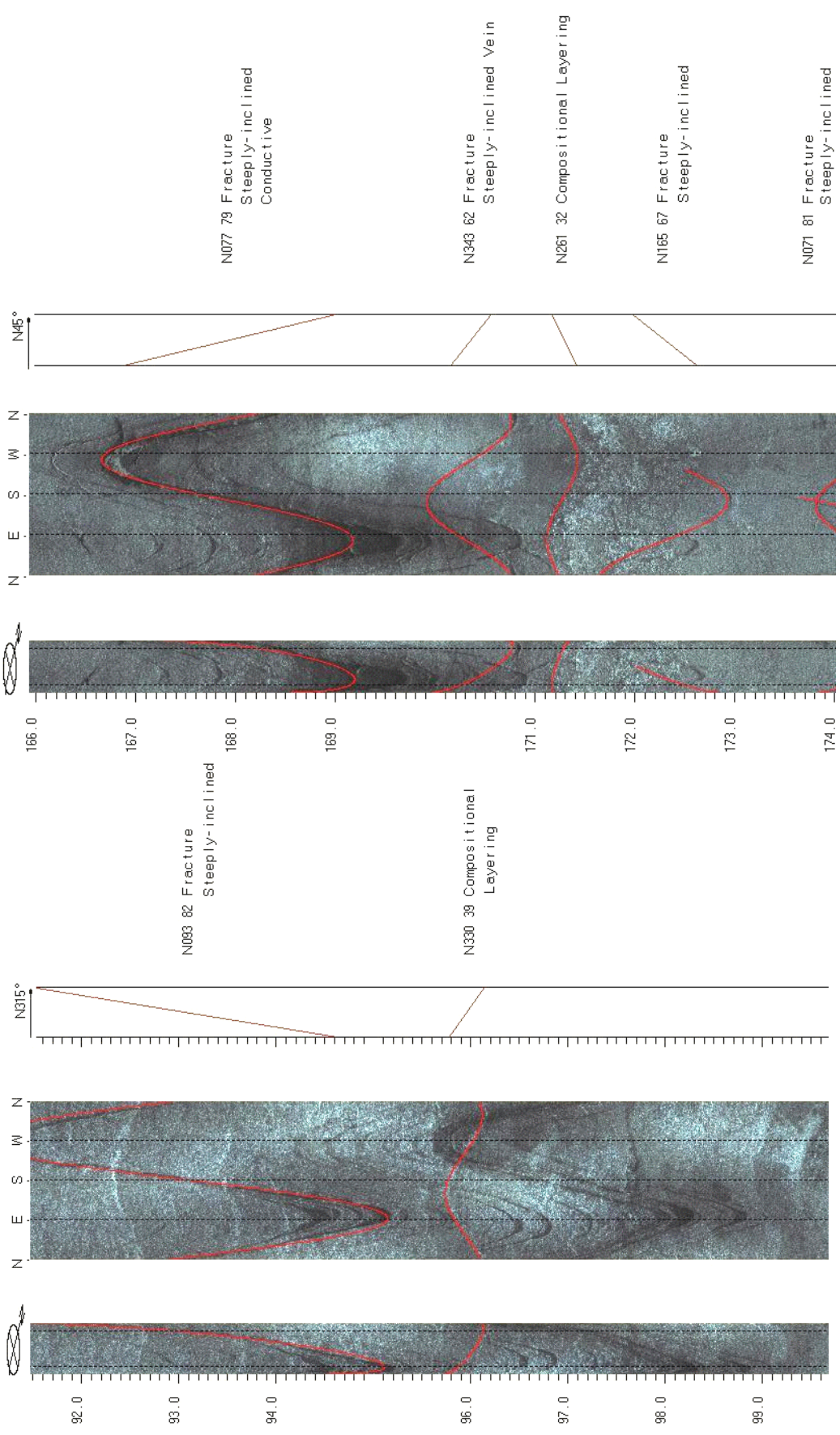

FIGURE 1D3. OPTV records of the 6-inch diameter well 7 showing bedrock structures and hydraulically-conductive features in diabase. Depth values are in feet below land surface.

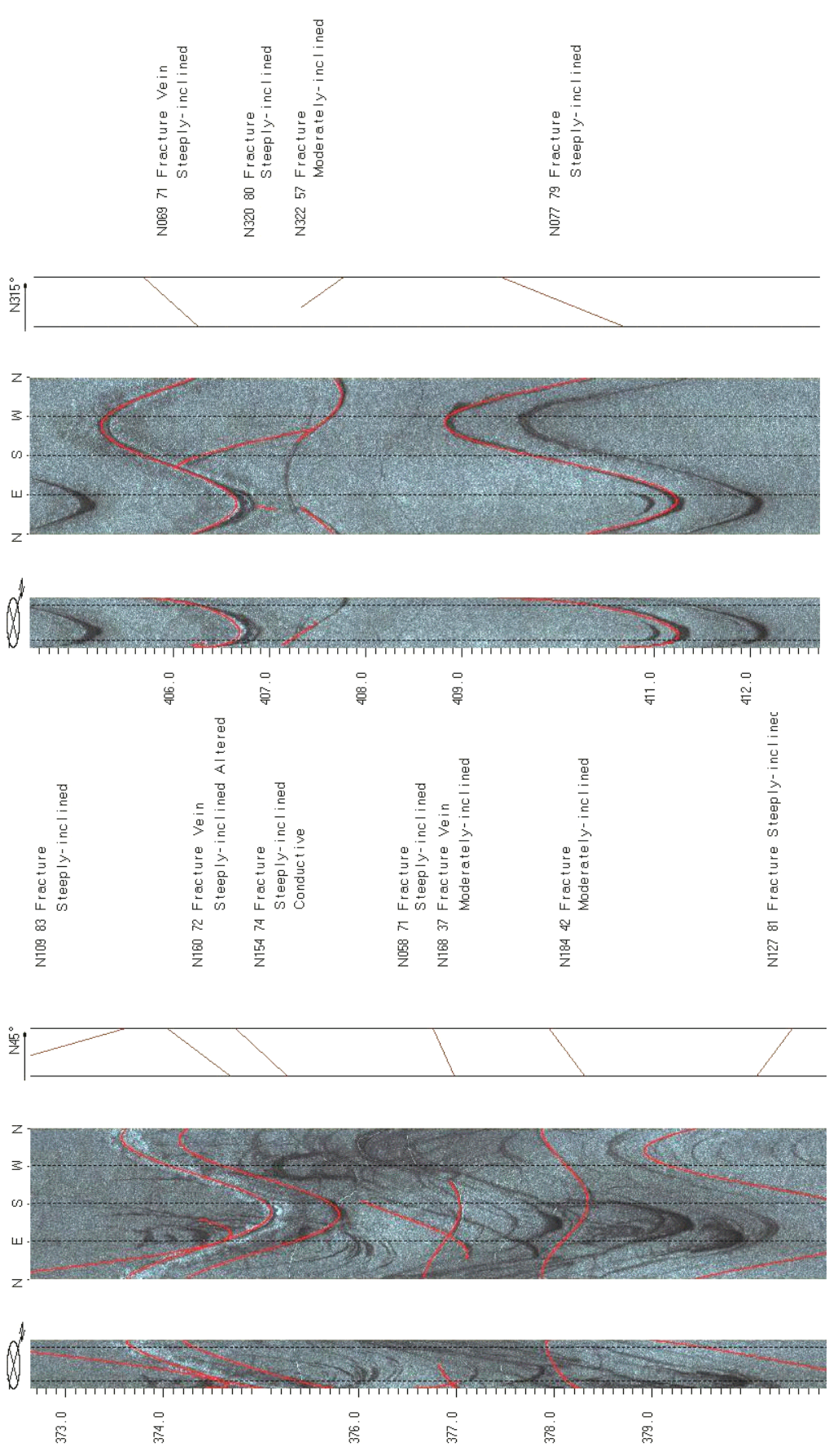

FIGURE 1D4. OPTV records of the 6-inch diameter well 5 showing bedrock structures and hydraulically-conductive features in diabase. Depth values are fin eet below land surface.

Wells 8 to 10 – Brunswick basalt of the Watchung zone overlying the Brunswick upper red zone

FIGURE 1E1. Map above shows wells 8 through 10 on the Essex County Country Club golf course, 350 Mt. Pleasant Ave, West Orange Twp., Essex County, NJ. Map below shows bedrock structures for each well based on a structural analysis of OPTV records.

Wells 8 to 10 – Brunswick basalt of the Watchung zone overlying the Brunswick upper red zone

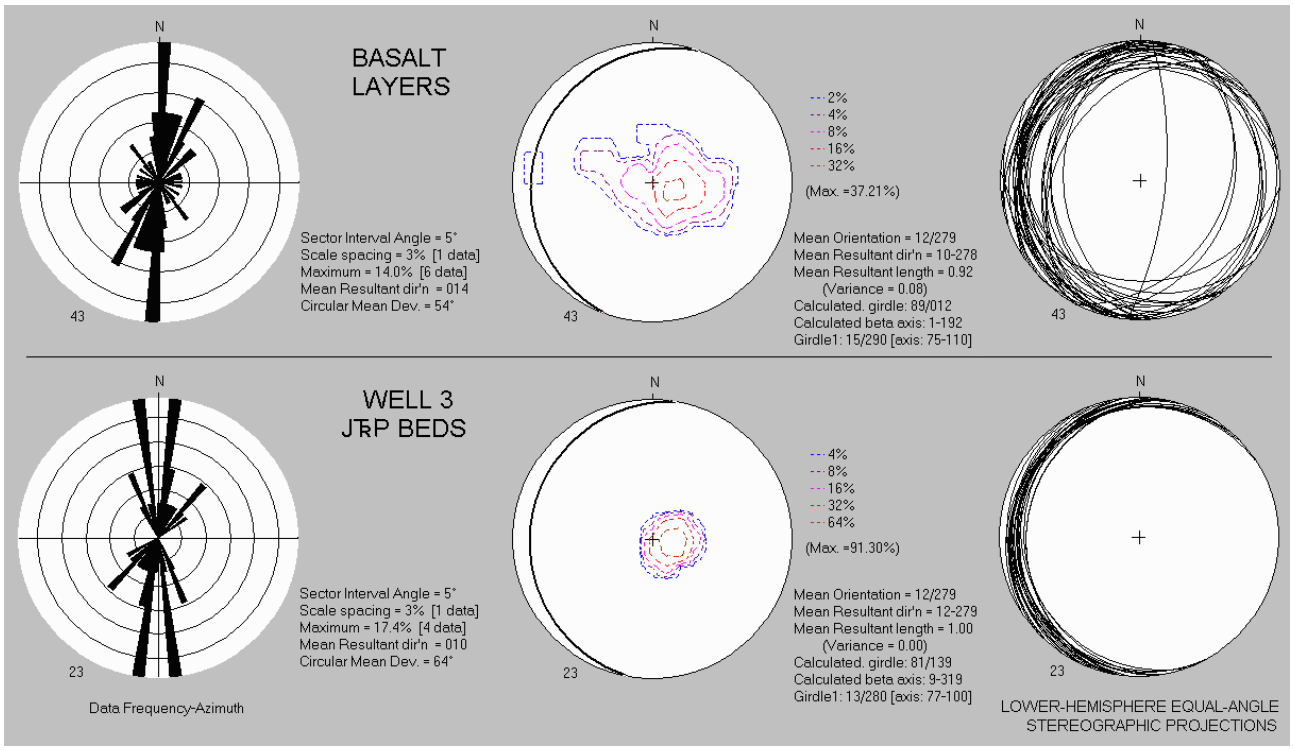

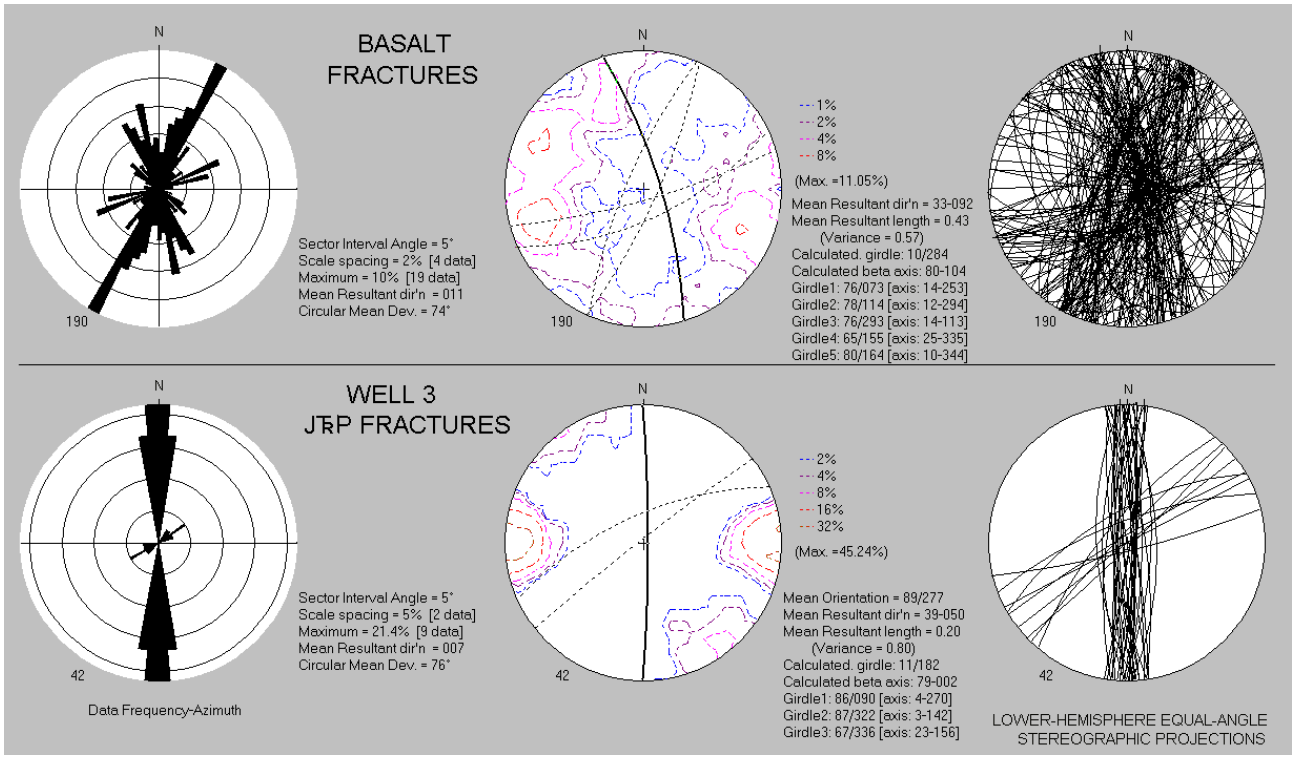

FIGURE 1E2. Structural analyses of OPTV records for wells 8 to10. Analysis above is for basalt layers and underlying sedimentary beds in the upper red zone of the Brunswick aquifer. Analysis below is for fractures in basalt and underlying sedimentary beds.

Well 8 – Brunswick basalt in the Watchung zone

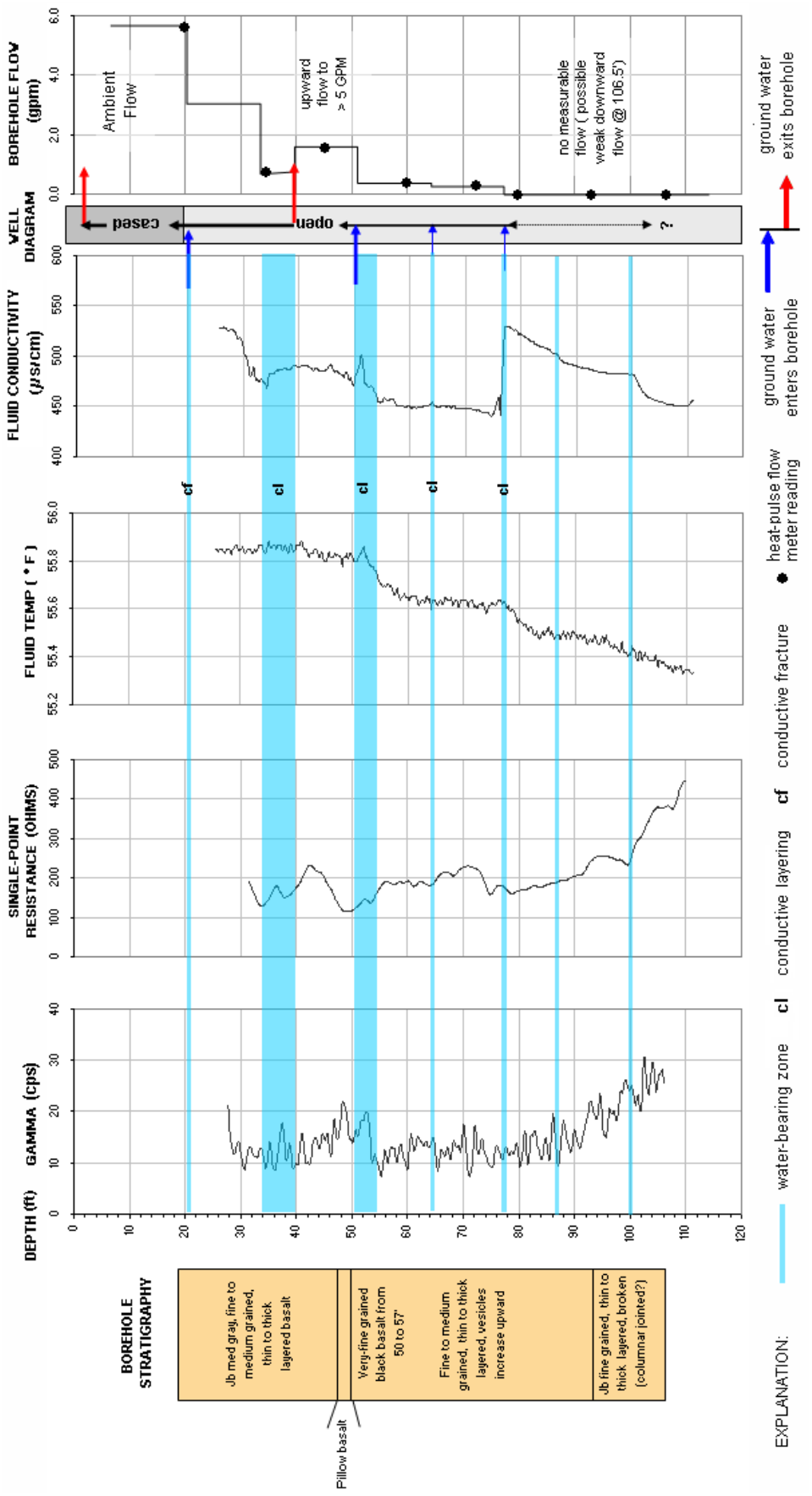

FIGURE 1E3. Stratigraphic and hydrogeologic sections based on geophysical logs for well 8 showing the vertical distribution and types of hydraulically-conductive features and water-bearing zones in basalt. Depth values are in feet below land surface.

Well 8 - Brunswick basalt in the Watchung zone

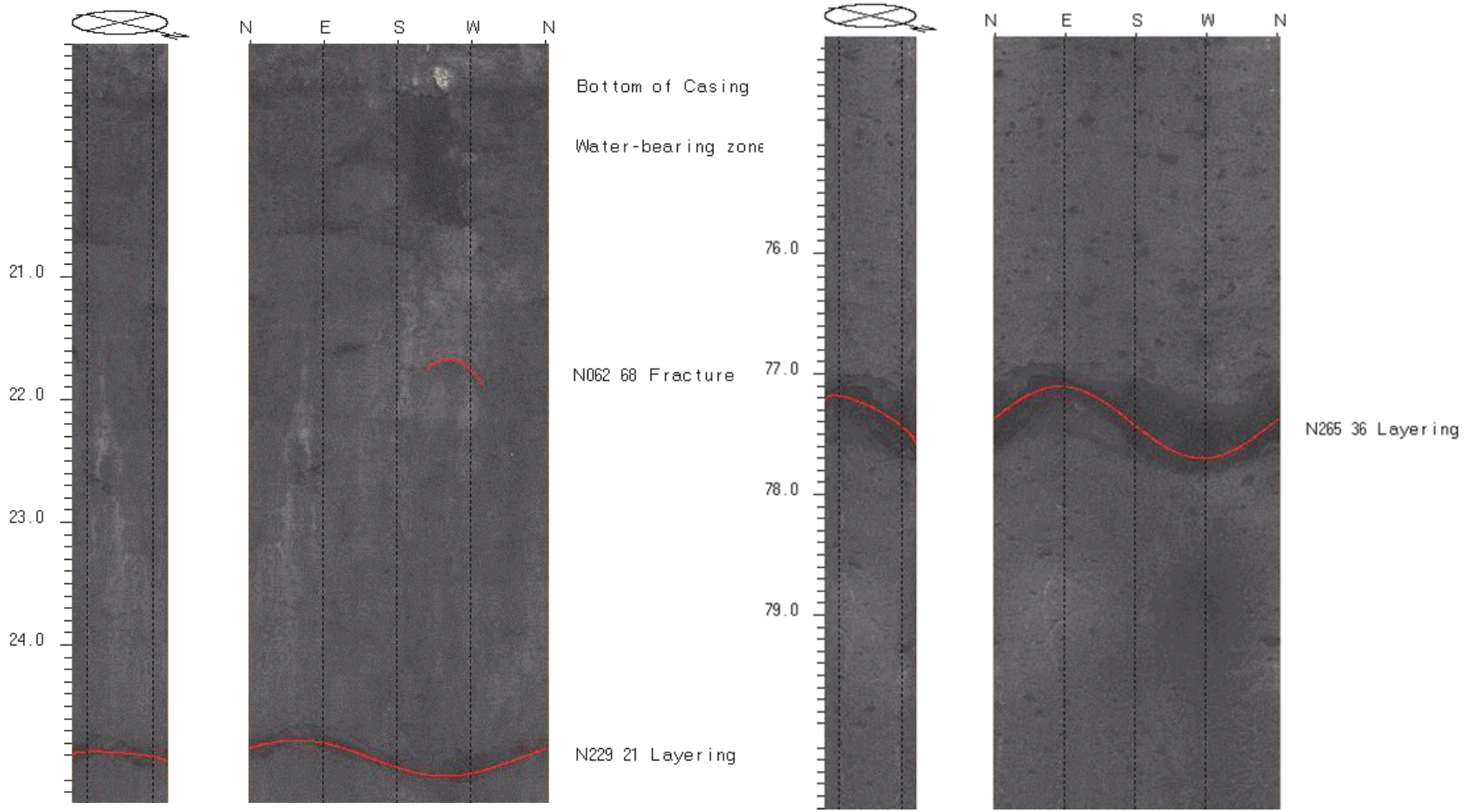

FIGURE 1E4. OPTV records of the 8-inch diameter well 8 showing bedrock structures and hydraulically-conductive features in basalt. Depth values are in feet below land surface..

Well 9 – Brunswick basalt of the Watchung zone

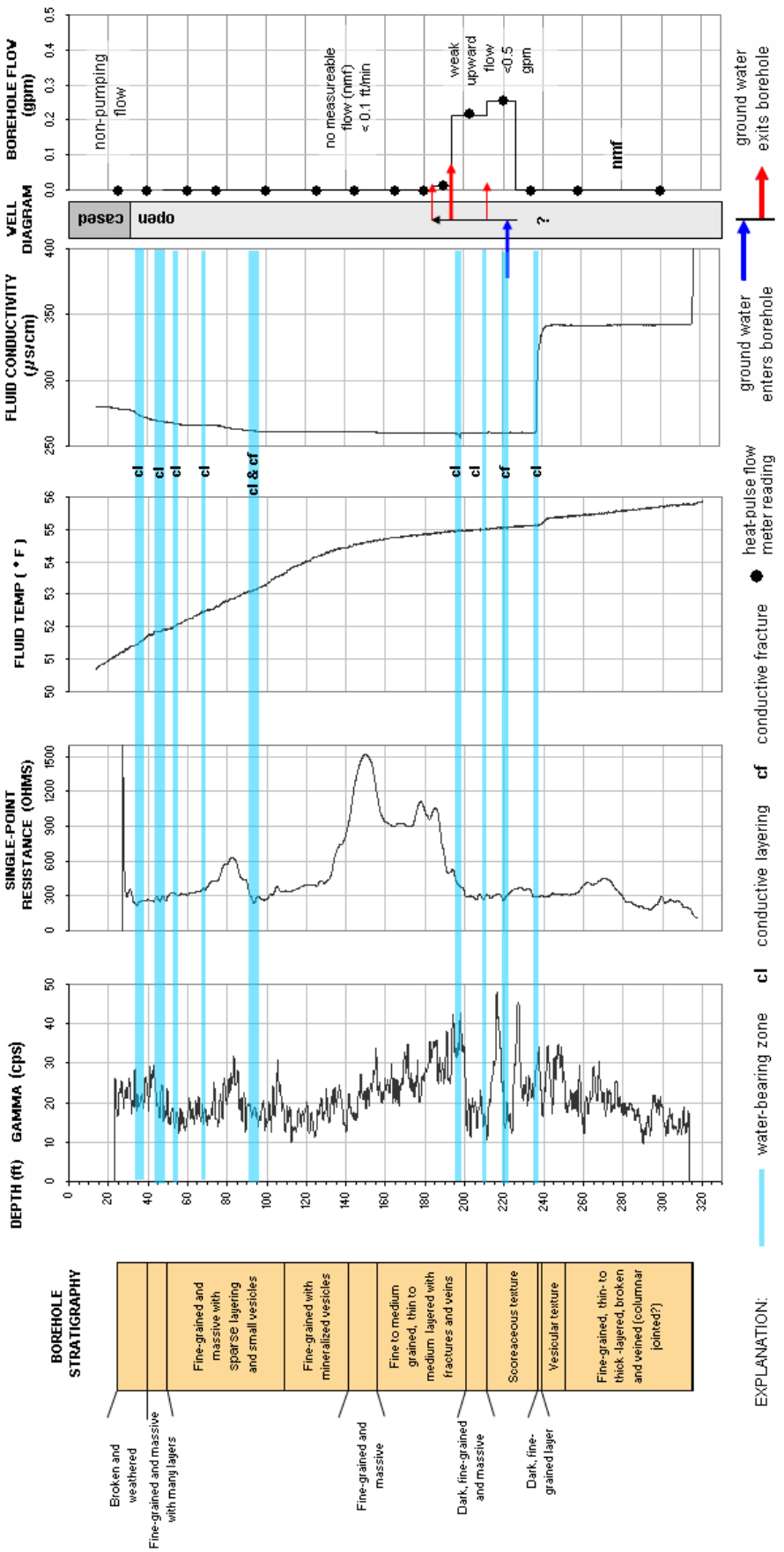

FIGURE 1E5. Stratigraphic and hydrogeologic sections based on geophysical logs for well 9 showing the vertical distribution and types of hydraulically-conductive features and water-bearing zones in basalt. Depth values are in feet below land surface.

Well 9 - Brunswick basalt in the Watchung zone

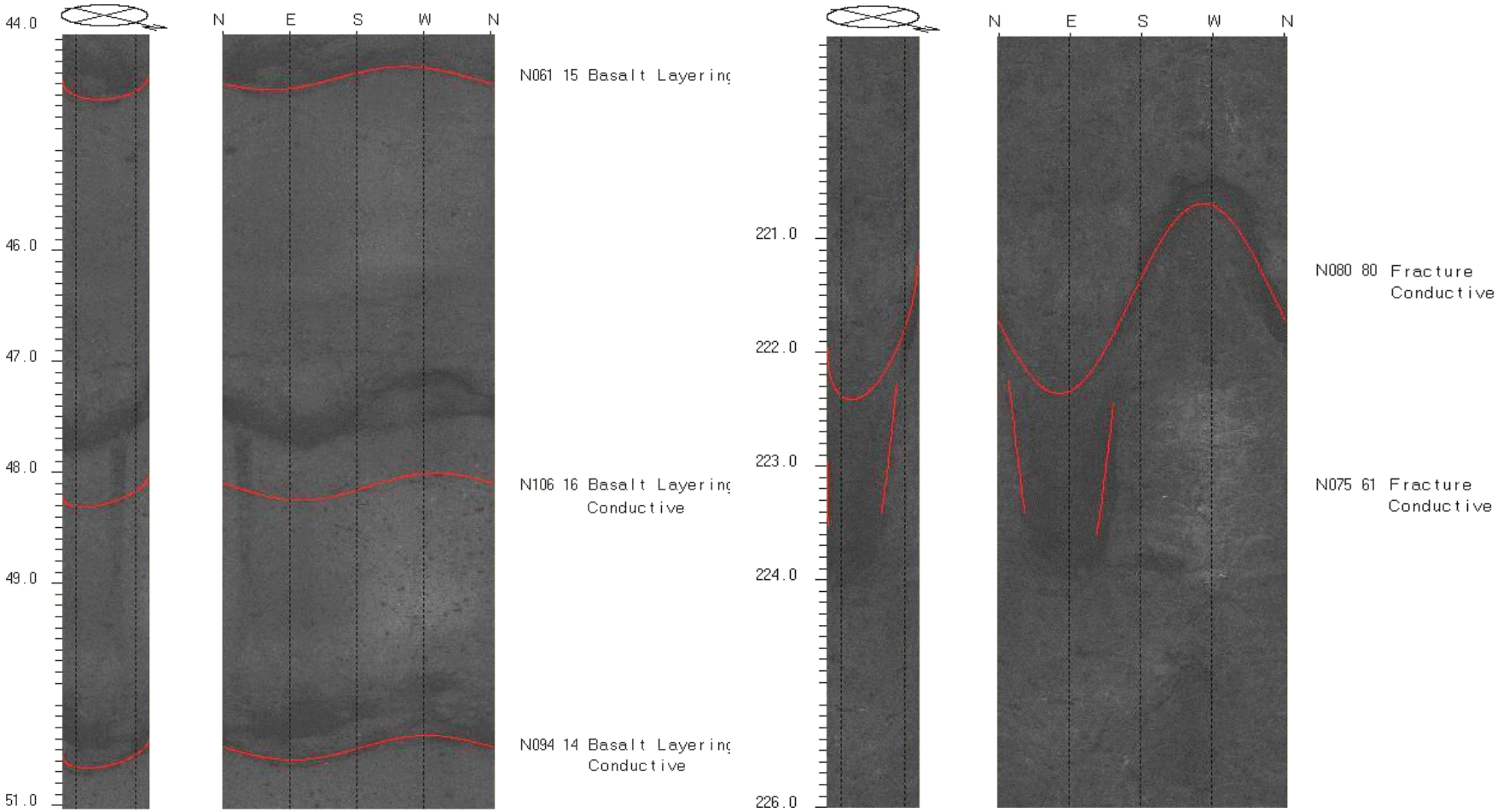

FIGURE 1E6. OPTV records of the 8-inch-diameter well 9 showing bedrock structures and hydraulically-conductive features in basalt. Depth values are feet below land surface.

Well 10 – Brunswick basalt of the Watchung zone overlying Brunswick upper red zone

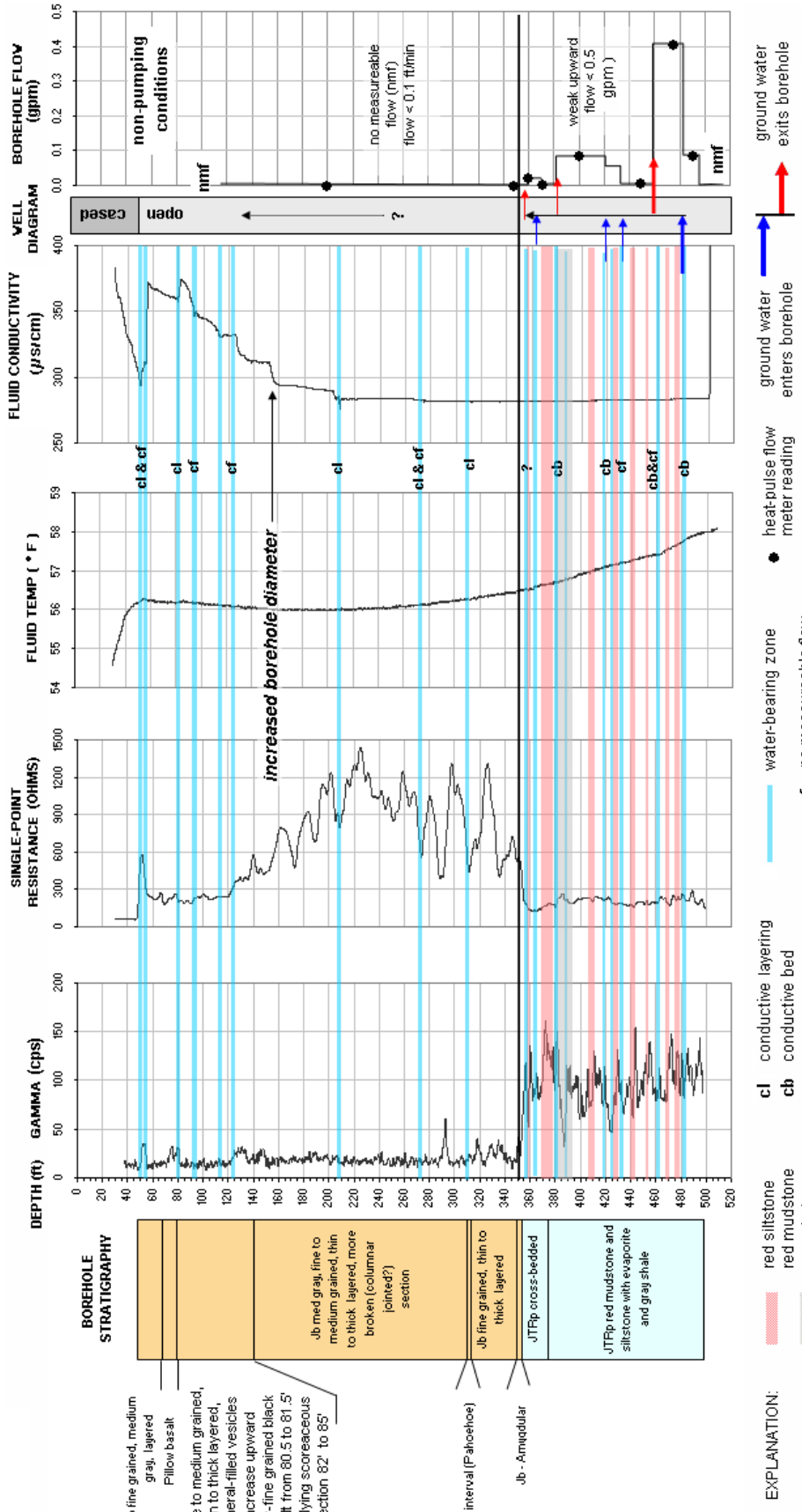

FIGURE 1E7. Stratigraphic and hydrogeologic sections based on interpretation of geophysical logs for well 10 showing the vertical distribution and types of hydraulically-conductive features and water-bearing zones in basalt, red mudstone and siltstone and gray sandstone. Depth values are in feet below land surface.

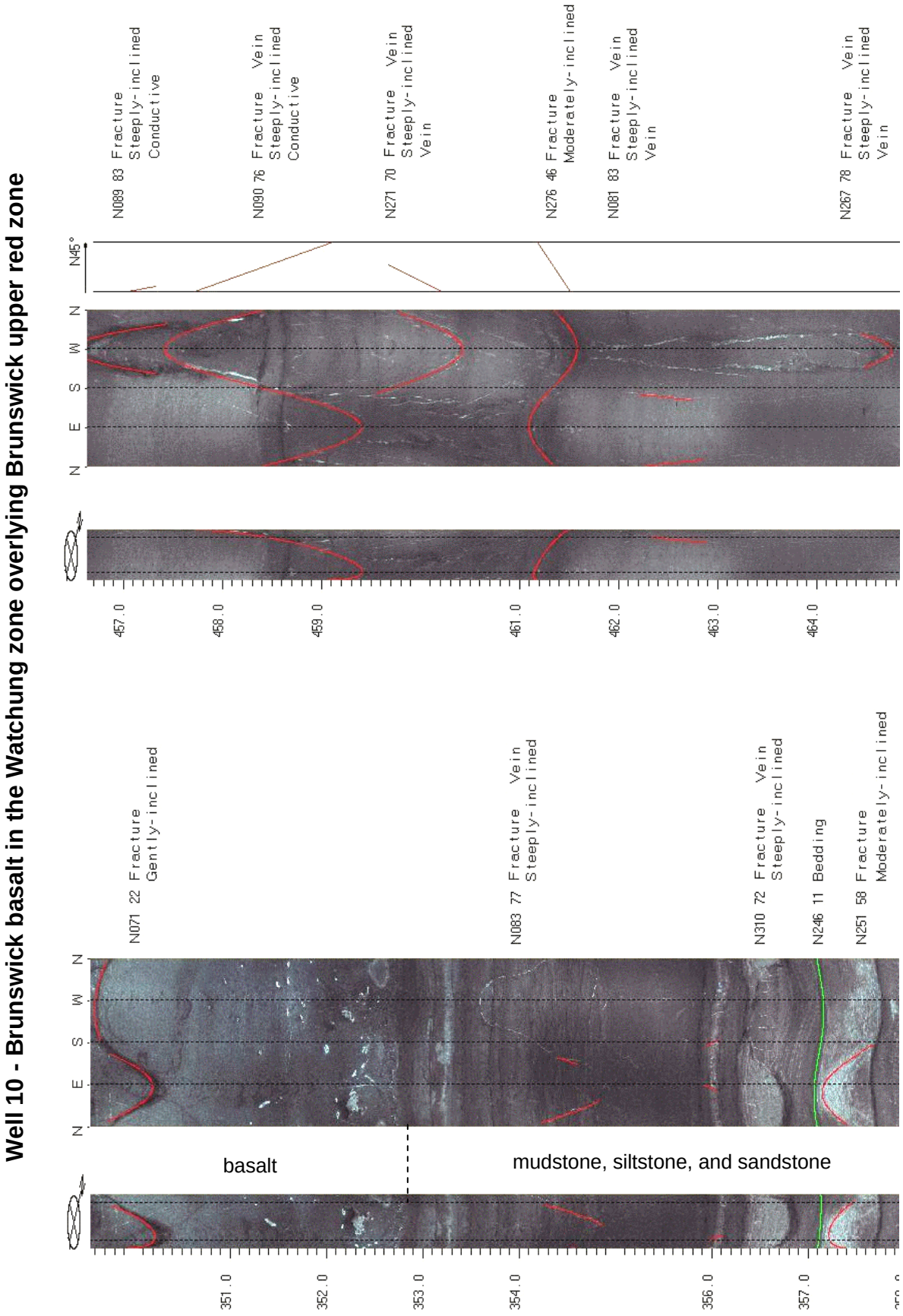

FIGURE 1E8. OPTV records for the 6-inch-diameter well 10 showing bedrock structures and hydraulically-conductive features in basalt and underlying mudstone, siltstone, and sandstone. Depth values are in feet below land surface.

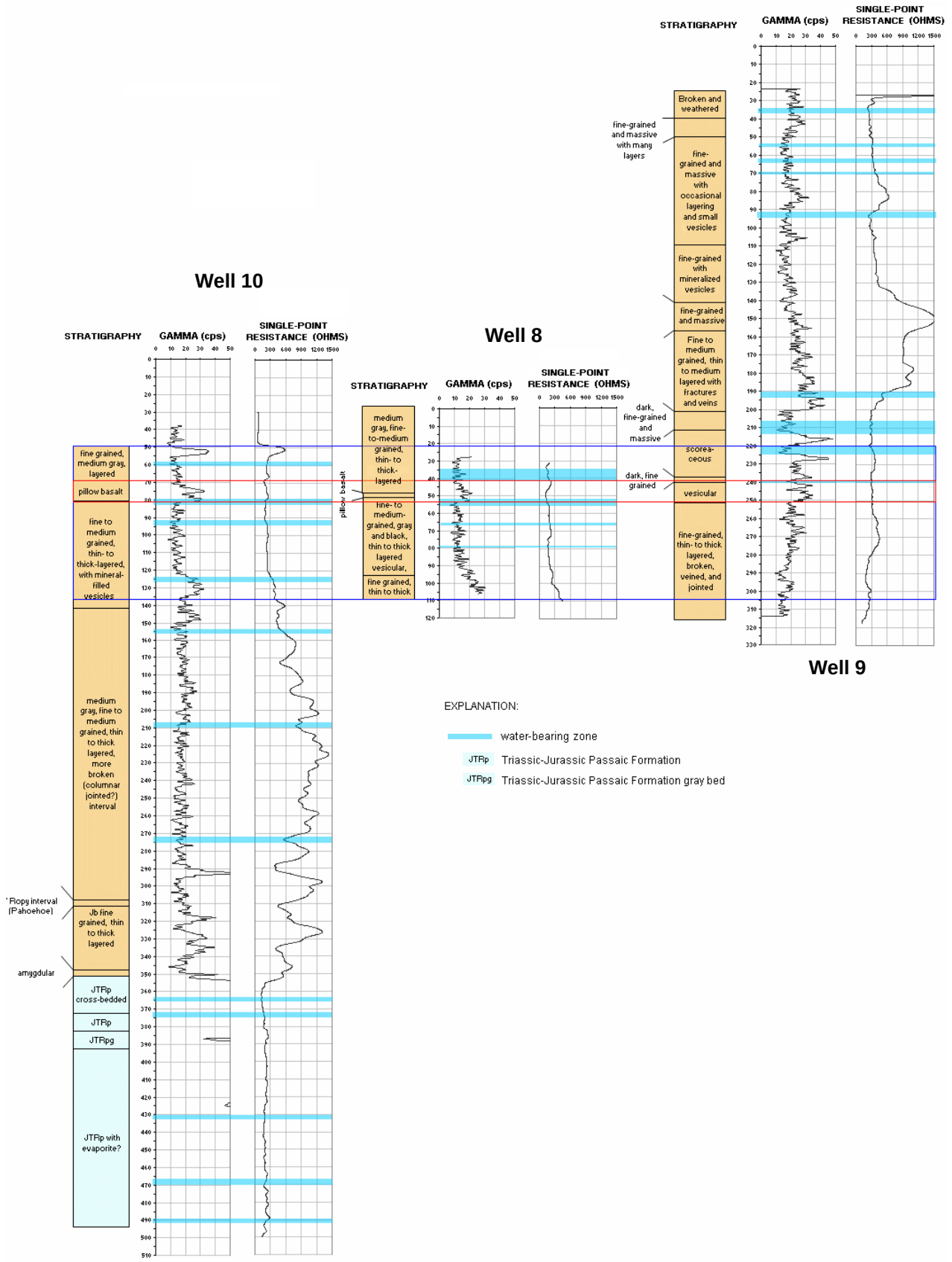

FIGURE 1E9. Correlation of hydro-stratigraphic sections for wells 8 through10 based on geophysical logs. Depth values are in feet below land surface.

Well 11 – Brunswick basalt of the Watchung zone overlying Brunswick upper red zone

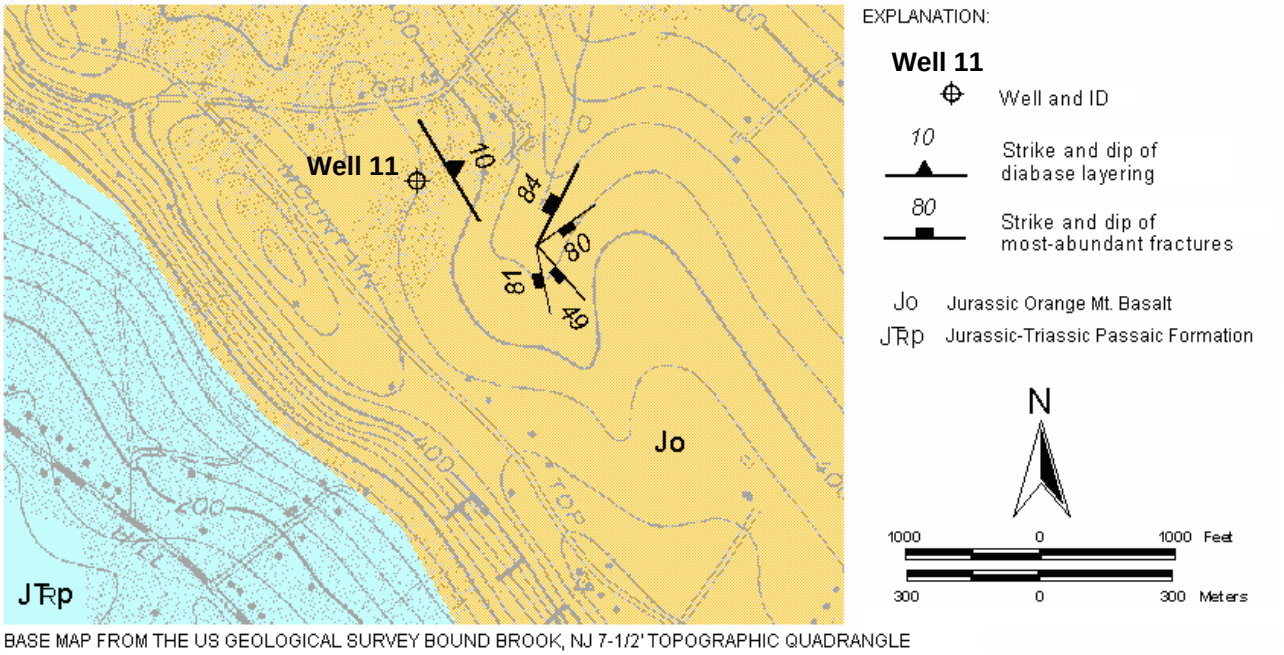

BASE MAP FROM THE US GEOLOGICAL SURVEY BOUND BROOK, NJ 7-1/2' TOPOGRAPHIC QUADRANGLE

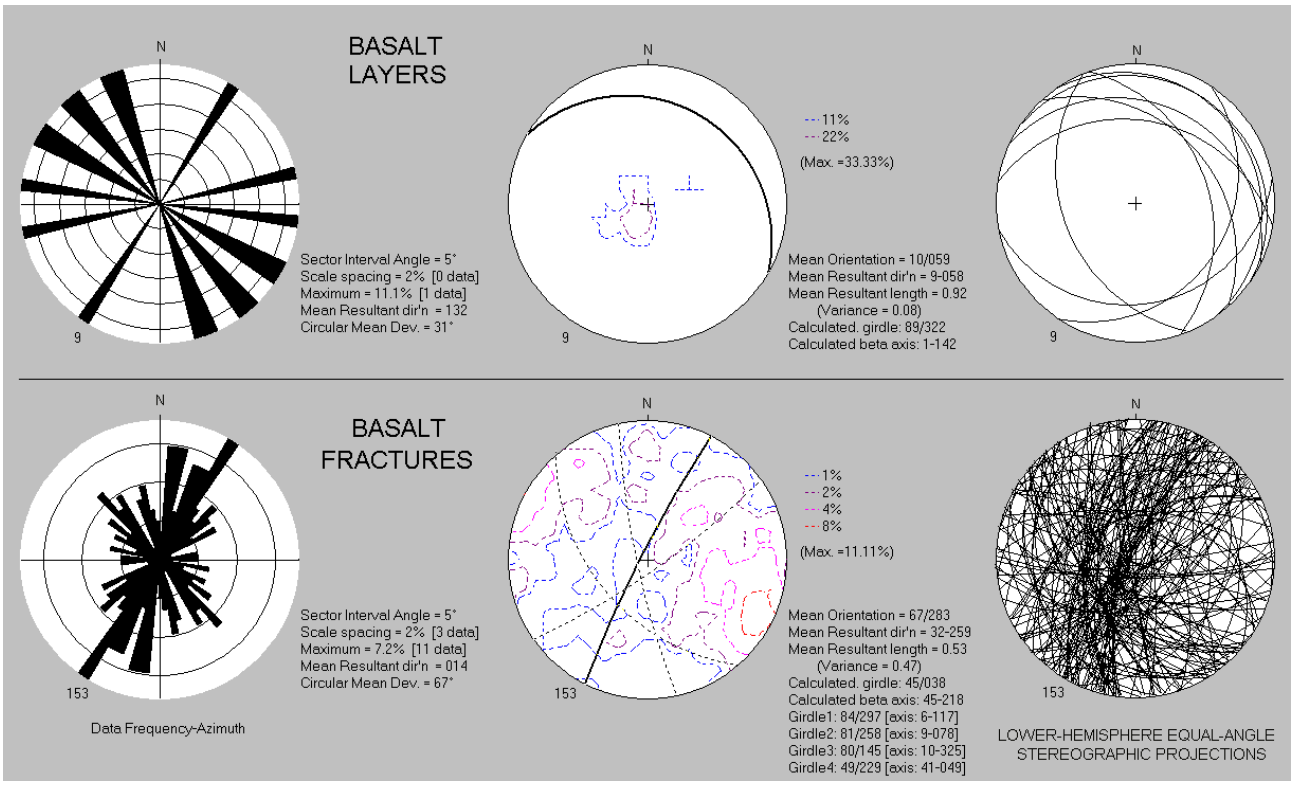

Figure 1F1. Map (above) shows the location of well 11 at 1163 Delaware Ave., Bridgewater Twp., Somerset County, NJ. Mapped bedrock structures are based on a structural analysis (bottom) of the OPTV record. Note that topographic ridges and surface streams parallel structural trends.

Well 11 – Brunswick basalt of the Watchung zone overlying mudstone and siltstone of the Brunswick upper red zone

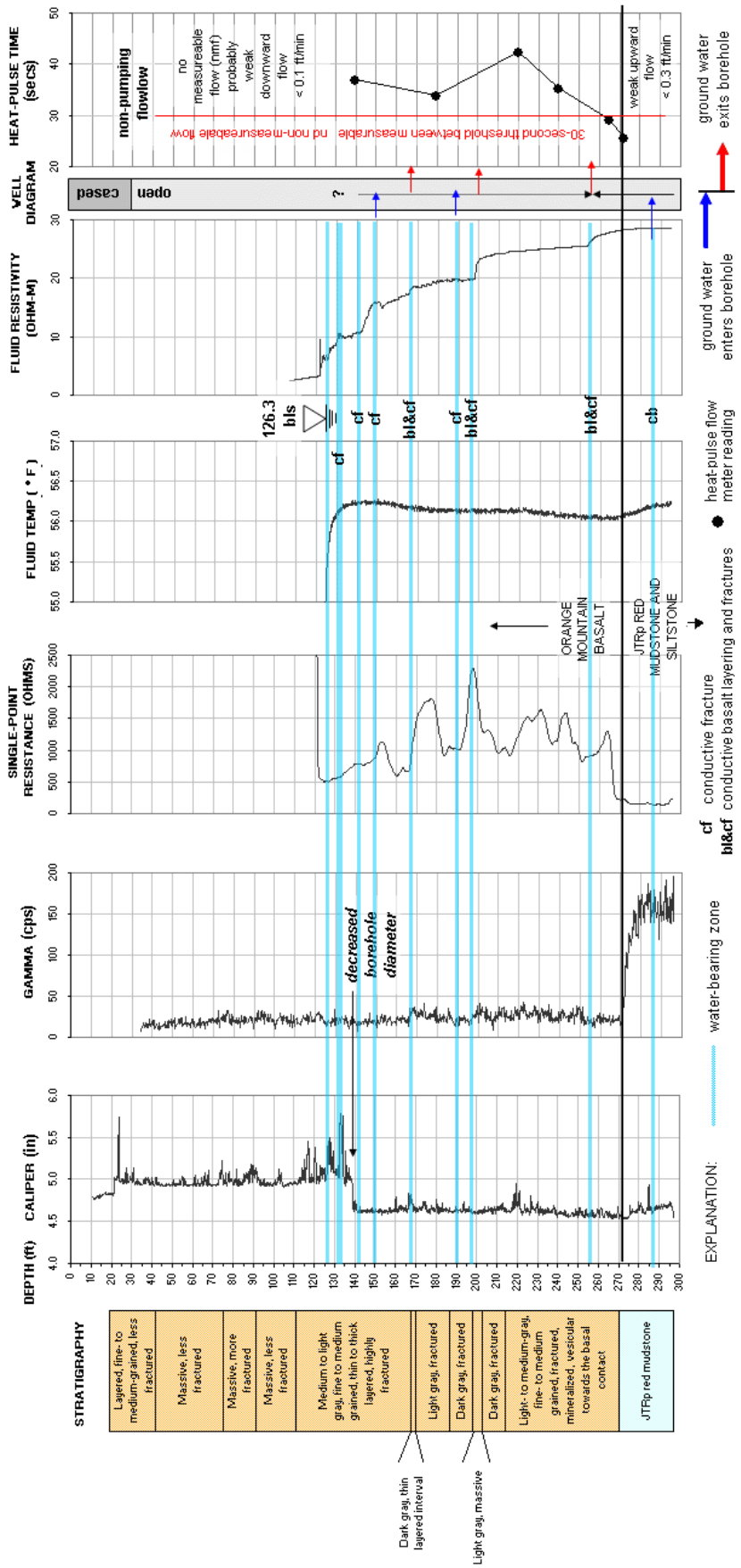

FIGURE 1F2. Stratigraphic and hydrogeologic sections based on geophysical logs for well 11 showing the vertical distribution and types of hydraulically-conductive features and water-bearing zones. Depth values are in feet below land surface.

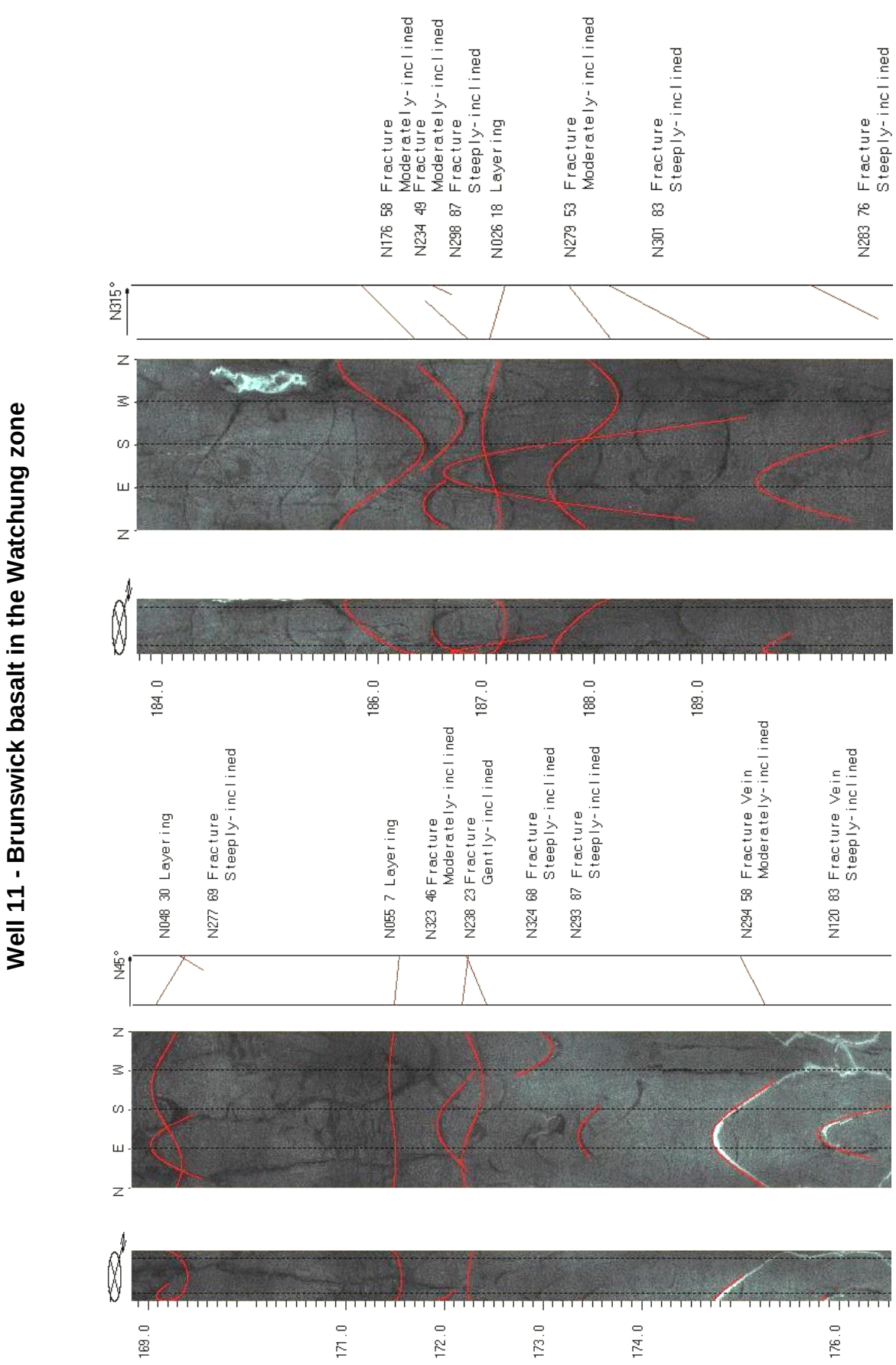

FIGURE 1F3. OPTV records of the 6-inch diameter well 11 showing bedrock structures in basalt. Depth values are in feet below land surface.

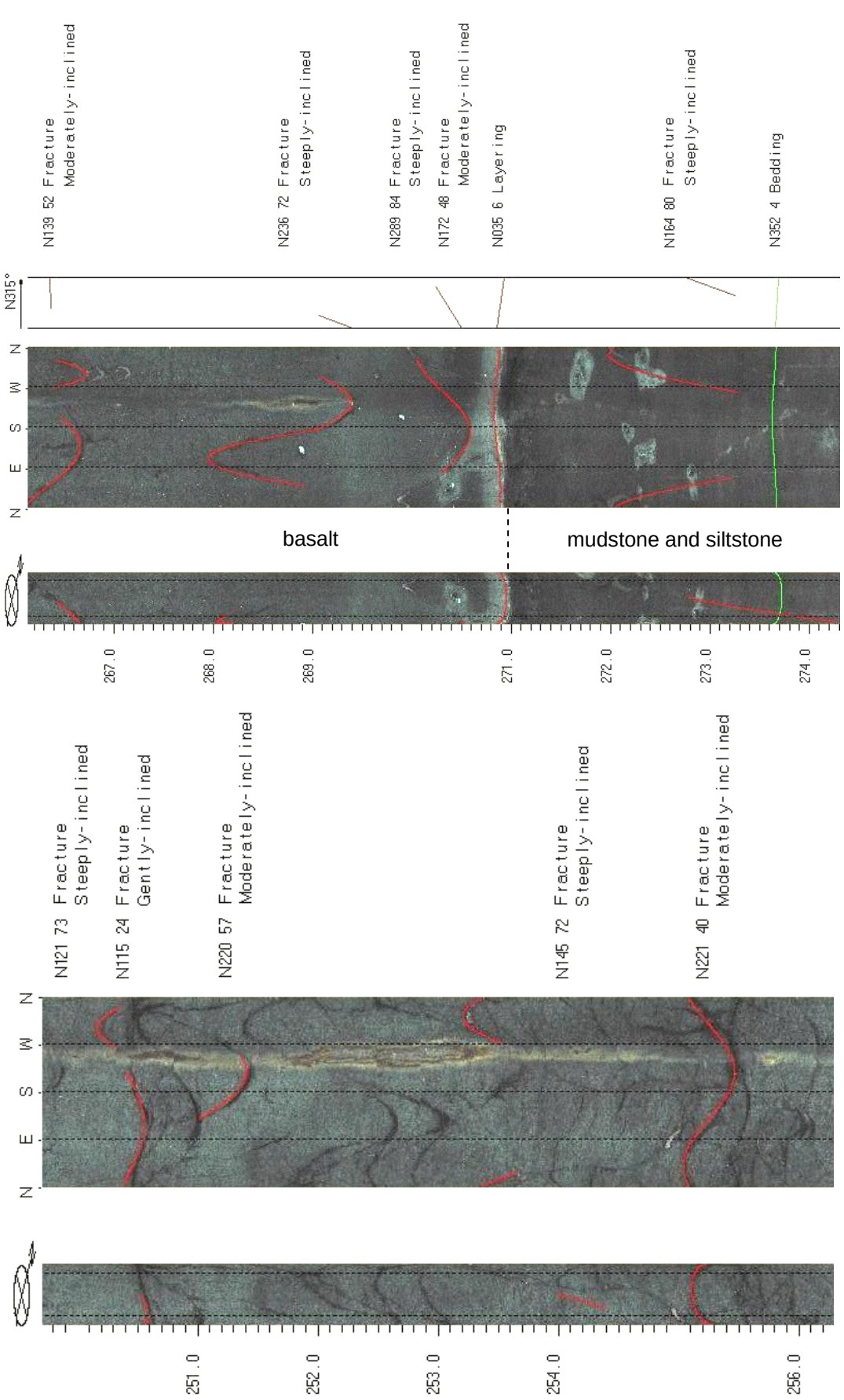

FIGURE 1F4. OPTV records of the 6-inch diameter well 11 showing bedrock structures in basalt (left and upper right) and underlying mudstone and siltstone of the Brunswick upper red zone (lower right). The stain seen on the borehole well in the image on the left is caused by the pump string resting against the borehole wall. Note the light-colored pockets of hydrothermal alteration in the shale and siltstone. Depth values are in feet below land surface.

Summary of Borehole Geophysical Studies in the Newark Basin, New Jersey:

Brunswick conglomerate and sandstone, and the Passaic flood tunnel workshaft geotechnical investigations

By Gregory C. Herman and John F. Curran, N.J. Geological Survey

Appendix 2 of

Contributions to the Geology and Hydrogeology of the Newark Basin

N.J. Geological Survey Bulletin 77

State of New Jersey
Department of Environmental Protection
Water Resource Management
New Jersey Geological Survey
2010

Wells 12 to 20 - Brunswick sandstone and conglomerate

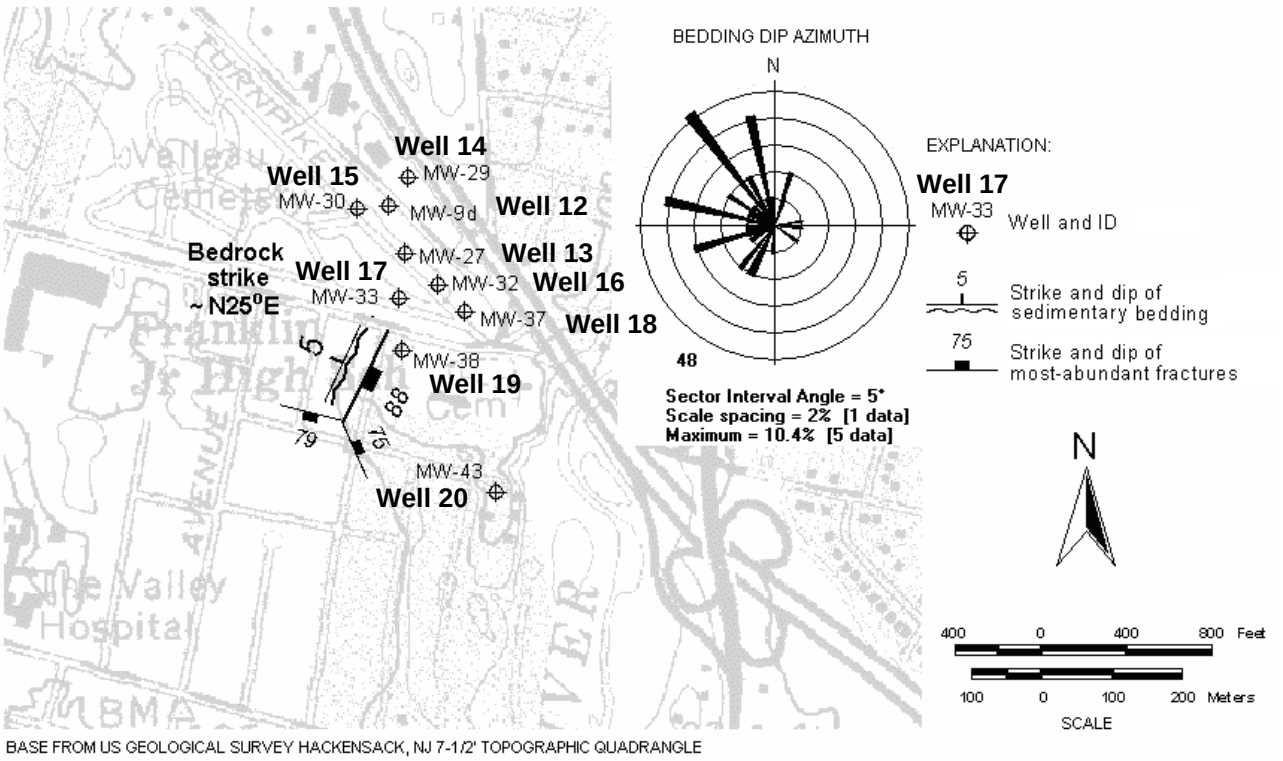

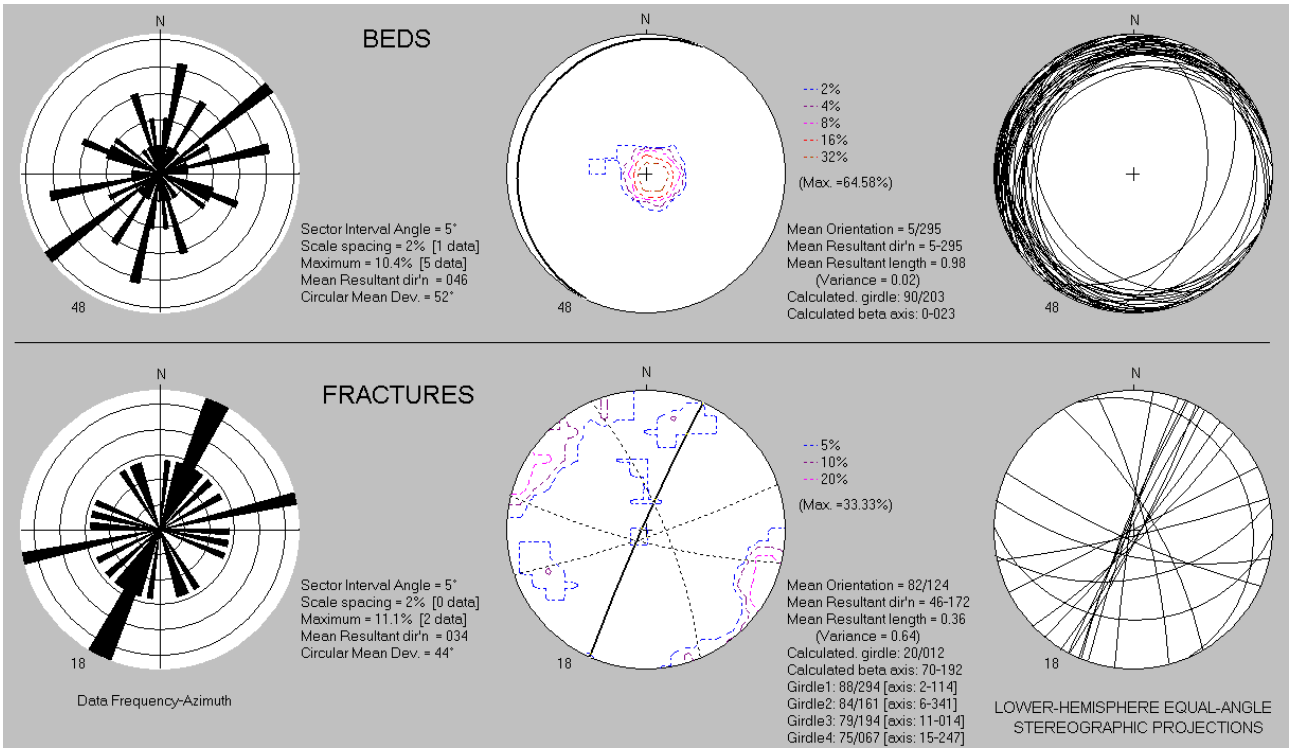

Figure 2A1. Map (above) shows wells 12 through 20 in the vicinity of the Ridgewood Shell Service Station, Ridgewood Twp., Bergen County, NJ. Mapped bedrock structures based on a structural analysis (below) of the OPTV records.

Wells 15 and 18 – Brunswick sandstone and conglomerate

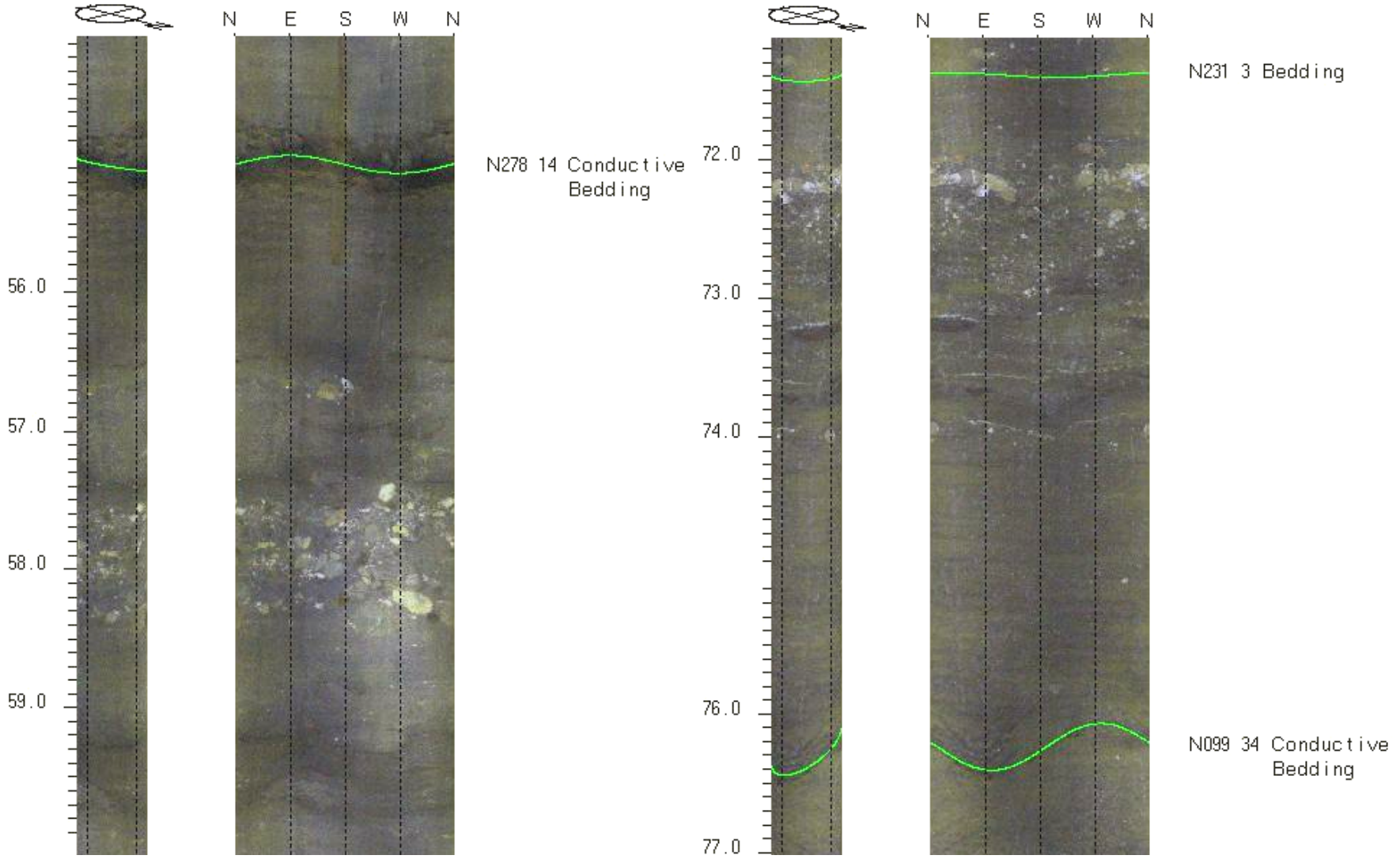

FIGURE 2A2. OPTV records of the 6-inch diameter wells 15 (left) and 18 (right) showing bedrock structures and hydraulically-conductive features in sandstone and conglomerate. Depth values are in feet below land surface.

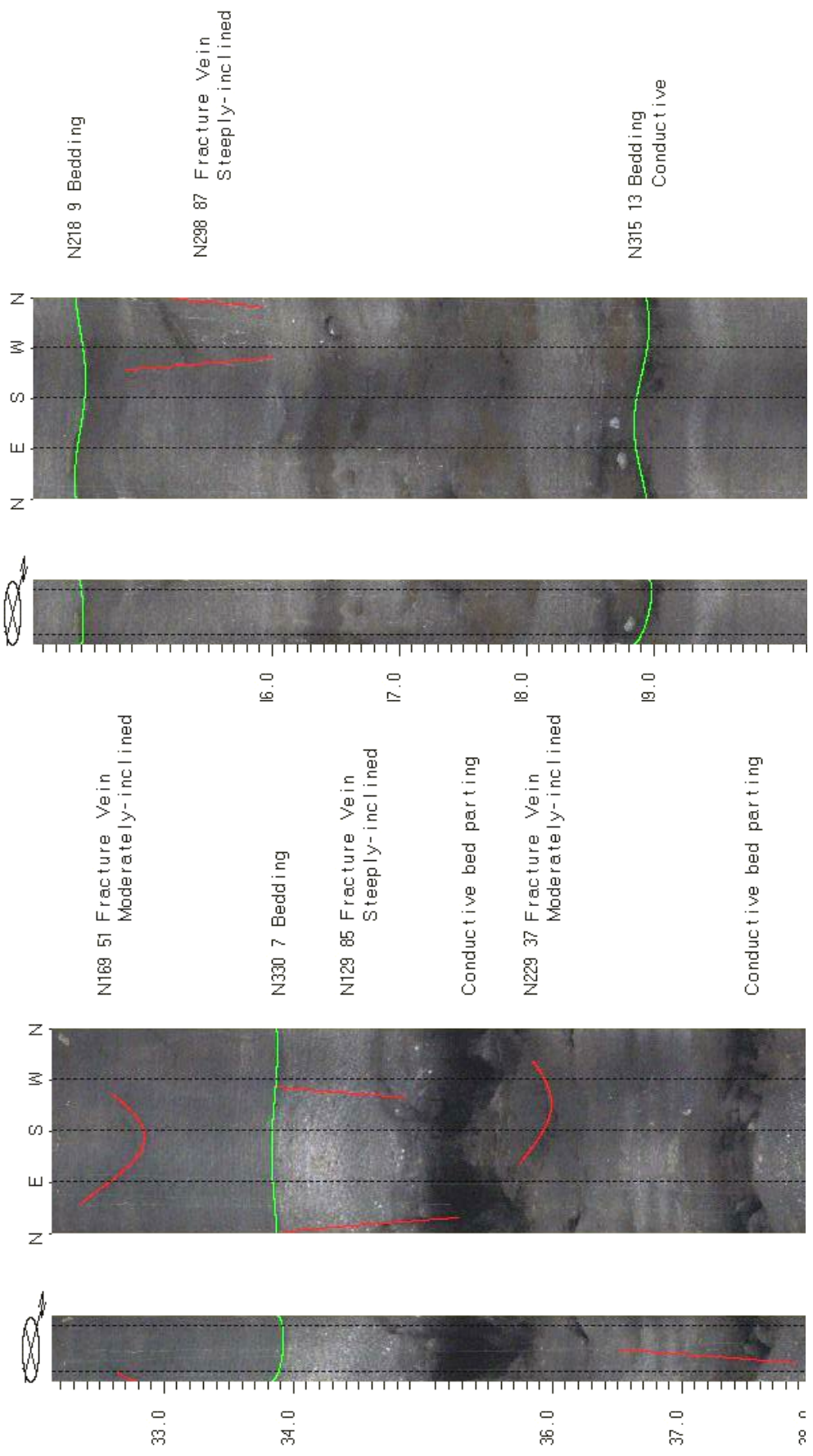

FIGURE 2A3. OPTV records of the 6-inch diameter well 12 showing bedrock structures and hydraulically-conductive features in sandstone and conglomerate. Depth values are in feet below land surface.

Wells 21 and 22 - Brunswick sandstone and conglomerate

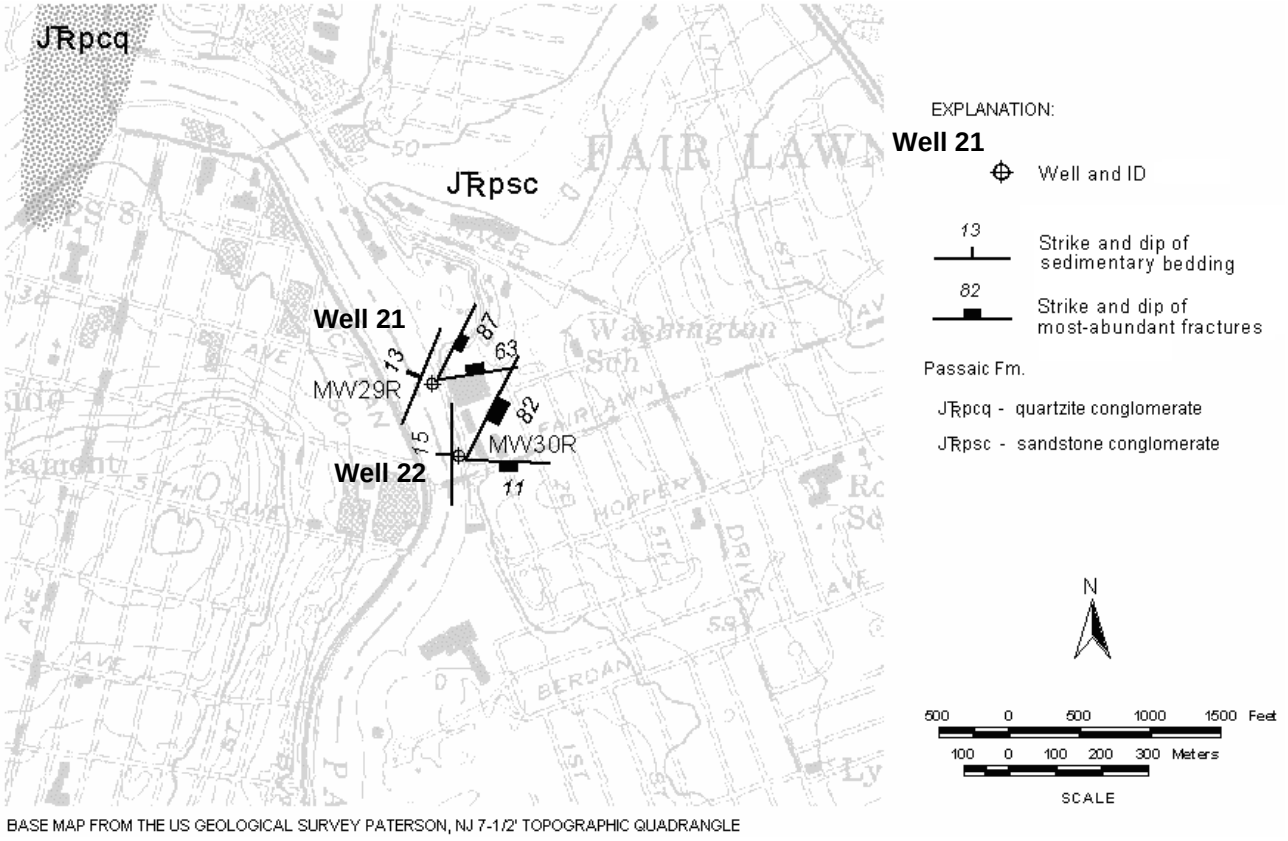

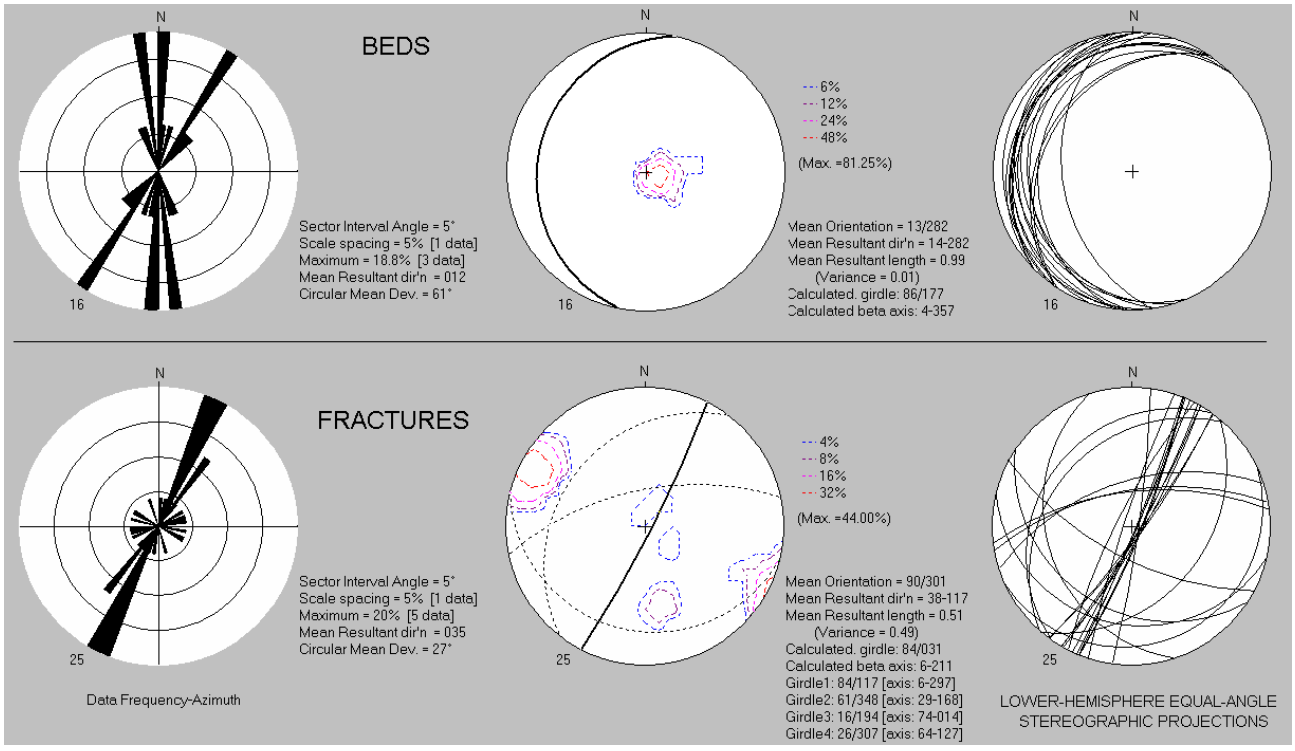

Figure 2B1. Map (above) shows wells 21 and 22 at the Sandoz Chemical Corp., Fairlawn Ave. and 3rd Street, Fairlawn Boro., Bergen County, NJ. Mapped bedrock structures based on a structural analysis (below) of the OPTV records.

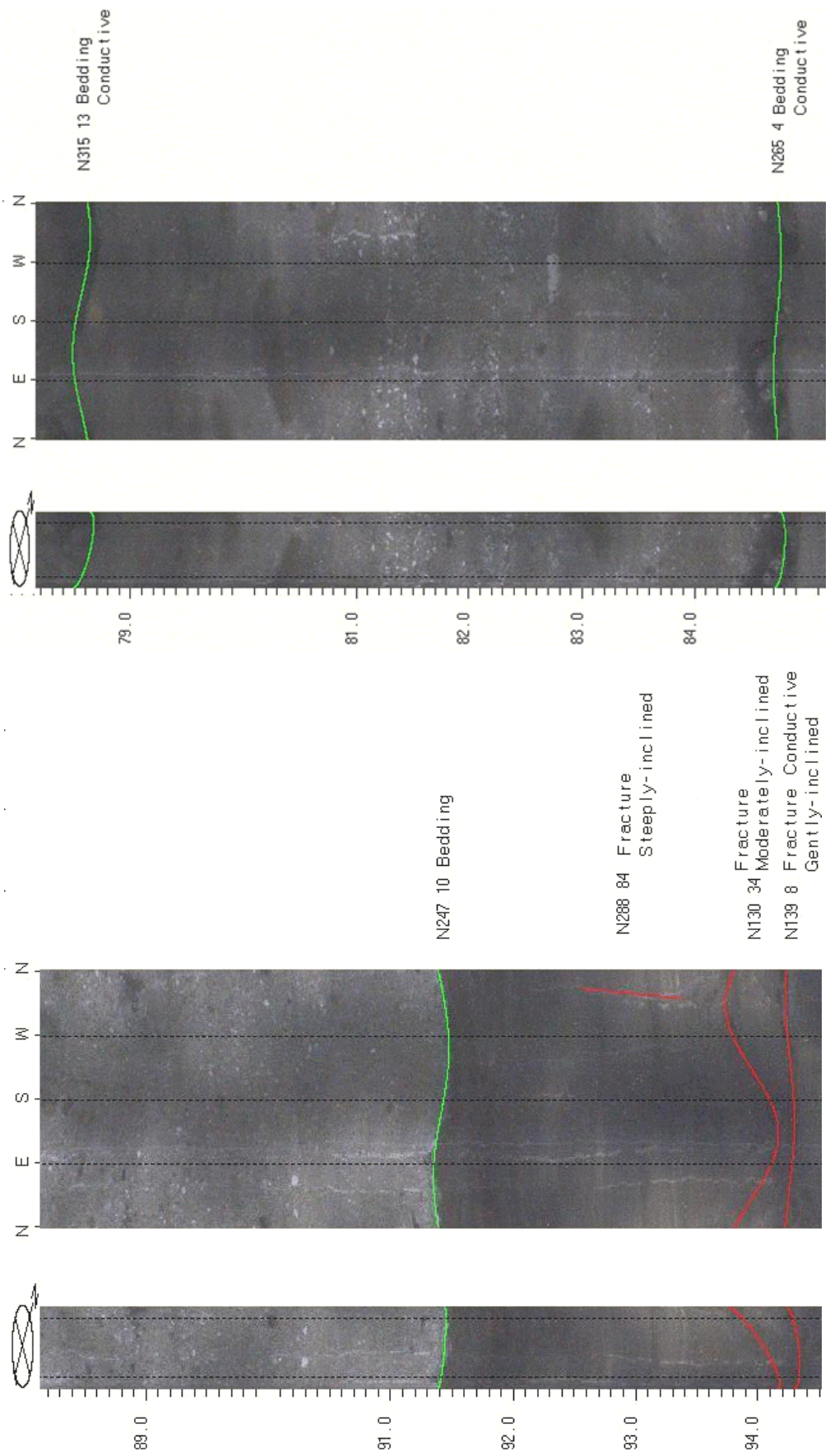

FIGURE 2B2. OPTV records of the 8-inch diameter well 21 showing bedrock structures and hydraulically-conductive features in sandstone and siltstone. Depth values are in feet below land surface.

Well 22 – Brunswick sandstone and conglomerate

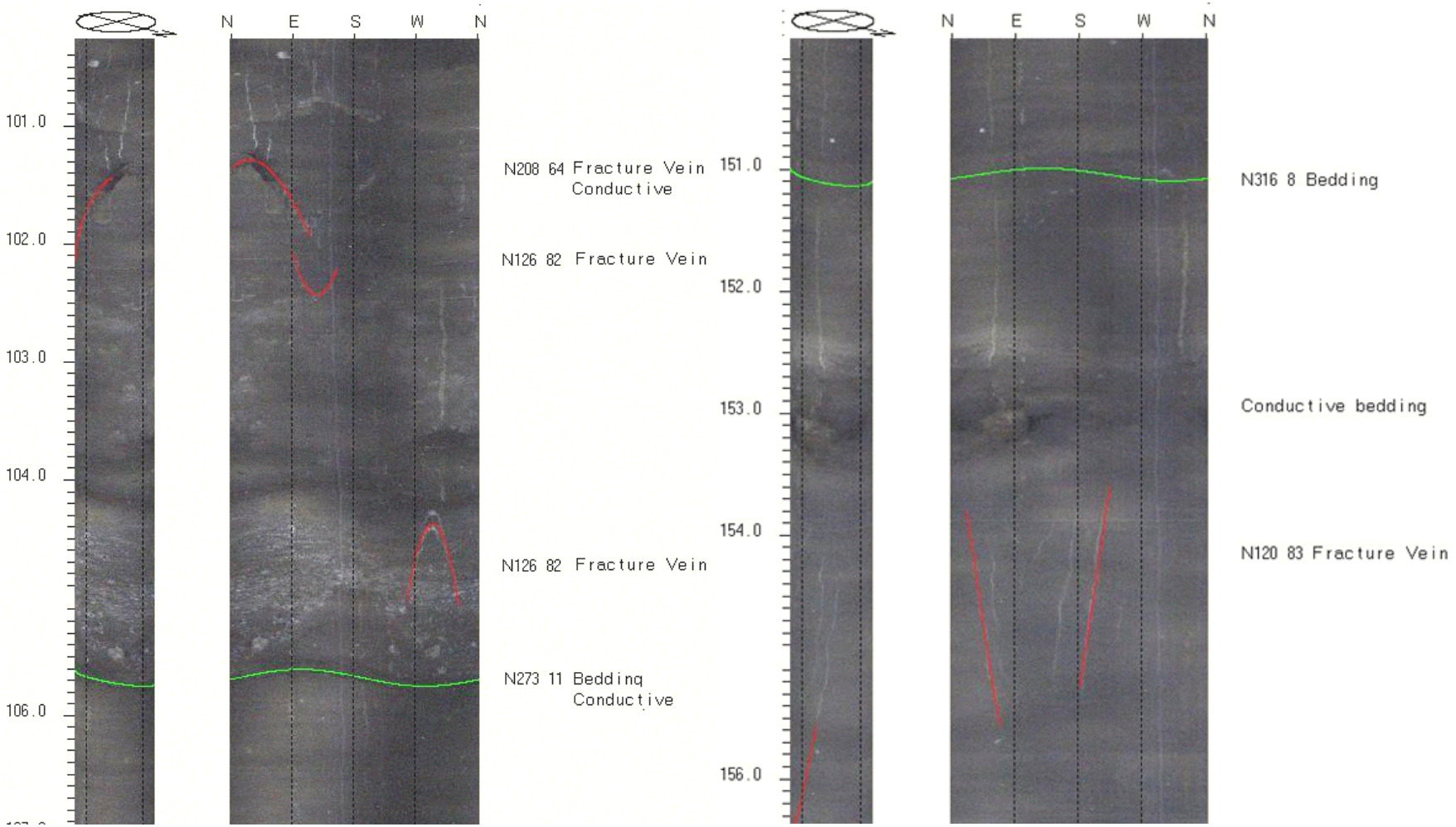

FIGURE 2B3. OPTV records of the 8-inch diameter well 22 showing bedrock structures and hydraulically-conductive features in sandstone and siltstone. Depth values are in feet below land surface.

Wells 23 to 25 - Brunswick sandstone

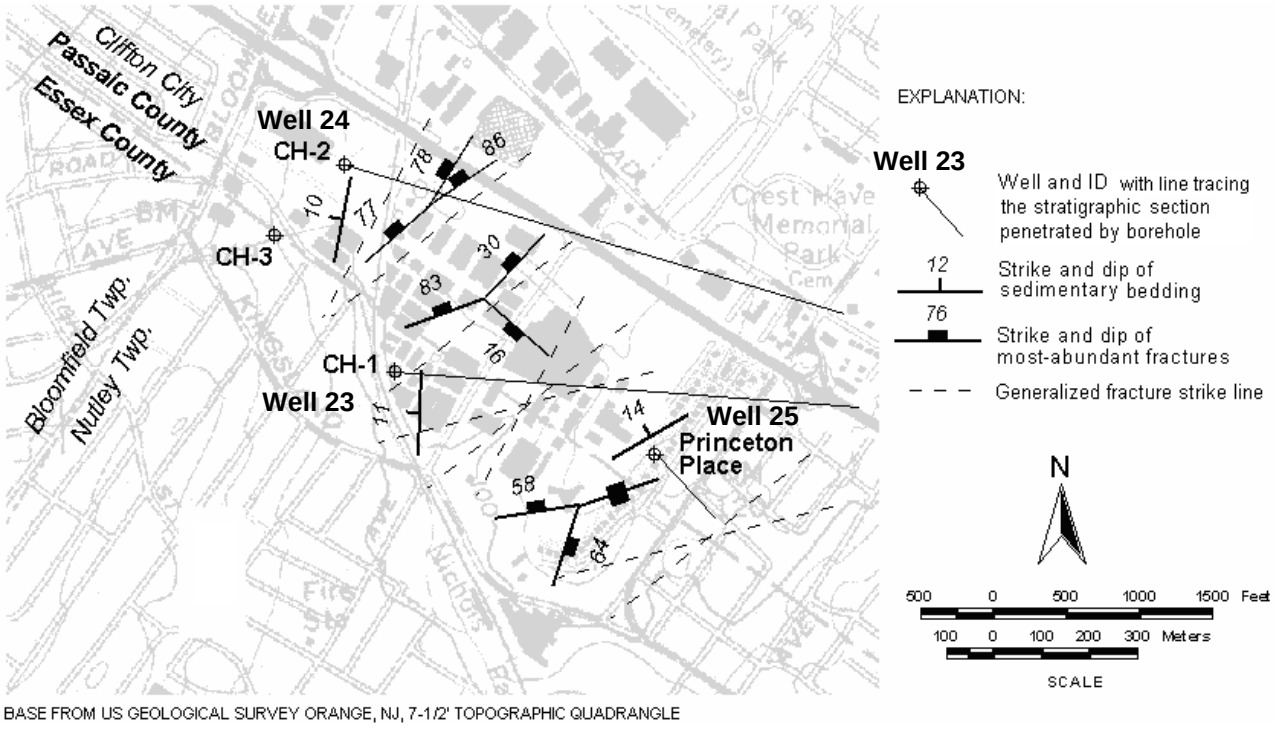

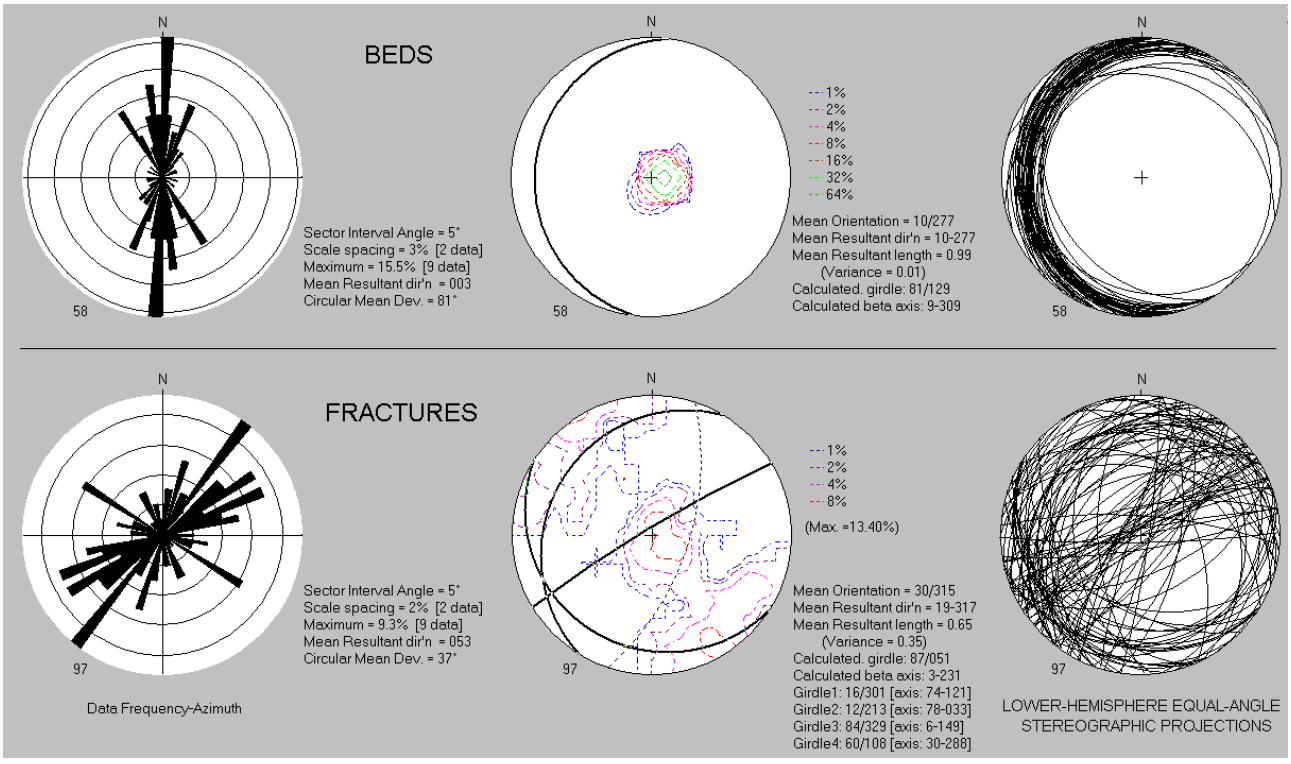

Figure 2C1. Map (above) shows wells 23 through 25 in the vicinity of the Hoffman-LaRoche facility, Clifton City, Passaic County and Nutley Twp., Essex County, NJ. Mapped bedrock structures based on a structural analysis (below) of the OPTV records.

Well 23 – Brunswick sandstone

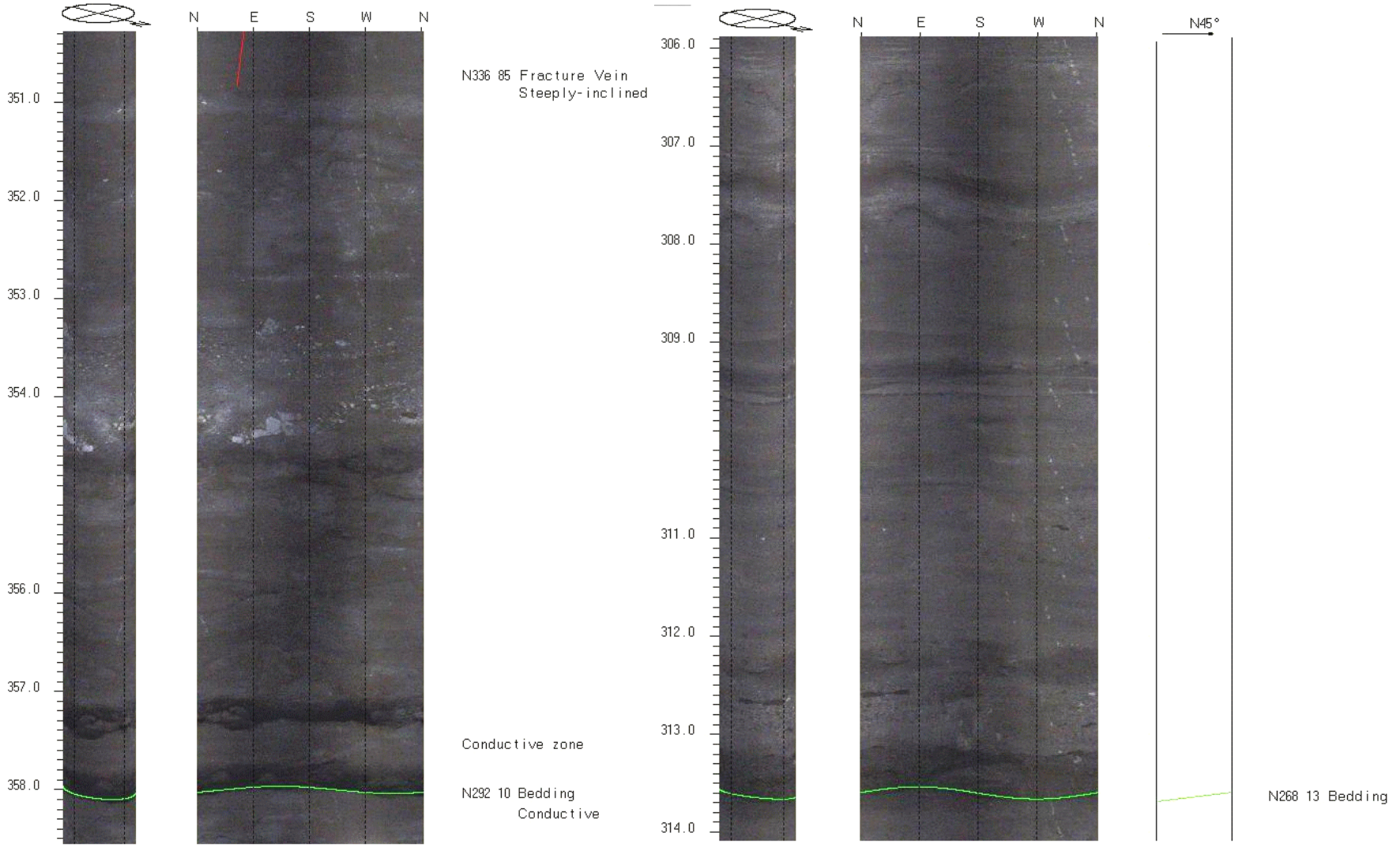

FIGURE 2C2. OPTV records of the 8-inch diameter well 23 showing bedrock structures and hydraulically-conductive features in sandstone. Depth values are in feet below land surface.

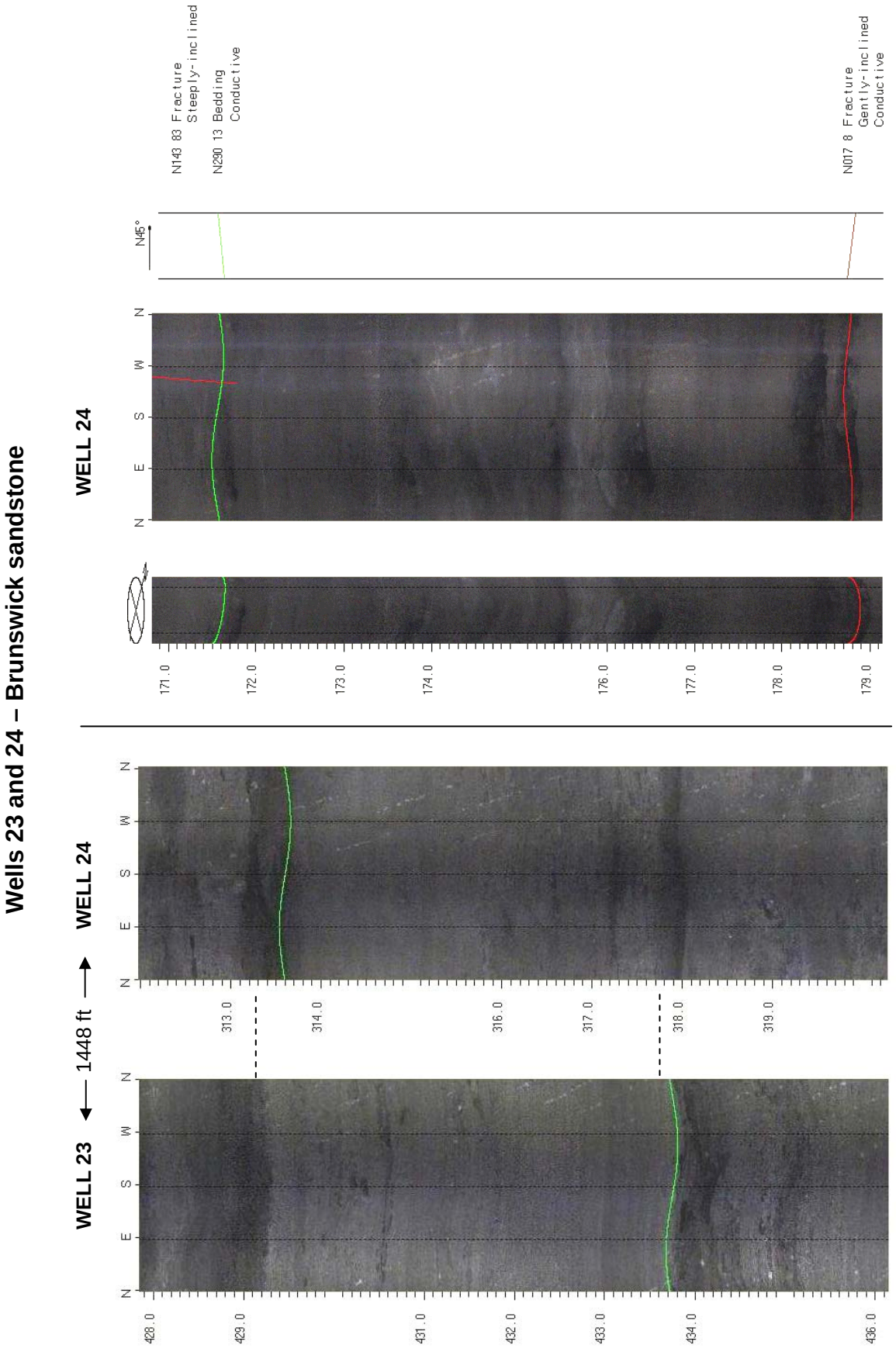

FIGURE 2C3. Stratigraphic correlation (left) for wells 23 and 24 based on OPTV records and an OPTV record for the 8-inch diameter well 24 (right) showing bedrock structures and hydraulically-conductive feature in sandstone and siltstone. Depth values are in feet below land surface.

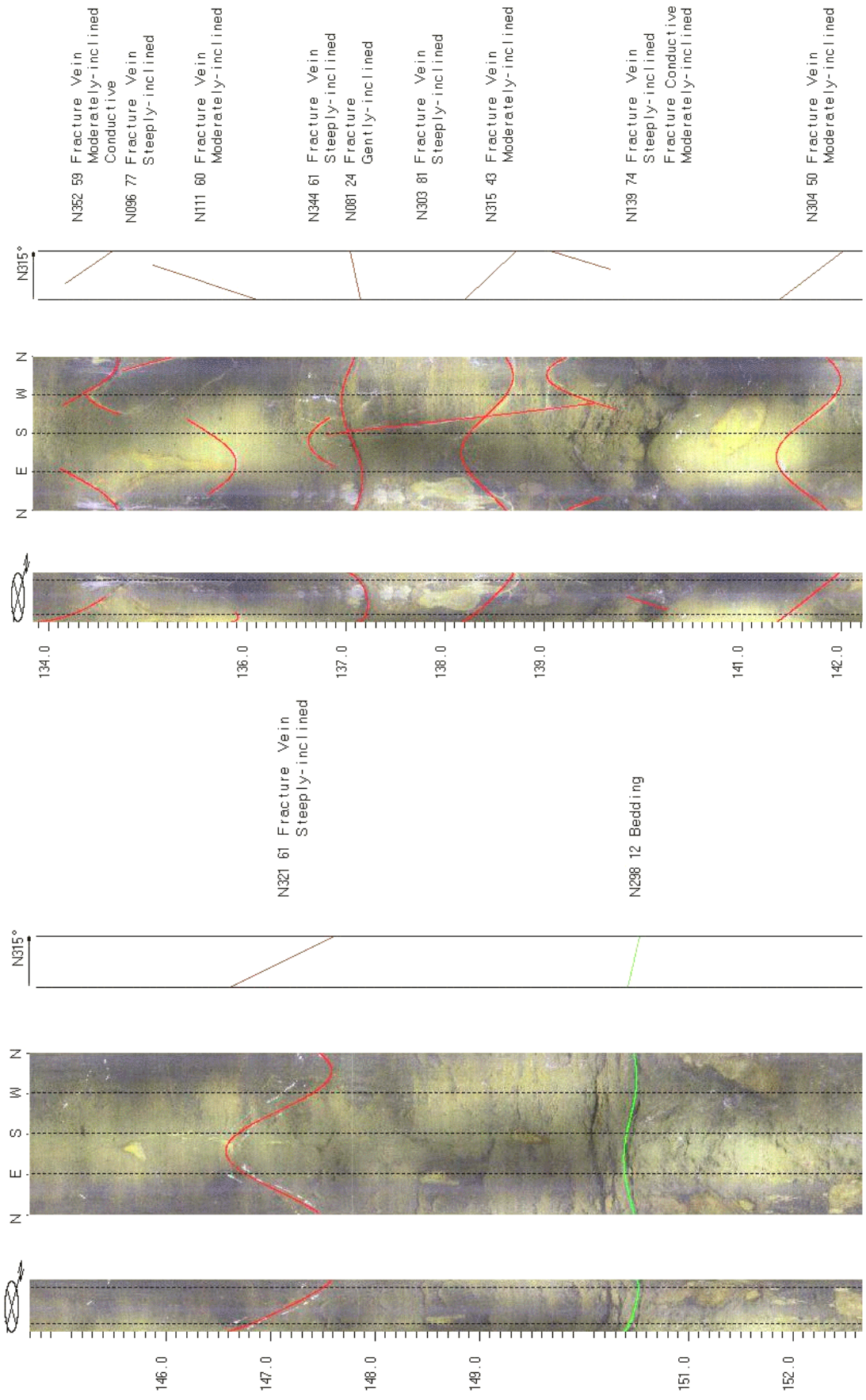

FIGURE 2C4. OPTV records of the 6-inch diameter well 25 showing bedrock structures and hydraulically-conductive features in sandstone. Depth values are in feet below land surface.

Wells 26 to 28 - Brunswick conglomerate

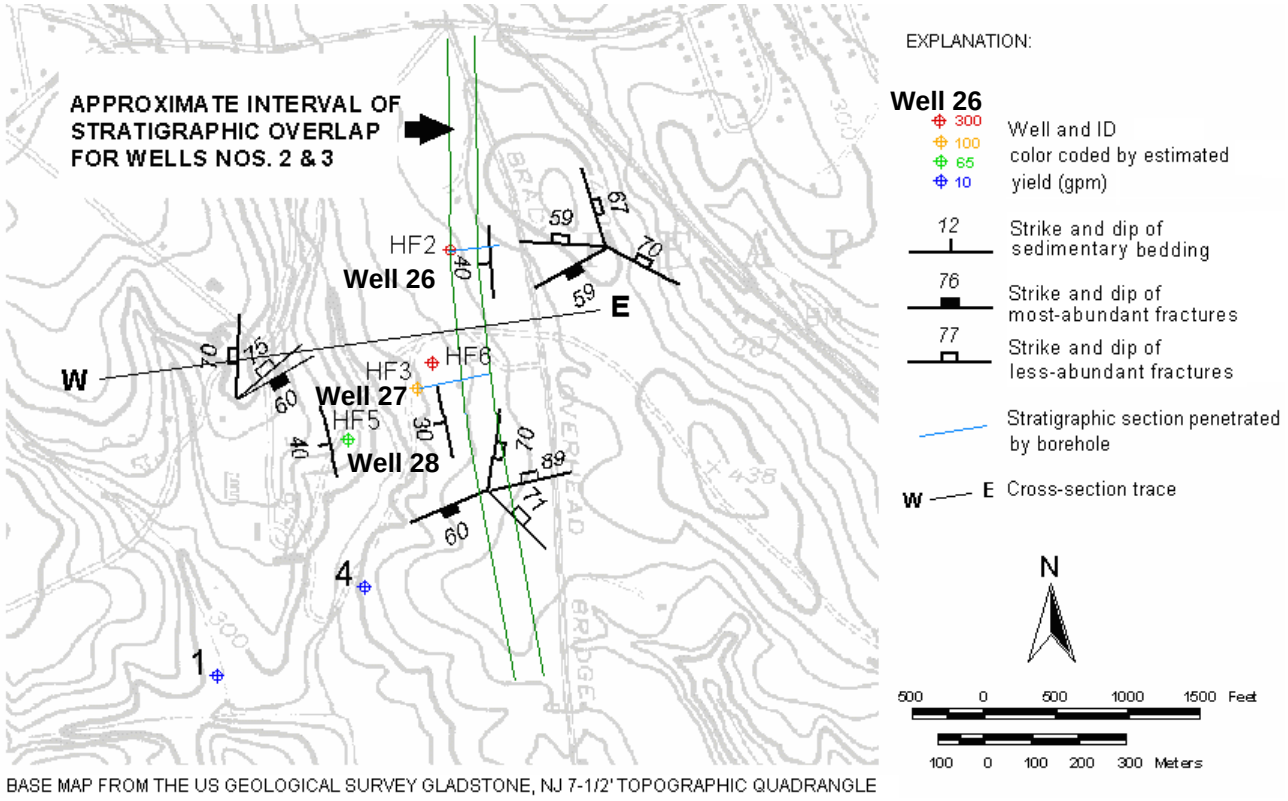

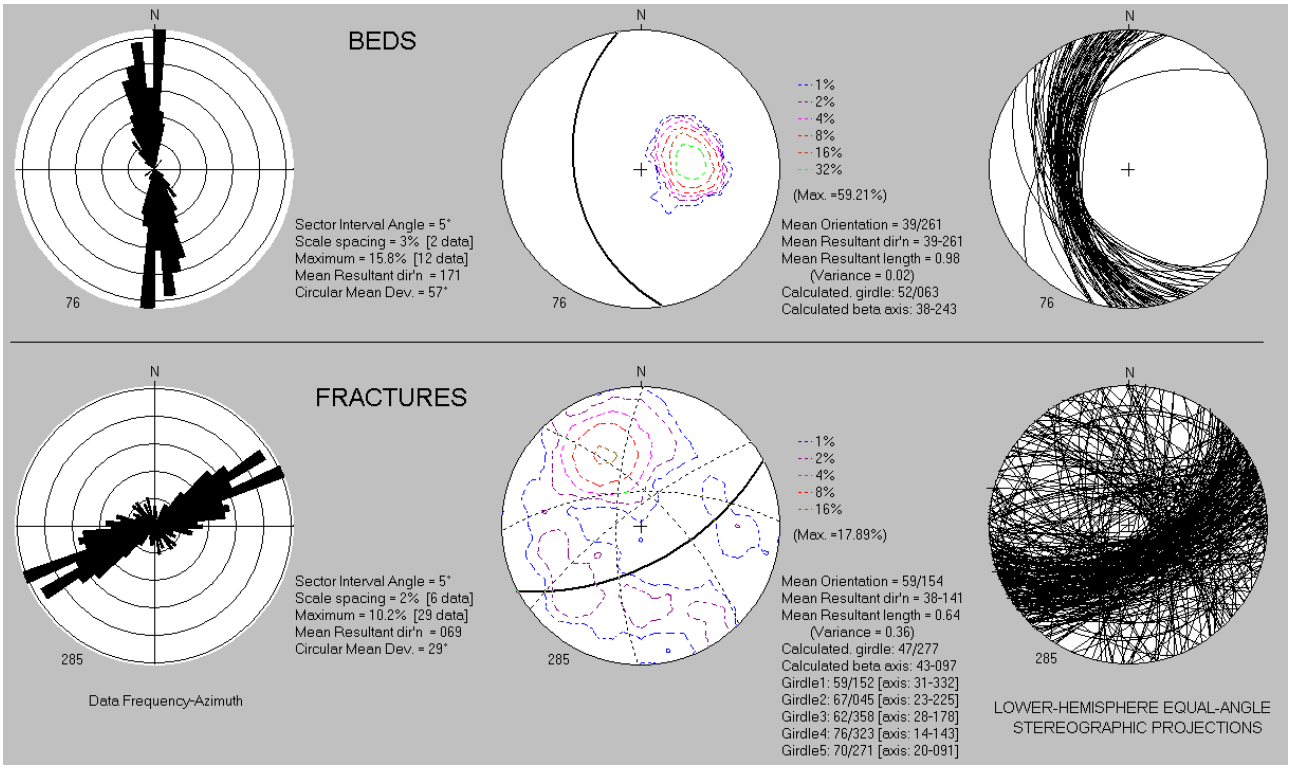

Figure 2D1. Map (above) shows wells 26 through 28 on the Hamilton Farms Golf Club, Bedminster Twp., Somerset County, NJ. Mapped bedrock structures based on structural analysis (below) of the OPTV records.

Wells 26 to 28 - Brunswick conglomerate

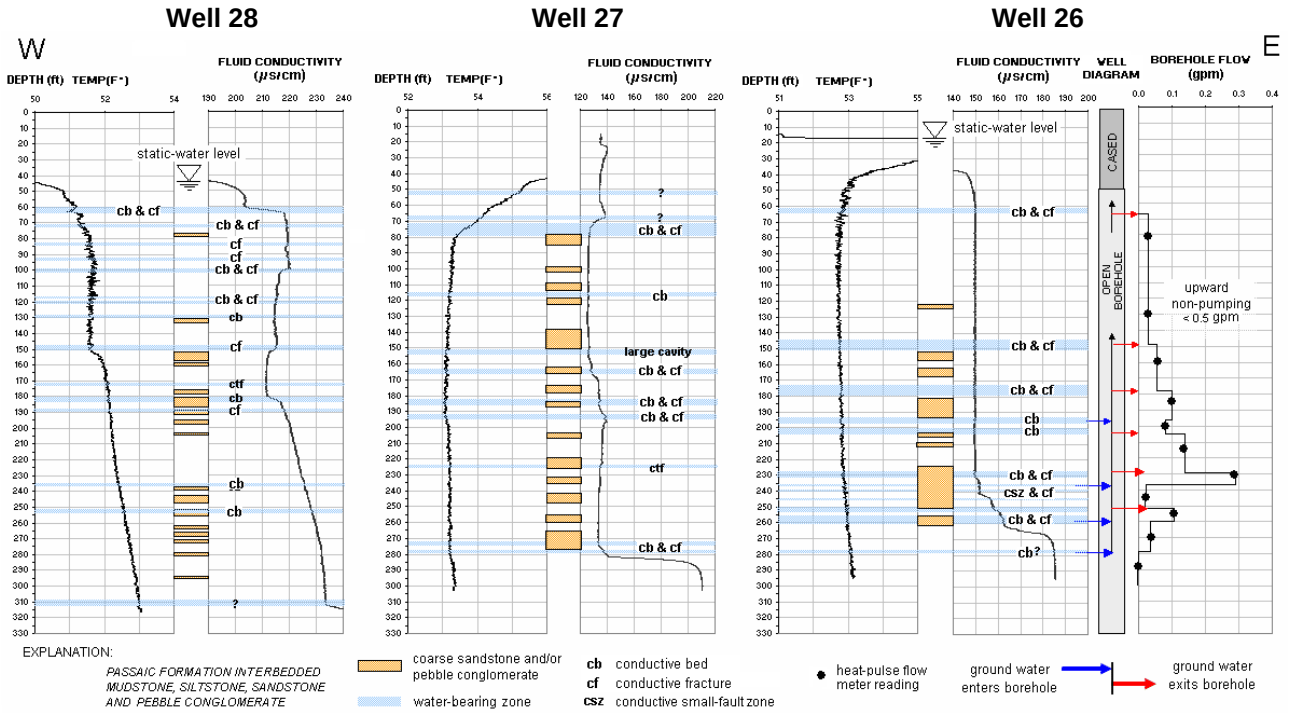

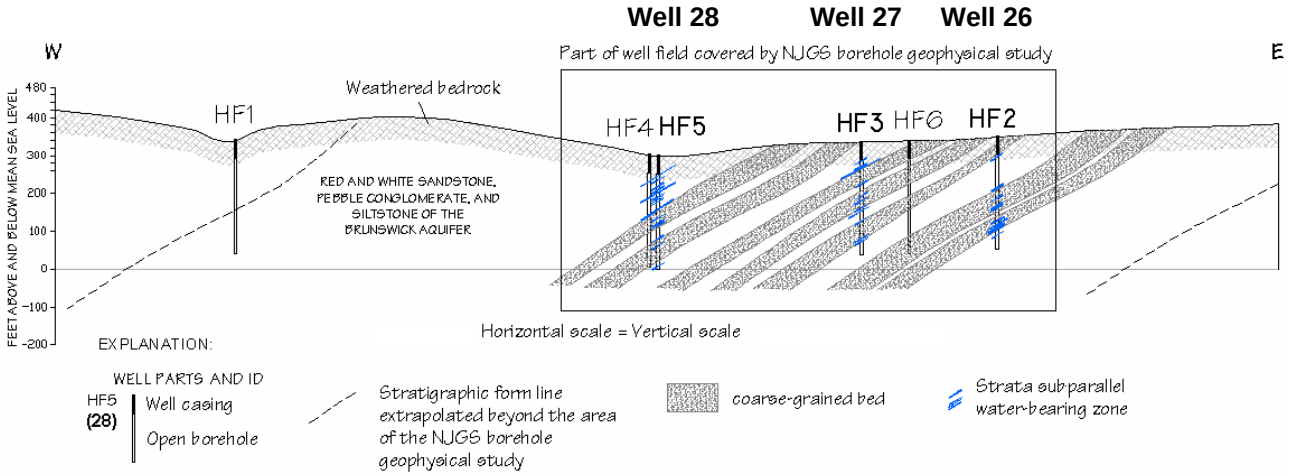

Figure 2D2. Hydrogeologic sections (above) based on geophysical logs for wells 26 through 28 showing the vertical distribution of hydraulically-conductive features and water-bearing zones in red and gray sandstone, conglomerate, siltstone and mudstone. Depth values are feet below land surface. The map trace for the hydrogeologic cross section (below) shown on figure 2D1.

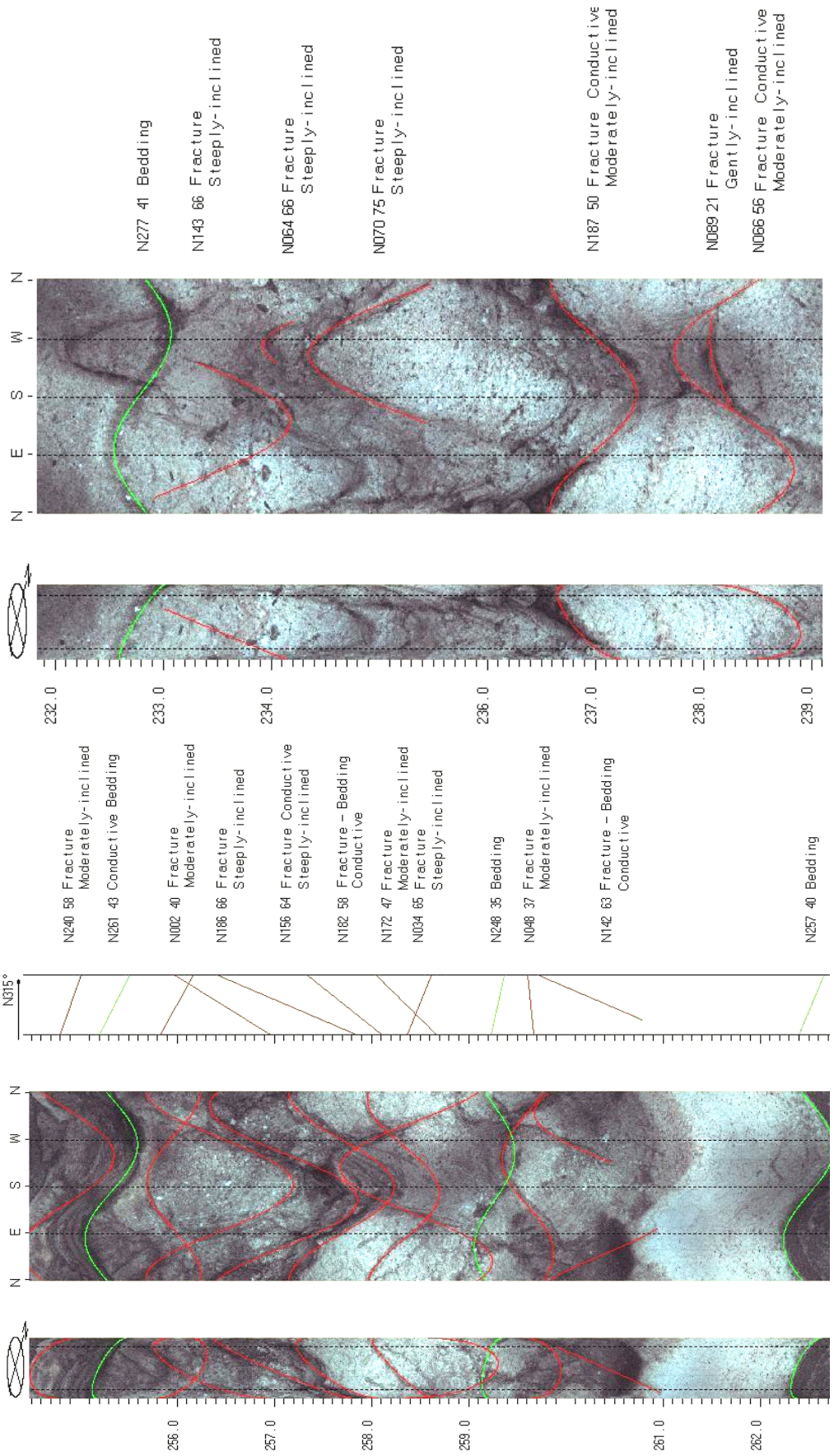

FIGURE 2D3. OPTV records of the 8-inch diameter well 26 showing bedrock structures and hydraulically-conductive features in conglomerate and sandstone. Depth values are in feet below land surface.

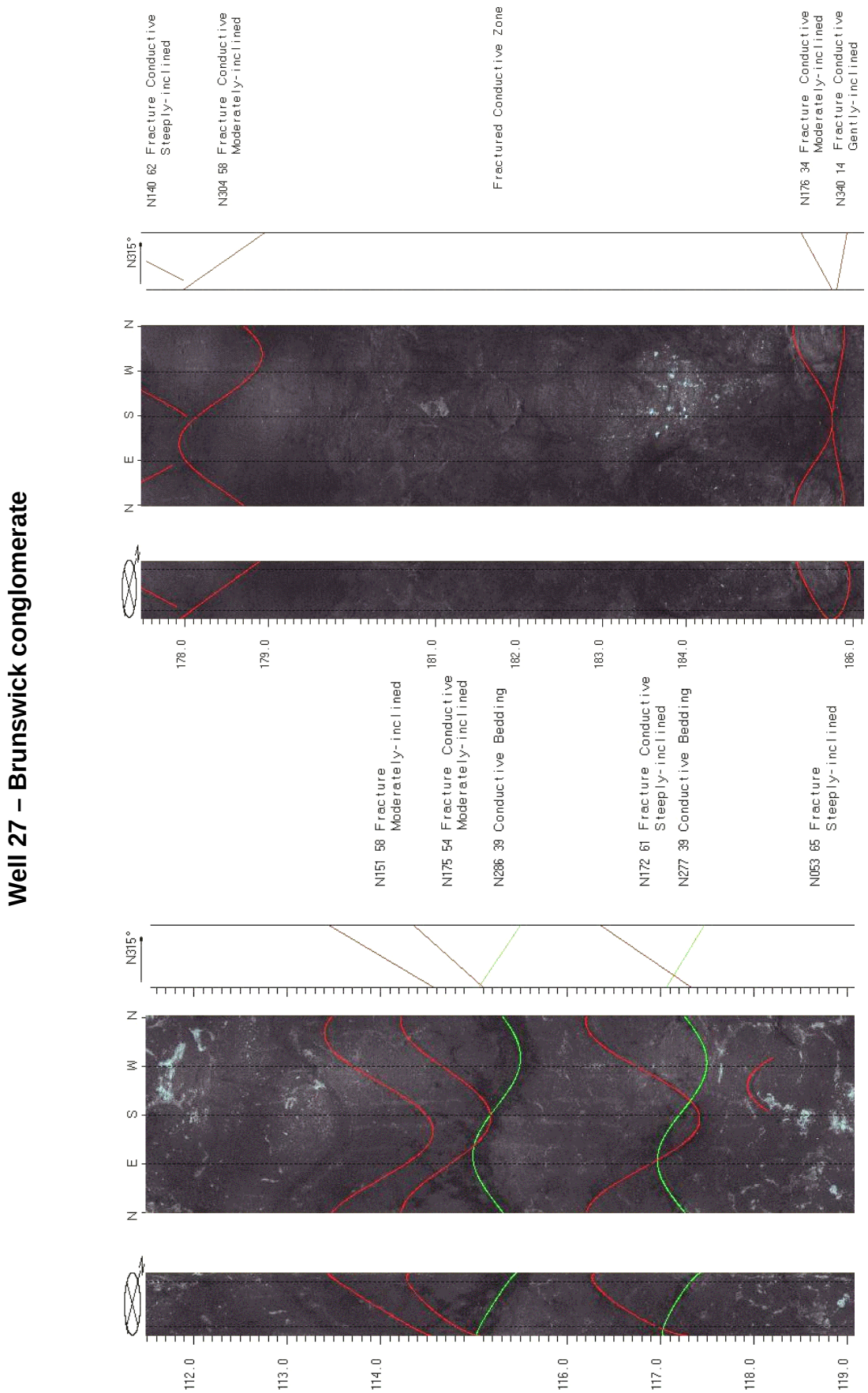

FIGURE 2D4. OPTV records of the 8-inch diameter well 27 showing bedrock structures and hydraulically-conductive features in conglomerate, sandstone and siltstone. Depth values are in feet below land surface.

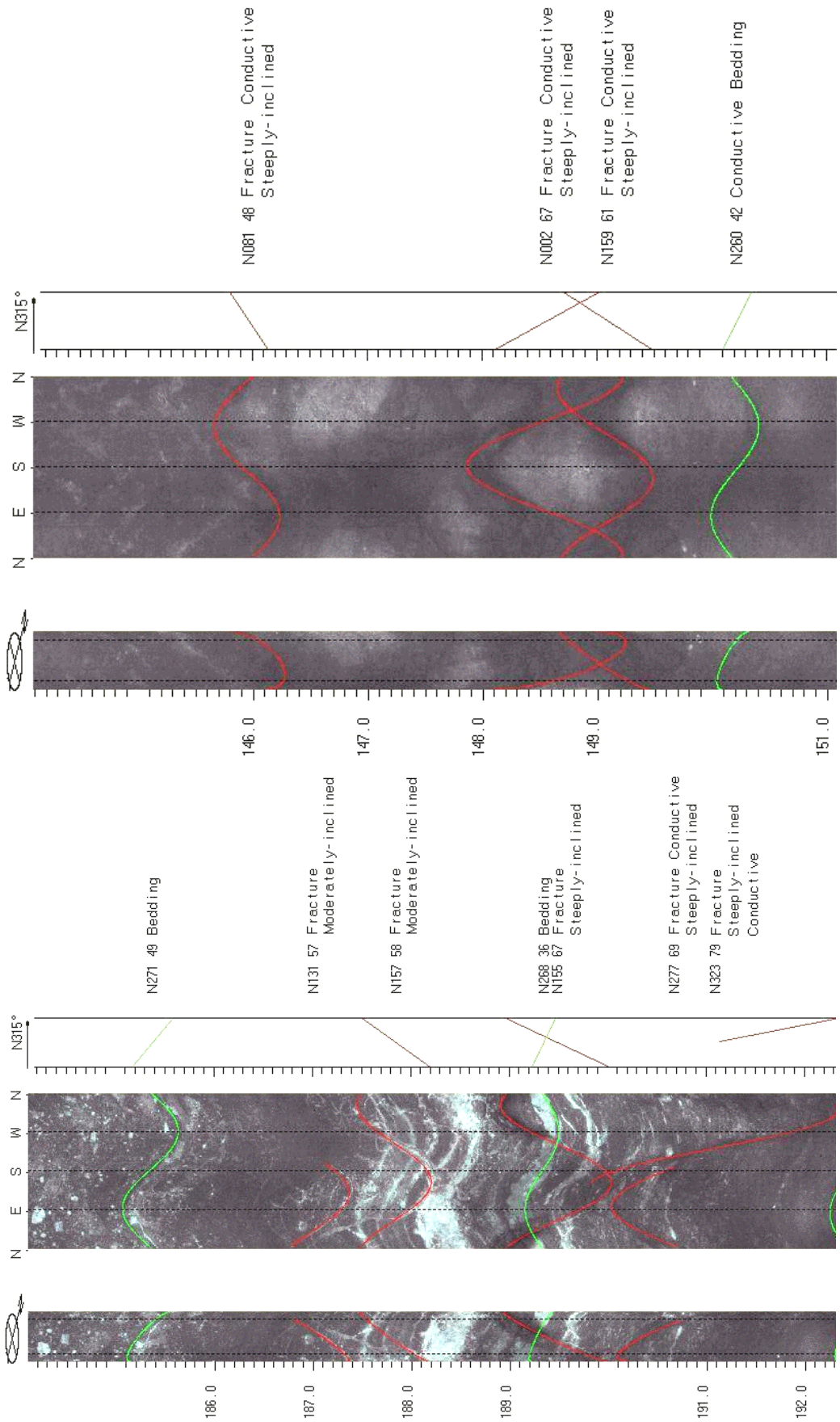

FIGURE 2D5. OPTV records of the 6-inch diameter well 28 showing bedrock structures and hydraulically-conductive features in conglomerate, sandstone, siltstone and mudstone. Depth values are in feet below land surface.

Wells 29 to 33 – Coarse-grained units in the Brunswick lower gray zone

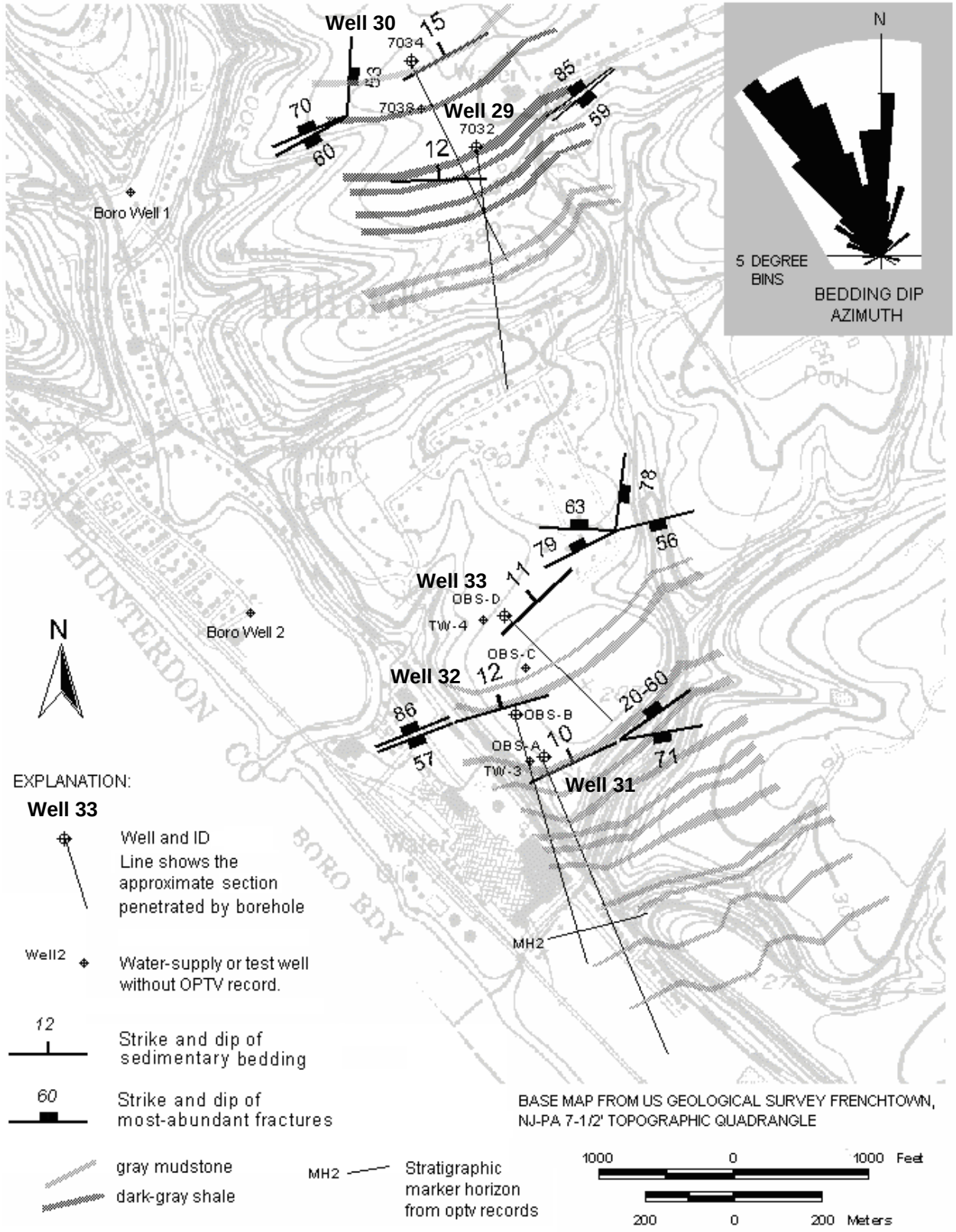

Figure 2E1. Map shows wells 29 through 33 in the vicinity of Milford Boro., Milford Twp., Hunterdon County, NJ. Mapped bedrock structures based on structural analyses of the OPTV records.

Wells 29 to 33 - Coarse-grained units in the Brunswick lower gray zone

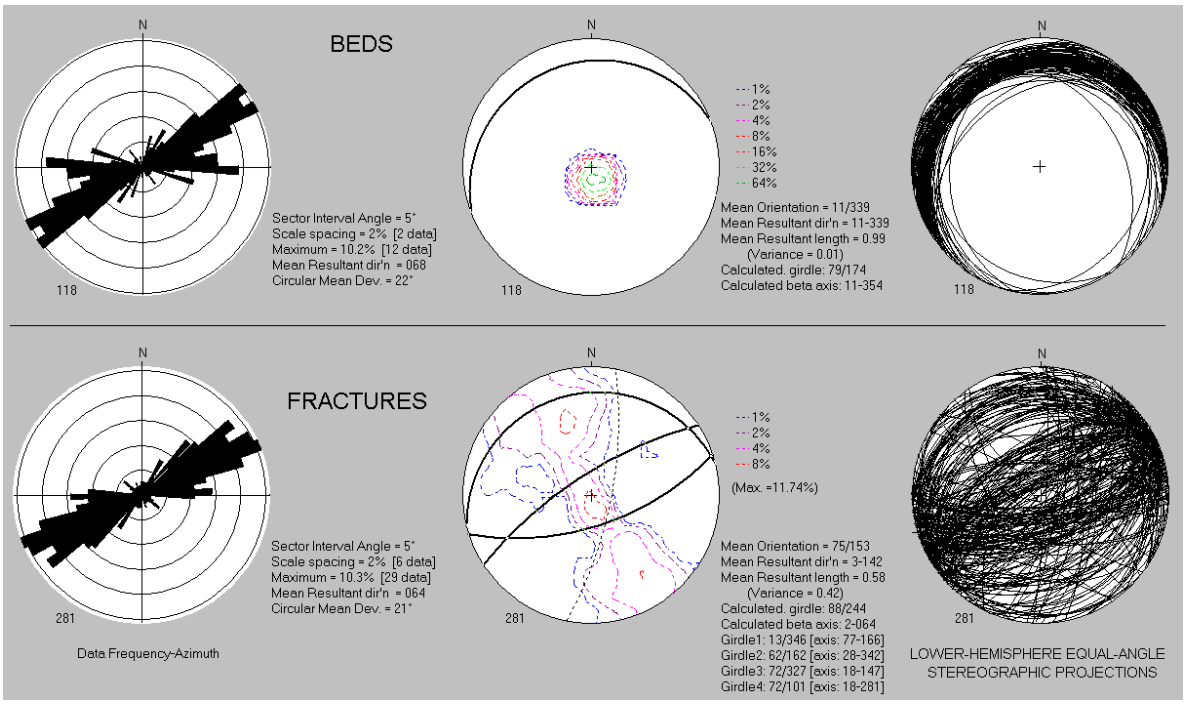

Well 29 - Coarse-grained units in the Brunswick lower gray zone

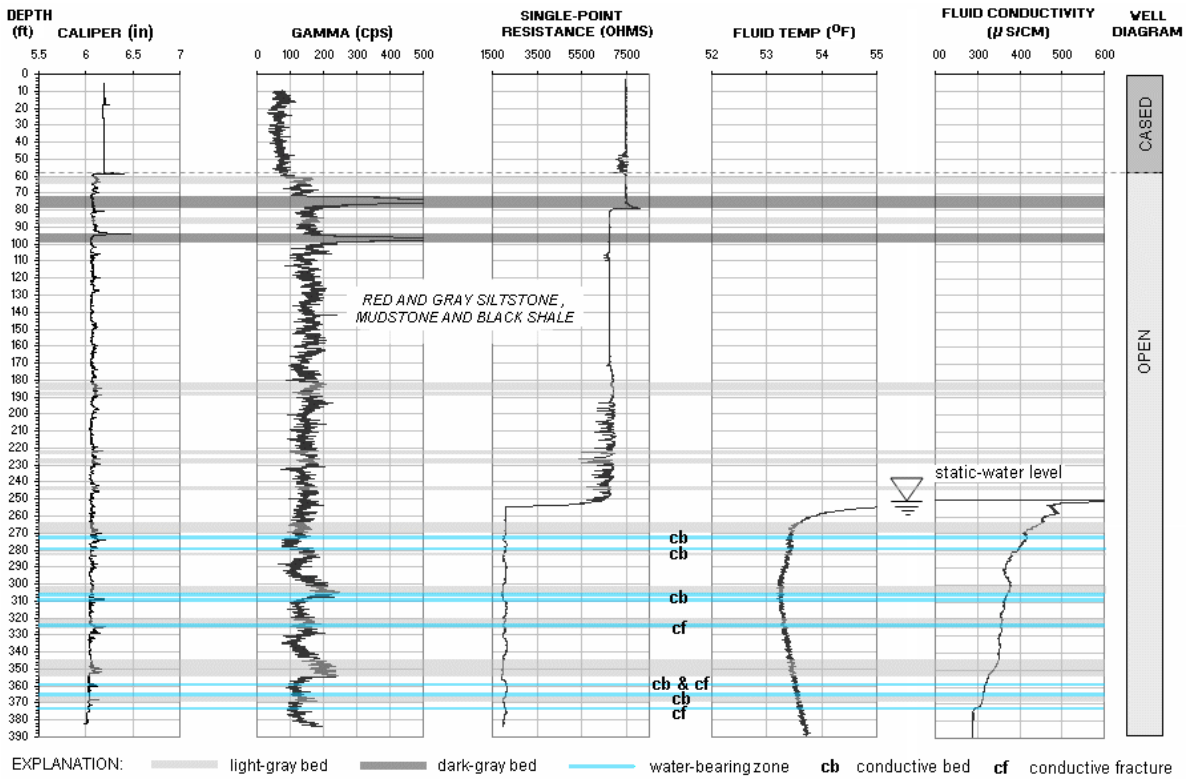

Figure 2E2. Structural analysis of OPTV records for wells 29 through 33 (above) and hydrogeologic section based on geophysical logs for well 29 (below) showing the vertical distribution and types of hydraulically-conductive features and water-bearing zones in siltstone, mudstone and shale. Depth values are in feet below land surface.

Well 30 - Coarse-grained units in the Brunswick lower gray zone

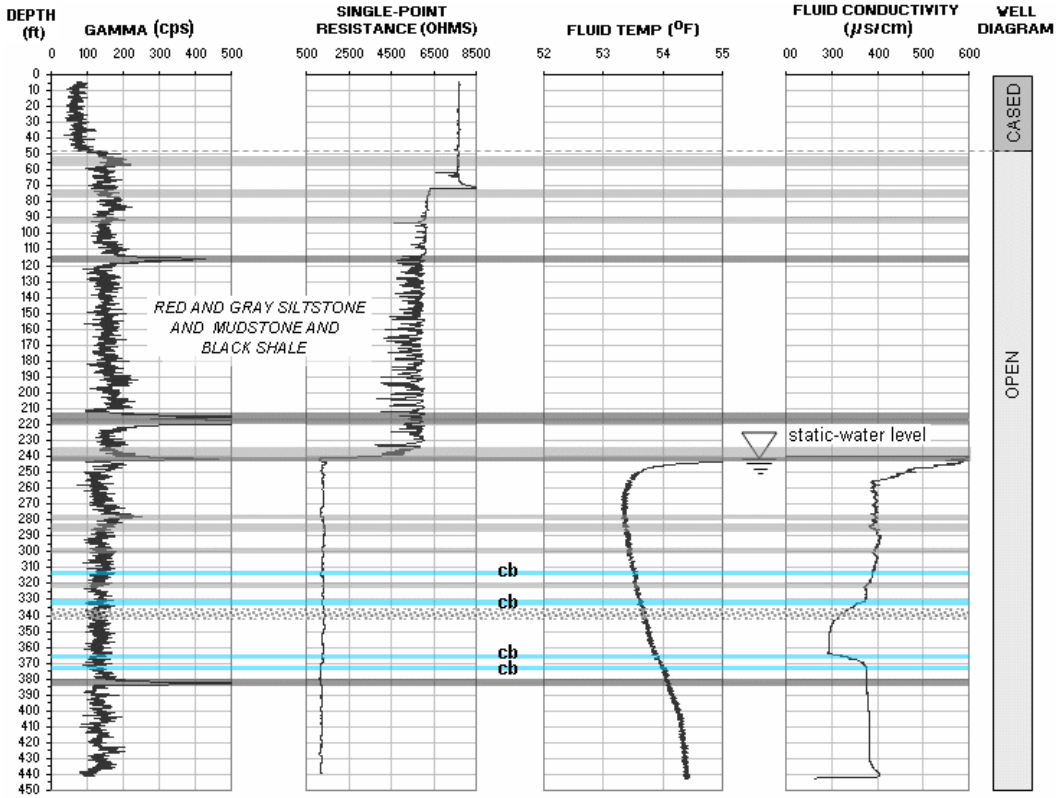

Well 31 - Coarse-grained units in the Brunswick lower gray zone

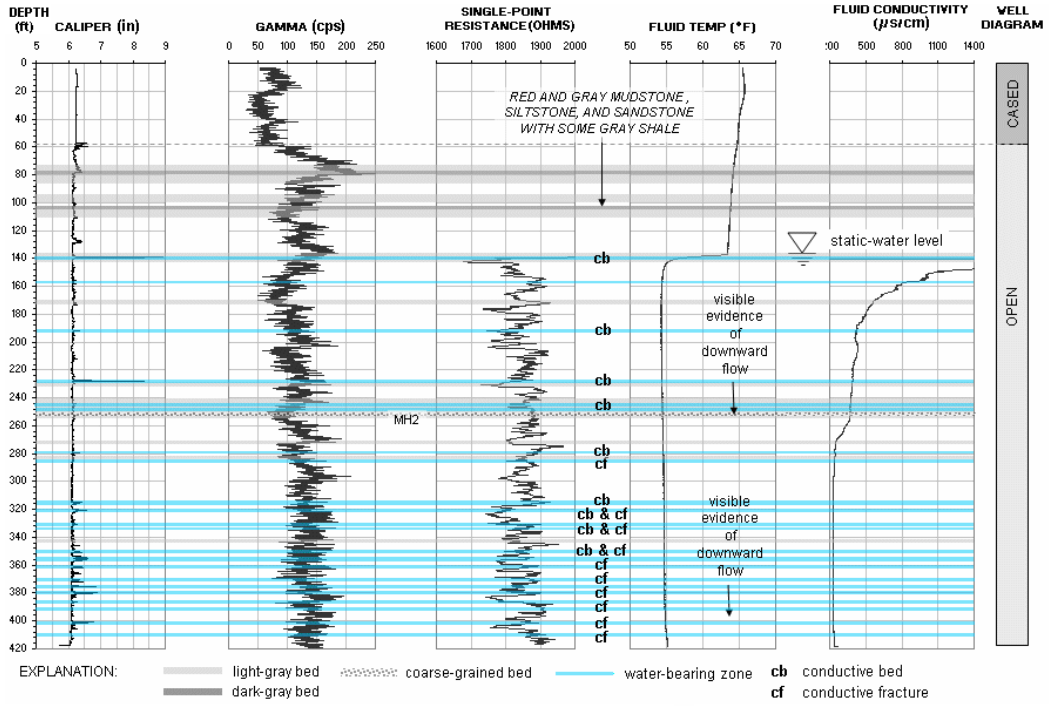

Figure 2E3. Hydrogeologic sections based on geophysical logs for wells 30 (above) and 31 (below) showing the vertical distribution and types of hydraulically-conductive features and water-bearing zones in siltstone, mudstone, shale and sandstone. Depth values are in feet below land surface.

Well 32 - Coarse-grained units in the Brunswick lower gray zone

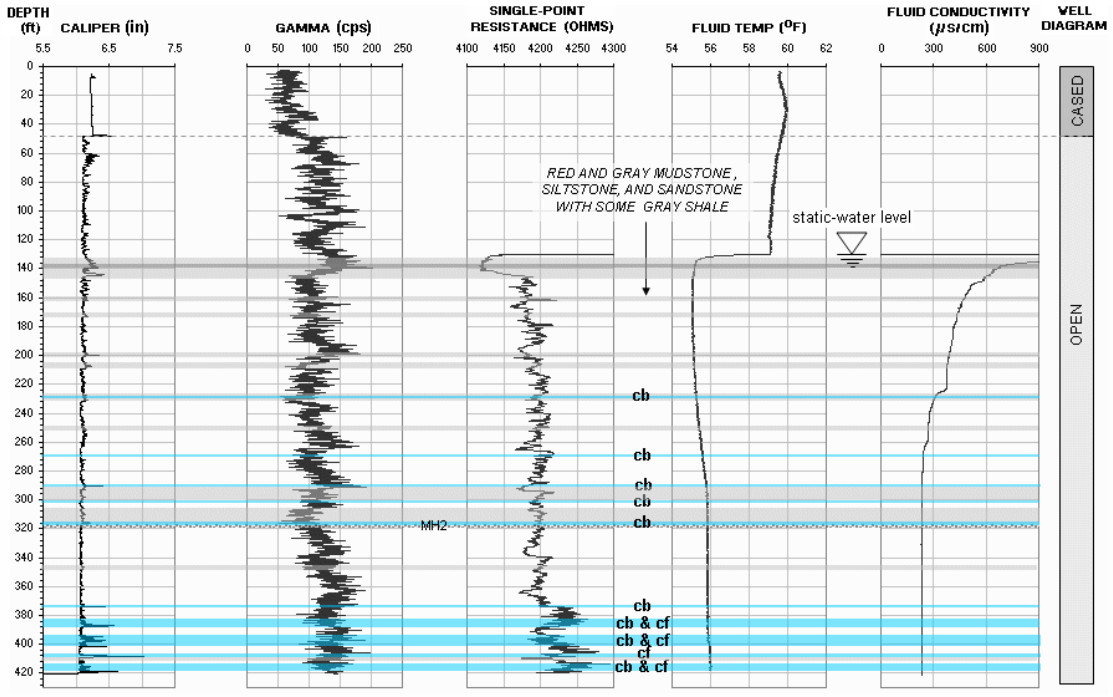

Well 33 - Coarse-grained units in the Brunswick lower gray zone

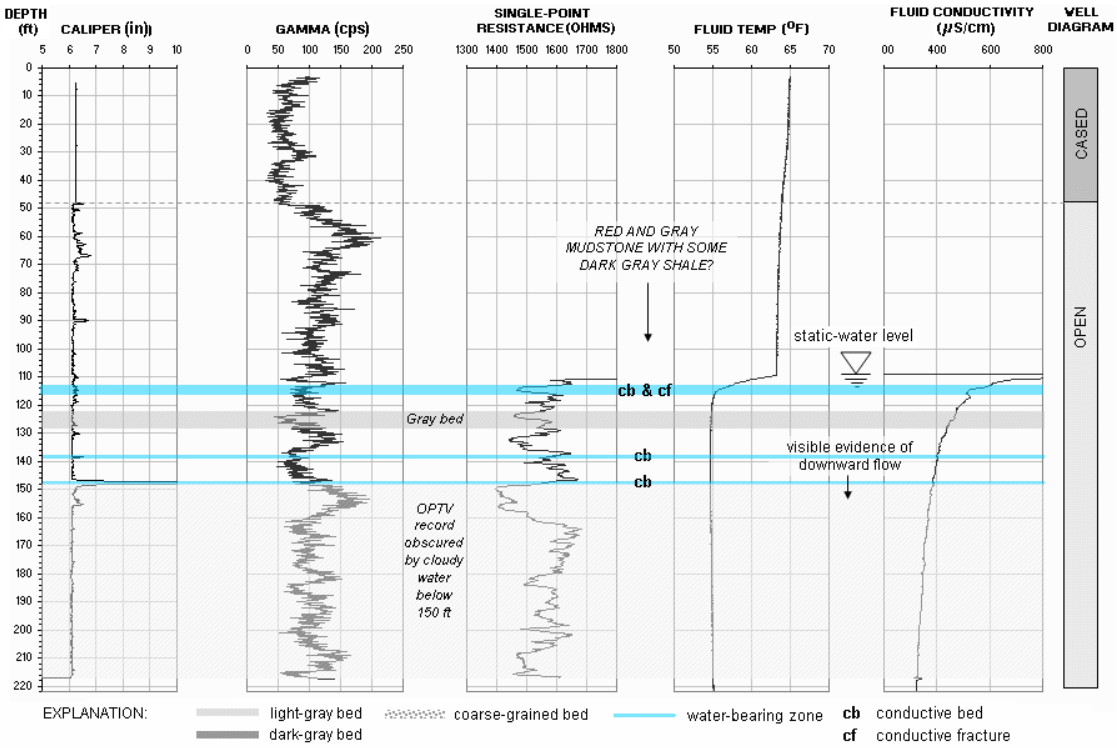

Figure 2E4. Hydrogeologic sections based on geophysical logs for wells 32 (above) and 33 (below) showing the vertical distribution and types of hydraulically-conductive features and water-bearing zones in siltstone, mudstone, shale and sandstone. Depth values are in feet below land surface.

Wells 29 and 30 – Coarse-grained units in the Brunswick lower gray zone

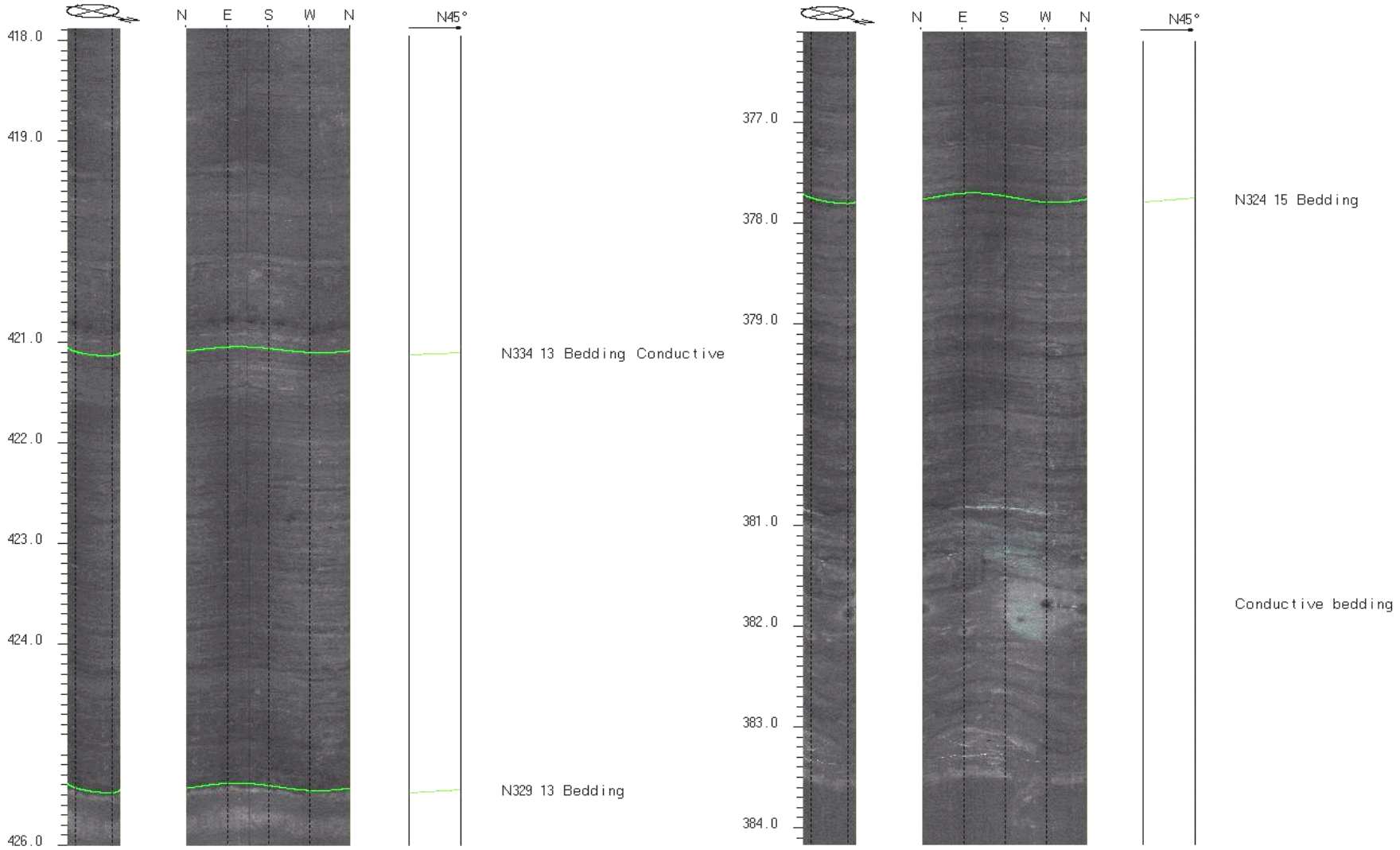

FIGURE 2E5. OPTV records of the 6-inch diameter wells 29 (left) and 30 (right) showing bedrock structures and hydraulically-conductive features in sandstone and siltstone. Depth values are in feet below land surface.

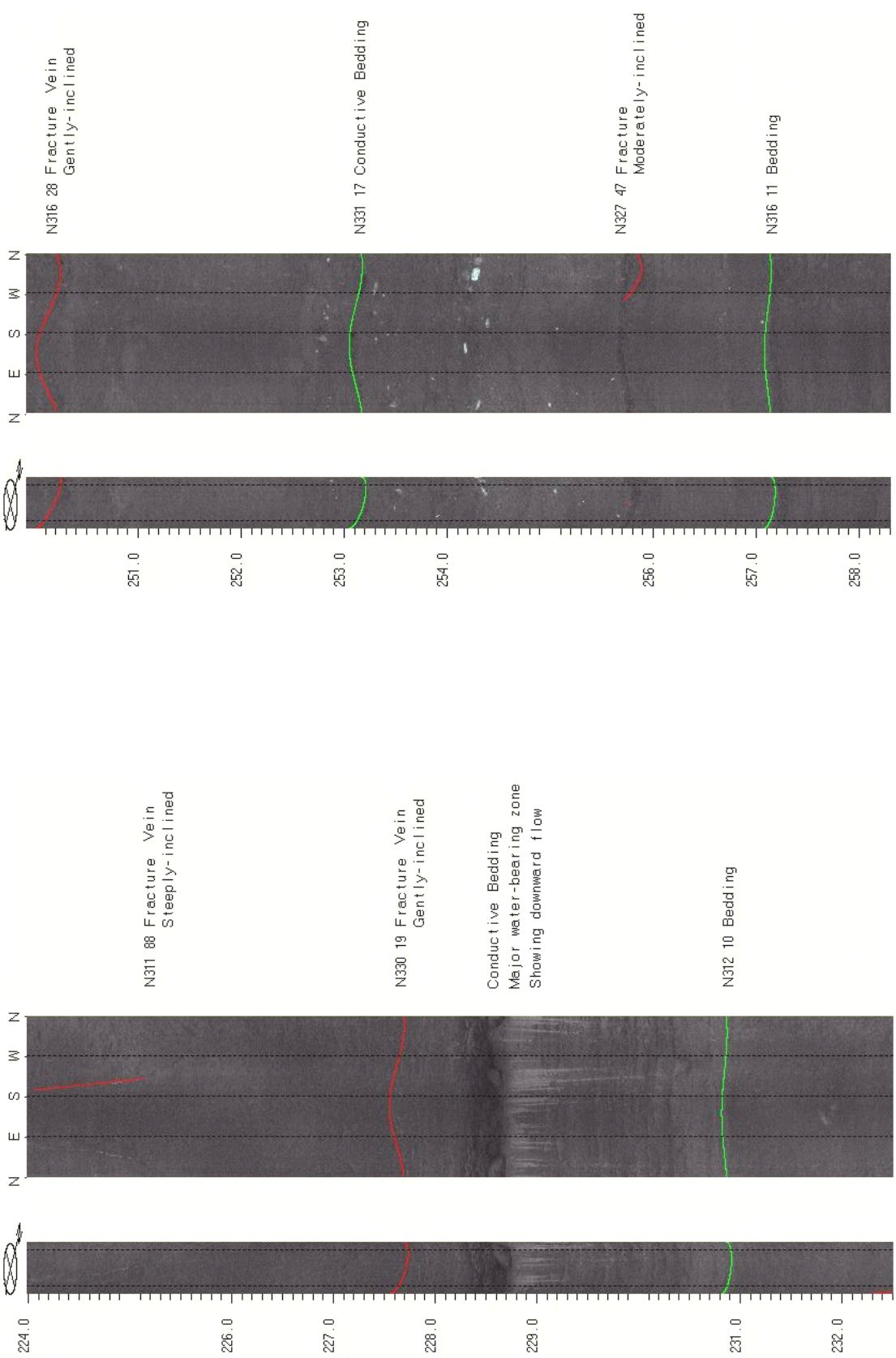

FIGURE 2E6. OPTV records of the 6-inch diameter well 31 showing bedrock structures and hydraulically-conductive features in sandstone and siltstone. Mineral deposits seen as light-colored stains on the borehole wall (left) emanate from conductive feature and taper downward in the direction of water flow. Depth values are in feet below land surface.

Wells 31 and 32 – Coarse-grained units in the Brunswick lower gray zone

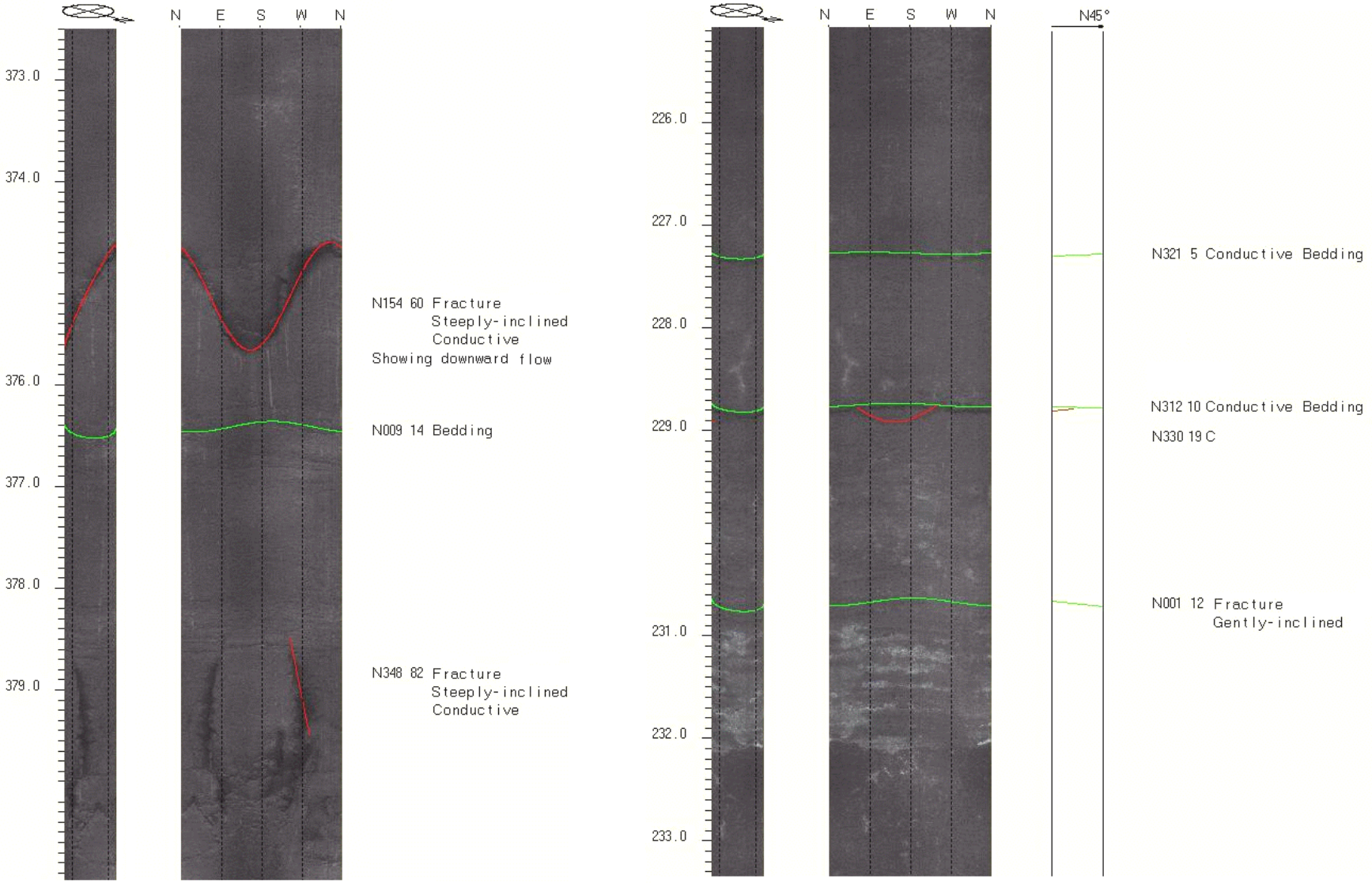

FIGURE 2E7. OPTV records of the 6-inch diameter wells 31 (left) and 32 (right) showing bedrock structures and hydraulically-conductive features in sandstone, siltstone and mudstone. Depth values are in feet below land surface.

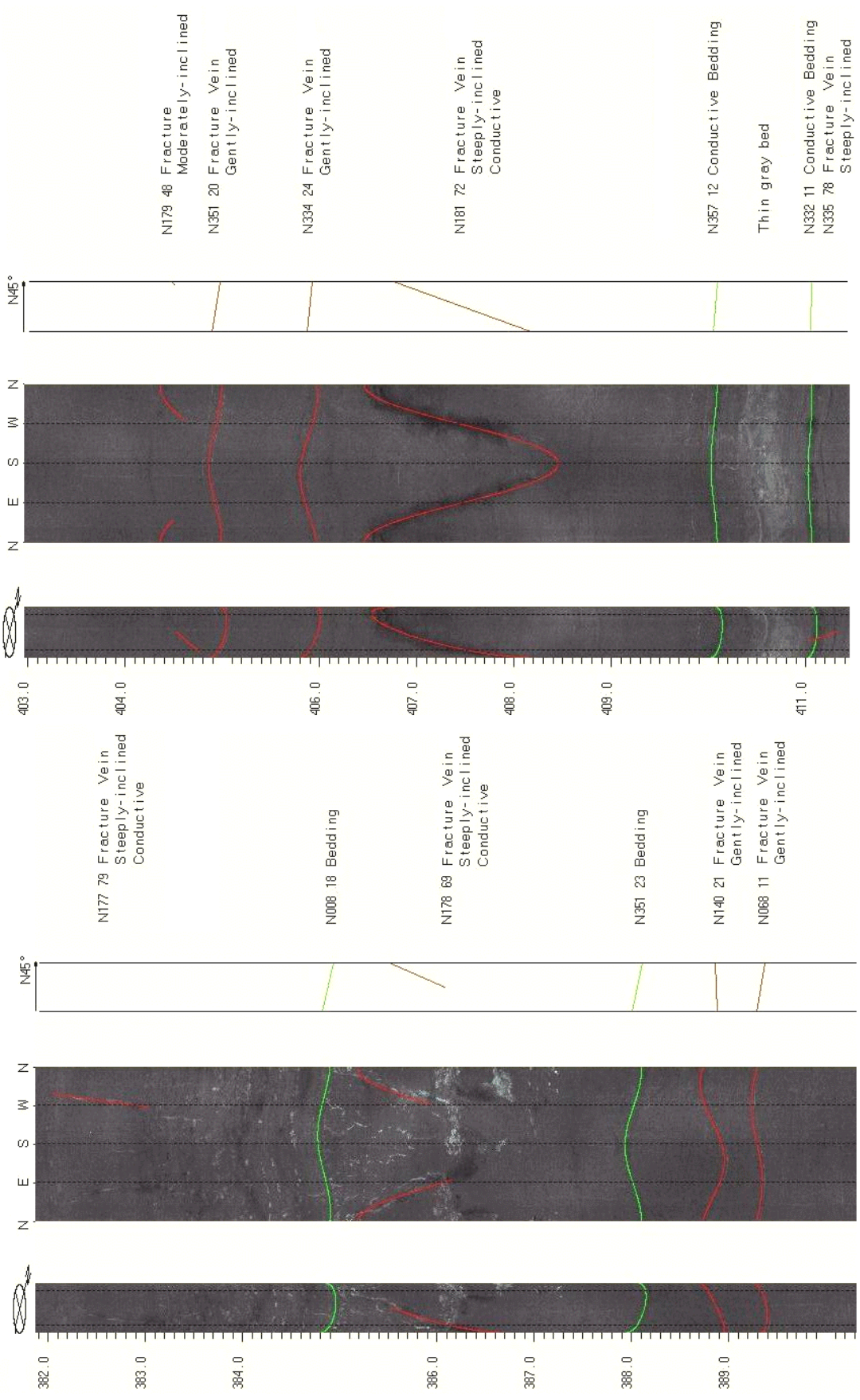

FIGURE 2E8. OPTV records of the 6-inch diameter well 32 showing bedrock structures and hydraulically-conductive features in conglomerate and sandstone. Depth values are in feet below land surface.

Wells 34 to 42 – Passaic flood tunnel workshaft geotechnical investigations

Flooding in New Jersey's Passaic river valley has seriously affected human habitation since the mid-19th century. Since then, the Army Corps of Engineers (ACE) proposed several flood control projects resulting in various subsurface geotechnical investigations conducted in the region from 1959 to 1983. A major flood in 1984 resulted in a new proposal for the Passaic River Flood Protection Plan that was accepted by local, State, and Federal officials. This plan called for construction of a dual-inlet water-diversion tunnel system that would prevent flooding by diverting floodwater through a tunnel connecting the upper watershed to a lower reach of the Passaic River. The U.S. Congress initially appropriated $60 million for the project. Subsurface investigations conducted during 1985-86 included the drilling of 45 rock cores along the proposed tunnel alignment (Phase 1 – fig. 2F1). A revised tunnel alignment (Phase 2 – fig. 2F1) was subsequently proposed based on analyses from Phase1 investigations. The revised tunnel system was about 20 miles long, 40 feet wide and as much as 450 feet below the surface extending to an outlet in the vicinity of Kearny Point in Newark Bay.

In 1990, the U.S. Congress authorized $1.2 billion for the Passaic River Flood Protection Project to be administered by the State of New Jersey and the ACE New York District. Phase 2 work included 154 additional rock cores and a set of detailed hydrogeological analyses conducted near workshafts along the tunnel alignment beginning in 1994. These analyses included detailed geological descriptions of bedrock core, geophysical logs of deep bedrock borings, and straddle packer-test studies for determining ground-water yield and aquifer parameters for specific bedrock intervals. The results of the hydrogeological analyses were summarized in a report by IT Corporation in 1995 and are recompiled here with a series of borehole-data summaries. The Passaic River Flood Protection Plan was abandoned by Federal and State legislators in the mid-1990s because of rising costs and local concerns of negative environmental impacts.

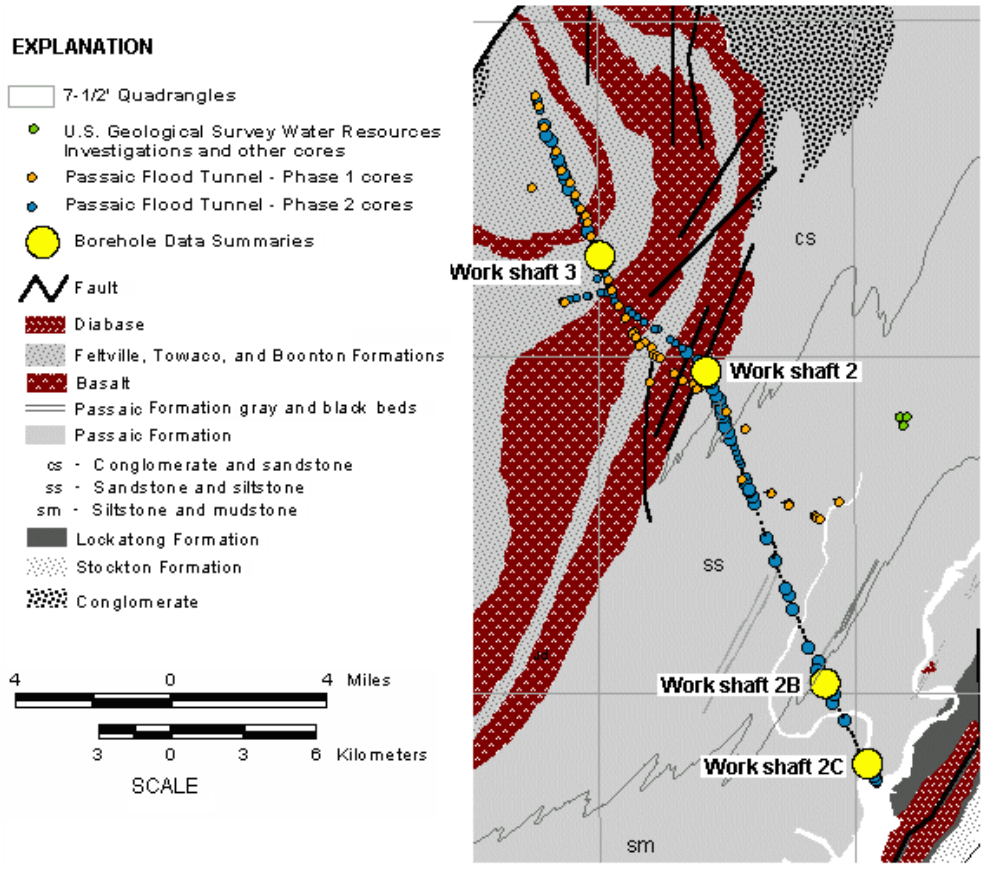

FIGURE 2F1 - Map showing location of rock cores and work shafts from the Army Corp. of Engineers Passaic flood tunnel project.

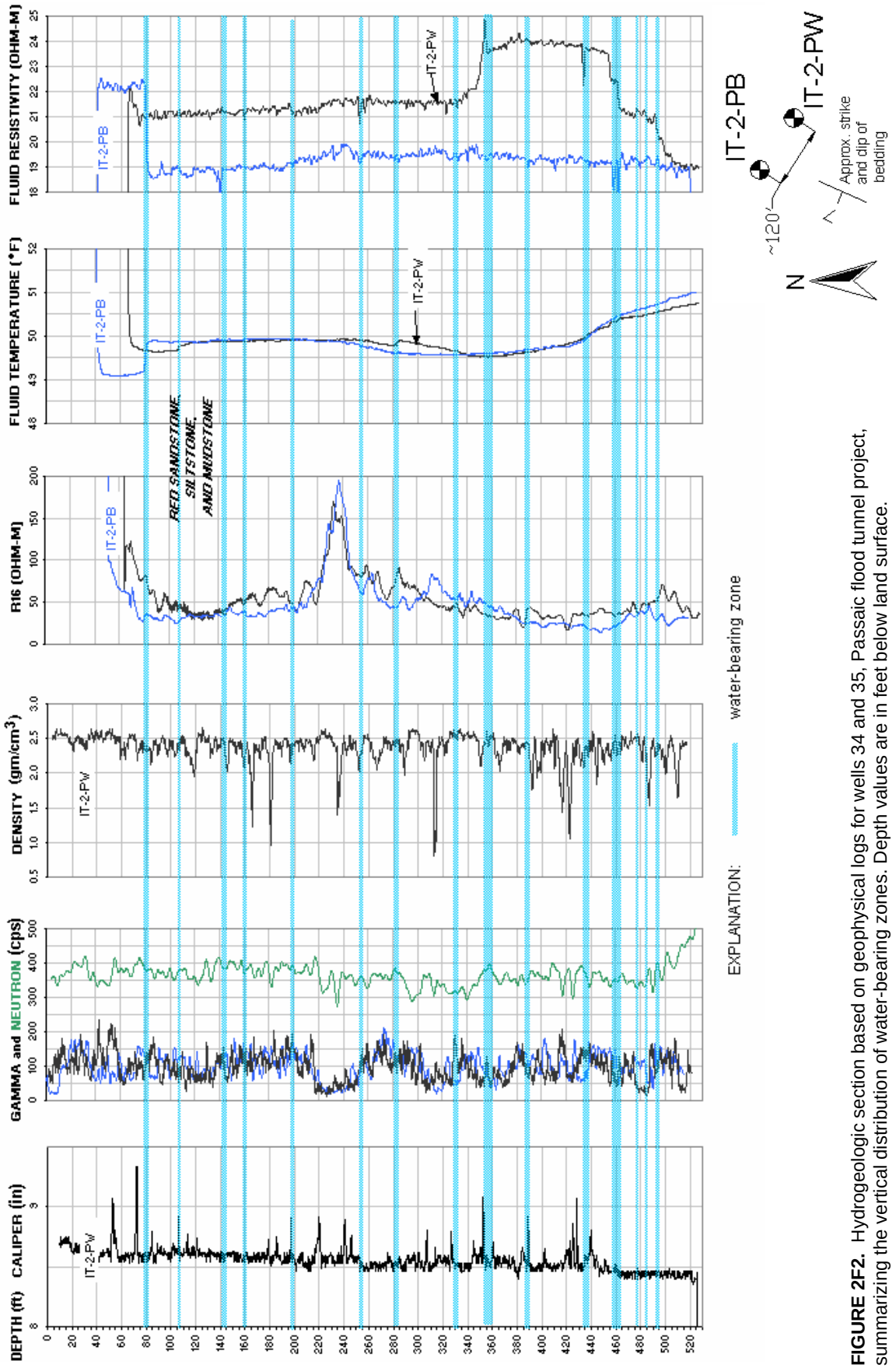

FIGURE 2F2. Hydrogeologic section based on geophysical logs for wells 34 and 35, Passaic flood tunnel project, summarizing the vertical distribution of water-bearing zones. Depth values are in feet below land surface.

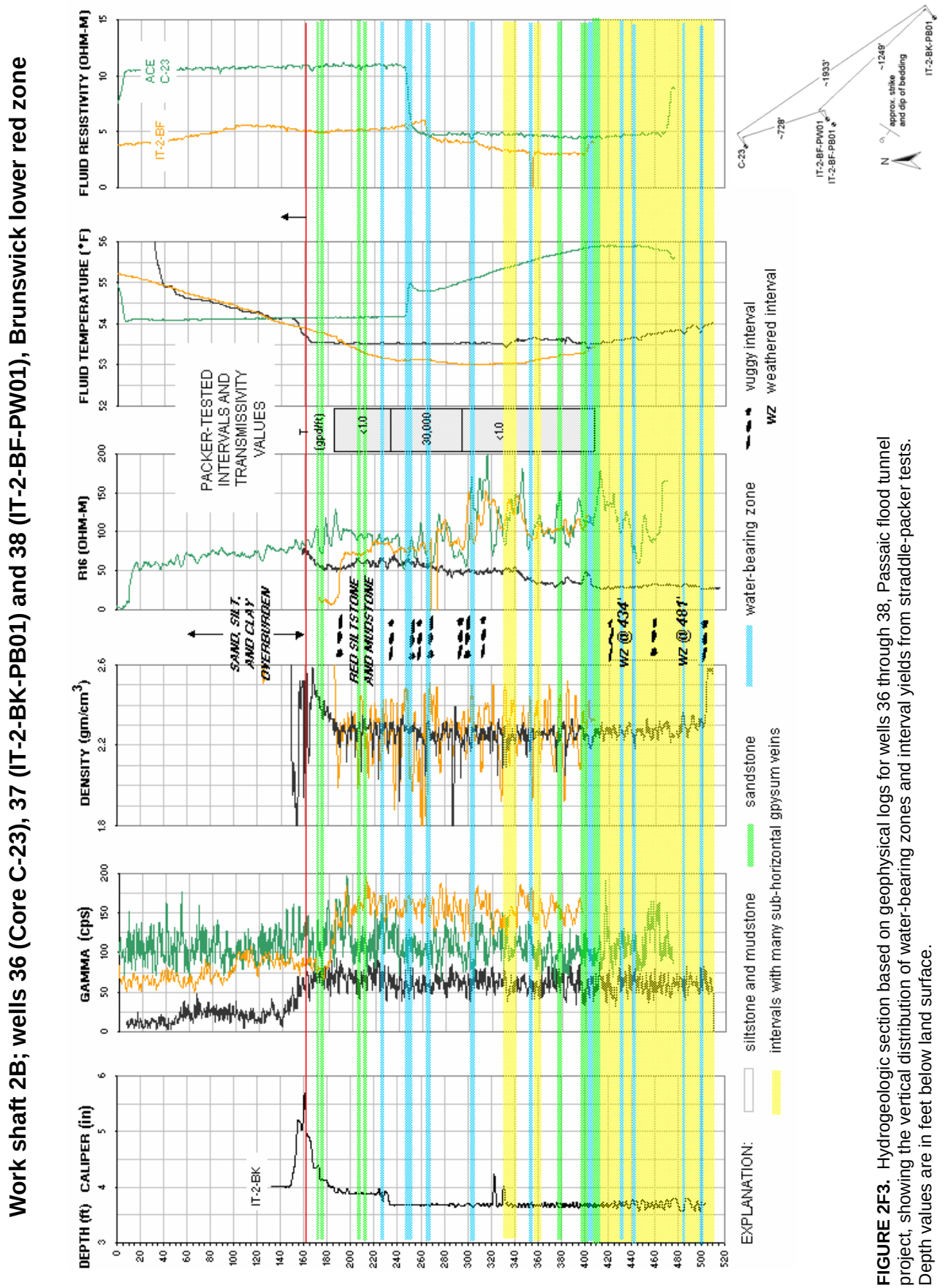

FIGURE 2F3. Hydrogeologic section based on geophysical logs for wells 36 through 38, Passaic flood tunnel project, showing the vertical distribution of water-bearing zones and interval yields from straddle-packer tests. Depth values are in feet below land surface.

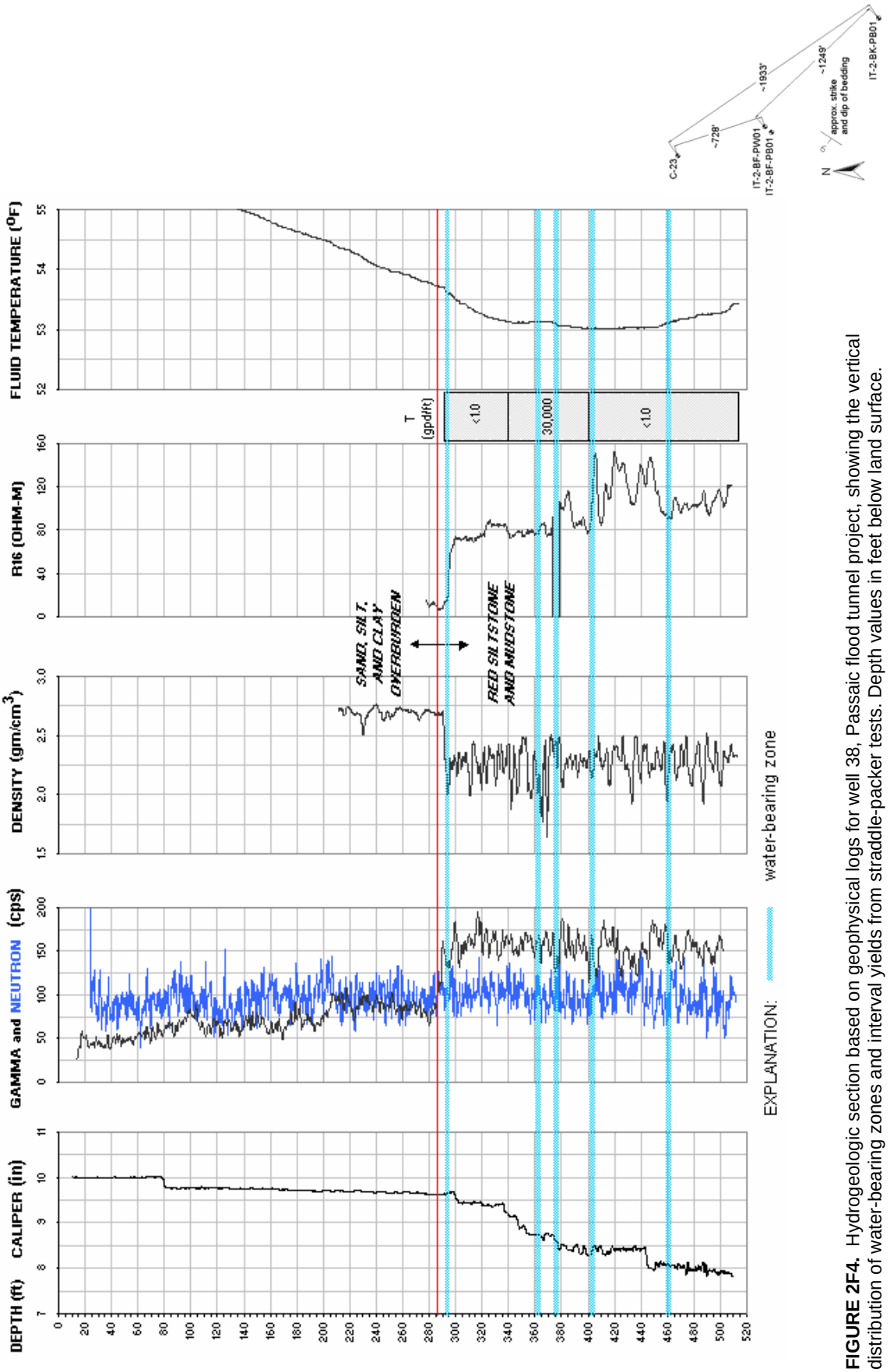

FIGURE 2F4. Hydrogeologic section based on geophysical logs for well 38, Passaic flood tunnel project, showing the vertical distribution of water-bearing zones and interval yields from straddle-packer tests. Depth values in feet below land surface.

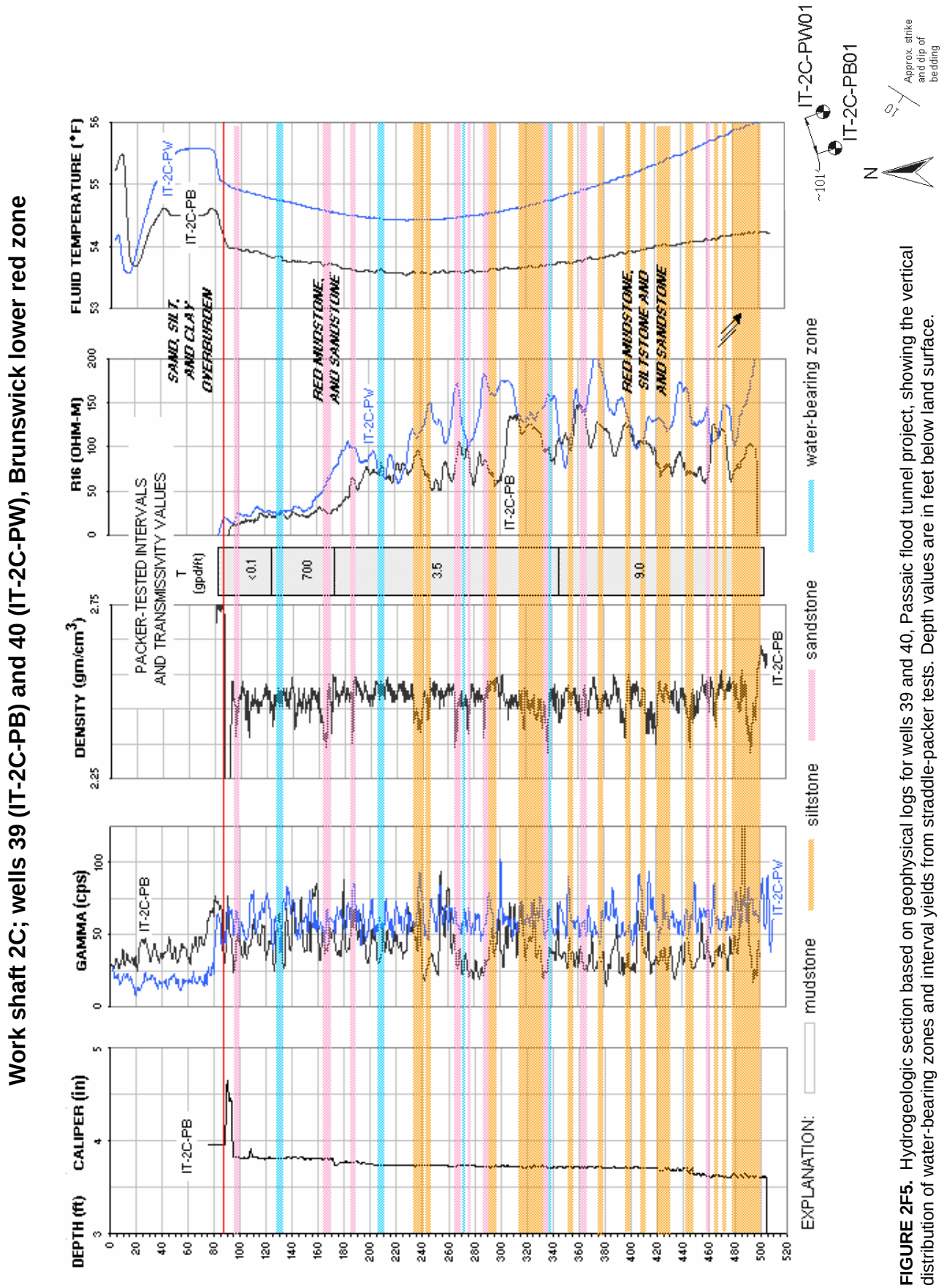

FIGURE 2F5. Hydrogeologic section based on geophysical logs for wells 39 and 40, Passaic flood tunnel project, showing the vertical distribution of water-bearing zones and interval yields from straddle-packer tests. Depth values are in feet below land surface.

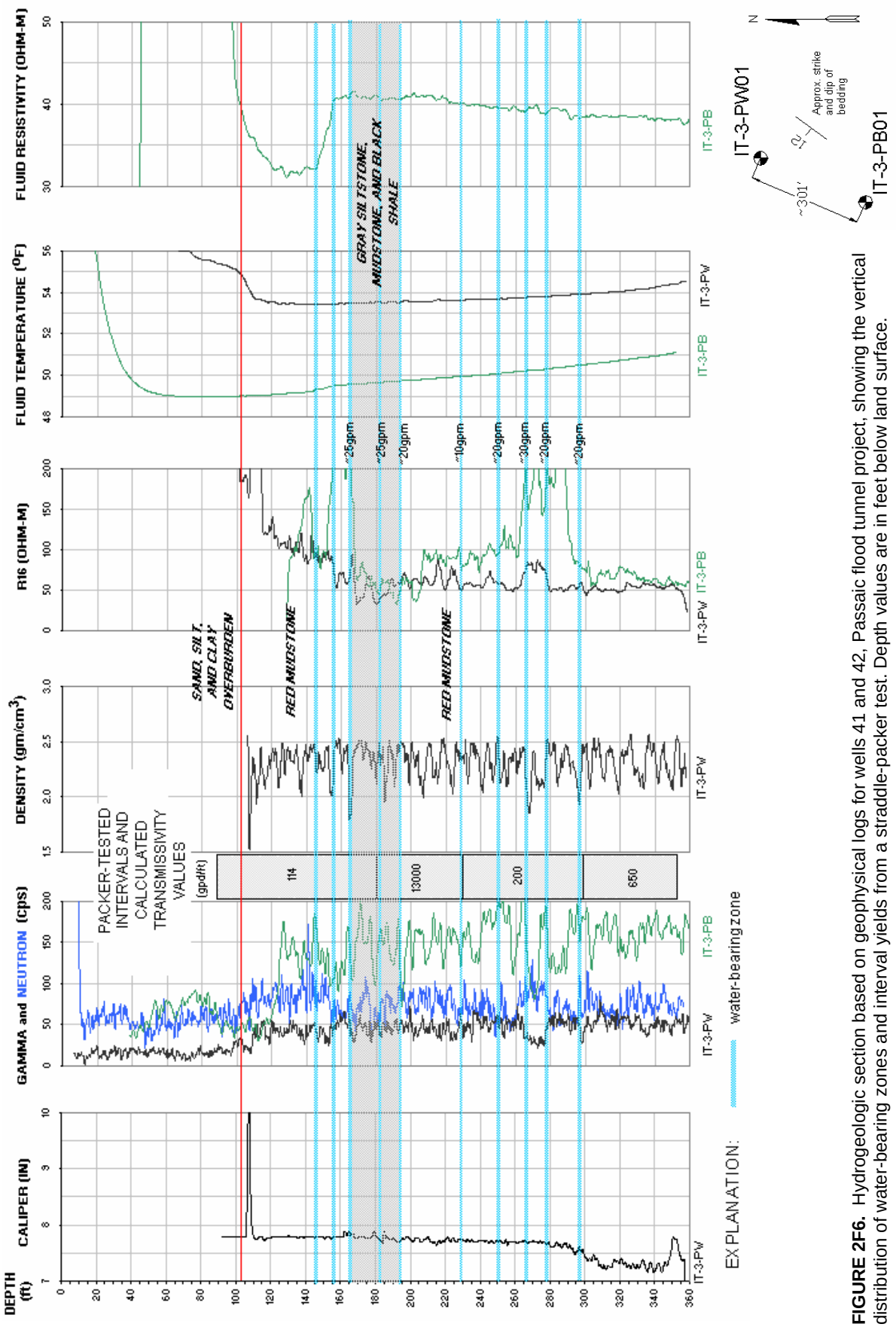

FIGURE 2F6. Hydrogeologic section based on geophysical logs for wells 41 and 42, Passaic flood tunnel project, showing the vertical distribution of water-bearing zones and interval yields from a straddle-packer test. Depth values are in feet below land surface.

Summary of Borehole Geophysical Studies in the Newark Basin, New Jersey:

Brunswick mudstone, siltstone and shale; middle red, middle gray, lower red and lower gray zones

By Gregory C. Herman and John F. Curran, N.J. Geological Survey

Appendix 3 of

Contributions to the Geology and Hydrogeology of the Newark Basin

N.J. Geological Survey Bulletin 77

State of New Jersey
Department of Environmental Protection
Water Resource Management
New Jersey Geological Survey
2010

Well 43 - Brunswick middle red zone

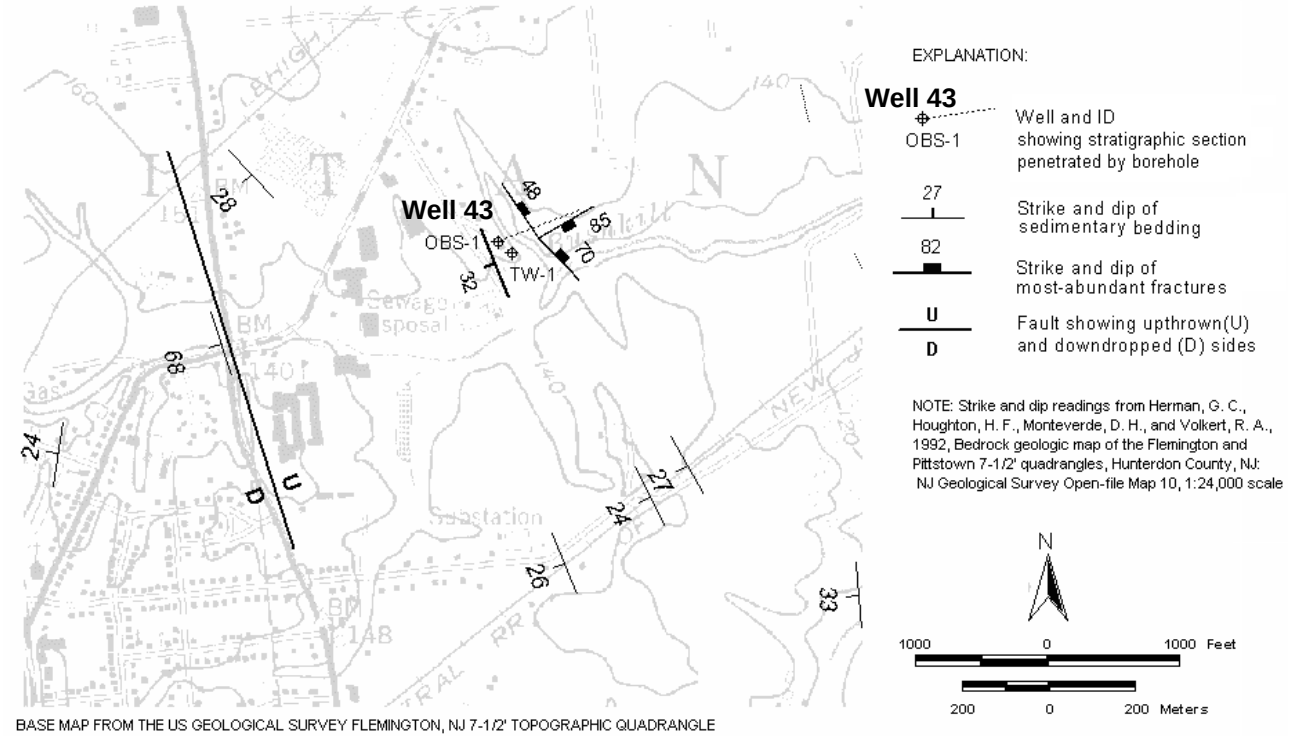

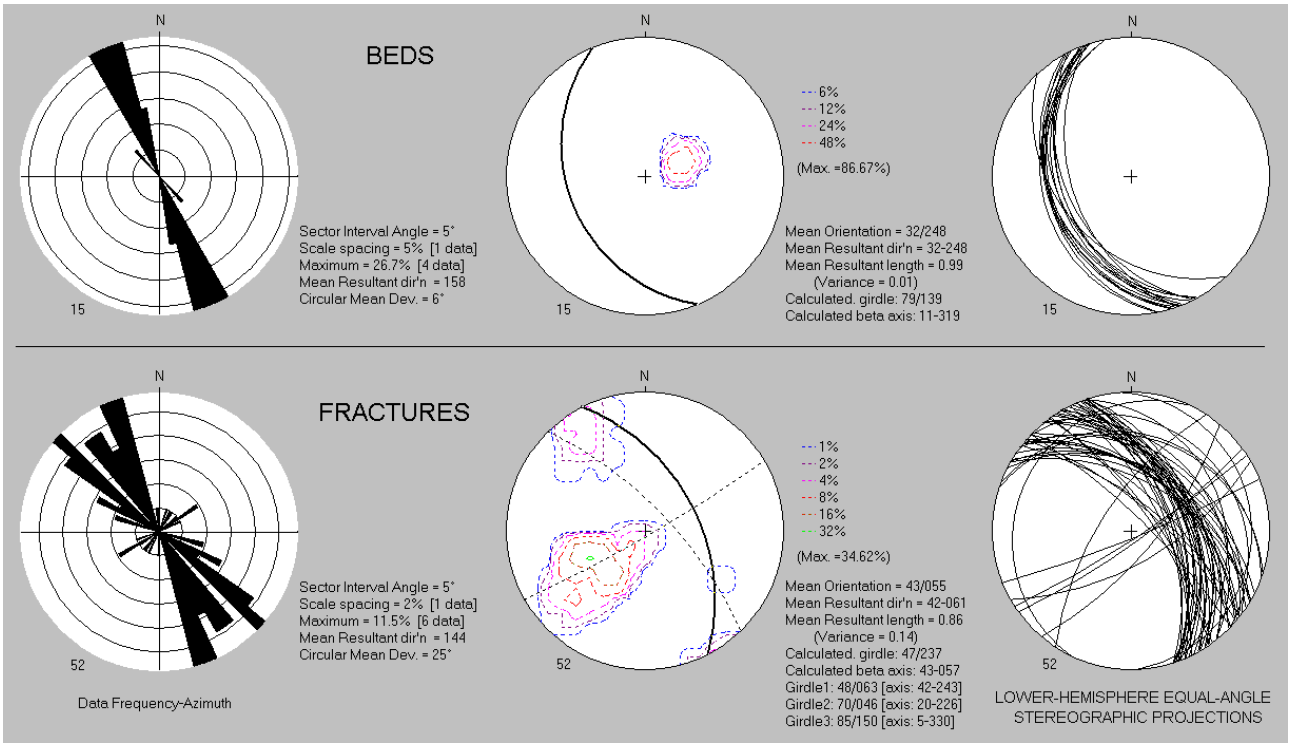

Figure 3A1. Map (above) shows well 43, Junction Rd., Raritan Twp., Hunterdon County, NJ. Bedrock structures mapped near the well are based on a structural analysis (below) of the OPTV record. Note how nearby topographic ridges and streams parallel the strike of structures.

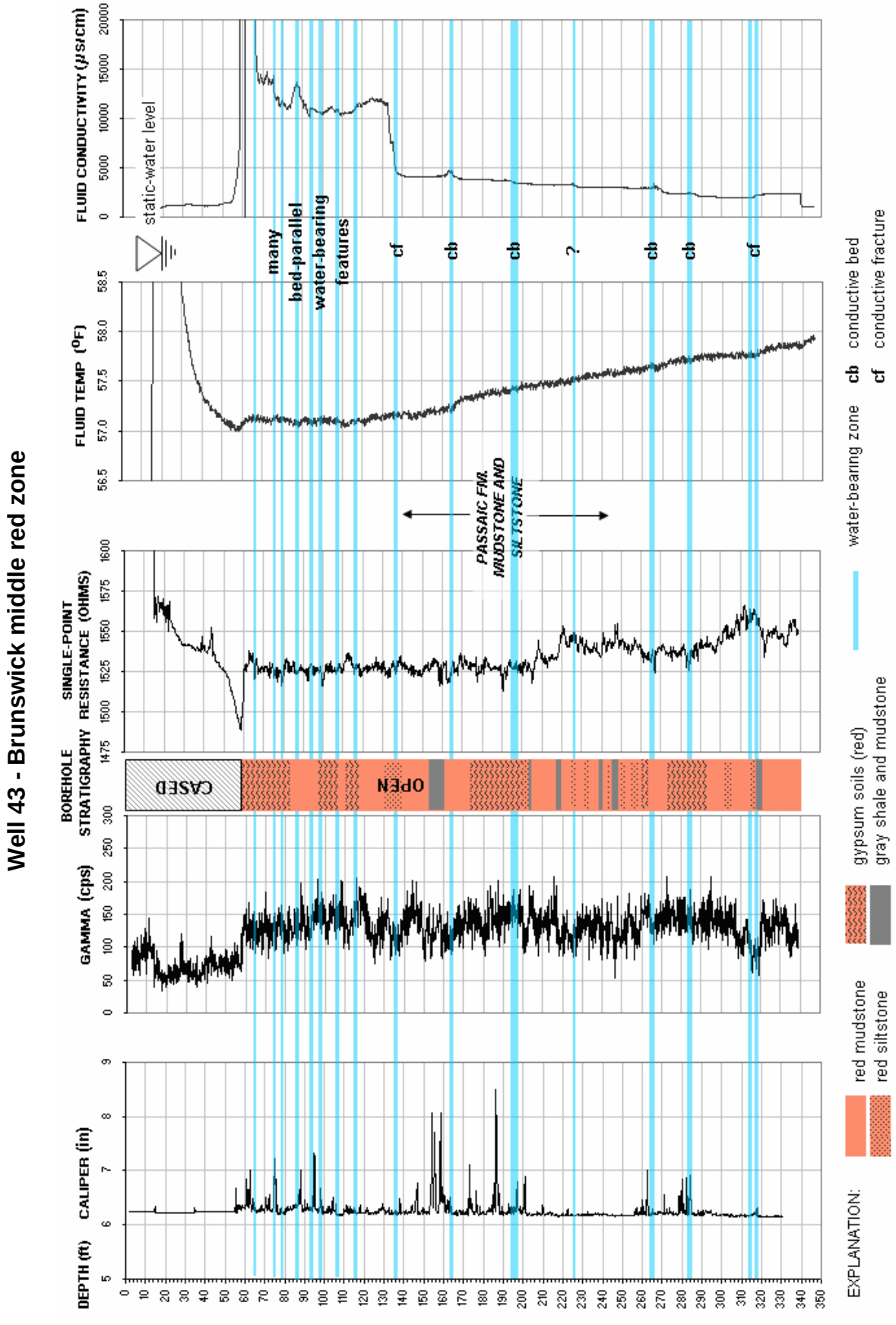

FIGURE 3A2. Hydrogeologic section based on geophysical logs for well 43 showing the vertical distribution and types of hydraulically-conductive features and water-bearing zones. Depth values are in feet below land surface.

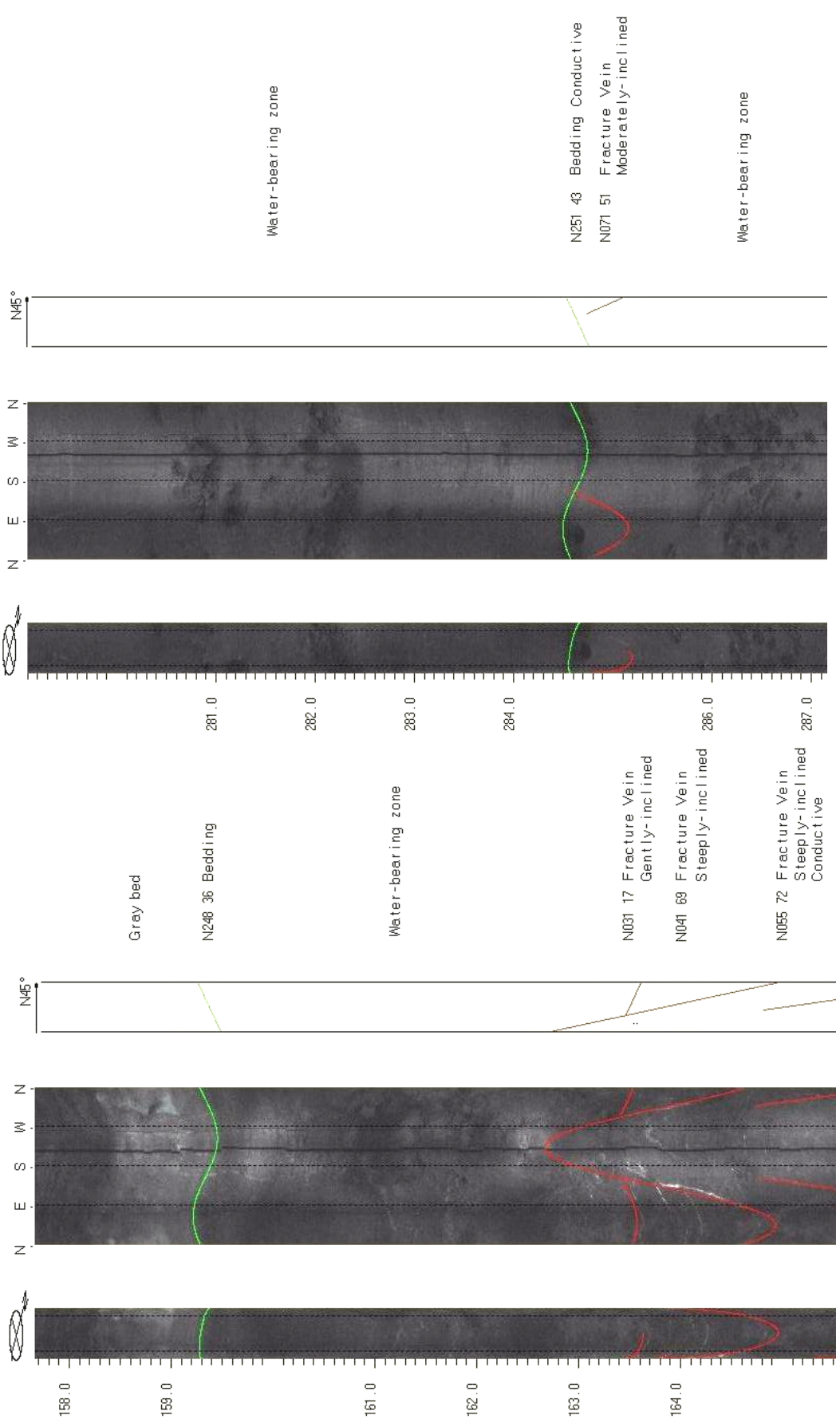

FIGURE 3A3. OPTV records of the 6-inch diameter well 43 showing bedrock structures and hydraulically-conductive features in red and gray mudstone. Depth values are in feet below land surface.

Well 44 - Brunswick middle red zone

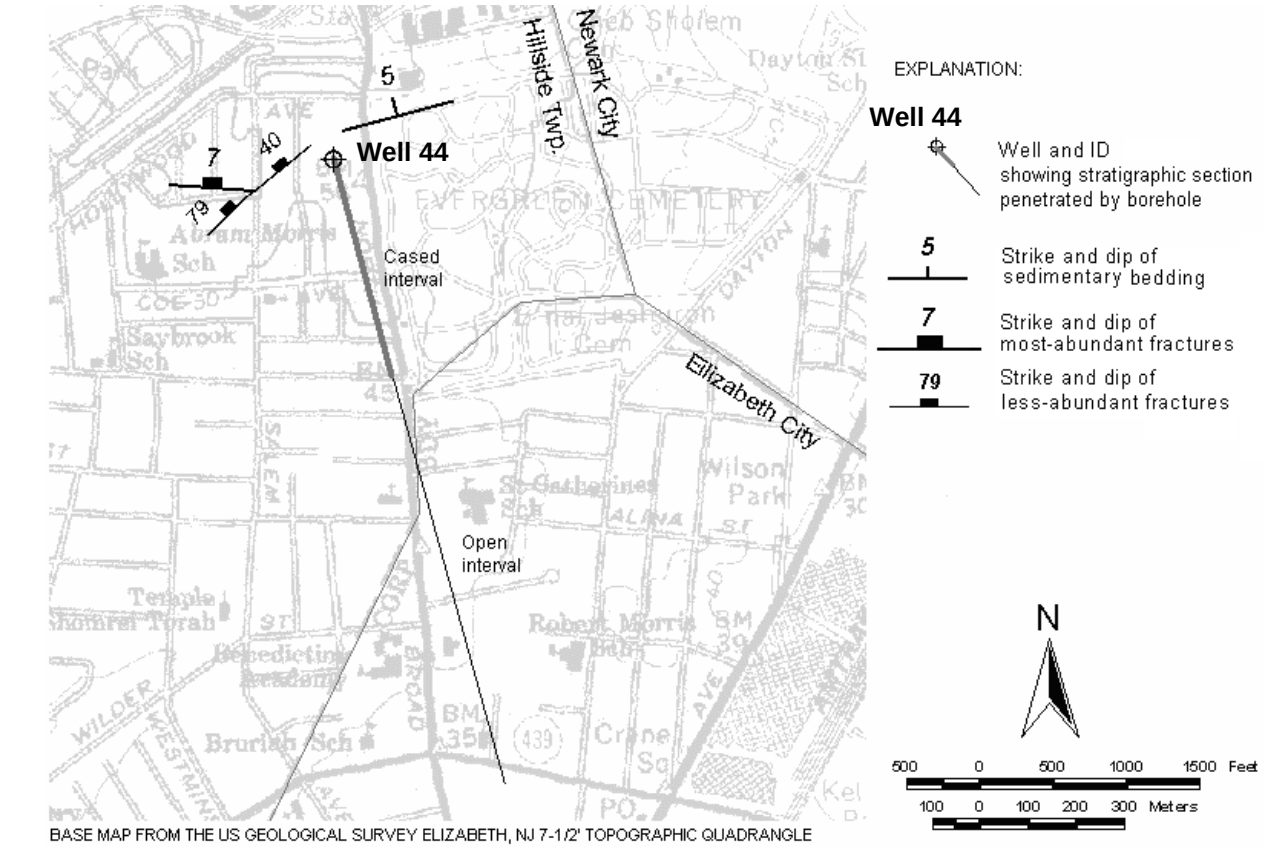

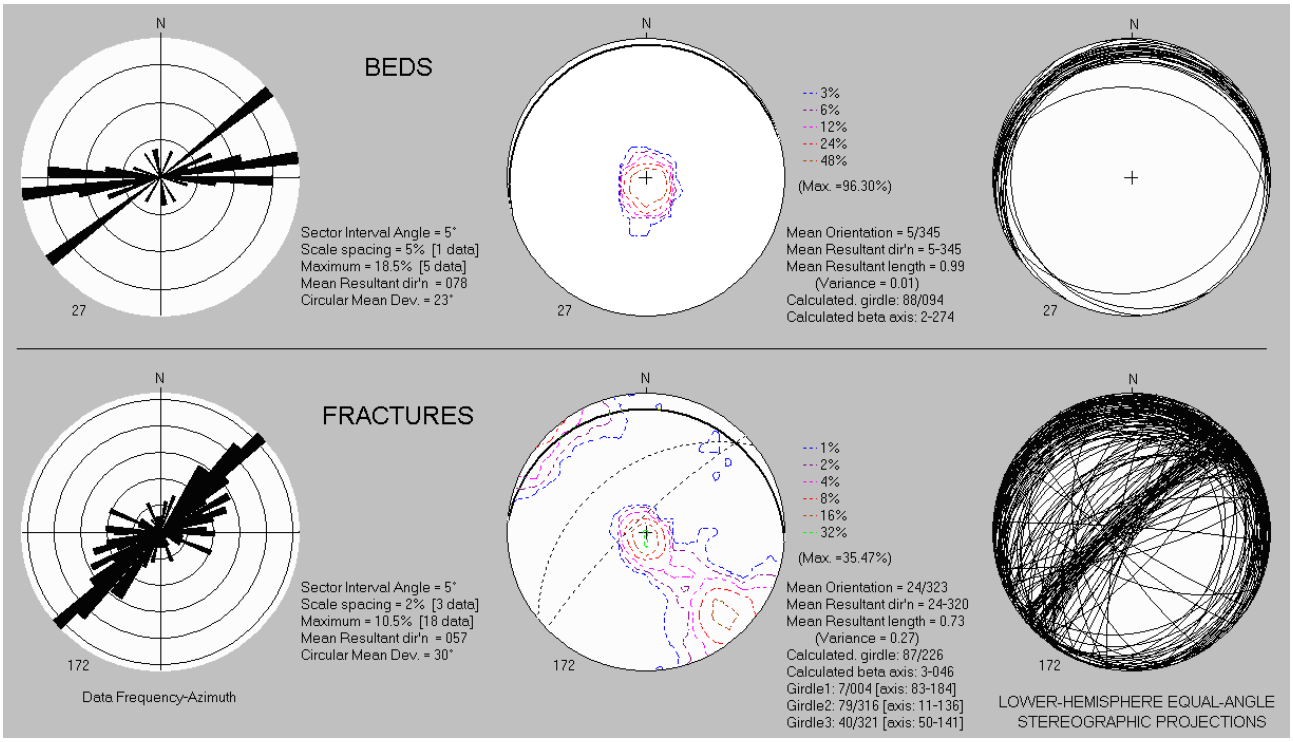

Figure 3B1. Map (above) shows well 44 at the Hillside Car Wash, 1260 North Broad St., Hillside Twp., Union County, NJ. Bedrock structures are based on a structural analysis (below) of the OPTV record.

Well 44 - Brunswick middle red zone

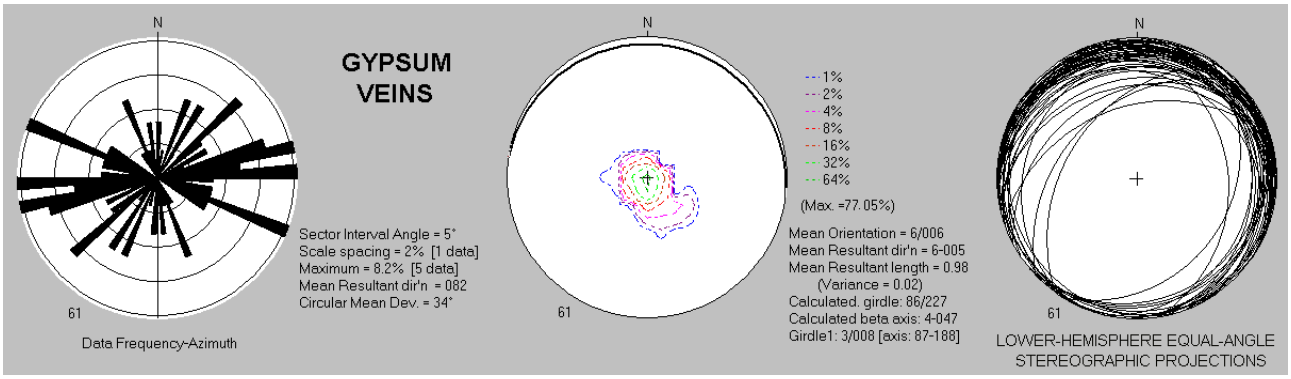

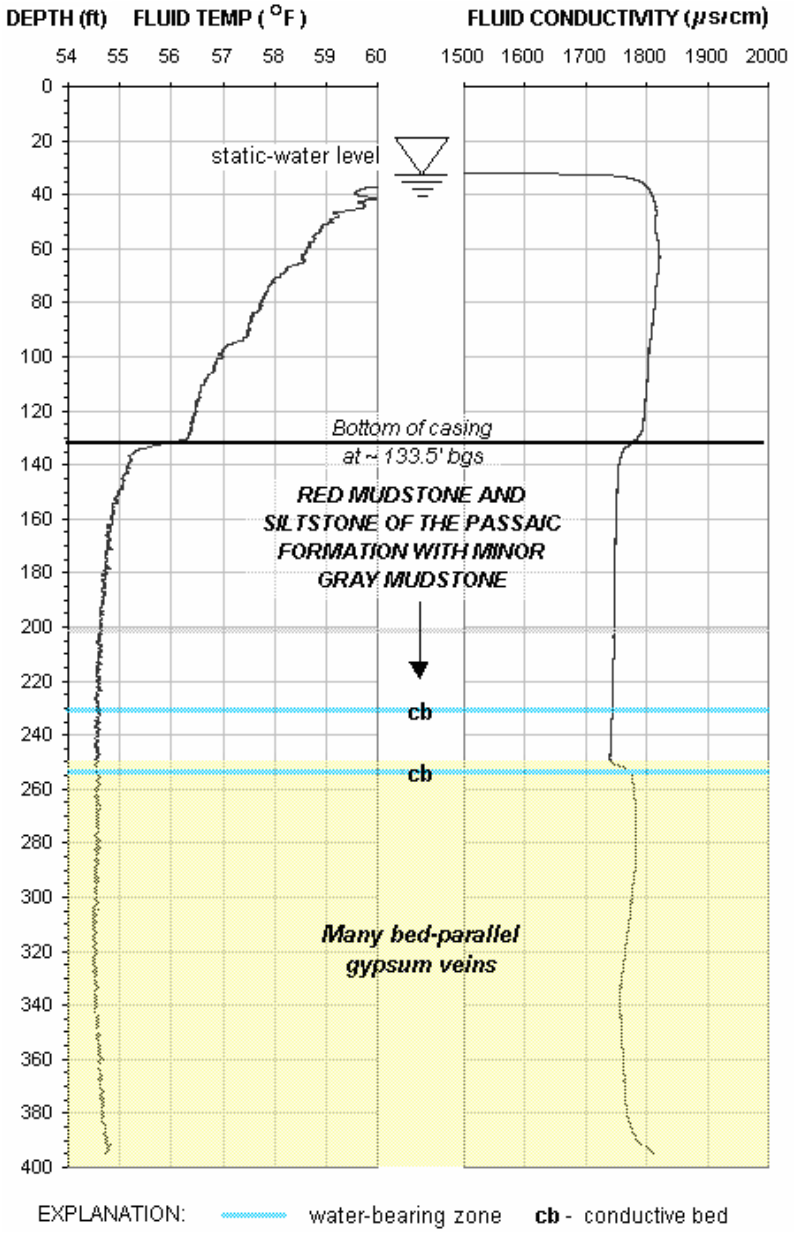

Figure 3B2. Structural analysis of gently-dipping gypsum veins from the OPTV record (above), and hydrogeologic section based on geophysical logs (below) showing the vertical distribution of hydraulically-conductive features, water-bearing zones, and the stratigraphic interval containing many gypsum veins. Depth values are in feet below land surface.

Well 43 - Brunswick middle red zone

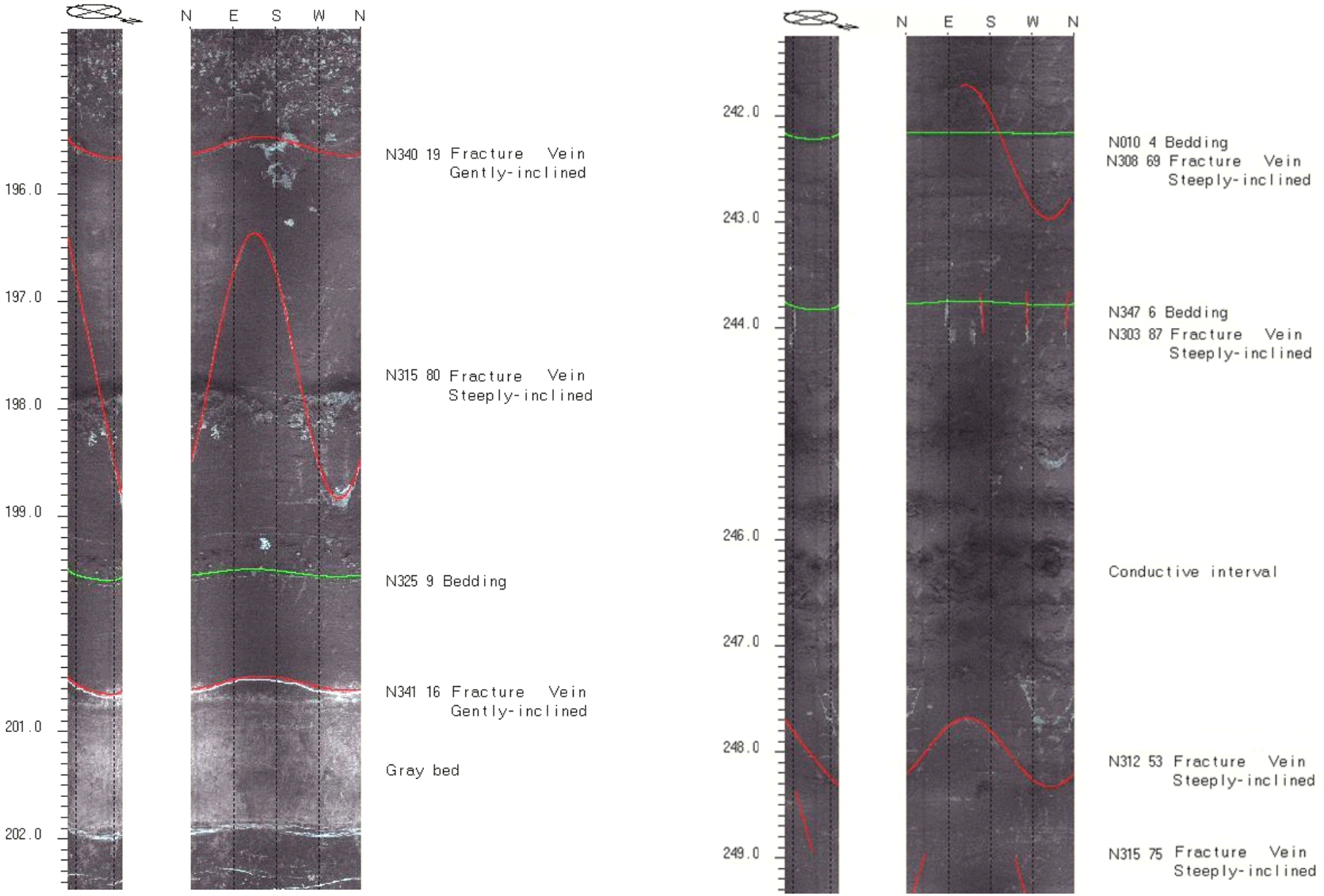

FIGURE 3B3. OPTV records of the 6-inch diameter well 44 showing bedrock structures and hydraulically-conductive features in red and gray mudstone. Depth values are in feet below land surface.

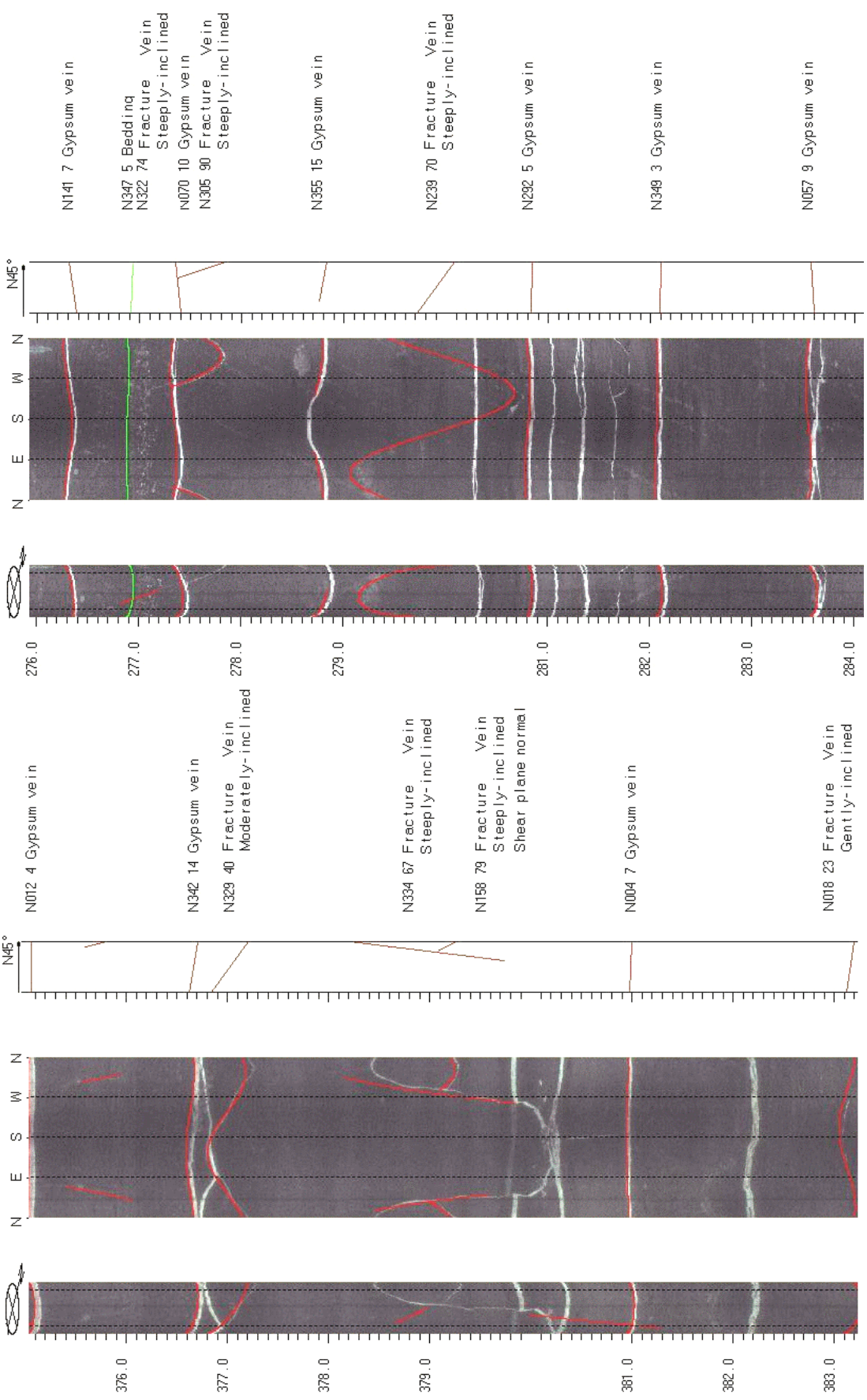

FIGURE 3B4. OPTV records of the 6-inch diameter well 43 showing bedrock structures in red mudstone. Depth values are in feet below land surface.

Wells 45 to 49 - Brunswick middle red zone

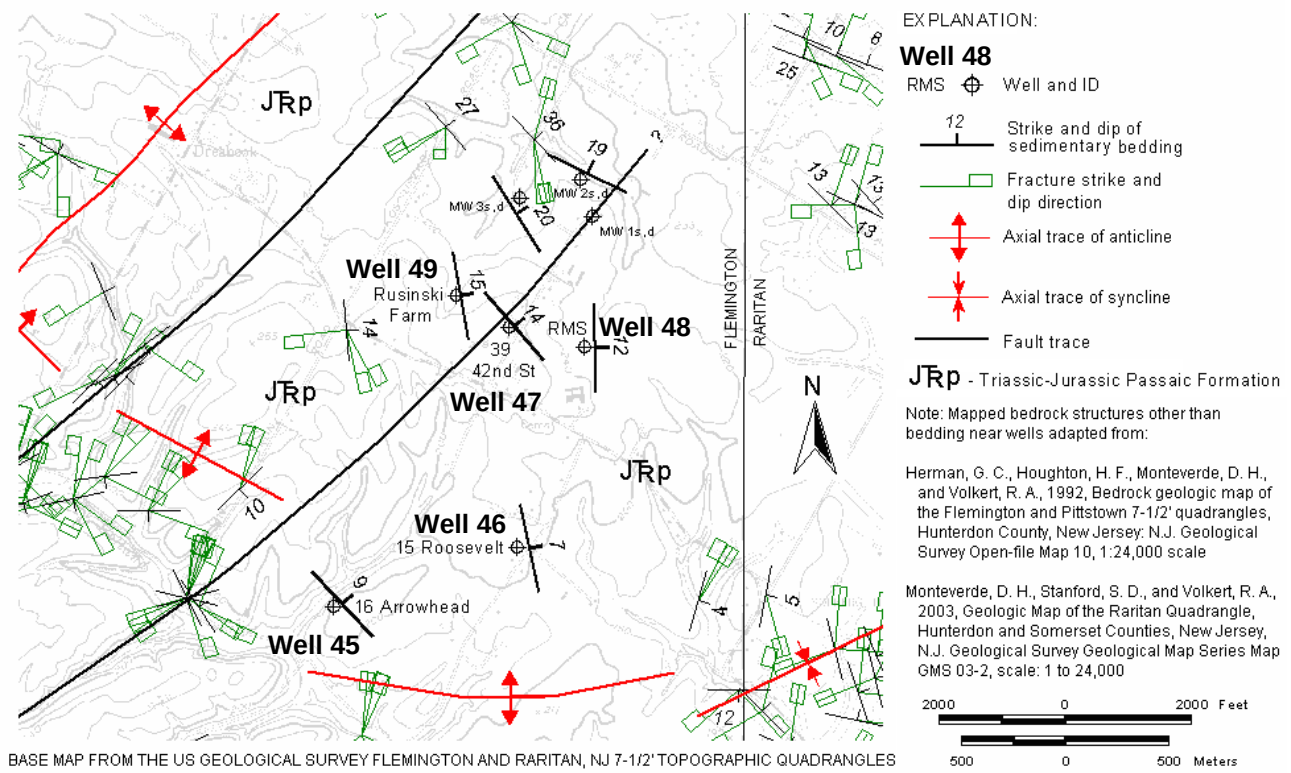

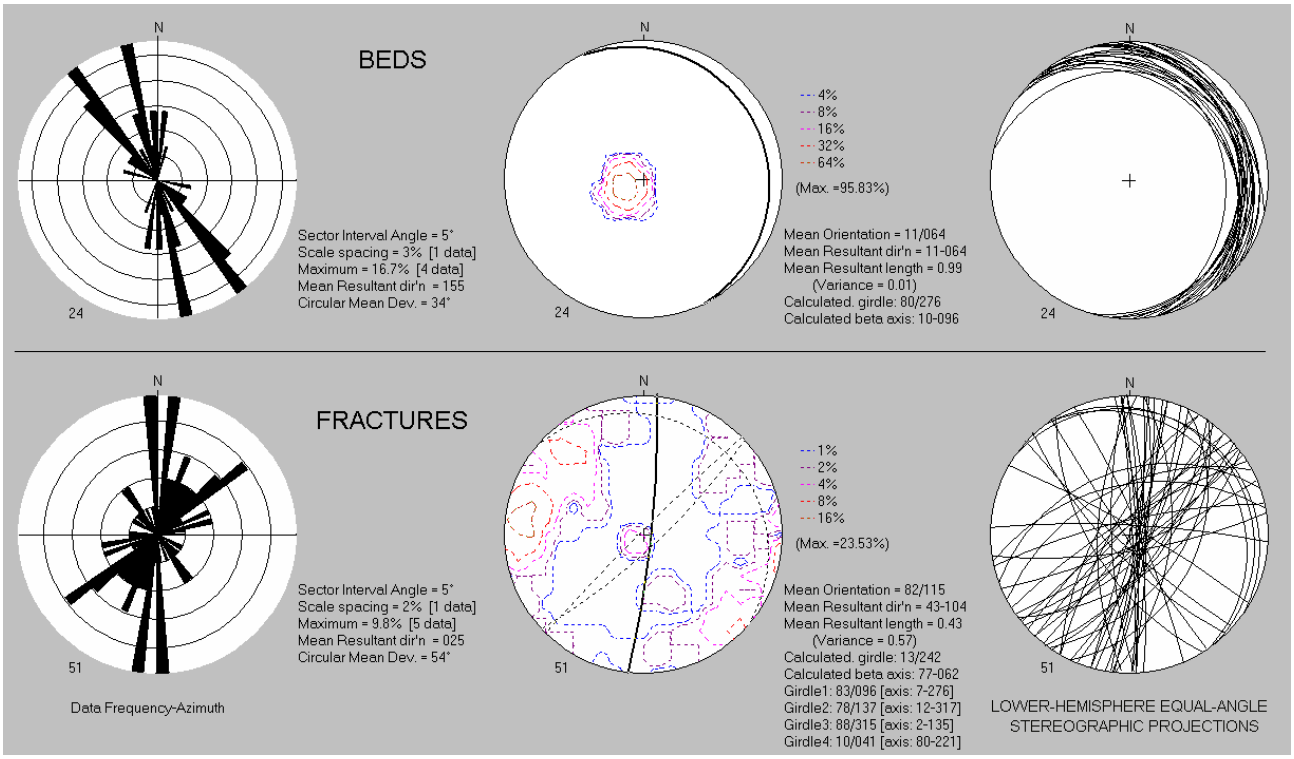

Figure 3C1. Map (above) shows wells 45 through 49 that were logged as part of a regional ground-water investigation in Readington Twp, Hunterdon County, NJ. The structural analysis (below) of the OPTV records summarizes bed and fracture orientations for the wells.

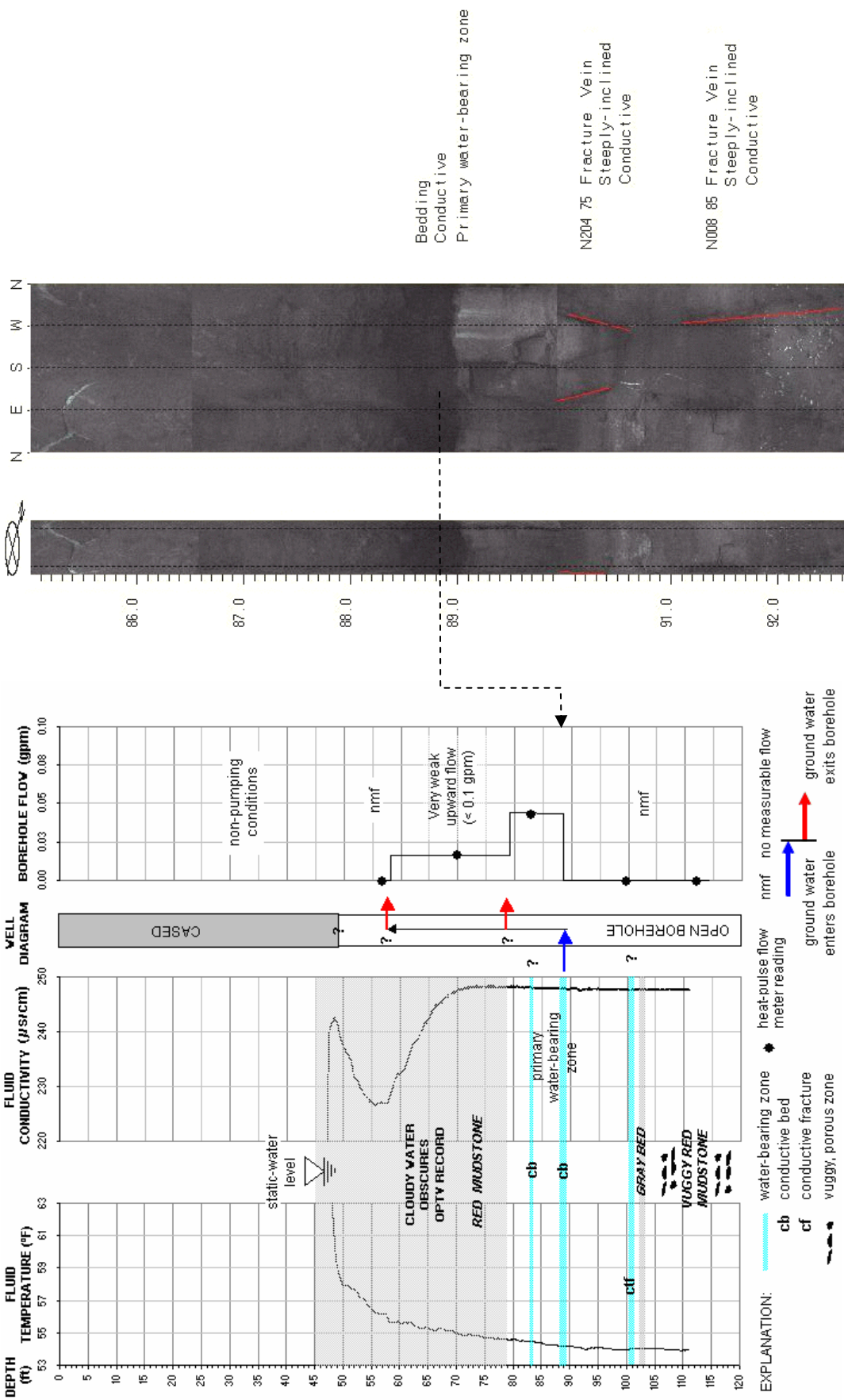

FIGURE 3C2. Hydrogeologic section based on geophysical logs (left) for well 45 at 16 Arrowhead Rd, Readington Twp, Hunterdon County, NJ. The section shows the vertical distribution and types of hydraulically-conductive features and water-bearing zones in red mudstone. An OPTV record of the 6-inch diameter well (right) shows the primary inflow zone. Light-colored mineral stains emanating from the conductive bed extend downward in response to periodic downward flows induced by pumping. Depth values are in feet below land surface.

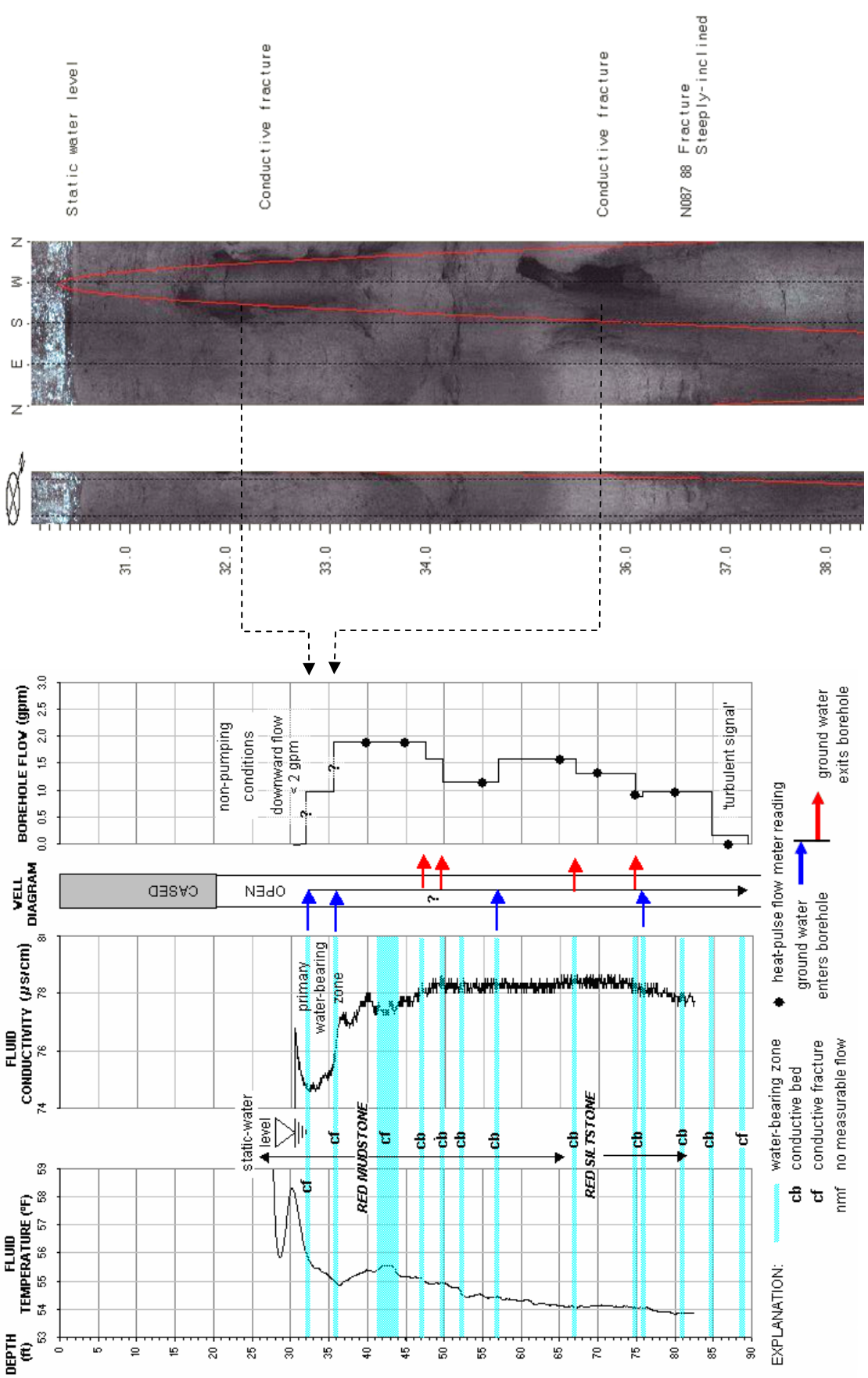

FIGURE 3C3. Hydrogeologic section based on geophysical logs (left) for well 46 at 15 Roosevelt Rd, Readington Twp, Hunterdon County, NJ. The section shows the vertical distribution and types of hydraulically-conductive features and water-bearing zones in red mudstone. An OPTV record of the 6-inch diameter well (right) shows primary inflow zones. Depth values are in feet below land surface.

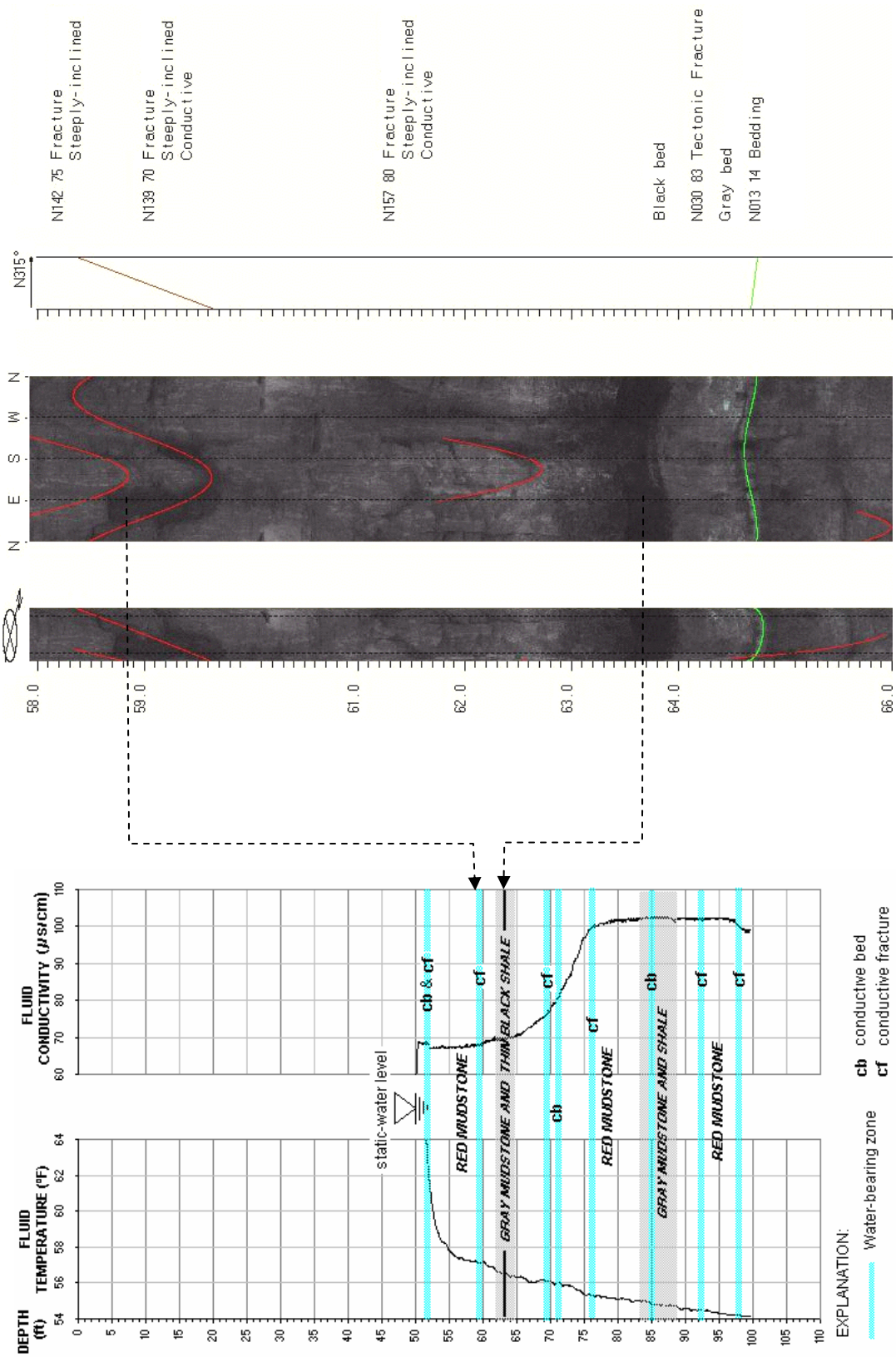

FIGURE 3C4. Hydrogeologic section based on geophysical logs (left) for well 47 at 139 42nd Street, Readington Twp, Hunterdon County, NJ. The section shows the vertical distribution and types of hydraulically-conductive features and water-bearing zones in red and gray mudstone and black shale. An OPTV record (right) of the 6-inch diameter well shows geologic structures and hydraulically-conductive features in red and gray mudstone. Depth values are in feet below land surface.

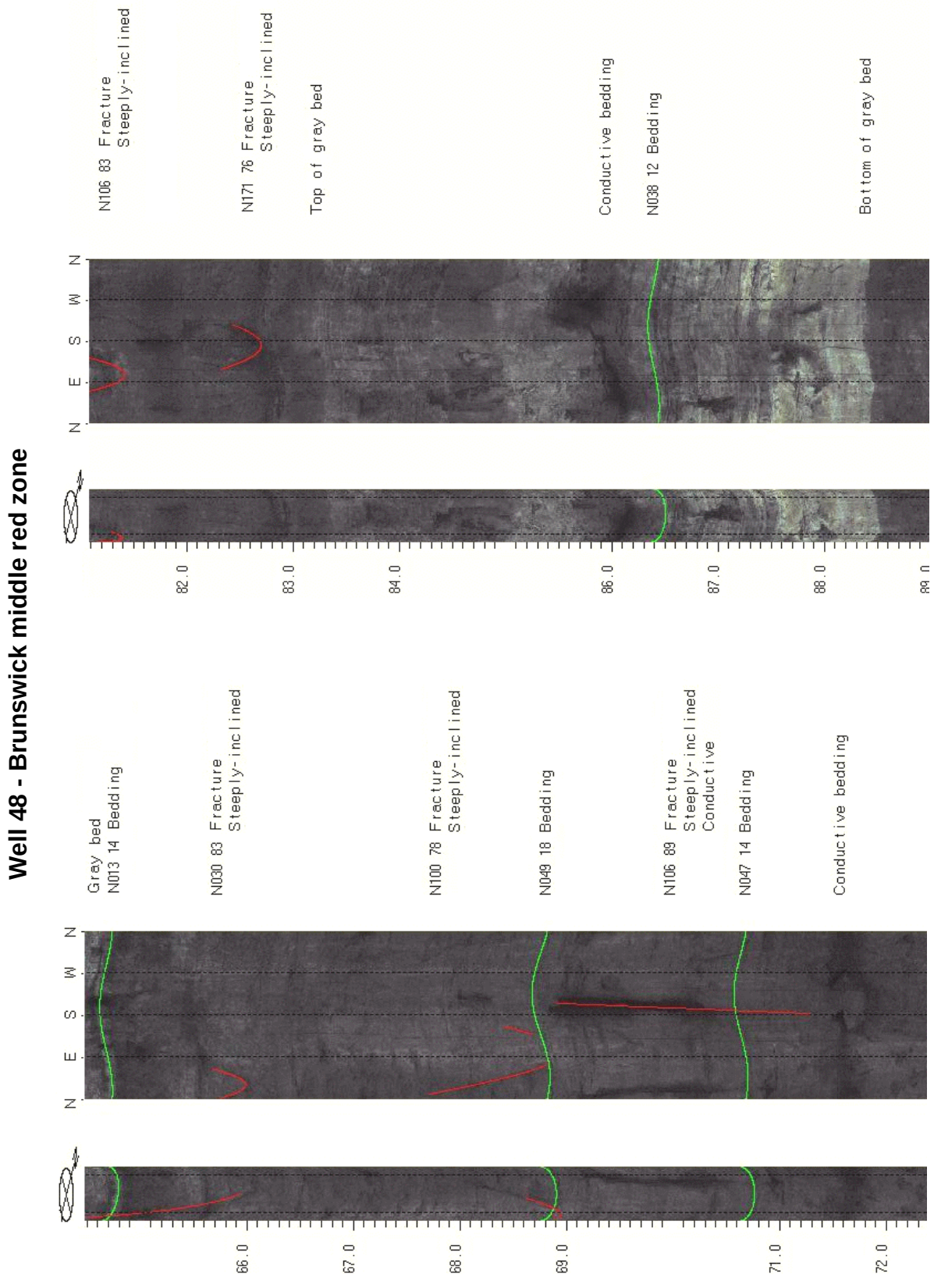

FIGURE 3C5. OPTV records of the 6-inch diameter well 48 at the Readington Middle School, Readington, Township, Hunterdon County, NJ showing geologic structures and conductive features in red and gray mudstone and gray shale. Depth values are in feet below land surface.

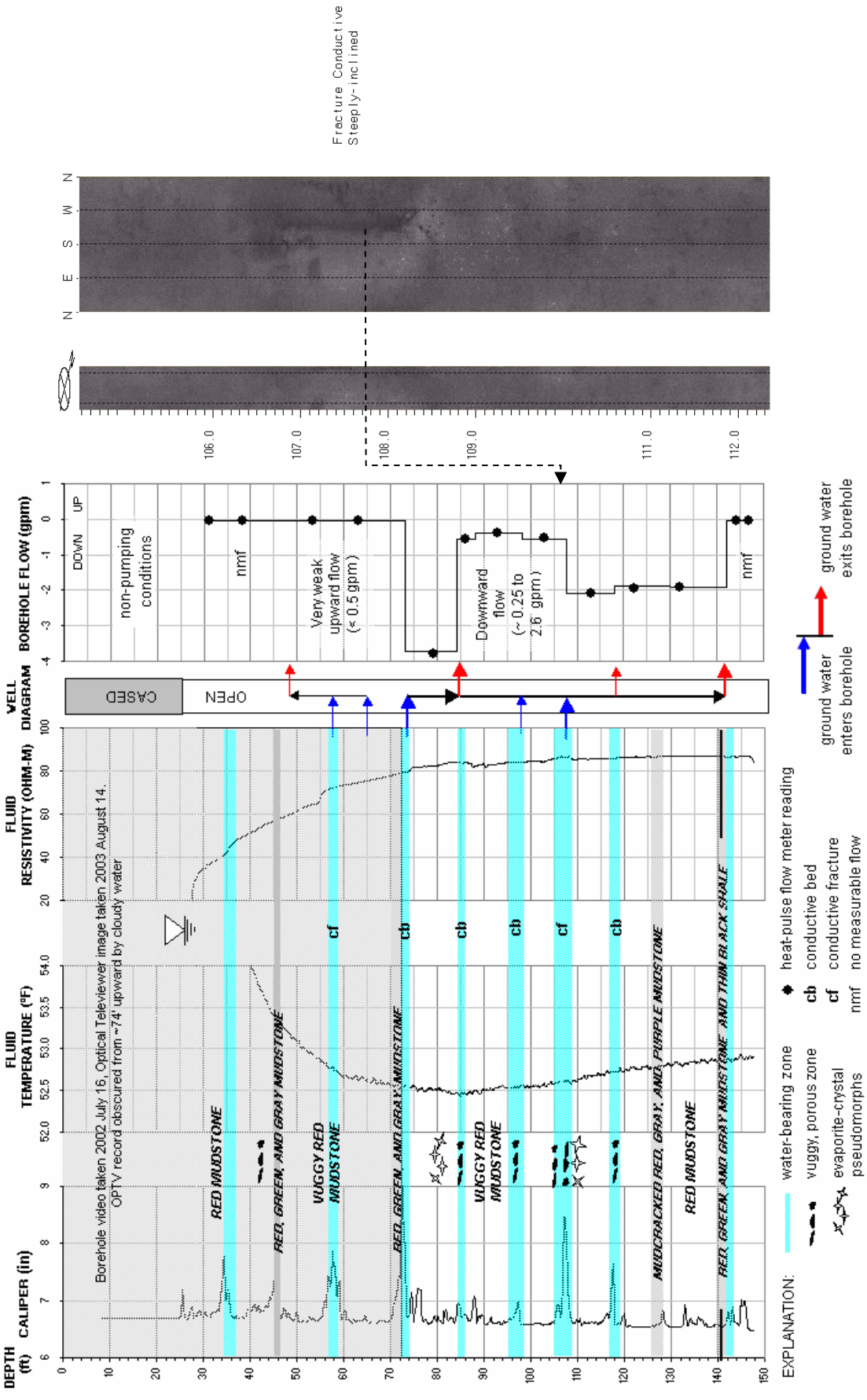

FIGURE 3C6. Hydrogeologic section based on geophysical logs (left) for well 49 at the Rusinski Farm, Readington Twp, Hunterdon County, NJ. The section shows the vertical distribution and types of hydraulically-conductive features and water-bearing zones in red and gray mudstone and black shale. An OPTV record (right) of the 6-inch diameter well shows a conductive fracture in red mudstone. Depth values are in feet below land surface.

Wells 50 to 54 - Brunswick middle red zone

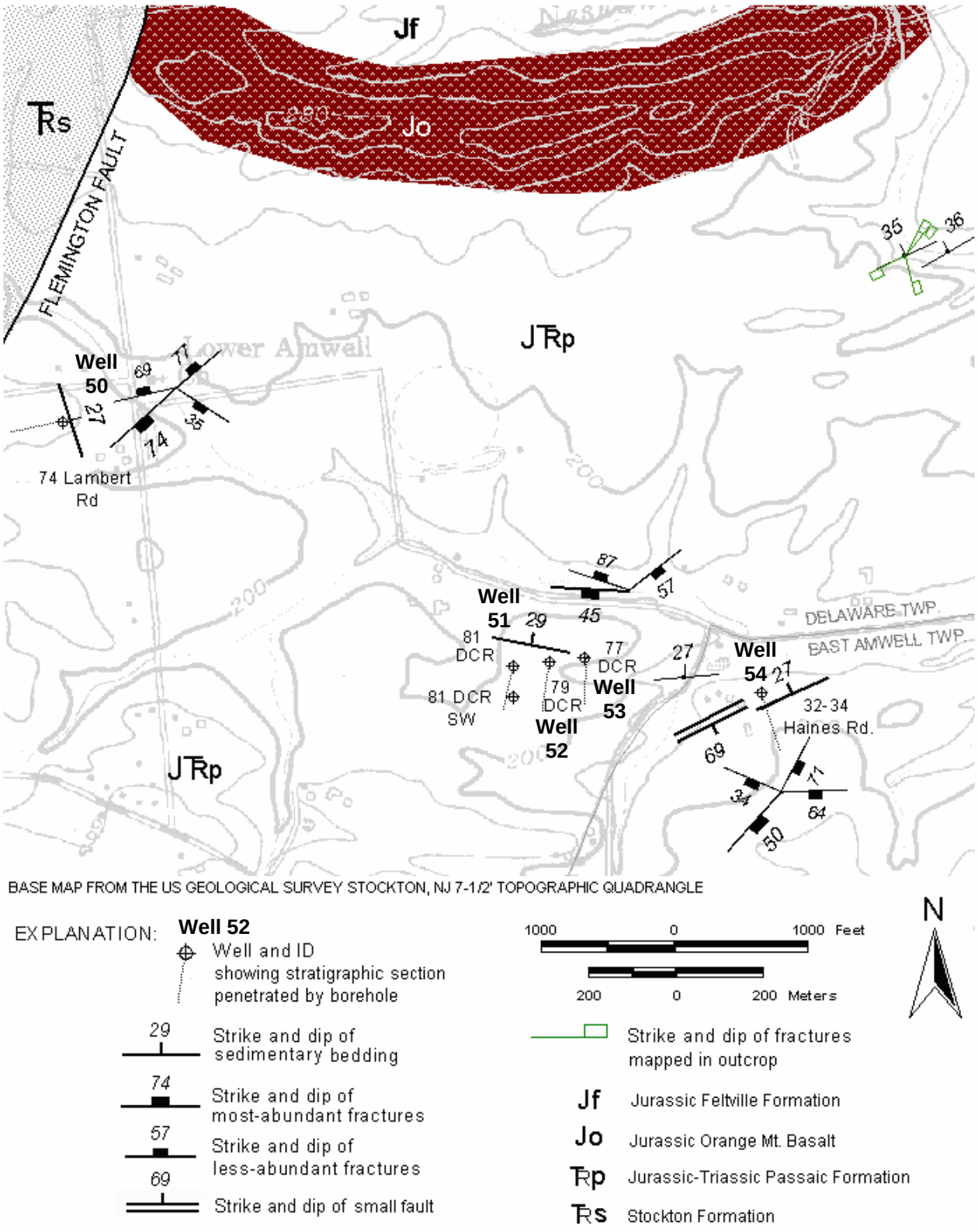

Figure 3D1. Map showing wells 50 through 54 as part of a regional arsenic-in-groundwater investigation in Delaware and East Amwell Twps., Hunterdon County, NJ.

Well 50 - Brunswick middle red zone

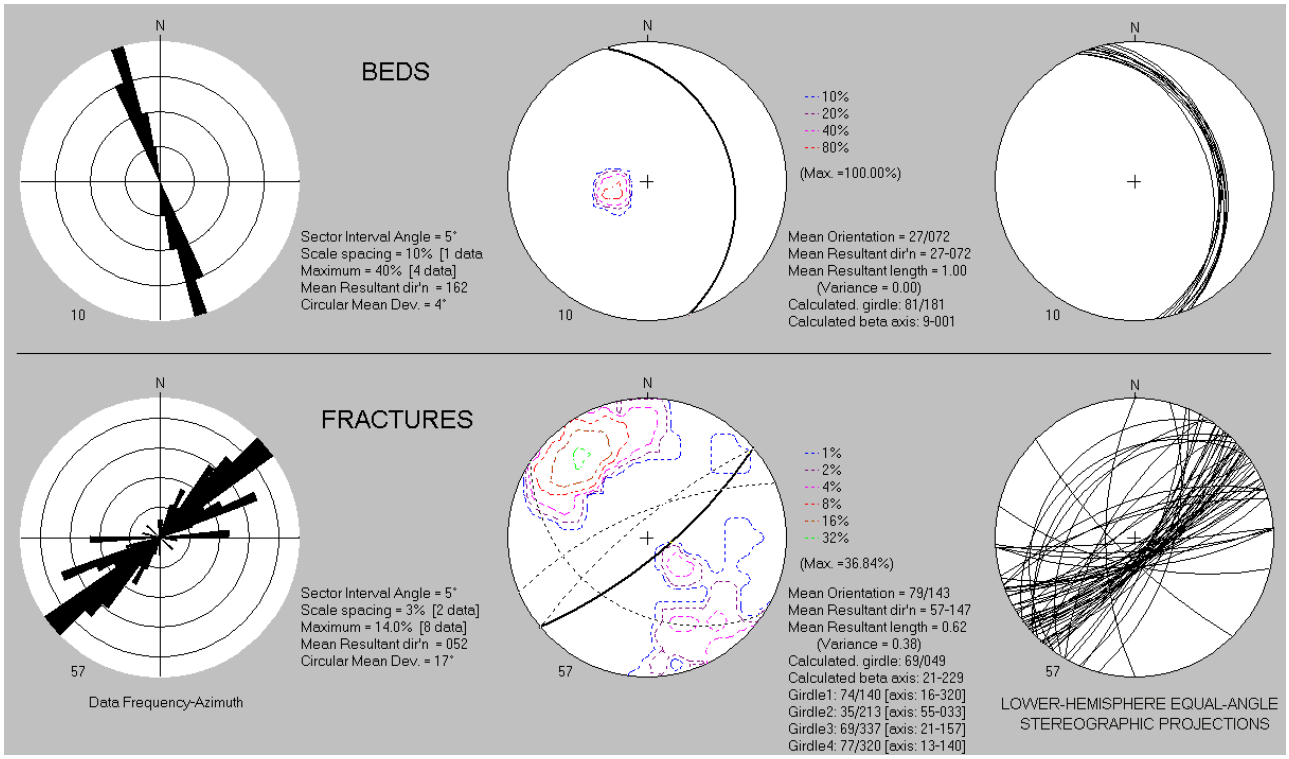

Wells 51 to 53 - Brunswick middle red zone

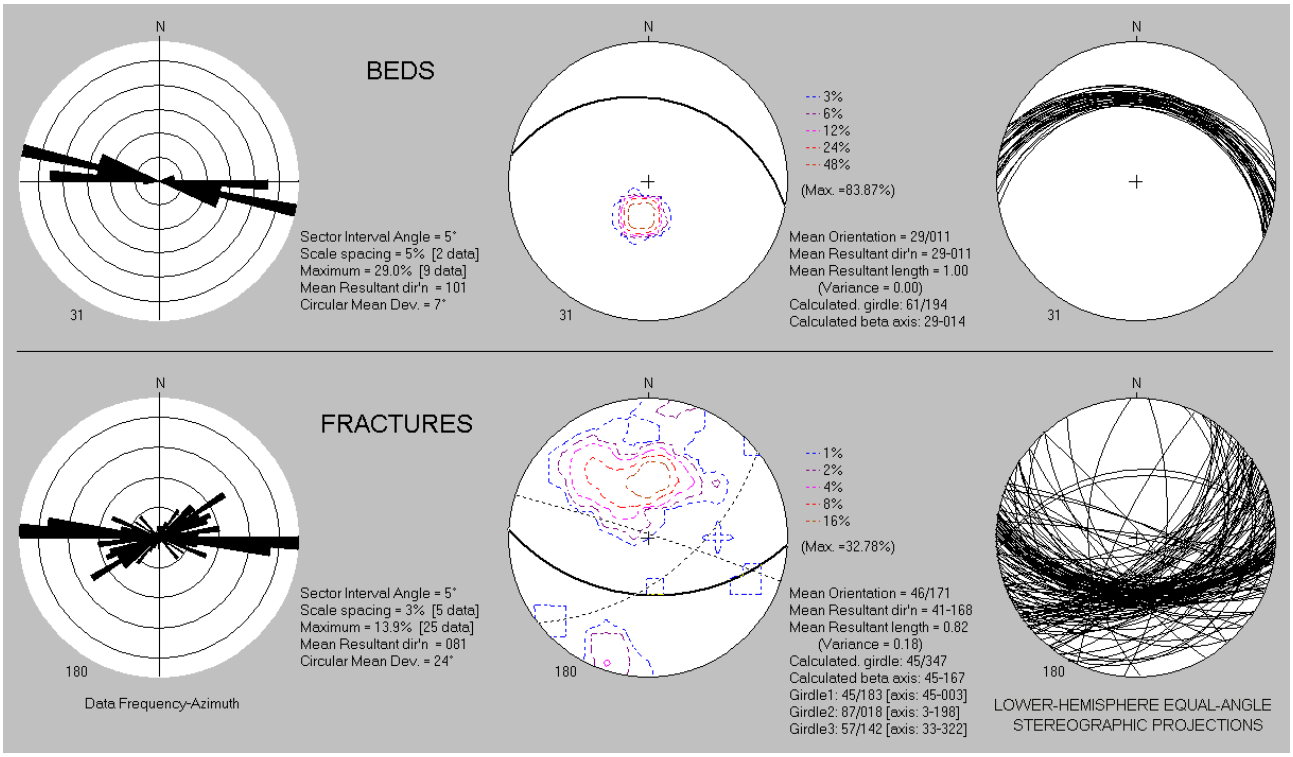

Figure 3D2. Structural analyses of OPTV records for wells 50 (above) and 51 to 53 (below) in Delaware and East Amwell Townships, Hunterdon County, NJ.

Well 54 - Brunswick middle red zone

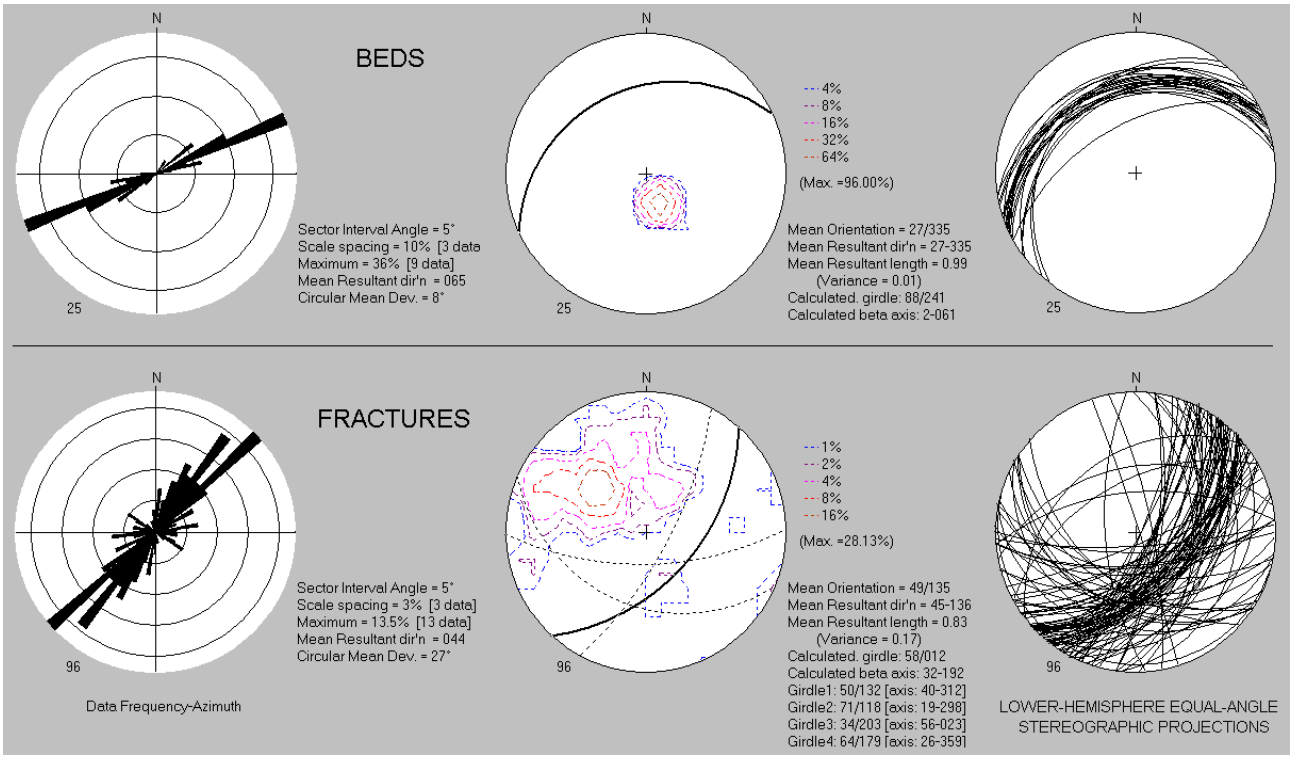

Well 50 - Brunswick middle red zone

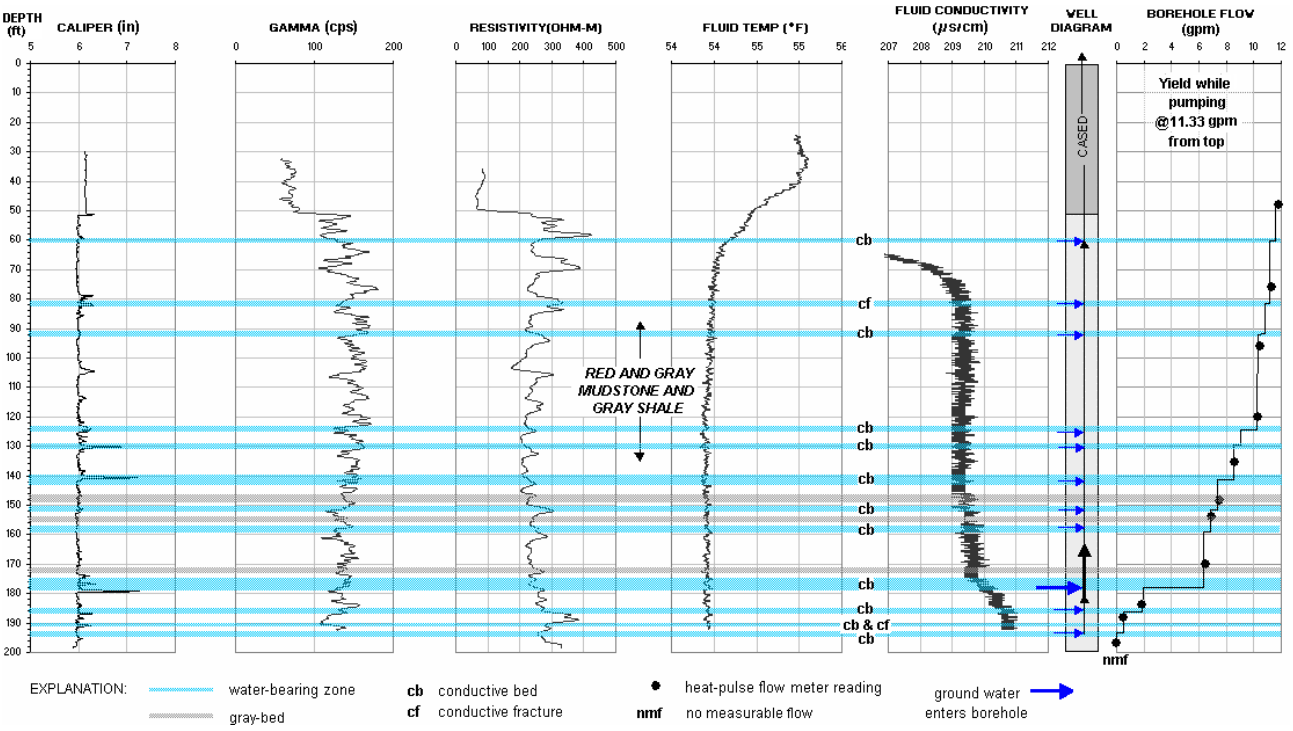

Figure 3D3. Structural analysis of the OPTV record for well 54 (above) and a hydrogeologic section for well 50 (below) based on geophysical logs. The section summarizes the vertical distribution and types of hydraulically-conductive features and water-bearing zones in red and gray mudstone and shale. Depth values are in feet below land surface.

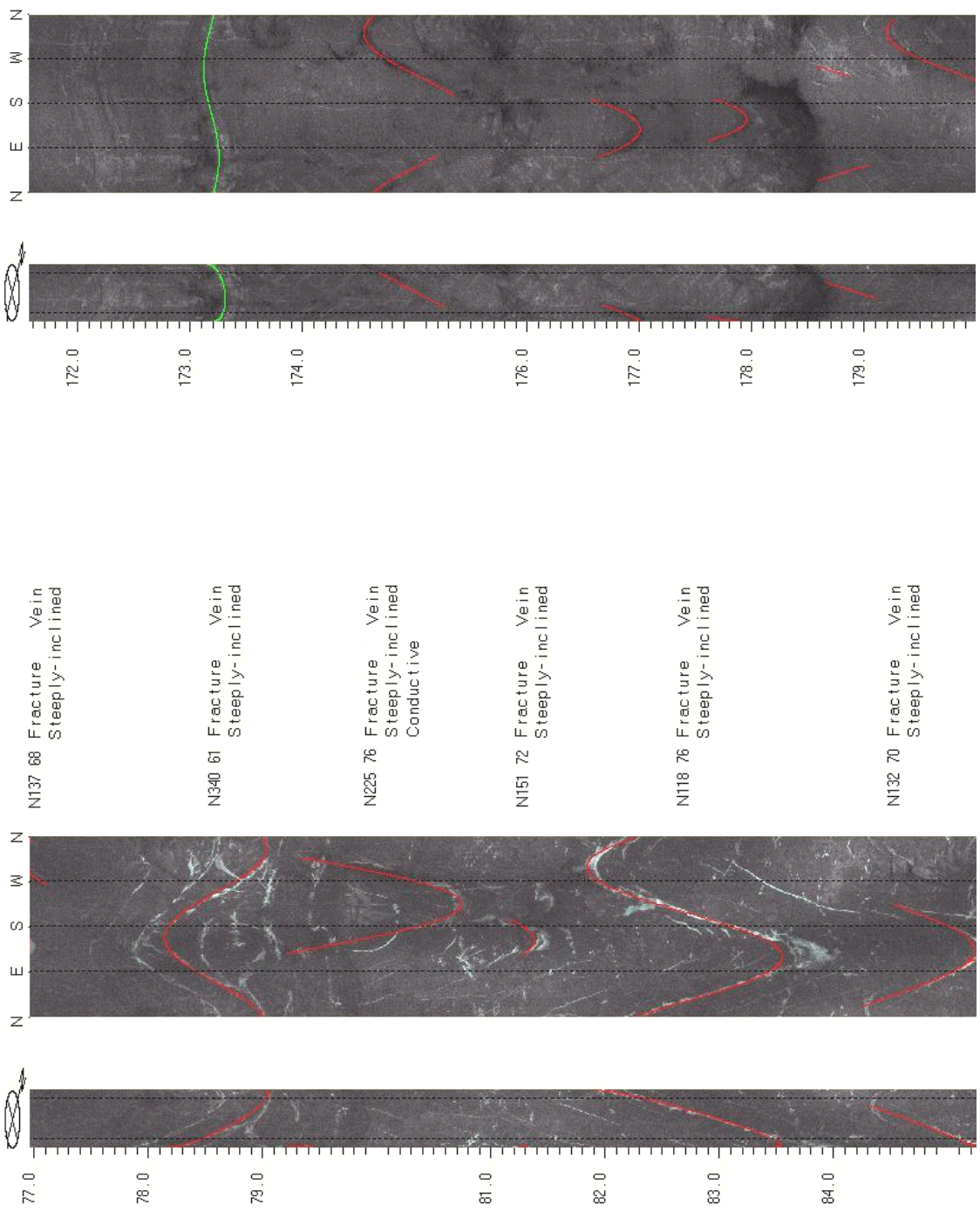

FIGURE 3D4. OPTV records of the 6-inch diameter well 50 at 74 Lambert Rd., Delaware Twp., Hunterdon County, NJ showing geologic structures and conductive features in red mudstone and gray shale. Depth values are in feet below land surface.

Well 51 - Brunswick middle red zone

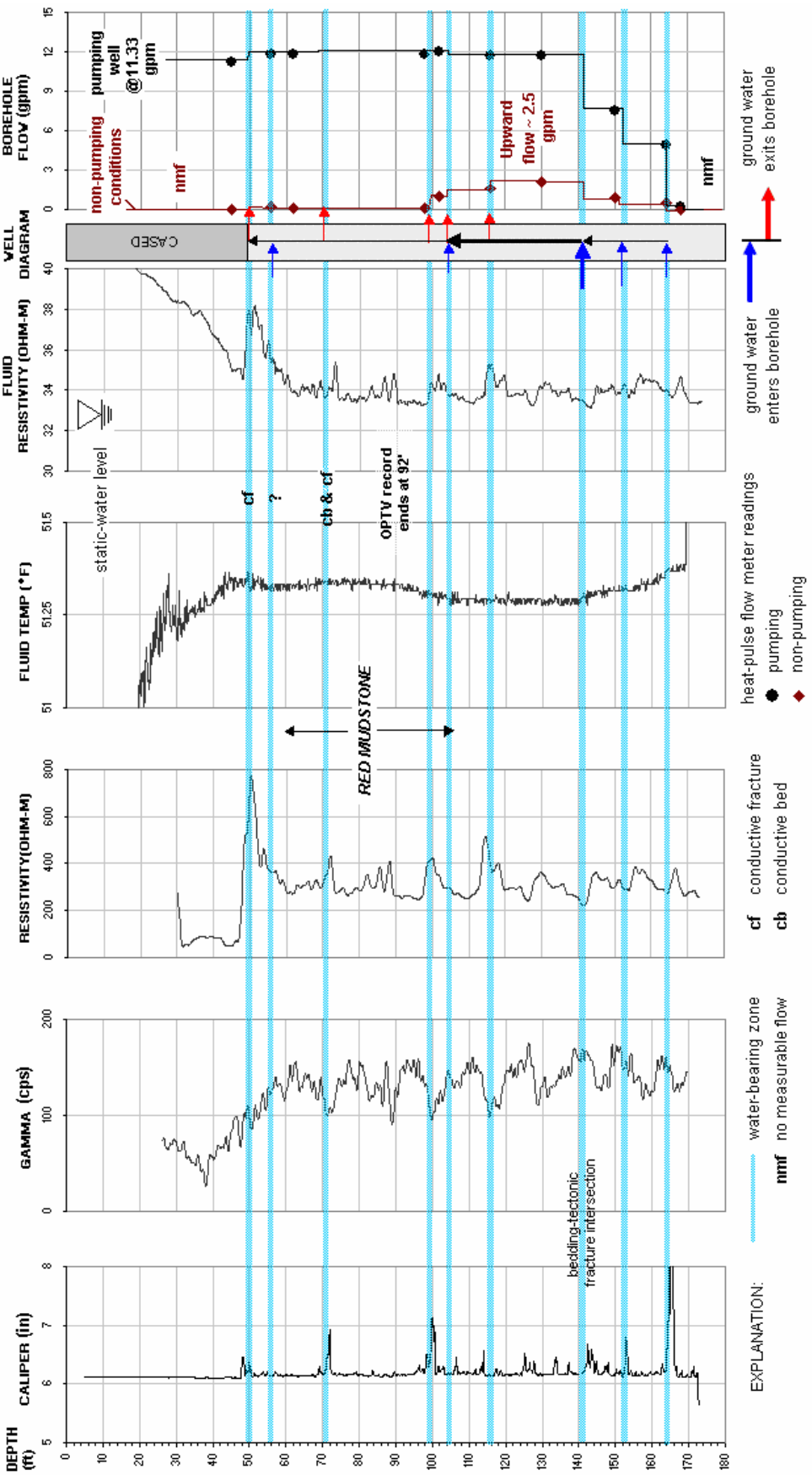

FIGURE 3D5. Hydrogeologic section based on geophysical logs for well 51 at 81 Dunkard Church Rd., Delaware Twp., Hunterdon County, NJ. The section shows the vertical distribution and types of hydraulically-conductive features and water-bearing zones in red mudstone. Depth values are in feet below land surface.

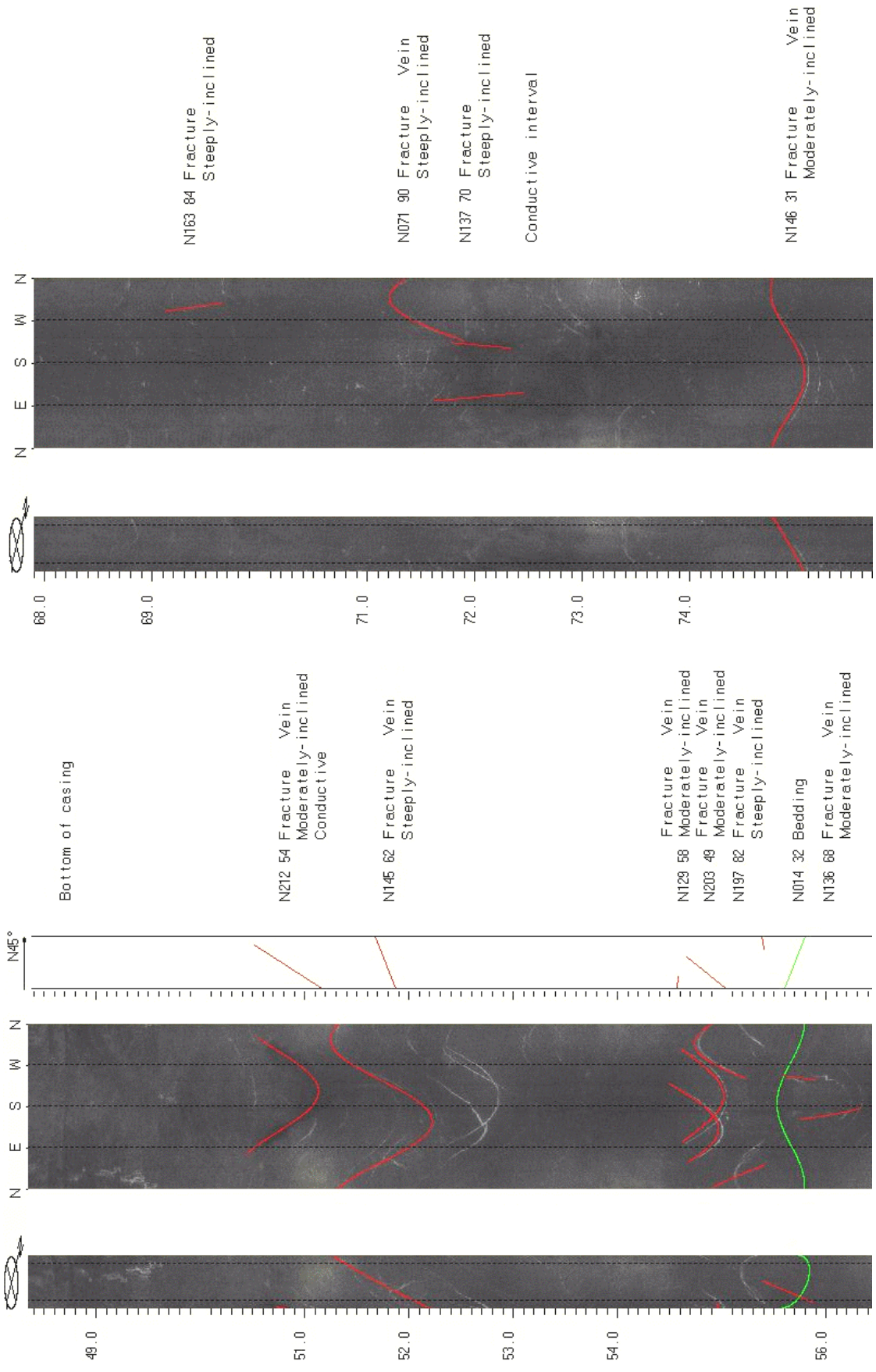

FIGURE 3D6. OPTV records of the 6-inch diameter well 51at 81 Dunkard Church Rd., Delaware Twp., Hunterdon County, NJ showing geologic structures and conductive features in red mudstone. Depth values are in feet below land surface.

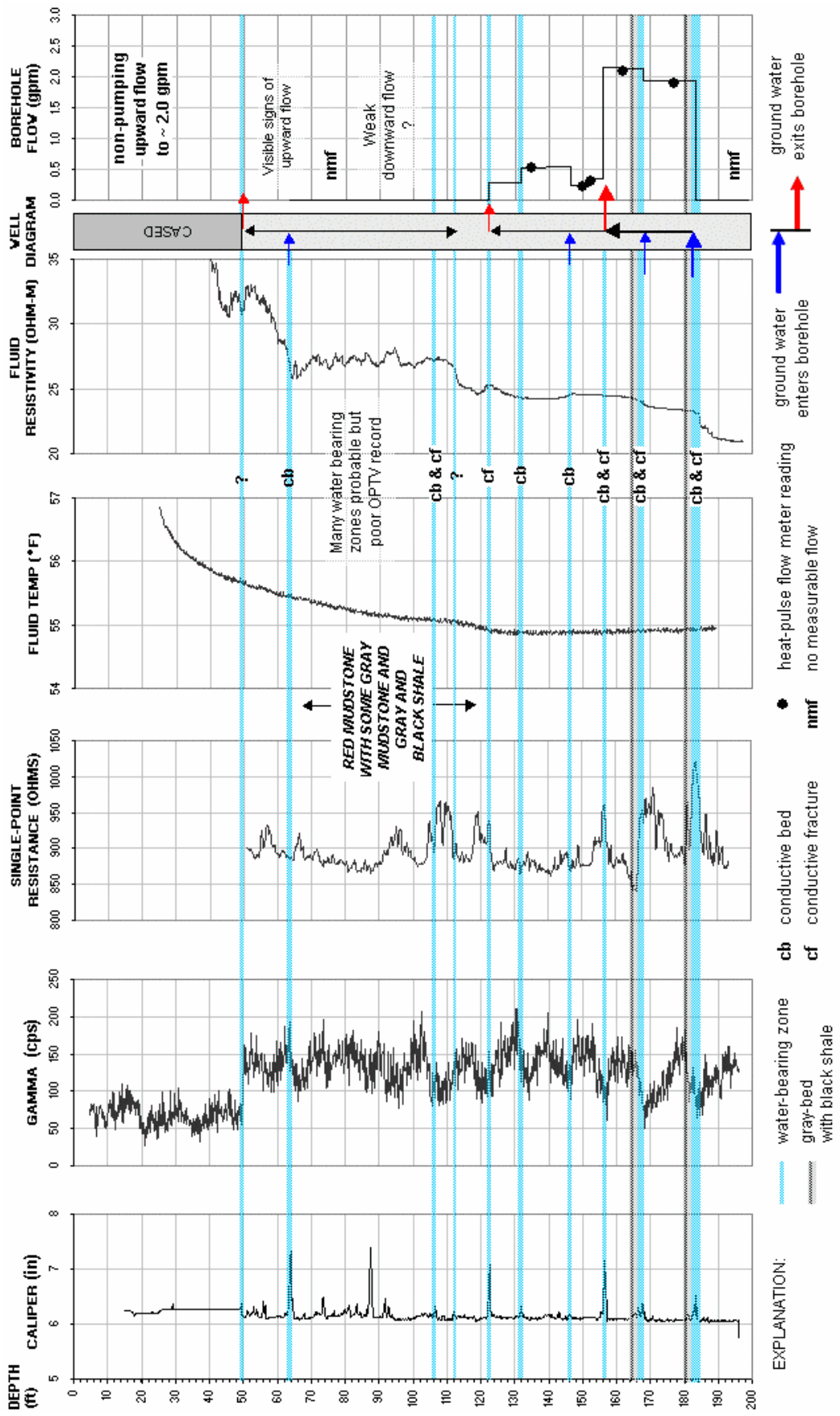

FIGURE 3D7. Hydrogeologic section based on geophysical logs for well 52 at 79 Dunkard Church Rd., Delaware Twp., Hunterdon County, NJ. The section shows the vertical distribution and types of hydraulically-conductive features and water-bearing zones in red and gray mudstone and black shale. Depth values are in feet below land surface.

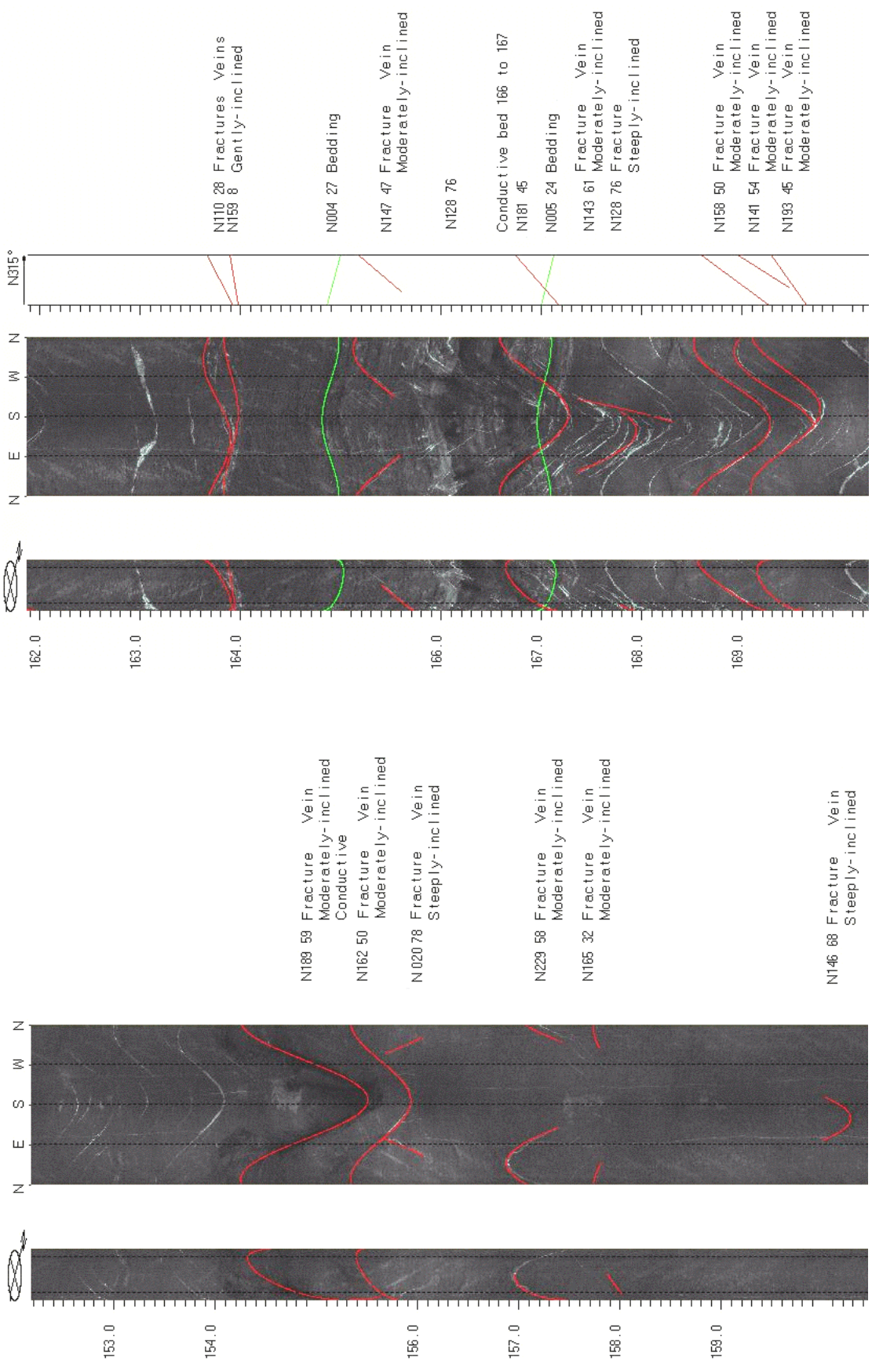

FIGURE 3D8. OPTV records of the 6-inch diameter well 52 at 79 Dunkard Church Rd., Delaware Twp., Hunterdon County, NJ showing geologic structures and conductive features in red and gray mudstone and gray shale. Depth values are in feet below land surface.

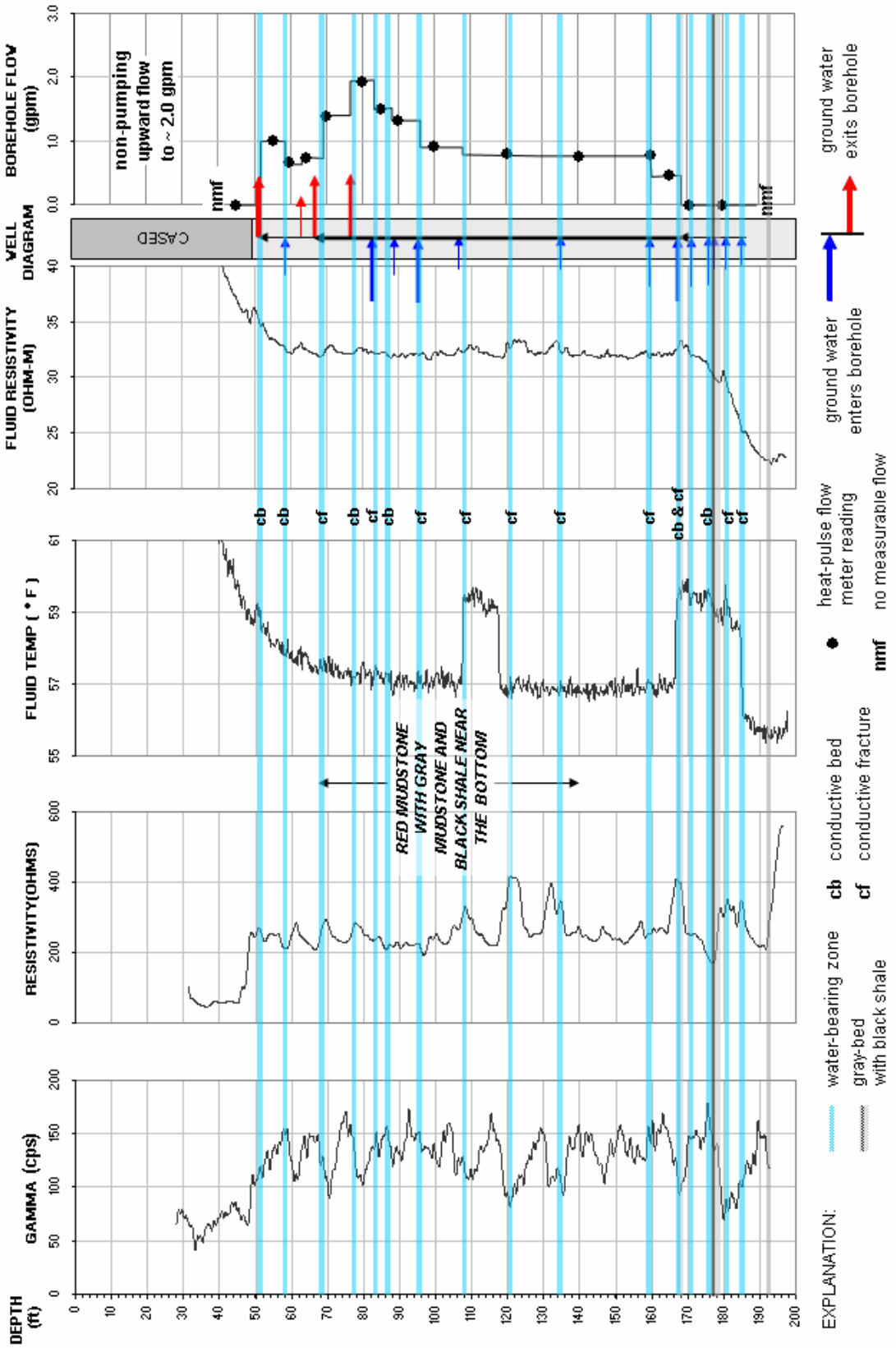

FIGURE 3D9. Hydrogeologic section based on geophysical logs for well 52 at 77 Dunkard Church Rd., Delaware Twp., Hunterdon County, NJ. The section shows the vertical distribution and types of hydraulically-conductive features and water-bearing zones in red and gray mudstone and black shale. Depth values are in feet below land surface.

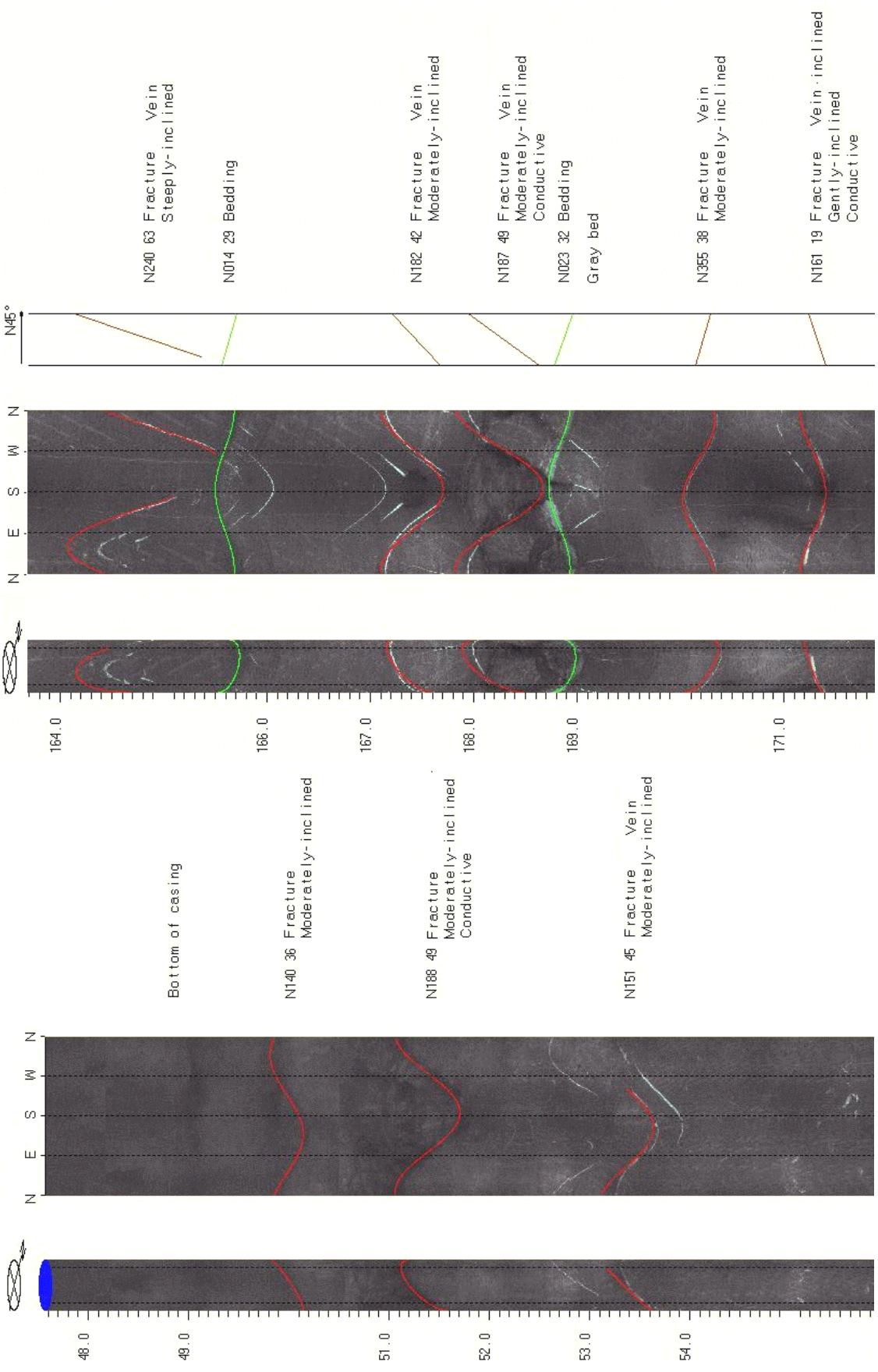

FIGURE 3D10. OPTV records of the 6-inch diameter well 51at 77 Dunkard Church Rd., Delaware Twp., Hunterdon County, NJ showing geologic structures and conductive features in red and gray mudstone and gray shale. Depth values are in feet below land surface.

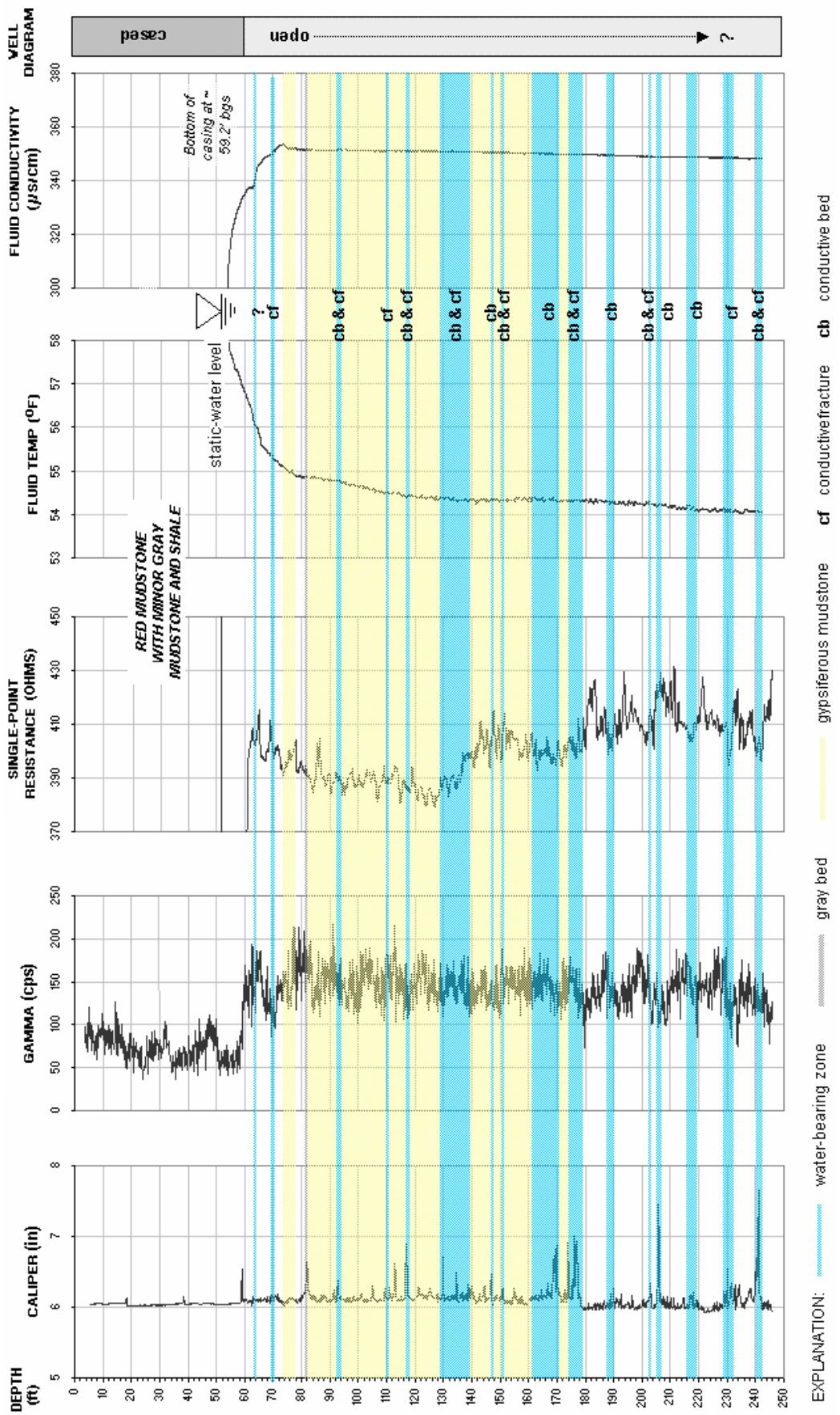

FIGURE 3D11. Hydrogeologic section based on geophysical logs for well 54 at 32-34 Haines Rd., East Amwell Twp., Hunterdon County, NJ. The section shows the vertical distribution and types of hydraulically-conductive features and water-bearing zones in red and gray mudstone and gray shale. Depth values are in feet below land surface.

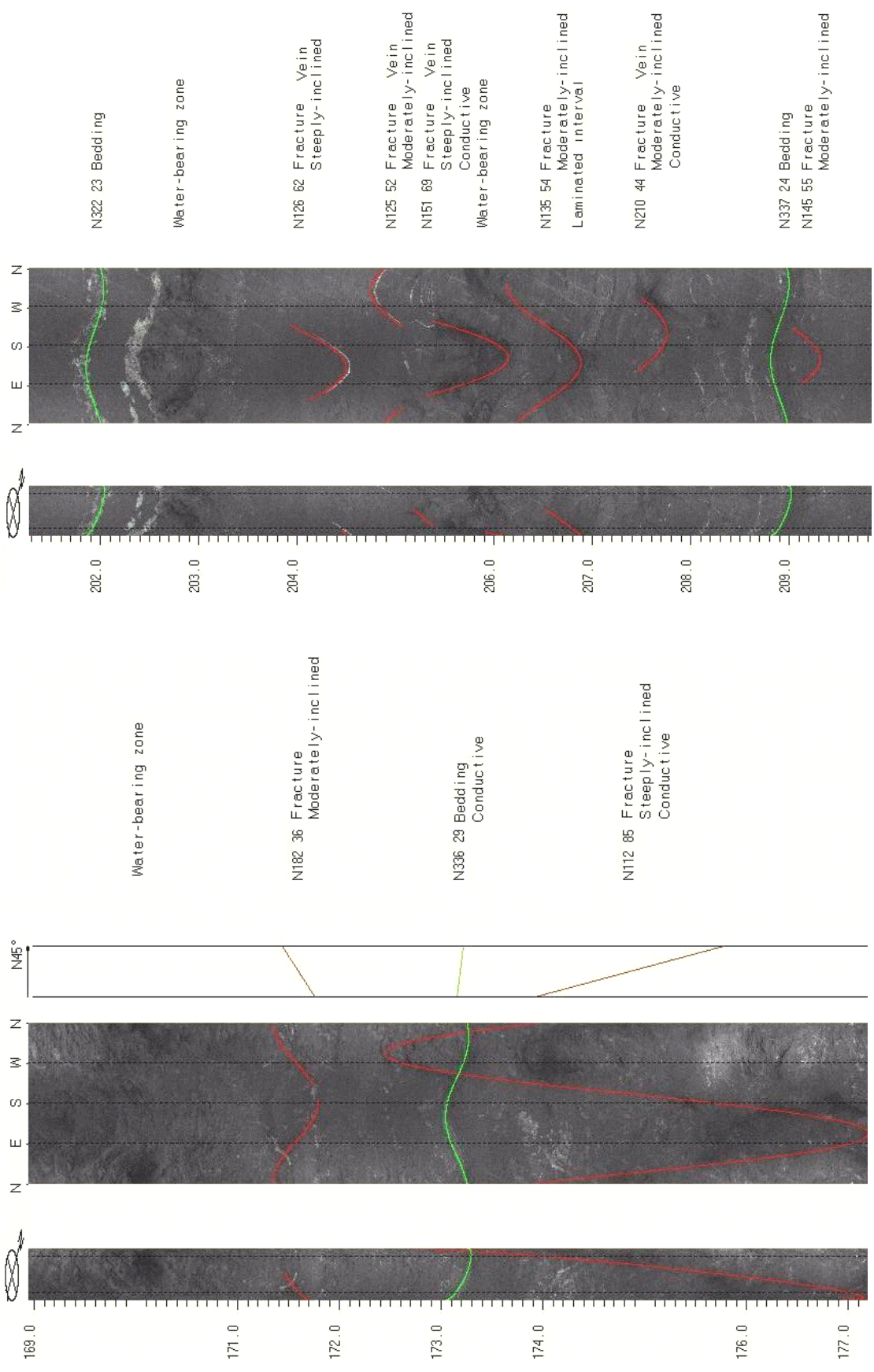

FIGURE 3D12. OPTV records of the 6-inch diameter well 54 at 32-34 Haines Rd., East Amwell Twp., Hunterdon County, NJ shows geologic structures and conductive features in red mudstone. Depth values are in feet below land surface.

Wells 52 and 53 - Brunswick middle red zone

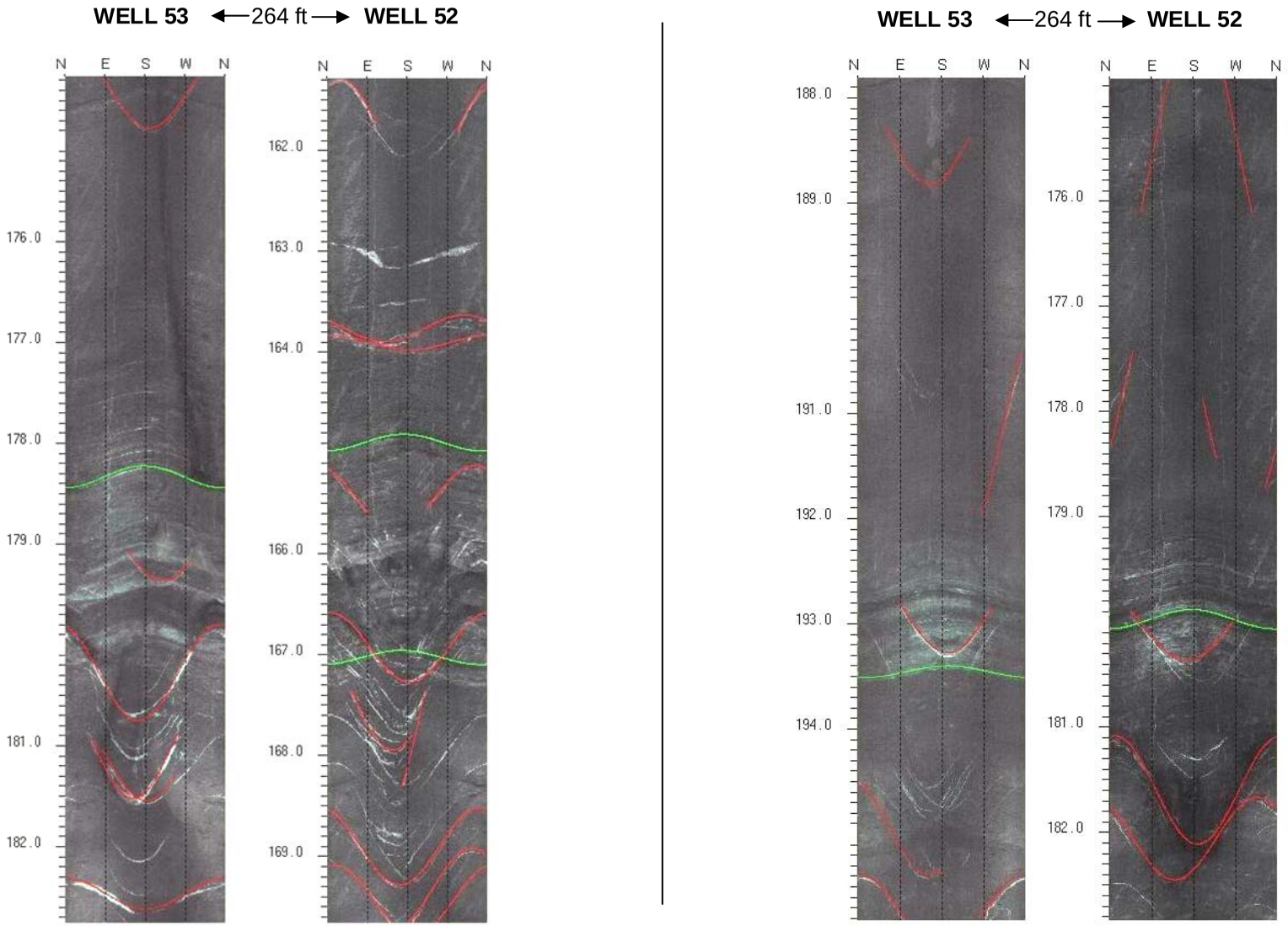

FIGURE 3D13. Stratigraphic correlation of wells 52 and 53 based on OPTV records, Dunkard Church Rd. Delaware Twp., Hunterdon County, NJ. Note the similar fracture sets occurring in the same stratigraphic intervals. Depth values are in feet below land surface.

Wells 52 to 54 - Brunswick middle red zone

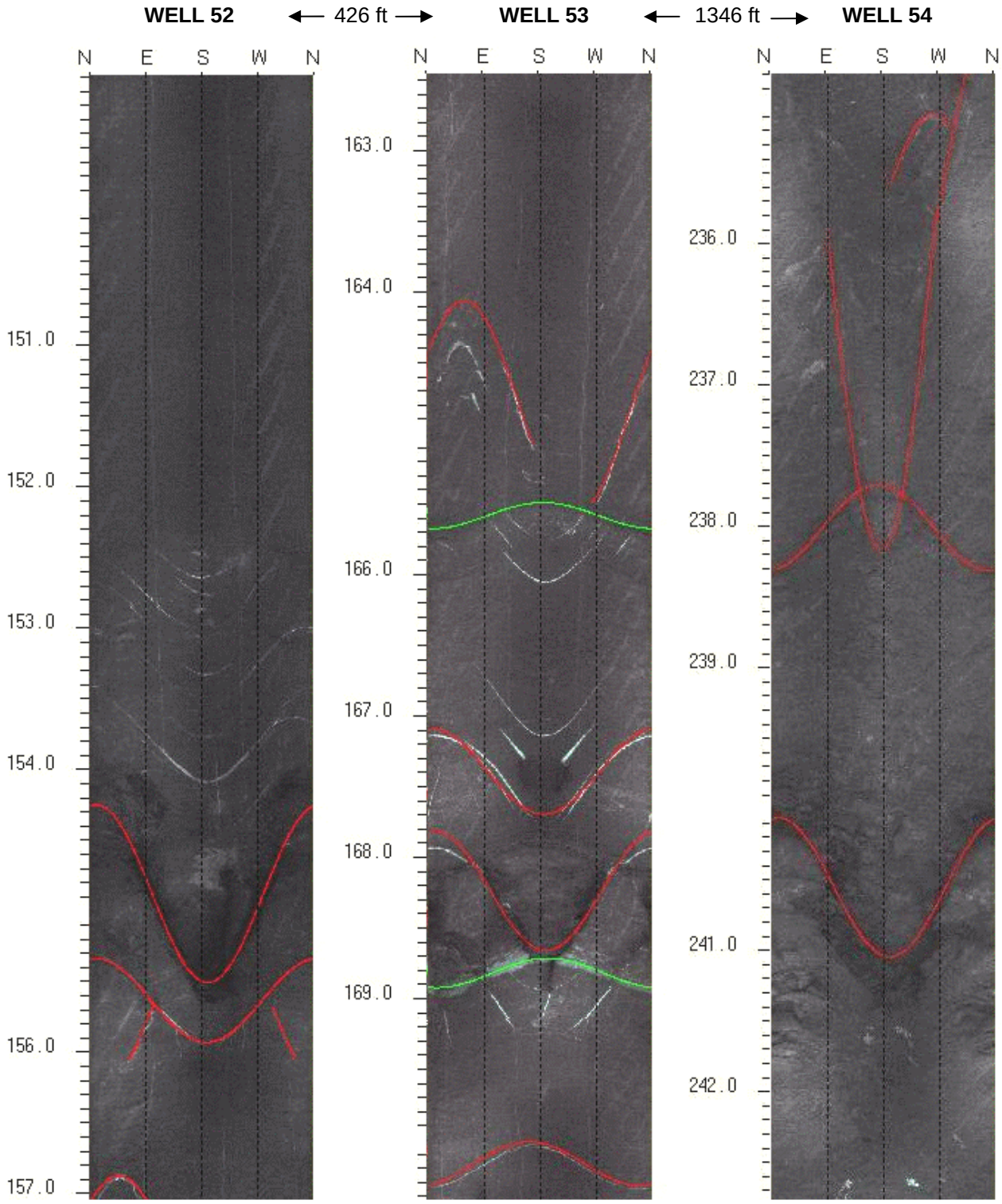

Figure 3D14. Stratigraphic correlation of wells based on OPTV records for wells 52 through 54, Dunkard Church Rd. Delaware Twp. and Lambert Rd., East Amwell Twp., Hunterdon County, NJ. Note the similar fracture sets occurring in the same stratigraphic intervals. Depth values are in feet below land surface.

Wells 55 to 60 - Brunswick middle red zone

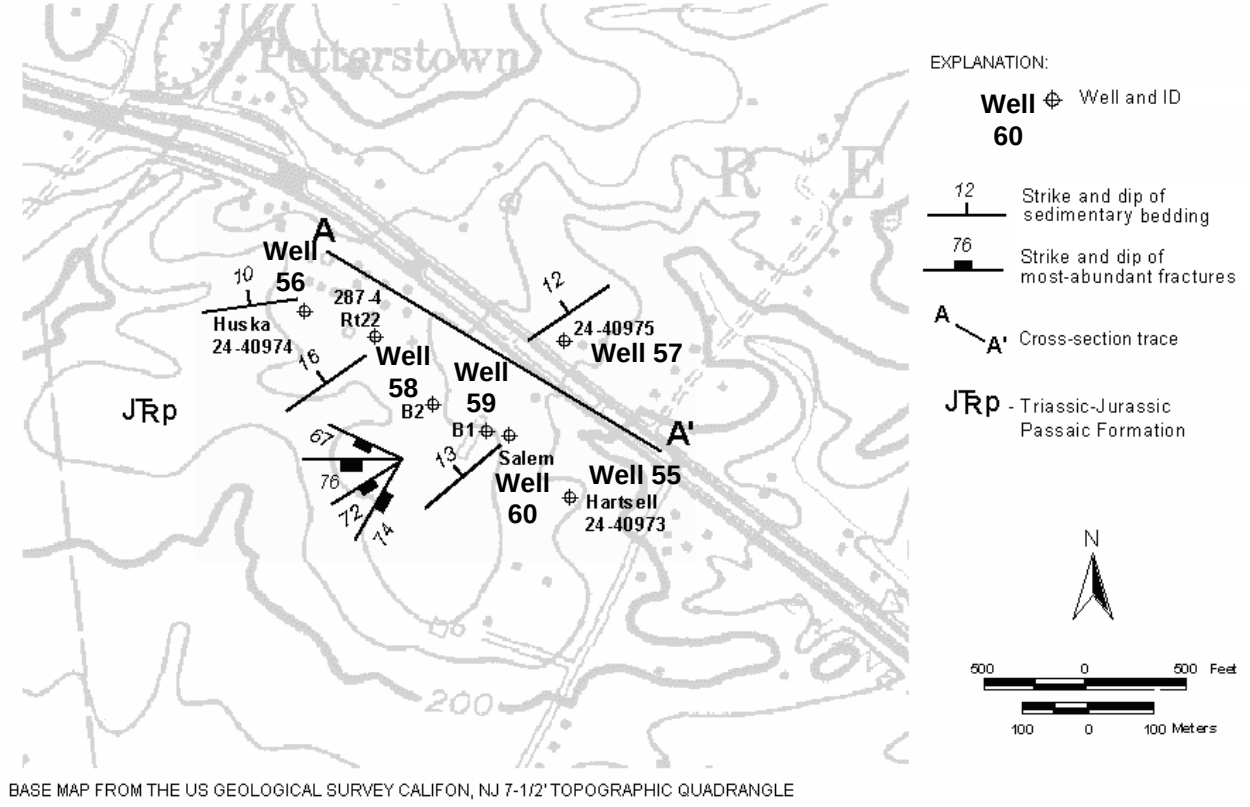

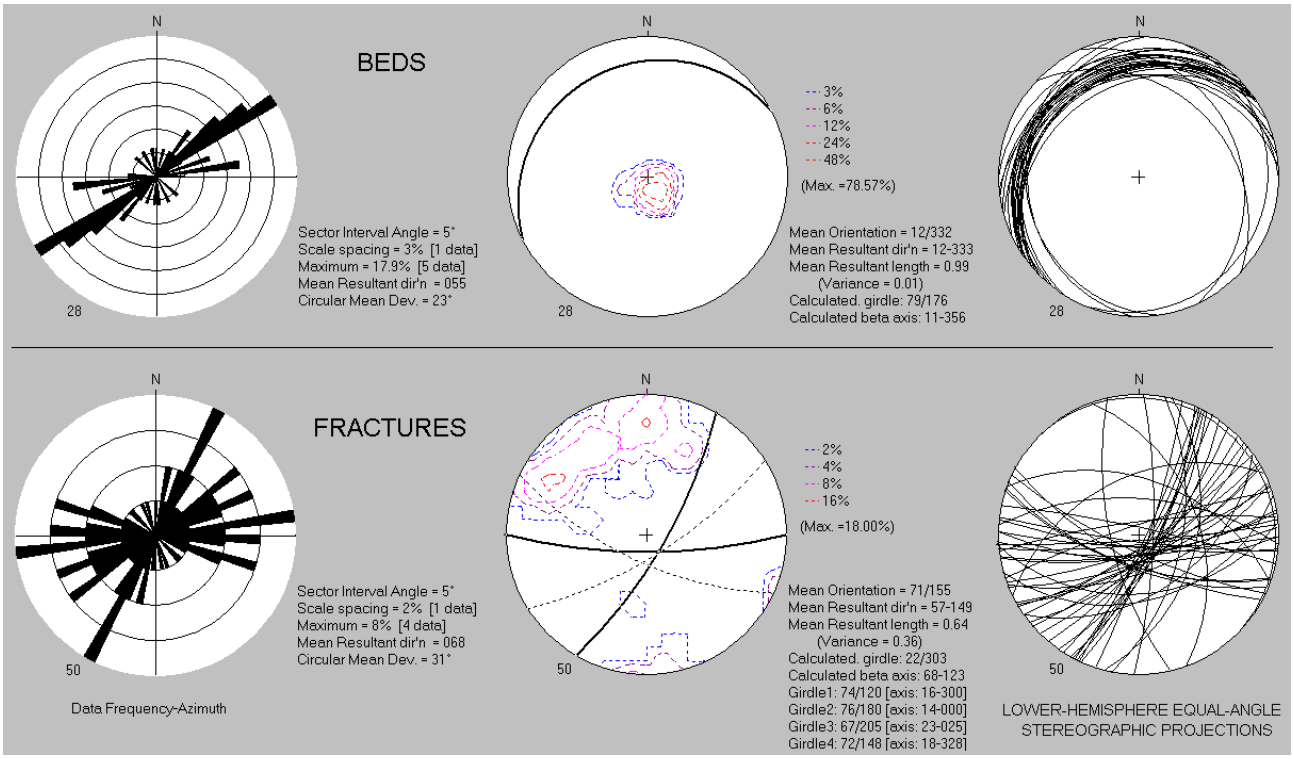

Figure 3E1. Map (above) shows wells 55 to 60 along Rt.22 near Potterstown, Readington Twp., Hunterdon County, NJ. Mapped bedrock structures are based on a structural analysis of beds and fractures (bottom) measured in OPTV records.

Wells 55 to 60 - Brunswick middle red zone

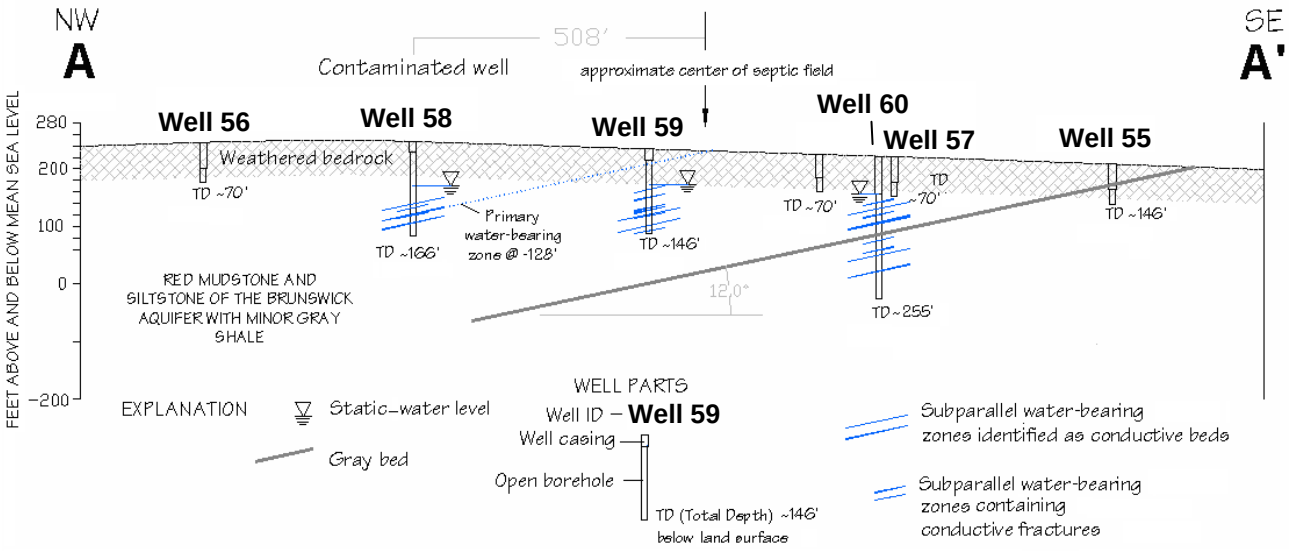

Well 58 - Brunswick middle red zone

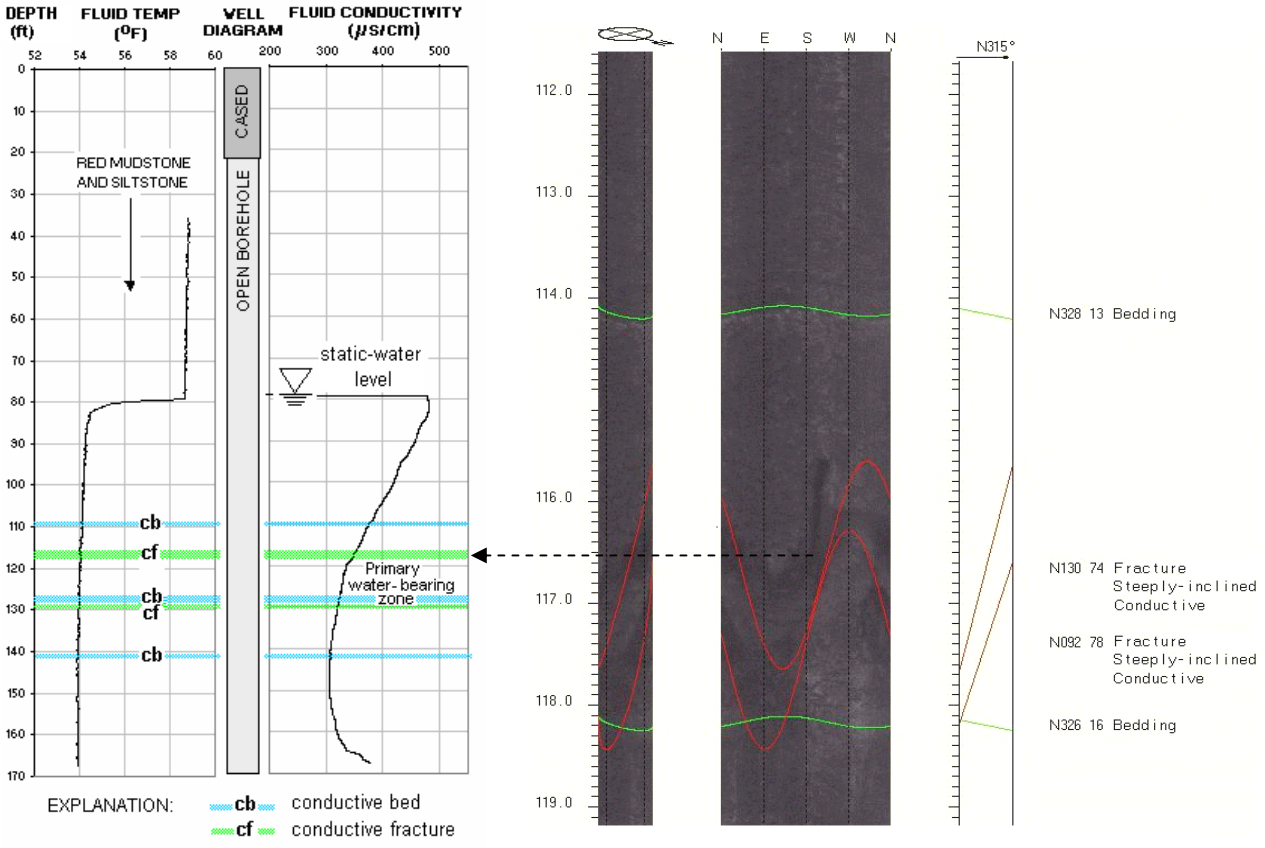

Figure 3E2. Hydrogeologic section (above) is based on geophysical logs for six wells along Rt.22 near Potterstown, Readington Twp, Hunterdon County, NJ. The hydrogeologic section for well 58 (below left) shows hydraulically-conductive features and water-bearing zones in red mudstone and siltstone. An OPTV record for well 58 (below right) shows conductive, steeply-dipping fractures in the 6-inch diameter domestic well. Depth values are in feet below land surface.

Well 59 - Brunswick middle red zone

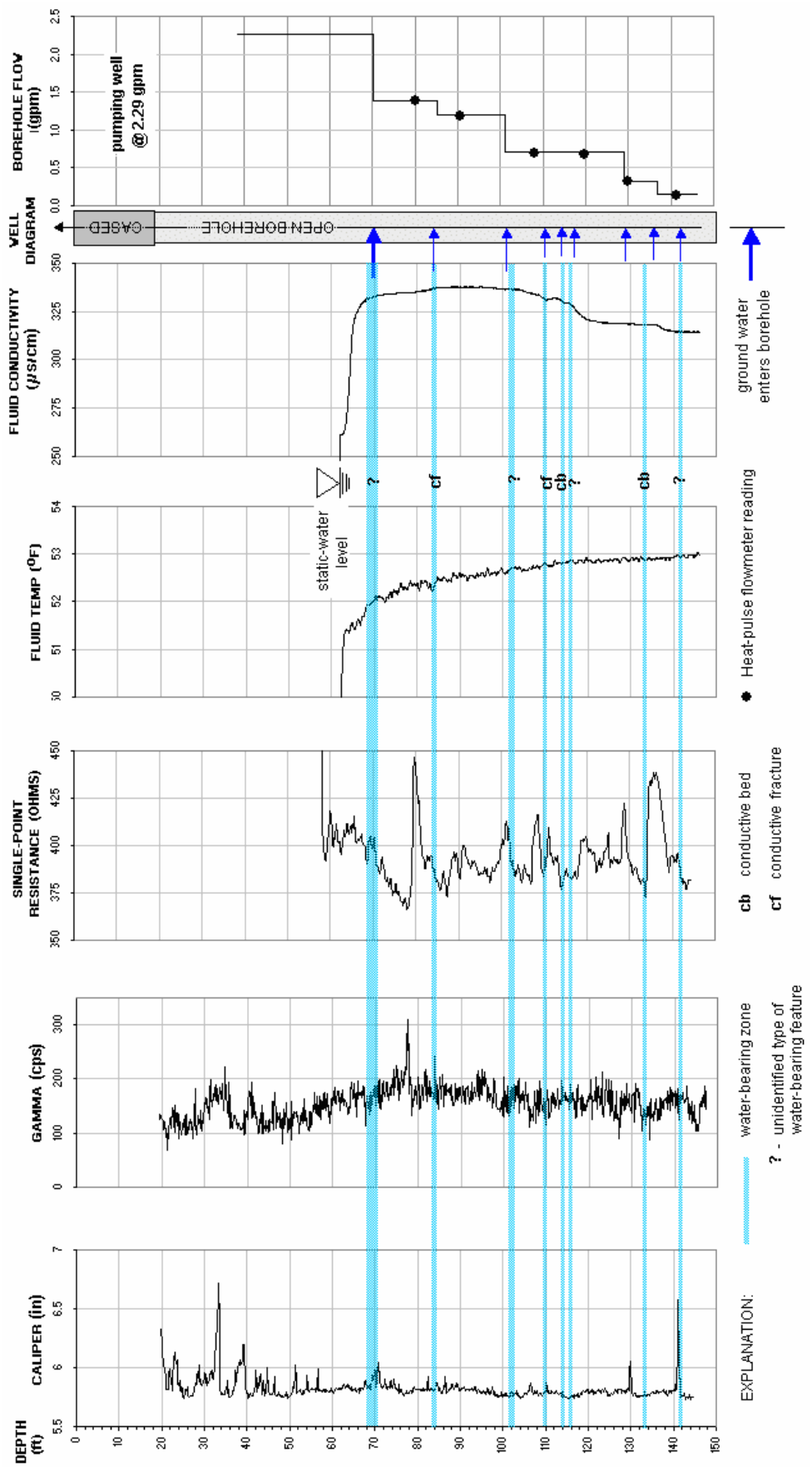

FIGURE 3E3. Hydrogeologic section based on geophysical logs for well 59 at Salem Industrial Park, Rt. 22 East, Readington Twp., Hunterdon County, NJ. The section shows the vertical distribution and types of hydraulically-conductive features and water-bearing zones in red mudstone and siltstone. Depth values are in feet below land surface.

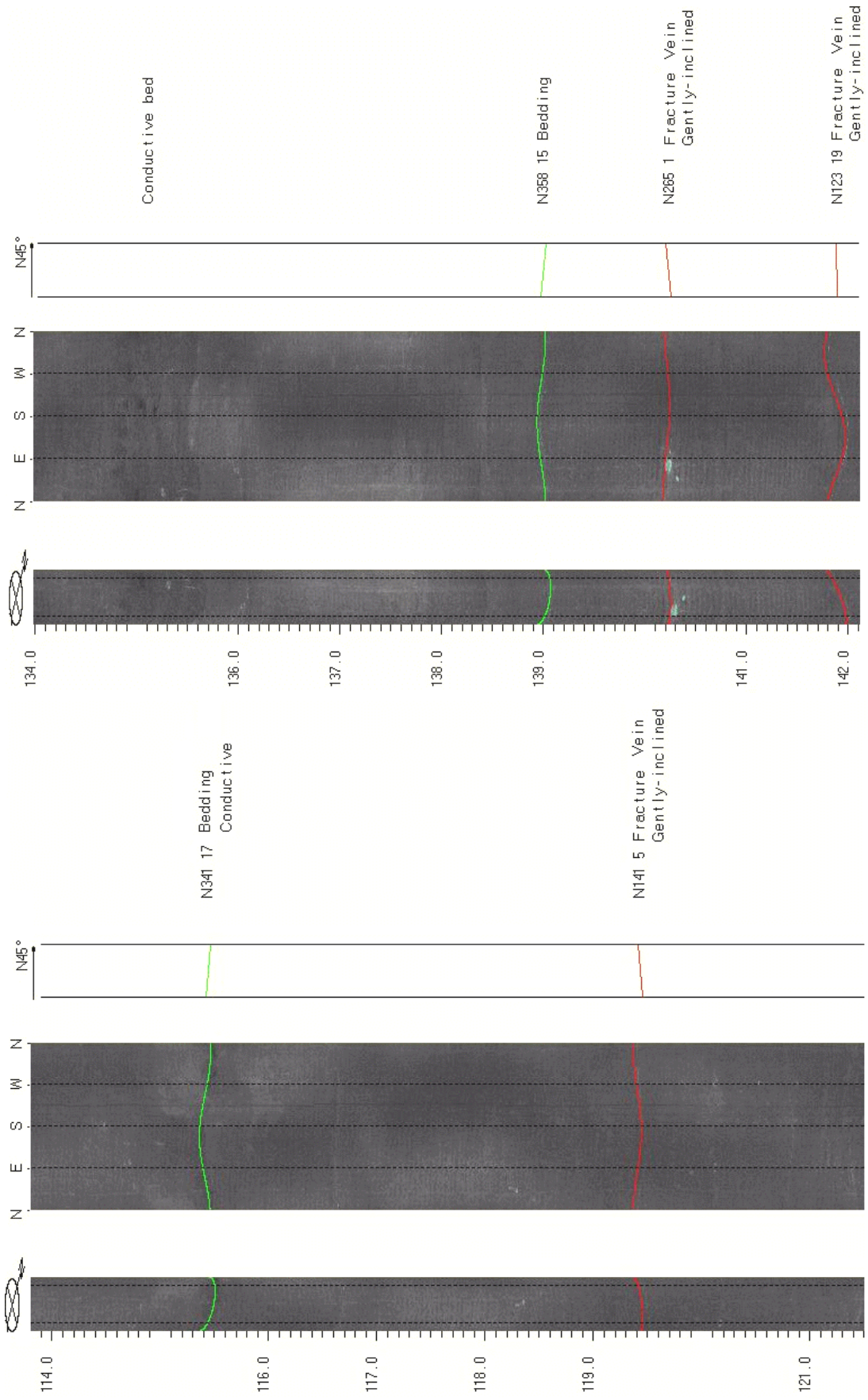

FIGURE 3E4. OPTV records of the 6-inch diameter well 59 at Salem Industrial Park, Rt. 22 East, Readington Twp., Hunterdon County, NJ showing geologic structures and conductive features in red mudstone. Depth values are in feet below land surface.

Well 60 - Brunswick middle red zone

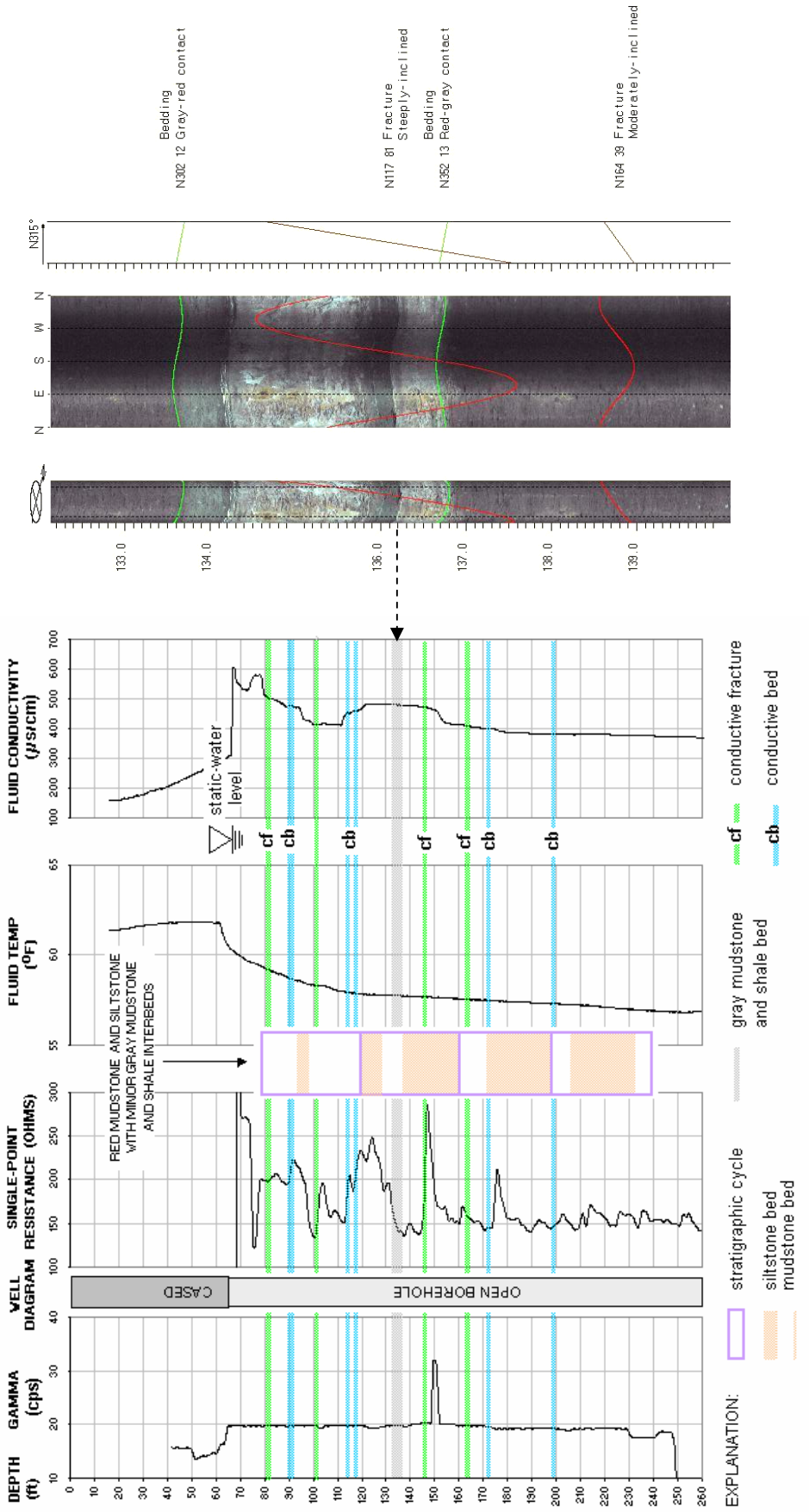

FIGURE 3E5. Hydrogeologic section (left) based on geophysical logs for well 60 at Salem Industrial Park, Rt. 22 East, Readington Twp., Hunterdon County, NJ. The section shows the vertical distribution and types of hydraulically-conductive features and water-bearing zones in red mudstone. An OPTV record for the 6-inch diameter well (right) shows a gray mudstone and shale bed. Depth values are in feet below land surface.

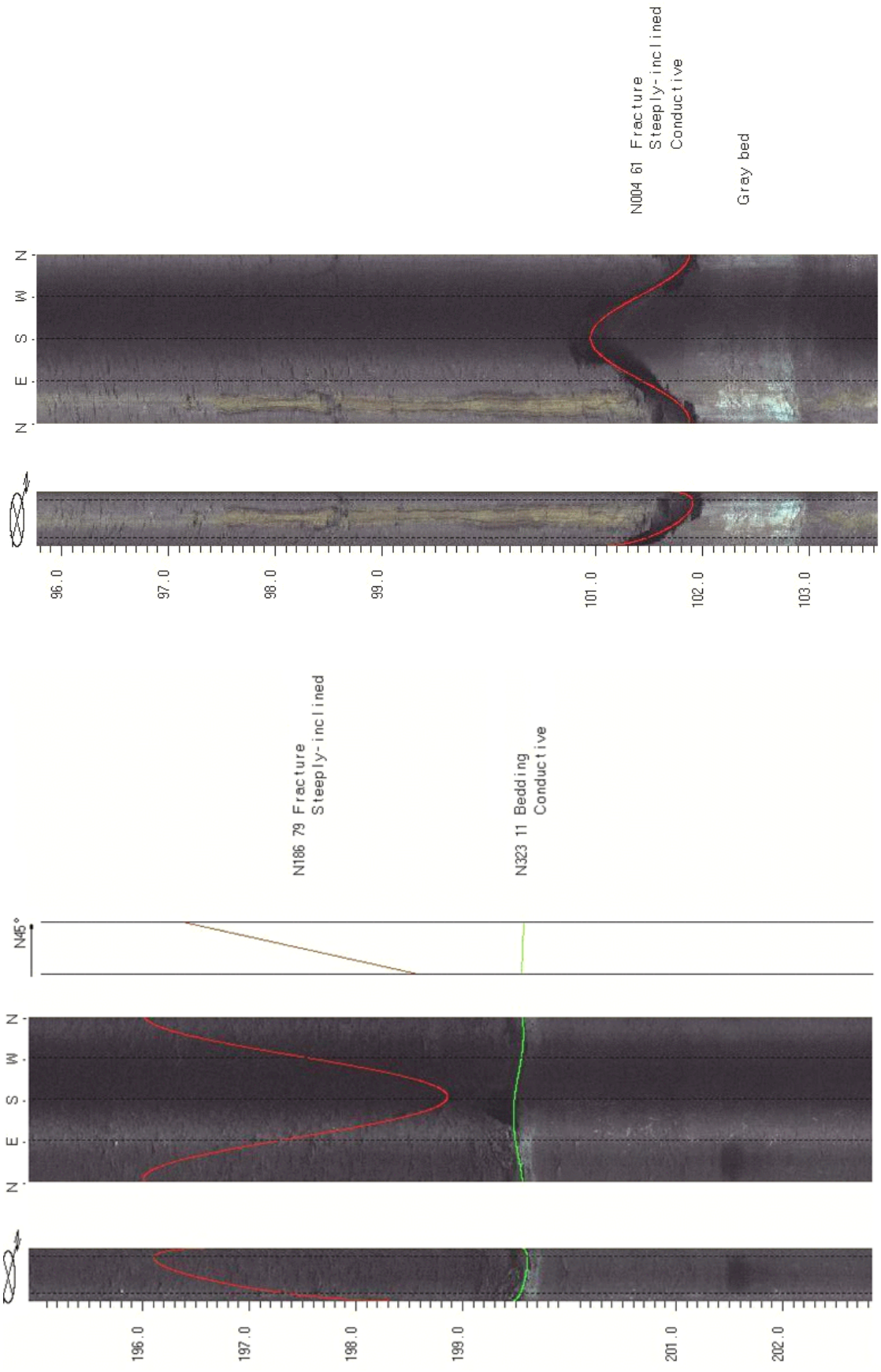

FIGURE 3E6. OPTV records of the 6-inch diameter well 60 at Salem Industrial Park, Rt. 22 East, Readington Twp., Hunterdon County, NJ showing geologic structures and conductive features in red mudstone and siltstone and a gray bed. Depth values are in feet below land surface.

Wells 61 to 67 - Brunswick middle red zone

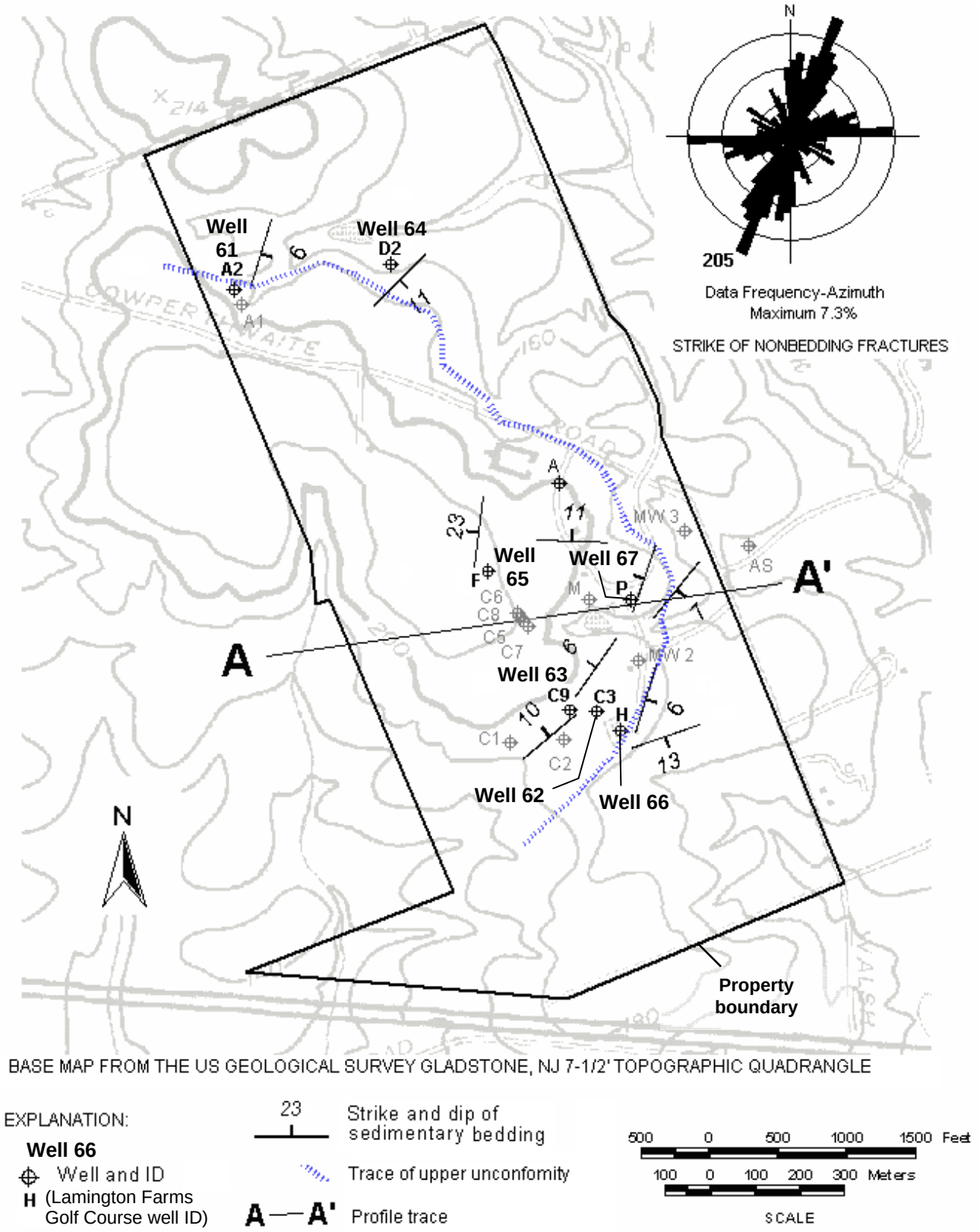

Figure 3F1. Map showing the location of wells 60 to 67 at Trump National Golf Course (formerly Lamington Farms Golf Course), Bedminster Twp., Somerset County, NJ.

Wells 61 to 67 - Brunswick middle red zone

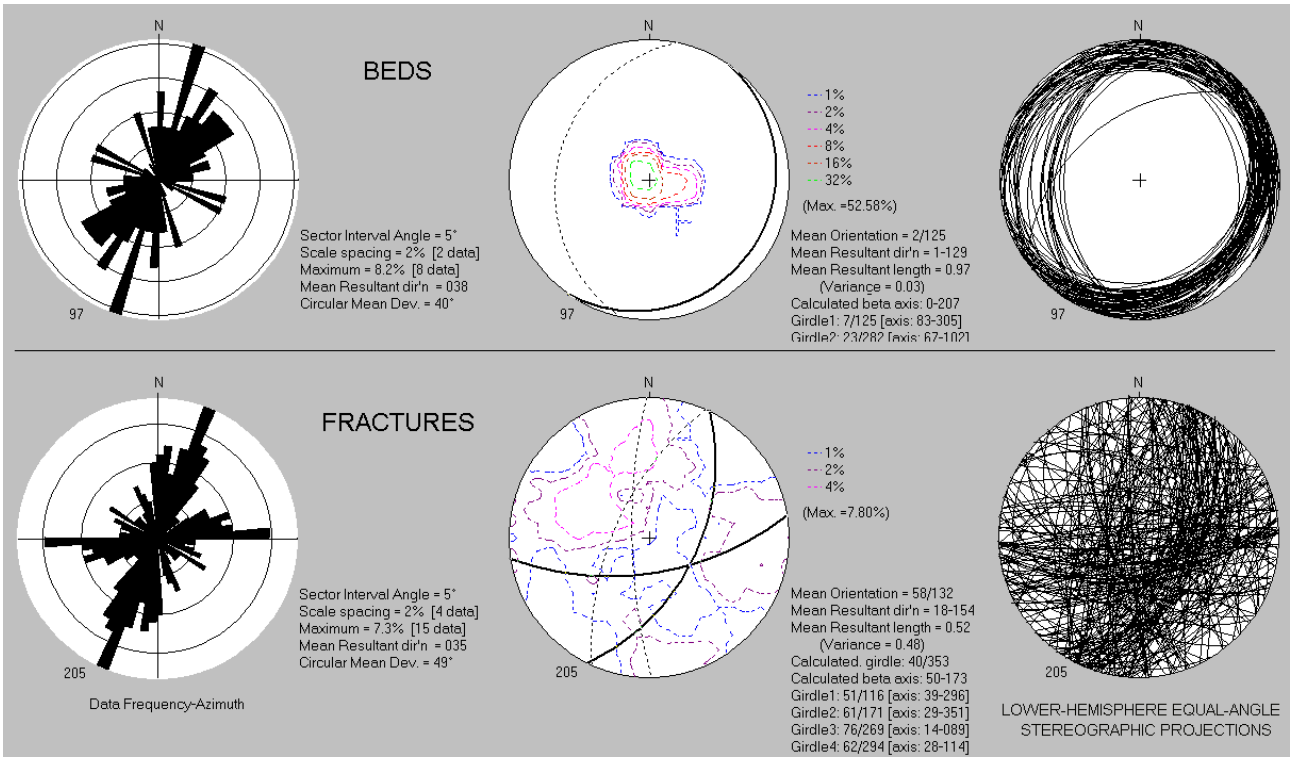

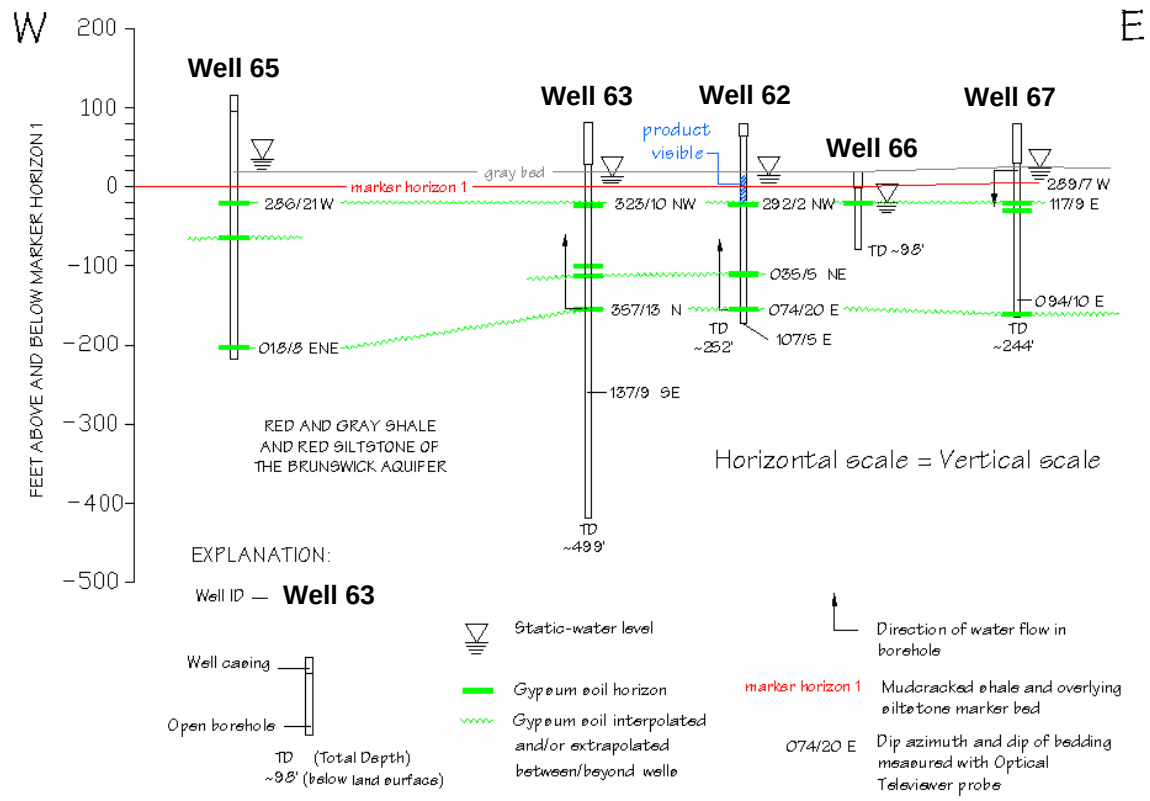

FIGURE 3F2. A structural analysis (above) of beds and fractures measured in OPTV records for wells 61 through 67. The geologic cross section (below) shows a correlation of gypsum-soil horizons identified in OPTV records and interpreted as stratigraphic unconformities. Note the opposing dips for strata above and below the soil horizons.

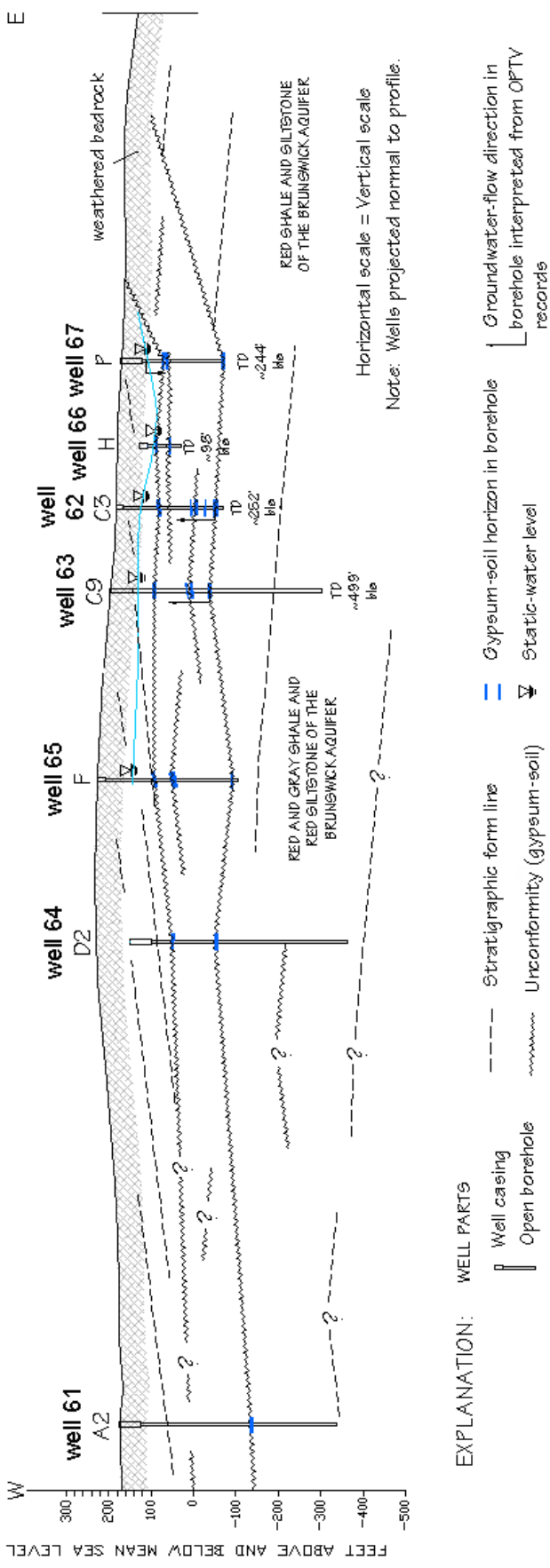

FIGURE 3F3. Hydrogeologic section based on seven wells at Trump National Golf Course, Bedminster Twp., Somerset County, NJ. Wells penetrate stratigraphic unconformities along extensive gypsum-soil beds. Stratigraphic sequences above and below the many unconformities dip in different directions.

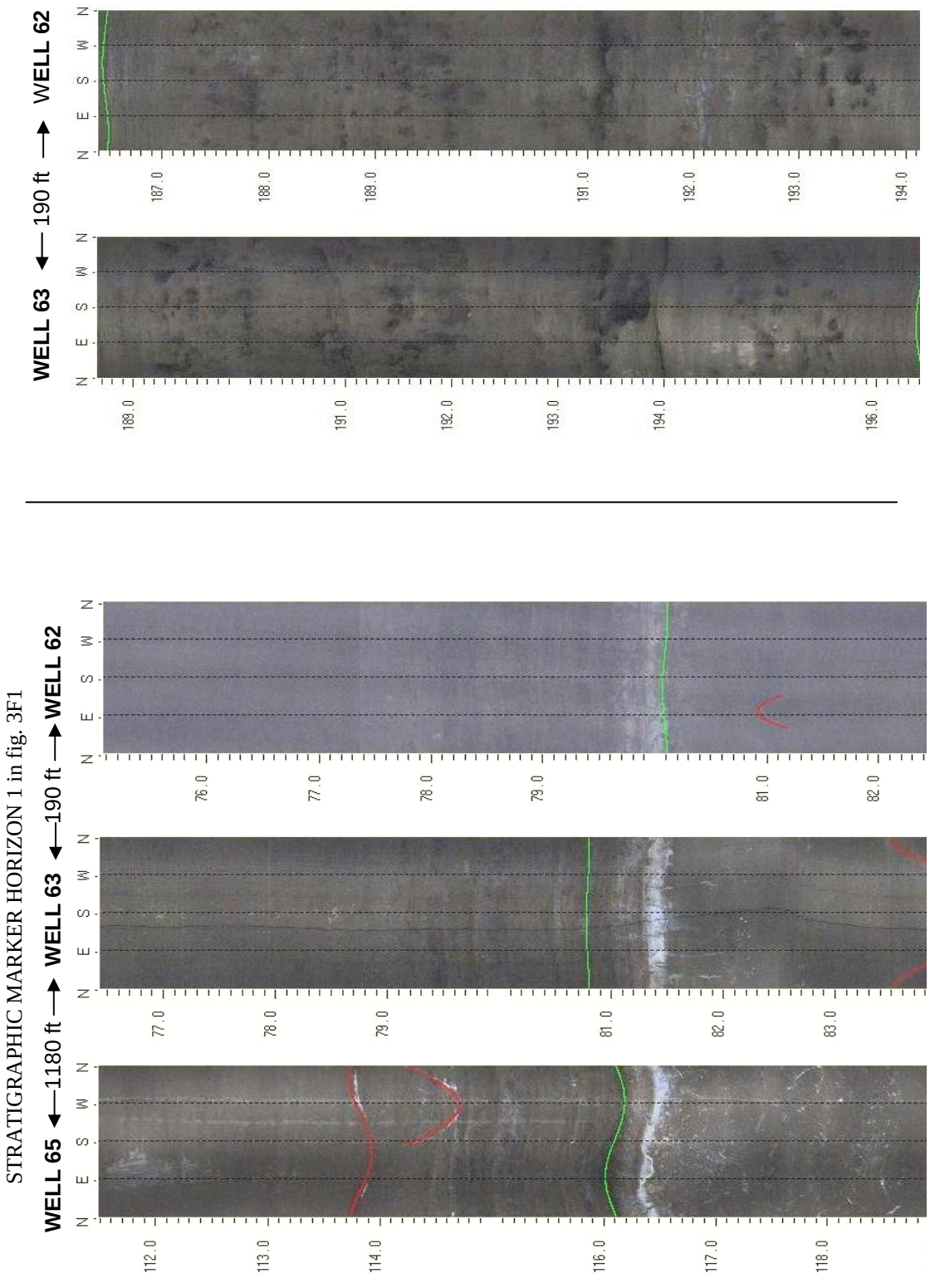

FIGURE 3F4. OPTV records for wells 62, 63 and 65 at Trump National Golf Course, Bedminster Twp., Somerset County, NJ showing stratigraphic marker horizon 1(left and fig. 3F2) and a correlation of a gypsum -soil horizon for wells 62 and 63 (right). Depth values are in feet below land surface.

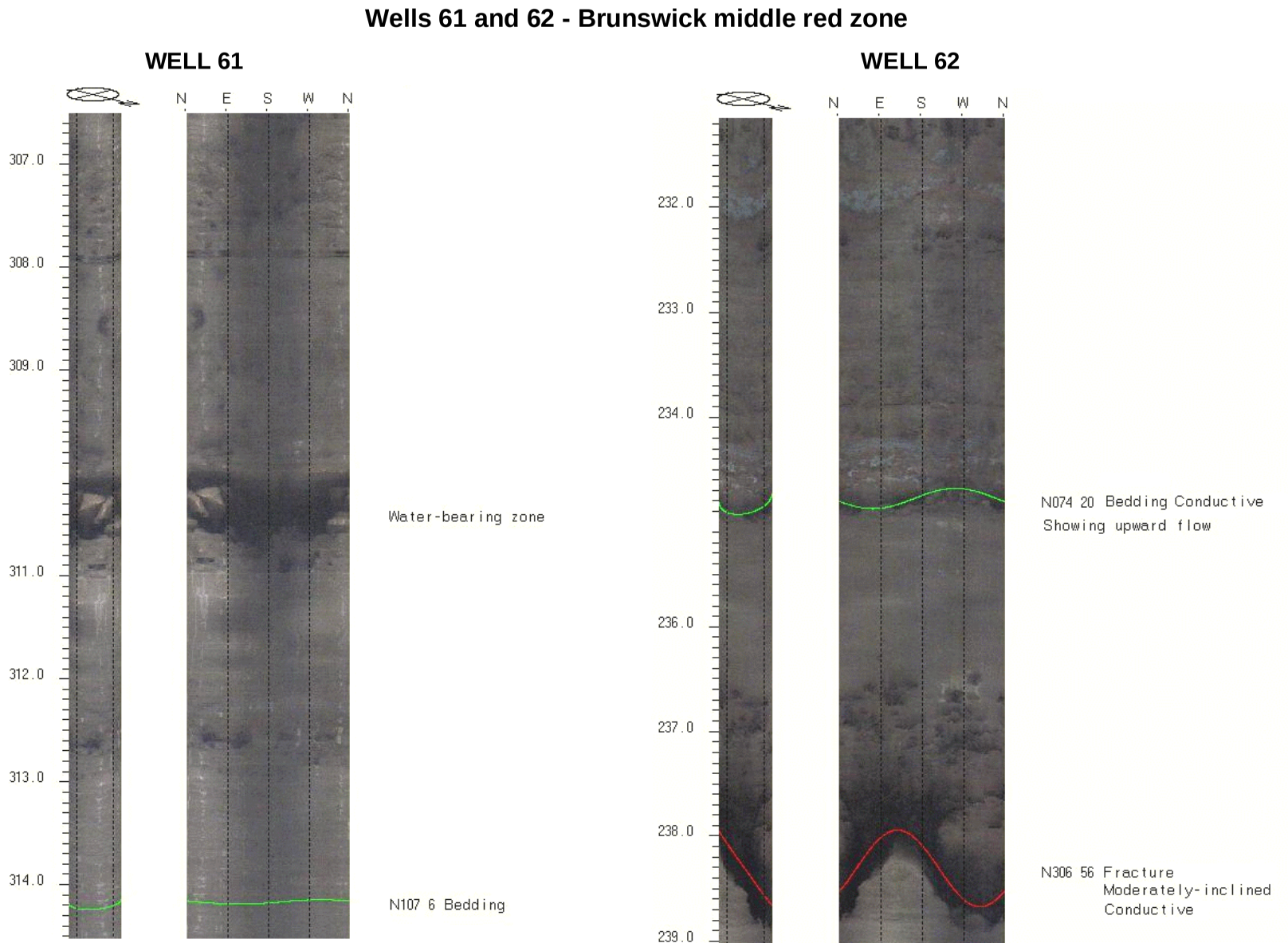

FIGURE 3F5. OPTV records of t6-inch diameter wells 61 and 62 showing geologic structures and hydraulically-conductive features in red mudstone with gypsum soils. Depth values are in feet below land surface.

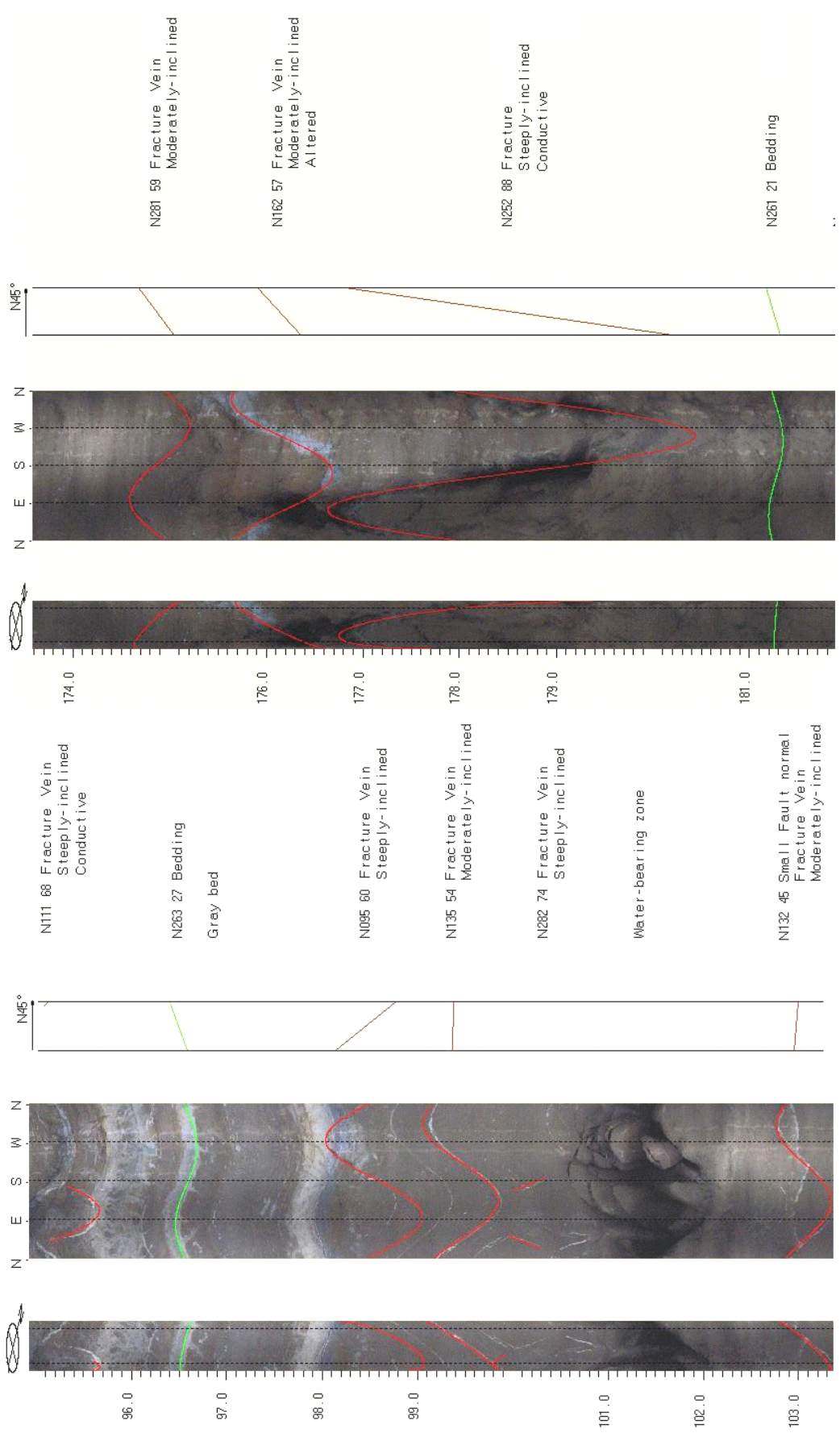

FIGURE 3F6. OPTV records of the 6-inch diameter well 65 at Salem Industrial Park, Rt. 22 East, Readington Twp., Hunterdon County, NJ showing geologic structures and hydraulically conductive features in red and gray mudstone. Depth values are in feet below land surface.

Wells 68 to 74 - Brunswick middle red and middle gray zones

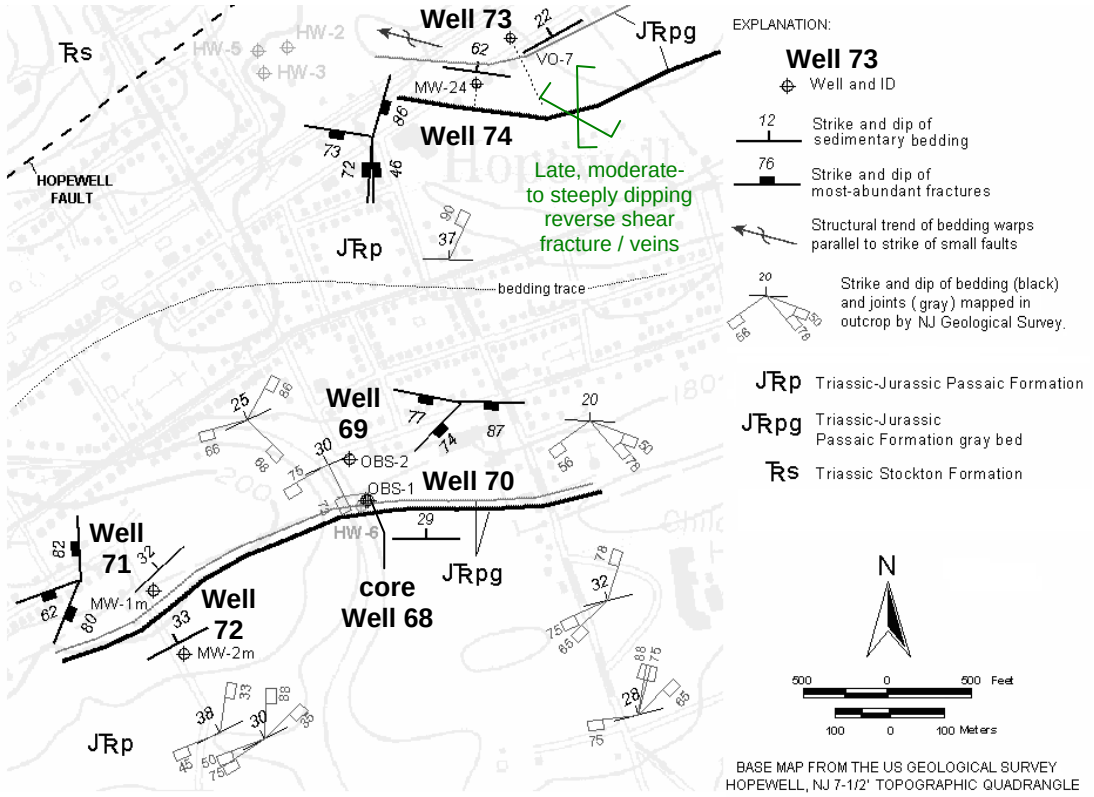

Wells 69 and 70 - Brunswick middle red and middle gray zones

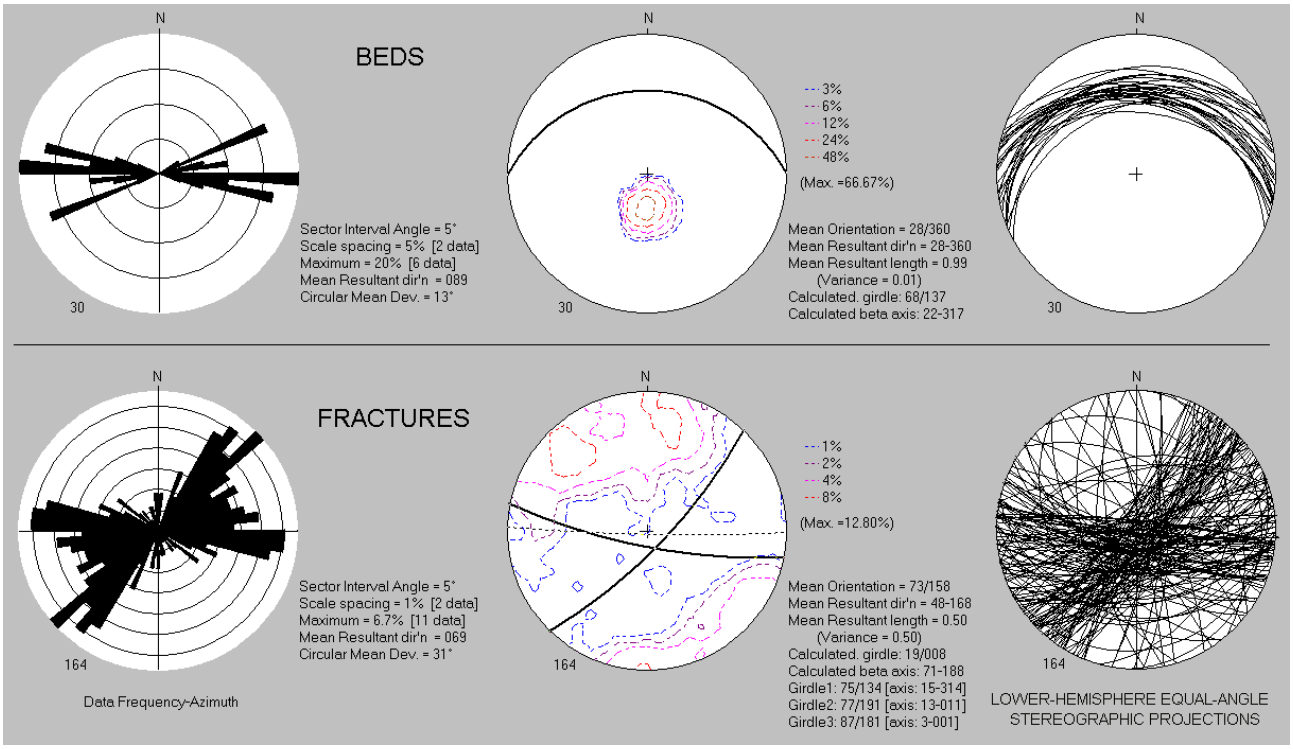

Figure 3G1. Map (above) shows wells 68 through 74 and nearby geological structures in Hopewell Borough, Mercer County, NJ. The strike and of bedding and fractures near each well are based on structural analyses of OPTV records. The structural analysis for wells 69 and 70 is shown below.

Wells 71 and 72 - Brunswick middle red and middle gray zones

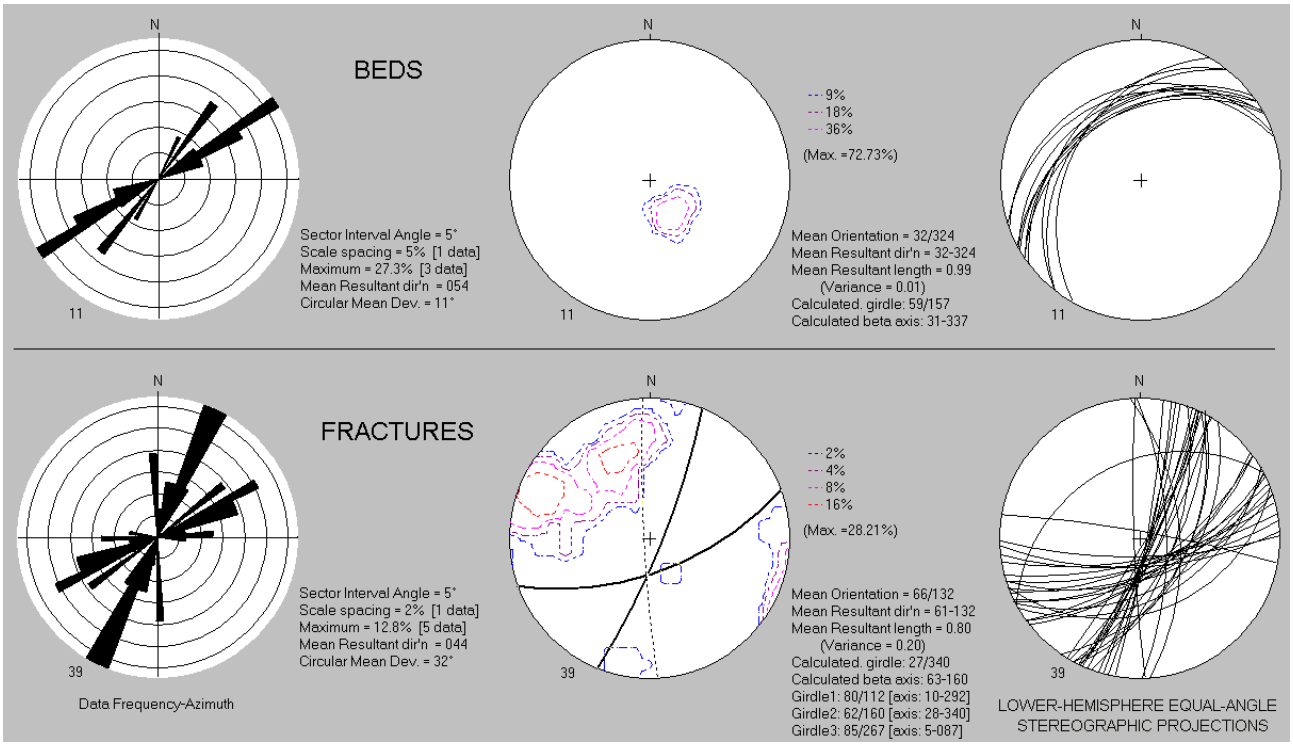

Wells 73 and 74 - Brunswick middle red and middle gray zones

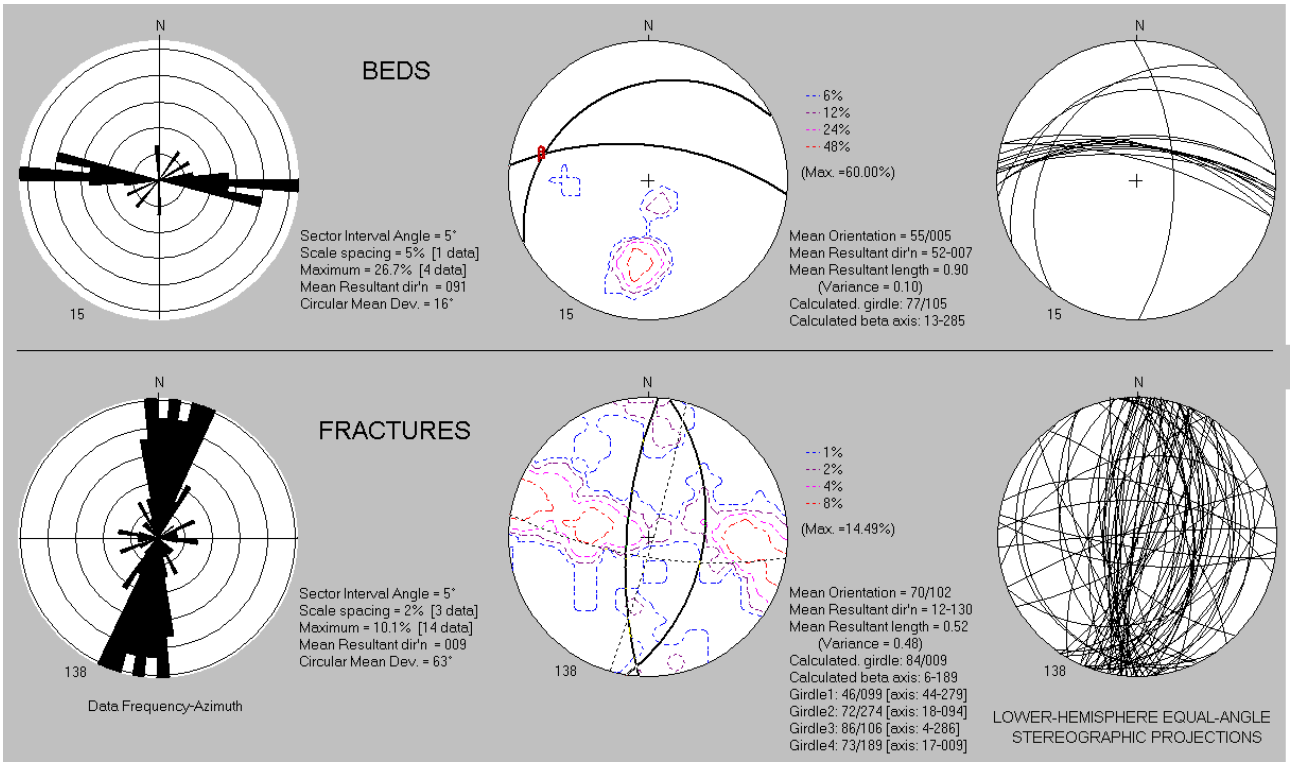

FIGURE 3G2. Structural analyses of beds and fractures measured in OPTV records for wells 71 and 72 (above) and wells 73 and 74 (below).

Wells 68 to 70 - Brunswick middle red and middle gray zones

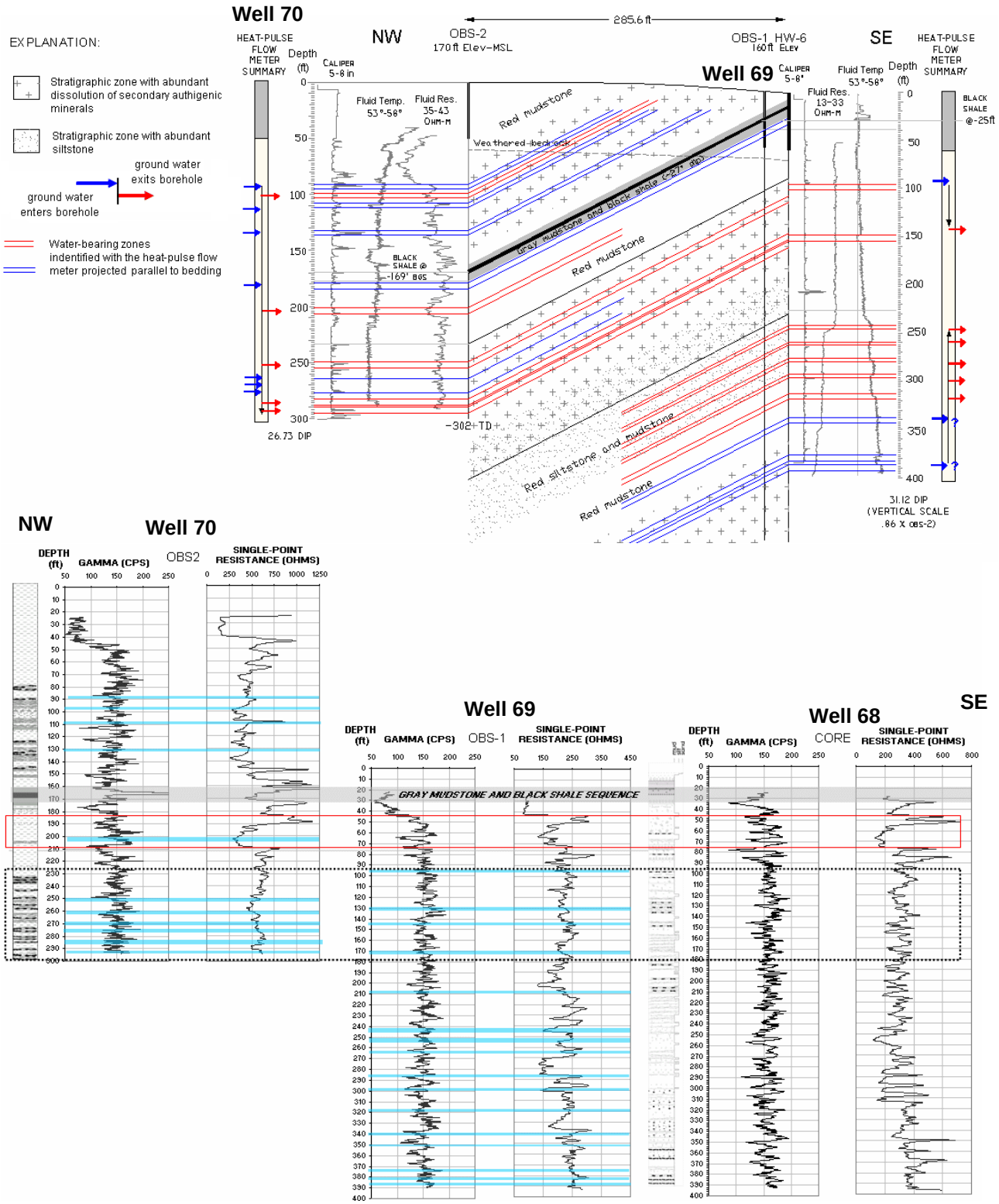

FIGURE 3G3. Hydrogeologic section (above) based on geophysical logs for wells 68 through 70 near Hopewell Borough supply well HW-6, Mercer County, NJ. Note the two directions of cross flow in well 68 under non-pumping conditions. Section below shows a stratigraphic correlation of wells 68 through 70 based on natural gamma-ray and single-point resistance logs. Depths are in feet below land surface.

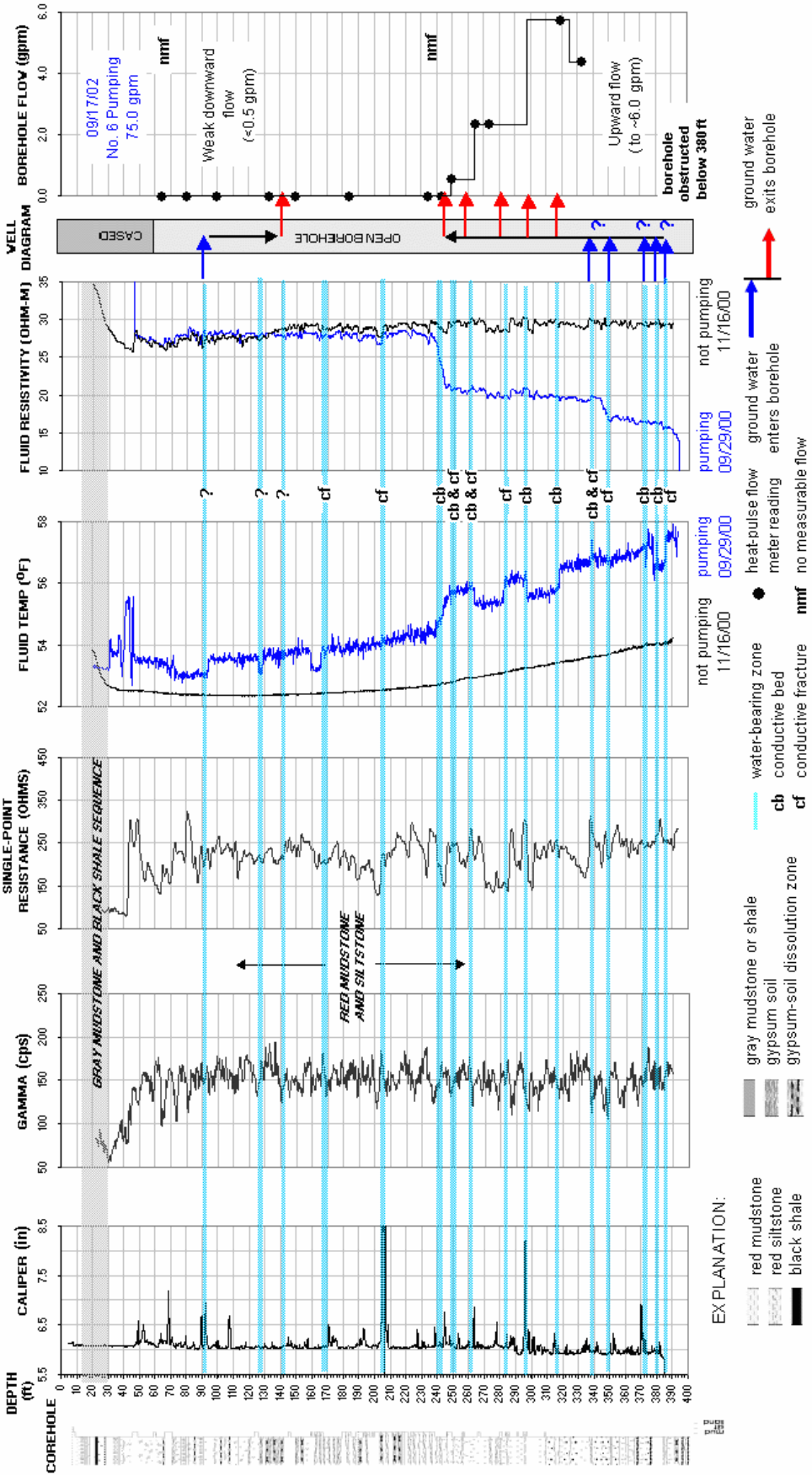

FIGURE 3G4. Hydrogeologic section based on geophysical logs for well 69, Hopewell Borough, Mercer County, NJ. County, NJ. The section shows the vertical distribution and types of hydraulically-conductive features and water-bearing zones in red and gray mudstone and siltstone with gray and black shale. Depths are in feet below land surface.

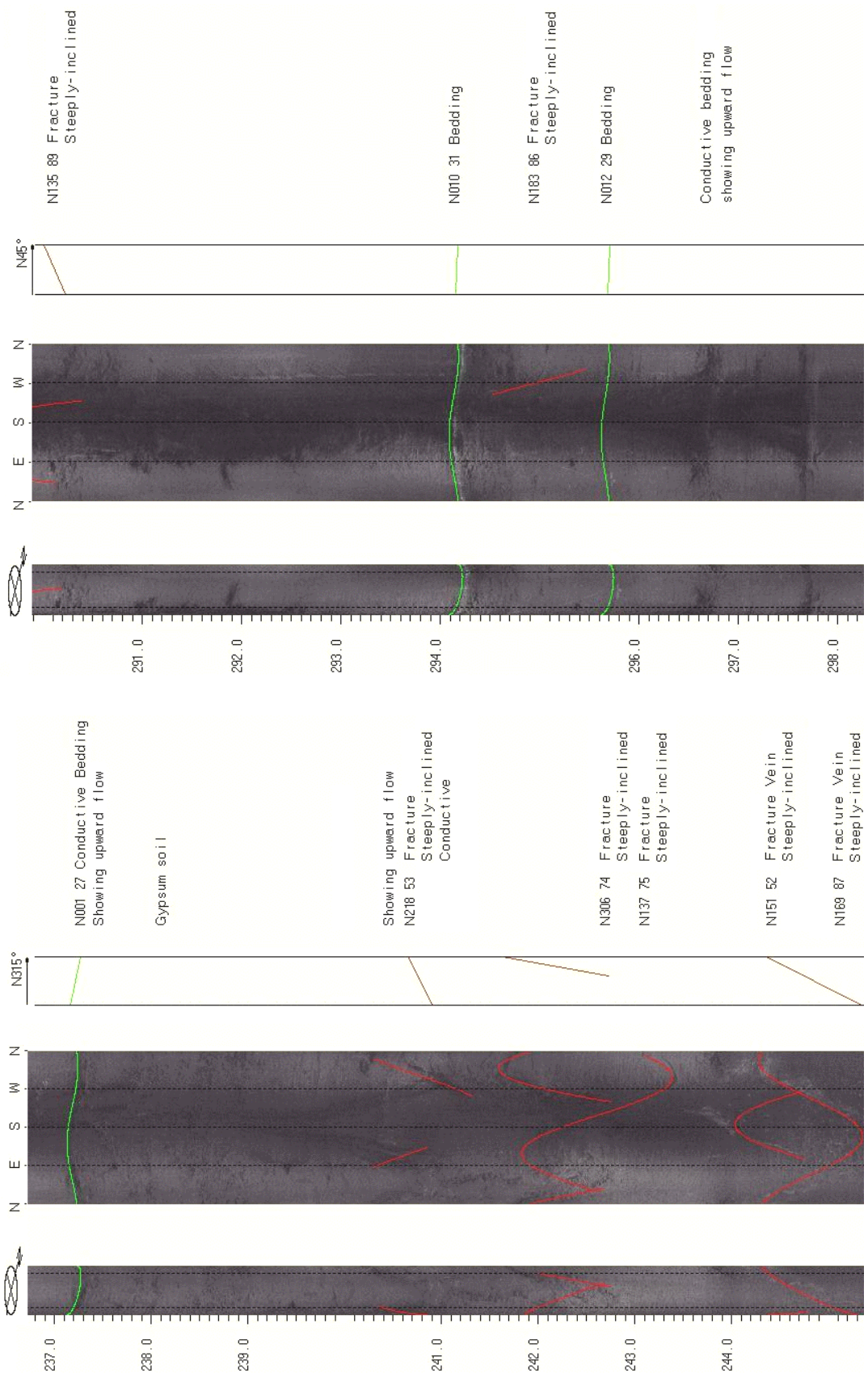

FIGURE 3G5. OPTV records of 6-inch diameter well 69 showing geologic structures and conductive features in red mudstone with gypsum soils. Mineral deposits seen as dark stains on the borehole wall emanate from conductive features and taper upward in the direction of natural cross flow. Depth values are in feet below land surface.

Well 70 - Brunswick middle red and middle gray zones

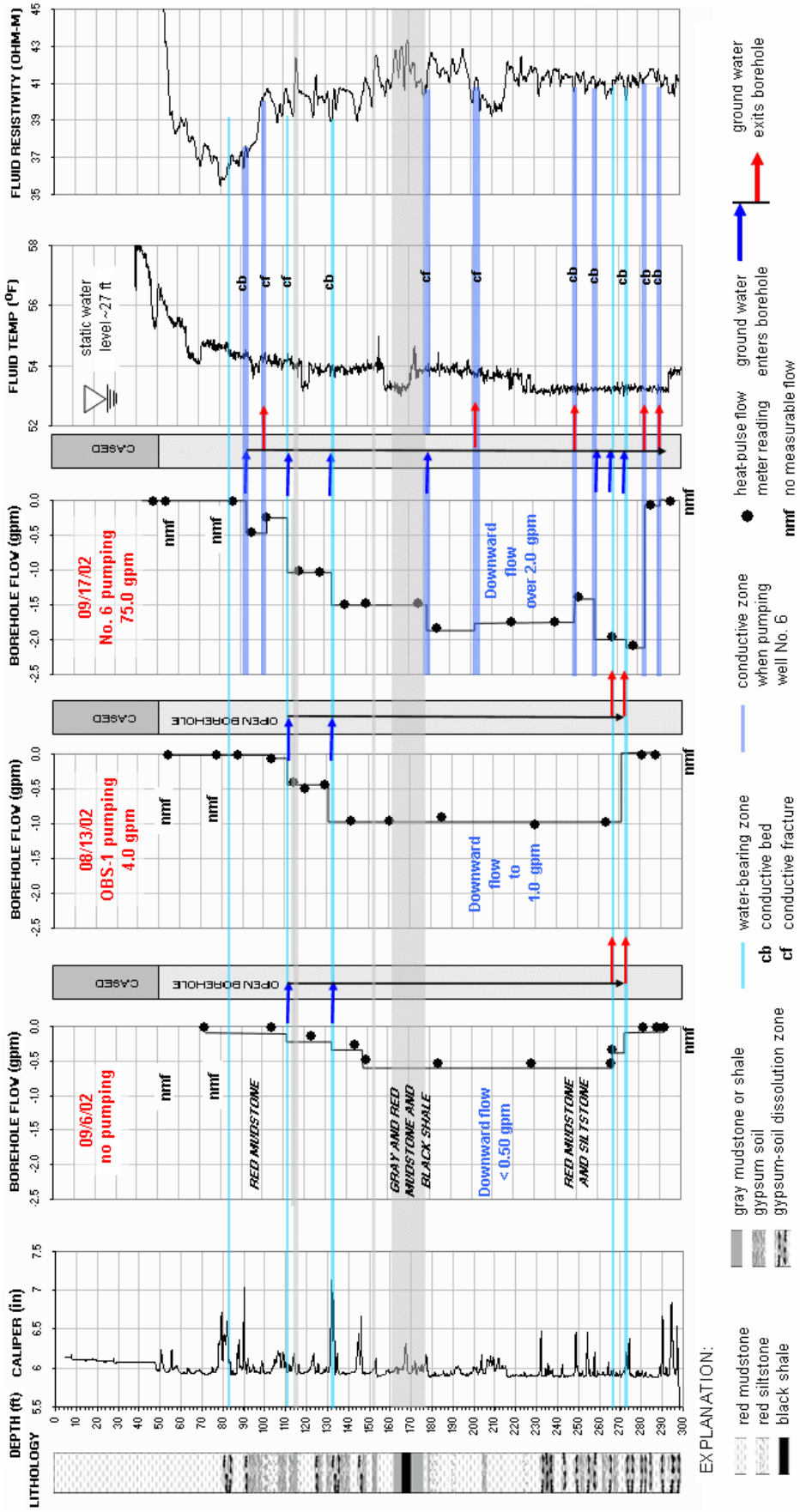

FIGURE 3G6. Hydrogeologic section based on geophysical logs for Well 70. A comparison of heat-pulse flow meter logs collected under pumping and non-pumping conditions shows that water-bearing zones have variable flow rates under variable-pumping conditions. Depth values are in feet below land surface.

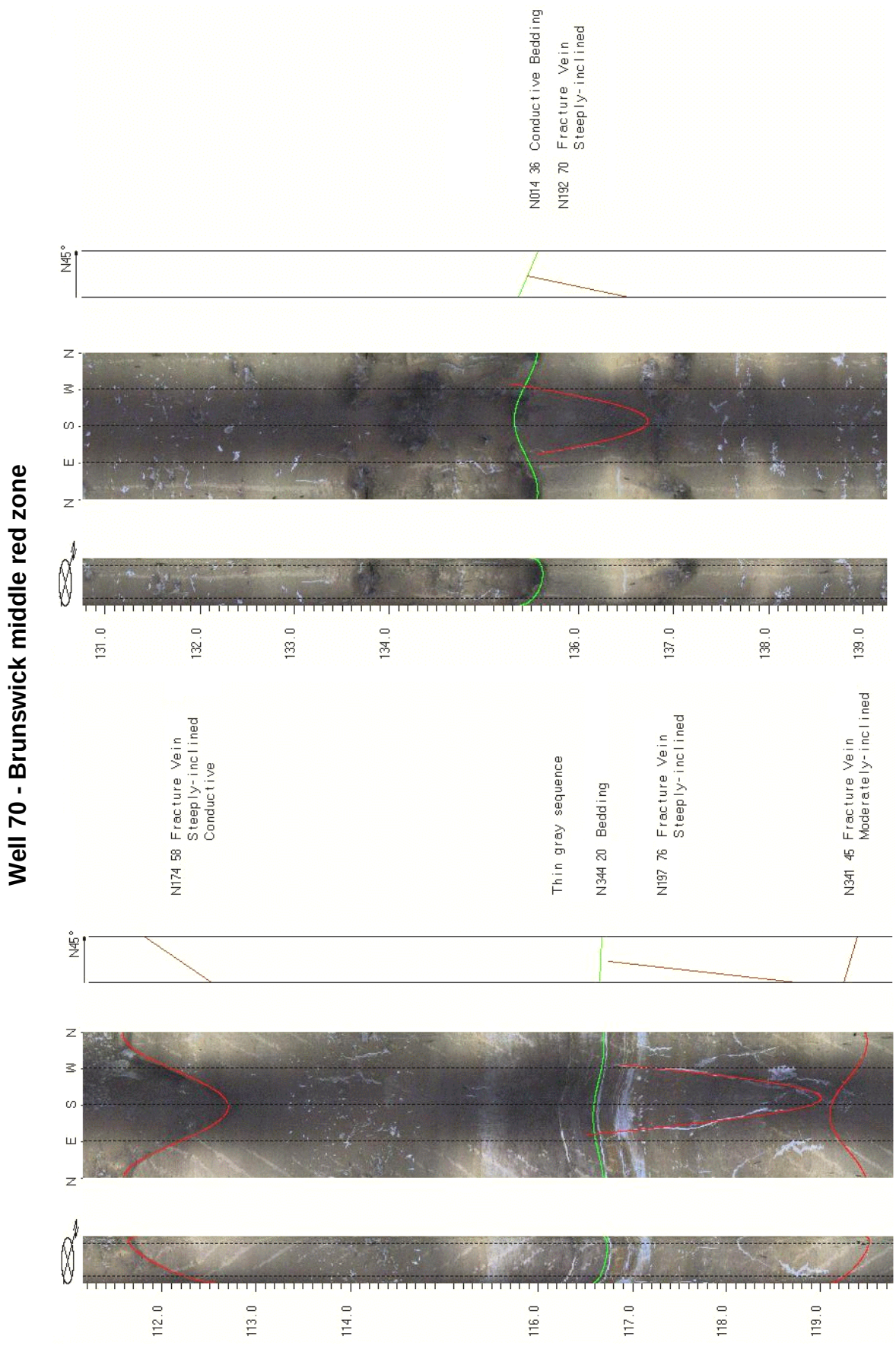

FIGURE 3G7. OPTV records of 6-inch diameter well 70 showing geologic structures and conductive features in red mudstone with gypsum soils and gray shale. Depth values are in feet below land surface.

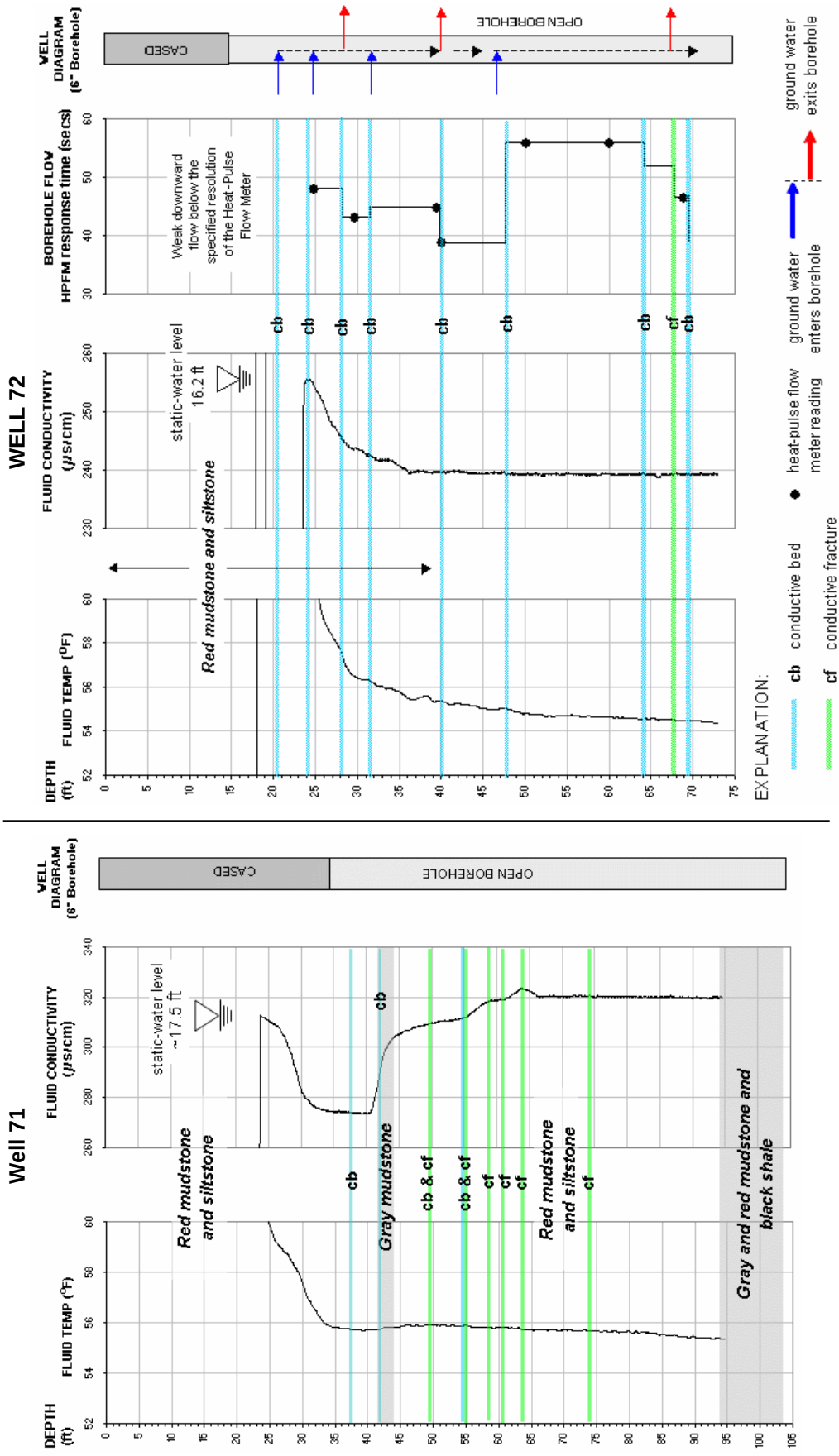

FIGURE 3G8. Hydrogeologic sections based on geophysical logs for wells 71(left) and 72 (right). The sections show the vertical distribution and types of hydraulically-conductive features and water-bearing zones in red and gray mudstone and siltstone with gray and black shale. Depth values are in feet below land surface.

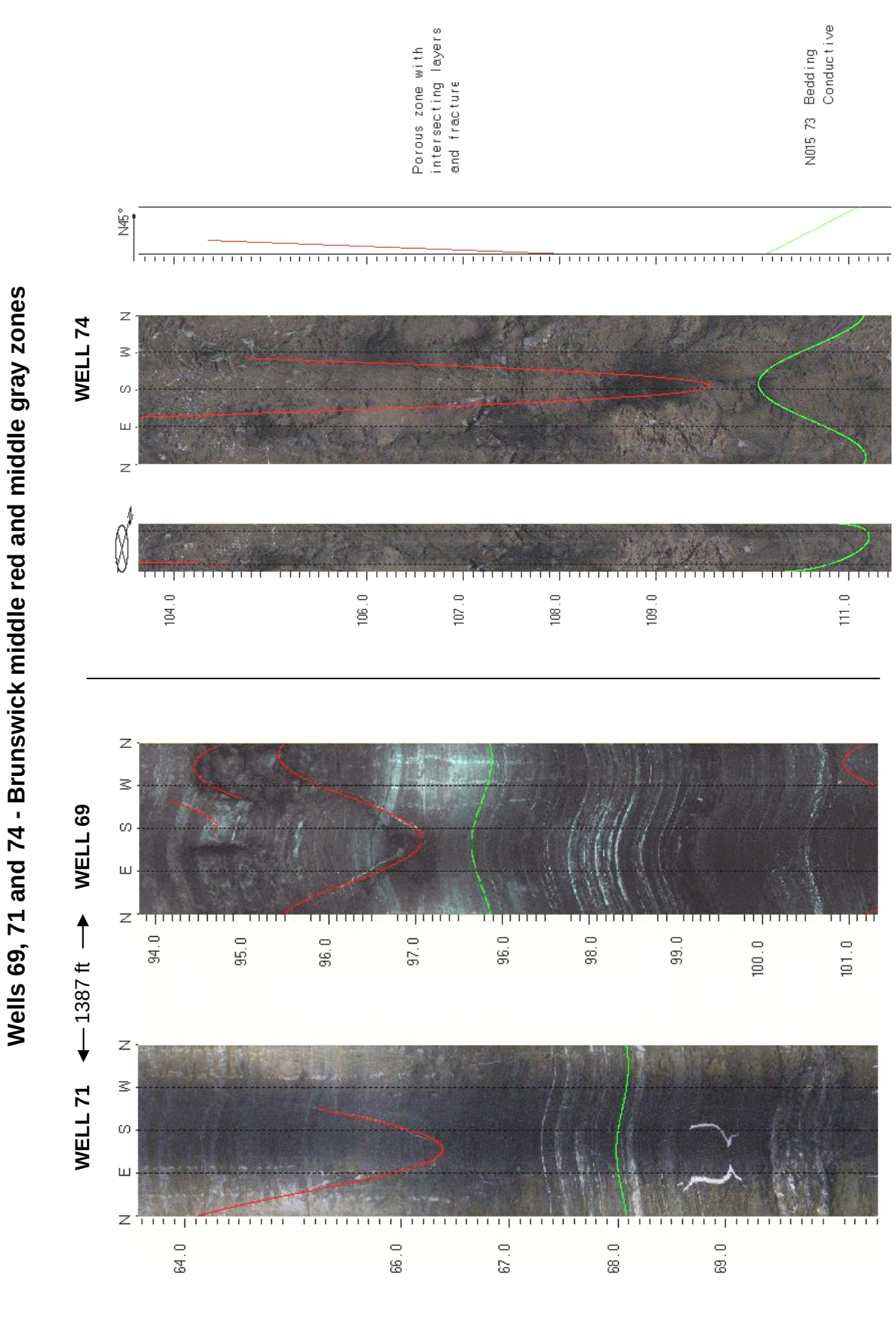

FIGURE 3G9. OPTV records for wells 69 and 71 (left) and well 74 (right). Left records show a stratigraphic correlation of gray- and black shale beds The right record shows a thick, conductive interval formed by the intersections of steeply-dipping fractures and moderately-dipping beds. Depth values are in feet below land surface.

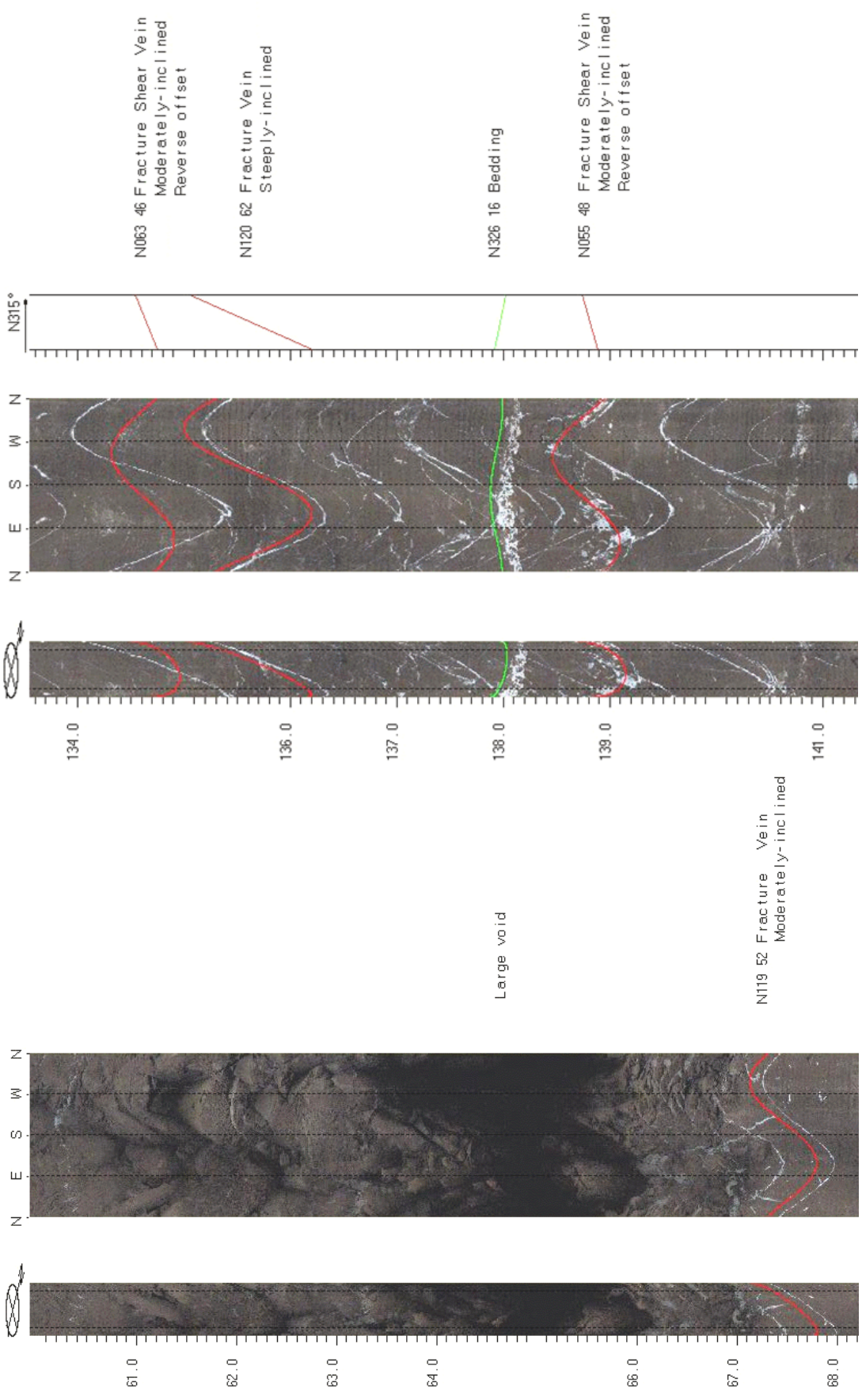

FIGURE 3G10. OPTV records for well 73 showing a large, bed-parallel void in red mudstone (left) and moderately dipping reverse-shear veins cutting steeply-dipping extension fractures in red mudstone (right). Depth values are in feet below land surface.

Well 75 - Brunswick middle gray zone

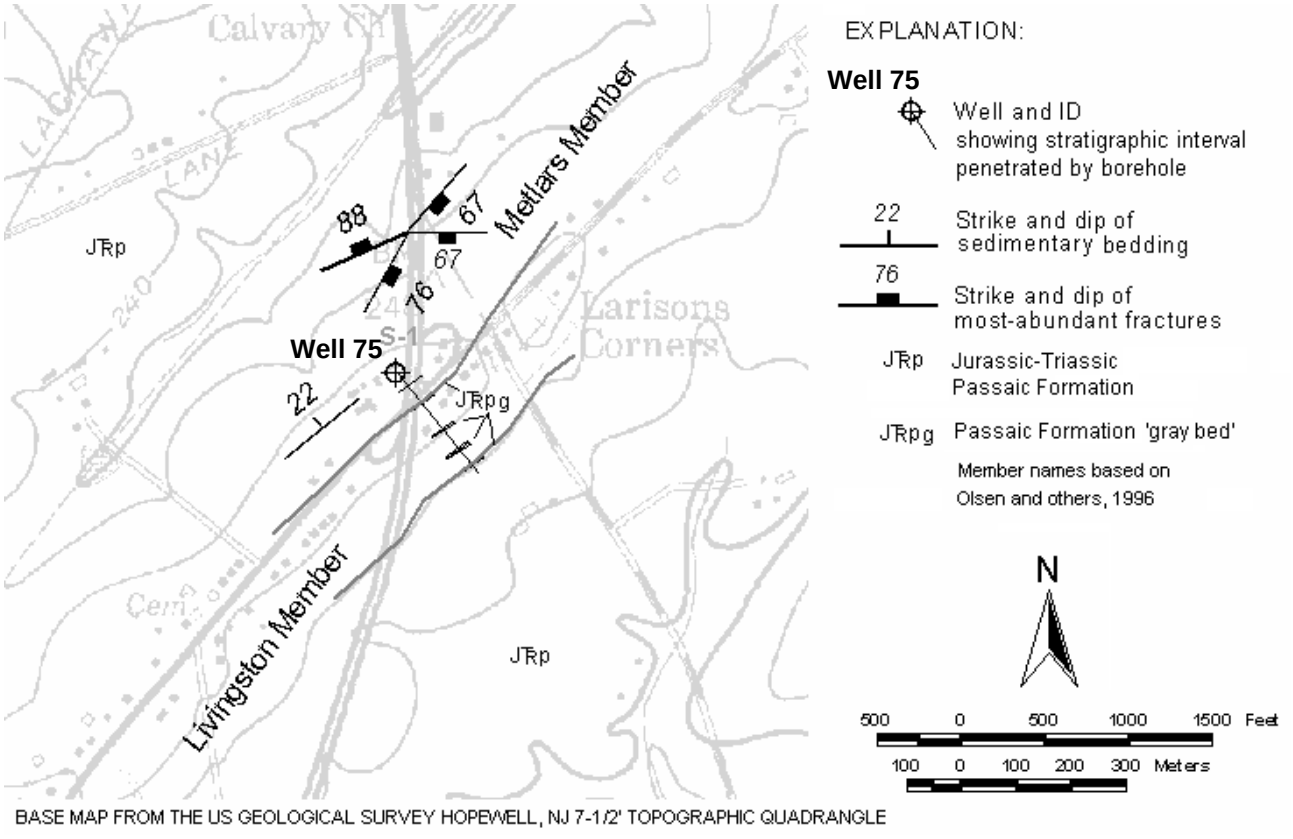

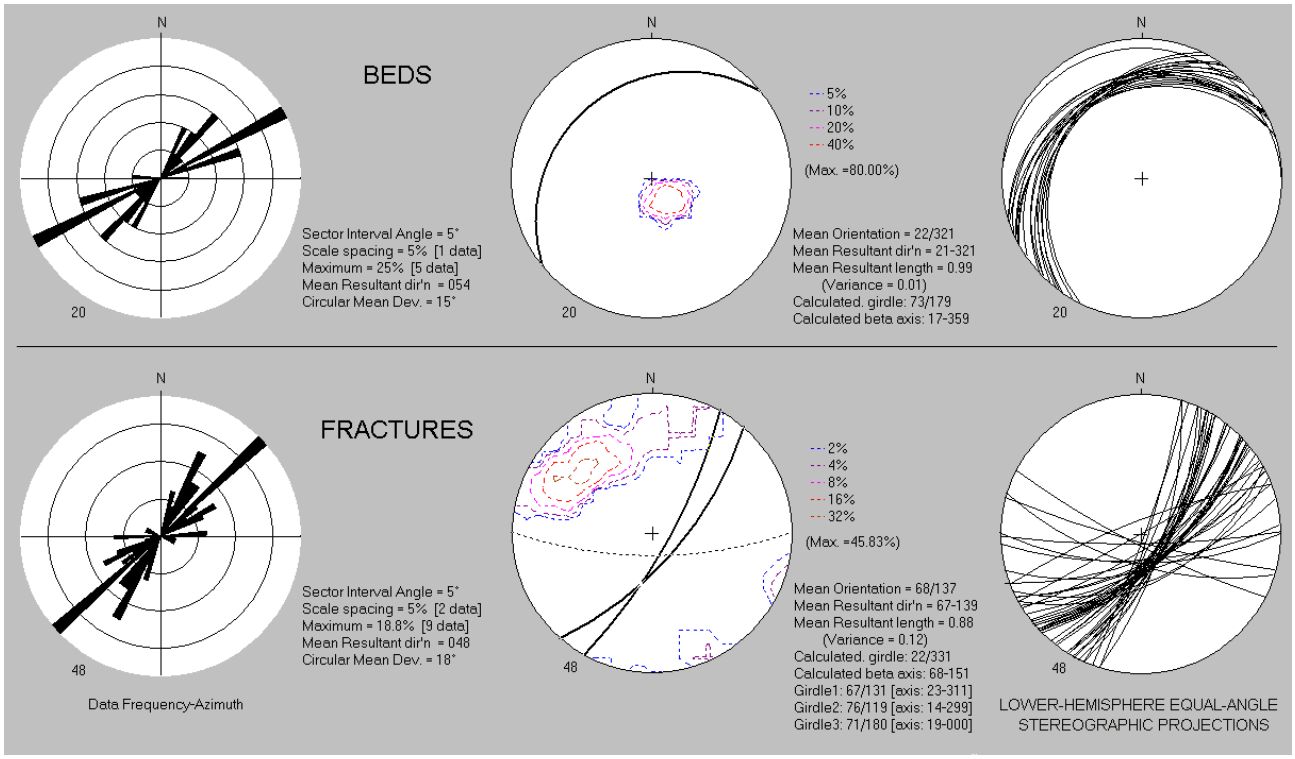

Figure 3H1. Map (above) shows well 75 at Larison's Corner, Rt. 202/31 N, East Amwell Twp., Hunterdon County, NJ. Mapped bedrock structures are based on a structural analysis of beds and fractures (bottom) measured in OPTV records.

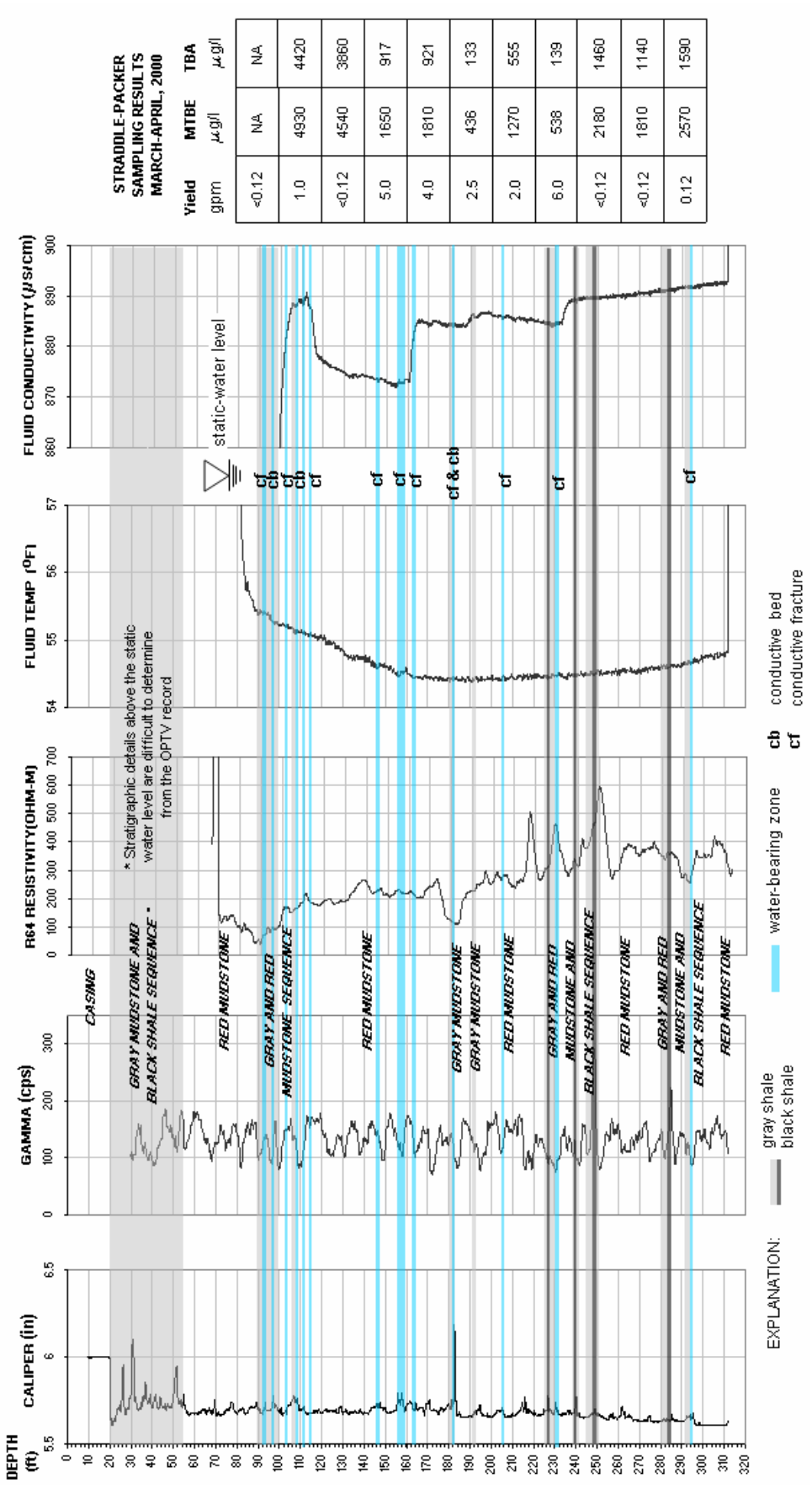

Yield gpm	MTBE µg/l	TBA µg/l
<0.12	NA	NA
1.0	4930	4420
<0.12	4540	3860
5.0	1650	917
4.0	1810	921
2.5	436	133
2.0	1270	555
6.0	538	139
<0.12	2180	1460
<0.12	1810	1140
0.12	2570	1590

FIGURE 3H2. Hydrogeologic section based on geophysical logs for well 57 at Schaffernoth Nursery, Larison's Corner, East Amwell Twp., Hunterdon County, NJ. The section shows the vertical distribution and types of hydraulically-conductive features and water-bearing zones in red and gray mudstone and gray and black shale. The straddle-packer results are part of a NJDEP BTEX investigation. Depth values are in feet below land surface. MTBE - Methyl tert-butyl ether, TBA - Tertiary butyl alcohol.

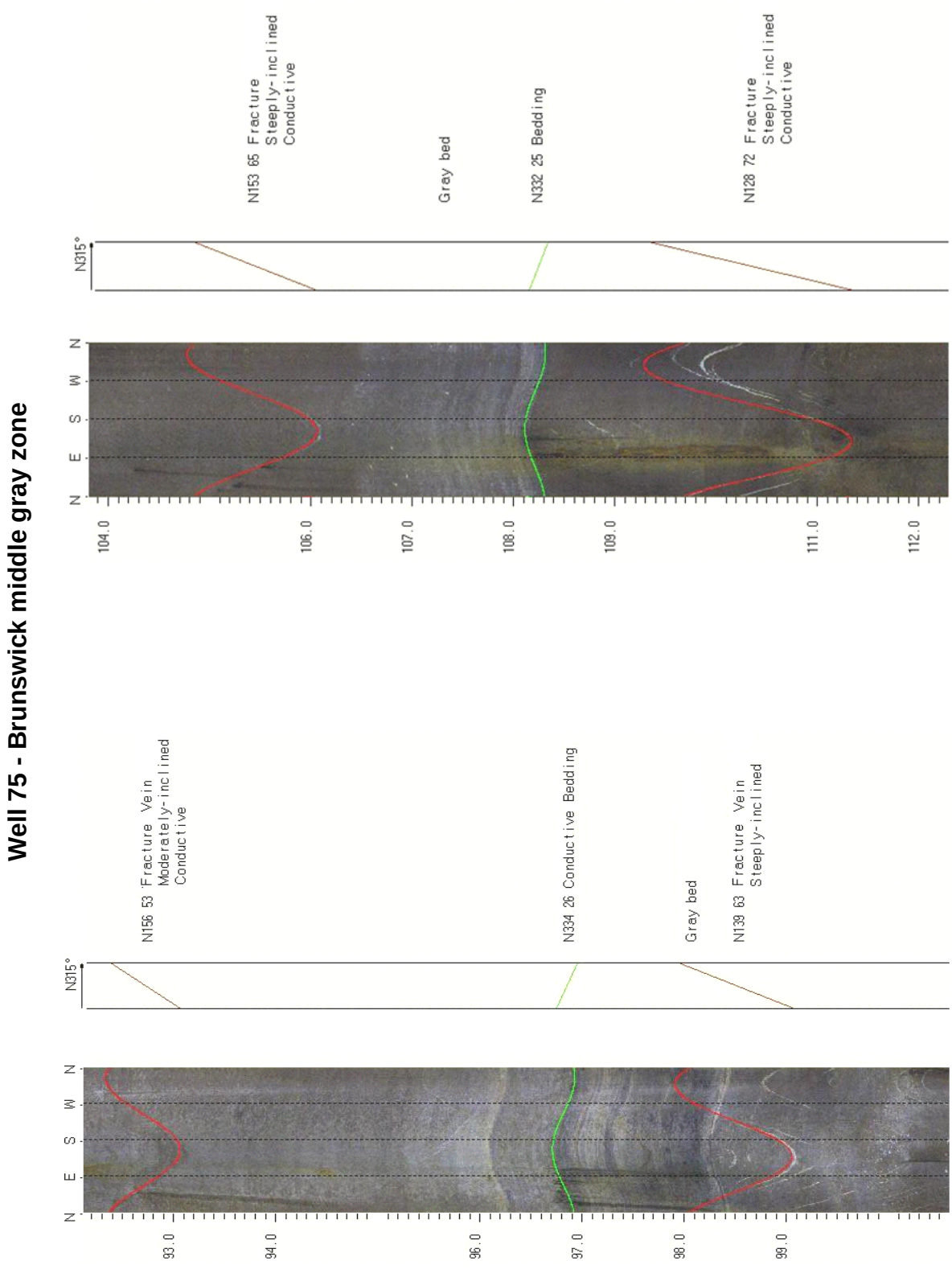

FIGURE 3H3. OPTV records of the 6-inch diameter well 75 showing geologic structures and conductive features in gray and black shale and red mudstone. Depth values are in feet below land surface.

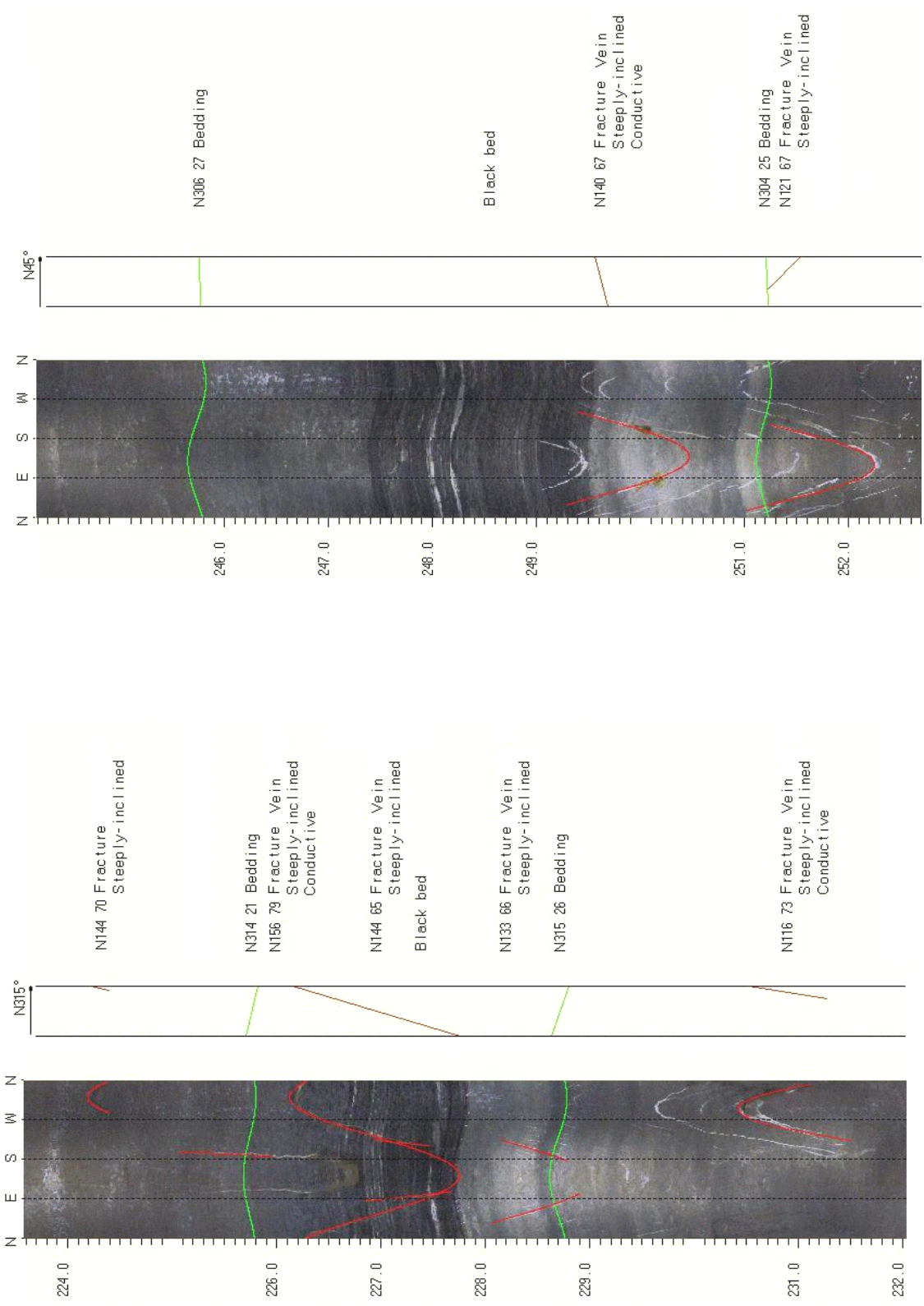

FIGURE 3H4. OPTV records of the 6-inch diameter well 75 showing geologic structures and conductive features in gray and black shale and red mudstone. Depth values are in feet below land surface.

Wells 76 to 78 - Brunswick middle gray zone

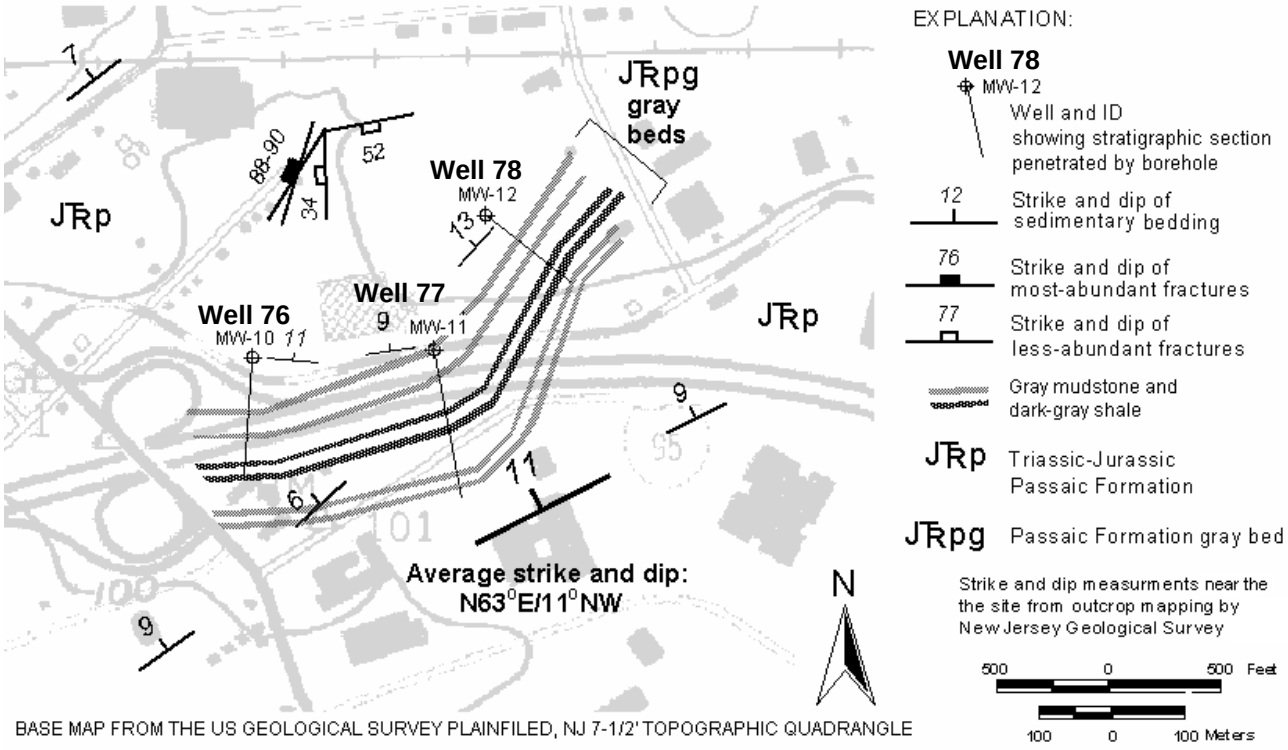

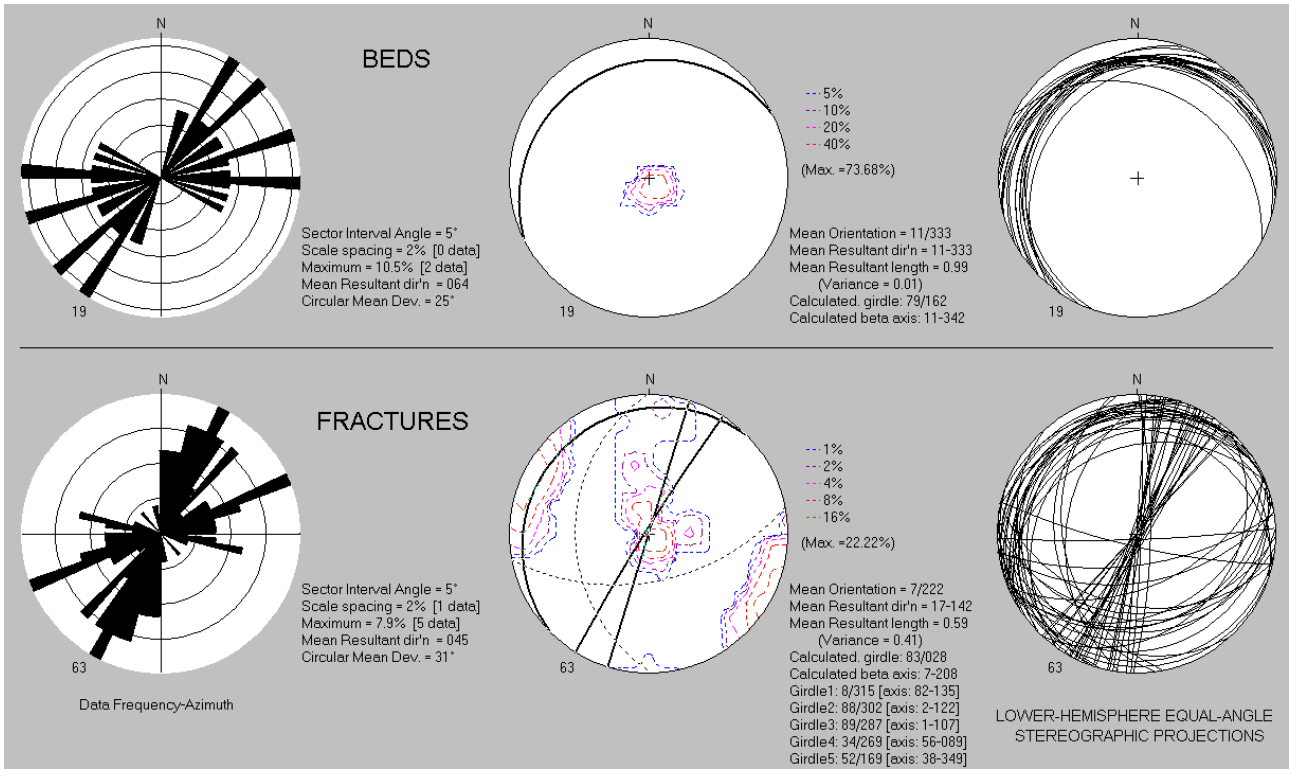

Figure 3I1. Map (above) shows wells 76 to 78 at the Home Depot, South Plainfield Boro, Middlesex County, NJ. Bedding and fractures mapped near the wells are based on a structural analysis (below) of the OPTV records for three monitoring wells.

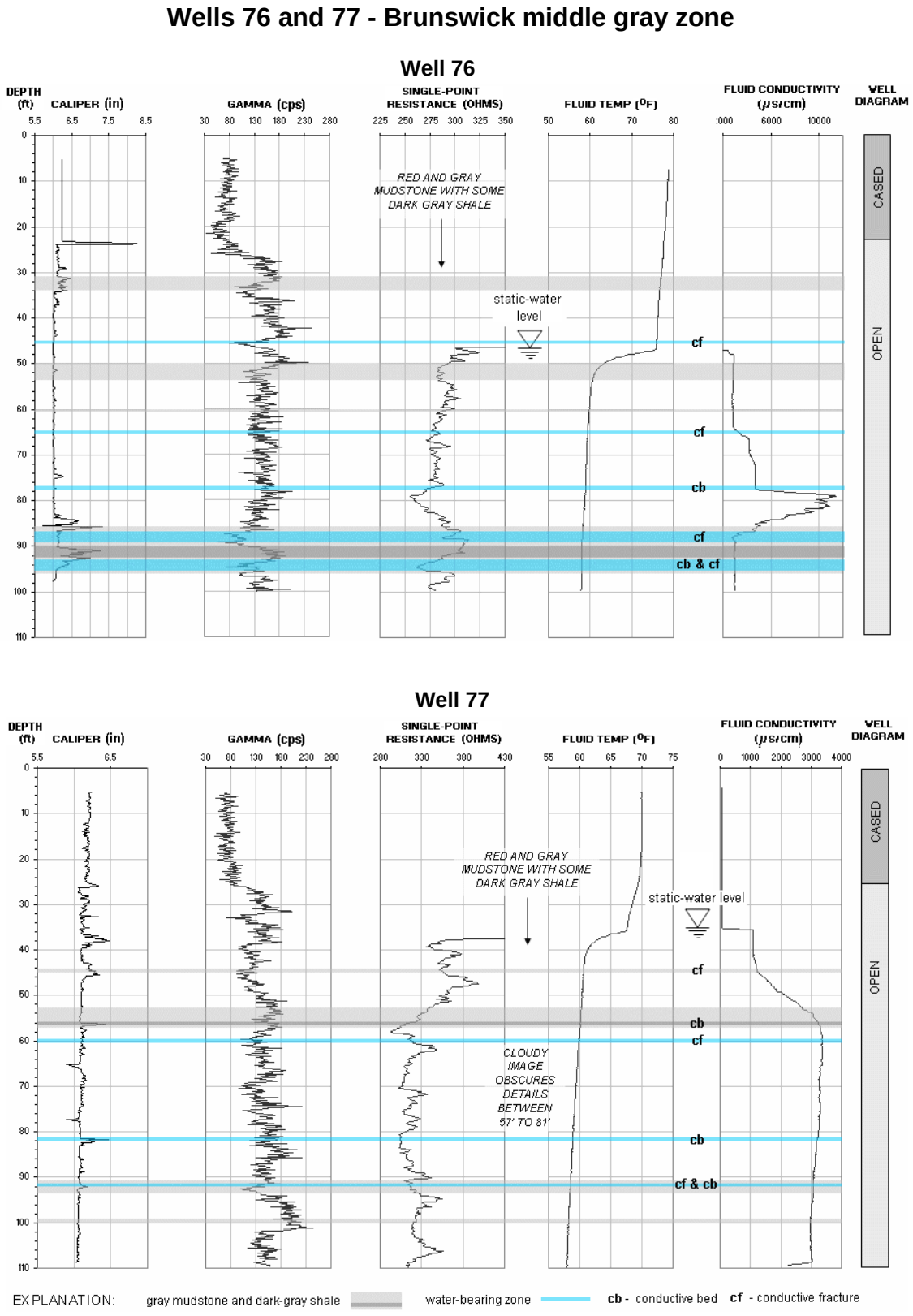

Figure 3I2. Hydrogeologic sections based on geophysical logs for wells 76 and 77 at the Home Depot, South Plainfield Boro, Middlesex County, NJ. The sections show the vertical distribution and types of hydraulically-conductive features and water-bearing zones in red, gray and black mudstone and shale. Depth values are in feet below land surface.

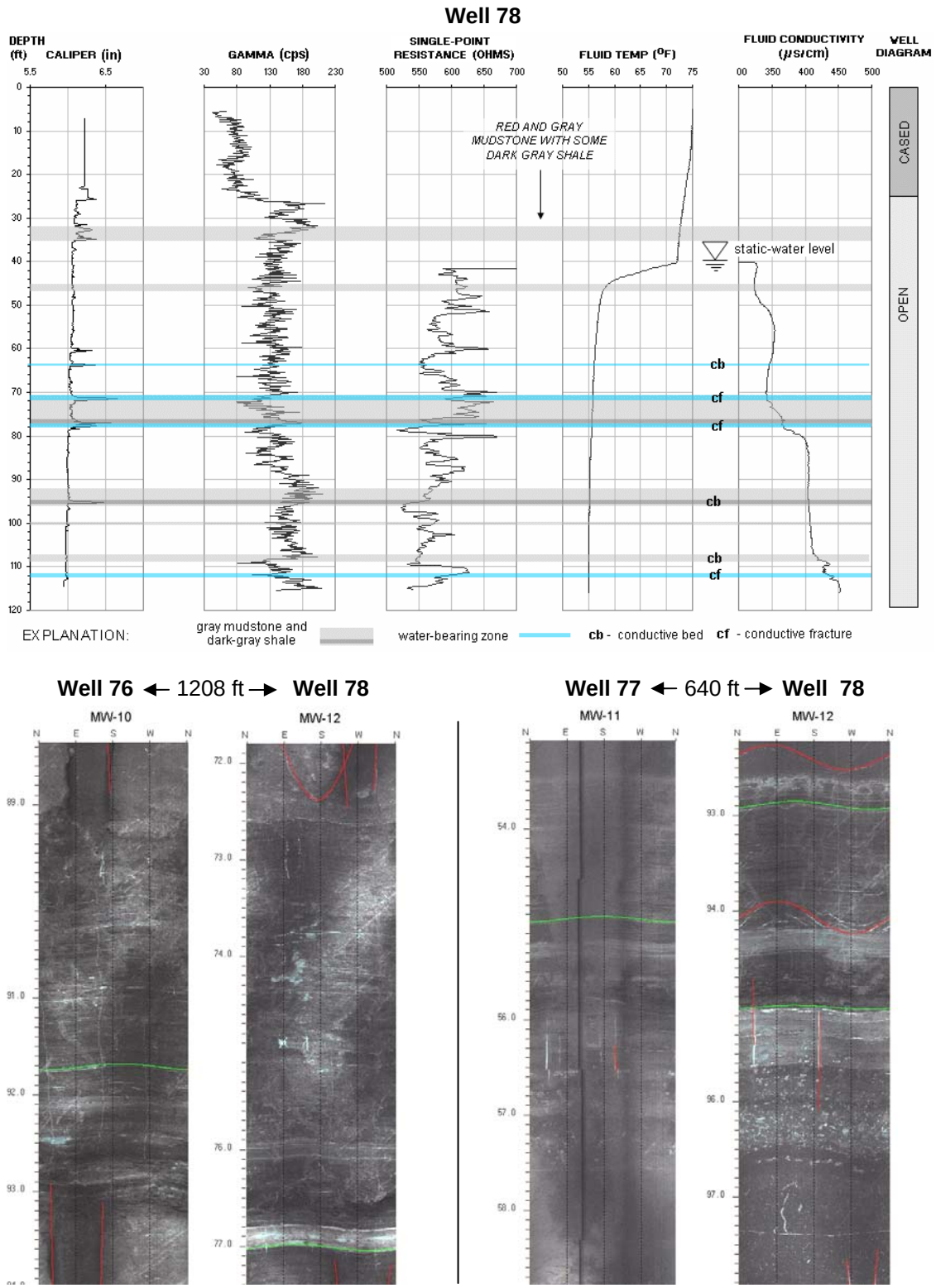

Figure 3I3. Hydrogeologic section (above) based on geophysical logs for well 78 at the Home Depot, South Plainfield Boro, Middlesex County, NJ. The section shows the vertical distribution and types of hydraulically-conductive features and water-bearing zones in red and gray mudstone and gray shale. Stratigraphic correlations (below) are based on OPTV records for wells 76 to 78. Depth values are in feet below land surface.

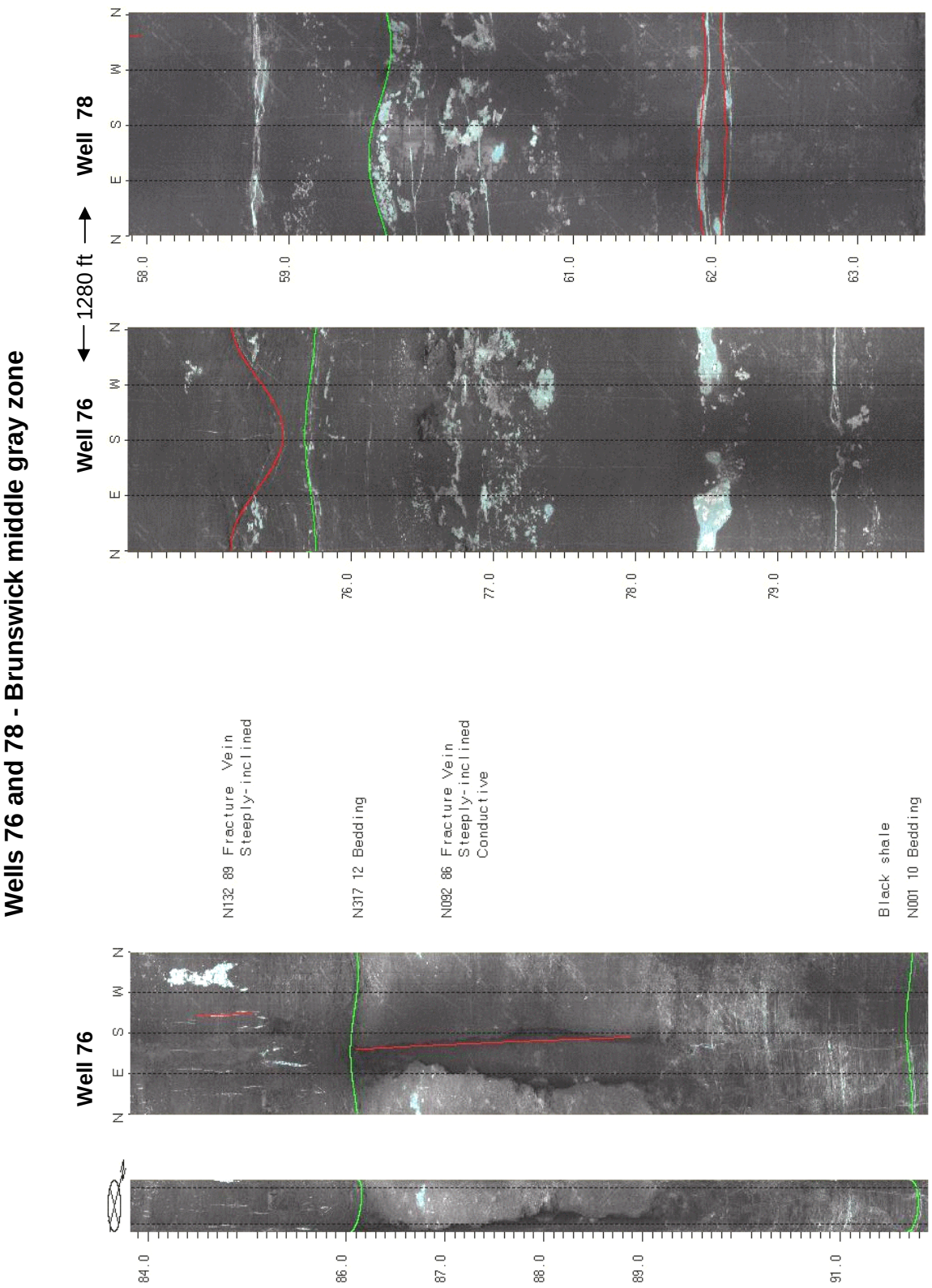

FIGURE 314. OPTV record of 6-inch diameter well 76 (left) showing geologic structures and conductive features in red and gray mudstone and gray shale. A stratigraphic correlation of wells 76 and 78 is shown at right. Depth values are in feet below land surface.

Wells 79 to 84 - Brunswick middle gray zone

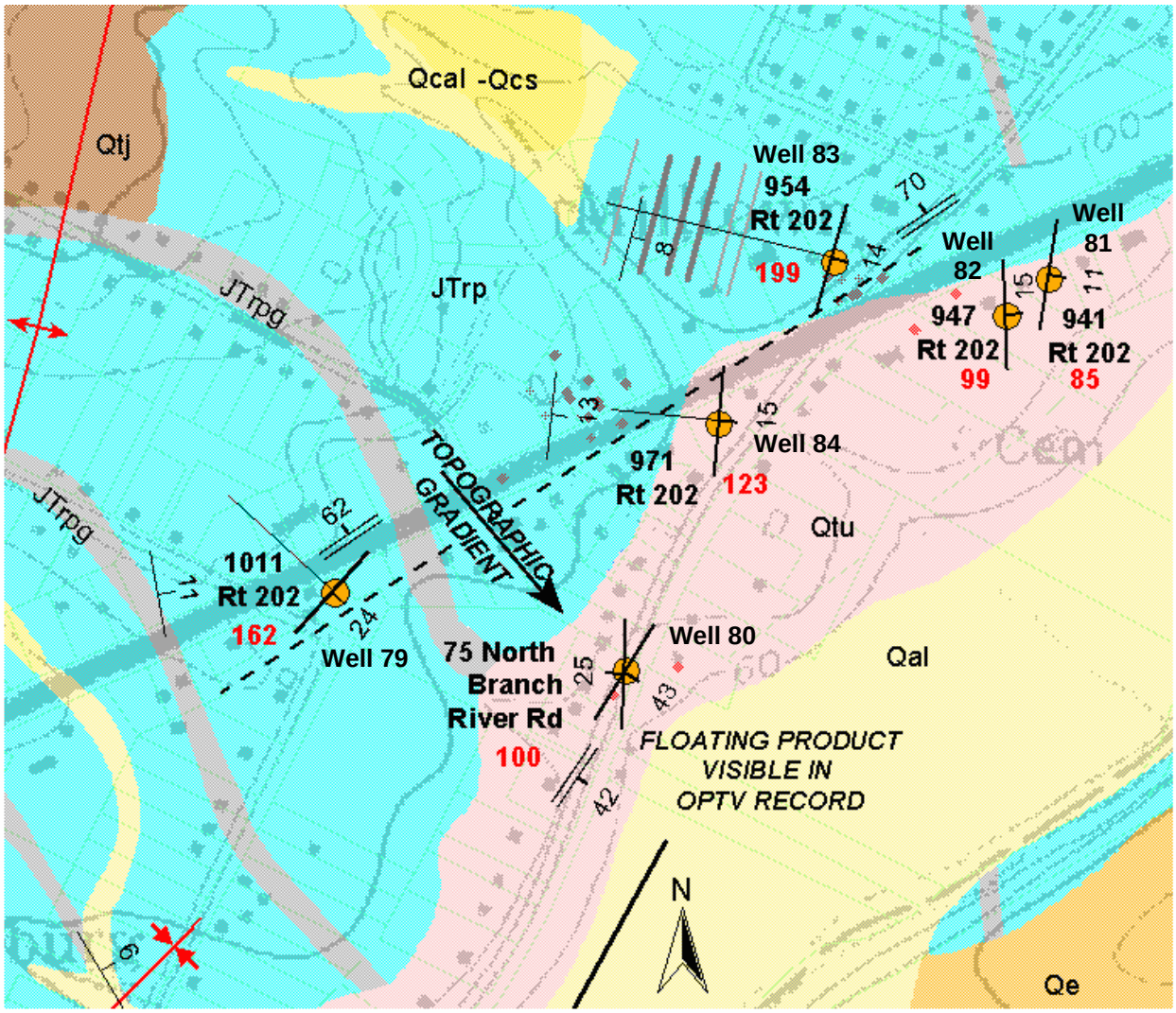

BASE MAP FROM THE US GEOLOGICAL SURVEY RARITAN, NJ 7-1/2' TOPOGRAPHIC QUADRANGLE

EXPLANATION:

Well 83 — Well with optical televiewer survey by the NJGS. Line trace shows the map distance of inclined strata that the well intercepts. Address and depth noted for each well. Projected map trace of gray and black shale beds intercepted by well shown.

24 — Bedding strike and dip

42 — Small fault strike and dip

Normal fault, dashed where inferred

Axial trace of anticline

Axial trace of syncline

500 0 500 Feet

100 0 100 200 Meters

Jurassic-Triassic bedrock	JTrp	Passaic Formation
	JTrpg	Passaic Formation gray bed sequence
Quaternary sand and gravel	Qal	Alluvium
	Qcal	Colluvium and alluvium
	Qcs	Shale colluvium
	Qe	Eolian deposits
	Qtj	Till
	Qtu	Upper terrace deposits

From NJGS Geologic Map Series GMS 03-2, Geologic Map of the Raritan Quadrangle, Hunterdon and Somerset Counties, New Jersey, Monteverde, D.H., Stanford, S.D., and Volkert, R.A., 2003.

Figure 3J1. Bedrock geology map showing wells 79 to 84 along Route 202, Branchburg Twp., Somerset County, NJ.

Wells 79 to 84 - Brunswick middle gray zone

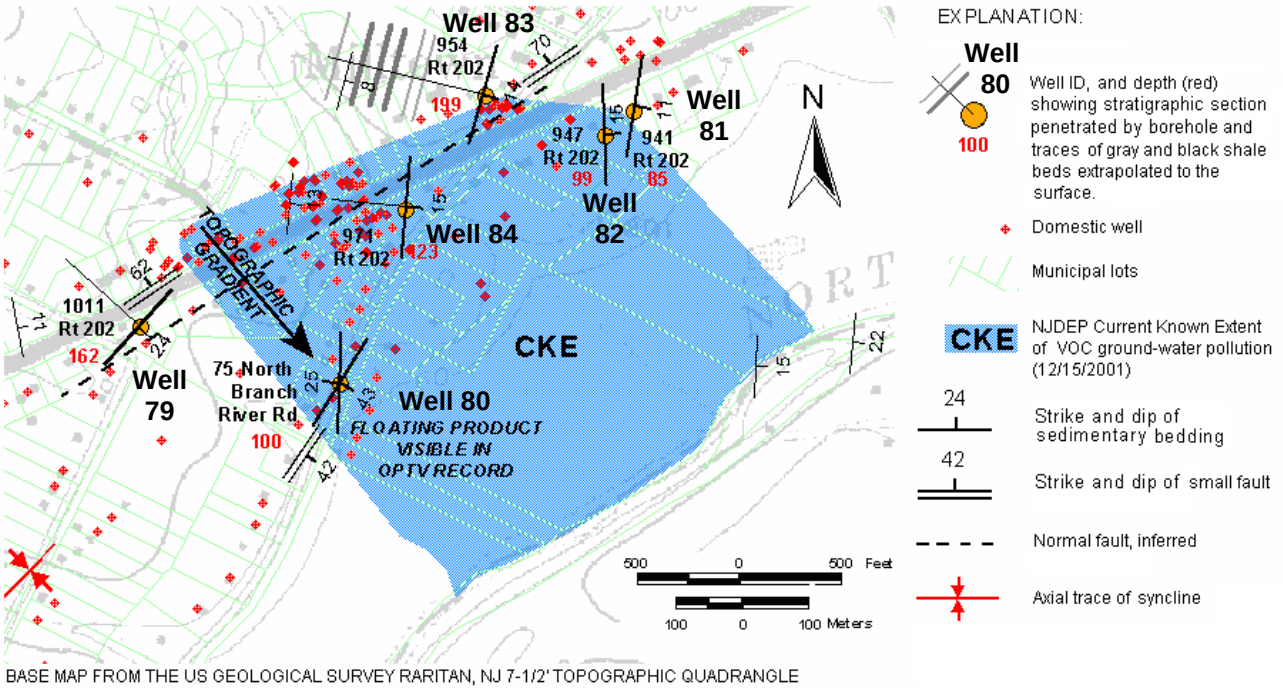

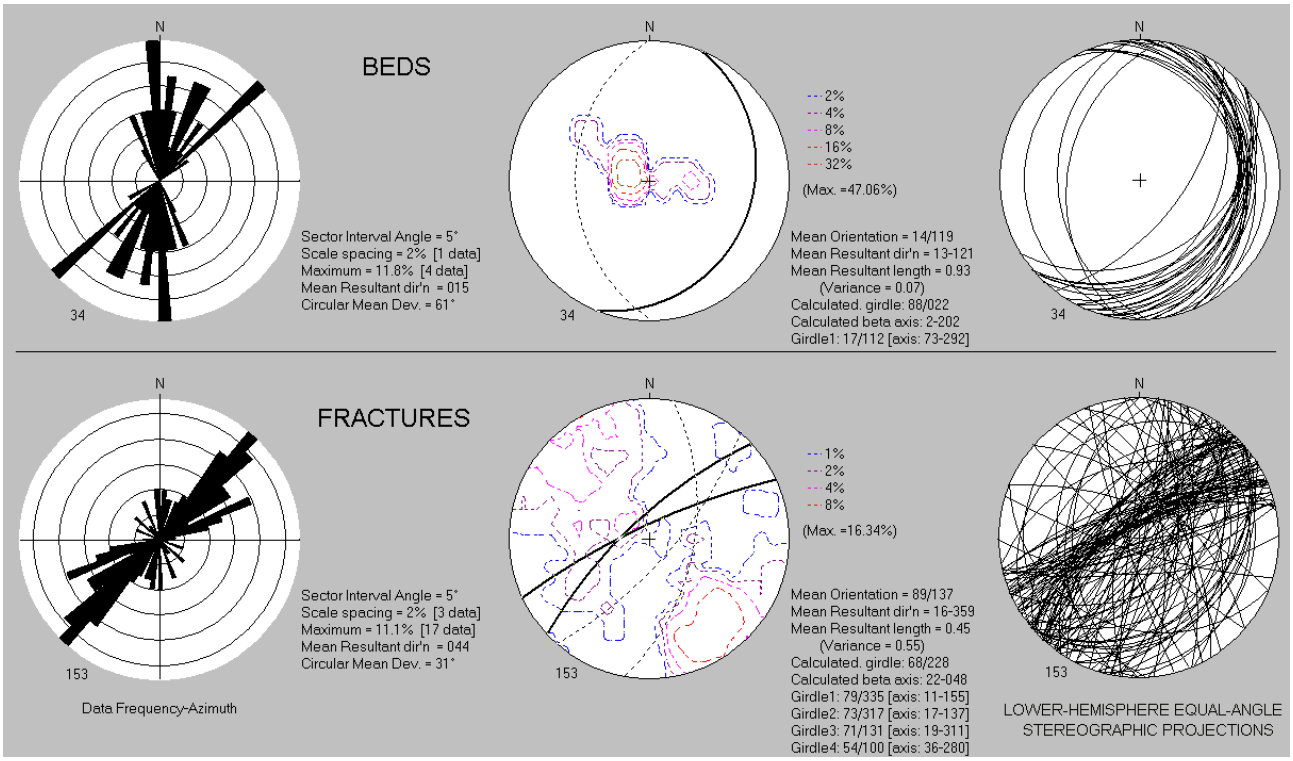

Figure 3J2. Map (above) showing the location of domestic wells and a volatile-organic-compound (VOC) plume near Route 202, Branchburg Twp., Somerset County, NJ. Structural analysis of OPTV records (below) shows bed and fracture orientations for wells 79 to 84.

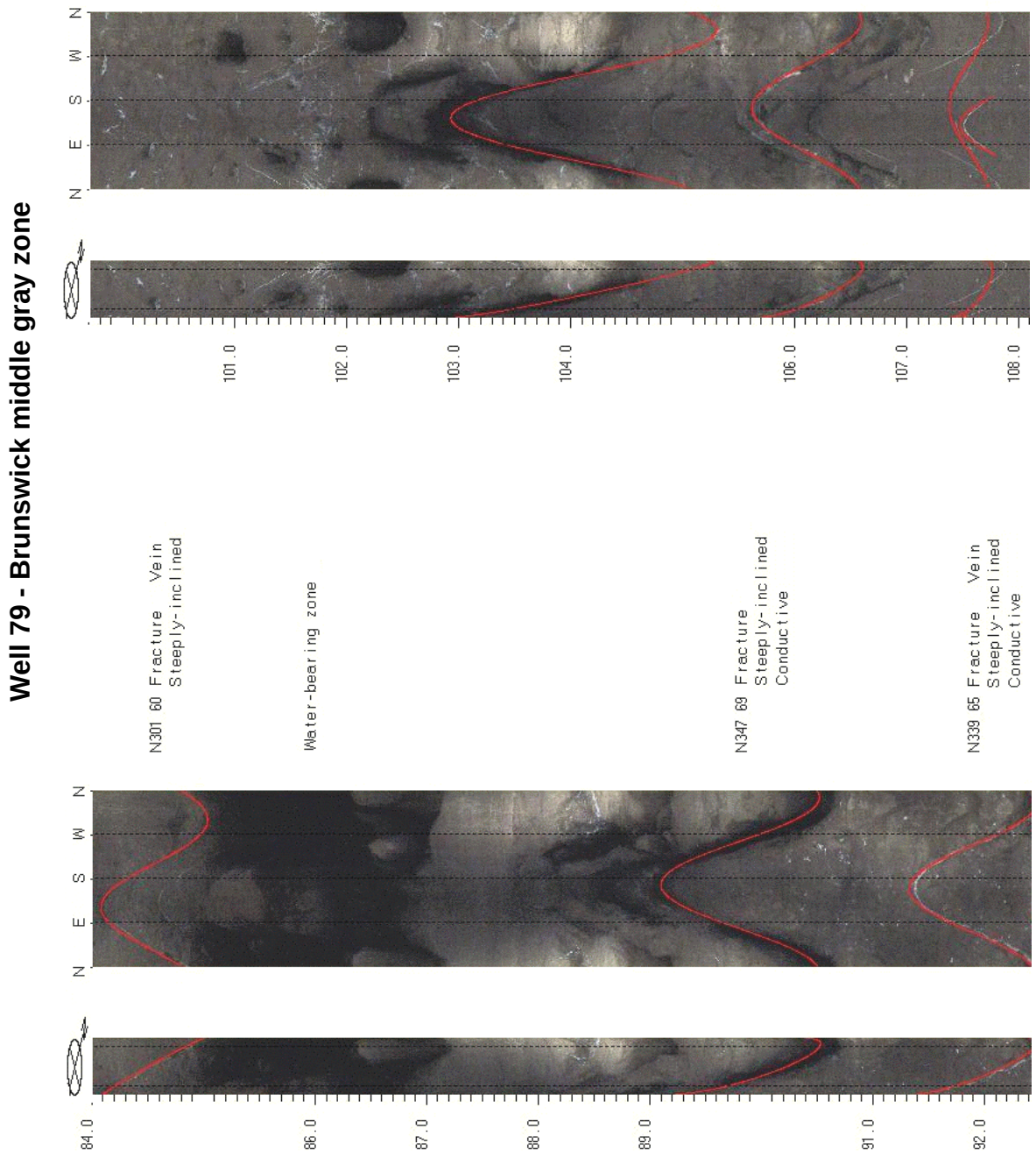

FIGURE 3J3. OPTV records of 6-inch diameter well 79 showing geologic structures and hydraulically-conductive features in red mudstone. Depth values are in feet below land surface.

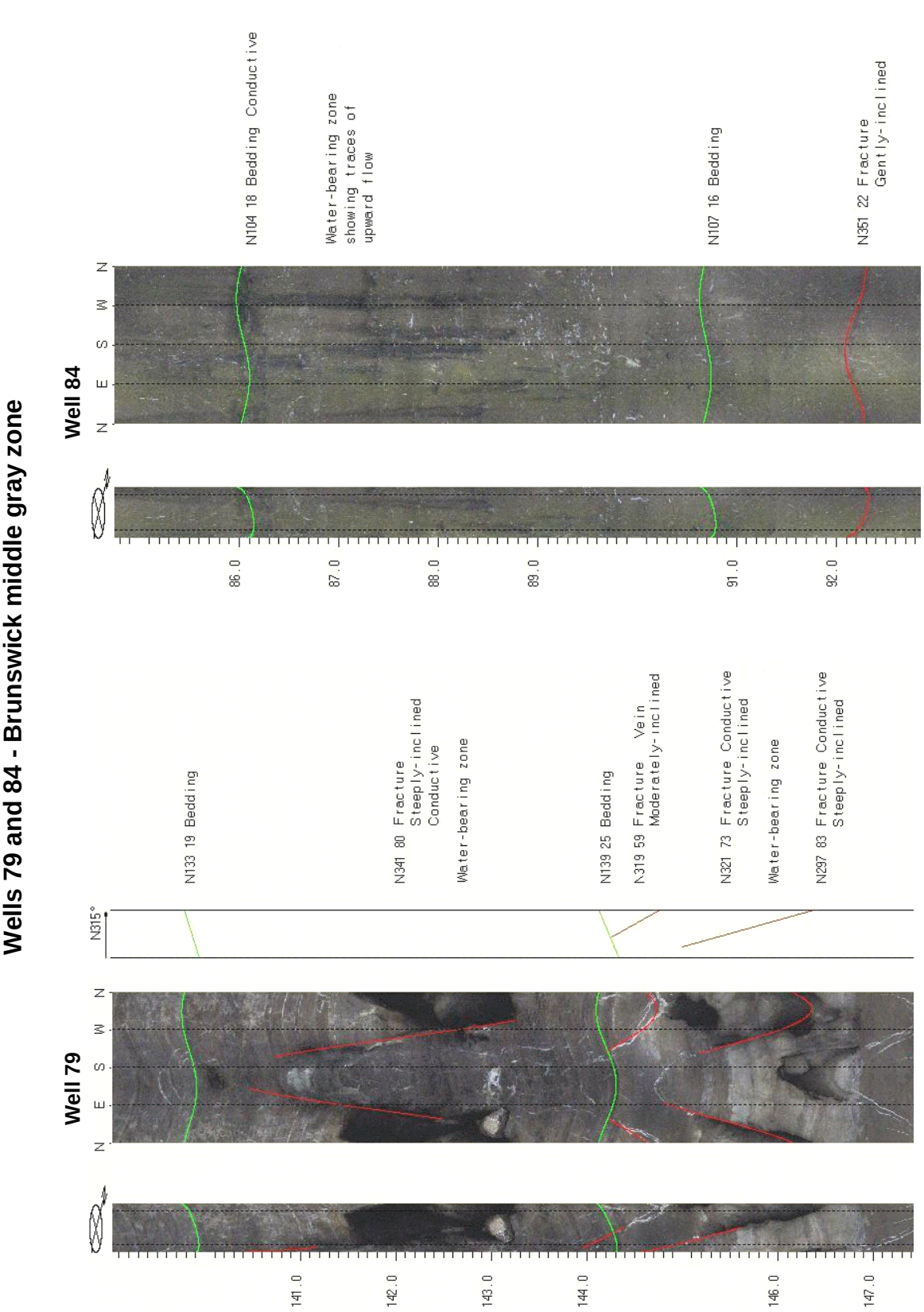

FIGURE 3J4. OPTV records of 6-inch diameter wells 79 (left) and 84 *right) showing geologic structures and hydraulically-conductive features in red mudstone and gray shale. Upward-tapering mineral stains emanating from conductive pores (right) indicate upward, non-pumping cross flow in well 84. Depth values are in feet below land surface.

Well 81 - Brunswick middle gray zone

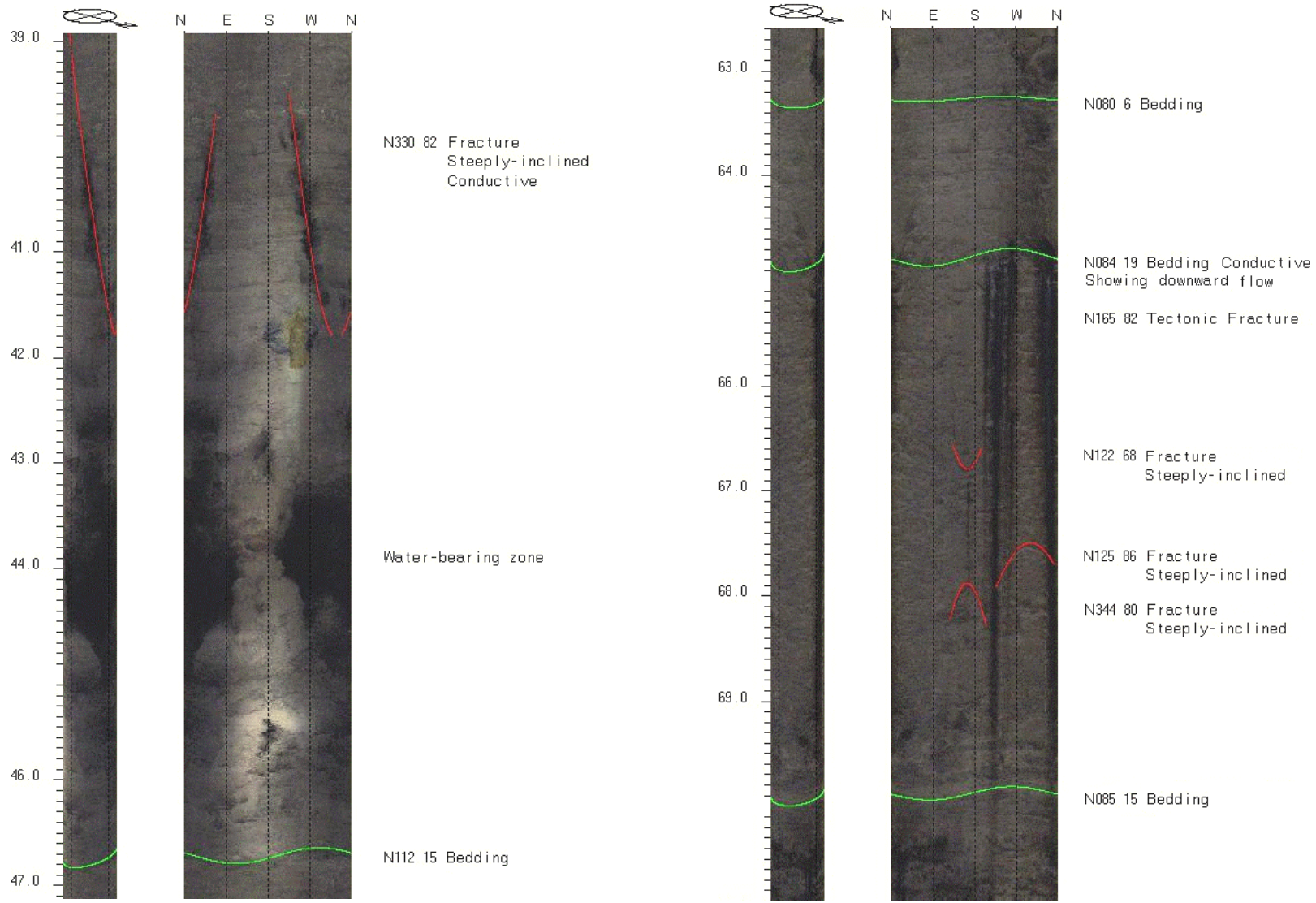

FIGURE 3J5. OPTV records of 6-inch diameter well 81showing geologic structures and hydraulically-conductive features in red and gray mudstone. Downward-tapering stains emanating from pores (right) may indicate pumping-induced flows. Depth values are in feet below land surface.

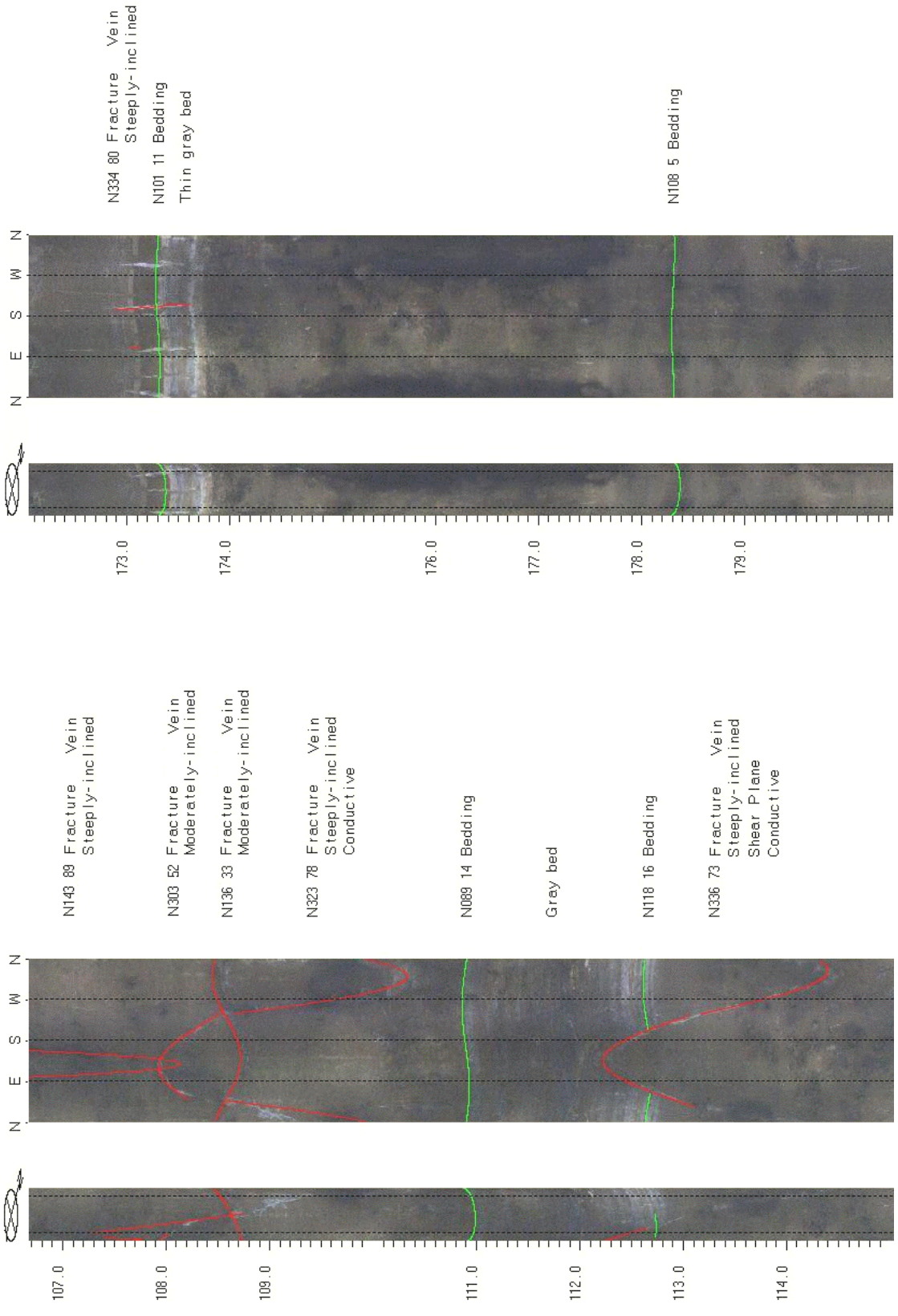

FIGURE 3J6. OPTV records of 6-inch diameter well 83 showing geologic structures and hydraulically-conductive features in red mudstone and gray shale. Note the shear plane (lower left) corresponding to the small-fault symbol mapped on figure 3J1. Depth values are in feet below land surface.

Wells 85 to 88 - Brunswick middle gray and lower red zones

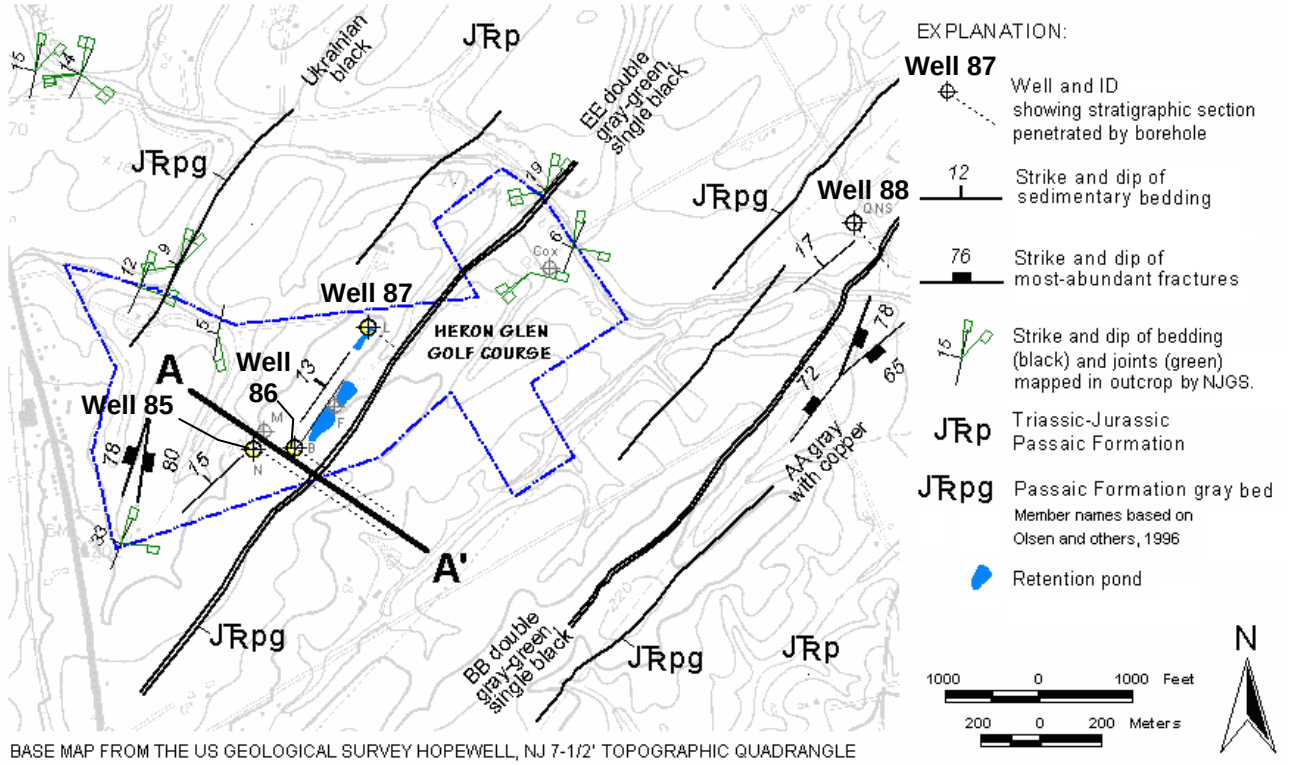

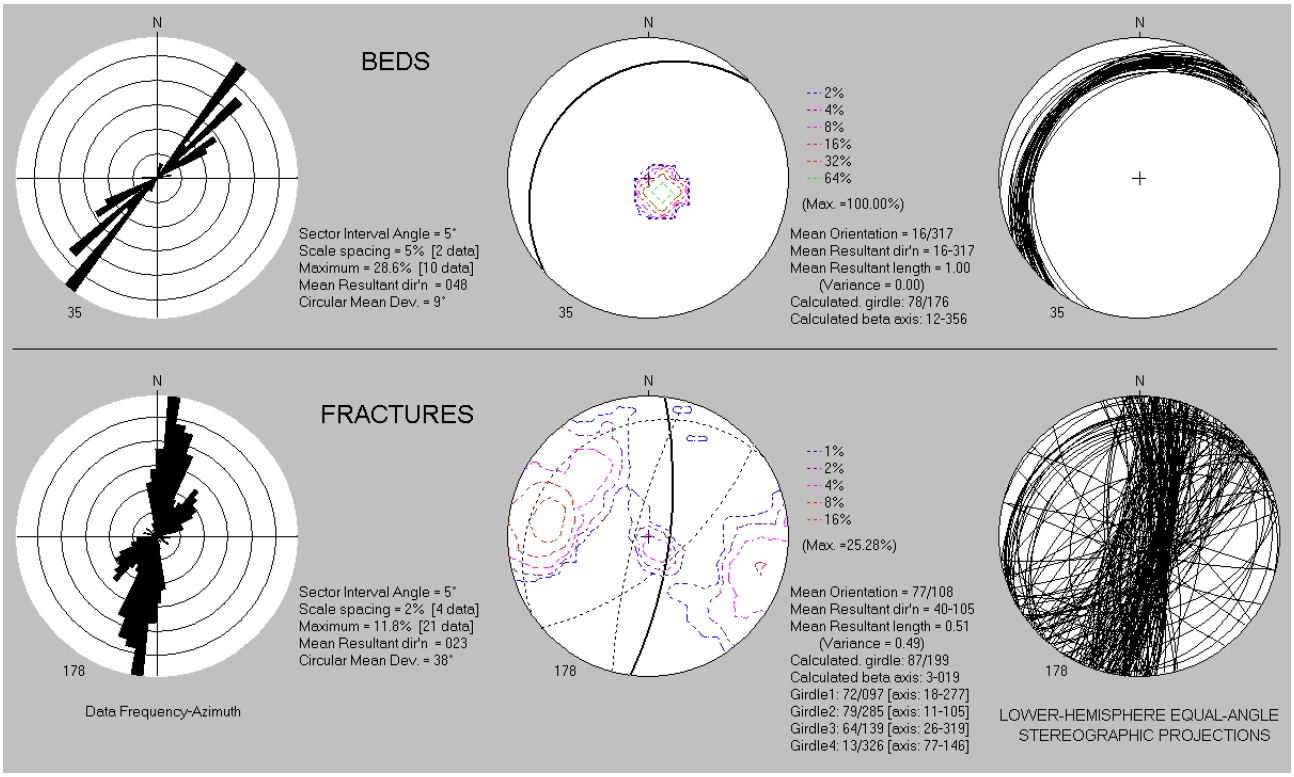

Figure 3K1. Map (above) showing wells 85 to 88 on and near the Heron Glen Golf Course, Rt. 202/31 N, Raritan Twp., Hunterdon County, NJ. Bedrock structures mapped near wells based on a structural analysis of OPTV data for wells 85 and 88 (below).

Wells 85 through 87 - Brunswick middle gray zone

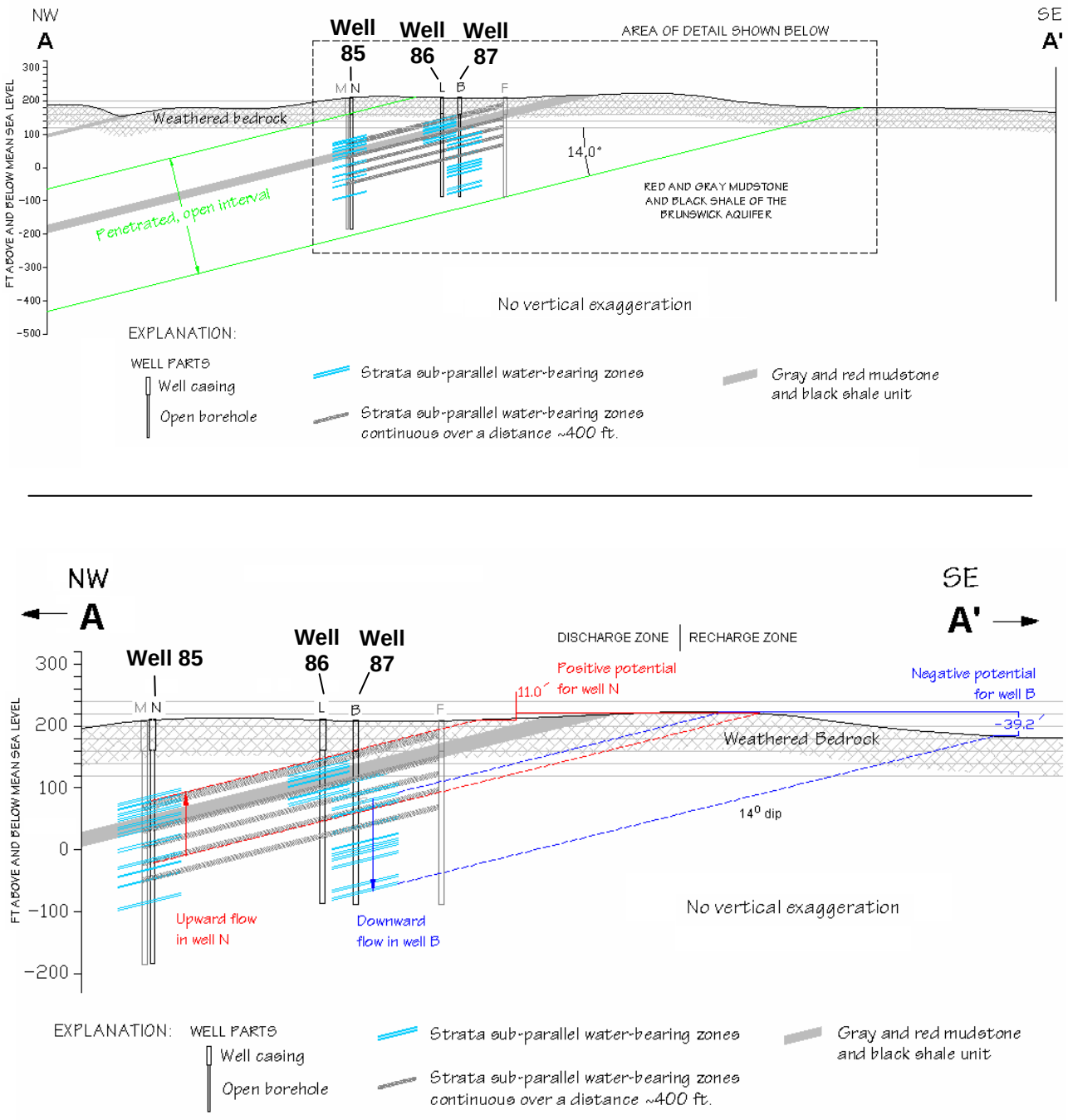

Figure 3K2. Hydrogeologic sections of the Heron Glen Golf Course well field, Rt. 202/31 N, Raritan Twp., Hunterdon County, NJ. Location of generalized section (above) shown on figure 3K1. Section details (below) show different cross-flow directions in wells 85 and 87 while pumping irrigation wells M and F at a combined rate of ~500 gpm. Flowing intervals are projected to land surface and shown in relation to topographic variations in the ground-water discharge and recharge zones.

Well 85 - Brunswick middle gray zone

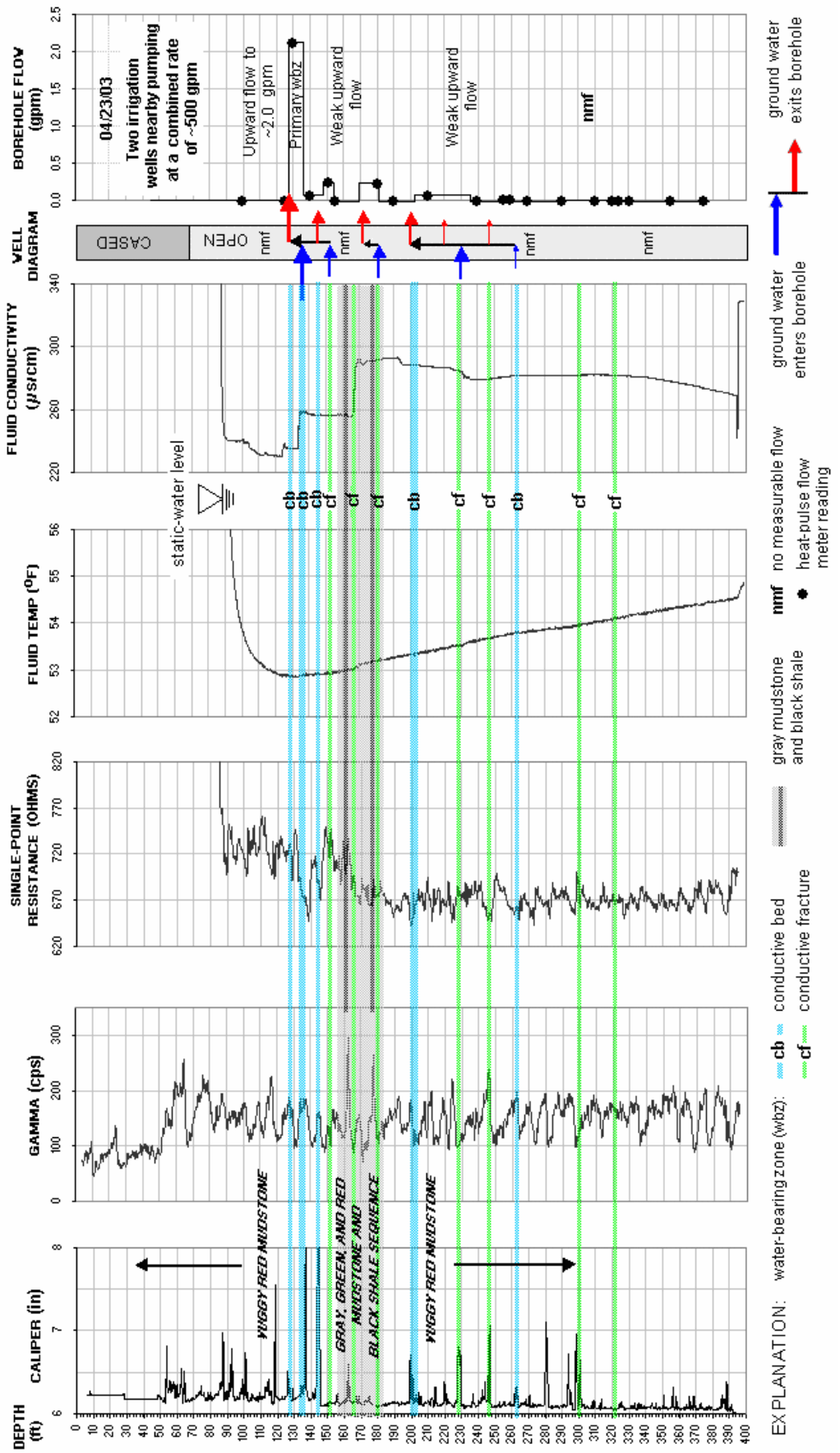

FIGURE 3K3. Hydrogeologic section based on geophysical logs for well 85 at the Heron Glen Golf Course, Rt. 202/31 N, Raritan Twp., Hunterdon County, NJ. The section shows the vertical distribution and types of hydraulically-conductive features and water-bearing zones in red and gray mudstone and gray and black shale. Depth values are in feet below land surface.

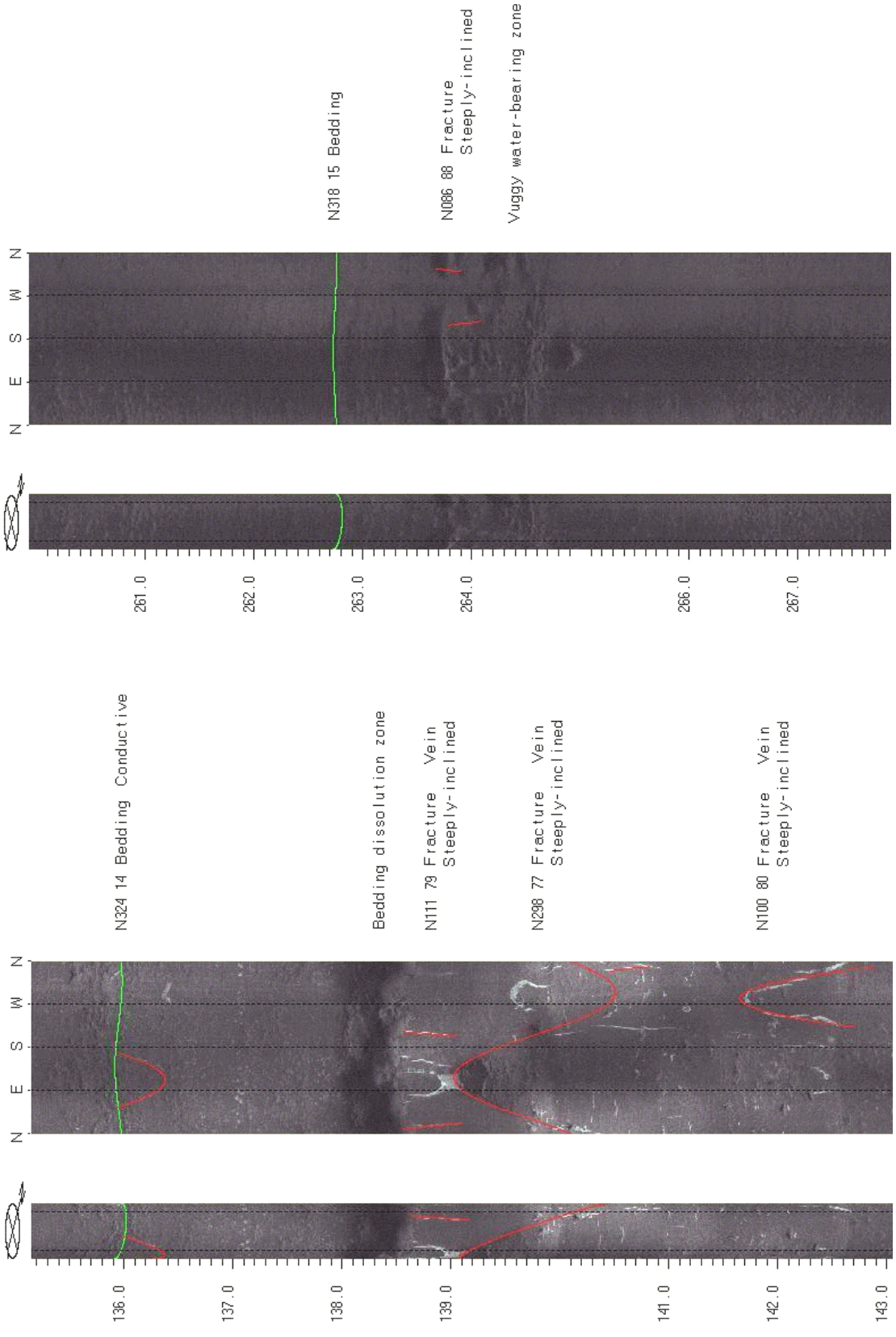

FIGURE 3K4. OPTV records of 6-inch diameter well 85 showing geologic structures and hydraulically-conductive features in red mudstone. Depth values are in feet below land surface.

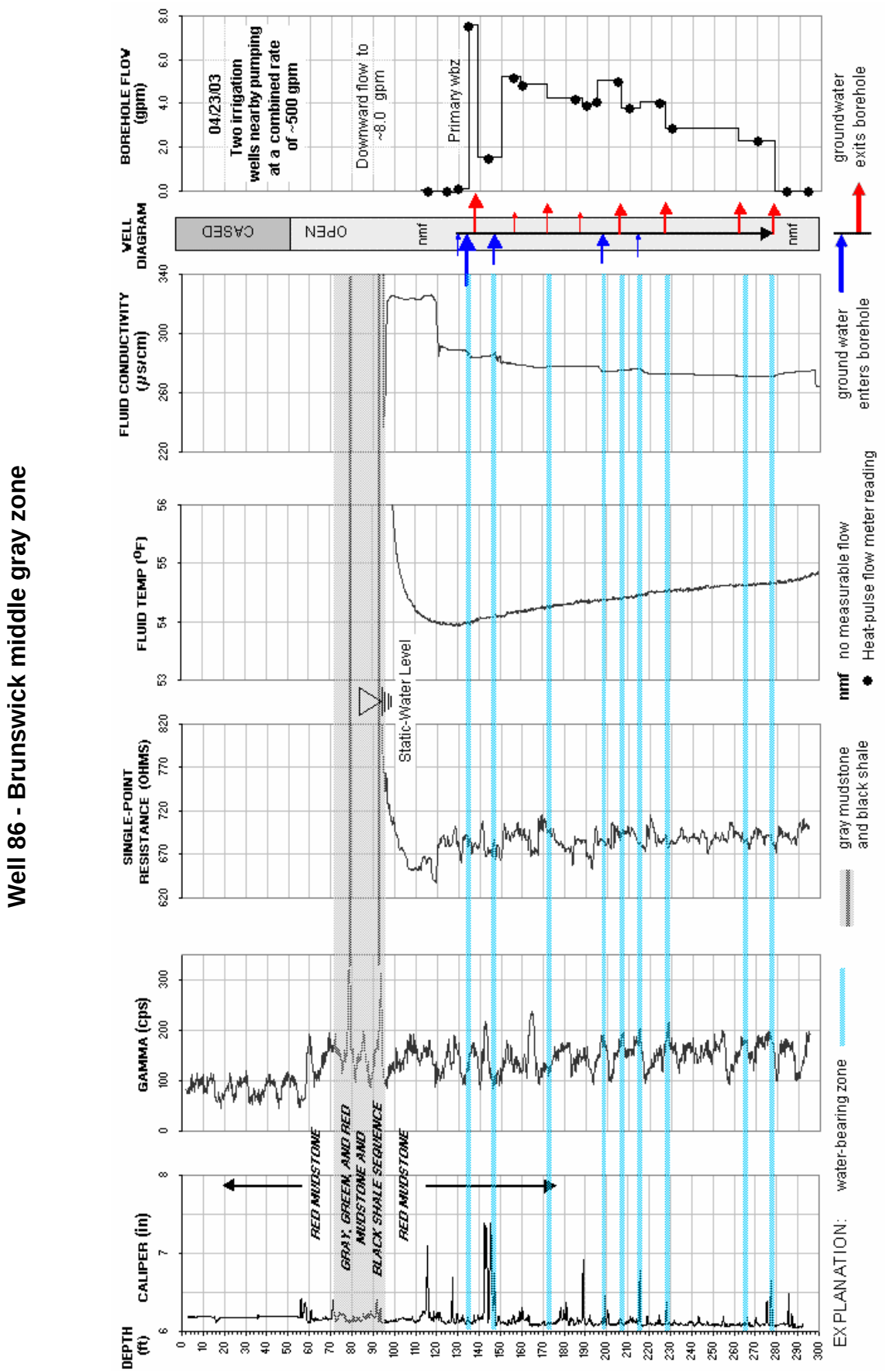

FIGURE 3K5. Hydrogeologic section based on geophysical logs for well 86 at the Heron Glen Golf Course, Rt. 202/31 N, Raritan Twp., Hunterdon County, NJ. The section shows the vertical distribution of water-bearing zones in red and gray mudstone and black shale. Depth values are in feet below land surface.

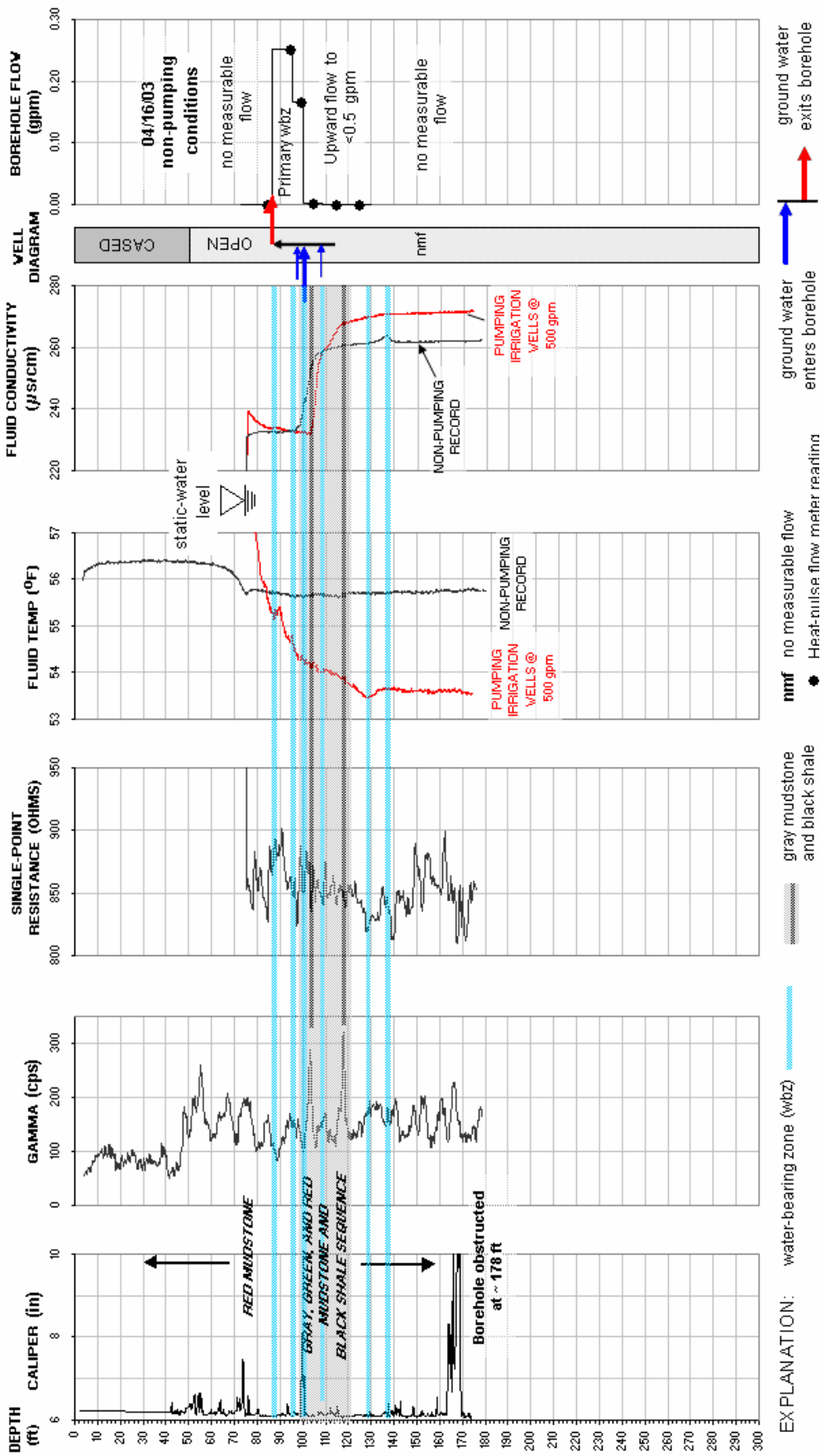

FIGURE 3K6. Hydrogeologic section based on geophysical logs for well 87 at the Heron Glen Golf Course, Rt. 202/31 N, Raritan Twp., Hunterdon County, NJ. The section shows the vertical distribution of water-bearing zones in red and gray mudstone and black shale. Depth values are in feet below land surface.

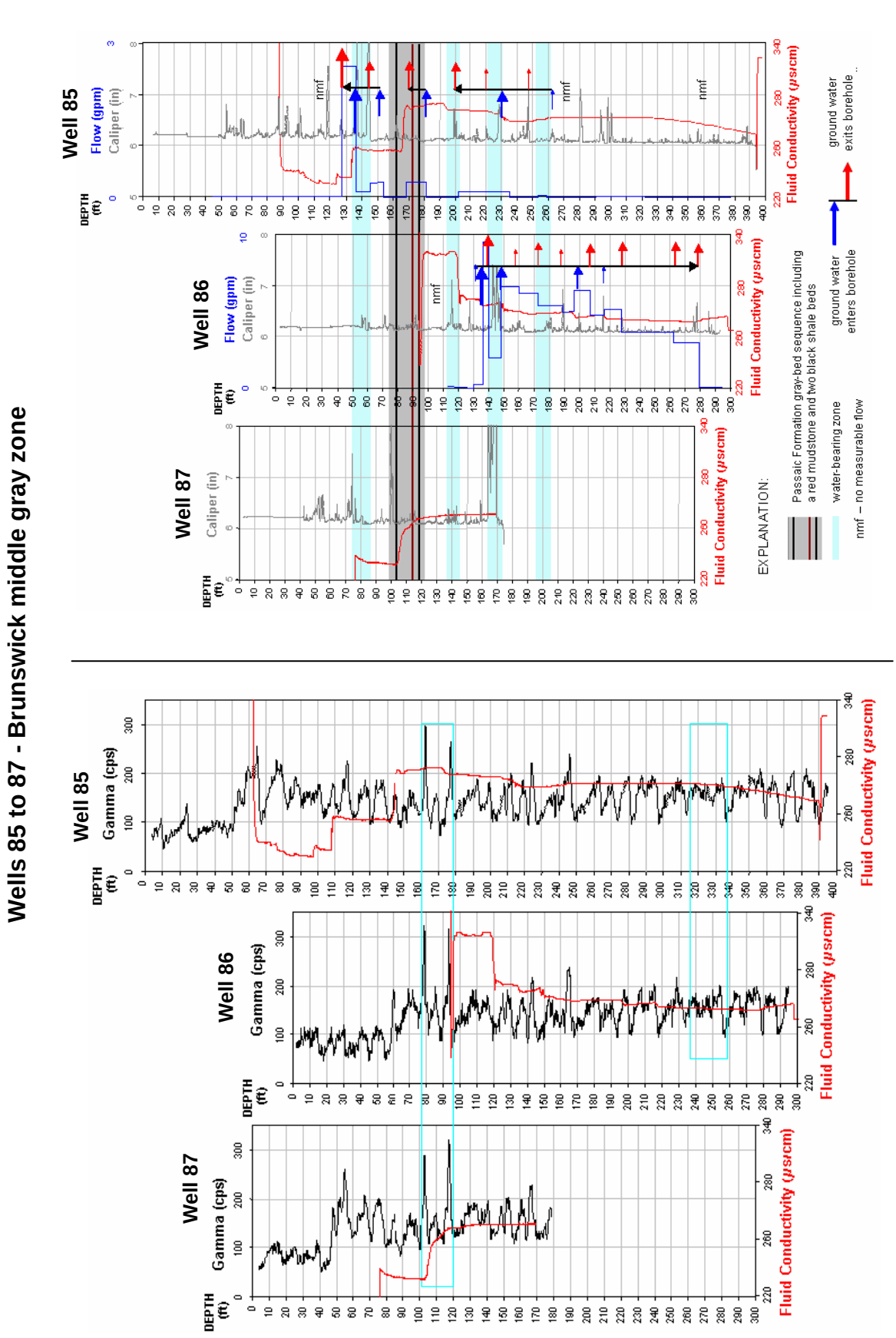

FIGURE 3K7. Stratigraphic correlation based on geophysical logs for wells 85 to 87 at the Heron Glen Golf Course, Rt. 202/31 N, Raritan Twp., Hunterdon County, NJ. The natural gamma logs (left) are used to establish the stratigraphic correlation. The caliper, fluid conductivity and flow logs (right) correlate water-bearing zones. Depth values are in feet below land surface.

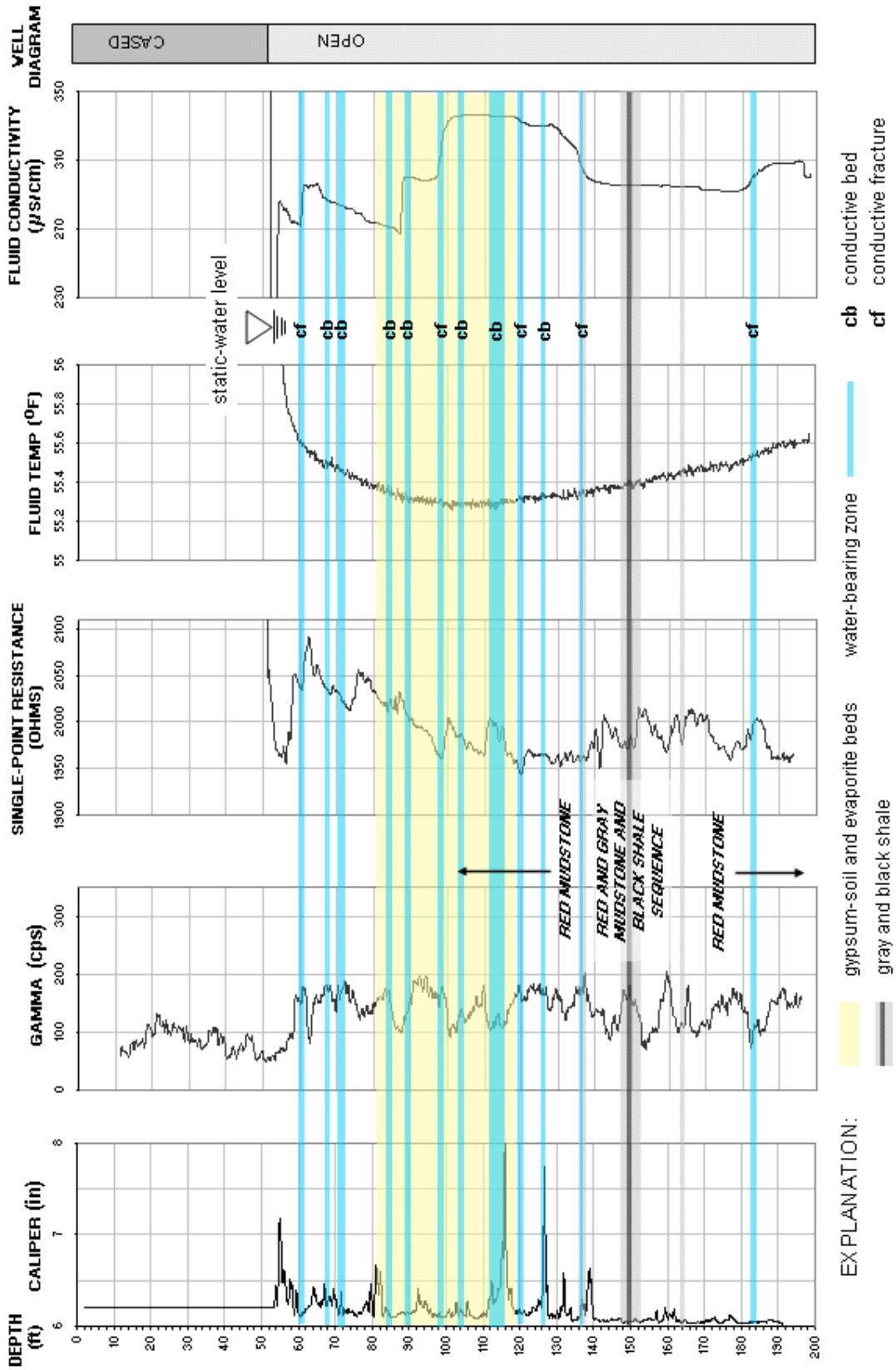

FIGURE 3K8. Hydrogeologic section based on geophysical logs for well 88, Reaville, Ave., Raritan Twp., Hunterdon County, NJ. The section shows the vertical distribution and types of hydraulically-conductive features and water-bearing zones in red and gray mudstone and gray and black shale. Depth values are in feet below land surface.

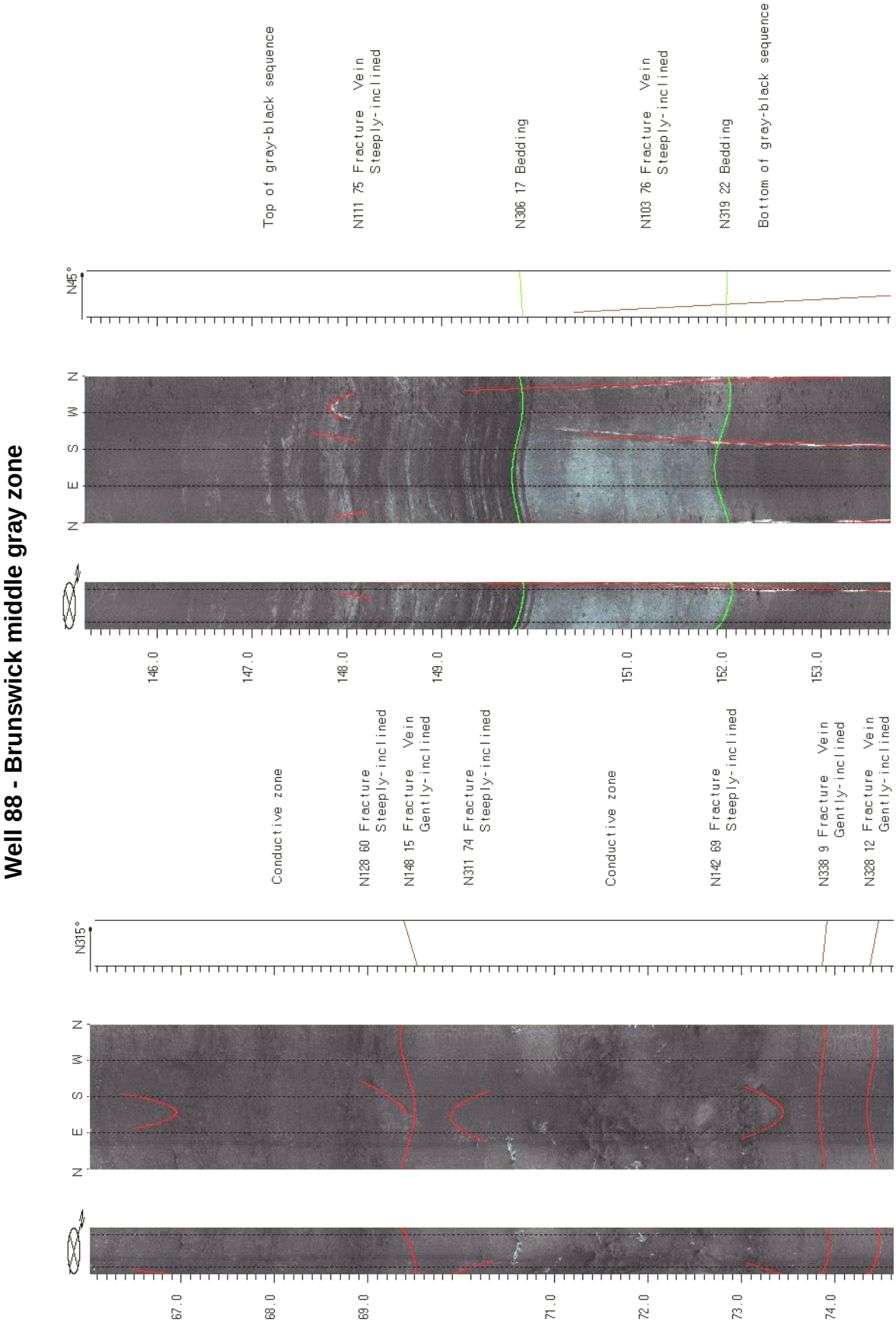

FIGURE 3K9. OPTV records of 6-inch diameter well 88 showing geologic structures and hydraulically-conductive features in red and gray mudstone and gray and black shale. Depth values are in feet below land surface.

Well 89 - Brunswick lower red zone

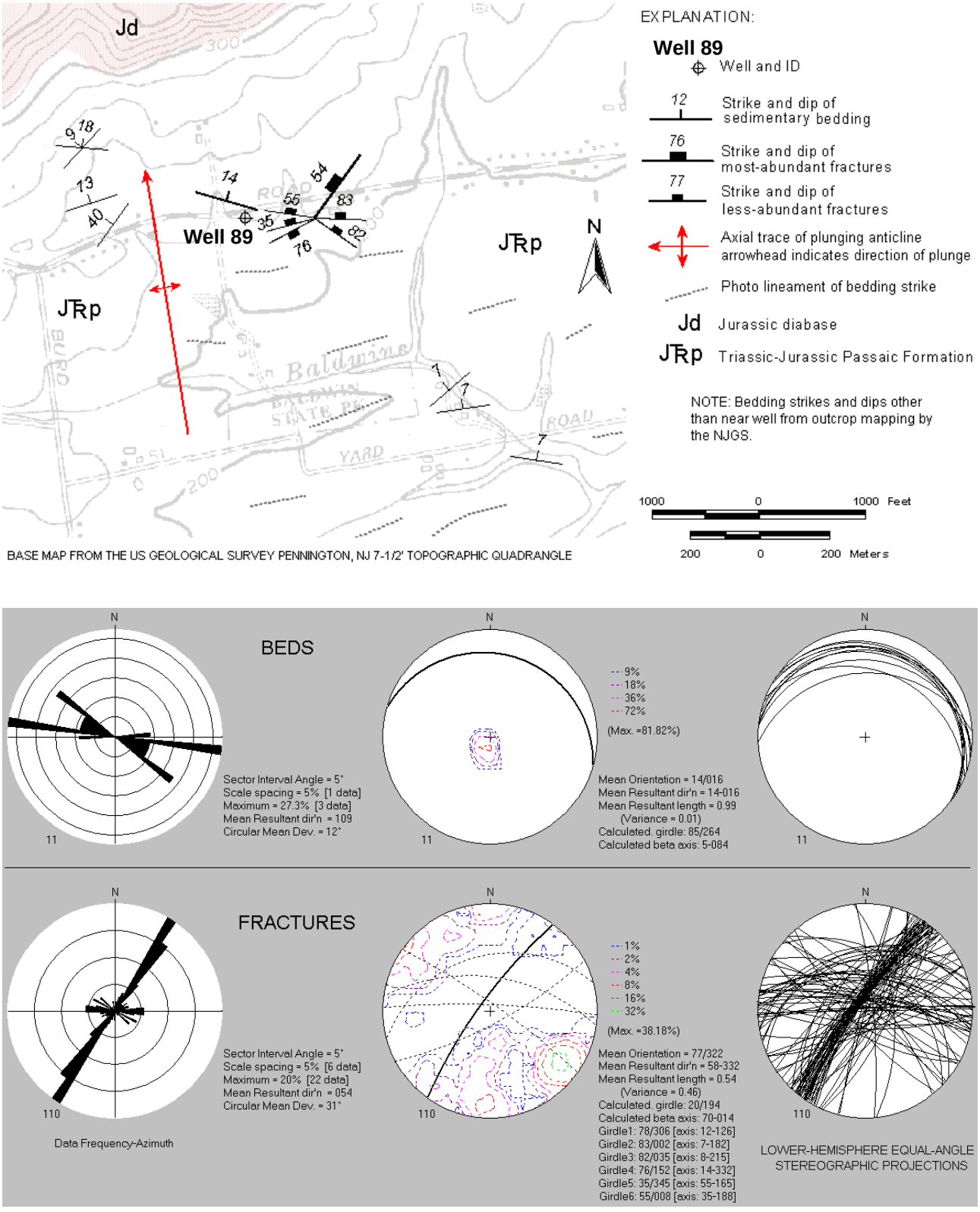

Figure 3L1. Map (above) showing well 89 off Woosamonsa Road at Harbat Farms, Hopewell Twp., Mercer County, NJ. Bedrock structures mapped near wells based on a structural analysis of OPTV data (below).

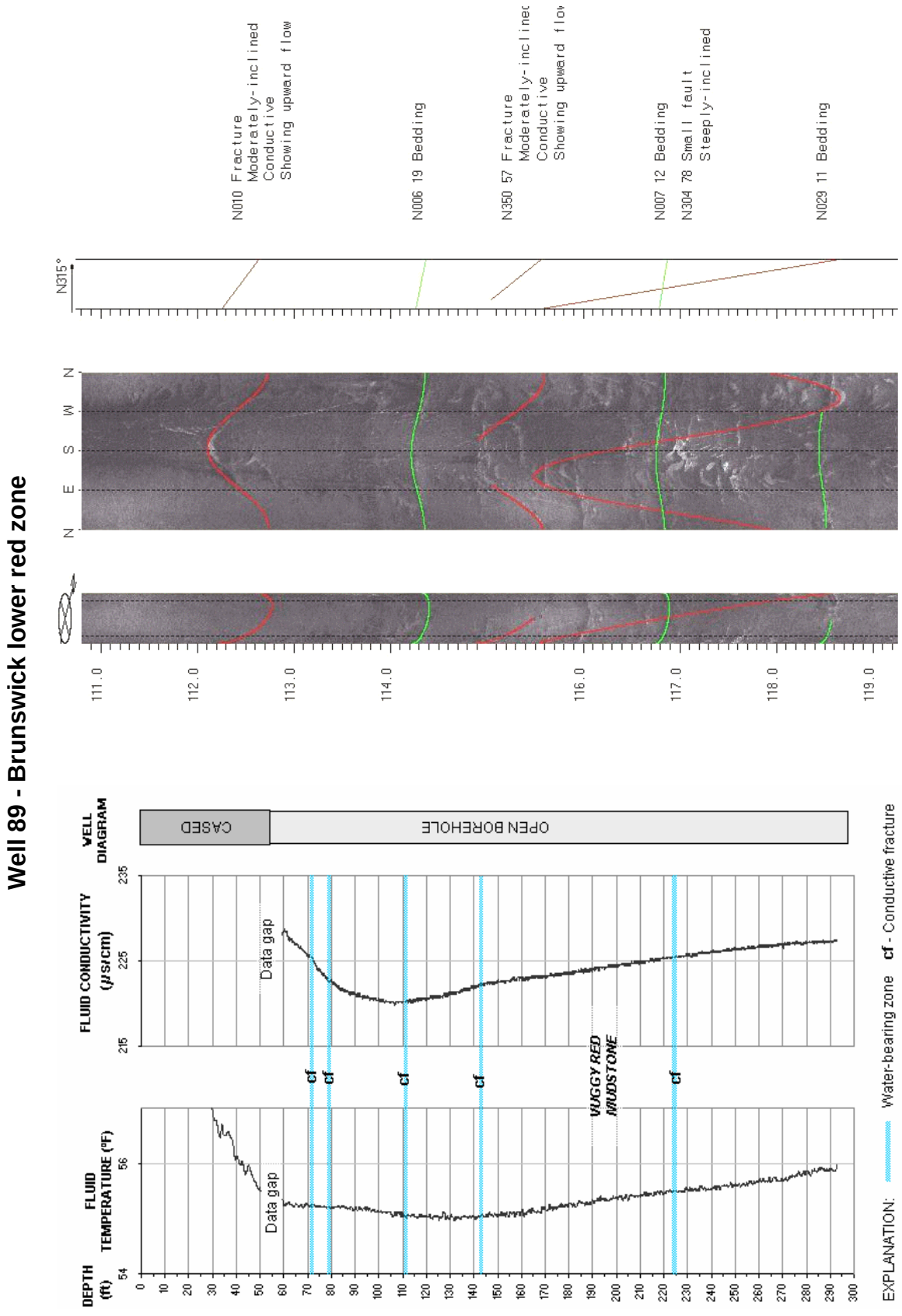

FIGURE 3L2. Hydrogeologic section (left) based on geophysical logs for well 89 at Harbat Farms, Woosamonsa Rd., Hopewell Twp., Mercer County, NJ., The section shows the vertical distribution and types of hydraulically-conductive features and water-bearing zones in red mudstone. OPTV record (right) shows geologic structures and hydraulically -conductive fractures. Depth values are in feet below land surface.

Wells 90 to 99 - Brunswick lower red zone

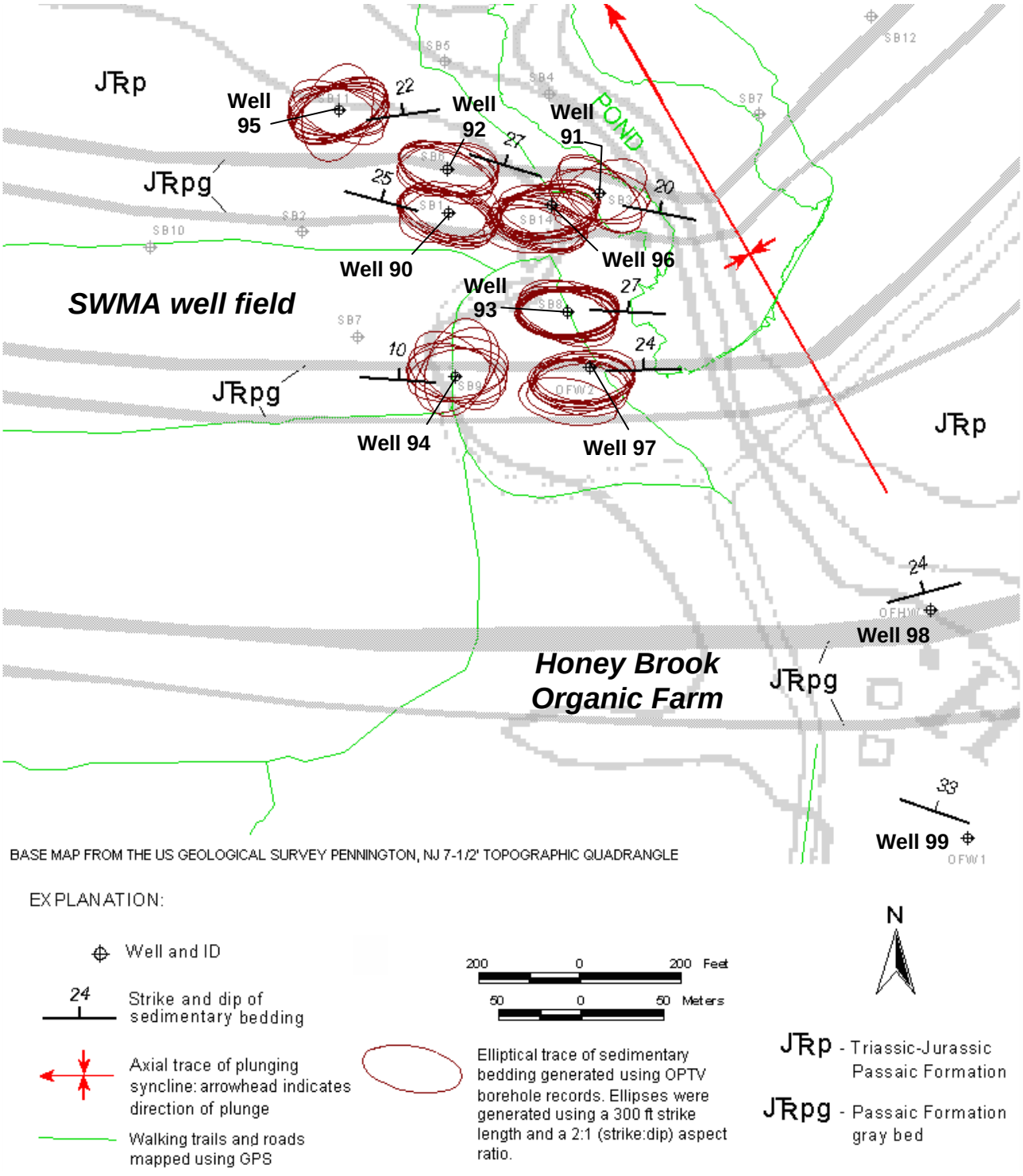

Figure 3M1. Map showing wells 90 to 99 at the Stony Brook-Millstone Watershed Association (SMWA) well field and the Honey Brook Organic Farm, Wargo Rd., Hopewell Twp., Mercer County, NJ. Bedding near wells based on structural analyses of OPTV data.

Wells 90 through 97 - Brunswick lower red zone

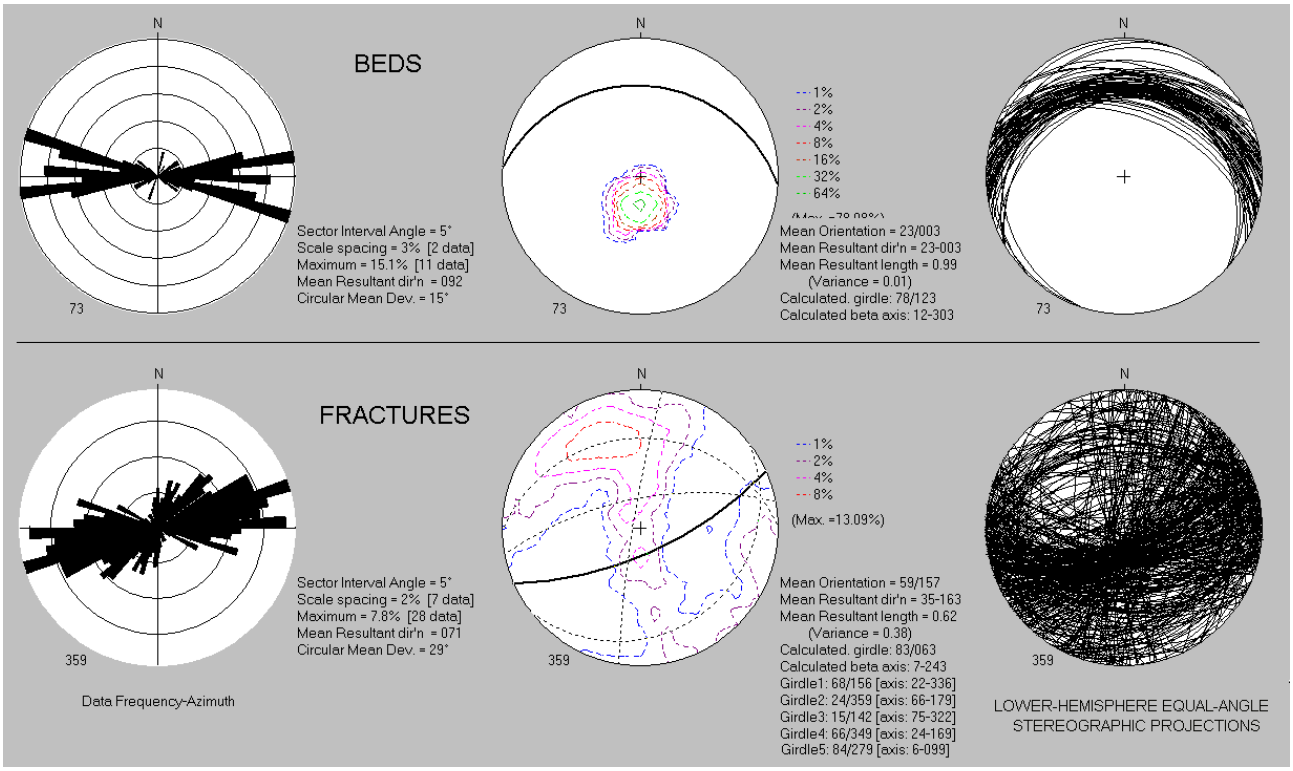

Wells 98 and 99 - Brunswick lower red zone

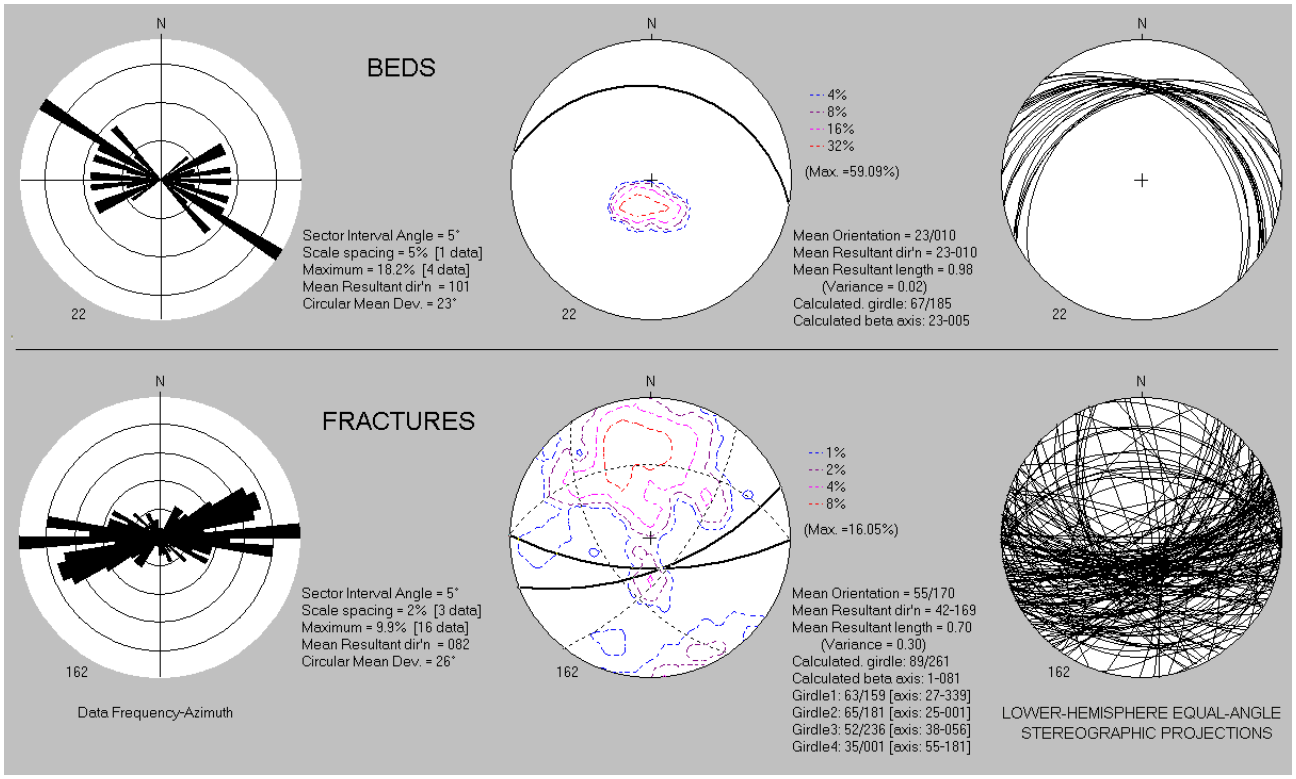

Figure 3M2. Structural analyses of OPTV records for wells 90 to 97 at the Stony Brook-Millstone Watershed Association well field (above) and wells 98 and 99 at the Honey Brook Organic Farm (below).

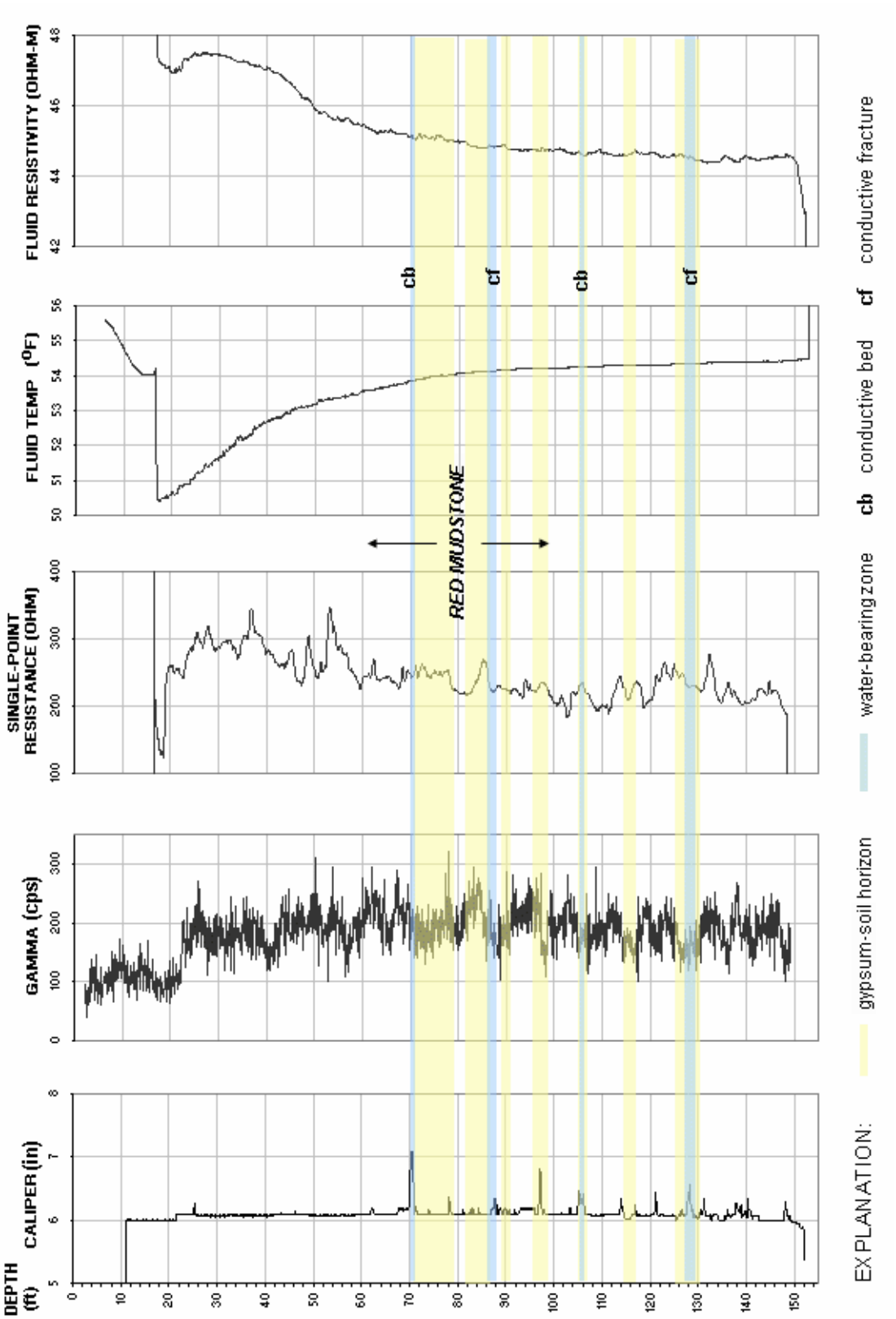

FIGURE 3M3. Hydrogeologic section based on geophysical logs for well 90 at the Stony Brook-Millstone Watershed Association well field, Wargo Rd., Hopewell Twp., Mercer County, NJ. The section shows the vertical distribution and types of hydraulically-conductive features and water-bearing zones in red mudstone. Depth values are in feet below land surface.

Well 91 - Brunswick lower red zone

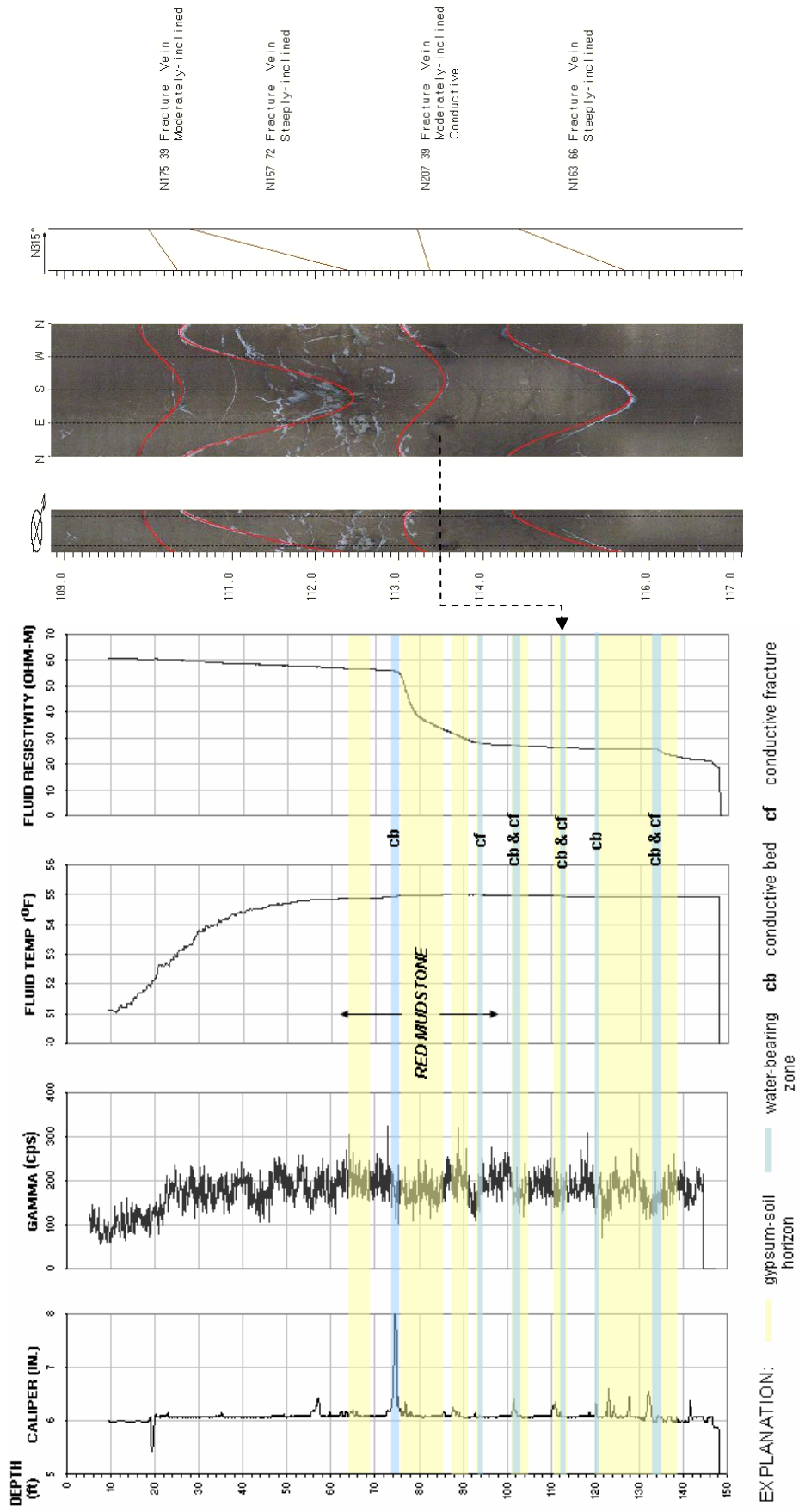

FIGURE 3M4. Hydrogeologic section (left) based on geophysical logs for well 91 at the Stony Brook-Millstone Watershed Association well field, Wargo Rd., Hopewell Twp., Mercer County, NJ. The section shows the vertical distribution and types of hydraulically-conductive features and water-bearing zones in red mudstone. OPTV record (right) shows geologic structures and hydraulically-conductive features in red mudstone. Depth values are in feet below land surface.

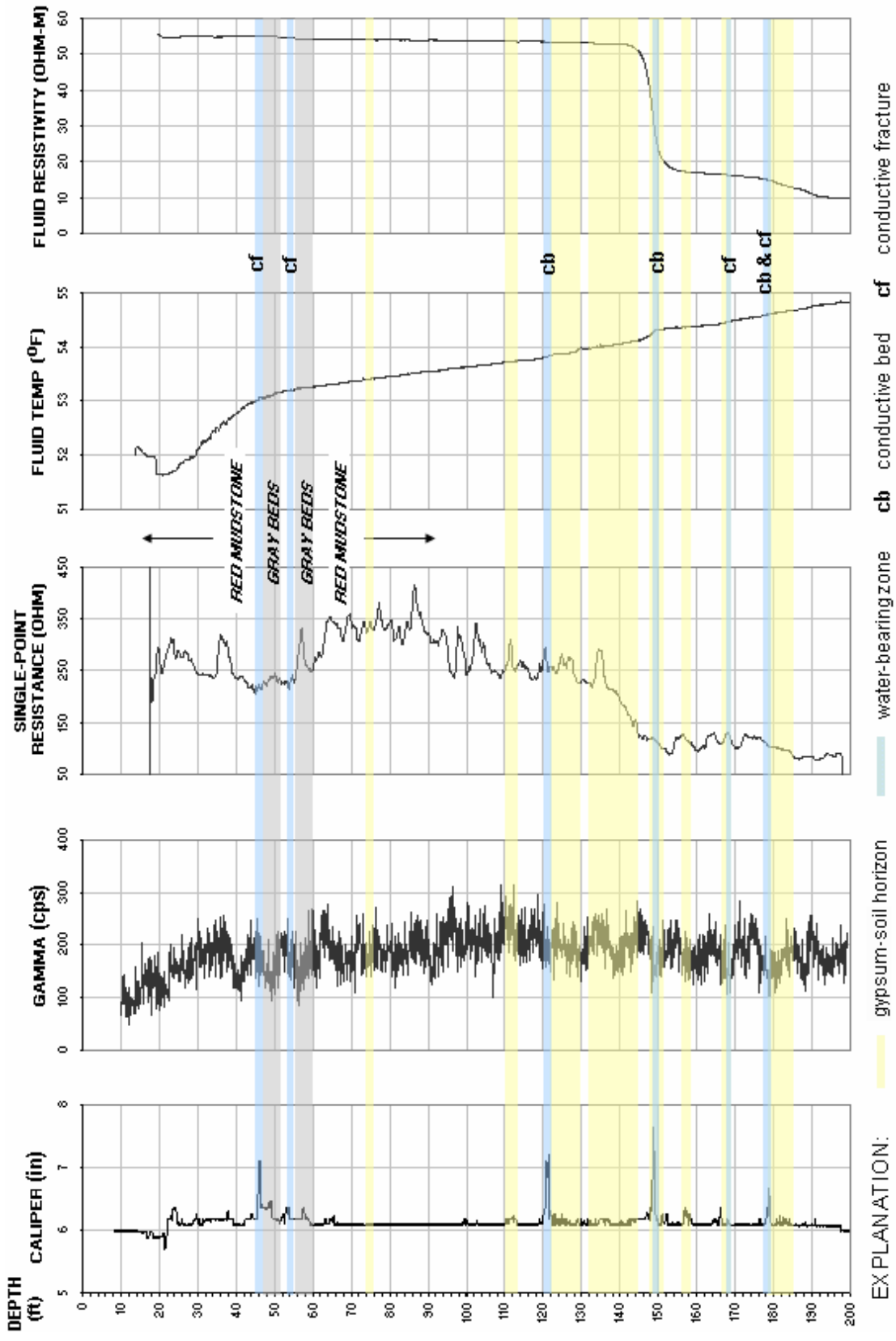

FIGURE 3M5. Hydrogeologic section based on geophysical logs for well 92 at the Stony Brook-Millstone Watershed Association well field, Wargo Rd., Hopewell Twp., Mercer County, NJ. The section shows the vertical distribution and types of hydraulically-conductive features and water-bearing zones in red and gray mudstone and gray and shale. Depth values are in feet below land surface.

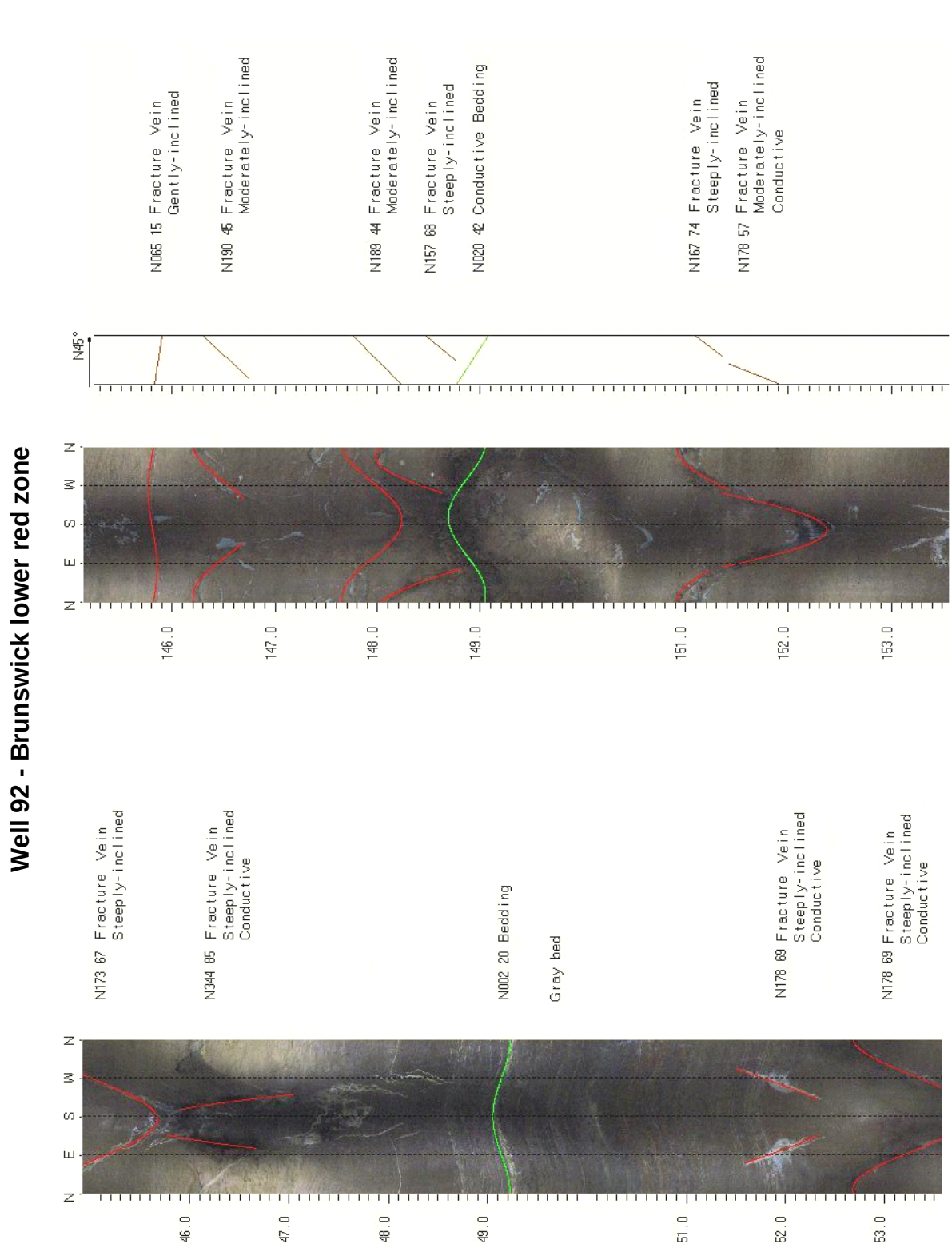

FIGURE 3M6. OPTV records of well 92 at the Stony Brook-Millstone Watershed Association well field showing geologic structures and hydraulically-conductive features in red and gray mudstone and gray shale. Depth values are in feet below land surface.

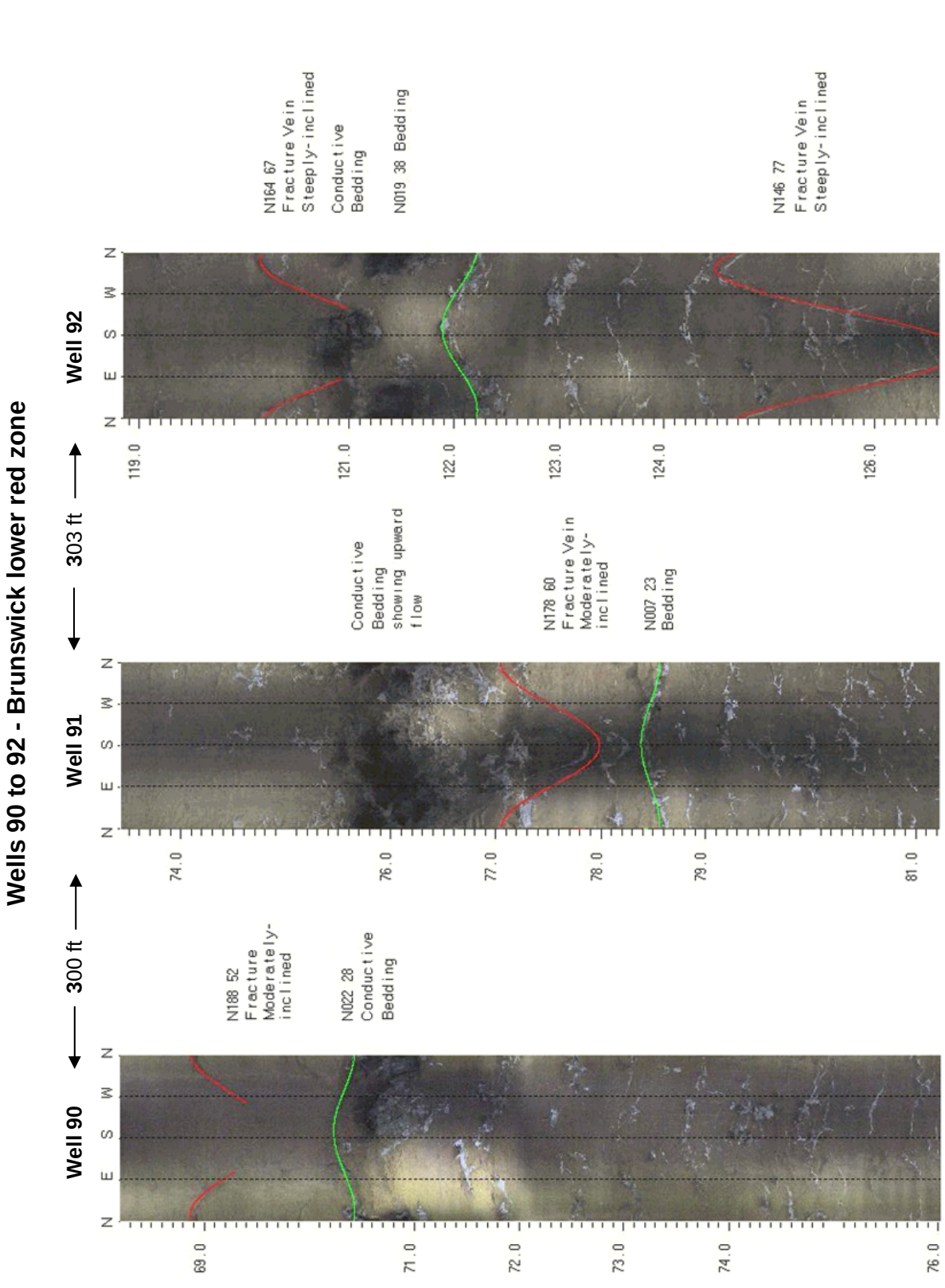

FIGURE 3M7. Stratigraphic correlation of wells 91 to 93 at the Stony Brook-Millstone Watershed Association well field based on OPTV records showing a major water-bearing zone in a gypsum-soil horizon and other geologic structures. Depth values are in feet below land surface.

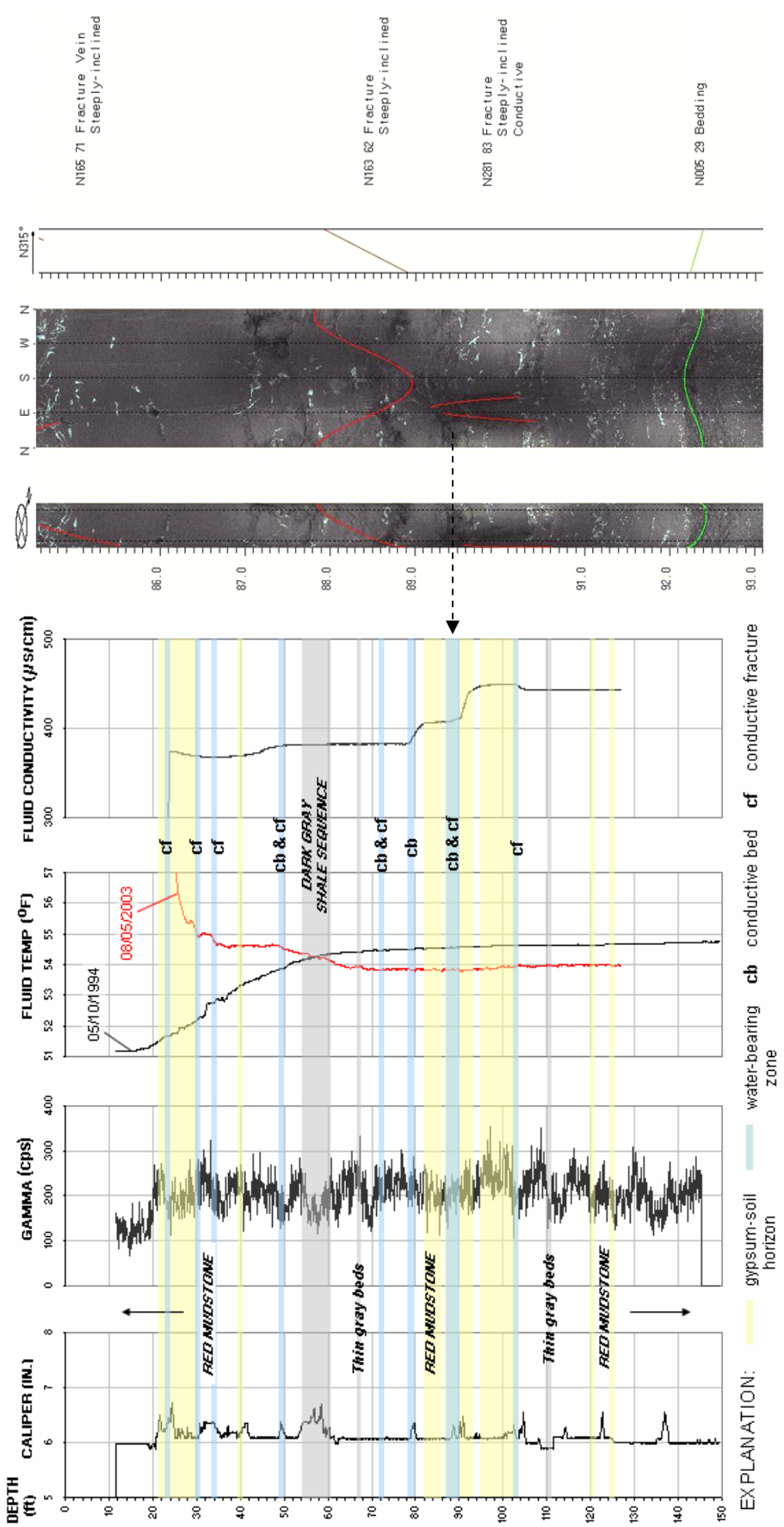

FIGURE 3M8. Hydrogeologic section (left) based on geophysical logs for well 93 at the Stony Brook-Millstone Watershed Association well field, Wargo Rd., Hopewell Twp., Mercer County, NJ. The section shows the vertical distribution and types of hydraulically-conductive features and water-bearing zones in red and gray mudstone and gray shale. OPTV record (right) shows geologic structures and hydraulically-conductive dissolution features in red mudstone with gypsum-soil horizons. Depth values are in feet below land surface.

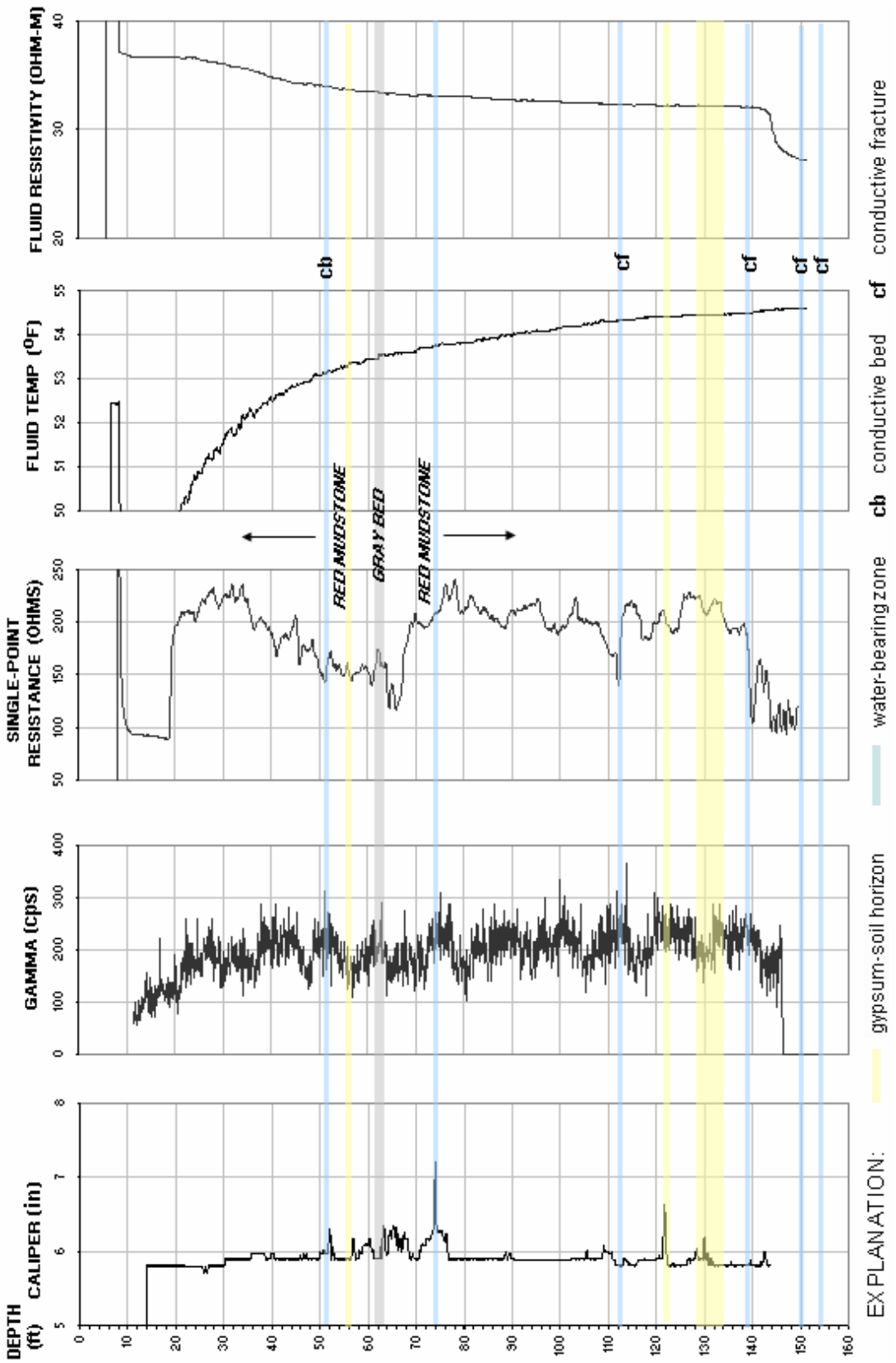

FIGURE 3M9. Hydrogeologic section based on geophysical logs for well 94 at the Stony Brook-Millstone Watershed Association well field, Wargo Rd., Hopewell Twp., Mercer County, NJ. The section shows the vertical distribution and types of hydraulically-conductive features and water-bearing zones in red and gray mudstone and gray shale. Depth values are in feet below land surface.

Well 95 - Brunswick lower red zone

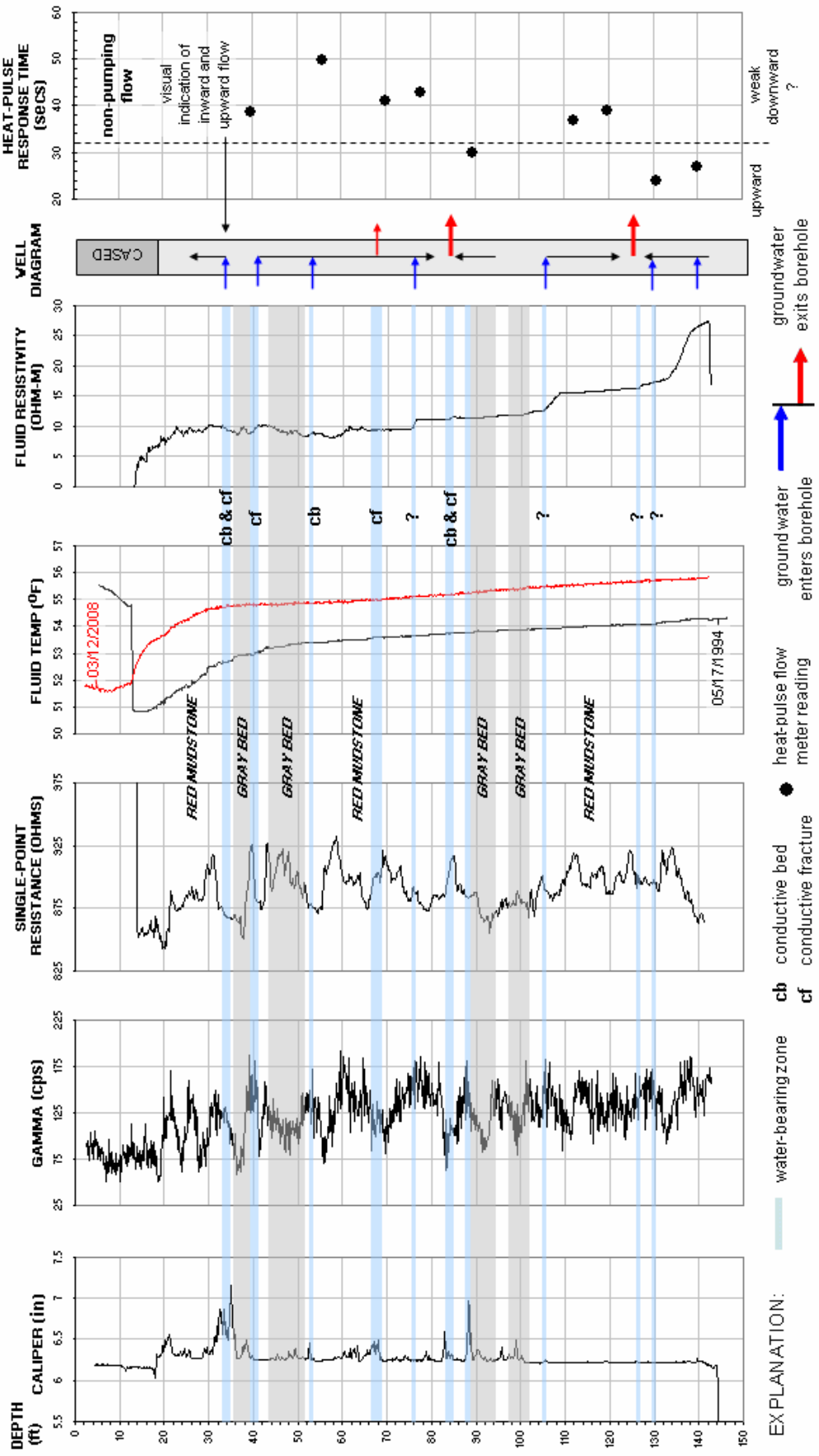

FIGURE 3M10. Hydrogeologic section based on geophysical logs for well 95 at the Stony Brook-Millstone Watershed Association well field, Wargo Rd., Hopewell Twp., Mercer County, NJ. The section shows the vertical distribution and types of hydraulically-conductive features and water-bearing zones in red and gray mudstone and gray shale. Depth values are in feet below land surface.

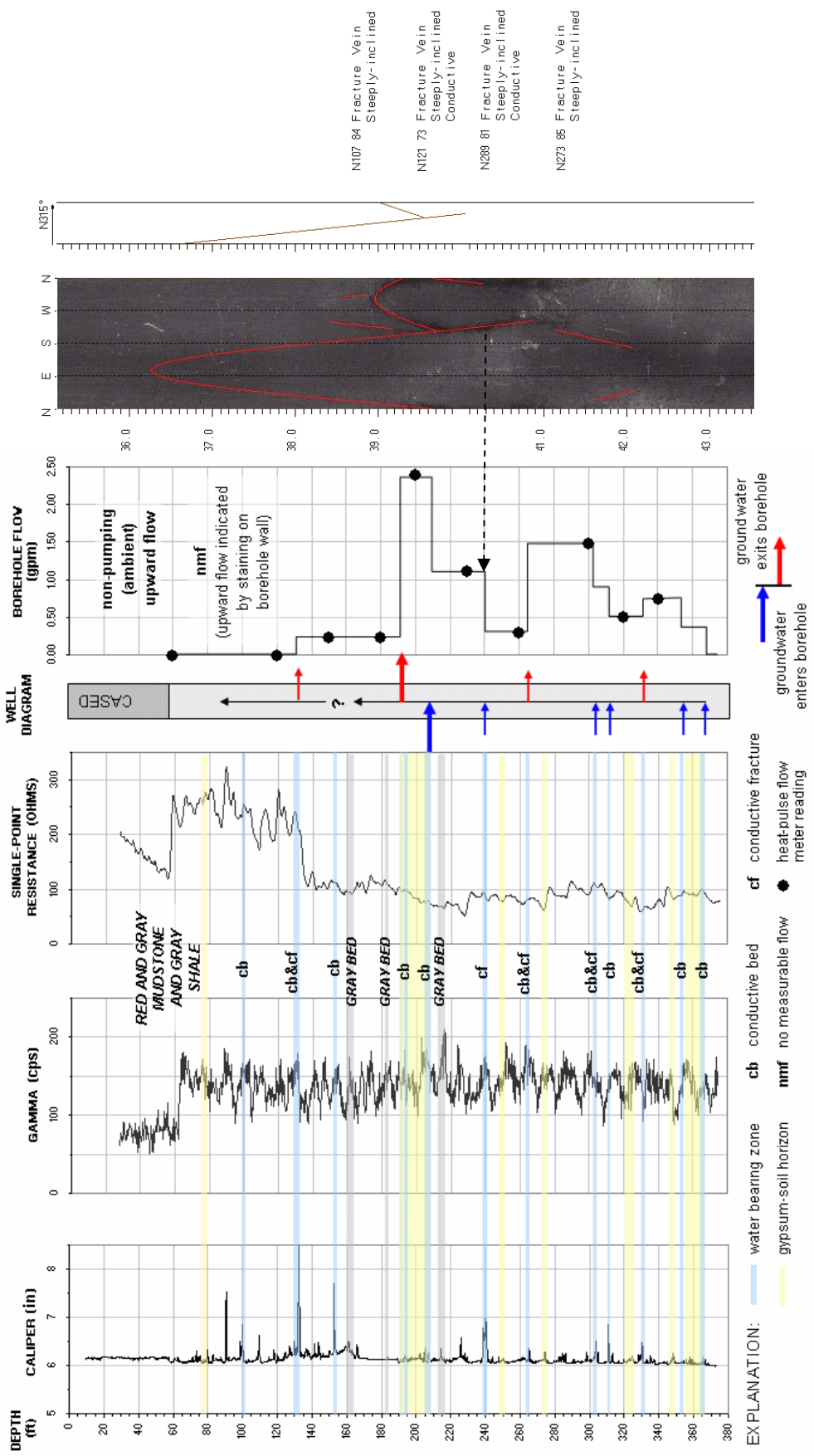

FIGURE 3M11. Hydrogeologic section (left) based on geophysical logs for well 93 at the Stony Brook-Millstone Watershed Association well field, Wargo Rd., Hopewell Twp., Mercer County, NJ. The section shows the vertical distribution and types of hydraulically-conductive features and water-bearing zones in red and gray mudstone and gray shale. OPTV record (right) shows geologic structures and hydraulically-conductive fractures in red mudstone. Depth values are feet below land surface.

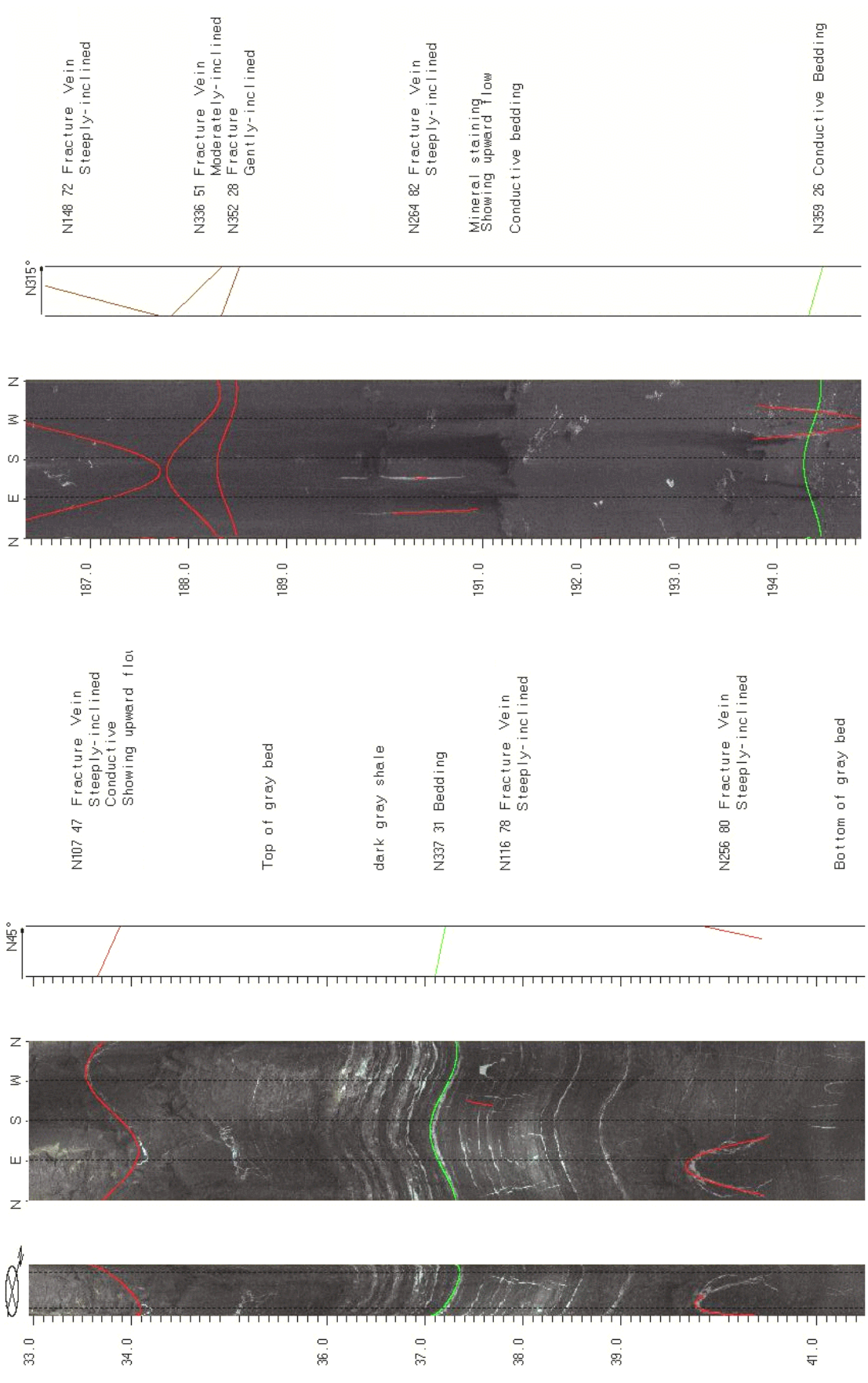

FIGURE 3M12. OPTV records of 6-inch diameter wells 95 (left) and 96 (right) at the Stony Brook-Millstone Watershed Association well field showing geologic structures and hydraulically-conductive features in red and gray mudstone and gray shale. Depth values are in feet below land surface.

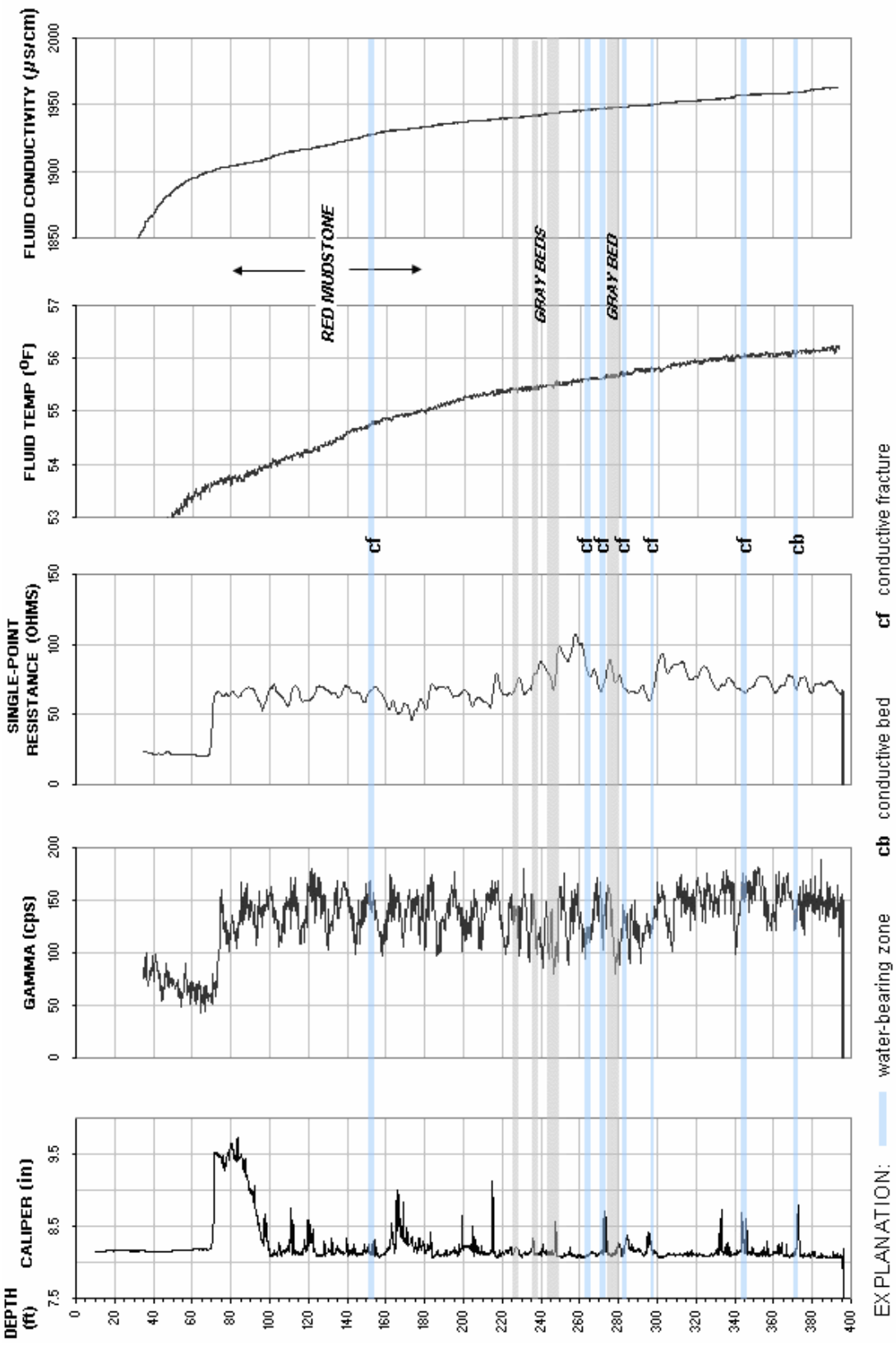

FIGURE 3M13. Hydrogeologic section based on geophysical logs for well 97 at the Stony Brook-Millstone Watershed Association well field, Wargo Rd., Hopewell Twp., Mercer County, NJ. The section shows the vertical distribution and types of hydraulically-conductive features and water-bearing zones in red and gray mudstone and gray shale. Depth values are in feet below land surface.

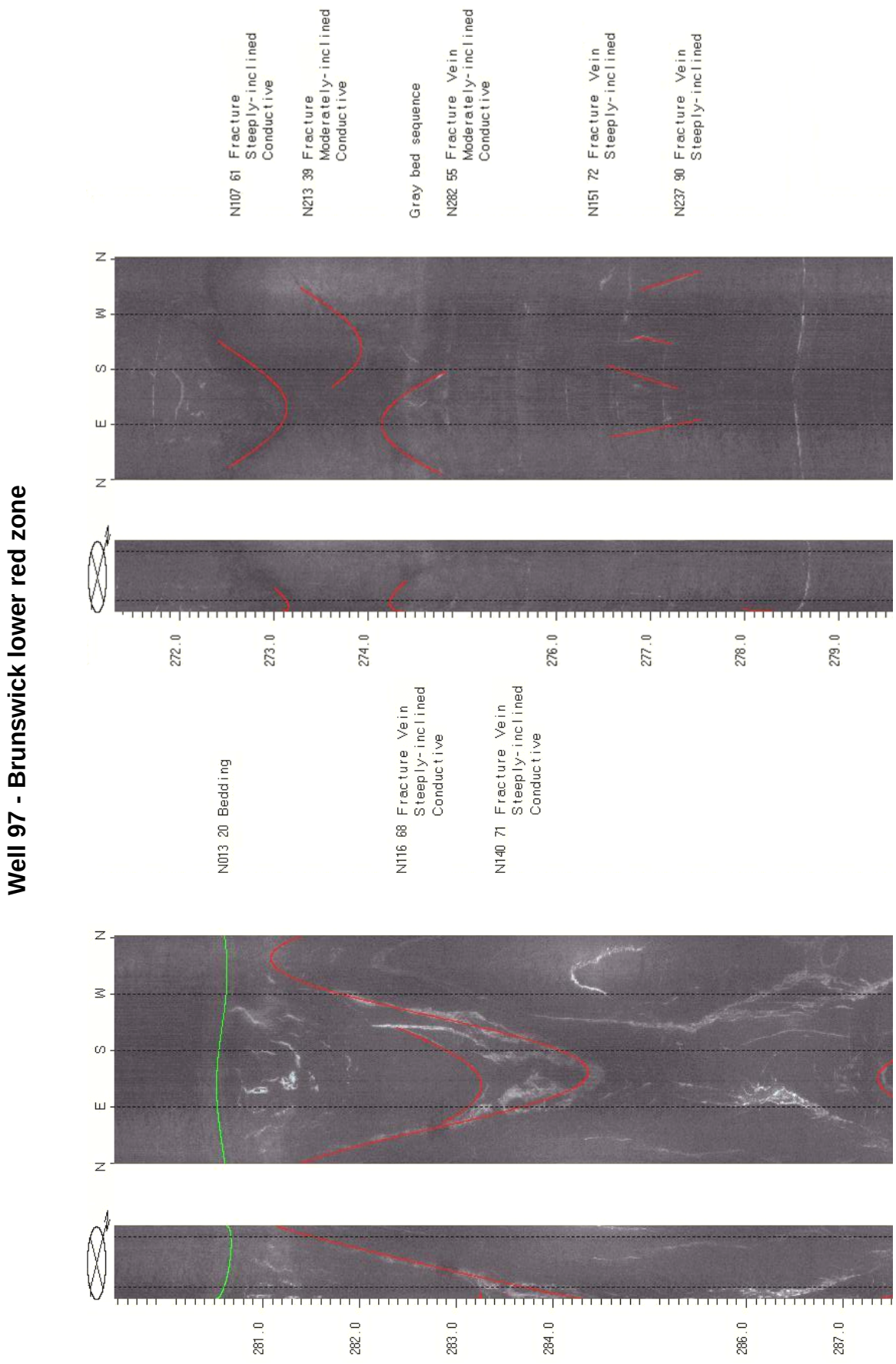

FIGURE 3M14. OPTV records of 8-inch diameter well 97 at the Stony Brook-Millstone Watershed Association well field showing geologic structures and hydraulically-conductive features in red and gray mudstone and gray shale. Depth values are in feet below land surface.

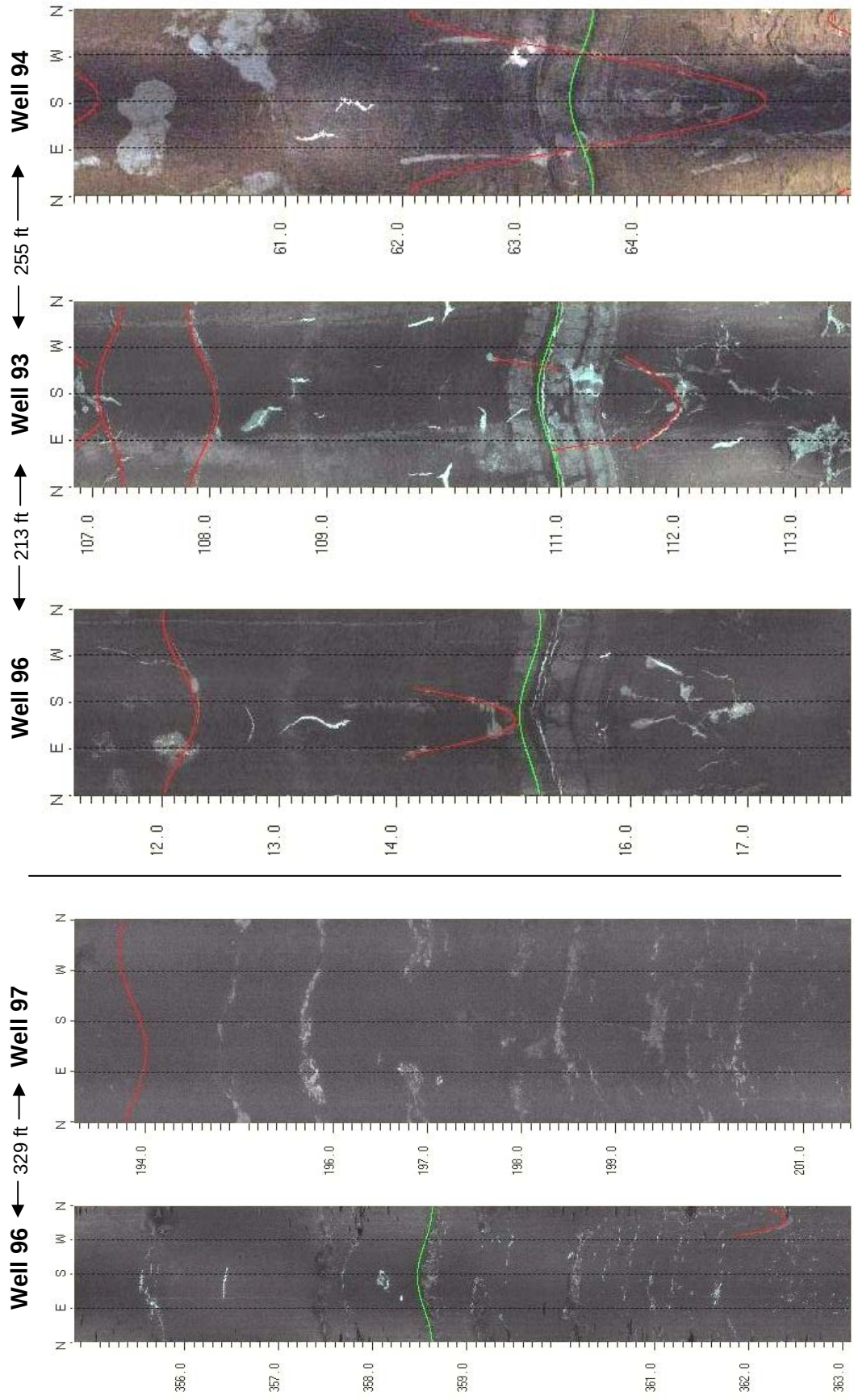

FIGURE 3M15. Stratigraphic correlation of wells 96 and 97 (left) and 96, 93 and 94 (right) based on OPTV records from the Stony Brook-Millstone Watershed Association well field. Depth values are in feet below land surface.

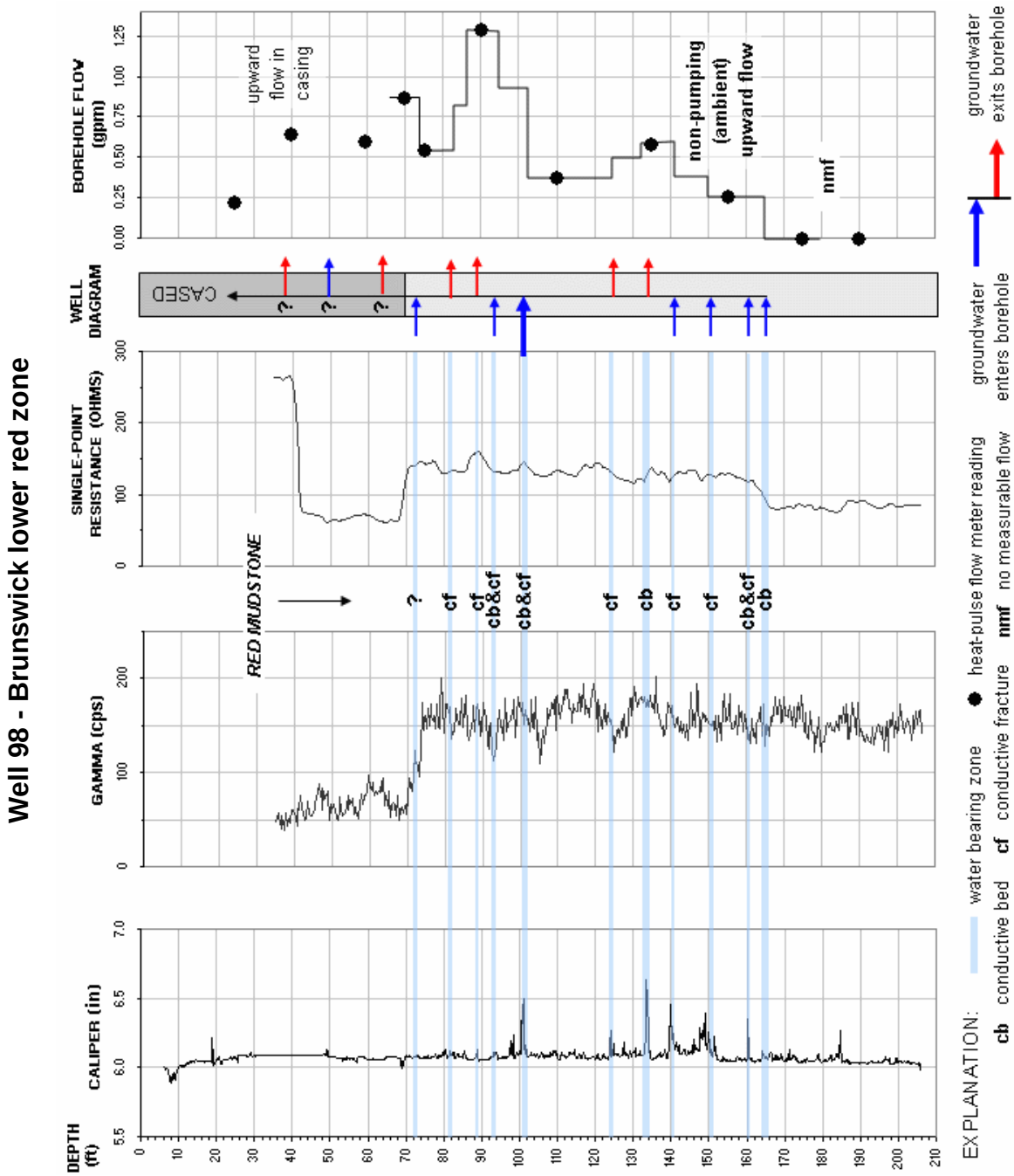

FIGURE 3M16. Hydrogeologic section based on geophysical logs for well 97 at the Stony Brook-Millstone Watershed Association well field, Wargo Rd., Hopewell Twp., Mercer County, NJ. The section shows the vertical distribution and types of hydraulically-conductive features and water-bearing zones in red and gray mudstone and gray shale. Depth values are feet below land surface.

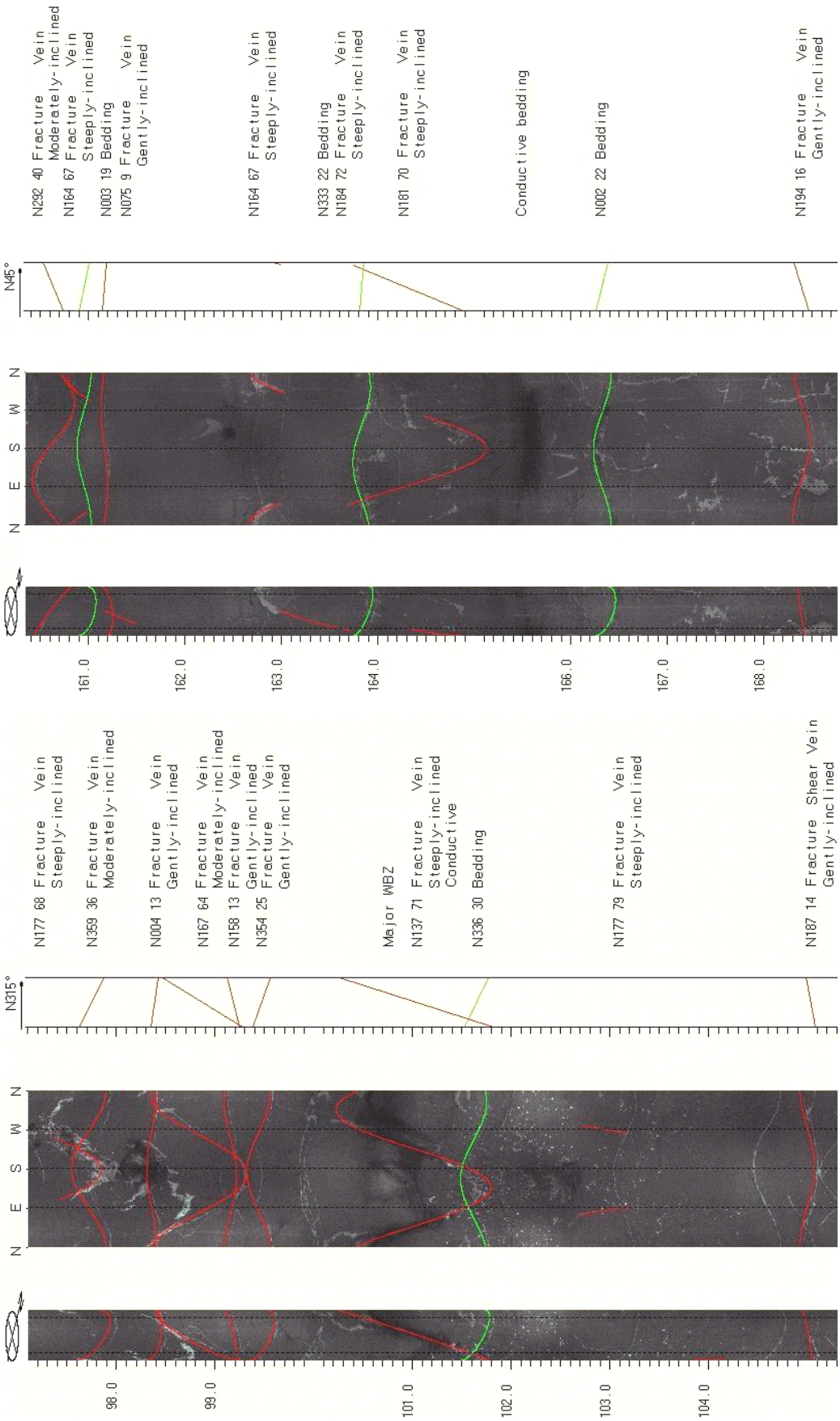

FIGURE 3M17. OPTV records of 6-inch diameter well 99 at the Honey Brook Organic Farm showing geologic structures and hydraulically-conductive features in red mudstone. Depth values are in feet below land surface.

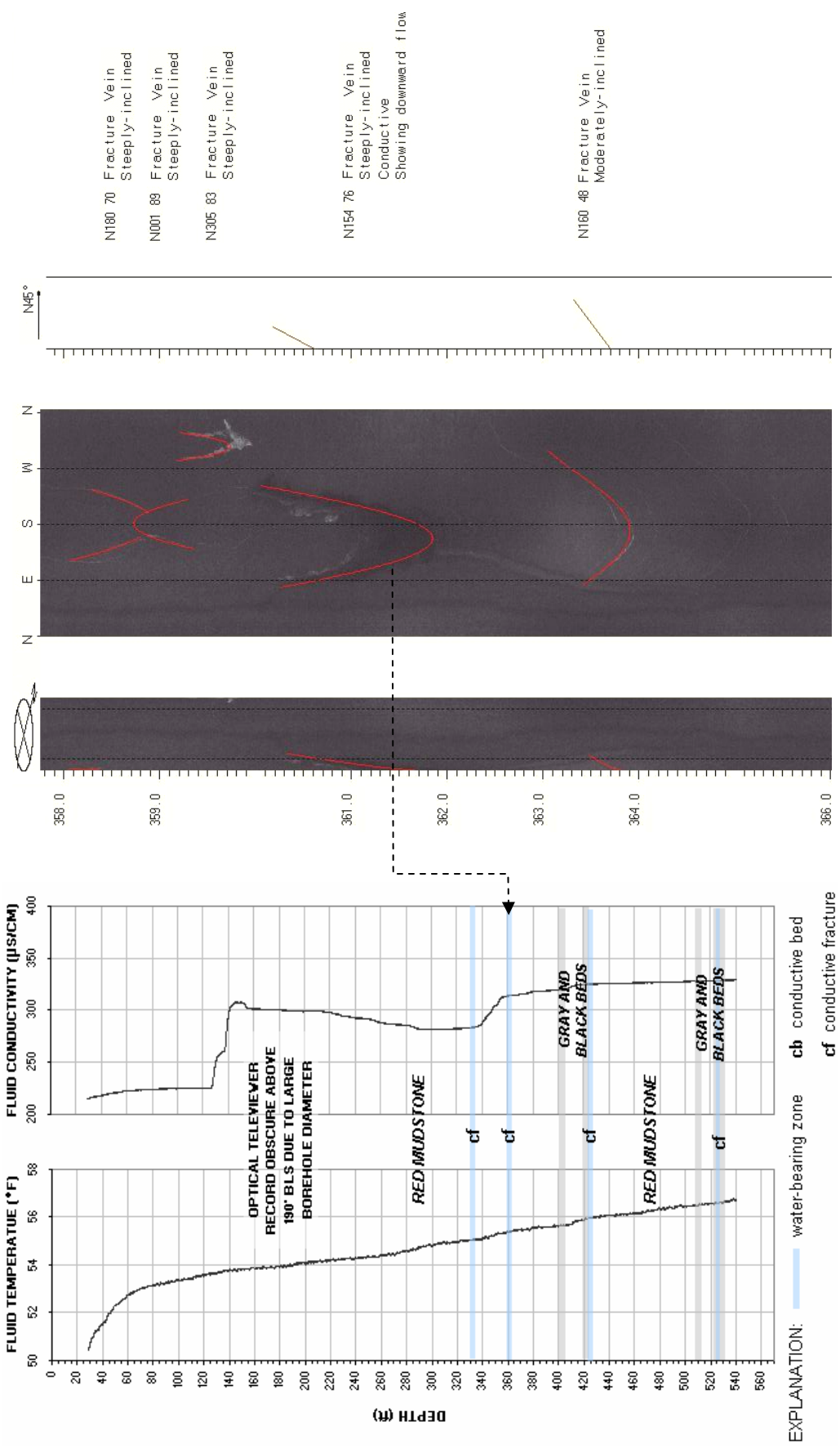

FIGURE 3M18. Hydrogeologic section (left) based on geophysical logs for well 99 at the Honey Brook Organic Farm, Wargo Rd., Hopewell Twp., Mercer County, NJ. The section shows the vertical distribution and types of hydraulically-conductive features and water-bearing zones in red and gray mudstone and gray and black shale. OPTV record (right) shows geologic structures and hydraulically-conductive fractures in red mudstone. Downward-tapering mineral stain on borehole wall indicates downward, non-pumping flow. Depth values are in feet below land surface.

Wells 90 to 104 - Brunswick lower red and lower gray zones

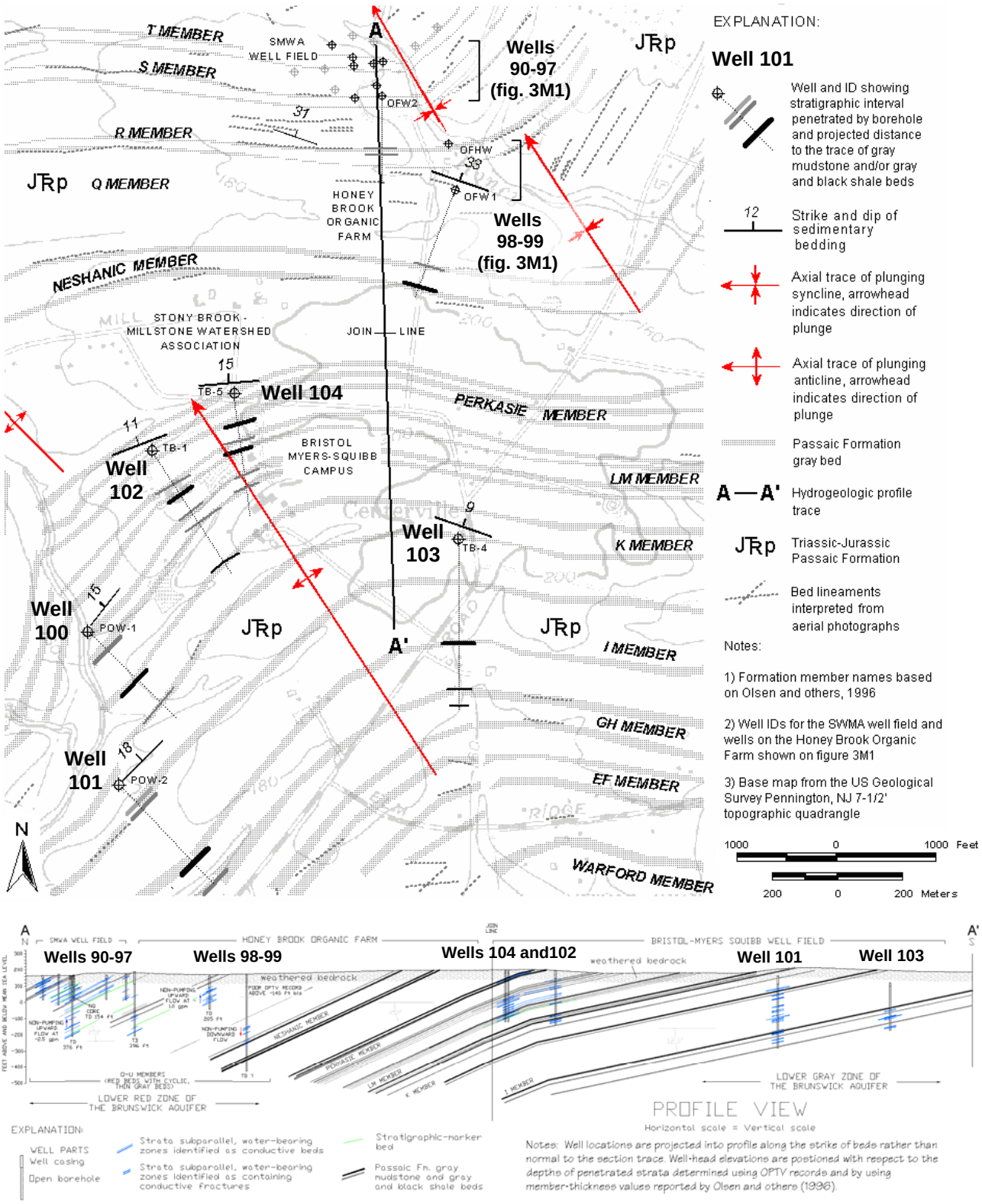

Figure 3N1. Map (above) shows wells 100 to 104 at the Bristol-Myers Squibb campus in Hopewell Twp., Mercer County, NJ in relation to wells at the Stony Brook-Millstone Watershed Association (SMWA) and the Honey Brook Organic Farm (Fig. 3M1). Details of hydrogeologic profile A-A' (below) are shown in figure 3N2.

Wells 90 to 104 - Brunswick lower red and lower gray zones

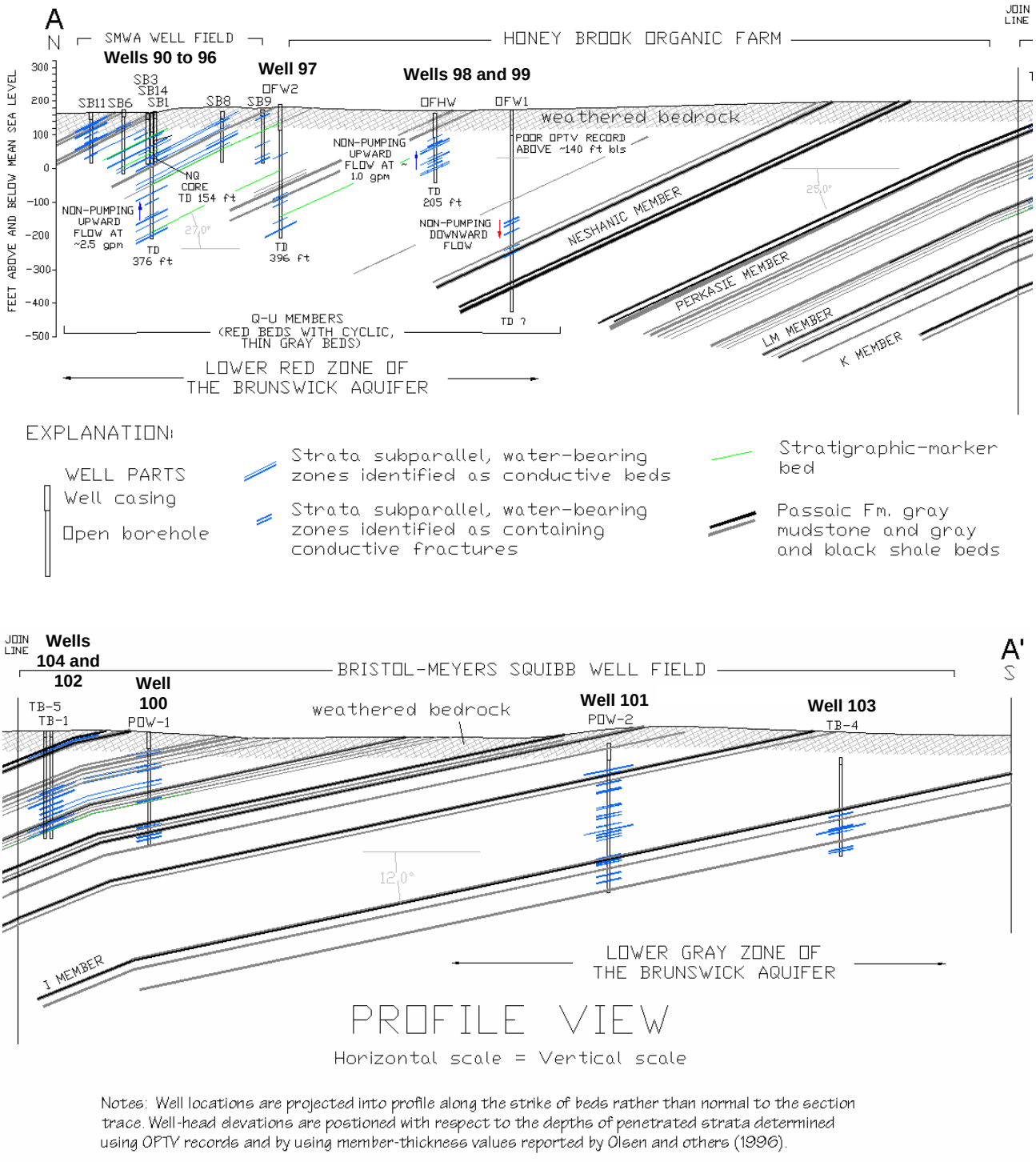

Notes: Well locations are projected into profile along the strike of beds rather than normal to the section trace. Well-head elevations are postioned with respect to the depths of penetrated strata determined using OPTV records and by using member-thickness values reported by Olsen and others (1996).

Figure 3N2. Hydrogeologic section A-A' for well fields at the Stony Brook-Millstone Watershed Association and Honey Brook Organic Farm (above) and the Bristol-Myers Squibb campus in Hopewell Twp., Mercer County NJ. The profile location and a composite section are shown in figure 3N1. The section shows the distribution of wells having OPTV records and stratigraphic water-bearing zones interpreted as conductive beds and fractures in the lower red (above) and lower gray (below) zones of the Brunswick aquifer. Stratigraphic-marker beds identified in OPTV records aid in positioning wells with respect to penetrated strata.

Wells 100 to 104 - Brunswick lower gray zone

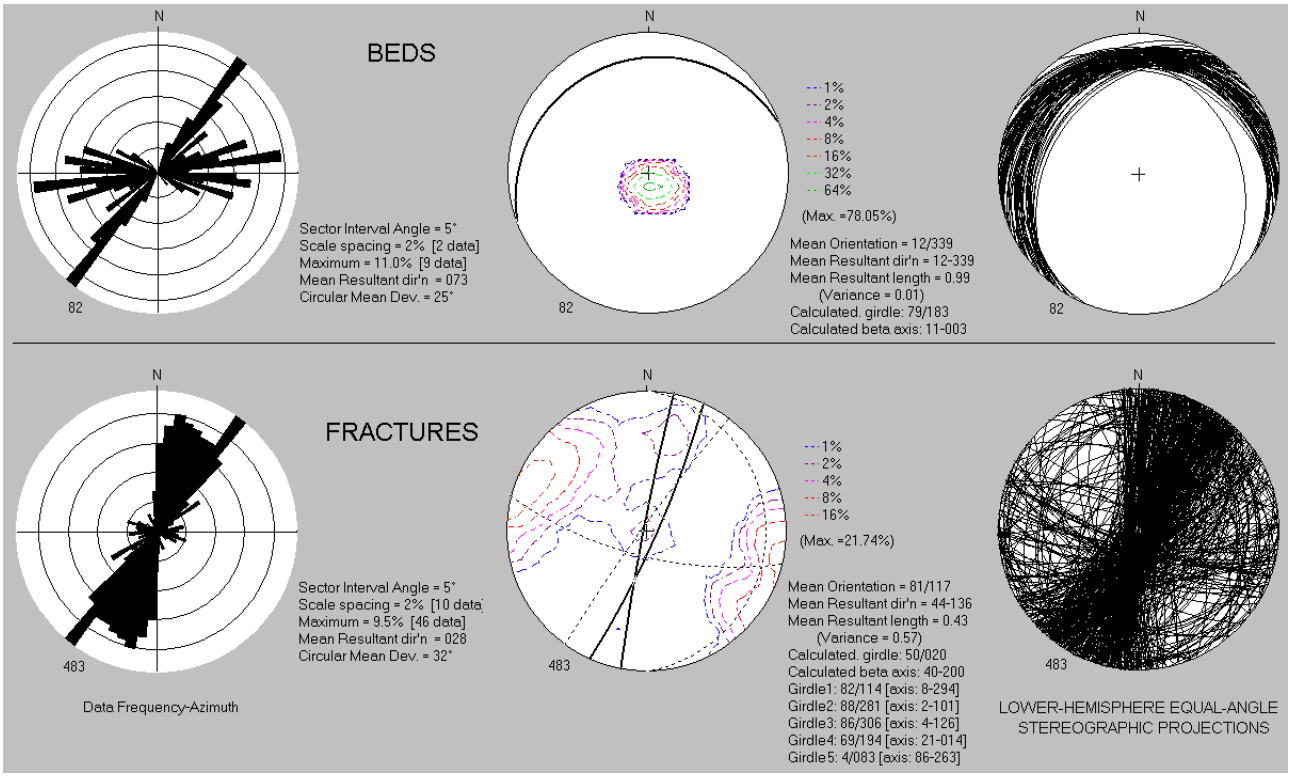

Wells 100 and 101 - Brunswick lower gray zone

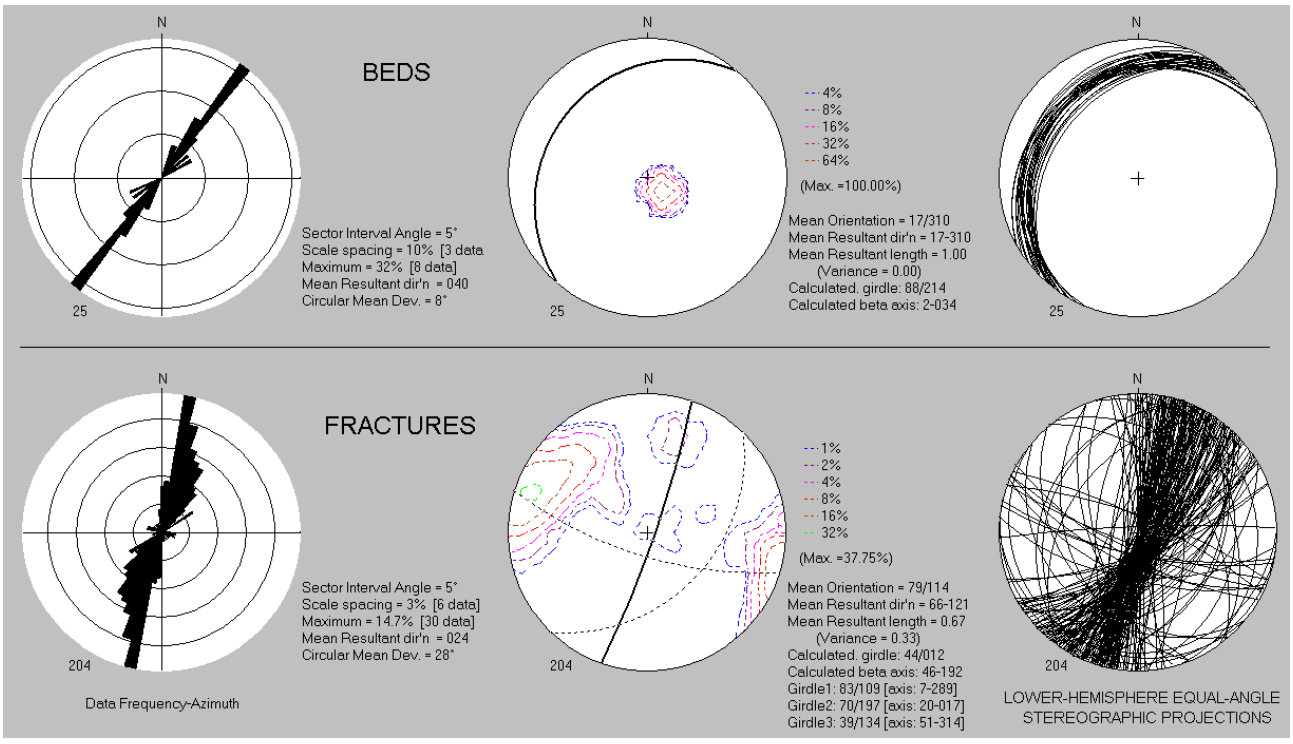

Figure 3N3. Structural analyses of OPTV for wells 100 to 104 (above) and wells 100 and 101 (below) at the Bristol-Myers Squibb campus in Hopewell Twp., Mercer County NJ.

Wells 102 and 104 - Brunswick lower gray zone

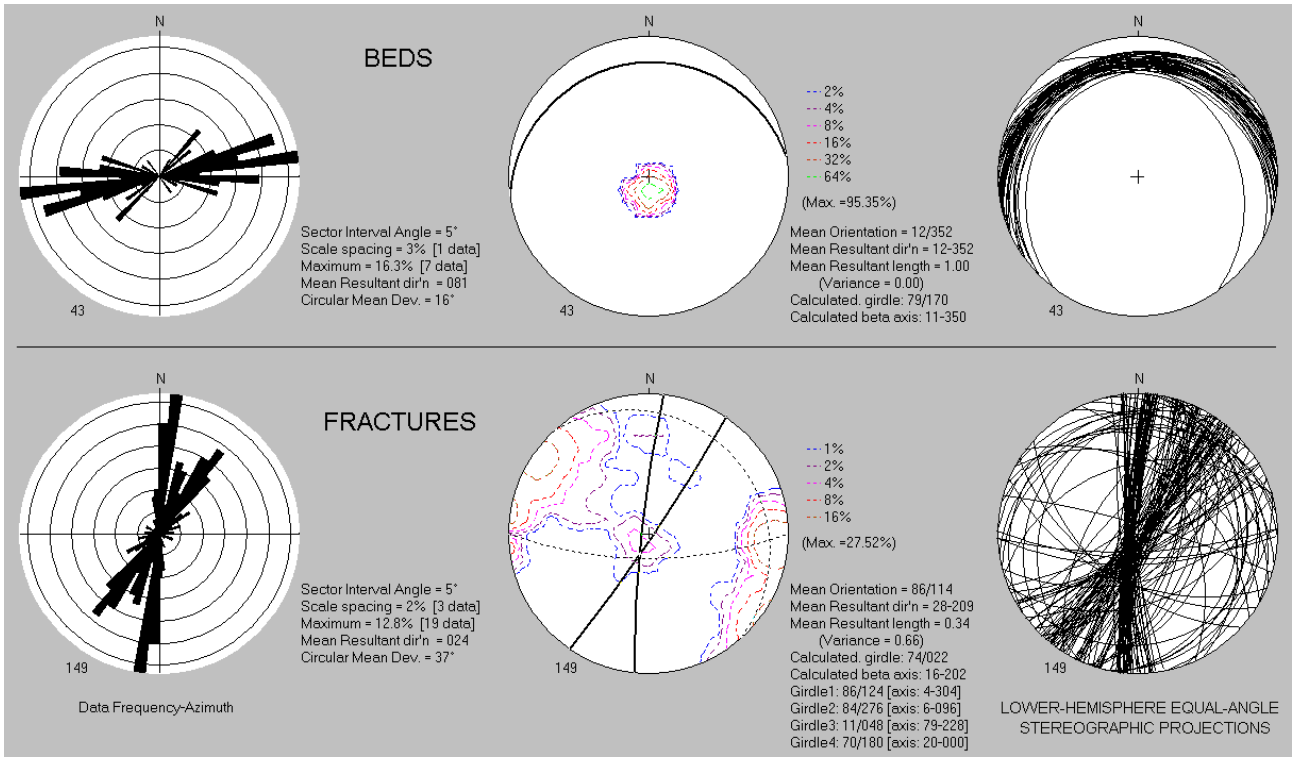

Well 103 - Brunswick lower gray zone

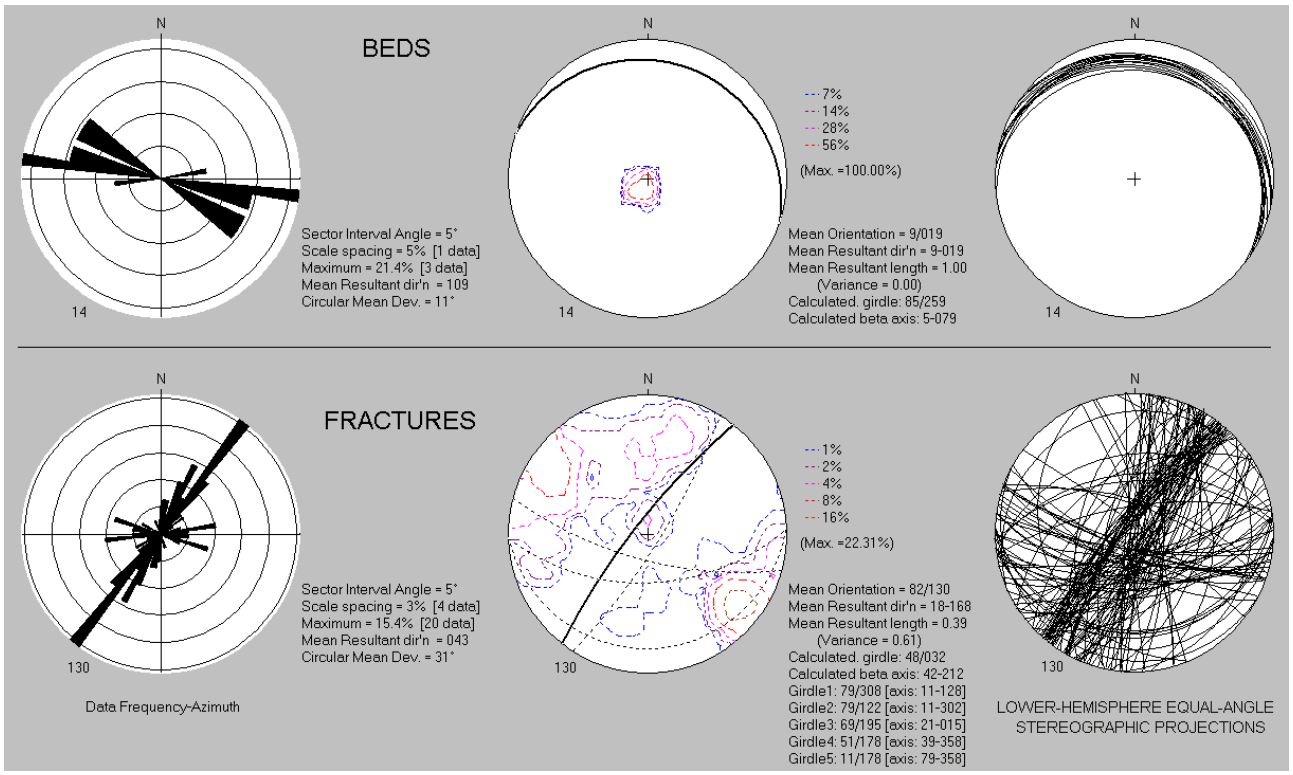

Figure 3N4. Structural analyses of OPTV for wells 100 and 104 (above) and wells 100 and 101 (below) at the Bristol-Myers Squibb campus in Hopewell Twp., Mercer County NJ.

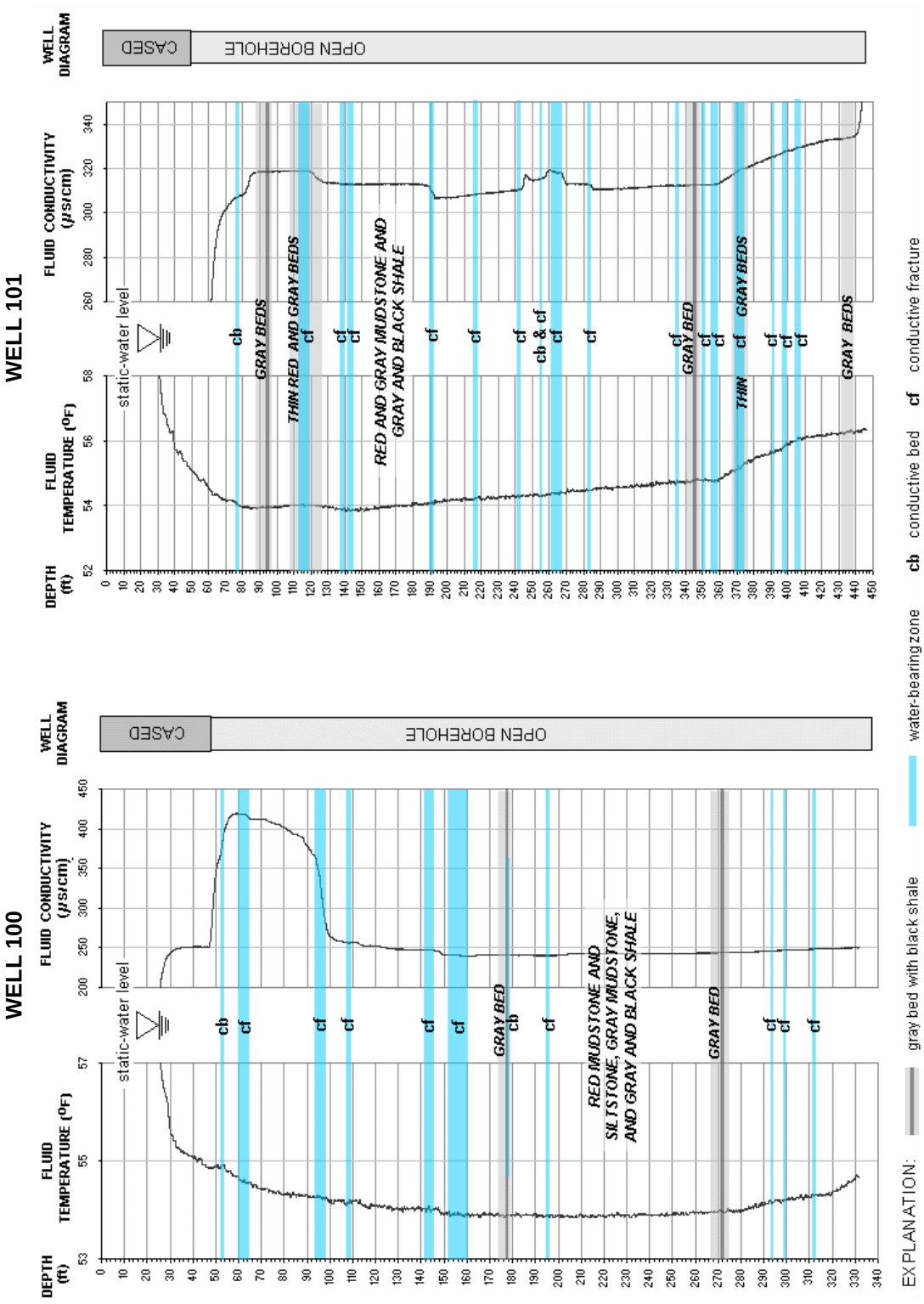

FIGURE 3N5. Hydrogeologic sections based on geophysical logs for wells 100 (left) and 101 (right) at the Bristol-Myers Squibb campus in Hopewell Twp., Mercer County NJ. The sections show the vertical distribution and types of hydraulically-conductive features and water-bearing zones in red mudstone and siltstone, gray mudstone, and gray and black shale. Depth values are in in feet below land surface.

Well 100 - Brunswick lower gray zone

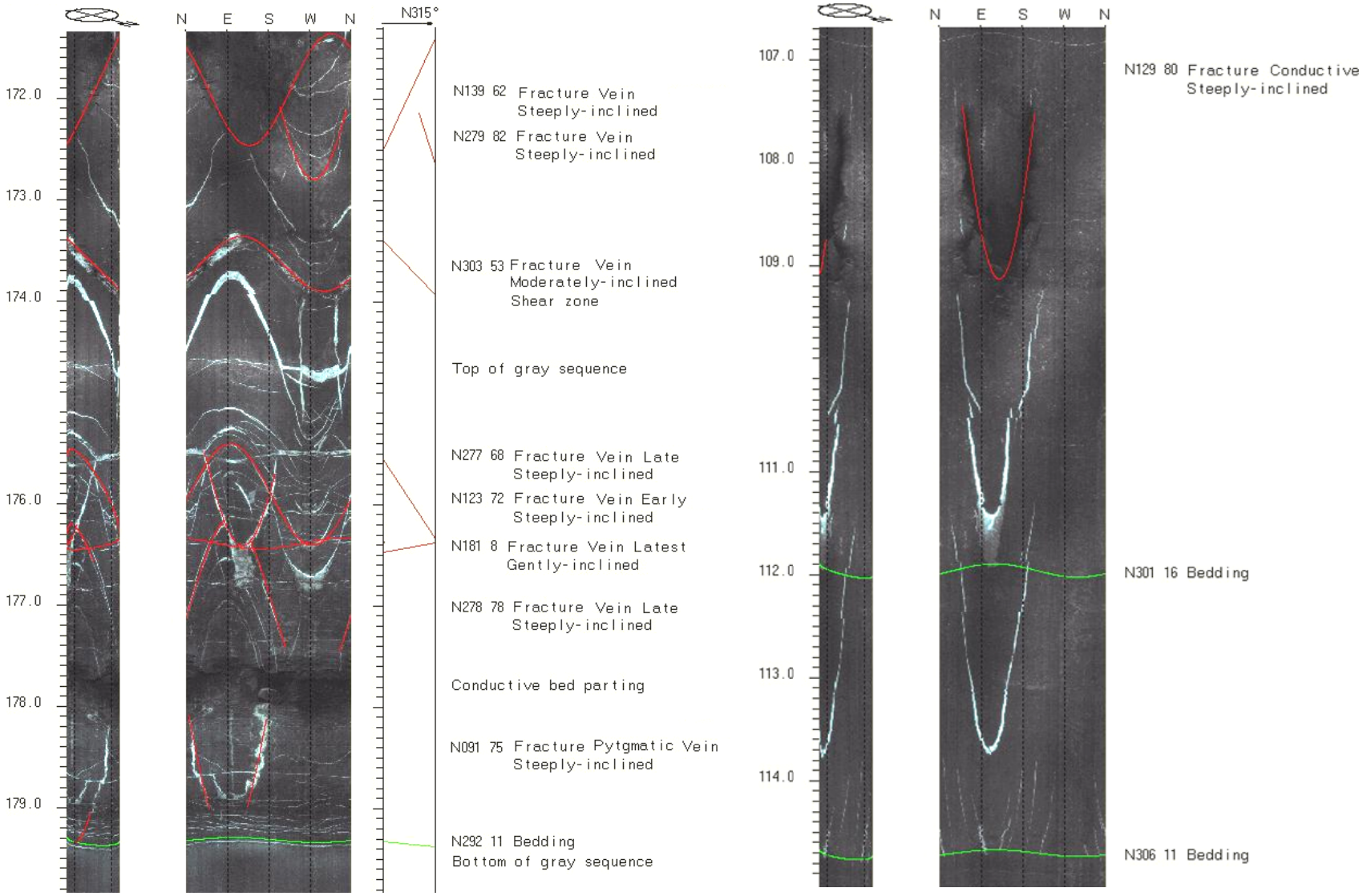

FIGURE 3N6. OPTV records of 6-inch diameter well 100 at the Bristol-Myers Squibb campus in Hopewell Twp., Mercer County NJ showing geologic structures and hydraulically-conductive features in red and gray mudstone and gray shale. Depth values are in feet below land surface.

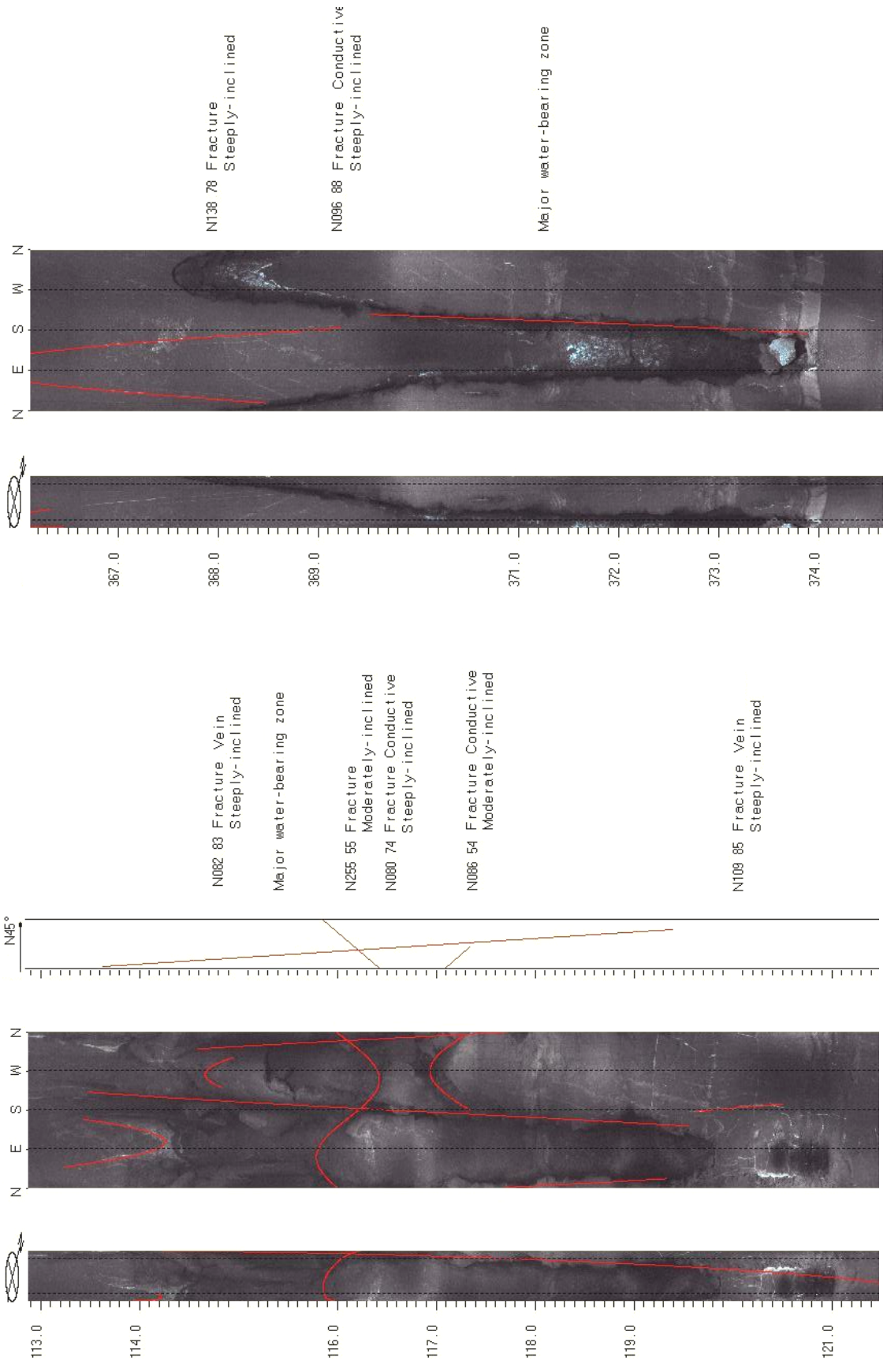

FIGURE 3N7. OPTV records of 6-inch diameter well 100 at the Bristol-Myers Squibb campus in Hopewell Twp., Mercer County NJ showing geologic structures and hydraulically-conductive features in red and gray mudstone and gray shale. Depth values are in feet below land surface.

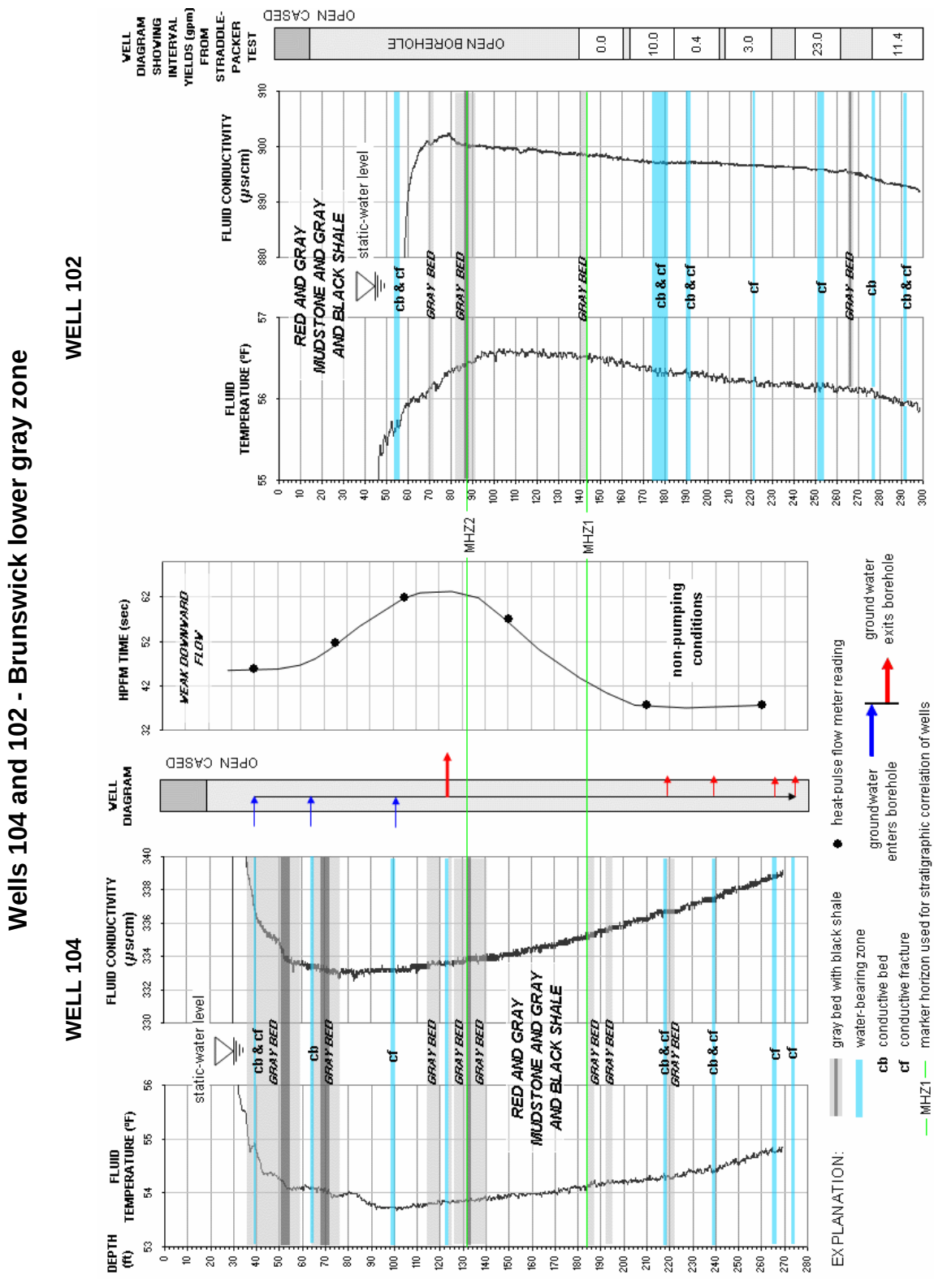

FIGURE 3N8. Hydrogeologic sections based on geophysical logs for wells 104 and 102 at the Bristol-Myers Squibb campus in Hopewell Twp., Mercer County NJ. The sections show the vertical distribution and types of hydraulically-conductive features and water-bearing zones in red and gray mudstone and gray and black shale. Depth values are feet below land surface.

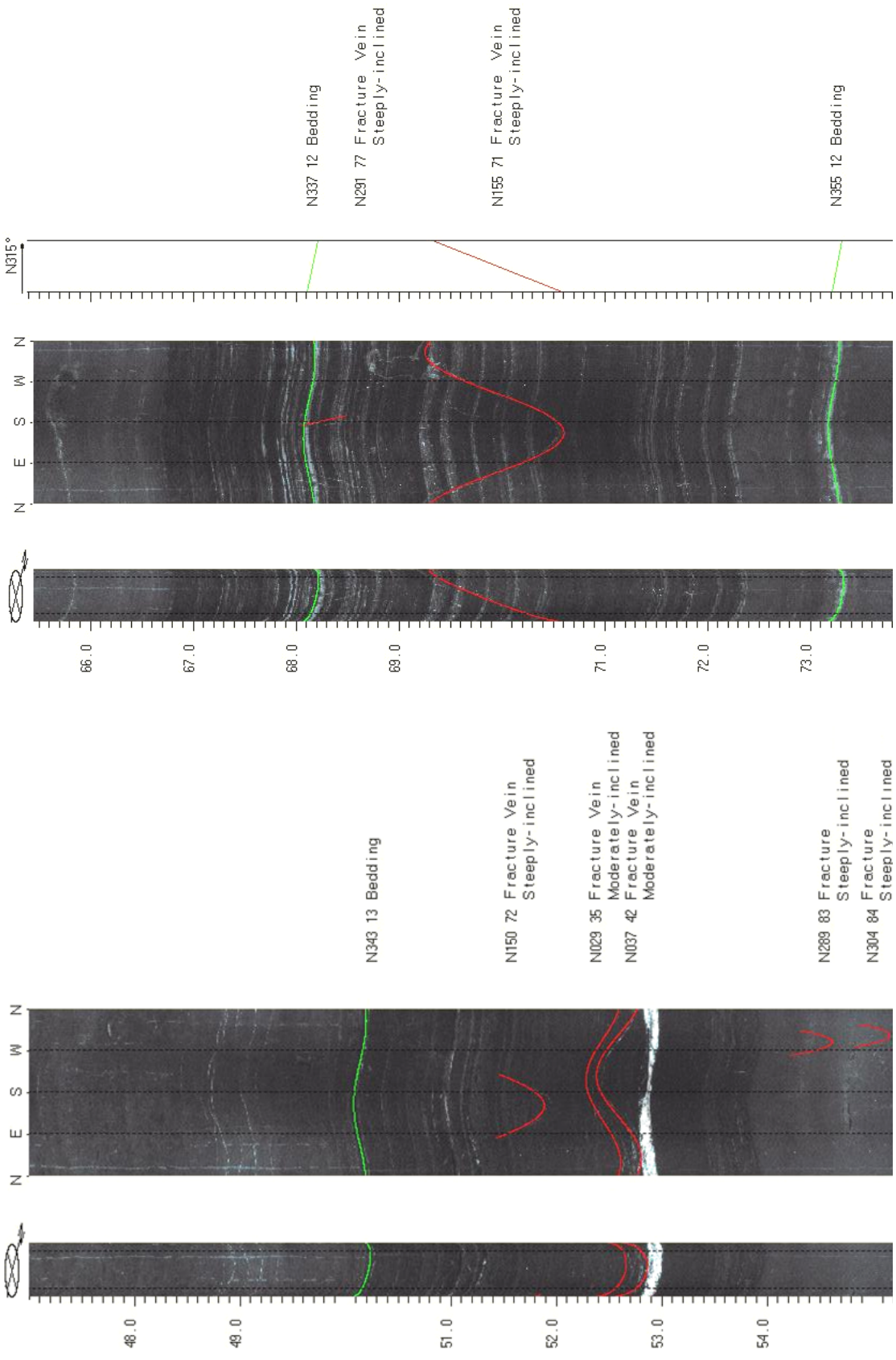

FIGURE 3N9. OPTV records of 6-inch diameter well 104 at the Bristol-Myers Squibb campus in Hopewell Twp., Mercer County NJ showing geologic structures in gray mudstone and gray and black shale. Depth values are in feet below land surface.

Well 102 - Brunswick lower gray zone

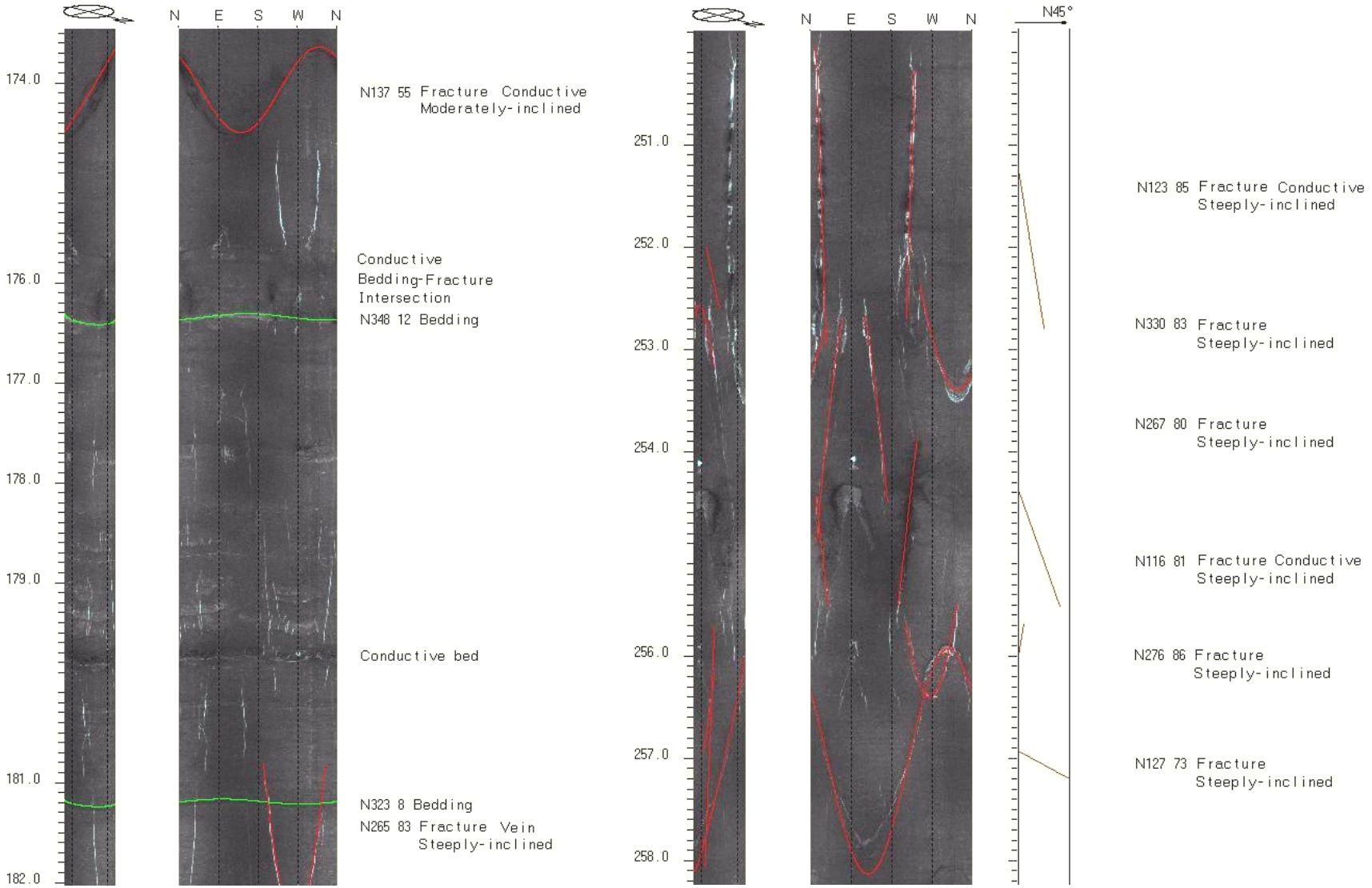

FIGURE 3N10. OPTV records of 6-inch diameter well 102 at the Bristol-Myers Squibb campus in Hopewell Twp., Mercer County NJ showing geologic structures and hydraulically-conductive features in red and gray mudstone. Depth values are in feet below land surface.

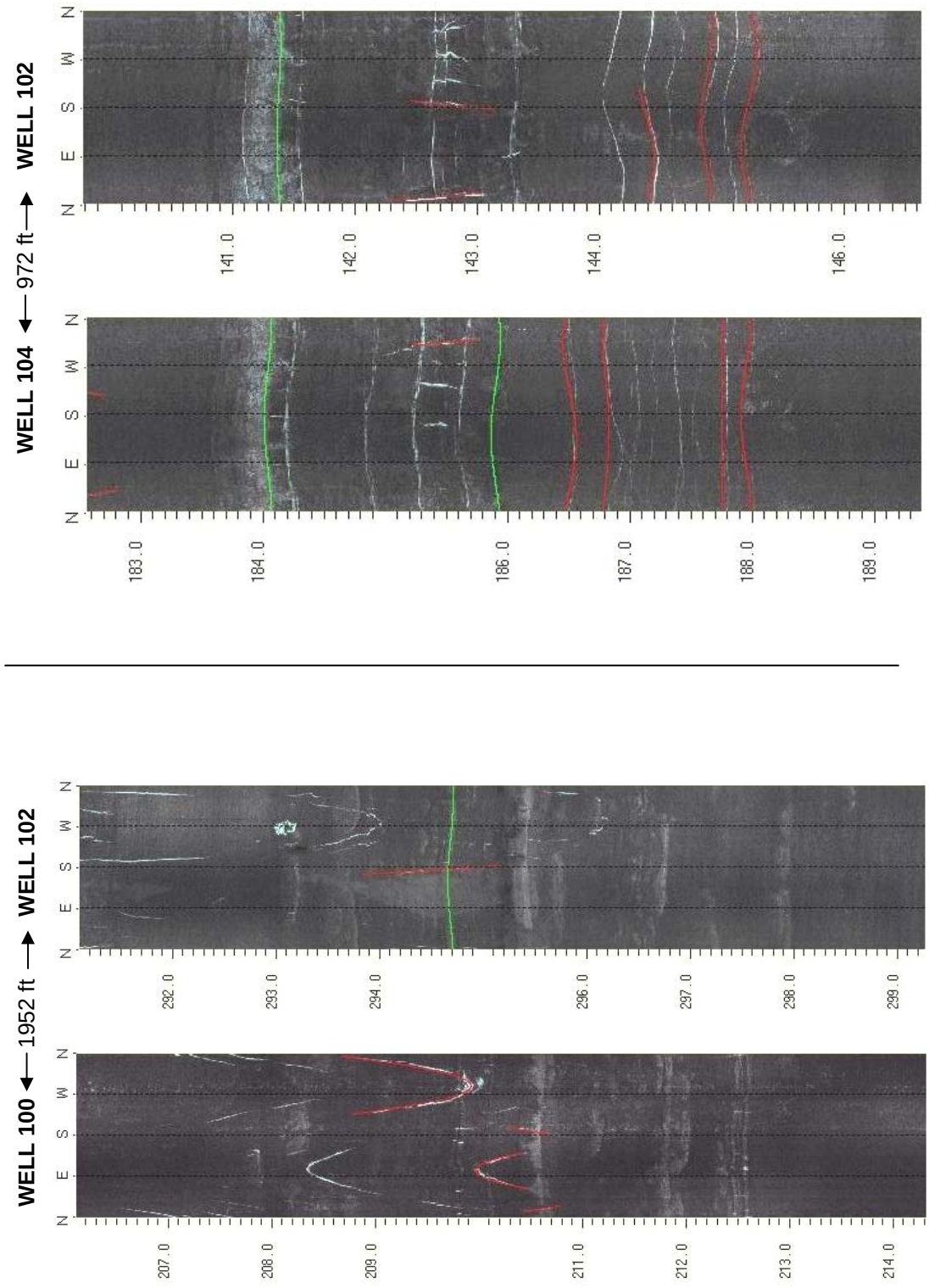

FIGURE 3N11. Stratigraphic correlation of wells 100, 102., and 104 based on OPTV records from the Bristol-Myers Squibb campus in Hopewell Twp., Mercer County NJ. Depth values are in feet below land surface.

Wells 101 and 103 - Brunswick lower gray zone

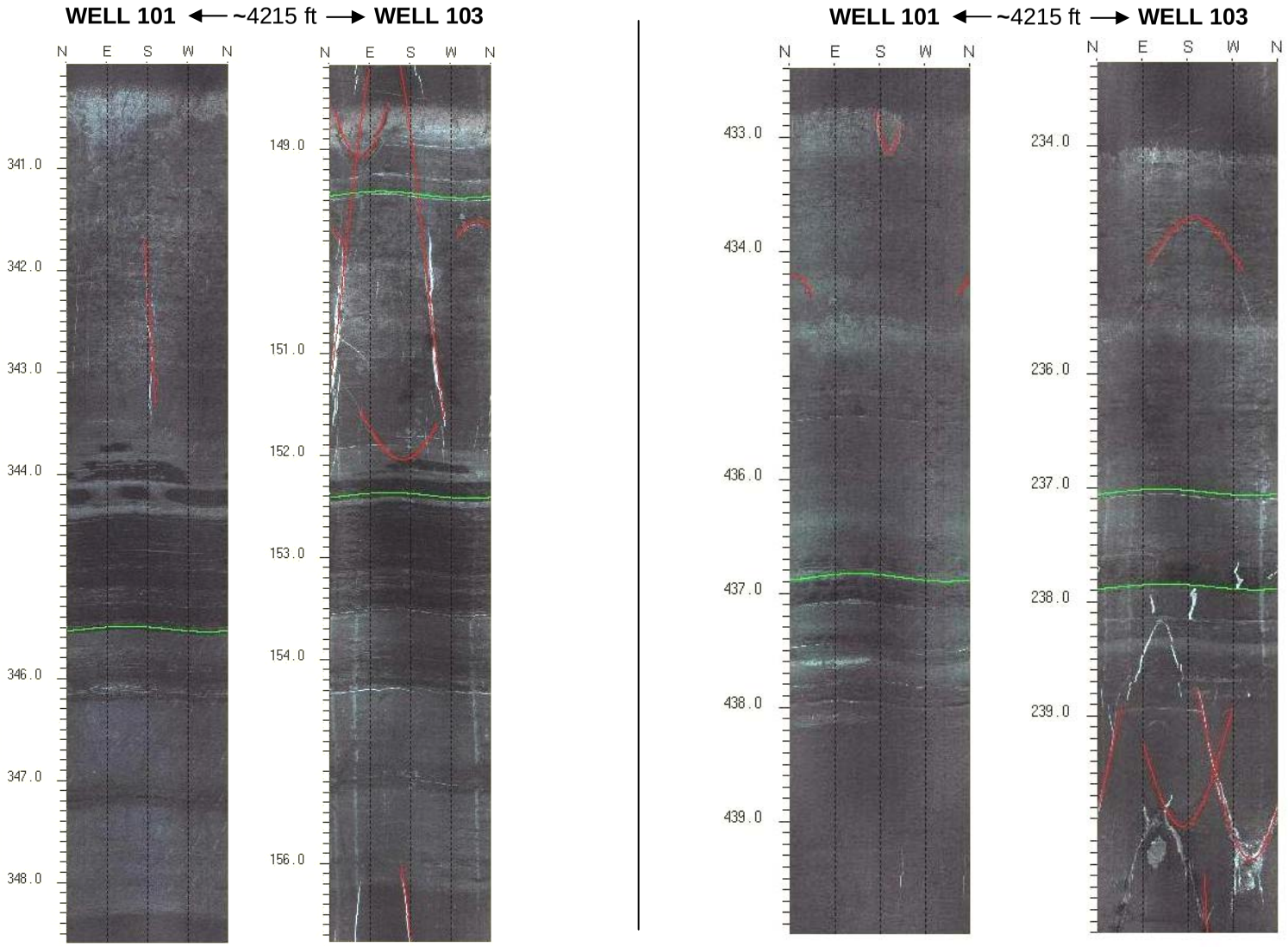

FIGURE 3N12. Stratigraphic correlation of wells 101 and 103 based on OPTV records from the Bristol-Myers Squibb campus in Hopewell Twp., Mercer County NJ. Depth values are in feet below land surface.

Wells 103 - Brunswick lower gray zone

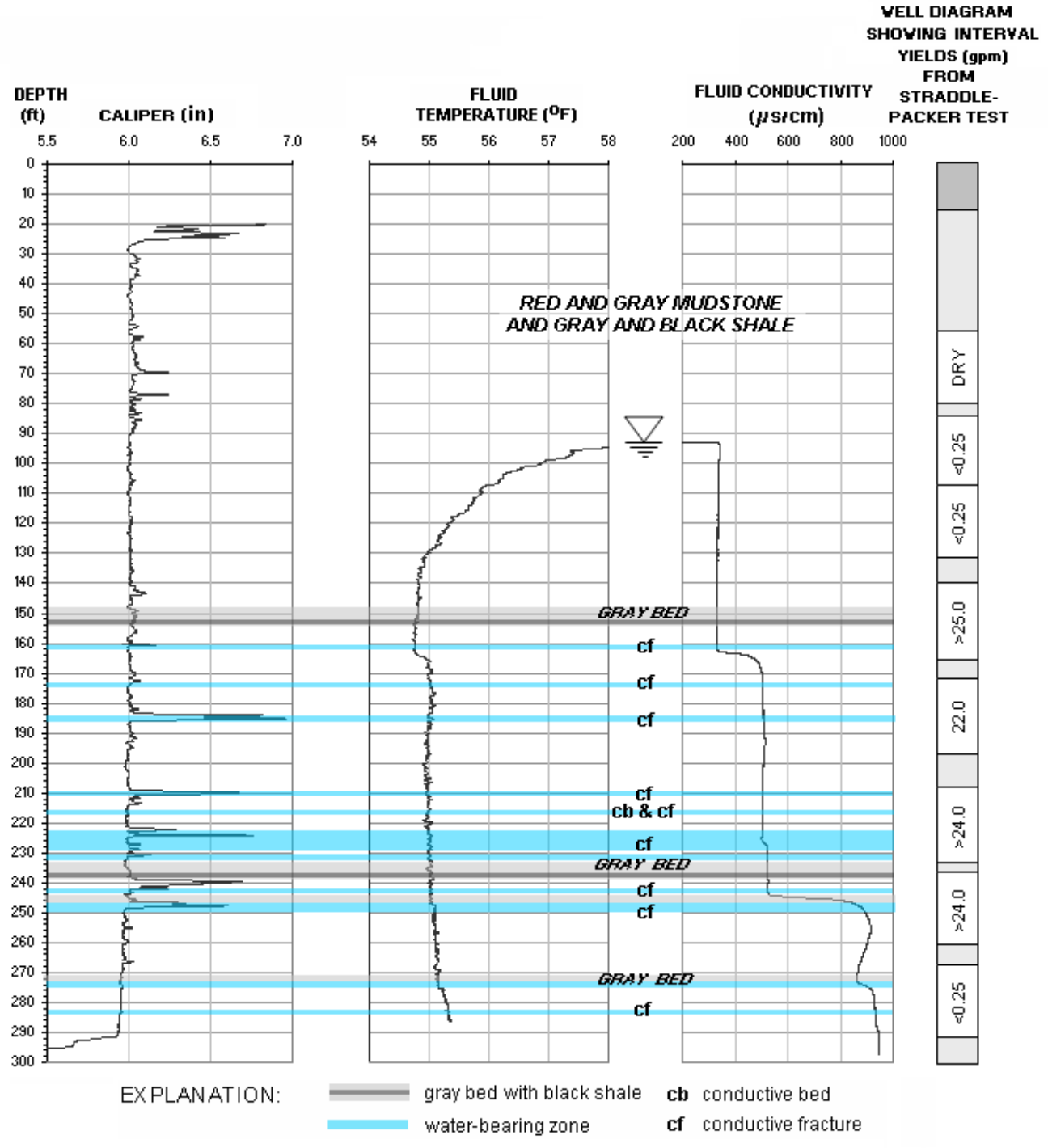

FIGURE 3N13. Hydrogeologic section based on geophysical logs for well 103 at the Bristol-Myers Squibb campus in Hopewell Twp., Mercer County NJ. The section shows the vertical distribution and types of hydraulically-conductive features and water-bearing zones in red and gray mudstone and gray and black shale. Depth values are in feet below land surface.

Well 103 - Brunswick lower gray zone

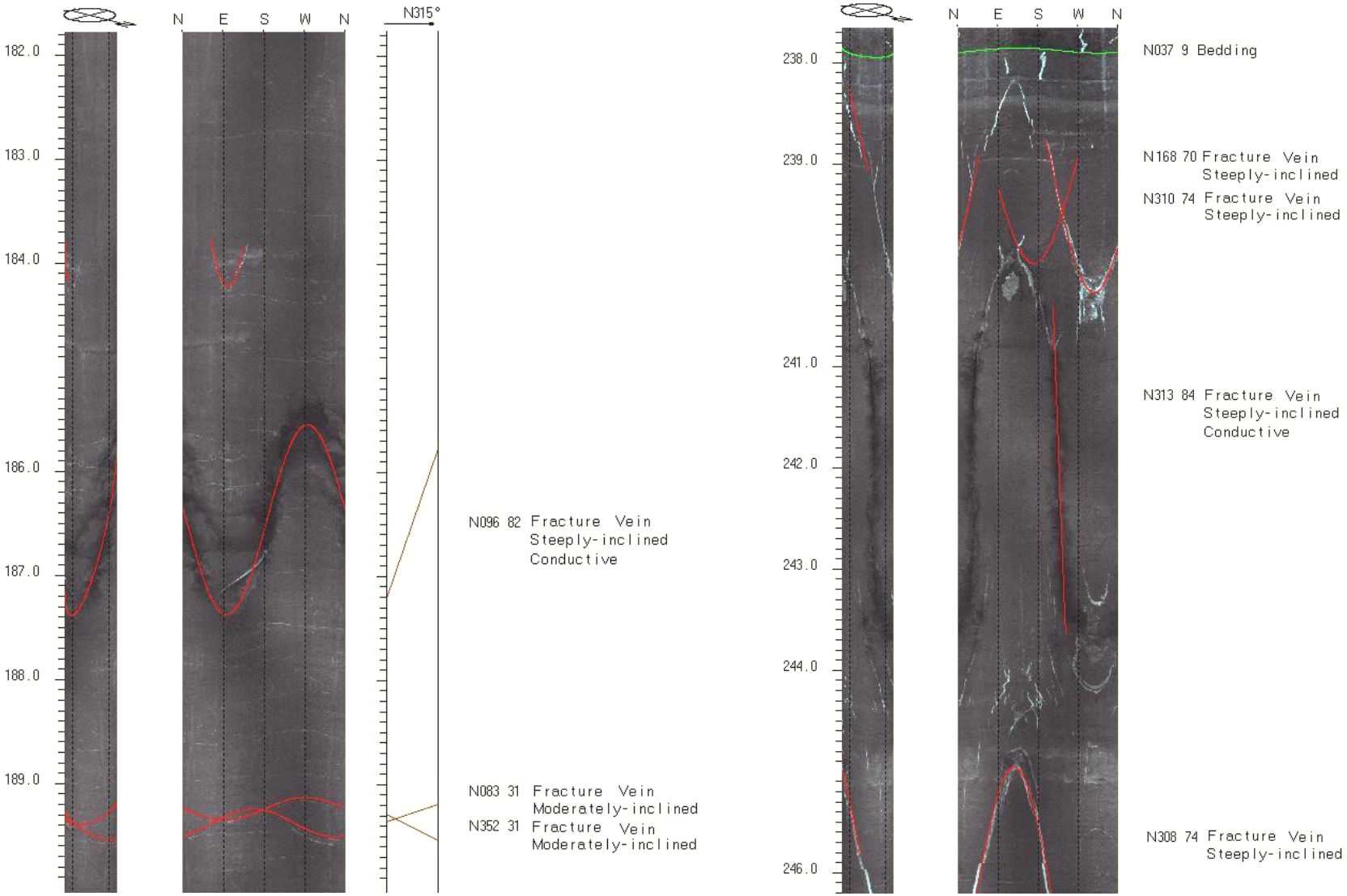

FIGURE 3N14. OPTV records of 6-inch diameter well 103 at the Bristol-Myers Squibb campus in Hopewell Twp., Mercer County NJ showing geologic structures and hydraulically-conductive features in red and gray mudstone and gray shale. Depth values are in feet below land surface.

Well 105 - Brunswick lower gray zone

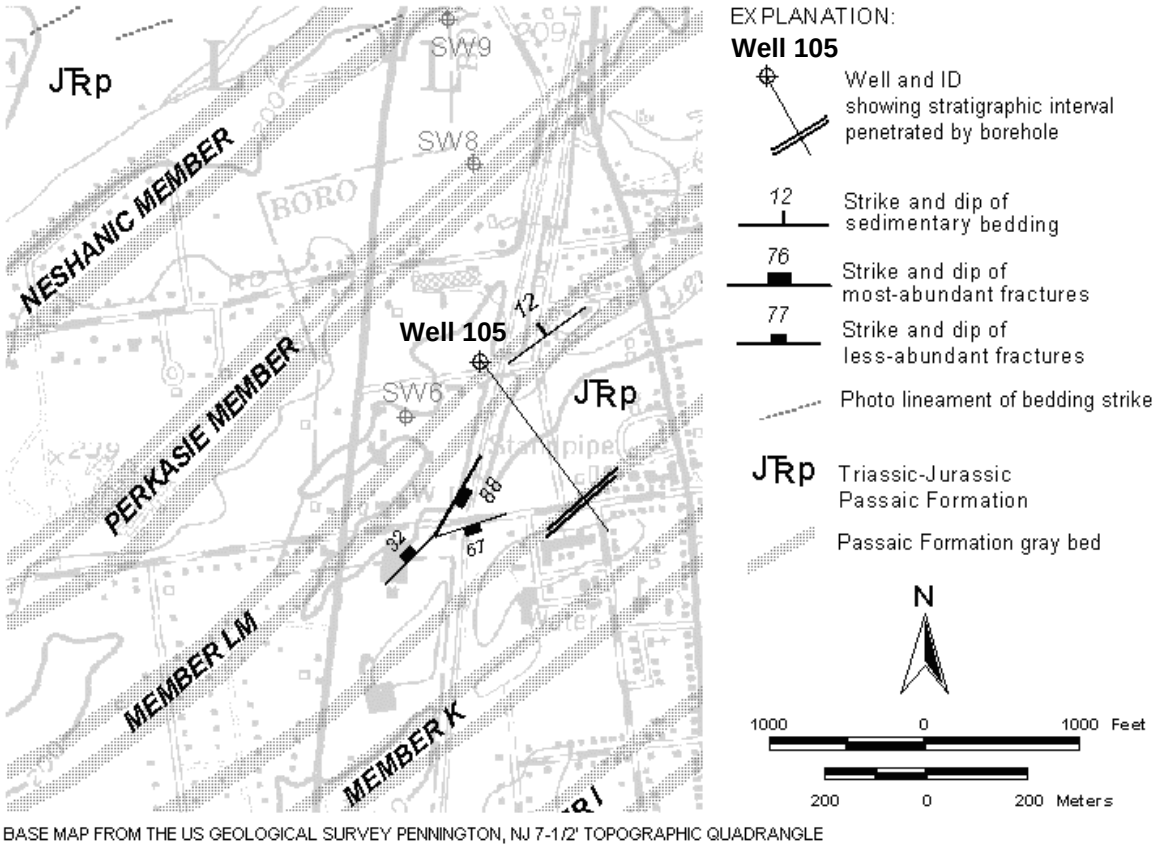

BASE MAP FROM THE US GEOLOGICAL SURVEY PENNINGTON, NJ 7-1/2' TOPOGRAPHIC QUADRANGLE

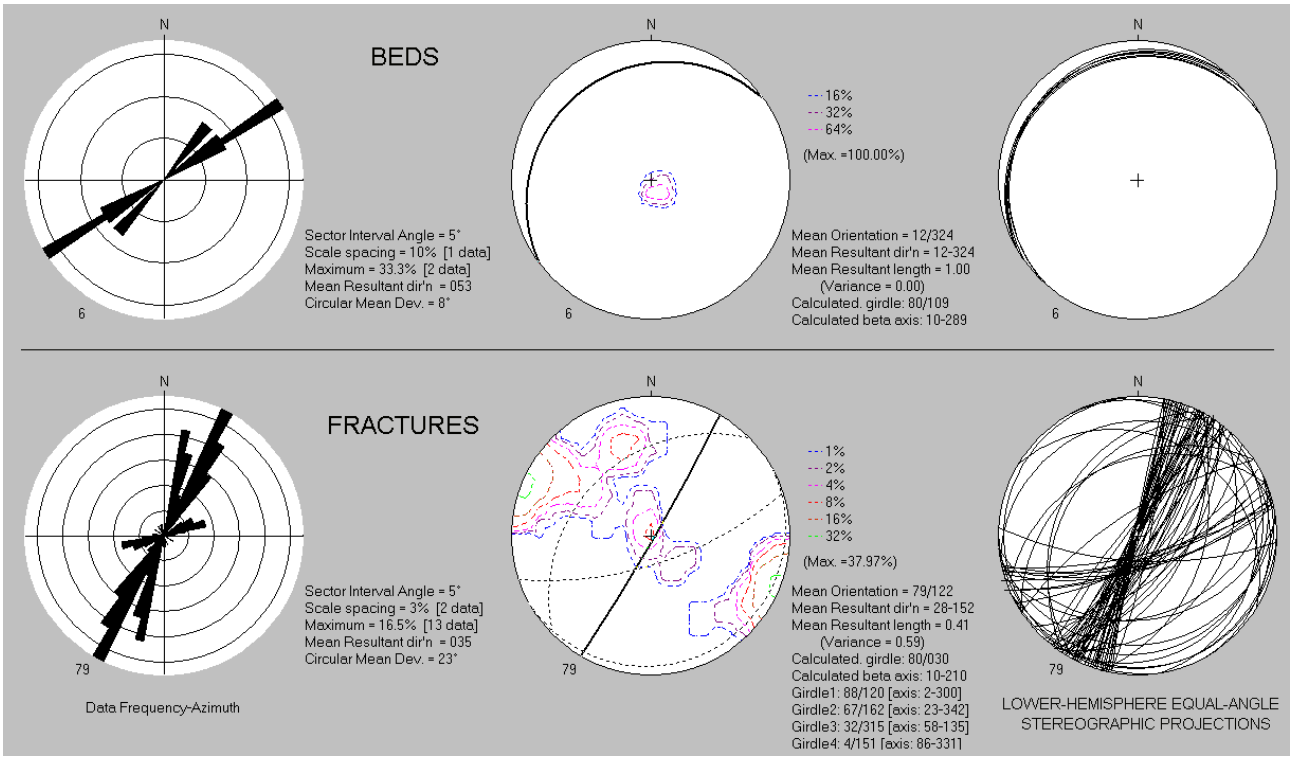

Figure 3O1. Map (above) showing well 105 in Pennington Boro, Mercer County, NJ. Bedrock structures mapped near wells based on a structural analysis of OPTV data (below).

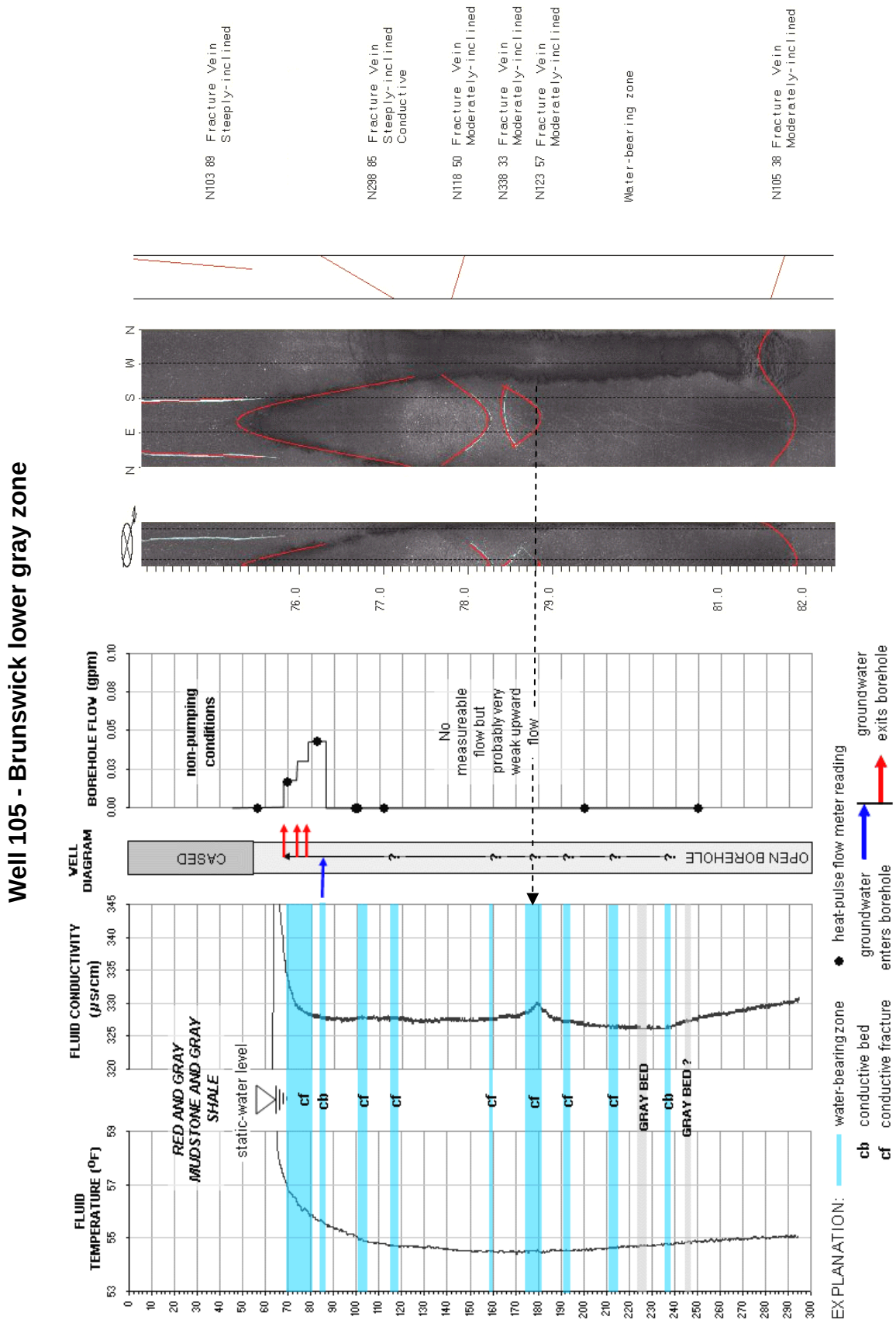

FIGURE 3O2. Hydrogeologic section (left) based on geophysical logs for well 105 in Pennington Boro, Mercer County, NJ, The section shows the vertical distribution and types of hydraulically-conductive features and water-bearing zones in red mudstone. OPTV record (right) shows geologic structures and hydraulically-conductive fracture. Depth values are in feet below land surface.

Wells 106 and 107 - Brunswick lower gray zone

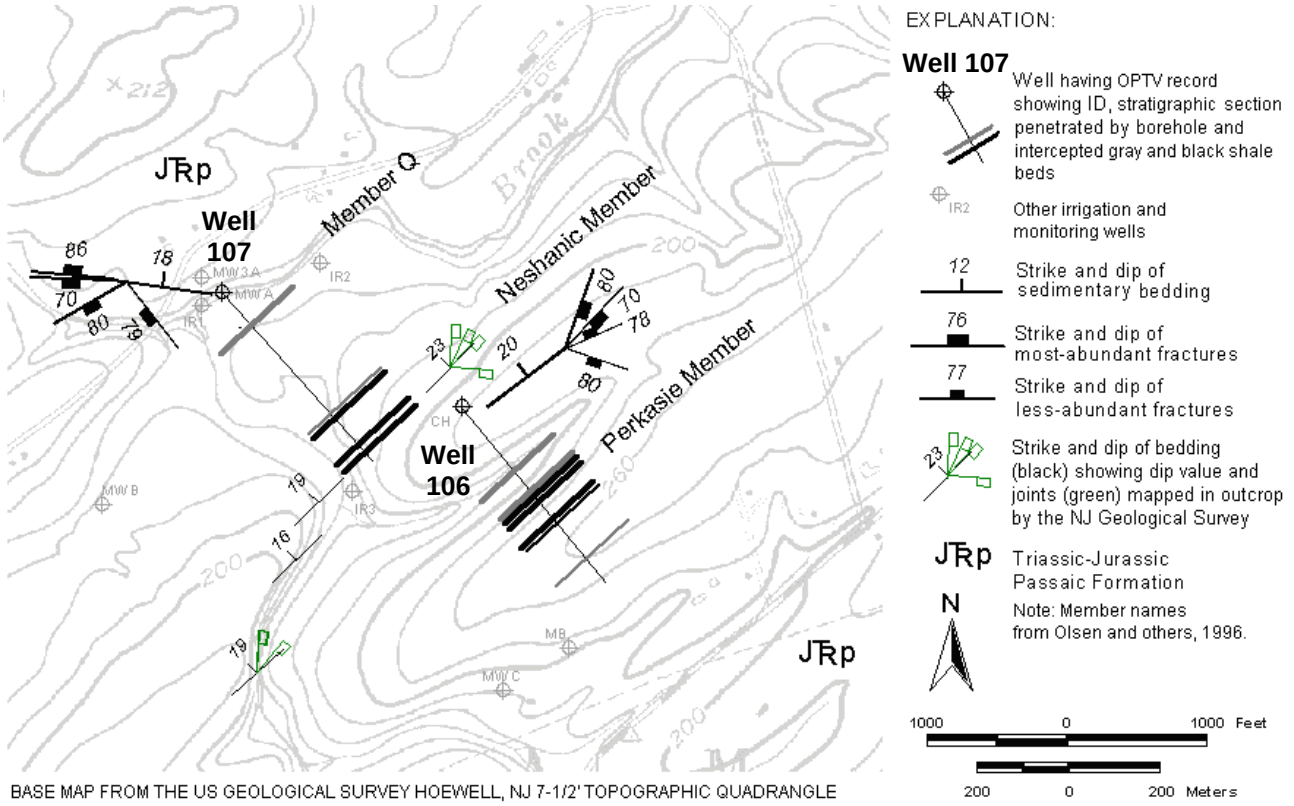

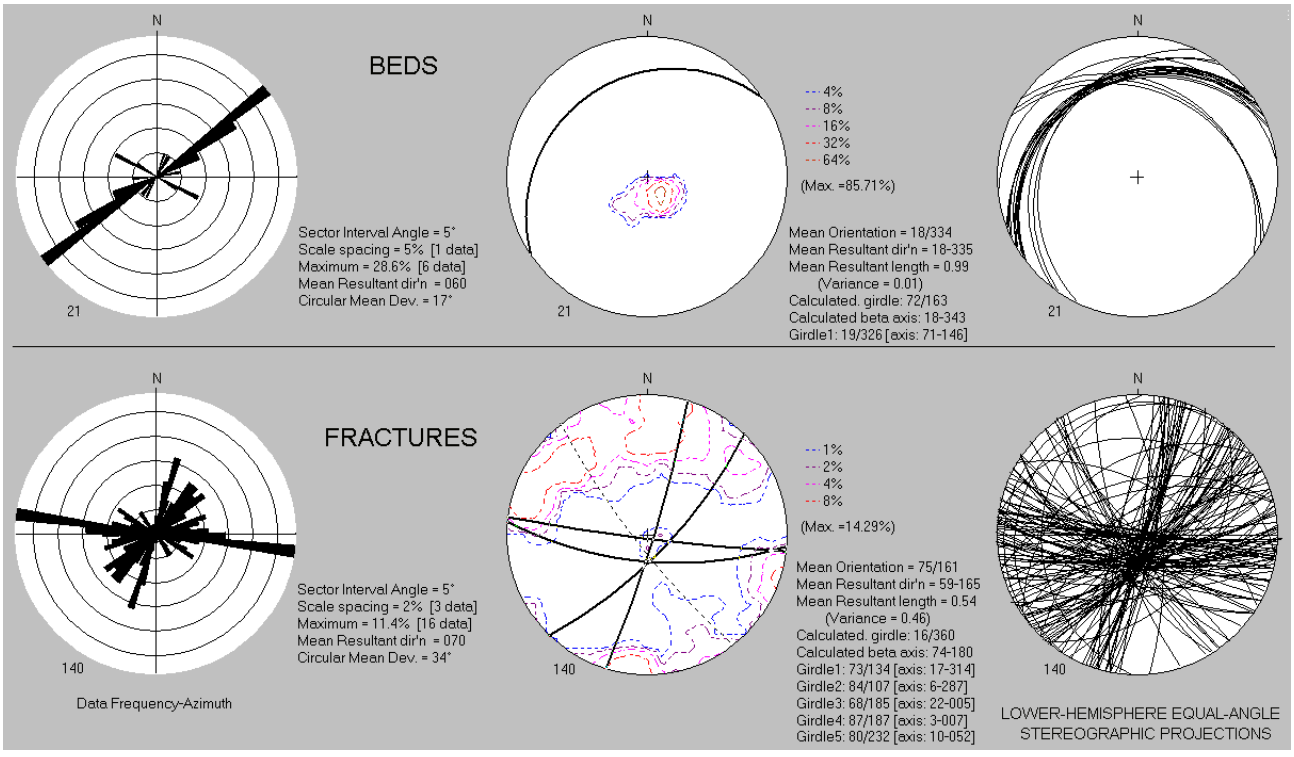

Figure 3P1. Map (above) showing wells 106 and 107 at the Ridge Golf Club, East Amwell Twp., Hunterdon County, NJ. Bedrock structures mapped near wells based on a structural analysis of OPTV data (below).

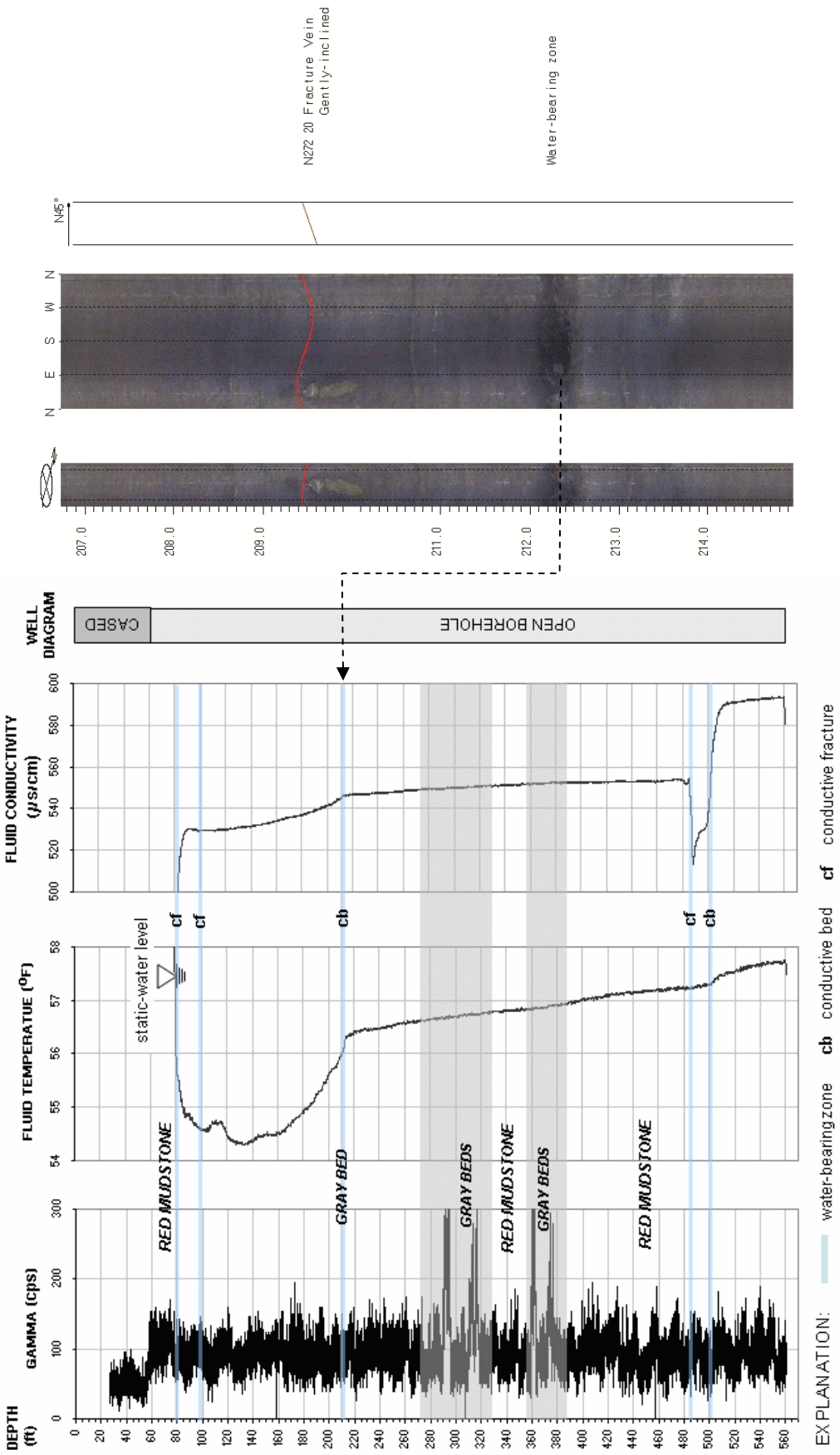

FIGURE 3P2. Hydrogeologic section (left) based on geophysical logs for well 106 at the Ridge Golf Club, East Amwell Twp., Hunterdon County, NJ., The section shows the vertical distribution and types of hydraulically-conductive features and water-bearing zones in red and gray mudstone and gray and black shale. OPTV record (right) shows geologic structures and a hydraulically-conductive bed. Depth values are in feet below land surface.

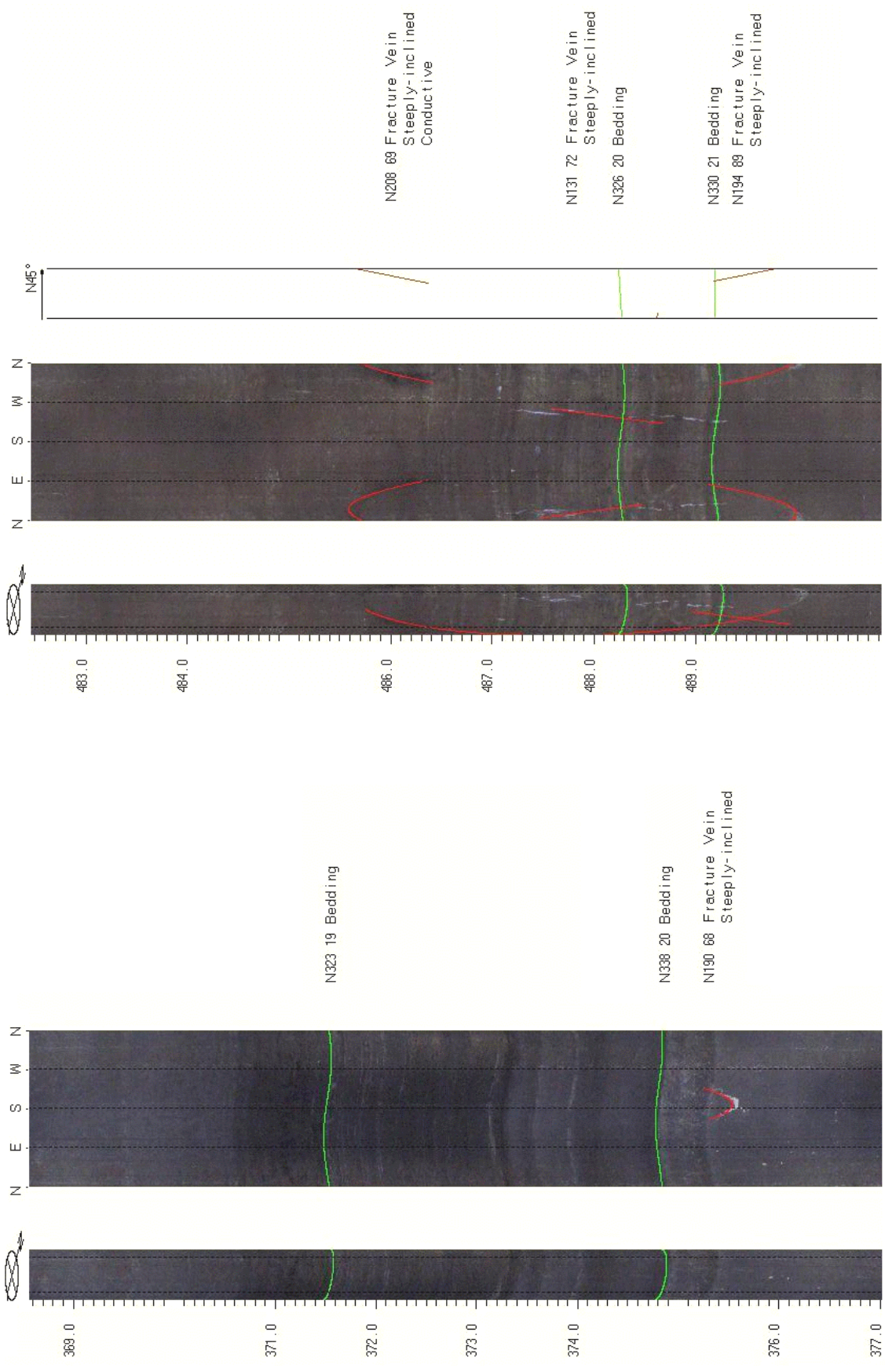

FIGURE 3P3. OPTV records of 6-inch diameter well 106 at the Ridge Golf Club, East Amwell Twp., Hunterdon County, NJ, showing geologic structures and hydraulically-conductive features in red and gray mudstone and gray and black shale. Depth values are in feet below land surface.

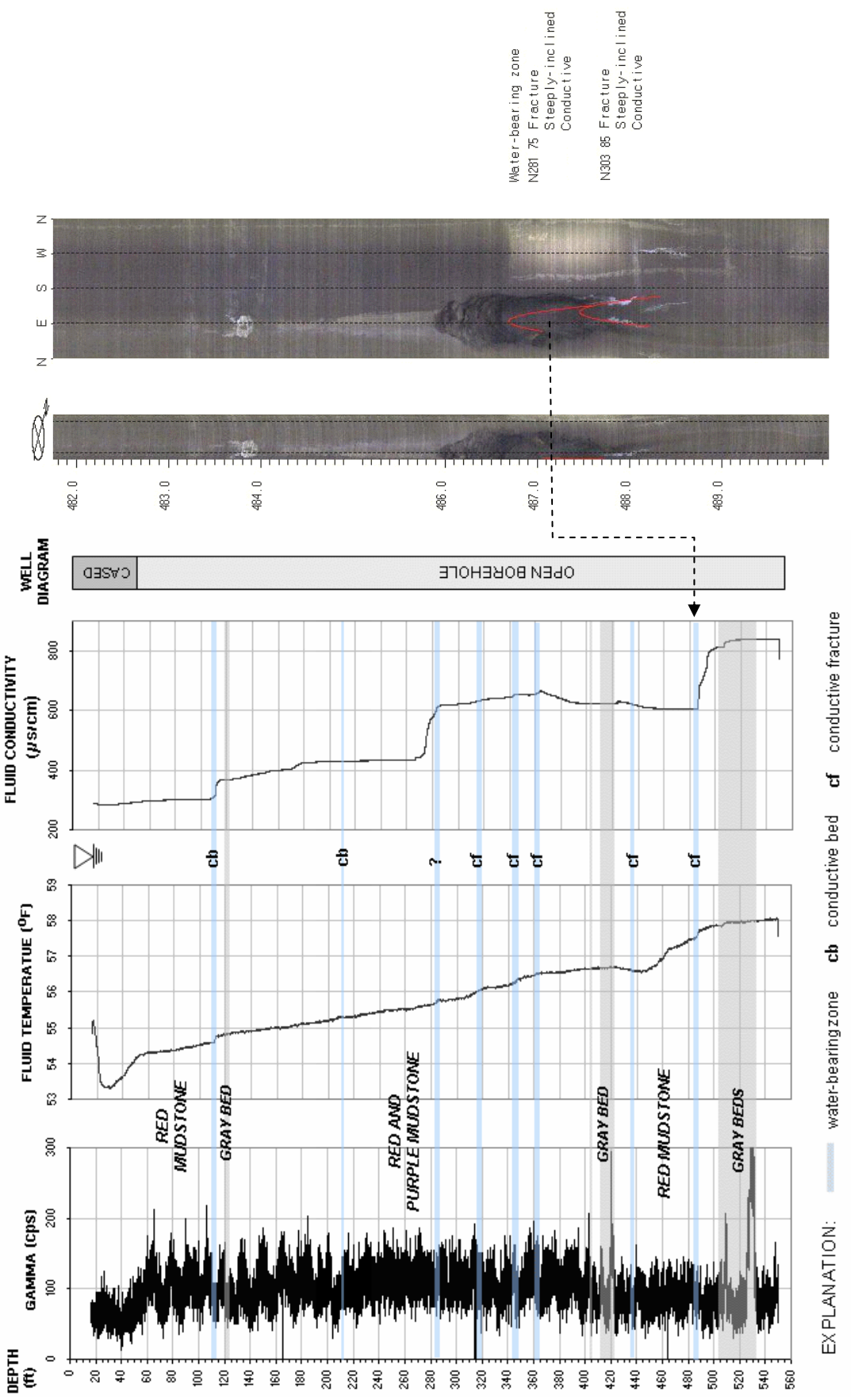

FIGURE 3P4. Hydrogeologic section (left) based on geophysical logs for well 107 at the Ridge Golf Club, East Amwell Twp., Hunterdon County, NJ. The section shows the vertical distribution and types of hydraulically-conductive features and water-bearing zones in red and gray mudstone and gray and black shale. OPTV record (right) shows hydraulically-conductive fracture. Depth values are in feet below land surface.

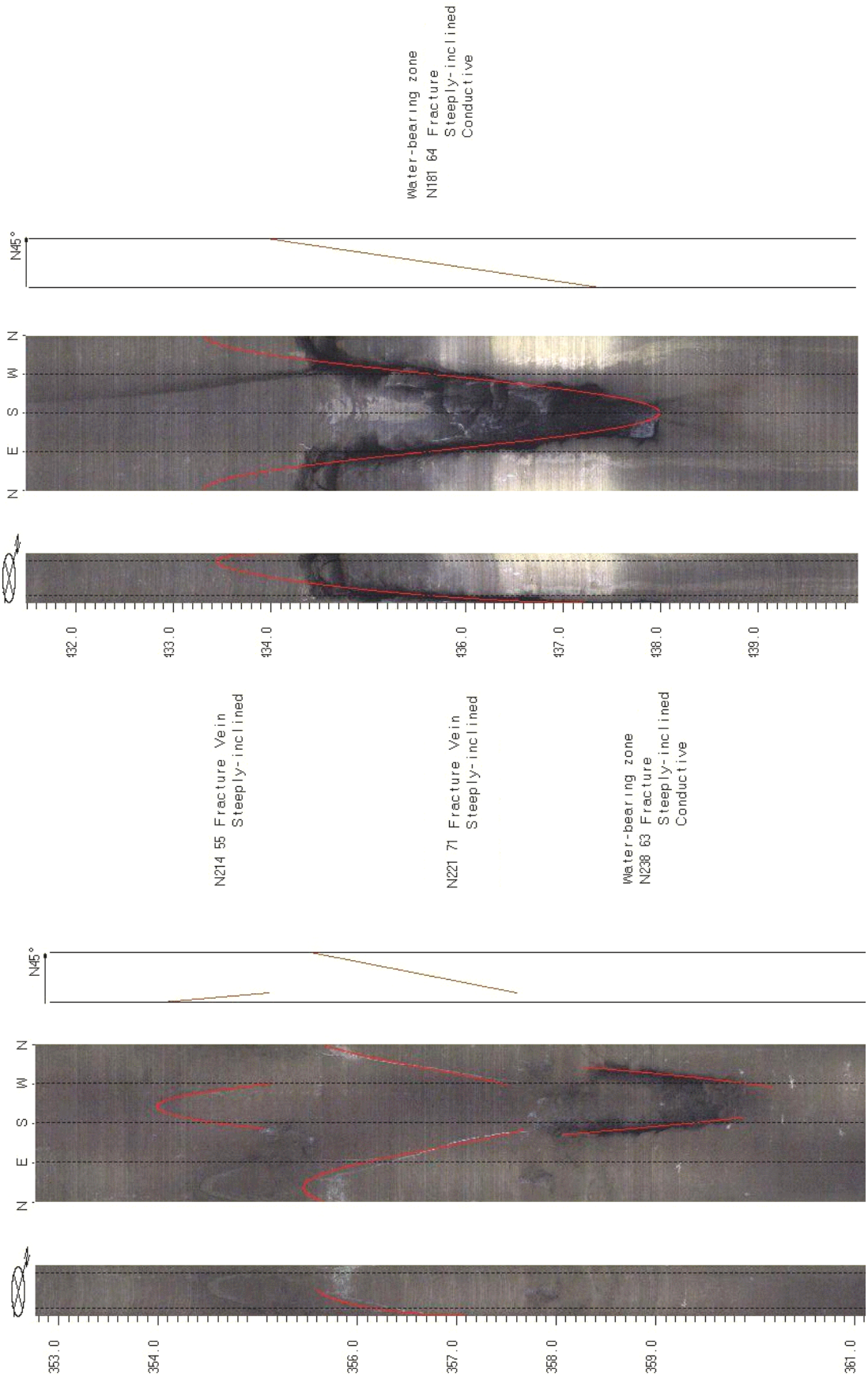

FIGURE 3P5. OPTV records of 6-inch diameter well 107 at the Ridge Golf Club, East Amwell Twp., Hunterdon County, NJ, showing geologic structures and hydraulically-conductive features in red and gray mudstone. Depth values are in feet below land surface.

Well 108 - Brunswick lower gray zone and Lockatong

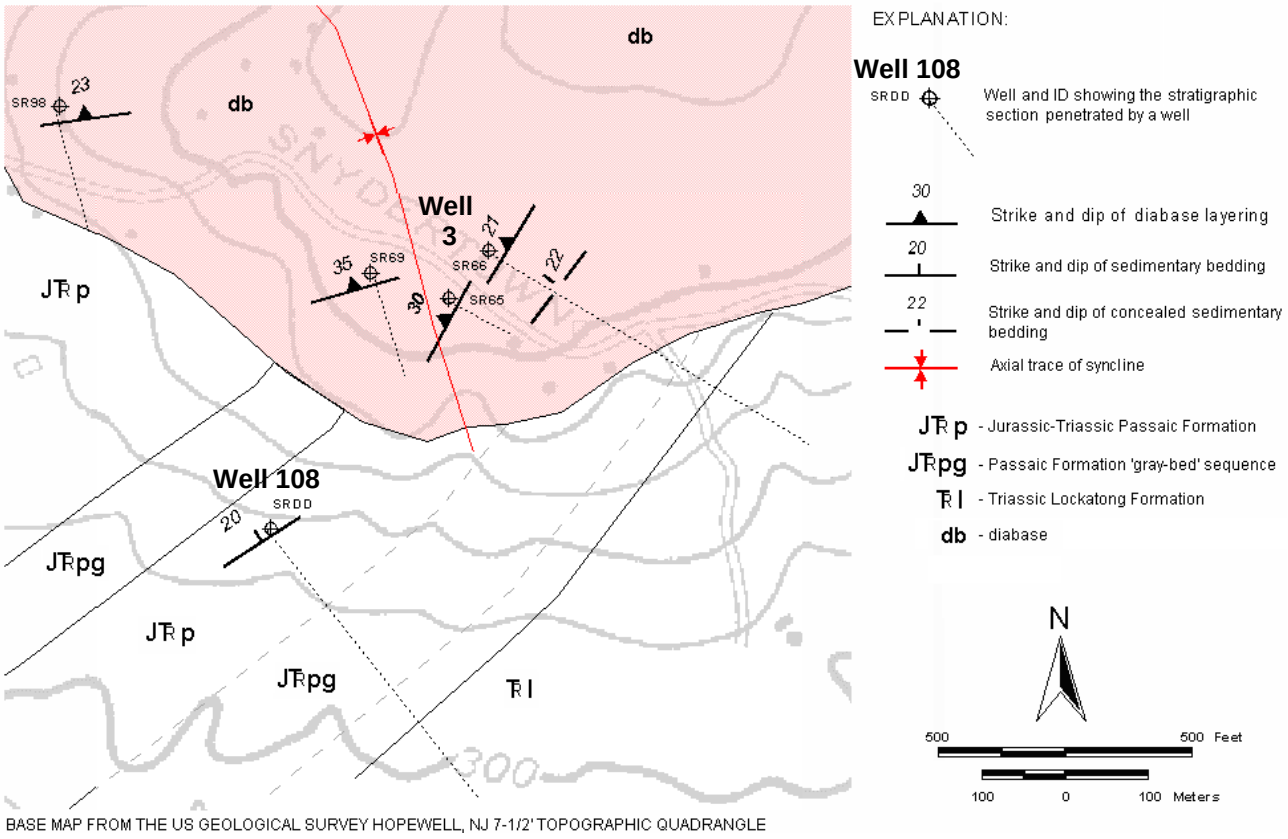

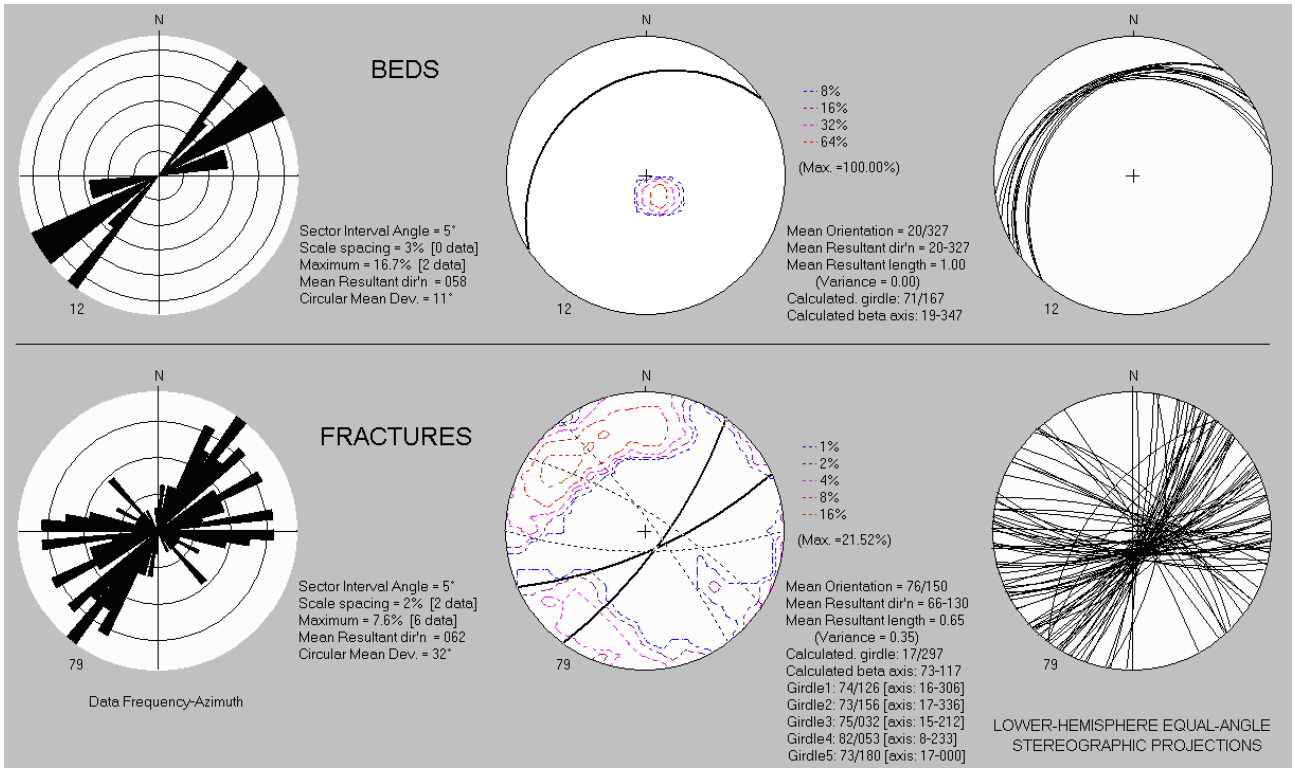

Figure 3Q1. Map (above) showing wells 108 and 3 off Snydertown Rd. in East Amwell Twp., Hunterdon County, NJ. Bedrock structures mapped near wells based on a structural analysis of OPTV data (below).

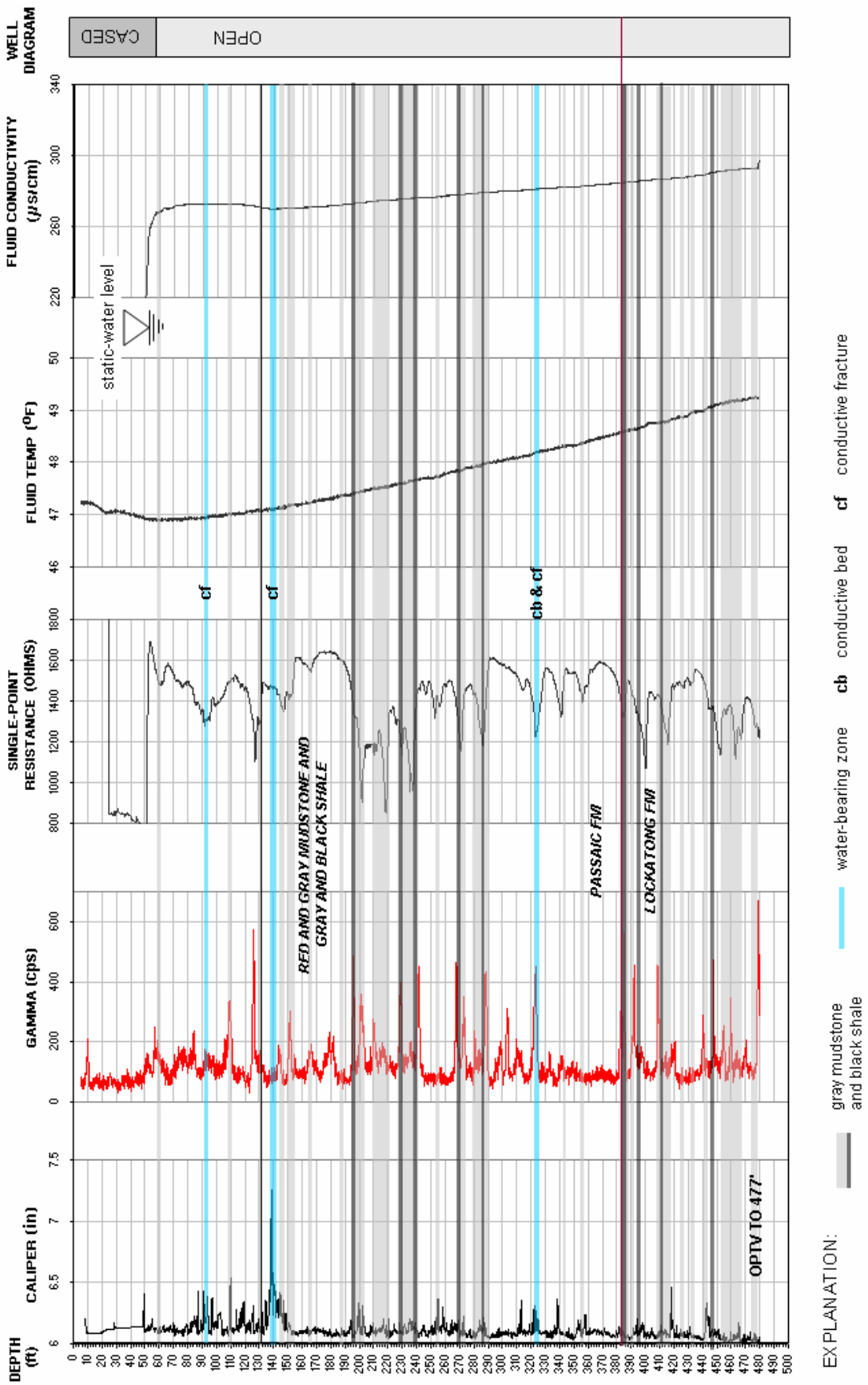

FIGURE 3Q2. Hydrogeologic section based on geophysical logs for well 108 off Snydertown Rd. in East Amwell Twp., Hunterdon County, NJ. The section shows the vertical distribution and types of hydraulically-conductive features and water-bearing zones in red and gray mudstone and gray and black shale. Depth values are in feet below land surface.

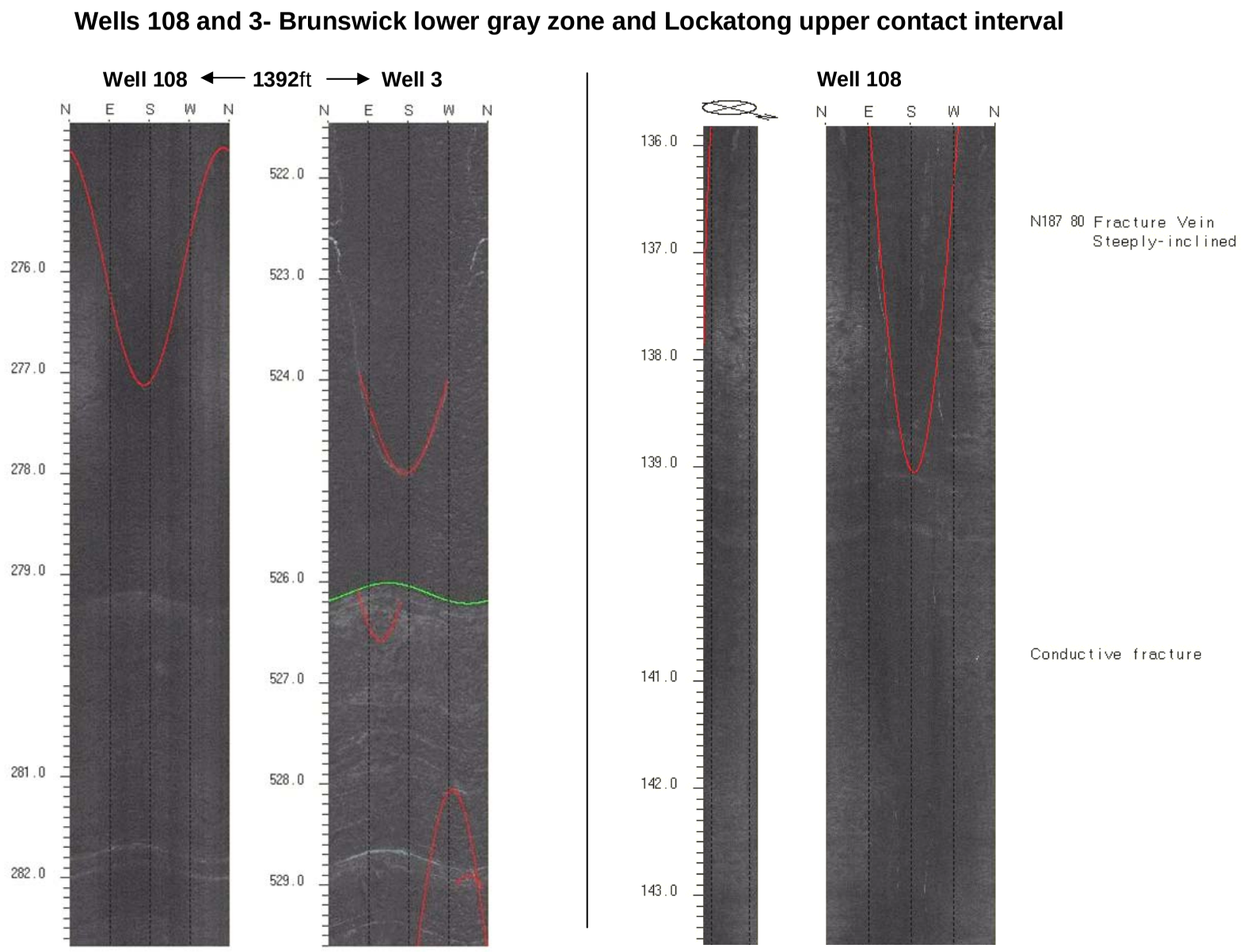

FIGURE 3Q3. Stratigraphic correlation based on OPTV records for wells 108 and 3 (left) near Snydertown Rd., East Amwell Twp., Hunterdon County, NJ. OPTV record (right) shows hydraulically-conductive fracture in 6-inch diameter well 108. Depth values are in feet below land surface.

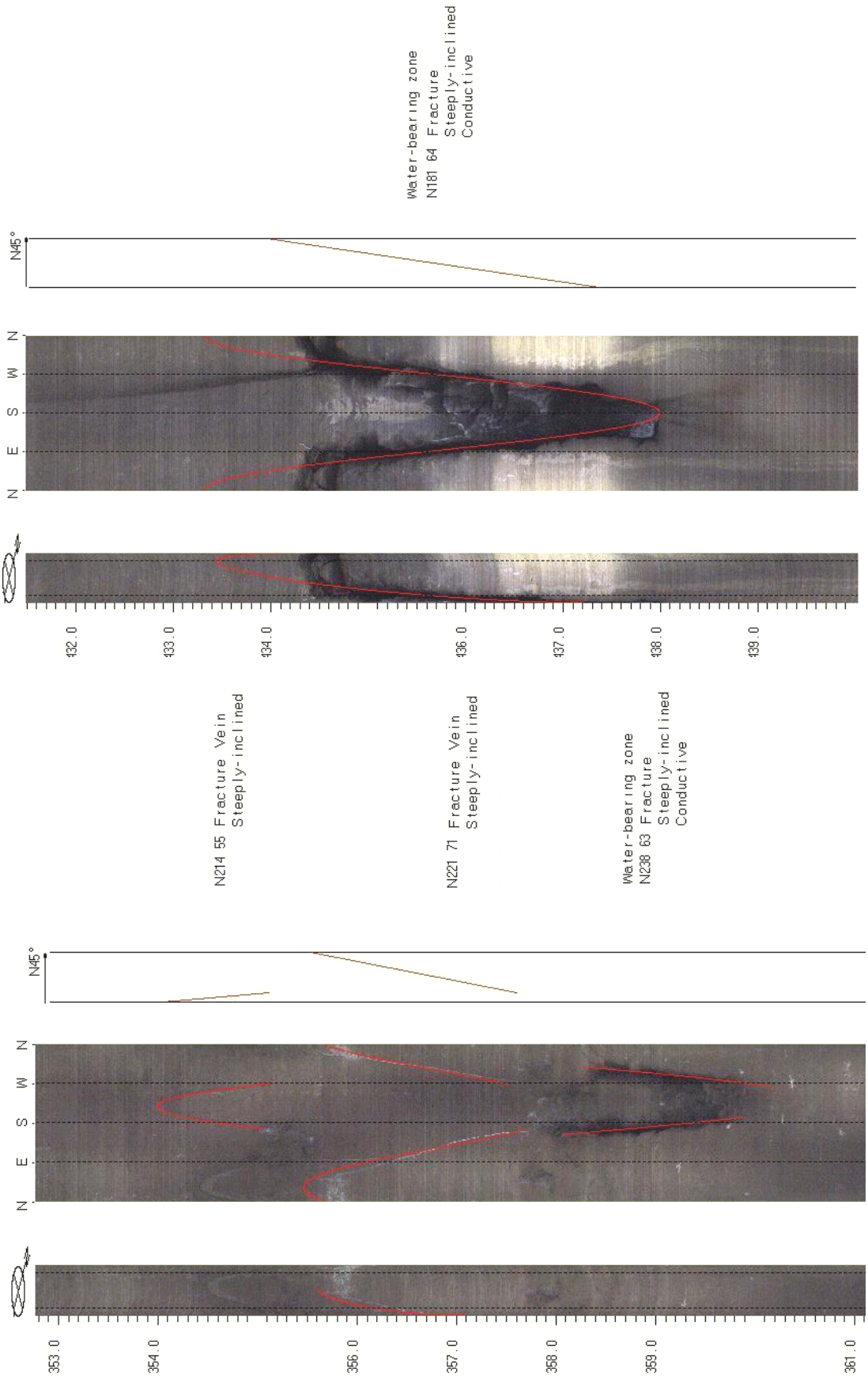

FIGURE 3P5. OPTV records of 6-inch diameter well 107 at the Ridge Golf Club, East Amwell Twp., Hunterdon County, NJ, showing geologic structures and hydraulically-conductive features in red and gray mudstone. Depth values are feet below land surface.

Well 108 - Brunswick lower gray zone and Lockatong

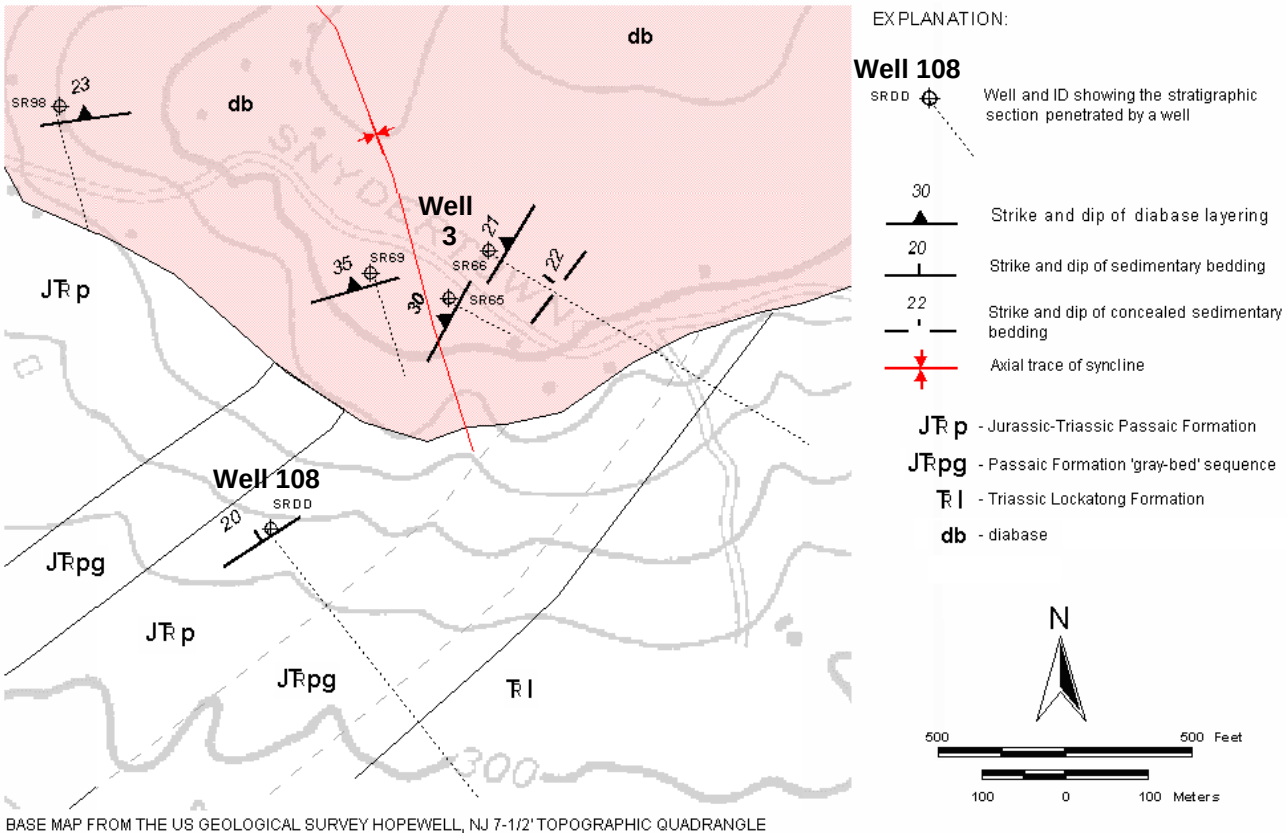

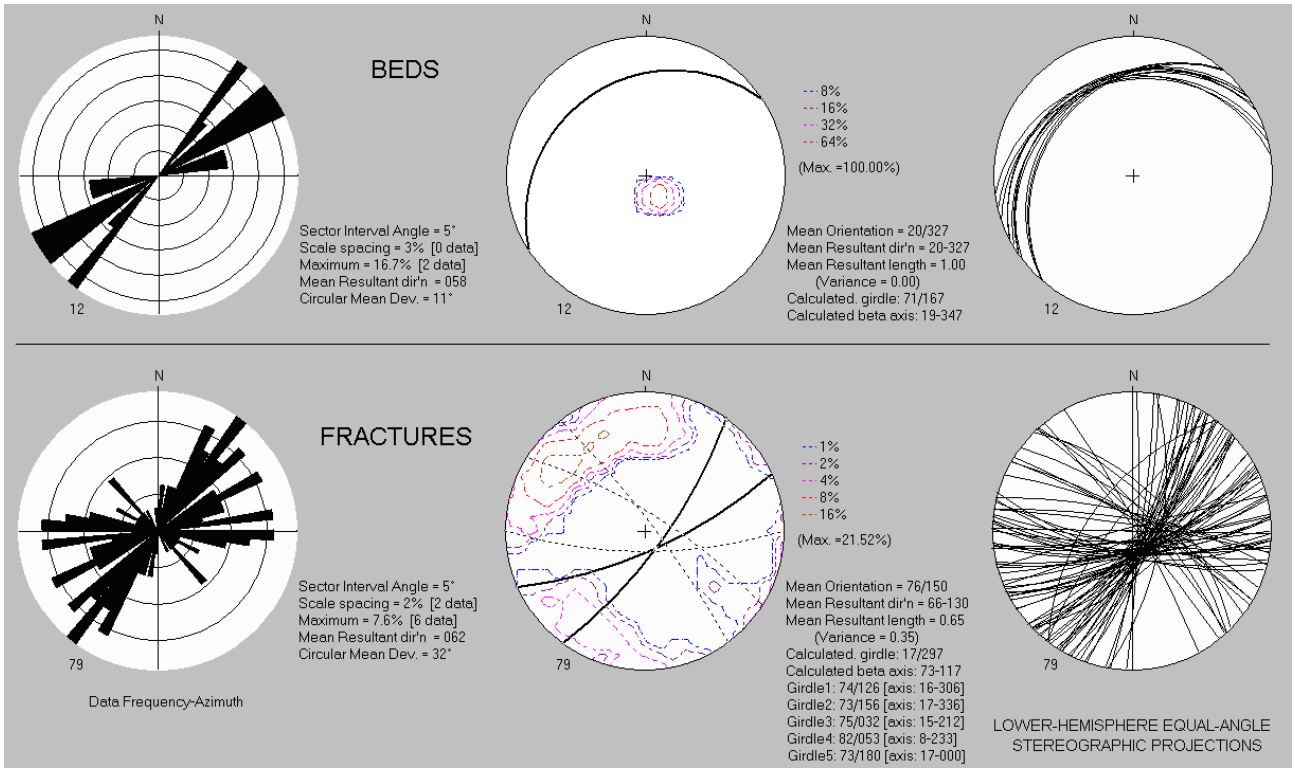

Figure 3Q1. Map (above) showing wells 108 and 3 off Snydertown Rd. in East Amwell Twp., Hunterdon County, NJ. Bedrock structures mapped near wells based on a structural analysis of OPTV data (below).

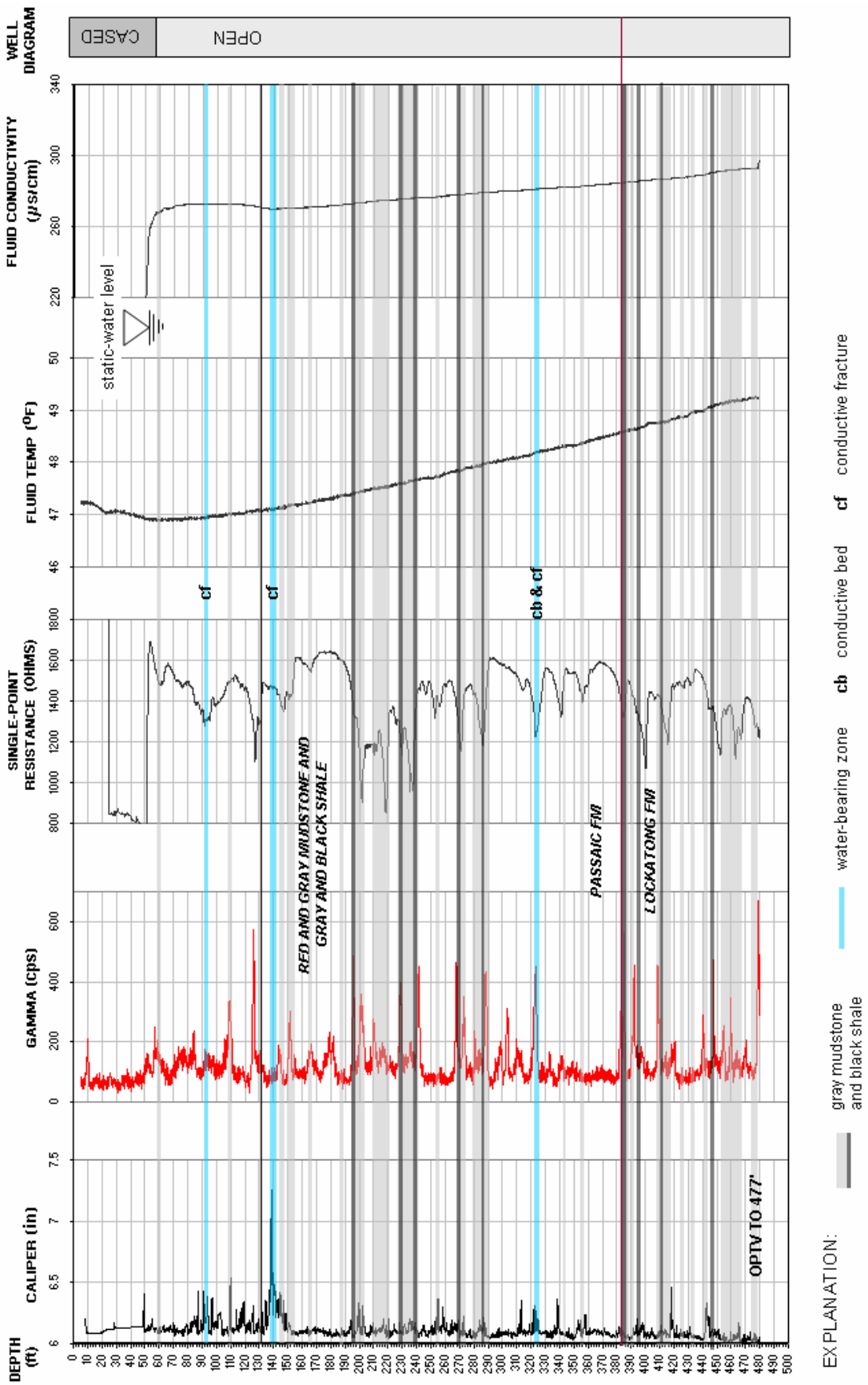

FIGURE 3Q2. Hydrogeologic section based on geophysical logs for well 108 off Snydertown Rd. in East Amwell Twp., Hunterdon County, NJ. The section shows the vertical distribution and types of hydraulically-conductive features and water-bearing zones in red and gray mudstone and gray and black shale. Depth values are in feet below land surface.

Wells 108 and 3- Brunswick lower gray zone and Lockatong upper contact interval

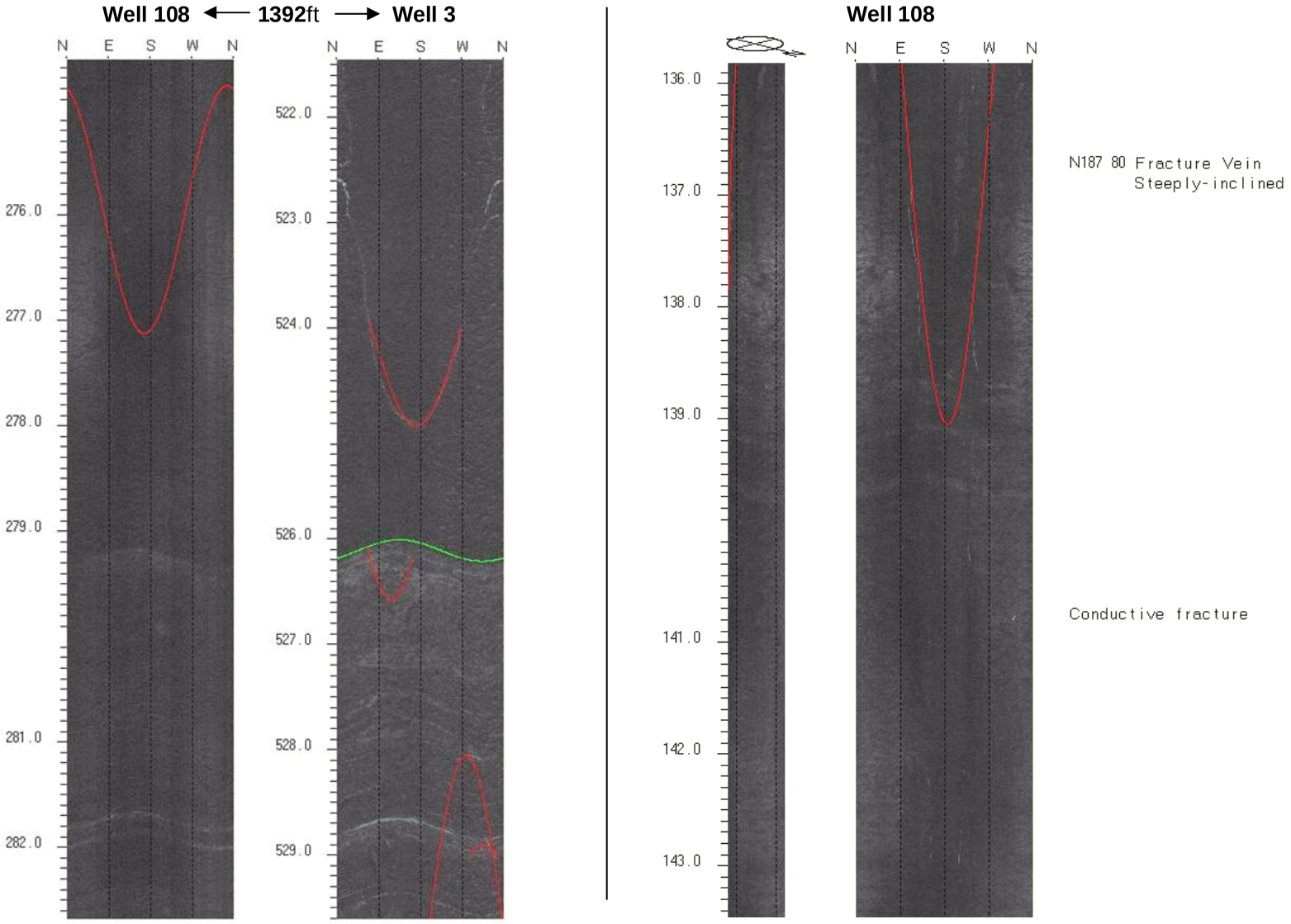

FIGURE 3Q3. Stratigraphic correlation based on OPTV records for wells 108 and 3 (left) near Snydertown Rd., East Amwell Twp., Hunterdon County, NJ. OPTV record (right) shows hydraulically-conductive fracture in 6-inch diameter well 108. Depth values are in feet below land surface.

Summary of Borehole Geophysical Studies in the Newark Basin, New Jersey:

Lockatong argillite and Stockton sandstone

By Gregory C. Herman and John F. Curran, N.J. Geological Survey

Appendix 4 of

Contributions to the Geology and Hydrogeology of the Newark Basin

N.J. Geological Survey Bulletin 77

State of New Jersey
Department of Environmental Protection
Water Resource Management
New Jersey Geological Survey
2010

Wells 109 and 110 – Lockatong argillite

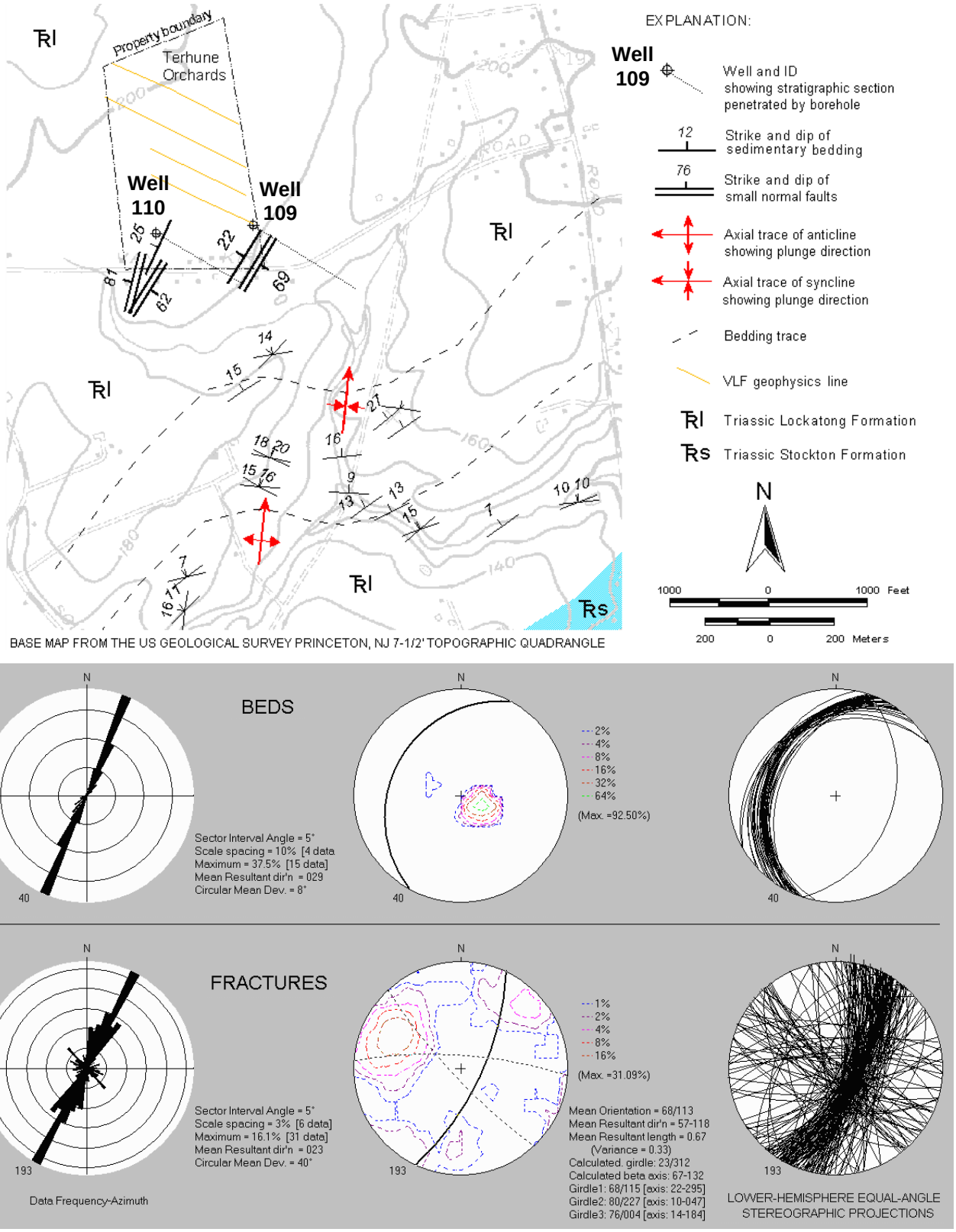

Figure 4A1. Map (above) showing wells 109 and 110 at Terhune Orchards, 42 Van Kirk Rd., Lawrence Twp., Mercer County, NJ. Bedrock structures mapped near wells based on a structural analysis of OPTV data (below).

Well 109 – Lockatong argillite

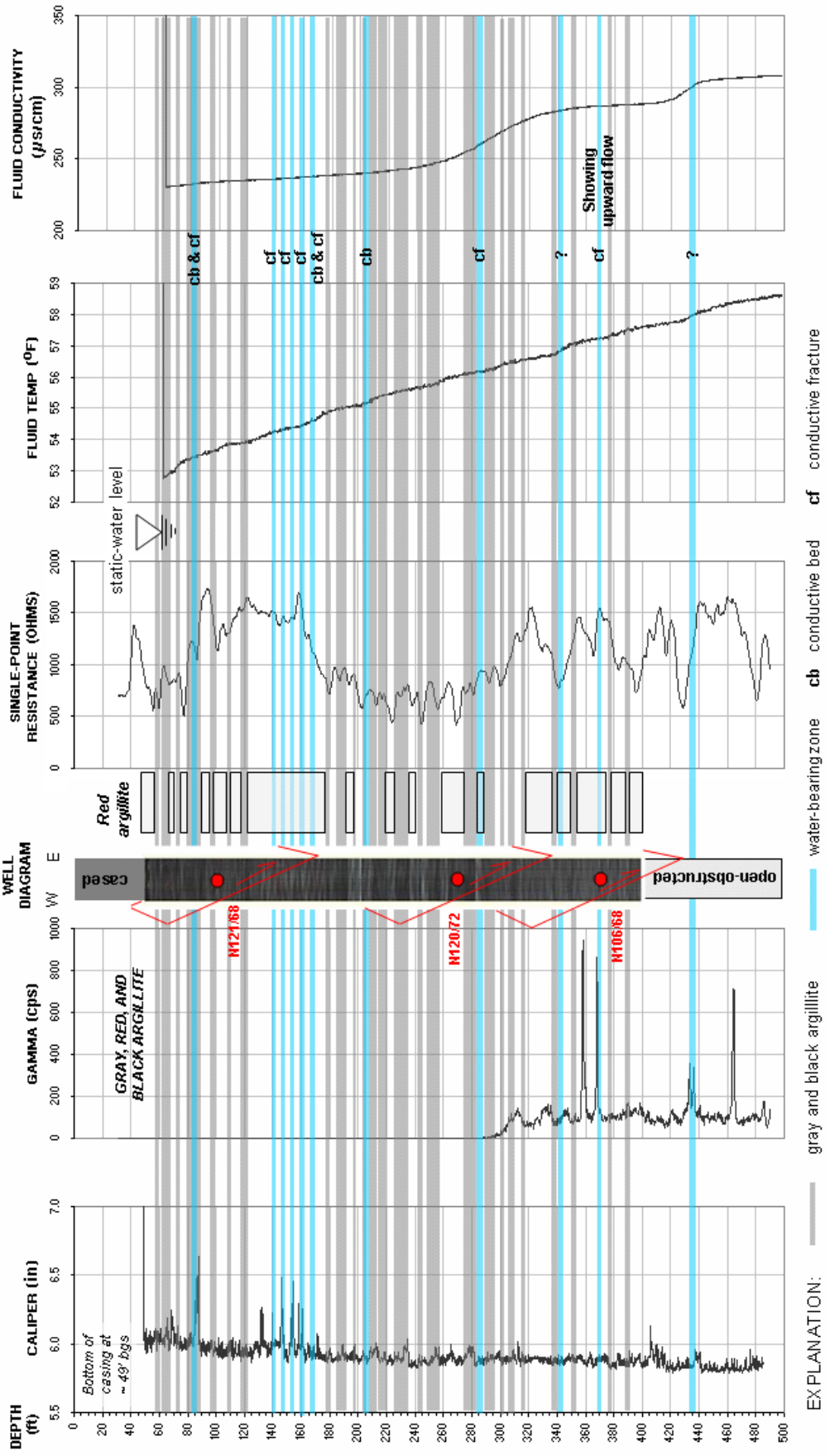

FIGURE 4A2. Hydrogeologic section based on geophysical logs for well 109 at Terhune Orchards, 42 Van Kirk Rd., Lawrence Twp., Mercer County, NJ. The section shows the vertical distribution and types of hydraulically-conductive features and water-bearing zones in Lockatong argillite. Depth values are in feet below land surface.

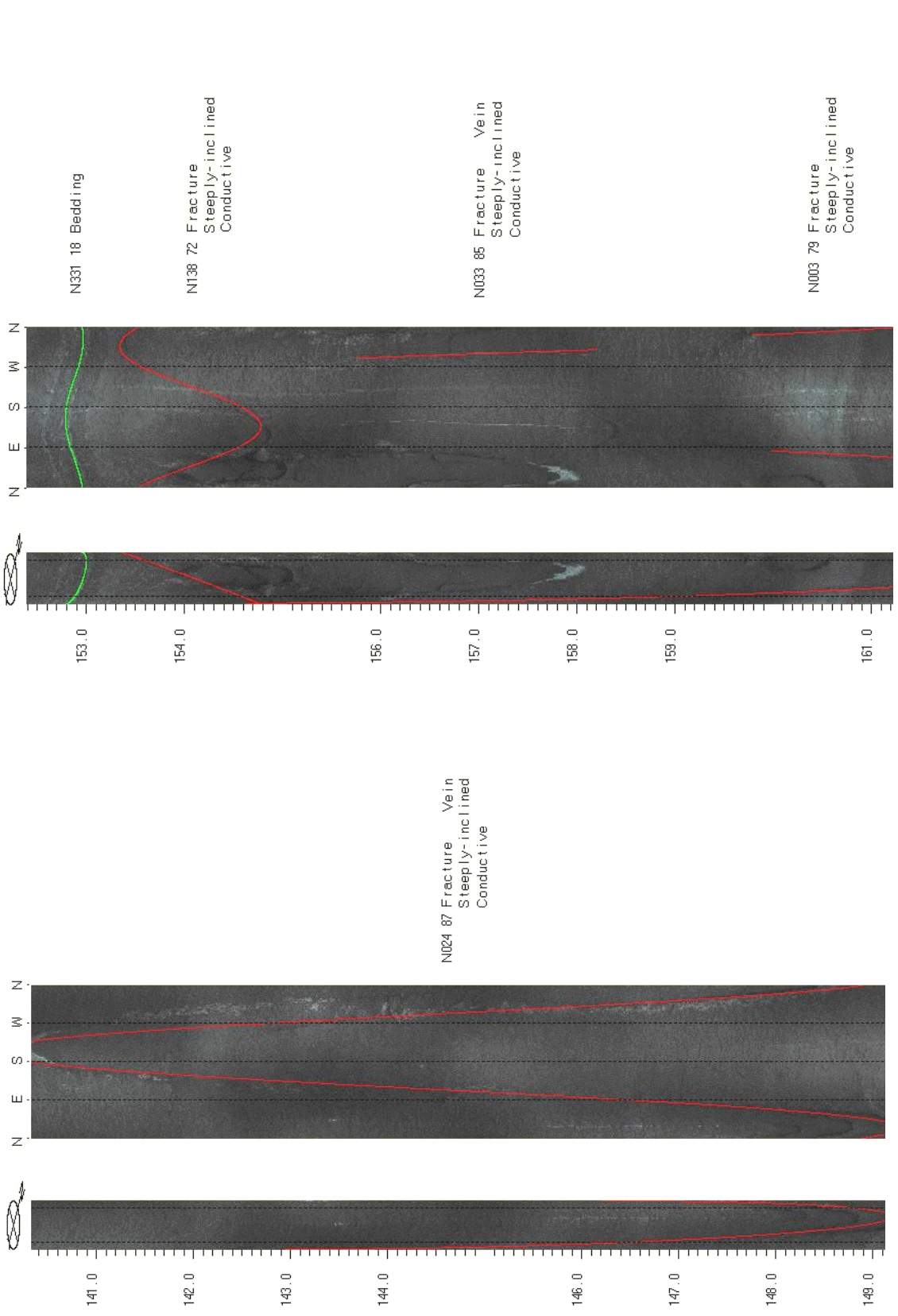

FIGURE 4A3. OPTV records of 6-inch diameter well 109 at Terhune Orchards, 42 Van Kirk Rd., Lawrence Twp., Mercer County, NJ showing geologic structures and hydraulically-conductive features in red argillite. Depth values are in feet below land surface.

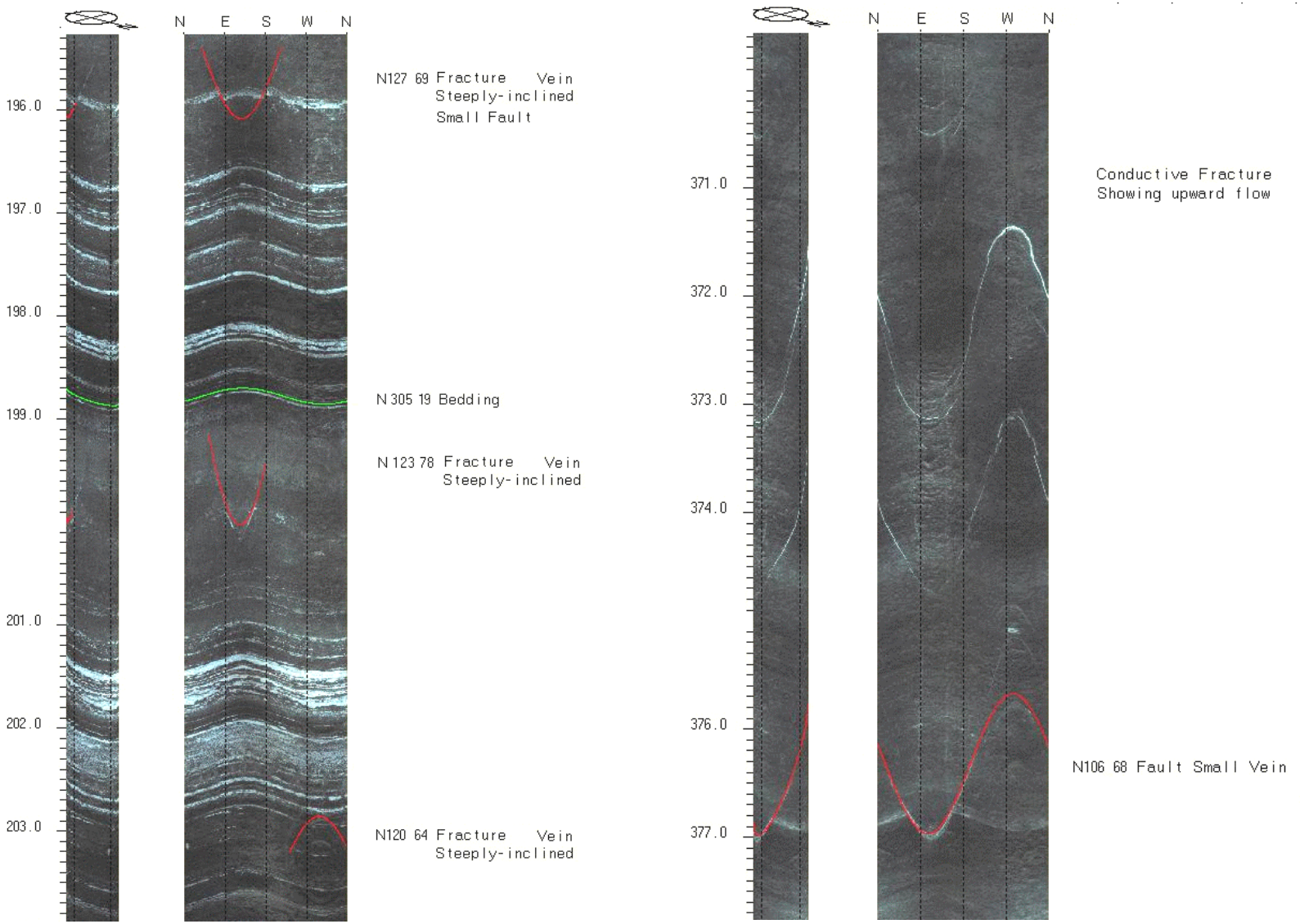

FIGURE 4A4. OPTV records of 6-inch diameter well 109 at Terhune Orchards, 42 Van Kirk Rd., Lawrence Twp., Mercer County, NJ showing geologic structures and hydraulically-conductive features in red argillite. Depth values are feet below land surface.

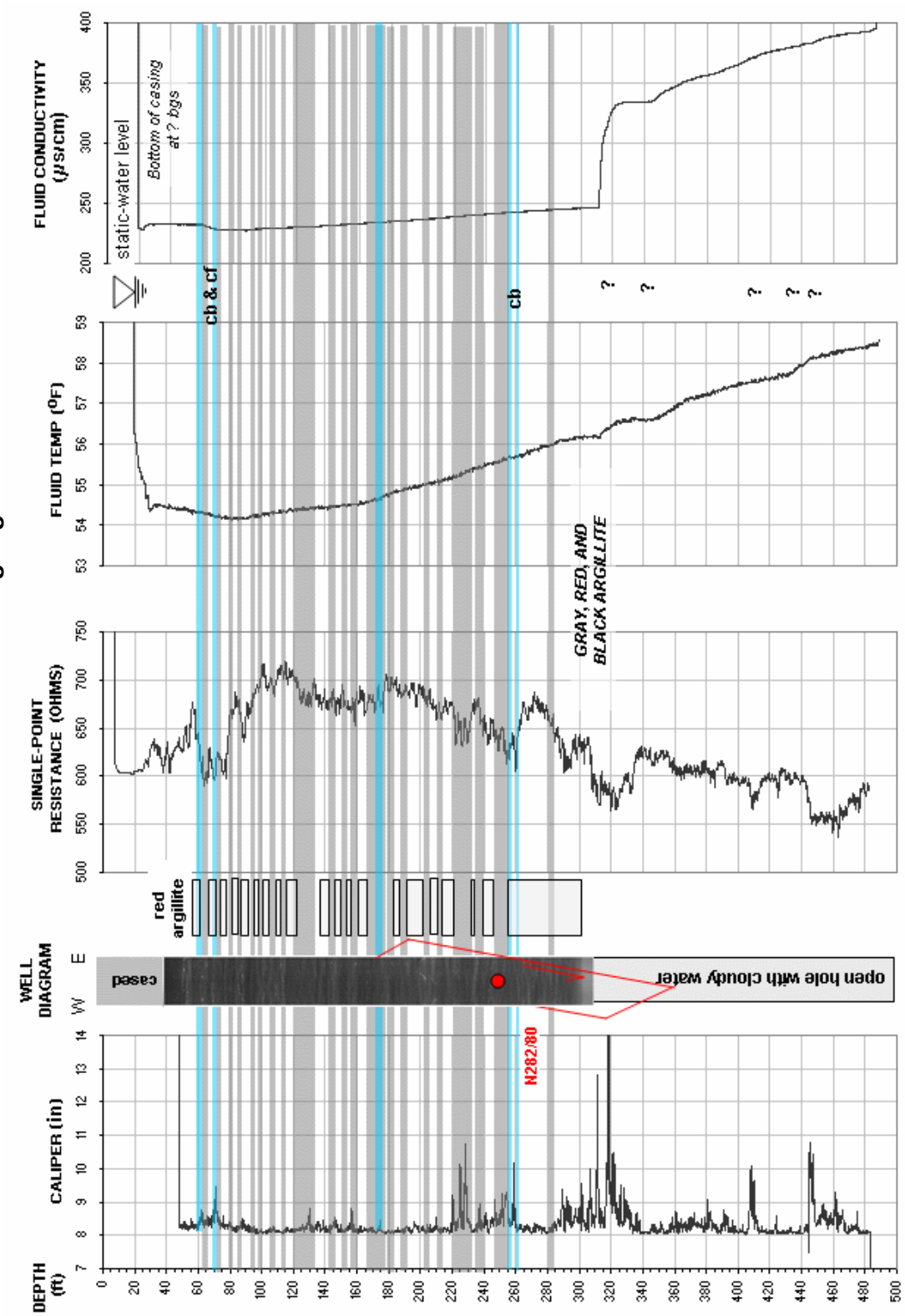

FIGURE 4A5. Hydrogeologic section based on geophysical logs for well 110 at Terhune Orchards, 42 Van Kirk Rd., Lawrence Twp., Mercer County, NJ. The section shows the vertical distribution and types of hydraulically-conductive features and water-bearing zones in Lockatong argillite. Depth values are in feet below land surface.

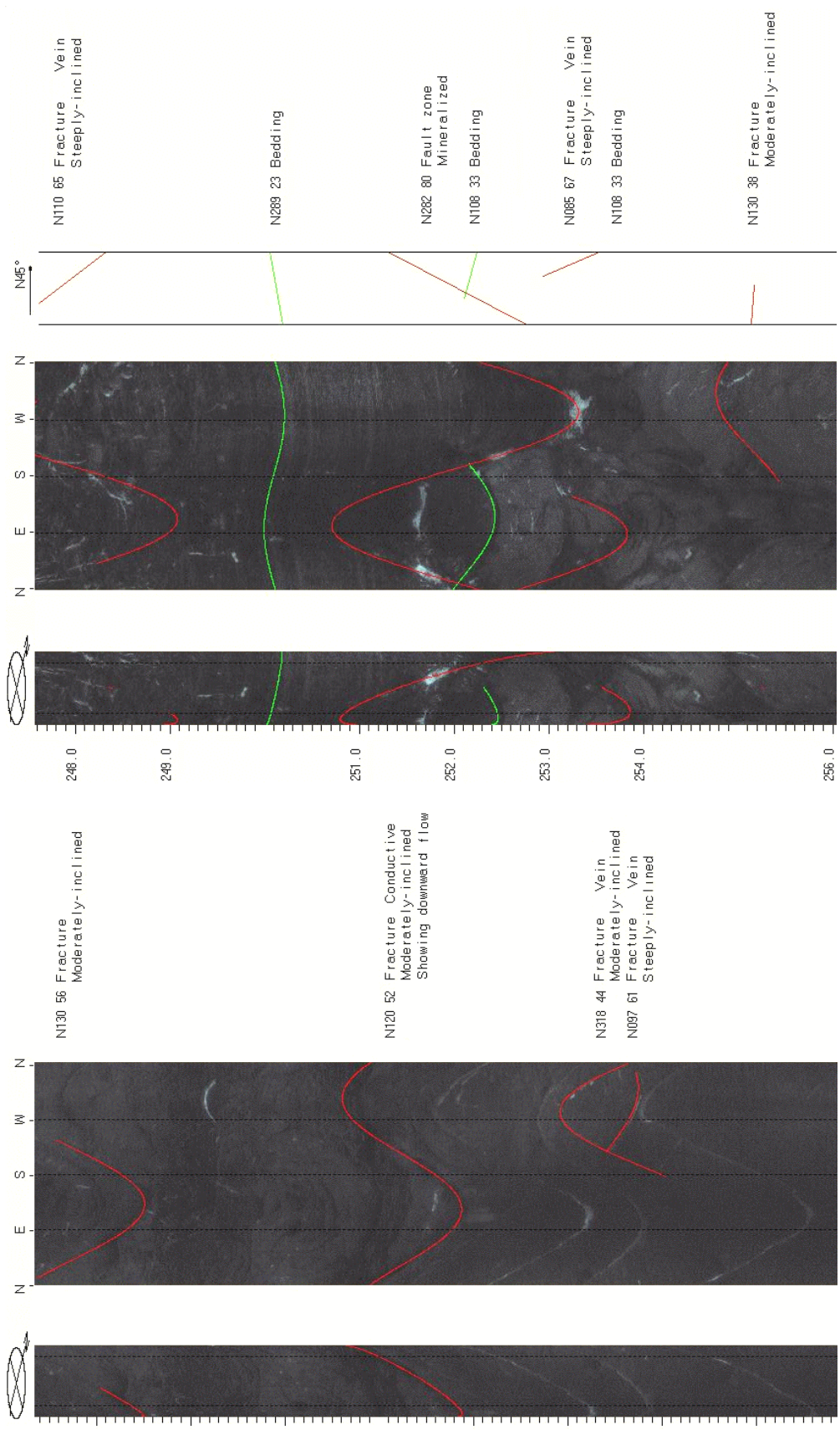

FIGURE 4A6. OPTV records of 8-inch diameter well 110 at Terhune Orchards, 42 Van Kirk Rd., Lawrence Twp., Mercer County, NJ showing geologic structures and hydraulically-conductive features in red and gray argillite. Depth values are in feet below land surface.

Wells 111 to 115 – Lockatong argillite

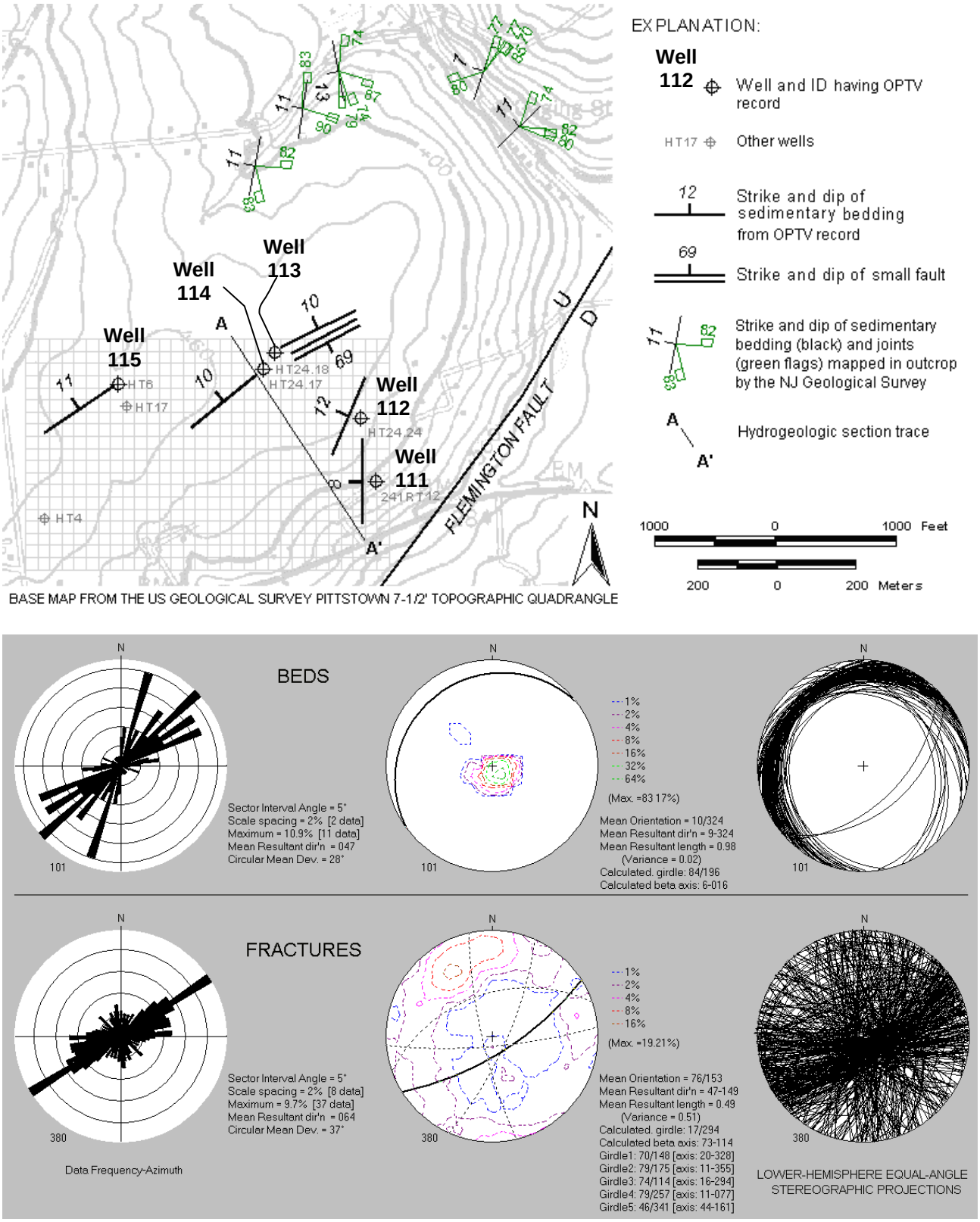

Figure 4B1. Map (above) showing wells 111 to115 at the Hilltop development, Raritan Twp., Hunterdon County, NJ. Bedrock structures mapped near wells based on structural analyses of OPTV data (below).

Wells 112 and 113 – Lockatong argillite

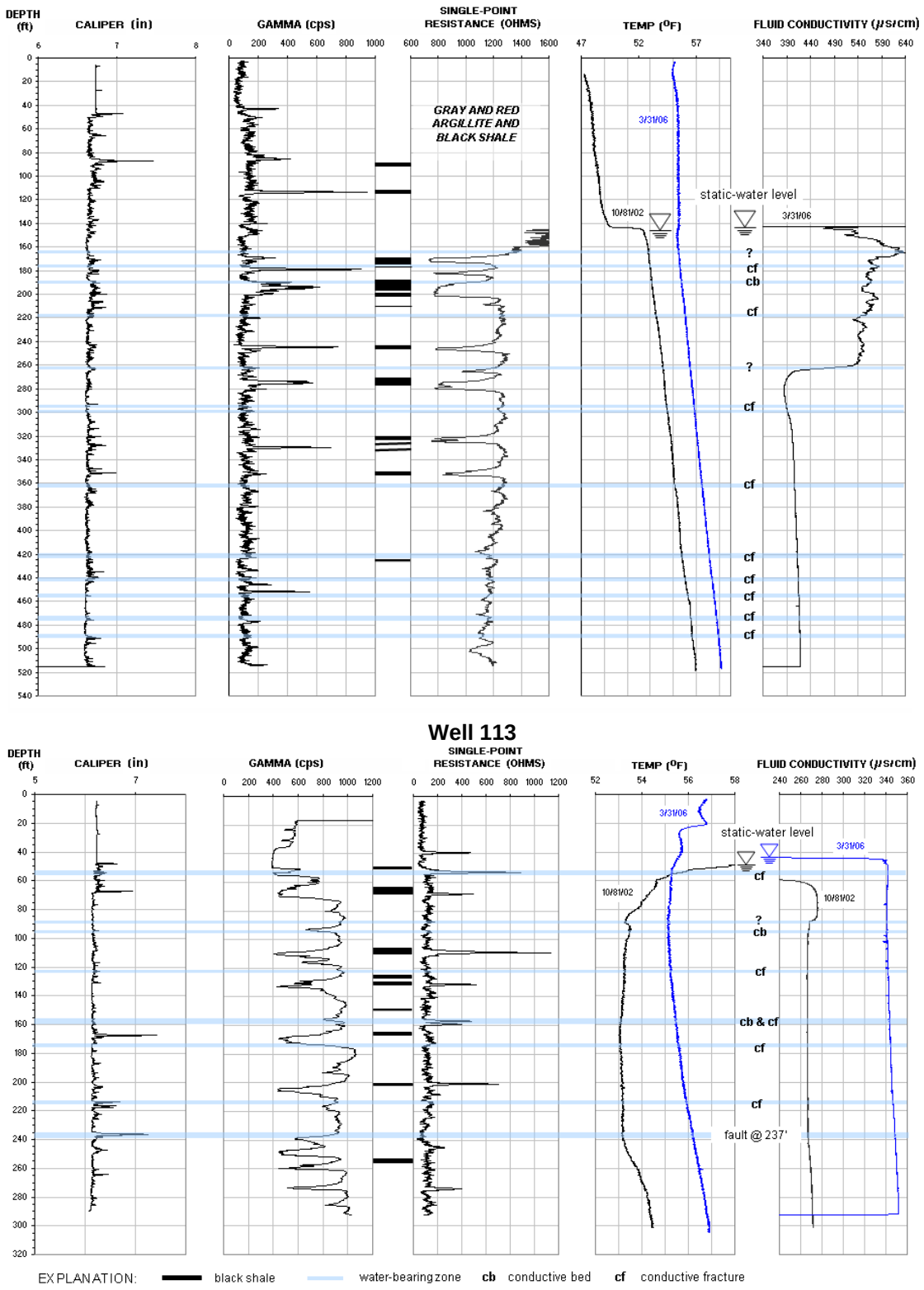

Figure 4B2. Hydrogeologic sections based on geophysical logs for wells 112 (above) and 113 (below). The sections summarize the profile distribution and types of hydraulically-conductive features in red and gray argillite and black shale. Depth values are in feet below land surface.

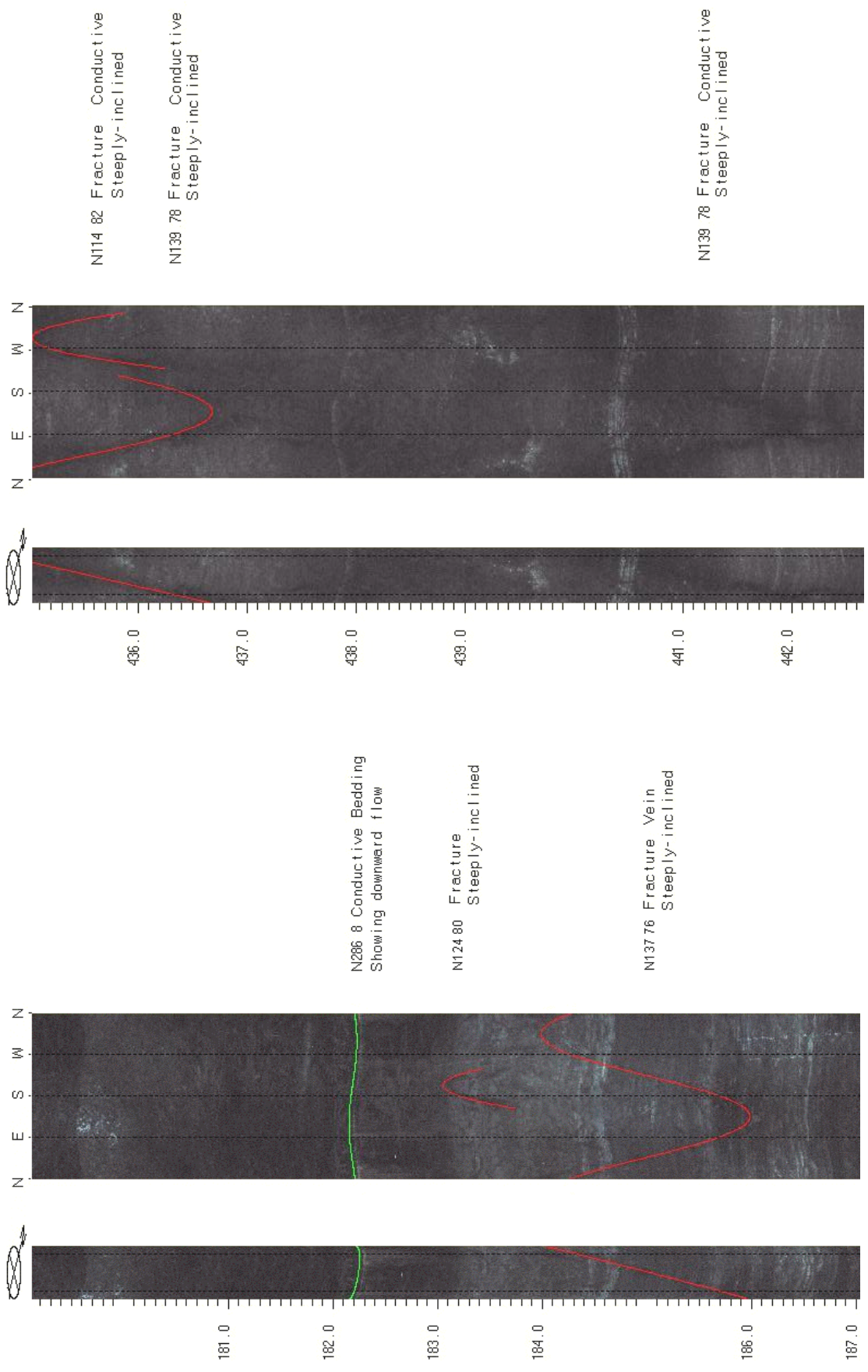

FIGURE 4B3 OPTV records of 6-inch diameter well 112 at the Hilltop development, Raritan Twp., Hunterdon County, NJ showing geologic structures and hydraulically-conductive features in gray and red argillite. Depth values are in feet below land surface.

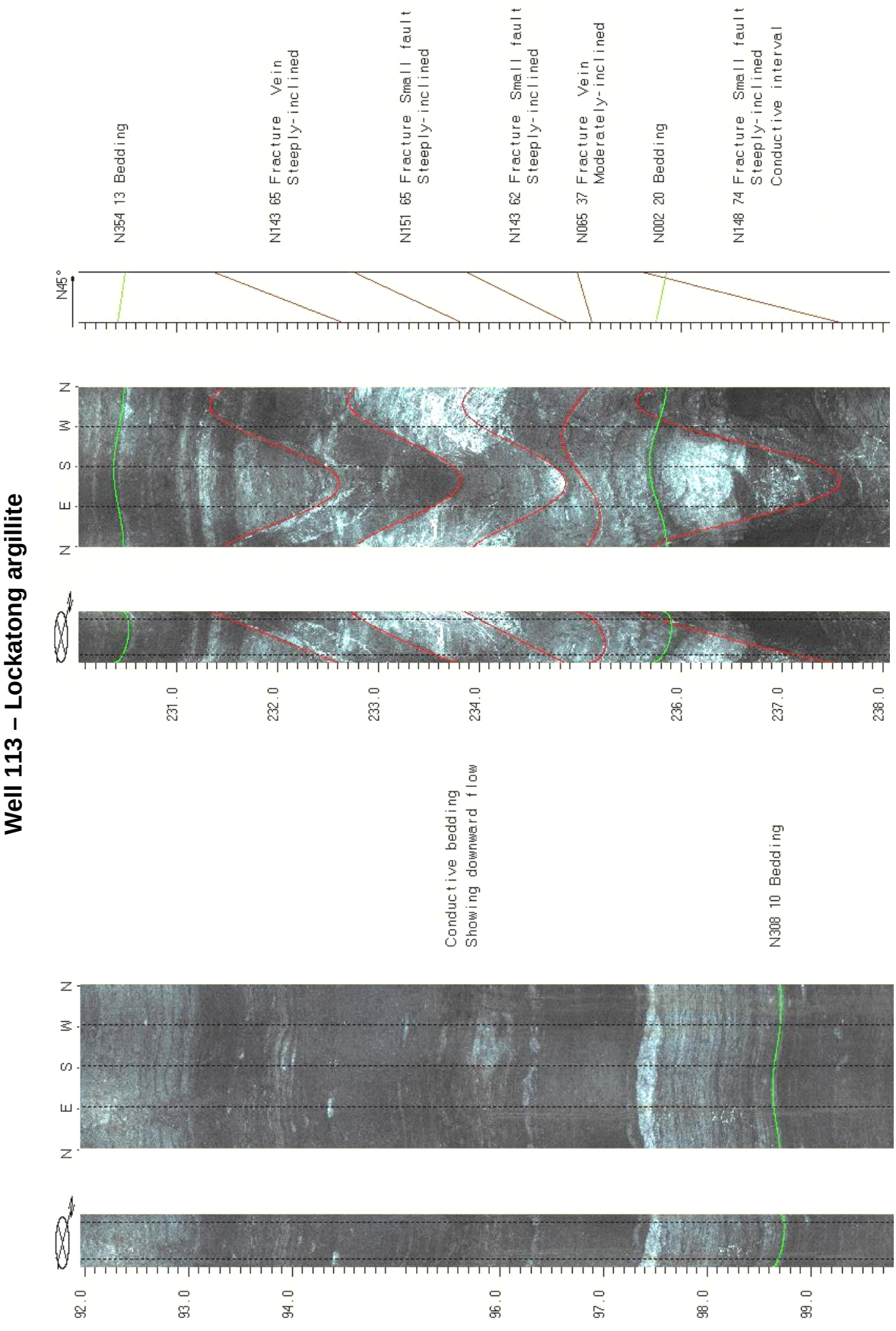

FIGURE 4B4. OPTV records of 6-inch diameter well 113 at the Hilltop development, Raritan Twp., Hunterdon County, NJ showing geologic structures and hydraulically-conductive features in gray and red argillite. Depth values are in feet below land surface.

Wells 114 and 115 – Lockatong argillite

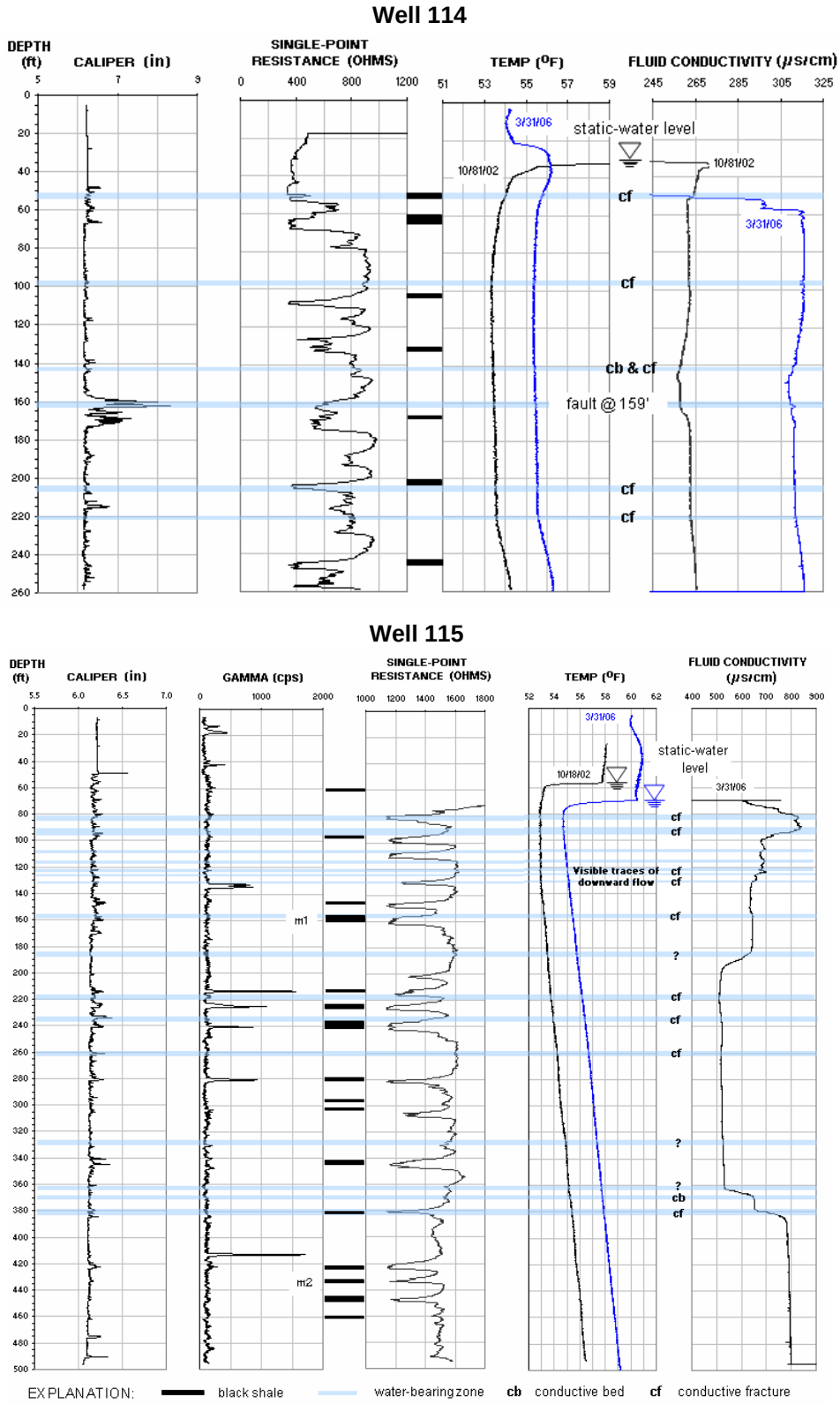

Figure 4B5. Hydrogeologic sections based on geophysical logs for wells 114 (above) and 115 (below). The sections summarize the distribution and types of hydraulically-conductive features in red and gray argillite and black shale. Depth values are in feet below land surface.

Well 114 – Lockatong argillite

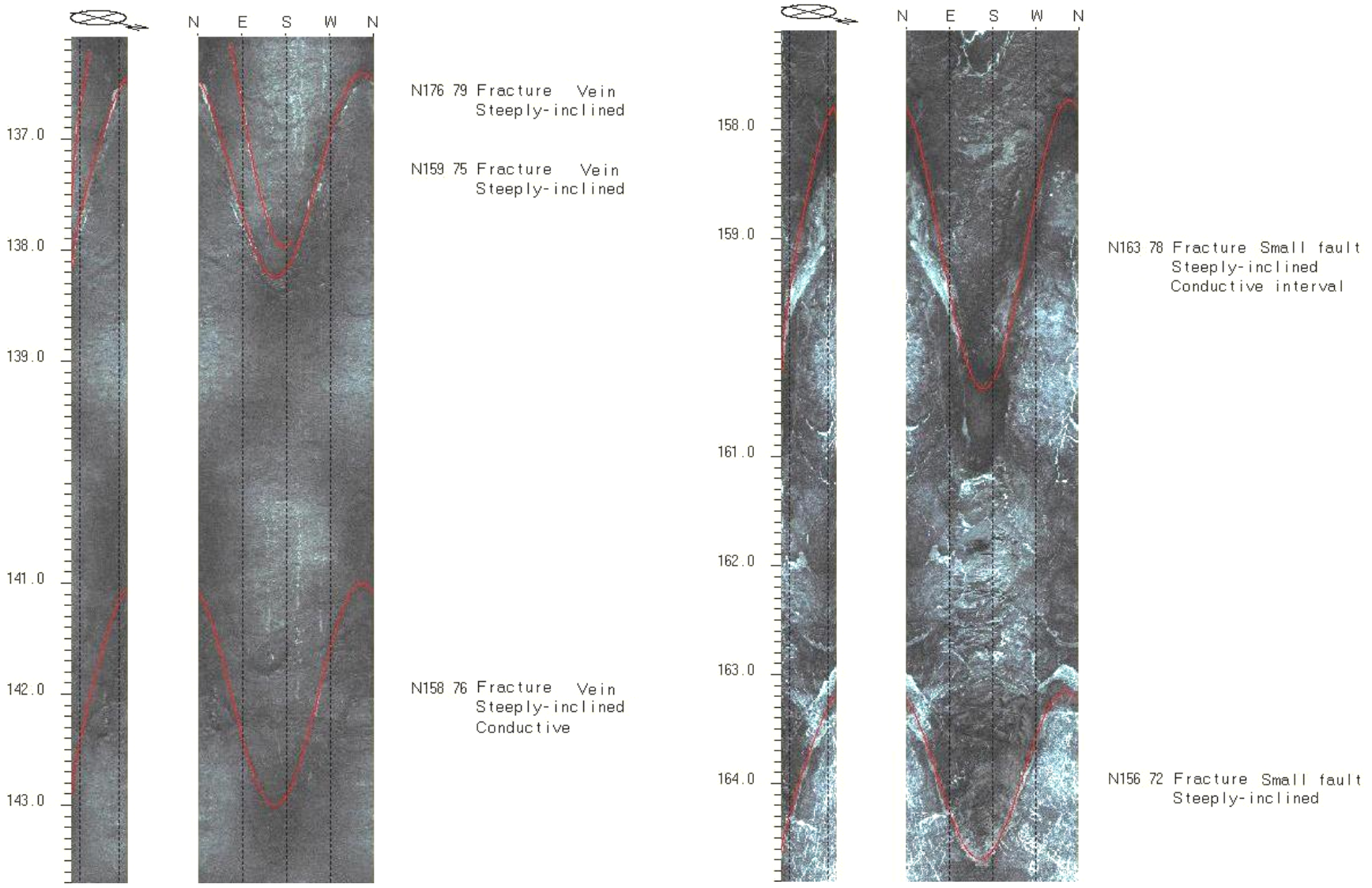

FIGURE 4B6. OPTV records of 6-inch diameter well 114 at the Hilltop development, Raritan Twp., Hunterdon County, NJ showing geologic structures and hydraulically-conductive features in gray and red argillite. Depth values are in feet below land surface.

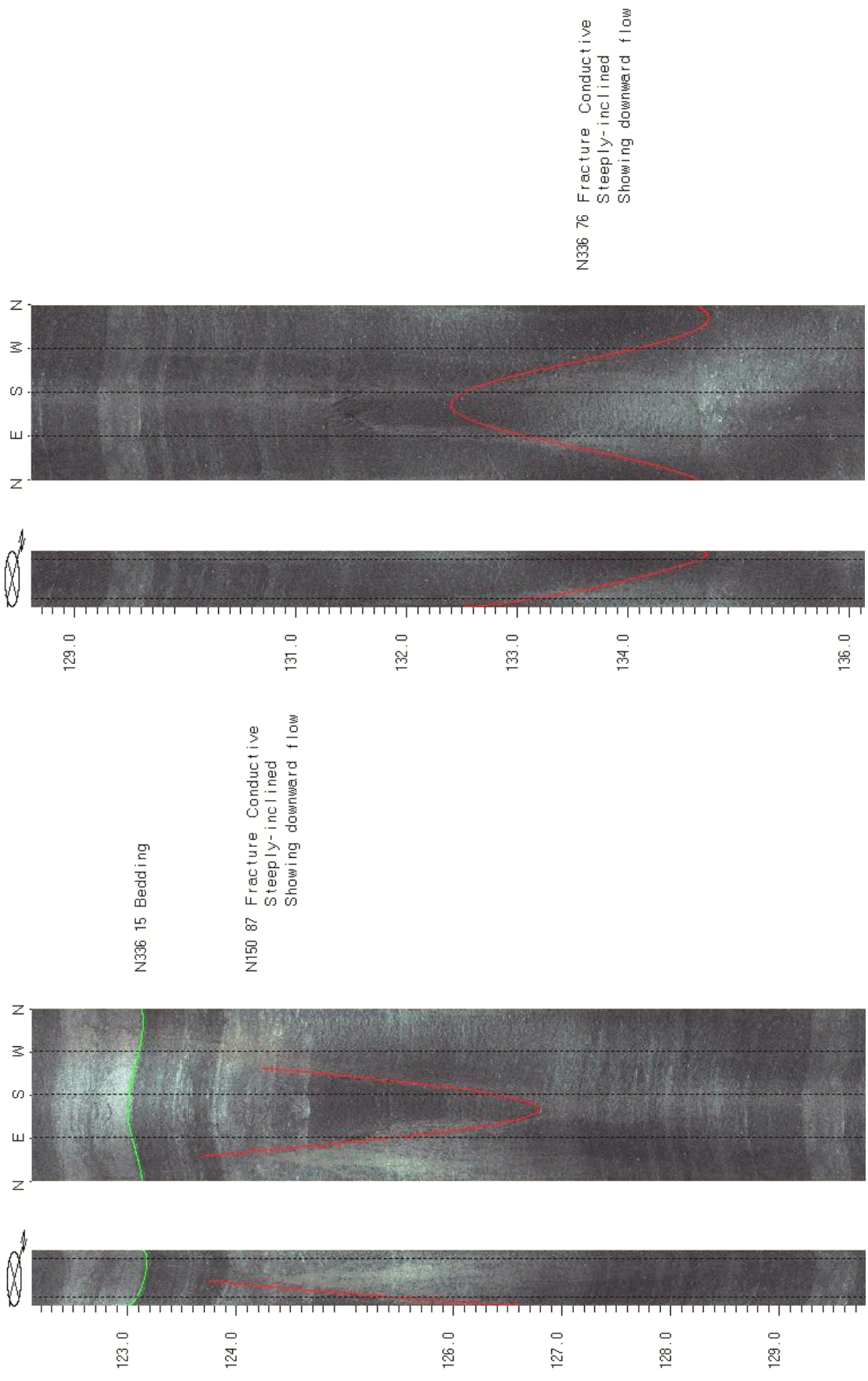

FIGURE 4B7. OPTV records of 6-inch diameter well 115 at the Hilltop development, Raritan Twp., Hunterdon County, NJ showing geologic structures and hydraulically-conductive features in gray and red argillite. Depth values are in feet below land surface.

Wells 111 to 115 – Lockatong argillite

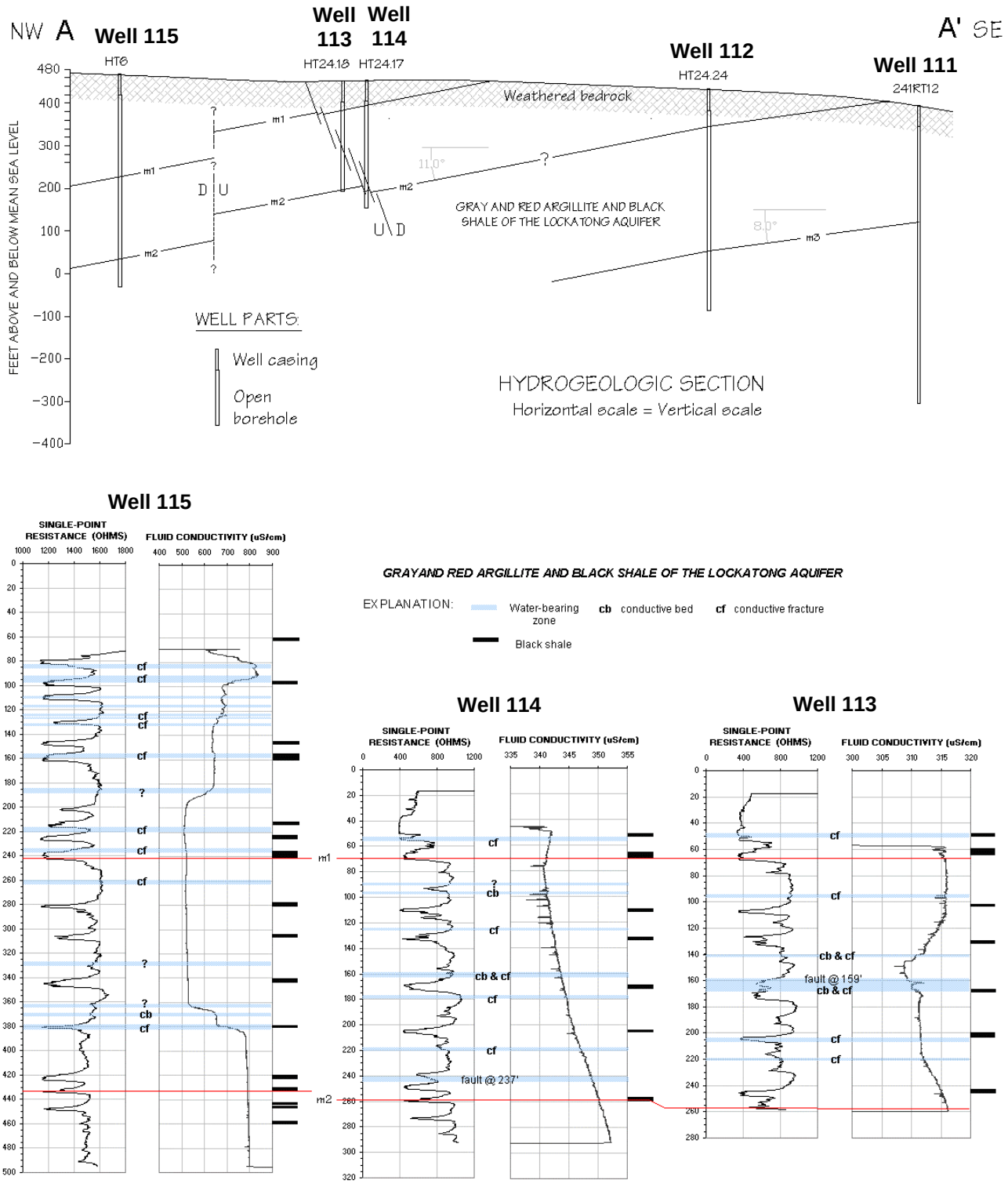

Figure 4B8. Hydrogeologic section (above) based on test wells 112 to 115 at the Hilltop development, Raritan Twp., Hunterdon County, NJ and a nearby domestic well. Stratigraphic marker horizons m1to m3 identified using OPTV records. Borehole geophysical records for well 112, 113 and 115 (below) show marker horizons m1 and m2 with respect to electrical resistance and fluid electrical-conductivity logs. Depth values (bottom) are in feet below land surface.

Wells 113 to 115 – Lockatong argillite

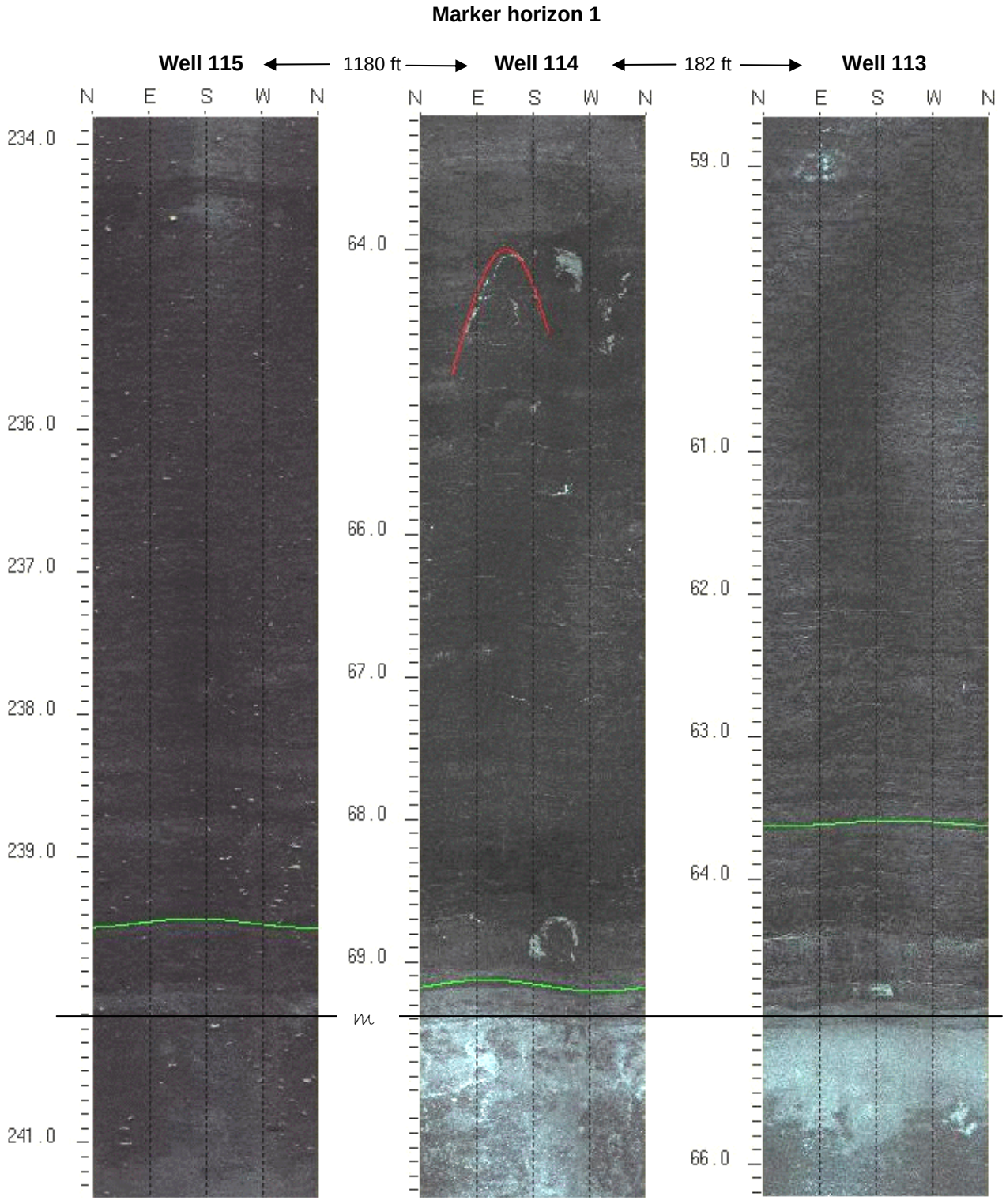

Figure 4B9. Stratigraphic correlation of wells 113 to115 at the Hilltop development, Raritan Twp., Hunterdon County, NJ based on OPTV records showing stratigraphic marker horizon m1in gray and red argillite. Depth values are in feet below land surface.

Wells 111 to 115 – Lockatong argillite

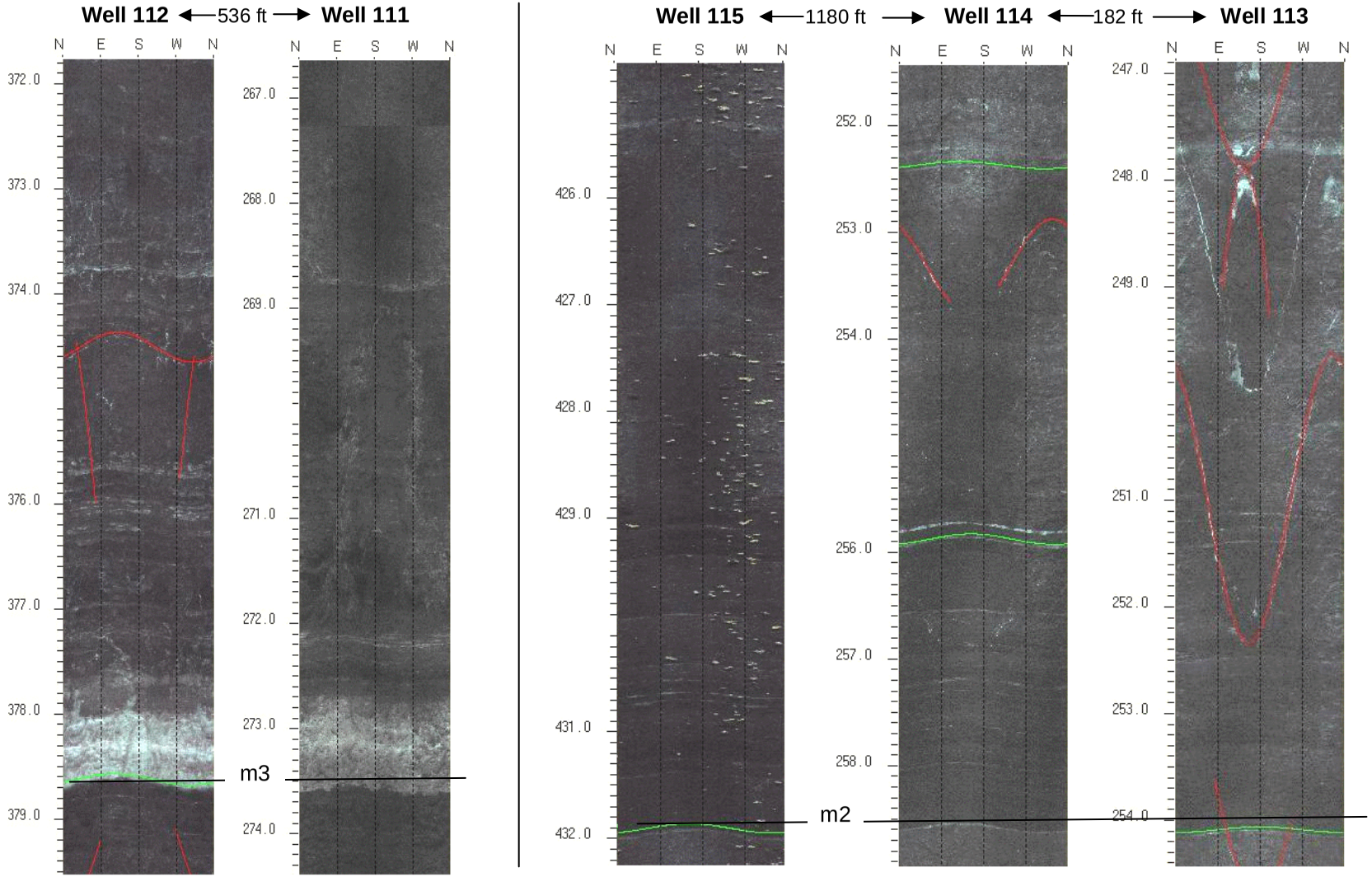

Figure 4B10. Stratigraphic correlation of wells 111and 112 (left, marker horizon m3) and wells 113 through 115 (right, marker horizon m2) at the Hilltop development, Raritan Twp., Hunterdon County, NJ. Correlations are based on OPTV records of gray and red argillite. Depth values are in feet below land surface.

Well 116 – Lockatong argillite overlying Stockton sandstone

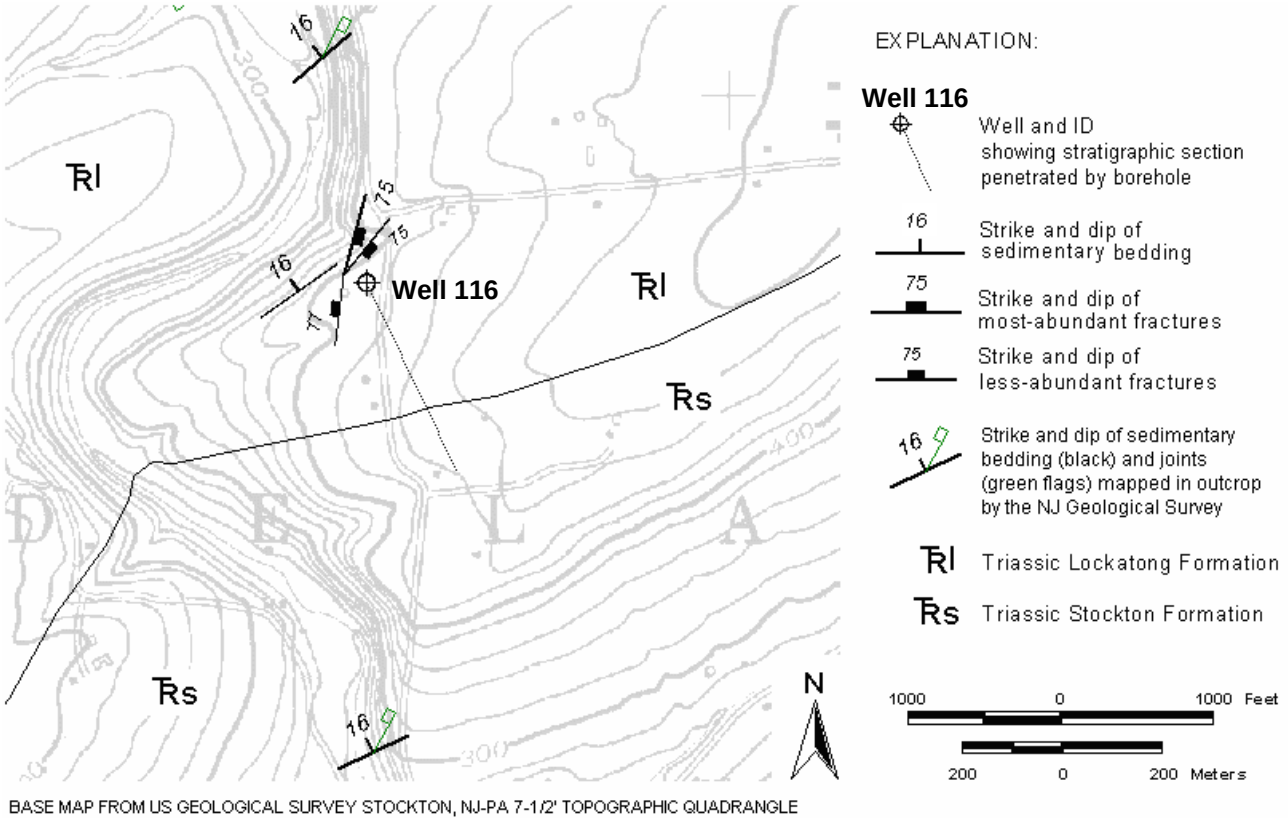

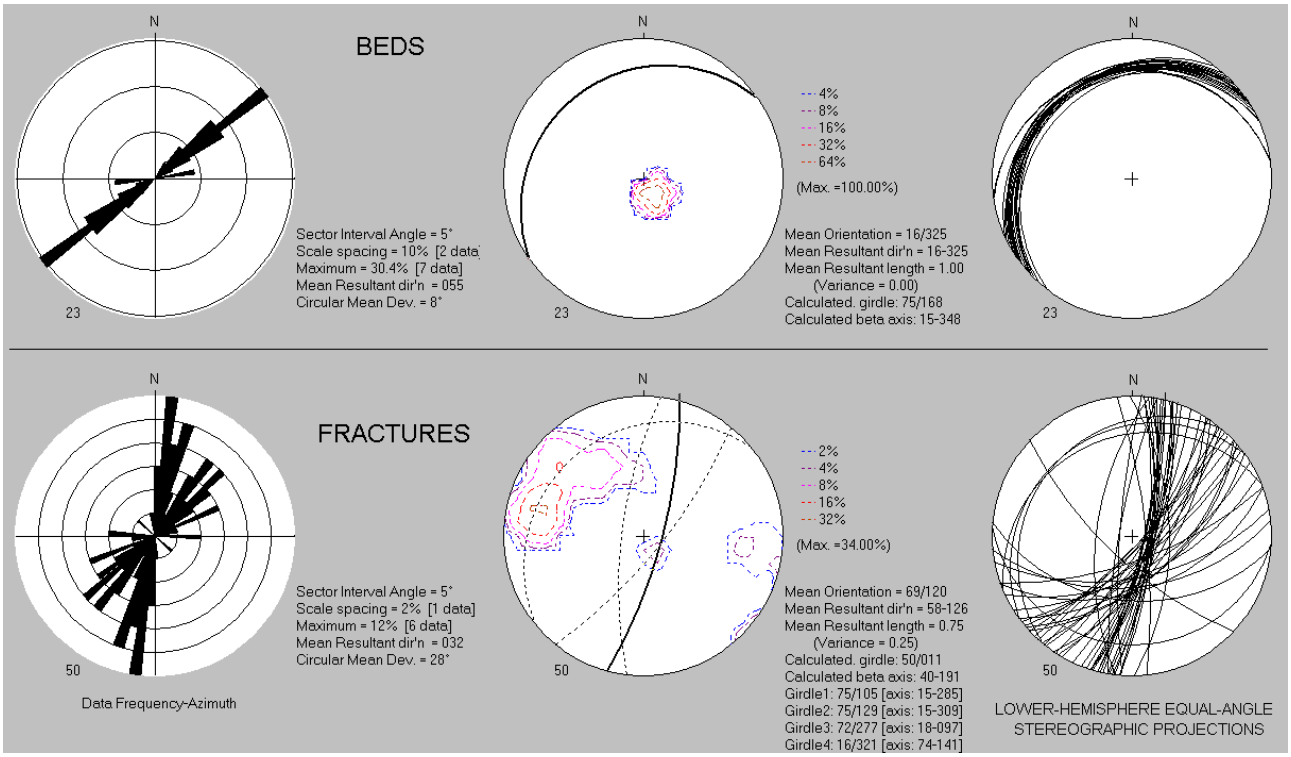

Figure 4C1. Map (above) showing wells 112 at Pine Hill Rd., Delaware Twp., Hunterdon County, NJ. Bedrock structures mapped near wells based on a structural analysis of OPTV data (below).

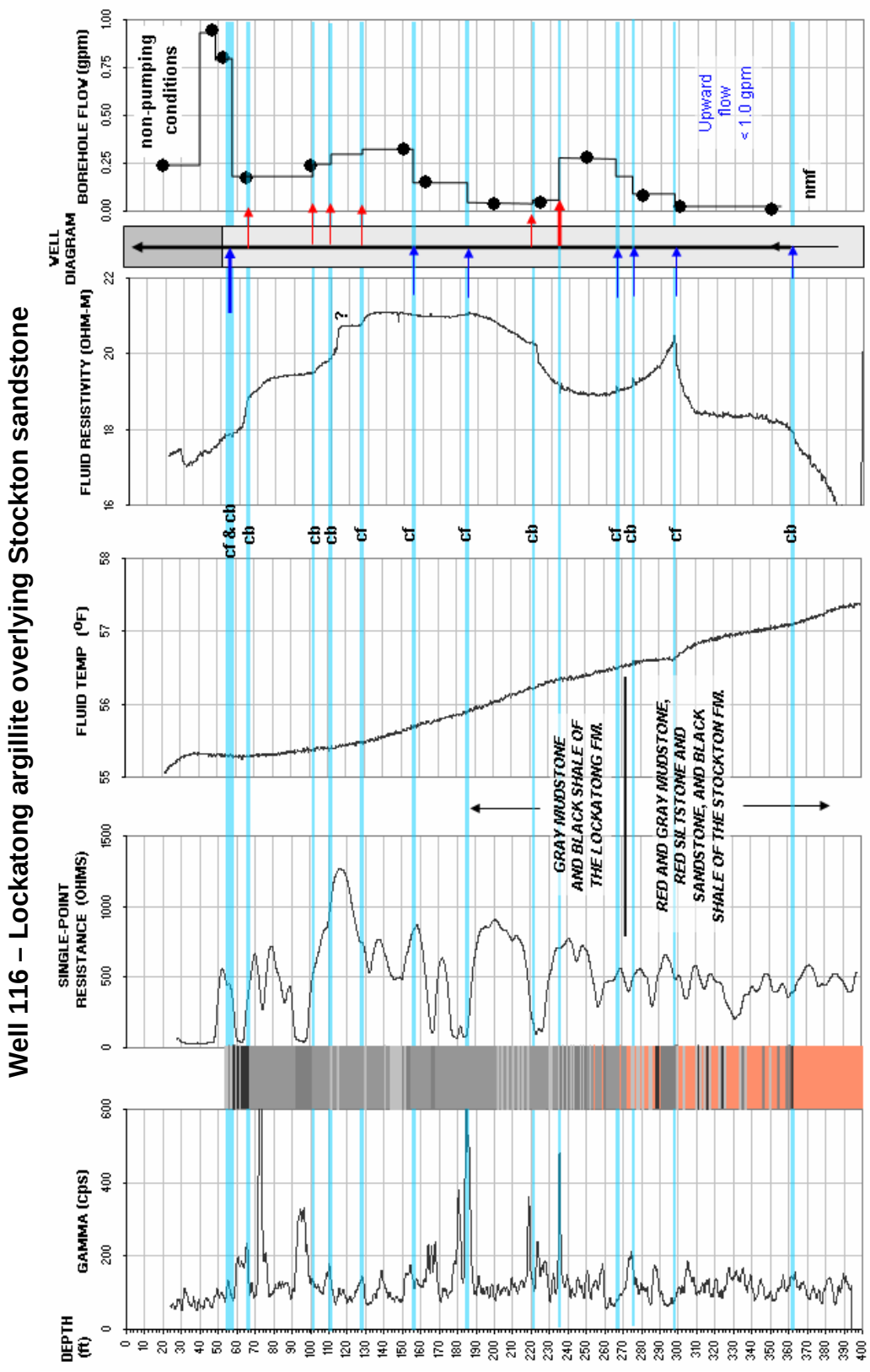

FIGURE 4C2. Hydrogeologic section based on geophysical logs for well 116 at Pine Hill Rd., Delaware Twp., Hunterdon County, NJ. The section shows the vertical distribution and types of hydraulically-conductive features and water-bearing zones in red and gray sandstone, siltstone and mudstone, and black shale. Depth values are in feet below land surface.

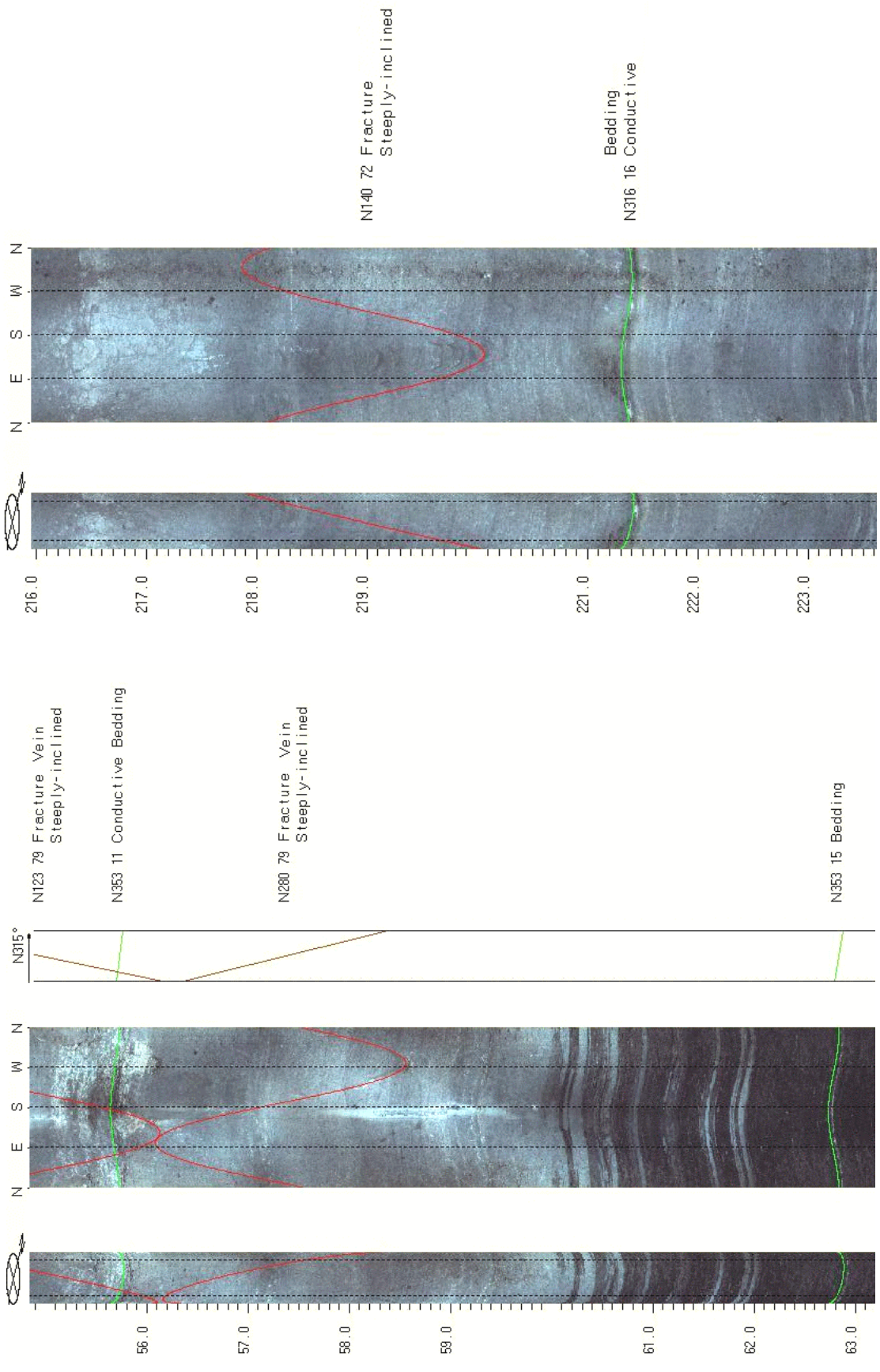

FIGURE 4C3. OPTV records of 6-inch diameter well 116 at Pine Hill Rd., Delaware Twp., Hunterdon County, NJ showing geologic structures and hydraulically-conductive features gray argillite siltstone, sandstone, argillite and black shale. Depth values are in feet below land surface.

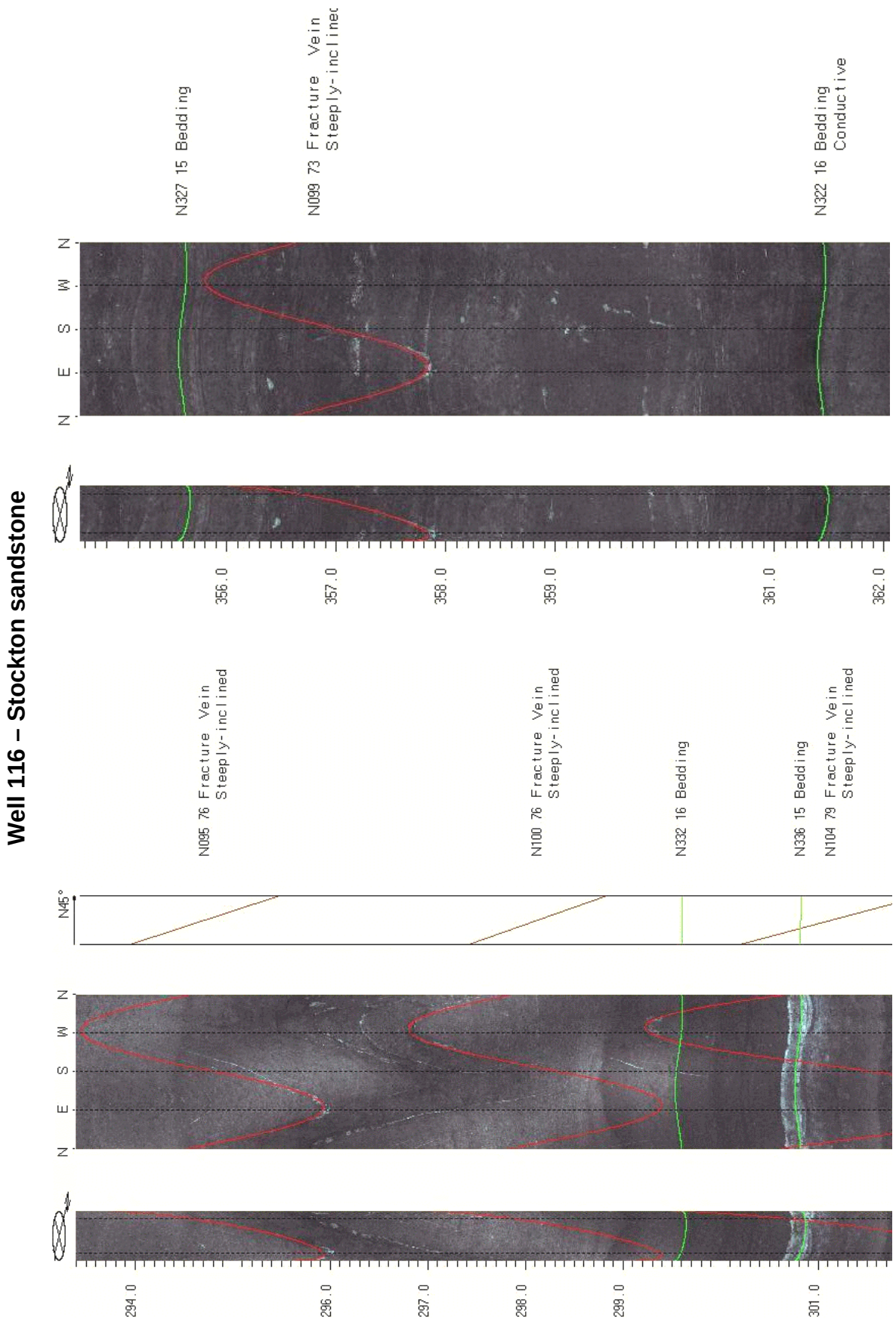

FIGURE 4C4. OPTV records of 6-inch diameter well 116 at Pine Hill Rd., Delaware Twp., Hunterdon County, NJ showing geologic structures and hydraulically-conductive features in red sandstone, siltstone, mudstone and gray siltstone. Depth values are in feet below land surface.

Wells 117 to 119 – Stockton sandstone

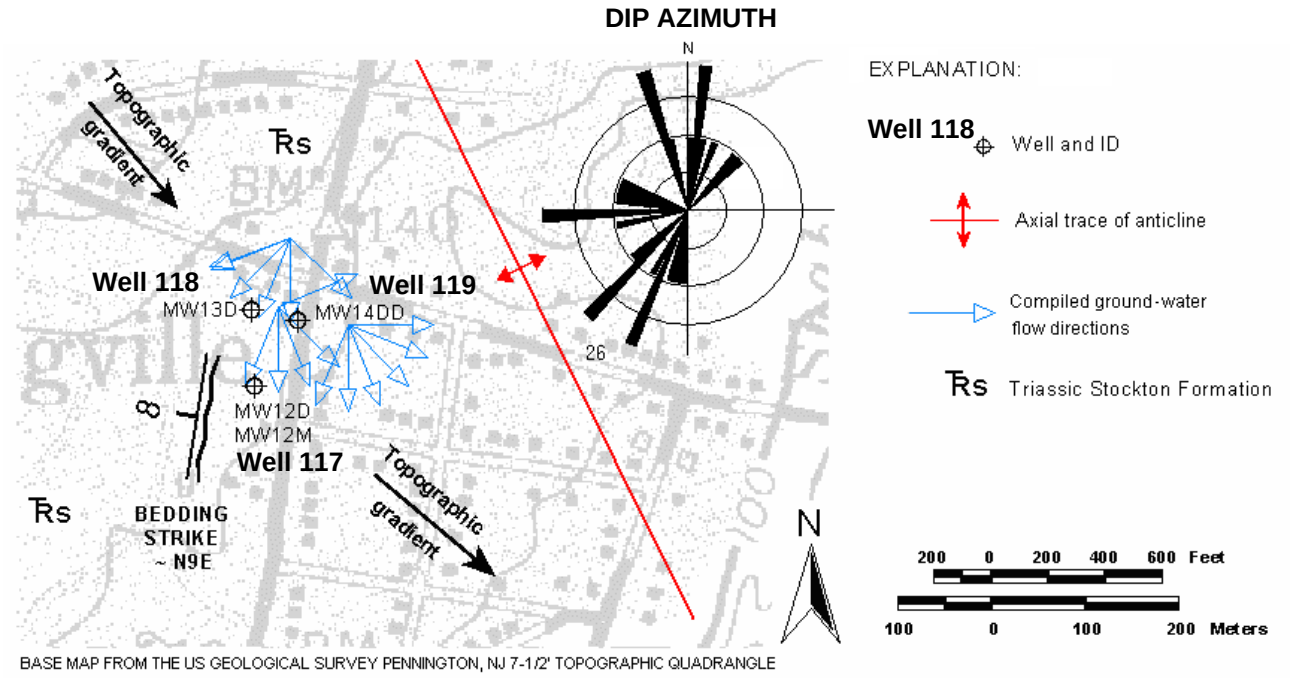

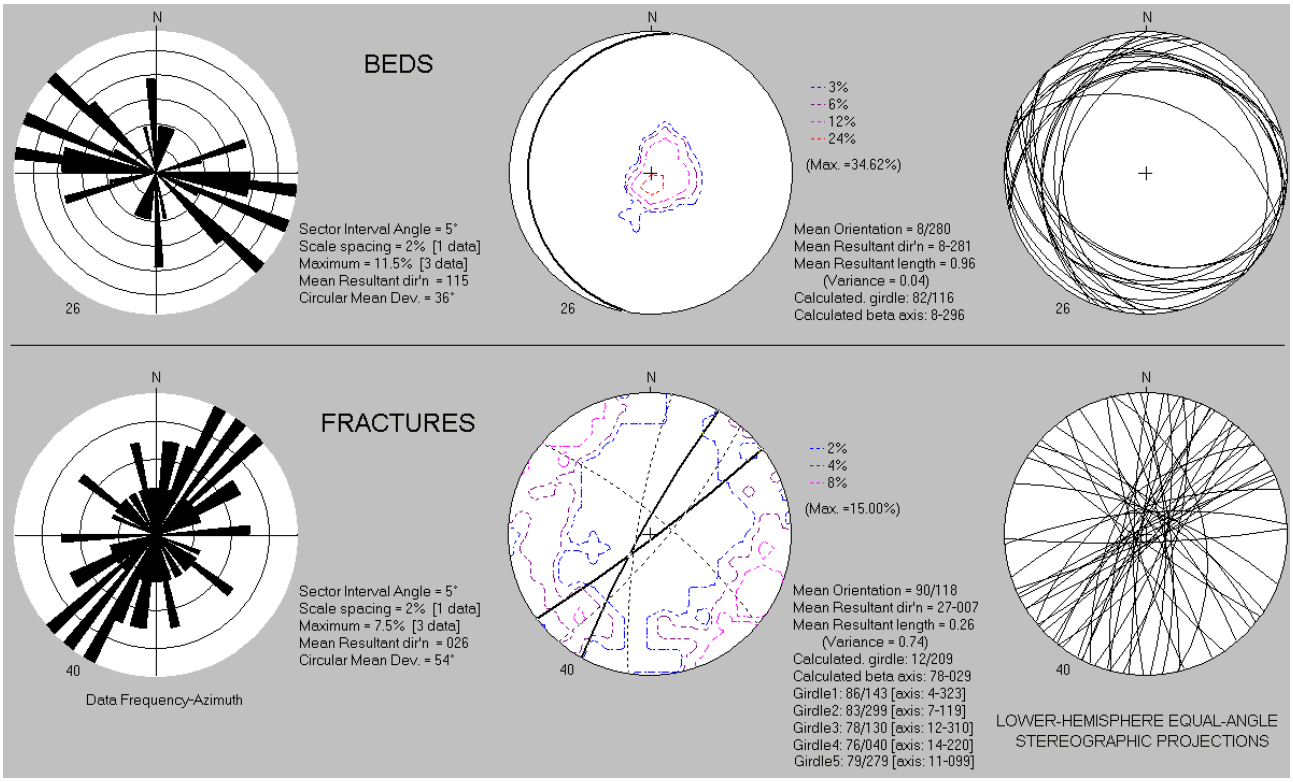

Figure 4D1. Map (above) shows wells 117 to 119 at Ewingville Rd. and Rt 31, Ewing Twp., Mercer County, NJ. Mapped structures based on structural analysis of OPTV records (below). Histogram on map shows dip azimuth of bedding for combined well records. Ground-water flow directions compiled from NJDEP case files for period 1987-2004.

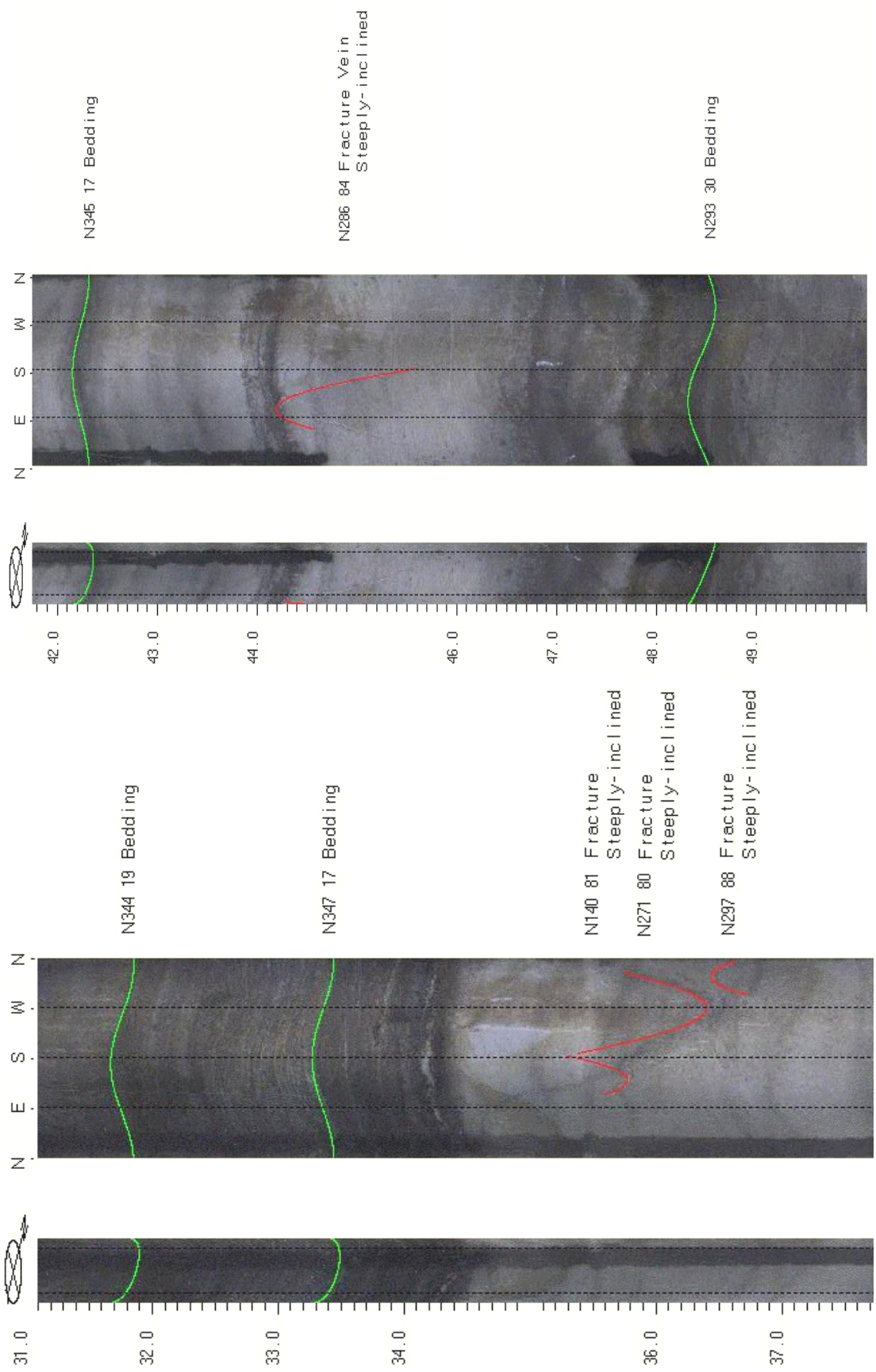

FIGURE 4D2. OPTV records of 6-inch diameter well 117 at Ewingville Rd. and Rt 31, Ewing Twp., Mercer County, NJ showing geologic structures and hydraulically-conductive features in sandstone and siltstone. Depth values are in feet below land surface.

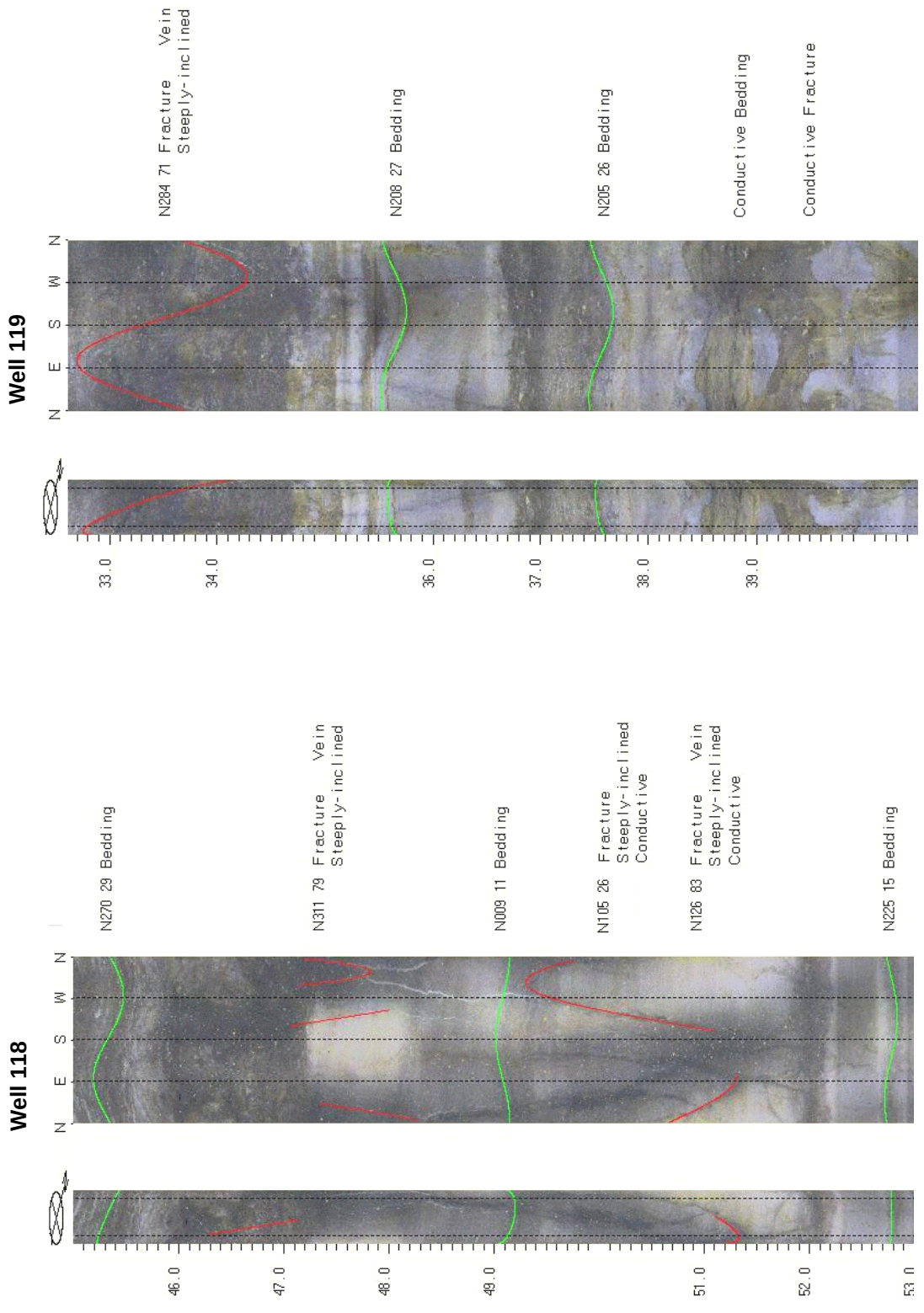

FIGURE 4D3. OPTV records of 6-inch diameter wells 118 and 119 at Ewingville Rd. and Rt 31, Ewing Twp., Mercer County, NJ showing geologic structures and hydraulically-conductive features in sandstone and siltstone. Depth values are in feet below land surface.

Wells 120 and 121 – Stockton sandstone

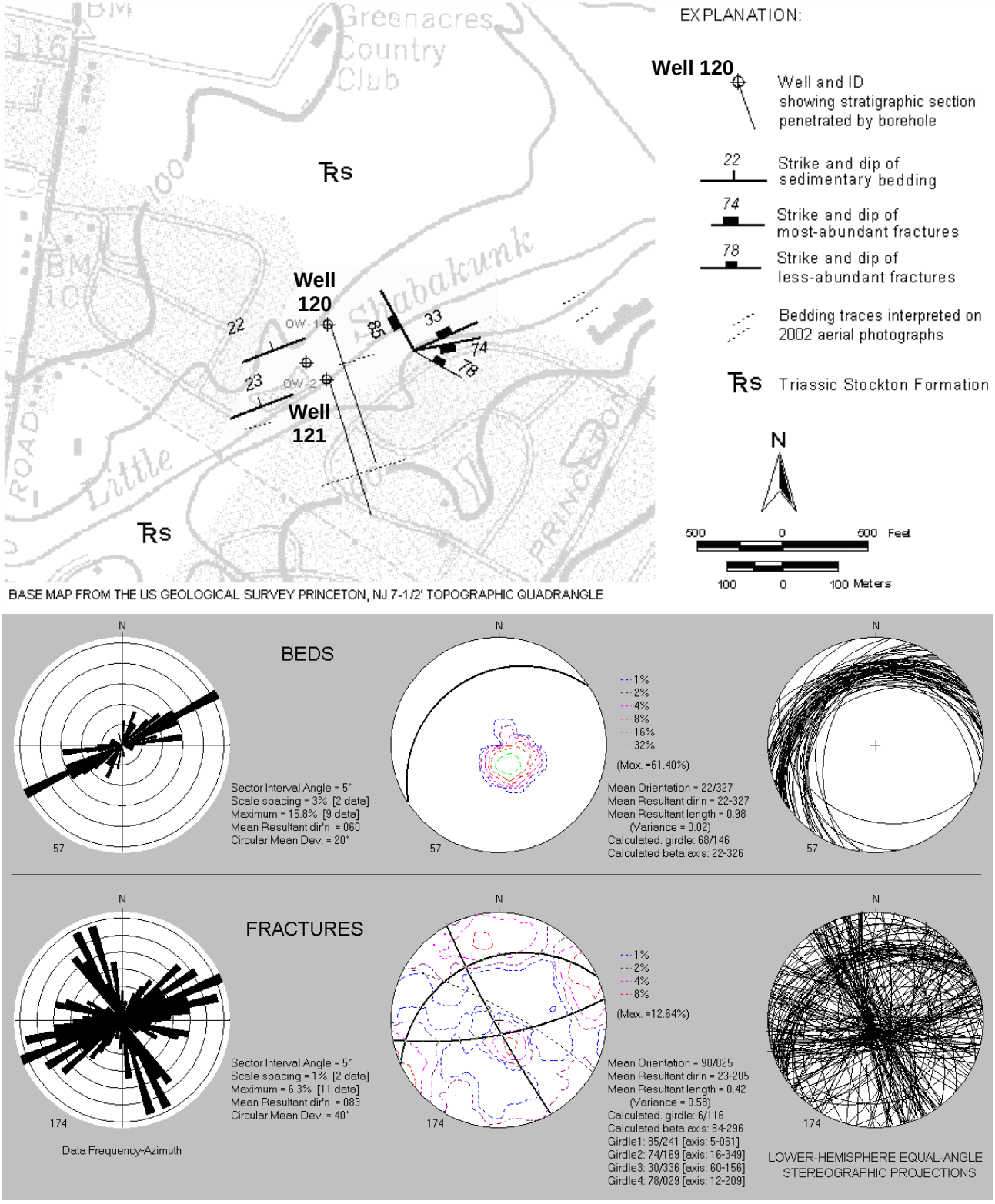

Figure 4E1. Map (above) shows wells 120 and 121 at the Greenacres Country Club, Rt. 206, Lawrence Twp., Mercer County, NJ. Structure strikes and dips on map based on structural analysis of beds and fractures in OPTV records (below).

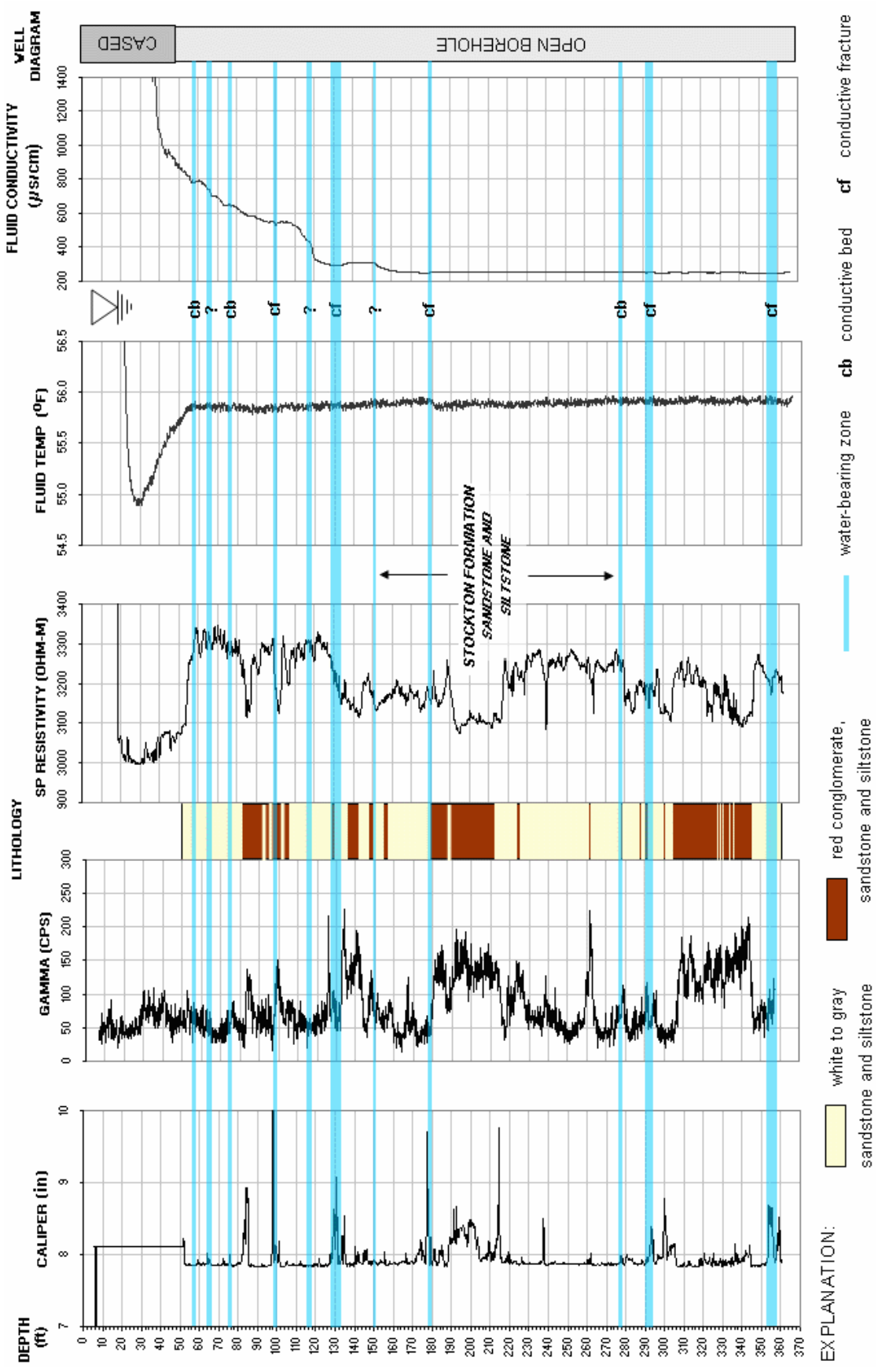

FIGURE 4E2. Hydrogeologic section based on geophysical logs for well 120 at the Greenacres Country Club, Rt. 206, Lawrence Twp., Mercer County, NJ. The section shows the vertical distribution and types of hydraulically-conductive features and water-bearing zones in red and gray sandstone, siltstone and mudstone and black shale. Depth values are in feet below land surface.

Wells 120 – Stockton sandstone

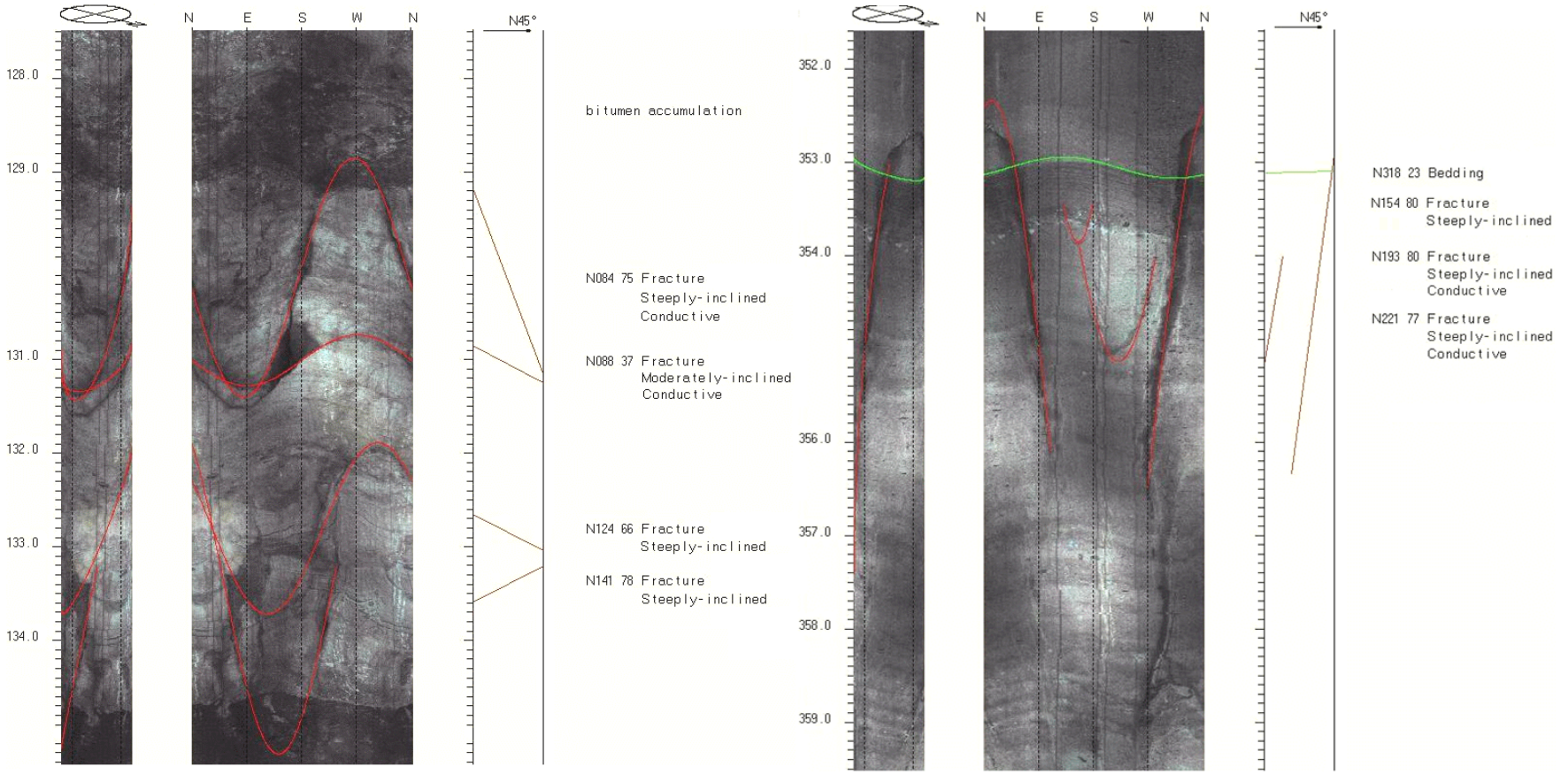

FIGURE 4E3. OPTV records of 8-inch diameter well 120 at the Greenacres Country Club, Rt. 206, Lawrence Twp., Mercer County, NJ showing geologic structures and hydraulically-conductive features in red gray sandstone and siltstone. Depth values are in feet below land surface.

Well 121 – Stockton sandstone

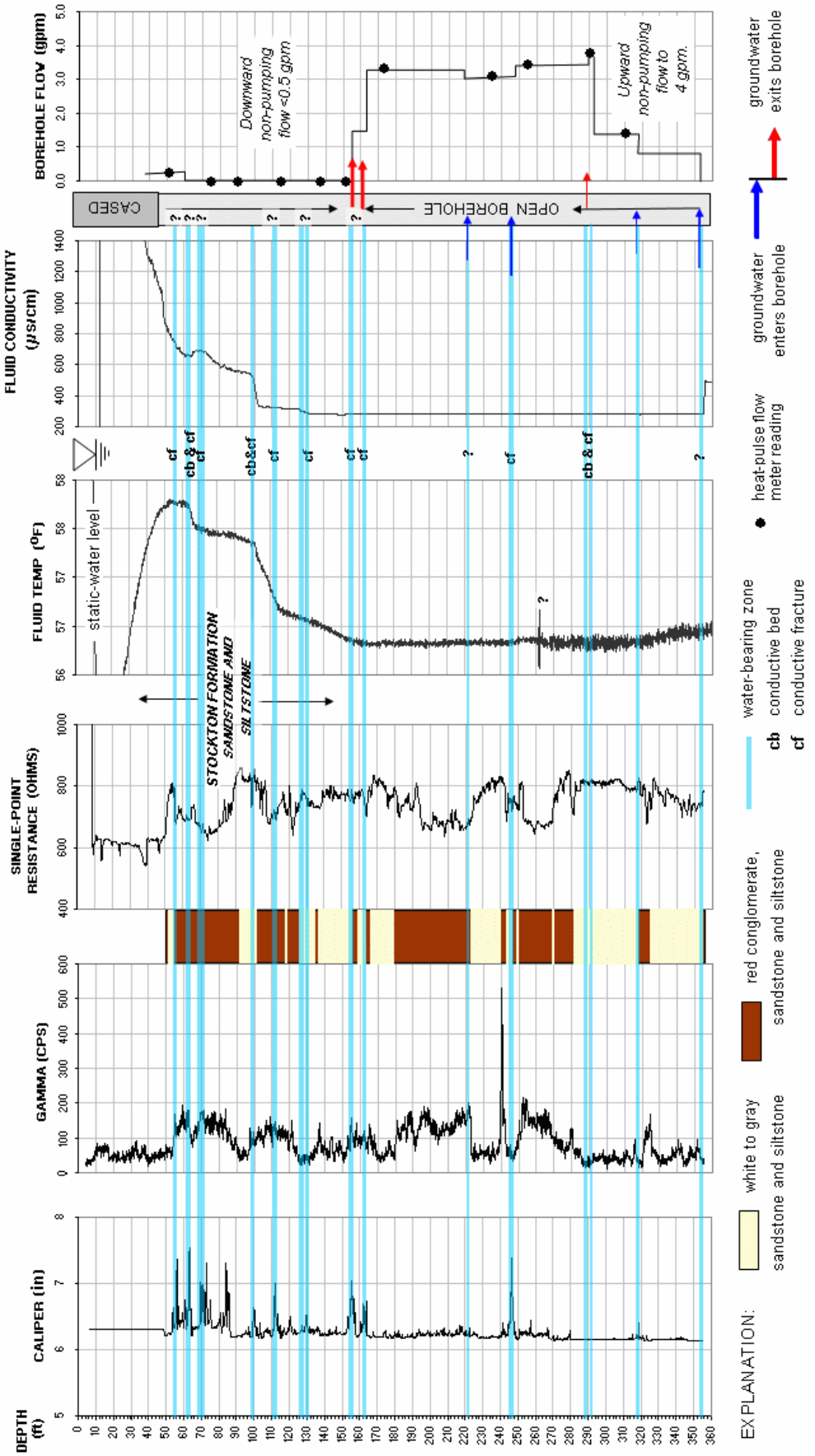

FIGURE 4E4. Hydrogeologic section based on geophysical logs for well 121 at the Greenacres Country Club, Rt. 206, Lawrence Twp., Mercer County, NJ. The section shows the vertical distribution and types of hydraulically-conductive features and water-bearing zones in red and gray sandstone, siltstone and mudstone and black shale. Depth values are in feet below land surface.

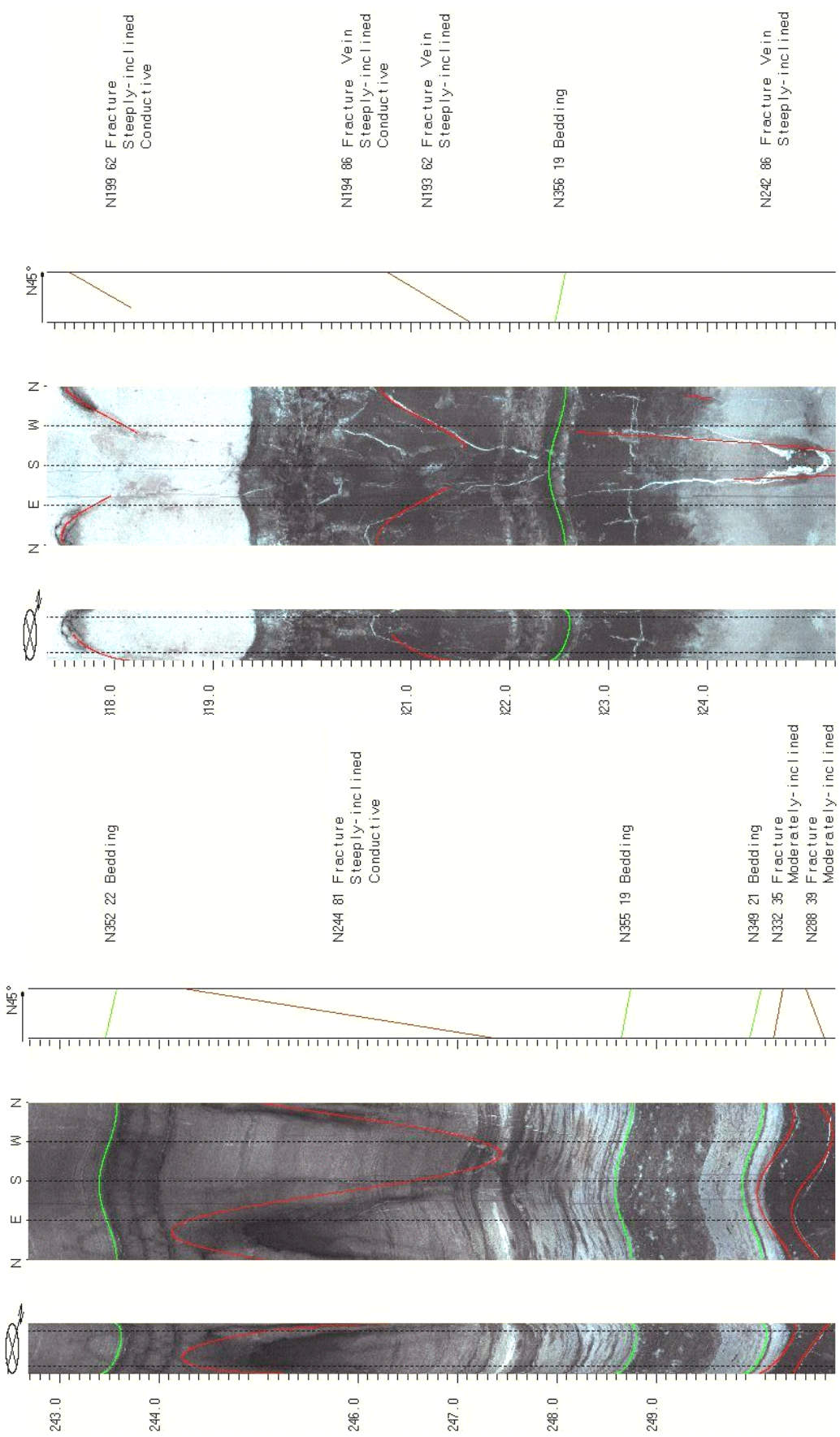

FIGURE 4E5. OPTV records of 6-inch diameter well 121 at the Greenacres Country Club, Rt. 206, Lawrence Twp., Mercer County, NJ showing geologic structures and hydraulically-conductive features in red gray sandstone and siltstone. Depth values are in feet below land surface.

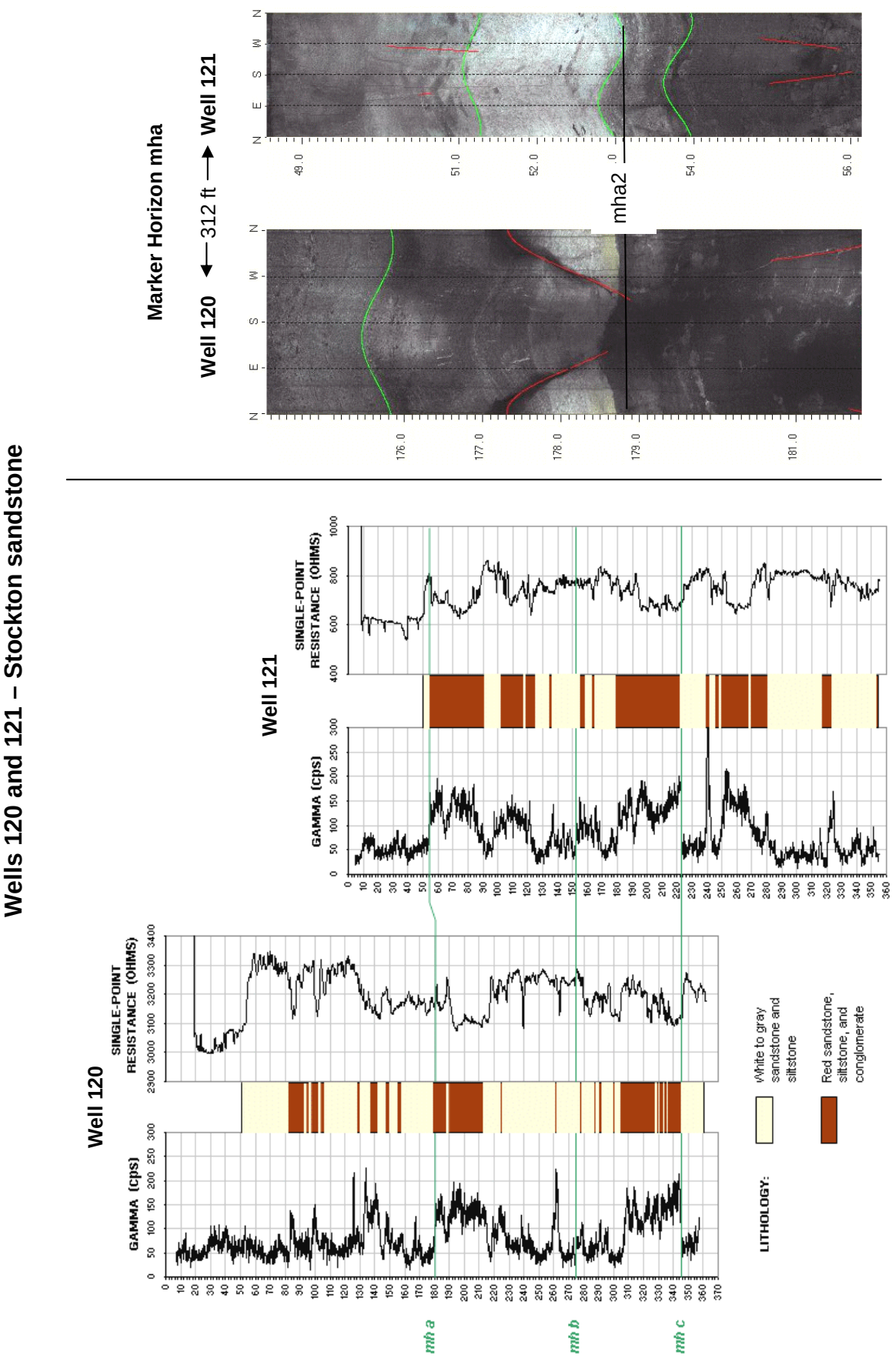

Figure 4E6. Stratigraphic correlation of wells 120 and 121 at the Greenacres Country Club, Rt. 206, Lawrence Twp., Mercer County, NJ based on natural gamma and electrical-resistivity logs (left) and OPTV records (right). Stratigraphic marker horizon mha is shown in both figures. Depth values are in feet below land surface.

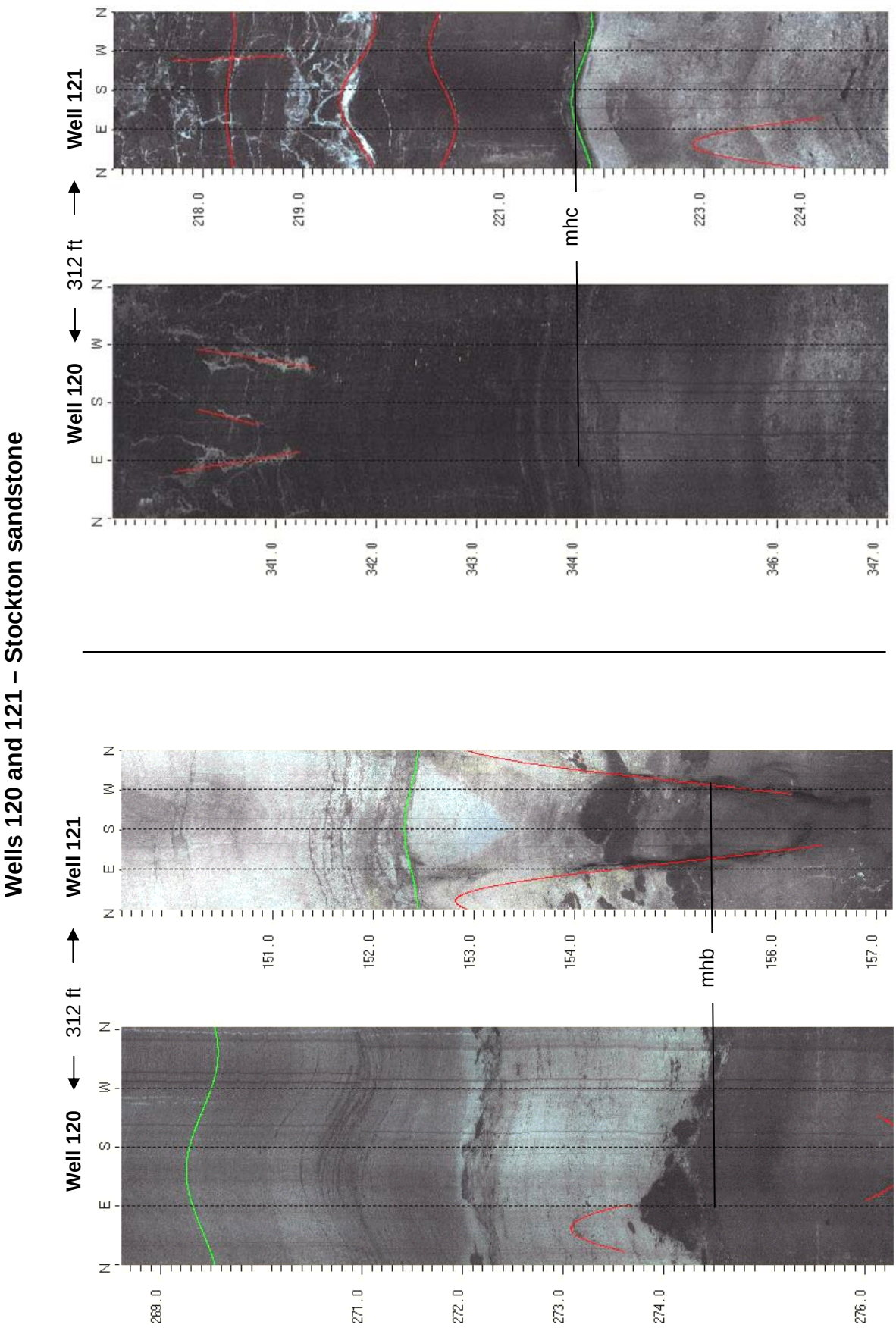

Figure 4E7. Stratigraphic correlation of wells 120 and 121 at the Greenacres Country Club, Rt. 206, Lawrence Twp., Mercer County, NJ based on OPTV records and showing stratigraphic marker horizons mhb (left) and mhc (right). Depth values are in feet below land surface.

Wells 122 to 124 – Stockton sandstone

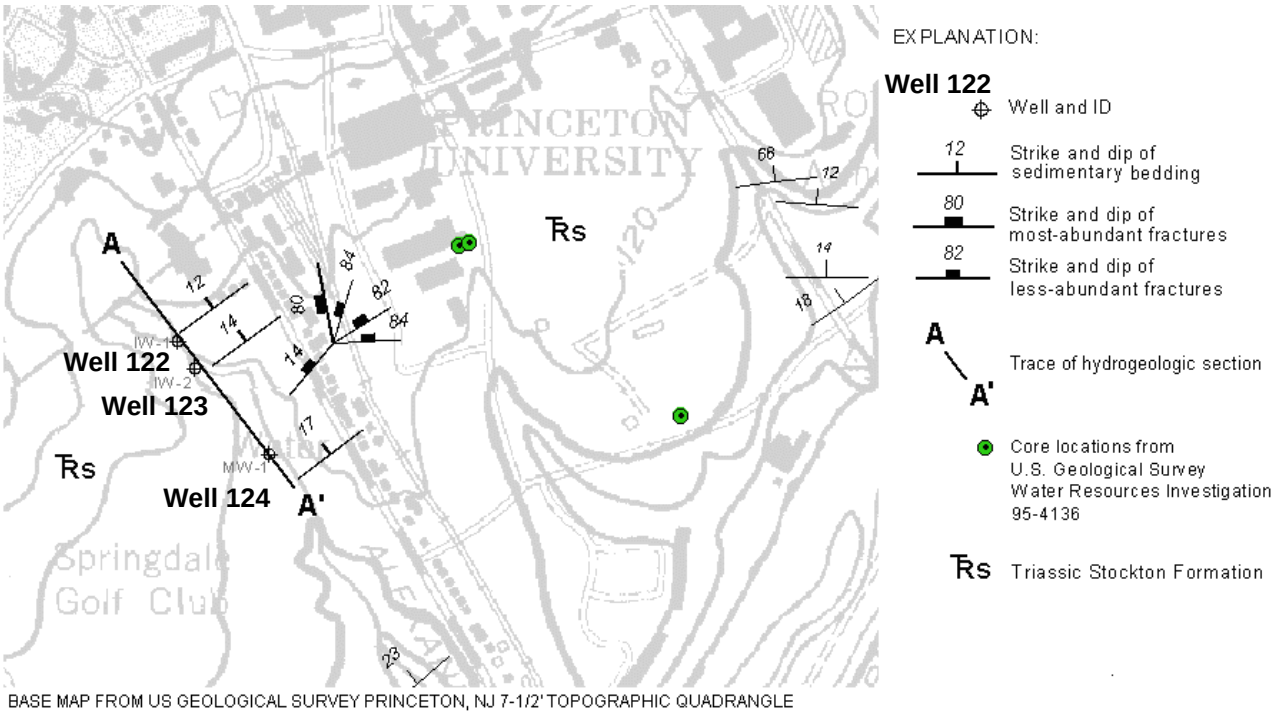

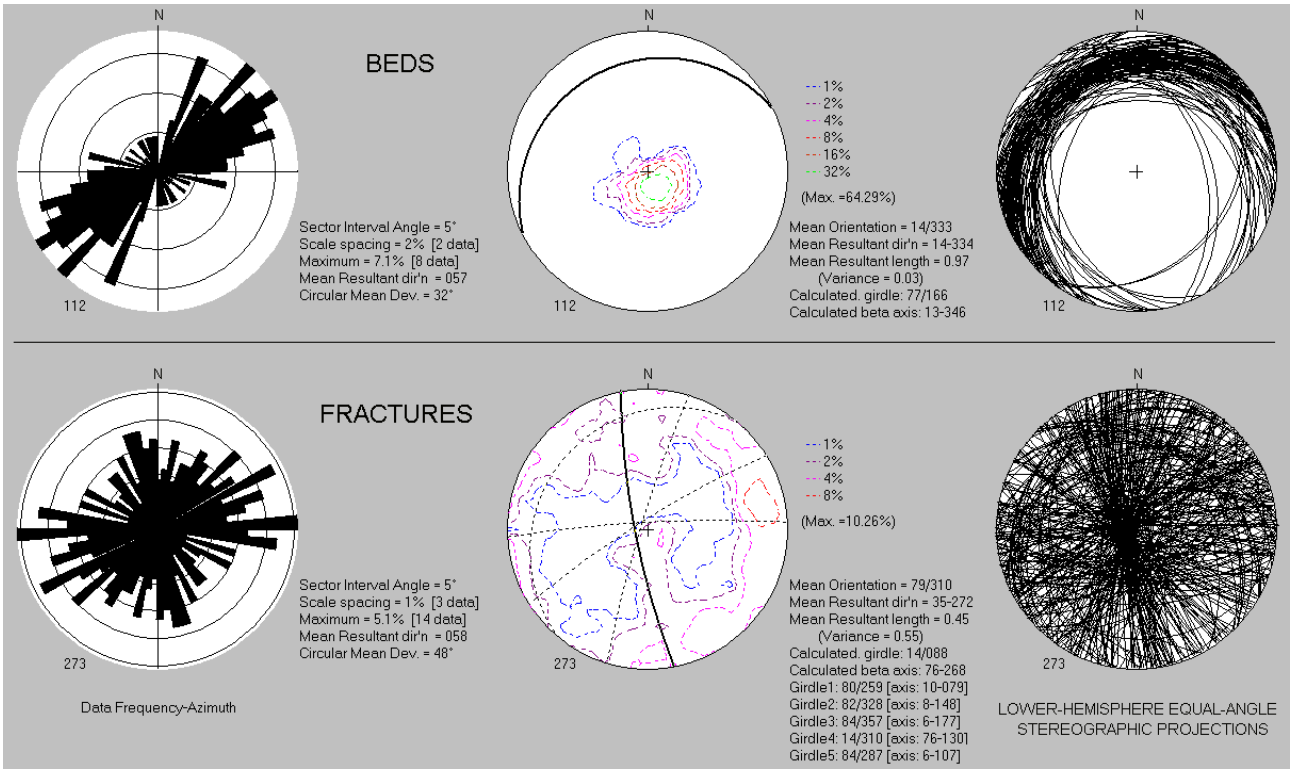

Figure 4F1. Map (above) shows wells 122 through 124 at the Springdale Golf Club, Princeton Twp., Mercer County, NJ. Structure strikes and dips near wells based on structural analysis of beds and fractures in OPTV records (below). Other bed orientations mapped in outcrop by the NJ Geological Survey.

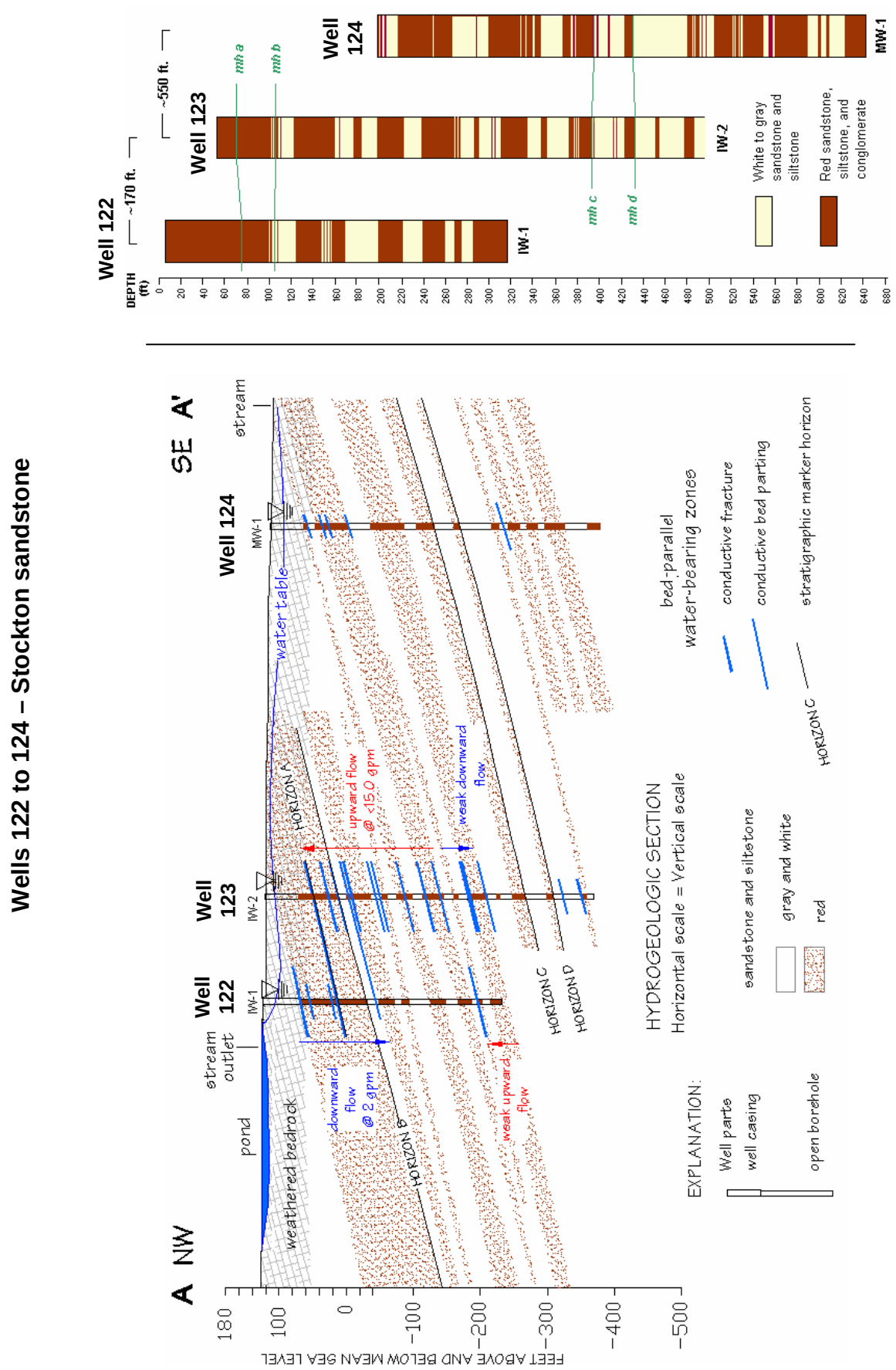

Figure 4F2. Hydrogeologic section (left) and stratigraphic section (right) showing stratigraphic correlation between wells 122 to 124 at the Springdale Golf Club, Princeton Twp., Mercer County, NJ. Depth valuyes for the sections on the right are in feet below land surface.

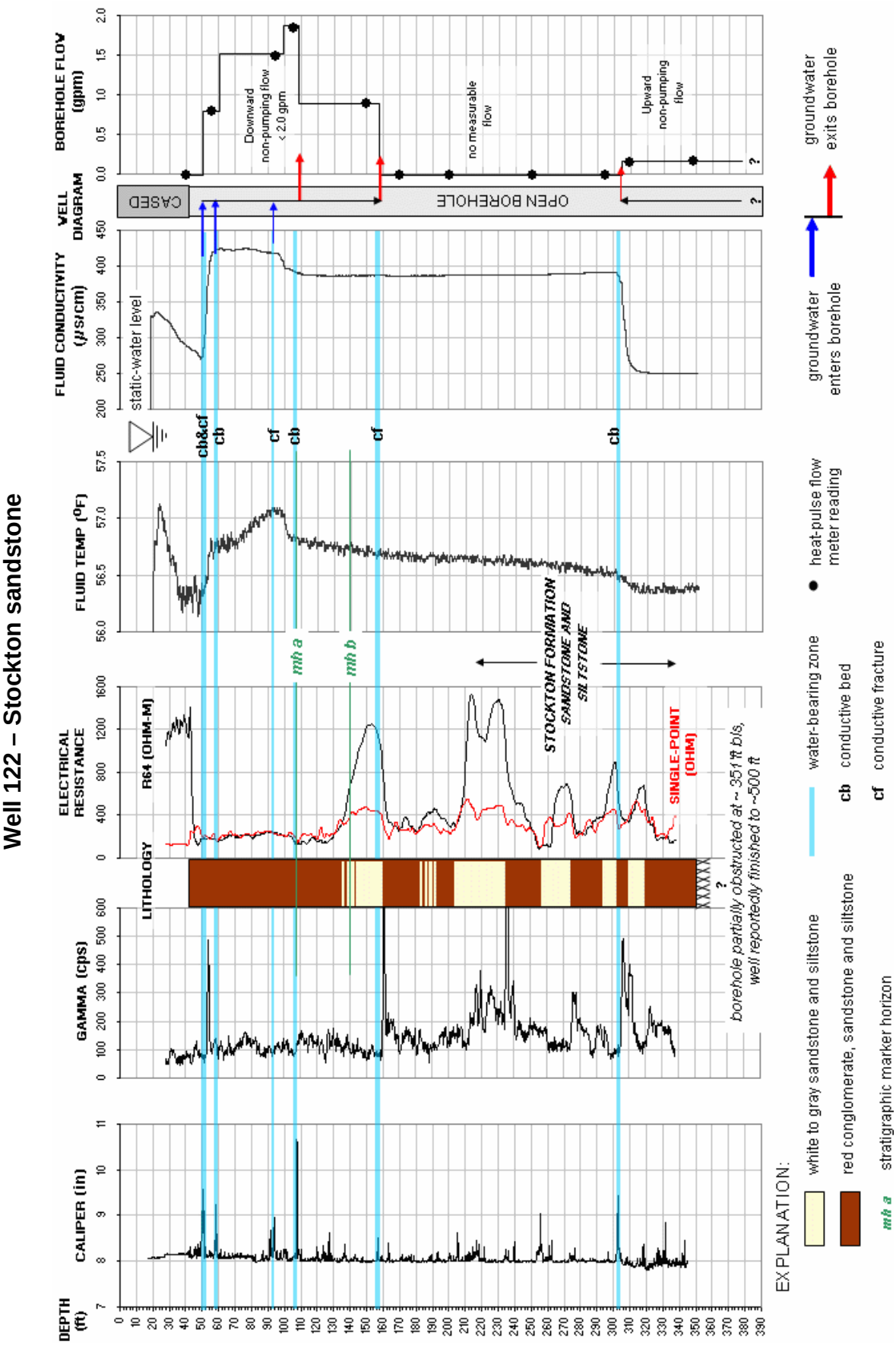

Figure 4F3. Hydrogeologic section based on geophysical logs summarizing the distribution and types of hydraulically-conductive features in well 122 at the Springdale Golf Club, Princeton Twp., Mercer County, NJ. Depth values are in feet below land surface.

Well 122 – Stockton sandstone

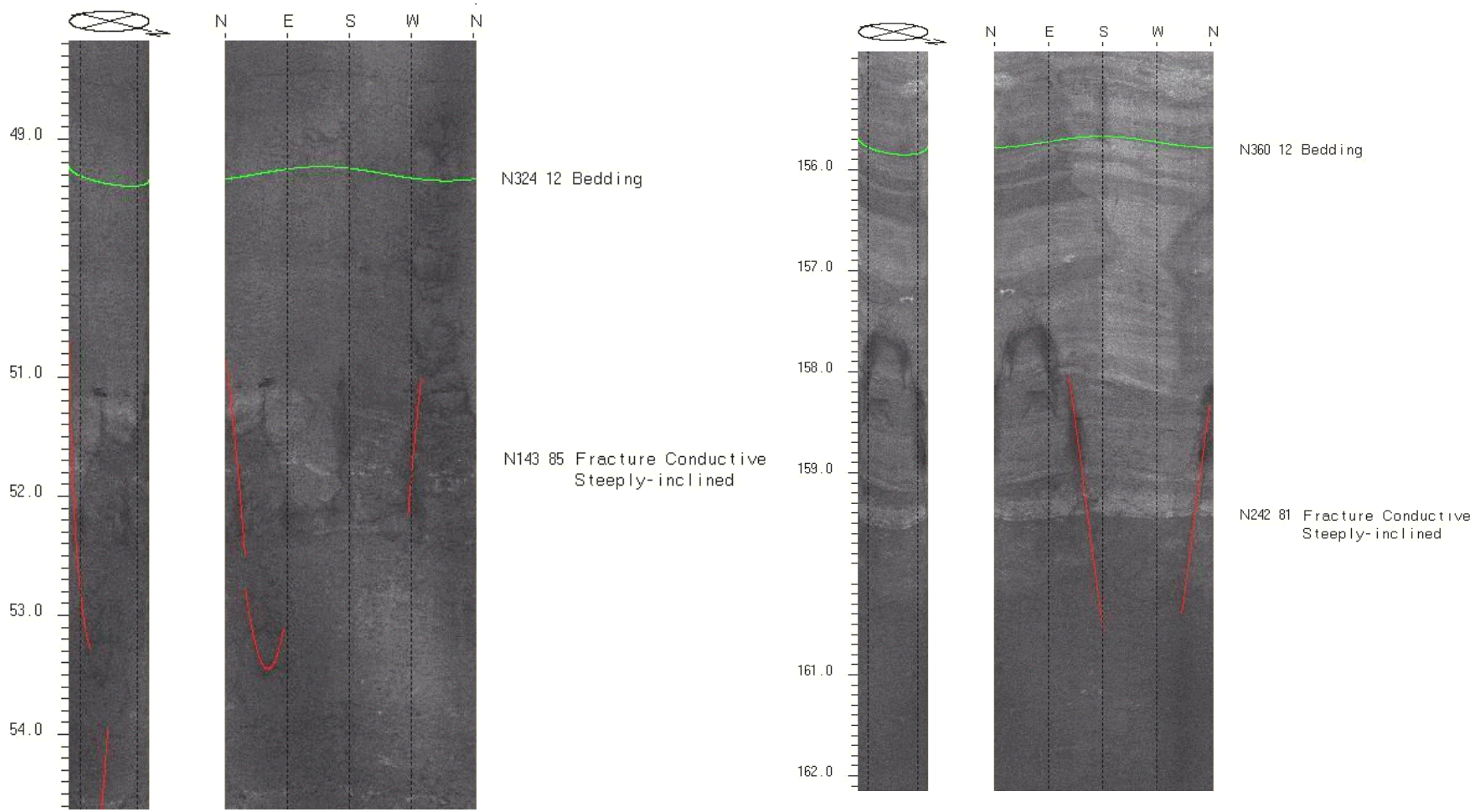

Figure 4F4. OPTV records of 8-inch diameter well 122 at the Springdale Golf Club, Princeton Twp., Mercer County, NJ showing geologic structures and hydraulically-conductive features in red gray and red sandstone and siltstone. Depth values are in feet below land surface.

S

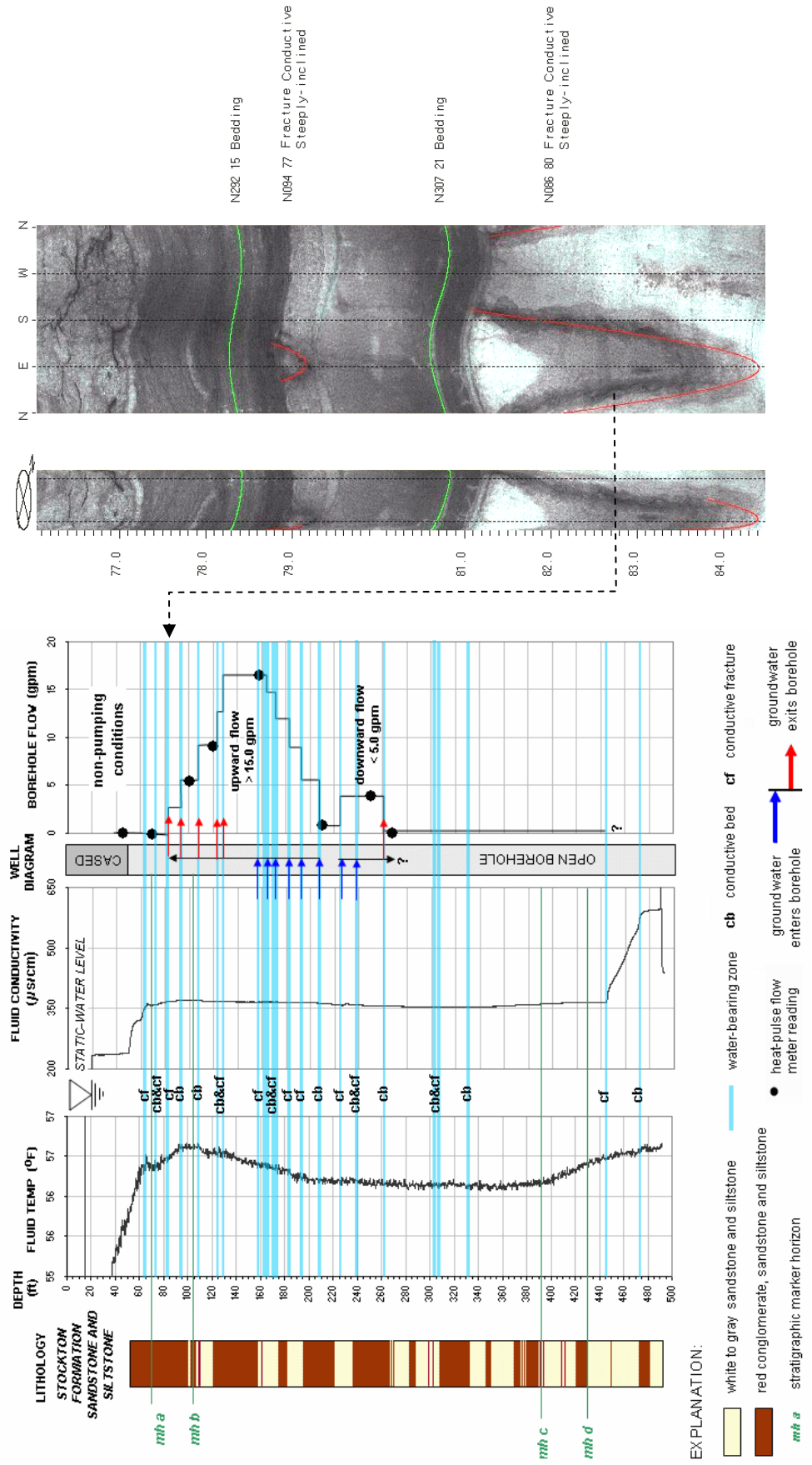

FIGURE 4F5. Hydrogeologic section based on geophysical logs (left) summarizing the distribution and types of hydraulically-conductive features in well 123 at the Springdale Golf Club, Princeton Twp., Mercer County, NJ. OPTV record of the 6-inch diameter well (right) shows geologic structures and hydraulically-conductive features in red and gray sandstone. Depth values are in feet below land surface.

Wells 123 – Stockton v sandstone

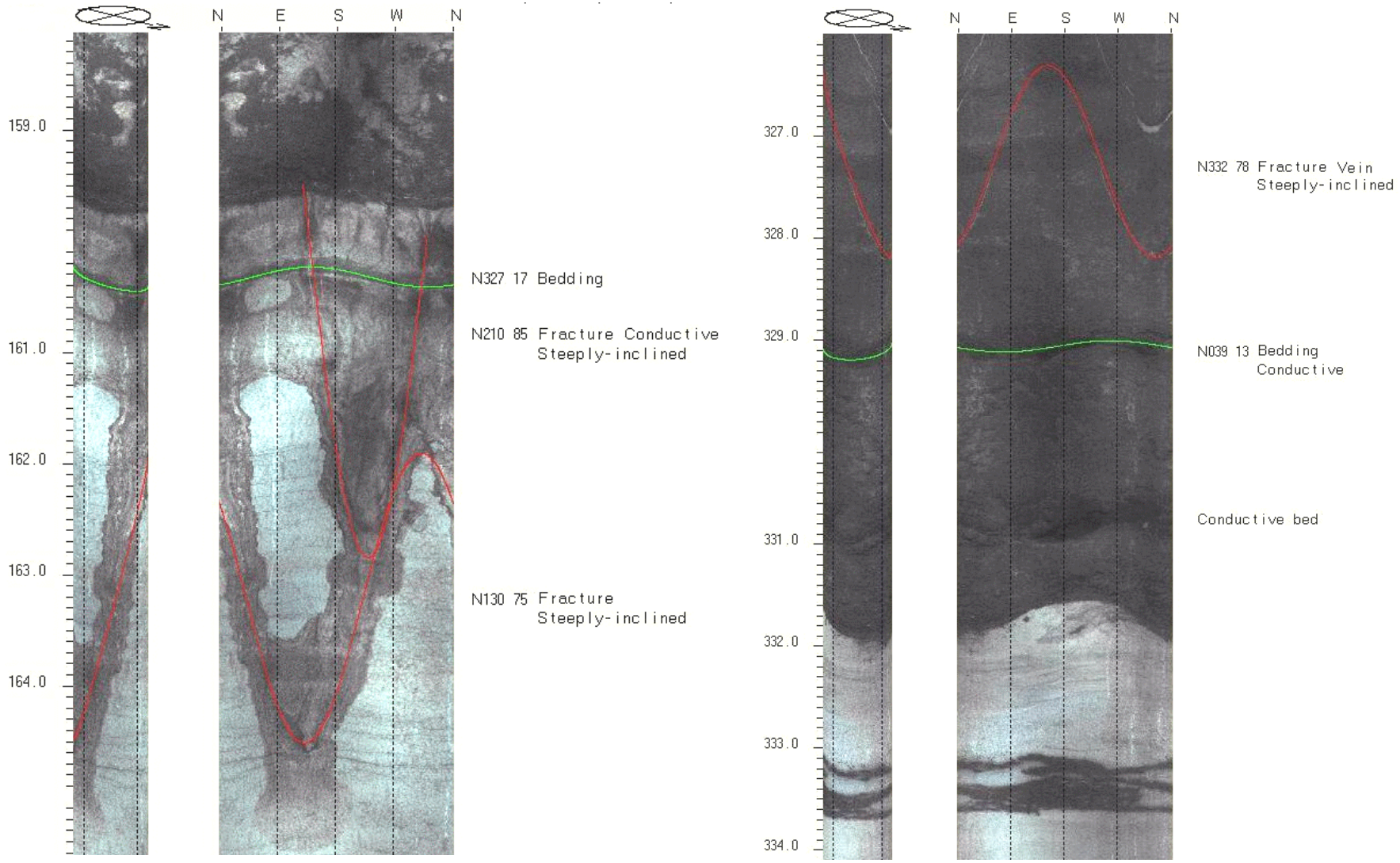

FIGURE 4F6. OPTV records of 8-inch diameter well 123 at the Springdale Golf Club, Princeton Twp., Mercer County, NJ showing geologic structures and hydraulically-conductive features in red gray and red sandstone and siltstone. Depth values are in feet below land surface.

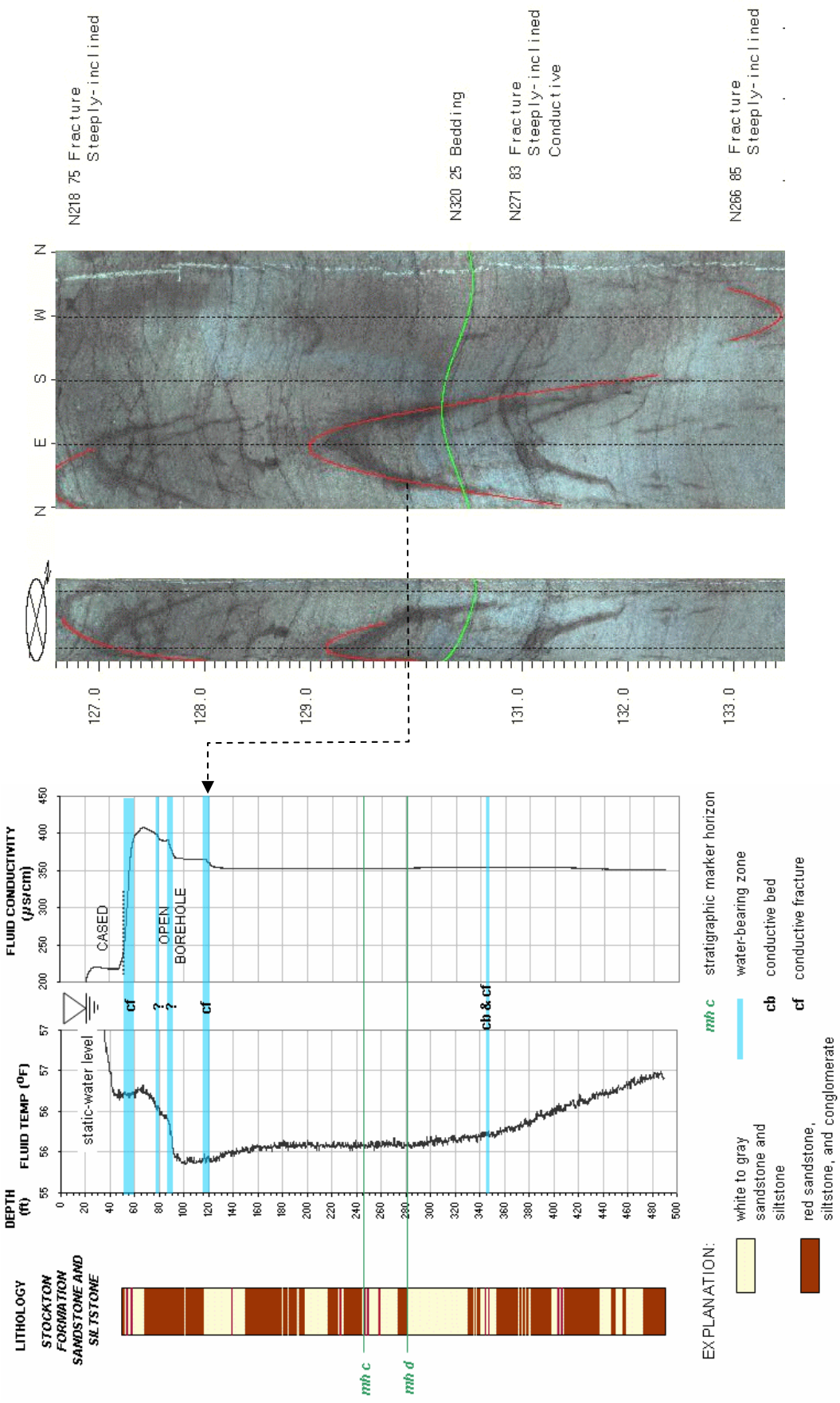

FIGURE 4F7. Hydrogeologic section based on geophysical logs (left) summarizing the distribution and types of hydraulically-conductive features in well 124 at the Springdale Golf Club, Princeton Twp., Mercer County, NJ. OPTV record of the 6-inch diameter well (right) shows geologic structures and hydraulically-conductive features in sandstone. Depth values are in feet below land surface.

Well 124 – Stockton sandstone

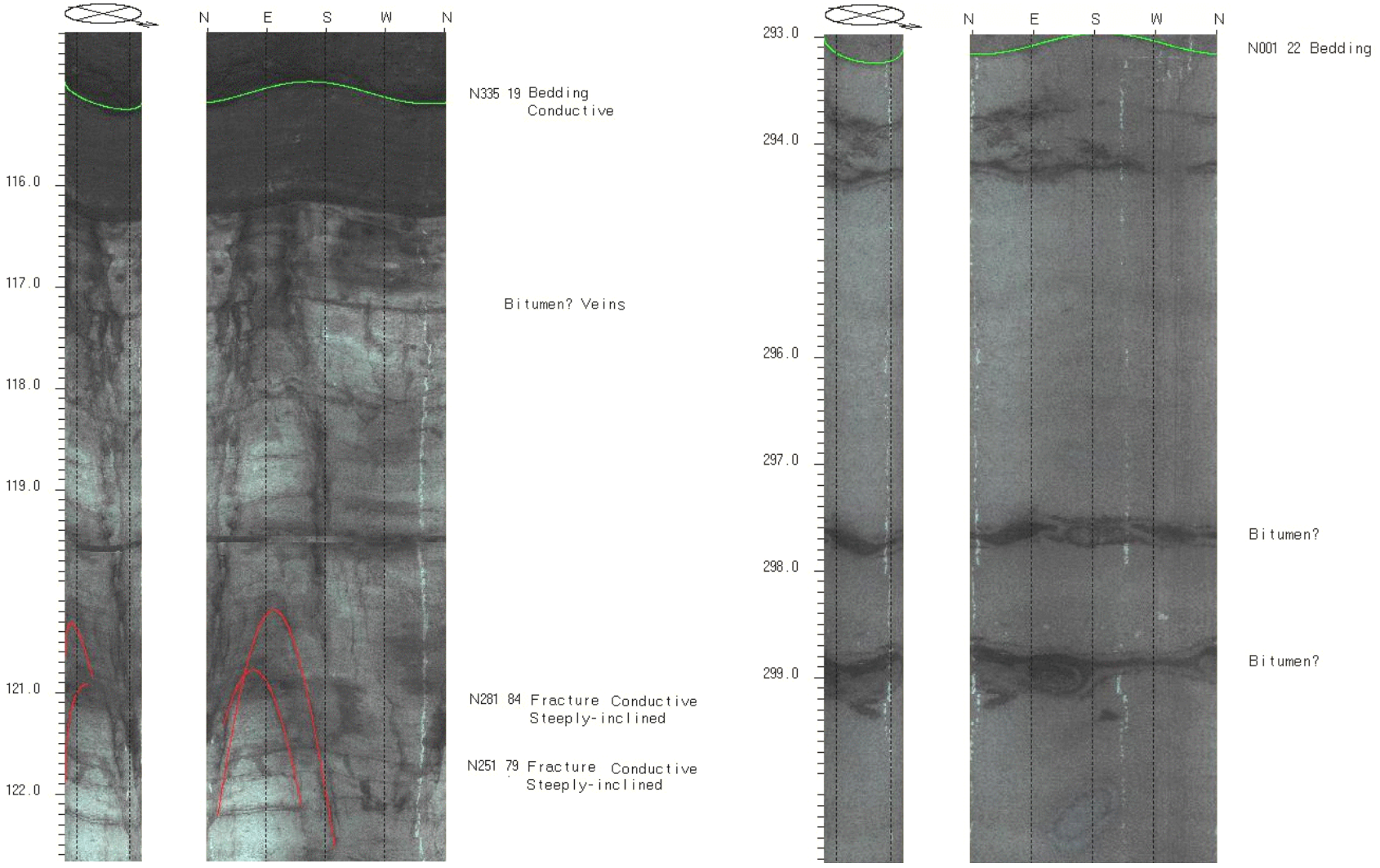

Figure 4F8. OPTV records of 6-inch diameter well 124 at the Springdale Golf Club, Princeton Twp., Mercer County, NJ showing geologic structures and hydraulically-conductive features in red gray and red sandstone and siltstone. Dark streaks and patches are probably relict hydrocarbons (bitumen) that highlight conductive paths. Depth values are in feet below land surface.

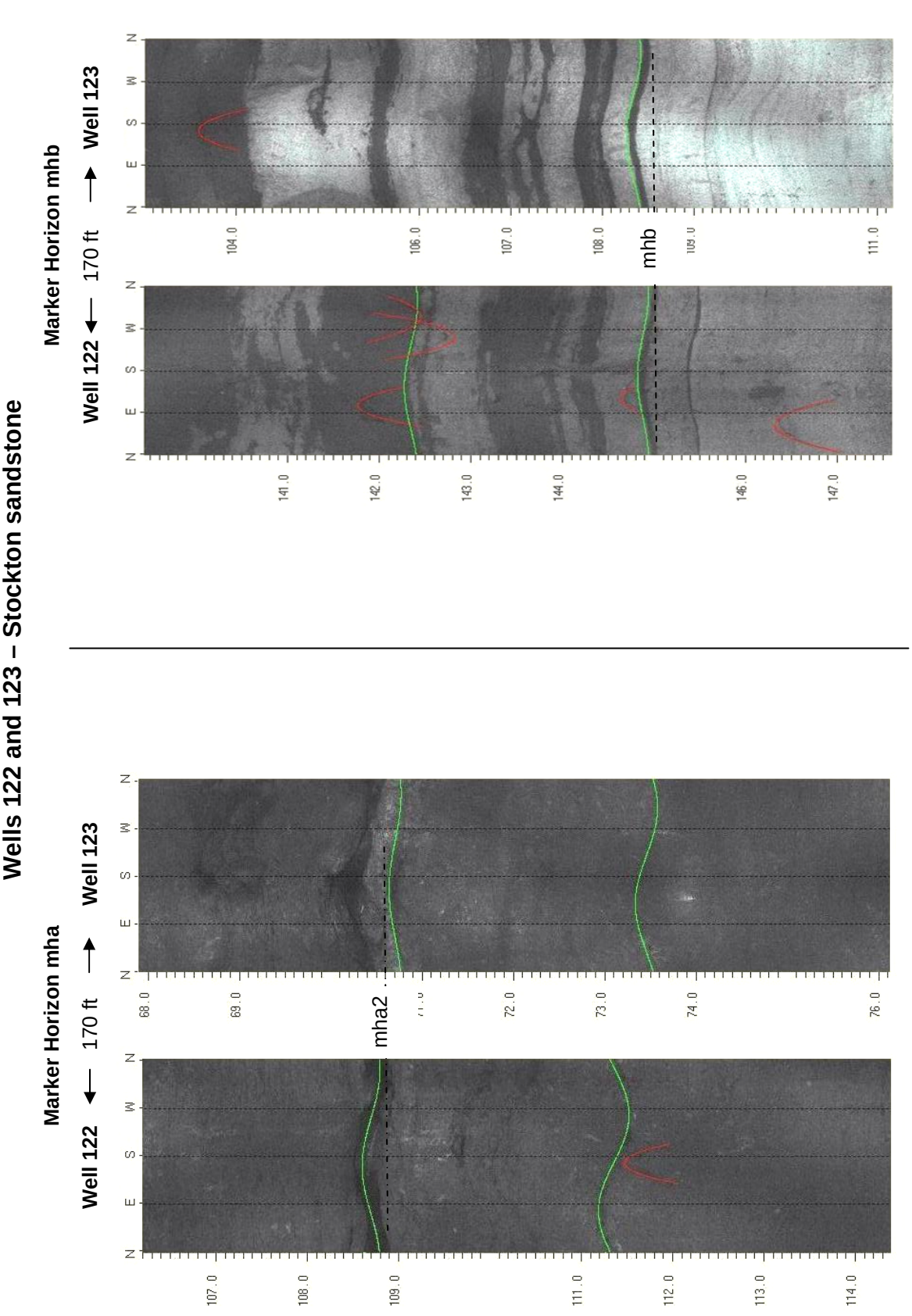

Figure 4F9. Stratigraphic correlation of wells 122 and 123 at the Springdale Golf Club, Princeton Twp., Mercer County, NJ based on OPTV records and showing stratigraphic marker horizons mha (left) and mhb (right). Depth values are in feet below land surface.

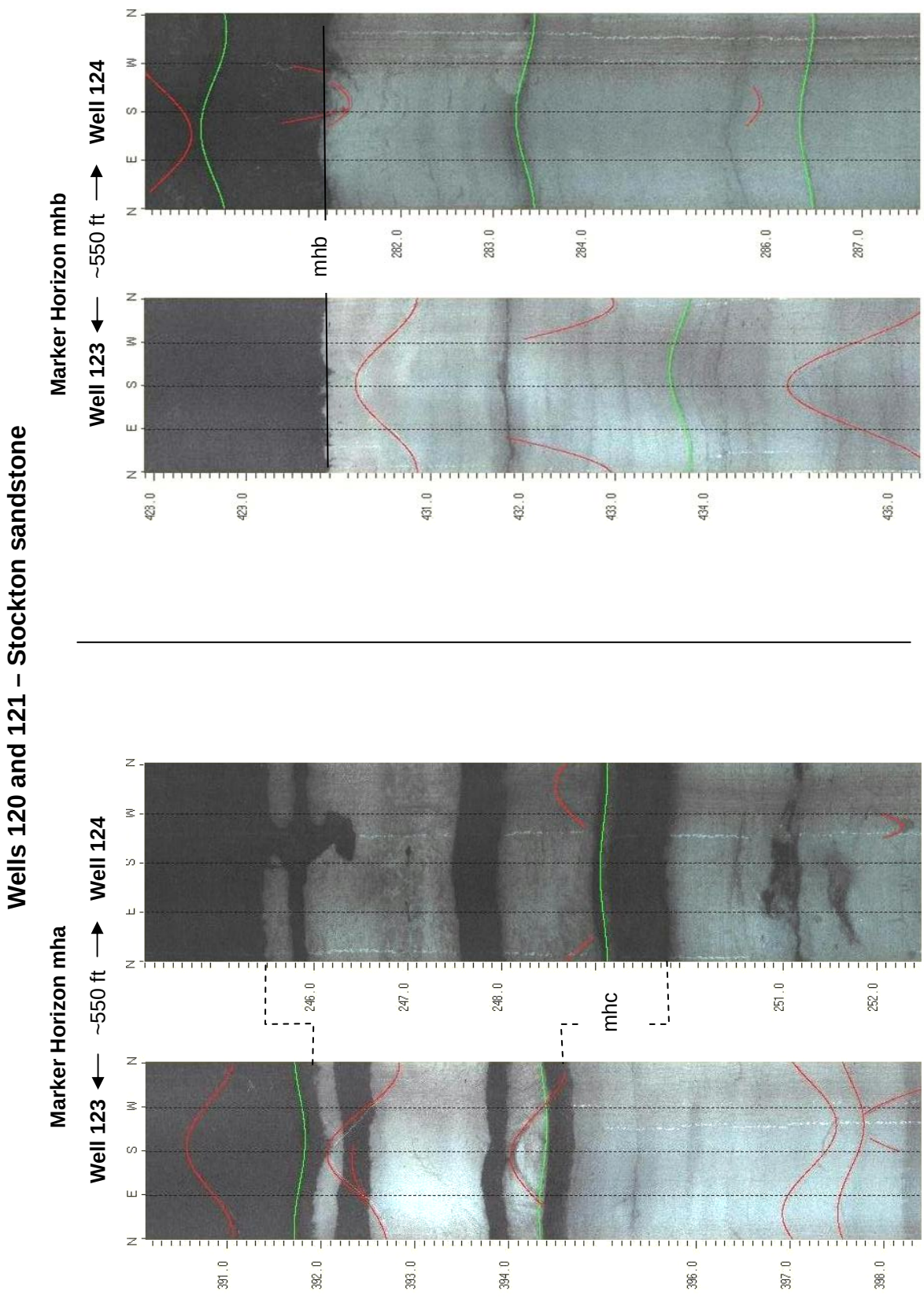

Figure 4F10. Stratigraphic correlation of wells 122 and 124 at the Springdale Golf Club, Princeton Twp., Mercer County, NJ based on OPTV records and showing stratigraphic marker horizons mhc (left) and mhd (right). Depth values are in feet below land surface.

Wells 125 to 127 – Stockton sandstone

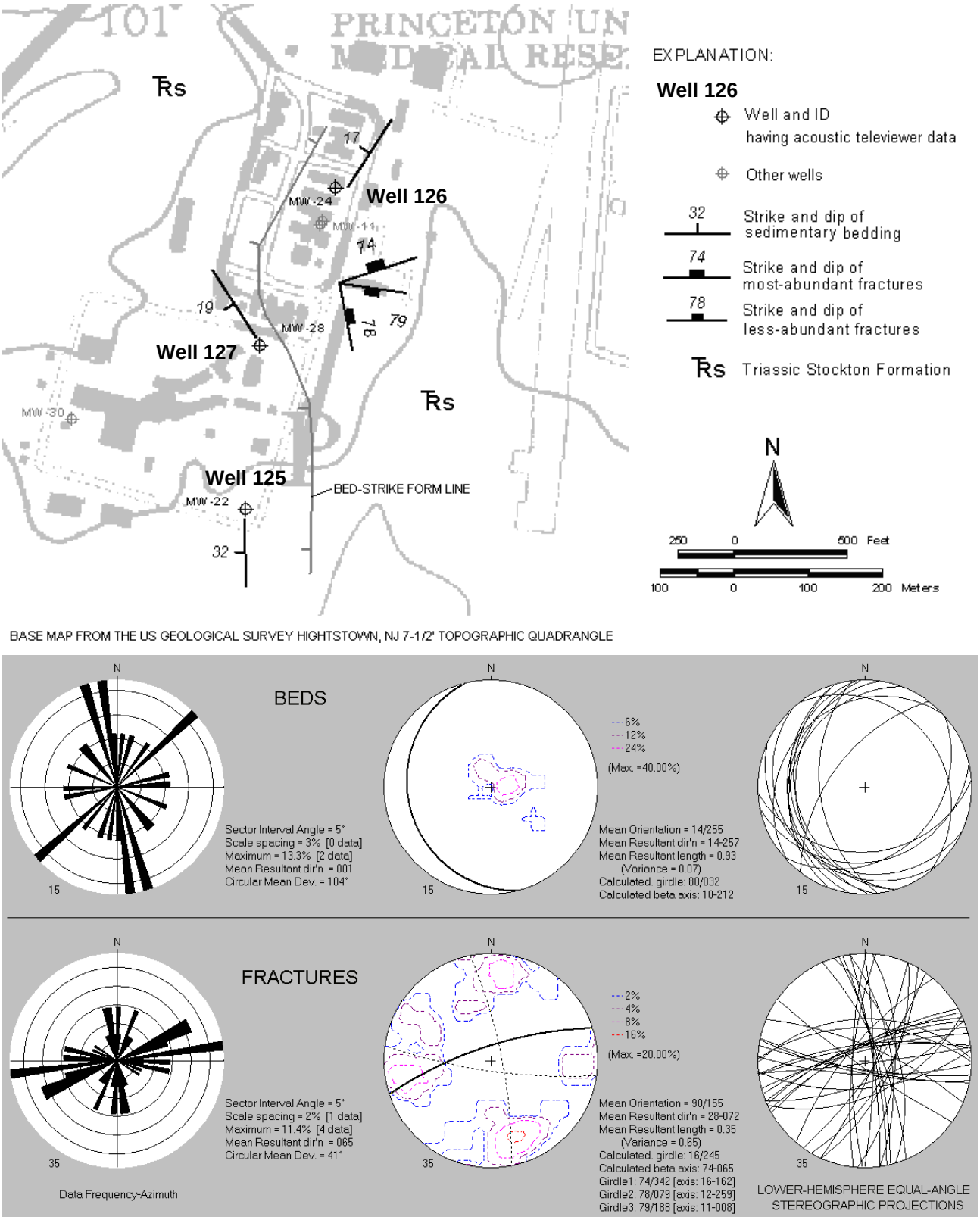

Figure 4G1. Map (above) showing wells 125 to127 at the Princeton Plasma Physics Laboratory, Princeton University Forrestal Campus, Plainsboro Twp., Mercer County, NJ. Mapped structures based on a structural analysis of ATV data (below).

Wells 125 and 126 – Stockton sandstone

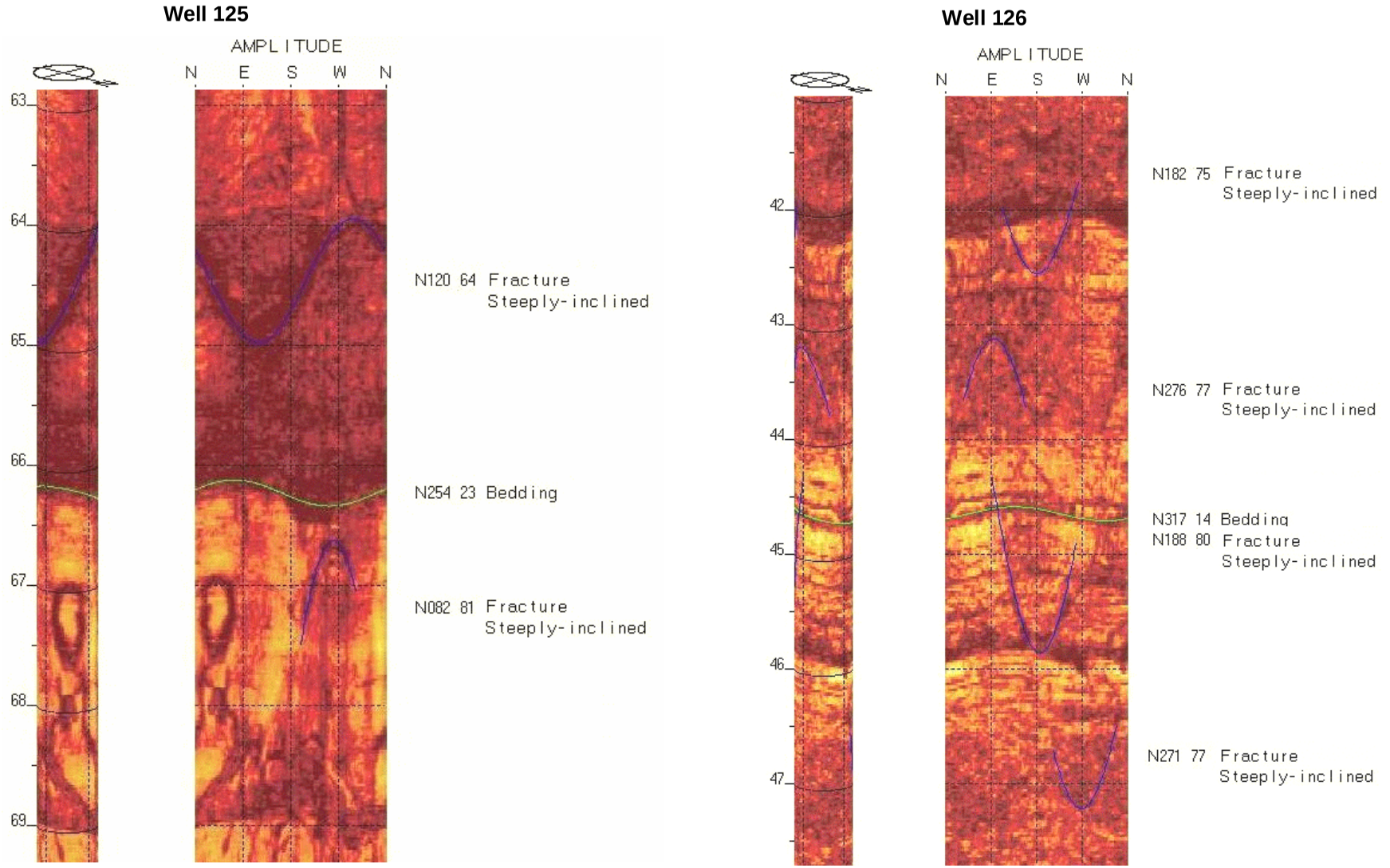

FIGURE 4G2. ATV records of 6-inch diameter wells 125 and 126 at the Princeton Plasma Physics Laboratory, Princeton University Forrestal Campus, Plainsboro Twp., Mercer County, NJ showing geologic structures in the Stockton aquifer. Depth values are in feet below land surface.

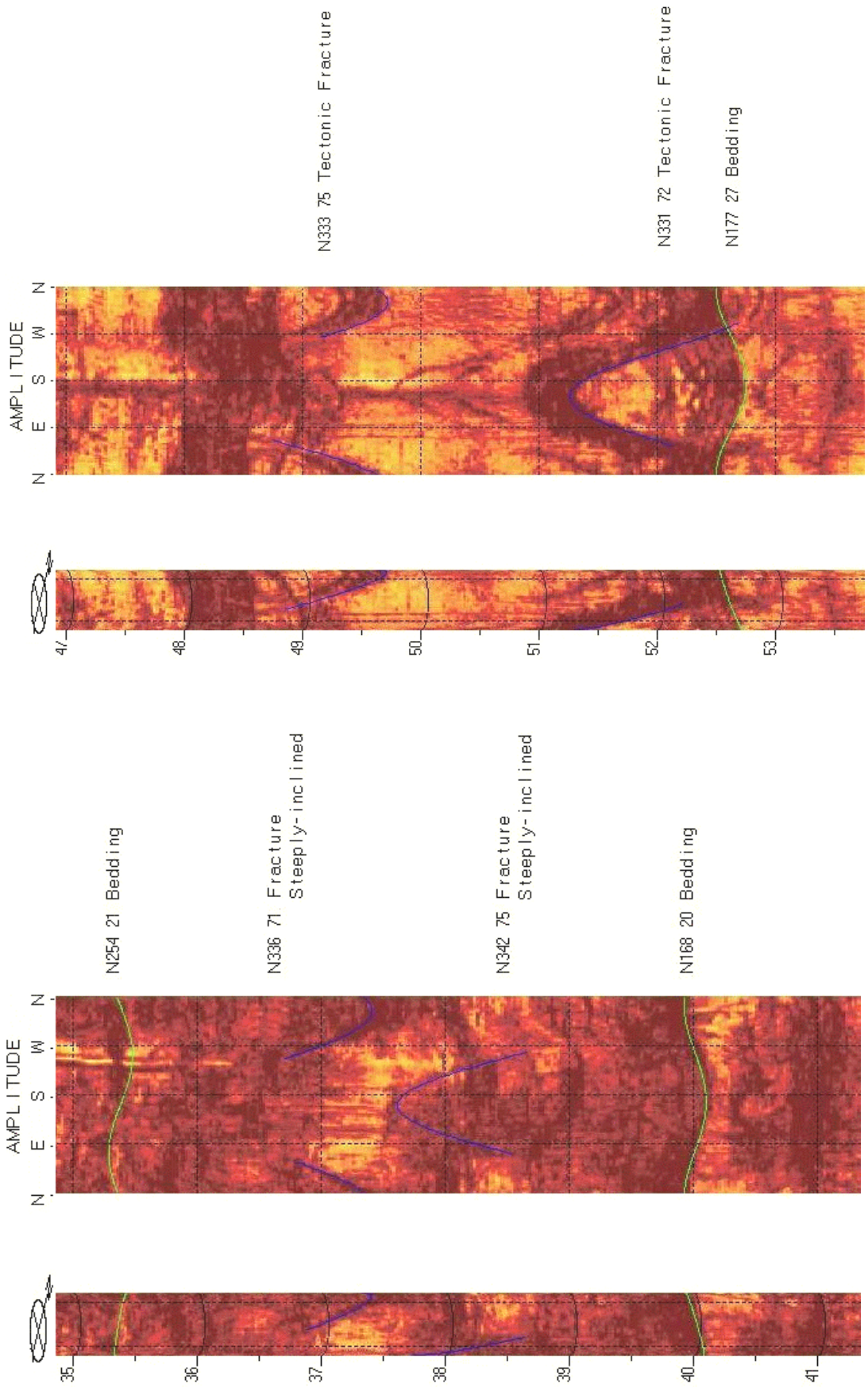

FIGURE 4G3. ATV records of 6-inch diameter well 127 at the Princeton Plasma Physics Laboratory, Princeton University Forrestal Campus, Plainsboro Twp., and Mercer County, NJ showing geologic structures in the Stockton aquifer. Depth values are in feet below land surface.